# Cover Picture

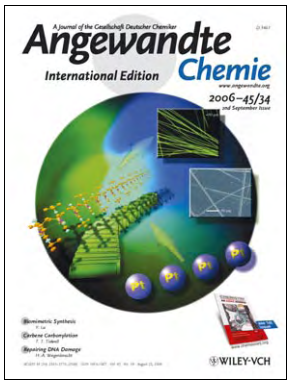


**Yinghui Sun, Kaiqi Ye, Hongyu Zhang, Junhu Zhang, Lan Zhao, Bao Li, Guangdi Yang, Bai Yang, Yue Wang,* Siu-Wai Lai, and Chi-Ming Che***

***Platinum(II)-to-platinum(II)*** interactions mediate and direct the formation of micro- and nanometer-scale molecular wires of $[Pt(CN\mathit{t}Bu)_2(CN)_2]$. The cover picture depicts models and microscopy images of the wires. Y. Wang, C.-M. Che, and co-workers describe in their Communication on page 5610 ff. the formation and photophysical properties of these photoluminescent molecular wires. An X-ray crystallographic study provides a structural basis for rationalizing the photoluminescent responses.

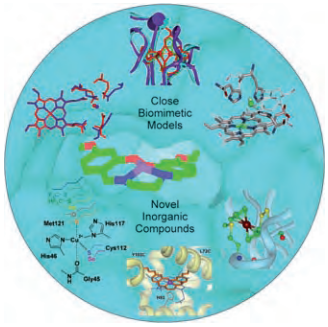


***Metalloenzymes***
Modern techniques from molecular biology can be used to modify metalloenzymes. In the Review on page 5588 ff., Y. Lu comments on the use of small stable proteins, and the introduction of non-natural amino acids and metal cofactors to produce better models of complex metalloproteins as well as novel structures.

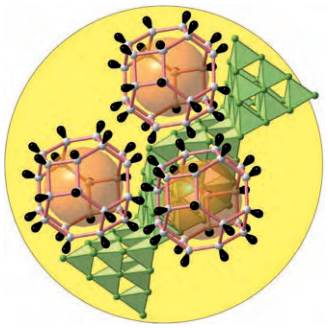

***Inorganic Structures***
In their Communication on page 5602 ff., M. Johnsson and co-workers describe how the structure of $Cu_{20}Sb_{35}O_{44}Cl_{37}$ is divided into a covalent part and an ionic part. The interface between the two parts is constituted by lone electron pairs belonging to $Sb^{3+}$ cations.

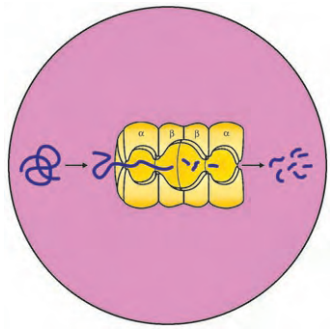

***Protein Engineering***
Multivalent chelator heads have been shown by R. Tampé and co-workers in their Communication on page 5702 ff. to act as synthetic gatekeepers that control the access to and the proteolytic activity of proteasome complexes.

# Contents

**The following Communications have been judged by at least two referees to be "very important papers" and will be published online at www.angewandte.org soon:**


*Jean-P. Leclerc, K. Fagnou**
**Palladium-Catalyzed Cross-Coupling Reactions of Diazine N-Oxides with Aryl Chlorides, Bromides, and Iodides**

*J. W. Lee, Jun-S. Lee, Young-T. Chang**
**Colorimetric Identification of Carbohydrates by a pH Indicator/pH-Change-Inducer Ensemble**

*Zhi-M. Cui, Q. Liu, Wei-G. Song*, Li-J. Wan**
**Insights into the Mechanism of Methanol-to-Olefin Conversion from Zeolites with Systematically Selected Framework Structures**

*J. A. Porco, Jr.,* S. Su, X. Lei, S. Bardhan, S. D. Rychnovsky*
**Total Synthesis and Structure Assignment of (+)-Hexacyclinol**

*S. Hiraoka, K. Harano, M. Shiro, Y. Ozawa, N. Yasuda, K. Toriumi, M. Shionoya**
**Isostructural Coordination Capsules with a Series of 10 Different $d^5$–$d^{10}$ Transition-Metal Ions**

*J. G. Cordaro, D. Stein, H. Rüegger, H. Grützmacher**
**Making the True "CP" Ligand**


## News


Chemistry: Whitesides honored ____ 5576

Medicinal Chemistry: Kubinyi recognized ____ 5576

Electrochemistry: Prize for Wang ____ 5576


## Books


Crystalline Molecular Complexes and Compounds — Frank H. Herbstein — *reviewed by A. Gavezzotti* ____ 5577

Value Creation — Florian Budde, Utz-Hellmuth Felcht, Heiner Frankemölle — *reviewed by A. Kleemann* ____ 5577


## Highlights

### Nitrogen-Substituted Ketenes


T. T. Tidwell* ____ 5580 – 5582

Blue, but Not a Mirage: Stable Aminoketenes by Carbene Carbonylation


**A true oasis**: The preparation of the first isolable aminoketenes by carbon monoxide addition to nitrogen-substituted carbenes (see scheme; Ar = 2,6-$i$Pr$_2$C$_6$H$_3$) fills a void in ketene chemistry in unexpected ways, and further provides a visual demonstration of ketene HOMO–LUMO interactions.

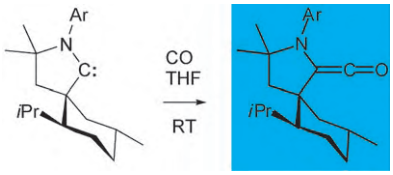


### DNA Repair


H.-A. Wagenknecht* ____ 5583 – 5585

The Search for Single DNA Damage among Millions of Base Pairs: DNA Glycosylases Trapped at Work


**Flipped out?** The location of base lesions by DNA glycosylases does not necessarily need complete base-flipping into the active site as recent structures of DNA-protein complexes show (see picture; oG = 8-oxoguanine).

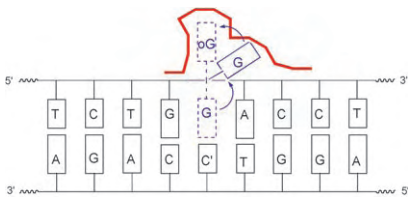




InterScience


© 2006 Wiley-VCH Verlag GmbH & Co. KGaA, Weinheim

# Reviews

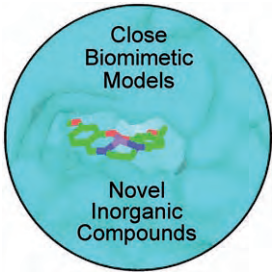


**One hand washes the other**: The methods of inorganic chemistry have for many years supported biology. It is now time to show what new biological techniques can do for inorganic chemistry.

*Chemical Biology*

Y. Lu* _____ **5588 – 5601**

Biosynthetic Inorganic Chemistry

# Communications

**The lone (ar)ranger**: The structure of $Cu_{20}Sb_{35}O_{44}Cl_{37}$ is divided up into two parts: ionically bonded $Cu^{+}$–$Cl^{-}$ supertetrahedra (green) and covalently bonded clusters that resemble zeolite β cages. The $Sb^{3+}$ ions (gray) lie at the vertices of the cages, while their lone pairs of electrons form surfaces that separate the covalent and ionic parts.

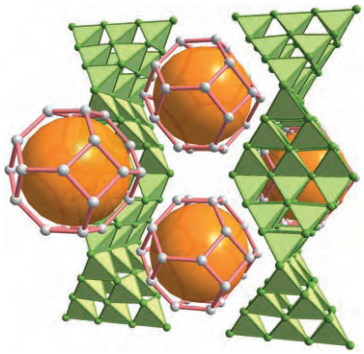

*Inorganic Chemistry*

Z. Mayerová, M. Johnsson,*
S. Lidin _____ **5602 – 5606**

Lone-Pair Interfaces That Divide Inorganic Materials into Ionic and Covalent Parts

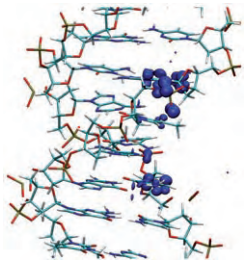

**Double or nothing**: Large-scale density functional calculations are used to study the formation of a large polaron on three proximal guanines (see picture). The formation was observed by step by step following of a proton-coupled charge transfer. The role played by the double proton transfer and a new and unexpected role for the tautomers of G and C were found.

*Charge Transfer*

F. L. Gervasio,* M. Boero,
M. Parrinello _____ **5606 – 5609**

Double Proton Coupled Charge Transfer in DNA

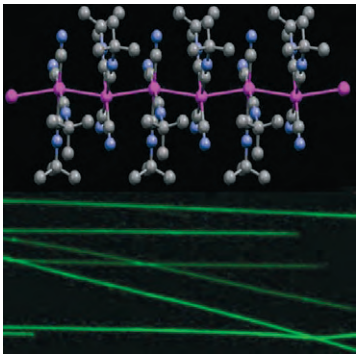

**Down to the wire**: $Pt^{II}\cdots Pt^{II}$ interactions provide the cohesive driving force for the construction of micro- and nanometer-scale luminescent wires, such as nanowires of $[Pt(CNtBu)_2(CN)_2]$ (see picture; Pt pink, N blue, C gray), which is a potential candidate for applications in nano-optical, electronic, and sensory devices.

*Nanowires*

Y. Sun, K. Ye, H. Zhang, J. Zhang, L. Zhao, B. Li, G. Yang, B. Yang, Y. Wang,* S.-W. Lai, C.-M. Che* _____ **5610 – 5613**

Luminescent One-Dimensional Nanoscale Materials with $Pt^{II}\cdots Pt^{II}$ Interactions

**For the USA and Canada:**
ANGEWANDTE CHEMIE International Edition (ISSN 1433-7851) is published weekly by Wiley-VCH PO Box 191161, D 69451 Weinheim, Germany. Air freight and mailing in the USA by Publications Expediting Inc. 200 Meacham Ave., Elmont, NY 11003. Periodicals postage paid at Jamaica NY 11431. US POSTMASTER: send address changes to *Angewandte Chemie*, Wiley-VCH, 111 River Street, Hoboken, NJ 07030. Annual subscription price for institutions: US$ 5685/5168 (valid for print and electronic / print or electronic delivery); for individuals who are personal members of a national chemical society prices are available on request. Postage and handling charges included. All prices are subject to local VAT/sales tax.


© 2006 Wiley-VCH Verlag GmbH & Co. KGaA, Weinheim

# The best in chemistry –

## for more than a hundred years

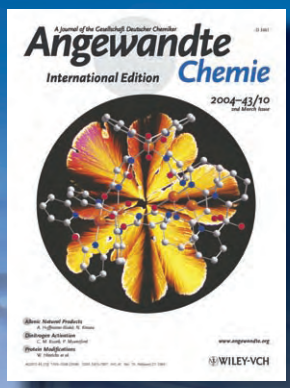


A Journal of the Gesellschaft Deutscher Chemiker

**Angewandte**
**International Edition** **Chemie**

**www.angewandte.org**

***1888:*** ***The beginning of a success story***

### Constant Innovations

***1962:*** *First issue of the International Edition*
***1976:*** *Graphical abstracts*
***1979:*** *Cover pictures*
***1988:*** *Centenary of Angewandte*
***1989:*** *Routine use of color*
***1991:*** *New section: Highlights*
***1992:*** *Computerized editorial tracking system*
***1995:*** *Internet service for readers*
***1998:*** *Regular press service; full-text online*
***2000:*** *New section: Essays; EarlyView: Communications available online ahead of the printed version*
***2001:*** *New section: Minireviews*
***2002:*** *Online submission of manuscripts*
***2003:*** *Weekly publication; new section: News; new layout*
***2004:*** *Backfiles (1962-1997); ManuscriptXpress: Online system for authors and referees*

### Angewandte's advisors...

***E. W. "Bert" Meijer***
*Technische Universiteit Eindhoven*

» ***Angewandte Chemie,*** *in its way of publishing, is as original as the chemistry described in the journal. It serves our society in a superb and attractive way. Many leading communications and comprehensive reviews have been published through the years and many of them are used in my teaching and cited in my own papers. It is a privilege to publish in and to be connected to a journal that is the trendsetter in chemistry of the highest standards.* «

***Angewandte Chemie International Edition*** *is a journal of the German Chemical Society (GDCh)*

GDCh

WILEY InterScience® DISCOVER SOMETHING GREAT

WILEY-VCH

12001404_gu

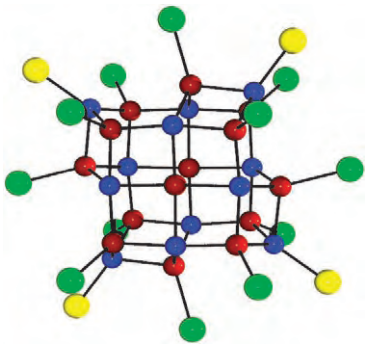

**A novel construction**: The reaction of $[FeCl_4]^-$ with $(Me_3Sn)_3N$ leads to the cluster $[Fe_{14}N_8(NSnMe_3)_4Cl_{12}]^{4-}$ (see picture; Fe red, N blue, Sn yellow, Cl green; Me groups omitted), which has a core built from 16 $Fe_2N_2$ rhombs. Mössbauer spectroscopy indicates the presence of 12 $Fe^{III}$ and 2 $Fe^{II}$ ions, and magnetic measurements suggest an $S = 2$ ground state for the cluster.


**Iron Nitride Clusters**

M. V. Bennett, R. H. Holm* . **5613 – 5616**

Self-Assembly of a Tetradecanuclear Iron Nitride Cluster


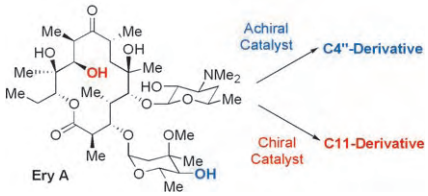


**Reversal**: Simple peptide-based nucleophilic catalysts can perturb the inherent reactivity hierarchy of the polyol natural product erythromycin A (see picture). Such catalyst-dependent modifications that reorganize natural product architecture may be of utility for generation of natural product analogs.


**Natural-Product Modification**

C. A. Lewis, S. J. Miller* **5616 – 5619**

Site-Selective Derivatization and Remodeling of Erythromycin A by Using Simple Peptide-Based Chiral Catalysts


**Twists in a spin**: RNA structural constraints have been obtained directly by exploiting the dependence of inter- and intranucleotide $^1H$–$^1H$ interactions on RNA conformation through the use of $^{13}C$ MAS solid-state NMR spectroscopy. The data provide evidence that $(CUG)_{97}$ RNA principally adopts an A-form helix conformation with a C3′-*endo* sugar pucker and an *anti* glycosidic torsion angle $\chi$ (see model).

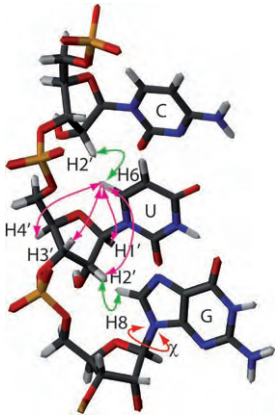



**Structure Determination**

K. Riedel, C. Herbst, S. Häfner, J. Leppert, O. Ohlenschläger, M. S. Swanson, M. Görlach, R. Ramachandran* **5620 – 5623**

Constraints on the Structure of $(CUG)_{97}$ RNA from Magic-Angle-Spinning Solid-State NMR Spectroscopy


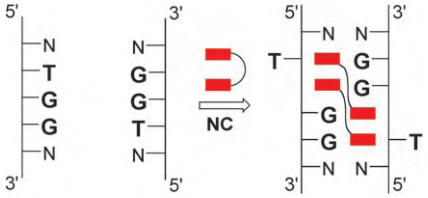


**A sticky end**: Two DNA strands that produce three contiguous mismatches (5′-TGG-3′/5′-TGG-3′ sequence) do not hybridize spontaneously, but are adhered by the mismatch-binding ligand naphthyridine carbamate dimer (**NC**; see picture, red rectangles: naphthyridine rings).


**DNA Hybridization**

T. Peng, C. Dohno, K. Nakatani* **5623 – 5626**

Mismatch-Binding Ligands Function as a Molecular Glue for DNA



© 2006 Wiley-VCH Verlag GmbH & Co. KGaA, Weinheim

# Contents


## Electron Transfer

M. P. Eng, B. Albinsson* — **5626 – 5629**

Non-Exponential Distance Dependence of Bridge-Mediated Electronic Coupling

**Donor chromophores** attached to oligo(phenyleneethynylene) molecular bridges of varying length have attenuation factors for electron tunneling $\beta$ that vary systematically with the donor–bridge (DB) energy gap (see picture). Investigations show that for bridges with ethynylene and vinylene repeating subunits, the electronic coupling increases with increasing donor–acceptor (DA) distance. A simple model accounts for this unexpected observation.

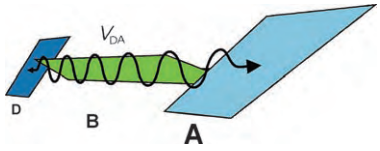


## Molecular Recognition

T. Ito, T. Yamaguchi* — **5630 – 5633**

Nonlinear Self-Excited Oscillation of a Synthetic Ion-Channel-Inspired Membrane

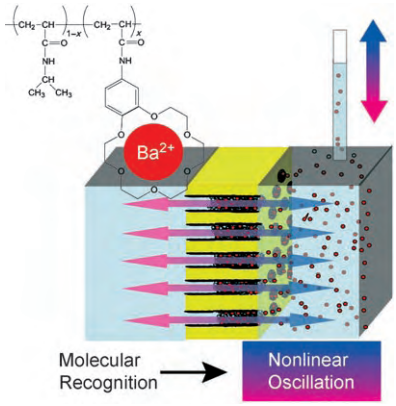


**In full swing**: Nonlinear oscillations by molecular signals are one of the inherent properties of life. An artificial ion-gating membrane, which was synthesized from a thermosensitive polymer and a crown ether, generated a relaxation oscillation similar to that of neurons in response to a specific ion signal (see picture).

## Protein Engineering

D. Sharma, Y. Cao, H. Li* — **5633 – 5638**

Engineering Proteins with Novel Mechanical Properties by Recombination of Protein Fragments

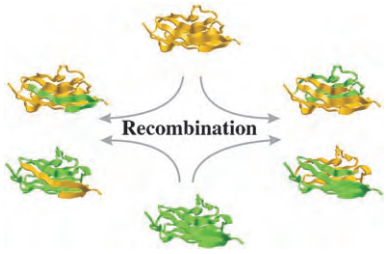


**The power of recombination**: A DNA-shuffling-based recombination technique was used to recombine protein fragments from two parent proteins to generate hybrid proteins, which can fold into three-dimensional structures similar to those of the parent proteins. These designed hybrid proteins are mechanically stable and display novel mechanical properties.

## Bismuth Clusters

P. C. Andrews,* G. B. Deacon, C. M. Forsyth, P. C. Junk, I. Kumar, M. Maguire — **5638 – 5642**

Towards a Structural Understanding of the Anti-Ulcer and Anti-Gastritis Drug Bismuth Subsalicylate

**The action of Pepto-Bismol** arising from the structure and hydrolysis of bismuth subsalicylate (BSS) is not yet understood. Two bismuth oxosalicylate clusters, $[Bi_{38}O_{44}(HSal)_{26}(Me_2CO)_{16}(H_2O)_2]$ (**1**) and $[Bi_9O_7(HSal)_{13}(Me_2CO)_5]$ (**2**), have been characterized which provide structural insight into the nature of BSS. A $Bi_9O_7$ cluster forms the core of **2** and is found at the heart of **1** (see picture; core Bi atoms: green, core O atoms: red).

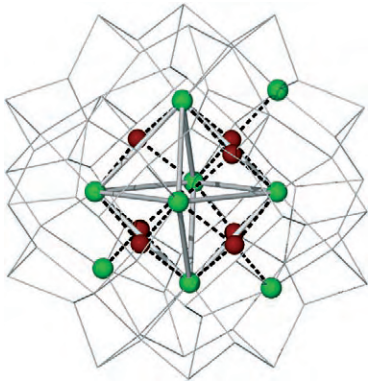



© 2006 Wiley-VCH Verlag GmbH & Co. KGaA, Weinheim

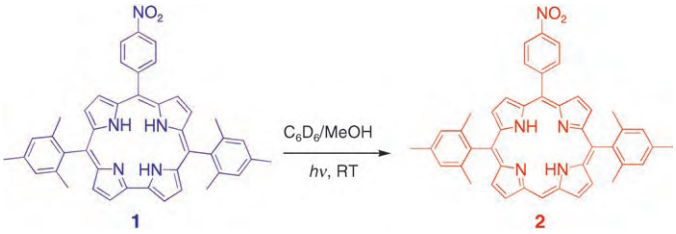


**As easy as $AB_2C$**: Irradiation of a solution of the free-base corrole **1** with a 400-W lamp led to its conversion into the corresponding *trans*-$AB_2C$-porphyrin **2** and an open-chain biliverdin-type by-product.

## Porphyrinoids

C. P. Gros, J.-M. Barbe,* E. Espinosa, R. Guilard* ——— **5642 – 5645**

Room-Temperature Autoconversion of Free-Base Corrole into Free-Base Porphyrin

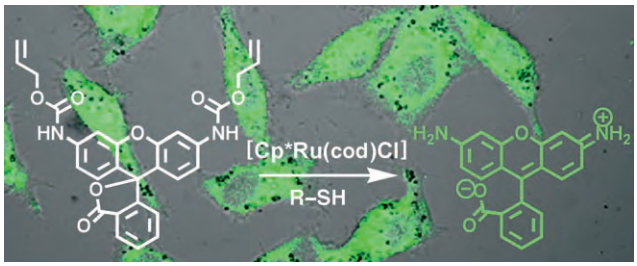


**Easy going**: A ruthenium-catalyzed release of amines from their respective allylcarbamates is disclosed and is a step towards the design of catalysts as tools for cellular biology. The reaction tolerates the combination of water, air, and thiols and can be performed inside living mammalian cells. Cp* = pentamethylcyclopentadienyl, cod = 1,5-cyclooctadiene.

## Bioorganometallic Chemistry

C. Streu, E. Meggers* ——— **5645 – 5648**

Ruthenium-Induced Allylcarbamate Cleavage in Living Cells

**Problem child**: The application of signaling DNA-aptamer technology to the development and execution of a high-throughput screen for an otherwise problematic target, adenosine deaminase (ADA), is reported. The approach employed a signaling DNA aptamer that reports on adenosine concentration (see scheme). The assay was robust in a screen of more than 44 000 molecules and revealed a new competitive inhibitor of the deaminase.

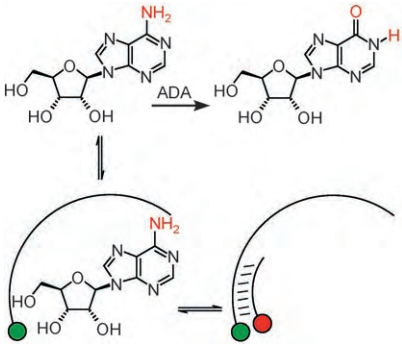


## Screening

N. H. Elowe, R. Nutiu, A. Allali-Hassani, J. D. Cechetto, D. W. Hughes, Y. Li,* E. D. Brown* ——— **5648 – 5652**

Small-Molecule Screening Made Simple for a Difficult Target with a Signaling Nucleic Acid Aptamer that Reports on Deaminase Activity

**Superduper**: A practical and cleaner synthetic protocol for various glycosides was established by means of a recyclable solid superacid promoter in supercritical carbon dioxide ($scCO_2$). Anomeric mixtures composed of α- and β-isomers were successfully separated by employing supercritical fluid chromatography (SFC) with $scCO_2$ and methanol. L = leaving group, P = protecting group, ROH = sphingosine, sugar, etc.

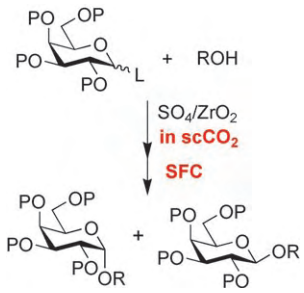


## Glycosidation

X.-B. Li, M. Ogawa, T. Monden, T. Maeda, E. Yamashita, M. Naka, M. Matsuda, H. Hinou, S.-I. Nishimura* **5652 – 5655**

Glycosidation Promoted by a Reusable Solid Superacid in Supercritical Carbon Dioxide


© 2006 Wiley-VCH Verlag GmbH & Co. KGaA, Weinheim

# Contents


## Thermoelectric Materials

X. Qiu, L. N. Austin, P. A. Muscarella, J. S. Dyck,* C. Burda* ——— **5656 – 5659**

Nanostructured $Bi_2Se_3$ Films and Their Thermoelectric Transport Properties

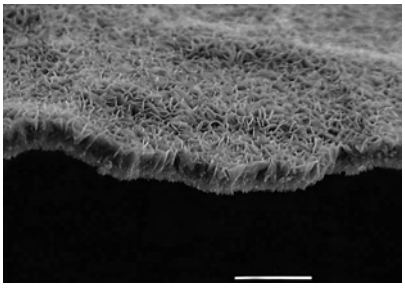

**A new strategy** to grow thermoelectric nanostructures on a wide variety of substrates is introduced. The synthesis involves the reduction of a selenium precursor to promote nucleation with bismuth ions to produce $Bi_2Se_3$ nanostructured films (see picture, scale bar 10 μm) under thermodynamic control. Thermoelectric transport measurements of the nanostructured films were performed from 6 to 300 K.

## Labeled Amino Acids

P. K. Mikhailiuk, S. Afonin, A. N. Chernega, E. B. Rusanov, M. O. Platonov, G. G. Dubinina, M. Berditsch, A. S. Ulrich,* I. V. Komarov* **5659 – 5661**

Conformationally Rigid Trifluoromethyl-Substituted α-Amino Acid Designed for Peptide Structure Analysis by Solid-State $^{19}F$ NMR Spectroscopy

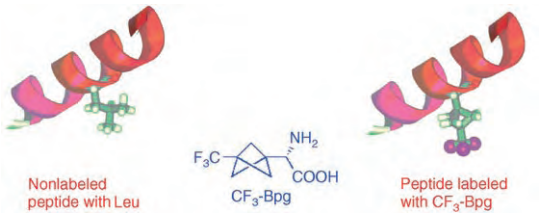


**Designing a sturdy label**: The fluorinated amino acid L-$CF_3$-Bpg (see picture), which was specifically designed as a $^{19}F$ NMR label for structure analysis of membrane-bound peptides, does not display the drawbacks of previously used labels. The amino acid can be readily incorporated into peptides and is particularly suitable as a substitute for Leu, Ile, and Met.

## Superlattices

Y. Yang, S. Liu, K. Kimura* ⎯ **5662 – 5665**

Superlattice Formation from Polydisperse Ag Nanoparticles by a Vapor-Diffusion Method

**A self-correction process** that is time- and pH-dependent results in growth of perfect superlattices from a bulk solution of hydrophilic Ag nanoparticles, despite their polydispersity, by a vapor-diffusion technique. After 12 weeks, three-dimensional rhombic superlattices are obtained (see picture).

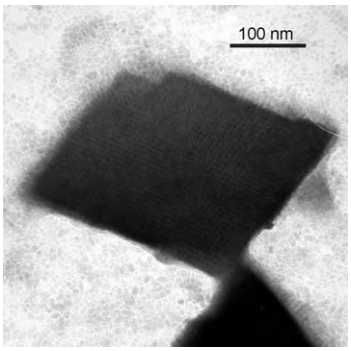


## Heterocycles

M. Pittelkow, T. K. Reenberg, K. T. Nielsen, M. J. Magnussen, T. I. Sølling, F. C. Krebs, J. B. Christensen* ——— **5666 – 5670**

Synthesis, Structure, and Properties of 4,7-Dimethoxybenzo[*c*]tellurophene: A Molecular Pyroelectric Material

**More than just curiosities**: The synthesis and characterization of a stable benzo[*c*]-tellurophene are presented. Te···Te interactions are shown to be one of the main driving forces for the crystal-packing properties of this electron-rich benzo[*c*]-tellurophene; furthermore, investigation of its pyroelectric properties reveals a secondary pyroelectric effect.



© 2006 Wiley-VCH Verlag GmbH & Co. KGaA, Weinheim

**The expanded phthalocyanine** dicarbahemiporphyrazine forms complexes in which the arene CH groups are in close proximity to the metal center. In the case of the copper adduct, one of the two C–H bonds is attacked by a solvent pyridine molecule, thereby forming a C–N bond (see picture; C gray, N blue, H light green). This reaction may proceed by oxidative nucleophilic substitution of hydrogen.

## Porphyrinoid Chemistry

R. Wu, A. Çetin, W. S. Durfee,*
C. J. Ziegler* ——— **5670 – 5673**

Metal-Mediated C–H Bond Activation in a Carbon-Substituted Hemiporphyrazine

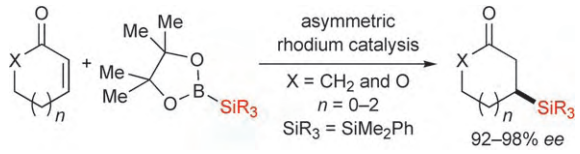


**Missing linkage**: A chiral cationic rhodium complex catalyzes the enantioselective conjugate addition of silyl anion equivalents to cyclic α,β-unsaturated ketones (X = $CH_2$) and esters (X = O; see scheme). This unprecedented catalytic process enables the asymmetric formation of a carbon–silicon bond, thus providing a facile access to α-chiral organosilicon compounds.

## Asymmetric Catalysis

C. Walter, G. Auer,
M. Oestreich* ——— **5675 – 5677**

Rhodium-Catalyzed Enantioselective Conjugate Silyl Transfer: 1,4-Addition of Silyl Boronic Esters to Cyclic Enones and Lactones

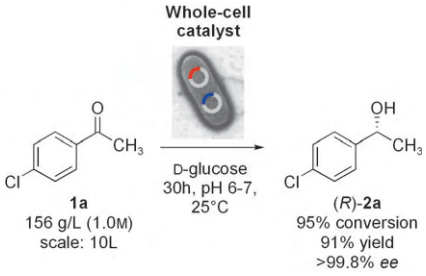


**Productive cells**: In a simple, highly efficient process for the synthesis of optically active alcohols, ketones are reduced by "designer cells" at high substrate concentrations and without the addition of an "external" cofactor in aqueous reaction medium. A wide range of *R* and *S* alcohols can be prepared with conversions of > 90% and enantioselectivities of > 99% *ee* (scheme shows results from the application on a 10-L scale).

## Enzyme Catalysis

H. Gröger,* F. Chamouleau, N. Orologas,
C. Rollmann, K. Drauz, W. Hummel,
A. Weckbecker, O. May* ——— **5677 – 5681**

Enantioselective Reduction of Ketones with "Designer Cells" at High Substrate Concentrations: Highly Efficient Access to Functionalized Optically Active Alcohols

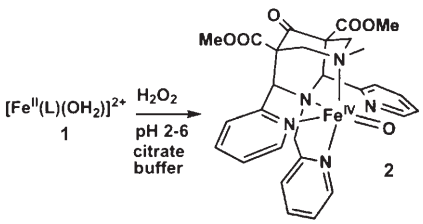


**A ferryl cation in water:** Iron(II) coordinated by the pentadentate ligand L reacts with $H_2O_2$ to form a low-spin $Fe^{IV}$=O complex with *S* = 1 (**2** in scheme) under conditions similar to those of the classical Fenton reaction. Complex **2** differs from a recently obtained high-spin aquated oxoiron(IV) species and demonstrates the role of the supporting polydentate ligand in controlling spin state and product formation.

## Coordination Chemistry

J. Bautz, M. R. Bukowski, M. Kerscher,
A. Stubna, P. Comba,* A. Lienke,
E. Münck,* L. Que, Jr.* ——— **5681 – 5684**

Formation of an Aqueous Oxoiron(IV) Complex at pH 2–6 from a Nonheme Iron(II) Complex and $H_2O_2$


© 2006 Wiley-VCH Verlag GmbH & Co. KGaA, Weinheim

# Contents


## Biosynthetic Pathways

M. S. Abdelfattah, J. Rohr* . . . . . **5685 – 5689**

Premithramycinone G, an Early Shunt Product of the Mithramycin Biosynthetic Pathway Accumulated upon Inactivation of Oxygenase MtmOII

**The unusual dodecaketide** premithramycinone G (see formula), which possesses a five-membered ring with two ketide chains in its tetracyclic structure, was accumulated upon inactivation of an early acting oxygenase of the mithramycin biosynthetic pathway. This unexpected structure allows novel hypothetic conclusions to be drawn regarding the early mithramycin pathway and suggestions for the involvement of three previously unassigned oxygenases.

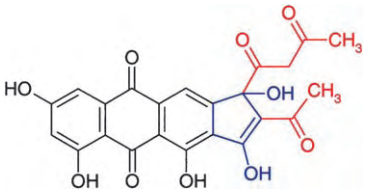


## Coordination Polymers

M. Scheer,* L. J. Gregoriades, A. V. Virovets, W. Kunz, R. Neueder, I. Krossing . . . . . **5689 – 5693**

Reversible Formation of Polymeric Chains by Coordination of Pentaphosphaferrocene with Silver(I) Cations

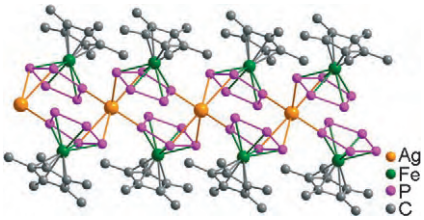


**A fragile coordination polymer**: The pentaphosphaferrocene $[Cp^*Fe(\eta^5\text{-}P_5)]$ reacts with the $Ag^I$ salt of the weakly coordinating anion $[Al\{OC(CF_3)_3\}_4]^-$ to yield a polymer comprising *cyclo*-$P_5$ moieties in an unprecedented 1,2,3-coordination mode (see figure). Analytical data and DFT calculations support the existence of a monomer/dimer/oligomer equilibrium in solution, which is entirely in favor of the monomer at room temperature and shifts to the dimer/oligomer at reduced temperatures.

## Asymmetric Rearrangement

M. E. Weiss, D. F. Fischer, Z.-q. Xin, S. Jautze, W. B. Schweizer, R. Peters* . . . . . **5694 – 5698**

Practical, Highly Active, and Enantioselective Ferrocenyl–Imidazoline Palladacycle Catalysts (FIPs) for the Aza-Claisen Rearrangement of *N*-*para*-Methoxyphenyl Trifluoroacetimidates

**Just a pinch of catalyst**: Just 0.05 mol% of a novel planar chiral ferrocenyl–imidazoline palladacycle catalyst (FIP) is sufficient to catalyze a highly efficient aza-Claisen rearrangement of *N*-*para*-methoxyphenyl trifluoroacetimidates and thereby provide access to chiral protected primary allylic amines with unprecedentedly high enantioselectivities (see scheme).

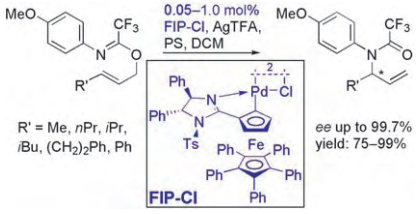


## Molecular Knots

M. Feigel,* R. Ladberg, S. Engels, R. Herbst-Irmer,* R. Fröhlich* . . . . . **5698 – 5702**

A Trefoil Knot Made of Amino Acids and Steroids

**Tying up the loose ends**: Cyclization of a linear hexapeptide made from alternating valine and α-aminodeoxycholanic acid units yielded two macrolactams: cyclo(valine-3-α-aminodeoxycholic acid amide)$_3$ and cyclo(valine-3-α-aminodeoxycholic acid amide)$_6$, the product of a cyclodimerization (see structure). X-Ray diffraction studies confirmed that the latter compound has the structure of a trefoil knot.

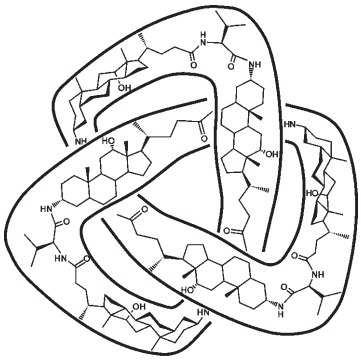



© 2006 Wiley-VCH Verlag GmbH & Co. KGaA, Weinheim

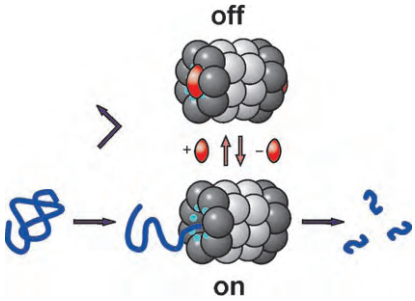


**Open sesame:** The proteasome complex is a nanodegradation machine that is essential for cellular protein turnover. A multivalent chelator head (MCH) was exploited for the specific binding to histidine-tagged proteasomes, even in crude cell lysates. Acting as synthetic gatekeepers, this MCH controls the access and thus the proteolytic activity of the nanomachinery.

***Nanobiotechnology***

K. Schulze, A. Mulder, A. Tinazli, R. Tampé* ——— **5702 – 5705**

Controlling the Activity of the 20S Proteasome Complex by Synthetic Gatekeepers

**Abstract art**: Bare $[MgO]^+$ ions can activate methane in a thermal ion/molecule reaction to afford $[MgOH]^+ + CH_3^{\bullet}$ as major products and $Mg^+ + CH_3OH$ in a side reaction. In conjunction with ab initio calculations, the results strongly support an hydrogen-atom abstraction mechanism which is assisted by a metal–carbon interaction (see scheme). Hydrocarbons (except methane) can also be activated by the magnesium-oxide cluster $[Mg_2O_2]^+$.

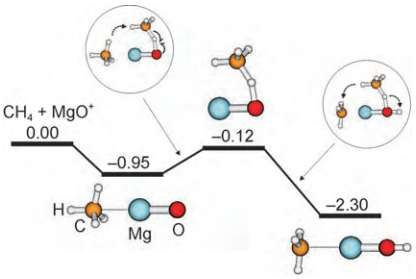


***Methane Activation***

D. Schröder,* J. Roithová* ——— **5705 – 5708**

Low-Temperature Activation of Methane: It also Works Without a Transition Metal

**Sources**

***Product and Company Directory***

You can start the entry for your company in "Sources" in any issue of *Angewandte Chemie*.

If you would like more information, please do not hesitate to contact us.

**Wiley-VCH Verlag – Advertising Department**
Tel.: 0 62 01 - 60 65 65
Fax: 0 62 01 - 60 65 50
E-Mail: MSchulz@wiley-vch.de

## Service

***Angewandte's Sister Journals*** ——— ***5710 – 5711***

***Keywords*** ——— ***5712***

***Authors*** ——— ***5713***

***Vacancies*** ——— ***A45***

***Preview*** ——— ***5715***

***For more information on Chemistry—An Asian Journal see www.chemasianj.org***


© 2006 Wiley-VCH Verlag GmbH & Co. KGaA, Weinheim

## Awarded...

### G. M. Whitesides receives Priestley Medal 2007

George M. Whitesides (Harvard University, Cambridge, MA, USA) will receive the highest honor of the American Chemical Society (ACS), the Priestley Medal, in recognition of distinguished service to chemistry. During the course of his career, Whitesides has made outstanding contributions to areas such as NMR spectroscopy, organometallic chemistry, organic synthesis with enzymes, materials and surface science, microfluidics, and nanotechnology, among others. In a Review recently published in *Angewandte Chemie*, Whitesides discussed the question of "*Why are proteins charged?*" by means of charge ladders and capillary electrophoresis.[1a] In much noted Essays, he has discussed the future of chemistry in general[1b] and that of nanoscience in particular.[1c] The ACS further recognizes his public service; for instance, he was recently involved in creating the National Academies' report entitled "Rising Above the Gathering Storm" for the US congress on the necessity of the advancement of education and science.

G. Whitesides

Whitesides completed his doctorate in 1964 at the California Institute of Technology (Pasadena) under the guidance of J. D. Roberts. He then accepted a position at Massachusetts Institute of Technology. He joined Harvard University in 1982. Whitesides is a member of the international advisory board of *Angewandte Chemie* and an honorary member of the editorial advisory board of *Small*.

### Skolnik Award for H. Kubinyi

With the Herman Skolnik Award, the Division of Chemical Information of the ACS honors outstanding contributions and achievements in the theory and practice of chemical information science. The 2006 prize has been awarded to Hugo Kubinyi (formerly BASF AG, Ludwigshafen, Germany) for his contributions to chemoinformatics, quantitative structure–activity relationships (QSAR),[2a,b] and combinatorial chemistry through his research into drug development. Kubinyi is the chairman of the editorial advisory board for the journal *QSAR & Combinatorial Science*. He is also an editor of the book series *Methods and Principles in Medicinal Chemistry* (Wiley-VCH) and a co-author of two volumes in this series.

H. Kubinyi

Kubinyi studied chemistry in Vienna and received his doctorate in 1965 from the Max Planck Institute for Biochemistry in Munich (Germany) under A. Butenandt (Nobel Prize in Chemistry in 1939) and E. Hecker. After a postdoctoral fellowship at the Deutsches Krebsforschungszentrum in Heidelberg, he began pharmaceutical research in 1966 at Knoll AG (Ludwigshafen), where he was responsible for the development of a partially synthetic heart glycoside.[2c] In 1985, Knoll AG was taken over by BASF. Kubinyi remained at BASF until his retirement in 2001. From 1987, he was responsible for molecular modeling, protein crystallization, and drug development, and after 1998 also for combinatorial chemistry. From 1986, he was also Professor of Pharmaceutical Chemistry at the University of Heidelberg.

### J. Wang honored with Cole–Parmer Award

Joseph Wang (Arizona State University, Tempe, USA) will receive the Cole–Parmer Award from the Division of Analytical Chemistry of the ACS for outstanding achievements in the area of electrochemistry. Wang received his doctorate from the Israel Institute of Technology (Haifa) in 1978. He then spent two years researching at the University of Wisconsin–Madison, and in 1980 he joined New Mexico State University (Las Cruces), where he was appointed professor in 2001. Since 2004, he is Professor of Chemical and Materials Engineering and Chemistry and Biochemistry at Arizona State University. His research areas include electrochemistry, biosensors,[3a] nanobiotechnology, microfluidics, and environmental monitoring. He recently reported in *Angewandte Chemie* on DNA-based amplified bioelectronic detection and coding of proteins,[3b] and discussed nanomaterial-based amplified transduction of biomolecular interactions in a Review published in *Small*.[3c] Wang is currently the chief editor of the journal *Electroanalysis* and the author of a book about analytical electrochemistry (Wiley 2006).

J. Wang


[1] a) I. Gitlin, J. D. Carbeck, G. M. Whitesides, *Angew. Chem.* **2006**, *118*, 3090; *Angew. Chem. Int. Ed.* **2006**, *45*, 3022; b) G. M. Whitesides, *Small*, **2005**, *1*, 172; c) G. M. Whitesides, *Angew. Chem.* **2004**, *116*, 2716; *Angew. Chem. Int. Ed.* **2004**, *43*, 3632.

[2] a) H. Kubinyi, *Chem. Unserer Zeit* **1986**, *20*, 191; b) H. Kubinyi, *Quant. Struct.-Act. Rel.* **2002**, *21*, 348; c) H. Kubinyi, D. Hotz, W. Steidle, *Liebigs Ann. Chem.* **1973**, 224.

[3] a) J. Wang, *Electroanalysis* **2005**, *17*, 7; b) J. Wang, G. Liu, B. Munge, L. Lin, Q. Zhu, *Angew. Chem.* **2004**, *116*, 2210; *Angew. Chem. Int. Ed.* **2004**, *43*, 2158; c) J. Wang, *Small*, **2005**, *1*, 1036.


DOI: 10.1002/anie.200603095


WILEY InterScience DISCOVER SOMETHING GREAT
© 2006 Wiley-VCH Verlag GmbH & Co. KGaA, Weinheim

Nitrogen-Substituted Ketenes

DOI: 10.1002/anie.200601643

# Blue, but Not a Mirage: Stable Aminoketenes by Carbene Carbonylation**

*Thomas T. Tidwell**

**Keywords:**
carbenes · carbonylation · ketenes · reactive intermediates · synthetic methods

Soon after the preparation and isolation of the first ketene in 1905[1a] efforts were made to prepare ketenes with highly electronegative heteroatom substituents, including examples with oxygen and halogen atoms bonded to the ketene.[1b–d,2,3] However, these efforts did not yield isolable ketenes, and it was apparent that these species were very reactive. Oxygen-substituted ketenes[2a,b] were however successfully generated and captured in situ with imines in [2+2] cycloaddition reactions.[2a] These compounds were much later directly observed by IR or UV spectroscopy in frozen matrices[2c] or as transient intermediates in solution,[2d] and were generated in the gas phase.[2e]

Halogen-substituted ketenes were an early target in ketene studies,[3a,b] but only in 1965–1966 was their generation conclusively demonstrated by trapping experiments,[3c–e] and even then the ketenes were not observed. Such compounds have only been observed in solution or matrices at low temperatures, or in the gas phase.[1b–d]

Although Staudinger speculated about the preparation of nitrogen-substituted ketenes,[2b] he apparently did not report any attempts directed toward their preparation. These compounds, however, ultimately proved to be of significant utility in the race to prepare penicillins.[4] The first reported successful preparation of a nitrogen-substituted ketene was evidently the reaction by Sheehan et al. of succinimidoacetyl chloride (**1**) with triethylamine, which generated ketene **2** as an unobserved intermediate. This intermediate was captured in situ by ketene–imine [2+2] cycloaddition with the thiazoline **3** to form **4**, which was used in the synthesis of a 5-phenyl penicillin **5** (Scheme 1).[4]

At the same time phthalimidoketene (**7**) was also generated by dehydrochlorination and trapped in situ by [2+2] cycloaddition wih imines, including benzylideneaniline (Scheme 2).[5a] The authors considered the possibility of ketene intermediates in these reactions,[5a] and it is now generally accepted that highly reactive ketenes are formed, but are too short-lived for direct observation.[1d,5c,d] Subsequently, the generation of nitrogen-substituted ketenes has been extensively examined, especially with regard to their use in β-lactam cyclization.[5b–d]

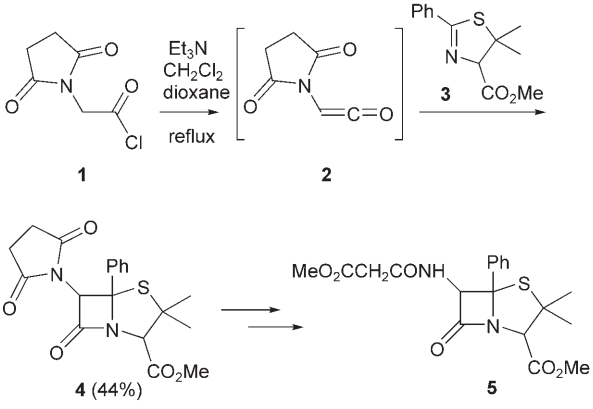


***Scheme 1.*** Preparation of a 5-phenyl penicillin **5** by ketene–imine [2+2] cycloaddition.

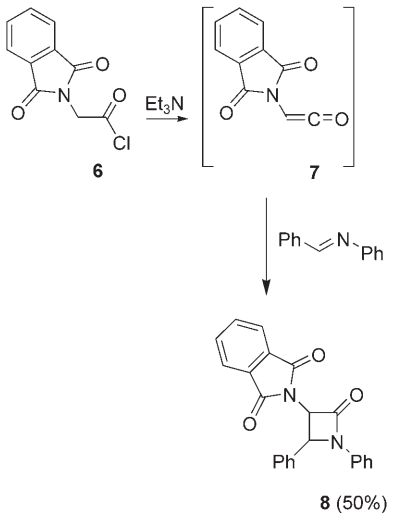


***Scheme 2.*** Phthalimidoketene generation and [2+2] cycloaddition.

The preparation of substituted phthalimidoketenes **10** was examined further by Winter and Pracejus by reaction of acid chlorides **9** with tertiary amines (Scheme 3), and for R = Bn, Ph, and *i*Pr, evidence for ketene formation in solution was provided in IR spectra by the observation of characteristic ketene bands at 2141, 2136, and 2125 $cm^{-1}$, respectively.[6] Dehydrochlorination of the acid chloride **9** (R = *t*Bu) with trimethylamine and subsequent distillation in high vacuum gave *tert*-butylphthalimidoketene (**10**, R = *t*Bu, m.p. 96–98 °C, IR absorption at 2134 $cm^{-1}$). The structure of **10** has

[*] Prof. T. T. Tidwell
Department of Chemistry
University of Toronto
Toronto, Ontario M5S 3H6 (Canada)
Fax: (+1) 416-978-3585
E-mail: ttidwell@chem.utoronto.ca

[**] Financial support by the Natural Sciences and Engineering Research Council of Canada is gratefully acknowledged.


InterScience
© 2006 Wiley-VCH Verlag GmbH & Co. KGaA, Weinheim

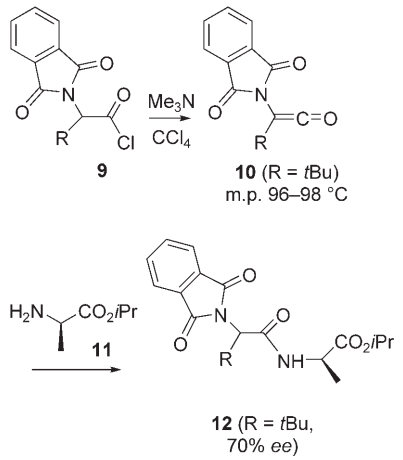


***Scheme 3.*** Formation of an isolable phthalimidoketene.

not been investigated by X-ray crystallography, but the steric stabilization from the two bulky groups and the delocalization of the nitrogen lone pair evidently permit this compound to be stable even in the solid state. Reaction of **10** (R = *t*Bu) with the *R*-alanine ester **11** at −62 °C gave the dipeptide **12** with 70 % *ee*. However, it appears that no aminoketenes were observed or isolated.

An explanation of the high reactivity of ketenes substituted with oxygen, nitrogen, and halogen substituents was provided by an observed correlation of computed isodesmic stabilization energies with substituent electronegativities; ketenes with electropositive substituents were better stabilized relative to those with electronegative substituents.[7] Ketenes were also shown to be stabilized by π-acceptor substituents and have a high electron density at C2, which would interact unfavorably with the lone pairs of the oxygen, nitrogen, and halogen substituents.

An early report of the isolation of a ketene with two nitrogen substituents by carbonylation of a stable carbene with carbon monoxide[8a] could not be substantiated experimentally and was calculated to be unfavorable energetically;[8b] nitrogen-substituted ketenes had thus remained as unobserved reactive intermediates. Unexpectedly, the route by carbene carbonylation has now proven to be successful[9a] in the first demonstration of the addition of carbon monoxide to stable amino-substituted acyclic carbenes **13a,b**[9b] and the cyclic carbene **15**,[9c] which reacted at room temperature in THF upon bubbling in carbon monoxide to form the stable ketenes **14a,b** and **16**, which each bear a single nitrogen substituent (Scheme 4).

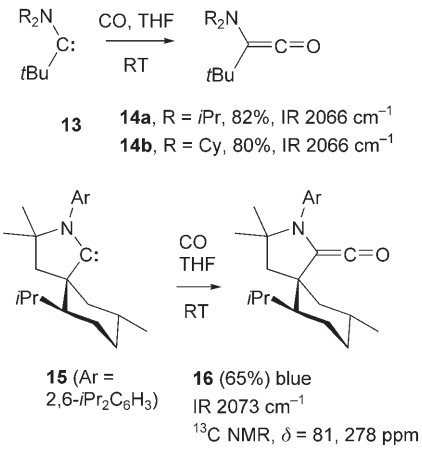


***Scheme 4.*** Stable aminoketenes by carbene carbonylation; Cy = cyclohexyl.

The ketenes **14** have the typical yellow color and IR and NMR spectra of ketenes, but **16** has an extraordinary blue color and a downfield NMR chemical shift for C2 of 278 ppm! The structures of the crystalline ketenes **14b** and **16** were determined by X-ray crystallography (Figures 1 and 2), and the structures **17** and **18** of the model aminoketene were calculated by using DFT methods (Scheme 5).

The structure of the flexible ketene **14b** showed a pyramidalized nitrogen atom (sum of the bond angles: 347.7°) with the nitrogen lone pair antiperiplanar to the C=C=O moiety. The calculated minimum-energy structure of **17** exhibited a similar geometry. However, for the rigid ketene **16** the X-ray structure showed a planar geometry for the nitrogen atom (sum of the bond angles: 357.3°) with the lone pair parallel to the C=C π system. The calculated structure of **18**, with a geometry similar to **16**, was not an energy minimum, and was 6.8 kcal mol$^{-1}$ less stable than **17**. The calculated singlet–triplet gaps for **17** and **18** are 23.9 and 17.0 kcal mol$^{-1}$, respectively, compared to a value of 51.8 kcal mol$^{-1}$ for $H_2C{=}C{=}O$, and the smaller gaps for **17** and **18** arise from increases in the HOMO energies, whereas the LUMOs are unaffected. The X-ray structure for **16** and the calculated structures of **17** and **18** show rather long bonds between the N atom and the ketenyl C atom (1.405, 1.443, and 1.409 A, respectively). These large bond lenths are indicative of little π bonding, and the blue color and long wavelength absorption (500–700 nm) of **16** was explained by the reduced HOMO–LUMO energy gap, which gives diradical character to this ketene.[9a] The remarkable $^{13}$C NMR chemical shift for the carbonyl carbon atom of **16** ($\delta = 278$ ppm) was explained by the reduced HOMO–LUMO energy gap, which results in an enhanced paramagnetic term.

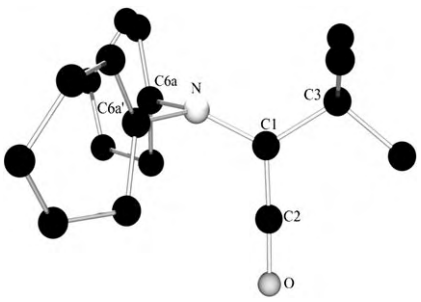


***Figure 1.*** X-ray structure for aminoketene **14b** (taken from reference [9a]).

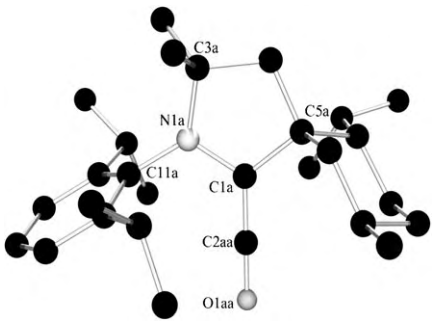


***Figure 2.*** X-ray structure for aminoketene **16** (taken from reference [9a]).

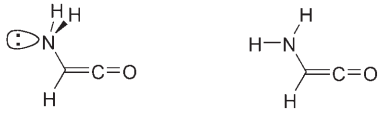


***Scheme 5.*** Computed structures of aminoketene.

The chemistry of carbenes and ketenes has been intertwined for almost a century, and early studies of the thermal


© 2006 Wiley-VCH Verlag GmbH & Co. KGaA, Weinheim

decarbonylation of ketenes played an important role in establishing the existence of carbenes as reactive intermediates.[10a] The photolysis and thermolysis of the parent ketene to form methylene remains one of the most-studied reactions of chemical physics after well over a half century.[10b,c] The synthesis of the ketenes **14** with pyramidyl, nonconjugating nitrogen atoms and **16** with a planar nitrogen atom that exhibits $\pi$ interaction with the ketene result from the unique properties of carbenes **13** and **15**. The readiness of these stable carbenes to react with carbon monoxide reveals a new attribute of these species, and has led to the preparation of new ketenes with startling properties. This development presages new discoveries still to come, including the preparation of still other new examples and the evaluation of the reactivities of these unique ketenes.

Published online: July 26, 2006


[1] a) H. Staudinger, *Ber. Dtsch. Chem. Ges.* **1905**, *38*, 1735 – 1739; b) for a historical account of the development of ketene chemistry, see: T. T. Tidwell, *Angew. Chem.* **2005**, *117*, 5926 – 5933; *Angew. Chem. Int. Ed.* **2005**, *44*, 5778 – 5785; c) for a review of recent developments in ketene chemistry, see: T. T. Tidwell, *Eur. J. Org. Chem.* **2006**, 563 – 576; d) T. T. Tidwell, *Ketenes*, 2nd ed., Wiley, Hoboken, **2006**.

[2] a) H. Staudinger, O. Kupfer, *Ber. Dtsch. Chem. Ges.* **1911**, *44*, 1638 – 1640; b) H. Staudinger, H. Schneider, *Helv. Chim. Acta* **1923**, *6*, 304 – 315; c) G. Maier, C. Rohr, *Liebigs Ann.* **1996**, 307 – 309; d) A. V. Fedorov, E. O. Danilov, A. G. Merzlikine, M. A. J. Rogers, D. C. Neckers, *J. Phys. Chem. A* **2003**, *107*, 3208 – 3214; e) T. Sugimura, *Eur. J. Org. Chem.* **2004**, 1185 – 1192.

[3] a) H. Staudinger, E. Anthes, H. Schneider, *Ber. Dtsch. Chem. Ges.* **1913**, *46*, 3539 – 3541; b) E. Ott, *Justus Liebigs Ann.* **1913**, *401*, 159 – 177; c) H. C. Stevens, D. A. Reich, D. R. Brandt, K. R. Fountain, E. J. Gaughan, *J. Am. Chem. Soc.* **1965**, *87*, 5257 – 5259; d) W. T. Brady, H. G. Liddell, W. L. Vaughn, *J. Org. Chem.* **1966**, *31*, 626 – 628; e) L. Ghosez, R. Montaigne, P. Mollet, *Tetrahedron Lett.* **1966**, 135 – 139.

[4] a) J. C. Sheehan, E. L. Buhle, E. J. Corey, G. D. Laubach, J. J. Ryan, *J. Am. Chem. Soc.* **1950**, *72*, 3829 – 3830; b) J. C. Sheehan, E. J. Corey, *J. Am. Chem. Soc.* **1951**, *73*, 4756 – 4759; c) J. C. Sheehan, *The Enchanted Ring*, MIT Press, Cambridge, **1982**.

[5] a) J. C. Sheehan, J. J. Ryan, *J. Am. Chem. Soc.* **1951**, *73*, 1204 – 1206; J. C. Sheehan, J. J. Ryan, *J. Am. Chem. Soc.* **1951**, *73*, 4367 – 4372; b) J. C. Sheehan, E. J. Corey, *Org. React.* **1957**, *9*, 388 – 408; c) C. Palomo, J. M. Aizpurua, *Science of Synthesis (Houben-Weyl)*, *Vol. 23.6* (Eds.: D. Bellus, R. Danheiser), Thieme, Stuttgart, **2006**; d) W. Reichen, *Chem. Rev.* **1978**, *78*, 569 – 588.

[6] S. Winter, H. Pracejus, *Chem. Ber.* **1966**, *99*, 151 – 159.

[7] a) L. Gong, M. A. McAllister, T. T. Tidwell, *J. Am. Chem. Soc.* **1991**, *113*, 6021 – 6028; b) M. A. McAllister, T. T. Tidwell, *J. Org. Chem.* **1994**, *59*, 4506 – 4515.

[8] a) S. N. Lyashchuk, Y. G. Skrypnik, *Tetrahedron Lett.* **1994**, *35*, 5271 – 5274; b) D. A. Dixon, A. J. Arduengo III, K. D. Dobbs, D. V. Khasnis, *Tetrahedron Lett.* **1995**, *36*, 645 – 648.

[9] a) V. Lavallo, Y. Canac, B. Donnadieu, W. W. Schoeller, G. Bertrand, *Angew. Chem.* **2006**, *118*, 3568 – 3571; *Angew. Chem. Int. Ed.* **2006**, *45*, 3488 – 3491; b) V. Lavallo, J. Mafhouz, Y. Canac, B. Donnadieu, W. W. Schoeller, G. Bertrand, *J. Am. Chem. Soc.* **2004**, *126*, 8670 – 8671; c) V. Lavallo, Y. Canac, C. Präsang, B. Donnadieu, G. Bertrand, *Angew. Chem.* **2005**, *117*, 5851 – 5855; *Angew. Chem. Int. Ed.* **2005**, *44*, 5705 – 5709.

[10] a) H. Staudinger, R. Endle, *Ber. Dtsch. Chem. Ges.* **1913**, *46*, 1437 – 1442; b) K. Knox, R. G. W. Norrish, G. Porter, *J. Chem. Soc.* **1952**, 1477 – 1486; c) W. F. Ross, G. B. Kistiakowsky, *J. Am. Chem. Soc.* **1934**, *56*, 1112 – 1115.


 © 2006 Wiley-VCH Verlag GmbH & Co. KGaA, Weinheim 

DNA Repair

DOI: 10.1002/anie.200602387

# The Search for Single DNA Damage among Millions of Base Pairs: DNA Glycosylases Trapped at Work

*Hans-Achim Wagenknecht**

**Keywords:**
base excision · base flipping · DNA damage · DNA · glycosylase

The maintenance of the genomic integrity by repairing DNA damage is critical and crucial for the survival of any living organism. DNA damage can occur spontaneously or be induced by chemicals or radiation and can have severe effects if not repaired.[1,2] DNA lesions yield mutations that interfere with cellular transactions and can lead to cancer in mammals.[3] To avoid such severe consequences, nature has evolved enzymatic DNA repair machineries.[4] They can be categorized[4] into 1) repair by direct reversal of damage, 2) base-excision repair (BER), 3) nucleotide-excision repair, 4) mismatch repair, and 5) repair of double-strand breaks.

Among these processes, the BER is well understood on the molecular level with respect to the enzymatic mechanism of DNA damage removal (Scheme 1).[5,6] BER proteins are primarily DNA glycosylases that hydrolyze the nucleosidic bond to the damaged DNA base yielding an abasic site. Subsequently, the deoxyribofuranoside is removed by β,δ-elimination. Monofunctional DNA glycosylases need a lyase as an additional enzyme to perform this reaction; bifunctional DNA glycosylases contain the catalytic lyase activity as a second function. Finally, the removed nucleotide is reinserted by DNA polymerases and ligases.

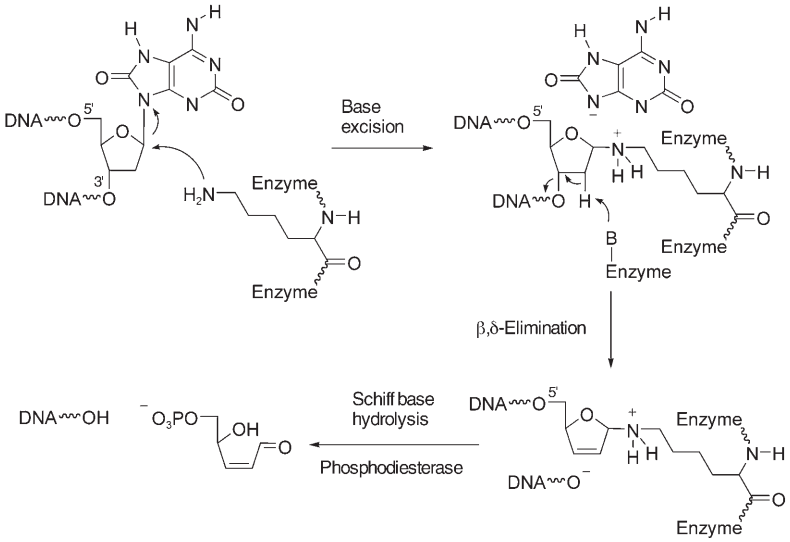


***Scheme 1.*** Principle mechanism of base excision by a bifunctional DNA glycosylase, such as hOGG1, through the Schiff base adduct formed between the protein and DNA. B = basic side chain of the enzyme.

In contrast to this profound understanding of the bioorganic details of the base excision mechanism, the actual damage recognition process remained poorly understood.[7] DNA glycosylases must check millions of base pairs of undamaged DNA to locate and then excise one single damaged nucleotide unit. It is hard to imagine that there are common characteristic properties among the various chemically different DNA modifications (such as deaminated, methylated, alkylated, or oxidized bases) that can be exploited by BER glycosylases to locate them.

It is obvious from the mechanism of glycosidic bond hydrolysis that, especially for enzymatic leaving-group activation, access of the DNA glycosylases to the damaged base, wich is normally hidden inside the base stack of the DNA duplex structure, is required. Hence, a common structural feature of all DNA glycosylases is the base-flipping of the damaged DNA base into an extrahelical pocket.[5–7] There, recognition of the modified base can take place by specific contacts to amino acids through electrostatic and stacking interactions as well as hydrogen bonding. It was proposed that these interactions in the protein-binding site discriminate between damaged or undamaged DNA bases.[5,6] Crystallographic data for a variety of BER protein–DNA complexes has evidenced that base flipping is a ubiquitous structural property of DNA glycosylases.[5–7]

The pure observation of base flipping as part of static protein structures does not answer the question of how DNA damage is recognized inside the DNA helix prior to the flipping process. In the late 1990s, several models were proposed of how these proteins locate

[*] Prof. H.-A. Wagenknecht
Institute for Organic Chemistry
University of Regensburg
93040 Regensburg (Germany)
Fax: (+49) 941-943-4617
E-mail: achim.wagenknecht@chemie.uni-regensburg.de
Homepage: http://www-oc.chemie.uni-regensburg.de/wagenknecht/


© 2006 Wiley-VCH Verlag GmbH & Co. KGaA, Weinheim

DNA damage.[8–10] In 1997, Verdine et al. divided the DNA lesions into strongly and not strongly helix-destabilizing lesions.[8] Of course, the target location of strongly helix-destabilizing lesions occurs through scanning of the surface of DNA until the protein detects a transiently extrahelical lesion. The protein then locks onto this lesion and catalyzes base excision. On the other hand, for intrahelical lesions that do not strongly destabilize the duplex structure, it was suggested that the protein checks both damaged and undamaged bases in the extrahelical enzyme pocket. This means that the enzyme migrates along the DNA helix exchanging one extrahelical base for the next until the base lesion is located. This base flipping of undamaged DNA bases represents a controversial aspect of this model for the search of DNA damage.

It is evident that the key information about DNA damage recognition would originate from structures of BER glycosylases in complexes with undamaged DNA targets. But how can an enzymatically active protein be trapped onto specific positions of an undamaged DNA target? In 2005, Verdine et al. presented the answer.[11] The published structure describes the protein complex consisting of human 8-oxoguanine (oG) glycosylase (hOGG1) and an undamaged DNA duplex. Verdine et al. previously reported a structure of inactivated hOGG1 bound to DNA containing oG.[12] The structure showed clearly the base-flipped situation of the oG moiety that is buried deeply into the active site of the protein where the nucleosidic hydrolysis takes place.

For the more-recent structure of hOGG1 bound to undamaged DNA, the group of Verdine developed and applied a cross-linking strategy to capture the protein onto an undamaged guanine.[13] The experimental setup for hOGG1 consists of two modifications (Figure 1):[11] 1) the counter cytosine to the target guanine in the DNA was modified with a short tether bearing a disulfide functionality. 2) The Asn 149 of hOGG1 was mutated to Cys. As a result, disulfide cross-linking was obtained between the protein and the DNA. It is very remarkable that the resulting structure of the hOGG1–DNA complex reveals that the undamaged guanine is indeed flipped out of the DNA helix. In contrast to the oG moiety, the undamaged guanine is not able to insert into the active site. Instead, it is placed in a nearby extrahelical binding pocket. This secondary binding site acts as a gatekeeper to the active site in order to guarantee that oG, but not the undamaged guanine, is cleaved off. This is an important result as it describes that protein-induced base flipping of undamaged DNA bases does occur and that the lesion discrimination takes place in an extrahelical position but not in the active site.

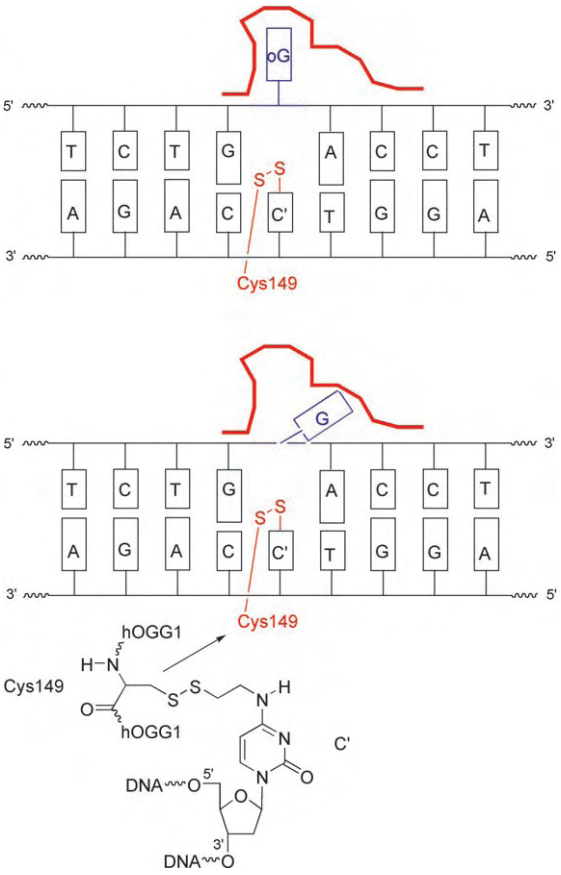


***Figure 1.*** Complex of hOGG1 (N149C mutant) with damaged DNA (top) and undamaged DNA (bottom) captured through a disulfide cross-link. The undamaged target guanine residue is flipped out but, in contrast to 8-oxoguanine, it is not inserted into the active site.

Although experimental evidence of the discussed structure of hOGG1 shows the processive migration of the BER enzyme while continuously base flipping, it still remains to be a matter of discussion. Especially with respect to the requirement of scanning millions of base pairs for a single damaged site, such a processive base flipping method seems to be too slow. The key question is if base extrusion is really needed for damage recognition.[7] An important general observation of BER is that all enzymes that flip bases out of the DNA duplex also bend the DNA quite significantly at the target site.[5,6] The question is whether such DNA distortions occur prior to, simultaneously with, or after base flipping. If DNA glycosylases are also able to bend undamaged DNA, one could envision an alternative induced-fit mechanism for the location of damaged sites. Such a mechanism was proposed by Tainer and co-workers.[9,10] The local conformational flexibility of the DNA duplex resulting from base damage, for example, *syn* conformations or wobble mispairs, may be sensed by BER enzymes through amino acids that induce a conformational strain onto the helix prior to the base-flipping event.

In fact, such a structural scenario was recently evidenced by the DNA–protein structure of MutM presented by Verdine and co-workers.[14] MutM represents a bacterial DNA glycosylase that recognizes oG and can therefore be regarded as the bacterial counterpart to the previously discussed hOGG1. Similar to hOGG1, a cross-linking strategy[13] was applied to capture enzymatically active MutM onto a damaged site and an undamaged guanine (Figure 2). For these studies, the phosphodiester backbone of the DNA within the protein binding site was modified with a thiol-containing tether. The cysteine-engineered Q166C mutant of MutM yielded a few interesting structures with a variety of trapped DNA targets. Similar to the hOGG1 complex, the structure of MutM with oG-containing DNA showed clearly that the damaged DNA base is flipped out into the extrahelical position. More

 © 2006 Wiley-VCH Verlag GmbH & Co. KGaA, Weinheim 

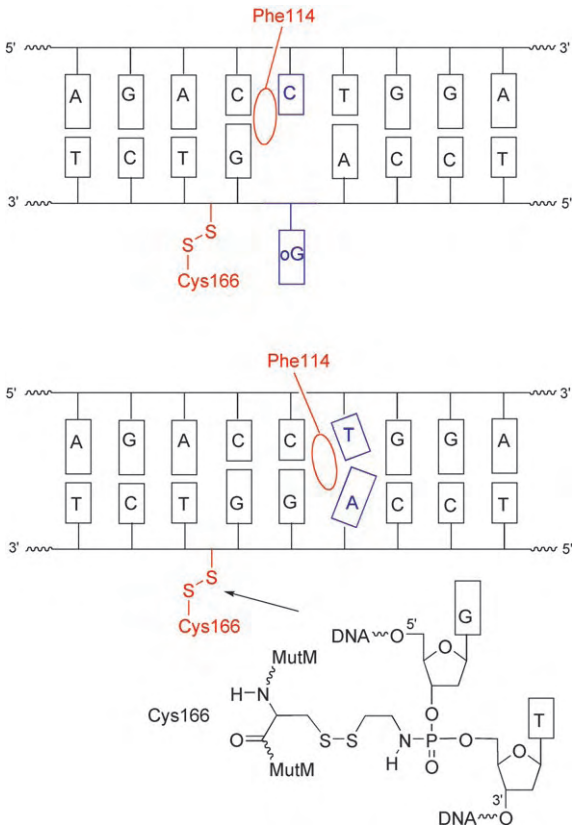


***Figure 2.*** Complex of MutM (Q166C mutant) with damaged DNA shows the base-flipped oG. Bottom: Example of interrogation complex of MutM (Q166C mutant) with undamaged DNA captured through a disulfide cross-link.

importantly, however, are the structural details of MutM trapped on undamaged DNA duplexes. In the latter cases, the structure revealed that the aromatic side chain of Phe114 is inserted into the DNA duplex next to the target base and that none of the bases are flipped out. The Phe114 side chain causes buckling at the intercalation site resulting in a kinetic preference for extruding oG rather than guanine. This means that the oG moiety is flipped out and that the undamaged guanine is not. This is a significant result not only as there is a positive selection towards extrusion of DNA lesions, but also a negative selection for extruding of undamaged bases.

Taken together, both discussed structures (hOGG1 and MutM) give new and important structural insights into the process of DNA damage location. The discrimination of damaged DNA bases from undamaged ones occurs by at least two mechanisms: 1) The conformational strain by the intercalation of the Phe114 side chain of MutM into the DNA helix yields a kinetic preference for the subsequent base flipping of the damaged over the undamaged base pair. This part of the damage location process is performed from outside the helix. 2) If the glycosylase makes an occasional mistake and attempts to flip an undamaged base to the active site, there are no dangerous consequences. This is shown in the case of hOGG1 in which the binding place in front of the active site is then able to discriminate thermodynamically between damaged and undamaged bases. In the future, it will be fascinating to see if there are more interesting DNA–protein structures that further refine this model of damage location.

Published online: August 4, 2006


[1] See, for example, D. Wang, S. A. Kreuzer, J. M. Essigmann, *Mutat. Res.* **1998**, *400*, 99–115.

[2] See, for example, E. C. Friedberg, L. D. McDaniel, R. A. Schultz, *Curr. Opin. Chem. Biol.* **2004**, *14*, 5–10.

[3] See, for example, A. Luch, *Nat. Rev. Cancer* **2005**, *5*, 113–125.

[4] See review and references therein: O. D. Schärer, *Angew. Chem.* **2003**, *115*, 3052–3082; *Angew. Chem. Int. Ed.* **2003**, *42*, 2946–2974.

[5] See review and references therein: S. S. David, S. D. Williams, *Chem. Rev.* **1998**, *98*, 1221–1261.

[6] See review and references therein: J. T. Stivers, Y. L. Jiang, *Chem. Rev.* **2003**, *103*, 2729–2759.

[7] See review and references therein: S. R. Rajski, B. A. Jackson, J. K. Barton, *Mutat. Res.* **2000**, *447*, 49–72.

[8] G. L. Verdine, S. D. Bruner, *Chem. Biol.* **1997**, *4*, 329–334.

[9] C. D. Mol, S. S. Parikh, C. D. Putnam, T. P. Lo, J. A. Tainer, *Annu. Rev. Biophys. Biomol. Struct.* **1999**, *28*, 101–128.

[10] S. S. Parikh, C. D. Mol, D. J. Hosfield, J. A. Tainer, *Curr. Opin. Struct. Biol.* **1999**, *9*, 37–47.

[11] A. Banerjee, W. Yang, M. Karplus, G. L. Verdine, *Nature* **2005**, *434*, 612–618.

[12] S. D. Bruner, D. P. G. Norman, G. L. Verdine, *Nature* **2000**, *403*, 859–866.

[13] G. L. Verdine, D. P. G. Norman, *Annu. Rev. Biochem.* **2003**, *72*, 337–366.

[14] A. Banerjee, W. L. Santos, G. L. Verdine, *Science* **2006**, *311*, 1153–1157.



© 2006 Wiley-VCH Verlag GmbH & Co. KGaA, Weinheim

Y. Lu

DOI: 10.1002/anie.200600168

Chemical Biology

# Biosynthetic Inorganic Chemistry

*Yi Lu**

**Keywords:**
biocatalysis · bioinorganic chemistry · biomimetic synthesis · protein design

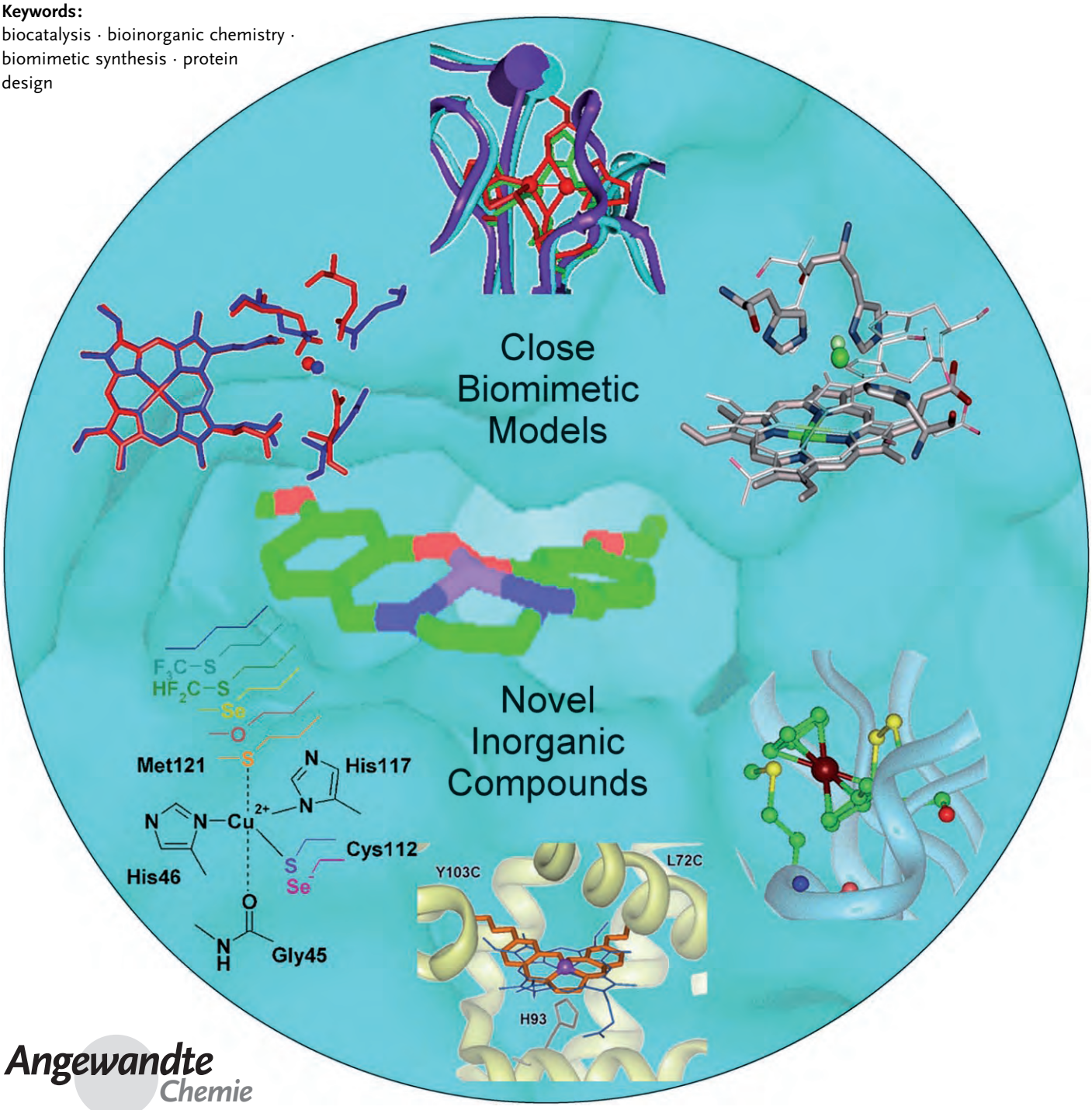




© 2006 Wiley-VCH Verlag GmbH & Co. KGaA, Weinheim

*Inorganic chemistry and biology can benefit greatly from each other. Although synthetic and physical inorganic chemistry have been greatly successful in clarifying the role of metal ions in biological systems, the time may now be right to utilize biological systems to advance coordination chemistry. One such example is the use of small, stable, easy-to-make, and well-characterized proteins as ligands to synthesize novel inorganic compounds. This biosynthetic inorganic chemistry is possible thanks to a number of developments in biology. This review summarizes the progress in the synthesis of close models of complex metalloproteins, followed by a description of recent advances in using the approach for making novel compounds that are unprecedented in either inorganic chemistry or biology. The focus is mainly on synthetic "tricks" learned from biology, as well as novel structures and insights obtained. The advantages and disadvantages of this biosynthetic approach are discussed.*

**From the Contents**

1. Introduction 5589

2. Application of Biosynthetic Inorganic Chemistry in Biomimetic Model Systems 5591

3. Biosynthetic Inorganic Chemistry for the Synthesis of New Inorganic Complexes 5595

4. Conclusions and Outlook 5598

## 1. Introduction

Metal ions play important roles in catalyzing numerous chemical and biological reactions, as the reactivity and diversity can be modulated at high levels by not only different metal ions, but also the different oxidation states of these same metal ions.[1–6] The successful synthesis and application of novel metal complexes or metalloenzymes can have a great impact on all areas of chemistry and biology, whether it is organic, medicinal, materials chemistry, or biochemistry and cell biology. An important example of such an impact is the development of metal catalysts for reactions such as nitrogen fixation, methane hydroxylation, and CO oxidation or insertion (Table 1).[7,8] These catalysts are key components for multibillion-dollar chemical industries that produce vital raw chemicals, such as fertilizers.

Interestingly, many of the reactions in Table 1 can be catalyzed by either synthetic catalysts or by biological enzymes. A closer look at the two systems suggests that the catalysts mediate the same reaction under different conditions: chemical systems generally operate at high temperatures and pressures in organic solvent, whereas biological systems work at ambient temperatures and pressures in water. Furthermore, biocatalysts often have high catalytic turnovers. Therefore, the question is not whether one can develop catalysts that can work under milder conditions with high turnovers, but rather how such catalysts can be developed.

A cursory look at the examples in Table 1 may lead one to conclude that one system may be better than the other; however, each system has its own advantages and disadvantages (Table 2). Chemical catalysts are generally smaller, easier to synthesize and characterize, cheaper to produce, and more resistant to harsh conditions such as high temperatures and pressures. These practical attributes make it difficult to replace catalysts with enzymes in industrial-scale synthesis, although enzymes possess a number of desirable features for catalysts. First, they form more-rigid active sites to stabilize the transition state and thus are more able to accelerate catalysis at ambient temperature and pressure. Second, they direct reactions towards a specific functional group of an organic substrate, thus eliminating or minimizing the need for protecting groups, which are often required in synthetic chemistry. Third, the catalytic site in enzymes is protected, which results in higher catalyst stability and higher turnover numbers. Fourth, enzymes achieve high regio-, stereo-, and enantioselectivity. Fifth, the complex protein framework is amenable to site-specific (as opposed to solvent-induced) modulation of the secondary coordination sphere of a metal-binding site. For example, the p$K_a$ values for glutamic acid in the same protein vary between 4.0 and 8.2, depending on the local electrostatic environment and hydrophobicity.[9] Finally, enzymes are environmentally benign, as they are synthesized and applied under physiological conditions in aqueous solvents and with biocompatible and biodegradable ligands.

Since each of the chemical and biological systems has its own advantages and disadvantages, one may wonder if the advantages of both systems can be combined. Towards this end, a number of synthetic biomimetic model systems for metalloproteins have been prepared from small organic molecules and characterized.[10] Such a synthetic approach has been very effective in the elucidation of structural and functional properties of metalloproteins.

Despite tremendous progress in biomimetic modeling, it is still relatively difficult to mimic some of the features of metalloproteins, for example, site-specific modulation of the secondary coordination sphere and the regio-, stereo-, and enantioselectivity of a system. Models that reproduce both the structure and the function of metalloproteins are rare. These challenges, like perhaps all obstacles in synthetic inorganic chemistry, can be overcome by ligand design. Prudent choice of ligand has repeatedly resulted in better models of metalloproteins,[10] especially when features in the secondary coordination sphere such as hydrogen-bonding

[*] Prof. Y. Lu
Department of Chemistry
University of Illinois at Urbana-Champaign
Urbana, IL 61801 (USA)
Fax: (+1) 217-244-3186
E-mail: yi-lu@uiuc.edu


© 2006 Wiley-VCH Verlag GmbH & Co. KGaA, Weinheim

***Table 1:*** Comparison of chemical and biological systems.

| Reaction | Chemical System | Biological System |
|---|---|---|
| nitrogen fixation | $\mathbf{N_{2(g)}} + 3\,H_{2(g)} \rightarrow 2\,\mathbf{NH_{3(g)}}$ ($\alpha$-Fe catalyst, 400–550 °C, 100 atm) | $\mathbf{N_2} + 8\,H^+ + 8\,e^- + 16\,MgATP \rightarrow 2\,\mathbf{NH_3} + H_2 + 16\,MgADP + 16\,P_i$ (nitrogenase) |
| methane hydroxylation | $\mathbf{CH_4} + H_2O \rightarrow CO + 3\,H_2$ (Ni catalyst, 700–900 °C, 1–25 bar) $CO + 2\,H_2 \rightarrow \mathbf{CH_3OH}$ (Cu/Zn Catalyst, 250–280 °C, 70–110 bar) | $\mathbf{CH_4} + O_2 + NADH + H^+ \rightarrow \mathbf{CH_3OH} + H_2O + NAD^+$ (methane monooxygenase) |
| CO oxidation | $\mathbf{CO} + H_2O \rightarrow \mathbf{CO_2} + H_2$ (Fe/Cu catalyst, $>200$ °C) | $\mathbf{CO} + H_2O \rightarrow \mathbf{CO_2} + 2\,H^+ + 2e^-$ (CO dehydrogenase) |
| CO insertion | $\mathbf{CH_3}OH + \mathbf{CO} \rightarrow \mathbf{CH_3CO}OH$ ($Rh(I)I_2(CO)_2]^-$, 120 °C, 30 atm) | $\mathbf{CH_3}$–[M] + **CO** + HS–CoA → $\mathbf{CH_3(CO)}$–S–CoA + $H^+$ + $[M^-]$[a] (acetyl-CoA synthase) |

[a] $\mathbf{CH_3}$–[M] is a corrinoid–iron–sulfur protein that acts in the reaction as a methyl group donor; HS-CoA is coenzyme A.

***Table 2:*** Advantages of chemical and biological systems.

| **Chemistry** Catalysts/Materials | **Biology** Enzymes/Biomaterials |
|---|---|
| easy to synthesize | mild conditions |
| easy to characterize | rigidity/protection |
| more robust | site-specific modulation of the 2nd coordination sphere |
| cheaper to produce | regio- and enantioselectivity environmentally friendly |
| approach: create new structures and functions by using a minimalist approach | approach: study native proteins and their variants |

were introduced.[11,12] The main difference between synthetic models and metalloproteins is that the synthetic models often contain water-insoluble organic ligands, whereas metalloproteins consist of polypeptides or proteins. Polypeptides and proteins are unusual organic molecules in that they are naturally soluble in water and can be synthesized under mild conditions. Through specific folding of the polypeptides and proteins, a rigid network can form that allows site-specific modulation of the secondary coordination sphere. This suggests that polypeptides or proteins were established in the course of evolution as ligands for metal-based catalysts or enzymes.

So why then should the ligands from biological systems not be used to synthesize model compounds? It used to be very difficult and expensive to make proteins and their variants, which rendered the use of such proteins as ligands impractical. However, advancements in biology, such as the development of cloning, protein expression, site-directed mutagenesis, and polymerase chain reaction, have made it possible to reduce dramatically the time required to synthesize proteins and change amino acid residues. Whereas it used to take many months or even many years to construct, express, and purify a series of proteins, it now takes a matter of weeks or even days; such progress is similar to that made in the computer industry (Figure 1). Furthermore, hundreds of milligrams or even grams of pure protein can now be

*Yi Lu received his BS degree from Beijing University (P.R. China) in 1986 and his PhD from the University of California at Los Angeles in 1992 under the guidance of Prof. Joan Selverstone Valentine. After two years of postdoctoral research at the California Institute of Technology in the group of Prof. Harry B. Gray, he began his independent career as an Assistant Professor in the Department of Chemistry at the University of Illinois at Urbana–Champaign, where he is now an Alumni Research Scholar Professor of Chemistry. His interests lie in bioinorganic chemistry.*

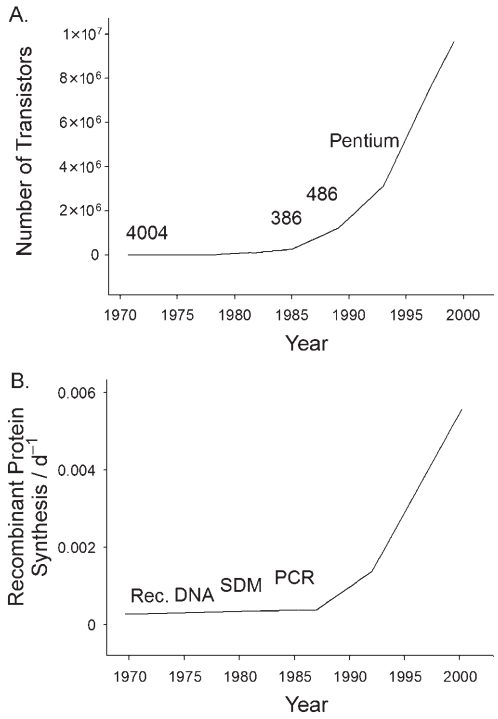


***Figure 1.*** Comparison of progresses made in the computer industry and biology. A) According to Moore's law, the number of transistors and thus the speed of a computer doubles approximately every 18 months. B) Estimated average speeds of cloning, expression, and purification of recombinant proteins (calculated as the inverse of number of days it takes to complete the process). Techniques such as recombinant DNA (Rec. DNA), site-directed mutagenesis (SDM), and the polymerase chain reaction (PCR) have significantly accelerated the biological progress.

 © 2006 Wiley-VCH Verlag GmbH & Co. KGaA, Weinheim 

prepared. Thanks to the progress in biotechnology, certain chemical synthesis steps in the production of pharmaceutical products can be replaced by biosynthesis. As a result, the number of synthesis steps is reduced, yields are increased, and less chemical waste is produced,[13,14] so that the difference in efficiency between the synthesis of small organic molecules and proteins is decreased. At the same time, progress in biophysics has made possible the routine characterization of metalloproteins by different spectroscopic techniques.[15–17] Advances in structural biology, such as the availability of high-energy synchrotron sources and high-field magnets and their associated methodology developments, have also made it possible to obtain three-dimensional crystal or NMR structures of proteins in a short period of time. Thus, it is now possible to synthesize and characterize novel inorganic compounds using small, stable, easy-to-produce proteins with characteristic scaffolds as "ligands".

The biosynthetic approach uses the same techniques as the biochemical studies of native enzymes and their mutant forms. However, the following examples below show that there are distinct differences between the two approaches: First, like all biomimetic approaches, the biosynthetic approach is a minimalist approach; it focuses on determining whether the necessary structural features identified in native enzymes are sufficient to confer the structure and function of the enzyme. Therefore, the two approaches are complementary. Second, stable, easy-to-produce, and well-characterized proteins are used in the biosynthetic approach, and successful models are often as good as, if not better than, the native enzymes for structural and functional studies. Third, biosynthetic models may offer additional advantages, since different metal-binding centers can be compared in the same protein framework. Finally, the biosynthetic approach allows synthesis of new compounds, with structures and reactivities unprecedented in either biology or inorganic chemistry.

## 2. Application of Biosynthetic Inorganic Chemistry in Biomimetic Model Systems

Biomimetic model systems combine the benefits of both chemistry and biology. In this process, one can learn the minimal structural features necessary to form metal-binding sites with desirable function and help to elucidate the structure–function relationship of target proteins. At the same time, new compounds with structures that are rare in inorganic chemistry may be synthesized, which expands our knowledge of coordination chemistry. The resulting compounds are often smaller and better defined structurally than the native proteins, and can therefore be used in practical applications.

Biosynthetic model systems with small, stable, and well-characterized proteins as ligands can achieve the same goals. Since they use the same ligands as target proteins and operate under almost the same physiological conditions, they can often result in closer models and are more readily usable in practical applications. A few examples will illustrate these features.

### 2.1. Inorganic Biosynthesis with the Same Protein Scaffold and Loop-Directed Mutagenesis

The $Cu_A$ center is a mixed-valence dinuclear copper center in which the copper ions are each coordinated to a histidine residue (His181 and His224) and bridged by the thiolate sulfur atoms of two cysteine ligands (Cys216 and Cys220, Figure 2A, top).[18–21] Weak ligands such as the thioether sulfur atom of methionine (Met227) and the backbone carbonyl oxygen atoms of isoleucine (Ile180), histidine (His224), and glutamate (Glu218) are also present in axial positions (Figure 2A, bottom). The $Cu_A$ center is unique in both inorganic chemistry and biology; it acts as an electron-transfer center in cytochrome *c* oxidase (C*c*O; a terminal oxidase in the respiratory chain of eukaryotic mitochondria and some aerobic bacteria)[22–26] and nitrous oxide reductase ($N_2OR$; an enzyme responsible for the reduction of $N_2O$ in denitrifying bacteria).[27,28] It was also the first biological system shown to contain a metal–metal bond.[29] Many coordination compounds containing metal–metal bonds are known with late transition metals; however few contain first-row transition metals such as copper.[30] Whereas dinuclear or multinuclear mixed-valence copper complexes in which the unpaired electron is completely localized (Class I) or partially delocalized (Class II) have been known for many years,[31,32] copper complexes, such as the $Cu_A$ center, with fully delocalized (Class III) mixed-valence states are rare.[33–40] In both cases, the synthesis of the $Cu_A$ center and elucidation of the structural features responsible for its functions are of great interest.

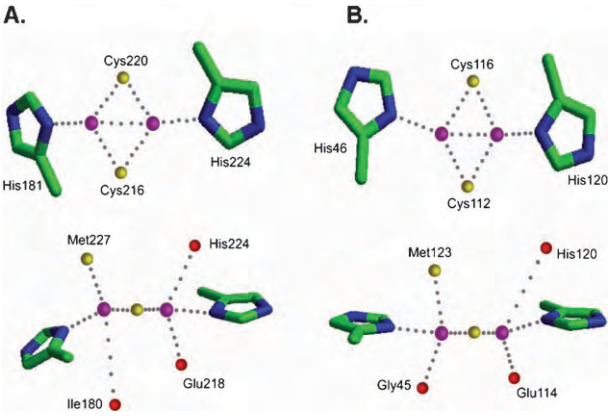


***Figure 2.*** Crystal structures of A) the $Cu_A$ center in cytochrome *c* oxidase from *P. denitrificans*; and B) a biosynthetic $Cu_A$ model in azurin. The top figures show the $Cu_A$ center with $Cu_2S_2$(Cys) in a plane and the bottom figures show the $Cu_A$ center viewed perpendicular to the plane.

A number of synthetic models with organic ligands have been reported for this purpose, most of which contain a dinuclear mixed-valence copper center and a copper–copper bond, but not bridging thiolate units.[33,34,38,39,41] A model compound that contains bridging thiolate residues but lacks a copper–copper bond also exists.[36] A dinuclear copper center containing a copper–copper bond and two bridging nitrogen atoms was also reported recently.[42] Stable, easy-to-make, and


© 2006 Wiley-VCH Verlag GmbH & Co. KGaA, Weinheim

well-characterized blue copper proteins such as amicyanin[43] and azurin[44] were used as ligands to make a closer model of the $Cu_A$ center. Blue copper proteins and proteins containing the $Cu_A$ center have been shown to share close structural homology.[45] Sequence alignment revealed that mononuclear blue copper proteins and dinuclear $Cu_A$ proteins differ mainly in a single loop between two β-strands. By replacing the loop in blue copper proteins with the corresponding loop in $Cu_A$ proteins (Figure 3), a close mimic of the $Cu_A$ center was

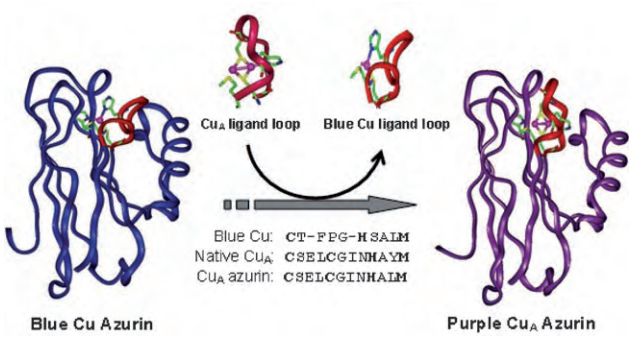


***Figure 3.*** Development of a biosynthetic $Cu_A$ model in azurin through loop-directed mutagenesis.

synthesized in blue copper proteins amicyanin[43] and azurin.[44] A high-resolution crystal structure showed that the $Cu_A$ center in the azurin model is almost identical to that of the native $Cu_A$ center, including structural features in the secondary coordination sphere, such as the nonbonding interactions between the thioether group of methionine residue and peptide carbonyl oxygen atoms (Figure 2B).[46]

The synthesis of a close model of a native protein is only one measure of the effectiveness of such an approach. How much insight is gained into the structure and function of the metal center is another important measure. The biosynthetic $Cu_A$ model also gives deeper insight in this regard. For example, a stopped-flow study of copper incorporation into metal-free $Cu_A$ azurin revealed a tetragonal intermediate and showed the importance of reductants in the formation of the final $Cu_A$ center.[47] Titration of different metal ions into the model protein suggests that the $Cu_A$ center as an $M^{II}M'^{I}$ center (M, M′ = any metal) is strongly favored regardless of the sequence of addition of metal ions.[48,49] Mutagenesis studies revealed that the conserved cysteine,[50] histidine,[51,52] and methinione[53] residues all play an important role in maintaining the structure and in fine-tuning the function. Surprisingly, the dinuclear copper structure remains largely intact, even when the histidine was replaced with residues incapable of coordinating to the copper (e.g. Ala and Gly), as evidenced by the similar characteristic purple color, as well as UV/Vis, magnetic circular dichroism (MCD), resonance Raman (RR), and electron nuclear double resonance (ENDOR) spectra.[51,52]

Until recently, there were not many examples of fully delocalized (Class III) dinuclear mixed-valence copper compounds. Even rarer is the reversible conversion between different classes, that is, between delocalized $[Cu^{1.5}\cdots Cu^{1.5}]$ and trapped valence $[Cu^{II}\cdots Cu^{I}]$ states. The study of the $Cu_A$ center in azurin provided an interesting example of a reversible transition between delocalized and trapped mixed-valence states that is triggered solely by a change in pH value.[54] The $Cu_A$ center is known to be the electron entry site in cytochrome *c* oxidase. However, its role in proton-coupled electron transfer has not been defined clearly. This work showed that protonation of the C-terminal His residue not only resulted in a trapped valance state of the $Cu_A$ center, but also caused a significant increase in the reduction potential.[54] Since the corresponding C-terminal His residue in cytochrome *c* oxidases is located along a major electron-transfer pathway from $Cu_A$ center to heme *a*, and since protonation can result in an increased reduction potential that prevents electron transfer from the $Cu_A$ center to heme *a*, the results strongly indicate that the $Cu_A$ center and the histidine residue may play important roles in proton-coupled electron transfer.[54]

These observations may be obtained from studies of native $Cu_A$ centers, in particular soluble fragments of C*c*O containing the $Cu_A$ center.[18–21] However, several studies have demonstrated that biosynthetic models can provide unique insights that are not readily obtainable from studies of either native enzymes or synthetic model compounds. For example, by using azurin as the "ligand" and replacing the ligand loop of the blue copper center with that of the $Cu_A$ center, two electron transfer (ET) centers may be placed in the same protein framework. High-resolution crystal structures showed that one of the copper atoms in the $Cu_A$ center overlays exactly with the blue copper center (Figure 4A).[46] Therefore,

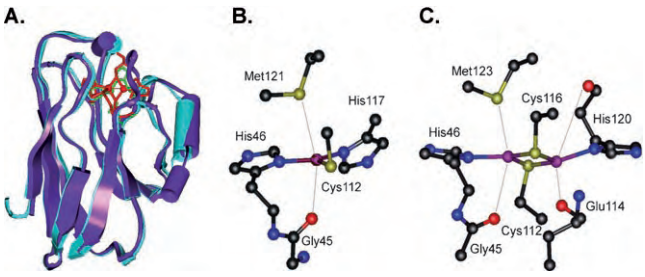


***Figure 4.*** A) Overlay of the crystal structures of blue copper azurin (in light blue) and the biosynthetic $Cu_A$ model in azurin (in purple). The copper site in the blue copper center (B) overlays almost exactly with one of the copper sites in the purple $Cu_A$ center (C).

this biosynthetic model provided a unique opportunity to compare the two ET centers in the same protein framework and exclude or at least minimize other factors that influence its properties. For example, the same series of mutations at a conserved axial methionine unit in the blue copper protein (Met121, Figure 4B) and the $Cu_A$ azurin (Met123, Figure 4C) indicate that the methionine residue has much less influence on the reduction potential of the $Cu_A$ center (< 25 mV) than of the blue copper center (> 170 mV).[53] In contrast, electron transfer from the same donor and at the same distance to the $Cu_A$ center is faster, despite its lower reduction potential, than to the blue copper center.[55] Thus, this work showed directly that the $Cu_A$ center is a more efficient ET center.

 © 2006 Wiley-VCH Verlag GmbH & Co. KGaA, Weinheim 

These findings may be important in understanding the different roles of the two copper centers. A much wider range of reduction potentials (> 600 mV) is required for blue copper proteins to transfer electrons to a variety of partners in many different biological systems.[20,21,56,57] In contrast, the $Cu_A$ center is part of cytochrome *c* oxidase, which is at the end of the respiration chain with very small differences (< 50 mV) in the potentials of the redox partners.[58] In this case, large variations in the potential could hinder the flow of electrons in the right direction. The diamond-shaped $Cu_2S_2$(Cys) core structure of $Cu_A$ provides a way to minimize changes in reduction potential through variations of the axial ligands. Despite the low driving force, however, the $Cu_A$ center still needs to transfer electrons to its partners at a desirable rate. Therefore, it has to optimize its structure by lowering its reorganization energy to be a more efficient ET center than the blue copper center.

Loop-directed mutagenesis, in which ligand loops of a template protein are swapped with those of a target protein that shares similar structural homology, was employed to make the biosynthetic models of the $Cu_A$ center described above. A preliminary survey of the protein structure data bank (PDB) suggests that this approach is not limited to specific cases but can be utilized generally to make biosynthetic models of many metalloproteins. For example, azurin, amicyanin, and $Cu_A$ proteins belong to a group with a common scaffold, called the Greek Key β-barrel. It is the second most abundant motif in the PDB, and a number of proteins with diverse active-site structures and functions, such as immunoglobin, beta-amylase, cytochrome *c* oxidase, nitrite reductase, and superoxide dismutase, contain the same scaffold (Figure 5).[59]

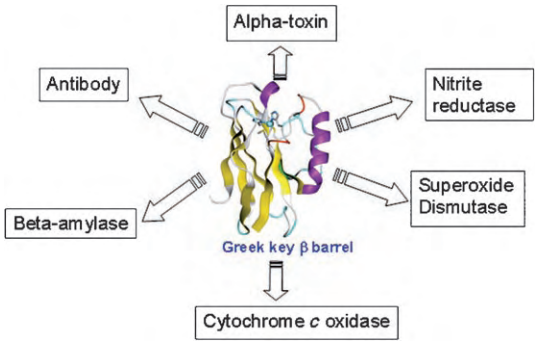


***Figure 5.*** The Greek Key β-barrel motif appears in more than 600 proteins of different classes with diverse functions. As most of the active sites are in the loop region, loop-directed mutagenesis can be used to construct novel metalloproteins.

Most of the active sites in these proteins reside within or between loops. Evidently, nature produced a thermodynamically stable scaffold upon which many different protein structures and functions can be conferred by simply swapping loops, which is much less disruptive to the protein structure than changing scaffolds. This "trick" is important for biosynthetic inorganic chemistry.

Another example of nature using the same protein scaffold for different functions are heme peroxidases.[60] All heme peroxidases contain a heme active site. However, manganese peroxidase (MnP) contains an additional $Mn^{II}$-binding site (Figure 6 A). $Mn^{II}$ oxidation plays a critical role in the function of MnP (Scheme 1) in the biodegradation of lignin, the second most abundant biopolymer on earth (after

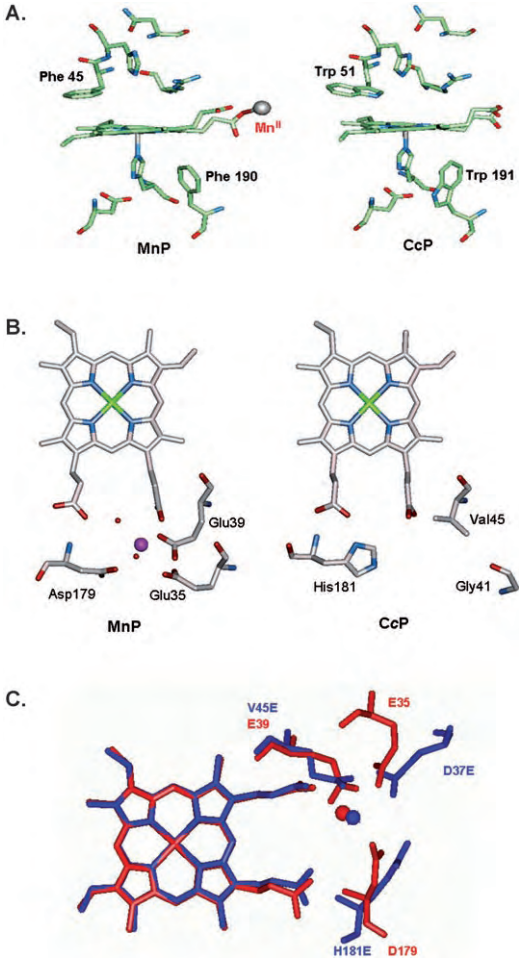


***Figure 6.*** A) Comparison of manganese peroxidase (MnP) and cytochrome *c* peroxidase (*Cc*P); B) Heme-manganese binding site in MnP and *Cc*P; C) Crystal structures of MnP (red) and a *Cc*P variant that mimics MnP (blue).

$$Fe^{III} + H_2O_2 \longrightarrow Fe^{IV}{=}O/Trp^{+\bullet} + H_2O$$

$$Fe^{IV}{=}O/Trp^{+\bullet} + Cc^{2+} \longrightarrow Fe^{IV}{=}O/Trp + Cc^{3+}$$

$$Fe^{IV}{=}O/Trp + 2\,H^+ + Cc^{2+} \longrightarrow Fe^{III}/Trp + Cc^{3+} + H_2O$$

$$Fe^{III} + H_2O_2 \longrightarrow Fe^{IV}{=}O/Por^{+\bullet}$$

$$Fe^{IV}{=}O/Por^{+\bullet} + Mn^{II} \longrightarrow Fe^{IV}{=}O/Por + Mn^{III}$$

$$Fe^{IV}{=}O/Por + 2\,H^+ + Mn^{II} \longrightarrow Fe^{III}/Por + Mn^{III} + H_2O$$

***Scheme 1.*** Catalytic cycles of *Cc*P (top) and MnP (bottom). Trp = tryptophan; Por = heme porphyrin.


© 2006 Wiley-VCH Verlag GmbH & Co. KGaA, Weinheim

cellulose), as well as being a key step in converting woody plants to small chemicals such as those in petroleum.[61] Interestingly, cytochrome *c* peroxidase (C*c*P) shares not only the same overall structure, but also a similar structure of the heme-binding site, the major differences being that C*c*P lacks the $Mn^{II}$-binding site and contains Trp instead of Phe around the heme-binding site (Figure 6A,B).[62] Several ligands to $Mn^{II}$ in MnP are absent in C*c*P. To convert C*c*P, an enzyme found in baker's yeast, into an MnP with similar function, the residues in C*c*P were replaced with the residues of MnP at the corresponding positions to give new C*c*P variants with enhanced MnP function (Figure 6C).[63–65] Furthermore, replacing the Trp residues in C*c*P with the Phe units from MnP showed that the Phe residues play different roles in MnP function; whereas the Trp191Phe mutation stabilized compound I (an intermediate), the Trp51Phe mutation increased the activity significantly, as it increased the reactivity of compound II, whose oxidation of $Mn^{II}$ is the rate-determining step in the reaction mechanism of MnP.[66,67]

### 2.2. Noncovalent Tuning of the Secondary Coordination Sphere through Inorganic Biosynthesis

The noncovalent tuning of the secondary coordination sphere of metal-binding sites is another "trick" of biological systems. For example, cytochrome P450 (Cyt P450) is one of the most efficient enzymes for asymmetric oxygen-transfer reactions, such as sulfoxidation, epoxidation, and hydroxylation, of a variety of substrates.[68] Its primary coordination sphere consists of a heme unit with a thiolate Cys as its proximal ligand (Figure 7A). In view of the importance of heme–thiolate ligation, the proximal ligand His in human myoglobin was changed to a Cys.[69,70] The spectrum of the resulting protein was similar to that of Cyt P450. The protein model also exhibited increased asymmetric sulfoxidation activity. However, the same His-to-Cys mutation alone in horse heart myoglobin (Mb) did not result in heme–thiolate ligation.[71] Instead, an additional mutation of the distal noncoordinating histidine to either a valine or isoleucine resulted in a P450-like protein with an iron(III) resting state (Figure 7B).[71] This effect, termed the *trans* effect by the authors, mimics the more hydrophobic environment of the Cyt P450 (Figure 7A) and contributes significantly to the binding of the axial ligand and to the stability.

Similarly, mutation of the axial His ligand to Cys in C*c*P resulted in a very unstable ligand that was rapidly oxidized to cysteic acid.[72] It was then recognized that a nonpolar residue next to the Cys unit is conserved in P450 proteins, while the analogous amino acid in C*c*P is an aspartic acid (Figure 7C). Thus, further mutation of this Asp residue to Leu resulted in a stable, pentacoordinate, high-spin heme with thiolate ligation.[73] The study also marked the first time a stable cyanidoferric complex and the ferrous state of a model P450 was obtained.[73,74]

Stable coordination of cysteine thiolate in the ferrous carbonyl derivative of an engineered protein was also obtained by mutations of the axial His and Met ligands in cytochrome $b_{562}$ to Cys and Gly, respectively (Figure 7D).[75] The key to success was the replacement of two glutamate residues (Glu4 and Glu8), which are electrostatically repelled from the heme propionate groups, with Ser. These studies demonstrated the importance of the secondary coordination sphere around the primary coordination ligands in stabilizing metal–ligand ligation.

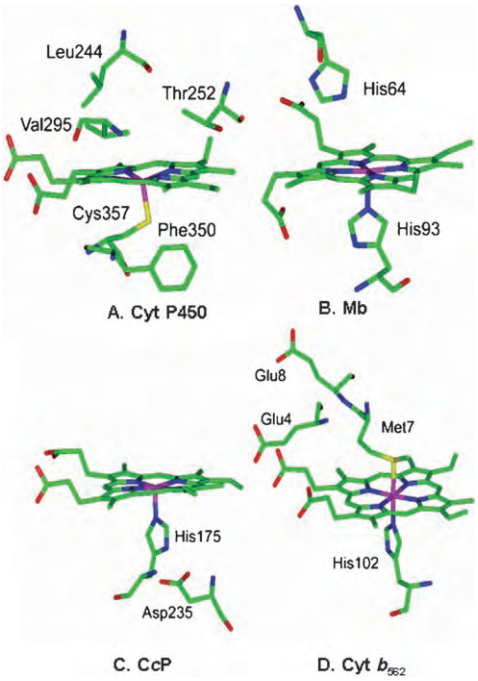


***Figure 7.*** Key structural differences of Cyt P450 (A), Mb (B), C*c*P (C), and Cyt $b_{562}$ (D).

### 2.3. Water and Hydrogen Bonding in Inorganic Biosynthesis

The third "trick" emerging from recent investigations on a number of metalloproteins is the precise positioning of hydrogen-bonding networks in fine-tuning the function and specificity of metalloproteins. For example, it has been shown that most heme enzymes go through a similar heme–peroxo intermediate and yet exhibit diverse enzymatic activities, such as monooxygenase (Cyt P450), heme oxygenase (HO), and oxidase (C*c*O). High-resolution crystal structures of both Cyt P450 and heme oxygenase revealed the presence of water molecules in the metal-binding sites (Scheme 2).[76,77] The number and exact location of the water molecules have been shown to be critical in forming hydrogen-bonding networks that can dramatically influence the reactivity. Although the exact nature of the hydrogen-bonding networks in C*c*O has not been revealed, functional studies of a biosynthetic model in myoglobin support their importance in fine-tuning the reactivity.[78] This work, complementary to work carried out using synthetic models,[79,80] is based on a structural comparison of myoglobin and heme–copper oxidase. Although both proteins contain heme, C*c*O contains a copper center that is approximately 4.7 Å from the heme iron center (Figure 8A). To make a biosynthetic model of C*c*O, His ligands were

 © 2006 Wiley-VCH Verlag GmbH & Co. KGaA, Weinheim 

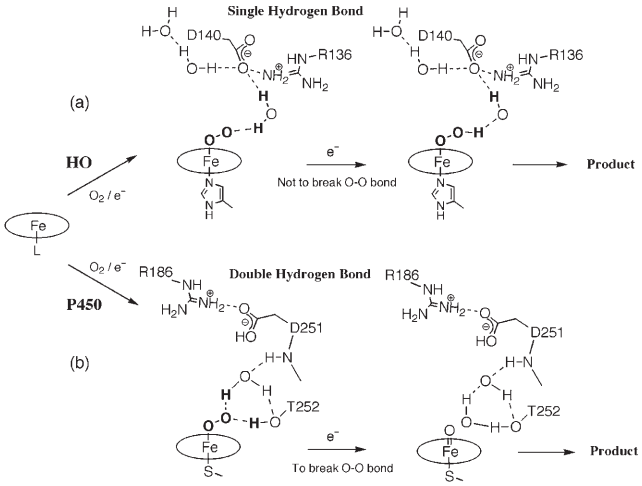


***Scheme 2.*** Proposed role of hydrogen bonds in HO and cyt P450. Adapted from reference [76].

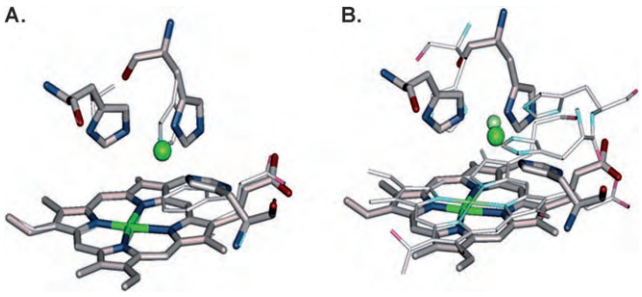


***Figure 8.*** A) Overlay of crystal structures of C*c*O (thick lines) with sperm whale Mb (thin lines). Mb lacks the $Cu_B$-binding site since it has one His, one Leu, and one Phe residue instead of three histidine residues as in C*c*O; B) Overlay of the crystal structure of C*c*O (thick lines) with a computer model of $Cu_B$Mb (Leu 28 His/Phe 43 Phe, thin lines).

introduced into the distal side of sperm whale Mb at the corresponding locations (Figure 8B).[81]

Spectroscopic studies indicate that the Mb model ($Cu_B$Mb) is very similar to C*c*O. Studies of this biosynthetic model also indicated that the presence of a copper ion has a critical influence on the redox potential of the heme Fe center[82,83] and can transform the oxygen-binding protein Mb into an oxygen-activating enzyme.[78,81] Interestingly, the protein model in Mb generates verdoheme, a key intermediate in HO, rather than producing a ferryl–heme as in C*c*O.[78] Control experiments indicated that protein instability or altered dynamics of the binding site were not the cause for this reaction, since replacement of $Cu^{II}$ or $Cu^{I}$ by redox-inactive ions such as $Zn^{II}$ and $Ag^{I}$, respectively, does not promote the HO reaction.[78] Since all reactions were carried out in the presence of catalase, the possibility of exogenous peroxide as the cause for verdoheme formation was also eliminated. More importantly, reaction of $Cu_B$Mb with $H_2O_2$ (equivalent in oxidation state to $2e^-$-reduced $O_2$ but possessing two extra protons) produces a ferryl species similar to that in C*c*O. Since HO results in verdoheme regardless of the presence of metal ions in the distal site, or through reaction pathways of either reduced heme with $O_2$ or oxidized heme with $H_2O_2$, the biosynthetic model $Cu_B$Mb is not simply an HO model. Rather, $Cu_B$Mb is at a branching point between HO and C*c*O (Scheme 3); the extra proton may promote either the C*c*O or the P450 reaction, but not the HO reaction. Therefore, such a biosynthetic model provides a unique opportunity to investigate which properties direct the enzyme activity.

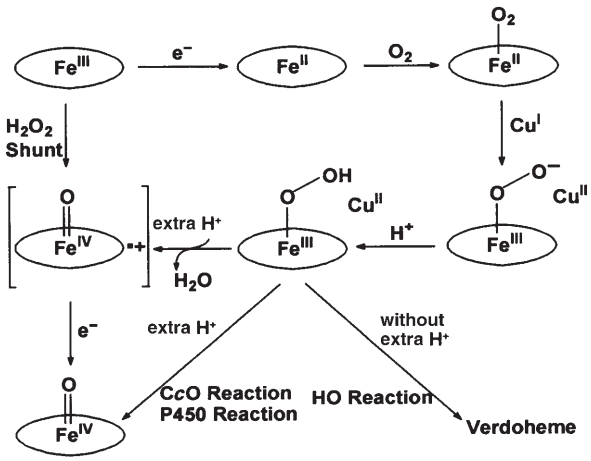


***Scheme 3.*** Hydrogen bonds and protons influence the reaction path of the common intermediate in heme enzymes. Adapted from reference [78].

## 3. Biosynthetic Inorganic Chemistry for the Synthesis of New Inorganic Complexes

Biosynthetic inorganic chemistry has been quite effective for making biomimetic models of complex metalloproteins and for revealing new insights into the structural features responsible for protein function. Its major advantage, however, is that it combines the benefits of inorganic chemistry and biology to produce new inorganic complexes with unprecedented structure and function.[84]

Natural metalloproteins normally consist of 20 amino acids, less than half of which can bind as ligands to metal ions. Furthermore, they employ only few metal ions and metal-containing prosthetic groups (e.g., cobalamins and heme groups). The use of nonnatural amino acids in metalloproteins will dramatically increase the number of possible ligand donor sets, and the introduction of inorganic compounds into proteins will lead to new and complex active sites. The net result will be a new, considerably expanded enzymology, which can draw from a large reservoir of artificial metalloproteins for various reaction types and rates.

Moreover, such endeavors can also result in new inorganic compounds with novel structure and activity. Especially important in this respect is the adaptation of inorganic catalysts for asymmetric reactions and for chemical transformations in water. Encapsulating these inorganic catalysts with proteins can fulfill both purposes, as the natural chiral environment of a protein can provide chiral discrimination. The hydrophobic interior of proteins provides a suitable surrounding for inorganic complexes that are active only in

 © 2006 Wiley-VCH Verlag GmbH & Co. KGaA, Weinheim 

organic solvent, while the hydrophilic exterior can increase the water solubility. These requirements can all be accomplished with minimal modification of the ligands and thus minimal effect on the catalyst reactivity.

### 3.1. Introducing Nonnatural Amino Acids into Metalloproteins

The properties of metalloproteins can be fine-tuned by introducing nonnatural amino acids into the metal-binding sites. For example, pyridine is a common ligand in synthetic models of metal-binding sites containing imidazole histidines in proteins.[10] The histidine ligands have been replaced by pyridine ligands in a newly designed heme protein with four α-helix units. The replacement of the two His ligands with two pyridyl ligands decreased the protein-binding affinity of ferric heme approximately 60 000-fold and increased the reduction potential of the heme by 287 mV.[85] These differences should be taken into consideration when using pyridines to model histidines in metalloproteins.

Perhaps the biggest advantage of using nonnatural amino acids in the metal-binding sites of proteins is the isostructural replacement of ligands or residues around the secondary coordination sphere, by which the electronic properties can be changed through substitution of a single atom or group. For example, both Cys and Met in blue copper protein proteins are conserved (Figure 9). Replacing the cysteine with

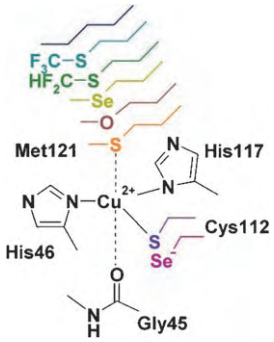


***Figure 9.*** Isostructural replacement of Cys and Met by nonnatural amino acids.

selenocysteine in azurin resulted in marked changes in the UV/Vis and EPR spectra (50-nm red shift of the visible charge transfer band and twofold increase in the hyperfine coupling constant),[86,87] with little effect on the reduction potential of the copper center.[86] In contrast, replacing the methionine with selenomethionine or norleucine resulted in little change in the UV/Vis and EPR spectra, but a dramatic increase in the reduction potentials (25 and 140 mV, respectively, over the native protein).[88]

In addition to ligands in the primary coordination sphere, residues in the secondary coordination sphere have also been replaced with nonnatural amino acids. For example, replacement of the OH group at the *para* position of a conserved Tyr unit near one of the Cys ligands of a rubredoxin with H, F, $NO_2$, and CN groups resulted in an increase in reduction potentials of the iron–sulfur center, with electron-withdrawing groups leading to more positive potentials (Figure 10 A).[89] Furthermore, a conserved hydrogen bond between the backbone amide groups and the cysteine ligand of the $Fe_4S_4$ clusters was found in high-potential iron–sulfur proteins (HiPIPs). Replacement of the backbone amide groups with an ester linkage eliminated these hydrogen bonds and lowered the reduction potential of the iron center by approximately 100 mV (Figure 10 B).[90]

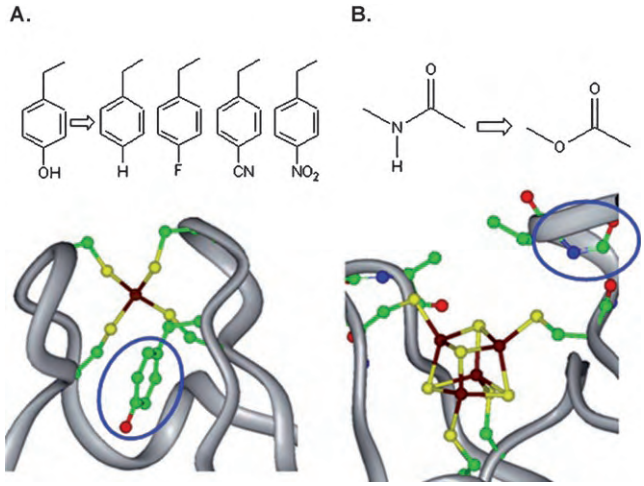


***Figure 10.*** Using nonnatural amino acids to probe the role of Tyr in the secondary coordination sphere in rubredoxin (A) and the backbone carbonyl oxygen atom in HiPIP (B).

Isostructural replacement of ligands has been a common practice in synthetic inorganic chemistry. Introducing nonnatural amino acids into metalloproteins finally allows biosynthetic inorganic chemistry to achieve a similar level of sophistication. Since proteins can provide a rigid network for the metal-binding sites, isostructural replacement often allows the introduction of ligands with little or no ability to coordinate to metal ions (e.g., replacement of Met with Ile) without affecting the overall characteristics of the metal-binding site. It also makes it easier to probe noncovalent interactions in the secondary coordination sphere (e.g., through replacement of a peptide bond with an ester linkage[90]). This approach can reveal the role of specific residues to an unprecedented level; it can be used to fine-tune coordination complexes. For example, the use of isostructural nonnatural amino acids at the Met position allowed deconvolution of different factors that influence the reduction potential of the blue copper azurin through this axial ligand.[88] A linear relationship between the reduction potential and the hydrophobicity of the side chains on the axial ligand pointed to hydrophobicity as the dominant factor in controlling the reduction potential[88] and could be helpful in developing similar compounds with predicted reduction potentials.

### 3.2. Introducing Nonnative Metal Cofactors into Proteins

The introduction of nonnative metal cofactors into proteins exemplifies the combination of the benefits of

 © 2006 Wiley-VCH Verlag GmbH & Co. KGaA, Weinheim 

biology and inorganic chemistry in biosynthetic inorganic chemistry. Three approaches have been applied towards this goal: noncovalent, single-covalent, and dual-covalent attachment.

The majority of native metal cofactors or prosthetic groups are incorporated into proteins through noncovalent interactions such as hydrogen bonding, as well as electrostatic and hydrophobic interactions. Because proteins have not been evolved to bind nonnative metal cofactors specifically, the introduction of these cofactors is a challenging task. The most successful approach thus far involves the replacement of the heme unit in heme proteins such as myoglobin with modified metalloporphyrins.[91–99] Since the modified metalloporphyrins are similar in structure to native heme groups, it is possible to confer novel reactivities to the protein through the introduction of new functional groups without severely changing the structure of the metal-binding site. For example, modifications to the two propionate groups in heme resulted in new functions such as protein–protein and protein–molecule recognition as well as electron-transfer properties and enhanced chemical reactivity (Figure 11 A),[99] which manifests itself for example in an enhanced P450-like dioxygen activation upon attachment of a flavin to one of the propionate groups.[102] Furthermore, when the heme is replaced with iron porphycene,[103] enhanced $O_2$-binding affinity is observed.

Many nonnative metal complexes do not resemble native metal cofactors. Conjugates of these metal complexes with biotin, however, can take advantage of the strong and specific binding between biotin and the protein avidin. In this way, biotinylated dirhodium(I) complexes have been introduced into avidin or the closely related protein streptavidin to produce novel catalysts for asymmetric hydrogenation with up to 96% enantiomeric excess (*ee*, Figure 11 B).[100,104–111] Another way to incorporate nonnative complexes is the design of metalloproteins based on the crystal structures of proteins and metal complexes. After careful inspection of the structures of myoglobin and $M^{III}$(salophen) complexes (M = Cr, Mn), modifications of both the protein and the metal complex gave a new protein that exhibited asymmetric sulfoxidation activity (Figure 11 C; salophen = *N*,*N*′-bis(salicylidene)-1,2-phenylenediamine dianion).[101,112–114] Finally, a mimetic protein with four helices has been designed de novo that selectively binds a metalloporphyrin.[115] This example marks the beginning of computationally developed, tailor-made metalloproteins with nonnative metal complexes.

Noncovalent attachment is not the only way in which native metal cofactors can be incorporated into proteins. There are also covalent attachment strategies, in which attachment is through either a single point (some protozoan mitochondrial cytochrome *c*[116]) or two points (most cytochrome *c*[117]). These strategies have also been applied to incorporate nonnative metal complexes.

For example, the introduction of 1,10-phenanthroline copper[120] or iron–edta[121] into proteins by single-point covalent attachment gave a sequence-specific nuclease (edta = ethylenediaminetetraacetate). Covalent attachment of a copper(II) 1,10-phenanthroline complex to a single cysteine residue in an adipocyte lipid-binding protein gave a catalyst that promotes highly enantioselective hydrolysis (with up to 86% *ee*) (Figure 12 A).[118,122] This strategy was also used to attach a ferrocene derivative covalently to azurin (Figure 12 B). This novel organometalloprotein increased the solubility of ferrocene and improved the stability of ferrocenium in water.[119] The secondary coordination sphere of the

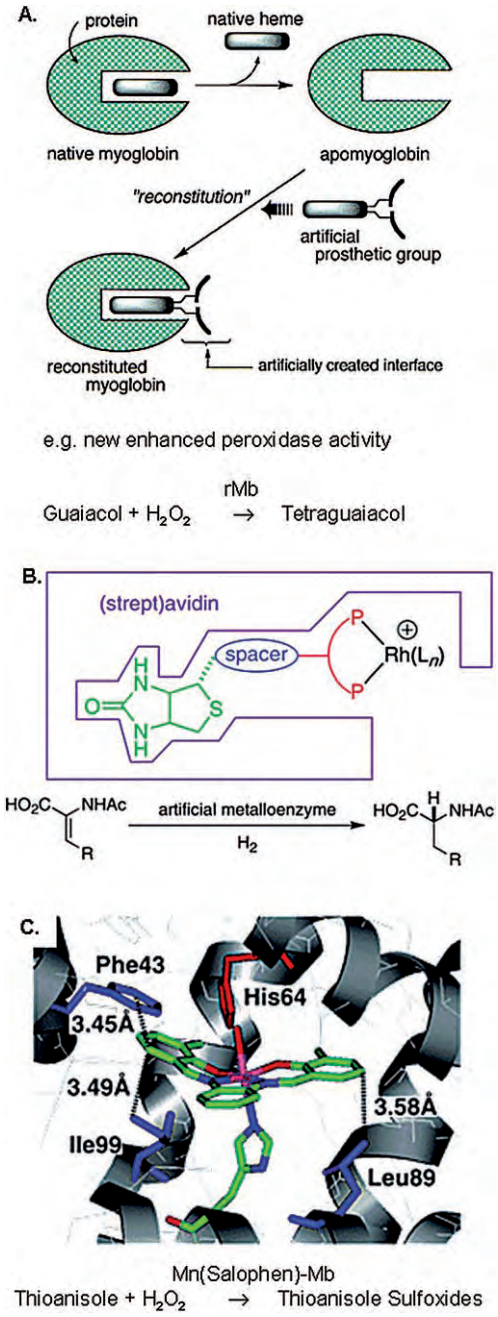


***Figure 11.*** Introducing nonnative metal-containing cofactors into proteins through noncovalent bonds. A) Replacing heme in Mb with a modified heme (adapted from reference [99]); B) Introducing organometallic complexes by taking advantage of strong noncovalent biotin and avidin interactions (adapted from reference [100]); C) Replacing heme in Mb with an Mn Schiff base complex (adapted from reference [113]).

 © 2006 Wiley-VCH Verlag GmbH & Co. KGaA, Weinheim 

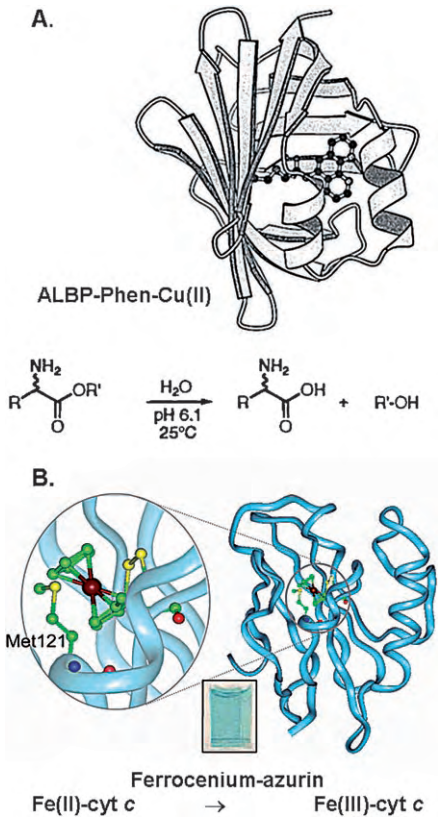


***Figure 12.*** Single-point covalent attachment of nonnative metal-containing cofactors to proteins. A) A computer model of an adipocyte lipid-binding protein–phenanthroline complex (ALBP-Phen) (adapted from reference [118]); B) A computer model of an azurin–ferrocene organometalloprotein.[119]

protein has also been used to fine-tune the reduction potential of ferrocene.[119]

Although single-point attachment allows the binding of nonnative metal complexes to proteins with minimum structural modifications, the conformational freedom of the complexes inside the protein may not be restricted enough to perform highly stereo- and enantioselective transformations. For example, an Mn(salen) complex coupled by single-point covalent attachment to a protein gave less than 10% *ee* (salen = *N*,*N*′-bis(salicylidene)ethylenediamine dianion).[123] When the complex is attached in a specific location of Mb by a dual-point covalent attachment, the enantioselectivity increased to 51% *ee* (Figure 13).[124] Clearly, such enantioselectivity is not yet useful for synthetic transformations; however, it is understandable given the fact that myoglobin has not evolved like other heme enzymes (e.g., Cyt P450) for asymmetric catalysis, and that the substrate binding site has not been modified to confer substrate selectivity. The principle demonstrated here is nonetheless important in guiding future research. For example, a combination of these covalent attachment strategies[123,124] with structure-based design or with directed evolution methods[125,126] will result in the next generation of asymmetric catalysts with even higher efficiencies and selectivities.

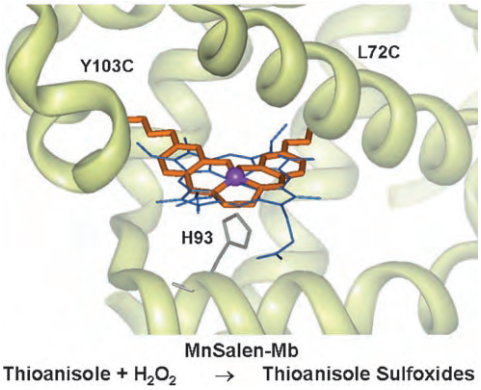


***Figure 13.*** Introducing nonnative metal-containing cofactors into proteins through dual-point covalent attachment. A computer model of Mb(L72C/Y103C) with a $Mn^{III}$salen complex covalently attached at two points and overlaid with heme in myoglobin (adapted from reference [124]).

## 4. Conclusions and Outlook

Biosynthetic inorganic chemistry is a natural extension of synthetic inorganic chemistry. Instead of using small organic molecules, small, stable, easy-to-make, and well-characterized proteins such as azurin and myoglobin are used as "ligands" for the synthesis of either biomimetic models or new compounds. The chemical and biological approaches each have advantages and disadvantages in terms of synthesis, characterization, and properties (Table 2).

*Synthesis.* A synthetic approach is generally faster and produces higher yields. However, recent developments in molecular biology and protein enzymology have enabled the routine production of hundreds of milligrams to grams of protein in the laboratory and even higher yields with industrial methods. By carrying out reactions with cells containing the desirable protein models, the power of natural amplification of genes and protein products can be exploited for biosynthesis and biocatalysis. One advantage of biosynthesis over small molecule synthesis, in which modification of the ligand might result in significant variations in yield and have associated cost and time investments, is that a similar modification of a protein ligand has a smaller influence on these parameters. These features make the speed and yield of biosynthesis closer to that of small molecule synthesis. In a few selected cases, it is even easier to synthesize biosynthetic models than some of the more complex synthetic models. For example, synthetic models of heme–copper oxidases require multistep syntheses that give relatively low yields.[79,80] The biosynthesis of heme–copper models in myoglobin[81] or cytochrome *c* peroxidase[127] proceeds with similar yields and preparation times as biosynthesis of other derivatives of the same proteins. Regardless of the complexity of the modifications, approximately 100 mg $L^{-1}$ of pure biosynthetic models can be obtained in less than a week. The routine production of gram quantities of protein is thus possible. Although the biosynthetic approach has been limited to a few cases in industry,[13,14] the gap between the two approaches is narrowing.

 © 2006 Wiley-VCH Verlag GmbH & Co. KGaA, Weinheim 

*Applications.* Biosynthesis is often carried out in air at ambient temperatures and pressures rather than in inert atmospheres at extreme temperatures and pressures, as are required for many syntheses of small molecules. Therefore, biosynthesis could help to save energy and equipment costs. Furthermore, biosynthesis is an environmentally benign approach, since biodegradable materials are utilized and water is the solvent. However, the products from biosyntheses are not as robust as synthetic compounds, which will make the long-term industrial use at high temperatures or pressures difficult. This problem can be overcome by using protein ligands that have been isolated from extremophilic organisms (which live at high temperatures or in organic solvents such as methanol).

A common criterion to evaluate the practical utility of catalysts is the mass ratio between the product and the catalyst. This is a good measure only if the catalysts are of similar type and are synthesized by similar methods. In this case, higher mass catalysts are generally more costly to synthesize and to dispose of, and therefore smaller compounds would be preferable to a chemically synthesized protein ligand of similar catalytic efficiency. However, biologically synthesized protein ligands can almost always be made at a much lower cost than their molecular weight would suggest, and disposing a biocompatible and biodegradable protein ligand is also much less costly than disposing a similarly sized organic ligand, which is often not biocompatible or biodegradable. In fact, the cost of synthesizing and disposing of a small protein (e.g., MW = 10000) by using recombinant protein expression systems is very similar to that of a much larger protein (e.g., MW = 100000). Therefore, multiple criteria are needed to evaluate different types of catalysts,[128] for example, mass ratio, catalyst accessibility and costs of synthesis and disposal, substrate scope, and, if applicable, enantioselectivity.

*Characterization.* Most metal-based spectroscopic techniques, such as electronic spectroscopy (UV/Vis), electron paramagnetic resonance (EPR), magnetic circular dichroism (MCD), resonance Raman (RR), and X-ray absorption spectroscopy (XAS), can be performed on both synthetic and biosynthetic compounds without much difference in data collection and interpretation. Even though recent developments in structural biology have made it possible to obtain three-dimensional structures of biosynthetic compounds routinely by using X-ray crystallography or NMR spectroscopy, it is still much easier to obtain structures of synthetic compounds with higher resolution. To overcome these limitations, one can use proteins with known 3D structures as ligands. In this way, it is easier to grow diffraction-quality crystals, and 3D structures can be obtained faster by comparing differences in the electron density map. The use of synchrotron sources to obtain diffraction data may also help to improve resolution.

*Properties.* Proteins provide a rigid network that helps to stabilize metal-binding or substrate-binding sites as a result of covalent bonds and noncovalent interactions (e.g., hydrogen bonds, electrostatic and hydrophobic forces) in the primary and secondary coordination spheres. They provide a better environment for regio- and stereoselective binding and catalysis, often without requiring protection of reactive functional groups. Because they consist of chiral natural amino acids, proteins are intrinsically enantioselective. Biosynthetic compounds with proteins can benefit from these features. Indeed, a number of biophysical studies show that biosynthetic models, such as a biosynthetic $Cu_A$ center in azurin (Figure 2B),[46] are as rigid as the native template proteins. Moreover, most synthetic modeling results in either structural or functional models of target native proteins. Because biosynthetic models use the same type of ligands and are synthesized and characterized under the same conditions as target proteins, they are often structural and functional models at the same time. Recent advances in synthetic chemistry have made it possible to design new organic ligands that provide a rigid network similar to that in proteins, including hydrogen-bonding interactions in the secondary coordination sphere.[11,12] Synthetic asymmetric catalysts have a wider range of activities and a broader substrate scope.[129] The wider range of activities arises mainly from the extensive choice of ligands, metals, and metal-containing cofactors. The broader substrate scope is attributable to a wide range of accessible reaction conditions, such as low temperatures, high pressures, and different organic solvents. Biosynthetic catalysts, however, are mostly restricted to only the 20 natural amino acids, physiologically available metals or metal-containing cofactors, physiological conditions, and water as solvent. These limitations make biocatalysts even more remarkable, and make it even more imperative to learn methods from nature to make better catalysts. The introduction of nonnatural amino acids and nonnative metal-containing cofactors into proteins is an important step in this direction.

In summary, recent advances in a number of areas in biology and chemistry have enabled the development of biosynthetic inorganic methods with comparable preparation times and yields to those of synthetic inorganic chemistry. In many cases, biosynthetic inorganic chemistry can produce close structural and functional models of more-complex metalloproteins and novel inorganic compounds. These developments, however, only demonstrate the potential that the biosynthetic approach has to offer; this potential is far from being realized. Although methodologies have been developed to introduce nonnative metal cofactors into proteins by noncovalent, single-, and double-covalent attachment, the use of these approaches in asymmetrically catalyzed syntheses of chiral intermediates for fine chemicals or pharmaceutical products is still lacking. In contrast to the field of asymmetric catalysis, which has had many years of development by a number of researchers, the field of biosynthetic inorganic chemistry is still in its infancy. Much more time and effort, including cross-fertilization of the synthetic and biosynthetic approaches, will be required before the full potential of biosynthetic inorganic chemistry can be realized.

*I wish to thank the members of my research group whose work has been cited in the references for their dedication and hard work, as well as Hee Jung Hwang, Thomas D. Pfister, Dewain Garner, and Natasha Yeung for help with the preparation of*

 © 2006 Wiley-VCH Verlag GmbH & Co. KGaA, Weinheim 

*figures in this review. The work of my group described in this review has been supported by the US National Science Foundation and the National Institutes of Health.*

Received: January 16, 2006
Published online: August 10, 2006

[1] S. J. Lippard, J. M. Berg, *Principles of Bioinorganic Chemistry*, University Science Books, Mill Valley, CA, **1994**.
[2] I. Bertini, H. B. Gray, S. J. Lippard, J. S. Valentine, *Bioinorganic Chemistry*, University Science Books, Sausalito, CA, **1994**.
[3] J. J. R. Fraústo da Silva, R. J. P. Williams, *The Biological Chemistry of the Elements, the Inorganic Chemistry of Life*, Clarendon Press, Oxford, **1991**.
[4] J. A. Cowan, *Inorganic Biochemistry, an Introduction*, VCH, New York, **1993**.
[5] W. Kaim, B. Schwederski, *Bioinorganic Chemistry: Inorganic Elements in the Chemistry of Life*, Wiley, Chichester, **1994**.
[6] R. H. Holm, E. I. Solomon, *Chem. Rev.* **1996**, *96*, 2237.
[7] *Ullmann's Encyclopedia of Industrial Chemistry*, 6th ed., 1998 Electronic Release, **1998**.
[8] *Riegel's Handbook of Industrial Chemistry*, 10th ed., **2003**.
[9] A. Fersht, *Structure and Mechanism in Protein Science: A Guide to Enzyme Catalysis and Protein Folding*, Freeman, New York, NY, **1999**.
[10] R. H. Holm, E. I. Solomon, *Chem. Rev.* **2004**, *104*, 347.
[11] R. I. Cukier, D. G. Nocera, *Annu. Rev. Phys. Chem.* **1998**, *49*, 337.
[12] A. S. Borovik, *Acc. Chem. Res.* **2005**, *38*, 54.
[13] B. A. Anderson, M. M. Hansen, A. R. Harkness, C. L. Henry, J. T. Vicenzi, M. J. Zmijewski, *J. Am. Chem. Soc.* **1995**, *117*, 12358.
[14] B. A. Anderson, M. M. Hansen, J. T. Vicenzi, M. J. Zmijewski, *Process Chem. Pharm. Ind.* **1999**, 263.
[15] *Inorganic Electronic Structure and Spectroscopy, Vol. I* (Eds.: E. I. Solomon, A. B. P. Lever), Wiley-Interscience, New York, **1999**.
[16] *Inorganic Electronic Structure and Spectroscopy, Vol. II* (Eds.: E. I. Solomon, A. B. P. Lever), Wiley-Interscience, New York, **1999**.
[17] *Physical Methods in Bioinorganic Chemistry: Spectroscopy and Magnetism* (Ed.: L. Que, Jr.), University Science Books, Mill Valley, CA, **2000**.
[18] C. Dennison, G. W. Canters, *Recl. Trav. Chim. Pays-Bas* **1996**, *115*, 345.
[19] H. Beinert, *Eur. J. Biochem.* **1997**, *245*, 521.
[20] A. J. Vila, C. O. Fernández in *Handbook on Metalloproteins* (Eds.: I. Bertini, A. Sigel, H. Sigel), Dekker, New York, NY, **2001**, p. 813.
[21] Y. Lu in *Biocoordination Chemistry, Vol. 8* (Eds.: L. Que, Jr., W. B. Tolman), Elsevier, Oxford, UK, **2004**, pp. 91.
[22] M. Saraste, *Q. Rev. Biophys.* **1990**, *23*, 331.
[23] B. G. Malmström, *Chem. Rev.* **1990**, *90*, 1247.
[24] G. T. Babcock, M. Wikstrom, *Nature* **1992**, *356*, 301.
[25] S. M. Musser, M. H. B. Stowell, S. I. Chan, *FEBS Lett.* **1993**, *327*, 131.
[26] J. A. García-Horsman, B. Barquera, J. Rumbley, J. Ma, R. B. Gennis, *J. Bacteriol.* **1994**, *176*, 5587.
[27] P. M. H. Kroneck, J. Riester, W. G. Zumft, W. E. Antholine, *Biol. Met.* **1990**, *3*, 103.
[28] W. G. Zumft, P. M. H. Kroneck, *Adv. Inorg. Biochem.* **1996**, *11*, 193.
[29] N. J. Blackburn, M. E. Barr, W. H. Woodruff, J. van der Oost, S. de Vries, *Biochemistry* **1994**, *33*, 10401.
[30] F. A. Cotton, R. A. Walton, *Multiple Bonds Between Metal Atoms*, Wiley, New York, **1982**.
[31] B. J. Hathaway in *Comprehensive Coordination Chemistry, the Synthesis, Reactions, Properties & Application of Coordination Compounds, Vol. 5*, 1st ed. (Eds.: G. Wilkinson, R. D. Gillard, J. A. McCleverty), Pergamon, Oxford, England, **1987**, p. 533.
[32] M. Dunaj-Jurco, G. Ondrejovic, M. Melnik, J. Garaj, *Coord. Chem. Rev.* **1988**, *83*, 1.
[33] C. Harding, V. McKee, J. Nelson, *J. Am. Chem. Soc.* **1991**, *113*, 9684.
[34] M. E. Barr, P. H. Smith, W. E. Antholine, B. Spencer, *J. Chem. Soc. Chem. Commun.* **1993**, 1649.
[35] C. Harding, J. Nelson, M. C. R. Symons, J. Wyatt, *J. Chem. Soc. Chem. Commun.* **1994**, 2499.
[36] R. P. Houser, V. G. Young, Jr., W. B. Tolman, *J. Am. Chem. Soc.* **1996**, *118*, 2101.
[37] D. D. LeCloux, R. Davydov, S. J. Lippard, *Inorg. Chem.* **1998**, *37*, 6814.
[38] C. He, S. J. Lippard, *Inorg. Chem.* **2000**, *39*, 5225.
[39] R. Gupta, Z. H. Zhang, D. Powell, M. P. Hendrich, A. S. Borovik, *Inorg. Chem.* **2002**, *41*, 5100.
[40] X.-M. Zhang, M.-L. Tong, X.-M. Chen, *Angew. Chem.* **2002**, *114*, 1071; *Angew. Chem. Int. Ed.* **2002**, *41*, 1029.
[41] D. D. LeCloux, R. Davydov, S. J. Lippard, *J. Am. Chem. Soc.* **1998**, *120*, 6810.
[42] S. B. Harkins, J. C. Peters, *J. Am. Chem. Soc.* **2004**, *126*, 2885.
[43] C. Dennison, E. Vijgenboom, S. de Vries, J. van der Oost, G. W. Canters, *FEBS Lett.* **1995**, *365*, 92.
[44] M. Hay, J. H. Richards, Y. Lu, *Proc. Natl. Acad. Sci. USA* **1996**, *93*, 461.
[45] G. J. Steffens, G. Buse, *Hoppe-Seyler's Z. Physiol. Chem.* **1979**, *360*, 613.
[46] H. Robinson, M. C. Ang, Y.-G. Gao, M. T. Hay, Y. Lu, A. H. J. Wang, *Biochemistry* **1999**, *38*, 5677.
[47] X. Wang, M. C. Ang, Y. Lu, *J. Am. Chem. Soc.* **1999**, *121*, 2947.
[48] M. T. Hay, R. M. Milberg, Y. Lu, *J. Am. Chem. Soc.* **1996**, *118*, 11976.
[49] M. T. Hay, Y. Lu, *J. Biol. Inorg. Chem.* **2000**, *5*, 699.
[50] H. J. Hwang, N. Nagraj, Y. Lu, *Inorg. Chem.* **2006**, *45*, 102–107.
[51] X. Wang, S. M. Berry, Y. Xia, Y. Lu, *J. Am. Chem. Soc.* **1999**, *121*, 7449.
[52] S. M. Berry, X. Wang, Y. Lu, *J. Inorg. Biochem.* **2000**, *78*, 89.
[53] H. J. Hwang, S. M. Berry, M. J. Nilges, Y. Lu, *J. Am. Chem. Soc.* **2005**, *127*, 7274.
[54] H. J. Hwang, Y. Lu, *Proc. Natl. Acad. Sci. USA* **2004**, *101*, 12842.
[55] O. Farver, Y. Lu, M. C. Ang, I. Pecht, *Proc. Natl. Acad. Sci. USA* **1999**, *96*, 899.
[56] H. B. Gray, B. G. Malmström, R. J. P. Williams, *J. Biol. Inorg. Chem.* **2000**, *5*, 551.
[57] E. I. Solomon, D. W. Randall, T. Glaser, *Coord. Chem. Rev.* **2000**, *200–202*, 595.
[58] B. E. Ramirez, B. G. Malmström, J. R. Winkler, H. B. Gray, *Proc. Natl. Acad. Sci. USA* **1995**, *92*, 11949.
[59] Y. Lu, S. M. Berry, T. D. Pfister, *Chem. Rev.* **2001**, *101*, 3047.
[60] A. Gengenbach, X. Wang, Y. Lu in *Fundamentals and Catalysis of Oxidative Delignification Processes, Vol. 785* (Ed.: D. S. Argyropoulos), American Chemical Society, Washington, DC, **2001**, p. 487.
[61] "Manganese and Its Role in Biological Processes": M. H. Gold, H. L. Youngs, M. D. S. Gelpke, *Met. Ions Biol. Syst.* **2000**, *37*, 559.
[62] M. Sundaramoorthy, K. Kishi, M. H. Gold, T. L. Poulos, *J. Biol. Chem.* **1994**, *269*, 32759.
[63] B. K. Yeung, X. Wang, J. A. Sigman, P. A. Petillo, Y. Lu, *Chem. Biol.* **1997**, *4*, 215.
[64] S. K. Wilcox, C. D. Putnam, M. Sastry, J. Blankenship, W. J. Chazin, D. E. McRee, D. B. Goodin, *Biochemistry* **1998**, *37*, 16853.

 © 2006 Wiley-VCH Verlag GmbH & Co. KGaA, Weinheim 

[65] X. Wang, Y. Lu, *Biochemistry* **1999**, *38*, 9146.
[66] A. Gengenbach, S. Syn, X. Wang, Y. Lu, *Biochemistry* **1999**, *38*, 11425.
[67] T. D. Pfister, A. J. Gengenbach, S. Syn, Y. Lu, *Biochemistry* **2001**, *40*, 14942.
[68] P. R. O. de Montellano, *Cytochrome P450 Structure, Mechanism, and Biochemistry*, 2nd ed., Plenum, New York, **1995**.
[69] S. Adachi, S. Nagano, Y. Watanabe, K. Ishimori, I. Morishima, *Biochem. Biophys. Res. Commun.* **1991**, *180*, 138.
[70] S. Adachi, S. Nagano, K. Ishimori, Y. Watanabe, I. Morishima, T. Egawa, T. Kitagawa, R. Makino, *Biochemistry* **1993**, *32*, 241.
[71] D. P. Hildebrand, J. C. Ferrer, H.-L. Tang, M. Smith, A. G. Mauk, *Biochemistry* **1995**, *34*, 11598.
[72] K. Choudhury, M. Sundaramoorthy, A. Hickman, T. Yonetani, E. Woehl, M. F. Dunn, T. L. Poulos, *J. Biol. Chem.* **1994**, *269*, 20239.
[73] J. A. Sigman, A. E. Pond, J. H. Dawson, Y. Lu, *Biochemistry* **1999**, *38*, 11122.
[74] R. Perera, M. Sono, J. A. Sigman, T. D. Pfister, Y. Lu, J. H. Dawson, *Proc. Natl. Acad. Sci. USA* **2003**, *100*, 3641.
[75] T. Uno, A. Yukinari, Y. Tomisugi, Y. Ishikawa, R. Makino, J. A. Brannigan, A. J. Wilkinson, *J. Am. Chem. Soc.* **2001**, *123*, 2458.
[76] H. Fujii, X. Zhang, T. Tomita, M. Ikeda-Saito, T. Yoshida, *J. Am. Chem. Soc.* **2001**, *123*, 6475.
[77] T. Matsui, M. Furukawa, M. Unno, T. Tomita, M. Ikeda-Saito, *J. Biol. Chem.* **2005**, *280*, 2981.
[78] J. A. Sigman, H. K. Kim, X. Zhao, J. R. Carey, Y. Lu, *Proc. Natl. Acad. Sci. USA* **2003**, *100*, 3629.
[79] J. P. Collman, R. Boulatov, C. J. Sunderland, L. Fu, *Chem. Rev.* **2004**, *104*, 561.
[80] E. Kim, E. E. Chufan, K. Kamaraj, K. D. Karlin, *Chem. Rev.* **2004**, *104*, 1077.
[81] J. A. Sigman, B. C. Kwok, Y. Lu, *J. Am. Chem. Soc.* **2000**, *122*, 8192.
[82] X. Zhao, N. Yeung, Z. Wang, Z. Guo, Y. Lu, *Biochemistry* **2005**, *44*, 1210.
[83] X. Zhao, M. J. Nilges, Y. Lu, *Biochemistry* **2005**, *44*, 6559.
[84] Y. Lu, *Curr. Opin. Chem. Biol.* **2005**, *9*, 118.
[85] H. K. Privett, C. J. Reedy, M. L. Kennedy, B. R. Gibney, *J. Am. Chem. Soc.* **2002**, *124*, 6828.
[86] S. M. Berry, M. D. Gieselman, M. J. Nilges, W. A. van der Donk, Y. Lu, *J. Am. Chem. Soc.* **2002**, *124*, 2084.
[87] M. Ralle, S. M. Berry, M. J. Nilges, M. D. Gieselman, W. A. van der Donk, Y. Lu, N. J. Blackburn, *J. Am. Chem. Soc.* **2004**, *126*, 7244.
[88] S. M. Berry, M. Ralle, D. W. Low, N. J. Blackburn, Y. Lu, *J. Am. Chem. Soc.* **2003**, *125*, 8760.
[89] D. W. Low, M. G. Hill, *J. Am. Chem. Soc.* **1998**, *120*, 11536.
[90] D. W. Low, M. G. Hill, *J. Am. Chem. Soc.* **2000**, *122*, 11039.
[91] T. Hayashi, A. Tomokuni, T. Mizutani, Y. Hisaeda, H. Ogoshi, *Chem. Lett.* **1998**, 1229.
[92] T. Hayashi, Y. Hitomi, T. Ando, T. Mizutani, Y. Hisaeda, S. Kitagawa, H. Ogoshi, *J. Am. Chem. Soc.* **1999**, *121*, 7747.
[93] T. Hayashi, T. Matsuda, Y. Hisaeda, *Chem. Lett.* **2003**, *32*, 496.
[94] H. Sato, T. Hayashi, T. Ando, Y. Hisaeda, T. Ueno, Y. Watanabe, *J. Am. Chem. Soc.* **2004**, *126*, 436.
[95] T. Hayashi, T. Nakagawa, K. Harada, T. Matsuo, Y. Hitomi, Y. Hisaeda, *Chem. Lett.* **2004**, *33*, 1512.
[96] H. Sato, M. Watanabe, Y. Hisaeda, T. Hayashi, *J. Am. Chem. Soc.* **2005**, *127*, 56.
[97] T. Hayashi, Y. Hitomi, T. Takimura, A. Tomokuni, T. Mizutani, Y. Hisaeda, H. Ogoshi, *Coord. Chem. Rev.* **1999**, *190–192*, 961.
[98] I. Hamachi, S. Shinkai, *Eur. J. Org. Chem.* **1999**, 539.
[99] T. Hayashi, Y. Hisaeda, *Acc. Chem. Res.* **2002**, *35*, 35.
[100] M. Skander, N. Humbert, J. Collot, J. Gradinaru, G. Klein, A. Loosli, J. Sauser, A. Zocchi, F. Gilardoni, T. R. Ward, *J. Am. Chem. Soc.* **2004**, *126*, 14411.
[101] T. Ueno, M. Ohashi, M. Kono, K. Kondo, A. Suzuki, T. Yamane, Y. Watanabe, *Inorg. Chem.* **2004**, *43*, 2852.
[102] T. Matsuo, T. Hayashi, Y. Hisaeda, *J. Am. Chem. Soc.* **2002**, *124*, 11234.
[103] T. Hayashi, H. Dejima, T. Matsuo, H. Sato, D. Murata, Y. Hisaeda, *J. Am. Chem. Soc.* **2002**, *124*, 11226.
[104] M. E. Wilson, G. M. Whitesides, *J. Am. Chem. Soc.* **1978**, *100*, 306.
[105] C.-C. Lin, C.-W. Lin, A. S. C. Chan, *Tetrahedron: Asymmetry* **1999**, *10*, 1887.
[106] J. Collot, J. Gradinaru, N. Humbert, M. Skander, A. Zocchi, T. R. Ward, *J. Am. Chem. Soc.* **2003**, *125*, 9030.
[107] C. M. Thomas, T. R. Ward, *Chem. Soc. Rev.* **2005**, *34*, 337.
[108] G. Klein, N. Humbert, J. Gradinaru, A. Ivanova, F. Gilardoni, U. E. Rusbandi, T. R. Ward, *Angew. Chem. Int. Ed.* **2005**, *44*, 7764.
[109] M. Skander, C. Malan, A. Ivanova, T. R. Ward, *Chem. Commun.* **2005**, 4815.
[110] T. R. Ward, *Chem. Eur. J.* **2005**, *11*, 3798.
[111] C. Letondor, N. Humbert, T. R. Ward, *Proc. Natl. Acad. Sci. USA* **2005**, *102*, 4683.
[112] M. Ohashi, T. Koshiyama, T. Ueno, M. Yanase, H. Fujii, Y. Watanabe, *Angew. Chem.* **2003**, *115*, 1035; *Angew. Chem. Int. Ed.* **2003**, *42*, 1005.
[113] T. Ueno, T. Koshiyama, M. Ohashi, K. Kondo, M. Kono, A. Suzuki, T. Yamane, Y. Watanabe, *J. Am. Chem. Soc.* **2005**, *127*, 6556.
[114] Y. Watanabe, T. Hayashi, *Prog. Inorg. Chem.* **2005**, *54*, 449.
[115] F. V. Cochran, S. P. Wu, W. Wang, V. Nanda, J. G. Saven, M. J. Therien, W. F. DeGrado, *J. Am. Chem. Soc.* **2005**, *127*, 1346.
[116] G. W. Pettigrew, J. L. Leaver, T. E. Meyer, A. P. Ryle, *Biochem. J.* **1975**, *147*, 291.
[117] R. A. Scott, A. G. Mauk, *Cytochrome c: A Multidisciplinary Approach*, University Science Books, Sausalito, CA, **1996**.
[118] R. R. Davies, M. D. Distefano, *J. Am. Chem. Soc.* **1997**, *119*, 11643.
[119] H. J. Hwang, J. R. Carey, E. T. Brower, A. J. Gengenbach, J. A. Abramite, Y. Lu, *J. Am. Chem. Soc.* **2005**, *127*, 15356.
[120] R. Chen, *Trends Biotechnol.* **2001**, *19*, 13.
[121] S. A. Datwyler, C. F. Meares, *Met. Ions Biol. Syst.* **2001**, *38*, 213.
[122] D. Qi, C.-M. Tann, D. Haring, M. D. Distefano, *Chem. Rev.* **2001**, *101*, 3081.
[123] M. T. Reetz, M. Rentzsch, A. Pletsch, M. Maywald, *Chimia* **2002**, *56*, 721.
[124] J. R. Carey, S. K. Ma, T. D. Pfister, D. K. Garner, H. K. Kim, J. A. Abramite, Z. Wang, Z. Guo, Y. Lu, *J. Am. Chem. Soc.* **2004**, *126*, 10812.
[125] M. T. Reetz, A. Zonta, K. Schimossek, K. Liebeton, K.-E. Jaeger, *Angew. Chem.* **1997**, *109*, 2961; *Angew. Chem. Int. Ed.* **1997**, *36*, 2830.
[126] M. T. Reetz, *Proc. Natl. Acad. Sci. USA* **2004**, *101*, 5716.
[127] J. A. Sigman, B. C. Kwok, A. Gengenbach, Y. Lu, *J. Am. Chem. Soc.* **1999**, *121*, 8949.
[128] E. N. Jacobsen, N. S. Finney, *Chem. Biol.* **1994**, *1*, 85.
[129] *Comprehensive Asymmetric Catalysis I–III*, *Vol. 1*, (Eds.: E. N. Jacobsen, A. Pfaltz, H. Yamamoto), Springer, New York, **1999**.

 © 2006 Wiley-VCH Verlag GmbH & Co. KGaA, Weinheim 

Inorganic Chemistry

DOI: 10.1002/anie.200600861

# Lone-Pair Interfaces That Divide Inorganic Materials into Ionic and Covalent Parts**

*Zuzana Mayerová, Mats Johnsson,* and Sven Lidin*

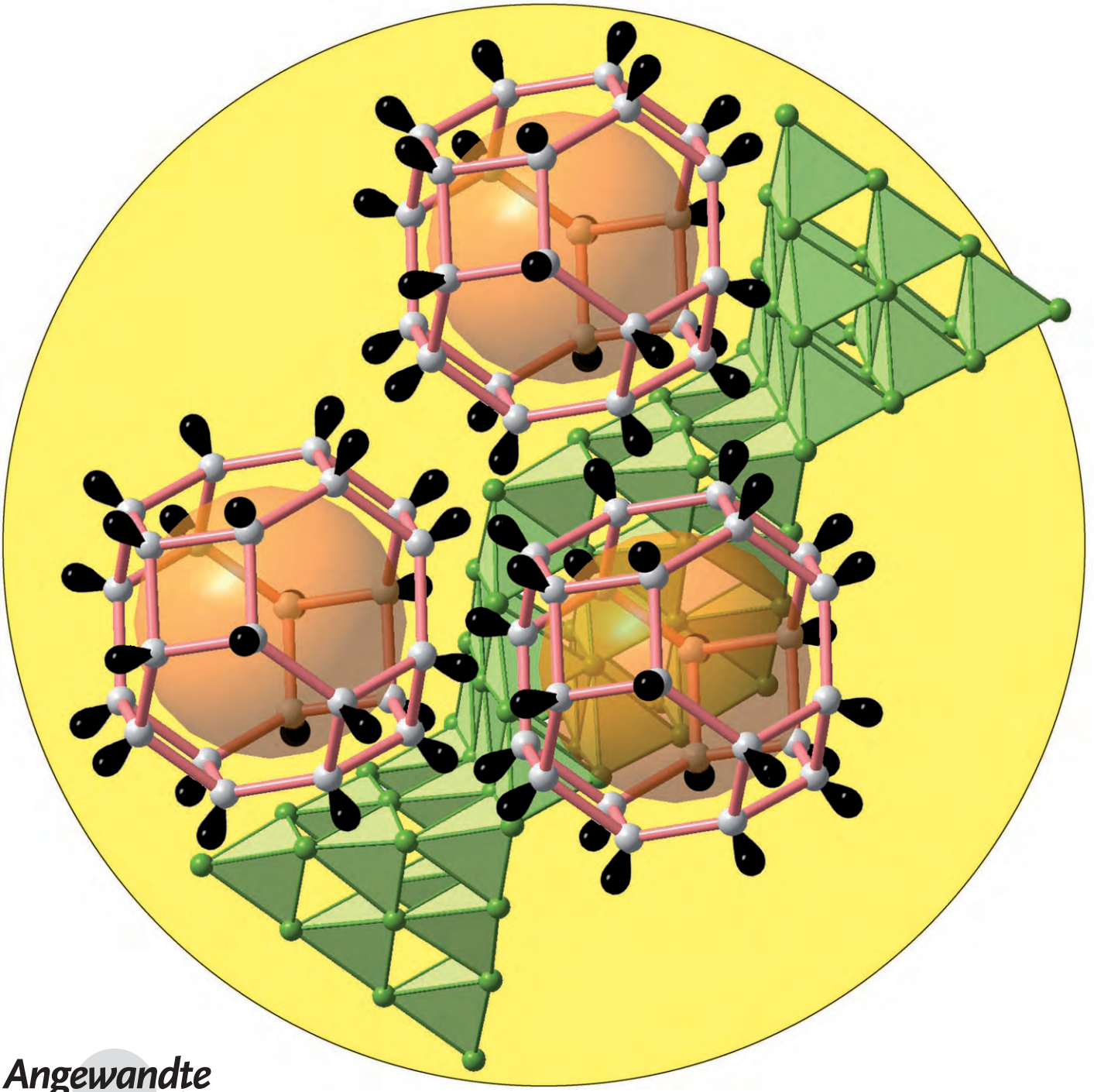



WILEY InterScience DISCOVER SOMETHING GREAT

© 2006 Wiley-VCH Verlag GmbH & Co. KGaA, Weinheim

Compounds containing main-group metals in low oxidation states frequently exhibit stereochemically active lone pairs. In particular, this is observed for compounds of $Sn^{II}$, $Pb^{II}$, $As^{III}$, $Sb^{III}$, $Bi^{III}$, and $Te^{IV}$. An intriguing phenomenon is the localization of such lone pairs to well-defined regions of the solid-state structures of these compounds, wherein the volumes of lone pairs form surfaces that separate regions of different kinds of chemical interaction.[1–5] Interestingly, lone pairs tend to aggregate and even more so they tend to aggregate together with negatively charged ions. Here we show a striking example of how this segregation effect can be used to template solid-state compounds with reduced dimensionality.

The new compound $Cu_{20}Sb_{35}O_{44}Cl_{37}$ (**1**) crystallizes in the tetragonal space group *I*4/*mmm*, with unit-cell parameters $a = 18.144(2)$ Å and $c = 15.795(2)$ Å. It features extensive disorder, indicative of a lowering of local symmetry. Alternative descriptions were also extensively checked. Reciprocal space was explored to detect any additional scattering features, but neither classical superstructure reflections, incommensurate satellites, nor diffuse scattering was observed. We therefore conclude that the translational cell is correct. The disorder features may be taken as an indication of twinning or local disorder; to distinguish between the two, several low-symmetry models were evaluated and discarded in favor of our final high-symmetry choice. In that case, disorder appears to be strictly local in nature and is best modeled by using a split model and/or large displacement parameters for the disordered part.

The crystal structure of **1** consists of two distinct parts: edge-sharing $[Cu_{10}Cl_{16}]^{6-}$ T3 supertetrahedra (the edge of the supertetrahedron consists of the edges of three $CuCl_4$ tetrahedra) that form infinite chains, and isolated, octahedral $[Sb_{35}Cl_5O_{44}]^{12+}$ clusters with pseudo-cubic symmetry. A schematic overview of the structure is displayed in Figure 1. The two parts of the structure, namely an anionic part and a cationic part, are separated by an interface made up from the lone pairs associated with $Sb^{III}$. The lone pairs act as terminators for the Sb–O network, essentially by generating a nonbonding shell surrounding the large $(Sb_{35}Cl_5O_{44})^{12+}$ cluster. This illustrates a general feature of lone-pair oxohalide systems. A chalcophile partial structure terminates by a nonbonding lone-pair skin that faces a halide layer forming the surface of a halophile substructure. This phenomenon is also seen in, for example, $CuSb_2O_3Br$ and $CuSbTeO_3Cl_2$.[6–7] In the present case, the relatively halophilic Cu associates exclusively with Cl, while the chalcophile Sb associates with O atoms. The association of terminal Cl ions and lone pairs to an interface region in the structure is hardly the sign of any mutual attraction, but this cohabitation is rather the effect of the expulsion of nonbonding parts to the surface of a structural entity.

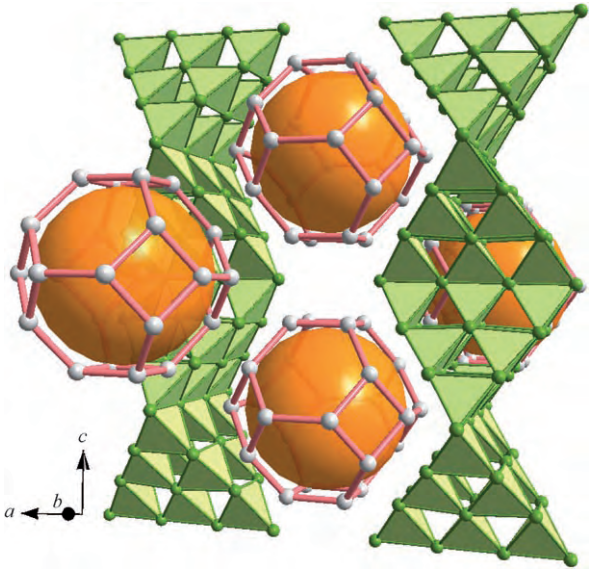


***Figure 1.*** Simplified view of the crystal structure for $Cu_{20}Sb_{35}O_{44}Cl_{37}$ (**1**) seen along the [010] axis. The covalently bonded clusters resembling zeolite β cages are placed in between sheets of ionically bonded supertetrahedra. Only Sb atoms (gray) and Cl atoms (green) are displayed. The orange spheres represent the void space within the clusters.

The Cu–Cl arrangement is simple but remarkable: $CuCl_4$ tetrahedra share Cl vertices to form T3 supertetrahedral $[Cu_{10}Cl_{20}]^{10-}$ units, much akin to the borosulfate and boroselenate T3 supertetrahedra reported by Krebs et al.[8–10] Recent research has focused on nanoclusters with large T*n* supertetrahedral units, as they have a potential to create novel low-density nanoporous crystalline solids with many interesting properties. Those studies concern chalcogenide clusters built of supertetrahedra of type T4 and T5.[11–13] The largest T5 units are represented by pseudo-T5 clusters in $(Cu_5In_{30}S_{54})^{13-}$ or T5 tetrahedra found in $Na_{26}Mn_{39}O_{55}$.[12–13] Larger supertetrahedral units may be obtained by combining different T*n* supertetrahedra and are known as supertetrahedra of supertetrahedra.[14] In all previously described compounds, the supertetrahedra are corner-sharing. The unique feature of the **1** is that the $[Cu_{10}Cl_{20}]^{10-}$ supertetrahedra share edges to form linear chains of the overall formulation $[(Cu_{10}Cl_{16})^{6-}]_\infty$. While edge-sharing is rather rare in tetrahedra, there is a facile local deformation mechanism for the accommodation of the accompanying strain in the T3 supertetrahedra that can clearly be seen in Figure 2. The Cu atoms that are located at the center of the three tetrahedra that form the edge of the supertetrahedron are displaced away from that edge towards the centre of the ensemble. The chains of supertetrahedra lie at the center of the isometric edges of the unit cell. Large cavities in the Cu–Cl packing are thus formed, which host the $[Sb_{35}Cl_5O_{44}]^{12+}$ clusters, centered at $\frac{1}{2}\,\frac{1}{2}\,0$ and at $0\,0\,\frac{1}{2}$.

[*] Z. Mayerová, Dr. M. Johnsson, Prof. Dr. S. Lidin
Department of Inorganic Chemistry
Stockholm University
106 91 Stockholm (Sweden)
Fax: (+46) 8152-187
E-mail: matsj@inorg.su.se

[**] This work was carried out through financial support from the European Union (HPHN-CT-2002-00193) and the Swedish Research Council. We thank Mr. Loïc Hugonin for help in creating the Frontispiece.

Supporting information for this article is available on the WWW under http://www.angewandte.org or from the author.

 © 2006 Wiley-VCH Verlag GmbH & Co. KGaA, Weinheim 

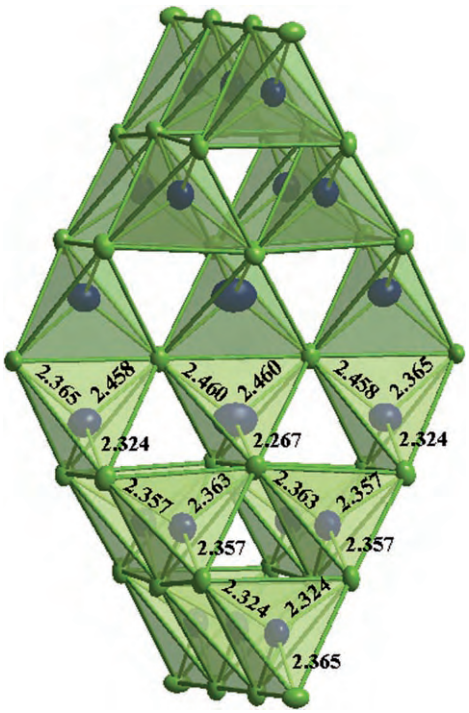


***Figure 2.*** Each supertetrahedron consists of 10 $CuCl_4$ distorted tetrahedra (Cu blue, Cl green). The distortion of the Cu–Cl bond lengths at the common edge of two supertetrahedra is shown. The Cu atoms are displaced away from that edge.

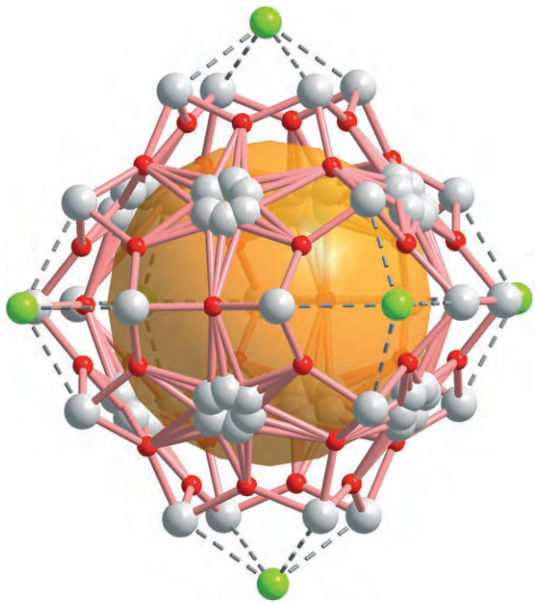

***Figure 3.*** Detailed view of the pseudo-cubic antimony oxochloride cluster outer shell (Sb gray, Cl green, O red). The shell forms a truncated octahedron with Sb at all vertices and at the centers of all hexagonal faces. Together with the oxygen atoms at all mid-edge positions, this forms an $Sb_{32}O_{36}$ cage equivalent to a β cage. Owing to the rather restrictive geometry of Sb–O distances and O-Sb-O angles, the Sb positions on the hexagonal faces are all split into six positions. All square faces are capped by Cl ions, which together form a large octahedron. The orange sphere represents the void space within the cluster.

***Figure 4.*** Relation between the outer and inner parts of the antimony oxochloride cluster. The two parts of the cluster are connected through the oxygen atoms of the inner shell and the six split Sb positions that lie at the center of the hexagonal planes of the outer shell. The oxygen positions are split to decrease the Sb–O strain in the outer layer. The inner part consists of a partly occupied central Sb atom surrounded by cubically arranged O atoms and an octahedron of partly occupied split Sb positions (Sb gray, O red).

The pseudo-cubic antimony oxochloride cluster consists of two shells: an outer shell that forms a truncated octahedron with Sb atoms at all vertices, and at the centers of all hexagonal faces with oxygen at all mid-edge positions forming an $Sb_{32}O_{36}$ cage equivalent to the β cages usually found in zeolites such as sodalite and similar to that found in compounds with the idealized composition $[(Te_{32}Ni_{30}X_3O_{90})^{5+}(Ni_4X_{13})^{5-}]$ (X = Cl, Br).[15–16] An idealized picture of this arrangement is shown in Figure 3. Owing to the rather restrictive geometry of Sb–O distances and O-Sb-O angles, the Sb positions on the hexagonal faces are all split into six positions. All square faces are capped by Cl ions, together forming a large octahedron. As a result of short distances along the *c* direction to neighboring clusters, the apical Cl positions are only half filled while the equatorial positions are all fully occupied. Within this large octahedral shell dwells the second entity, an $O_8$ cube capped on all faces by Sb with almost-half occupancies. In the center of this unit, there is another Sb position with a relatively low occupancy (ca. 1/6). This arrangement, formally $Sb_7O_8$, but rather closer to $Sb_3O_8$ by composition, is shown in Figure 4. This inner part of the cluster is bonded to the partially occupied Sb atoms of the outer shell, generating a large number of possible configurations related by minor rotational adjustments. We modeled this part of the structure with split positions to generate admissible Sb–O distances. The central Sb atom was assumed to be distributed over several positions as well in response to the presence or absence of the six apical Sb atoms, but given the rather low occupancy and the high symmetry of this position it was deemed prudent to model this atom by using a single position. Because of the unconstrained partial occupancies, the total composition of the cluster was in fact $Sb_{34.67}Cl_5O_{44}$, while overall charge balance would dictate $[Sb_{35}Cl_5O_{44}]^{12+}$.

 © 2006 Wiley-VCH Verlag GmbH & Co. KGaA, Weinheim 

The Sb atoms that make up the β cages behave more or less as expected for $Sb^{III}$. The Sb atoms that occupy the vertices of the truncated octahedron form the apices of squat trigonal pyramids. Together with their stereochemically active lone pair (E), this makes up a set of $SbO_3E$ tetrahedra. If the Cl atoms that complete the octahedron are taken into account, the coordination is still an unsurprising $SbClO_3E$ trigonal bipyramid for these atoms. The Sb site at the center of the hexagonal window of the truncated octahedron is rather more troubled. This position is not ideally suited for an Sb atom, neither when considering distances nor when considering geometry. The result is a split of this position into six distinct locations, each with three suitable Sb–O distances within the hexagonal ring and one Sb–O distance to an oxygen atom that belongs to the entity in the center of the cluster. The general coordination is then, not unexpectedly, again a trigonal-bipyramidal $SbO_4E$, but this is rather strained having three oxygen atoms coplanar with the central Sb atom (such a coordination is also observed in $Sb_8O_{11}Cl_2$).[17] The coordination of the Sb atoms in the inner cluster is a $SbO_4E$ square pyramid (this type of coordination was previously observed for $Sb^{III}$ in, for example, the compound $BaSbO_2Cl$).[18]

It is still unclear if there is a positive interaction between lone-pair aggregates and negatively charged ions or if the agglomeration is simply an effect of mutual expulsion from the bonded regions of the structure. A simple but typical example is tetragonal BiOCl in which Bi and O form a covalently bonded oxidic sheet that terminates on both sides by layers of $Bi^{III}$ lone pairs. The Cl ions are found in the regions outside these sheets.[19] The Cl region of the structure may actually be intercalated by alkali metals as in $Cs_xBi_{2-x}Pb_xO_2Cl_2$ to form a second, ionically bonded substructure.[20] Lone pairs define the boundary between the two regions of different interactions.

In summary, lone pairs separate two structurally very different regions in the compound $Cu_{20}Sb_{35}O_{44}Cl_{37}$ (**1**) described. The halophile copper forms a relatively simple structure of edge-sharing T3 supertetrahedra that form infinite chains along the tetragonal *c* direction. Interspersed between these $[Cu_{10}Cl_{16}{}^{6-}]_\infty$ columns are covalent entities, namely $[Sb_{35}Cl_5O_{44}]^{12+}$ clusters. If the interconnectivity of the $[Cu_{10}Cl_{16}{}^{6-}]_\infty$ columns is ignored and the center of the supertetrahedra are considered as the loci of negatively charged clusters, the whole ensemble may be regarded as a fluorite-type packing of clusters. While the $[Cu_{10}Cl_{16}{}^{6-}]_\infty$ columns terminate by an outer layer of Cl ions, the $[Sb_{35}Cl_5O_{44}]^{12+}$ clusters present a surface covered by $Sb^{III}$ lone pairs, and in the typical fashion of lone-pair oxohalides, we find a dividing region; in this case, in the shape of undulating tubes built from lone pairs and halide ions.

## Experimental Section

$Sb_2O_3$ (Aldrich), CuCl (ABCR), $SbCl_3$ (ACROS organics), and amorphous $SiO_2$ (prepared by hydrolysis of TEOS (ACROS organics) and subsequent calcinations) were used as starting materials for the synthesis of $Cu_{20}Sb_{35}O_{44}Cl_{37}$ (**1**). A mixture of $SiO_2$, $Sb_2O_3$, and CuCl in 1:1:1 molar ratio was placed in a sealed evacuated silica tube and subsequently heat-treated in a muffle furnace at 500 °C for 93 h. The product was a mixture of a yellow powder, transparent yellow crystals, and yellow-green single crystals of $Cu_{20}Sb_{35}O_{44}Cl_{37}$. As single crystals of **1** were found only in one end of the silica tubes, chemical transport appears to be involved in the growth mechanism. The crystals used for analyses were selected manually on the basis of color and morphology. The compound was also synthesized as a powder from a stoichiometric mixture of $Sb_2O_3/SbCl_3/CuCl$ (44:17:60).

Single-crystal X-ray diffraction data on **1** were collected at 290 K on an STOE IPDS diffractometer equipped with an image plate and graphite-monochromatized $Mo_{K\alpha}$ radiation ($\lambda = 0.71073$ Å) from a rotating anode. The intensities of the reflections were integrated by using the software provided by the manufacturer, and absorption correction was carried out numerically, after crystal shape optimization.[21–22] The structures were solved by direct methods (SHELXS97) and refined by full-matrix least squares on $|F|$ using the program Jana2000.[23–24] All illustrations were made with the program Diamond.[25] 24 807 reflections, of which 1783 were unique, were collected in the region $2.24 < \theta < 27.98°$; space group *I*4/*mmm*; unit cell dimensions $a = 18.144(2)$ Å, $c = 15.795(2)$ Å, $Z = 2$, $V = 5199.37(99)$ Å$^3$. All fully occupied atomic positions except oxygen were refined using anisotropic displacement parameters. $R = 0.0639$ for 1.556 reflections with $I > 3\sigma(I)$ and 0.0714 for 1.783 reflections; $wR = 0.0997$ and $S = 1.83$ (the goodness of fit on $|F|$). Crystal data, details of structure determination, atomic coordinates, equivalent isotropic displacement parameters, and bond lengths are given in the Supporting Information. Further details on the crystal structural investigations may be obtained from the Fachinformationszentrum Karlsruhe, 76344 Eggenstein-Leopoldshafen, Germany (fax: (+49) 7247-808-666; e-mail: crysdata@fiz-karlsruhe.de), on quoting the depository number CSD-416247.

The chemical composition of the products were confirmed by using energy-dispersive spectrometry (EDS, LINK AN10000) in a scanning electron microscope (SEM, JEOL 820). See Supporting Information for the measured chemical composition.

Received: March 6, 2006
Revised: April 25, 2006
Published online: July 28, 2006

**Keywords:** antimony · cluster compounds · halides · interfaces · structure elucidation

[1] H. Katzke, Y. Oka, Y. Kanke, K. Kato, T. Yao, *Z. Kristallogr.* **1999**, *214*, 284–289.
[2] C. Särnstrand, *Acta Crystallogr. Sect. B* **1978**, *34*, 2402–2407.
[3] W. Altenburger, W. Hiller, I. R. Jahn, *Z. Kristallogr.* **1987**, *181*, 227–234.
[4] J. A. Alonso, *J. Chem. Soc. Dalton Trans.* **1998**, *12*, 1947–1950.
[5] J. A. Alonso, E. Gutérrez-Puebla, A. Jerez, A. Monge, C. Ruiz-Valero, *J. Chem. Soc. Dalton Trans.* **1985**, 1633–1635.
[6] Z. Mayerová, M. Johnsson, S. Lidin, *J. Solid State Chem.* **2005**, *178*, 3487–3491.
[7] R. Becker, M. Johnsson, R. Kremer, P. Lemmens, *Solid State Sci.* **2003**, *5*, 1411–1416.
[8] A. Hammerschmidt, P. zum Hebel, F. Hiltmann, B. Krebs, *Z. Anorg. Allg. Chem.* **1996**, *622*, 76–84.
[9] B. Krebs, H. Diercks, *Z. Anorg. Allg. Chem.* **1984**, *518*, 101–114.
[10] P. zum Hebel, B. Krebs, M. Gruene, W. Mueller-Warmuth, *Solid State Ionics* **1990**, *43*, 133–142.
[11] C. Wang, Y. Li, X. Bu, N. Zheng, O. Zivkovic, C.-S. Yang, P. Feng, *J. Am. Chem. Soc.* **2001**, *123*, 11 506–11 507.
[12] X. Bu, N. Zheng, Y. Li, P. Feng, *J. Am. Chem. Soc.* **2002**, *124*, 12 646–12 647.
[13] A. Möller, P. Amann, V. Kataev, N. Schitter, *Z. Anorg. Allg. Chem.* **2004**, *630*, 890–894.

 © 2006 Wiley-VCH Verlag GmbH & Co. KGaA, Weinheim 

[14] H. Li, J. Kim, M. O'Keeffe, O. M. Yaghi, *Angew. Chem.* **2003**, *115*, 1863 – 1865; *Angew. Chem. Int. Ed.* **2003**, *42*, 1819 – 1821.
[15] L. Pauling, *Z. Kristallogr. Kristallgeom. Kristallphys. Krista* **1930**, *74*, 213 – 225.
[16] M. Johnsson, S. Lidin, K. W. Törnroos, H.-B. Bürgi, P. Millet, *Angew. Chem.* **2004**, *116*, 4292 – 4295; *Angew. Chem. Int. Ed.* **2004**, *43*, 4292 – 4295.
[17] S. Menchetti, C. Sabelli, R. Trosti-Ferroni, *Acta Crystallogr. Sect. C* **1984**, *40*, 1506 – 1510.
[18] F. Thuillier-Chevin, P. Maraine, G. Perez, *Rev. Chim. Miner.* **1980**, *17*, 102 – 109.
[19] F. A. Bannister, *Mineral. Mag. J. Mineral. Soc.* **1935**, *149*, 49 – 58.
[20] D. O. Charkin, P. S. Berdonosov, A. M. Moisejev, R. R. Shagiakhmetov, V. A. Dolgikh, P. Lightfoot, *J. Solid State Chem.* **1999**, *147*, 527 – 535.
[21] X-RED, Version 1.07, STOE & Cie GmbH, Darmstadt, Germany, **1996**.
[22] X-SHAPE revision 1.09, STOE & Cie GmbH, Darmstadt, Germany, **1997**.
[23] G.-M. Sheldrick, SHELXS-97—Program for the Solution of Crystal Structures, Göttingen, **1997**.
[24] V. Petříček, M. Dusek, Institute of Physics AVCR, Praha, Czech Republic, **2000**.
[25] K. Brandenburg, DIAMOND Release 2.1e, Crystal Impact GbR, Bonn, Germany, **2000**.

 © 2006 Wiley-VCH Verlag GmbH & Co. KGaA, Weinheim 

Charge Transfer

DOI: 10.1002/anie.200602106

# Double Proton Coupled Charge Transfer in DNA**

*Francesco Luigi Gervasio,* Mauro Boero, and Michele Parrinello*

Charge transfer processes in DNA play an important role in oxidatively generated damage and possibly in repairing mechanisms.[1–3] Furthermore, if conductive, DNA could be used in nanoelectronic devices.[4–6] Unfortunately, the many experiments conducted have provided contradictory results, with conductivities that cover the entire range from metallic to insulator.[7–11] Such experiments are technically difficult as they require handling of single molecules or small bundles of DNA and fine control of their contact to the metallic leads and to the supporting surfaces. Despite experimental difficulties, a general consensus has been reached.[1,12] In particular, experiments on chemically modified or photosensitizer intercalated DNA have demonstrated that wet DNA and DNA bundles can carry charge.[1,13,14] On the other hand, long DNA helices deposited on mica surfaces or in dry conditions were found to be insulators or wide-bandgap semiconductors.[12] These results are not unexpected as the intrinsic randomness of DNA, induced by distortions and defects, can affect its conducting properties. Moreover, oxidation plays an important role as a parasitic event relative to hole (positive radical) migration.[15,16]

As discussed in reference [17], charge transportation in duplex DNA takes place when the Fermi energies of the electrodes fall between the HOMO and the LUMO of the constituents and can occur through two possible mechanisms: a) a coherent single-step transportation from donor to acceptor (superexchange limit)[18] or b) multistep charge hopping.[19,20]

Both mechanisms have been observed in wet DNA. In these experiments, the charge is injected site selectively by either intercalating an oxidizing agent or introducing some modification into the DNA. Similarly a charge sink can be created by the introduction of a modified base or of a GGG sequence; the effect of such modifications is to lower the ionization potential (IP) with respect to that of an isolated G, thus making the site an effective hole trap.[21] By using this approach, Giese et al. determined the effect of the bridge length on the efficiency of hole transfer by varying the number of $(A:T)_n$ base pairs between the charge injection site and the GGG.[22] An exponential decay of the charge-transfer efficiency was observed as a function of the interposed $(A:T)_n$ sequence for $n < 4$,[23] in agreement with a single-step superexchange-mediated transfer mechanism. Similar results have been reported by Nakatanu and Saito in reference [1]. In DNA sequences containing isolated G:C sites between the source and sink, the charge was shown to hop reversibly between all guanines.[24]

Although the role of fluctuations in modulating DNA conductivity and a possible polaron-like hopping mechanism has been investigated in several experiments,[20,25–28] our knowledge of the microscopic changes induced by the charge defect and its transfer is mostly based on indirect evidence. Different localization mechanisms have been proposed: a change in the tilt angle of the bases, a rearrangement of the solvation shell, a fluctuation in the position of counterions, and a change in the protonation state of G. The first was hypothesized on the basis of simplified theoretical models.[29] The importance of the polarization of the solvent shell has been shown to play a role in the charge transfer in poly(A:T).[30] The ion-gated charge-hopping mechanism was proposed from first-principles simulations that showed a correlation between the charge localization and the position

[*] Dr. F. L. Gervasio, Prof. M. Parrinello
Computational Science
Department of Chemistry and Applied Biosciences
ETH Zurich
USI Campus
Via Giuseppe Buffi 13, 6900 Lugano (Switzerland)
Fax: (+41) 586-664-817
E-mail: fgervasi@phys.chem.ethz.ch
Homepage: www.rgp.ethz.ch
Prof. M. Boero
Center for Computational Sciences
University of Tsukuba
1-1-1 Tennodai, Tsukuba, Ibaraki 305-8576 (Japan)

[**] We acknowledge generous grants from the Earth Simulator Center (ES-JAMSTEC)–Yokohama and from the Swiss National Supercomputing Centre(CSCS) which have made this calculation possible. M.B. is grateful to Takashi Ikeda and Masaru Hirata for their valuable help. F.L.G. is grateful to Y. Mantz for his valuable help.

 InterScience © 2006 Wiley-VCH Verlag GmbH & Co. KGaA, Weinheim 

of the counterion and it was supported by indirect experimental evidence.[31] The proton-coupled charge-transfer mechanism received most attention and different groups found experimental and theoretical supporting evidence.[32–35] In this scenario, the charge hopping is linked to the proton transfer from G to C.

Recently, by performing first-principles dynamical simulations on a crystalline poly-d(GpCp) fiber, we found that the hole can indeed be localized by a proton transfer from G to C.[35] However, we did not observe directly the hole migrating from one site to another as a consequence of a specific change. The same is also true for all the other first-principles calculations performed on realistic models.[31,36,37] Experimentally, only indirect evidence has been reported and the issue remains controversial and much debated.

Herein we report the direct observation of charge transfer from a GGG to a G site upon deprotonation of the latter. This was obtained by a large-scale first-principles quantum-mechanical (QM) simulation coupled to a molecular mechanics (MM) simulation (QM/MM) on a fully hydrated 38-base-pair B-DNA d(5′ACGCACGTCGCATAATATTACGT GGGTATTATATTAGC-3′). The chosen sequence is the same as that used in the experiments of Giese and coworkers[38] The structure was equilibrated at room temperature for 10 ns in a box $38\times41\times154$ Å$^3$ with 5902 water molecules and $Na^+$ counterions, for a total of 20265 atoms, by using the Amber99 force field.[39] QM/MM calculations were performed within DFT.[40,41] We performed seven different QM/MM molecular-dynamics simulations starting from uncorrelated structures extracted from the MM run. The quantum subsystem was taken to be the central segment d(5′GTGGG-3′), which, to reduce the computational cost, was in some of the calculations replaced by d(5′GTGG-3′). The QM subsystem included the sugar–phosphate backbone for a total of 303 atoms and was terminated with four capping hydrogen atoms. The classical MM part included the remaining 19962 atoms.

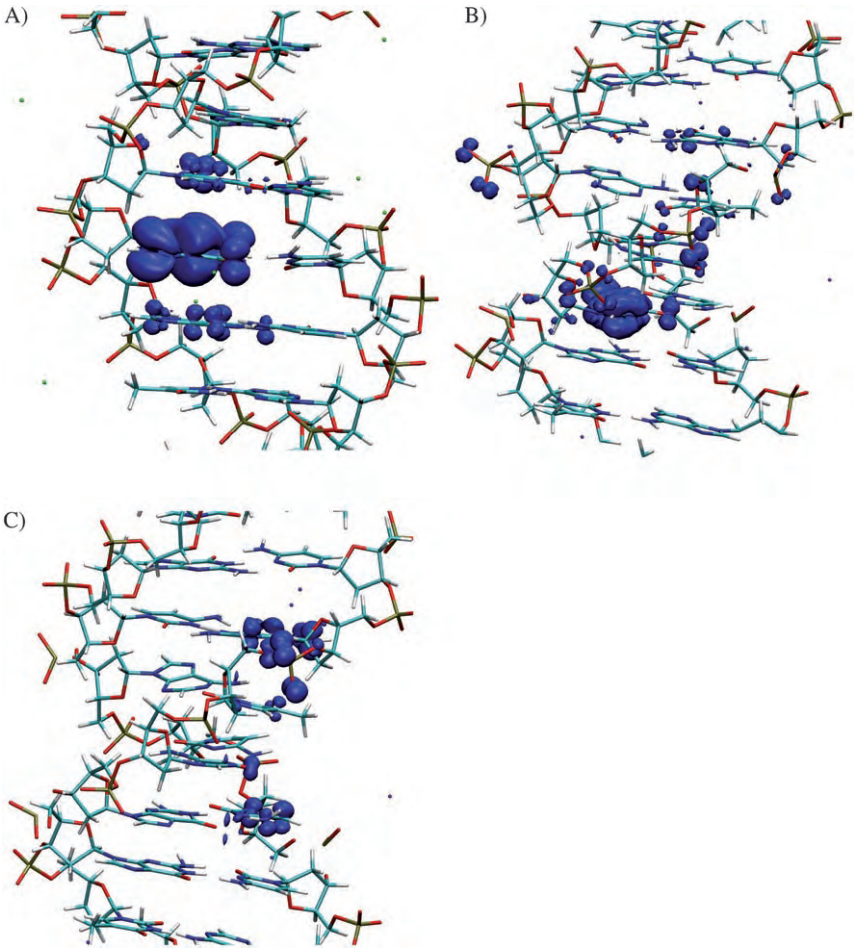


***Figure 1.*** Details of the three-dimensional structure of the B-DNA 38mer and of the spin density isosurface (in blue) associated with the radical cation state. A) In the initial state, the hole is localized on the GGG. B) When the isolated G undergoes double proton transfer, the hole is transferred through the sugar–phosphate backbone. C) The isolated G is deprotonated and the hole is localized on it. The isosurfaces shown have a value of $5\times10^{-2}$ e Å$^3$.

The present-day exchange and correlation functionals used in DFT have well-known drawbacks in describing radical states. The most severe is the incomplete cancellation of the electron self-interaction, which artificially favors charge delocalization.[42] Thus, in the case of delocalized states, special care was taken to check the robustness of our results. We repeated our calculations by using the self-energy corrections introduced in reference [43] in which adjustable parameters were fitted to reproduce the distribution of the spin density of a guanine pair stacked at 3.5 and 9 Å obtained with a correlated (MP2) ab initio calculation.[44]

Another important indicator of the quality of the theoretical treatment of open-shell systems is the expectation value of the square total spin operator, $\langle S^2\rangle$. In the present work, it was calculated for all the relevant states following reference [45]. Starting from five different geometries obtained from the classical molecular dynamics run, we removed one electron and performed 2-ps QM/MM equilibrations at 300 K. In Figure 1 A, a typical spin-density, which is the difference between the density of the spin up and spin down electron, is shown. In agreement with previous Hartree–Fock ab initio calculations and with experimental results,[46,21] the hole is localized on the three proximal guanines with a density peak on the central G. The difference between calculations performed on different initial geometries is mainly seen in the amount of spin density localized on the sugar–phosphate backbone of the guanines. We are confident that the localization pattern for the hole is not affected by electron self-interaction problems as very similar results were obtained by Hartree–Fock calculations, which are self-interaction free by construction, on a duplex 4mer 5′-XGGG-3′, where X = T,C.[46,21] This is in good agreement with previous reports of a large polaron state.[20,47,30] During the dynamics, the calculated $\langle S^2\rangle$ turns out to be about 0.8, very

 © 2006 Wiley-VCH Verlag GmbH & Co. KGaA, Weinheim 

close to the correct value for a doublet (0.75), indicating that, in this case, the spin polarization is correctly described by DFT.

We now focus on the hole-hopping mechanism. As we obtained similar localization patterns with the larger and smaller QM subsystems (d(5′GTGGG-3′) and d(5′GTGG-3′)), we used the latter to speed up the calculations. Our goal is to understand how a hole, which is initially localized on the stacked GGG triplet, reversibly hops to a different isolated G, which is separated from the GGG by an AT bridge. It is clear that the hopping will not occur without some change in the structure or solvation of the isolated G as the GGG triplet is a more favorable trap configuration for a hole than a single G.[21] Taking our cue from electron paramagnetic resonance (EPR) experiments[48] and from the results of our former full quantum calculation in which a proton-coupled charge localization was observed,[35] we studied the energetics and the effects on the atomic and electronic structure of the deprotonation of an isolated G by means of our recently developed metadynamics method. This approach is able to escape local minima by overcoming large free-energy barriers and makes it possible to reconstruct the free energy surface in the space of a chosen set of relevant collective variables (CVs).[49] Herein, starting from two independent configurations, we performed two metadynamics simulations by using as CVs the distance of the $N^1$ hydrogen atom of G from the $N^3$ of C and the coordination number[16] of the hydrogen atom with respect to the $N^3$ of C (see Figure 2).

Figure 2 shows the schematic view of the initial and final state of the isolated G. Initially it does not possess any radical

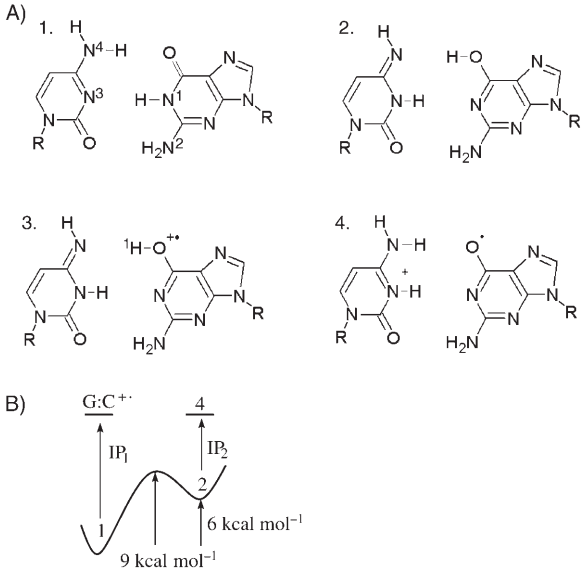


***Figure 2.*** A) Mechanism for the charge transfer from the GGG sink to the isolated G. 1. Initially, the isolated G has a neutral Watson–Crick pair character. 2. The reaction proceeds with a double proton transfer. 3. The hole (radical cation) is transferred from the GGG sink to the isolated G. 4. The final state. B) Qualitative representation of free-energy profiles of the reaction. The free energies reported were obtained on the full QM/MM system with metadynamics. The adiabatic ionization potentials are $IP_1 = 6.9$ eV and $IP_2 = 6.5$ eV. These values were calculated on a gas phase G:C pair by relaxing the geometry with B3LYP functional and a 6-31++G* gaussian basis set.

character, hence the G $N^1$ proton is not acidic (Figure 2.1). As the reaction proceeds, the proton is transferred from this G base to the nearby paired C base and, simultaneously, the $H^4$ proton belonging to C is transferred to G (C*:G*, Figure 2.2). This double proton exchange makes the final state energetically more favorable than a single proton transfer ($G_{-H}$) : C-$H^+$. Indeed G, in contrast to $G^+$, is not acidic and the single proton exchange is highly unfavorable, whereas the double proton exchange, resulting in the formation of two neutral species, is more likely.[50–52] It is important to notice that the metadynamics is acting only on $H^1$, thus the double proton transfer that we observe is spontaneous and cannot be ascribed to an artificial bias. Soon after the proton transfer, the hole is transferred from the GGG triplet to the isolated G (Figure 2.3). In Figure 1B, a snapshot of the intermediate stage is shown. When the isolated G has radical character, the $H^4$ proton is transferred back to the C. This has the effect of further localizing the charge, in agreement with reference [35] (Figure 1C and Figure 2.4). To verify this mechanism, we calculated the adiabatic ionization potential of C:G and C*:G* with a B3LYP/6-31++G(d) calculation in the gas phase. The IPs are 6.9 eV and 6.5 eV for C:G and C*:G*, respectively. In agreement with the QM/MM calculations, relaxing the geometry of C*:G* in the radical cation state we obtain ($G_{-H}$): C-$H^+$ (Figure 2B).

This mechanism was preserved and the pathway was substantially unchanged during runs starting from different initial coordinates and reversibly repeats itself even when a different collective variable is used. In all these calculations, we checked that the self-interaction corrections have little effect. The intermediate state resulting from our simulations (Figure 1B) is in agreement with the coherent single-step-transfer picture suggested by experiments performed on G:C bases separated by a single A:T bridging pair.[13] Before the hole transfer, the free-energy barrier to double proton transfer is around 9 kcal mol$^{-1}$ (Figure 2B), in agreement with the 10 kcal mol$^{-1}$ obtained with correlated ab initio calculations for an isolated G:C pair.[50] Once the isolated guanine has radical character, the free-energy profile along the hydrogen atom dissociation coordinate agrees with that of references [35, 53]. In this case, the two protonation states have a very similar stability and the interconversion barrier is around 6 kcal mol$^{-1}$.

Our calculation provides an important insight into the details of the mechanism that are not directly accessible to experimental probes. We observe directly the proton-coupled charge transfer, a mechanism already proposed on the basis of multiple H/D isotope-effect studies on the charge mobility[34,32] and indirectly shown by us in a previous theoretical paper.[35] Moreover, we find a new and unexpected role for the tautomers of G and C generated by double proton transfer. We observe that the double proton transfer is sufficient to trigger charge hopping from a nearby site even if the nearby site is a GGG triplet, a much better hole trap than an isolated G. We also show that at short donor–acceptor distances, the charge is transferred in a single step.

Received: May 26, 2006
Published online: August 3, 2006

 © 2006 Wiley-VCH Verlag GmbH & Co. KGaA, Weinheim 

**Keywords:** density functional calculations · DNA damage · electron transfer · molecular dynamics · nucleobases


[1] "Long-Range Charge Transfer in DNA I–II": *Topics in Current Chemistry, Vol. 236–237* (Ed.: G. B. Schuster), Springer, Heidelberg, **2004**.

[2] T. Douki, J. L. Ravanat, D. Angelov, J. R. Wagner, J. Cadet, *Top. Curr. Chem.* **2004**, *236*, 1 – 25.

[3] E. M. Boon, *Proc. Natl. Acad. Sci. USA* **2003**, *100*, 12543 – 12547.

[4] C. Dekker, M. A. Ratner, *Phys. World* **2001**, *14*, 29 – 33.

[5] M. D. Ventra, M. Zwolak, *Encyclopedia of Nanoscience and Nanotechnology*, American Scientific Publishers, New York, **2004**.

[6] S. O. Kelley, N. M. Jackson, M. G. Hill, J. K. Barton, *Angew. Chem.* **1999**, *111*, 991 – 996; *Angew. Chem. Int. Ed.* **1999**, *38*, 941 – 945.

[7] R. Holmlin, P. Dandliker, J. Barton, *Angew. Chem.* **1997**, *109*, 2830 – 2848; *Angew. Chem. Int. Ed. Engl.* **1997**, *36*, 2714 – 2730.

[8] H. W. Fink, C. Schonenberger, *Nature* **1999**, *398*, 407 – 410.

[9] A. Y. Kasumov, M. Kociak, S. Gueron, B. Reulet, V. T. Volkov, D. V. Klinov, H. Bouchiat, *Science* **2001**, *291*, 280 – 282.

[10] D. Porath, A. Bezryadin, S. deVries, C. Dekker, *Nature* **2000**, *403*, 635 – 638.

[11] C. Gomez-Navarro, F. Moreno-Herrero, P. J. de Pablo, P. J. Colchero, J. G. Herrero, A. M. Bar, *Proc. Natl. Acad. Sci. USA* **2002**, *99*, 8484 – 8487.

[12] R. G. Endres, D. L. Cox, R. R. P. Singh, *Rev. Mod. Phys.* **2004**, *76*, 195 – 214.

[13] B. Giese, *Annu. Rev. Biochem.* **2002**, *71*, 51 – 70.

[14] K.-H. Yoo, D. H. Ha, J. O. Lee, J. W. Park, J. Kim, J. J. Kim, H. Y. Lee, T. Kawai, H. Y. Choi, *Phys. Rev. Lett.* **2001**, *87*, 198102 – 198104.

[15] B. Giese, M. Spichty, *ChemPhysChem* **2000**, *1*, 195 – 198.

[16] F. L. Gervasio, A. Laio, M. Iannuzzi, M. Parrinello, *Chem. Eur. J.* **2004**, *10*, 4846 – 4852.

[17] M. Bixon, J. Jortner, *J. Chem. Phys.* **2005**, *319*, 273 – 282.

[18] A. Nitzan, *Annu. Rev. Phys. Chem.* **2001**, *52*, 681 – 750.

[19] D. Ly, Y. Kan, B. Armitage, G. B. Schuster, *J. Am. Chem. Soc.* **1996**, *118*, 8747 – 8748.

[20] G. B. Schuster, *Acc. Chem. Res.* **2000**, *33*, 253 – 260.

[21] Y. Yoshioka, Y. Kitagawa, Y. Takano, K. Yamaguchi, T. Nakamura, I. Saito, *J. Am. Chem. Soc.* **1999**, *121*, 8712 – 8719.

[22] B. Giese, J. Amaudrut, A. K. Köhler, M. Spormann, S. Wessely, *Nature* **2001**, *412*, 318 – 320.

[23] When the number of A:T bridging bases exceeds four, the distance dependence of charge-transfer efficiency changes from an exponential-decay regime to a very slowly decreasing linear regime. This change was interpreted by the onset of a different mechanism, namely an a-hopping mechanism. In this regime the adenine are oxidized and act as charge carriers (see reference [13].

[24] B. Giese, S. Wessely, *Angew. Chem.* **2000**, *112*, 3632 – 3634; *Angew. Chem. Int. Ed.* **2000**, *39*, 3490 – 3491.

[25] M. A. O'Neill, H. C. Becker, C. Wan, J. K. Barton, A. H. Zewail, *Angew. Chem.* **2003**, *115*, 6076 – 6080; *Angew. Chem. Int. Ed.* **2003**, *42*, 5896 – 5900.

[26] C. Wan, T. Fiebig, S. O. Kelley, C. R. Tradway, J. K. Barton, A. Zewail, *Proc. Natl. Acad. Sci. USA* **1999**, *96*, 6014 – 6019.

[27] D. Ly, L. Sanii, G. B. Schuster, *J. Am. Chem. Soc.* **1999**, *121*, 9400 – 9410.

[28] P. T. Henderson, D. Jones, G. Hampikian, Y. Kan, G. B. Schuster, *Proc. Natl. Acad. Sci. USA* **1999**, *96*, 8353 – 8358.

[29] R. Bruinsma, G. Grüner, M. R. D'Orsogna, J. Rudnik, *Phys. Rev. Lett.* **2000**, *85*, 4393 – 4396.

[30] E. M. Conwell, *Proc. Natl. Acad. Sci. USA* **2005**, *102*, 8795 – 8799.

[31] R. N. Barnett, C. L. Cleveland, A. Joy, U. Landman, G. Schuster, *Science* **2001**, *294*, 567 – 571.

[32] B. Giese, S. Wessely, *Chem. Commun.* **2001**, 2108 – 2109.

[33] S. Steenken, *Biol. Chem.* **1997**, *378*, 1293 – 1297.

[34] V. Shafirovich, A. Dourandin, N. E. Geacintov, *J. Phys. Chem. B* **2001**, *105*, 8431 – 8435.

[35] F. L. Gervasio, M. Boero, A. Laio, M. Parrinello, *Phys. Rev. Lett.* **2005**, *94*, 158103.

[36] F. L. Gervasio, P. Carloni, M. Parrinello, *Phys. Rev. Lett.* **2002**, *89*, 108102.

[37] A. Hübsch, R. G. Endres, D. L. Cox, R. R. P. Singh, *Phys. Rev. Lett.* **2005**, *94*, 178102.

[38] E. Meggers, M. E. Michel-Beyerle, B. Giese, *J. Am. Chem. Soc.* **1998**, *120*, 12950 – 12955.

[39] W. D. Cornell, P. Cieplak, C. I. Bayly, I. R. Gould, K. M. Merz, Jr., D. M. Ferguson, D. C. Spellmeyer, T. Fox, J. W. Caldwell, P. A. Kollmann, *J. Am. Chem. Soc.* **1995**, *117*, 5179 – 5197.

[40] A. Laio, J. VandeVondele, U. Roethlisberger, *J. Chem. Phys.* **2002**, *116*, 6941 – 6947.

[41] All calculations were performed in the local spin density formulation, as implemented in the cpmd code.[54] Hamprecht–Cohen–Tozer–Handy gradient corrections on the exchange-correlation function were included.[55] The interaction between valence electrons and ionic cores was described by martins-troullier pseudopotentials.[56] the kohn-sham valence orbitals were expanded in a plane wave basis set with an energy cutoff of 70 ry.

[42] J. Laegsgaard, K. Stokbro, *Phys. Rev. Lett.* **2001**, *86*, 2834.

[43] J. VandeVondele, M. Sprik, *Phys. Chem. Chem. Phys.* **2005**, *7*, 1363 – 1367.

[44] By using $\alpha = 0.8$ and $\beta = 0.5$, we are able to reproduce both a situation in which the hole is delocalized on two stacked guanines when the distance is 3.5 Å and one where the hole is localized when the distance is 9 Å. Similar results were obtained for a stacked benzene couple.

[45] J. Wang, A. D. Becke, V. H. Smith Jr., *J. Chem. Phys.* **1995**, *102*, 3477 – 3480.

[46] H. Sugiyama, I. Saito, *J. Am. Chem. Soc.* **1996**, *118*, 7063 – 7068.

[47] A. Omerzu, M. Licer, T. Mertelj, V. V. Kabanov, D. Mihailovic, *Phys. Rev. Lett.* **2004**, *93*, 218101.

[48] K. Hildebrand, D. Schulte-Frohlinde, *Free Radical Res. Commun.* **1990**, *11*, 195 – 206.

[49] A. Laio, A. Rodriguez-Fortea, F. L. Gervasio, M. Ceccarelli, M. Parrinello, *J. Phys. Chem. B* **2005**, *109*, 6714 – 6721.

[50] L. Gorb, Y. Podolyan, P. Dziekonski, W. A. Sokalski, J. Leszczynski, *J. Am. Chem. Soc.* **2004**, *126*, 10119 – 10129.

[51] V. Zoete, M. Meuwly, *J. Chem. Phys.* **2004**, *121*, 4377 – 4387.

[52] A. Abo-Riziq, L. Grace, E. Nir, M. Kabelac, P. Hobza, M. S. de Vries, *Proc. Natl. Acad. Sci. USA* **2005**, *102*, 20 – 23.

[53] M. Hutter, T. Clark, *J. Am. Chem. Soc.* **1996**, *118*, 7574 – 7577.

[54] CPMD V3.5, Copyright IBM Corp 1990 – 2001, Copyright MPI fuer Festkoerperforschung, Stuttgart, **1997–2001**.

[55] F. A. Hamprecht, A. J. Cohen, D. J. Tozer, N. C. Handy, *J. Chem. Phys.* **1998**, *109*, 6264 – 6271.

[56] N. Troullier, J. L. Martins, *Phys. Rev. B* **1991**, *43*, 1993 – 2006.


 © 2006 Wiley-VCH Verlag GmbH & Co. KGaA, Weinheim 

Nanowires

DOI: 10.1002/anie.200601588

# Luminescent One-Dimensional Nanoscale Materials with $Pt^{II}\cdots Pt^{II}$ Interactions**

*Yinghui Sun, Kaiqi Ye, Hongyu Zhang, Junhu Zhang, Lan Zhao, Bao Li, Guangdi Yang, Bai Yang, Yue Wang,* Siu-Wai Lai, and Chi-Ming Che**

Self-assembly of organic and inorganic molecules into one-dimensional (1D) micrometer- and nanometer-scale architectures has become a useful approach for the fabrication of materials with extraordinary properties and applications.[1–12] Noncovalent intermolecular interactions are widely regarded as an efficient approach to construct molecular assemblies with well-defined structures in the micro- and nanoscopic size regime and involve hydrogen-bonding, π–π stacking, electrostatic, and van der Waals interactions. The size and structure of nanoscale aggregates can be significantly varied through manipulation of intermolecular interactions by the judicious choice of the solvent and/or functionalization of the precursor molecules.[3–7] On the contrary, the use of weak metal···metal interactions in the construction of 1D nanostructures remains sparse.[13] Herein, we report luminescent 1D inorganic micro- and nanowires from $[Pt(CNtBu)_2(CN)_2]$ that are aggregated and directed by $Pt^{II}\cdots Pt^{II}$ interactions. The precursor $[Pt(CNtBu)_2(CN)_2]$ was synthesized in high yield by stirring $K_2PtCl_4$ and excess *tert*-butyl isocyanide in water at room temperature.[14] This partially dealkylated complex is stable towards air and moisture at room temperature. Slow diffusion of diethyl ether vapor into a solution of $[Pt(CNtBu)_2(CN)_2]$ in acetonitrile resulted in the formation of light green, long rodlike crystals, which exhibit strong green emission under UV light (Figure 1).

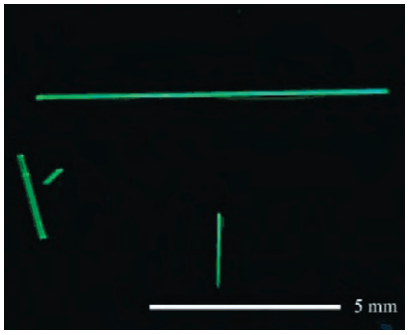


***Figure 1.*** Photographic image of $[Pt(CNtBu)_2(CN)_2]$ crystals excited with UV light ($\lambda_{ex} = 365$ nm).

The molecular structure of $[Pt(CNtBu)_2(CN)_2]$ was determined by X-ray crystallography (Figure 2). The two CN and CN*t*Bu ligands respectively adopt *cis* geometry (Figure 2a). In the crystal packing diagram, $[Pt(CNtBu)_2(CN)_2]$ units stack in pairs along the *a* axis with a C(8)-Pt(1)-Pt(2)-C(4) torsion angle of 125.20° (Figure 2b), and this pattern extends continuously with adjacent pairs to form infinite linear stacks of square-planar $Pt^{II}$ molecules along the *a* axis with $Pt^{II}\cdots Pt^{II}$ distances of 3.354(1) Å. This pattern is similar to those observed in other extended linear-chain platinum(II) complexes.[15] Figure 2c displays a view of a $[Pt]_n$ chain aligned as a 1D coordination wire. The $[Pt]_n$ chains are packed along the *a* axis to result in the formation of rod-type crystals (Figure 2d). Nonclassical hydrogen bonding for the intermolecular C–H···N≡C interactions are observed (H···N 2.66–2.74 Å; angle C–H···N 144.9–154.2°; see Supporting Information), through which bundles of $[Pt]_n$ chains are held together in the crystal structure of $[Pt(CNtBu)_2(CN)_2]$ (see Supporting Information). These structural features encouraged us to explore the possibility of employing $[Pt(CNtBu)_2(CN)_2]$ as a building block for the construction of 1D micrometer- and nanometer-sized wires and fibers based on $Pt^{II}\cdots Pt^{II}$ interactions.

First, an evaporation approach was employed for the aggregation of $[Pt(CNtBu)_2(CN)_2]$ molecules into luminescent wires. Following evaporation of a solution of $[Pt(CNtBu)_2(CN)_2]$ in acetonitrile ($10^{-4}$ M) in air on a silicon substrate, an emission microscope image was recorded that revealed the formation of wires assembled with high length/diameter aspect ratios (Figure 3a). The diameter of the $Pt^{II}$ wires generated is approximately 25 μm, and their lengths can be more than 1000 μm. To obtain luminescent wires with smaller diameters, an approach of injection reprecipitation was employed. Luminescent wires of micrometer and nanometer diameters were prepared by controlling the volume of the solution of the complex in acetonitrile injected into water. Figure 3 b and c show the topographic features of luminescent wires observed by optical microscopy and scanning electron

[*] Y. Sun, K. Ye, H. Zhang, J. Zhang, L. Zhao, B. Li, G. Yang, B. Yang, Prof. Dr. Y. Wang
Key Laboratory for Supramolecular Structure and Materials of the Ministry of Education
College of Chemistry
Jilin University
Changchun 130012 (P.R. China)
Fax: (+86) 431-519-3421
E-mail: yuewang@jlu.edu.cn
Dr. S.-W. Lai, Prof. Dr. C.-M. Che
Department of Chemistry and
HKU-CAS Joint Laboratory on New Materials
University of Hong Kong
Pokfulam Road, Hong Kong SAR (P.R. China)
Fax: (+852) 2857-1586
E-mail: cmche@hku.hk

[**] This work was supported by the National Natural Science Foundation of China, the Major State Basic Research Development Program (2002CB613401), and the Program for Changjiang Scholars and Innovative Research Teams in Universities (IRT0422). We are grateful for financial support from the Research Grants Council of the Hong Kong SAR, China (HKU 7039/03P), the National Natural Science Foundation of China/Research Grants Council Joint Research Scheme (N_HKU 742/04), and the University Development Fund (Nanotechnology Research Institute Program) and Strategic Research Theme (Nano-biotechnology) of the University of Hong Kong.

Supporting information for this article is available on the WWW under http://www.angewandte.org or from the author.


WILEY InterScience DISCOVER SOMETHING GREAT
© 2006 Wiley-VCH Verlag GmbH & Co. KGaA, Weinheim

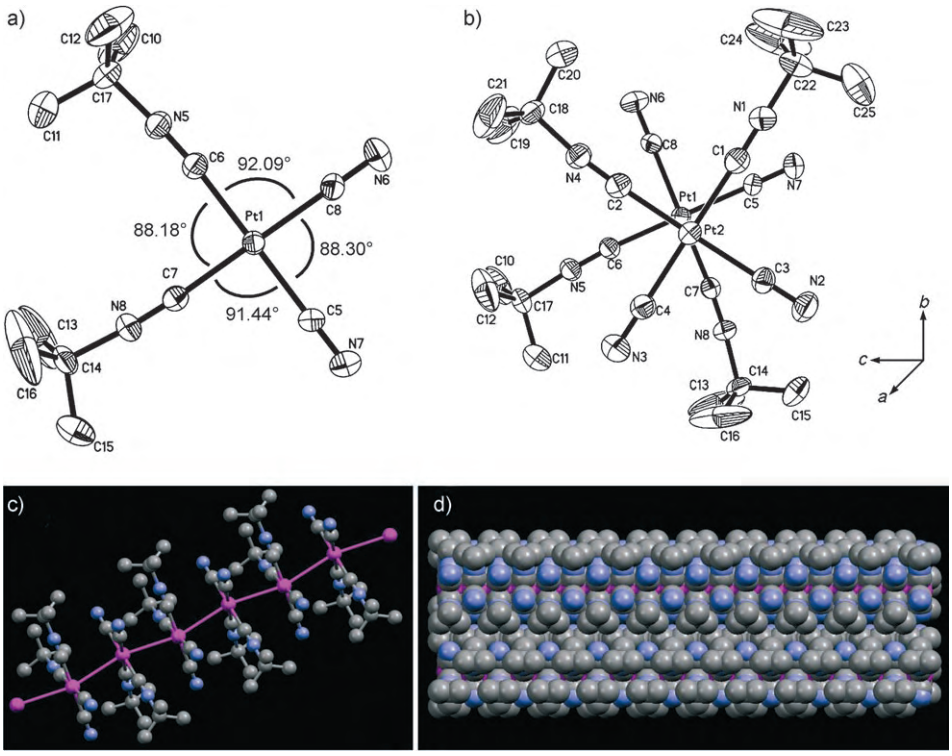


***Figure 2.*** Crystal structure of $[Pt(CNtBu)_2(CN)_2]$. a) ORTEP drawing with thermal ellipsoids shown at the 30% probability level. b) View along the *a* axis showing the relative orientation of two adjacent $[Pt(CNtBu)_2(CN)_2]$ molecules (H atoms labels omitted for clarity). c) Side view of molecular wire showing metal–metal interactions (Pt pink, N blue, C gray). d) Crystal packing diagram of $[Pt]_n$ chains.

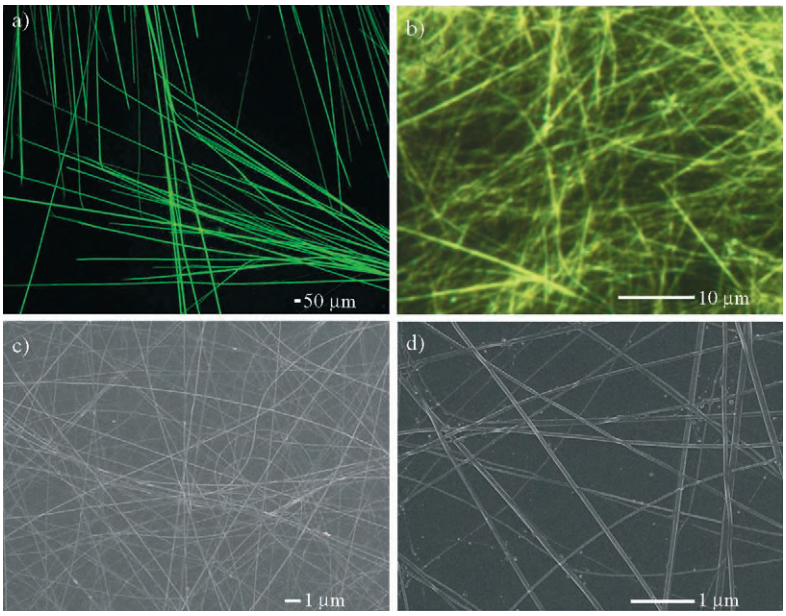


***Figure 3.*** Emission microscopy images (a, b; upon excitation at 365 nm) and scanning electron micrographs (c, d; under different magnification) of luminescent $[Pt(CNtBu)_2(CN)_2]$ wires formed a) on a silicon substrate by slowly evaporating a solution of $[Pt(CNtBu)_2(CN)_2]$ in acetonitrile ($10^{-4}$ M); by injecting 200 μL (b) and 50 μL (c, d) of a solution of $[Pt(CNtBu)_2(CN)_2]$ in acetonitrile ($9.6\times10^{-3}$ M) into 10 mL of water followed by transferring the mixture onto a silicon substrate. In parts (c, d), a platinum layer was sputtered onto the surface to increase the conductivity.

microscopy (SEM), respectively. The diameter of the wires formed was sensitive to the volume of the solution: 200 μL of $[Pt(CNtBu)_2(CN)_2]$ in acetonitrile afforded luminescent wires with diameters of around 500 nm, whereas 50 μL of the solution gave wires with diameter of approximately 70 nm.

Upon excitation at 365 nm with a UV lamp, $[Pt(CNtBu)_2(CN)_2]$ nanowires exhibited an intense emission at $\lambda_{max} = 560$ nm at 298 K (see Supporting Information). However, when the wires were dissolved in acetonitrile a colorless solution was obtained. Figure 4 a shows the emission spectra of a solution of $[Pt(CNtBu)_2(CN)_2]$ in acetonitrile recorded at different temperatures (from 298 to 77 K). At 298 K the solution was non-emissive, but an emission with $\lambda_{max} = 542$ nm developed at a temperature of 220 K. Upon lowering the temperature, aggregation of $[Pt(CNtBu)_2(CN)_2]$ in acetonitrile at 220 K was observed, and the emission at $\lambda = 542$ nm is attributed to the $^3[5d_\sigma^*, 6p_\sigma]$ electronic excited state of $[Pt(CNtBu)_2(CN)_2]$ aggregates.[16–18] As the temperature of the solution of $[Pt(CNtBu)_2(CN)_2]$ was further decreased to 77 K, the emission at $\lambda = 542$ nm was resolved into two bands at 584 and 530 nm with lifetimes ($\tau$) of 2.5 and 3.5 μs, respectively. Variation of the excitation wavelength resulted in a change in the relative intensity of the two emission bands at 530 and 584 nm (see Supporting Information). These results suggest that the emissions at $\lambda = 530$ and 584 nm originate from different $[Pt(CNtBu)_2(CN)_2]_n$ species. Previous work revealed that the emission properties of $[Pt(CN)_4]^{2-}$ in solution are affected by the concentration of the complex and can be attributed to the $^1[5d_\sigma^*, 6p_\sigma]$ and $^3[5d_\sigma^*, 6p_\sigma]$ excited states of $\{[Pt(CN)_4]^{2-}\}_n$ for different values of $n$.[19] The emission spectra of $[Pt(CNtBu)_2(CN)_2]$ nanowires showed a temperature dependence (Figure 4 b) similar to that recorded in acetonitrile solution. The solid-state emission at 562 nm at 298 K resolved into two peak maxima at 545 and 597 nm upon decreasing the temperature to 77 K. We also found that the emission spectrum of [Pt-

 © 2006 Wiley-VCH Verlag GmbH & Co. KGaA, Weinheim 

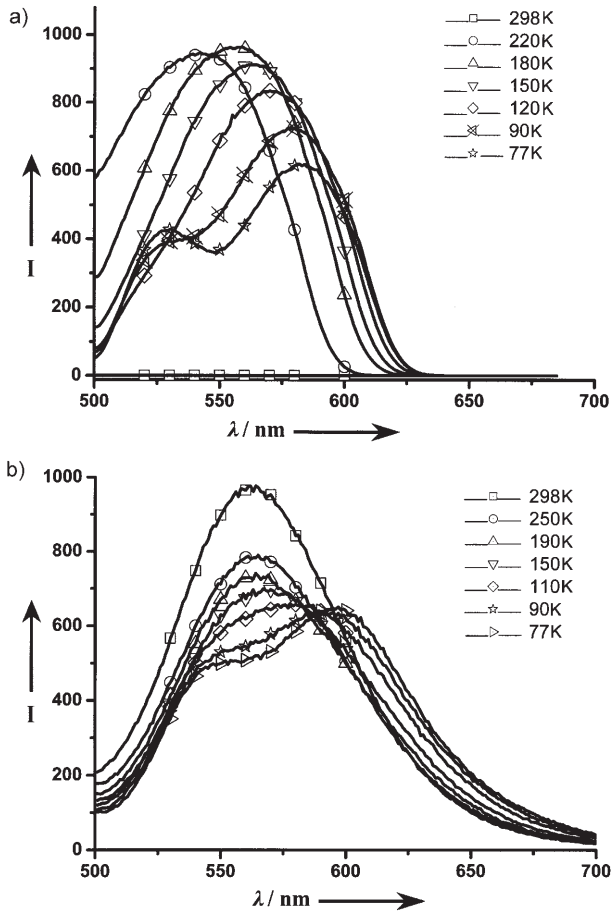


***Figure 4.*** Emission spectra of a) a solution of $[Pt(CNtBu)_2(CN)_2]$ in acetonitrile ($5.0\times10^{-4}$ M) and b) $[Pt(CNtBu)_2(CN)_2]$ nanowires at different temperatures. The nanowires were formed by injecting 200 μL of a solution of $[Pt(CNtBu)_2(CN)_2]$ in acetonitrile ($9.6\times10^{-3}$ M) into 10 mL of water followed by transferring the mixture onto a silicon substrate.

$(CNtBu)_2(CN)_2]$ nanowires at 77 K depends on the excitation wavelength (see Supporting Information).

The relationships between the excitation and emission spectra were examined. For a glassy solution of $[Pt(CNtBu)_2(CN)_2]$ in benzonitrile ($5.66\times10^{-5}$ M) at 77 K, the emission spectra recorded at different excitation wavelengths showed a gradual shift in emission maximum (see Supporting Information). Upon excitation of the glassy solution at 475 nm, an emission peak at 547 nm and a shoulder at 610 nm were observed. Upon shifting the excitation wavelength to higher energy, the corresponding emission maximum was also blue-shifted. A series of excitation spectra were recorded while monitoring different emission wavelengths: an intense band was found with a spectral profile resembling the $[nd_\sigma^*\rightarrow(n+1)p_\sigma]$ transition of dinuclear $d^8$ or $d^{10}$ metal systems,[16,20] and the excitation peak maximum shifted from 480 nm to 464, 452, 433, and 428 nm upon changing the emission wavelength from 570 nm to 547, 534, 520, and 502 nm, respectively. We tentatively assign the different photophysical properties to the $[5d_\sigma^*\rightarrow6p_\sigma]$ electronic excited states of $[Pt(CNtBu)_2(CN)_2]_n$ aggregates.

Exposure of $[Pt(CNtBu)_2(CN)_2]$ nanowires to the vapor of volatile organic compounds (VOCs) resulted in changes in the emission properties (Figure 5). A shift of the emission maximum from 562 to 533 nm was observed with a concomitant increase in emission intensity. Such solvatochromism was reversible, and the emission spectrum was restored to its

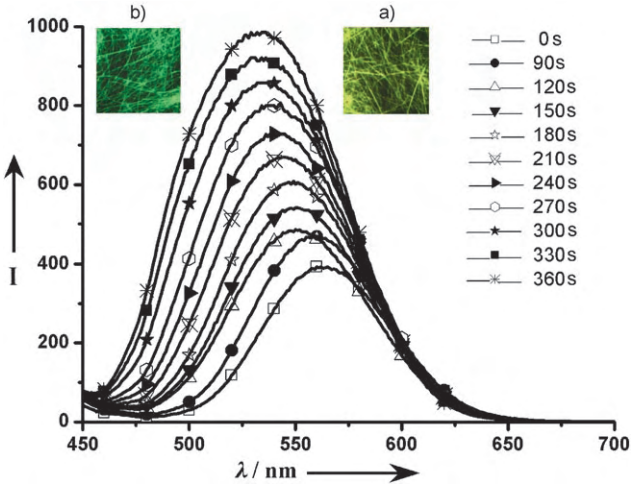


***Figure 5.*** Room-temperature emission spectra of $[Pt(CNtBu)_2(CN)_2]$ nanowires recorded after exposure of the sample to acetonitrile vapor at different time intervals. The wires were formed by injecting 200 μL of a solution of $[Pt(CNtBu)_2(CN)_2]$ in acetonitrile ($9.6\times10^{-3}$ M) into 10 mL of water followed by transferring the mixture onto a silicon substrate. Insets: Emission microscopy images of luminescent wires before (a) and after (b) exposure to acetonitrile vapor.

original profile after the sample was placed in air for 15 days or under vacuum for 10 h. Subtle environmental changes can perturb the weak $Pt^{II}\cdots Pt^{II}$ interactions and subsequently affect the $^3[5d_\sigma^*,6p_\sigma]$ emissive properties.[16–18] Previous studies have demonstrated that the $^3[5d_\sigma^*,6p_\sigma]$ excited states of dinuclear and linear-chain $Pt^{II}$ compounds are sensitive to temperature and atmospheric factors.[15a,17,21,22] Here, we examined the vapochromic behavior of the crystals obtained by diffusing diethyl ether vapor into a solution of $[Pt(CNtBu)_2(CN)_2]$ in acetonitrile. These bright yellow crystals of $[Pt(CNtBu)_2(CN)_2]$ in the dry state showed an intense emission with $\lambda_{max}=534$ nm ($\tau=0.85$ μs; quantum yield $\Phi=0.33$) at 298 K, however, at 77 K two emission peaks with maxima at $\lambda=510$ ($\tau=0.47$ μs) and 569 nm ($\tau=1.65$ μs) were observed. Exposure of the crystals to acetonitrile vapor only resulted in a change in the emission intensity with no shift of the emission maximum (see Supporting Information). We propose that the micro- and nanostructures of $[Pt(CNtBu)_2(CN)_2]$ species exhibit large surface areas, which would enhance the contact between $[Pt(CNtBu)_2(CN)_2]$ molecules and the organic solvent molecules.

To examine the effect of acetonitrile vapor upon the crystal structure and packing of $[Pt(CNtBu)_2(CN)_2]$, X-ray diffraction data were collected under different conditions. Crystals were grown by diffusion of diethyl ether into a solution of $[Pt(CNtBu)_2(CN)_2]$ in acetonitrile at room temperature. Crystal **1** was isolated from the solution mixture (acetonitrile and diethyl ether) and kept in air at room temperature for 15 days, and the X-ray crystal data were

 © 2006 Wiley-VCH Verlag GmbH & Co. KGaA, Weinheim 

collected at 298 K. Crystal **2** was isolated from the solution and encapsulated in epoxy resin, and the X-ray data were immediately recorded at 298 K. For crystal **2**, although we could not precisely locate the coordinates of some carbon and nitrogen atoms at 298 K, the coordinates of the Pt atom and coordinated carbon atoms could be accurately determined. On the basis of the two sets of X-ray crystal data, the intermolecular $Pt^{II}\cdots Pt^{II}$ distances in the two structures were found to be similar (3.354(1) Å for crystal **1**; 3.3525(2) Å for crystal **2**) but there are slight variations in the bond angles ($\measuredangle$ *t*BuNC-Pt-CN*t*Bu = 88.18° for crystal **1** and 92.11° for crystal **2**; $\measuredangle$ NC-Pt-CN = 88.30° (**1**) and 98.52° (**2**); $\measuredangle$ *t*BuNC-Pt-CN = 91.44, 92.09° (**1**) and 83.46, 85.91° (**2**)) around the $Pt^{II}$ center (see Supporting Information). This observation is consistent with the finding that exposure of dry crystals of $[Pt(CNtBu)_2(CN)_2]$ to acetonitrile vapor affects the emission intensity, but the variation in the emission maximum is small (see Supporting Information).

In conclusion, we have demonstrated that $[Pt(CNtBu)_2(CN)_2]$ molecules can form micrometer- and nanometer-scale luminescent wires. Weak $Pt^{II}\cdots Pt^{II}$ interactions are useful cohesive force for the construction of 1D functional nanomaterials. Recent work has revealed that 1D nanorods can be obtained from cyclometalated platinum(II) complexes.[13b] More importantly, $Pt^{II}\cdots Pt^{II}$ interactions not only induce the formation of 1D nanostructures but are also responsible for the intense green $^3[5d_\sigma^*, 6p_\sigma]$ emission of the self-assembled $[Pt(CNtBu)_2(CN)_2]$ wires.

Received: April 22, 2006
Revised: June 21, 2006
Published online: July 28, 2006

**Keywords:** cyanides · luminescence · metal–metal interactions · nanostructures · platinum

[1] J. P. Hill, W. Jin, A. Kosaka, T. Fukushima, H. Ichihara, T. Shimomura, K. Ito, T. Hashizume, N. Ishii, T. Aida, *Science* **2004**, *304*, 1481 – 1483.
[2] J. Huang, R. B. Kaner, *J. Am. Chem. Soc.* **2004**, *126*, 851 – 855.
[3] B.-K. An, D.-S. Lee, J.-S. Lee, Y.-S. Park, H.-S. Song, S. Y. Park, *J. Am. Chem. Soc.* **2004**, *126*, 10232 – 10233.
[4] P. Yan, A. Chowdhury, M. W. Holman, D. M. Adams, *J. Phys. Chem. B* **2005**, *109*, 724 – 730.
[5] R. Harada, Y. Matsuda, H. Okawa, T. Kojima, *Angew. Chem.* **2004**, *116*, 1861 – 1864; *Angew. Chem. Int. Ed.* **2004**, *43*, 1825 – 1828.
[6] M. L. Bushey, T.-Q. Nguyen, C. Nuckolls, *J. Am. Chem. Soc.* **2003**, *125*, 8264 – 8269.
[7] T.-Q. Nguyen, R. Martel, P. Avouris, M. L. Bushey, L. Brus, C. Nuckolls, *J. Am. Chem. Soc.* **2004**, *126*, 5234 – 5242.
[8] K. L. Niece, J. D. Hartgerink, J. J. J. M. Donners, S. I. Stupp, *J. Am. Chem. Soc.* **2003**, *125*, 7146 – 7147.
[9] H. Fu, D. Xiao, J. Yao, G. Yang, *Angew. Chem.* **2003**, *115*, 2989 – 2992; *Angew. Chem. Int. Ed.* **2003**, *42*, 2883 – 2886.
[10] H. Liu, Q. Zhao, Y. Li, Y. Liu, F. Lu, J. Zhuang, S. Wang, L. Jiang, D. Zhu, D. Yu, L. Chi, *J. Am. Chem. Soc.* **2005**, *127*, 1120 – 1121.
[11] H. Liu, Y. Li, S. Xiao, H. Gan, T. Jiu, H. Li, L. Jiang, D. Zhu, D. Yu, B. Xiang, Y. Chen, *J. Am. Chem. Soc.* **2003**, *125*, 10794 – 10795.
[12] H. Yao, C. A. Michaels, S. J. Stranick, T. Isohashi, K. Kimura, *Lett. Org. Chem.* **2004**, *1*, 280 – 287.
[13] a) M. Enomoto, A. Kishimura, T. Aida, *J. Am. Chem. Soc.* **2001**, *123*, 5608 – 5609; b) W. Lu, V. A. L. Roy, C.-M. Che, *Chem. Commun.* **2006**, DOI:10.1039/B607422G.
[14] L. Malatesta, F. Bonati, *Isocyanide Complexes of Metals*, Wiley, London, **1969**, p. 169.
[15] a) C. E. Buss, K. R. Mann, *J. Am. Chem. Soc.* **2002**, *124*, 1031 – 1039; b) V. W.-W. Yam, K. M.-C. Wong, N. Zhu, *J. Am. Chem. Soc.* **2002**, *124*, 6506 – 6507.
[16] D. M. Roundhill, H. B. Gray, C. M. Che, *Acc. Chem. Res.* **1989**, *22*, 55 – 61.
[17] B.-H. Xia, C.-M. Che, D. L. Phillips, K.-H. Leung, K.-K. Cheung, *Inorg. Chem.* **2002**, *41*, 3866 – 3875.
[18] C.-M. Che, L. G. Butler, H. B. Gray, R. M. Crooks, W. H. Woodruff, *J. Am. Chem. Soc.* **1983**, *105*, 5492 – 5494.
[19] J. W. Schindler, R. C. Fukuda, A. W. Adamson, *J. Am. Chem. Soc.* **1982**, *104*, 3596 – 3600.
[20] a) S.-W. Lai, H.-W. Lam, W. Lu, K.-K. Cheung, C.-M. Che, *Organometallics* **2002**, *21*, 226 – 234; b) W.-F. Fu, K.-C. Chan, K.-K. Cheung, C.-M. Che, *Chem. Eur. J.* **2001**, *7*, 4656 – 4664.
[21] C. L. Exstrom, J. R. Sowa, Jr., C. A. Daws, D. Janzen, K. R. Mann, G. A. Moore, F. F. Stewart, *Chem. Mater.* **1995**, *7*, 15 – 17.
[22] C. E. Buss, C. E. Anderson, M. K. Pomije, C. M. Lutz, D. Britton, K. R. Mann, *J. Am. Chem. Soc.* **1998**, *120*, 7783 – 7790.

 © 2006 Wiley-VCH Verlag GmbH & Co. KGaA, Weinheim 

*Iron Nitride Clusters*

DOI: 10.1002/anie.200601570

# Self-Assembly of a Tetradecanuclear Iron Nitride Cluster**

*Miriam V. Bennett and R. H. Holm**

Recently, we reported the synthesis, structures, and certain electronic properties of the first examples of molecular mid-valent high-nuclearity iron nitride clusters.[1] Four clusters were obtained by self-assembly, $[Fe_4N_2Cl_{10}]^{4-}$ (**1**), $[Fe_{10}N_8Cl_{12}]^{5-}$ (**2**), and their bromide analogues (Scheme 1). This work was motivated in part by the revelation, from high-resolution protein crystallography, of a light atom X at the centre of the $Fe_6$ portion of the $MoFe_7S_9X$ cluster core in the iron–molybdenum cofactor (FeMoco) of nitrogenase.[2] Consideration of the electronic properties of the cofactor in three

[*] Dr. M. V. Bennett, Prof. R. H. Holm
Department of Chemistry and Chemical Biology
Harvard University
Cambridge, MA 02138 (USA)
Fax: (+1) 617-496-9289
E-mail: holm@chemistry.harvard.edu

[**] This research was supported by National Institutes of Health Grant GM 28856, and conducted in part at the Center for Materials Science and Engineering at M.I.T. M.V.B. is supported by a National Institutes of Health N.R.S.A. Fellowship.

Supporting information for this article is available on the WWW under http://www.angewandte.org or from the author.


© 2006 Wiley-VCH Verlag GmbH & Co. KGaA, Weinheim

oxidation states has led to the order of likelihood of N > O > C for the identity of atom X.[3] Subsequent electron nuclear double resonance (ENDOR) and electron spin echo envelope modulation (ESEEM) evidence has been interpreted as disfavoring nitrogen as atom X.[4] Shortly after the discovery of atom X, it was found that this atom does not exchange under enzyme turnover conditions with dinitrogen, suggesting that it serves a structural and/or electronic role in the cofactor.[4] In a chemical context, the presence of atom X requires that any synthesis of a cluster analogue of FeMoco incorporate atom X at some stage, and raises the possibility of a template effect in the construction of the cluster core.[5] Further, the presence of atom X implies the existence of a new class of clusters that possibly includes the generalized fragment $Fe_n(\mu_n\text{-}X)$.

We have pursued the exploratory synthesis of iron nitride clusters in a continuing attempt to disclose structures and structural principles that may be relevant to a synthetic analogue of FeMoco and its biosynthetic precursor(s). The desired clusters possess nuclearities exceeding two, differentiating them from various binuclear species with Fe-N-Fe bridges,[6–10] and are devoid of the carbonyl ligands present in interstitial low-valent clusters such as $[Fe_5(\mu_5\text{-}N)(CO)_{14}]^-$[11] and $[Fe_6(\mu_6\text{-}N)(CO)_{15}]^{3-}$.[12] The cluster products in the assembly system of $[FeCl_4]^-$ and $(Me_3Sn)_3N$ in acetonitrile are primarily controlled by the molar ratio of the reactants (Scheme 1), although the reactant ratio is not necessarily

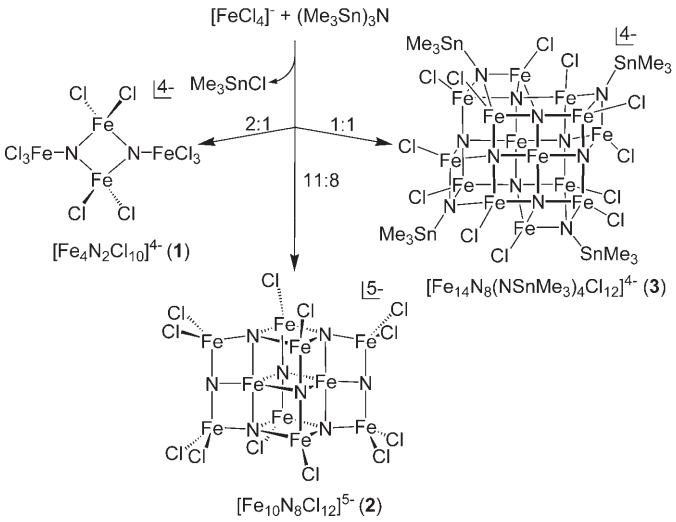


***Scheme 1.*** Formation of clusters **1**–**3** in self-assembly systems with the indicated molar ratios of $[FeCl_4]^-$:$(Me_3Sn)_3N$.

expressed in the product composition. Clusters **1** and **2** were isolated as $Et_4N^+$ salts at $[FeCl_4]^-$:$(Me_3Sn)_3N$ ratios of 2:1 (72% yield) and 11:8 (37% yield).[1] Herein, a 1:1 stoichiometry affords the nitrido cluster $[Fe_{14}N_8(NSnMe_3)_4Cl_{12}]^{4-}$ (**3**; 18% yield), as well as two other clusters, $[Fe_8N_2(NSnMe_3)_6Cl_8]^{2-}$ and the prismane $[Fe_6(NSnMe_3)_6Cl_6]^-$, as highly air- and proton-sensitive $Et_4N^+$ salts. The formation of these two additional clusters from the mother liquor containing **3** presumably contributes to the relatively low yield of **3**.

Cluster **3** contains several unique features (Figure 1).[13] Charge balance dictates a mixed-valent formulation of $12\,Fe^{III} + 2\,Fe^{II}$; consequently, this is the first iron nitride cluster to contain ferrous ions. The cluster has crystallo-

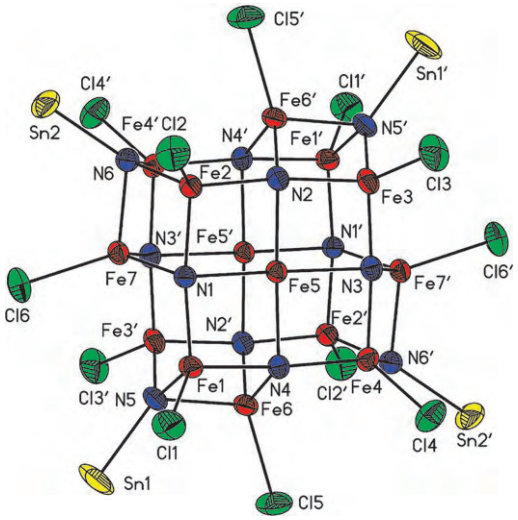


***Figure 1.*** The structure of cluster **3**; thermal ellipsoids are set at 50% probability; primed and unprimed atoms are related by an inversion center; methyl groups are omitted for clarity. Selected interatomic distances [Å] and angles [°]: Fe-Cl 2.239(8) (∅ of 6), Sn-N 2.100(2) (∅ of 2), Fe-($\mu_3$-N) 1.969(4) (∅ of 6), Fe-($\mu_4$-N) 1.902(12) (∅ of 12), Fe5···Fe5′ 2.783(2), Fe5-($\mu_4$-N) 2.004(6) (∅ of 4); N-Fe5-N 89.6(3) (∅ of 4) and 171.0(2) (∅ of 2), Fe1,2-($\mu_3$-N)-Fe3′,4′ 117.4(4) (∅ of 2), Fe5-($\mu_4$-N)-Fe 119.3(6) (∅ of 4: Fe6-Fe7), Fe1–4-($\mu_4$-N)-Fe1–4 170(1) (∅ of 4), ($\mu_3$-N)-Fe-($\mu_4$-N) 114(1) (∅ of 4: Fe1–Fe4) 95.9(1) (∅ of 4: Fe1–Fe4), ($\mu_4$-N)-Fe-($\mu_4$-N) 95.9(6) (∅ of 4: Fe1–Fe4), ($\mu_3$-N)-Fe-($\mu_4$-N) 96.2(3) (∅ of 4: Fe6–Fe7), ($\mu_4$-N)-Fe-($\mu_4$-N) 109.0(4) (∅ of 4: Fe6–Fe7), Sn-($\mu_3$-N)-Fe 120(2) (∅ of 6). In an interior rhomb (Fe1N1Fe5N4): Fe1-N1 1.893(5), Fe1-N4 1.918(5), Fe5-N1 2.003(5), Fe5-N4 2.001(5), Fe1···Fe5 2.694(1), N1···N4 2.829(2); N1-Fe1-N4 95.8(2), N1-Fe5-N4 89.9(2), Fe1-N1-Fe5 87.4(2), Fe1-N4-Fe5 86.8(2). In an exterior rhomb (Fe1N4Fe6N5): Fe1-N4 1.918(5), Fe1-N5 1.969(5), Fe6-N4 1.904(5), Fe6-N5 1.969(5), Fe1···Fe6 2.590(1), N4···N5 2.884(2); N4-Fe1-N5 95.8(2), N4-Fe6-N5 96.2(2), Fe1-N4-Fe6 85.3(2), Fe1-N5-Fe6 82.2(2). ∅ = average.

graphically imposed inversion symmetry, but has nearly ideal noncrystallographic $C_{4h}$ symmetry. It contains eight interior $\mu_4$-nitrogen atoms that are bound only to iron atoms, and four exterior $\mu_3$-nitrogen atoms that are each bound to the tin atom of one $SnMe_3$ moiety and three iron atoms. The four independent $\mu_4$-nitrogen atoms (N1–N4) occupy butterfly-shaped ($C_{2v}$ symmetry) environments, as exemplified by the angles Fe1-N1-Fe2 = 171.2(3)° and Fe5-N1-Fe7 = 119.2(2)°. The two independent $\mu_3$-nitrogen atoms (N5 and N6) occur in trigonal pyramidal $SnNFe_3$ fragments. All iron atoms except Fe5/Fe5′ occur in highly distorted tetrahedral $Fe(\mu_3\text{-}N)(\mu_4\text{-}N)_2Cl$ units. The tin sites are more nearly tetrahedral.

The inner $Fe_8N_8$ portion of the $[Fe_{14}(\mu_4\text{-}N)_8(\mu_3\text{-}N)_4]^{4+}$ core may be described as a close-packed cube; the remaining Fe6/Fe6′ and N5/N5′, and Fe7/Fe7′ and N6/N6′ atoms are displaced outward from adjacent cube faces. The $Fe_5N_4$ face defined by Fe1–Fe5 and N1–N4, and its symmetry equivalent

 © 2006 Wiley-VCH Verlag GmbH & Co. KGaA, Weinheim 

are parallel and nearly planar. Within each of these $Fe_5N_4$ faces, the atoms are connected into four edge-sharing $Fe_2N_2$ rhombs. The $Fe_4$ and $N_4$ planes of each $Fe_5N_4$ face are perfectly planar, and the dihedral angle between them is 0.6°.

The Fe6/Fe6′, Fe7/Fe7′, N5/N5′, and N6/N6′ atoms define a nearly perfect $Fe_4N_4$ plane, which is located between the two $Fe_5N_4$ faces and extends beyond them to form the exterior of the cluster. The three planes are connected through four pairs of edge-sharing $Fe_2N_2$ rhombs. As typical examples of the geometry, the dihedral angle between the planes of the exterior rhombs sharing an Fe6–N5 edge is 115.3°, and the dihedral angle between the planes of the exterior and interior rhombs sharing an Fe1–N4 edge is 118.5°. Thus, the cluster is built from 16 $Fe_2N_2$ rhombs.

The $Fe_4N_2$ sides of the inner $Fe_8N_8$ cube are also nearly planar and intersect at right angles. For example, the atom deviation from the $Fe_4N_2$ plane defined by Fe1, Fe2, Fe3′, Fe4′, N1, and N3′ is 0.048 Å, and the dihedral angle between this plane and that defined by Fe1′, Fe2, Fe3, Fe4′, N1, and N3′ is 89.8°. The Fe6/Fe6′, Fe7/Fe7′, N5/N5′, and N6/N6′ atoms lie 0.92–1.13 Å above the side $Fe_4N_2$ planes.

The nexus of each $Fe_5N_4$ face of the cluster is the Fe5/Fe5′ site, which lies on the pseudo-fourfold axis. These iron atoms have square planar coordination environments, with an average Fe–($\mu_4$-N) distance of 2.004(6) Å and an average N-Fe-N angle of 89.7(3)°. The Fe5 atom deviates by 0.224(1) Å from the $Fe_4(1–4)N_4(1–4)$ plane of the face, and by 0.158(3) Å from the $N_4$ plane, in the direction of Fe5′. As a result, the Fe5···Fe5′ separation is 2.783(2) Å, 0.58 Å shorter than the Fe1···Fe3′ distance of 3.364(1) Å between the faces. The N1···N3′ distance between directly opposite nitrogen atoms is 3.098(7) Å.

The $Fe_2N_2$ rhomb emerges as the dominant structural feature of **3**. The dimensions of two typical rhombs are given in Figure 1. An apparent manifestation of the rigid connectivity of the fused rhomb core is the large departure from tetrahedral geometry at the iron sites. At the Fe1 site, for example, the three Cl-Fe-N angles and the N1-Fe1-N5 angle are in the range 114.1(2)–116.3(2)°, while the remaining N1-Fe1-N4 and N4-Fe1-N5 angles are constrained to 95.8(2)° by their inclusion in two different $Fe_2N_2$ rhombs. The Fe1–N1 and Fe1–N4 bond lengths in the first rhomb average to 1.91(2) Å, while the Fe1–N5 distance in the second rhomb is 1.969(5) Å. The same situation (but with different metric parameters) applies to the other tetrahedral iron sites.

Likewise, the square planar geometry at the Fe5 site is the result of rigid rhomb connectivity. It is probable that this site contains $Fe^{II}$ ions, as the Fe5–N bond lengths are similar to the average $Fe^{II}$–N bond lengths in the complexes [Fe(OEP)] (OEP = 2,3,7,8,12,13,17,18-octaethylporphyrinato; 2.00(2) Å),[14] [Fe(TPP)] (TPP = 5,10,15,20-tetraphenylporphyrinato; 1.966(2) Å),[15] and $[Fe(OMP)]^{2-}$ (OMP = 5,5,10,10,15,15,20,20-octamethylporphyrinogenato; 1.93(1) Å),[16] which all have square planar coordination geometries and $S = 1$ ground states. (Note that with the more flexible porphyrinogenato ligands, the $Fe^{II}$–N bond distances in square planar complexes are approximately 0.04–0.05 Å longer than the $Fe^{III}$–N values.[16,17]) The mean Fe–Cl distance of 2.240(9) Å within the 12 $FeN_3Cl$ fragments is consistent with the expected value for an $Fe^{III}$ ion in a (distorted) tetrahedral site, as judged by the $Fe^{III}$–Cl distances of 2.24–2.27 Å in **1**[1] and of 2.29–2.33 Å in salts of $[FeCl_4]^{2-}$.[18]

Initial magnetic measurements suggest an $S = 2$ ground state for **3**. At 295 K, the value of $\chi_M T$ is 5.89 $cm^3 K mol^{-1}$ in an applied field of 0.05 T. $\chi_M T$ remains nearly constant to 115 K, and decreases to 4.80 $cm^3 K mol^{-1}$ at 5 K (see Supporting Information). Variable-field magnetization data at 2.0 K reveal that the magnetization approaches saturation at a value of approximately $4N\mu_B$ in a field of 5 T. The $S = 2$ ground state may arise from 12 antiferromagnetically coupled $S = {}^5/_2$ $Fe^{III}$ ions that are additionally coupled to two $S = 1$ $Fe^{II}$ ions. Accordingly, square planar $Fe^{II}N_4$ complexes, such as those mentioned above and phthalocyaninatoiron(II),[19] usually have triplet ground states.

The Mössbauer spectrum of $(Et_4N)_4$**3** at 4.2 K was fit under the assumption of a 6:1 site ratio: a doublet at an isomer shift of $\delta = 0.38$ mm $s^{-1}$ with a quadrupole splitting of $\Delta E_Q = 0.77$ mm $s^{-1}$ corresponds to the majority $Fe^{III}$ ions, and a doublet at $\delta = 0.48$ mm $s^{-1}$ with $\Delta E_Q = 2.11$ mm $s^{-1}$ corresponds to the minority $Fe^{II}$ ions (see Supporting Information). This fitting is compatible with the oxidation state assignment from the analysis of the magnetic data.

Several common features are emerging for iron nitride clusters. In structural terms, all of the clusters are built by the edge-sharing of $Fe_2N_2$ rhombs. In binuclear and cluster iron nitride complexes, the five nitrogen-centered structural elements in Scheme 2 have been identified, and the coordination environment of the iron atoms in Scheme 2 b–e is tetrahedral, square planar, or trigonal bipyramidal. The presence of $Fe_2N_2$ rhombs is reminiscent of iron sulfide cluster chemistry, in which twelve structural types result from the edge- and/or vertex-sharing of $Fe_2S_2$ rhombs.[20,21] Although three iron oxidation states (II, III, and IV) are found in iron nitride clusters, only two (II and III) are found in weak-field iron sulfide clusters. Lastly, in all of the binary iron nitride phases, except FeN, the atomic ratio of iron to nitrogen is greater than one, which is also the case in **1**–**3**. However, the structural elements noted here do not occur in $Fe_2N$, $Fe_3N$, $Fe_4N$, or $Fe_{16}N_2$.[22,23] The present work represents a further step in elucidating the synthetic and structural chemistry of iron nitride clusters.

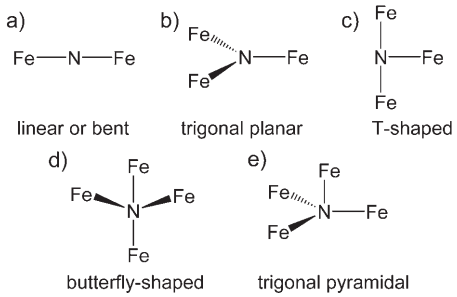


***Scheme 2.*** Structural elements (idealized) found in iron nitride clusters with nuclearities of 2 (a), 4 (b), 10 (c–e), and 14 (d).

 © 2006 Wiley-VCH Verlag GmbH & Co. KGaA, Weinheim 

## Experimental Section

All manipulations were carried out under a dinitrogen atmosphere in a glovebox. Anhydrous acetonitrile (Burdick & Jackson; < 10 ppm water) was dried over molecular sieves (4 Å). Diethylether and THF were distilled from sodium benzophenone ketyl and stored over molecular sieves (4 Å).

$(Et_4N)_4$**3**: A pale yellow solution of $(Et_4N)[FeCl_4]$[24] (0.33 g, 1.01 mmol) in acetonitrile (0.85 mL) was added to an emulsion of $(Me_3Sn)_3N$[25] (0.52 g, 1.02 mmol) in acetonitrile (0.85 mL). The black solution was stirred for 5 min and allowed to stand at room temperature for 11 h. The black mother liquor was decanted from black rectangular plates of other cluster products. The decanted solution was left standing for an additional 24 h, over which time large black truncated rhombohedra separated. The crystalline solid was collected by carefully decanting the mother liquor, washed with THF (5 × 3 mL) and ether (3 × 3 mL), and dried under vacuum to afford 0.033 g (18%) of product. Elemental analysis (%) calcd for $C_{44}H_{116}Cl_{12}Fe_{14}N_{16}Sn_4$: C 20.71, H 4.55, Cl 16.67, Fe 30.64, N 8.78, Sn 18.61; found: C 20.65, H 4.60, Cl 16.74, Fe 30.58, N 8.75, Sn 18.49.

Received: April 20, 2006
Published online: July 21, 2006

**Keywords:** cluster compounds · iron · nitrides · self-assembly · tin

[1] M. V. Bennett, S. Stoian, E. L. Bominaar, E. Münck, R. H. Holm, *J. Am. Chem. Soc.* **2005**, *127*, 12378 – 12386.
[2] O. Einsle, F. A. Tezcan, S. L. A. Andrade, B. Schmid, M. Yoshida, J. B. Howard, D. C. Rees, *Science* **2002**, *297*, 1696 – 1700.
[3] V. Vrajmasu, E. Münck, E. L. Bominaar, *Inorg. Chem.* **2003**, *42*, 5974 – 5988.
[4] H.-I. Lee, P. M. C. Benton, M. Laryukhin, R. Y. Igarashi, D. R. Dean, L. C. Seefeldt, B. M. Hoffman, *J. Am. Chem. Soc.* **2003**, *125*, 5604 – 5605.
[5] S. C. Lee, R. H. Holm, *Proc. Natl. Acad. Sci. USA* **2003**, *100*, 3595 – 3600.
[6] T. Jüstel, T. Weyhermüller, E. Bill, M. Lengen, A. X. Trautwein, P. Hildebrandt, *Angew. Chem.* **1995**, *107*, 744; *Angew. Chem. Int. Ed. Engl.* **1995**, *34*, 669 – 672.
[7] T. Jüstel, M. Müller, T. Weyhermüller, C. Kressl, E. Bill, P. Hildebrandt, M. Lengen, M. Grodzicki, A. X. Trautwein, B. Nuber, K. Wieghardt, *Chem. Eur. J.* **1999**, *5*, 793 – 810.
[8] M. Li, M. Shang, N. Ehlinger, C. E. Schulz, W. R. Scheidt, *Inorg. Chem.* **2000**, *39*, 580 – 583.
[9] T. A. Betley, J. C. Peters, *J. Am. Chem. Soc.* **2004**, *126*, 6252 – 6254.
[10] S. D. Brown, J. C. Peters, *J. Am. Chem. Soc.* **2005**, *127*, 1913 – 1923.
[11] R. Hourihane, T. R. Spalding, G. Ferguson, T. Deeney, P. Zanello, *J. Chem. Soc. Dalton Trans.* **1993**, 43 – 46.
[12] R. Della Pergola, C. Bandini, F. Demartin, E. Diana, L. Garlaschelli, P. L. Stanghellini, P. Zanello, *J. Chem. Soc. Dalton Trans.* **1996**, 747 – 754.
[13] Diffraction-quality crystals were obtained from the second crop collected from the mother liquor, as described above. Crystal data for $(Et_4N)_4$**3**·5 MeCN: $C_{54}H_{131}Cl_{12}Fe_{14}N_{21}Sn_4$, $M_r = 2756.91$, $T = 193$ K, monoclinic, space group $C2/c$, $a = 23.991(3)$, $b = 18.450(3)$, $c = 23.450(3)$ Å, $\beta = 94.268(3)°$, $V = 10351(2)$ Å$^3$, $Z = 4$, $\rho_{calcd} = 1.769$ g cm$^{-3}$, $R_1 = 0.0584$, $wR_2 = 0.1140$, 37311 reflections (12872 independent), 492 parameters, 0 restraints. Data were collected on a Bruker APEX diffractometer using graphite-monochromated $Mo_{K\alpha}$ ($\lambda = 0.71073$ Å) radiation, and were corrected for Lorentz, polarization, and absorption effects. Structures were solved by direct methods and refined against all data using SHELXTL 5.0. CCDC-604928 contains the supplementary crystallographic data for this paper. These data can be obtained free of charge from The Cambridge Crystallographic Data Centre via www.ccdc.cam.ac.uk/data_request/cif.
[14] S. H. Strauss, M. E. Silver, K. M. Long, R. G. Thompson, R. A. Hudgens, K. Spartalian, J. A. Ibers, *J. Am. Chem. Soc.* **1985**, *107*, 4207 – 4215.
[15] N. Li, Z. Su, P. Coppens, J. Landrum, *J. Am. Chem. Soc.* **1990**, *112*, 7294 – 7298.
[16] J. Bachmann, D. G. Nocera, *J. Am. Chem. Soc.* **2005**, *127*, 4730 – 4743.
[17] D. Jacoby, C. Floriani, A. Chiesi-Villa, C. Rizzoli, *J. Chem. Soc. Chem. Commun.* **1991**, 220 – 222.
[18] J. W. Lauher, J. A. Ibers, *Inorg. Chem.* **1975**, *14*, 348 – 352.
[19] C. G. Barraclough, R. L. Martin, S. Mitra, R. C. Sherwood, *J. Chem. Phys.* **1970**, *53*, 1643 – 1648.
[20] R. H. Holm, in *Bio-coordination Chemistry*, *Vol. 8*, (Eds.: L. Que, Jr., W. A. Tolman), Elsevier, Oxford **2004**, pp. 61 – 90.
[21] P. V. Rao, R. H. Holm, *Chem. Rev.* **2004**, *104*, 527 – 559.
[22] H. Jacobs, D. Rechenbach, U. Zachwieja, *J. Alloys Compd.* **1995**, *227*, 10 – 17.
[23] B. Eck, R. Dronskowski, M. Takahashi, S. Kikkawa, *J. Mater. Chem.* **1999**, *9*, 1527 – 1537.
[24] N. S. Gill, *J. Chem. Soc.* **1961**, 3512 – 3515.
[25] K. Sisido, S. Kozima, *J. Org. Chem.* **1964**, *29*, 907 – 909.

 © 2006 Wiley-VCH Verlag GmbH & Co. KGaA, Weinheim 

*Natural-Product Modification*

DOI: 10.1002/anie.200601490

# Site-Selective Derivatization and Remodeling of Erythromycin A by Using Simple Peptide-Based Chiral Catalysts**

*Chad A. Lewis and Scott J. Miller**

Medicinal chemistry relies on the efficient generation of analogs of lead compounds. Natural products represent a special class of leads since they have survived eons of natural selection and generally evolved to perform a specific function.[1] Yet, natural products are difficult to modify efficiently

[*] C. A. Lewis,[+] Prof. S. J. Miller[+]
Department of Chemistry
Boston College
Chestnut Hill, MA 02467 (USA)
E-mail: scott.miller@yale.edu

[+] Current address
Department of Chemistry
Yale University
P.O. Box 208107
New Haven, CT 06520 (USA)
Fax: (+1) 203-432-6144

[**] We thank the National Institute of General Medical Sciences for support (R01-GM-068649).

Supporting information for this article is available on the WWW under http://www.angewandte.org or from the author.


WILEY InterScience DISCOVER SOMETHING GREAT
© 2006 Wiley-VCH Verlag GmbH & Co. KGaA, Weinheim

by chemical methods because of their complexity and multifunctional nature.[2] Enzymatic catalysts have been applied in this context.[3] However, the range of reactions that may be employed, and the specificities they exhibit, often lead to a limited set of natural-product analogs. Using peptide-based catalysts, we report herein unique examples of small-molecule, chiral catalyst-dependent, site-selective modifications of a natural product polyol, erythromycin A.

The selective derivatization of polyols is a special challenge to asymmetric catalysis. Unlike enantioselective catalysis, wherein competing reaction pathways present equivalent activation barriers in the absence of a chiral catalyst (e.g., desymmetrization as shown in Scheme 1a), regioselective, "site-selective" catalysis presents the additional challenge of unequal reaction barriers (Scheme 1b). Thus, if a desired polyol derivative requires modification of a hydroxy group of lower inherent reactivity relative to others, then increased demands are placed on a chiral catalyst: the rate of functionalization at the desired, less reactive site must be sufficiently enhanced to overcome and surpass the inherent rate of the more reactive site in order to achieve a selective reaction (i.e., $\Delta\Delta G^{\ddagger}(2) \gg \Delta\Delta G^{\ddagger}(3)$). For natural-product modification, the viability of any approach therefore requires that catalysts are able to affect reversals of the inherent reactivity of individual sites within the molecule. In this sense, the catalyst introduces an element of "double diastereodifferentiation," as catalyst architecture may enhance inherent reactivity in a "matched" sense.[4] Alternatively, in the case of a desired reversal of innate selectivity, one wishes to find powerful catalysts that are "mismatched," in order to fully overcome the native kinetic preference.

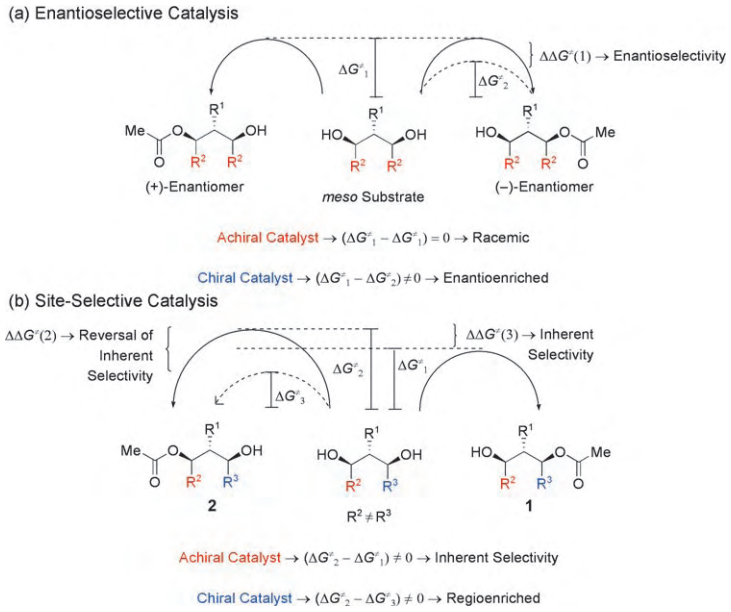


***Scheme 1.*** a) Reaction coordinate for the enantioselective desymmetrization of a *meso* substrate. With an achiral catalyst, the two hydroxy groups react at equal rates. A chiral catalyst may accelerate one pathway leading to enantioselectivity. b) In a site-selective reaction, the two hydroxy groups are of unequal reactivity. Achiral catalysts lead to a product distribution that reflects the inherent reactivity of the two sites ($\Delta\Delta G^{\ddagger}(3)$; **1** is the major product). To form the product of functionalization at the less reactive site (**2**), $\Delta\Delta G^{\ddagger}(2)$ must be large to overcome the lower reactivity, and further favor the formation of the "minor" product.

As a prototype polyol for study of site-selective catalysis, we began with erythromycin A (**3**), an antibiotic with a storied history in both medicinal and synthetic chemistry.[5] We then chose to explore the fundamental process of alcohol acylation, a typical "group transfer" process that could lead to classes of analogs wherein hydroxy groups are converted to unique esters. We have reported that low molecular weight peptide-based catalysts are effective enantioselective catalysts for various group transfers, including acylation,[6] phosphorylation,[7] and sulfinylation.[8] The common chiral catalyst scaffold for group transfer is exemplified by nucleophilic, histidine-based catalysts as shown in Scheme 2.

We initially demonstrated that indeed, the hydroxy group array of **3** provides a range of relative reactivities. The reactivity hierarchy was initially established in the seminal report of Abbott Laboratories, employing pyridine as solvent and catalyst.[9] In our own studies, we found the Abbott results to be entirely reproducible. Furthermore, we established that the achiral catalyst *N*-methylimidazole (NMI) afforded similar results. Indeed, the C2′-hydroxy group undergoes acylation first, due in part to the autocatalytic vicinal tertiary amine, to give the 2′-monoacetate **4** as the major product when a limiting quantity of acetic anhydride ($Ac_2O$) is used (Equation (1) in Scheme 3). Indeed, this site undergoes acylation even in the absence of a catalyst. The next most reactive position is the C4″-hydroxy, as evidenced by preferential formation of the C2′,C4″-diacetate when NMI is used with additional $Ac_2O$; this diacetate is converted to C4″-monoacetate **5** when the reaction is quenched with MeOH, which autocatalytically cleaves the C2′-acetate group (Equation (2) in Scheme 3). Finally, the least reactive secondary site, the C11-OH, acylates such that an Ery A-triacetate (not shown) forms, but only after prolonged reaction time. The tertiary alcohols of **3** are substantially less reactive under these conditions. Under catalysis by NMI (10 mol%), or when pyridine is employed as solvent, the inherent selectivity for **5**/**6**

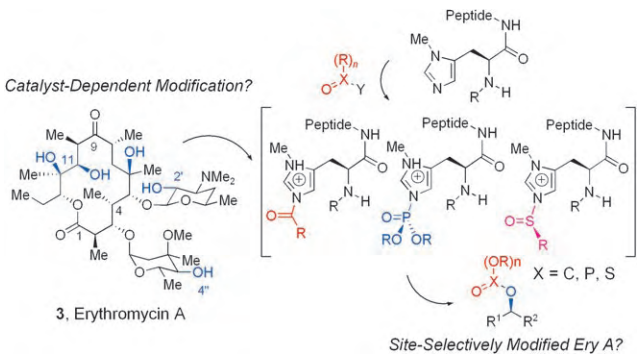


***Scheme 2.***


© 2006 Wiley-VCH Verlag GmbH & Co. KGaA, Weinheim

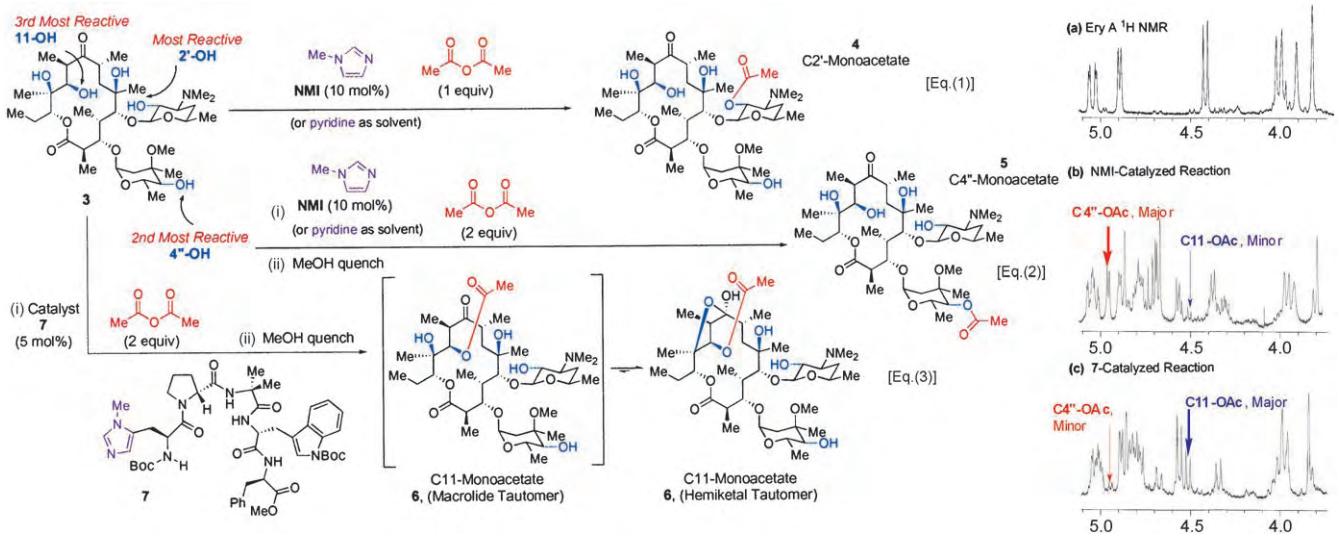


***Scheme 3.*** Reactions of **3** and $^1$H NMR spectra (400 MHz) of a) erythromycin A in a diagnostic ppm window, b) the unpurified reaction mixture when NMI is used as catalyst, and c) of the unpurified reaction mixture when peptide **7** is used as catalyst. Both spectra (b) and (c) are recorded prior to methanolysis. Boc = *tert*-butoxycarbonyl.

may be extracted to be approximately 4:1, although the ratio is strongly dependent on overall extent of conversion. It is notable that with NMI as catalyst, even after 3 days, < 30 % of **3** is converted to **5** and **6** (via **4**). Isolation of large quantities of **6** is therefore difficult.

Our goal then became the identification of a small-molecule catalyst that would reverse the inherent reactivity such that the C11-OH group is modified preferentially over the more reactive C4″-OH of **3**. We examined 137 peptide catalyst candidates, chosen at random from our catalyst libraries. Shown in Scheme 3 are typical $^1$H NMR spectra (400 MHz) of the reaction mixtures when $Ac_2O$ is employed with different catalysts. Notably, many of the peptides examined exhibit NMI or pyridine-like behavior, favoring the C4″-monoacetate **5**, after MeOH quench (Scheme 3b). However, when peptides disposed toward the adoption of β-turn-like structures are employed (e.g., **7**),[10] a reversal of inherent selectivity is observed.[11] In addition, the peptide-catalyzed reactions are generally significantly faster than those promoted by pyridine or NMI. The major product formed under catalysis by **7**, following MeOH quench, is clearly the C11-derivative **6** (Scheme 3c and Equation (3)). We estimate by $^1$H NMR integration that catalyst **7** delivers a ratio of **5**/**6** of ca. 1:5.[12]

Notably, peptide **7** provides not only a catalyst-dependent derivatization of a unique, inherently less reactive hydroxy. In addition, C11-monoacetate **6** exists almost exclusively as its hemiketal tautomer. Everett and co-workers have rationalized hemiketalization of C11-acetate derivatives of erythromycin as a consequence of the loss of a macrolide-stabilizing hydrogen bond between the C11-OH and the C9-carbonyl in native erythromycin.[13] Independent of the structural basis of the tautomerization, the site-selective catalysis results in skeletal reorganization of the natural product.[14] Such reactions, wherein a chiral catalyst not only modifies a unique, inherently disfavored site, but also reorganizes the natural product structure, may be of particular value to the generation of diverse, natural product-derived compounds.

Catalyst **7** appears general for additional group transfers. For example, a dramatic reversal is observed with octanoyl anhydride, setting the stage for site-selective "lipidation" of natural products (Table 1, entry 1). Whereas reaction with pyridine delivers **8a**/**9a** with greater than 10:1 selectivity, catalyst **7** strongly reverses the selectivity such that **9a** is the major product with selectivity of 1:9. Transfer of the β-alanyl moiety via the mixed anhydride also provides a strong reversal (Table 1, entry 2). Achiral catalysts favor **8b** (5:1 over **9b**), while catalyst **7** delivers high selectivity for **9b** (1: > 10). The transfer of functionalized reagents implies the potential for selective labeling of natural products at specific sites. Selective transfer of an alkenyl group is illustrated in entry 3, wherein catalyst **7** reverses the inherent selectivity such that **9c** is the preferred product (5:1 selectivity, **9c**/**8c**). Smaller substrates appear to provide less drastic reversals. Propionyl transfer with achiral catalysts leads to modest selectivity for the inherently favored **8d** (2:1), whereas catalyst **7** favors formation of **9d** (1:3.5, Table 1, entry 4). Notably, in all cases peptide **7** is a far more active catalyst than the achiral catalysts, leading to isolation of C11-derivatized material. While chromatographic separations of compounds at the diester stages are difficult and can limit yields of isolated **9**, in all cases methanolysis of the C2′-OH-derived esters leads to C11-monoesters with excellent purity.

These findings illustrate the potential of chiral catalyst-dependent, site-selective modification of polyol natural products. In addition, the discovery of catalyst-dependent modifications that reorganize natural product architecture may be of additional utility in the science of natural product analog generation. The mechanistic basis of these transformations is a frontier area of chiral catalysis, and studies of catalyst interactions with polyfunctional substrates are underway.[15]

 © 2006 Wiley-VCH Verlag GmbH & Co. KGaA, Weinheim 

***Table 1:*** Site-selective reactions of erythromycin A with achiral catalyst versus **7**.

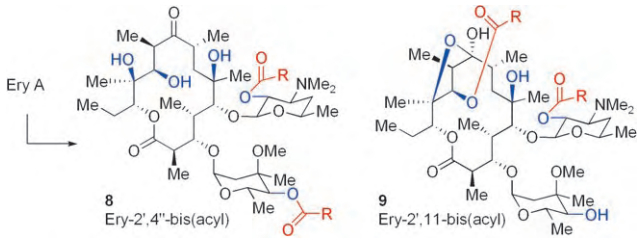


| Entry | | Achiral cat.[a] **8**:**9**[b] | Cat. **7**[c] **8**:**9** (yield of **9**) |
|---|---|---|---|
| 1<br>**8a**, **9a**:<br>R = $(CH_2)_6CH_3$ | 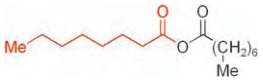 | > 10:1[b] | 1:9<br>(58%) |
| 2<br>**8b**, **9b**:<br>R = $(CH_2)_2NHBoc$ | 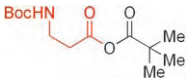 | 5:1[b] | 1: > 10<br>(53%) |
| 3<br>**8c**, **9c**:<br>R = $(CH_2)_2CH{=}CH_2$ | 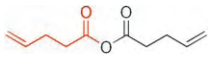 | 2:1[b] | 1:5<br>(56%) |
| 4<br>**8d**, **9d**:<br>R = Et | 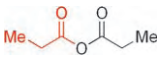 | 2:1[b] | 1:3.5<br>(28%) |

[a] Reaction catalyzed by pyridine as solvent. Reactions catalyzed by NMI provide similar ratios. [b] Reactions with pyridine or NMI are generally sluggish and not preparatively useful. Consistent with the reports of Abbott Laboratories,[9] the yields of **8** (R = Me) under conditions promoted by pyridine is about 70% after 3 days reaction time. Yields of **9** under catalysis by pyridine are extremely low and difficult to quantify. Thus, peptide **7** provides unique access to **9**. [c] Yields are determined from isolated material after chromatography. In cases where co-elution with minor components occurs, conversion into the corresponding C11-monoester following methanolysis of the C2′-OH-ester delivers pure compounds for full characterization. See Supporting Information for details.

## *Experimental Section*

General procedure for the acylation of erythromycin A: Erythromycin A (**3**, 100 mg, 0.136 mmol) was dissolved in $CHCl_3$ (100 mM, 1.36 mL) in a flame-dried vial. Triethylamine (5 equiv, 93.0 μL, 0.681 mmol) and the catalyst (5 mol%, 20.0 mM in $CH_2Cl_2$, 0.340 mL, 6.81 μmol) were then added sequentially. For less reactive anhydrides, 10 mol% catalyst is employed (see Supporting Information for details.) Acetic anhydride (10 equiv, 128 μL, 1.36 mmol) was added and the reaction was allowed to stir at 25 °C. Reaction progress was monitored by $^1$H NMR (400 MHz) by removing 100 μL aliquots followed by a methanol quench. The resulting solutions were passed through a silica gel plug eluting with a $CHCl_3$/MeOH (95/5 v/v) solvent system and concentrated under high vacuum. After an appropriate time interval, the full reaction mixture was quenched by addition of methanol and passed through a silica gel plug and concentrated to dryness. If complete cleavage of the labile 2′-acetyl was desired, the unpurified reaction mixture was redissolved in MeOH and allowed to stir for 72 h. After concentration of the reaction mixture, reaction selectivity was analyzed by $^1$H NMR (400 MHz). Individual products were isolated by silica gel column chromatography ($CHCl_3$/MeOH/$NH_4OH$, 14 M; 95/5/1 v/v/v) and/or semipreparative HPLC techniques.

Received: April 14, 2006
Revised: June 12, 2006
Published online: July 21, 2006

**Keywords:** asymmetric catalysis · erythromycin · nucleophiles · peptides · site-selectivity

[1] J. Clardy, C. Walsh, *Nature* **2004**, *432*, 829–837.
[2] J. Y. Ortholand, A. Ganesan, *Curr. Opin. Chem. Biol.* **2004**, *8*, 271–280.
[3] U. Abel, C. Koch, M. Speitling, F. G. Hansske, *Curr. Opin. Chem. Biol.* **2002**, *6*, 453–458.
[4] S. Masamune, W. Choy, J. S. Petersen, L. R. Sita, *Angew. Chem.* **1985**, *97*, 1–31; *Angew. Chem. Int. Ed. Engl.* **1985**, *24*, 1–30.
[5] J. M. McGuire, R. L. Bunch, R. C. Anderson, H. E. Boaz, E. H. Flynn, H. M. Powell, J. W. Smith, *Antibiot. Chemother.* **1952**, *2*, 281–283.
[6] G. T. Copeland, S. J. Miller, *J. Am. Chem. Soc.* **2001**, *123*, 6496–6502.
[7] B. R. Sculimbrene, S. J. Miller, *J. Am. Chem. Soc.* **2001**, *123*, 10125–10126.
[8] J. W. Evans, M. B. Fierman, S. J. Miller, J. A. Ellman, *J. Am. Chem. Soc.* **2004**, *126*, 8134–8135.
[9] P. H. Jones, E. J. Baker, E. K. Rowley, T. J. Perun, *J. Med. Chem.* **1972**, *15*, 631–634.
[10] For several lead references to the structure-nucleating effects of D-Pro and Aib, see: a) T. S. Haque, J. C. Little, S. H. Gellman, *J. Am. Chem. Soc.* **1996**, *118*, 6975–6985; b) I. L. Karle, S. K. Awasthi, P. Balaram, *Proc. Natl. Acad. Sci. USA* **1996**, *93*, 8189–8193; c) C. Toniolo, M. Crisma, F. Formaggio, C. Peggion, *Biopolymers* **2001**, *60*, 396–419.
[11] A table of the catalysts that were screened, reflecting their diverse performance, may be found in the Supporting Information.
[12] The ratios are supported by both NMR analysis and yields of isolated products; see Supporting Information.
[13] J. R. Everett, E. Hunt, J. W. Tyler, *J. Chem. Soc. Perkin Trans. 2* **1991**, 1481–1487.
[14] M. D. Burke, E. M. Berger, S. L. Schreiber, *Science* **2003**, *302*, 613–618.
[15] For examples of mechanistic studies of asymmetric reactions catalyzed by peptides related to **7**, see: a) M. M. Vasbinder, E. R. Jarvo, S. J. Miller, *Angew. Chem.* **2001**, *113*, 2906–2909; *Angew. Chem. Int. Ed.* **2001**, *40*, 2824–2827; b) M. B. Fierman, D. J. O'Leary, W. E. Steinmetz, S. J. Miller, *J. Am. Chem. Soc.* **2004**, *126*, 6967–6971.

 © 2006 Wiley-VCH Verlag GmbH & Co. KGaA, Weinheim 

Structure Determination

DOI: 10.1002/anie.200600769

# Constraints on the Structure of $(CUG)_{97}$ RNA from Magic-Angle-Spinning Solid-State NMR Spectroscopy**

*Kerstin Riedel, Christian Herbst, Sabine Häfner, Jörg Leppert, Oliver Ohlenschläger, Maurice S. Swanson, Matthias Görlach, and Ramadurai Ramachandran**

Expansions of short nucleotide sequence repeats are associated with a number of neuromuscular diseases.[1–3] CTG triplet repeat expansions in the 3′ noncoding region of the myotonic dystrophy protein kinase (DMPK) gene give rise to transcripts harboring CUG triplet repeat expansions on the RNA level. Repeats containing $>50$ CUG triplets cause in *trans*-dominant fashion the most frequent form of adult-onset muscular dystrophy (DM1). The current model for DM1 pathogenesis strongly suggests that such repeats fold into large stable double-stranded RNA hairpins, which bind and sequester muscleblind (MBNL) proteins that are involved in the alternative splicing of a number of pre-mRNAs. As a consequence, the MBNL proteins are unavailable to the splicing machinery, and a number of important muscular pre-mRNAs, for example, for the chloride channel ClC-1 and the insulin receptor, are aberrantly spliced; this process ultimately leads to the clinical manifestations of DM1.

To decipher the structural basis of DM1, which could potentially permit the development of suitable drugs that would interfere with the sequestration of MBNL proteins by CUG repeats, we have recently initiated, as a first step, a magic-angle-spinning (MAS) solid-state NMR study of a $\approx$100-kDa RNA composed of 97 CUG repeats ($(CUG)_{97}$). $^{15}N$-$^{15}N$ chemical-shift correlation experiments have enabled us to show the presence of canonical GC base pairs in this RNA.[4] In addition, analysis of the observed $^{13}C$ chemical shifts for the sugar carbon atoms suggested that $(CUG)_{97}$ adopts an A-form helix conformation with a C3′-*endo* sugar pucker and an *anti* conformation of the glycosidic torsion angle $\chi$.[5] Herein, we have explored the possibility of obtaining structural information directly by exploiting the dependence of inter- and intranucleotide $^1H$–$^1H$ distances on RNA conformation. Since the extraction of $^1H$–$^1H$ distances by direct $^1H$ observation techniques is still difficult in the solid state, we have utilized in this study the potential of proton–proton dipolar-coupling-mediated chemical-shift correlation spectroscopy of low-gamma nuclei[6–13] for mapping the spatial proximity of the sugar and aromatic protons in $(CUG)_{97}$.

The radio frequency (RF) pulse sequence[13] and a schematic representation of the double-stranded $(CUG)_{97}$ employed are shown in Figure 1. Longitudinal $^1H$ magnetization exchange mediated by proton–proton dipolar coupling is allowed to take place during the spin diffusion period $\tau_{mix}$. The experiment is carried out with a very short CP contact time ($\approx$100 μs) and a proton spin diffusion mixing time, $\tau_{mix}$, of 100–200 μs. This time regime minimizes relayed magnetization transfers during the CP and $\tau_{mix}$ periods and, hence, crosspeaks with appreciable intensities are expected only between proton-attached $^{13}C$ sites that are connected by $^1H$–$^1H$ distances of less than $\approx$3 Å.[8–13] $^{13}C$ homonuclear isotropic chemical-shift correlation spectra of a uniformly {$^{15}N$,$^{13}C$}-labeled sample of $(CUG)_{97}$ obtained with different short proton spin diffusion mixing times are shown in Figure 2. The resonance assignments indicated are based on our recent studies.[5,14] The expected crosspeaks arising from direct or relayed magnetization transfers originating from sugar proton–sugar proton dipolar interactions and corresponding to intranucleotide proton–proton distances of $<3.0$ Å are seen. By contrast, crosspeaks between the aromatic and sugar C1′ and C4′ carbon atoms, which would reflect the spatial proximity of the corresponding attached protons, are essentially absent.

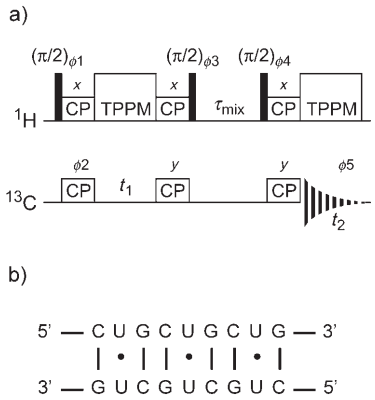


***Figure 1.*** a) CPMAS pulse sequence employed for proton spin diffusion based isotropic chemical-shift correlation of the protonated carbon sites in RNA. The RF pulse and the receiver phases were cycled as $\phi1=(y,-y)$, $\phi2=(-y,-y,y,y)$, $\phi3=(4\times y,4\times -y)$, $\phi4=(8\times y,8\times -y)$, and $\phi5=(x,-x,-x,x,-x,x,x,-x,-x,x,x,-x,x,-x,-x,x)$. High-power two-pulse phase modulation (TPPM) decoupling was employed in the $t_1$ and $t_2$ time periods and phase-sensitive 2D spectra were generated as described by States et al.[18] b) Schematic representation of a section of the double-stranded $(CUG)_{97}$ RNA.

[*] K. Riedel, C. Herbst, S. Häfner, Dr. J. Leppert, Dr. O. Ohlenschläger, Dr. M. Görlach, Dr. R. Ramachandran
Research Group Molecular Biophysics/NMR Spectroscopy
Leibniz Institute for Age Research
Fritz Lipmann Institute
Beutenbergstrasse 11, 07745 Jena (Germany)
Fax: (+49) 3641-656-225
E-mail: raman@fli-leibniz.de
Prof. Dr. M. S. Swanson
Department of Molecular Genetics and Microbiology
Powell Gene Therapy Center
College of Medicine
University of Florida
1600 SW Archer Road, Gainesville, FL 32610-0266 (USA)

[**] This study has been funded in part by a PhD fellowship to Kerstin Riedel from the Stiftung Stipendien-Fonds des Verbandes der Chemischen Industrie e.V. and a grant from the Deutsche Forschungsgemeinschaft (grant no.: GO474/6-1).


InterScience
© 2006 Wiley-VCH Verlag GmbH & Co. KGaA, Weinheim

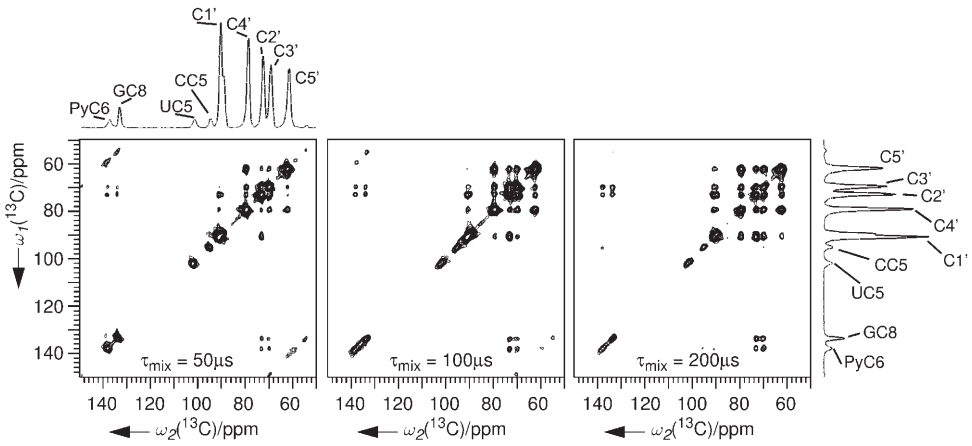


***Figure 2.*** Experimental $^{13}C$-$^{13}C$ chemical-shift correlation spectra of the hydrated, uniformly {$^{15}N$,$^{13}C$}-labeled $(CUG)_{97}$ RNA. Mixing times were as indicated; spinning speed: 10000 Hz; data acquisition in the direct dimension: 10 ms; CP contact time: 75 µs; recycle time: 1 s; $\omega_1$ spectral width: 30000 Hz; 160 $t_1$ increments with 64 transients per increment were employed. The RF carrier was kept at the center of the spectral region. Chemical shifts are referenced with respect to external adamantane ($\delta_{CH} = 29.5$ ppm with respect to tetramethylsilane). The assignments of the different resonances are indicated on the spectral projection shown.

It is known that in A-form helical RNA (Figure 3) sequential H1′···H6/H8 distances are larger than 3 Å.[15] In a proton spin diffusion based $^{13}C$-$^{13}C$ chemical-shift correlation spectrum, this would be reflected by the absence of the corresponding crosspeaks between the aromatic and sugar C1′ carbon atoms. By contrast, B-form helices are characterized by short internucleotide H1′···H5′/H5″ distances of about 2 Å. Hence, the absence of strong crosspeaks between the C1′ and C5′ carbon atoms with a $\tau_{mix}$ period of 50 µs, similar to that between the C1′ and C2′ carbon atoms, is consistent with an A-form helix. By using standard RNA conformations, that is, C3′-*endo* and C2′-*endo* sugar puckers and various torsion angles $\chi$, we have evaluated the intranucleotide distances between aromatic and sugar protons with molecular modeling (Table 1). From these results, it can be deduced that the absence of crosspeaks between the aromatic and sugar C1′ carbon atoms indicates a $\chi$ angle, describing the relative orientation of the base and the sugar moiety across the glycosidic bond, in the *anti* range.

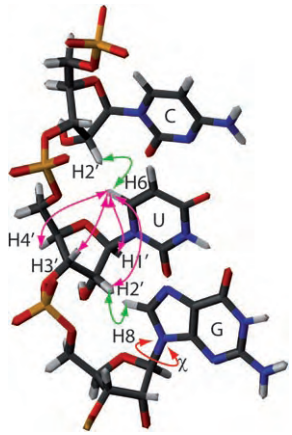


***Figure 3.*** Representative intra- and internucleotide $^1H$–$^1H$ dipolar interactions in a double-stranded A-form helical RNA. For clarity, only one strand of the RNA, modelled with SYBYL software, is shown.

In the spectra shown in Figure 2, crosspeaks arising from dipolar interactions involving aromatic (H6/H8) and sugar (H2′ and H3′) protons can be clearly observed. In a uniformly labeled sample these crosspeaks could, in principle, arise both from intra- and internucleotide $^1H$–$^1H$ dipolar interactions. Since A-form RNA helices are characterized by internucleotide H2′···H8/H6 and H3′···H8/H6 distances in the range of 1.5–2.5 Å and 2.5–4 Å,[15] respectively, the corresponding crosspeaks seen in Figure 2 can arise from sequential interactions. However, it is equally possible that when the $\chi$ angle is in the *anti* range, one could also observe crosspeaks arising from intranucleotide correlations (Table 1).

To identify the origin of the sugar–aromatic crosspeaks seen in Figure 2, we have carried out further experiments employing a $(CUG)_{97}$ sample that has been specifically labeled with [$^{13}C$]U. Figure 4 shows the correlation spectrum for this sample with a $\tau_{mix}$ period of 200 µs. In this case all the crosspeaks arising from internucleotide $^1H$–$^1H$ dipolar interactions are not detectable due to specific U labeling, so crosspeaks in the spectrum of such a sample can only arise from intranucleotide $^1H$–$^1H$ dipolar interactions. No such crosspeaks between the aromatic C6 and sugar C2′ carbon atoms are detected (Figure 4). This indicates that the corresponding crosspeak in Figure 2 can only arise from sequential, internucleotide $^1H$–$^1H$ dipolar interactions, as

***Table 1:*** Distance ranges for H6/H8 to sugar protons as extracted from models of riboG and riboU generated with SYBYL software.

| $\chi$ | for C2′-*endo* | | | | for C3′-*endo* | | | |
|---|---|---|---|---|---|---|---|---|
| | Purine H8/Pyrimidine H6 to | | | | | | | |
| | H1′ | H2′ | H3′ | H4′ | H1′ | H2′ | H3′ | H4′ |
| 0°, *syn* | 2.7–3.1 | 3.2–3.5 | 5.2–5.5 | 5.6–6.0 | 2.7–3.1 | 2.5–2.6 | 4.3–4.5 | 5.4–5.7 |
| 45° | 2.3–2.7 | 4.1–4.3 | 5.7–6.1 | 5.5–5.9 | 2.3–2.7 | 3.6–3.7 | 5.1–5.2 | 5.4–5.8 |
| 90°, high *syn* | 2.4–2.8 | 4.6–4.8 | 5.9–6.3 | 5.0–5.4 | 2.4–2.7 | 4.3–4.4 | 5.1–5.3 | 5.1–5.6 |
| 135° | 2.8–3.2 | 4.4–4.7 | 5.7–6.1 | 4.4–4.9 | 2.9–3.2 | 4.5–4.7 | 4.5–4.8 | 4.6–5.1 |
| 180°, *anti* | 3.4–3.7 | 3.7–4.1 | 5.1–5.6 | 4.1–4.7 | 3.5–3.7 | 4.0–4.4 | 3.4–3.8 | 4.2–4.6 |
| 225° | 3.7–4.0 | 2.7–3.1 | 4.4–4.9 | 4.3–4.8 | 3.7–3.9 | 3.1–3.6 | 2.2–2.6 | 4.2–4.5 |
| 270°, high *anti* | 3.6–3.9 | 1.7–2.3 | 4.0–4.6 | 4.8–5.3 | 3.6–3.9 | 1.9–2.5 | 2.1–2.3 | 4.5–4.8 |
| 315° | 3.3–3.6 | 2.0–2.5 | 4.4–4.9 | 5.4–5.8 | 3.2–3.6 | 1.5–2.0 | 3.1–3.3 | 5.0–5.3 |


© 2006 Wiley-VCH Verlag GmbH & Co. KGaA, Weinheim

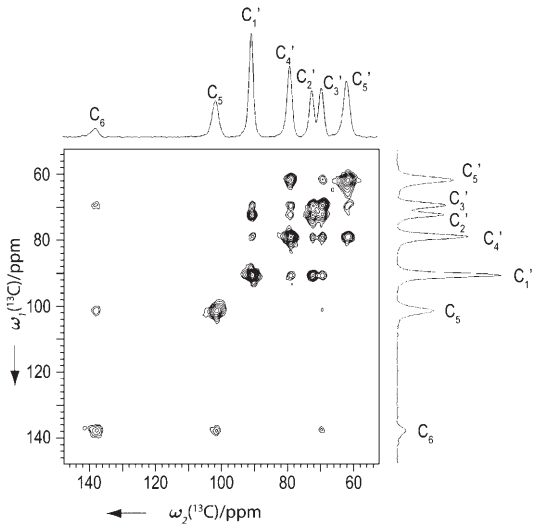


***Figure 4.*** Experimental $^{13}C$-$^{13}C$ chemical-shift correlation spectrum of the hydrated [$^{13}C$]U-labeled $(CUG)_{97}$ RNA sample. Mixing time: 200 μs; CP contact time: 100 μs; 160 $t_1$ increments with 512 transients per increment were employed. For further details see the legend to Figure 2.

expected for A-form helical RNAs. The crosspeak between the aromatic C6 and sugar C3′ carbon atoms (Figure 4) indicates a C3′-*endo* sugar conformation for U. With the $\chi$ angle in the *anti* range and in a C2′-*endo* conformation, the H6···H3′ distance is always larger than that between the H6 and H2′ protons and this would result first in the appearance of the crosspeak between the aromatic C6 and sugar C2′ carbon atoms. This is not the case here, even with lower mixing times (data not shown), and this again suggests a C3′-*endo* sugar conformation for U, as expected for A-form helices.

The data presented herein provide further clear evidence for the conclusions deduced from $^{13}C$ chemical-shift analysis, namely, that $(CUG)_{97}$ principally adopts an A-form helix conformation with a C3′-*endo* sugar pucker and an *anti* glycosidic torsion angle $\chi$. They also demonstrate that strong dipolar interactions between spatially proximal $^{1}H$ nuclei can be effectively exploited for extracting RNA conformation constraints from $^{13}C$ MAS solid-state NMR spectroscopy. On the other hand, and as pointed out earlier by Lange et al.,[8] short-range distance measurements by using low-gamma nuclei typically do not provide structural information. The present approach is also applicable even for the study of uniformly labeled samples. To minimize the effects of conformation averaging/flexibility, it would be advantageous to carry out these experiments at the lowest temperature possible. Further studies will have to be carried out to obtain additional structural constraints for generating a well-defined MAS-NMR-spectroscopically derived 3D structure of $(CUG)_{97}$. However, the A-form helix conformation of $(CUG)_{97}$, as deduced from our earlier studies and as further substantiated herein, has meanwhile been corroborated with an X-ray crystal study on an 18-base-pair RNA containing 6 CUG repeats.[16]

Although to reduce data acquisition time we have carried out only two-dimensional $^{13}C$-$^{13}C$ chemical-shift correlation experiments, it should be possible to extend this approach to three dimensions, for example, to obtain $^{15}N/^{13}C$-edited $^{13}C$-$^{13}C$ correlation spectra. Such experiments would be useful for resolving spectral overlaps. The approach adopted herein can also be extended to study systems by using different labeling schemes. Conceptually similar to the approach used in structure determinations of RNA molecules by liquid-state NMR spectroscopy,[17] in which a fast classification of the predominant $\chi$ conformation is achieved by an analysis of the intensities of the H1–H8/H6 NOE crosspeaks, the analysis of proton spin diffusion induced $^{13}C$-$^{13}C$ chemical-shift correlation spectra in the short-mixing-time regime should allow the characterization of the torsion angle $\chi$, the sugar pucker, and the helical regions of large RNA systems through MAS solid-state NMR spectroscopy. While proton–proton dipolar couplings have been successfully employed recently for the extraction of structural constraints from MAS solid-state NMR studies of peptides and proteins, distance estimates involving nonexchangeable protons have been exploited herein for the first time in the study of nucleic acids. Although structural studies of RNAs are typically carried out with solution-state NMR spectroscopy, this study clearly indicates that even large RNA systems are, in principle, amenable for investigations with MAS solid-state NMR spectroscopy.

## Experimental Section

RNA samples were prepared by using appropriately labeled ribonucleoside triphosphates as described earlier.[4] A hydrated, undiluted {$^{15}N$,$^{13}C$}-labeled RNA sample of $(CUG)_{97}$[4] (8.5 mg) and a hydrated, specifically [$^{13}C$]U-labeled $(CUG)_{97}$ sample (5 mg) were used. Experiments were carried out at about −15 °C on a 500-MHz wide-bore Varian Unity Inova solid-state NMR spectrometer equipped with a 5-mm DOTY supersonic triple-resonance probe.

Received: February 28, 2006
Revised: May 15, 2006
Published online: July 20, 2006

**Keywords:** helical structures · magic-angle spinning · NMR spectroscopy · RNA · structure elucidation

[1] K. R. Nykamp, M. S. Swanson, *Prog. Mol. Subcell. Biol.* **2004**, *35*, 57–77.
[2] L. P. W. Ranum, J. W. Day, *Am. J. Hum. Genet.* **2004**, *74*, 793–804.
[3] L. P. W. Ranum, J. W. Day, *Trends Genet.* **2004**, *20*, 506–512.
[4] J. Leppert, C. R. Urbinati, S. Häfner, O. Ohlenschläger, M. S. Swanson, M. Görlach, R. Ramachandran, *Nucleic Acids Res.* **2004**, *32*, 1177–1183.
[5] K. Riedel, J. Leppert, S. Häfner, O. Ohlenschläger, M. Görlach, R. Ramachandran, *J. Biomol. NMR* **2004**, *30*, 389–395.
[6] M. Wilhelm, H. Feng, U. Tracht, H. W. Spiess, *J. Magn. Reson.* **1998**, *134*, 255–260.
[7] I. de Boer, L. Bosman, J. Raap, H. Oschkinat, H. J. M. de Groot, *J. Magn. Reson.* **2002**, *157*, 286–291.
[8] A. Lange, S. Luca, M. Baldus, *J. Am. Chem. Soc.* **2002**, *124*, 9704–9705.

 © 2006 Wiley-VCH Verlag GmbH & Co. KGaA, Weinheim 

[9] A. Lange, K. Seidel, L. Verdier, S. Luca, M. Baldus, *J. Am. Chem. Soc.* **2003**, *125*, 12640 – 12648.
[10] A. Lange, S. Becker, K. Seidel, L. Verdier, K. Giller, O. Pongs, M. Baldus, *Angew. Chem.* **2005**, *117*, 2125 – 2129; *Angew. Chem. Int. Ed.* **2005**, *44*, 2089 – 2092.
[11] R. Tycko, Y. Ishii, *J. Am. Chem. Soc.* **2003**, *125*, 6606 – 6607.
[12] B. Reif, B. J. van Rossum, F. Castellani, K. Rehbein, A. Diehl, H. Oschkinat, *J. Am. Chem. Soc.* **2003**, *125*, 1488 – 1489.
[13] K. Riedel, J. Leppert, O. Ohlenschläger, M. Görlach, R. Ramachandran, *J. Biomol. NMR* **2005**, *31*, 331 – 336.
[14] K. Riedel, J. Leppert, O. Ohlenschläger, M. Görlach, R. Ramachandran, *J. Biomol. NMR* **2005**, *31*, 49 – 57.
[15] B. Furtig, C. Richter, J. Wöhnert, H. Schwalbe, *ChemBioChem* **2003**, *4*, 936 – 962.
[16] B. H. M. Mooers, J. S. Logue, J. A. Berglund, *Proc. Natl. Acad. Sci. USA* **2005**, *102*, 16626 – 16631.
[17] P. B. Moore, *Acc. Chem. Res.* **1995**, *28*, 251 – 256.
[18] D. J. States, R. A. Haberkorn, D. J. Ruben, *J. Magn. Reson.* **1982**, *48*, 286 – 292.

 © 2006 Wiley-VCH Verlag GmbH & Co. KGaA, Weinheim 

DNA Hybridization

DOI: 10.1002/anie.200601190

# Mismatch-Binding Ligands Function as a Molecular Glue for DNA**

*Tao Peng, Chikara Dohno, and Kazuhiko Nakatani**

Single-stranded DNA (ssDNA) hybridizes with another ssDNA unit having the complementary base sequence. The high sequence specificity in the hybridization is one of the most important properties of DNA as a genetic material, and also characterizes DNA as the unique component of the molecular architecture.[1–5] The formation of a double-stranded DNA (dsDNA) molecule of fully matched base sequences is highly energetically favorable and proceeds spontaneously at a temperature below the melting temperature ($T_m$) of the duplex, and therefore it is difficult to turn the hybridization on and off under isothermal conditions. Studies toward controlling or modulating the DNA hybridization with photochemical[6–9] and electronic reactions[10,11] of chemically modified oligonucleotides have been reported. Herein, we describe an approach to turn on duplex formation of two natural, unmodified ssDNA sequences that do not spontaneously hybridize with each other by a mismatch-binding ligand (MBL).

Recent studies on the binding of an MBL to the $(CGG)_n$ trinucleotide repeat revealed a novel mode of ligand binding to a mismatched DNA duplex.[12,13] The naphthyridine carbamate dimer (**NC**) selectively binds to the 5′-CGG-3′/5′-CGG-3′ sequence (CGG/CGG), which involves a G–G mismatch flanked by two C–G base pairs, with a 2:1 **NC**/DNA stoichiometry. The binding of **NC** to the CGG/CGG sequence induced two cytosines to be out of the π stack, as evidenced by the selective cleavage at the unpaired cytosine triggered by the addition of hydroxylamine.[12] We anticipated that the flipped-out cytosine in the **NC**-bound CGG/CGG triad could be substituted with other nucleotide bases such as thymine, and therefore **NC** could stabilize the 5′-TGG-3′/5′-TGG-3′ (TGG/TGG) sequence that consists of three contiguous T–G, G–G, and G–T mismatches (Figure 1). As the hybridization of two ssDNA molecules to produce the TGG/TGG sequence would be energetically unfavorable, these ssDNA sequences could be adhered by binding of **NC** to the TGG/TGG sequence.

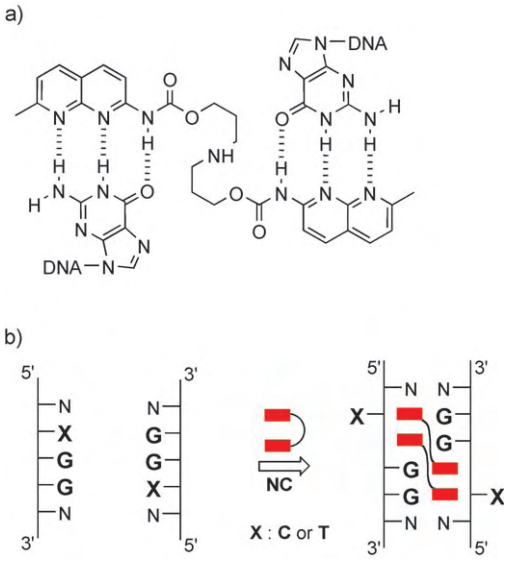


***Figure 1.*** a) **NC** and its hydrogen-bonding pattern to a guanine–guanine mismatch. b) Schematic representation of the binding of **NC** to the XGG/XGG sequence. Red rectangles: naphthyridine rings.

The binding of **NC** was first investigated for 5′-TGG-3′/5′-CGG-3′ (TGG/CGG) where one cytosine of the CGG/CGG sequence was substituted with thymine. The 11-mers 5′-d(CCCATGGTCCG)-3′ (**T1**) and 5′-d(CGGACGG-TGGG)-3′ (**C1**; 5 μM) produced a duplex (**T1**/**C1**) containing a TGG/CGG sequence with a $T_m$ of 35.7 °C in sodium cacodylate buffer. In the presence of **NC**, the $T_m$ of the **NC**-bound **T1**/**C1** was 71.1 °C, which shows an increase in $T_m$ of 35.4 K (Figure 2). The transition from dsDNA to ssDNA is monophasic, regardless of the presence of **NC**. The transition occurred somewhat less cooperatively in the presence of **NC**. The melting kinetics may not be as simple as those in the

[*] Dr. T. Peng, Dr. C. Dohno, Prof. K. Nakatani
Department of Regulatory Bioorganic Chemistry
The Institute of Scientific and Industrial Research (SANKEN)
Osaka University
8-1 Mihogaoka, Ibaraki 567-0047 (Japan)
Fax: (+81) 6-6879-8459
E-mail: nakatani@sanken.osaka-u.ac.jp

[**] This work was supported by a Grant-in-Aid for Scientific Research (A) from the Japan Society for the Promotion of Science, Health and Labor Sciences Research Grants for Research on Advanced Medical Technology from the Ministry of Health, Labor, and Welfare, and CREST, Japan Science and Technology Agency.

Supporting information for this article is available on the WWW under http://www.angewandte.org or from the author.

 © 2006 Wiley-VCH Verlag GmbH & Co. KGaA, Weinheim 

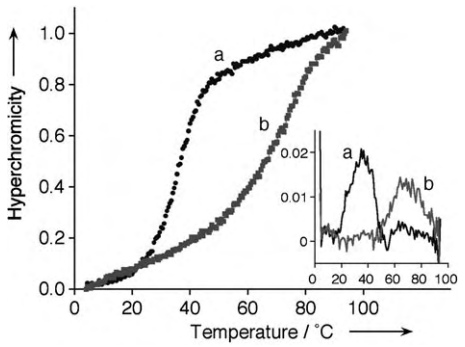


***Figure 2.*** Thermal denaturation profile of **T1** and **C1** (5 μM each) in the absence (a) and presence (b) of **NC** (100 μM). The absorbance at 260 nm was measured in sodium cacodylate buffer (10 mM, pH 7.0) containing 0.1 M NaCl. The temperature was increased from 4 to 94 °C at a rate of 1 °C min$^{-1}$. The absorbance was measured with an interval of 1 °C. Measurements were carried out at least three times. The average of three data sets of denaturation profiles was used for the plots. Inset: differential plots of the melting profiles.

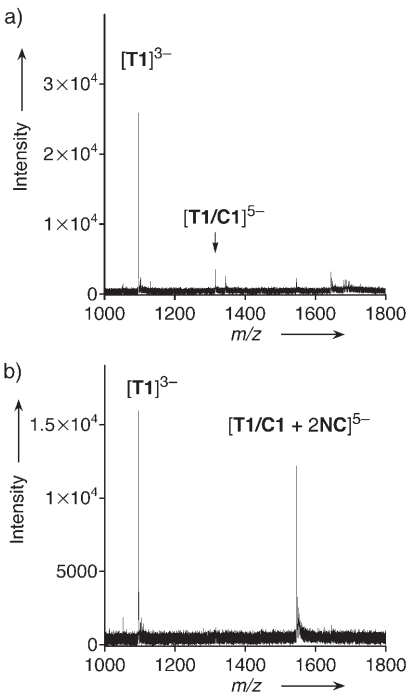


***Figure 3.*** CSI-TOF MS of **T1** and **C1** in the a) absence and b) presence of **NC** (40 μM). Samples contained 20 μM of each strand in 50% aqueous methanol and ammonium acetate (100 mM). Ions in the range of *m*/*z* from 1000 to 1800 are shown for clarity. The sample solution was cooled at −10 °C during the injection with a flow rate of 0.5 mL h$^{-1}$.

absence of **NC**, because this transition involves the dissociation of four components, two DNA strands (**T1** and **C1**) and two **NC** molecules. The thermal denaturation profiles showed that in the temperature range between 45 and 55 °C, **T1** and **C1** were present as single-stranded forms in the absence of **NC** but as an **NC**-bound duplex form in the presence of **NC**.

The cold-spray ionization time-of-flight mass spectrometry (CSI-TOF MS)[12,14] of **T1** and **C1** showed ions corresponding to a 3− ion of a single-stranded form ([**T1**]$^{3-}$, *m*/*z*: found: 1096.2; calcd: 1096.2) and a 5− ion of a duplex form ([**T1**/**C1**]$^{5-}$, *m*/*z*: found: 1344.8; calcd: 1344.6; Figure 3a). On addition of **NC** to the duplex with a 2:1 molar ratio, the intensity of the ions corresponding to [**T1**]$^{3-}$ became weaker with the concomitant appearance of a new ion corresponding to the 5− ion of a 2:1 complex of **NC** and the duplex ([**T1**/**C1** + 2**NC**]$^{5-}$, *m*/*z*: found: 1546.3; calcd: 1545.9; Figure 3b). On increasing the concentration of **NC**, the intensity of the ion corresponding to [**T1**/**C1** + 2**NC**]$^{5-}$ became strong with a concomitant decrease of the intensity of [**T1**]$^{3-}$ (see Supporting Information). Complexes of **NC** bound to **T1**/**C1** with 1:1 and/or 3:1 stoichiometries were not detected. These results clearly showed that the binding of **NC** to the duplex **T1**/**C1** proceeded in an exclusive stoichiometry of 2:1. This stoichiometry of **NC** binding is the characteristic feature that is observed for the binding of **NC** to the CGG/CGG sequence[12] and the binding of the related MBL naphthyridine azaquinolone to the CAG/CAG sequence. The structure of the latter complex has been determined by NMR spectroscopy.[13] These findings suggested that the thymine in the **NC**-bound **T1**/**C1** would most likely be out of the π stack.

The T component in the extrahelical position could be preferentially oxidized with potassium permanganate ($KMnO_4$) compared to that in the intrahelical position.[15] The resulting thymine glycol (Tg) can be degraded with hot piperidine, eventually leading to strand cleavage.[16–18] The oxidation of **T1**/**C1** with $KMnO_4$ followed by treatment with hot piperidine was examined (Scheme 1). The duplex **T1**/**C1** (12.5 μM) did not react with $KMnO_4$ (0.2 mM) at 0 °C for

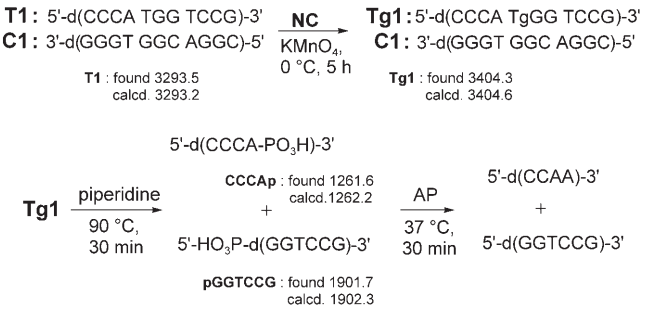


***Scheme 1.*** The oxidation of **T1**/**C1** by $KMnO_4$ upon binding of **NC**. AP = alkaline phosphatase.

320 min, as judged by reversed-phase HPLC analysis (see Supporting Information). In contrast, the TGG-containing DNA **T1** was consumed by 70% in the presence of **NC** (40 μM) and converted into the 11-mer DNA 5′-d(CCCA-TgGGTCCG)-3′ (**Tg1**) which contained a Tg unit.[16] After isolation by HPLC, **Tg1** was treated with hot piperidine to give two products corresponding to oligomers 5′-d(CCCA)-$PO_3$H-3′ (**CCCAp**) and 5′-$HO_3$P-d(GGTCCG)-3′ (**pGGTCCG**). All DNA products were identified by MALDI-TOF mass spectrometry (Scheme 1). Although the duplex **T1**/**C1** contained two kinds of thymine residues, only that in the TGG/CGG sequence was reactive to $KMnO_4$ upon **NC** binding. These results clarified the finding that the T unit in the TGG/CGG sequence was in the extrahelical position in the **NC**-bound complex.

 © 2006 Wiley-VCH Verlag GmbH & Co. KGaA, Weinheim 

Having confirmed that 1) **NC** could stabilize the duplex containing two contiguous T–G and G–G mismatches in **T1**/**C1** and 2) the T component was in the extrahelical position in the **NC**-bound TGG/CGG sequence, the binding of **NC** to the three contiguous mismatches T–G, G–G, and G–T in the TGG/TGG sequence was investigated. The 11-mers 5′-d(CCTTTGGTCAG)-3′ (**T2**) and 5′-d(CTGATGGAAGG)-3′ (**T3**) that had a 5′-TGG-3′ sequence were present as single-stranded forms at room temperature, as shown by the denaturation profile, because the possible duplex **T2**/**T3** should involve three contiguous mismatches (Figure 4a). At

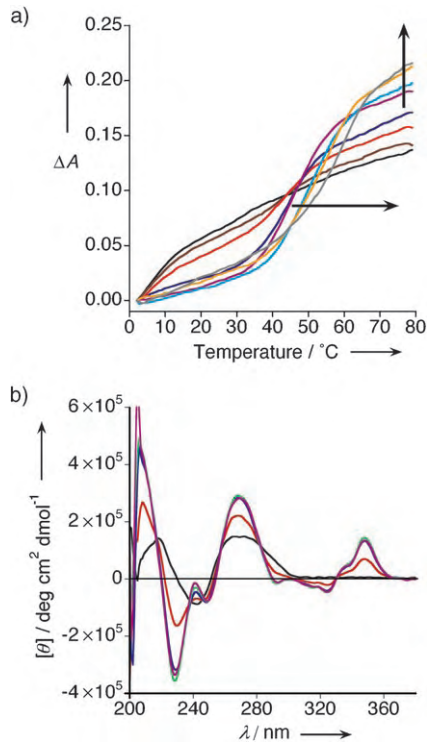


***Figure 4.*** a) Thermal denaturation profile of **T2** and **T3** (5 μM each) with different concentrations of **NC** (0 (black), 2.5 (brown), 5 (red), 10 (blue), 20 (purple), 40 (cyan), 60 (yellow), and 100 μM (gray)). The vertical arrow indicates the increase in $\Delta A$ with increasing **NC** concentration. The horizontal arrow indicates the increase in melting temperature with increasing **NC** concentration. b) CD spectrum of **T2** and **T3** (5 μM each) measured in sodium cacodylate buffer (10 mM, pH 7.0) and NaCl (100 mM) at 25 °C in the absence (black) and presence of **NC** at 5 μM (red), 10 μM (blue), 15 μM (green), and 20 μM (purple).

increasing concentrations of **NC**, the transition from dsDNA to ssDNA became apparent and shifted toward a higher-temperature region. Notably, the $T_m$ value for **T2** and **T3** reached 58.8 °C in the presence of 100 μM **NC**, thus showing the formation of a stable, **NC**-bound **T2**/**T3** duplex at room temperature.

The transition of ssDNA to dsDNA of **T2** and **T3** during titration with **NC** was monitored by circular dichroism (CD) spectroscopy (Figure 4b). Without **NC**, the CD spectrum of the mixture of **T2** and **T3** showed a positive band at 272 nm and a negative band at 250 nm. After addition of **NC**, the ellipticity of the positive band increased on increasing the amount of **NC** from one to four molar equivalents. In addition, the induced CD bands observed at 348 and 324 nm also changed their magnitude in response to the **NC** concentration. The change in CD involved the isodichroic points, and showed the transition of single-stranded **T2** and **T3** to the **NC**-bound duplex. The formation of the **NC**-bound duplex was further supported by CSI-TOF MS observations which indicated a 2:1 complex of **NC** with **T2**/**T3**. Again, the stoichiometry was exclusively 2:1. A selective strand cleavage of the 11-mer 5′-d(GCAATGGTTGC)-3′ (**T4**) at the T component in the TGG/TGG sequence was also confirmed by $KMnO_4$ oxidation upon binding of **NC** to the **T4**/**T4** duplex followed by heating with piperidine. In contrast, the protection of the other two T units from oxidation by $KMnO_4$ indicated that these components are in the intrahelical position (see Supporting Information).

The results described herein showed that **NC** could stabilize not only the two contiguous T–G and G–G mismatches in the TGG/CGG sequence, but also the three contiguous T–G, G–G, and G–T mismatches in the TGG/TGG sequence. By choosing an appropriate DNA sequence, two ssDNA molecules that do not spontaneously hybridize with each other could be adhered by the binding of **NC** to the TGG/TGG sequence. On the basis of **NC** binding to the CGG/CGG sequence, we used the TGG/TGG sequence in which the C component is substituted with another pyrimidine nucleotide base. In fact, the C component in the CGG/CGG sequence could be substituted with purine bases A and G, as evidenced by the CSI-TOF MS of the **NC**-bound complex for the AGG/AGG and GGG/GGG sequences. These results will be reported elsewhere. The molecule **NC** represents a new class of substances that function as molecular glue, not only in DNA hybridization but also in modulating the DNA secondary structure.

Received: March 25, 2006
Revised: May 26, 2006
Published online: July 21, 2006

**Keywords:** DNA · hybridization · mass spectrometry · nucleotides

[1] E. Winfree, F. Liu, L. A. Wenzler, N. C. Seeman, *Nature* **1998**, *394*, 539–544.
[2] B. Yurke, A. J. Turberfield, A. P. Mills, Jr., F. C. Simmel, J. E. Neumann, *Nature* **2000**, *406*, 605–608.
[3] H. Yan, S. H. Park, G. Finkelstein, J. H. Reif, T. H. LaBean, *Science* **2003**, *301*, 1882–1884.
[4] M. Endo, T. Majima, *Angew. Chem.* **2003**, *115*, 5922–5925; *Angew. Chem. Int. Ed.* **2003**, *42*, 5744–5747.
[5] S. Liao, N. C. Seeman, *Science* **2004**, *306*, 2072–2074.
[6] B. Ghosn, F. R. Haselton, K. R. Gee, W. T. Monroe, *Photochem. Photobiol.* **2005**, *81*, 953–959.
[7] H. Asanuma, T. Ito, T. Yoshida, X. Liang, M. Komiyama, *Angew. Chem.* **1999**, *111*, 2547–2549; *Angew. Chem. Int. Ed.* **1999**, *38*, 2393–2395.
[8] H. Asanuma, X. Liang, T. Yoshida, A. Yamazawa, M. Komiyama, *Angew. Chem.* **2000**, *112*, 1372–1374; *Angew. Chem. Int. Ed.* **2000**, *39*, 1316–1318.
[9] X. G. Liang, H. Asanuma, M. Komiyama, *J. Am. Chem. Soc.* **2002**, *124*, 1877–1883.

 © 2006 Wiley-VCH Verlag GmbH & Co. KGaA, Weinheim 

[10] K. Hamad-Schifferli, J. J. Schwartz, A. T. Santos, S. G. Zhang, J. M. Jacobson, *Nature* **2002**, *415*, 152 – 155.
[11] J. Yang, J. Y. Lee, H.-P. Too, G.-M. Chow, *Biophys. Chem.* **2006**, *120*, 87 – 95.
[12] T. Peng, K. Nakatani, *Angew. Chem.* **2005**, *117*, 7446 – 7449; *Angew. Chem. Int. Ed.* **2005**, *44*, 7280 – 7283.
[13] K. Nakatani, S. Hagihara, Y. Goto, A. Kobori, M. Hagihara, G. Hayashi, M. Kyo, M. Nomura, M. Mishima, C. Kojima, *Nat. Chem. Biol.* **2005**, *1*, 39 – 43.
[14] K. Yamaguchi, *J. Mass Spectrom.* **2003**, *38*, 473 – 490.
[15] H. Hayatsu, T. Ukita, *Biochem. Biophys. Res. Commun.* **1967**, *29*, 556 – 561.
[16] C. M. Rubin, C. W. Schmid, *Nucleic Acids Res.* **1980**, *8*, 4613 – 4620.
[17] A. M. Maxam, W. Gilbert, *Methods Enzymol.* **1980**, *65*, 499 – 560.
[18] J. A. Gogos, M. Karayiorgou, H. Aburatani, F. C. Kafatos, *Nucleic Acids Res.* **1990**, *18*, 6807 – 6814.

 © 2006 Wiley-VCH Verlag GmbH & Co. KGaA, Weinheim 

Electron Transfer

DOI: 10.1002/anie.200601379

# Non-Exponential Distance Dependence of Bridge-Mediated Electronic Coupling**

*Mattias P. Eng and Bo Albinsson**

Long-range electron transfer (ET) and triplet-energy transfer (TET) are governed by the through-bond electronic coupling ($V_{DA}$). As this coupling is of the exchange type and is related to orbital overlap, it is generally believed to decay exponentially with distance [Eq. (1)].

$$V_{DA} = V_0 \exp\left(-\frac{\beta}{2} R_{DA}\right) \quad (1)$$

In Equation (1), $R_{DA}$ is the donor–acceptor (D–A) separation, $V_0$ is the electronic coupling at contact distance, and $\beta$ is an attenuation factor characteristic of the intervening medium. This simple expression has been used to analyze the distance dependence for electron and energy transfer in a vast number of donor–bridge–acceptor (DBA) systems for which characteristic $\beta$ values have been suggested.[1–5] In addition, it is expected that the electronic coupling is proportional to the inverse of the energy gap between the relevant bridge and donor states [Eq. (2)].

$$V_{DA} = \frac{V_{DB} V_{BA}}{\Delta} \left(\frac{v}{\Delta}\right)^{m-1} \quad (2)$$

[*] M. P. Eng, Prof. B. Albinsson
Chalmers University of Technology
Department of Chemical and Biological Engineering
412 96 Göteborg (Sweden)
Fax: (+46) 317-723-858
E-mail: balb@chalmers.se

[**] This work is supported by grants from the Swedish Research Council (VR).

Supporting information for this article is available on the WWW under http://www.angewandte.org or from the author.

This relation, first derived by McConnell,[6] gives the through-bond donor–acceptor interaction for a chain of $m$ identical units with nearest neighbor interactions $v$ and energy gaps $\Delta$ between the relevant donor and bridge localized states. For $v/\Delta \ll 1$, it can easily be shown that Equation (2) leads to exponential distance dependence. In DBA systems with π-conjugated bridges ("wires"), it is more difficult to dissect the bridge into well-defined chain elements and the validity of Equations (1) and (2) might be questioned. In general, experimental studies of the distance dependence of ET and TET are analyzed with Equation (1) and the estimated $\beta$ values regarded as bridge-specific parameters. We will show in this communication that: 1) $\beta$ is not a bridge-specific parameter for π-conjugated bridges; 2) Equation (1) is not valid in cases for which the energy of the bridge states vary strongly with bridge length, that is, the distance dependence of the exchange interaction might be non-exponential.

We have been interested for quite some time in understanding bridge-mediated electronic coupling. Carefully designed DBA systems with porphyrin donors and acceptors and with different bridging structures have been investigated experimentally. The metallation states of the porphyrins were varied to allow selective studies of ET, TET, and singlet-energy transfer, SET. In one set of systems with constant D–A separation, the donor–bridge energy-gap dependence was mapped out,[7] and in another set the distance dependence was investigated.[8–10] In parallel to the experimental studies, we have developed a DFT-based quantum-mechanical method to calculate the electronic coupling for ET, TET, and SET. In particular, the calculations for TET were shown to give excellent quantitative agreement with the experiments if an appropriate conformational-averaging procedure was employed.[8] Inspired by the success of the calculations, we have expanded our study to include other important π-conjugated bridges and to specifically investigate how the distance dependence for the TET electronic coupling varies with the donor–bridge energy gap for a set of oligo(phenyleneethenylene) (OPE) bridges.

The electronic coupling $V_{DA}$ was deduced from the TD-B3LYP/6-31G(d)-calculated (Gaussian 03[11]) energy splitting of the two lowest triplet states of the symmetric donor–bridge–donor (DBD) molecules as described in the Supporting Information. Calculating the values of $V_{DA}$ for OPE bridges with edge–edge separations of between 12 and 37 Å ($x = 2$–5) and linear fits of $\ln V_{DA}$ versus $R_{DA}$ yielded the $\beta$ values. This was done for the seven different donors (Table 1), which have calculated lowest triplet energies of between 15450 $cm^{-1}$ and 4660 $cm^{-1}$. The fits are excellent (Figure 1a) and the slopes vary systematically with the variation of the donor–bridge energy gap. This shows that $\beta$ is sensitive to the appended donor and acceptor and, thus, is not a bridge-specific parameter. In fact, from the McConnell model the $\beta$ values are expected to vary with the donor–bridge energy gap as described in Equation (3).

$$\beta = \frac{2}{R_0} \ln\left|\frac{\Delta}{v}\right| \quad (3)$$


InterScience DISCOVER SOMETHING GREAT
© 2006 Wiley-VCH Verlag GmbH & Co. KGaA, Weinheim

***Table 1:*** Model systems for mapping out the donor–bridge energy gap dependence of $\beta$ for the OPE bridge structure (see Table 2).

| Donor | | $E_D(T_1)$ [cm$^{-1}$] | $\beta$ [Å$^{-1}$] |
|---|---|---|---|
| 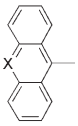 | Acr (X = N) | 15 450 | 0.10 |
| | A (X = CH) | 14 520 | 0.18 |
| 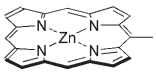 | ZnPor | 14 340 | 0.19 |
| 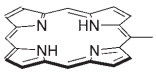 | $H_2$Por | 11 720 | 0.32 |
| 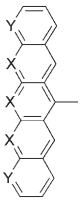 | P5N (X = Y = N) | 8770 | 0.39 |
| | P3N (X = N, Y = CH) | 6100 | 0.43 |
| | P (X = Y = CH) | 4660 | 0.47 |

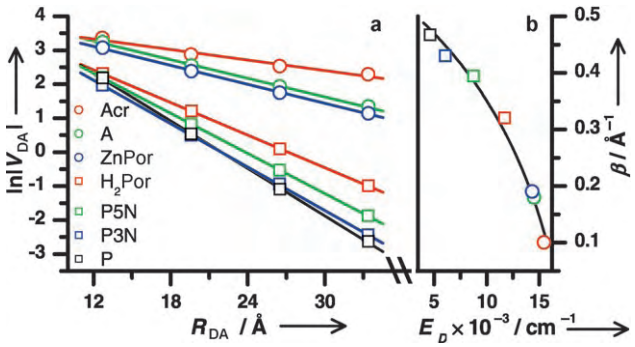


***Figure 1.*** a) ln $V_{DA}$ versus $R_{DA}$ for the OPE bridges with acridine (Acr), anthracene (A), zinc(II) porphine (ZnPor), free-base porphine ($H_2$Por), 4,5,6,7,8-pentaazapentacene (P5N), 5,6,7-triazapentacene (P3N), and pentacene (P) as donor chromophores. b) The obtained $\beta$ values plotted versus the calculated donor excitation energy (symbols) and the fit of Equation (3) to the data (solid line).

In Equation (3), $\Delta = E_{B'} - E_D$, $E_{B'}$ and $R_0$ are the (hypothetical) triplet energy and length of the repeating unit, respectively, and $E_D$ is the triplet energy of the donor. Figure 1b shows this variation along with a best fit to Equation (3) to yield values for the bridge unit coupling, $v = 2944$ cm$^{-1}$ and $E_{B'} = 19\,884$ cm$^{-1}$.[12] The coupling between the subunits of the OPE bridge is quite substantial as expected for a π-conjugated system, but the ratio $v/\Delta = 0.15$ is still small enough to give an exponential dependence on distance. It should be noted that the triplet energy of the bridge subunit extracted from the fit is significantly smaller than the triplet energy of phenyleneethynylene (26 123 cm$^{-1}$), which demonstrates that estimating the effective energy gap in the superexchange model is quite difficult and, thus, use of Equation (3) for quantitative predictions might yield misleading results.

In another study, we calculated $V_{DA}$ for the pentacene donor (P) with different bridging structures (see Supporting Information) Pentacene was chosen because it has the lowest triplet energy among the donors shown in Table 1 to allow for bridges that have low triplet energies.

In Table 2 the investigated bridges along with the resulting $\beta$ values are listed, and the calculated electronic coupling is displayed in Figure 2. The approximate exponential dependence on distance found for the OPE bridge was also observed for the OTP and OPV bridges. However, for the bridges with non-aromatic repeating structures, OE, Ph-OE, OV, and Ph-OV, different behavior was observed. All these bridges show distinct non-exponential distance dependence; the electronic coupling increases with increasing distance in certain regions. Clearly, the data from these bridges cannot be analyzed with the McConnell superexchange model.

***Table 2:*** Model systems for mapping out the variation of $|V_{DA}|$ with the bridge structure.[a,b]

| Bridge | | $E(T_1)$ range [cm$^{-1}$] | $\beta$ [Å$^{-1}$] |
|---|---|---|---|
| 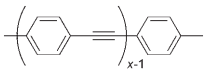 | OPE | 21 600–16 100 | 0.47 |
| 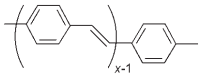 | OPV | 18 500–13 000 | 0.42 |
| | OTP | 18 700–11 200 | 0.37 |
| | OE | 27 200–7800 | –[c] |
| 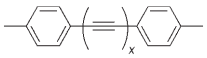 | Ph-OE | 21 600–8700 | –[c] |
| | OV | 22 400–5700 | –[c] |
| 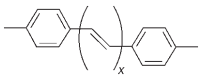 | Ph-OV | 18 500–4900 | –[c] |

[a] Donor/Acceptor: Pentacene, $E(T_1) = 4660$ cm$^{-1}$. [b] OPE is oligo(phenyleneethenylene) ($x = 2$–5), OPV is oligo(phenylenevinylene) ($x = 2$–5), OTP is oligo(thiophene) ($x = 2$–5), OE is oligo(ethylene) ($x = 2$–11), Ph-OE is phenyl end capped oligo(ethylene) ($x = 1$–8), OV is oligo(vinylene) ($x = 2$–10), and Ph-OV is phenyl end capped oligo(vinylene) ($x = 1$–10). [c] Non-exponential, see text.

As an alternative to the superexchange model, which dissects the bridge into subunits, the molecular bridges could be regarded as a single tunneling barrier of width $R_{DA}$ and height $\Delta E$. In contrast to the superexchange model, the variation of $\Delta E$ with $R_{DA}$ has to be considered explicitly. For this simple model the electronic coupling is given by Equation (4).[13]

$$V_{DA} = \frac{\alpha}{\Delta E} \exp(-\rho\sqrt{\Delta E} R_{DA}) \qquad (4)$$

 © 2006 Wiley-VCH Verlag GmbH & Co. KGaA, Weinheim 

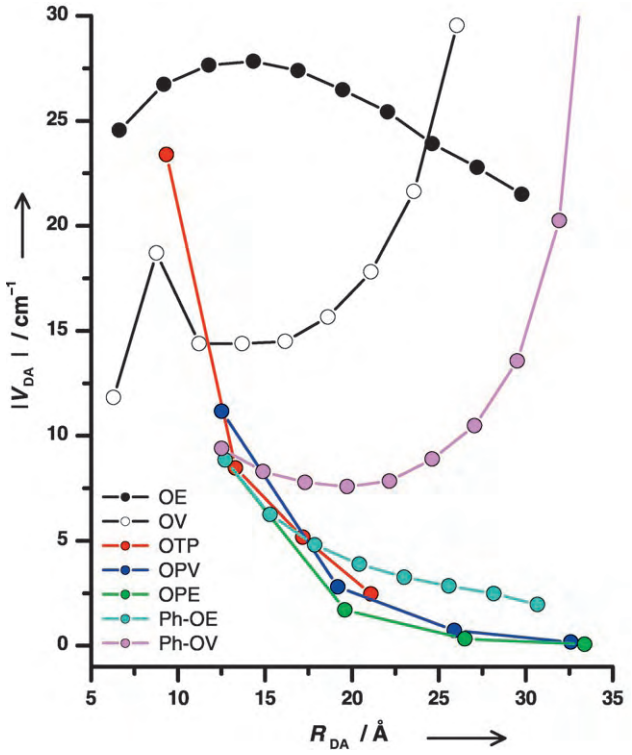


***Figure 2.*** The calculated electronic coupling $|V_{DA}|$ versus $R_{DA}$ for pentacene as donor chromophore with the various bridges. The electronic coupling for the OE-bridge has been multiplied by a factor of 0.15.

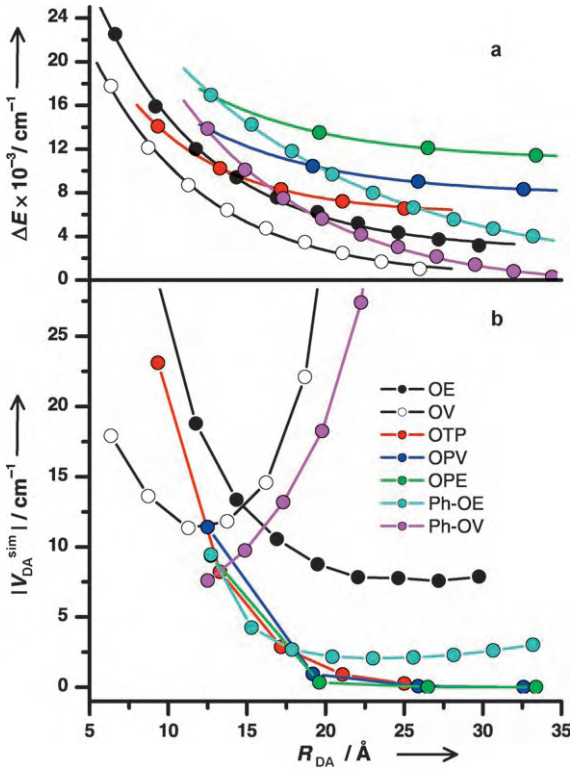


***Figure 3.*** a) The calculated energy barrier for tunneling $\Delta E$ versus $R_{DA}$ for various bridges with pentacene as donor chromophore and exponential fits to Equation S1 in the Supporting Information. b) The simulated electronic coupling $|V|_{DA}^{sim}$ derived by using Equation (4) and the calculated $\Delta E$ values; $\rho = 0.0057$ Å$^{-1}$ cm$^{1/2}$ (two tunneling electrons).

In Equation (4), $\alpha$ is a system-specific parameter related to the donor–bridge coupling but not dependent on $R_{DA}$; $\rho$, at least in principle, is related to the effective mass of the virtual tunneling electron(s). Simulations show that Equation (4) can qualitatively describe the anomalous behavior of the OE, Ph-OE, OV, and Ph-OV bridges as well as the normal exponential behavior of the OPE, OPV, and OTP bridges (Figure 3). The distance dependence of the electronic coupling is easily accessible through Equation (4) once the distance dependence of the triplet excitation energy is known. In Figure 3a the calculated tunneling barriers, $\Delta E$ (estimated from the difference between the energies of the lowest triplet states of the bridges and pentacene), are shown together with exponential fits. The calculated energies agree almost quantitatively with the experimental energies in those cases for which the information is available (see Supporting Information). Figure 3b shows the distance dependence of the electronic coupling estimated from Equation (4) by using the calculated triplet energies and by assuming a common decay parameter, $\rho = 0.0057$ Å$^{-1}$ cm$^{1/2}$, which corresponds to the mass of two (virtual) tunneling electrons. The simulated electronic coupling has an approximately exponential distance dependence for the OPE, OPV, and OTP bridges but shows more complex behavior for the other four bridges. This is qualitatively the same distance dependence as that observed in the quantum-mechanical calculations and below we present our reasoning for this unexpected agreement.

From Equation (4) a local $\beta$ value can be analytically calculated for the tunneling model [Eq. (5)].

$$\beta^{loc} = -2\frac{d \ln V_{DA}}{dR} = 2\frac{d\Delta E}{dR}\left(\frac{1}{\Delta E} + \frac{\rho R}{2\sqrt{\Delta E}}\right) + 2\rho\sqrt{\Delta E} \qquad (5)$$

The first term of this equation gives a negative contribution that tends to zero as $R$ increases and the second term gives a positive contribution that tends to $2\rho\Delta E_{\infty}^{1/2}$, which is the limiting $\beta$ value for a bridge long enough to show negligible variations in the energy gap. If the variation of the bridge energy is large (i.e., large $d\Delta E/dR$) the attenuation factor ($\beta^{loc}$) is negative. In regions where $\Delta E$ varies quickly with distance, the pre-exponential factor of Equation (4) causes the electronic coupling to increase over a limited $R_{DA}$ range. This variation is qualitatively what has been observed for the OE, Ph-OV, and OV bridges and we conclude that in certain cases it is necessary to use a model, such as Equation (4), that allows for the interplay between the donor–bridge energy gap and donor–acceptor distance.

The simple tunneling model is not expected to give quantitative results but it is not possible to obtain correct results from the superexchange model either. In particular, for small values of $\Delta E$ the electronic coupling increases rapidly both in the tunneling model and in the quantum-mechanical calculations. This behavior is expected because at

 © 2006 Wiley-VCH Verlag GmbH & Co. KGaA, Weinheim 

near degeneracy, the wavefunctions of the bridge and donor mix strongly and the identities of the different chromophores are lost. Experimentally, in such a situation ($\Delta E < 3000\ cm^{-1}$), a non-coherent hopping mechanism is difficult to avoid and the rate for ET or TET is no longer dictated by the direct transfer between the donor and acceptor but through a relay mechanism involving states populated at the bridge.[14] However, as can be seen in both Figure 2 and Figure 3, the anomalous distance dependence is also observed in situations for which the barrier exceeds 10000 $cm^{-1}$ and we believe that the strong distance dependence of the excitation energies of the bridges is responsible for this effect.

In this study, we have calculated the bridge-mediated electronic coupling for TET, but the results are expected to be general for any exchange-type coupling. There are several reasons for calculating the TET couplings: 1) there are no or small solvent-reorganization energies, which for ET processes add additional distance dependence; 2) bridge and donor state energies are easily accessible; 3) there is very good correlation between the experimentally determined and calculated couplings for OPE-bridged porphyrin systems.[8]

Wasielewski and co-workers recently reported two cases for which anomalous distance dependence were experimentally observed.[14,15] Electron transfer mediated by OPV and fluorene oligomers showed a strongly non-exponential dependence on distance. However, both of these cases involve switching between a superexchange mechanism and a non-coherent hopping mechanism that uses bridge-localized states.[15] In contrast, for the systems studied in this paper (Table 2), the donor–bridge energy gap is too large to have significant contributions from a hopping mechanism, at least for the shorter members of the OE, OV, Ph-OE, and Ph-OV series. Thus, the reason for non-exponential distance dependence is different in this case.

Many experimental studies report very shallow distance dependencies for π-conjugated bridges[2,16] and also for ET in DNA.[17] In addition, the bridge-energy dependence of the $\beta$ values has been suggested in a few experimental studies (most notably in DNA systems),[18] but, to the best of our knowledge, a quantitative demonstration of Equation (3) has not been previously reported. For TET between zinc and free base porphyrins through the OPE bridge, we determined experimentally a $\beta$ value of 0.45 $Å^{-1}$.[8,19] This is quite different from the $\beta$ value (0.11 $Å^{-1}$) previously obtained for this bridge with $[Ru(terpy)_2]$/$[Os(terpy)_2]$ (terpy is 2,2′,6′,2″-terpyridine) donor–acceptor couple by Harriman et al.[2] This difference can entirely be ascribed to the difference in donor–bridge energy gaps [Equation (3)] and, thus, it shows experimentally the importance of not treating $\beta$ as a bridge parameter but a system-specific parameter. We believe that the results presented in this communication are important for the future interpretation of ET and TET reactions.

Received: April 7, 2006
Revised: May 11, 2006
Published online: July 26, 2006

**Keywords:** conjugation · density functional calculations · donor–acceptor systems · electron transfer · electron tunneling

[1] S. Creager, C. J. Yu, C. Bamdad, S. O'Connor, T. MacLean, E. Lam, Y. Chong, G. T. Olsen, J. Y. Luo, M. Gozin, J. F. Kayyem, *J. Am. Chem. Soc.* **1999**, *121*, 1059–1064.
[2] A. Harriman, A. Khatyr, R. Ziessel, A. C. Benniston, *Angew. Chem.* **2000**, *112*, 4457–4460; *Angew. Chem. Int. Ed.* **2000**, *39*, 4287–4290.
[3] A. Helms, D. Heiler, G. McLendon, *J. Am. Chem. Soc.* **1992**, *114*, 6227–6238.
[4] S. B. Sachs, S. P. Dudek, R. P. Hsung, L. R. Sita, J. F. Smalley, M. D. Newton, S. W. Feldberg, C. E. D. Chidsey, *J. Am. Chem. Soc.* **1997**, *119*, 10563–10564.
[5] J. F. Smalley, S. B. Sachs, C. E. D. Chidsey, S. P. Dudek, H. D. Sikes, S. E. Creager, C. J. Yu, S. W. Feldberg, M. D. Newton, *J. Am. Chem. Soc.* **2004**, *126*, 14620–14630.
[6] H. McConnell, *J. Chem. Phys.* **1961**, *35*, 508.
[7] K. Kilså, J. Kajanus, A. N. Macpherson, J. Mårtensson, B. Albinsson, *J. Am. Chem. Soc.* **2001**, *123*, 3069–3080.
[8] M. P. Eng, T. Ljungdahl, J. Mårtensson, B. Albinsson, *J. Phys. Chem. B* **2006**, *110*, 6483–6491.
[9] K. Pettersson, A. Kyrychenko, E. Rönnow, T. Ljungdahl, J. Mårtensson, B. Albinsson, *J. Phys. Chem. A* **2006**, *110*, 310–318.
[10] K. Pettersson, J. Wiberg, T. Ljungdahl, J. Mårtensson, B. Albinsson, *J. Phys. Chem. A* **2006**, *110*, 319–326.
[11] M. J. Frisch, et al., see reference [1] in Supporting Information, Gaussian, Inc., Pittsburgh PA, **2003**.
[12] Based on the assumption that $R_0 = 6.9$ Å (estimated from calculations).
[13] G. Gamov, *Nature* **1928**, *122*, 805–806.
[14] W. B. Davis, W. A. Svec, M. A. Ratner, M. R. Wasielewski, *Nature* **1998**, *396*, 60–63.
[15] R. H. Goldsmith, L. E. Sinks, R. F. Kelley, L. J. Betzen, W. Liu, E. A. Weiss, M. A. Ratner, M. R. Wasielewski, *Proc. Natl. Acad. Sci. USA* **2005**, *102*, 3540–3545.
[16] F. Giacalone, J. L. Segura, N. Martin, J. Ramey, D. M. Guldi, *Chem. Eur. J.* **2005**, *11*, 4819–4834.
[17] S. O. Kelley, J. K. Barton, *Chem. Biol.* **1998**, *5*, 413–425.
[18] F. D. Lewis, J. Q. Liu, W. Weigel, W. Rettig, I. V. Kurnikov, D. N. Beratan, *Proc. Natl. Acad. Sci. USA* **2002**, *99*, 12536–12541.
[19] It should be noted that the experimentally determined $\beta$ values are averages of the conformational distribution of the OPE bridge whereas the values in this article are calculated for planar bridges. Please see reference [8] for a discussion.

 © 2006 Wiley-VCH Verlag GmbH & Co. KGaA, Weinheim 

Molecular Recognition

DOI: 10.1002/anie.200600298

# Nonlinear Self-Excited Oscillation of a Synthetic Ion-Channel-Inspired Membrane

*Taichi Ito and Takeo Yamaguchi**

Nonlinear phenomena are crucially important in future science and engineering. Some researchers have achieved nonlinear oscillations such as the Belousov–Zhabotinskii reaction,[1] chemical reactions on catalysts,[2] rhythmic swelling phenomena of hydrogels,[3] permeation phenomena of membranes,[4,11] swinging motions of lipids,[5] fluorescence oscillation of quantum dots,[6] synthetic metabolators,[7] and rhythmic drug-delivery systems.[8] We have developed a synthetic ion-channel-inspired biomembrane, which we call a molecular recognition ion-gating membrane.[9] This membrane could control both hydrostatic pressure-driven flow[9b,c] and osmotic pressure[9a] in response to $Ba^{2+}$ ions. Herein, we report that our gating membrane generated nonlinear self-excited oscillation in response to $Ba^{2+}$ ions (see Figure 1) by combining these two functions of the membrane.

The response mechanism of the gating membrane is described as follows. A copolymer of *N*-isopropylacrylamide (NIPAM) and benzo[18]crown-6-acrylamide (BCAm) was grafted onto the pore surface of the porous substrate membrane. Poly(NIPAM) is a thermosensitive polymer,[10a] which acts as an actuator of pore opening and closing through its volume phase transition. BCAm[10b] has a crown ether receptor, which works as an ion sensor. Thus, the membrane forms a complex with $Ba^{2+}$, which has a high complex formation constant with crown ether receptors and causes its grafted copolymer to swell. This swelling controls the pore size and hydrostatic flow.[9b,c] Furthermore, the complexed $Ba^{2+}$ ions work as fixed membrane charges, which generate Donnan potential and osmotic pressure.[9a,e]

The present oscillator was inspired by the so-called Teorell oscillator,[11] in which hydrostatic and electroosmotic pressure-driven flow pass back and forth through a negatively charged, glassy, porous membrane, driven by both a constant ion concentration gradient and a constant electric current. Consequently, the oscillator (Figure 1) has a solution chamber and a solvent chamber, with the membrane placed between these two chambers. A capillary was attached to the solution chamber, which was filled with an aqueous ionic solution.

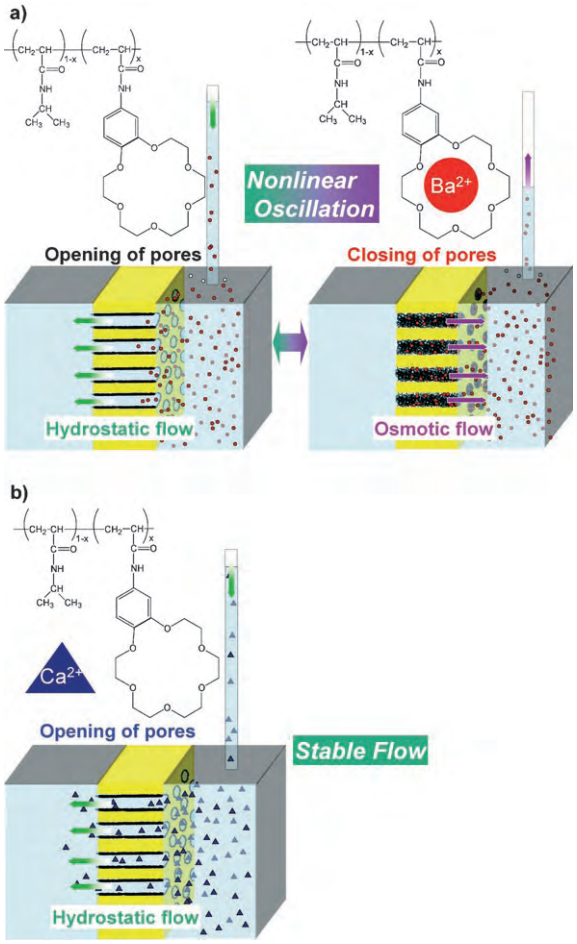


***Figure 1.*** The concept of a nonlinear self-excited oscillator using a molecular recognition ion-gating membrane in response to a specific ion signal. a) The case of aqueous $BaCl_2$ solution. b) The case of aqueous $CaCl_2$ solution. A trace amount of free crown ether was loaded inside the membrane before experimentation.

Thus, the resulting osmotic inflow from the solvent chamber increased the water level in the capillary. In the case of $Ba^{2+}$, the ions enter the membrane with the hydrostatic flow, and the membrane closes its pores and stops the hydrostatic flow. At the same time, the water level in the capillary decreases. After the pores close, the osmotic flow generated by the Donnan potential pours into the membrane in the opposite direction to the hydrostatic flow. This osmotic flow eliminates the complexed ions from the membrane; simultaneously, the water level in the capillary gradually increases. When the captured ions are fully eliminated, the pores of the membrane reopen and the hydrostatic flow reenters the membrane. This cycle repeats without external stimuli; therefore, a nonlinear self-excited oscillation occurs. In comparison, other ions such as $Ca^{2+}$ do not form complexes with the membrane. Consequently, the membrane does not generate an osmotic flow, and oscillation does not occur.

The membrane was prepared by a peroxide plasma graft polymerization method, as described in an earlier publication[2b] and the Supporting Information. SEM images of the membrane prepared in the present study are shown in Figure 2. Nanosized, ionic-stimulus-responsive pores were

[*] Dr. T. Ito,[+] Prof. T. Yamaguchi
Department of Chemical System Engineering
The University of Tokyo
7-3-1 Hongo, Bunkyo-ku, Tokyo 113-8656 (Japan)
Fax: (+81) 3-5841-7227
E-mail: yamag@chemsys.t.u-tokyo.ac.jp
[+] Present address: Department of Chemical Engineering
Massachusetts Institute of Technology (USA)

Supporting information for this article is available on the WWW under http://www.angewandte.org or from the author.


WILEY InterScience DISCOVER SOMETHING GREAT
© 2006 Wiley-VCH Verlag GmbH & Co. KGaA, Weinheim

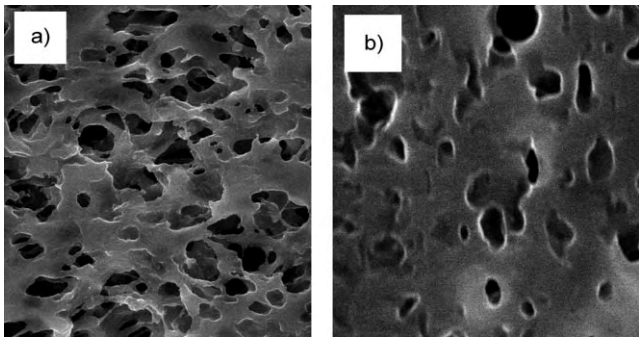


***Figure 2.*** SEM images of membrane surfaces a) before plasma graft polymerization, b) after plasma graft polymerization.

formed successfully. Then, filtration experiments were performed using previously reported methods.[9b,c] Osmotic flow was measured without attaching the capillary. The concentration of $Ba^{2+}$ ions was increased from 0 to 100 mM in both filtration experiments and osmotic flow measurements. Finally, oscillation experiments were performed using a pressure sensor (Keyence, AP-12A) to measure the hydraulic pressure resulting from changes in the water level, which was recorded by a personal computer at intervals of 1 s. The cross-sectional area of the attached capillary was 0.024 $cm^2$. The solvent chamber and the solution chamber were filled with pure water and aqueous $BaCl_2$, $CaCl_2$, or KCl solution of different concentrations between 0 and 100 mM, respectively. In some of the experiments, the membrane was immersed in aqueous benzo[18]crown-6 (10 mM) and then washed thoroughly with pure water. The temperature was maintained at 41 °C in all the experiments. If a fluctuation of the water level was observed, it meant that the intended nonlinear oscillation was obtained.

Figure 3 shows the dependence of both the hydrostatic flow (■), measured by filtration experiments, and the osmotic flow (○) on $BaCl_2$ concentration. This relationship indicates that both the pore-opening and pore-closing states can exist, depending on the value of the hydrostatic pressure, when the

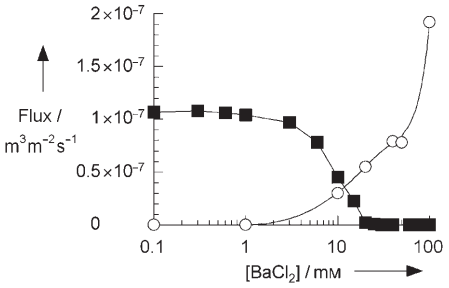


***Figure 3.*** The hydrostatic and osmotic volume flux through the molecular recognition ion-gating membrane. The permeation volume fluxes through the membrane of aqueous $BaCl_2$ solutions of different concentrations were measured at different applied pressures at 41 °C. At $\Delta P = 30$ kPa (306.1 cm $H_2O$) (■), hydrostatic pressure permitted the flow from the ion-fed side into the membrane despite the closure of the pores of the membrane. In contrast, at $\Delta P = 0$ kPa (0 cm $H_2O$) (○), osmotic pressure generated the volume flux from the pure water side into the ion-fed side. Hence, the direction of volume flux depended on the applied hydrostatic pressure.

$BaCl_2$ concentration is around 20 mM. Thus, both hydrostatic and osmotic flow can be generated, and the water level of the attached capillary can increase or decrease. This finding indicates that the proposed oscillation phenomena can occur in this region.

Following from the above results, oscillation experiments were performed using aqueous $BaCl_2$ solutions with concentrations between 20 and 50 mM. However, the water level in the capillary increased monotonically. In the case of $CaCl_2$, the water level decreased monotonically, and became constant at zero. As a result, the nonlinear self-excited oscillation did not occur.

To trigger the oscillation, we added a 10 mM solution of benzo[18]crown-6 to the pure water chamber. The oscillation occurred against 100 mM $BaCl_2$ solution. After this oscillation, the membrane was cleaned carefully with pure water several times; oscillation experiments against a 40 mM $BaCl_2$ solution were performed on the sixth, eighth, 25th, 26th, and 28th days after the addition of crown ether. Although only trace amounts of crown ether remained in the membrane because of the repeated washes in pure water at each time point, oscillations in water level occurred as shown in Figure 4. The oscillation disappeared on the 28th day. Over time, the water level gradually increased during the nonlinear oscillation. The increases in water level indicate osmotic flow resulting from both the closing of the pores and the Donnan potential, while the decreases in water level indicate hydrostatic flow resulting from opening of the pores. The continual switch of the water level shows that opening and closing of the pores occurred autonomously and alternately without external stimuli.

To focus on the oscillation periods, they were random. Although not uniform, the oscillations on the sixth day were relatively regular (see Figure 4a). The period of osmotic flow was always about 1100 s. That of hydrostatic flow was initially about 250 s; it then decreased to about 1 s with increasing water level. This result indicates that the pore-closing mode is slow and the pore-opening mode is very fast; therefore, this oscillation is classified as a relaxation oscillation, which consists of a fast mode and a slow mode. The amplitude of the oscillation was almost constant (see Figure 4a–d). The quantity of ions that the hydrostatic flow supplied to the membrane in one wave can be estimated as about 10.5 μmol from the average amplitude of 1.8 cm $H_2O$ in Figure 4a. In contrast, the total amount of crown ether receptor that was contained in the membrane was 7.3 μmol, as estimated from the amount of grafted poly(NIPAM-*co*-BCAm). These values almost coincide; hence, it is speculated that the amplitude was determined by the mass balance of membrane crown ether receptors and signal ions.

In contrast, the water level decreased monotonically in the case of $CaCl_2$ or KCl (Figure 5), because the pores were always open at 41 °C and a concentration of 40 mM.[9b,c] Only the complex formation constant of $Ba^{2+}$ with crown ether receptors was high enough to generate osmotic pressure and close the pores.

The reproducibility of these phenomena is an especially important point in the field of nonlinear science. After the procedure described above, we reloaded the free crown ether and repeated the same experiments, and the same types of

 © 2006 Wiley-VCH Verlag GmbH & Co. KGaA, Weinheim 

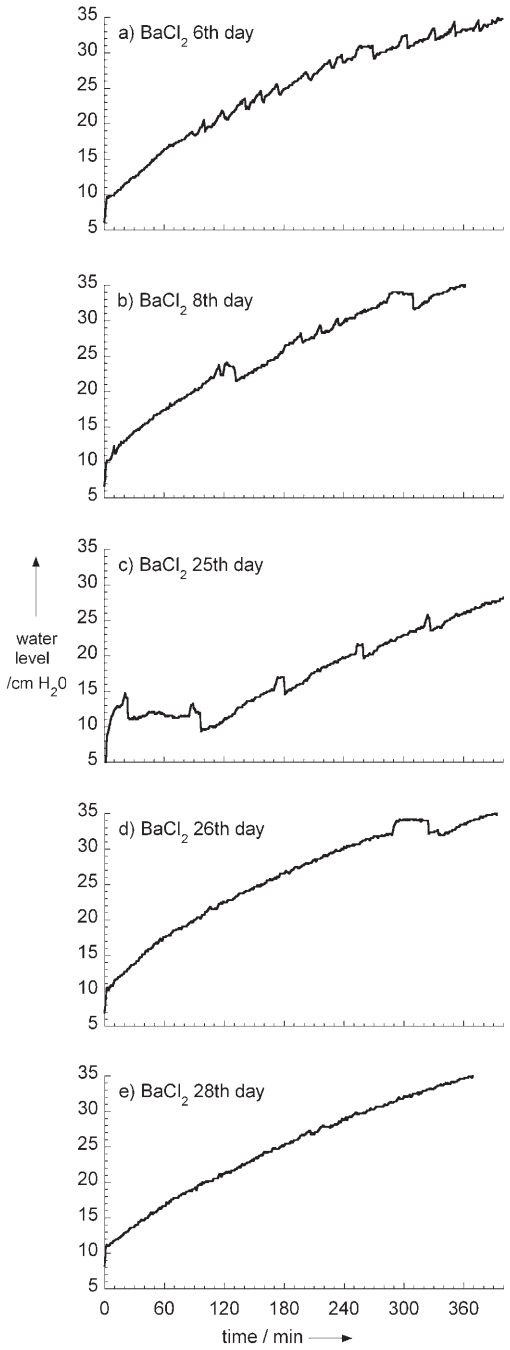


***Figure 4.*** Nonlinear oscillations of the molecular recognition ion-gating membrane. The time course of the water level was measured at 41 °C. The concentration of $BaCl_2$ was 40 mM. The measurements were performed on the a) 6th day, b) 8th day, c) 25th day, d) 26th day, and e) 28th day after the addition of 10 mM crown ether.

oscillations were observed. However, we could not control the oscillation periods and the water level at which the oscillation started. The amplitude was the same as that seen in Figure 4. Consequently, these oscillations are thought to be very sensitive to the initial concentration distribution of the loaded crown ethers inside the gating membrane. We speculate that the loaded crown ethers were transported to the membrane by the osmotic flow, where they may have

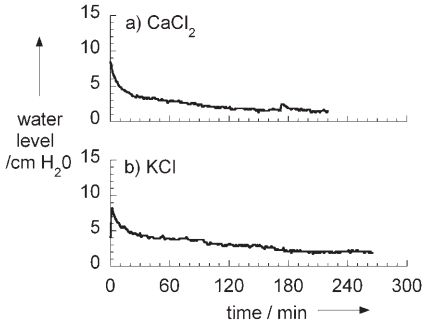


***Figure 5.*** Monotonous decrease of the water level without oscillation measured at 41 °C. The concentration of a) $CaCl_2$ or b) KCl was 40 mM. The measurements were performed on the same day with the addition of 10 mM crown ether.

eliminated $Ba^{2+}$ ions that were complexed with crown ether receptors in the grafted copolymer. The details of the oscillation mechanism are still unclear, so further research is ongoing.

In summary, the molecular recognition ion-gating membrane opened and closed its pores autonomously and alternately in response to $Ba^{2+}$ ions; namely, the membrane generated a nonlinear self-excited oscillation like an ion channel of a biomembrane. This oscillation was a typical relaxation oscillation. By changing the receptor moiety of the grafted polymer,[12] various gating membrane oscillation systems that respond to other molecular signals could be designed in the future. This type of oscillator is expected to lead to novel dynamic devices such as pulsatile drug-delivery systems, new affinity separation systems, microchips to handle information nonlinearly, and actuators that respond to various molecular signals.

Received: January 23, 2006
Revised: May 12, 2006
Published online: July 20, 2006

**Keywords:** crown compounds · ion channels · membranes · molecular recognition · nonlinear oscillation

[1] a) A. N. Zaikin, A. M. Zhabotinsky, *Nature* **1970**, *225*, 535–537; b) G. Nicolis, I. Prigogine, *Self-Organization in Nonequilibrium Systems*, Wiley, New York, **1977**.
[2] a) G. Ertl, *Science* **1991**, *254*, 1750–1755; b) H. H. Rotermund, W. Engel, M. Kordesch, G. Ertl, *Nature* **1990**, *343*, 355–357.
[3] a) V. E. Shashoua, *Nature* **1967**, *215*, 846–847; b) A. Katchalsky, R. Spangler, *Q. Rev. Biophys.* **1968**, *1*, 127–175; c) Y. Osada, H. Okuzaki, H. Hori, *Nature* **1992**, *355*, 242–244; d) R. Yoshida, H. Ichijo, T. Hakuta, T. Yamaguchi, *Macromol. Rapid Commun.* **1995**, *16*, 305–310; e) R. Yoshida, T. Takahashi, T. Yamaguchi, H. Ichijo, *J. Am. Chem. Soc.* **1996**, *118*, 5134–5135.
[4] a) K. Yoshikawa, S. Maeda, H. Kawakami, *Ferroelectrics* **1988**, 86, 281–298; b) R. Larter, *Chem. Rev.* **1990**, *90*, 355–381; c) R. P. Rastogi, R. C. Srivastava, S. N. Singh, *Chem. Rev.* **1993**, *93*, 1945–1990; d) S. Kihara, K. Maeda, *Prog. Surf. Sci.* **1994**, 47, 1–54; e) N. Minoura, S. Aiba, Y. Fujiwara, *J. Am. Chem. Soc.* **1993**, *115*, 5902–5906; f) A. Higuchi, M. Hara, *J. Phys. Chem.* **1996**, *100*, 2183–2188.
[5] S. M. Nomura, T. Harada, K. Yoshikawa, *Phys. Rev. Lett.* **2002**, *88*, 093903.

 © 2006 Wiley-VCH Verlag GmbH & Co. KGaA, Weinheim 

[6] A. Komoto, S. Maenosono, Y. Yamaguchi, *Langmuir* **2004**, *20*, 8916 – 8923.
[7] a) E. Fung, W. W. Wong, J. K. Suen, T. Bulter, S. G. Lee, J. C. Liao, *Nature* **2005**, *435*, 118 – 122; b) D. Sprinzak, M. B. Elowitz, *Nature* **2005**, *438*, 443 – 448.
[8] a) R. A. Siegel, C. G. Pitt, *J. Controlled Release* **1995**, *33*, 173 – 188; b) G. P. Misra, R. A. Siegel, *J. Controlled Release* **2002**, *81*, 1 – 6; c) A. P. Dhanarajan, G. P. Misra, R. A. Siegel, *J. Phys. Chem. A* **2002**, *106*, 8835 – 8838.
[9] a) T. Ito, T. Yamaguchi, *J. Am. Chem. Soc.* **2004**, *126*, 6202 – 6203; b) T. Ito, T. Hioki, T. Yamaguchi, T. Shinbo, S. Nakao, S. Kimura, *J. Am. Chem. Soc.* **2002**, *124*, 7840 – 7846; c) T. Yamaguchi, T. Ito, T. Sato, T. Shinbo, S. Nakao, *J. Am. Chem. Soc.* **1999**, *121*, 4078 – 4079; d) S. Okajima, Y. Sakai, T. Yamaguchi, *Langmuir* **2005**, *21*, 4043 – 4049; e) H. Ohashi, N. Miyaoi, T. Yamaguchi, unpublished results.
[10] a) Y. Hirokawa, T. Tanaka, *J. Chem. Phys.* **1984**, *81*, 6379 – 6380; b) M. Irie, Y. Misumi, T. Tanaka, *Polymer* **1993**, *34*, 4531 – 4535.
[11] a) T. Teorell, *J. Gen. Physiol.* **1959**, *42*, 831 – 845; b) T. Teorell, *J. Gen. Physiol.* **1959**, *42*, 847 – 863; c) Y. Kobatake, H. Fujita, *J. Chem. Phys.* **1964**, *40*, 2212 – 2218; d) Y. Kobatake, H. Fujita, *J. Chem. Phys.* **1964**, *40*, 2219 – 2222; e) R. P. Rastogi, G. Srinivas, R. C. Srivastava, P. C. Pandey, A. P. Mishra, A. R. Singh, *J. Colloid Interface Sci.* **1995**, *175*, 262 – 275; f) R. P. Rastogi, G. P. Mishra, P. C. Pandey, K. Bala, K. Kumar, *J. Colloid Interface Sci.* **1999**, *217*, 275 – 287.
[12] a) K. Sumaru, M. Kameda, T. Kanamori, T. Shinbo, *Macromolecules* **2004**, *37*, 4949 – 4955; b) A. Matsumoto, T. Kurata, D. Shiino, K. Kataoka, *Macromolecules* **2004**, *37*, 1502 – 1510; c) Z. R. Lu, P. Kopeckova, J. Kopecek, *Macromol. Biosci.* **2003**, *3*, 296 – 300; d) E. Kokufata, Y. Q. Zhang, T. Tanaka, *Nature* **1991**, *351*, 302 – 304.

 © 2006 Wiley-VCH Verlag GmbH & Co. KGaA, Weinheim 

Protein Engineering

DOI: 10.1002/anie.200600382

# Engineering Proteins with Novel Mechanical Properties by Recombination of Protein Fragments**

*Deepak Sharma, Yi Cao, and Hongbin Li**

The mechanical properties of proteins are crucial in living cells as proteins serve as basic units in cells to constantly sense, generate, and bear mechanical forces.[1,2] Outside the cell, nature exploits the mechanical features of proteins and produces a variety of materials with superb mechanical properties (e.g. spider dragline silk[3,4]) which often outperform man-made materials. Studies of the mechanics of proteins are not only important in understanding fundamental biophysical principles underlying various biological processes,[5] but they also underscore the great potential in engineering protein-based advanced materials and using proteins as building blocks for the bottom-up construction of functional nanomechanical devices.[6]

Despite the great significance of mechanical proteins, the investigation of the mechanical design of these proteins at the single-molecule level was not possible until the development of single-molecule force spectroscopy techniques a few years ago.[7–11] Since then, single-molecule atomic force microscopy (AFM) has become the workhorse in the field of protein nanomechanics.[5,12–15] Initial single-molecule AFM studies focused on naturally occurring mechanical proteins that are placed under stretching force under physiological conditions, such as the immunoglobulin (Ig) domains of the giant muscle protein titin and the fibronectin type III domains from fibronectin and tenascin.[7,10,11,16–19] Recently, non-mechanical proteins have also been studied by single-molecule force spectroscopy in the search for mechanically stable protein folds and to expand the toolbox of mechanical proteins.[20–25] With the increasing understanding of the relationship between protein structure and protein mechanical stability, scientists have attempted to engineer or modify the mechanical properties of proteins. Such efforts are limited to site-directed mutagenesis.[19,26–28] With the advent of nanobiotechnology, it is desired to engineer novel multifunctional mechanical proteins that combine desired mechanical properties with other functional properties, such as enzymatic activity. Site-directed mutagenesis may not suffice for such challenges. Here, we demonstrate the feasibility and the first attempt towards engineering novel mechanical proteins through DNA-shuffling-based recombination.

Recombination is an important mechanism for proteins to acquire novel functions. Recombination offers the advantage of combining beneficial mutations from multiple parents into a single offspring and has been exploited extensively by nature during evolution in improving protein traits such as enzymatic activity. This method has also been used extensively in the directed-evolution of proteins in the laboratory and has become one of the most important strategies in engineering proteins with novel functions.[29,30] Recombination is based on DNA-shuffling of proteins sharing high sequence homology and identity. Recent developments have extended this method to proteins that are distantly related and share low sequence homology.[31,32] Here, as a proof of principle, we demonstrate the feasibility of using this powerful method to engineer proteins with novel mechanical stability. This will serve as the first step towards engineering multifunctional proteins in which mechanical stability is combined with desired additional functionality.

We used the 27th and 32nd immunoglobulin domains (I27 and I32, following the nomenclature by Labeit[33]) from human cardiac titin as the parent model proteins to construct

[*] Dr. D. Sharma, Y. Cao, Prof. Dr. H. Li
Department of Chemistry
The University of British Columbia
2036 Main Mall
Vancouver BC, V6T1Z1 (Canada)
Fax: (+1) 604-822-2847
E-mail: Hongbin@chem.ubc.ca

[**] This work was supported by the Natural Sciences and Engineering Research Council of Canada, Canada Research Chairs program, Canada Foundation for Innovation, and Peter Wall Institute for Advanced Studies and by start-up fund from the University of British Columbia. Y.C. was supported in part by the Laird Fellowship.

Supporting information for this article is available on the WWW under http://www.angewandte.org or from the author.

 © 2006 Wiley-VCH Verlag GmbH & Co. KGaA, Weinheim 

hybrid proteins by recombining different fragments from the two parents. I27 and I32 are good model systems for mechanical proteins and have been studied extensively by single-molecule AFM.[7,11,16,27] It was shown that I27 unfolds at a force of ≈200 pN while I32 is mechanically more stable and unfolds at a force of ≈300 pN.[11,16] The big difference in their mechanical stability may have interesting ramifications for the mechanical properties of hybrid recombinant proteins.

Extensive single-molecule atomic force microscopy studies,[11,26–28,34,35] in conjunction with steered molecular dynamics simulations,[36–39] revealed the critical importance of the A′ and G β strands (referred to as the A′G patch) to the mechanical stability of the I27 domain. When I27 is stretched from its N and C termini, a shear force is applied to the hydrogen-bonding network in the A′G patch, which forms the force-bearing parts of I27 and constitutes the strongest mechanical resistance to unfolding. This shear topology of the hydrogen-bonding network seems to be a common feature among stable mechanical proteins,[11,22,25,28] and suggests that mechanical stability may be a rather local phenomenon. Hence, it seems possible to modulate the mechanical properties of I27-like proteins by shuffling the A′G patch among I27 homologous proteins. Here, we show that, by interchanging the force-bearing A′ and G strands or the presumably non-force-bearing C, D, and E strands between I27 and I32, we can successfully generate mechanically stable, hybrid proteins. To the best of our knowledge, this is the first successful recombination approach to impart novel mechanical properties to proteins.

I27 and I32 share a high sequence homology (identity 42%, similarity 57%, according to the program CLUSTALW, Figure 1A). Although the three-dimensional structure of I32 has not yet been determined, co-evolution and similar functional properties suggest that I32 shares high structural homology with I27. Structural homology modeling using the web-based package Swiss-Model by First Approach Mode (URL: http://swissmodel.expasy.org/) showed that I32 adopts a β-sandwich structure (Figure 1B, green) that is similar to that of I27[40] (Figure 1B, yellow). The hybrid proteins were designed such that they contain both A′ and G β strands from the same parent (Figure 1B) to have minimal disruption of interactions between these two strands, which are presumably important for the mechanical stability. Crossover points were selected at the loops to minimize the interference of the packing of the β-sandwich structure. Using this approach, we shuffled the fragments of both proteins (see the Experimental Section) and constructed four hybrids, I27-A′G-I32, I32-A′G-I27, I27-CDE-I32 and I32-CDE-I27, where the force-bearing A′ and G strands (for the first two hybrids) or non-force-bearing C, D, and E strands (for the latter two hybrids) are interchanged between I27 and I32 (Figure 1B). I27-A′G-I32 stands for a hybrid protein in which A′ and G strands come from I32, while the rest come from parent protein I27. I27-CDE-I32 stands for a hybrid protein in which the C, D, and E strands come from I32, and the remaining come from I27. The other two hybrid proteins are named accordingly (Figure 1B).

To efficiently screen and test the mechanical properties of the hybrid proteins, we constructed a polyprotein containing the recombined hybrid Ig domain flanked by four tandem

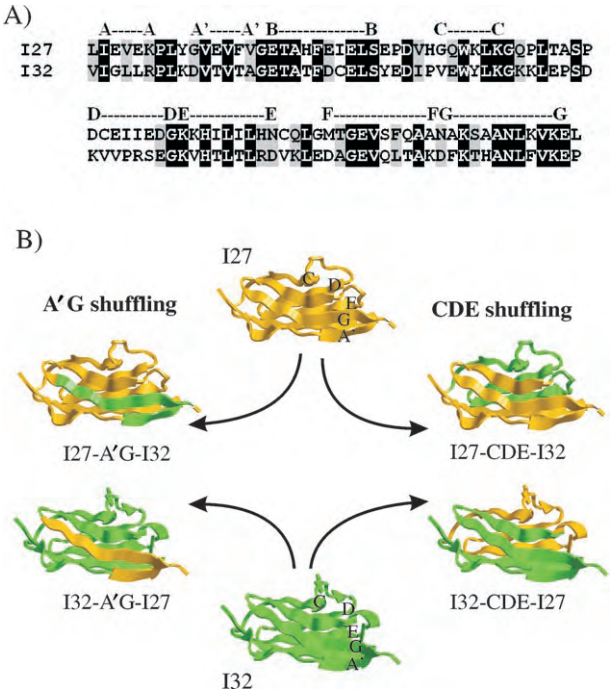


***Figure 1.*** Engineering novel mechanical proteins by recombination of protein fragments from I27 and I32. A) Sequence alignment between parent proteins I27 and I32 shows high sequence homology (57% similarity) between the two proteins. Gray shading indicates homology, inverse text (white on black background) indicates identity. B) Designed hybrid Ig domains. Middle column shows the three-dimensional structures of I27 (Protein Database code: 1TIT,[40] yellow) and I32 (green). I32 structure was obtained by homology modeling (see text). By interchanging the A′ and G β strands between I27 and I32, we designed hybrid proteins I27-A′G-I32 and I32-A′G-I27 (left column). Interchanging the C, D, and E β strands between I27 and I32 resulted in hybrid proteins I27-CDE-I32 and I32-CDE-I27 (right column). In the hybrid proteins, the fragments coming from the wild-type I27 are shown in yellow, while those from wild-type I32 are shown in green.

GB1 domains at the N and C termini (Figure 2A), as described in the Experimental Section. The well-characterized GB1 protein[25] serves as an internal caliper for identifying single-molecule stretching events[41] as well as pinning down the mechanical signature of the hybrid Ig domains. A 1-μL droplet of the purified polyprotein solution (≈100 ng) was deposited on a clean glass cover slip, and the polyprotein was stretched between an AFM tip and glass substrate in phosphate-buffered saline (PBS).

Stretching $(GB1)_4$-I27-A′G-I32-$(GB1)_4$ results in force–extension curves having a characteristic sawtooth pattern like those in Figure 2B. Individual force peaks correspond to the mechanical unraveling of the individual protein domains being stretched.[7,11] The last force peak corresponds to the stretching of the fully unfolded polypeptide and its subsequent detachment from the surface of the glass substrate or AFM tip. Fits according to the worm-like chain model (WLC)[42] of polymer elasticity are shown as dotted lines (Figure 2B).

If we observe five or more unfolding events of GB1 in one force–extension curve, we are certain that one I27-A′G-I32

 © 2006 Wiley-VCH Verlag GmbH & Co. KGaA, Weinheim 

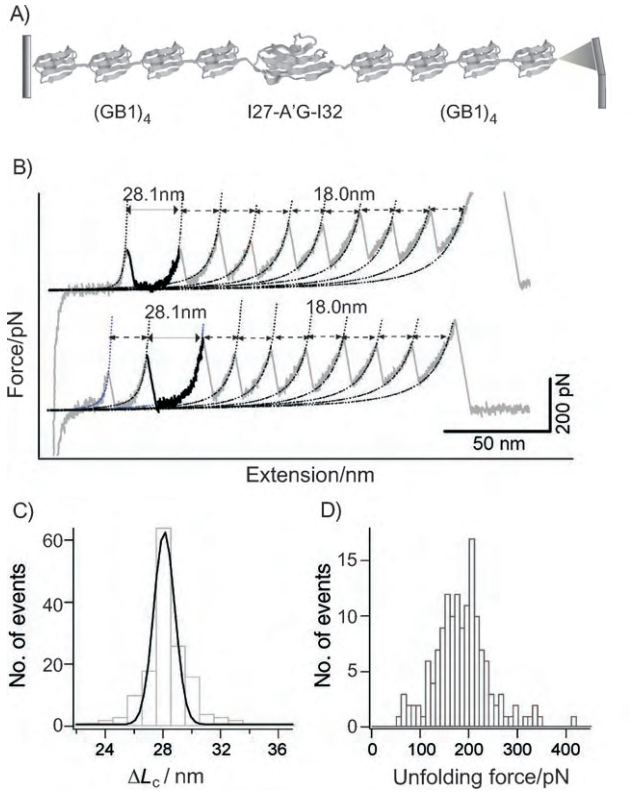


***Figure 2.*** Mechanical properties for the hybrid I27-A′G-I32 protein. A) Representation of the chimera polyprotein $(GB1)_4$-I27-A′G-I32-$(GB1)_4$ being stretched between the AFM tip and glass substrate. B) Two representative force–extension curves for stretching chimera polyprotein $(GB1)_4$-I27-A′G-I32-$(GB1)_4$. Dotted lines correspond to WLC fits to the force–extension data. Contour length increments $\Delta L_c$ between consecutive unfolding events are indicated between WLC fits. The force peaks corresponding to the mechanical unfolding events of GB1 are in gray, while the unfolding event with $\Delta L_c \approx 28$ nm corresponds to the unfolding of the folded hybrid I27-A′G-I32 protein (in black). C) Histogram of $\Delta L_c$ for the unfolding of the hybrid I27-A′G-I32, which corresponds to the events in black in Figure 2B. A Gaussian fit to the histogram shows an average $\Delta L_c$ of $28.1 \pm 0.7$ nm, confirming that I27-A′G-I32 acquires a folded structure similar to that of the wild-type I27. D) Unfolding force frequency histogram for the recombined I27-A′G-I32 shows an average unfolding force of $\approx 178 \pm 44$ pN ($n = 149$) at a pulling speed of 400 nm s$^{-1}$.

domain has been stretched, since I27-A′G-I32 is flanked by $(GB1)_4$ on both termini. The unfolding events of GB1 can be readily recognized[25] by their characteristic contour length increment ($\Delta L_c$) of $\approx 18$ nm. Similarly, the unfolding of I27-A′G-I32 can be identified by its own characteristic $\Delta L_c$ value. The contour length increment is an intrinsic structural parameter of a folded protein and can be used to infer structural information about a protein.[34,43] I27-A′G-I32 comprises 89 amino acids (aa) and is 32 nm long when it is fully stretched (89aa × 0.36 nm per aa = 32 nm), the same as wild-type (wt-) I27 and wt-I32. If the hybrid protein folds into a stable three-dimensional structure similar to that of I27 and I32, the distance between the N and C termini of the hybrid Ig domain in the folded state will be also similar to that of I27 and I32, which is $\approx 4.3$ nm.[40] The complete mechanical unfolding of the hybrid protein will result in $\Delta L_c \approx 28$ nm (32 nm − 4.3 nm = 27.7 nm), similar to that of I27 and I32 (Table 1). Therefore, the mechanical unfolding of the folded hybrid Ig domain will manifest itself in the force–extension curve as an unfolding event with $\Delta L_c \approx 28$ nm. Indeed, in the

***Table 1:*** Mechanical properties of the recombined hybrid proteins.

| | Unfolding force (±SD) [pN] | Contour length increment (±SD) [nm] |
|---|---|---|
| wt-I27[a] | 204(±26) | 28.1 ± 0.2 |
| wt-I32[b] | 298(±24) | 28 |
| I27-A′G-I32 | 178(±44) | 28.1(±0.7) |
| I27-CDE-I32 | 212(±35) | 27.9(±0.6) |
| I32-A′G-I27 | 229(±87) | 28.0(±0.6) |
| I32-CDE-I27 | 147(±40) | 28.1(±0.6) |

[a] Reference [11]. [b] Reference [16].

force–extension recordings of $(GB1)_4$-I27-A′G-I32-$(GB1)_4$ having more than five GB1 unfolding events ($\Delta L_c \approx 18$ nm), we always observe one unfolding event with contour length increment of $\approx 28$ nm, in good agreement with the polyprotein we constructed. A histogram of $\Delta L_c$ for these events shows an average of 28.1 nm for $\Delta L_c$ (Figure 2C). Therefore, these events correspond to the mechanical unfolding of I27-A′G-I32, indicating that I27-A′G-I32 is folded and mechanically resistant. An unfolding force histogram shows an average unfolding force of $\approx 178$ pN ($n = 149$) (Figure 2D).

Similarly, we observed unfolding events with $\Delta L_c \approx 28$ nm (Figure 3A, C, and E) in force–extension curves of all other three recombined hybrid Ig domains. These events correspond to the mechanical unfolding of the designed hybrid Ig

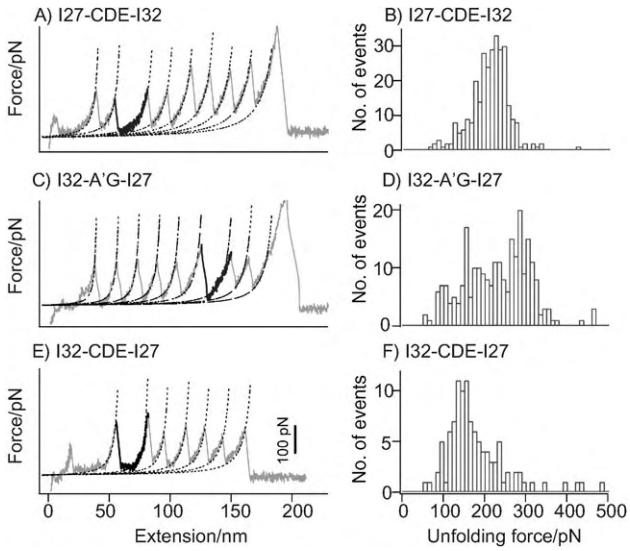


***Figure 3.*** Typical force–extension curves and unfolding force histograms for the recombined hybrid Ig domains: A), B) for I27-CDE-I32, C), D) for I32-A′G-I27, and E), F) for I32-CDE-I27. In A), C), and E) the unfolding events of hybrid Ig domains are in black, while the unfolding of GB1 domains are in gray. Approximations by the WLC model are shown as dotted lines. The average unfolding force is $212 \pm 35$ pN ($n = 293$) for I27-CDE-I32, $229 \pm 87$ pN ($n = 255$) for I32-A′G-I27, and $147 \pm 40$ pN ($n = 107$) for I32-CDE-I27.

 © 2006 Wiley-VCH Verlag GmbH & Co. KGaA, Weinheim 

domains. The unfolding force histograms of the three hybrid proteins are shown in Figure 3B, D, and F. These results confirmed that all the three recombined hybrid Ig domains are folded and mechanically resistant. The fact that the contour length increment (see the Supporting Information) is similar to that of the wt-I27 and wt-I32 indicates that these three hybrid Ig domains acquired three-dimensional structures that are similar to those of the wild-type domains. The mechanical properties of the four hybrid Ig domains are summarized in Table 1. It is evident that the four hybrid Ig domains show novel and diverse mechanical stability, with unfolding forces ranging from $\approx$150 pN to 230 pN, which is different from that of the parent wt-I27 and wt-I32. The distribution of the unfolding forces for the hybrids (I27-A′G-I32, I27-CDE-I32, and I32-CDE-I27) is slightly broader than that of wt-I27 and wt-I32. This broadening may have resulted from the fact that the loading rate for the stretching of hybrid Ig domains varies due to the unfolding of the fingerprint GB1 domains in the construct. However, the unfolding force distribution of I32-A′G-I27 is significantly broader, suggesting its uniqueness to I32-A′G-I27.

To ensure that such a broad distribution for I32-A′G-I27 is not an artifact caused by the AFM methodology we used, we have constructed a polyprotein chimera [GB1-(I32-A′G-I27)]$_4$ (see the Supporting Information) and carried out single-molecule AFM measurements. The use of GB1 in this polyprotein chimera allows us to identify the mechanical unfolding events of I32-A′G-I27 unambiguously. (The force–extension curves of this polyprotein chimera, as well as the unfolding force histogram of I32-A′G-I27, are shown in the Supporting Information.) The unfolding force histogram of I32-A′G-I27 shows a broad distribution, which is in close agreement with the result shown in Figure 3D. This result corroborates that the broad distribution of unfolding forces is indeed an intrinsic property of the recombined I32-A′G-I27 domain. However, its molecular origin remains unknown. Much more in-depth experimental and simulation efforts will be required to find a molecular-level explanation for such a broad distribution. These efforts will involve the illustration of the three-dimensional structure of the protein, detailed molecular dynamics simulation of the mechanical unfolding process, and site-directed mutagenesis.

Our conclusion that all four engineered hybrid Ig domains are folded is further corroborated by structural evaluation using far-UV circular dichroism (CD) spectroscopy. Figure 4 shows the far-UV CD spectra of the four isolated hybrid Ig domains, which were expressed as individual monomers (see the Experimental Section). The CD spectra of the four engineered Ig domains are characteristic of a predominantly β-sheet secondary structure and are similar to that of the parent protein I27 reported previously.[44] In addition, CD measurements (see the Supporting Information) on the polyprotein chimera [GB1-(I32-A′G-I27)]$_4$ showed that the flanking of recombined Ig domain with GB1 does not change the secondary structure of Ig domains. These results confirm that the engineered hybrid domains are indeed folded into structures similar to those of the wild-type parent proteins and that the novel mechanical properties of the engineered proteins indeed result from recombination.

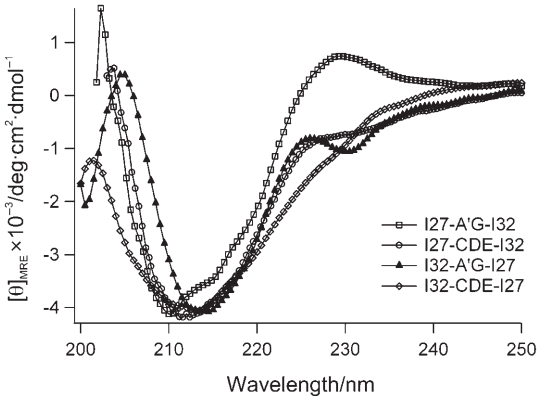


***Figure 4.*** Far-UV CD spectra for the recombined hybrid Ig domains. Spectra were obtained using a cuvette (path length 0.2 cm) at a scan rate of 20 nm min$^{-1}$. Each curve was obtained by averaging three scans. CD spectra of all four designed hybrid proteins are typical of β-sheet proteins.

Previous studies have identified that the A′G patch is the key element that imparts the mechanical resistance to I27.[26,36–38,45] Owing to the high structural homology between I27 and I32, we expect that the same rule also applies to I32. The backbone hydrogen bonds linking A′ and G β strands are identified to be the main origin of the mechanical strength. If A′G is the sole region important for mechanical stability, one would expect that I27-A′G-I32 and I32-CDE-I27 will be mechanically as stable as the wt-I32, as the force-bearing A′G patch of wt-I32 is preserved in both hybrid Ig domains. Similarly, the mechanical stability of I32-A′G-I27 and I27-CDE-I32 would be similar to that of the wt-I27. However, both I27-A′G-I32 and I32-CDE-I27 unfold at much lower forces than wt-I32 (178 pN and 147 pN versus the expected 300 pN for wt-I32), while I32-A′G-I27 is mechanically stronger than wt-I27 (229 pN versus the expected 200 pN for wt-I27). These results clearly suggest that the A′G patch may not be the only structural region responsible for the mechanical stability of Ig domains. Additional interactions and structures that are coupled to the A′G patch may also play important roles in determining the mechanical stability of Ig domains. For example, the hydrophobic packing of the two β sheets may also be one important factor in determining the mechanical stability of Ig domains. This finding resembles those found in recombination-based directed evolution of enzymes: although the active site of an enzyme is composed of only a few key residues, structures distant from the active site as well as those adjacent ones can have a profound effect on the outcome of the enzymatic activities.[30,46]

These "unexpected" results reveal richer structural information and details that one can utilize to further tailor the mechanical and other functional properties of proteins through protein-engineering tools. This perspective offers great promise for engineering proteins with much more diverse mechanical stability and functionality from two parent proteins with well-defined mechanical stability.

In summary, we have demonstrated the first successful attempt to engineer novel mechanically stable proteins by shuffling protein fragments among two homologous parent

 © 2006 Wiley-VCH Verlag GmbH & Co. KGaA, Weinheim 

proteins. We showed that by recombination the four designed hybrid Ig domains based on I27 and I32 fold into three-dimensional structures that are similar to the wild-type parent proteins. In addition the hybrid Ig domains are mechanically stable. The methodology demonstrated here is an exciting new application of the powerful recombination technique in the field of protein mechanics and opens a new way to tailor proteins' mechanical properties. This study also serves as the first step towards engineering mechanical proteins with multiple functionalities, which will find useful applications in bionanotechnology by serving as building blocks for nanomechanical devices. Future work will involve combining high-accuracy homology modeling and experimental recombination work to extend the current methodology to a series of homologous Ig domains with the aim of constructing a combinatorial mechanical protein library.

## Experimental Section

wt-I27 and I32, carrying a 5′ *BamH*I and a 3′ *Bgl*II and *Kpn*I restriction site, were amplified from an Ig8-GFP plasmid[21] encoding I27 to I34 of human cardiac titin and GFP (a generous gift from Dr. Matthias Rief) using standard PCR techniques and subcloned into pUC19 vector to generate pUC19-I27 and pUC19-I32, respectively.

Plasmid containing the designed hybrid I27-A′G-I32 gene was generated using the megaprimer method.[47] DNA that encodes residues 15–78 of I27 was amplified using wt-I27 as a template. Forward and reverse primers for this PCR encode the A′ strand (residues 11–14) and the G strand (residues 79–88) of I32, respectively. Both primers are flanked with sequences of wt-I27 (one to four residues) at their 5′ and 3′ ends. Amplified product was gel-purified and subsequently used as megaprimer to generate pUC19-I27-A′G-I32 using pUC19-I27 as the PCR template. Similarly, pUC19-I32-A′G-I27 was constructed.

pUC19-I27-CDE-I32 and pUC19-I32-CDE-I27 were generated as follows: Restrictions sites ApaI and AgeI were introduced into I27 and I32 after residues 28 and 67, respectively, by site-directed mutagenesis, leading to plasmids pUC19-I27(a-a) and pUC19-I32 (a-a). Insert encoding residues 29–66 of I27, which corresponds to the CDE region along with its adjacent loops, was obtained after digestion of pUC19-I27(a-a) with ApaI and AgeI. The insert was then ligated into the pUC19-I32(a-a) vector, which was linearized by *Apa*I and *Age*I restriction enzymes, to produce pUC19-I32-CDE-I27. pUC19-I27-CDE-I32 was obtained similarly. All sequences were confirmed by DNA sequencing.

Protein expression was carried out in pQE80L expression vector. $(GB1)_4$ polyprotein gene was obtained by a procedure similar to that described previously for $(GB1)_8$.[25] For expression of I27-A′G-I32, pUC19-I27-A′G-I32 was digested with restriction enzymes *BamH*I and *Kpn*I. The insert released was subcloned into vector pQE80L-$(GB1)_4$, which was digested with enzymes *Bgl*II and *Kpn*I, to generate pQE80L-$(GB1)_4$-I27-A′G-I32. $(GB1)_4$ flanked with *BamH*I and *Kpn*I was further subcloned into pQE80L-$(GB1)_4$-I27-A′G-I32 digested with *Bgl*II and *Kpn*I. The other three hybrid protein expression vectors were constructed in a similar fashion. The expression vector contained an N-terminal six-residue histidine tag to facilitate purification of expressed proteins. Two additional Cys residues were included at the 3′ end of the gene. The polyprotein was expressed in DH5α strain and purified using Ni-NTA (NTA = nitrilotriacetic acid; *N*,*N*-bis(carboxymethyl)glycine) affinity chromatography. The protein samples were kept in PBS buffer containing 200 mM imidazole with 5 mM 1,4-dithiothreitol to prevent air-oxidation of cysteine residues at 4 °C.

For circular dichroism (CD) studies, individual hybrid Ig domains were directly subcloned into the pQE80L expression vector using restriction sites BamHI and KpnI. Proteins were expressed in DH5α strain and purified using Ni-NTA affinity chromatography. Proteins were eluted in PBS buffer containing 200 mM imidazole. Eluted proteins were extensively dialyzed against 0.5 × PBS before CD measurements.

Single-molecule AFM experiments were carried out on a custom-built atomic force microscope, which was constructed as described previously.[48] The spring constant of each individual cantilever ($Si_3N_4$ cantilevers from Vecco, with a typical spring constant of 40 pN nm$^{-1}$) was calibrated in solution using the equipartition theorem before and after each experiment.[49,50] All the force–extension measurements were carried out in PBS buffer. A 1-μL droplet of the polyprotein solution ($\approx$100 ng) was placed on a clean glass cover slip covered by PBS buffer. It was allowed to absorb for 5 min and was then stretched between the AFM tip and glass substrate at a pulling speed of 400 nm s$^{-1}$.

CD spectra in the far-UV range were recorded on a Jasco-J810 spectropolarimeter flushed with nitrogen gas. The spectra were recorded in a cuvette with a path length of 0.2 cm at a scan rate of 20 nm min$^{-1}$. For each protein sample an average of three scans was reported. Data was corrected for buffer contributions. Results are expressed as mean residue ellipticity ($\theta_{MRE}$), calculated according to Equation (1), where $\theta_{obs}$ is the observed ellipticity (in deg), $d$ is path length (in cm), $C$ is concentration of protein samples (M), and $n$ is total number of amino acids in the protein.

$$\theta_{MRE} = (100\,\theta_{obs})/[d\,C\,(n-1)] \quad (1)$$

Received: January 29, 2006
Revised: May 12, 2006
Published online: July 20, 2006

**Keywords:** protein engineering · protein structures · scanning probe microscopy · single-molecule studies

[1] G. Bao, S. Suresh, *Nat. Mater.* **2003**, *2*, 715.
[2] A. S. Tatham, P. R. Shewry, *Trends Biochem. Sci.* **2000**, *25*, 567.
[3] N. Becker, E. Oroudjev, S. Mutz, J. P. Cleveland, P. K. Hansma, C. Y. Hayashi, D. E. Makarov, H. G. Hansma, *Nat. Mater.* **2003**, *2*, 278.
[4] J. C. van Hest, D. A. Tirrell, *Chem. Commun.* **2001**, 1897.
[5] T. E. Fisher, A. F. Oberhauser, M. Carrion-Vazquez, P. E. Marszalek, J. M. Fernandez, *Trends Biochem. Sci.* **1999**, *24*, 379.
[6] D. S. Goodsell, *Bionanotechnology*, Wiley-Liss, Hoboken, **2004**.
[7] M. Rief, M. Gautel, F. Oesterhelt, J. M. Fernandez, H. E. Gaub, *Science* **1997**, *276*, 1109.
[8] M. S. Kellermayer, S. B. Smith, H. L. Granzier, C. Bustamante, *Science* **1997**, *276*, 1112.
[9] L. Tskhovrebova, J. Trinick, J. A. Sleep, R. M. Simmons, *Nature* **1997**, *387*, 308.
[10] A. F. Oberhauser, P. E. Marszalek, H. P. Erickson, J. M. Fernandez, *Nature* **1998**, *393*, 181.
[11] M. Carrion-Vazquez, A. F. Oberhauser, S. B. Fowler, P. E. Marszalek, S. E. Broedel, J. Clarke, J. M. Fernandez, *Proc. Natl. Acad. Sci. USA* **1999**, *96*, 3694.
[12] M. Carrion-Vazquez, A. F. Oberhauser, T. E. Fisher, P. E. Marszalek, H. B. Li, J. M. Fernandez, *Prog. Biophys. Mol. Biol.* **2000**, *74*, 63.
[13] R. B. Best, D. J. Brockwell, J. L. Toca-Herrera, A. W. Blake, D. A. Smith, S. E. Radford, J. Clarke, *Anal. Chim. Acta* **2003**, *479*, 87.
[14] X. Zhuang, M. Rief, *Curr. Opin. Struct. Biol.* **2003**, *13*, 88.
[15] B. Samori, G. Zuccheri, P. Baschieri, *ChemPhysChem* **2005**, *6*, 29.

 © 2006 Wiley-VCH Verlag GmbH & Co. KGaA, Weinheim 

[16] H. Li, W. A. Linke, A. F. Oberhauser, M. Carrion-Vazquez, J. G. Kerkvliet, H. Lu, P. E. Marszalek, J. M. Fernandez, *Nature* **2002**, *418*, 998.
[17] A. F. Oberhauser, C. Badilla-Fernandez, M. Carrion-Vazquez, J. M. Fernandez, *J. Mol. Biol.* **2002**, *319*, 433.
[18] S. P. Ng, R. W. Rounsevell, A. Steward, C. D. Geierhaas, P. M. Williams, E. Paci, J. Clarke, *J. Mol. Biol.* **2005**, *350*, 776.
[19] D. J. Brockwell, G. S. Beddard, J. Clarkson, R. C. Zinober, A. W. Blake, J. Trinick, P. D. Olmsted, D. A. Smith, S. E. Radford, *Biophys. J.* **2002**, *83*, 458.
[20] G. Yang, C. Cecconi, W. A. Baase, I. R. Vetter, W. A. Breyer, J. A. Haack, B. W. Matthews, F. W. Dahlquist, C. Bustamante, *Proc. Natl. Acad. Sci. USA* **2000**, *97*, 139.
[21] H. Dietz, M. Rief, *Proc. Natl. Acad. Sci. USA* **2004**, *101*, 16192.
[22] D. J. Brockwell, G. S. Beddard, E. Paci, D. K. West, P. D. Olmsted, D. A. Smith, S. E. Radford, *Biophys. J.* **2005**, *89*, 506.
[23] R. B. Best, B. Li, A. Steward, V. Daggett, J. Clarke, *Biophys. J.* **2001**, *81*, 2344.
[24] C. Cecconi, E. A. Shank, C. Bustamante, S. Marqusee, *Science* **2005**, *309*, 2057.
[25] Y. Cao, C. Lam, M. Wang, H. Li, *Angew. Chem.* **2006**, *45*, 658; *Angew. Chem. Int. Ed.* **2006**, *45*, 642.
[26] H. Li, M. Carrion-Vazquez, A. F. Oberhauser, P. E. Marszalek, J. M. Fernandez, *Nat. Struct. Biol.* **2000**, *7*, 1117.
[27] P. M. Williams, S. B. Fowler, R. B. Best, J. L. Toca-Herrera, K. A. Scott, A. Steward, J. Clarke, *Nature* **2003**, *422*, 446.
[28] H. Li, J. M. Fernandez, *J. Mol. Biol.* **2003**, *334*, 75.
[29] J. D. Bloom, M. M. Meyer, P. Meinhold, C. R. Otey, D. MacMillan, F. H. Arnold, *Curr. Opin. Struct. Biol.* **2005**, *15*, 447.
[30] C. A. Voigt, C. Martinez, Z. G. Wang, S. L. Mayo, F. H. Arnold, *Nat. Struct. Biol.* **2002**, *9*, 553.
[31] J. A. Bittker, B. V. Le, J. M. Liu, D. R. Liu, *Proc. Natl. Acad. Sci. USA* **2004**, *101*, 7011.
[32] K. E. Griswold, Y. Kawarasaki, N. Ghoneim, S. J. Benkovic, B. L. Iverson, G. Georgiou, *Proc. Natl. Acad. Sci. USA* **2005**, *102*, 10082.
[33] S. Labeit, B. Kolmerer, *Science* **1995**, *270*, 293.
[34] M. Carrion-Vazquez, P. E. Marszalek, A. F. Oberhauser, J. M. Fernandez, *Proc. Natl. Acad. Sci. USA* **1999**, *96*, 11288.
[35] S. B. Fowler, R. B. Best, J. L. Toca Herrera, T. J. Rutherford, A. Steward, E. Paci, M. Karplus, J. Clarke, *J. Mol. Biol.* **2002**, *322*, 841.
[36] M. Gao, H. Lu, K. Schulten, *J. Muscle Res. Cell Motil.* **2002**, *23*, 513.
[37] H. Lu, B. Isralewitz, A. Krammer, V. Vogel, K. Schulten, *Biophys. J.* **1998**, *75*, 662.
[38] H. Lu, K. Schulten, *Biophys. J.* **2000**, *79*, 51.
[39] E. Paci, M. Karplus, *Proc. Natl. Acad. Sci. USA* **2000**, *97*, 6521.
[40] S. Improta, A. S. Politou, A. Pastore, *Structure* **1996**, *4*, 323.
[41] H. Li, A. F. Oberhauser, S. D. Redick, M. Carrion-Vazquez, H. P. Erickson, J. M. Fernandez, *Proc. Natl. Acad. Sci. USA* **2001**, *98*, 10682.
[42] J. F. Marko, E. D. Siggia, *Macromolecules* **1995**, *28*, 8759.
[43] H. Dietz, M. Rief, *Proc. Natl. Acad. Sci. USA* **2006**, *103*, 1244.
[44] A. S. Politou, D. J. Thomas, A. Pastore, *Biophys. J.* **1995**, *69*, 2601.
[45] D. K. West, D. J. Brockwell, P. D. Olmsted, S. E. Radford, E. Paci, *Biophys. J.* **2006**, *90*, 287.
[46] C. R. Otey, J. J. Silberg, C. A. Voigt, J. B. Endelman, G. Bandara, F. H. Arnold, *Chem. Biol.* **2004**, *11*, 309.
[47] G. Sarkar, S. S. Sommer, *Biotechniques* **1990**, *8*, 404.
[48] J. M. Fernandez, H. Li, *Science* **2004**, *303*, 1674.
[49] E. L. Florin, M. Rief, H. Lehmann, M. Ludwig, C. Dornmair, V. T. Moy, H. E. Gaub, *Biosens. Bioelectron.* **1995**, *10*, 895.
[50] J. L. Hutter, J. Bechhoefer, *Rev. Sci. Instrum.* **1993**, *64*, 3342.

 © 2006 Wiley-VCH Verlag GmbH & Co. KGaA, Weinheim 

Bismuth Clusters

DOI: 10.1002/anie.200600469

# Towards a Structural Understanding of the Anti-Ulcer and Anti-Gastritis Drug Bismuth Subsalicylate**

*Philip C. Andrews,* Glen B. Deacon, Craig M. Forsyth, Peter C. Junk, Ish Kumar, and Melissa Maguire*

Bismuth subsalicylate (BSS), commonly marketed as colloidal suspensions under the commercial names of "Bismatrol", and "Pepto-Bismol", is one of several bismuth compounds regularly used for the therapeutic treatment of a variety of gastrointestinal ailments including duodenal and peptic ulcers, ulcerative colitis, and diarrhea.[1–7] In conjunction with antibiotic compounds such as tetracycline, clarithromycin, and amoxicillin, BSS (as well as bismuth subcitrate (CBS) and ranitidine bismuth citrate) has been effective in the treatment and eradication of *Helicobacter pylori*, the bacterium linked to gastritis and ulceration implicated in the development of gastric cancer and gastric lymphoma.[8–13] It is estimated that at least half of the world's population is infected with *H. pylori* and, without treatment, it is present in its host for life.[14–16] The medical and social impact of *H. pylori* was acknowledged by the award of the 2005 Nobel Prize in Physiology and Medicine to Marshall and Warren.

Despite the efficacy of these bismuth formulations, the mechanism of action of bismuth compounds in the body, either in their interaction with bacteria, the urease *H. pylori* produces, or the localized environment around gastric lesions, is largely unknown. As a first step there have been attempts to model the structures of BSS (and CBS) through the formation and structural elucidation of a variety of bismuth carboxylates.[2,17,18] The most important of these are tris-substituted bismuth salicylate $[Bi(Hsal)_3]$ ($H_2sal = (2\text{-}HO)C_6H_4COOH$) "trapped" by chelating amines, for example, $[Bi(Hsal)_3(bpy)]_2\cdot(C_7H_8)_2$, (bpy = 2,2′-bipyridine),[19] bismuth thiosalicylate complexes,[20] and the structurally uncharacterized $[Bi(Hsal)_3]$ compound.[21,22] These model compounds, however, do not address the "sub" part of subsalicylate which, as the name infers, requires partial hydrolysis of the $BiL_3$ species and concomitant hydroxide/oxide formation, resulting in the typical insolubility of these compounds. Since the hydrolysis or partial neutralization process is not easily

[*] Dr. P. C. Andrews, Prof. G. B. Deacon, Dr. C. M. Forsyth, Assoc. Prof. P. C. Junk, I. Kumar, M. Maguire
School of Chemistry
Monash University
Clayton, Melbourne, VIC 3800 (Australia)
Fax: (+61) 3-9905-4597
E-mail: Phil.Andrews@sci.monash.edu.au

[**] We thank the Australian Research Council for financial support and Monash University Centre for Green Chemistry for seed funding. We are indebted to Dr. Ian Grey from the Minerals Division of CSIRO Australia for many useful discussions on the structures of bismuth oxide.


WILEY InterScience DISCOVER SOMETHING GREAT
© 2006 Wiley-VCH Verlag GmbH & Co. KGaA, Weinheim

controlled under heterogeneous conditions, BSS, as a pharmaceutical formulation, raises interesting compositional and structural questions. Its high degree of insolubility has made the definitive determination of its nature extremely difficult.

We report here the reproducible synthesis and characterization of two bismuth oxosalicylate clusters of high nuclearity, $[Bi_{38}O_{44}(HSal)_{26}(Me_2CO)_{16}(H_2O)_2]\cdot(Me_2CO)_4$ (**1**) and $[Bi_9O_7(HSal)_{13}(Me_2CO)_5]\cdot(Me_2CO)_{1.5}$ (**2**). Our study provides structural insights into the nature of BSS and establishes a basis for more meaningful studies into its mode of action and biological activity.

Colorless crystals of **1** and **2** grew slowly over four to five days upon dissolution of $[Bi(Hsal)_3]$ in reagent-grade acetone. The product from the solvent-free reaction of $BiPh_3$ with salicylic acid[21] analyzes with relative consistency to be the $[Bi(Hsal)_3]$ species. Hydrolysis at this stage is most likely precluded, or minimized, by the temperature of the reaction and the use of carefully dried reagents. $[Bi(Hsal)_3]$ formed by this method is almost entirely soluble in warm acetone, and slow evaporation provides a reasonable yield of colorless crystals. Complete evaporation of the mother liquor results in a loss of integrity of the crystals as lattice and bound solvent is lost and the crystals become opaque.

Single-crystal X-ray diffraction on a variety of crystals from several reaction mixtures indicates that crystals of **2**, with nine bismuth atoms in the central oxide core, initially predominate with co-crystallization of a relatively small amount of the very large cluster **1**, which has 38 bismuth atoms. However, extended crystal growth times leads to a predominance of the larger cluster which appears to be the least soluble and most thermodynamically stable form. To date we have collected data on 15 crystals and as yet have not found any other cluster species by single-crystal X-ray diffraction. Powder XRD patterns on the bulk sample differed from those generated from the single-crystal data, most likely because of the loss of lattice and bound solvent molecules from **1** and **2**.

We assume that hydrolysis occurs as a result of water in the acetone and that the rate of hydrolysis and crystal growth determines the degree of oxide formation. Elemental analyses (C, H) on one fresh dried sample of crystalline material analyzed correctly for **1**. However, repeated analyses on several samples of the air-dried crystals provided inconsistent results, owing to the loss of acetone and/or $H_2O$. This is a strong indication, along with the crystallographic results, that a mixture of clusters is obtained and underscores the difficulty in comprehensive characterization.

MALDI mass spectrometry in acetone with 0.1% trifluoroacetic acid (TFA) confirms the presence of a $Bi_9$ cluster having the same nuclearity as the initial isolated cage, as well as other fragmentation species. This was the case whether an added matrix was used or not. The highest $m/z$ values are for $[Bi_9O_7(Hsal)_{10}(Me_2CO)_3(H_2O)_9]^{3+}$ (1233), $[Bi_9O_7(Hsal)_{10}(H_2O)_6]^{3+}$ (1157), and $[Bi_8O_6(Hsal)_9(Me_2CO)_2(H_2O)]^{3+}$ (1045). Other prominent peaks are listed in the experimental description. $^1H$ and $^{13}C$ NMR spectra, recorded in dilute solutions in [$D_6$]acetone, indicate just the salicylate ligand. At 30 °C all the proton signals are broad with no defined splitting, but four equal intensity resonances are observed for 2-$HOC_6H_4COO^-$. Though there is some further broadening of the signals as the temperature is lowered, one ligand environment dominates. At −80 °C the proton resonances become sharp, the splitting is more defined, and there is some movement in the chemical-shift values, but only one ligand environment is visible.

The crystal structures of **1** and **2** are shown in Figure 1a and Figure 1b, respectively. The oxide core of **1** adopts a well-defined octahedral cluster of edge-shared cubes at the crystallographic origin and resembles a small block of the fluorite structure when Bi–O contacts are included out to 3.1 Å, which is well within the sum (4.0 Å) of the van der

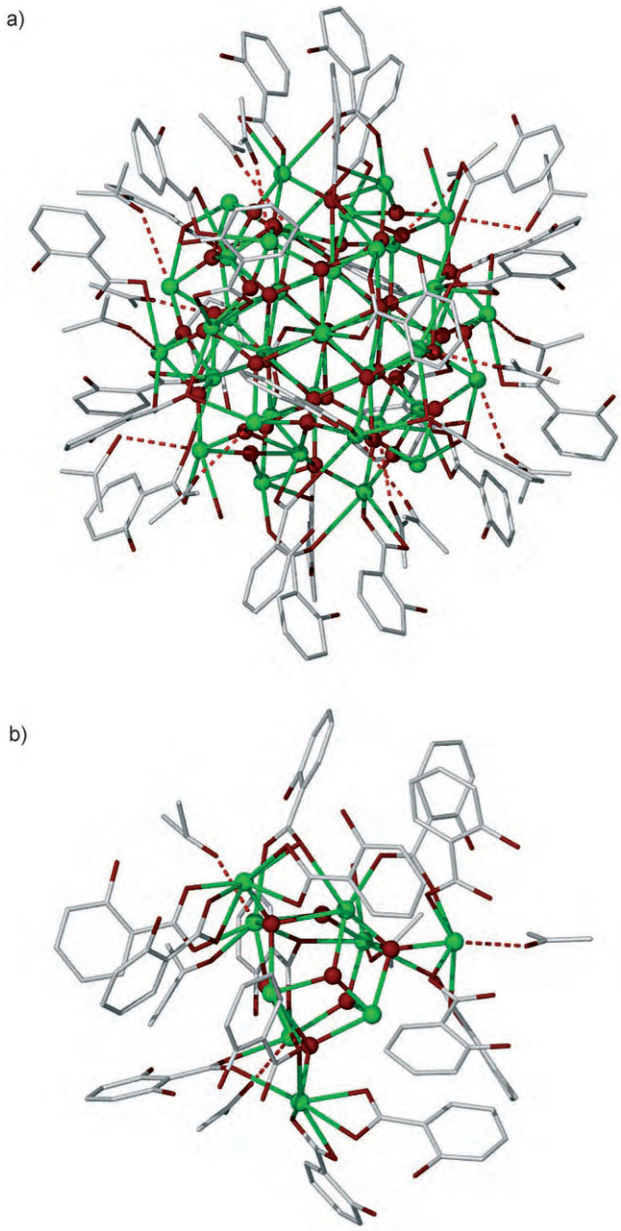


***Figure 1.*** a) Molecular structure of $[Bi_{38}O_{44}(HSal)_{26}(Me_2CO)_{16}(H_2O)_2]$ (**1**) showing the shrouding of the $Bi_{38}O_{44}$ core (green = Bi, red = O) by 26 salicylate ligands (stick structures). b) Molecular structure of $[Bi_9O_7(HSal)_{13}(Me_2CO)_5]$ (**2**) showing the shrouding of the $Bi_9O_7$ core (green = Bi, red = O) by 13 salicylate ligands (stick structures).

 © 2006 Wiley-VCH Verlag GmbH & Co. KGaA, Weinheim 

Waals radii for Bi and O.[23,24] The cubes are almost regular though the location of each Bi atom in each cube is well displaced from the center, presumably as a result of the lone pairs of electrons. This arrangement corresponds to the high-temperature (> 717 °C) oxygen-deficient $\delta$ phase of $Bi_2O_3$, the phase that has sparked significant interest in materials science recently owing to its extremely high oxide mobility.[25] This phase contrasts with the formally lower-temperature β phase identified for the large silanolate cluster $[Bi_{22}O_{26}(OSiMe_2tBu)_{14}]$, which was isolated from the hydrolysis of $Bi(OSiMe_2tBu)_3$ in benzene.[26] While inorganic ternary bismuth oxide clusters of high nuclearity are not unexpected,[27–29] similar metal–organic compounds of bismuth, including those with ethoxide, trifluoroacetate, phosphonate, and citrate ligands are now apparent.[30–34] In addition, Whitmire and co-workers have recently incorporated bismuth and salicylate anions and dianions into several structurally characterized heterobimetallic clusters containing Al or a series of transition metals,[35–38] generally of low nuclearity.

Mehring and co-workers have proposed a set of rules to describe the growth pattern of bismuth oxo clusters, including homometallic oxo clusters containing 4, 9, 18, 20, and 22 bismuth atoms, in addition to several larger heterobimetallic clusters incorporating sodium which were derived from partial hydrolysis of bismuth silanolates.[39] They deduced that the structural building block for the bismuth-rich clusters is the $[Bi_6O_8]^{2+}$ polyhedron, which has six octahedral Bi atoms with the eight O atoms located over all of the triangular faces. The structures of both **1** and **2** appear to conform to this. Thus, at the heart of the cluster in **1** is a central $Bi_6$ octahedron in which the six Bi atoms, Bi(6,9,13) and symmetry equivalents, are bound to only oxide atoms. Surrounding this are four further $Bi_6$ octahedra, which share edges with each of the four equatorial edges of the central $Bi_6$, thus forming a planar cross of five octahedra. Above and below this plane are four further $Bi_6$ octahedra, joined at a single vertex (i.e. each doubly edge sharing), which is also one of the axial Bi atoms of the central $Bi_6$ octahedron. Thus, each of these four octahedra shares four edges with neighboring $Bi_6$ octahedra. This accounts for all 38 Bi atoms (24 external and 14 internal). The $Bi_9$ clusters comprise a central $Bi_6$ octahedron but with only seven of the eight trigonal faces capped by an O atom, as shown in Figure 2a. The hole is covered by a $\mu_3$-$\eta^1$:$\eta^1$:$\eta^1$-salicylate: Bi(2,5,6) by O(16,17) and Bi(11,14,16) by O(61,62). Three additional Bi atoms protrude from the core and are all connected through a bridging $\mu_4$-O atom.

The cores of **1** and **2** are surrounded by 26 and 13 salicylate ligands, respectively. The bonding to the outlying $Bi^{III}$ centers corresponds to highly complex bridging modes (see below) with no evidence of any interactions with the *ortho* hydroxy oxygen atoms. This is similar to the bonding in $[Bi(Hsal)_3(bpy)]_2\cdot(C_7H_8)_2$ and in contrast to that in $[Bi(Hsal)(sal)(phen)]_2\cdot(C_7H_8)_2$[19] (phen = 1, 10-phenanthroline). If one considers all Bi–O bond lengths in the structures up to 3.1 Å, three broad categories become evident: very short bonds (shortest 2.06 Å in **1** and 2.09 Å in **2**) primarily found in the oxide core, and medium and long bonds resulting from asymmetric coordination of the carboxylate ligands. In **1** the coordination numbers of the Bi atoms are either six (2 × Bi), seven (10 × Bi), or eight (7 × Bi). The bismuth atoms Bi(6,10,13) and their symmetry equivalents bond only to core oxygen atoms and are all eight-coordinate. The three independent Bi atoms are bonded to 19 O atoms; O(12) is bound to all three, and a further three oxygen atoms are bound to two such Bi atoms. Bi(6,9,13)–O bond lengths range from 2.252(10) to 3.056(10) Å and do not include the shortest Bi–O bond lengths. Twelve of the remaining Bi atoms in the asymmetric unit each have three Bi–O core bond lengths shorter than 2.25 Å, whilst the other four have three comparable with the shortest distance seen for Bi(6,9,13)–O and at least one much shorter. The shortest $Bi-O_{core}$ bond length is 2.059(9) Å, for Bi(3)–O(6), and there are four others below 2.10 Å. Eight Bi atoms, Bi(2,5,10,18) and their symmetry equivalents, are bound mainly to core O atoms with seven-coordinate Bi(5) and eight-coordinate Bi(10) each having six core O atoms.

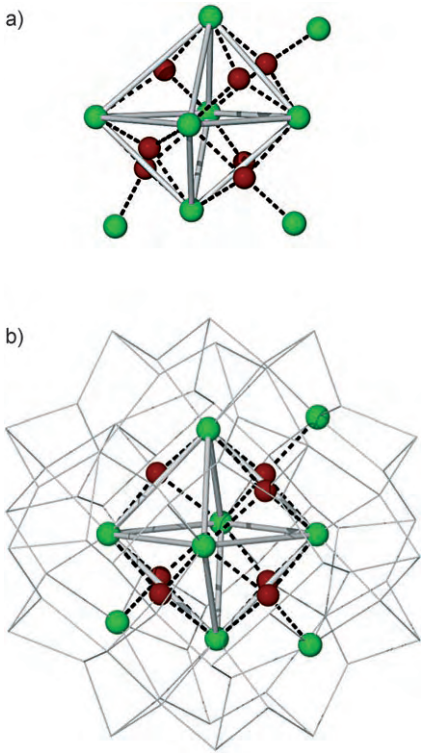


***Figure 2.*** a) Structure of the $Bi_9O_7$ core of $[Bi_9O_7(HSal)_{13}(Me_2CO)_5]$ (**2**), showing the octahedral arrangement of the Bi atoms with seven octahedral faces capped by an oxygen atom. Three Bi atoms extend the core bound to a capping O atom. b) Structure of the $Bi_{38}O_{44}$ core of $[Bi_{38}O_{44}(HSal)_{26}(Me_2CO)_{16}(H_2O)_2]$ (**1**), with $Bi_9O_7$ at the heart of the core; colors as in Figure 1.

Salicylate ligands are bonded to all Bi atoms except Bi(6,19,13) and their symmetry equivalents. The variation in carboxylate bonding modes is extraordinary, even though, as stated earlier, binding of the OH group of $Hsal^-$ does not occur. Thus, $\mu_4$-$\eta^1$:$\eta^1$:$\eta^1$:$\eta^1$, $\mu_3$-$\eta^2$:$\eta^2$:$\eta^1$, $\mu_3$-$\eta^2$:$\eta^1$:$\eta^1$, $\mu_3$-$\eta^1$:$\eta^1$:$\eta^1$, $\mu$-$\eta^2$:$\eta^1$ (with the $CO_2$ group perpendicular or coplanar with the Bi···Bi vector) and $\mu$-$\eta^1$:$\eta^1$, involving only one carboxylate oxygen, are all observed. The carboxylate bonding modes in **2** are less complex, with only $\mu_3$-$\eta^1$:$\eta^1$:$\eta^1$ and $\mu$-$\eta^2$:$\eta^1$ predominating. Surprisingly, none of the most common bonding

 © 2006 Wiley-VCH Verlag GmbH & Co. KGaA, Weinheim 

modes—simple chelation, O,O′ bridging, and unidentate—are observed. The Bi–$O_{Hsal}$ bond lengths cover a narrower range, 2.415(9)–3.066(10) Å, than the Bi–$O_{core}$ bond lengths, and there are always at least three Bi–$O_{core}$ bonds shorter than the shortest Bi–$O_{Hsal}$ distance around each bismuth atom. In at least two cases where there is chelation to a bismuth atom (as part of a more complex carboxylate binding mode), the two Bi–$O_{Hsal}$ distances differ by 0.5–0.6 Å. Two water ligands, Bi–$O(23)_{H_2O}$ 2.647(10) Å, with a distance typical for $Bi^{III}$–$OH_2$,[40] are attached to the $Bi_{38}$ cage. In addition, 16 acetone ligands are coordinated to the cage, four of which bridge two bismuth atoms unsymmetrically (0.13, 0.17 Å). The range of Bi–O distances, 2.815(10)–3.089(10) Å, is at the top end of the Bi–O bond lengths, and can be related to the ready loss of acetone and crystallinity on drying.

Of all the bismuth oxo coordination clusters observed thus far in the solid state, those with nine Bi atoms seem to occur most regularly. From Mehring's study $[Bi_9O_7(OSiMe_3)_{13}]$ was characterized, while $[Bi_9O_7(OC_6F_5)_{13}]$[41,42] and its thf solvate[41] were obtained upon hydrolysis and elimination of bis(pentafluorophenyl) ether from dimeric $[Bi(OC_6F_5)_3$-$(toluene)]_2$.[42] Apart from the obvious differences in the bonding modes of carboxylate with silanolate and phenolate, these clusters are essentially isostructural with **2** and display relatively high thermodynamic stability.

Interestingly, as Figure 2b graphically depicts, the core of **2** lies at the heart of **1.** This information, coupled with the presence of the Bi-coordinated solvent molecules in **1** and **2**, reveals a possible process for hydrolysis and core formation, and indicates that complex **2** gives rise to complex **1**. These structures provide an insight into the nature of bismuth subsalicylate and plausibly other basic bismuth medicinals which we propose are based on bismuth oxide cores. The capacity for cluster building, shown by the relationship between **1** and **2** and extrapolated to larger clusters, accounts for the near insolubility of these species.

## Experimental Section

*o*-Hydroxybenzoic acid (salicylic acid) (0.44 g, 3.0 mmol) was ground together with $BiPh_3$ (0.44 g, 1.0 mmol) in a mortar and pestle and dried in vacuo. The mixture was heated at 120 °C for 6 h and the resulting white powder dissolved in warm reagent-grade acetone and filtered. Slow evaporation of the solvent produced a crop of colorless crystals, which were separated by hand and identified as the oxosalicylate bismuth clusters **1** and **2** through single-crystal X-ray diffraction. Further analysis was conducted on the air-dried opaque material which was collected after complete solvent removal and washing with toluene. Yield 147 mg (air-dried, microcrystalline material) m.p. >240 °C (decomp to gray powder). $^1$H NMR (400.13 MHz, [D$_6$]acetone, 30 °C): $\delta = 11.02$ (1H, PhO*H*), 7.79 (1H, *o*-H), 7.35 (1H, *p*-H), 6.84, 6.67 ppm (2H, *m*-H). $^{13}$C NMR (100.62 MHz, [D$_6$]acetone, 30 °C): $\delta = 206.9$ (C=O), 162.3 (*q*-C), 136.3 (p-C), 131.7 (*o*-C), 119.8 (*m*-C), 118.2 (*m*-C), 116.3 ppm (*q*-C). Attenuated total reflectance(ATR) IR: $\tilde{\nu} = 3375$ (w, br), 3050 (w, br), 1681 (w), 1619 (m), 1588 (m), 1522 (m), 1478 (s), 1143 (s), 1375 (s), 1336 (s, sh), 1303 (s), 1240 (s), 1216 (s), 1156 (s), 1141 (s) 1090 (m), 1029 (m), 860 (m), 808 (m), 750 (m), 701 (m), 663 cm$^{-1}$ (m). MS (MALDI, acetone + 0.1% TFA, no matrix): *m*/*z*: 1233 $[Bi_9O_7$-$(Hsal)_{10}(Me_2CO)_3(H_2O)_9]^{3+}$, 1157 $[Bi_9O_7(Hsal)_{10}(H_2O)_6]^{3+}$, 1045 $[Bi_8O_6(Hsal)_9(Me_2CO)_2(H_2O)]^{3+}$, 887 $[Bi_3(Hsal)_7(Me_2CO)_2(H_2O)_4]^{2+}$, 767 $[Bi_3O(Hsal)_5(Me_2CO)_2(H_2O)_5]^{2+}$, 716 $[Bi(Hsal)_3Na(Me_2CO)$-$(H_2O)]^+$, 627 $[Bi_5O_4(Hsal)_4(Me_2CO)_2(H_2O)_6]^{3+}$, 510 $[Bi_2(Hsal)_4$-$(H_2O)_3]^{2+}$, 417.9 $[Bi_2]^+$, 208.9 $[Bi]^+$. Elemental analysis for **1**–($H_2O$ and acetone) (%) calcd for $C_{182}H_{164}O_{122}Bi_{38}$: C 17.85, H 1.35; found C 17.97, H 1.13.

Crystalline samples of compounds **1** and **2** were mounted upon glass fibers in highly viscous oil at 123(2) K. Data were collected on Bruker ApexII Kappa CCD (**1**) and Enraf-Nonius Kappa CCD (**2**) diffractometers (graphite-monochromated $Mo_{K\alpha}$ X-ray radiation ($\lambda = 0.71073$ Å)) and corrected for absorption using the SADABS (**1**) and the DENZO-SMN packages (**2**). Structural solution and refinements were carried out using the SHELX suite of programs with the graphical interface X-Seed. Both structures were severely affected by the large heavy-atom content, and therefore data were not as precise as preferred. However, the connectivity of both structures is unambiguous. For compound **1**, all Bi atoms and salicylate ligands bound in the central core were refined anisotropically, while all other non-H atoms were refined isotropically. Examination of the anisotropic displacement parameters suggested rotational disorder in some of the aromatic rings, but this could not be adequately modeled with the current data. One aromatic ring C(37)–C(42) and some of the lattice acetone molecules were restrained with optimal geometries. For compound **2**, only the Bi atoms could sustain anisotropic refinement, and therefore all other non-H atoms were refined isotropically. Crystal data for **1**: $C_{242}H_{254}Bi_{38}O_{144}$, $M_r = 13407.86$, $0.13 \times 0.10 \times 0.10$ mm, orthorhombic, space group *Pbca* (No. 61), $a = 31.302(1)$, $b = 30.795(1)$, $c = 31.584(1)$ Å, $V = 30409(11)$ Å$^3$, $Z = 4$, $\rho_{calcd} = 2.928$ g cm$^3$, $F_{000} = 24048$, $\mu = 21.994$ mm$^{-1}$, $2\theta_{max} = 55.0°$, 172443 reflections collected, 34804 unique ($R_{int} = 0.108$). Final GOF = 1.010, $R_1 = 0.0490$, $wR_2 = 0.0871$, *R* indices based on 21680 reflections with $I > 2\sigma(I)$ (refinement on $F^2$) $R_1 = 0.107$, $wR_2 = 0.106$ (all data). Crystal data for **2**: $C_{221}H_{207}Bi_{18}O_{107}$, $M_r = 8336.51$, $0.20 \times 0.15 \times 0.15$ mm, triclinic, space group $P\bar{1}$ (No. 2), $a = 16.485(3)$, $b = 28.643(6)$, $c = 28.853(6)$ Å, $\alpha = 68.99(3)$, $\beta = 79.27(3)$, $\gamma = 75.78(3)°$, $V = 12256(4)$ Å$^3$, $Z = 2$, $\rho_{calcd} = 2.259$ g cm$^{-3}$, $F_{000} = 7766$, $\mu = 12.966$ mm$^{-1}$, $2\theta_{max} = 56.5°$, 178890 reflections collected, 57507 unique ($R_{int} = 0.2130$). Final GOF = 0.941, $R_1 = 0.0891$, $wR_2 = 0.1440$, *R* indices based on 24017 reflections with $I > 2\sigma(I)$ (refinement on $F^2$), 1536 parameters, 0 restraints. CCDC-289350 for compound **1** and CCDC-289351 for compound **2** contain the supplementary crystallographic data for this paper. These data can be obtained free of charge from The Cambridge Crystallographic Data Centre via www.ccdc.cam.ac.uk/data_request/cif.

Received: February 4, 2006
Revised: May 22, 2006
Published online: July 25, 2006

**Keywords:** bismuth oxide · bismuth · oxo ligands · salicylate ligands · solid-state structures

[1] F. L. Suarez, J. Furne, J. Stiehm, C. Garten, M. D. Levitt, *Dig. Dis. Sci.* **2000**, *45*, 1444.
[2] G. G. Briand, N. Burford, *Chem. Rev.* **1999**, *99*, 2601.
[3] P. J. Sadler, H. Li, H. Sun, *Coord. Chem. Rev.* **1999**, 689.
[4] R. Iffland, *Bismuth, Handbook on Metals in Clinical and Analytical Chemistry* (Eds.: H. G. Seiler, A. Sigel, H. Sigel), Marcel Dekker, New York, **1994**.
[5] H. L. DuPont, C. D. Ericsson, *N. Engl. J. Med.* **1993**, *328*, 1821.
[6] D. Figueroa-Quintanilla, E. Salazar-Lindo, R. B. Sack, *N. Engl. J. Med.* **1993**, *328*, 1653.
[7] D. W. Bierer, T. Klapötke, *Biol. Met.* **1988**, *1*, 69.
[8] J. Houghton, J. G. Fox, T. C. Wang, *Eur. J. Gastroenterol. Hepatol.* **2002**, *17*, 495.

 © 2006 Wiley-VCH Verlag GmbH & Co. KGaA, Weinheim 

[9] S. Marchi, F. Costa, M. Bellini, C. Belcari, M. G. Mumolo, A. Tornar, R. Spisni, E. Torelli, G. Maltinti, *Eur. J. Gastroenterol. Hepatol.* **2002**, *13*, 547.
[10] N. Chiba, *Can. J. Gastro.* **2000**, *14*, 885.
[11] D. Y. Graham, G. M. Lew, D. G. Evans, P. D. Klein, *Ann. Intern. Med.* **1991**, *115*, 266.
[12] T. E. Sox, C. A. Olsen, *Antimicrob. Agents Chemother.* **1989**, *33*, 2075.
[13] A. Slikkerveer, F. A. de Wolff, *Med. Toxicol. Adverse Drug Exp.* **1989**, *4*, 303.
[14] B. Noonan, R. A. Alm, *Curr. Drug Targets: Infect. Disord.* **2002**, *2*, 331.
[15] P. Ruggerio, S. Peppoloni, D. Berti, R. Rappuoli, G. Del Giudice, *Expert Opin. Invest. Drugs* **2002**, *11*, 1127.
[16] M. J. Blaser, *Sci. Am.* 2005, 292, 38.
[17] N. Burford, M. D. Eelman, D. E. Mahony, M. Morash, *Chem. Commun.* **2003**, 146, and references therein.
[18] G. G. Briand, N. Burford, *Adv. Inorg. Chem.* **2000**, *50*, 285.
[19] J. H. Thurston, E. M. Marlier, K. H. Whitmire, *Chem. Commun.* **2002**, 2834.
[20] N. Burford, M. D. Eelman, T. S. Cameron, *Chem. Commun.* **2002**, 1402.
[21] P. C. Andrews, G. B. Deacon, W. R. Jackson, M. Maguire, N. Scott, B. W. Skelton, A. H. White, *J. Chem. Soc. Dalton Trans.* **2002**, 4634.
[22] J. H. Thurston, K. H. Whitmire, *Inorg. Chem.* **2002**, *41*, 4194.
[23] N. C. Norman, *Chemistry of Arsenic, Antimony and Bismuth*, Blackie, London, **1998**.
[24] S. C. Nyberg, C. H. Faerman, *Acta Crystallogr. Sect. B* **1985**, *41*, 274.
[25] J. A. Switzer, M. G. Shumsky, E. W. Bohannan, *Science* **1999**, *284*, 293.
[26] D. Mansfeld, M. Mehring, M. Schürmann, *Angew. Chem.* **2005**, *117*, 250; *Angew. Chem. Int. Ed.* **2005**, *44*, 245.
[27] T. E. Crumpton, C. Greaves, *J. Mater. Chem.* **2004**, *14*, 2433.
[28] J. Wang, Y. Li, *Chem. Commun.* 2003, 2320.
[29] E. N. Christensen, M.-A. Chevallier, J. Skibstedb, B. B. Iversena, *J. Chem. Soc. Dalton Trans.* **2000**, 265.
[30] J. H. Thurston, D. C. Swenson, L. Messerle, *Chem. Commun.* **2005**, 4228.
[31] B. Kugel, W. Frank, *Z. Anorg. Allg. Chem.* **2002**, *628*, 2178.
[32] M. Mehring, M. Schürmann, *Chem. Commun.* **2001**, 2354.
[33] E. Asato, K. Katsura, M. Mikuriya, U. Turpeinen, I. Mutikainen, J. Reedijk, *Inorg. Chem.* **1995**, *34*, 2447.
[34] W. Li, L. Jin, N. Zhu, X. Hou, F. Deng, H. Sun, *J. Am. Chem. Soc.* **2003**, *125*, 12408.
[35] J. H. Thurston, A. Kumar, C. Hofmann, K. H. Whitmire, *Inorg. Chem.* **2004**, *43*, 8427.
[36] J. H. Thurston, D. Trahan, T. Ould-Ely, K. H. Whitmire, *Inorg. Chem.* **2004**, *43*, 3299.
[37] J. H. Thurston, K. H. Whitmire, *Inorg. Chem.* **2003**, *42*, 2014.
[38] J. H. Thurston, K. H. Whitmire, *Inorg. Chem.* **2002**, *41*, 4194.
[39] M. Mehring, D. Mansfield, S. Paalasmaa, M. Schürmann, *Chem. Eur. J.* **2006**, *12*, 1767.
[40] A search of the Cambridge Crystallographic Database (CSD version 5.26) gave an average Bi–O(water) distance of 2.652 Å.
[41] C. M. Jones, M. D. Burkart, K. H. Whitmire, *Chem. Commun.* **1992**, 1638.
[42] K. H. Whitmire, S. Hoppe, O. Sydora, J. L. Jolas, C. M. Jones, *Inorg. Chem.* **2000**, *39*, 85.

 © 2006 Wiley-VCH Verlag GmbH & Co. KGaA, Weinheim 

Porphyrinoids

DOI: 10.1002/anie.200601580

# Room-Temperature Autoconversion of Free-Base Corrole into Free-Base Porphyrin**

*Claude P. Gros, Jean-Michel Barbe,* Enrique Espinosa, and Roger Guilard**

Corrole chemistry has attracted a renewed interest as a result of recently reported synthetic procedures for the preparation of various *meso*- and β-substituted monocorroles as well as of cofacial biscorrole systems.[1–10] Moreover, metal complexes of corroles can serve as catalysts for the reduction of dioxygen[11] and epoxidation,[12] as well as gas sensors.[13,14]

Corrole macrocycles are generally less stable in solution than their porphyrin analogues. Indeed, a photocatalyzed ring opening of the corrole usually occurs in the presence of dioxygen, leading to the corresponding biliverdin species when the free-base corrole is substituted at the 10-*meso* position by an aryl group (e.g. phenyl).[15,16] It was suggested that the cleavage of the direct C–C bond occurs via the formation of a dioxetan intermediate.[15,16] Metalation provides a way to stabilize the corrole ring,[9,17] but it has been shown that insertion of nickel into a face-to-face biscorrole or porphyrin-corrole dyads leads to the formation of an oxocorrole by insertion of an oxo group at one of the *meso* positions.[18]

Free-base corroles are photosensitive, and investigation into their photochemistry, for example, may be problematic. Therefore, great care must be taken to obtain reproducible spectra.[16,19,20] Free-base *meso*-triaryl corroles (e.g. phenyl, *p*-nitrophenyl) showed a diminished and broadened Soret band when left in solution in methylene chloride and exposed to air and light during a few hours.[4,19] On the other hand, perfluorophenylcorrole is thermally more stable than regular corroles as a result of the presence of electron-withdrawing groups; nevertheless, this system decomposes after a few hours of light exposure.[4,19] Many instabilities have been observed, but until now no decomposition product has been

[*] Dr. C. P. Gros, Dr. J.-M. Barbe, Dr. E. Espinosa, Prof. Dr. R. Guilard
LIMSAG UMR 5633
Université de Bourgogne
Faculté des Sciences Mirande
9, Avenue A. Savary BP 47870
21 078 Dijon Cedex (France)
Fax: (+33) 380-396-117
E-mail: jmbarbe@u-bourgogne.fr
Roger.Guilard@u-bourgogne.fr
Homepage: www.u-bourgogne.fr/limsag

[**] The French Ministry of Research (MENRT) and the CNRS (UMR 5633) are gratefully acknowledged. The authors are also grateful to Dr. Anne Chartogne (EU Mass Spectrometry Technologies Centre, Waters Corporation, Almere, The Netherlands) for accurate mass measurements (Q-TOF Premium MS instrument, ESI mode) and to Mrs. Julie Morel for the synthesis of the corrole precursors.

Supporting information for this article is available on the WWW under http://www.angewandte.org or from the author.


© 2006 Wiley-VCH Verlag GmbH & Co. KGaA, Weinheim

identified and fully characterized; the only exception was an open-chain tetrapyrrole structure reported by some of us[15] and by Paolesse et al.[16]

We report here the first example of an autoconversion of a free-base $A_2B$-corrole into its $AB_2C$-porphyrin analogue at room temperature. The 5,15-dimesityl-10-nitrophenylcorrole free base (**1**) was prepared according to a published procedure.[21] To our surprise, a solution of **1** in benzene/methanol slowly converted at room temperature in the presence of air into the corresponding *trans*-$AB_2C$-porphyrin **2** (Scheme 1).

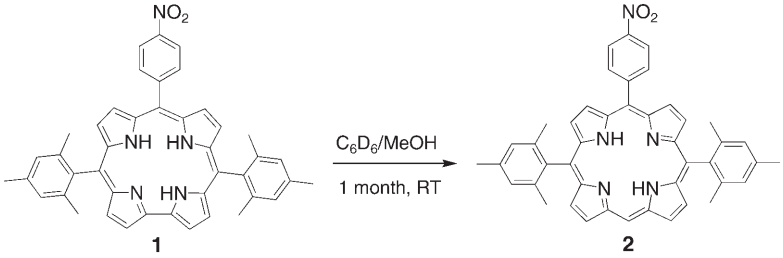


1 2

***Scheme 1.*** Autoconversion at room temperature of the free-base corrole **1** into the free-base porphyrin **2**.

The formation of the porphyrin analogue **2** was observed by mass spectrometry (MALDI-TOF), which showed a molecular pattern centered at *m*/*z* 667.8 (compared to *m*/*z* 655.3 for the monocorrole), and confirmed by X-ray crystallography (Figure 1).[22] Compounds **1** and **2** cocrystallize, occupying the same unit-cell regions and showing site-occupation factors of 0.50:0.50. Owing to the direct $C_{pyr}$–$C_{pyr}$ bond between two pyrrolic groups in **1**, their orientation in the macrocyclic moiety is different to those in **2**. The rest of the atoms of both compounds share the same positions in the crystal structure (Figure 1). Further structural features related to the different orientations of the two pyrrolic groups concern the dissimilar attractive NH···N and repulsive H···H interactions that take place in the macrocyclic cavities of **1** and **2** as a result of the extra hydrogen atom $H(N_{pyr})$, which points to this region in the free-base corrole.

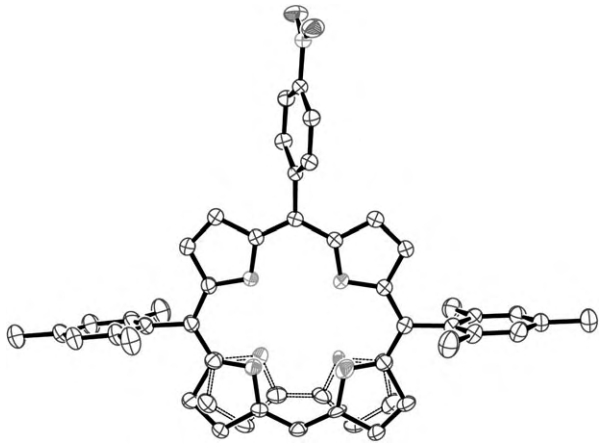

***Figure 1.*** ORTEP view showing the molecular structure of the cocrystallized corrole **1** (background) and porphyrin **2** (foreground). Ellipsoids are drawn at the 50% probability level. Hydrogen atoms are omitted for clarity. N pale gray; O dark gray; C white.

Note that separation of **1** and **2** by column chromatography on silica gel or alumina was impossible because of their similar elution characteristics. However, porphyrin **2** was successfully isolated in 19% yield by irradiating (400-W visible light) a solution of **1** (40 mg) in benzene/methanol (5:1) at room temperature during 48 h. The conversion reaction was monitored by UV/Vis and $^1$H NMR spectroscopy as well as MALDI-TOF mass spectrometry by following the total disappearance of the corrole molecular ion peak at *m*/*z* 655.4 and the appearance of the porphyrin molecular ion peak at *m*/*z* 667.8 (see Supporting Information). The $^1$H NMR spectrum of **2** ($C_6D_6$) shows the characteristic patterns of a porphyrin macrocycle (see Table 1) with a singlet for a *meso* hydrogen atom at $\delta = 9.78$ ppm, while the electronic absorption spectrum ($CH_3CN$) displays a Soret band at $\lambda_{max} = 412$ nm ($\varepsilon = 176\,000$ cm M$^{-1}$) and four Q bands at 508 ($\varepsilon = 11\,000$), 541 (2700), 583 (3700), and 638 nm (1400 cm M$^{-1}$).

***Table 1:*** $^1$H NMR data for compounds **2** and **3**.

**2**: $^1$H NMR (500 MHz, $C_6D_6$): $\delta = 9.78$ (s, 1H, *meso*), 8.96 (d, 2H, β-H), 8.93 (d, 2H, β-H), 8.88 (d, 2H, β-H), 8.58 (d, 2H, β-H), 8.04 (d, 2H, $H_o$-nitro-Ph), 7.61 (d, 2H, $H_m$-nitro-Ph), 7.26 (s, 4H, H-Mes), 2.51 (s, 6H, $CH_3$-Mes), 1.96 (s, 12H, $CH_3$-Mes), −2.28 ppm (s, 2H, NH).

**3**: $^1$H NMR (500 MHz, $CDCl_3$): $\delta = 11.25$ (s, 2H, NH pyr), 11.15 (s, 2H, NH pyr), 6.80 (s, 4H, H-Mes), 6.38 (d, 4H, β-H), 5.98 (d, 2H, β-H), 5.70 (d, 2H, β-H), 2.25 (s, 6H, $CH_3$-Mes), 2.01 ppm (s, 12H, $CH_3$-Mes).

Our first thought was that the 5-*meso*-carbon atom originated from a methanol molecule (one of the two crystallization solvents). To further confirm this hypothesis, four parallel experiments were carried out in benzene solutions with $^{13}CH_3OH$, $CD_3OD$, $CH_3OD$, and $CH_3OH$, respectively, as cosolvents. In all cases, a molecular ion peak at *m*/*z* 667.8 was observed, showing clearly that the *meso*-carbon atom at the 5-position of porphyrin **2** did not originate from a methanol molecule. Furthermore, no signal for the $^{13}$C-*meso*-carbon atom was observed in the $^{13}$C NMR spectrum of the isolated porphyrin **2** (obtained from benzene/$^{13}CH_3OH$ solution).

This unexpected result led us to further investigate the plausible reaction sequences leading to porphyrin **2** from corrole **1**. Our attention was drawn by the systematic presence of a molecular peak at *m*/*z* 554.3 in MALDI-TOF mass spectra corresponding to a red-violet polar compound (see Supporting Information). The appearance of this peak as well as the increase in its intensity was shown to be concomitant with the formation of the porphyrin macrocycle (see Supporting Information). Spectral characterization allowed identification of this by-product as an open-chain biliverdin-type structure **3** (Mes =

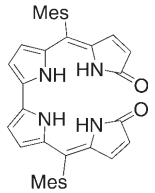


3

 © 2006 Wiley-VCH Verlag GmbH & Co. KGaA, Weinheim 

mesityl). From accurate mass measurements carried out on the molecular ion, the molecular formula $C_{36}H_{34}N_4O$ was proposed (calculated for $C_{36}H_{34}N_4O$: 554.2682; found: 554.2684). Accordingly, this result demonstrates that the nitrophenyl substituent is the leaving group of the oxidation reaction. Compound **3** displays a $^1$H NMR spectrum characteristic of a $C_2$-symmetric molecule (see Table 1). The electronic absorption spectrum shows a breakdown of the aromatic system and no Soret band ($\lambda_{max}$ ($CH_2Cl_2$): 372 (100%), 540 (44%), 661 nm (43%)). A possible mechanism based on these data for the conversion of corrole into porphyrin and the parallel oxidation reaction is proposed in the Supporting Information. A 2π+2π cycloaddition of the corrole macrocycle is thought to occur to first give a spirocyclobutane intermediate, which is then split, after oxidation, into the porphyrin system **2** and the biliverdin derivative **3**.

Although there are a few examples of thermal splitting reactions of octaphyrins into porphyrin moieties during metalation reactions (at $T > 100\,^\circ$C),[23–25] no similar reaction was described before in corrole chemistry. In summary, we have reported the first example of room-temperature autoconversion of free-base $A_2B$-corrole to free-base $AB_2C$-porphyrin. As corroles become candidates for a wide variety of applications, their stability in solution has to be delineated. Further work is currently under progress on other free-base corrole derivatives that bear different electron-donating or electron-withdrawing substituents at the *meso*- or β-positions to fully identify the key intermediates of this conversion and to further confirm this mechanism.

Received: April 21, 2006
Revised: May 22, 2006
Published online: July 20, 2006

**Keywords:** corrole · nitrogen heterocycles · oxidation · photochemistry · porphyrinoids

[1] a) J.-M. Barbe, F. Burdet, E. Espinosa, C. P. Gros, R. Guilard, *J. Porphyrins Phthalocyanines* **2003**, *7*, 365; b) R. Guilard, J.-M. Barbe, C. Stern, K. M. Kadish in *The Porphyrin Handbook*, *Vol. 18* (Eds.: K. M. Kadish, K. M. Smith, R. Guilard), Academic Press, Boston, **2003**, p. 303.
[2] M. Bröring, C. Hell, *Chem. Commun.* **2001**, 2336.
[3] a) J. P. Collman, R. A. Decreau, *Tetrahedron Lett.* **2003**, *44*, 1207; b) R. A. Decreau, J. P. Collman, *Tetrahedron Lett.* **2003**, *44*, 3323.
[4] G. R. Geier III, J. F. B. Chick, J. B. Callinan, C. G. Reid, W. P. Auguscinski, *J. Org. Chem.* **2004**, *69*, 4159.
[5] A. Ghosh, *Angew. Chem.* **2004**, *116*, 1952; *Angew. Chem. Int. Ed.* **2004**, *43*, 1918.
[6] Z. Gross, N. Galili, I. Saltsman, *Angew. Chem.* **1999**, *111*, 1530; *Angew. Chem. Int. Ed.* **1999**, *38*, 1427.
[7] a) D. T. Gryko, *Eur. J. Org. Chem.* **2002**, 1735; b) D. T. Gryko, B. Koszarna, *Org. Biomol. Chem.* **2003**, *1*, 350.
[8] a) R. Guilard, C. P. Gros, F. Bolze, F. Jérôme, Z. Ou, J. Shao, J. Fischer, R. Weiss, K. M. Kadish, *Inorg. Chem.* **2001**, *40*, 4845; b) R. Guilard, D. T. Gryko, G. Canard, J.-M. Barbe, B. Koszarna, S. Brandès, M. Tasior, *Org. Lett.* **2002**, *4*, 4491; c) R. Guilard, F. Jérôme, J.-M. Barbe, C. P. Gros, Z. Ou, J. Shao, J. Fischer, R. Weiss, K. M. Kadish, *Inorg. Chem.* **2001**, *40*, 4856.
[9] a) R. Paolesse in *The Porphyrin Handbook*, *Vol. 2* (Eds.: K. M. Kadish, K. M. Smith, R. Guilard), Academic Press, New York, **2000**, p. 201; b) R. Paolesse, A. Marini, S. Nardis, A. Froiio, F. Mandoj, D. J. Nurco, L. Prodi, M. Montalti, K. M. Smith, *J. Porphyrins Phthalocyanines* **2003**, *7*, 25.
[10] a) C. Jeandon, R. Ruppert, H. J. Callot, *J. Org. Chem.* **2006**, *71*, 3111; b) C. Jeandon, R. Ruppert, H. J. Callot, *Chem. Commun.* **2004**, 1090.
[11] a) K. M. Kadish, L. Frémond, F. Burdet, J.-M. Barbe, C. P. Gros, R. Guilard, *J. Inorg. Biochem.* **2006**, *100*, 858; b) K. M. Kadish, L. Frémond, Z. P. Ou, J. Shao, C. Shi, F. C. Anson, F. Burdet, C. P. Gros, J.-M. Barbe, R. Guilard, *J. Am. Chem. Soc.* **2005**, *127*, 5625.
[12] G. Golubkov, J. Bendix, H. B. Gray, A. Mahammed, I. Goldberg, A. J. DiBilio, Z. Gross, *Angew. Chem.* **2001**, *113*, 2190; *Angew. Chem. Int. Ed.* **2001**, *40*, 2132.
[13] J.-M. Barbe, G. Canard, S. Brandès, F. Jérôme, G. Dubois, R. Guilard, *Dalton Trans.* **2004**, 1208.
[14] C. Di Natale, D. Salimbeni, R. Paolesse, A. Macagnano, A. D'Amico, *Sens. Actuators B* **2000**, *65*, 220.
[15] C. Tardieux, C. P. Gros, R. Guilard, *J. Heterocycl. Chem.* **1998**, *35*, 965.
[16] R. Paolesse, F. Sagone, A. Macagnano, T. Boschi, L. Prodi, M. Montalti, N. Zaccheroni, F. Bolletta, K. M. Smith, *J. Porphyrins Phthalocyanines* **1999**, *3*, 364.
[17] C. Erben, S. Will, K. M. Kadish in *The Porphyrin Handbook*, *Vol. 2* (Eds.: K. M. Kadish, K. M. Smith, R. Guilard), Academic Press, New York, **2000**, p. 233.
[18] F. Jérôme, J.-M. Barbe, C. P. Gros, R. Guilard, J. Fischer, R. Weiss, *New J. Chem.* **2001**, *25*, 93.
[19] T. Ding, E. A. Aleman, D. A. Modarelli, C. J. Ziegler, *J. Phys. Chem. A* **2005**, *109*, 7411.
[20] B. Ventura, A. D. Esposti, B. Koszarna, D. T. Gryko, L. Flamigni, *New J. Chem.* **2005**, *29*, 1559.
[21] D. T. Gryko, K. Jadach, *J. Org. Chem.* **2001**, *66*, 4267.
[22] Red-purple single crystals of the co-crystallized compounds **1** and **2** were obtained by slow diffusion of methanol into a solution of **1** in $C_6D_6$. A high-quality specimen of dimensions $0.50 \times 0.15 \times 0.10$ mm$^3$ was used for the X-ray diffraction experiment. Data were collected at $T = 115(2)$ K up to $\theta_{max} = 27.63°$ with graphite monochromatized $Mo_{K\alpha}$ radiation ($\lambda = 0.71073$ Å) on a Nonius KappaCCD diffractometer,[26] equipped with a nitrogen jet stream low-temperature system (Oxford Cryosystems). No significant decay of intensity was observed during the data collection. No diffractometer or temperature problems occurred during the experiment. Data reduction was performed by using the DENZO software.[27] No absorption corrections were applied. The structure was solved by direct methods (SIR97 program)[28] and refined by full-matrix least-squares on $F^2$ (SHELXL-97 program)[29] using the complete set of reflections. All non-hydrogen atoms were refined with anisotropic thermal parameters. All hydrogen atoms of **1** and **2**, except two H($N_{pyr}$) hydrogen atoms of **1** and one H($N_{pyr}$) atom of **2**, were located by Fourier synthesis and placed at calculated positions using a riding model. All deuterium atoms of the disordered solvent molecules were placed at calculated positions using a riding model, however only some of them were located in the Fourier synthesis. Two global isotropic thermal factors were refined, one for hydrogen atoms and the other for deuterium atoms. Compounds **1** and **2** co-crystallize with a $C_6D_6$ solvent molecule $0.5(Cor)\cdot 0.5(Por)\cdot C_6D_6$ in the triclinic system (space group $P\bar{1}$), $a = 8.1405(2)$ Å, $b = 15.7733(4)$ Å, $c = 15.8787(5)$ Å, $\alpha = 73.239(1)°$, $\beta = 81.074(1)°$, $\gamma = 82.885(1)°$, $V = 1921.85(9)$ Å$^3$, $Z = 2$, $\rho_{calcd} = 1.279$ g cm$^{-3}$, $\mu(Mo_{K\alpha}) = 0.079$ mm$^{-1}$, 13902 collected reflections, 8842 independent reflections ($R_{int} = 0.0370$), and 612 refined parameters. At the convergence, the final agreement factors are $R(F) = 0.0634$ and 0.1078 and $R_w(F^2) =$

 © 2006 Wiley-VCH Verlag GmbH & Co. KGaA, Weinheim 

0.1521 and 0.1739, for $I > 2\sigma(I)$ and all data, respectively. The largest Fourier difference peak and hole are 0.311 and $-0.322\ e\ Å^{-3}$. Compounds **1** and **2** occupy the same unit cell regions, showing site-occupation factors of 0.50:0.50. Following this structural feature, the solvent molecule is also disordered over two close positions with equivalent site-occupation factors of 0.50:0.50. CCDC 603366 contains the supplementary crystallographic data for this paper. These data can be obtained free of charge from The Cambridge Crystallographic Data Centre via www.ccdc.cam.ac.uk/data_request/cif.

[23] Y. Tanaka, W. Hoshino, S. Shimizu, K. Youfu, N. Aratani, N. Maruyama, S. Fujita, A. Osuka, *J. Am. Chem. Soc.* **2004**, *126*, 3046.

[24] E. Vogel, M. Michels, L. Zander, J. Lex, N. S. Tuzun, K. N. Houk, *Angew. Chem.* **2003**, *115*, 2964; *Angew. Chem. Int. Ed.* **2003**, *42*, 2857.

[25] L. Latos-Grazynski, *Angew. Chem.* **2004**, *116*, 5234; *Angew. Chem. Int. Ed.* **2004**, *43*, 5124.

[26] COLLECT, Data Collection Software, BV Nonius, Delft, The Netherlands, **1998**.

[27] DENZO Software (Z. Otwinowski, W. Minor, *Methods Enzymol.* **1997**, *276*, 307).

[28] A. Altomare, M. C. Burla, M. Camalli, G. L. Cascarano, C. Giacovazzo, A. Guagliardi, A. G. G. Moliterni, G. Polidori, R. Spagna, *J. Appl. Crystallogr.* **1999**, *32*, 115.

[29] SHELXL97 Program, G. M. Sheldrick, SHELXL97, University of Göttingen, Germany, **1997**.

 © 2006 Wiley-VCH Verlag GmbH & Co. KGaA, Weinheim 

*Bioorganometallic Chemistry*

DOI: 10.1002/anie.200601752

# Ruthenium-Induced Allylcarbamate Cleavage in Living Cells**

*Craig Streu and Eric Meggers**

Organometallics are increasingly gaining attention as tools in chemical biology owing to their distinguished physicochemical properties, reactivities, and three-dimensional structures.[1] Along these lines, the exceptional ability of organometallic compounds to catalyze a wide variety of chemical transformations has not yet been sufficiently exploited for chemical biology, but could yield bioactive molecules with novel properties.[2–4] For example, such catalysts could eventually be used to amplify signals by turning over a substrate multiple times, catalytically label or deactivate target biomolecules, or release prodrugs and all this in a cellular environment. However, designing catalysts which work under physiological conditions is a significant challenge owing to the combined presence of air, water, and a plethora of cellular components such as millimolar concentrations of thiols, which are prone to poison organometallic catalysts, especially under protic and aerobic conditions.[5]

With respect to this new aspect of bioorganometallic chemistry, we herein disclose a ruthenium-catalyzed release of amines from their allylcarbamates that tolerates the combination of water, air, and thiols, and we demonstrate the utility of this cleavage reaction in living mammalian cells.[6–10]

In the course of screening several organometallic catalysts for a variety of reactions, we found that the complex [Cp*Ru(cod)Cl] (Cp* = pentamethylcyclopentadienyl, cod = 1,5-cyclooctadiene; **1**) catalyzes the cleavage of allylcarbamates **2** to their respective amines **3** in the presence of an excess of thiophenol in an open flask experiment, tolerating water and air (Scheme 1).[11,12] For example, the reaction of *p*-methylaniline allylcarbamate **2a** (200 mM) with 5 equivalents of thiophenol in the presence of 10 mol% ruthenium catalyst **1**, carried out in MeOH/$H_2O$ (95:5) under air and overnight at room temperature, provides *p*-methylaniline in 86% yield if isolated as the *tert*-butoxycarbonyl (Boc)-protected amine, and 89% yield according to GC analysis (Table 1, entry 1). This deprotection is quite general as it works under the same conditions with high yields also for allylcarbamates of an electron-acceptor-substituted aniline (**2b**, 85% yield) and a primary (**2c**, 94%, isolated as the Boc-protected amine), as well as a secondary amine (**2d**, 87% yield; Scheme 1).[13]

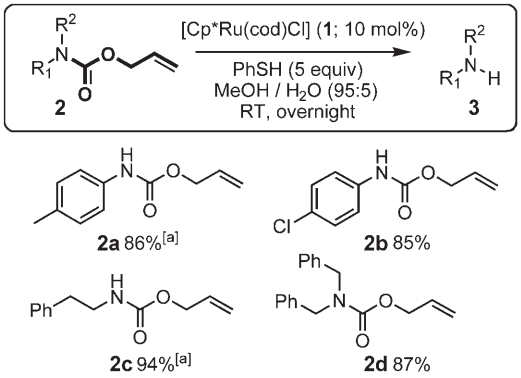


***Scheme 1.*** Reaction of compounds **2** to form the respective amines **3**. [a] Isolated as the Boc-protected amine.

The influence of air, water, and aliphatic thiols on the GC-determined yields of this ruthenium-catalyzed cleavage is shown for substrate **2a** in Table 1. Accordingly, yields are not significantly affected by air and water (Table 1, entries 1–3). In contrast, omitting thiophenol prevents the carbamate cleavage completely in the presence of water and air (Table 1, entry 4). Most importantly for cellular applications, the cleavage reaction can be performed in the presence of

[*] C. Streu, Prof. E. Meggers
Department of Chemistry
University of Pennsylvania
231 South 34th Street, Philadelphia, PA 19104 (USA)
Fax: (+1) 215-746-0348
E-mail: meggers@sas.upenn.edu
Homepage: http://www.sas.upenn.edu/~meggers/

[**] We gratefully acknowledge support from the National Institutes of Health (confocal fluorescence microscope: 1S10RR021113-01) and the group of Prof. Gary A. Molander (GC measurements).

Supporting information for this article is available on the WWW under http://www.angewandte.org or from the author.

 © 2006 Wiley-VCH Verlag GmbH & Co. KGaA, Weinheim 

***Table 1:*** Catalytic cleavage of allylcarbamate **2a** to *p*-methylaniline with [Cp*Ru(cod)Cl].[a]

| Entry | Thiol | Solvent | Atm. | *T* | Yield |
|---|---|---|---|---|---|
| 1 | PhSH | MeOH/$H_2O$ (95:5) | air | RT | 89% |
| 2 | PhSH | MeOH | air | RT | 93% |
| 3 | PhSH | MeOH/$H_2O$ (95:5) | argon | RT | 96% |
| 4 | no thiols | MeOH/$H_2O$ (95:5) | air | RT | 0% |
| 5 | PhSH and $PhCH_2CH_2SH$ | MeOH/$H_2O$ (95:5) | air | RT | 93% |
| 6 | $PhCH_2CH_2SH$ | MeOH/$H_2O$ (95:5) | air | RT | 34% |
| 7 | $PhCH_2CH_2SH$ | MeOH/$H_2O$ (95:5) | air | 37°C | 67% |

[a] General reaction conditions: **2a** (200 mM), [Cp*Ru(cod)Cl] (20 mM), thiol (1 M; each), at room temperature (20–23°C) overnight. Yields were determined by GC analysis.

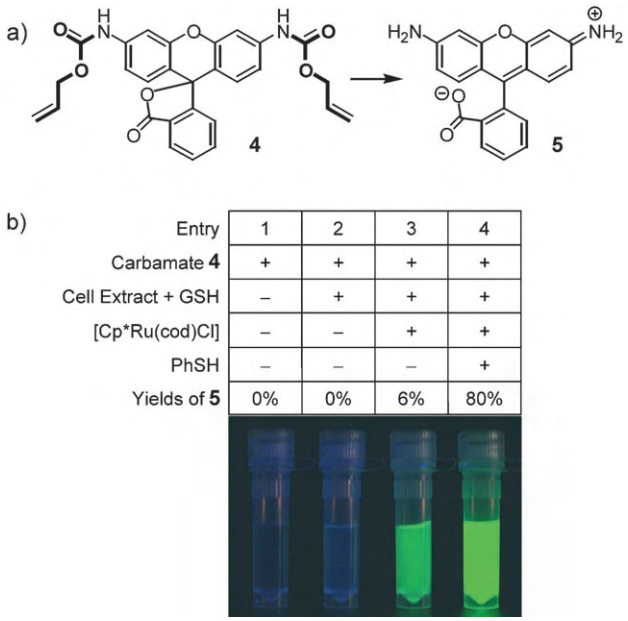


***Figure 1.*** Influence of cell extract on the ruthenium-catalyzed allylcarbamate cleavage. a) Ruthenium-catalyzed deprotection of the caged fluorophore **4** to rhodamine 110 (**5**). b) Fluorescence development with **4**. Reaction conditions: Entry 1: **4** (0.5 mM) in DMSO/$H_2O$ (1:1). Entry 2: **4** (0.5 mM), in DMSO/cell extract (1:1), and GSH (3.5 mM), yielding an overall pH of 7.0. Entry 3: Same as entry 2, but with additional [Cp*Ru(cod)Cl] at 100 μM. Entry 4: Same as entry 2, but with additional [Cp*Ru(cod)Cl] at 100 μM and 3.5 mM PhSH. Reaction mixtures were shaken at 120 rpm for 2.5 h at 37°C. Yields were then determined by comparing the fluorescence of diluted samples with a standard curve of different concentrations of rhodamine 110. For the shown vials, the solutions were diluted 20-fold with $H_2O$/MeOH (1:1) and excited with a long-wavelength UV lamp.

aliphatic thiols, such as benzeneethanethiol, with virtually no influence on the yield of the reaction (93%; Table 1, entry 5). However, if performed at room temperature, the aromatic thiol is necessary because substitution for an aliphatic thiol leads to a significant reduction in yield (34%; Table 1, entry 6). Interestingly, increasing the temperature to 37°C provides the released amine with an improved yield of 67% by using the aliphatic thiol benzeneethanethiol as the only nucleophile.

To evaluate the carbamate cleavage under conditions that more closely resemble a physiological environment, the bis-allyloxycarbonyl-protected rhodamine 110 (**4**; Figure 1a) was synthesized.[14] This caged fluorophore is virtually nonfluorescent (Figure 1b, entry 1) and stable in the presence of *E. coli* cell extract (Figure 1b, entry 2).[15] However, upon allylcarbamate deprotection, strongly green-fluorescent rhodamine 110 (**5**) is released (Figure 1a). This allows for monitoring of the ruthenium-catalyzed reaction by fluorescence analysis. For example, the reaction of **4** with **1** (20 mol%) in the presence of cell extract and an additional glutathione (GSH; 3.5 mM)[16] leads to the release of the fluorophore with a yield for **5** of 6% at 37°C (Figure 1b, entry 3). Under the same conditions, but with additional thiophenol, the yield increases to 80% as measured after 2.5 h (Figure 1b, entry 4), resulting in a turnover number of 8. These results demonstrate that [Cp*Ru(cod)Cl] is able to catalyze the cleavage of allylcarbamates under biological conditions consisting of millimolar concentrations of GSH as well as a plethora of cellular components from the whole-cell extract.

Finally, the caged fluorophore **4** was used as a tool to investigate the ruthenium-induced allylcarbamate cleavage in living mammalian cells. For this, cultured HeLa cells were loaded with caged fluorophore **4** by incubating the HeLa cells with **4** (100 μM) for half an hour, followed by washing the cells with phosphate-buffered saline (PBS) buffer solution, and the subsequent addition of fresh media. Thereafter, catalyst **1** was added to the medium in final concentrations as low as 20 μM. Fluorescence should now only develop inside the cell where the caged fluorophore **4** is located. Indeed, observing the changes in fluorescence by live-cell imaging with a confocal fluorescence microscope demonstrates that green fluorescence increases in intensity by around 10-fold over a time period of 15 minutes within the cytoplasm of the cells (Figure 2a and b). For comparison, in the absence of thiophenol, the fluorescence increases more modestly by around 3.5-fold, indicating that thiophenol is beneficial, although not absolutely required, for the induction of fluorescence. This is consistent with our model experiments in cell extract (see Figure 1).

Additional cell-staining experiments with the red fluorescent membrane carbocyanine dye $DiIC_{18}$(5) illustrate that the fluorescence only develops in the interior of the cell (Figure 2c–f). In control experiments, we verified that no fluorescence evolves in the absence of ruthenium complex **1** or the absence of the caged fluorophore **4** (data not shown). Together, these experiments demonstrate that ruthenium complex **1** is capable of passing through the cell membrane and inducing the cleavage of allylcarbamates within living cells. Notably, cytotoxicity experiments with the 3-(4,5-dimethylthiazol-2-yl)-2,5-diphenyltetrazolium bromide (MTT) method verify that treatment with the organoruthenium compound **1**, thiophenol, and the caged fluorophore **4** does not influence the viability of the cells (see the Supporting Information).

 © 2006 Wiley-VCH Verlag GmbH & Co. KGaA, Weinheim 

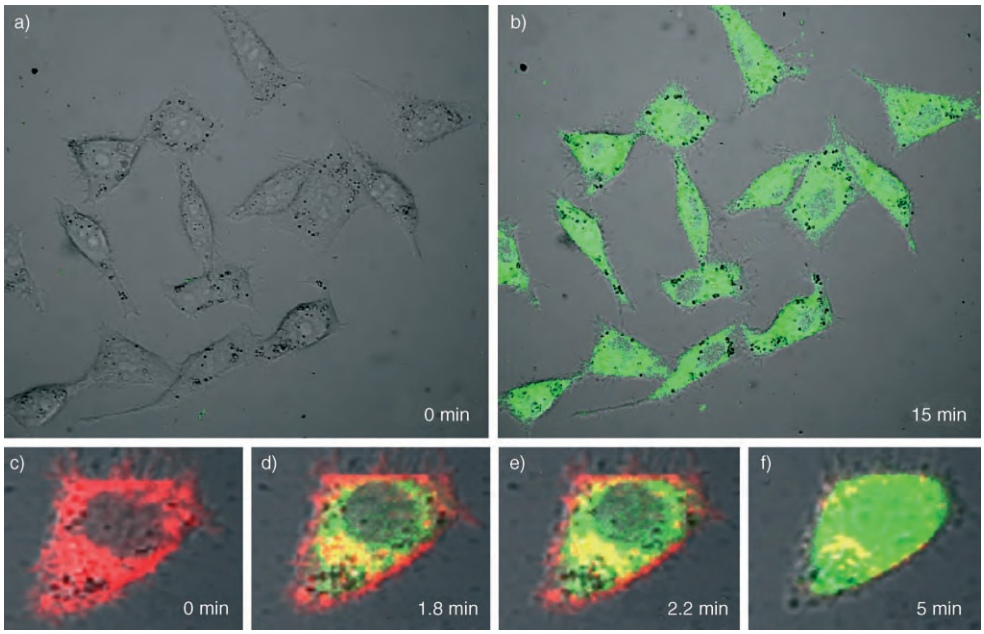


***Figure 2.*** Fluorescence microscopy imaging of ruthenium-induced uncaging of allylcarbamate-protected rhodamine 110 (**4**) inside HeLa cells. Shown are superimposed phase-contrast and fluorescence images. Images a) and b): Cells were preincubated with **4** (100 μM) for 30 min, washed with PBS buffer solution, and then treated with [Cp*Ru(cod)Cl] (20 μM) and thiophenol (500 μM). The shown images are a) right after this addition and b) after 15 min. Images c)–f): Cells were preincubated with **4** (100 μM) for 30 min and at the same time with the membrane carbocyanine dye $DiIC_{18}$(5) (Molecular Probes). After washing with PBS buffer solution, cells were treated with [Cp*Ru(cod)Cl] (40 μM) and thiophenol (100 μM). The shown images are c) right after this addition and d)–f) after the indicated times.

In conclusion, [Cp*Ru(cod)Cl] has been shown to be capable of inducing the uncaging of amines from their respective allylcarbamates under physiological conditions such as in living mammalian cells. The described reaction is an encouraging starting point towards the goal of designing catalytic organometallics as tools in chemical biology.

Received: May 3, 2006
Published online: July 20, 2006

**Keywords:** bioorganometallic chemistry · cleavage reactions · homogeneous catalysis · mammalian cells · ruthenium

[1] For bioorganometallic chemistry and medicinal organometallic chemistry, see: a) K. Severin, R. Bergs, W. Beck, *Angew. Chem.* **1998**, *110*, 1722–1743; *Angew. Chem. Int. Ed.* **1998**, *37*, 1634–1654; b) D. B. Grotjahn, *Coord. Chem. Rev.* **1999**, *190*, 1125–1141; c) (Ed.: G. Jaouen), *J. Organomet. Chem.* **1999**, *589*, 1–126; d) N. Metzler-Nolte, *Angew. Chem.* **2001**, *113*, 1072–1076; *Angew. Chem. Int. Ed.* **2001**, *40*, 1040–1043; e) R. H. Fish, G. Jaouen, *Organometallics* **2003**, *22*, 2166–2177; f) R. Stodt, S. Gencaslan, I. M. Müller, W. S. Sheldrick, *Eur. J. Inorg. Chem.* **2003**, 1873–1882; g) D. Schlawe, A. Majdalani, J. Velcicky, E. Heßler, T. Wieder, A. Prokop, H.-G. Schmalz, *Angew. Chem.* **2004**, *116*, 1763–1766; *Angew. Chem. Int. Ed.* **2004**, *43*, 1731–1734; h) D. R. Van Staveren, N. Metzler-Nolte, *Chem. Rev.* **2004**, *104*, 5931–5985; i) I. Ott, B. Kircher, R. Gust, *J. Inorg. Biochem.* **2004**, 485–489; j) *Bioorganometallics* (Ed.: G. Jaouen), Wiley-VCH, Weinheim, **2005**; k) Y. K. Yan, M. Melchart, A. Habtemariam, P. J. Sadler, *Chem. Commun.* **2005**, 4764–4776; l) C. S. Allardyce, A. Dorcier, C. Scolaro, P. J. Dyson, *Appl. Organomet. Chem.* **2005**, *19*, 1–10; m) F. Wang, A. Habtemariam, E. P. L. van der Geer, R. Fernandez, M. Melchart, R. J. Deeth, R. Aird, S. Guichard, F. P. A. Fabbiani, P. Lozano-Casal, I. D. H. Oswald, D. I. Jodrell, S. Parsons, P. J. Sadler, *Proc. Natl. Acad. Sci. USA* **2005**, *102*, 18269–18274; n) P. J. Dyson, G. Sava, *Dalton Trans.* **2006**, 1929–1933; o) U. Schatzschneider, N. Metzler-Nolte, *Angew. Chem.* **2006**, *118*, 1534–1537; *Angew. Chem. Int. Ed.* **2006**, *45*, 1504–1507; p) J. É. Debreczeni, A. N. Bullock, G. E. Atilla, D. S. Williams, H. Bregman, S. Knapp, E. Meggers, *Angew. Chem.* **2006**, *118*, 1610–1615; *Angew. Chem. Int. Ed.* **2006**, *45*, 1580–1585; q) A. F. Peacock, A. Habtemariam, R. Fernandez, V. Walland, F. P. A. Fabbiani, S. Parsons, R. E. Aird, D. I. Jodrell, P. J. Sadler, *J. Am. Chem. Soc.* **2006**, *128*, 1739–1748; r) Y. K. Yan, M. Melchart, A. Habtemariam, A. F. A. Peacock, P. J. Sadler, *J. Biol. Inorg. Chem.* **2006**, *11*, 483–488.

[2] Catalytic hydrogenation of membrane lipids has been demonstrated in living cyanobacteria, plant, and mammalian cells. See, for example: a) L. Vigh, F. Joó, Á. Cséplö, *Eur. J. Biochem.* **1985**, *146*, 241–244; b) S. Benkö, H. Hilkmann, L. Vigh, W. J. van Blitterswijk, *Biochim. Biophys. Acta* **1987**, *896*, 129–135; c) L. Vigh, D. A. Los, I. Horváth, N. Murata, *Proc. Natl. Acad. Sci. USA* **1993**, *90*, 9090–9094; d) I. Horváth, A. Glatz, V. Varvasovszki, Z. Török, T. Páli, G. Balogh, E. Kovács, L. Nádasdi, S. Benkö, F. Joó, L. Vigh, *Proc. Natl. Acad. Sci. USA* **1998**, *95*, 3513–3518.

[3] For small synthetic molecules with superoxide dismutase activity in vivo, see: a) D. Salvemini, Z.-Q. Wang, J. L. Zweier, A. Samouilov, H. Macarthur, T. P. Misko, M. G. Currie, S. Cuzzocrea, J. A. Sikorski, D. P. Riley, *Science* **1999**, *286*, 304–306; b) D. P. Riley, *Chem. Rev.* **1999**, *99*, 2573–2587.

[4] Organometallics have recently been used to catalyze protein modifications in a test tube. For an overview, see: a) J. M. Antos, M. B. Francis, *Curr. Opin. Chem. Biol.* **2006**, *10*, 253–262; b) J. H. Maarseveen, J. N. H. Reek, J. W. Back, *Angew. Chem.*

 © 2006 Wiley-VCH Verlag GmbH & Co. KGaA, Weinheim 

**2006**, *118*, 1873 – 1875; *Angew. Chem. Int. Ed.* **2006**, *45*, 1841 – 1843.
[5] Testing of many organometallic compounds in our laboratory for catalysis under these conditions has revealed that not the individual components alone, but rather in combination, causes serious problems for most organometallic catalysts.
[6] For an overview of organometallic catalysis in water, see: *Aqueous-Phase Organometallic Catalysis* (Eds.: B. Cornils, W. A. Herrmann), 2nd ed., Wiley-VCH, Weinheim, **2004**.
[7] For some air- and moisture-tolerant transition metal catalysts, see: B. D. Sherry, F. D. Toste, *Chemtracts* **2005**, *18*, 14 – 28.
[8] For transition metal catalyzed C–C bond formations in water and under air, see: C.-J. Li, *Acc. Chem. Res.* **2002**, *35*, 533 – 538.
[9] For transition-metal-catalyzed carbon–sulfur bond formations, see: T. Kondo, T. Mitsudo, *Chem. Rev.* **2000**, *100*, 3205 – 3220.
[10] For ruthenium-catalyzed reactions in the presence of thiols, see, for example: a) Y. Inada, Y. Nishibayashi, M. Hidai, S. Uemura, *J. Am. Chem. Soc.* **2002**, *124*, 15172 – 15173; b) T. Kondo, Y. Kanda, A. Baba, K. Fukuda, A. Nakamura, K. Wada, Y. Morisaki, T. Mitsudo, *J. Am. Chem. Soc.* **2002**, *124*, 12960 – 12961.
[11] Catalyst **1** has previously been shown to catalyze the allylation of thiols with allylcarbonates in MeCN and under an atmosphere of argon: T. Kondo, Y. Morisaki, S. Uenoyama, K. Wada, T. Mitsudo, *J. Am. Chem. Soc.* **1999**, *121*, 8657 – 8658.
[12] In the course of the reaction, PhSH is converted into allylphenylsulfide and $CO_2$ is released. Mechanistically, this reaction is related to the ruthenium-catalyzed addition of nucleophiles to allylic carbonates which is postulated to proceed through the formation of a π-allylruthenium species. See, for example: B. M. Trost, F. D. Toste, A. B. Pinkerton, *Chem. Rev.* **2001**, *101*, 2067 – 2096.
[13] It is noteworthy that we obtain as a side product the partial oxidation of PhSH to the disulfide. However, in the presence of an excess of thiol, no negative influence on the yield of the carbamate cleavage is observed.
[14] For uncaging rhodamine dyes, see, for example: a) S. P. Leytus, L. L. Melhado, W. F. Mangel, *Biochem. J.* **1983**, *209*, 299 – 307; b) S. S. Chandran, K. A. Dickson, R. T. Raines, *J. Am. Chem. Soc.* **2005**, *127*, 1652 – 1653.
[15] In contrast, the corresponding bis-allylcarbonate derivative is hydrolyzed rapidly under these conditions.
[16] Glutathione is present in virtually all mammalian cells at millimolar concentrations: N. Kaplowitz, T. Y. Aw, M. Ookhtens, *Annu. Rev. Pharmacol. Toxicol.* **1985**, *25*, 714 – 744.

 © 2006 Wiley-VCH Verlag GmbH & Co. KGaA, Weinheim 

Screening

DOI: 10.1002/anie.200601695

# Small-Molecule Screening Made Simple for a Difficult Target with a Signaling Nucleic Acid Aptamer that Reports on Deaminase Activity**

*Nadine H. Elowe, Razvan Nutiu, Abdellah Allali-Hassani, Jonathan D. Cechetto, Donald W. Hughes, Yingfu Li,* and Eric D. Brown**

Conventional approaches to small-molecule screening are currently being challenged by the availability of vast amounts of genomic sequence information and a plethora of potential targets. This challenge has precipitated a need for new screening paradigms that emphasize simplicity, capacity, and parallelization. Herein we report the application of signaling DNA-aptamer technology for the development and execution of a high-throughput screen for an otherwise problematic target, adenosine deaminase (ADA). The approach employed a signaling DNA aptamer that reports on adenosine concentration over the course of the enzymatic reaction. The assay was extremely robust in a screen of more than 44000 molecules and revealed a new competitive inhibitor of the deaminase. Nucleic acid aptamers have proven worthy as a routinely selectable species for a wide variety of small molecules and so this proof-of-principle work has broad

[*] N. H. Elowe,[+] Dr. A. Allali-Hassani,[#] Dr. J. D. Cechetto, Dr. Y. Li, Dr. E. D. Brown
Department of Biochemistry and Biomedical Sciences
McMaster University
Hamilton, ON L8N 3Z5 (Canada)
Fax: (+1) 905-525-9033
E-mail: liying@mcmaster.ca
ebrown@mcmaster.ca

R. Nutiu, Dr. D. W. Hughes, Dr. Y. Li
Department of Chemistry
McMaster University
Hamilton, ON L8N 3Z5 (Canada)
Fax: (+1) 905-522-9033

[+] Current address:
Novartis Institutes for BioMedical Research, Diabetes and Metabolism
100 Technology Square
Cambridge, MA 02139 (USA)

[#] Current address:
Structural Genomics Consortium
University of Toronto
100 College Street, Floor 3A, Room 351
Toronto, ON M5G 1L5, (Canada)

[**] We thank Jan Blanchard for her help with mass spectrometry and comments on the manuscript. This work was supported by Ontario Research and Development Challenge Fund, Natural Sciences and Engineering Research Council, and MDS Sciex. E.D.B. and Y.L. hold Canada Research Chairs.

Supporting information for this article is available on the WWW under http://www.angewandte.org or from the author.


WILEY InterScience DISCOVER SOMETHING GREAT
© 2006 Wiley-VCH Verlag GmbH & Co. KGaA, Weinheim

applicability and potential for the development of enzymatic assays suitable for a chemical genomic approaches.

Aptamers are single-stranded DNA and RNA molecules derived from random libraries that are capable of binding to diverse biological targets, such as small-molecule metabolites, peptides, hormones, or proteins, with high affinity and specificity. Aptamers have found diverse utility ranging from research[1] to diagnostic and therapeutic applications.[2,3] Nucleic acid aptamers were first shown to have promise as a displaceable ligand in compound screening in which a panel of a dozen naphthalensulfonic acids were tested for their capacity to compete a $^{32}$P-labeled aptamer from platelet-derived growth factor.[4] An interesting property of nucleic acid aptamers is that they are known to undergo conformational changes upon target binding.[5] This characteristic is emerging as exploitable for the design of signaling probes that report on the interaction of aptamers with their targets and thus, signaling aptamers have genuine potential in assay development and small-molecule screening.[6,7] Recently, we reported a proof-of-concept study in which the enzyme activity of alkaline phosphatase was monitored in real time by using a signaling DNA aptamer with a higher affinity for adenosine than for AMP.[8] The assay employed a "structure-switching" aptamer in which adenosine binding induced a state of high fluorescence through release of a quenching group. The assay was amenable to screening in a 96-well plate and was sensitive to known inhibitors of alkaline phosphatase. Thus, signaling nucleic acid systems have begun to show real promise as reporter systems that can be tailored with relative ease to a variety of assays. In the work reported herein, we have rigorously tested this potential in an automated, high-throughput screen (HTS) of ADA against a small-molecule library of more than 44000 compounds.

ADA is a key enzyme in purine metabolism, catalyzing the irreversible deamination of adenosine/deoxyadenosine to inosine/deoxyinosine. ADA is a ubiquitous enzyme best known for its role in certain types of severe combined immunodeficiency diseases.[9] The enzyme has both cytosolic and extracelluar forms in which the latter is associated with CD26, which is strongly upregulated in T-cell activation.[10] Increasingly, extracellular adenosine is recognized to have a role in attenuating immunity and inflammation, and thus inhibitors of ADA may have real potential for clinical applications.[11] Despite growing interest in this target, ADA does not have a simple, homogenous, and sensitive assay amenable to HTS. Common methods measure ammonia produced[12] or the change in adenosine concentration by monitoring absorbance at 265 nm.[13] The former is not easily automated and the short-wavelength detection of the latter is prone to interference from the intrinsic absorbance of screening compounds. A long-wavelength coupled assay system has also been described,[14] but it is inherently cumbersome owing to the need for three coupling enzymes. Thus, none of the assays described to date could be considered ideal for small-molecule screening.

To develop a screening assay for ADA, we employed a fluorescence-signaling aptamer with high affinity for adenosine and virtually no affinity for inosine (Figure 1 A).[15,16] The fluorescence signal in this system is derived from a fluorescein

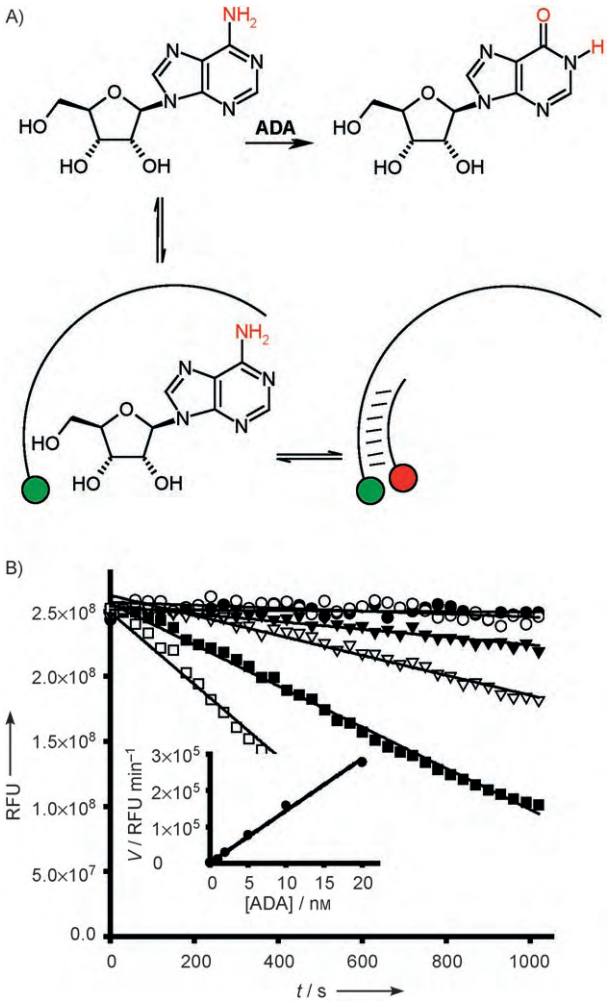


***Figure 1.*** A) Fluorescence-signaling aptamer assay for screening. The fluorescein-labeled aptamer, depicted as an arc with a green-filled circle (Fluorescein-5′-TCACTGACCTGGGGGAGTATTGCGGAGGAAGGT), complexes with either adenosine or a quenching oligonucleotide (5′-CCCAGGTCAGTG-Dabcyl; arc with red-filled circle) resulting in the exclusion of the other. The fluorescein-labeled aptamer has little affinity for inosine. Thus as adenosine is transformed to inosine by ADA, the aptamer becomes available to complex with the quenching group and reports on the progress of the reaction with decreasing fluorescence over time. Inhibition of ADA maintains high adenosine concentration and the highly fluorescent adenosine–aptamer complex is therefore formed. B) Assay linearity with time and enzyme concentration. Assays were run with varying enzyme concentration (● No ADA; ○ 1 nM ADA; ▼ 2 nM ADA; ▽ 5 nM ADA; ■ 10 nM ADA; □ 20 nM ADA) and with 500 μM adenosine, 20 nM aptamer, 40 nM QDNA, 5 mM $MgCl_2$, 300 mM NaCl in 25 mM 2-[4-(2-hydroxyethyl)-1-piperazinyl]ethanesulfonic acid (HEPES) buffer solution at pH 8.0. The reaction was initiated with the addition of an adenosine and DNA mixture and monitored over time, with excitation at 485 nm and measuring emission at 530 nm. RFU = relative fluorescence units. $V$ = reaction velocity.

group present at the 5′-end of the DNA aptamer and determined by the ratio of two different structural states, the adenosine-bound and free forms of the aptamer. Only the latter is capable of complexing with antisense DNA containing a dabcyl quenching group (QDNA). As adenosine is converted to inosine, the QDNA-bound form of the aptamer

 © 2006 Wiley-VCH Verlag GmbH & Co. KGaA, Weinheim 

predominates, resulting in a decrease in fluorescence. Real-time monitoring of the adenosine-dependent fluorescent signal provided a convenient and homogeneous assay of ADA activity that was optimized in this work for linearity with time and enzyme concentration (Figure 1B). An enzyme concentration of 10 nM fell in the linear range of the latter and had a robust signal for HTS. For the sensitive detection of competitive inhibitors,[17] we chose a substrate concentration equal to the $K_m$ for adenosine (500 μM; data not shown). Work with a known inhibitor of ADA, *erythro*-9-(2-hydroxy-3-nonyl)adenine (EHNA), confirmed that the assay conditions faithfully reported on the activity and inhibition of adenosine deaminase. Dose–response relationships for EHNA were virtually superimposable by using either the signaling aptamer assay or a HPLC method that measures adenosine turnover directly (Figure 2).

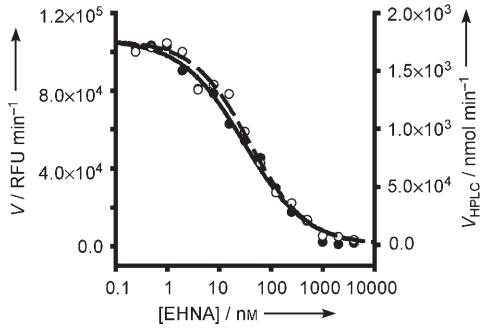


***Figure 2.*** Dose–response analysis for the known inhibitor EHNA determined by using the fluorescence-signaling aptamer assay and a direct determination of adenosine turnover by HPLC. Data for the signaling aptamer method (——) and the HPLC determination (– – –) were fit to the dose–response equation described in the Experimental Section, and $IC_{50}$ values of $30 \pm 5$ and $39 \pm 7$ nM, respectively, were obtained. Reactions contained 10 nM ADA, 500 μM adenosine, and varying EHNA concentrations (4% final DMSO v/v). The signaling aptamer assay also included 20 nM fluorescent aptamer, 40 nM QDNA, 5 mM $MgCl_2$, and 300 mM NaCl in 25 mM HEPES buffer solution at pH 8.0, whereas the reactions prepared for analysis by HPLC were in 25 mM HEPES buffer at pH 8.0 and 100 mM KCl. These were quenched with 0.2 N HCl, 3 min after initiation with adenosine and ultrafiltered through a membrane with a molecular-weight cutoff at 3000 g mol$^{-1}$ and the filtrate analyzed. Inosine and residual adenosine, as detected at 250 nm, were separated by HPLC on a reverse-phase column, over a buffer solution gradient from 100% 30 mM $KH_2PO_4$ to 30% acetonitrile/water (1:1 v/v) over 9 mL at a flow rate of 1 mL min$^{-1}$.

By using the assay described, we screened a diverse collection of 44400 commercial compounds in duplicate. Figure 3A shows a replicate plot of screening data in which the quality of the screen is evident in the high correspondence of duplicate determinations. More evidence of the quality of this screen is evident in Figure 3B, which shows a plot of the signal from high-control wells (no inhibitor added) and low-control wells (2 μM EHNA). We calculated a *Z′*-factor for the high and low controls of 0.51. This parameter is a statistical measure of the quality of the screening data in which a value of 0.5 or greater indicates a very workable signal window and

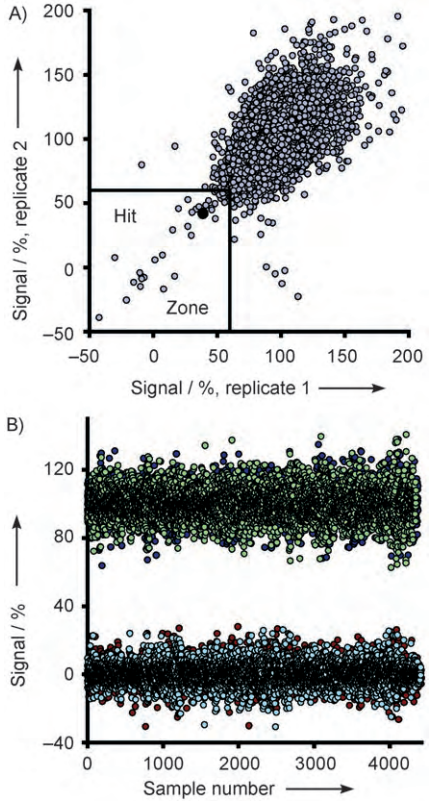


***Figure 3.*** Primary screen of ADA. A) Plot of duplicate data from a screen of 44400 compounds (Maybridge plc, Cornwall, UK). Each 75-μL reaction contained 10 μM library compound (4% v/v final dimethyl sulfoxide content), 10 nM ADA, 500 μM adenosine, 20 nM aptamer, 40 nM QDNA, 25 mM HEPES buffer, pH 8.0, 5 mM $MgCl_2$ and 300 mM NaCl. The outlined hit zone was 3σ from the mean of the data and defined as 60% residual signal. Coordinates of the defined ADA inhibitor, MAC-0038732, are highlighted in black. B) Plot of the percent residual signal of the high-control data (dark-blue- and light-green-filled circles) and low-control data (burgundy- and light-blue-filled circles) of the first and second replicates, respectively, of the screen. The calculated Z′-factor for this screen was 0.51. Neat DMSO was added to wells containing high controls, whereas low controls contained 2 μM EHNA.

limited variation associated with the high and low control data.[18]

Some 47 screening "hits" were selected based on a hit zone three standard deviations below the mean of the data. These compounds were subsequently analyzed in a series of secondary assays as summarized in Scheme 1. Retesting of the hit compounds under primary screening conditions confirmed that 12 compounds were repeatable hits. The compound screening literature has few analyses that would make for an objective analysis of hit and confirmation rates.[19] Nevertheless, with a hit rate of about 0.1% (47 of 44400) of compounds screened and confirmation rate of 26% (12 of 47), we conclude, based on our own screening experience,[20–23] that the signaling aptamer assay proved to be quite tractable and well behaved in primary screening. The activity of these 12 compounds was further evaluated in the fluorescence-signaling aptamer assay by using additives that are commonly used to test for promiscuous or nonspecific inhibitors, such as

 © 2006 Wiley-VCH Verlag GmbH & Co. KGaA, Weinheim 

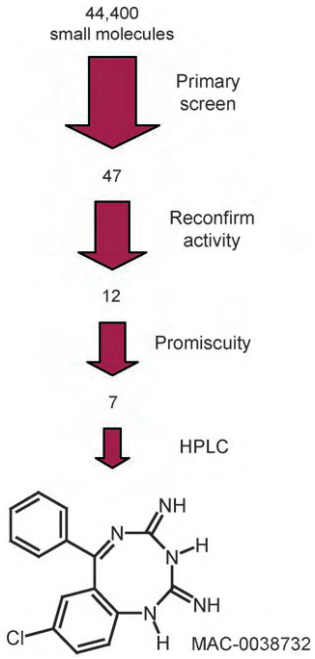


***Scheme 1.*** Workflow resulting in the identification of MAC-0038732, a new inhibitor of adenosine deaminase.

reducing agent 1,4-dithio-D,L-threitol (DTT), detergent (Triton X-100), and bovine serum albumin (BSA). Promiscuous electrophilic compounds are frequently sensitive to the inclusion of excess DTT or BSA in the reaction mixture,[20] whereas the attenuation of compound activity in the presence of detergent is often an indication of promiscuous inhibition through compound aggregation.[24,25] Of the confirmed 12 hits, the inhibitory activity of seven of the compounds was not significantly perturbed in the presence of any of the three agents tested (1 mM DTT, 0.01% (v/v) Triton X-100, and 0.1 mg mL$^{-1}$ BSA). The remaining five compounds were discarded as they exhibited promiscuous behavior.

The remaining seven compounds were analyzed by using an HPLC assay as a direct test for inhibited ADA. HPLC analysis showed that one of these compounds, MAC-0038732 (Scheme 1), was indeed an inhibitor of adenosine deaminase. Interestingly, analysis by mass spectrometry revealed that the identity of the active molecule (297.1 Da) was not that predicted for the structure in the compound database (315 Da). Indeed, NMR spectroscopic analysis of the active molecule indicated a structure that was consistent with cyclization of the biguanidine functionality to form an imine (for details see the Supporting Information) with the loss of a water molecule. Steady-state kinetic analysis of the inhibition of ADA by MAC-0038732 revealed competitive inhibition with respect to adenosine and a $K_i$ of 2 μM (data not shown). The six remaining compounds showed, through the HPLC assay, no inhibition. Careful examination of the signaling aptamer assay revealed that these compounds were falsely positive as a result of interference with the fluorescence signal. Two of these compounds were highly fluorescent and obscured the output of the signaling aptamer assay, whereas the remaining four compounds could quench the aptamer–adenosine fluorescence signal. Although these six compounds revealed a potential shortcoming in the signaling aptamer assay, namely interference with the fluorescent reporter system, we note herein that relatively few compounds were problematic (6 out of 44400) and that these false positives were easily identified in secondary screening.

The new inhibitor (MAC-0038732) of adenosine deaminase discovered in this work is a cyclized imine with an extraordinary eight-membered ring containing a biguanidine moiety. The compound has notable similarity to a deaminase inhibitor reported by Wang and Hosmane (seven-membered ring containing a biguanidine system),[26] which was 100-fold less potent ($K_i$ of 200 μM) but was also a competitive inhibitor. Together, these molecules present an interesting case that large biguanidine-containing ring systems may merit further exploration for their capacity to inhibit ADA. Indeed, ADA inhibitors reported to date are largely nucleoside analogues such as EHNA.[27] MAC-0038732 and other non-nucleoside inhibitors[28] represent fresh approaches to this emerging target in inflammation and immunity.

In conclusion, we report the first use of an aptamer in high-throughput compound screening. Described is the use of a fluorescence-signaling aptamer system in a simple, automated, and homogeneous assay of an otherwise problematic target, adenosine deaminase. The small-molecule screen was robust and yielded a new competitive inhibitor of adenosine deaminase. The work has broad implications for emerging genome-scale screening paradigms in which the goal is to streamline assay development and implementation with universal assay methodologies. Although genome-scale assay parallelization and throughput have great potential for transforming small-molecule screening, these approaches await considerable technological advancements. This is particularly true in biochemical screens for inhibitory compounds in which methods are needed that are in harmony with proteomic approaches and simplify the establishment of assays amenable to automation and throughput. The ability to routinely select aptamers as assay reagents coupled with the performance of fluorescence-signaling aptamers, as demonstrated in the work described herein, suggests that nucleic acid aptamers have exciting potential for this purpose.

Received: April 29, 2006
Published online: July 20, 2006

**Keywords:** adenosine deaminase · assays · DNA structures · inhibitors · small-molecule screening

[1] R. R. Breaker, *Nature* **2004**, *432*, 838.
[2] S. E. Osborne, I. Matsumura, A. D. Ellington, *Curr. Opin. Chem. Biol.* **1997**, *1*, 5.
[3] S. M. Nimjee, C. P. Rusconi, B. A. Sullenger, *Annu. Rev. Med.* **2005**, *56*, 555.
[4] L. S. Green, C. Bell, N. Janjic, *Biotechniques* **2001**, *30*, 1094.
[5] T. Hermann, D. J. Patel, *Science* **2000**, *287*, 820.
[6] J. S. Hartig, S. H. Najafi-Shoushtari, I. Grune, A. Yan, A. D. Ellington, M. Famulok, *Nat. Biotechnol.* **2002**, *20*, 717.

 © 2006 Wiley-VCH Verlag GmbH & Co. KGaA, Weinheim 

[7] J. Srinivasan, S. T. Cload, N. Hamaguchi, J. Kurz, S. Keene, M. Kurz, R. M. Boomer, J. Blanchard, D. Epstein, C. Wilson, J. L. Diener, *Chem. Biol.* **2004**, *11*, 499.
[8] R. Nutiu, J. M. Yu, Y. Li, *ChemBioChem* **2004**, *5*, 1139.
[9] M. B. Aldrich, M. R. Blackburn, R. E. Kellems, *Biochem. Biophys. Res. Commun.* **2000**, *272*, 311.
[10] J. Kameoka, T. Tanaka, Y. Nojima, S. F. Schlossman, C. Morimoto, *Science* **1993**, *261*, 466.
[11] J. Linden, *Annu. Rev. Pharmacol. Toxicol.* **2001**, *41*, 775.
[12] G. Giusti, B. Galanti, *Adenosine Deaminase: Colorimetric Method*, *Vol. 4*, 3rd ed., Verlag Chemie, Weinheim, **1984**.
[13] F. Heinz, *Adenosine Deaminase:UV-Method*, *Vol. 4*, 3rd ed., Verlag Chemie, Weinheim, **1984**.
[14] H. M. Oosthuizen, J. P. Ungerer, S. H. Bissbort, *Clin. Chem.* **1993**, *39*, 2182.
[15] D. E. Huizenga, J. W. Szostak, *Biochemistry* **1995**, *34*, 656.
[16] R. Nutiu, Y. Li, *J. Am. Chem. Soc.* **2003**, *125*, 4771.
[17] R. A. Copeland, *Anal. Biochem.* **2003**, *320*, 1.
[18] J. H. Zhang, T. D. Chung, K. R. Oldenburg, *J. Biomol. Screening* **1999**, *4*, 67.
[19] J. H. Zhang, X. Wu, M. A. Sills, *J. Biomol. Screening* **2005**, *10*, 695.
[20] J. E. Blanchard, N. H. Elowe, C. Huitema, P. D. Fortin, J. D. Cechetto, L. D. Eltis, E. D. Brown, *Chem. Biol.* **2004**, *11*, 1445.
[21] N. H. Elowe, J. E. Blanchard, J. D. Cechetto, E. D. Brown, *J. Biomol. Screening* **2005**, *10*, 653.
[22] X. Li, M. Zolli-Juran, J. D. Cechetto, D. M. Daigle, G. D. Wright, E. D. Brown, *Chem. Biol.* **2004**, *11*, 1423.
[23] M. Zolli-Juran, J. D. Cechetto, R. Hartlen, D. M. Daigle, E. D. Brown, *Bioorg. Med. Chem. Lett.* **2003**, *13*, 2493.
[24] S. L. McGovern, E. Caselli, N. Grigorieff, B. K. Shoichet, *J. Med. Chem.* **2002**, *45*, 1712.
[25] A. J. Ryan, N. M. Gray, P. N. Lowe, C. W. Chung, *J. Med. Chem.* **2003**, *46*, 3448.
[26] L. Wang, R. S. Hosmane, *Bioorg. Med. Chem. Lett.* **2001**, *11*, 2893.
[27] G. Bastian, M. Bessodes, R. P. Panzica, E. Abushanab, S. F. Chen, J. D. Stoeckler, R. E. Parks, Jr., *J. Med. Chem.* **1981**, *24*, 1383.
[28] T. Terasaka, T. Kinoshita, M. Kuno, I. Nakanishi, *J. Am. Chem. Soc.* **2004**, *126*, 34.

 © 2006 Wiley-VCH Verlag GmbH & Co. KGaA, Weinheim 

Glycosidation

DOI: 10.1002/anie.200602161

# Glycosidation Promoted by a Reusable Solid Superacid in Supercritical Carbon Dioxide**

*Xue-Bing Li, Masato Ogawa, Toshiki Monden, Takahiro Maeda, Eri Yamashita, Mariko Naka, Masao Matsuda, Hiroshi Hinou, and Shin-Ichiro Nishimura**

Functional roles of glycoconjugates are of growing importance owing to carbohydrate-mediated signal transductions, which are crucial steps for a variety of biological phenomena such as cellular differentiation, aging, immune systems, infections, and malignant alterations of cells. Synthetic studies of carbohydrates are indispensable both for elucidating essential structures of the functional glycoconjugates and for producing therapeutic reagents of carbohydrate-related diseases.[1]

Glycosidation is one of the most important reactions in chemical synthesis of glycoconjugates.[2] In recent years, although there has been an increasing interest in environmentally more-sustainable chemical processes,[3] a practical and cleaner chemical synthetic process of carbohydrates has been discussed very little except for a few pioneering efforts.[4] The advent of a highly efficient, safe, and environmentally benign method for the glycosidation is strongly expected because this key technology will allow for practical and industrial scale production of natural and unnatural glycosides. Enzyme-assisted synthesis has been recognized to be a much more sustainable and efficient strategy than pure chemical protocols in terms of the construction of various seeds libraries for the discovery and research of therapeutic reagents.[5] However, the present potentials are not high enough for large scale synthesis of drug candidates required for the following clinical trials.

[*] Dr. X.-B. Li, T. Monden, T. Maeda, E. Yamashita, M. Naka, Dr. M. Matsuda, Dr. H. Hinou, Prof. Dr. S.-I. Nishimura
Division of Advanced Chemical Biology
Graduate School of Advanced Life Science
Frontier Research Center for Post-Genome Science and Technology
Hokkaido University
N21, W11, Sapporo 001-0021 (Japan)
Fax: (+81) 11-706-9042
E-mail: shin@glyco.sci.hokudai.ac.jp

M. Ogawa
Department of Technical Engineering
Faculty of Science, Hokkaido University
N10, W8, Sapporo 060-0010 (Japan)

[**] This work was supported by a grant for the National Project "Research and Development on Glycocluster Controlling Biomolecules" from the New Energy and Industrial Technology Development Organization (NEDO).

Supporting information for this article is available on the WWW under http://www.angewandte.org or from the author.


WILEY InterScience DISCOVER SOMETHING GREAT
© 2006 Wiley-VCH Verlag GmbH & Co. KGaA, Weinheim

In the present study, our interest is focused on the feasibility of recyclable solid-superacid-promoted glycosidation in supercritical fluids (SCFs). Solid superacids are industrially potent catalysts that can act both as Lewis acids and Brønstead acids. SCFs used as reaction media for homogeneous catalysts or as compressed carriers for heterogeneous catalysts have great potential for manipulation of a variety of catalytic reactions.[3] As $CO_2$ has a critical point close to ambient temperature ($T_c = 31.3\,°C$, $P_c = 7.4$ MPa) and is nonflammable, nontoxic, and inexpensive, supercritical (sc)$CO_2$ has received immense interest as an alternative reaction media to petroleum-derived common organic solvents used in large-scale chemical synthesis. However, there has been no example of the glycosidation by means of $scCO_2$ as a reaction media. Although it seemed that this might be owing to the poor solubility of polar biomolecules, such as amino acids and sugars toward $scCO_2$, recent reports[6] on the improved solubility of some sugar acetates in $scCO_2$ greatly motivated us to challenge "green" replacement of conventional synthetic protocols by using hazardous promoters and flammable/toxic organic solvents.[7] We hypothesized that the use of a nonpolar $scCO_2$ may promote glycosidation by increasing the interaction of relatively polar species such as sugar derivatives and alcohols on the surface of solid acid catalysts. Furthermore, this effect will encourage the phase separation of contaminated $H_2O$, which appears to reduce the yields of the glycosidation due to hydrolysis of the products/intermediates through rehydration at the glycoside bonds. We thought that an original and desired apparatus suited for monitoring glycosidation process must allow for investigating versatile and general conditions of solid-superacid-promoted cleaner glycosidation in $scCO_2$.

To monitor the solubility of typical glycosyl donors and acceptors toward $scCO_2$, a novel apparatus with a quartz-window-equipped reactor was developed and examined in this study. Figure 1 shows schematic view of the apparatus used for glycosidation in supercritical fluids. In addition to the convenient quartz window, it should also be noted that a tailored stirrer connected with the reactor allowed for accelerating heterogeneous solid-acid-promoted glycosidation of various donors and acceptors with different solubility to $scCO_2$. As indicated in Figure 2, the reaction promoted by sulfated zirconia ($SO_4/ZrO_2$),[8] one of the common and industrially available solid superacid catalysts, was successfully monitored through the quartz window by using 3D digital fine scope. In accordance with the progress of the glycosidation, the reaction mixture exhibited a significant phase-transition state from emulsion to a clear supercritical fluidic phase, suggesting the existence of some sweet spots in the individual reaction condition. The present synthetic system made possible a precise optimization study for searching for suitable reaction conditions. We finally concluded that all the glycosidation reactions between donors **1**,[9] **2**,[10] **3**,[11] and acceptors **4**–**8** by using $SO_4/ZrO_2$ proceeded smoothly in $scCO_2$ under just over the critical point at 34 °C and 8.0 MPa for 6 h.

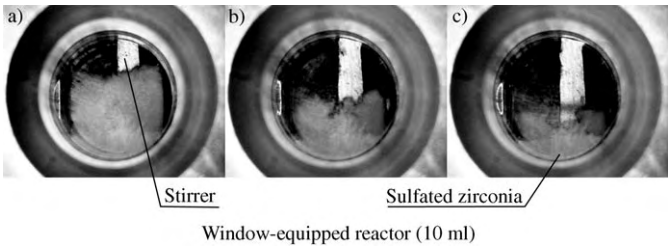


***Figure 2.*** Photographs showing the process of the dissolution of glycosyl donor **1** (126 mg) and acceptor **4** (17 mg) during the glycosidation promoted by sulfated zirconia (126 mg) in $scCO_2$ at 34 °C: a) a mixture of solid materials before addition of $CO_2$; b) most of the donor and acceptor substrates were dissolved in $scCO_2$ at a pressure of 7.5 MPa; c) at a pressure of 8.0 MPa, only sulfated zirconia remained in the solid state.

Table 1 indicates the results of glycosidation of 2,3,4,6-tetra-*O*-acetyl-α-D-galactopyranosyl trichloroacetimidate **1** with acceptors **4**–**7**. Coupling of **1** with all acceptors in $scCO_2$ gave only β-glycosides **9**,[12] **10**,[13] **11**, and **12** in 76–87 % yields, suggesting that the reactions proceeded by neighboring

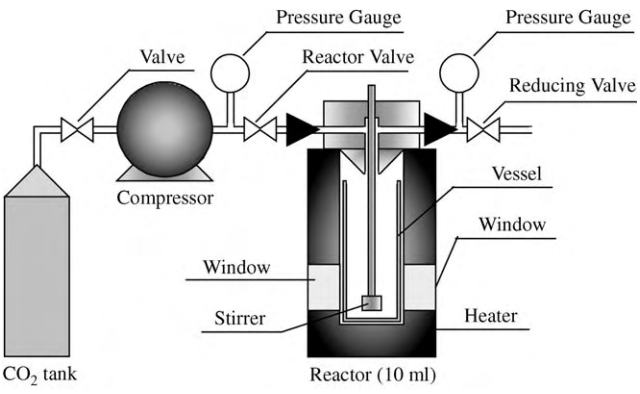


***Figure 1.*** Equipment used for glycosidation reactions in $scCO_2$. The tailored SCF synthesizer is composed of a window-equipped stainless-steel 10-mL reactor with a circulatory heating apparatus, a high pressure pump, a pressure regulator, and a motor-driven stirrer.

***Table 1:*** Glycosidations of glycosyl donor **1** with various glycosyl acceptors promoted by sulfated zirconia in $scCO_2$.[b]

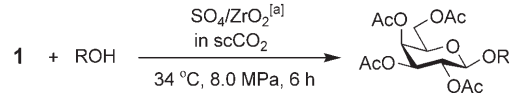


| Entry | Acceptor | Products | Yield [%][c] | α/β ratio[d] |
|---|---|---|---|---|
| 1 | **4** | **9** | 85 | 0/1 |
| 2 | **5** | **10** | 87 | 0/1 |
| 3 | **6** | **11** | 76 | 0/1 |
| 4 | **7** | **12** | 81 | 0/1 |

[a] $SO_4/ZrO_2$ was obtained commercially from Wako Pure Chemical Industries, Ltd. and activated by heating at 650 °C for 2 h before use. [b] Glycosidations were carried out by use of 1.1 equiv of alcohol and 100 wt % of $SO_4/ZrO_2$ to the donor **1**. [c] Yield of isolated product after purification by SFC. [d] The stereochemistry (α/β ratio) was determined by SFC and $^1H$ NMR spectroscopy (500 MHz).

 © 2006 Wiley-VCH Verlag GmbH & Co. KGaA, Weinheim 

group participation mechanism as observed in the reactions of common donors having 2-*O*-acyl protections conducted in common organic solvents. Glycosidation by using glycosyl donors **2** and **3** protected by *O*-benzyl groups were also examined under the same conditions, in $scCO_2$ at 34 °C and 8.0 MPa. The results summarized in Table 2 suggest that both

***Table 2:*** Glycosidations of glycosyl donor **2** or **3** with various glycosyl acceptors promoted by sulfated zirconia in $scCO_2$.[b]

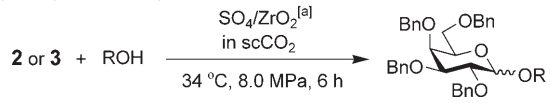


| Entry | Donor | Acceptor | Products | Yield [%][c] | α/β ratio[d] |
|---|---|---|---|---|---|
| 1 | **2** | **4** | **13** | 86 | 79/21 |
| 2 | **2** | **5** | **14** | 91 | 81/19 |
| 3 | **2** | **7** | **15** | 80 | 72/28 |
| 4 | **2** | **8** | **16** | 54 | 68/32 |
| 5 | **3** | **4** | **13** | 88 | 24/76 |
| 6 | **3** | **5** | **14** | 82 | 45/56 |
| 7 | **3** | **7** | **15** | 78 | 32/68 |
| 8 | **3** | **8** | **16** | 51 | 37/63 |

[a] $SO_4/ZrO_2$ was obtained commercially from Wako Pure Chemical Industries, Ltd. and activated by heating at 650 °C for 2 h before use. [b] Glycosidations were carried out by use of 1.1 equiv of alcohol and 100 wt% of $SO_4/ZrO_2$ to the donor **2** or **3**. [c] Yield of isolated product after purification by SFC. [d] The stereochemistry (α/β ratio) was determined by SFC and $^1H$ NMR spectroscopy (500 MHz). Bn = benzyl.

glycosyl donors **2** and **3** were efficiently activated by $SO_4/ZrO_2$ in $scCO_2$ and afforded the expected glycosides **13**,[14] **14**,[15] **15**,[16] and **16**[17] in 51–91% yields as a mixture of stereoisomers. These results indicate that the combination of $SO_4/ZrO_2$ with SFC did not work for the improvement of stereoselectivity in the selected glycosidation. The crude products, which contained solid catalyst, were recovered free from any solvent and thus they were dissolved in a small amount of methanol and subjected to simple filtration to separate the reusable catalyst. To minimize the use of organic solvents in the whole synthetic protocols, we decided to employ supercritical fluid chromatography (SFC) with $scCO_2$ as the mobile phase for the final purification of the glycosides instead of common silica gel chromatography. As indicated in Figure 3, it was revealed that SFC, by using $scCO_2$ under methanol-gradient (5–50%) at 30 °C and 14 MPa, allowed for separation of the mixture of α/β glycosides. Yields of the isolated products represent similar characteristics that are observed in the conventional methods with common organic solvents.

In conclusion, we have reported the first example of the cleaner chemical synthesis of glycosides in supercritical fluid ($scCO_2$). Our results show that $CO_2$ can provide significant advantages in reusable heterogeneous solid acid ($SO_4/ZrO_2$)-promoted glycosidation of common glycosyl donors with various acceptors over a wide range of temperatures and pressures. All of our glycosidation reactions show that there is a clear preference for glycoside formation over their hydrolytic by-products.[18] Purification of the stereoisomers of the glycosides by means of SFC allowed for totally sustainable and environmentally friendly protocol for the practical and large-scale synthesis of biologically and industrially important glycoconjugates. We are currently investigating the versatility of the present protocols by the combined use of SCF and SFC in the combinatorial synthesis of glycoside-based drug seeds libraries as well as the construction of commercially available SCF synthesizer that can be implemented in existing organic synthesis and carbohydrate chemistry laboratories (compounds used in this study are listed in Scheme 1).

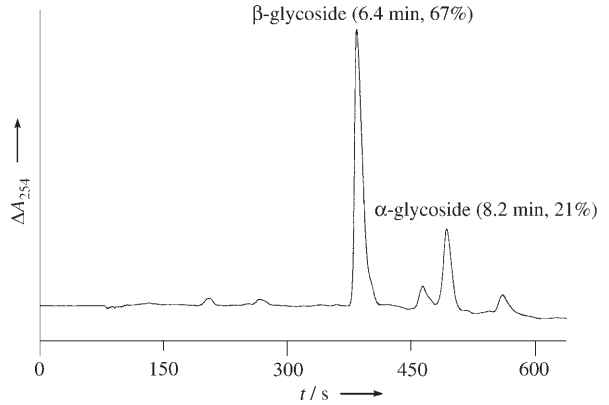


***Figure 3.*** SFC profile for the separation of the anomeric mixture of the glycosides produced by the glycosidation of 2,3,4,6-*tetra*-*O*-benzyl-α-D-galactopyranosyl imidate (**3**) with *n*-octylalcohol (**4**). Purification was performed with a Gilson SF3 SFC system equipped with Chiralpak AD (4.6×250 $mm^2$, Daicel Chemical Industries, Ltd.) under a $scCO_2$–MeOH gradient program (MeOH, 5% (0 min)→50% (15 min), flow rate = 2.5 $mL\,min^{-1}$) at 14 MPa and 30 °C. Monitoring of the compounds was carried out with a UV detector at 254 nm or an evaporative light scattering detector (ELSD) in cases for the purification of O-acetylated products derived from glycosyl donor **1**).

## *Experimental Section*

A quartz vessel charged with glycosyl donor (1 equiv), accepter (1.1 equiv), and sulfated zirconia (100 wt% of the donor) was attached to the reactor (10 mL) as shown in Figure 2. The reactor was heated to 34 °C and $CO_2$ was introduced successively from a reservoir by a high-pressure pump. The start of the reaction is defined as the time at which the $CO_2$ pressure reaches 8.0 MPa. After stirring the reaction mixture at 34 °C and 8.0 MPa for 6 h, the reactor was cooled to 20 °C and $CO_2$ was then slowly leaked out. The residual solid in the vessel was washed out with methanol. Sulfated zirconia was recovered by filtration. The filtrate was evaporated to give a residue that was subjected to SFC for the isolation and analysis (yield and α/β ratio) of the product.

Received: May 31, 2006
Published online: July 26, 2006

**Keywords:** chromatography · glycosidation · green chemistry · superacidic systems · supercritical fluids

 © 2006 Wiley-VCH Verlag GmbH & Co. KGaA, Weinheim 

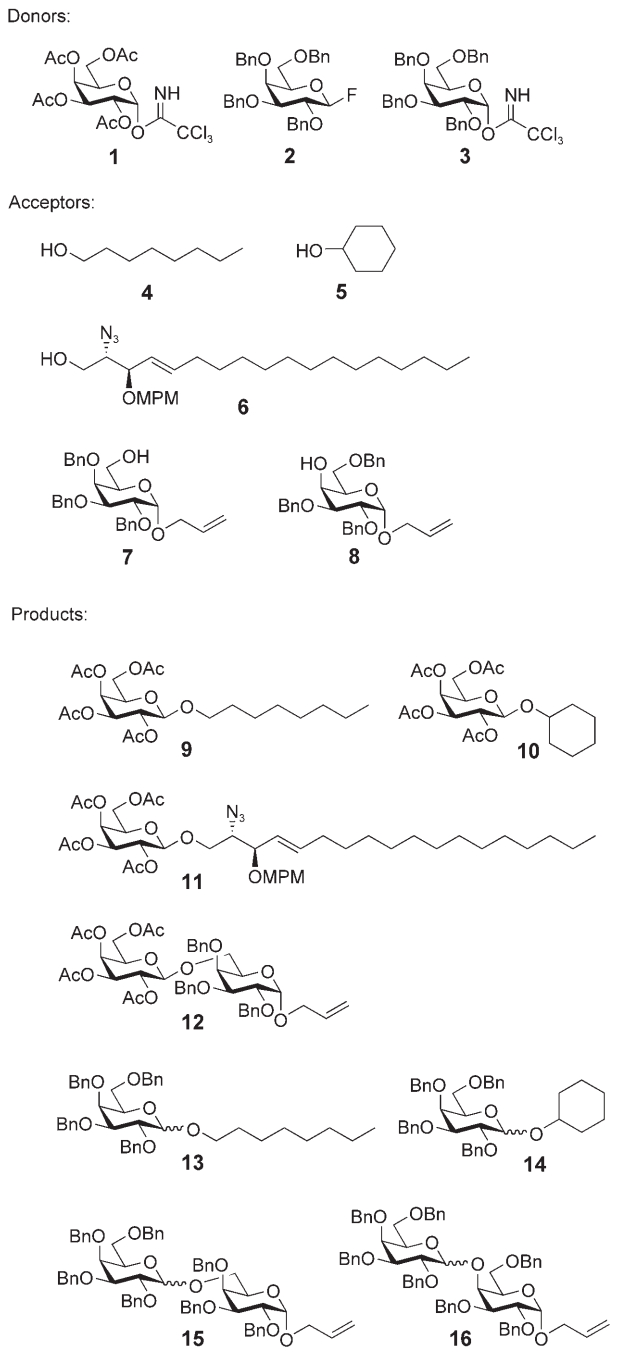


***Scheme 1.*** Chemical structures of glycosyl donors, acceptors, and products used in this study. MPM = 4-methoxybenzyl


[1] R. A. Dwek, *Chem. Rev.* **1996**, *96*, 683.

[2] For selected reviews on chemical glycosidation, see: a) R. R. Schmidt, *Angew. Chem.* **1986**, *98*, 213; *Angew. Chem. Int. Ed. Engl.* **1986**, *25*, 212; b) P. Sinaÿ, *Pure Appl. Chem.* **1991**, *63*, 519; c) K. Toshima, K. Tatsuta, *Chem. Rev.* **1993**, *93*, 1503; d) G.-J. Boons, *Tetrahedron* **1996**, *52*, 1095; e) B. G. Davis, *J. Chem. Soc. Perkin Trans. 1* **2000**, 2137; f) B. Fraser-Reid, J. C. López, A. M. Gómez, C. Uriel, *Eur. J. Org. Chem.* **2004**, 1387.

[3] For example, see: a) P. G. Jessop, T. Ikariya, R. Noyori, *Nature* **1994**, *368*, 231; b) P. T. Anastas, T. C. Williams, *Green Chemistry: Designing Chemistry for the Environment*, Oxford University Press, Oxford, **1998**; c) P. E. Savage, *Chem. Rev.* **1999**, *99*, 603; d) A. Baiker, *Chem. Rev.* **1999**, *99*, 453.

[4] a) K. Sasaki, S. Matsumura, K. Toshima, *Tetrahedron Lett.* **2004**, *45*, 7043; b) H. Nagai, K. Sasaki, S. Matsumura, K. Toshima, *Carbohydr. Res.* **2005**, *340*, 337.

[5] Enzyme-assisted synthesis of glycoconjugates, for example, see: a) C. Unverzagt, H. Kunz, J. C. Paulson, *J. Am. Chem. Soc.* **1990**, *112*, 9308; b) C. Unverzagt, *Angew. Chem.* **1996**, *108*, 2507; *Angew. Chem. Int. Ed. Engl.* **1996**, *35*, 2350; c) K. M. Koeller, C.-H. Wong, *Chem. Rev.* **2000**, *100*, 4465; d) M. Meldal, F.-I. Auzanneau, O. Hindsgaul, M. M. Palcic, *J. Chem. Soc. Chem. Commun.* **1994**, 1849; e) O. Seitz, C.-H. Wong, *J. Am. Chem. Soc.* **1997**, *119*, 8766; f) S. K. George, T. Schwientek, B. Holm, C. A. Reis, H. Clausen, J. Kihlberg, *J. Am. Chem. Soc.* **2001**, *123*, 11117; g) N. Bezay, G. Dudziak, A. Liese, H. Kunz, *Angew. Chem.* **2001**, *113*, 2350; *Angew. Chem. Int. Ed.* **2001**, *40*, 2292; h) M. Fumoto, H. Hinou, H. Ohta, T. Ito, K. Yamada, A. Takimoto, H. Kondo, H. Shimizu, T. Inazu, Y. Nakahara, S. -I. Nishimua, *J. Am. Chem. Soc.* **2005**, *127*, 11804.

[6] a) P. Raveendran, S. L. Wallen, *J. Am. Chem. Soc.* **2002**, *124*, 7274; b) V. K. Potluri, J. Xu, R. Enick, E. Beckman, A. D. Hamilton, *Org. Lett.* **2002**, *4*, 2333.

[7] In general, chemical glycosidation is promoted by means of many hazardous promoters such as trimethylsilyl trifluoromethanesulfonate (TMSOTf), $BF_3{\cdot}Et_2O$, $Cp_2HfCl_2{\cdot}AgClO_4$, AgOTf, and *N*-iodosuccimide/trifluoromethanesulfonic acid (NIS/TfOH) in petroleum-derived common organic solvents such as dichloromethane, dichloroethane, toluene, ether, tetrahydrofuran, and acetonitrile. As for the novel approaches in this area, see: a) K.-S. Ko, F. A. Jaipuri, N. L. Pohl, *J. Am. Chem. Soc.* **2005**, *127*, 13162; b) D. M. Ratner, E. R. Murphy, M. Jhunjhunwala, D. A. Synder, K. F. Jensen, P. H. Seeberger, *Chem. Commun.* **2005**, 578; c) B. Mukhopadhyay, S. V. Maurer, N. Rudolph, R. M. van Well, D. A. Russel, R. A. Field, *J. Org. Chem.* **2005**, *70*, 9059.

[8] a) S.-I. Nishimura, Patent WO PCT/JP99/04261, **1999**; b) H. Nagai, K. Kawahara, S. Matsumura, K. Toshima, *Tetrahedron Lett.* **2001**, *42*, 4159; c) K. Toshima, H. Nagai, K. Kasumi, K. Kawahara, S. Matsumura, *Tetrahedron* **2004**, *60*, 5331.

[9] S. Sato, Y. Ito, T. Nukada, Y. Nakahara, T. Ogawa, *Carbohydr. Res.* **1987**, *167*, 197.

[10] T. Mukaiyama, Y. Murai, S.-I. Shoda, *Chem. Lett.* **1981**, 431.

[11] R. R. Schmidt, J. Michel, *J. Carbohydr. Chem.* **1985**, *4*, 141.

[12] D. S. K. Tsui, P. A. J. Gorin, *Carbohydr. Res.* **1985**, *144*, 137.

[13] H. Kondo, S. Aoki, Y. Ichikawa, R. L. Halcomb, H. Ritzen, C.-H. Wong, *J. Org. Chem.* **1994**, *59*, 864.

[14] A. Bülow, T. Meyer, T. K. Olszewski, M. Bols, *Eur. J. Org. Chem.* **2004**, 323.

[15] H. Uchiro, K. Miyazaki, T. Mukaiyama, *Chem. Lett.* **1997**, 403.

[16] P. A. Gent, R. Gigg, *J. Chem. Soc. Perkin Trans. 1* **1975**, 1972.

[17] Compound **16** was hydrogenated and characterized as known compounds that were reported previously, see: H. A. El-Shenawy, C. Schuerch, *Carbohydr. Res.* **1984**, *131*, 227.

[18] To achieve much higher yields and stereoselective glycosidation by using the present SCF-SFC synthesis, we are now evaluating feasibility of many other solid Lewis acid catalysts and the results will be reported shortly.


 © 2006 Wiley-VCH Verlag GmbH & Co. KGaA, Weinheim 

Thermoelectric Materials

DOI: 10.1002/anie.200600848

# Nanostructured $Bi_2Se_3$ Films and Their Thermoelectric Transport Properties**

*Xiaofeng Qiu, Leah N. Austin, Philip A. Muscarella, Jeffrey S. Dyck,* and Clemens Burda**

Since the discovery of the thermoelectric effect by Thomas Johann Seebeck in 1821, solid-state thermoelectric materials have long held the promise of becoming the next generation of energy converters thanks to their small size, light weight, reliability, and potential for higher conversion efficiencies.[1] However, bulk thermoelectric materials seem to have reached their performance limit; most materials exhibit an optimum thermoelectric figure of merit ($ZT$) of about 1 at room temperature, which equates to only around 10% of the Carnot efficiency. Since the 1960s, the efficiencies of bulk thermoelectric materials have been improved only marginally. To promote the economic potential of these materials and to support the full development of the associated technological applications, improvements in thermoelectric efficiencies leading to $ZT \geq 3$ at room temperature are required. It was not until the early 1990s that Dresselhaus and co-workers demonstrated theoretically that it is possible to increase the $ZT$ values drastically by decreasing the size of thermoelectric materials.[2–5] However, the practical difficulties in synthesizing, testing, and utilizing structures smaller than 100 nm make the production of nanoscale thermoelectric materials a real challenge. Therefore, methods that provide reproducible and stable nanostructured thermoelectric films and reliable thermoelectric measurements are of great importance. We have developed chemically grown nanostructured thermoelectric films, the building and testing of which is a significant step towards better thermoelectric materials.

Only a few nanostructured thermoelectric devices with significant improvement of $ZT$ values have been reported. Venkatasubramanian et al. successfully prepared $Bi_2Te_3$/$Sb_2Te_3$ superlattice thin films by molecular-beam epitaxy and obtained a $ZT$ value of 2.4 at room temperature.[6] Harman et al. achieved a $ZT$ value of 2.0 at 300 K with PbSeTe-based quantum-dot superlattice structures grown by a similar method.[7] However, the techniques that were used to produce these superlattice structures are very delicate and exceedingly expensive and therefore are unlikely to be applicable to large-scale production. In the meantime, a cheaper and easier pressure-injection method using an alumina template was developed to prepare Bi and $Bi_{1-x}Sb_x$ alloy nanowire arrays and their thermoelectric properties were investigated.[8–11] A related template-based electrochemical method was used to produce a group of high-$ZT$ thermoelectric materials.[12–15] The alumina-template-based nanowire arrays are an important step towards establishing nanostructures with possible high thermoelectric performance. However, no significant improvement in $ZT$ value was reported and the template materials were suspected to cause complications for transport measurements.[16]

Herein, we introduce an alternative strategy to grow nanostructures on a wide variety of substrates and perform thermoelectric measurements on these nanostructured films. The synthesis is based on a previously reported $Bi_2Se_3$ preparation[17,18] and a method by Vayssieres for growing thin films.[19] The synthesis involves the reduction of a selenium precursor ($Na_2SeSO_3$) by ascorbic acid to promote nucleation with nitrilotriacetic acid (NTA) coordinated $Bi^{3+}$, which deposits $Bi_2Se_3$ nanostructures on the substrates. Since the reduction potential of ascorbic acid is pH-dependent and the equilibrium between NTA and $Bi^{3+}$ determines the availability of free $Bi^{3+}$ ions, the growth of $Bi_2Se_3$ can be thermodynamically controlled. Other important parameters such as temperature and reaction time also provide further control over the nanostructure growth. Another very important factor is the surface charge density, which alters the interfacial tension.[19] Control of this parameter was accomplished by adjusting the pH value and the ionic strength of the reaction mixture. This method allows the production of films with different composition, grain size, and thickness, as well as deposition on substrates of any size, shape, and composition. This versatility constitutes an important improvement in the preparation of thermoelectric thin films and opens up the possibility for a range of applications.

To avoid the complications of unwanted parallel electrical and thermal conductance from substrates, all $Bi_2Se_3$ thin films herein were grown on glass substrates, although the results did not depend on the choice of substrate. The thin films prepared by this method exhibit hexagonal structure (JCPDS file: 33-214), as shown in Figure 1. No impurity phases were detected in the X-ray data. The stable baseline and sharp diffraction peaks indicate that the thin film produced shows significant coverage of the substrate and is highly crystalline. Ensuring reproducibly high quality films was a major concern in developing the presented experiments, since only continuous and highly crystalline thin films allow successful measurements.

Figure 2 shows the scanning electron microscopy (SEM) images of the $Bi_2Se_3$ nanostructured thin films. The growth process of the films can be monitored by taking images at different stages of the growth (Scheme 1). Initially, a few

[*] L. N. Austin, P. A. Muscarella, Prof. J. S. Dyck
Department of Physics
John Carroll University
20700 North Park Blvd.
University Heights, OH 44118 (USA)
Fax: (+1) 216-397-4499
E-mail: jdyck@jcu.edu
X. Qiu, Prof. C. Burda
Center for Chemical Dynamics and Nanomaterials Research
Department of Chemistry
Case Western Reserve University
10900 Euclid Avenue, Cleveland, OH 44106 (USA)
Fax: (+1) 216-368-3006
E-mail: burda@case.edu

[**] C.B. acknowledges support from the NSF (#CHE-0239688), an ACS-PRF (#45359-AC10), and the Ohio Board of Regents.

 InterScience © 2006 Wiley-VCH Verlag GmbH & Co. KGaA, Weinheim 

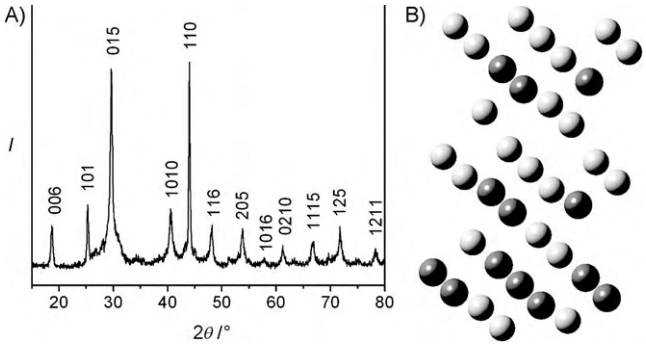


***Figure 1.*** A) XRD pattern of the prepared nanostructured $Bi_2Se_3$ thin film. B) 3D crystal structure of $Bi_2Se_3$; black: Bi, gray: Se.

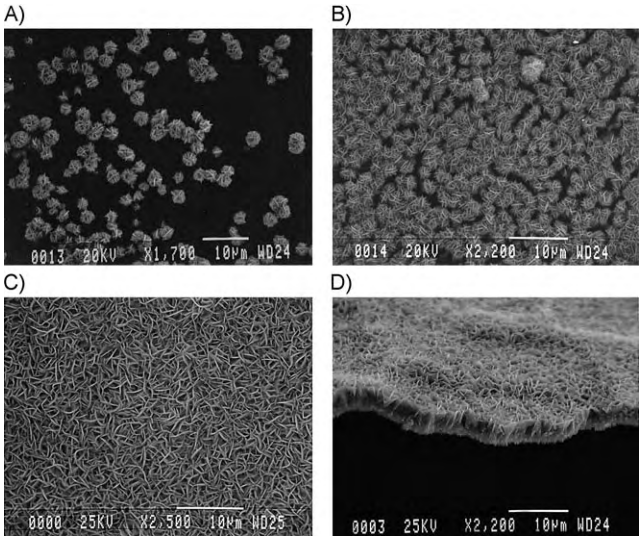


***Figure 2.*** SEM images of the synthesized films showing the increasing coverage of the substrate. A) After 5 min. B) After 30 min. C) After 120 min. D) Cross-sectional view of the thin film.

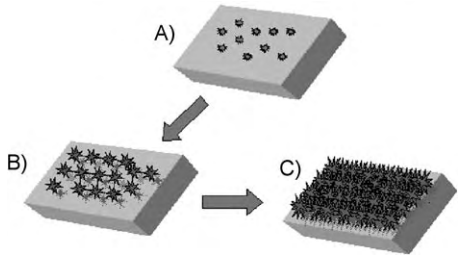


***Scheme 1.*** Steps observed during film growth. A) Initial nucleation; B) Coalescence; C) Lamella-structured film formation.

$Bi_2Se_3$ nucleation centers form and quickly develop into starlike structures (Scheme 1, step A and Figure 2a). As the number of nucleation centers increases, the rapidly developing starlike structures start to grow into each other (Scheme 1, step B and Figure 2b). After a growth time of typically 3 h, the individual island structures coalesce and form a continuous lamella-structured film (Scheme 1, step C and Figure 2c). The thickness of the individual lamella structures does not change during the growth period and remains in the range 30–80 nm. This observation indicates that the surface charge density may be at a maximum; thus the interfacial tension results in a minimum.[19] Under such conditions the lamella thickness remains less than 100 nm. Furthermore, the thickness of the film is very uniform but can be varied by changing the concentrations of the precursors. This indicates that the growth along the film surface is uniform, which in turn supports a more uniform charge-carrier transport through the nanostructured film.

To perform reproducible thermoelectric measurements and obtain reliable data from the nanostructured thin films requires synthetic reproducibility. A major concern in the measurements is to avoid additional conductance from substrates as well as other side effects; therefore, the prepared thin films should be grown on a substrate with very low electrical and thermal conductance. This requirement constitutes a problem for most electrochemical deposition techniques. We used glass slides as substrates to avoid parallel currents through substrates or other chemical residues of the synthesis that were encountered in earlier experiments.[16]

Figure 3 displays the resistance ($R$) and Seebeck coefficient ($S$) of a $Bi_2Se_3$ film from 6 to 300 K. These data are representative of values obtained for these films. The Seebeck coefficient is negative and has linear temperature dependence. Negative values of $S$ indicate $n$-type conduction, which is expected for $Bi_2Se_3$, which typically has a high density of selenium vacancies.[20] The value at room temperature ($-119\ \mu V K^{-1}$) is larger by a factor of two than that found for bulk, single crystals with electron concentration $n \approx 10^{20}\ cm^{-3}$ grown by the Bridgman method,[21] and very similar to that reported for polycrystalline $Bi_2Se_3$ with $n \approx 10^{19}\ cm^{-3}$ grown by metal–organic chemical vapor deposition (MOCVD).[22] The thermoelectric figure of merit is determined by a dimensionless parameter $ZT = S^2 T/\rho\kappa$, in which $\rho$ is the electrical resistivity and $\kappa$ is the thermal conductivity. Enhanced $S$ values can directly contribute to an increase of the $ZT$ value.

Electrical-resistance measurements of the thin films were also performed over a wide temperature range, and it was

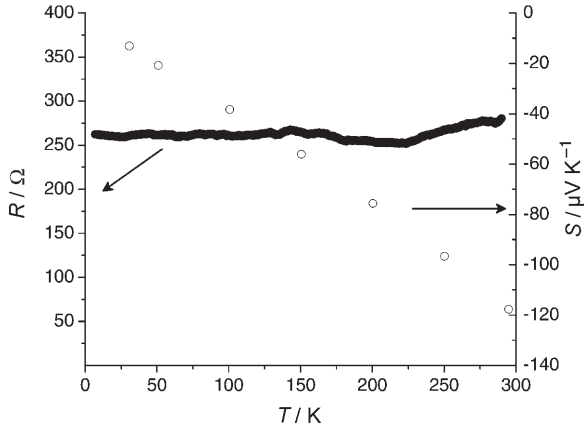


***Figure 3.*** Solid circles, left axis: Electrical resistance ($R$) of a nanostructured $Bi_2Se_3$ thin film from 6 to 300 K. Open circles, right axis: Seebeck coefficients ($S$) between 30 and 300 K for the same $Bi_2Se_3$ thin film. The negative temperature dependence of $S$ indicates dominant $n$-type conduction.

 © 2006 Wiley-VCH Verlag GmbH & Co. KGaA, Weinheim 

found that $R$ has a minimal dependence on temperature. The resistance increases about 30 Ω as the temperature rises from 6 to 300 K. To calculate $\rho$, one needs to know the exact current density. For mesoporous thin films, it is extremely difficult to measure the exact cross-sectional area precisely. However, quite certainly, $\rho$ of the thin film is higher than that of a single crystal. A higher electrical resistivity will counteract the $ZT$ enhancement that results from a larger Seebeck coefficient. Unfortunately, this situation is common for nanoscale thermoelectric materials since an increase in S generally means an increase in $\rho$.

The nanostructured films should efficiently reduce the thermal conductivity $\kappa$ of the thin film. It is evident from the relationship $ZT = S^2 T/\rho\kappa$ that a decrease in $\kappa$ enhances the thermoelectric figure of merit. The thermal conductivity $\kappa_{tot}$ is the sum of components deriving from electronic ($\kappa_{el}$) and lattice ($\kappa_{lat}$) contributions. The electronic thermal contribution can be ignored for our measurements, since the electrical resistivity is high. Therefore, only the lattice thermal conductivity is relevant in this case and $\kappa_{tot} \approx \kappa_{lat}$. Furthermore, the lamella-type structures will drastically increase the density of boundaries in the film, thus causing boundary phonon scattering and a further decrease in $\kappa_{lat}$.[23] Therefore, the experimental $\kappa_{lat}$ value for our nanostructured thin films should certainly be lower than the known value for single bulk crystals ($\kappa_{lat} = 1.33\ W m^{-1} K^{-1}$ in the direction perpendicular to the $c$ axis at room temperature), which makes the total thermal conductivity $\kappa_{tot}$ of the presented film much lower than the bulk value. Future experiments will be aimed at determining the thermal conductivity; it is expected that the significant decrease of the $\kappa$ value allows the ultimate $ZT$ value to be improved. Furthermore, the ease with which the thin film structures can be chemically controlled provides additional possibilities to increase $ZT$ values.

In summary, we have introduced a new chemical method to produce nanostructured films for thermoelectric studies and applications. Varying the synthetic parameters allows control of the scale, morphology, and composition of the films and enables the thermoelectric transport properties to be optimized reliably and less expensively. This method should also allow large-scale production of functional thin films for applications such as catalysis and energy conversion.

## Experimental Section

The glass substrate ($22 \times 40\ mm^2$; Corning Glass Works (USA)) was cut into strips ($2 \times 8\ mm^2$) with a diamond cutter, cleaned with ethanol, acetone, and distilled water, and then dried in air. A typical precursor solution is composed of nitrilotriacetic acid (NTA; 4.0 g; Aldrich, 99 + %), ascorbic acid (1.0 g; Aldrich, 99 %), $Bi(NO_3)_3 \cdot 5H_2O$ (0.5 g; Sigma-Aldrich, 99.99 %), and freshly made $Na_2SeSO_3$ solution (8 mL). The glass slides were placed into a teflon-capped flask and heated at 60 °C for 2 h. A uniform film was formed on the surface of the glass slides. The thin films were rinsed several times with distilled water to remove any excess precipitates and then dried.

The phase purity of the thin films was analyzed with a Scintag X-1 Advanced X-ray diffractometer (XRD, 2.4° min$^{-1}$, $Cu_{K\alpha}$ radiation), and the morphology of the thin films was characterized with a JOEL JFM-840 scanning electron microscope (20 kV, JEOL, Japan).

The electrical resistance ($R$) and Seebeck coefficient ($S$) were measured in the plane of the film as a function of temperature upon warming. The sample thickness was typically in the range 1–5 μm. The sample temperature was controlled with a closed-cycle helium refrigerator equipped with a radiation shield, and the sample space was kept at pressures below $10^{-5}$ Torr. Electrical resistance was measured in a four probe configuration by using a SRS 830 lock-in amplifier (Stanford Research Systems, Inc. USA) with an excitation frequency of 16 Hz. The excitation currents, determined with a Keithley 195 A multimeter (Keithley Instruments Inc. USA), were kept below 50 μA to prevent sample damage and heating. The average warming rate for the resistance measurements was less than 1 K min$^{-1}$. For the measurements of the Seebeck coefficients, one end of the sample was thermally anchored with GE 7031 varnish (Cambridge Magnetic Refrigeration, UK) to a copper cold sink, and a miniature strain gauge mounted at the free end of the sample served as heater. Thermal gradients with magnitude of less than 5 % of the absolute temperature were measured with the aid of fine copper-constantan thermocouples, and the copper legs of the thermocouples were used to measure the sample voltage. Keithley 2182 nanovoltmeters (Keithley Instruments Inc. USA) were used to measure the sample voltage and thermocouple voltages. Seebeck coefficients were determined from the slope of plots of sample voltage versus $\Delta T$ while holding the cold end of the sample at a constant temperature. Electrical contacts to the sample were made by using colloidal silver paste (Ted Pella, USA) to avoid heating the sample with solder.

Received: March 6, 2006
Published online: July 21, 2006

**Keywords:** nanostructures · thermoelectric materials · thin films · transport properties

[1] F. J. DiSalvo, *Science* **1999**, *285*, 703 – 706.
[2] L. D. Hicks, M. S. Dresselhaus, *Phys. Rev. B* **1993**, *47*, 12727 – 12731.
[3] L. D. Hicks, M. S. Dresselhaus, *Phys. Rev. B* **1993**, *47*, 16631 – 16634.
[4] M. S. Dresselhaus, Y. M. Lin, S. B. Cronin, O. Rabin, M. R. Black, D. Dresselhaus, T. Koga, *Semicond. Semimetals* **2001**, *71*, 1 – 121.
[5] Y. M. Lin, M. S. Dresselhaus, *Phys. Rev. B* **2003**, *68*, 075304.
[6] R. Venkatasubramanian, E. Silvola, T. Colpitts, B. O'Quinn, *Nature* **2001**, *413*, 597 – 602.
[7] T. C. Harman, P. J. Taylor, M. P. Walsh, B. E. LaForge, *Science* **2002**, *297*, 2229 – 2232.
[8] Z. Zhang, J. Y. Ying, M. S. Dresselhaus, *J. Mater. Res.* **1998**, *13*, 1745 – 1748.
[9] Y. M. Lin, S. B. Cronin, J. Y. Ying, M. S. Dresselhaus, J. P. Heremans, *Appl. Phys. Lett.* **2000**, *76*, 3944 – 3946.
[10] O. Rabin, Y. M. Lin, M. S. Dresselhaus, *Appl. Phys. Lett.* **2001**, *79*, 81 – 83.
[11] Y. M. Lin, O. Rabin, S. B. Cronin, J. Y. Ying, M. S. Dresselhaus, *Appl. Phys. Lett.* **2002**, *81*, 2403 – 2405.
[12] A. L. Prieto, M. S. Sander, M. S. Martín-González, R. Gronsky, T. Sands, A. M. Stacy, *J. Am. Chem. Soc.* **2001**, *123*, 7160 – 7161.
[13] M. Martín-González, A. L. Prieto, R. Gronsky, T. Sands, A. M. Stacy, *Adv. Mater.* **2003**, *15*, 1003 – 1006.
[14] A. L. Prieto, M. Martín-González, J. Keyani, R. Gronsky, T. Sands, A. M. Stacy, *J. Am. Chem. Soc.* **2003**, *125*, 2388 – 2389.
[15] M. Martín-González, G. J. Snyder, A. L. Prieto, R. Gronsky, T. Sands, A. M. Stacy, *Nano Lett.* **2003**, *3*, 973 – 977.
[16] R. F. Service, *Science* **2004**, *306*, 806 – 807.
[17] X. F. Qiu, J. J. Zhu, L. Pu, Y. Shi, Y. D. Zheng, H. Y. Chen, *Inorg. Chem. Commun.* **2004**, *7*, 319 – 321.

 © 2006 Wiley-VCH Verlag GmbH & Co. KGaA, Weinheim 

[18] X. F. Qiu, C. Burda, R. L. Fu, L. Pu, H. Y. Chen, J. J. Zhu *J. Am. Chem. Soc.* **2004**, *126*, 16276 – 16277.
[19] L. Vayssieres, *Int. J. Nanotechnol.* **2004**, *1*, 1 – 41.
[20] J. Horak, J. Navratil, Z. Stary, *J. Phys. Chem. Solids* **1987**, *48*, 1227 – 1233.
[21] J. Navratil, J. Horak, T. Plechacek, S. Kamba, P. Lostak, J. S. Dyck, W. Chen, C. Uher, *J. Solid State Chem.* **2004**, *177*, 1704 – 1712.
[22] A. Al Bayaz, A. Giani, A. Foucaran, F. Pascal-Delannoy, A. Boyer, *Thin Solid Films* **2003**, *441*, 1 – 5.
[23] M. S. Toprak, C. Stiewe, D. Platzek, S. Williams, L. Bertini, E. Muller, C. Gatti, Y. Zhang, M. Rowe, M. Muhammed, *Adv. Funct. Mater.* **2004**, *14*, 1189 – 1196.

 © 2006 Wiley-VCH Verlag GmbH & Co. KGaA, Weinheim 

*Labeled Amino Acids*

DOI: 10.1002/anie.200600346

# Conformationally Rigid Trifluoromethyl-Substituted α-Amino Acid Designed for Peptide Structure Analysis by Solid-State $^{19}$F NMR Spectroscopy

*Pavel K. Mikhailiuk, Sergii Afonin, Alexander N. Chernega, Eduard B. Rusanov, Maxim O. Platonov, Galina G. Dubinina, Marina Berditsch, Anne S. Ulrich,* and Igor V. Komarov**

The incorporation of specifically fluorine-labeled L-α-amino acids (FAAs) into polypeptides is a prerequisite for analyzing them by $^{19}$F NMR spectroscopy. The advantages of observing this isotope arise from its high sensitivity, the absence of biological background signals, its wide range of chemical shifts, and strong dipolar interactions.[1,2] An FAA is usually incorporated into a peptide by solid-phase peptide synthesis (SPPS), though some other methods have also been developed.[1,3] In most NMR applications the FAAs simply serve to probe qualitative changes in the local environment.[1] Only recently, FAAs have been incorporated into membrane-bound peptides to determine explicit structural parameters in terms of orientational constraints and/or interatomic distances by solid-state $^{19}$F NMR spectrosopy.[4,5] These solid-state NMR studies are particularly informative about membrane-active peptides, as they can reveal their conformation, alignment, and dynamic behavior in a lipid bilayer under quasi-native conditions.[4] However, only a limited number of FAAs are applicable to this approach, as they must meet certain structural requirements.[5] All of the compounds (**1**–**6**) used in the past face certain drawbacks in terms of either their structural interpretation and/or their chemical incorporation into peptides.

Here we report the design, synthesis, and characterization of a novel FAA that avoids the problems of **1**–**6** and is ideally

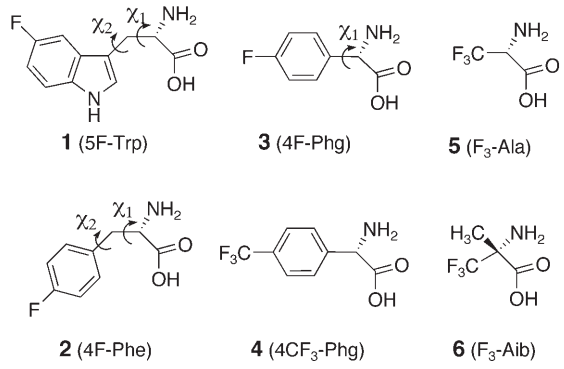


suited as a label for structure analysis of membrane-bound peptides by solid-state $^{19}$F NMR spectroscopy. The principles of its design are based on the known advantages and disadvantages of the previously used FAAs,[4,5] given that the following criteria have to be satisfied. First, the $^{19}$F reporter group has to be rigidly attached to the peptide backbone in a well-defined position with respect to the molecular framework. Any conformational flexibility of the side chain around $\chi_1$ and $\chi_2$ would make the structural interpretation of the NMR parameters ambiguous, as is the case for **1** and **2**.[4d,5,6] In **3** and **4** the position of the $^{19}$F reporter group is well-defined, but analysis of the chemical shift anisotropy of the single $^{19}$F substituent in **3** must still take into account the value of $\chi_1$.[4c,e,5,7] Fast rotation of the $CF_3$ group in **4** renders all $^{19}$F interactions axially symmetric and colinear with the $C_\alpha$–$C_\beta$ bond, which makes it ideal for orientational analysis.[4a,b,5] While the chemical shift of a monofluorinated FAA is difficult to reference,[2,5,8] this problem does not arise when the absolute dipolar splitting of a $CF_3$ group is analyzed.[4a,b,5]

It is also important that the FAA should not disturb the structure and function of a peptide. Finally, the FAA should

[*] Dr. M. Berditsch, Prof. A. S. Ulrich
Universität Karlsruhe (TH)
Institut für Organische Chemie
Fritz-Haber-Weg 6, 76133 Karlsruhe (Germany)
Fax: (+49) 721-608-48-23
E-mail: anne.ulrich@ibg.fzk.de
P. K. Mikhailiuk, Dr. M. O. Platonov, Dr. G. G. Dubinina, Prof. I. V. Komarov
Department of Chemistry
Kyiv National Taras Shevchenko University
Volodymyrska 64, 01033 Kyiv (Ukraine)
Fax: (+38) 044-225-12-73
and
Enamine Ltd.
Matrosova 23, Kiev 01103 (Ukraine)
E-mail: ik214@yahoo.com
Homepage: http://www.enamine.net
Dr. A. N. Chernega, Dr. E. B. Rusanov
Institute of Organic Chemistry of NAS of Ukraine
Murmanska 5, 02094 Kyiv (Ukraine)
Dr. S. Afonin
Forschungszentrum Karlsruhe
Institut für biologische Grenzflächen
Hermann-von-Helmholtz-Platz 1
76344 Eggenstein-Leopoldshafen (Germany)

Supporting information for this article is available on the WWW under http://www.angewandte.org or from the author.

 © 2006 Wiley-VCH Verlag GmbH & Co. KGaA, Weinheim 

be chemically stable and sufficiently reactive, and should maintain its L configuration during peptide synthesis. Even under optimized conditions of Fmoc-SPPS the previously used FAAs were found to racemize (**3, 4**), to eliminate HF (**5**), or to be highly unreactive (**6**).[5,7]

In search of a rigid L-amino acid that would satisfy all of the above-mentioned criteria, we focused on the bicyclo-[1.1.1]pentane system. Placing $CF_3$ and aminocarboxylate moieties at the bridgehead positions of this skeleton yields the $^{19}$F-labeled amino acid **7** (3-(trifluoromethyl)bicyclopent-[1.1.1]-1-ylglycine, $CF_3$-Bpg) as the target. The $C_\alpha$–$C_\beta$ and C–$CF_3$ bonds in **7** are colinear; the side chain can rotate only around these bonds. In contrast to **3** and **4**, in **7** the $CF_3$ group and the α-carbon atom are separated by a saturated bicyclic cage. This should make **7** less prone to racemization, since the transmission of electronic effects across the bicyclo-[1.1.1]pentane cage is far less pronounced than through an aromatic ring.[9] Neither degradation by the loss of HF (as in **5**) nor an unusually low reactivity of the aminocarboxylate moiety as a result of steric hindrance (as in **6**), are expected for **7** under SPPS conditions.

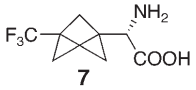

**7**

The synthesis of **7** commences from **8** and proceeds via [1.1.1]propellane **9**[10,11] as the key intermediate (Scheme 1). Addition of $CF_3I$ at the "inverted" carbon atoms of **9** led to compound **10**,[12] which was treated directly with *t*BuLi to generate the carbanion and then with methylformate to produce aldehyde **11**. A mixture of compound **11** and the corresponding hemiacetal **12** was used in the Strecker synthesis with (*R*)-α-phenylglycinol as the chiral auxiliary.[13] Products **13** and **14** were separated chromatographically. The X-ray crystal structure of **14**[14] confirmed the absolute configuration at the newly formed chiral center to be *S* (Figure 1).

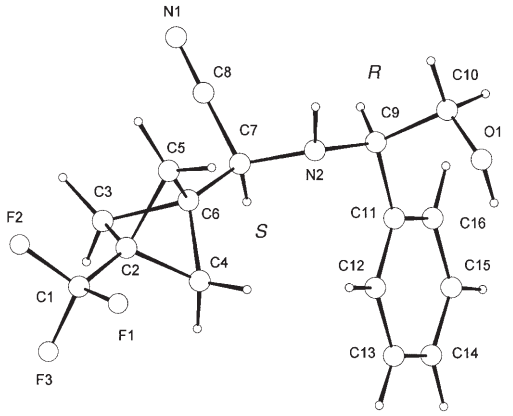

***Figure 1.*** Molecular structure of **14**.

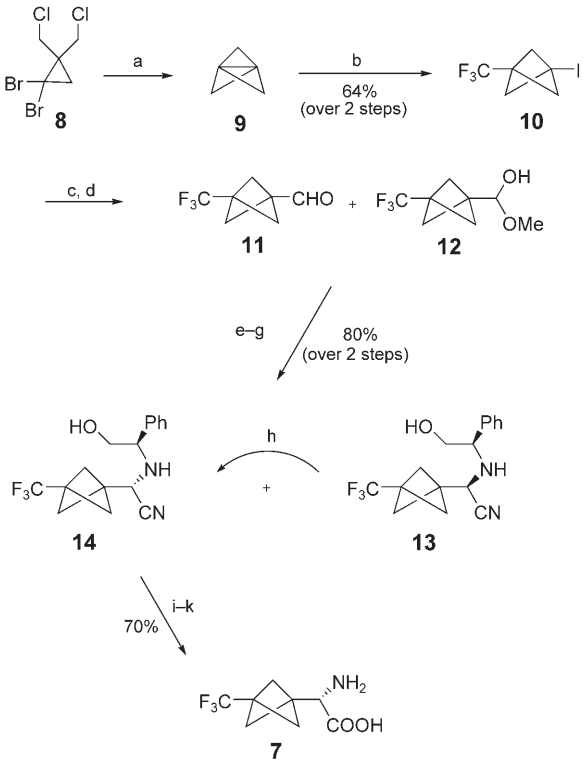

***Scheme 1.*** Reagents and conditions: a) MeLi, pentane, −78 °C, 0.5 h; b) $CF_3I$, pentane, RT, 20 h; c) *t*BuLi, $Et_2O$, −78 °C, 1 h; d) $CH_3OCHO$, $Et_2O$, −78 °C→RT, 3 h; e) (*R*)-α-phenylglycinol, $CH_2Cl_2$, RT, 2 h; f) $(CH_3)_3SiCN$, RT, 10 h; g) chromatographic separation; h) MeOH, reflux, 3 h; i) $Pb(OAc)_4$, $CH_2Cl_2$, 0 °C, 5 min; j) 6 M HCl, reflux, 2 h; k) chromatography on Dowex-50.

Monitoring the asymmetric Strecker reaction by HPLC we found that the initial **14**/**13** ratio was 1:1. However, equilibration of purified **13** in MeOH led to isomerization, giving a **14**/**13** ratio of 4:1. Repetition of the isomerization–separation procedure provided **14** in 80 % yield. The desired L amino acid **7** was obtained from **14** by cleavage of the PhCH–$CH_2OH$ bond and hydrolysis of the intermediate Schiff base. Compound **7** was optically pure (> 95 % *ee*), as evidenced by the $^1$H NMR spectrum of the corresponding methyl ester in the presence of a chiral lanthanide shift reagent.

To examine the suitability of **7** as a $^{19}$F-labeled amino acid for the analysis of peptides by NMR spectroscopy ($^{19}$F NMR label), we first compared its calculated properties[15] with those of the nonpolar proteinogenic amino acids and the aforementioned $^{19}$F-labeled compounds. The shape and steric volume of **7** resemble closely the corresponding values of Leu, Ile, Met, Trp, and Phe. The similarity to Pro, Val, and Ala is poorer. The nonaromatic character of **7** constitutes its main difference to Trp and Phe. If one considers the values of octanol/water partition coefficients, a substitution of Leu, Ile, or Met by **7** would cause minimal change in the mean hydrophobicity, which is an important prerequisite for the proper folding of a polypeptide.[16] According to all parameters it is apparent that **7** is closer to the natural nonpolar amino acids than any of the previously used phenylglycine derivatives (**3, 4**).

To address the suitability of **7** experimentally, the new FAA was incorporated in the 21-mer sequence of the antimicrobial peptide PGLa in the very same way as **3** and **4** had been previously used as $^{19}$F NMR labels.[4a,b,h] The substituted positions were Ile 9 (**15**), Ala 10 (**16**), Ile 13 (**17**), and Ala 14 (**18**). Previously, the FAAs **3** and **4** had racemized

 © 2006 Wiley-VCH Verlag GmbH & Co. KGaA, Weinheim 

completely under the SPPS conditions used to produce PGLa.[4a,b,5,7] Now, all of the synthetic peptides containing **7** were obtained as single diastereomers, as shown by HPLC/MS. It is known that PGLa assembles as an α helix when bound to a lipid bilayer and permeabilizes bacterial membranes.[4a,b] The biological activity of **15**–**18** was tested by bacterial-growth inhibition assays, which can respond strongly to single-point mutations (see the Supporting Information). This proved that none of the labeled analogues display any functional deviations from the wild-type peptide, suggesting that the new building block **7** did not induce any structural perturbations. Structure analysis of the labeled peptides **15**–**18** by circular dichroism proved that no distortion was induced by the new unit in any of the positions examined (see Figure 2).

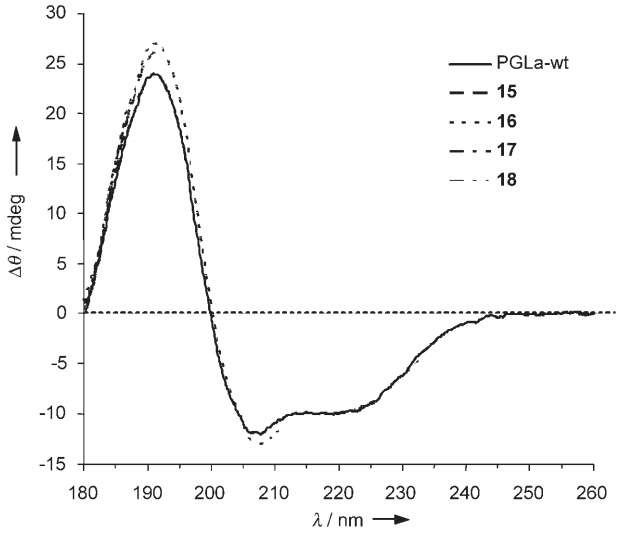


***Figure 2.*** Circular dichroism spectra of the PGLa wild-type peptide and its L-$CF_3$-Bpg-labeled analogues **15**–**18** in the presence of sodium dodecyl sulfate micelles (5 mmol), normalized to the peptide concentration.

Finally, we reconstituted the labeled peptides into mechanically oriented phospholipid bilayers for a comprehensive solid-state $^{19}$F NMR analysis. In brief, **15**–**18** behaved the same way as the PGLa analogues that had been previously labeled with **3** and **4**.[4a,b,5,7] Namely, 1) they bind to and uniformly align in 1,2-dimyristoyl-*sn*-glycero-3-phosphocholine (DMPC) bilayers; 2) they rotate around the bilayer normal; 3) they realign in a concentration-dependent manner; and 4) for a given concentration the labeled positions exhibit the expected dipolar coupling and sign compatible with the known α-helical conformation. Therefore, we conclude that $CF_3$-Bpg satisfies all chemical and conformational requirements as a good labeling unit for peptide structure analysis by solid-state $^{19}$F NMR spectroscopy.

In summary, we have synthesized the novel conformationally rigid fluorinated L α-amino acid **7** ($CF_3$-Bpg). The overall yield of the synthesis is 35 %, which makes it attractive for an intermediate-scale production of **7**.[17] This amino acid was designed as a label for membrane-bound peptides and can be used to study their alignment, structure, and dynamics by means of solid-state $^{19}$F NMR spectroscopy.

Received: January 26, 2006
Revised: May 15, 2006
Published online: July 25, 2006

**Keywords:** amino acids · fluorine · membrane-active peptides · NMR spectroscopy

[1] M. A. Danielson, J. J. Falke, *Annu. Rev. Biophys. Biomol. Struct.* **1996**, *25*, 163.
[2] a) A. S. Ulrich, *Prog. Nucl. Magn. Reson. Spectrosc.* **2004**, *46*, 1; b) A. S. Ulrich in *Encyclopedia of Spectroscopy and Spectrometry* (Eds.: J. Lindon, G. Tranter, J. Holmes), Academic Press, New York, **2000**, p. 813.
[3] a) C. Frieden, S. D. Hoetzli, J. G. Bann, *Methods Enzymol.* **2004**, *380*, 400; b) T. L. Hendrickson, V. de Crécy-Lagard, P. Schimmel, *Annu. Rev. Biochem.* **2004**, *73*, 147.
[4] a) R. W. Glaser, C. Sachse, U. H. N. Dürr, P. Wadhwani, S. Afonin, E. Strandberg, A. S. Ulrich, *Biophys. J.* **2005**, *88*, 3392; b) R. W. Glaser, C. Sachse, U. H. N. Dürr, P. Wadhwani, A. S. Ulrich, *J. Magn. Reson.* **2004**, *168*, 153; c) S. Afonin, U. H. N. Dürr, R. W. Glaser, A. S. Ulrich, *Magn. Reson. Chem.* **2004**, *42*, 195; d) S. L. Grage, J. Wang, T. A. Cross, A. S. Ulrich, *Biophys. J.* **2002**, *83*, 3336; e) J. Salgado, S. L. Grage, L. H. Kondejewski, R. N. McElhaney, R. S. Hodges, A. S. Ulrich, *J. Biomol. NMR* **2001**, *21*, 191; f) O. Toke, R. D. O'Connor, T. K. Weldeghiorghis, W. L. Maloy, R. W. Glaser, A. S. Ulrich, J. Schaefer, *Biophys. J.* **2004**, *87*, 675; g) O. Toke, W. L. Maloy, S. J. Kim, J. Blazyk, J. Schaefer, *Biophys. J.* **2004**, *87*, 662; h) E. Strandberg, P. Wadhwani, P. Tremoulihac, U. H. N. Dürr, A. S. Ulrich, *Biophys. J.* **2006**, *90*, 1676.
[5] A. S. Ulrich, P. Wadhwani, U. H. N. Dürr, S. Afonin, R. W. Glaser, C. Sachse, P. Tremouilhac, M. Berditchevskaia in *NMR Spectroscopy of Biological Solids* (Ed.: A. Ramamoorthy), CRC, Boca Raton, **2006**.
[6] M. Cotten, C. Tian, D. D. Busath, R. B. Shirts, T. A. Cross, *Biochemistry* **1999**, *38*, 9185.
[7] S. Afonin, R. W. Glaser, M. Berditchevskaia, P. Wadhwani, K. H. Gührs, U. Möllmann, A. Perner, A. S. Ulrich, *ChemBioChem* **2003**, *4*, 1151.
[8] a) R. W. Glaser, A. S. Ulrich, *J. Magn. Reson.* **2003**, *164*, 104; b) R. Ulrich, R. W. Glaser, A. S. Ulrich, *J. Magn. Reson.* **2003**, *164*, 115.
[9] W. Adcock, Y. Baran, A. Filippi, M. Speranza, N. A. Trout, *J. Org. Chem.* **2005**, *70*, 1029.
[10] R. Pellicciari, M. Raimondo, M. Marinozzi, B. Natalini, G. Costantino, C. Thomsen, *J. Med. Chem.* **1996**, *39*, 2874.
[11] K. B. Wiberg, S. T. Waddell, *J. Am. Chem. Soc.* **1990**, *112*, 2194.
[12] J. L. Adcock, A. A. Gack, *J. Org. Chem.* **1992**, *57*, 6206.
[13] T. K. Chakraborty, G. V. Reddy, K. A. Hussain, *Tetrahedron Lett.* **1991**, *32*, 7597.
[14] CCDC-293724 contains the supplementary crystallographic data for this paper. These data can be obtained free of charge from The Cambridge Crystallographic Data Centre via www.ccdc.cam.ac.uk/data_request/cif.
[15] The physical properties of the amino acids (see the Supporting Information) were calculated by QikProp (www.schrodinger.com).
[16] C. Branden, J. Tooze, *Introduction to Protein Structure*, Garland Publishing, New York, **1999**.
[17] Compound **7** is available at Enamine Ltd (http://www.enamine.net).

 © 2006 Wiley-VCH Verlag GmbH & Co. KGaA, Weinheim 

Superlattices

DOI: 10.1002/anie.200601233

# Superlattice Formation from Polydisperse Ag Nanoparticles by a Vapor-Diffusion Method**

*Yang Yang, Shuman Liu, and Keisaku Kimura**

Plenteous development of synthetic methods affords more and more possibilities to endow nanoparticles with controlled morphology and surface properties that can be manipulated as "artificial atoms". Assembly of these nanoparticles would provide an opportunity to investigate and further tailor their collective physical properties.[1]

Superlattice formation by metal or semiconductor nanoparticles is currently being explored by strategies of bottom-up assembly, which include solvent evaporation of metal nano-organosols on a substrate,[1,2] crystallization of nanoparticles from bulk solution by sedimentation or precipitation,[3] wet deposition by supramolecular interactions between the nanoparticles and a surface,[2d,4] and organization of nanoparticles at oil/water interfaces.[5] In most cases, obtaining superlattice structures strongly depends on highly monodisperse nanoparticles as building blocks. Recently, we reported that hydrophilic metal nanoparticles are excellent components for formation of two- or three-dimensional (2D or 3D) superlattices at the air/water interface by adjusting the concentration of the electrolyte.[6] Herein, we use hydrophilic mercaptosuccinic acid (MSA)-capped Ag nanoparticles as an example and report facile superlattice formation by vapor diffusion of hydrogen chloride (HCl) into their bulk aqueous solution. This new approach can induce the construction of perfect superlattice structure at air/water interfaces under relatively mild conditions and, in particular, high monodispersity of the initial nanoparticle ensemble is not strictly required.

A transmission electron microscopy (TEM) image of the as-prepared MSA-capped Ag nanoparticles (Figure 1a) and their size histogram (Figure 1b) show that they are roughly spherical with an average diameter of 4.8 nm. The full width at half-maximum (fwhm) calculated from the distribution is about 1.4 nm, so the size polydispersity is up to 29%. The selected-area electron diffraction (SAED) pattern (inset to Figure 1a) shows that the as-prepared Ag nanoparticles consist of a face-centered cubic (fcc) phase (for XRD and FTIR data, see Supporting Information). Figure 1c shows the model of an MSA-capped Ag nanoparticle. On the basis of such a structure, the MSA-capped Ag nanoparticle can be considered to be a macromolecule with good solubility in water and is likely to be modifiable by reaction of the carboxylate groups.[7]

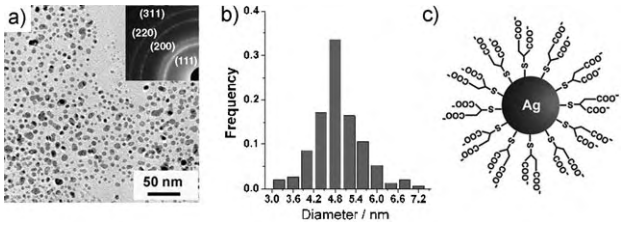


***Figure 1.*** a) TEM image of as-prepared MSA-capped Ag nanoparticles. The inset shows the corresponding SAED pattern. b) Particle size histogram. c) Model of an MSA-capped Ag nanoparticle.

First, we transformed the hydrophilic Ag nanoparticles into organosols by means of the cation surfactant cetyltrimethylammonium bromide ($C_{16}H_{33}(CH_3)_3NBr$, CTAB) through electrostatic interaction. In addition to changing the particle surface from hydrophilic to hydrophobic, the formation of $MSA^-$–$CTA^+$ anion–cation pairs effectively neutralizes the charge of the carboxylate groups of MSA. The reduced surface charge is beneficial for the balance between local electrostatic repulsion and dispersion forces required as driving force for self-assembly. However, the high polydispersity of the particles prevented superlattice formation at the air/water interface after solvent evaporation (Supporting Information). Alternatively, we adopted our previous method for growing colloidal crystals of MSA-capped metal nanoparticles from bulk aqueous solution by directly adding a concentrated solution of HCl,[6] which can convert the MSA molecules on the particle surface from the carboxylate to the acid state and thus decrease the repulsive forces among the nanoparticles. However, we failed to obtain any superlattice structures, and the polydispersity of the starting Ag nanoparticles (TEM observations) probably again prevented superlattice formation.

Since MSA-capped nanoparticles can be regarded as artificial macromolecules, the method for the formation of colloidal crystals from bulk solution has certain similarities with practical procedures for macromolecule crystallization. For crystallization of biological macromolecules such as protein/solvent systems, vapor diffusion methods that increase the concentration of precipitating agents or alter physical properties, e.g. the pH value, are currently far more popular than other approaches such as bulk crystallization.[8] The vapor diffusion technique is ideal for screening a large range of conditions and permits considerable flexibility in varying conditions by modification of the precipitant concentration in the reservoir. Hence, we utilized a similar strategy involving gradual diffusion of HCl gas into the concentrated aqueous solution of MSA-capped Ag nanoparticles.

[*] Dr. Y. Yang, Dr. S. Liu, Prof. K. Kimura
Department of Material Science
Graduate School of Material Science
University of Hyogo
3-2-1 Koto, Kamigori-cho, Ako-gun, Hyogo 678-1297 (Japan)
Fax: (+81) 791-580-161
E-mail: kimura@sci.u-hyogo.ac.jp

[**] The Japan Society for the Promotion of Science is gratefully acknowledged for financial support of this work and for a postdoctoral fellowship (P04402). This work was also supported in part by a Grant-in-Aid for Scientific Research (S: 16101003) and Scientific Research in Priority Areas, Molecular Spins (15087210) from MEXT.

Supporting information for this article is available on the WWW under http://www.angewandte.org or from the author.


InterScience
© 2006 Wiley-VCH Verlag GmbH & Co. KGaA, Weinheim

The crystallization of Ag nanoparticles was carried out in a glass vial (vial A) in which MSA-capped Ag nanoparticle powder (6.0 mg) was dissolved in distilled water (3.0 mL; pH 5.8–6.0); HCl solution (4.0 mL) was placed in another glass vial of the same dimensions (vial B). Then vials A and B were stored in a closed vessel of suitable volume. With 1.0 M HCl solution in vial B, assembled structures visible to the naked eye formed at the air/water interface after about two weeks, while some black precipitate was also observed at the bottom of vial A.

TEM images revealed that most structures formed at the air/water interface consisted of an Ag nanoparticle monolayer over a large area. However, the size of the nanoparticles in the layer was not uniform, so the domain of ordered arrangement was rather small. When the growth period was up to three weeks, 2D superstructures formed at the air/water interface (Figure 2a). A magnified image and the corresponding size histogram are presented in Figure 2b and c, respectively. It can be clearly seen that the MSA-capped Ag nanoparticles organize into a 2D-ordered compact structure. The fast Fourier transform (FFT, inset in Figure 2b) pattern also indicates that the assembly consists of nanoparticle lattices with hexagonal symmetry and long-range order. The average diameter of the particles is about 4.8 nm, and the polydispersity is reduced to 13% in the superlattice. The interparticle gap estimated from Figure 2b is about 1.2 nm, approximately equal to twice the length of the MSA molecule (ca. 0.6 nm), and indicates the absence of chain interdigitation of the MSA layers among adjacent particles. This result agrees well with the mechanism previously proposed for superlattice formation by MSA-capped Au nanoparticles, that is, hydrogen bonds among MSA molecules connect adjacent nanoparticles.[6b,c]

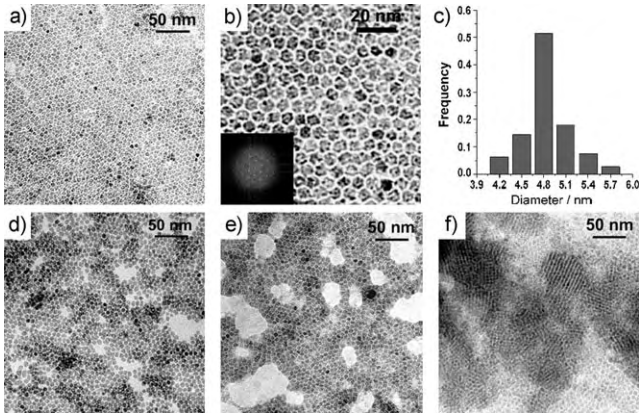


***Figure 2.*** Morphological evolution with aging time for 1.0 M HCl solution in vial B. a) 3, d) 4, e) 5, and f) 7–12 weeks. b) Enlarged image of (a) and corresponding FFT. c) Particle size histogram of (a).

Clearly, the degree of order of the initially formed close-packed 2D structure improves as growth proceeds. Whitesides and Boncheva previously proposed that a sufficient degree of reversibility is required for a self-assembly system to form highly ordered arrays.[9] In our system, the air/water interface not only offers an important alternative scaffold for organization of Ag nanoparticles, but also retains sufficient reversibility to correct errors in the self-assembly process. When the polydisperse hydrophobic Ag nanoparticles assemble into a monolayer at the air/water interface, two important events are likely to happen in this highly dynamic process. First, the particles in the minority whose sizes are different from those of other component particles can be gradually repelled towards the boundary of the superlattice. Second, a particle trapped in a metastable site can be released back into bulk solution owing to its diffusive nature in a suspension (inadequate solvation). Such a particle can possibly reenter the lattice as a building block once the most stable position has been found. These two processes, which act continually during the aging time, will significantly narrow the size distribution in the superstructure, remove lattice defects, and improve the lattice symmetry in the formed superlattice. Simultaneously, the gradual diffusion of HCl into the bulk suspension produces more hydrophobic nanoparticles at a slow rate, which will act as new building blocks and themselves undergo the self-correction process for further growth of the superlattice.

The TEM images shown in Figure 2d and 2e demonstrate the morphological evolution of the superstructures formed at the air/water interface for growth times of four and five weeks. Comparing the contrast of these two images shows that the hexagonal close-packed (hcp) superlattice structure gradually grows from mono- to bi- to multilayer. After growth over a period of seven weeks (the pH in vial A had decreased to 0.4–0.6), many 3D superlattice aggregates were visible (Figure 2f). The close-packed Ag nanoparticles in these superstructures mimic the stacking of atoms in the crystal, and this leads to the appearance of many lattice planes in the colloidal crystal. However, all these 3D superlattices are shapeless and their size is relatively small. Investigation by TEM revealed that this amorphous appearance was hardly changed by further extending superlattice growth to three months. At this time the pH value in vial A was in the range of 0.4–0.6, almost the same as one month earlier, that is, HCl diffusion from vial B to vial A was close to the equilibrium state. Note that the final pH value in vial A is sufficient for superlattice formation according to our previous studies on direct addition of HCl to the bulk solution.

When the initial concentration of HCl in vial B was increased from 1.0 to 3.0 M, assembled structures were found at the air/water interface after only about one week. The shorter time for the appearance of assemblies indicates a faster HCl diffusion from vial B to A. However, unlike the result obtained with 1.0 M HCl solution, most of the formed structures were a mass of particle aggregates, as well as small monolayer domains, according to TEM observations. No large areas of continuous monolayer could be observed. Similarly, the nanoparticle arrangement in these structures was random, and periodic stacking did not take place in the initial stage. Over a growth period of four weeks, the ordering of particle arrangements was partially improved. Figure 3a is a typical image of the structure formed at this stage, from which it can be seen that the particle size in both mono- and multilayers has become uniform, and the particles are inclined to assemble into hcp structures due to the self-

 © 2006 Wiley-VCH Verlag GmbH & Co. KGaA, Weinheim 

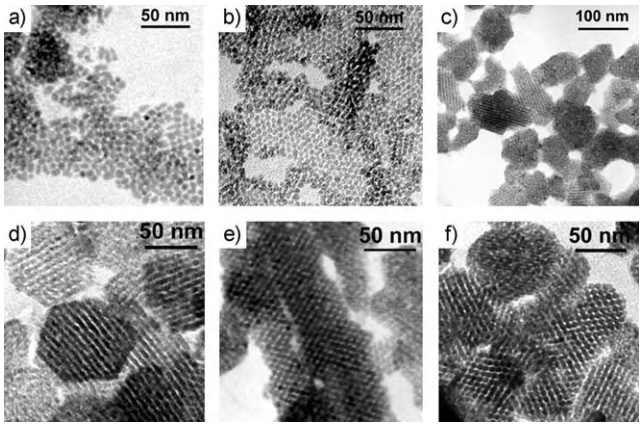


***Figure 3.*** Morphological evolution with aging time for 3.0 M HCl solution in vial B. a) 4, b) 6, and c) 10–12 weeks. d–f) Typical superlattice morphologies during growth for 10–12 weeks.

correction process. After a growth time of 6 weeks, the appearance of ordered mono- and multilayers was observed (Figure 3b). During about 10–12 weeks of growth, a large number of 3D superlattices formed at the air/water interface (Figure 3c). Each 3D superlattice is made up of ordered close-packed nanoparticle, and the superlattices are mostly faceted plate crystals with average size in the range of 50–100 nm. Various shapes of 3D superlattices could be found when different areas of the TEM sample were inspected. Figure 3d–f show three representative morphologies of the 3D superlattices formed under these conditions: hexagonal, clubbed, and round shapes, respectively. In each case, the packing of Ag nanoparticles in the superlattice is very regular.

We further increased the concentration of HCl in vial B to 6.0 M. As expected, the time needed for visible assembly formation at the air/water interface decreased, to 3–4 d. The majority of structures were aggregates composed of randomly arranged nanoparticles. However, the number of aggregates formed in the visual field was smaller than with an initial HCl concentration of 3.0 M. Until six weeks from the beginning, we found some slightly disordered 3D superlattices. A relatively large one is presented in Figure 4a. The observed change in contrast indicates the thickness of overlapping Ag nanoparticle layers is not uniform. The packing of Ag nanoparticles in the thick area is already ordered with the appearance of a regular lattice. However, the particles are not yet well organized in the thin area, which can be assumed to be the origin of further growth of the 3D superlattice. On the basis of self-correction under vapor diffusion, the size of the 3D superlattice became larger and larger with more Ag nanoparticles orderly stacked and overlapping along this direction. Figure 4b and 4c show 3D superlattices for increasing growth time. In every growth stage, the 3D superlattices have the same rhombic shape but with gradually increasing size. After 12 weeks of growth, the cross diameter of the Ag nanoparticle superlattice can attain 1–2 μm. Its thickness was estimated to be 0.2–0.3 μm on the basis of SEM investigations.

Figure 5a and 5b show low- and high-resolution TEM images of a perfectly rhombic 3D superlattice after a growth period of 12 weeks. Compared to the structure shown in Figure 4a, organization of the nanoparticles is much more orderly. The average size of component nanoparticles is still 4.8 nm, but the size polydispersity is reduced from the original 29% to 8% in the superlattice. The projected positions of Ag nanoparticles show a slightly elongated hexagonal structure, which is confirmed by the inset FFT pattern. To discriminate between fcc and hcp structures, further TEM investigation of these superlattices was carried out. Two different arrangements of Ag nanoparticles are found in the superlattice (Figure 5c,d and e,f). Both the observed packing of Ag nanoparticles and the FFT patterns of these arrangements (see insets) are consistent with those expected for the (100) and (110) projections of an fcc superlattice. Especially the strict fourfold symmetry that is apparent in Figure 5d excludes the possibility of an hcp structure.[3b,10] Tilted TEM experiments were performed on the sample grown for 12 weeks. By tilting the 3D superlattice to −15 or +15°, TEM images repeatedly demonstrated that the stacking of Ag nanoparticles in the multilayers always appears to be periodic along various orientations, that is, the 3D superlattice is highly ordered (Supporting Information).

The above investigations show that gradual alteration of pH is particularly beneficial for superlattice formation at the air/water interface no matter which initial concentration of HCl in the reservoir is employed. Increasing the HCl concentration from 1.0, to 3.0, and to 6.0 M increased the

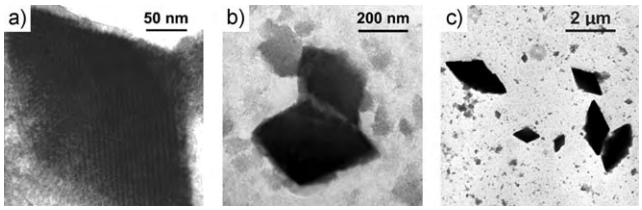


***Figure 4.*** Morphological evolution with aging time for 6.0 M HCl solution in vial B. a) 6, b) 8, and c) 12 weeks.

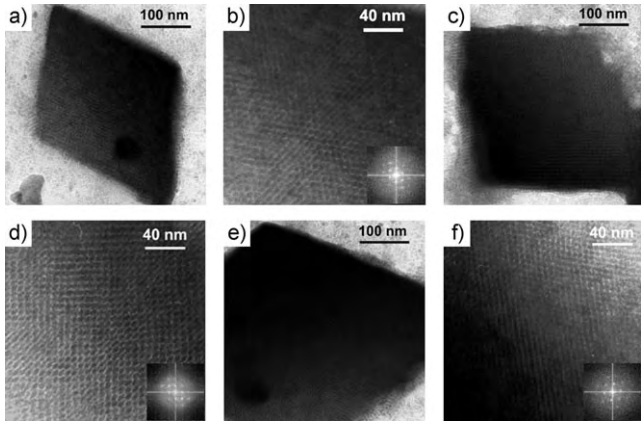


***Figure 5.*** a, c, e) TEM images of three typical 3D rhombic superlattices with 6.0 M HCl solution in vial B during growth of 12 weeks. b, d, f) Enlarged images of (a), (c), and (e), respectively, with corresponding FFT.

 © 2006 Wiley-VCH Verlag GmbH & Co. KGaA, Weinheim 

rate of diffusion of HCl into the bulk solution of Ag nanoparticles. Accordingly, the appearance of aggregates at the air/water interface became faster and faster. However, at this stage the formed aggregates are random in each case owing to the size polydispersity. By time-dependent self-correction processing, ordered 2D or 3D superlattices began to form at later stages.

Conversely, the time required for superlattice formation was increased by increasing the initial HCl concentration. Since self-correction of the assembly strongly relies on the air/water interface, slower formation of aggregates provides the Ag nanoparticles with sufficient opportunity to self-assemble, restructure, and order themselves into a crystalline lattice at such an interface. Note that, even when 6.0 M HCl solution is used for diffusion, the production of solvates is much milder than with direct addition of concentrated HCl solution. Excessively fast growth will lead to many irregular structures isolated from the air/water interface. This could be the reason why formation of colloidal crystals by direct addition of HCl solution strongly depends on a narrow size distribution of starting nanoparticles and their formation is quite sensitive to the conditions. On the other hand, a lower production rate of building blocks is inclined to form 2D network or 3D crystals of small size. At relatively high diffusion rate, 3D superlattices of large size and characteristic crystal shape become dominant due to full crystal growth, possibly favored by the reduced number of initial nuclei of colloidal crystals. Even if the pH in the hydrosol reaches the same value, the structures formed at the air/water interface under different diffusion conditions are diverse. Thus, the pathway leading to supersaturation and the kinetics of the process may be as important as the final conditions achieved.[8]

In summary, a new vapor diffusion method to build superlattices from polydisperse MSA-capped Ag nanoparticles has been developed. Long-term observations for up to three months demonstrated that superlattice morphology can be controlled by a time- and pH- dependent self-correction process. This represents an economical and general strategy for superlattice creation from water-soluble metal or semiconductor nanoparticles stabilized by molecules bearing carboxylate groups, and is also beneficial for a better understanding of the self-assembly process.

## Experimental Section

Preparation of MSA-capped Ag nanoparticles:[7b] With vigorous stirring, freshly prepared aqueous $NaBH_4$ solution (60 mL, 0.2 M) was added through a syringe at a rate of 2.0 mL min$^{-1}$ to water/methanol mixture (250 mL) containing $AgNO_3$ (1.25 mmol) and MSA (97%, 2.5 mmol) at 0 °C. The resulting dark brown, flocculent precipitate was separated and thoroughly washed with 20% water/methanol and pure ethanol in turn, followed by freeze-drying, to yield about 0.25 g of black powder.

Ag nanoparticles were crystallized in a glass vial of 5 cm in height and 1.5 cm in diameter (vial A), in which the as-prepared MSA-capped Ag nanoparticle powder (6.0 mg) was dissolved in distilled water (3.0 mL) to form a dark brown solution. HCl solution (4.0 mL) was placed in another glass vial (vial B). The concentration of HCl solution in vial B was set at 1.0, 3.0, or 6.0 M. Then vials A and B were stored in a closed vessel of suitable volume (50 mL) and left in the dark for three months. The species formed at the air/water interface in vial A were sampled after certain times for morphology observations.

TEM images and corresponding SAED patterns were obtained at 200 kV acceleration voltage. The Ag nanoparticle superstructures formed at the air/water interface were directly transferred to a carbon-coated copper support grid for TEM and SAED experiments. The mean particle size of Ag nanoparticles was estimated by measuring the diameters of at least 200 individual particles. SEM images were taken at 15 kV acceleration voltage. X-ray diffraction (XRD) was performed with $Cu_{K\alpha 1}$ radiation ($\lambda = 1.54056$ Å) at 40 kV and 20 mA.

Received: March 29, 2006
Revised: April 28, 2006
Published online: July 26, 2006

**Keywords:** nanoparticles · self-assembly · silver · superlattices

[1] a) H. Weller, *Curr. Opin. Colloid Interface Sci.* **1998**, *3*, 194; b) C. P. Collier, T. Vossmeyer, J. R. Heath, *Annu. Rev. Phys. Chem.* **1998**, *49*, 371; c) C. B. Murray, C. R. Kagan, M. G. Bawendi, *Annu. Rev. Mater. Sci.* **2000**, *30*, 545; d) B. O. Dabbousi, C. B. Murray, M. F. Rubner, M. G. Bawendi, *Chem. Mater.* **1994**, *6*, 216; e) P. C. Ohara, J. R. Heath, W. M. Gelbart, *Angew. Chem.* **1997**, *109*, 1120; *Angew. Chem. Int. Ed. Engl.* **1997**, *36*, 1078; f) S. A. Harfenist, Z. L. Wang, R. L. Whetten, I. Vezmar, M. M. Alvarez, *Adv. Mater.* **1997**, *9*, 817; g) M. P. Pileni, *J. Phys. Chem. B* **2001**, *105*, 3358; h) S. Stoeva, K. J. Klabunde, C. M. Sorensen, I. Dragieva, *J. Am. Chem. Soc.* **2002**, *124*, 2305; i) F. X. Redl, K. S. Cho, C. B. Murray, S. O'Brien, *Nature* **2003**, *423*, 968; j) E. V. Shevchenko, D. V. Talapin, N. A. Kotov, S. O'Brien, C. B. Murray, *Nature* **2006**, *439*, 55.

[2] a) A. Taleb, C. Petit, M. P. Pileni, *Chem. Mater.* **1997**, *9*, 950; b) A. L. Rogach, D. V. Talapin, E. V. Shevchenko, A. Kornowski, M. Haase, H. Weller, *Adv. Funct. Mater.* **2002**, *12*, 653; c) S. I. Stoeva, B. L. V. Prasad, S. Uma, P. K. Stoimenov, V. Zaikovski, C. M. Sorensen, K. J. Klabunde, *J. Phys. Chem. B* **2003**, *107*, 7441; d) M.-C. Daniel, D. Astruc, *Chem. Rev.* **2004**, *104*, 293.

[3] a) C. B. Murray, C. R. Kagan, M. G. Bawendi, *Science* **1995**, *270*, 1335; b) D. V. Talapin, E. V. Shevchenko, A. Kornowski, N. Gaponik, M. Haase, A. L. Rogach, H. Weller, *Adv. Mater.* **2001**, *13*, 1868.

[4] a) L. M. Demer, D. S. Ginger, S.-J. Park, Z. Li, S.-W. Chung, C. A. Mirkin, *Science* **2002**, *296*, 1836; b) A. K. Boal, F. Ilhan, J. E. DeRouchey, T. Thurn-Albrecht, V. M. Rotello, *Nature* **2000**, *404*, 476; c) A. Sanyal, T. B. Norsten, O. Uzun, V. M. Rotello, *Langmuir* **2004**, *20*, 5958.

[5] a) Y. Lin, H. Skaff, T. Emrick, A. D. Dinsmore, T. P. Russell, *Science* **2003**, *299*, 226; b) W. H. Binder, *Angew. Chem.* **2005**, *117*, 5300; *Angew. Chem. Int. Ed.* **2005**, *44*, 5172.

[6] a) K. Kimura, S. Sato, H. Yao, *Chem. Lett.* **2001**, 372; b) S. H. Wang, S. Sato, K. Kimura, *Chem. Mater.* **2003**, *15*, 2445; c) S. H. Wang, H. Yao, S. Sato, K. Kimura, *J. Am. Chem. Soc.* **2004**, *126*, 7438.

[7] a) S. H. Chen, K. Kimura, *Langmuir* **1999**, *15*, 1075; b) S. H. Chen, K. Kimura, *Chem. Lett.* **1999**, 1169; c) J. Tominaga, S. Sato, H. Yao, K. Kimura, *Chem. Lett.* **2002**, 950.

[8] A. McPherson, *Crystallization of Biological Macromolecules*, Cold Spring Harbor, Cold Spring Harbor, **1999**.

[9] G. M. Whitesides, M. Boncheva, *Proc. Natl. Acad. Sci. USA* **2002**, *99*, 4769.

[10] a) L. Motte, F. Billoudet, E. Lacaze, J. Douin, M. P. Pileni, *J. Phys. Chem. B* **1997**, *101*, 138; b) Z. L. Wang, *Adv. Mater.* **1998**, *10*, 13.

 © 2006 Wiley-VCH Verlag GmbH & Co. KGaA, Weinheim 

Heterocycles

DOI: 10.1002/anie.200601298

# Synthesis, Structure, and Properties of 4,7-Dimethoxybenzo[*c*]tellurophene: A Molecular Pyroelectric Material**

*Michael Pittelkow, Theis K. Reenberg, Kim T. Nielsen, Magnus J. Magnussen, Theis I. Sølling, Frederik C. Krebs, and Jørn B. Christensen**

The formation of molecular crystals that possess a polar axis in the solid state is largely an unexplored area, and no generic understanding is available to this day. Materials with a polar axis (a permanent dipole moment in the solid state) potentially possess ferroelectric, piezoelectric, and pyroelectric properties.[1] Pyroelectric solids are used as the key material in a variety of components, which range from microphones and infrared detectors to frequency-doubling crystals in laser technology, just to mention a few.[2] Examples of the design and synthesis of organic materials with pyroelectric properties are scarce because of the difficulties in predicting the crystalline properties of matter.[3] An organic material must crystallize in one of the ten polar point groups to exhibit pyroelectric properties.[4] Although most organic molecules possess a permanent dipole moment, few crystallize in a polar space group. Generally, derivatives based on *meta*-disubstituted benzene have proven to be useful as they have a tendency to crystallize in one of these ten required polar point groups and, thus, exhibit a pyroelectric effect.[5] Apart from this rather vague design rule, little is known about the structural features that promote crystallization in a polar point group, and it is only on the odd and unexpected occasion that novel pyroelectric materials appear.[2a,b]

Herein, we describe the synthesis, structure, and properties of an unusually stable Te-containing heterocyclic compound that crystallizes in a polar space group and possesses pyroelectric properties: 4,7-dimethoxybenzo[*c*]tellurophene (**9**; Scheme 1).

The highly reactive *o*-quinoid heterocycles benzo[*c*]-furan,[6] benzo[*c*]thiophene,[7] and benzo[*c*]selenophene[8] have been the object of considerable interest both from a synthetic and a theoretical perspective.[9] A particularly interesting application of these types of compounds is their role as precursors for low-band-gap conducting polymers.[10] Cava and co-workers first reported benzo[*c*]tellurophenes (Scheme 1),[11–12] whose properties constitute a largely untouched area of tellurium-based heterocyclic chemistry[13–14] largely as a result of the lack of synthetic procedures and the inherent instability of the parent heterocycle.

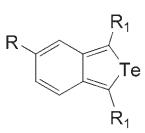


**1**: R=H, $R_1$=H
**2**: R=OMe, $R_1$=H
**3**: R=$NO_2$, $R_1$=H
**4**: R=H, $R_1$=$CO_2$Et
**5**: R=H, $R_1$=$CO_2$Bn
**6**: R=H, $R_1$=*p*-Me$C_6H_4SO_2$

***Scheme 1.*** Benzo[*c*]tellurophenes prepared by Cava and co-workers.

The treatment of **7**[15] with elemental Te and NaI in methoxyethanol yields the orange 4,7-dimethoxy-1,3-dihydrobenzo[*c*]tellurophene diiodide (**8**) in 64% yield (Scheme 2). Attempts to eliminate HI from **8** to yield **9** by using $Et_3N$ in benzene gave a 2:1 mixture of the desired product **9** (major product) and 1,3-dihydro-4,7-dimethoxybenzo[*c*]tellurophene (**10**; minor product; isolated after removal of **9** by reaction with maleic anhydride), as seen by $^1$H NMR spectroscopic analysis. As we were not able to separate the two products, **8** was converted into the bistrifluoroacetate **11** by treatment with $CF_3CO_2Ag$ in anhydrous benzene.[16] Elimination from **11** to the desired product **9** was achieved by using $Et_3N$ in benzene. Compound **9** was purified by column chromatography on silica gel in 72% yield. The benzo[*c*]tellurophene (**9**) was stable in the solid form at room temperature and ambient atmosphere for (at least) several months in the dark (no darkening of the product was observed). It was also stable in solution with benzene and heptane, but it decomposed in $CHCl_3$ after a few hours to give

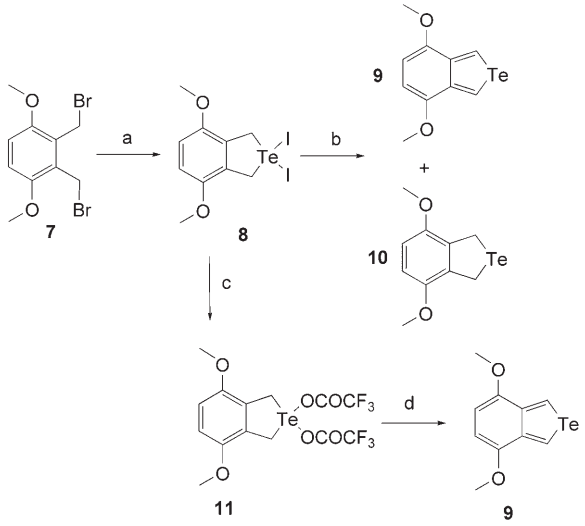


***Scheme 2.*** Synthesis of 4,7-dimethoxybenzo[*c*]tellurophene (**9**). Reagents and conditions: a) NaI, Te, methoxyethanol (64%); b) $Et_3N$, benzene; c) $CF_3COOAg$, benzene (99%); d) $Et_3N$, benzene (72%).

[*] M. Pittelkow, Dr. T. K. Reenberg, M. J. Magnussen, T. I. Sølling, Dr. J. B. Christensen
Department of Chemistry
University of Copenhagen
Universitetsparken 5, 2100 Copenhagen (Denmark)
Fax: (+45) 3532-0212
E-mail: jbc@kiku.dk
K. T. Nielsen, Dr. F. C. Krebs
The Danish Polymer Center
RISØ National Laboratory
P.O. Box 49, 4000 Roskilde (Denmark)

[**] We thank Associate Professor Lars Henriksen and Theis Brock-Nannestad for useful discussions and Professor Klaus Bechgaard for conducting the cyclic voltammetry experiments.

Supporting information for this article is available on the WWW under http://www.angewandte.org or from the author.


InterScience
© 2006 Wiley-VCH Verlag GmbH & Co. KGaA, Weinheim

a gray precipitate (probably elemental Te). Elemental analysis, cyclic voltammetry, and $^1$H and $^{13}$C NMR, UV/Vis, and IR spectroscopy (see the Supporting Information) were used to characterize **9**. Cyclic voltammetry of **9** showed that the heterocycle was oxidized irreversibly and had an oxidation potential of 0.65 eV in $CH_2Cl_2$ with $n$Bu$_4$PF$_6$ as the electrolyte and Pt versus the standard calomel electrode as the reference. However, we did not observe any polymerization of the monomer during the oxidation process.

Final proof of the structure of **9** came from the single-crystal X-ray structure (Figure 1). Needle-shaped yellow crystals were grown by slow evaporation of a solution of **9** in benzene at room temperature in the dark.

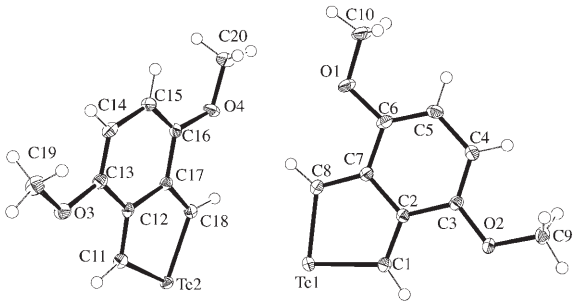


***Figure 1.*** Asymmetric unit cell of the X-ray structure of **9** at 100 K.

The structure of **9** is as expected, planar, and shows similarity in bond lengths and angles with the tellurophene[17] and bitellurophene.[18] These data also agree well with microwave spectroscopic data recorded for tellurophene.[19] The crystal packing of **9** exhibits few similarities with the only reported structure of a benzo[*c*]selenophene.[20]

There are two molecules in the asymmetric unit (Figure 1). At a first glance, these seem to be located randomly in space. More information is evident in the crystal packing, in which a $C_2$ axis materializes and Te–Te interactions are the dominant force (Figures 2 and 3). In fact, the Te–Te distance is 4.06–4.10 Å, which is approximately 0.2 Å shorter than the van der Waal distance of Te (4.30 Å). The benzo[*c*]tellurophene cores are tilted with an angle of approximately 48° with respect to the $C_2$ axis and are arranged two by two. The vector of the molecular dipole has a significant component in the direction of the polar axis (*b* axis). The vector sums of the molecular dipoles cancel in the *a*–*c* plane, whereas the vector sum gives a net dipole moment along the *b* axis, which results in a permanent polarization in the solid state. The distance between two Te atoms in benzo[*c*]tellurophene molecules that are stacked on top of each other is approximately 5.4 Å, which is too large to be accounted for by the van der Waal radius of Te. However, the distance that separates two layers of benzo[*c*]tellurophenes can be attributed to π–π interactions (ca. 3.5–3.6 Å) between the aromatic cores.[21] The unit cell is shown in Figure 2 and shows the molecular tilt with the *b* axis. Four molecules form a tilted square with twofold symmetry, with a distance between all Te atoms in the tilted square of 4.06–4.10 Å. This type of structure with a short Te–Te interaction and a polar space group has also been seen for the structure of 9-(9′-*H*-fluoren-9′-ylidene)-9*H*-telluroxanthene and could be a more general property of organotellurium compounds.[24]

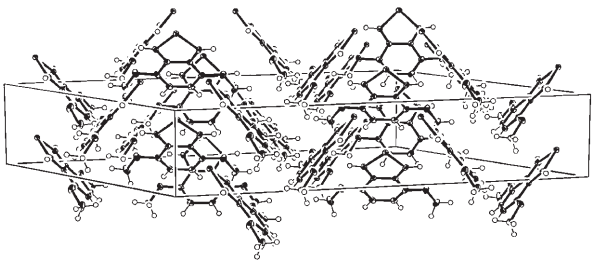

***Figure 2.*** The crystal packing of **9** at 100 K. It can be seen how all the molecules are pointing in the same direction.

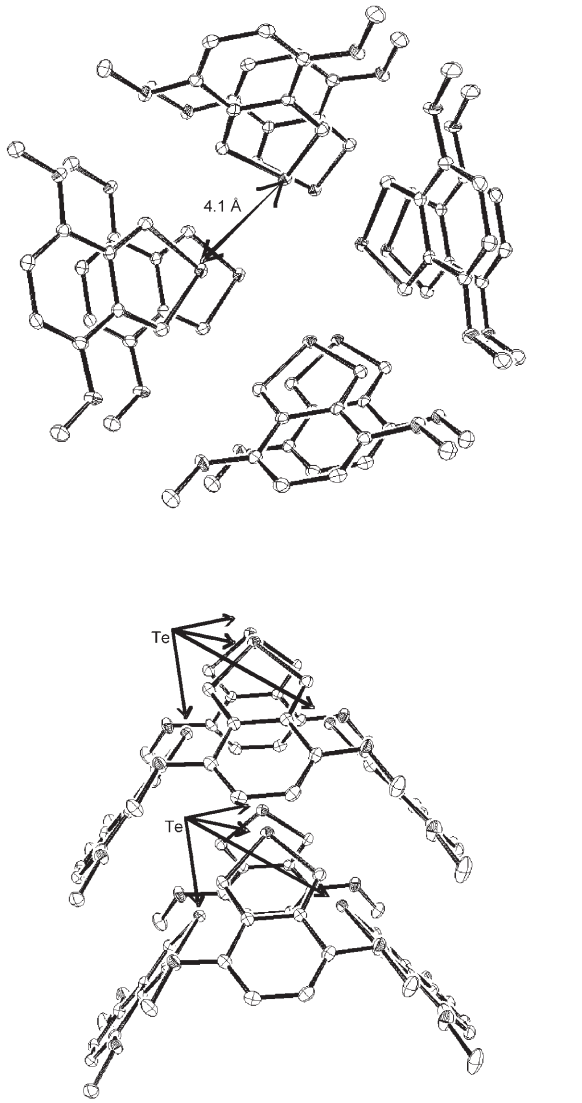


***Figure 3.*** Two views of a section of the crystal structure of **9** at 100 K. Top: the Te–Te interactions looking down the $C_2$ axis. Bottom: the placement of the Te atoms in space (perpendicular to the $C_2$ axis). The hydrogen atoms have been removed for clarity.

 © 2006 Wiley-VCH Verlag GmbH & Co. KGaA, Weinheim 

The fact that all the benzo[*c*]tellurophene molecules point in the same direction in space introduces a permanent polarization into the crystal, thus prompting us to investigate the pyroelectric properties. The pyroelectric effect can be divided into three contributions: primary, secondary, and tertiary effects. The primary effect has origin in abrupt atomic or molecular movements within the crystals as a function of the temperature that leads to changes in the polarization in the material. This behavior is often observed in connection with phase transitions in which the spontaneous polarization either appears, cancels, or changes radically; for example, if the symmetry changes from polar to nonpolar. The secondary effect is due to the change in polarization as a function of the thermal expansion (change of the volume as a function of the temperature) of the unit cell. The tertiary effect is coupled to the piezoelectric properties that pyroelectric materials invariably have. By ensuring homogenous heating of the material and careful design of the detector geometry the tertiary effect can be eliminated from the experiment.

We investigated the X-ray structure as a function of the temperature to determine whether the observed pyroelectric effect is a primary or secondary effect. Therefore, the X-ray diffraction data of **9** were recorded at 100, 150, 200, 250, 300, 323, 343, and 373 K. An exothermic phase transition was observed at about 353 K, as shown by differential scanning calorimetry (DSC; see the Supporting Information). The X-ray data could be collected at 343 K, but the crystal blackened and its edges became rounded upon heating to 373 K. No diffraction could be observed when the temperature was lowered back down to 343 K. This behavior indicates that the observed crystal structure may not be an equilibrium structure. We, however, rule out the possibility of polymorphism as all diffraction disappears after the heating step to 373 K. We observed a decrease in the diffraction intensity as a function of time when collecting data at 343 K, and no diffraction was observed after 2 h. It, therefore, seems plausible that **9** loses tellurium at high temperature.

The structural refinement of **9** was unproblematic at all temperatures, except at 323 K, for which we employed constraints on the molecular geometry by forcing the benzene ring to approach a hexagonal geometry.

If the pyroelectric effect is a primary effect, a structural change as a function of the temperature, which affects the polarization, has to be observed. A change in the polarization can only happen if the angle between the $C_2$ axis and the plane of the molecule changes. We have plotted the angle between the least-squares-fitted plane and the $C_2$ axis as a function of the temperature for one of the molecules in the asymmetric unit cell (the same results were obtained for the other molecule in the asymmetric unit; see the Supporting Information). No significant changes were observed which means that a primary pyroelectric effect can be excluded.

In Figure 4, the polar axes of the unit cell and the cell volume is plotted as a function of the temperature, thus clearly indicating a secondary pyroelectric effect.

The secondary pyroelectric effect is solely due to the thermal expansion of the material with temperature. Compound **9** expands when heated, and as the dipoles in the unit cell stay constant the polarization decreases, thus giving the secondary pyroelectric effect as [Eq. (1)]:[2b]:

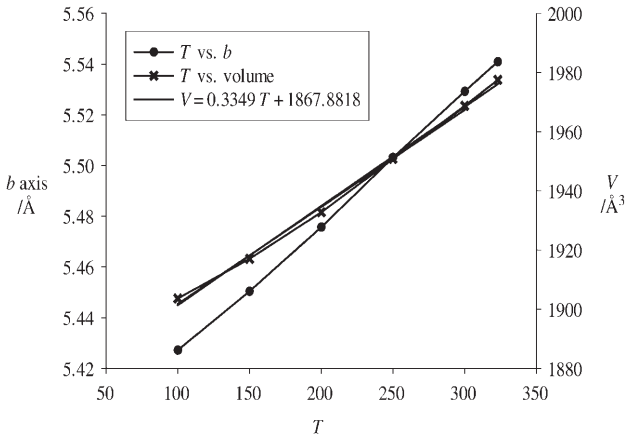


***Figure 4.*** Length of the *b* axis and the volume of the unit cell as a function of temperature.

$$\frac{dP(T)}{dT} = p_2(T) = -\frac{Z}{a\,T^2 + 2\,b\,T + \frac{b^2}{a}}\mu\cos(\theta) \qquad (1)$$

where $P$, $aT^2+2bT+b^2/a$, $T$, $Z$, $\mu$, and $\theta$ are the polarization, the derivatives of the linear thermal expansion with respect to the temperature, the temperature, the molecular entities per unit cell, the molecular dipole moment, and the angle between the molecular plane and the $C_2$ axis, respectively. The dipole moment of the molecules can be enhanced in the solid state, as reported previously,[2c] but this amounts to only minor changes in the overall magnitude of the pyroelectric effect.

The dipole moments of the single molecules and the unit cells were calculated at the B3LYP/3-21G level of theory using the Gaussian 98 suite of programs.[22] The molecular coordinates from the X-ray crystal structures were used as input, and the results are summarized in Table 1. We observe that the dipole moment stays relatively constant with temperature, except for when the temperature was raised to near the phase transition.

***Table 1:*** Calculated dipole moments.[a]

| *T* [K] | $\mu$ [D][b] | $\mu$ [D][c] |
|---|---|---|
| 100 | 2.17 | 15.96 |
| 150 | 2.16 | 14.10 |
| 200 | 2.19 | 12.92 |
| 250 | 2.16 | 13.47 |
| 300 | 2.18 | 12.89 |
| 323 | 2.59 | 15.96 |

[a] B3LYP/3-21G. [b] Single molecule. [c] Component along the *b* axis in a single unit cell, the value is equal to the total dipole moment of one unit cell.

On the basis of the equation for the thermal expansion (Figure 4) and the calculated dipole moment (Table 1), it becomes possible to calculate the pyroelectric effect as a function of the temperature (Figure 5).

 © 2006 Wiley-VCH Verlag GmbH & Co. KGaA, Weinheim 

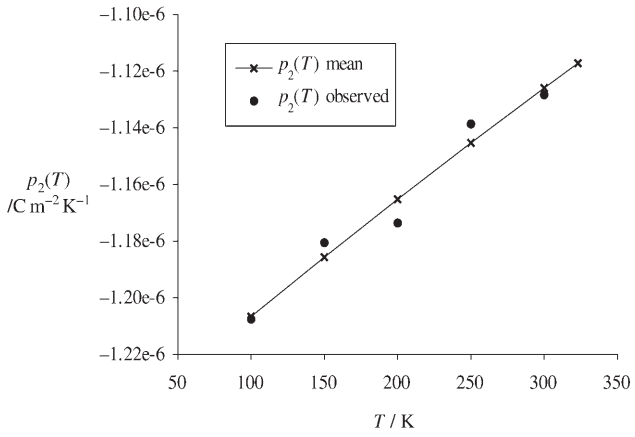


***Figure 5.*** The calculated secondary pyroelectric coefficient as a function of the temperature. The $p_2(T)$ calculated is the secondary pyroelectric coefficient calculated by use of Equation (1), the calculated dipole moments from Table 1, the thermal expansion from Figure 4, and the angle between the molecular plane and the $C_2$ axis. The $p_2(T)$ mean is the secondary pyroelectric coefficient calculated by use of equation above, the mean value of the calculated dipole moments from Table 1, the thermal expansion from Figure 4, and the mean angle between the molecular plane and the $C_2$ axis.

From the point of view of application, primary pyroelectric materials have the advantage that large effects are seen near the phase transition, and therefore very sensitive detector systems can be designed. Their disadvantage is that the operation of the detector system is limited to temperatures near the phase transition. The application of the secondary pyroelectric effect in a detector system has the advantage that it can work over a large temperature range, and organic systems generally have high merit factors.[2b]

We are puzzled by the stability of **9** relative to the other known 1,3-unsubstituted benzo[*c*]tellurophenes, which decompose upon isolation.[11–12] We speculate that the stability of **9** is due to the steric effect that the methoxy groups in the 4- and 7-positions impose on the 1- and 3-positions of the heterocycle. This steric effect prevents these reactive positions from polymerizing, and we consider this to be a *peri* effect.[23]

To summarize, we have presented the synthesis and characterization of a stable benzo[*c*]tellurophene derivative, including the first crystal structure of this type of heterocycle. In addition, we observe an unusual stabilizing effect of the electron-donating methoxy substituents in the 4- and 7-positions. The pyroelectric properties of **9** have been investigated, and a secondary effect was found. This discovery suggests that tellurium-containing heterocycles could be attractive in materials science.

## Experimental Section

All synthetic procedures and characterization data are given in the Supporting Information. Atomic coordinates and further crystallographic details have been deposited with the Cambridge Crystallographic Data Centre, University Chemical Laboratory, Lensfield Road, Cambridge CB2 1EW, England. CCDC 299607–299612 contain the supplementary crystallographic data for this paper. These data can be obtained free of charge from The Cambridge Crystallographic Data Centre via www.ccdc.cam.ac.uk/data_request/cif.

Received: April 3, 2006
Published online: July 21, 2006

**Keywords:** density functional calculations · heterocycles · molecular pyroelectrics · X-ray diffraction

[1] D. Y. Curtin, I. C. Paul, *Chem. Rev.* **1981**, *81*, 525–541.
[2] For examples, see: a) S. Matyjasik, Y. V. Shaldin, *Phys. Solid State* **1997**, *39*, 1454–1456; b) F. C. Krebs, P. S. Larsen, J. Larsen, C. S. Jacobsen, C. Boutton, N. Thorup, *J. Am. Chem. Soc.* **1997**, *119*, 1208–1216; c) G. K. H. Madsen, F. C. Krebs, B. Lebech, F. K. Larsen, *Chem. Eur. J.* **2000**, *6*, 1797–1804; d) A. Faldt, F. C. Krebs, N. Thorup, *J. Chem. Soc. Perkin Trans. 2* **1997**, 2219–2227.
[3] a) J. D. Dunitz, A. Gavezzotti, *Angew. Chem.* **2005**, *117*, 1796–1819; *Angew. Chem. Int. Ed.* **2005**, *44*, 1766–1787; b) "Crystal Design: Structure and Function": G. R. Desiraju in *Perspectives in Supramolecular Chemistry*, *Vol. 7*, Wiley-VCH, **2003**.
[4] S. T. Liu, *Landolt-Börnstein, Numerical Data and Functional Relationships in Science and Technology*, *Vol. 11/III* (Ed.: K.-H. Hellwege), Springer, New York, **1979**, pp. 471–494.
[5] a) A. D. Mighell, J. R. Rodgers, *Acta Crystallogr. Sect. A* **1980**, *36*, 321–326; b) J. C. Wilson, *Acta Crystallogr. Sect. A* **1988**, 44, 715–724.
[6] For a general review about the synthesis of benzo[*c*]furans, see: "Science of Synthesis": P. G. Steel in *Houben-Weyl*, *Vol. 10* (Ed.: E. J. Thomas), Thieme, Stuttgart, **2001**, pp. 87–130.
[7] For a general review about the synthesis of benzo[*c*]thiophenes, see: "Science of Synthesis": J. T. Gilchrist, S. J. Higgins in *Houben-Weyl*, *Vol. 10* (Ed.: E. J. Thomas), Thieme, Stuttgart, **2001**, pp. 185–210.
[8] For a general review about the synthesis of benzo[*c*]selenophenes, see: "Science of Synthesis": P. J. Murphy in *Houben-Weyl*, *Vol. 10* (Ed.: E. J. Thomas), Thieme, Stuttgart, **2001**, pp. 301–205.
[9] "Furans and Their Benzo derivatives": a) F. M. Dean in *Comprehensive Heterocyclic Chemistry*, *Vol. 4* (Eds.: A. R. Katritzky, C. V. Rees), Pergamon, Elmsford, **1984**, pp. 531–712; b) W. Friedrichsen, *Adv. Heterocycl. Chem.* **1980**, *26*, 135.
[10] F. Wudl, M. Kobayashi, A. J. Heeger, *J. Org. Chem.* **1984**, *49*, 3382–3384.
[11] E. H. Mørkved, M. V. Lakshmikantham, M. P. Cava, *Tetrahedron lett.* **1996**, *51*, 9149–9150.
[12] Z. Huang, M. V. Lakshmikantham, M. Lyon, M. P. Cava, *J. Org. Chem.* **2000**, *65*, 5413–5415.
[13] a) M. R. Detty, M. B. O'Regan in *Tellurium-Containing Heterocycles*, *Vol. 53*, Wiley, New York, **1994**; b) "Science of Synthsis": P. J. Murphy in *Houben-Weyl*, *Vol. 10* (Ed.: E. J. Thomas), Thieme, Stuttgart, **2001**, pp. 343–346.
[14] a) N. Petragnani, H. A. Stefani, *Tetrahedron* **2005**, *61*, 1613–1616; b) G. Zeni, D. S. Lüdtke, R. B. Panatieri, A. L. Braga, *Chem. Rev.* **2006**, *106*, 1032–1076.
[15] J. Eskildsen, T. Christensen, T. K. Reenberg, U. Larsen, J. B. Christensen, *Org. Prep. Proced.* **2000**, *32*, 398–400.
[16] Preparation of $CF_3COOAg$: J. G. Traynham, J. S. Dehn, *J. Org. Chem.* **1958**, *23*, 1545–1546.
[17] Crystal structure of α-tellurophene carboxylic acid: L. Fanfani, A. Nunzi, P. F. Zanazzi, A. R. Zanzari, M. A. Pellinghelli, *Cryst. Struct. Comm.* **1972**, *1*, 273–278.
[18] Crystal structure of 2,2′-bitellurophene: T. Otsubo, S. Inoue, H. Nozoe, T. Jigami, F. Ogura, *Synth. Met.* **1995**, *69*, 537–538.
[19] Microwave spectrum of tellurophene: R. D. Brown, J. G. Crofts, *Chem. Phys.* **1973**, *1*, 217–219.

 © 2006 Wiley-VCH Verlag GmbH & Co. KGaA, Weinheim 

[20] Crystal structure of a benzo[*c*]selenophene derivative: E. Aqad, M. V. Lakshmikantham, M. P. Cava, G. A. Broker, R. D. Rogers, *Org. Lett.* **2003**, *5*, 2519 – 2521.
[21] C. A. Hunter, J. K. M. Sanders, *J. Am. Chem. Soc.* **1990**, *112*, 5525 – 5534.
[22] Gaussian 98 (Revision A.11.3), J. Frisch, G. W. Trucks, H. B. Schlegel, G. E. Scuseria, M. A. Robb, J. R. Cheeseman, V. G. Zakrzewski, J. A. Montgomery, Jr., R. E. Stratmann, J. C. Burant, S. Dapprich, J. M. Millam, A. D. Daniels, K. N. Kudin, M. C. Strain, O. Farkas, J. Tomasi, V. Barone, M. Cossi, R. Cammi, B. Mennucci, C. Pomelli, C. Adamo, S. Clifford, S. J. Ochterski, G. A. Petersson, P. Y. Ayala, Q. Cui, K. Morokuma, D. K. Malick, A. D. Rabuck, K. Raghavachari, J. B. Foresman, J. Cioslowski, J. V. Ortiz, B. B. Stefanov, G. Liu, A. Liashenko, P. Piskorz, I. Komaromi,R. Gomperts,R. L. Martin,D. J. Fox,T. Keith, M. A. Al-Laham, C. Y. Peng, A. Nanayakkara, C. Gonzalez, M. Challacombe, P. M. W. Gill, B. Johnson,W. Chen, M. W. Wong, J. L. Andres, M. Head-Gordon, E. S. Replogle, J. A. Pople, Gaussian, Inc., Pittsburgh, PA, **1998**.
[23] V. Balasubramaniyan, *Chem. Rev.* **1966**, *66*, 567 – 641.
[24] A. Levy, P. U. Biedermann, S. Cohen, I. Agranat, *J. Chem. Soc. Perkin Trans. 2* **2001**, 2329 – 2341.

 © 2006 Wiley-VCH Verlag GmbH & Co. KGaA, Weinheim 

Porphyrinoid Chemistry

DOI: 10.1002/anie.200601765

# Metal-Mediated C–H Bond Activation in a Carbon-Substituted Hemiporphyrazine**

*Ruoqiu Wu, Anıl Çetin, William S. Durfee,* and Christopher J. Ziegler**

Unlike many C–H bond activations,[1] nucleophilic substitution reactions on aromatic rings with hydride as the leaving group can be difficult to achieve. Nucleophilic substitution of arenes by halide loss has been known for many decades. However, C–H aromatic substitutions have been known only since the late 1970s and proceed only under certain reaction conditions.[2] Electron-withdrawing substituents are required on the aromatic ring, and frequently only strong nucleophiles such as $NH_2^-$ can readily attack. Alternative methods can be used to assist replacement of an aromatic hydride. Vicarious nucleophilic aromatic substitution can be used in the activation of arene C–H bonds, which is promoted by loss of HX.[3] In addition, oxidants can also be employed to effect loss of hydride in a process known as oxidative nucleophilic substitution of hydrogen (ONSH).[4] Herein, we present an unusual nucleophilic aromatic substitution with the relatively weak nucleophile pyridine in the dicarbahemiporphyrazine macrocycle, which may occur through an ONSH mechanism. Upon metalation with copper, nucleophilic attack of the internal carbon atom with pyridine is promoted by the reduction of the metal from $Cu^{II}$ to $Cu^{I}$. This reaction proceeds under very mild conditions in air and represents a potential new means to activate C–H bonds with transition metals.

The metalation of porphyrin analogues and isomers with interior carbon positions has become an area of significant activity.[5] The chemistry of the N-confused porphyrins,[6] benziporphyrins,[7] and azuliporphyrins[8] all involve macrocycles in which an aromatic C–H bond is in close proximity to the metal binding site. The interior C–H bond can remain intact upon metal binding, as observed in the Mn,[9] Fe,[10] and Zn[11] complexes of N-confused porphyrins.[6] The exact nature of this C–H metal "agostic" interaction is still under investigation, but the proximity of a metal center to this carbon atom activates it toward nucleophilic and electrophilic attack. Indirect evidence of such metal-mediated chemistry has been seen in the copper-mediated oxidative degradation of an N-confused porphyrin[12] and silver-catalyzed C–N bond formation in *m*-benziporphyrin.[13]

In the early 1950s, Elvidge and Linstead reported the synthesis of the hemiporphyrazine macrocycle (Scheme 1).[14]

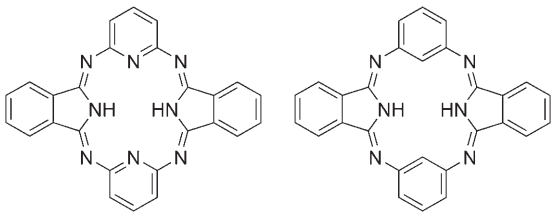


***Scheme 1.*** The structures of hemiporphyrazine (left) and the N-deficient analogue dicarbaporphyrazine (right).

The hemiporphyrazines bear a superficial resemblance to phthalocyanine, but the phthalocyanines are aromatic systems of 18 π electrons while the hemiporphyrazines are systems of 20 π electrons.[15] Linstead et al. later prepared a series of porphyrazine derivatives in which one or two of the central metal-binding nitrogen atoms were replaced with CH groups. In one case, 2,6-diaminopyridine was replaced by 1,3-diaminobenzene, and the macrocycle **1** is thus doubly N-deficient.[16] This molecule can be considered as a dicarbahemiporphyrazine (dchp).

Although there are only two nitrogen atoms within the core of the ring, macrocycle **1** does bind metal ions (Scheme 2,

[*] R. Wu, Dr. W. S. Durfee
Department of Chemistry
Buffalo State College
1300 Elmwood Ave., Buffalo, NY 14222 (USA)
Fax: (+1) 716-878-4028
E-mail: durfeews@buffalostate.edu
A. Çetin, Dr. C. J. Ziegler
Department of Chemistry
University of Akron
190 E. Buchtel Commons, Akron, OH 44325 (USA)
Fax: (+1) 330-972-7370
E-mail: ziegler@uakron.edu

[**] This work was supported by the donors of the Petroleum Research Fund, administered by the American Chemical Society (W.S.D.). We acknowledge NSF grant CHE-0116041, which was used to purchase the Bruker–Nonius diffractometer, and the Kresge Foundation and donors to the Kresge Challenge Program at The University of Akron for funds used to purchase the NMR instruments used in this work.


WILEY InterScience DISCOVER SOMETHING GREAT
© 2006 Wiley-VCH Verlag GmbH & Co. KGaA, Weinheim

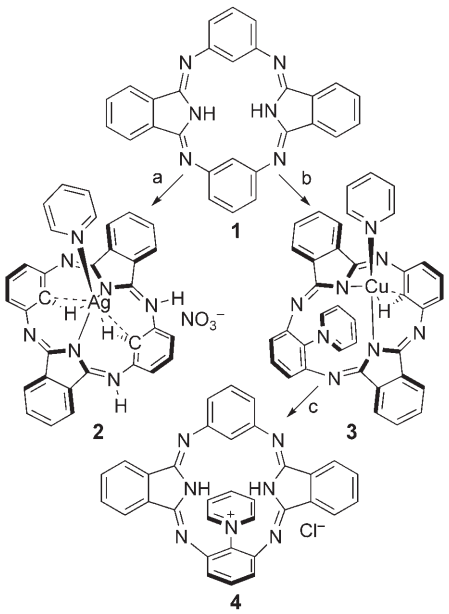


***Scheme 2.*** Synthesis of compounds **2**, **3**, and **4**, starting from **1**. Reagents: a) $AgNO_3$, pyridine, MeOH, air; b) $Cu^{I}$ or $Cu^{II}$ salt, pyridine, MeOH, air; c) $CH_2Cl_2$, air.

Figure 1).[17] The reaction of **1** with $AgNO_3$ afforded [Ag(dchp)py]$NO_3$ (**2**; py = pyridine), a pseudo-three-coordinate $Ag^{I}$ species. The presence of an $NO_3^-$ counterion in the unit

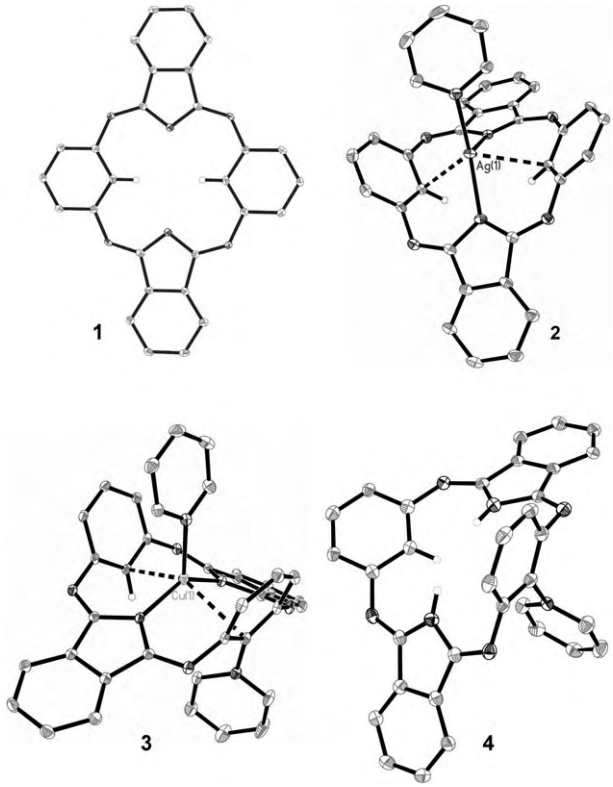


***Figure 1.*** Thermal-ellipsoid diagrams (35% probability level) of all reactants and products from Scheme 2 (C light gray, N dark gray). Hydrogen atoms have been omitted for clarity, with the exception of the internal CH groups and NH groups.

cell of **2** indicates that the ligand binds to the $Ag^{I}$ cation in a neutral tautomeric form.[17] We believe that two of the external nitrogen atoms are protonated in this complex to achieve charge balance. This situation is in contrast to that of **3** (see below), in which the positive charges of the pyridinium moiety and the $Cu^{I}$ ion are balanced by the negative charges of the two deprotonated core nitrogen atoms. The metal–macrocycle Ag–N bond lengths in **2** are relatively large (ca. 2.36 Å), in part owing to the steric interaction of the benzene rings. The Ag–C distances are 2.62 and 2.71 Å, which are too large for a strong silver–arene interaction,[18] but the carbon atoms are within close proximity of the metal ion. The metal center is located out of the plane of the macrocycle (from the plane of the four *meso* nitrogen atoms) by 1.35 Å, which represents a larger distance than seen in the metallo-N-confused porphyrins.[6] Compound **2** is diamagnetic, and the $^{109}Ag$ NMR spectroscopic signal of this compound is observed at $\delta = 377$ ppm.

The reactions of **1** with a variety of Cu salts such as $Cu(CH_3COO)_2{\cdot}2H_2O$ and $[Cu(CH_3CN)_4]BF_4$ in the presence of air and pyridine did not produce stable $Cu^{II}$ compounds. Instead, the macrocycle reacted with pyridine after metalation to form the species [Cu(dchp-py)(py)] (**3**).[17] Species **3** is a $Cu^{I}$ compound in which a pyridine molecule has formed a C–N bond at one of the two internal CH positions. We isolated two crystal forms of this complex from different solvents. As in the Ag compound, the $Cu^{I}$ center is pseudo-three-coordinate and bound to both of the internal nitrogen atoms from the ring and one axial pyridine ligand, with Cu–N bond lengths ranging between 2.03 and 2.08 Å.

Both the remaining interior C–H bond and the new C–N bond are in close proximity to the metal center in this new complex, with average Cu–C(H) and Cu–C(N) bond lengths of about 2.41 Å and 2.74 Å, respectively. As in species **2**, the metal center in **3** is located out of the plane of the macrocycle by 0.77 Å, which is just over half of the corresponding distance observed in compound **2**. The $^1H$ NMR chemical shift of the proton in the interior C–H bond changes slightly from that of the unmetalated ligand **1**, moving from $\delta = 6.77$ to 7.31 ppm. We believe that this reaction proceeds through $Cu^{II}$-assisted elimination of hydride, and the hydride reduces the metal center to $Cu^{I}$, which is more stable in the low-coordinate environment of the ligand.[19] An alternate mechanism to ONSH might involve the initial formation of a highly oxidized $Cu^{III}$ center with a metal–carbon bond (by activation of one of the internal CH groups). Chelation of pyridine and reductive elimination would then produce the pyridine adduct **3**.

Recrystallization of **3** in dichloromethane in air resulted in the loss of pyridine and demetalation to yield the free ligand. The free-base species $H_2$dchp-py (**4**) retains the pendant pyridine moiety at the interior carbon position.[17] The C–N bond length in this species is 1.46 Å, which is identical to that seen in both crystal forms of the copper complex. We believe that dioxygen reacts with **3** and the solvent (dichloromethane) to produce $CuCl_2$ and the protonated free base **4**.

In conclusion, metalation of the dicarbahemiporphyrazine **1** with the redox-active metal copper activates an interior C–H bond toward nucleophilic substitution. This reaction

 © 2006 Wiley-VCH Verlag GmbH & Co. KGaA, Weinheim 

proceeds through an ONSH mechanism in which the $Cu^{II}$ center accepts a hydride and is reduced to $Cu^{I}$. We are continuing our investigations into the metal complexes of both singly and doubly N-deficient hemiporphyrazines.

## Experimental Section

Dicarbahemiporphyrazine (dchp, **1**) was synthesized as described in the literature.[14,16] Crystals of the planar dicationic form of **1** were grown from a mixture of formic acid and diethyl ether (1:1).

**2**: $AgNO_3$ (102 mg, 0.6 mmol) was added to a solution of **1** (132 mg, 0.3 mmol) in pyridine (10 mL), and the mixture was stirred for 30 minutes at room temperature. The resulting solution was filtered, and the filtrate was layered with diethyl ether. Orange-red crystals of **2** were collected after four days. Yield: 0.082 g (40%). $^1$H NMR (300 MHz, [D$_5$]pyridine): $\delta = 8.32$ (q, $J = 3.0$ Hz, 4H), 8.11 (d, $J = 7.2$ Hz, 1H), 7.98 (t, $J = 3.6$ Hz, 1H), 7.91 (m, 2H) 7.36 (s, 5H), 7.12 (dd, $J = 2.4$, 5.1 Hz, 0.5H), 6.91 (s, 0.5H), 6.80 (d, $J = 6.6$ Hz, 0.5H), 6.70 (d, $J = 7.5$ Hz, 0.5H), 6.62 (m, 0.5H), 6.45 ppm (dd, $J =$ 2.1, 7.8 Hz, 0.5H); $^{109}$Ag NMR (14.0 MHz, [D$_5$]pyridine): $\delta =$ 377.1 ppm; high-res. ESI-MS (positive ion): $m/z$: 547.0 $[Ag(dchp)]^+$. The material loses the axially coordinated solvent rapidly, with only 0.5 equivalents of pyridine remaining after standing. Elemental analysis (%) calcd for $C_{30.5}H_{24.5}N_{7.5}O_5Ag$: C 53.58, H 3.58, N 15.36; found: C 53.60, H 3.07, N 15.37.

**3**: Compound **3** was synthesized by three different routes. All reactions were carried out aerobically. Route 1: Compound **1** (439 mg, 1 mmol) was dissolved in hot *n*-butanol (30 mL), and a solution of $Cu(CH_3CO_2)_2{\cdot}2H_2O$ (399 mg, 2 mmol) in methanol (5 mL) was added. The resulting mixture was heated at reflux for 12 h. The resulting brown precipitate was collected by filtration and washed with methanol and diethyl ether. The product was then dissolved in pyridine (10 mL), and diethyl ether was allowed to diffuse into the solution. Deep red crystals of **3** were collected after several days and were suitable for X-ray diffraction (crystal **3a**). Route 2: Compound **1** (132 mg, 0.3 mmol) was dissolved in pyridine (10 mL), and $Cu(CH_3CO_2)_2{\cdot}2H_2O$ (120 mg, 0.6 mmol) was added to the solution with stirring. The mixture turned to deep red almost immediately and was heated at reflux for 24 h. After the mixture had been filtered, the resulting solution was layered with diethyl ether. Deep red single crystals were collected after several days. Single crystals for X-ray diffraction were grown from toluene/methanol (1:1, crystal **3b**). Route 3: Compound **1** (132 mg, 0.3 mmol) and $[Cu(CH_3CN)_4]BF_4$ (124 mg, 0.4 mmol) were mixed in pyridine (10 mL). The mixture was stirred at room temperature for 30 minutes. Diethyl ether was allowed to diffuse into the resulting solution, and the crystals that formed after several days were identical to those from Route 1. Yield (from Route 1): 0.312 g, 48%. $^1$H NMR (300 MHz, [D$_6$]DMSO): $\delta = 8.34$ (s, 4H), 8.18 (t, $J = 7.8$ Hz, 1H), 7.92 (d, $J =$ 7.3 Hz, 2H), 7.74 (t, $J = 7.4$ Hz, 2H), 7.64 (m, 4H), 7.46 (m, 4H), 7.31 (s, 1H), 7.21 (m, 4H), 6.98 (t, $J = 7.8$ Hz, 1H), 6.87 (t, $J = 7.8$ hz, 1H), 6.57 (d, $J = 7.8$ Hz) 2H), 6.42 ppm (d, $J = 7.8$ Hz, 2H); $^{13}$C NMR (75.4 MHz, [D$_6$]DMSO): $\delta = 170.2$, 164.8, 150.1, 149.9, 147.8, 147.4, 144.8, 140.1, 138.3, 136.1, 133.7, 130.6, 130.2, 126.3, 123.7, 121.5, 120.7, 118.4, 117.2 ppm; high-res. ESI-MS (positive ion): $m/z$: 516.2 $[H_2dchp\text{-}py]^+$. Elemental analysis (%) calcd for $C_{83}H_{67}N_{16}O_5Cu_2$: C 66.65, H 4.51, N 14.98; found: C 66.20, H 4.31, N 15.96.

**4**: Compound **1** (132 mg, 0.3 mmol) and $Cu(CH_3CO_2)_2{\cdot}2H_2O$ (120 mg, 0.6 mmol) were mixed in pyridine (10 mL). The solution turned to deep red immediately and was heated at reflux for 24 h. The resulting solution was slowly layered with $CH_2Cl_2$. The resultant solution turned from red to blue upon oxidation with air. Yellow-orange crystals of **4** were collected after several days. Yield: 0.016 g (10%). $^1$H NMR (300 MHz, [D$_6$]DMSO): $\delta = 11.17$ (s, 2H), 10.09 (s, 0.5H), 9.62 (d, $J = 6.0$ Hz, 1H), 9.19 (d, $J = 6.0$ Hz, 1H), 8.93 (s, 1H), 8.50 (m, 2H), 8.36 (d, $J = 7.3$ Hz, 2H), 8.14 (t, $J = 6.0$ Hz, 1H), 8.05 (t, $J = 6.0$ Hz, 1H), 7.62 (m, 8H), 7.44 (m, 2H), 7.34 (d, $J = 8.1$ Hz, 2H), 7.07 (d, $J = 6.9$ Hz, 1H), 6.87 (m, 1H), 6.78 ppm (d, $J = 7.9$ Hz, 2H); $^{13}$C NMR (75.4 MHz, [D$_6$]DMSO): $\delta = 169.5$, 166.8, 148.7, 147.9, 138.8, 137.0, 136.5, 132.9, 131.6, 131.3, 129.2, 128.6, 125.4, 122.1, 122.0, 118.8, 117.2, 116.9 ppm; high-res. ESI-MS (positive ion): $m/z$: 516.2 $[Hdchp\text{-}py]^+$. Elemental analysis (%) calcd for $C_{33}H_{32}N_7OCl_3$: C 61.64, H 4.08, N 15.25; found: C 61.44, H 4.10, N 14.48.

Received: May 5, 2006
Published online: July 20, 2006

**Keywords:** agostic interactions · arene activation · metalation · porphyrinoids · structure elucidation

[1] B. A. Arndtsen, R. G. Bergman, T. A. Mobley, T. H. Peterson, *Acc. Chem. Res.* **1995**, *28*, 154; C. G. Jia, T. Kitamura, Y. Fujiwara, *Acc. Chem. Res.* **2001**, *34*, 633; W. D. Jones, *Acc. Chem. Res.* **2003**, *36*, 140.
[2] M. Mąkosza, J. Winiarski, *Acc. Chem. Res.* **1987**, *20*, 282.
[3] M. Mąkosza, A. Kwast, *Eur. J. Org. Chem.* **2004**, *10*, 2125; S. Florio, P. Lorusso, R. Luisi, C. Granito, L. Ronzini, L. Troisi, *Eur. J. Org. Chem.* **2004**, *10*, 2118; M. D. Drew, D. A. Jackson, N. J. Lawrence, J. Liddle, R. G. Pritchard, *Chem. Commun.* **1997**, 189.
[4] M. Mąkosza, K. Wojciechowski, *Chem. Rev.* **2004**, *104*, 2631.
[5] *The Porphyrin Handbook, Vol. II* (Eds.: K. M. Kadish, K. M. Smith, R. Guilard), Academic Press, New York, **2000**.
[6] J. D. Harvey, C. J. Ziegler, *Coord. Chem. Rev.* **2003**, *247*, 1; P. J. Chimielewski, L. Latos-Grażyński, *Coord. Chem. Rev.* **2005**, *249*, 2510.
[7] M. Stępień, L. Latos-Grażyński, *Acc. Chem. Res.* **2005**, *38*, 88.
[8] T. D. Lash, *Synlett* **2000**, *3*, 279; T. D. Lash, D. A. Colby, G. M. E. Ferrence, *J. Org. Chem.* **2003**, *68*, 4533.
[9] J. D. Harvey, C. J. Ziegler, *Chem. Commun.* **2003**, *23*, 2890.
[10] W.-C. Chen, C.-H. Hung, *Inorg. Chem.* **2001**, *40*, 5070.
[11] H. Furuta, T. Ishizuka, A. Osuka, *J. Am. Chem. Soc.* **2002**, *124*, 5622.
[12] H. Furuta, H. Maeda, A. Osuka, *Org. Lett.* **2002**, *4*, 181.
[13] M. Stepien, L. Latos-Grażyński, *J. Am. Chem. Soc.* **2002**, *124*, 3838.
[14] J. A. Elvidge, J. P. Linstead, *J. Chem. Soc.* **1952**, 5008.
[15] F. Fernández-Lázaro, T. Torres, B. Hauschel, M. Hanack, *Chem. Rev.* **1998**, *98*, 563.
[16] P. F. Clark, J. A. Elvidge, R. P. Linstead, *J. Chem. Soc.* **1954**, 2490; J. A. Elvidge, J. H. Golden, *J. Chem. Soc.* **1957**, 700; R. P. Smirnov, *Izv. Vyssh. Uchebn. Zaved. Khim. Khim. Tekhnol.* **1967**, *10*, 1169.
[17] Crystal data for **1**: triclinic, space group $P\bar{1}$, $a = 5.0864(12)$, $b =$ 11.867(3), $c = 12.441(3)$ Å, $\alpha = 71.651(4)$, $\beta = 89.775(4)$, $\gamma =$ 78.614(4)°, $V = 697.4(3)$ Å$^3$, $Z = 1$, $\rho = 1.482$ g cm$^{-3}$, $R_1 = 0.0665$, $wR_2 = 0.1298$ (for 3200 reflections, $I_o > 2\sigma(I_o)$). Crystal data for **2**: triclinic, space group $P\bar{1}$, $a = 8.7694(13)$, $b = 13.3129(19)$, $c =$ 14.937(2) Å, $\alpha = 73.503(2)$, $\beta = 81.501(2)$, $\gamma = 73.782(2)$°, $V =$ 1601.1(4) Å$^3$, $Z = 2$, $\rho = 1.463$ g cm$^{-3}$, $R_1 = 0.0472$, $wR_2 = 0.1029$ (for 7400 reflections, $I_o > 2\sigma(I_o)$). Crystal data for **3a**: monoclinic, space group $P2_1/c$, $a = 14.2673(11)$, $b = 13.1552(10)$, $c =$ 24.0192(13) Å, $\beta = 126.441(3)$, $V = 3626.7(4)$ Å$^3$, $Z = 4$, $\rho =$ 1.349 g cm$^{-3}$, $R_1 = 0.0438$, $wR_2 = 0.1013$ (for 8715 reflections, $I_o > 2\sigma(I_o)$). Crystal data for **3b**: monoclinic, space group $P2_1/n$ $a = 10.2762(11)$, $b = 43.463(5)$, $c = 16.4235(17)$ Å, $\beta =$ 101.059(2)°, $V = 7199.1(13)$ Å$^3$, $Z = 4$, $\rho = 1.394$ g cm$^{-3}$, $R_1 =$ 0.0568, $wR_2 = 0.1208$ (for 17298 reflections, $I_o > 2\sigma(I_o)$). Crystal data for **4**: $P\bar{1}$, $a = 8.5234(11)$, $b = 13.7264(17)$, $c =$ 14.0816(18) Å, $\alpha = 91.287(2)$, $\beta = 97.805(2)$, $\gamma = 96.667(2)$°, $V =$ 1620.0(4) Å$^3$, $Z = 2$, $\rho = 1.413$ g cm$^{-3}$, $R_1 = 0.0814$, $wR_2 = 0.2100$ (for 6313 reflections, $I_o > 2\sigma(I_o)$). Data were collected at 100 K (Bruker-AXS SMART CCD diffractometer with $Mo_{K\alpha}$ radia-

 © 2006 Wiley-VCH Verlag GmbH & Co. KGaA, Weinheim 

tion, $\lambda = 0.71073$ Å) and corrected for absorption (empirical SADABS). The structures were solved by direct methods and refined by full-matrix least-squares procedures (SHELX97). CCDC-603061–603065 contains the supplementary crystallographic data for this paper. These data can be obtained free of charge from The Cambridge Crystallographic Data Centre via www.ccdc.cam.ac.uk/data_request/cif.

[18] K. Shelly, D. C. Finster, Y. J. Lee, W. R. Scheidt, C. A. Reed, *J. Am. Chem. Soc.* **1985**, *107*, 5955; I. F. , Jr., Taylor, E. A. Hall, E. L. Amma, *J. Am. Chem. Soc.* **1969**, *91*, 5745.

[19] K. M. Kadish, C. Araullo, G. B. Maiya, D. Sazou, J.-M. Barbe, R. Guilard, *Inorg. Chem.* **1989**, *28*, 2528.

 © 2006 Wiley-VCH Verlag GmbH & Co. KGaA, Weinheim 

Asymmetric Catalysis

DOI: 10.1002/anie.200601747

# Rhodium-Catalyzed Enantioselective Conjugate Silyl Transfer: 1,4-Addition of Silyl Boronic Esters to Cyclic Enones and Lactones**

*Christian Walter, Gertrud Auer, and Martin Oestreich**

Silicon connected to a stereogenic carbon atom is an important functional group in asymmetric synthesis. The synthetic equivalence of silicon and oxygen, which is achieved by the stereospecific oxidative degradation of a C–Si bond,[1] as well as several stereoselective C–C bond-forming reactions involving α-chiral silanes[2] underscore the synthetic potential of silicon. Conversely, the number of effective methods for the direct enantioselective formation of C–Si bonds is limited[3] and, therefore, novel asymmetric transition-metal-catalyzed reactions will certainly plug a "synthetic hole".

The 1,4-addition of stoichiometric amounts of silicon-based cuprate reagents to prochiral α,β-unsaturated carbonyl compounds is one of the standard C–Si bond-forming reactions.[4] Although copper-catalyzed variants are available today,[5,6] their extension to chirally modified catalysts has so far failed.[7] Copper-catalyzed conjugate silyl transfer of disilanes has also been reported, but again only for a racemic series.[8] To date, the palladium-catalyzed enantioselective 1,4-disilylation[9] of acyclic enones using disilanes has remained the sole example (**B**→**A**, Scheme 1).[10] The importance of β-silyl carbonyl compound **A** (either as a masked aldol itself or as a functionalized precursor for the preparation of α-chiral silanes)[2b] has resulted in the development of alternative catalyst-controlled routes towards **A**. These approaches, however, rely on the more established rhodium-catalyzed enantioselective formation of C–C bonds[11] (**C**→**A**, Scheme 1) and copper-catalyzed enantioselective formation of C–H bonds[12] (**D**→**A**, Scheme 1).[13]

Inspired by the rhodium-catalyzed 1,4-addition of aryl boronic acids,[14] and aware of the diverse transition-metal-catalyzed chemistry of Si–B compounds,[15] we envisioned a rhodium-catalyzed (asymmetric) conjugate silyl transfer through the use of silyl boronic esters as the silyl anion source.[16] Herein we report an unprecedented conjugate C–Si bond-forming reaction, which, for the first time, enables the catalytic asymmetric 1,4-addition of nucleophilic silicon to cyclic α,β-unsaturated carbonyl compounds with excellent levels of stereoinduction.

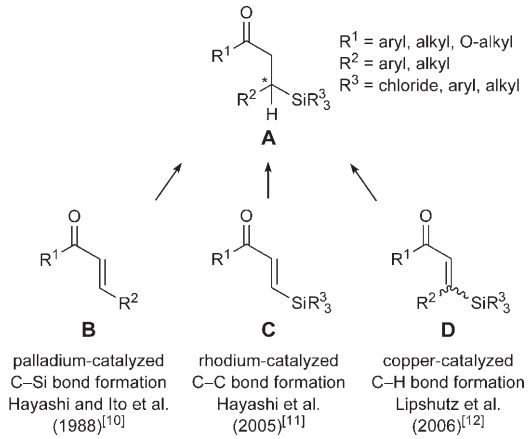


***Scheme 1.*** Strategies for the transition-metal-catalyzed enantioselective construction of α-chiral β-silylated carbonyl compounds.

Our search for catalysts that would facilitate silyl transfer from pinacol-derived silyl boronic ester **11**[17] to 2-cyclohexenone (**2**) commenced with a systematic screening of rhodium (pre)catalysts (Scheme 2 and Table 1). For this, typical reaction conditions for the rhodium-catalyzed 1,4-addition of aryl boronic acids served as a reasonable reference point (1,4-dioxane/$H_2O$ solvent mixtures at elevated reaction temperatures).[14] Two crucial observations emerged from these initial investigations: Both the presence of a base and the absence of strongly coordinating counterions were critical for product formation. Replacement of chloride by weakly or noncoordinating perchlorate led to the achiral cationic catalyst [(dppp)Rh(cod)]$ClO_4$.[18]

We were pleased to find that a combination of this catalyst (5.0 mol%) and an equimolar amount of the free bidentate ligand dppp (5.0 mol%) in the presence of triethylamine as the base (1.0 equiv) promoted the desired 1,4-addition—KOH (1.0 equiv) performed equally well[19] (Scheme 2 and Table 1). The rhodium-catalyzed silyl transfer from **11** (2.5 equiv) to cyclic enones **1–3** in aqueous 1,4-dioxane at 50 °C afforded racemic products **6–8** in good yields (Table 1, entries 1–3). Acyclic enone **4** was less reactive under identical reaction conditions and required double the amount of catalyst and ligand, which then gave *rac*-**9** in good yield

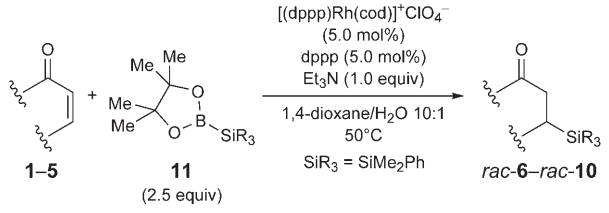


***Scheme 2.*** Rhodium-catalyzed conjugate silyl transfer (see Table 1). dppp = 1,3-bis(diphenylphosphanyl)propane, cod = 1,5-cyclooctadiene.

[*] Dipl.-Chem. C. Walter,[+] Dr. G. Auer, Prof. Dr. M. Oestreich[+]
Institut für Organische Chemie und Biochemie
Albert-Ludwigs-Universität Freiburg
Albertstrasse 21, 79104 Freiburg im Breisgau (Germany)
Fax: (+49) 761-203-6100
E-mail: martin.oestreich@orgmail.chemie.uni-freiburg.de

[+] New address:
Organisch-Chemisches Institut
Westfälische Wilhelms-Universität Münster
Corrensstrasse 40, 48149 Münster (Germany)
Fax: (+49) 251-83-36501
E-mail: martin.oestreich@uni-muenster.de

[**] Financial support for this work was provided by the Deutsche Forschungsgemeinschaft (Emmy Noether-Programm, 2001-2006), the Fonds der Chemischen Industrie, and the Aventis Foundation (Karl-Winnacker-Stipendium, 2006-2008). We thank Gerd Fehrenbach for performing the HPLC analyses.

 © 2006 Wiley-VCH Verlag GmbH & Co. KGaA, Weinheim 

***Table 1:*** Rhodium-catalyzed conjugate silyl transfer (see Scheme 2).

| Entry | Substrate | Product | Yield [%][a] |
|---|---|---|---|
| 1 | **1** | 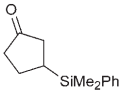 *rac*-**6** | 82 |
| 2 | **2** | 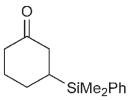 *rac*-**7** | 76 |
| 3 | **3** | 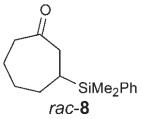 *rac*-**8** | 81 |
| 4[b] | 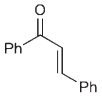 **4** | 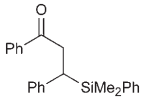 *rac*-**9** | 77 |
| 5 | 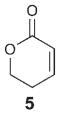 **5** | 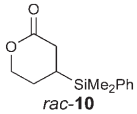 *rac*-**10** | 76 |

[a] Yield of analytically pure product isolated by flash chromatography on silica gel. [b] $[(dppp)Rh(cod)]^{+}ClO_4^{-}$ (10 mol%) and dppp (10 mol%).

(Table 1, entry 4). Besides cyclic α,β-unsaturated ketones **1**–**3**, lactone **5** displayed similar reactivity and provided *rac*-**10** cleanly (Table 1, entry 5).

We then addressed the elusive enantioselective 1,4-addition of nucleophilic silicon to cyclic substrates by using the chiral catalyst $[((S)\text{-binap})Rh(cod)]ClO_4$[18] (5.0 mol%) with additives (*S*)-binap (5.0 mol%) and triethylamine (1 equiv)[19] (Scheme 3 and Table 2). To our delight, conjugate silylation of cyclic enones **1**–**3** proceeded with remarkably high enantioselectivities (Table 2, entries 1–3). Unfortunately, the yields of the isolated products (*S*)-**6**–(*S*)-**8** decreased with increasing ring size.[20] Thus, α,β-unsaturated lactone **5** underwent the silyl transfer with excellent enantioselectivity and in reasonable yield (Table 2, entry 4) whereas acyclic enone **4** was completely inert under these reaction conditions. The absolute configuration of (*S*)-**6**[21] and (*S*)-**7**[22] was assigned unambiguously by comparison with reported data, while those of (*S*)-**8** and (*S*)-**10** were assigned on the basis of similar HPLC characteristics on a chiral stationary phase and the sign of the optical rotation.[22]

We generally used catalyst and ligand loadings of 5.0 mol% in these reactions. We reduced the amount of $[((S)\text{-binap})Rh(cod)]ClO_4$ and (*S*)-binap to 1.0 mol% for the

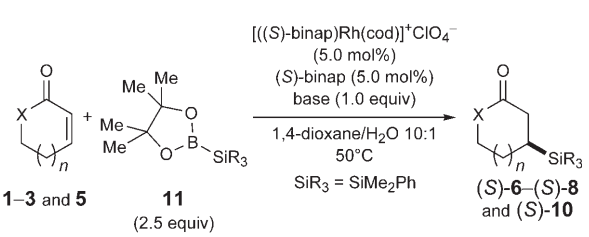


***Scheme 3.*** Catalytic asymmetric conjugate silyl transfer (see Tables 2 and 3). binap = 2,2′-bis(diphenylphosphanyl)-1,1′-binaphthyl.

***Table 2:*** Catalytic asymmetric conjugate silyl transfer (see Scheme 3).

| Entry | Substrate | *n* | X | Base | Product | Yield [%][a] | *ee* [%][b] | $[\alpha]_D$[c] |
|---|---|---|---|---|---|---|---|---|
| 1 | **1** | 0 | $CH_2$ | $Et_3N$ | (*S*)-**6** | 70 | 97 | −131 |
| 2 | **2** | 1 | $CH_2$ | $Et_3N$ | (*S*)-**7** | 45 | 96 | −85.8 |
| 3 | **3** | 2 | $CH_2$ | $Et_3N$ | (*S*)-**8** | 22 | 92 | −66.9 |
| 4 | **5** | 1 | O | $Et_3N$ | (*S*)-**10** | 58 | 96 | −38.1 |

[a] Yield of analytically pure product isolated by flash chromatography on silica gel. [b] HPLC analysis on Daicel columns provided baseline separation of the enantiomers: Chiralpak AD-H column (*n*-heptane/*i*PrOH 300:1 at 20°C) for **6**: $t_r$ = 21.8 min for (*S*)-**6** and 23.7 min for (*R*)-**6**; Chiralpak AD-H column (*n*-heptane/*i*PrOH 100:1 at 20°C) for **7**: $t_r$ = 9.48 min for (*S*)-**7** and 10.7 min for (*R*)-**7**; Chiralcel OD-H column (*n*-heptane/*i*PrOH 100:1 at 20°C) for **8**: $t_r$ = 13.5 min for (*S*)-**8** and 14.9 min for (*R*)-**8**; Chiralpak AD-H column (*n*-heptane/*i*PrOH 100:1 at 20°C) for **10**: $t_r$ = 19.5 min for (*S*)-**10** and 20.5 min for (*R*)-**10**. [c] *c* = 2.21 for (*S*)-**6**, 2.86 for (*S*)-**7**, 1.07 for (*S*)-**8**, and 1.77 for (*S*)-**10** in $CHCl_3$ at 20°C.

thus far best reaction **1**→(*S*)-**6** (70%, 97% *ee*), which resulted in a substantial decrease in the yield and, importantly, the enantioselectivity (47%, 85% *ee*). An excess of the free ligand, (*S*)-binap, was indispensable to ensure high enantioselectivities. The catalyst alone induced distinctly diminished enantioselection (55%, 74% *ee*).

The influence of the base on the yield and stereoinduction of related rhodium-catalyzed processes is known.[14,19] A brief survey of different organic and inorganic bases confirmed these findings for **1**→(*S*)-**6** (Table 3). Sterically hindered

***Table 3:*** Influence of the base on enantioselectivity (see Scheme 3).

| Entry | Substrate | *n* | Base | Product | Yield [%] | *ee* [%] |
|---|---|---|---|---|---|---|
| 1 | **1** | 0 | TMP | (*S*)-**6** | 75 | 96 |
| 2 | **1** | 0 | morpholine | (*S*)-**6** | 0 | – |
| 3 | **1** | 0 | $K_3PO_4$ | (*S*)-**6** | 71 | 98 |
| 4 | **1** | 0 | KOH | (*S*)-**6** | 68 | 59 |
| 5 | **2** | 1 | KOH | (*S*)-**7** | 45 | 78 |

2,2,6,6-tetramethylpiperidine (TMP) was comparable with triethylamine (Table 3, entry 1). In contrast, (*S*)-**6** was not produced when morpholine was used as the base (Table 3, entry 2). Inorganic bases such as $K_3PO_4$ and KOH also gave different results: stereoinduction as high as 98% *ee* was obtained with the former (Table 3, entry 3), whereas a pronounced negative effect was seen with the latter for **1** as well as **2** (Table 3, entries 4 and 5).

In summary, we have presented a novel transition-metal-catalyzed C–Si bond-forming reaction. In the presence of cationic rhodium complexes, the Si–B fragment functions as an equivalent of nucleophilic silicon, which is efficiently transferred onto acyclic as well as cyclic α,β-unsaturated carbonyl compounds. Chiral $[((S)\text{-binap})Rh(cod)]ClO_4$ has effected an unprecedented asymmetric 1,4-addition to cyclic acceptors in high enantiomeric excesses. This transformation might also pave the way for synthetically useful tandem processes. Extension of this line of research including mechanistic investigations[23] is our current focus.

## *Experimental Section*

General procedure: A Schlenk tube equipped with a magnetic stir bar in an argon atmosphere was charged with the rhodium catalyst

 © 2006 Wiley-VCH Verlag GmbH & Co. KGaA, Weinheim 

(5.0 mol%) and the ligand (5.0 mol%). The compounds were then dissolved in deoxygenated 1,4-dioxane/$H_2O$ 10:1 (ca. 0.5 M based on substrate). The α,β-unsaturated acceptor (1.0 equiv), the silyl boronic ester (2.5 equiv), and the base (1.0 equiv) were then added and the reaction mixture maintained at 50 °C for 16 h. After cooling the mixture to room temperature, silica gel was added and the solvents were evaporated under reduced pressure. The residue was subjected to flash column chromatography on silica gel using cyclohexane/ethyl acetate solvent mixtures as the eluent.

Received: May 3, 2006
Published online: July 21, 2006

**Keywords:** asymmetric catalysis · boron · homogeneous catalysis · rhodium · silicon

[1] G. R. Jones, Y. Landais, *Tetrahedron* **1996**, *52*, 7599 – 7662.
[2] a) Surprisingly, general reviews on the preparation and chemistry of α-chiral silanes are not reported in the literature; b) I. Fleming in *Science of Synthesis*, *Vol. 4* (Ed.: I. Fleming), Thieme, Stuttgart, **2002**, pp. 927 – 946.
[3] T. Hayashi in *Comprehensive Asymmetric Catalysis*, *Vol. 1* (Eds.: E. N. Jacobsen, A. Pfaltz, H. Yamamoto), Springer, Heidelberg, **1999**, pp. 319 – 333.
[4] a) R. K. Dieter in *Modern Organocopper Chemistry* (Ed.: N. Krause), Wiley-VCH, Weinheim, **2002**, pp. 79 – 144; b) I. Fleming in *Organocopper Reagents. A Practical Approach* (Ed.: R. J. K. Taylor), Oxford Academic Press, New York, **1994**, pp. 257 – 292.
[5] B. H. Lipshutz, J. A. Sclafani, T. Takanami, *J. Am. Chem. Soc.* **1998**, *120*, 4021 – 4022.
[6] M. Oestreich, B. Weiner, *Synlett* **2004**, 2139 – 2142.
[7] G. Auer, B. Weiner, M. Oestreich, *Synthesis* **2006**, 2113 – 2116.
[8] a) H. Ito, T. Ishizuka, J.-i. Tateiwa, M. Sonoda, A. Hosomi, *J. Am. Chem. Soc.* **1998**, *120*, 11196 – 11197; b) C. T. Clark, J. F. Lake, K. A. Scheidt, *J. Am. Chem. Soc.* **2004**, *126*, 84 – 85.
[9] a) T. Hayashi, Y. Matsumoto, Y. Ito, *Tetrahedron Lett.* **1988**, *29*, 4147 – 4150; b) S. Ogoshi, S. Tomiyasu, M. Morita, H. Kurosawa, *J. Am. Chem. Soc.* **2002**, *124*, 11598 – 11599.
[10] a) T. Hayashi, Y. Matsumoto, Y. Ito, *J. Am. Chem. Soc.* **1988**, *110*, 5579 – 5581; b) Y. Matsumoto, T. Hayashi, Y. Ito, *Tetrahedron* **1994**, *50*, 335 – 346.
[11] T. Hayashi, R. Shintani, K. Okamoto, *Org. Lett.* **2005**, *7*, 4757 – 4759.
[12] B. H. Lipshutz, N. Tanaka, B. R. Taft, C.-T. Lee, *Org. Lett.* **2006**, *8*, 1963 – 1966.
[13] Shortly after submission of this manuscript, a paper appeared reporting a chiral Lewis acid catalyzed conjugate addition of carbon nucleophiles to α,β-unsaturated β-silyl imide substrates: E. P. Balskus, E. N. Jacobsen, *J. Am. Chem. Soc.* **2006**, *128*, 6810 – 6812.
[14] K. Yoshida, T. Hayashi in *Modern Rhodium-Catalyzed Organic Reactions* (Ed.: P. A. Evans), Wiley-VCH, Weinheim, **2005**, pp. 55 – 77.
[15] a) M. Suginome, Y. Ito, *Chem. Rev.* **2000**, *100*, 3221 – 3256; b) I. Beletskaya, C. Moberg, *Chem. Rev.* **2006**, *106*, 2320 – 2354.
[16] Significant progress has been made in enantioselective Si–B chemistry: a) for reagent- and catalyst-controlled palladium-catalyzed addition to allenes, see: M. Suginome, T. Ohmura, Y. Miyake, S. Mitani, Y. Ito, M. Murakami, *J. Am. Chem. Soc.* **2003**, *125*, 11174 – 11175; b) for catalyst-controlled platinum-catalyzed addition to cyclic 1,3-dienes, see: M. Gerdin, C. Moberg, *Adv. Synth. Catal.* **2005**, *347*, 749 – 753.
[17] M. Suginome, T. Matsuda, Y. Ito, *Organometallics* **2000**, *19*, 4647 – 4649.
[18] a) G. Giordano, R. H. Crabtree, *Inorg. Synth.* **1979**, *19*, 218 – 220; b) K. Tani, T. Yamagata, S. Otsuka, H. Kumobayashi, S. Akutagawa, *Org. Synth.* **1989**, *67*, 33 – 43.
[19] R. Itooka, Y. Iguchi, N. Miyaura, *J. Org. Chem.* **2003**, *68*, 6000 – 6004.
[20] The diminished reactivity of [((*S*)-binap)Rh(cod)]$ClO_4$ compared to [(dppp)Rh(cod)]$ClO_4$ might indicate that electron-rich phosphines will enhance the reaction rate. A survey of chiral ligands will be the subject of future investigations.
[21] $[\alpha]_D = +105$ ($c = 3.08$ in $CHCl_3$ at 20 °C) for (*R*)-**7** (personal communication from Professor Pierre Deslongchamps): a) S. Trudeau, P. Deslongchamps, *J. Org. Chem.* **2004**, *69*, 832 – 838; b) G. Sarakinos, E. J. Corey, *Org. Lett.* **1999**, *1*, 811 – 814.
[22] R. W. Barnhart, X. Wang, P. Noheda, S. H. Bergens, J. Whelan, B. Bosnich, *J. Am. Chem. Soc.* **1994**, *116*, 1821 – 1830.
[23] T. Hayashi, M. Takahashi, Y. Takaya, M. Ogasawara, *J. Am. Chem. Soc.* **2002**, *124*, 5052 – 5058.

 © 2006 Wiley-VCH Verlag GmbH & Co. KGaA, Weinheim 

*Enzyme Catalysis*

DOI: 10.1002/anie.200503394

# Enantioselective Reduction of Ketones with "Designer Cells" at High Substrate Concentrations: Highly Efficient Access to Functionalized Optically Active Alcohols**

*Harald Gröger,* Francoise Chamouleau, Nicolas Orologas, Claudia Rollmann, Karlheinz Drauz, Werner Hummel, Andrea Weckbecker, and Oliver May**

The cofactor-dependent asymmetric reduction of ketones catalyzed by alcohol dehydrogenases represents a valuable method for the synthesis of optically active alcohols.[1] For the

[*] Dr. H. Gröger, Dr. F. Chamouleau, Dr. N. Orologas, C. Rollmann, Dr. O. May
Degussa AG
Service Center Biocatalysis
P.O. Box 1345, 63403 Hanau (Germany)
Fax: (+49) 618-159-2961
E-mail: harald.groeger@degussa.com
oliver.may@degussa.com

Prof. Dr. K. Drauz
Degussa AG
Corporate Center Innovation Management
P.O. Box 1345, 63403 Hanau (Germany)

Prof. Dr. W. Hummel, A. Weckbecker
Institute for Molecular Enzyme Technology
Heinrich-Heine University
Research Centre Jülich
Wilhelm-Johnen-Strasse, 52426 Jülich (Germany)

[**] The authors thank the Federal Ministry of Education and Research (BMBF) for support of the project "Entwicklung eines biokatalytischen und nachhaltigen Verfahrens zur industriellen Herstellung enantiomerenreiner Amine und Alkohole unter besonderer Berücksichtigung der Atomökonomie" within the program "Biotechnologie 2000 – Nachhaltige BioProduktion". We thank Dr. F.-R. Kunz and Dr. M. Janik and their teams (Degussa, AQura GmbH) for carrying out chiral HPLC and GC analyses as well as recording NMR spectra.

Supporting information for this article is available on the WWW under http://www.angewandte.org or from the author.


© 2006 Wiley-VCH Verlag GmbH & Co. KGaA, Weinheim

in situ regeneration of the cofactor, which is used in catalytic amounts owing to its high price, substrate-coupled[2] as well as enzyme-coupled[3] techniques are available. For the competitive application of this enzymatic technology on an industrial scale, in particular when one considers the high efficiency of the established metal-catalyzed hydrogenation as the benchmark,[4] it is essential to carry out biocatalytic reduction processes at high substrate concentrations and (preferably) in the absence of "external" cofactor. However, to date most of the biocatalytic syntheses based on the enzyme-coupled approach do not fulfill these requirements; they proceed with substrate concentrations of $<50\,g\,L^{-1}$, often even $<10\,g\,L^{-1}$. Accordingly, only a few examples have been reported that show a potential for technical applications or that already have been carried out on an industrial scale.[3,5]

One of these exceptions is the whole-cell-catalyzed reduction of ethyl 4-chloro-3-oxobutyrate developed by Shimizu et al., which proceeds at impressive substrate concentrations of 250 $g\,L^{-1}$ in a biphasic solvent system consisting of *n*-butyl acetate and an aqueous buffer solution (89% conversion, >99% *ee*).[3a,b] This reaction proceeds in the presence of a very low, catalytic amount of the expensive cofactor.[3a,b] In addition, Weuster-Botz et al. recently reported a new method based on the use of ionic liquids (which are, however, currently still expensive) with maximum substrate concentrations of $\approx 20\,g\,L^{-1}$ based on the total volume of solvents.[3c] The Matsuyama group described reductions with substrate concentrations of 30–50 $g\,L^{-1}$ in the presence of a recombinant whole-cell catalyst containing an alcohol dehydrogenase (ADH) and a formate dehydrogenase.[3d] One disadvantage of formate dehydrogenase used for the cofactor regeneration is its low specific activity of at most $\approx 10\,U\,mg^{-1}$ of purified enzyme, which leads to an unfavorable substrate/catalyst ratio.

In the following we report a simple, highly efficient, and broadly applicable process for the synthesis of optically alcohols complementing the previous processes. This process is characterized by the use of "designer cells" (with high overexpression of the required enzymes), which operate in pure aqueous media at high substrate concentrations of $>100\,g\,L^{-1}$ without an added "external" cofactor to furnish a broad range of (functionalized) *R* and *S* alcohols with conversions of typically >90% and enantioselectivities of >99% *ee* in most cases.

As we were interested in developing an efficient "tailor-made" whole-cell catalyst for the desired asymmetric reduction according to the process shown in Scheme 1, alcohol dehydrogenases (ADHs) with a high specific activity were chosen. An ADH from *Lactobacillus kefir* as an *R*-specific alcohol dehydrogenase[6a,b] and an ADH from *Rhodococcus erythropolis* as an *S*-specific alcohol dehydrogenase[6c,d] turned out to be particularly useful owing to their high specific activities, which exceed 1000 $U\,mg^{-1}$ for a range of substrates. These enzymes are also already available in recombinant form, which is required for technical applications.[6] Since an efficient whole-cell catalyst also relies on a cofactor-regenerating enzyme with high activity, glucose dehydrogenases with an activity of several hundred U per milligram of purified protein were chosen. The coexpression of the corresponding

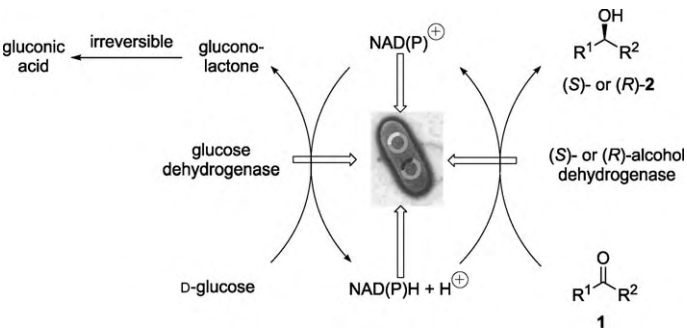


***Scheme 1.*** General reaction scheme of the target process.

alcohol dehydrogenase with a glucose dehydrogenase proceeded very successfully when the *E. coli* strain DSM14459 was used as a host organism.

We demonstrated this concept in the design of the *S*-enantioselective whole-cell catalyst (Scheme 2). A one-plasmid strategy was applied: genes that encode the alcohol dehydrogenase from *Rhodococcus erythropolis* and glucose dehydrogenase from *Bacillus subtilis*[6e] were ligated into one plasmid (pNO14c). The *E. coli* strain DSM14459 was used as a host organism. Both required enzymes were overexpressed and obtained with good activities of 32 $U\,mg^{-1}$ of crude

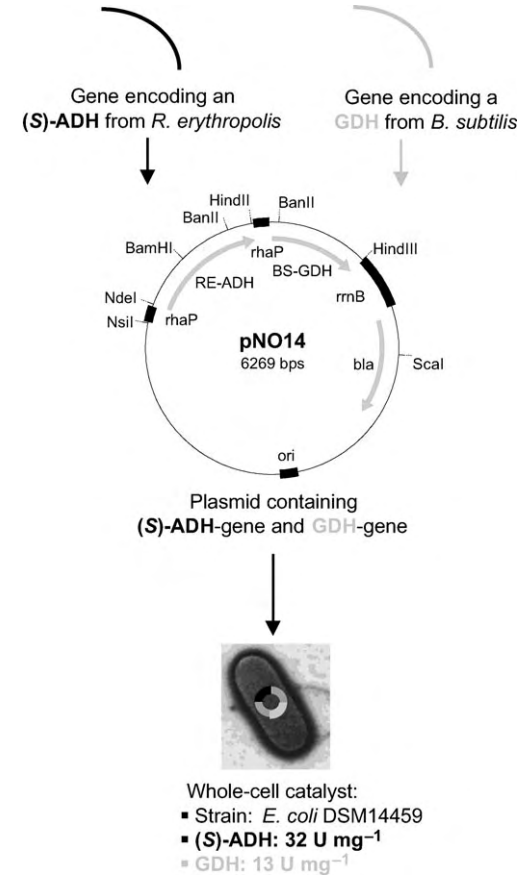


***Scheme 2.*** Concept of the "designer bugs"-whole-cell catalysts (recombinant microorganisms overexpressing the genes of the desired enzymes).

 © 2006 Wiley-VCH Verlag GmbH & Co. KGaA, Weinheim 

protein for the recombinant *S*-alcohol dehydrogenase from *R. erythropolis* [(*S*)-RE-ADH] and 13 U mg$^{-1}$ of crude protein for the recombinant glucose dehydrogenase from *B. subtilis* (BS-GDH). The analoguous *R*-selective whole-cell catalyst was constructed in the same manner by using *E. coli* DSM14459 as host organism, but in this case two plasmids were used (pNO5c/pNO8c), which contain genes encoding the above-mentioned ADH from *L. kefir* [(*R*)-LK-ADH] and a glucose dehydrogenase from *Thermoplasma acidophilum* (TA-GDH),[6f] respectively.

With respect to possible applications of these designer cells, we carried out the reaction in pure water or aqueous buffer solution. The solubility limit was exceeded and a second phase or an emulsion formed. This concept proved to be highly suitable for the envisioned asymmetric reductions, which also proceeded without addition of "external" cofactor. High conversion was obtained in the initial studies, which were carried out with the model substrate 4-chloroacetophenone (**1a**) at a concentration of 500 mM (78 g L$^{-1}$; Scheme 3). Interestingly, conversions of > 95 % were obtained with both the *R*- and *S*-selective whole-cell catalysts. A potential negative effect resulting from high substrate concentrations and subsequent destabilization caused by interactions at the extended phase interface does not occur or is negligible. In addition, the presence of an organic phase is expected to contribute significantly to cell-membrane permeability, which is essential for mass transfer.

Next, preparative conversions at high substrate concentrations were carried out with different types of substrates. Typically the substrate concentrations were 1.0 M or greater—significantly more than 100 g of substrate per L of reaction volume. The process operation was very economical and straightforward: Besides the substrate and glucose, only the whole-cell catalyst (as wet biomass) was needed to start the reaction; added cofactor was not required (or only in very small amounts in exceptional cases). The reaction with the model substrate **1a** proceeded at a substrate concentration of 1.0 M (156 g L$^{-1}$) in the presence of the *S*-selective whole-cell catalyst with a high conversion of 94 % and an excellent enantioselectivity of > 99.8 % *ee* (Table 1, entry 1). Addition of cofactor was not required.

A range of further ketones were reduced to the corresponding *S*- and *R*-enantiomeric forms of alcohols **2**, and again added cofactor was not necessary. The reaction also proceeded with acetophenone-type substrates bearing sterically demanding substituents. The *R*-selective whole-cell catalyst was used to convert 4-phenoxyacetophenone (1.0 M; 212 g L$^{-1}$) into the desired (*R*)-**2b** with a conversion of > 95 % and an enantioselectivity of > 99.4 % *ee* (Table 1, entry 2). After simple extractive workup the product (*R*)-**2b** was obtained with high purity in 88 % yield.

***Table 1:*** Preparative examples.

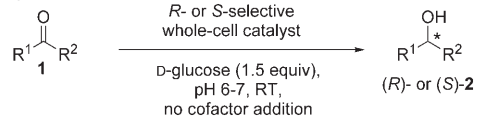


| Entry | Product | Abs. config.[a] | Biocatalyst[b] (amount in g L$^{-1}$) | Substrate conc. [g L$^{-1}$] | *t* [h] | Conv. [%] | *ee* [%] |
|---|---|---|---|---|---|---|---|
| 1[c] | 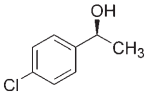 | (*S*)-**2a** | (*S*)-ADH/GDH (52) | 156 | 31 | 94 | > 99.8 |
| 2 | 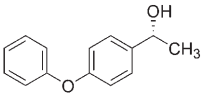 | (*R*)-**2b** | (*R*)-ADH/GDH (52) | 212 | 25 | > 95 | > 99.4 |
| 3 | 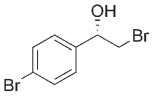 | (*S*)-**2c** | (*R*)-ADH/GDH (52) | 140 | 26 | 94 | 97 |
| 4 | 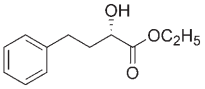 | (*S*)-**2d** | (*S*)-ADH/GDH (51) | 210 | 27 | 93 | 96 |
| 5 | 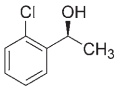 | (*S*)-**2e** | (*S*)-ADH/GDH (48) | 156 | 76 | 95 | > 99.4 |

[a] Absolute configuration. [b] Used as wet biomass. [c] Glucose (3 equiv) was added.

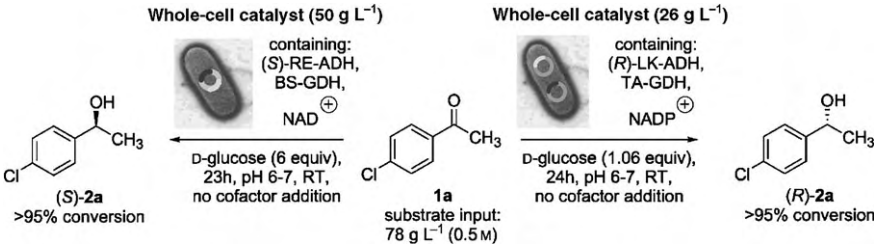


***Scheme 3.*** Initial conversions at substrate concentrations of 500 mM.

We also examined substrates bearing further functional groups, which thus allow subsequent transformations. α-Halogenated acetophenones are particularly interesting, as the corresponding alcohols of type **2c** may be converted under standard conditions into optically active epoxides, which are also of commercial interest. To test this, we examined the bioreduction of 2-bromo-1-(4-bromophenyl)ethanone. As the biocatalyst, the *R*-enantioselective strain *E. coli* DSM14459, containing the ADH from *L. kefir*, was chosen. The reaction proceeded highly efficiently at a substrate concentration of 0.5 M (140 g L$^{-1}$) providing the desired alcohol (*S*)-**2c** with a conversion of 94 % and an enantioselectivity of 97 % *ee* (Table 1, entry 3).

The enantioselective reduction of sterically demanding α-keto esters was also possible. Ethyl 4-phenyl-2-oxobutyrate

 © 2006 Wiley-VCH Verlag GmbH & Co. KGaA, Weinheim 

(1.02 M; 210 g L$^{-1}$) was transformed into (*S*)-**2d** with a conversion of 93% and an enantioselectivity of 96% ee (Table 1, entry 4). The biocatalyst in this case was the strain *E. coli* DSM14459 containing the *S*-enantioselective ADH from *R. erythropolis*.

Notably, the biocatalysts were also suitable for the reduction of *ortho*-substituted acetophenones. This type of substrate is often problematic in chemocatalytic reductions. The biocatalytic reduction with the *R*-selective whole-cell catalyst provided (*R*)-**2e** with a significantly decreased enantioselectivity of 90% *ee*; this reaction was also carried at a high substrate concentration of 156 g L$^{-1}$, and a conversion of >95% was obtained after a prolonged reaction time of 53 h. In contrast the analogous *S*-selective whole-cell catalyst led to the formation of (*S*)-**2e** with >99% *ee* and a conversion of 95%; however, an extended reaction time of 76 h was required (Table 1, entry 5). In the reduction reactions studied, which are also suitable for the conversion of purely aliphatic ketones, there were no limitations arising from the low solubility of the ketones in the aqueous reaction media.

The high reaction rates, conversions, and enantioselectivities along with the simple operation at high substrate concentrations allowed a fast scaleup of the process. As an example we tested the reduction of **1a** on a 10-L scale (Scheme 4). When the reaction was conducted at a substrate

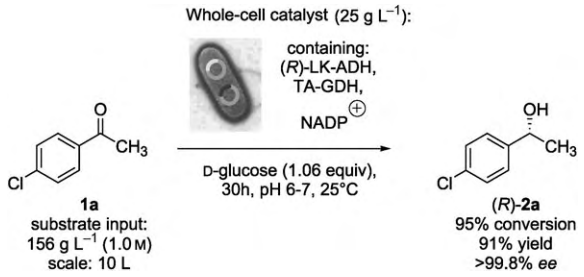


***Scheme 4.*** Application of the process on a 10-L scale.

concentration of 1.0 M (156 g L$^{-1}$) in the presence of the *R*-selective whole-cell catalyst, a conversion of 95% was observed after a reaction time of 30 h. Subsequent filtration (after the pH had been lowered and a filter aid added, in analogy to a related protocol[7] in order to avoid emulsion formation in downstream processing), extraction, and evaporation of solvent gave (*R*)-**2a** as a crude product in 91% yield with a purity of 95% and an excellent enantiomeric excess of >99.8% *ee* (Scheme 4). The reaction was carried out at a low biocatalyst concentration of 25 g of wet biomass per liter.

In summary, we have devised a practical biocatalytic reduction concept suitable for upscaling that is based on the use of a tailor-made whole-cell catalyst in a pure aqueous reaction medium and proceeds at >100 g L$^{-1}$. This methodology was used to furnish the desired (functionalized) optically active *R* and *S* alcohols with high conversions (>90%) and excellent enantioselectivities (>99% *ee* and partly even >99.8% *ee*). This process technology has been also established on a technical scale (after optimization), and the reduction of other substrates is being examined.

## Experimental Section

General experimental protocol for the preparation of the whole-cell-catalyst strains: Chemically competent cells of *E. coli* DSM14459[8a] were transformed with the plasmid pNO14c (see Scheme 2) or the plasmids pNO5c and pNO8c (see the Supporting Information) according to the procedure described in reference [8b] (for the gene sequences of the plasmids, see the Supporting Information). The plasmid pNO14c encoded for an alcohol dehydrogenase from *R. erythropolis*[6c,d] and a glucose dehydrogenase from *B. subtilis*.[6e] These dehydrogenases genes were under the control of a rhamnose promotor.[8c] The plasmids pNO5c and pNO8c encoded for an alcohol dehydrogenase from *L. kefir* and a glucose dehydrogenase from *T. acidophilum*, respectively. Active cells were prepared, for example, by incubation of a single colony of *E. coli* DSM14459 (pNO14c) or *E. coli* DSM14459 (pNO5c, pNO8c) in 2 mL of an LB medium with antibiotics supplement (50 μg L$^{-1}$ of ampicillin and also 20 μg mL$^{-1}$ of chloramphenicol in the case of the *R*-selective whole-cell catalyst) with shaking (250 rpm) at 37 °C for 18 h. This culture was diluted 1:100 with fresh LB medium containing rhamnose (2 g L$^{-1}$) as the inductor, antibiotics supplement (50 μg L$^{-1}$ of ampicillin and also 20 μg mL$^{-1}$ of chloramphenicol in the case of the *R*-selective whole-cell catalyst) and 1 mM of $ZnCl_2$, and incubated with shaking (250 rpm) for 18 h at 30 °C. The cells were harvested by centrifugation (10000 g, 10 min, 4 °C), the supernatant was discarded, and cell pellets, which could be stored at −20 °C, were used in the biotransformation experiments.

General experimental protocol for the biocatalytic reduction of ketones: A Titrino reaction apparatus was filled with 20 mL of an aqueous phosphate buffer solution (0.2 M; adjusted to pH 7.0), the *R*- or *S*-enantioselective whole-cell catalyst of type *E. coli* DSM14459 [containing either (*S*)-RE-ADH or (*R*)-LK-ADH as well as a glucose dehydrogenase; cell concentration ≈50 g of wet biomass per liter (see Table 1)], D-glucose (typically 1.5 equiv based on the amount of ketone), and 20 mmol (0.5 M) or 40 mmol (1.0 M) of the corresponding ketone (see Table 1). Water was added until a volume of 40 mL was reached. The reaction mixture was stirred at room temperature for the set reaction time, and the pH was maintained at ≈6.5 by dosage of aqueous sodium hydroxide (5 M NaOH). After the reaction time given in Table 1 the conversion was determined by HPLC and NMR spectroscopy. The workup was carried out by lowering the pH to <3 with concentrated hydrochloric acid, adding 3.0 g of the filter-aid material Celite Hyflo Supercel to the reaction mixture, and then filtering. The filter cake was washed with methyl *tert*-butyl ether (3 × 50 mL), and the aqueous phase was extracted with the resulting organic fractions. The collected organic phases were dried over magnesium sulfate and concentrated to dryness to deliver the desired optically active alcohol in high purity, even as a crude product, of typically at least 93%. If necessary, the purity of the products can be further improved by means of standard purification methods such as, for example, distillation and chromatography.

Received: September 25, 2005
Revised: March 2, 2006
Published online: July 21, 2006

**Keywords:** alcohols · asymmetric catalysis · cofactors · enzyme catalysis · reductions

[1] Reviews: a) K. Nakamura, T. Matsuda in: *Enzyme Catalysis in Organic Synthesis*, *Vol. 3*, 2nd ed. (Eds.: K. Drauz, H. Waldmann), Wiley-VCH, Weinheim, **2002**, pp. 991 – 1047; b) W. Hummel, *Adv.*

 © 2006 Wiley-VCH Verlag GmbH & Co. KGaA, Weinheim 

*Biochem. Eng./Biotechnol.* **1997**, *58*, 146–184; c) K. Faber, *Biotransformations in Organic Chemistry*, 5th ed., Springer, Berlin, **2004**, chap. 2.2.3, pp. 192–197.

[2] For selected contributions on substrate-coupled cofactor regeneration with 2-propanol in the asymmetric enzymatic reduction of ketones, see: a) W. Stampfer, B. Kosjek, C. Moitzi, W. Kroutil, K. Faber, *Angew. Chem.* **2002**, *114*, 1056–1059; *Angew. Chem. Int. Ed.* **2002**, *41*, 1014–1017; b) M. Wolberg W. Hummel, C. Wandrey, M. Müller, *Angew. Chem.* **2000**, *112*, 4476–4478; *Angew. Chem. Int. Ed.* **2000**, *39*, 4306–4308; c) M. Amidjojo, D. Weuster-Botz, *Tetrahedron: Asymmetry* **2005**, *16*, 899–901.

[3] a) N. Kizaki, Y. Yasohara, J. Hasegawa, M. Wada, M. Kataoka, S. Shimizu, *Appl. Microbiol. Biotechnol.* **2001**, *55*, 590–595; b) M. Kataoka, K. Kita, M. Wada, Y. Yasohara, J. Hasegawa, S. Shimizu, *Appl. Microbiol. Biotechnol.* **2003**, *62*, 437–445; c) H. Pfründer, M. Amidjojo, U. Kragl, D. Weuster-Botz, *Angew. Chem.* **2004**, *116*, 4629–4631; *Angew. Chem. Int. Ed.* **2004**, *43*, 4529–4531; d) A. Matsuyama, H. Yamamoto, Y. Kobayashi, *Org. Process Res. Dev.* **2002**, *6*, 558–561.

[4] R. Noyori, T. Okhuma, *Angew. Chem.* **2001**, *113*, 40–75; *Angew. Chem. Int. Ed.* **2001**, *40*, 40–73.

[5] Review: A. Liese, K. Seelbach, C. Wandrey, *Industrial Biotransformations*, Wiley-VCH, Weinheim, **2000**.

[6] a) W. Hummel, M.-R. Kula (FZ Jülich GmbH), EP 456107, **1991**; b) A. Weckbecker, W. Hummel in *Microbial Enzymes and Biotransformations, Methods in Biotechnology, Vol. 17* (Ed.: J. L. Barredo), Humana Press, Totowa, **2004**, pp. 241–253; c) W. Hummel, K. Abokitse, H. Gröger (Degussa AG), EP 1499716, **2003**; d) K. Abokitse, W. Hummel, *Appl. Microbiol. Biotechnol.* **2003**, *62*, 380–386; e) W. Hilt, G. Pfleiderer, P. Fortnagel, *Biochim. Biophys. Acta* **1991**, *1076*, 298–304; f) J. R. Bright D. Byrom, M. J. Danson, D. W. Hough, P. Towner, *Eur. J. Biochem.* **1993**, *211*, 549–554.

[7] R. L. Hanson, S. Goldberg, A. Goswami, T. P. Tully, R. N. Patel, *Adv. Synth. Catal.* **2005**, *347*, 1073–1080.

[8] a) O. May, K. Liebeton, J. Eck (Degussa AG), WO 2003042412, **2003**; b) J. Sambrook, E. F. Fritsch, T. Maniatis, *Molecular Cloning: A Laboratory Manual*, 2nd ed., Cold Spring Harbor Laboratory Press, Cold Spring Harbor, **1989**; c) T. Stumpp, B. Wilms, J. Altenbuchner, *BIOspektrum* **2000**, *6*, 33–36.

 © 2006 Wiley-VCH Verlag GmbH & Co. KGaA, Weinheim 

Coordination Chemistry

DOI: 10.1002/anie.200601134

# Formation of an Aqueous Oxoiron(IV) Complex at pH 2–6 from a Nonheme Iron(II) Complex and $H_2O_2$**

*Jochen Bautz, Michael R. Bukowski, Marion Kerscher, Audria Stubna, Peter Comba,* Achim Lienke, Eckard Münck,* and Lawrence Que, Jr.**

The oxidation chemistry of iron(II) in water has been discussed since the days of Fenton and his discovery of the ability of iron(II) salts together with hydrogen peroxide to oxidize organic substrates in acidic aqueous solutions.[1–3] The involvement of hydroxyl radicals[4] and/or iron(IV) species[5] has been suggested on the basis of experimental observations, and DFT calculations support the latter.[6] More recently, oxoiron(IV) intermediates have been identified in the catalytic cycle of taurine α-ketoglutarate dioxygenase (TauD)[7,8] and characterized for several synthetic nonheme complexes,[9–14] including two high-resolution crystal structures.[10,13] On the basis of the spectroscopic signatures of these precedents, similar intermediates in other systems can be analyzed.

Although oxoiron(IV) complexes are generally synthesized in organic solvents, there are two reports of syntheses in aqueous media. In the first case, the previously characterized

[*] Dr. J. Bautz, Dr. M. Kerscher, Prof. Dr. P. Comba
Anorganisch-Chemisches Institut
Universität Heidelberg
INF 270, 69120 Heidelberg (Germany)
Fax: (+49) 6226-548-453
E-mail: peter.comba@aci.uni-heidelberg.de

Dr. A. Stubna, Prof. Dr. E. Münck
Department of Chemistry
Carnegie Mellon University
Pittsburgh, PA 15213 (USA)
Fax: (+1) 412-268-1061
E-mail: emunck@cmu.edu

Dr. M. R. Bukowski, Prof. Dr. L. Que, Jr.
Department of Chemistry and
Center for Metals in Biocatalysis
University of Minnesota
207 Pleasant Street SE, Minneapolis, MN 55455 (USA)
Fax: (+1) 612-624-7029
E-mail: que@chem.umn.edu

Dr. A. Lienke
Unilever Research and Development
Olivier van Noortlaan 120
3133 AT Vlaardingen (The Netherlands)

[**] This work was supported by the German Science Foundation and Unilever (P.C.), and the US National Institutes of Health (GM-33162 to L.Q. and EB-001475 to E.M.).

Supporting information for this article (electrospray mass spectral data, $H_2O_2$ concentration dependence, and Eyring plots for the formation of **2**) is available on the WWW under http://www.angewandte.org or from the author.


© 2006 Wiley-VCH Verlag GmbH & Co. KGaA, Weinheim

complex $[Fe^{IV}(O)(N4Py)]^{2+}$ (N4Py = bis(2-pyridylmethyl)-bis(2-pyridyl)methylamine) was found to form in a 3:1 $H_2O$/MeCN (v/v) mixture from the reaction of its iron(II) precursor with several oxidants including $H_2O_2$, but a detailed mechanistic study of the latter reaction was not reported.[15] In the second case, an aqueous high-spin oxoiron(IV) complex was identified from the reaction of $[Fe(H_2O)_6]^{2+}$ with ozone in acidic aqueous solution in an effort to clarify the nature of the oxidant involved in the classical Fenton reaction.[16] We now report a mechanistic study of the reaction of $H_2O_2$ with a nonheme iron(II) complex bearing a pentadentate bispidine ligand in water to form an $S=1$ oxoiron(IV) complex under conditions similar to those of the classical Fenton reaction.

The reaction of $[Fe^{II}(L)(SO_4)]$[17] (**1**) with PhIO or $H_2O_2$ in water at 25 °C affords the pale blue-green species **2** with an absorption maximum $\lambda_{max}$ at 715 nm ($\varepsilon = 400\ cm^{-1}M^{-1}$), a feature that suggests the formation of an $S=1$ oxoiron(IV) complex (Figure 1).[9–14] High-resolution electrospray mass

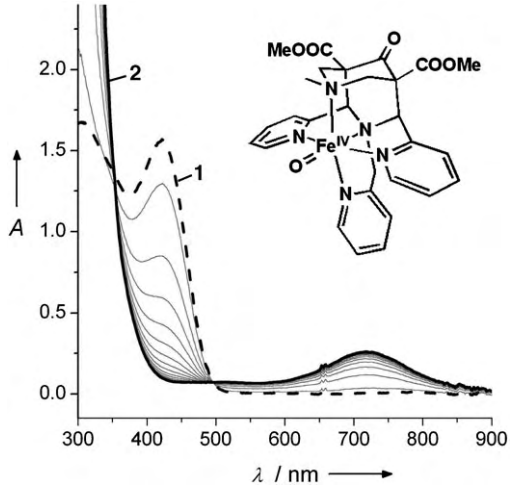


***Figure 1.*** The reaction of 1 mM $[Fe^{II}(L)(SO_4)]$ (**1**; -----) with 10 equiv $H_2O_2$ at 0 °C in 50 mM citrate buffer (pH 5.4) to form $[Fe^{IV}(L)(O)]^{2+}$ (**2**; ——).

spectrometry of the aqueous solution (see the Supporting Information) reveals several ions at *m/z* 293.5741, 302.5790, and 692.1623, which can be assigned to the complexes $[Fe^{IV}(L)(O)]^{2+}$, $[Fe^{IV}(L)(O)+H_2O]^{2+}$, and $[Fe^{IV}(L)(O)+H_2O+BF_4]^{+}$, respectively. The incorporation of water in the latter two ions results from hydration of the backbone carbonyl on the ligand framework and is a feature of the bispidine ligand that has been observed previously in the X-ray crystal structure of the iron(II) starting material.[17] With PhIO as oxidant, the formation of **2** is evidenced by the appearance of a Mössbauer doublet (Figure 2a) that represents 90 % of the total iron in the sample. These data, together with a measurement of the absorbance at 715 nm for the Mössbauer sample, establish an extinction coefficient of $400\ M^{-1}\ cm^{-1}$ for **2**.

The Mössbauer analysis of **2** shows that it belongs to a new family of low-spin oxoiron(IV) complexes with $S=1$.[9–14] We have recorded its Mössbauer spectra at a number of temperatures and applied magnetic fields (4.2 K: 0, 1.0, 2.5, 4.0, 6.0,

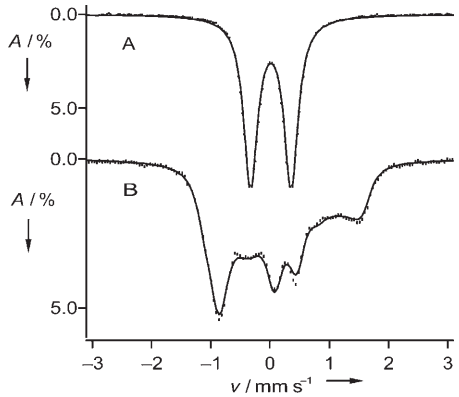


***Figure 2.*** Mössbauer spectra of **2** at 4.2 K, obtained by oxidation of **1** with PhIO in $H_2O$, recorded for $B=0$ T (A) and $B=8.0$ T (B). The solid lines are spectral simulations generated from Equation (1) with parameters $D=+23(2)\ cm^{-1}$, $E/D=0$ (fixed), $g_e=2.0$, $A_x/g_n\beta_n=-22(2)$ T, $A_y/g_n\beta_n=-20(2)$ T, $A_z/g_n\beta_n\approx-5$ T, $\Delta E_Q=0.69(1)\ mm\,s^{-1}$, $\eta=0.5$, $\delta=0.02(1)\ mm\,s^{-1}$ (relative to Fe metal at 298 K), and $\Gamma=0.29\ mm\,s^{-1}$ (Lorentzian full width at half maximum). Approximately 90 % of the $^{57}Fe$ in the sample can be attributed to **2**; the remainder appears to belong to a high-spin $Fe^{III}$ species, as indicated by spectra recorded with velocity of $\pm 11\ mm\,s^{-1}$ (data not shown).

and 8.0 T; 35 K: 8.0 T; 100 K: 8.0 T). The spectra recorded at 4.2 K for $B=0$ T (A) and $B=8.0$ T (B) are shown in Figure 2. The zero-field spectrum consists of a doublet with quadrupole splitting $\Delta E_Q=0.69\ mm\,s^{-1}$ and isomer shift $\delta=0.02\ mm\,s^{-1}$. The small isomer shift firmly establishes **2** as an $Fe^{IV}$ complex. The solid lines drawn through the data are spectral simulations based on the commonly used $S=1$ Hamiltonian [Eq. (1)] using the parameters listed in Figure 2. These parameters are quite similar to those reported recently for related oxoiron(IV) complexes.[9–14]

$$\mathbf{H} = \mathbf{D}(S_z^2 - 2/3) + E(S_x^2 - S_y^2) + g_e\beta\mathbf{B}\,\mathbf{S} + \mathbf{S}\,\mathbf{A}\,\mathbf{I} - g_n\beta_n\mathbf{B}\,\mathbf{I} + H_Q \qquad (1)$$

$H_Q$ describes the quadrupole splitting of the excited state nucleus, and all other symbols have their conventional meanings. The simulations of all the other recorded spectra have the same quality as those shown in Figure 2. We tested whether the data can be simulated with an $S=2$ Hamiltonian, which is appropriate for a high-spin $Fe^{IV}$ center. The data set at 4.2 K can be simulated well with an $S=2$ Hamiltonian, but very poor simulations result when the parameters obtained at low temperature are applied to the data at 35 and 100 K. This suggests, as anticipated, that **2** does indeed exhibit an $S=1$ ground state. It is appropriate to test the spin state of other $Fe^{IV}$=O complexes, because for related complexes the large zero-field splitting parameters $D$ have been found to reflect a low-lying $S=2$ configuration.[14,18] DFT calculations on the $S=1$ complex $[Fe^{IV}(O)(TMC)(NCMe)]^{2+}$ ($D=28\ cm^{-1}$) suggest a low-lying $S=2$ configuration at $2900\ cm^{-1}$ (see the Supporting Information of reference [14]; TMC = 1,4,8,11-tetramethyl-1,4,8,11-tetraazacyclotetradecane). The $D$ value obtained for **2** ($23\ cm^{-1}$) suggests an $S=2$ excited state at slightly higher energy (when both complexes are assumed to have similar covalency).

 © 2006 Wiley-VCH Verlag GmbH & Co. KGaA, Weinheim 

With $H_2O_2$ as oxidant, **2** is formed in variable yield, depending on the pH value employed (Figure 3), as indicated by the intensity of the band at 715 nm. The transformation of **1** ($\lambda_{max} = 405$ nm) at pH 5.4 (50 mM citrate buffer) to **2** ($\lambda_{max} = 715$ nm) occurs over the course of 80 s at 0 °C with an

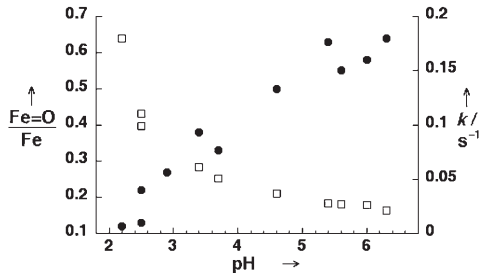


***Figure 3.*** pH dependence of the yield (●, left) and the rate of formation of **2** (□, right) at 0 °C in 50 mM citrate buffer.

isosbestic point at 490 nm and no other chromophoric intermediates (Figure 1). The transformation exhibits pseudo-first-order behavior with excess $H_2O_2$, and a first-order dependence of the formation rate on $H_2O_2$ concentration is observed, as studied by the development of the band at 715 nm (see the Supporting Information). Thus, **1** reacts with $H_2O_2$ and appears likely to convert directly into **2** under these conditions.

To obtain further mechanistic insight into the formation of **2**, the yields and kinetics were investigated at pH 2–6 in 50 mM citrate buffer (Figure 3). Remarkably, **2** can be formed over this pH range, and the yield of **2** increases linearly from pH 2 to 6, reaching a maximum of approximately 60 % conversion at pH 6. Once formed, **2** is stable for a period of hours, even at low pH values. Interestingly, despite its larger yield at higher pH values, the rate of reaction as monitored either by the disappearance of **1** (at 400 nm) or by the appearance of **2** (at 715 nm) decreases with increasing pH value.

The temperature dependence for the rate of formation of the oxoiron(IV) complex was determined at pH 3.4, 5.4, and 6.3 (see the Supporting Information). Eyring plots reveal an activation enthalpy $\Delta H^{\neq}$ of 34 kJ mol$^{-1}$ and an activation entropy $\Delta S^{\neq}$ of $-150$ J K$^{-1}$ mol$^{-1}$ (Table 1). The activation enthalpy is 20 kJ mol$^{-1}$ smaller and the activation entropy is at least twofold larger than the corresponding values for the formation of [$Fe^{IV}$(O)(TMP)] ($H_2$TMP = *meso*-tetramesitylporphin) and $[Fe^{IV}(O)(TPA)]^{2+}$ (TPA = tris(2-pyridylmethyl)amine) from their peroxoiron(III) precursors (Table 1).[19–21] These differences suggest a divergence in the mechanisms of oxoiron(IV) formation. Since the latter complexes are very likely generated by O–O bond homolysis of their peroxoiron(III) precursors, we postulate that **2** forms directly from the reaction of **1** with $H_2O_2$ by iron(II)-promoted O–O bond heterolysis. (As pointed out by a reviewer, the observed kinetics are also consistent with rate-determining formation of $[Fe^{II}(L)(H_2O_2)]^{2+}$, followed by rapid steps leading to the formation of the $Fe^{IV}$=O species; however, ligand exchange at a kinetically labile high-spin iron(II) center would be expected to be facile and not rate-determining.) Indeed, the smaller activation enthalpy determined experimentally for the conversion of **1** into **2** approaches values calculated by DFT for the conversion of $Fe^{II}$–OOR intermediates into $Fe^{IV}$=O complexes in pterin-dependent and 2-oxoglutarate-dependent nonheme iron enzymes.[22–24]

The reaction of **1** with $H_2O_2$ in water clearly exhibits an outcome different from the analogous reaction in MeOH, in which a purple $Fe^{III}$–OOH intermediate is observed.[25] The latter requires 1.5 equivalents of $H_2O_2$ in a two-step process that involves an $Fe^{III}$–OH intermediate (Scheme 1, top).[26] For the reaction of **1** with $H_2O_2$ in aqueous media, there is no evidence for the formation of an $Fe^{III}$–OOH chromophore that in turn decays to form **2**. Instead, Figure 1 shows an isosbestic point near 500 nm, a fact that supports the direct conversion of **1** into **2**. The observed second-order kinetic behavior and the large and negative entropy of activation support a mechanism in which $H_2O_2$ binds to the iron(II) center of **1** in a preequilibrium step and then undergoes O–O bond cleavage in a rate-determining step to form **2**. In this process, the proton migrates from the proximal to the

***Table 1:*** Activation parameters for the conversion of **1** (1 mM) into **2** with $H_2O_2$ (10 equiv) in 50 mM citrate buffer and related reactions.

| Reaction | Solvent | $\Delta H^{\neq}$ [kJ mol$^{-1}$] | $\Delta S^{\neq}$ [J mol$^{-1}$ K$^{-1}$] | Ref. |
|---|---|---|---|---|
| **1**→**2** | pH 3.4 | 32(4) | −149(14) | this work |
| | pH 5.4 | 34(2) | −150(6) | this work |
| | pH 6.3 | 35(2) | −148(8) | this work |
| | mean: | 34 | −150 | |
| $[Fe^{III}(OOtBu)(TPA)(NCMe)]^{2+} \rightarrow [Fe^{IV}(O)(TPA)(NCMe)]^{2+}$ | MeCN | 52(1) | −74(3) | [20] |
| $[Fe^{III}(OOtBu)(TPA)(NCMe)]^{2+} + PyO \rightarrow [Fe^{IV}(O)(TPA)(OPy)]^{2+}$ [a] | MeCN | 50(2) | −42(10) | [20] |
| $[Fe^{III}(\kappa^2\text{-}OOC(CH_3)_2OH)(TPA)]^{2+} \rightarrow [Fe^{IV}(O)(TPA)]^{2+}$ | acetone | 54(3) | −35(13) or −42(12) | [21] |
| $[(TMP)Fe^{III}\text{–}O\text{–}O\text{–}Fe^{III}(TMP)] \rightarrow 2[Fe^{IV}(O)(TMP)]$ | toluene | 61 | −60 | [19] |
| Calcd for $Fe^{II}(OOR) \rightarrow Fe^{IV}(O)$ in nonheme iron enzymes | | 12–20 | | [22–24] |

[a] OPy = Pyridine *N*-oxide.

 © 2006 Wiley-VCH Verlag GmbH & Co. KGaA, Weinheim 

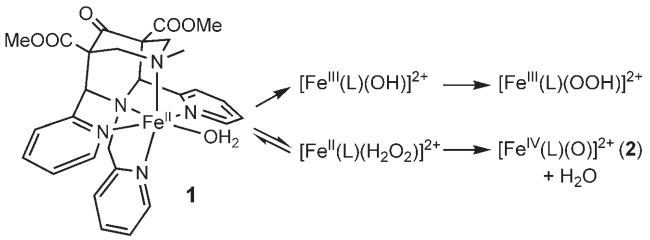


***Scheme 1.*** Proposed mechanisms for the reaction of **1** with $H_2O_2$ in methanol (top) and aqueous media (bottom).

terminal oxygen atom of the bound $H_2O_2$ molecule (Scheme 1, bottom). It is currently unclear why at higher pH values a higher yield of **2** is obtained despite the slower rate of formation; this trend may, however, reflect the inhibition at higher pH values of side reactions that promote the decay of **2**. Indeed, the isosbestic points in the conversion of **1** into **2** were lost at longer time intervals at low pH values.

In summary, we have identified an iron(II) complex **1** that reacts with $H_2O_2$ at acidic pH values to form a low-spin oxoiron(IV) complex by O–O bond cleavage. This complex differs from the high-spin aquated oxoiron(IV) species recently obtained from the reaction of $[Fe(H_2O)_6]^{2+}$ with ozone at pH 1,[16] and demonstrates the role of the supporting polydentate ligand in controlling the spin state and directing the outcome of the reaction. Although DFT calculations support the direct formation of $Fe^{IV}$=O from $[Fe(H_2O)_6]^{2+}$ and $H_2O_2$ under Fenton conditions,[6] the preponderance of evidence appears to support the involvement of hydroxyl radicals in aqueous Fenton chemistry.[2,3,16] However, the results reported herein demonstrate that the species $[FeO]^{2+}$ formulated by Bray and Gorin[5] more than 70 years ago can also occur with the support of the pentadentate ligand L.

Received: March 22, 2006
Published online: July 21, 2006

**Keywords:** coordination modes · iron · N ligands · oxidation · oxo ligands

[1] H. J. H. Fenton, *J. Chem. Soc.* **1894**, *65*, 889.
[2] C. Walling, *Acc. Chem. Res.* **1975**, *8*, 125.
[3] C. Walling, *Acc. Chem. Res.* **1998**, *31*, 155.
[4] F. Haber, J. Weiss, *Proc. R. Soc. London Ser. A* **1934**, *147*, 332.
[5] W. C. Bray, M. H. Gorin, *J. Am. Chem. Soc.* **1932**, *54*, 2124.
[6] F. Buda, B. Ensing, M. C. M. Gribnau, E. J. Baerends, *Chem. Eur. J.* **2001**, *7*, 2775.
[7] J. M. Bollinger, Jr., J. C. Price, L. M. Hoffart, E. W. Barr, C. Krebs, *Eur. J. Inorg. Chem.* **2005**, 4245.
[8] C. Krebs, J. C. Price, J. Baldwin, L. Saleh, M. T. Green, J. M. Bollinger, Jr., *Inorg. Chem.* **2005**, *44*, 742.
[9] C. A. Grapperhaus, B. Mienert, E. Bill, T. Weyhermüller, K. Wieghardt, *Inorg. Chem.* **2000**, *39*, 5306.
[10] J.-U. Rohde, J.-H. In, M. H. Lim, W. W. Brennessel, M. R. Bukowski, A. Stubna, E. Münck, W. Nam, L. Que, Jr., *Science* **2003**, *299*, 1037.
[11] M. H. Lim, J.-U. Rohde, A. Stubna, M. R. Bukowski, M. Costas, R. Y. N. Ho, E. Münck, W. Nam, L. Que, Jr., *Proc. Natl. Acad. Sci. USA* **2003**, *100*, 3665.
[12] V. Balland, M.-F. Charlot, F. Banse, J.-J. Girerd, T. A. Mattioli, E. Bill, J.-F. Bartoli, P. Battioni, D. Mansuy, *Eur. J. Inorg. Chem.* **2004**, 301.
[13] E. J. Klinker, J. Kaizer, W. W. Brennessel, N. L. Woodrum, C. J. Cramer, L. Que, Jr., *Angew. Chem.* **2005**, *117*, 3756; *Angew. Chem. Int. Ed.* **2005**, *44*, 3690.
[14] M. R. Bukowski, K. D. Koehntop, A. Stubna, E. L. Bominaar, J. A. Halfen, E. Münck, W. Nam, L. Que, Jr., *Science* **2005**, *310*, 1000.
[15] C. V. Sastri, M. S. Seo, M. J. Park, K. M. Kim, W. Nam, *Chem. Commun.* **2005**, 1405.
[16] O. Pestovsky, S. Stoian, E. L. Bominaar, X. Shan, E. Münck, L. Que, Jr., A. Bakac, *Angew. Chem.* **2005**, *117*, 7031; *Angew. Chem. Int. Ed.* **2005**, *44*, 6871; Erratum: O. Pestovsky, S. Stoian, E. L. Bominaar, X. Shan, E. Münck, L. Que, Jr., A. Bakac, *Angew. Chem.* **2006**, *118*, 348; *Angew. Chem. Int. Ed.* **2006**, *45*, 340.
[17] H. Börzel, P. Comba, K. S. Hagen, Y. D. Lampeka, A. Lienke, G. Linti, M. Merz, H. Pritzkow, L. V. Tsymbal, *Inorg. Chim. Acta* **2002**, *337*, 407.
[18] J. C. Schöneboom, F. Neese, W. Thiel, *J. Am. Chem. Soc.* **2005**, *127*, 5840.
[19] A. L. Balch, *Inorg. Chim. Acta* **1992**, *198–200*, 297.
[20] J. Kaizer, M. Costas, L. Que, Jr., *Angew. Chem.* **2003**, *115*, 3799; *Angew. Chem. Int. Ed.* **2003**, *42*, 3671.
[21] A. Mairata i Payeras, R. Y. N. Ho, M. Fujita, L. Que, Jr., *Chem. Eur. J.* **2004**, *10*, 4944.
[22] A. Bassan, M. R. A. Blomberg, P. E. M. Siegbahn, *Chem. Eur. J.* **2003**, *9*, 4055.
[23] T. Borowski, A. Bassan, P. E. M. Siegbahn, *Chem. Eur. J.* **2004**, *10*, 1031.
[24] A. Bassan, T. Borowski, P. E. M. Siegbahn, *Dalton Trans.* **2004**, 3153.
[25] M. R. Bukowski, P. Comba, C. Limberg, M. Merz, L. Que, Jr., T. Wistuba, *Angew. Chem.* **2004**, *116*, 1303; *Angew. Chem. Int. Ed.* **2004**, *43*, 1283.
[26] G. Roelfes, M. Lubben, K. Chen, R. Y. N. Ho, A. Meetsma, S. Genseberger, R. M. Hermant, R. Hage, S. K. Mandal, V. G. Young, Jr., Y. Zang, H. Kooijman, A. L. Spek, L. Que, Jr., B. L. Feringa, *Inorg. Chem.* **1999**, *38*, 1929.

 © 2006 Wiley-VCH Verlag GmbH & Co. KGaA, Weinheim 

*Biosynthetic Pathways*

DOI: 10.1002/anie.200600511

# Premithramycinone G, an Early Shunt Product of the Mithramycin Biosynthetic Pathway Accumulated upon Inactivation of Oxygenase MtmOII

*Mohamed S. Abdelfattah and Jürgen Rohr**

Mithramycin (**1**, MTM, Scheme 1, also known as mithramycin A, mithracin, and plicamycin) is an aureolic acid anticancer agent produced by various soil bacteria of the genus *Streptomyces*, including *Streptomyces argillaceus* (ATCC12956). It inhibits the growth of cancer cells by cross-linking GC-rich DNA, thereby shutting down specificity protein (Sp1 or Sp3) dependent pathways towards proto-oncogenes, such as c-*myc*,[1] *APC*,[2] and c-*src*.[3] The last gene is also associated with the unique hypocalcemic activity of mithramycin.[3] MTM has become a popular biochemical tool to study Sp-dependent signal-transduction pathways, but because of its toxic side effects is rarely used as an anticancer agent, except for the treatment of tumor hypercalcemia refactory to other chemotherapy.[4–8] However, MTM was recently identified as a potential lead drug against neurological diseases,[9,10] arthritis,[11] and for the treatment of hematologic disorders.[12] All these new applications require only very small, less-toxic concentrations of the drug, although the mode-of-action in these contexts remains obscure.

The biosynthesis of MTM has been studied intensively during the past couple of years,[13–18] and combinatorial biosynthetic efforts have already revealed various new MTM analogues, some with apparently advantageous biological activity profiles.[19–21] The biosynthesis of MTM proceeds through a type II polyketide synthase (PKS) mediated condensation of multiple acyl-CoA units to the formation of the first isolable tetracyclic intermediates demethylpremithramycinone and premithramycinone (**2**), which in turn is glycosylated and C-methylated to give premithramycin B (**3**). The final steps in mithramycin biosynthesis are an oxidative cleavage of the fourth ring of **3**, followed by decarboxylation and reduction of the 4′-keto group, catalyzed by oxygenase MtmOIV and ketoreductase MtmW, respectively (Scheme 1).[20,22,23] However, virtually nothing is known about the post-PKS steps prior to the formation of **2**; particularly unclear is the role of the products of the three oxygenase encoding genes *mtmOI*, *mtmOII*, and *mtmOIII*.[13] Here, we describe the isolation, structure elucidation, and putative biosynthetic impact of a novel early shunt product of mithramycin biosynthesis, premithramycinone G (**4**, Figure 1 and Scheme 2), which is accumulated by the MtmOII$^-$ mutant *S. argillaceus* M7OII.[13]

Gene inactivation of post-PKS enzymes does not only present a very useful tool for the elucidation of biosynthetic pathways by analysis of accumulated intermediates or shunt products, but also has the potential to generate new "non-natural" natural products with better or altered biological activities.[24] However, this approach only gave one clear result in regard to the oxygenases of the mithramycin pathway. Four oxygenase genes (*mtmOI*, *mtmOII*, *mtmOIII*, and *mtmOIV*) were identified in the MTM gene cluster and inactivated by insertion of resistance cassettes. While the

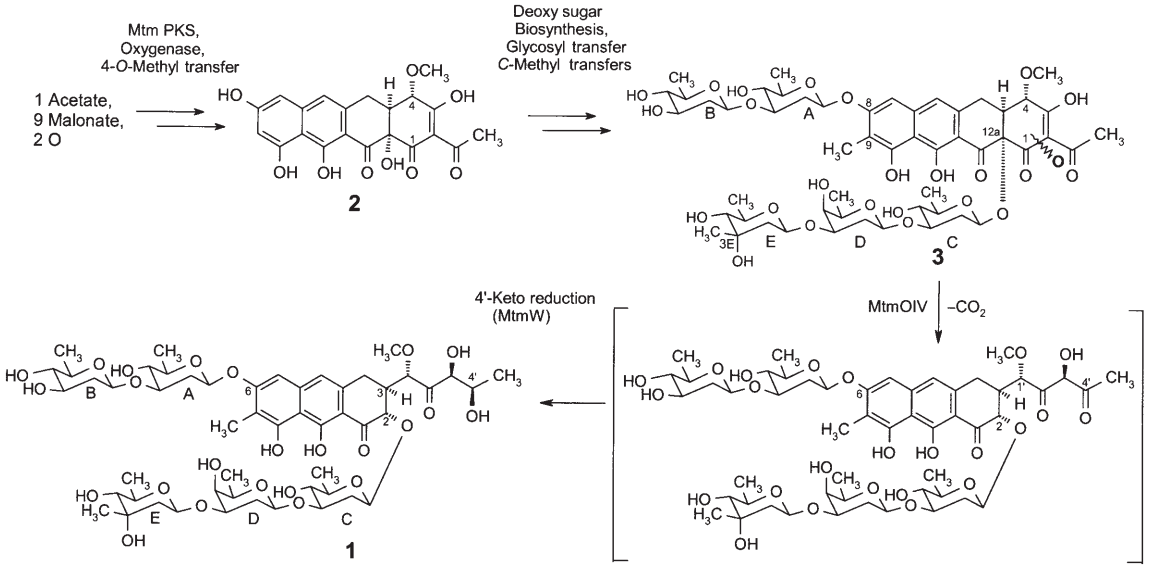


***Scheme 1.*** Biosynthetic pathway of mithramycin (MTM, **1**) showing intermediates premithramycinone (**2**) and premithramycin B (**3**), as well as the late oxidative rearrangement catalyzed by MtmOIV.

[*] Dr. M. S. Abdelfattah, Prof. Dr. J. Rohr
University of Kentucky
Department of Pharmaceutical Sciences
College of Pharmacy
725 Rose Street, Lexington, KY 40536-0082 (USA)
Fax: (+1) 859-257-7564
E-mail: jrohr2@email.uky.edu


© 2006 Wiley-VCH Verlag GmbH & Co. KGaA, Weinheim

inactivation of *mtmOIV* resulted in clear evidence of the action of the corresponding enzyme MtmOIV,[22,23] the inactivation of neither *mtmOI* nor *mtmOIII* appear to have any consequence for mithramycin biosynthesis.[13] Inactivation of *mtmOII* resulted in the "non-producing" mutant strain M7OII, which generated an unstable compound.[13,14]

After several attempts to isolate this unstable, putative early intermediate of the mithramycin biosynthesis failed, we designed a gene complementation experiment, in which TcmH, an early acting oxygenase from the tetracenomycin gene cluster, intercepted the intermediate and led to the formation of premithramycinone H (**5**). These experiments provided vague, indirect conclusions on the role of MtmOII in MTM biosynthesis.[25] We were now able to isolate a novel shunt product directly from the M7OII mutant which gives unexpected new evidence of the role of MtmOII in mithramycin biosynthesis.

Analysis of the crude extract of the *S. argillaceus* M7OII mutant strain by HPLC/MS (Figure 1) showed the presence

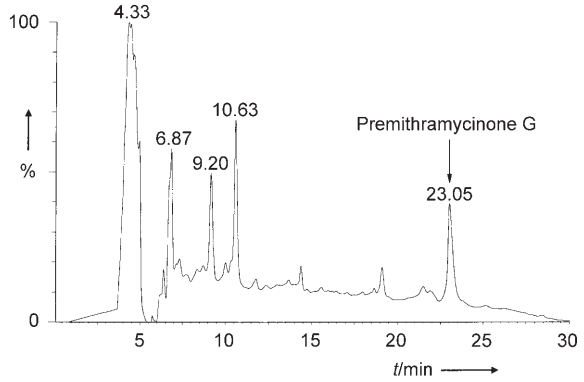


***Figure 1.*** HPLC/MS analysis of the crude extract of the M7OII mutant.

of a major product (which we later named premithramycinone G) with a UV spectrum significantly different from any known intermediate of the MTM biosynthesis. It is produced in amounts of 2.5 mg $L^{-1}$ and has a molecular weight of $M_r$ = 452 g $mol^{-1}$, based on the deprotonated molecular ion peak at $m/z$ = 451 in the negative mode APCI-MS spectrum. Its molecular weight was also confirmed by ESI-MS operated in the positive mode ($m/z$ 475 $[M+Na]^+$ and 453 $[M+H]^+$), and high-resolution EIMS ($m/z$ 452.3667, 8%; calcd 452.3671) revealed its molecular formula unambiguously as $C_{23}H_{16}O_{10}$.

The $^1$H NMR spectrum of premithramycinone G (Table 1) showed two *meta*-coupled aromatic protons at $\delta$ = 7.66 and 7.02 ppm as well as one singlet at $\delta$ = 8.61 ppm. Two groups of signals at $\delta$ = 3.38 and 3.21 ppm for one methylene group as well as two methyl groups at $\delta$ = 2.80 and 2.20 ppm were observed in the aliphatic region. The $^{13}$C NMR spectrum showed all 23 signals, of which 17 resulted from quaternary carbon atoms including 5 carbonyl groups ($\delta$ = 206.1, 199.1, 196.2, 188.2, and 183.3 ppm), while the aliphatic region showed only three methine, one methylene, and two methyl groups. Database searches gave no hits matching these NMR data and molecular weight. 2D NMR studies (HSQC and CIGAR-HMBC,[26,27] Scheme 2) finally revealed structure **4**

***Table 1:*** $^1$H and $^{13}$C NMR data as well as incorporation of [1,2-$^{13}C_2$]acetate data (* = enriched C atoms) of **4**.[a]

| Position | Premithramycinone G (**4**) | |
|---|---|---|
| | $\delta_H$ | $\delta_C$ |
| 1* | – | 77.4 (27.5) |
| 2* | – | 112.7 (30.1) |
| 3* | – | 186.4 (30.1) |
| 3a* | – | 121.3 (36.0) |
| 4* | – | 166.3 (36.0) |
| 4a* | – | 119.7 (28.0) |
| 5* | – | 188.2 (28.0) |
| 5a* | – | 111.8 (33.4) |
| 6* | – | 166.4 (33.4) |
| 7* | 7.02 (d, 1.80 Hz, 1H) | 109.9 (32.6) |
| 8* | – | 166.5 (32.6) |
| 9* | 7.66 (d, 1.80 Hz, 1H) | 109.0 (30.1) |
| 9a* | – | 137.5 (30.1) |
| 10* | – | 183.3 (35.2) |
| 10a* | – | 124.7 (35.2) |
| 11* | 8.61 (s, 1H) | 114.9 (31.4) |
| 11a* | – | 152.1 (31.4) |
| 1′* | – | 196.2 (27.5) |
| 2′ | 3.38, 3.21 (dd, 12.1 Hz, 2H) | 59.2 |
| 3′ | – | 206.1 |
| 4′ | 2.20 (s, 3H) | 31.2 |
| 1″* | – | 199.1 (29.3) |
| 2″* | 2.80 (s, 3H) | 32.9 (29.3) |

[a] 9.4 T, [$D_5$]pyridine; chemical shifts in ppm (multiplicity; $J$ in Hz; $J_{C,C}$ from the incorporation experiment with [1,2-$^{13}C_2$]acetate).

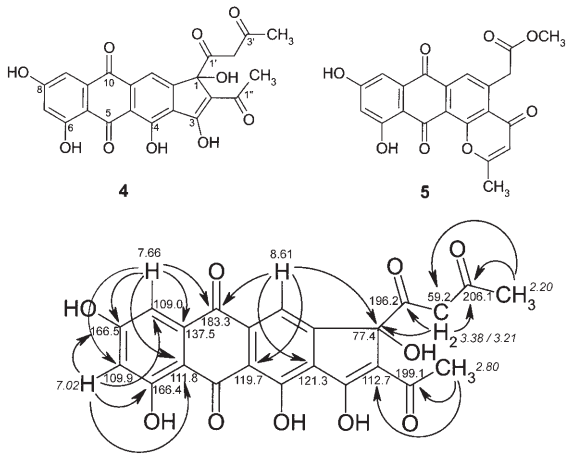


***Scheme 2.*** Top: Structures of premithramycinone G (**4**) and premithramycinone H (**5**); bottom: $^{2,3}J_{C,H}$ couplings observed in the HMBC spectrum of **4**.

for premithramycinone G, a novel molecule with an unprecedented framework derived from 1,3,4,6,8-pentahydroxy-1*H*-cyclopenta[*b*]anthracene-5,10-dione. In the HMBC spectrum, the singlet aromatic proton at $\delta$ = 8.61 ppm showed $^3J_{C,H}$ couplings with the carbon atoms at $\delta$ = 183.3, 121.3, 119.7, and 77.4 ppm. The other two aromatic protons in the *meta* positions at $\delta$ = 7.66 and 7.02 ppm, respectively, showed $^3J_{C,H}$ couplings with carbon signals at $\delta$ = 183.3, 111.8, and 109.9 ppm and with those at $\delta$ = 111.8 and 109.0 ppm. The position of the acyl group at C2 was confirmed by the $^3J_{C,H}$ coupling between the methyl protons at $\delta$ = 2.80 ppm

 © 2006 Wiley-VCH Verlag GmbH & Co. KGaA, Weinheim 

and the quaternary carbon atom at $\delta = 112.7$ ppm. The long-range correlation in the HMBC spectrum between the methylene group of the butane-2,4-dione side chain and the carbon atom at $\delta = 77.40$ ppm revealed the position of this side chain. Structure **4** and its $^{13}C$ NMR assignments were further confirmed by incorporation experiments with doubly $^{13}C$-labeled acetate.

Premithramycinone G (**4**) contains 23 carbon atoms, that is, 3 more than the decaketide-derived aglycon of MTM. Thus, **4** must be viewed as a dodecaketide-derived compound, which relates it to the group of benanomicin/pradimicin-type antifungal antibiotics.[28–34] However, an incorporation experiment with [1,2-$^{13}C$]acetate showed that only the first 10 acetate units of **4** were $^{13}C$-enriched, while 3 carbon atoms of the oxobutyryl side chain did not appear to be labeled (Scheme 3). These results may indicate that the three unlabeled carbon atoms derive either from another biosynthetic pool (for example, acetoacetate from incompletely degraded fatty acids) or are acetate-derived, but come in at a much later stage of the biosynthesis pathway, which was not (or no longer) affected by the exogenously fed $^{13}C$-labeled acetate—possibly after the closure of the first three rings of the molecule. Recently, Hertweck et al. also discussed a possible sequence for the biosynthesis of enterocin that envisions a cyclization reaction prior to further chain-elongation steps.[35]

The fact that this "dodecaketide"-derivative **4** accumulated upon inactivation of oxygenase MtmOII allows the conclusion to be drawn that MtmOII is somewhat involved in controling the chain length. Similar findings were very recently reported by Hunter and co-workers, who observed the accumulation of polyketide shunt products with altered chain lengths in the oxytetracycline pathway upon inactivation of oxygenase OtcC.[36] They concluded that OtcC is an essential partner of the polyketide synthase complex. Thus, it is possible that MtmOII contributes to controling the chain length in MTM biosynthesis by acting as an essential component of the PKS complex. In the absence of MtmOII, the correct regiospecificity in the cyclization step leading to the formation of the fourth ring is also disturbed, which likely occurs normally after α oxidation (possibly through MtmOI) followed by reduction by 2-oxoacyl-ACP reductase MtmTII. A similar role was also proposed by Li and Piel for GrhO2, an enzyme of the griseorhodin A pathway with 50% amino acid identity and 61% similarity to MtmTII.[37] Furthermore, the missing MtmOII might allow the ACP-bound ester carbonyl group to react with 3-oxobutyrate (in **6**, Scheme 3), which resembles the "lower" oxobutyryl side chain of the biosynthetic intermediate **7**, that is, its normal reaction partner (Scheme 3). Since *mtmTII* is located immediately downstream of *mtmOII*, it is also possible that its encoded ketoreductase was inactivated by a polar effect together with the inactivation of MtmOII. As a consequence, the newly introduced α-keto group can undergo the shunt aldol condensation leading to the five-membered ring found in **4**. This presumably spontaneous cyclization most likely happens after the chain elongation.

In the normal MTM biosynthesis it is likely that MtmOII catalyzes an epoxidation reaction either simultaneously with or shortly after the correct fourth cyclization to give the tetracyclic premithramycin framework. This reaction introduces the oxygen atom in the 2-position of **1** (= 12a-position of **2**); this oxygen atom is not found in either shunt pathway resulting from the inactivation of MtmOII. A possible mechanism for this is epoxidation followed by a reductive opening of the epoxide. A similar sequence of events was discussed in the context of the reaction cascade catalyzed by oxygenase TcmG in the biosynthesis of tetracenomycin C,[38]

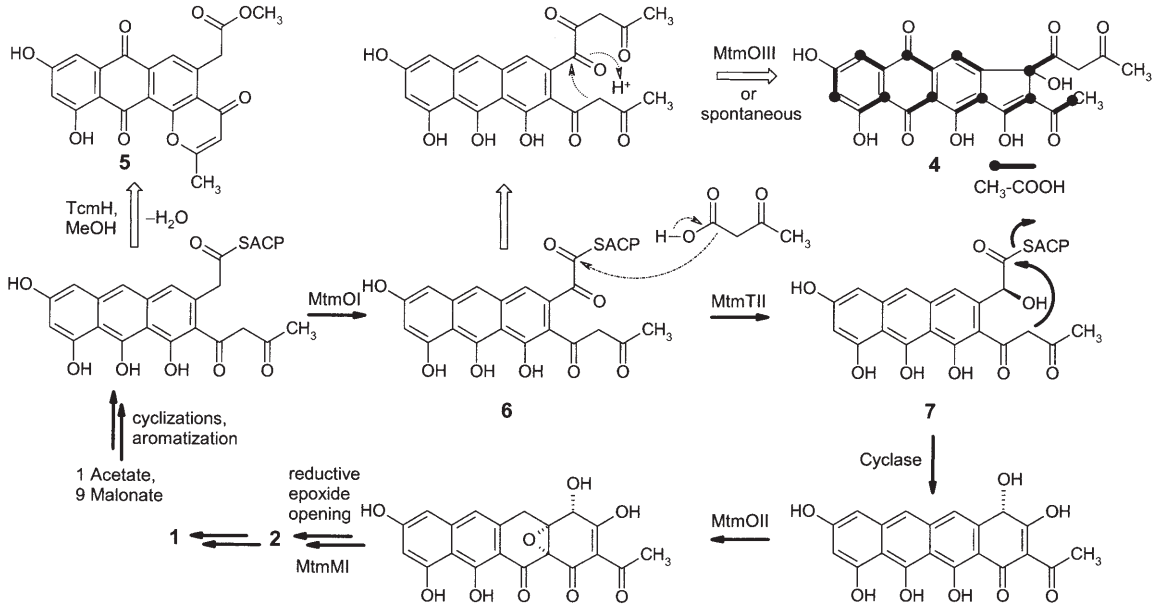


***Scheme 3.*** Hypothetical early pathway (thick black arrows) to MTM (**1**) and shunt pathways (open and dotted arrows) to **4** and **5** with the concluded hypothetical new roles of oxygenases MtmOI, MtmOII, and MtmOIII, as well as ketoreductase MtmTII. The structural formula of **4** shows the carbon enrichments after feeding MtmOII$^-$-mutant *S. argillaceus* M7OII with [1,2-$^{13}C_2$]acetate.

 © 2006 Wiley-VCH Verlag GmbH & Co. KGaA, Weinheim 

and can be proposed for the introduction of the tertiary alcohol function during the biosynthesis of tetracycline. The latter reaction may be catalyzed by oxygenase OxyL,[39] which shows 48% amino acid identity and 63% similarity to MtmOII. Finally, if MtmOII is a component of a multienzyme complex it may also prevent spontaneous cyclizations and the spontaneous or MtmOIII-catalyzed anthrone oxidation to give the anthraquinone shunt-products premithramycinone G (**4**) and H (**5**). These reactions only occur in the absence of MtmOII.

As mentioned previously, the oxidation pattern of **4** along with the role suggested here of MtmOII in the mithramycin biosynthetic pathway also allows first conclusions to be drawn regarding the roles of oxygenases MtmOI and MtmOIII, whose involvements in MTM biosynthesis have so far remained unclear. As shown in Scheme 3, it is necessary that one of these two enzymes, presumably MtmOI, oxidizes the carbon atom in the α-position to the acyl-ACP ester carbonyl group, which eventually becomes the O atom in the 1′-position of **1** (= 4-position of **2** and **3**, = 1-position of **4**). MtmOIII normally does not participate in MTM biosynthesis, but might however be responsible for the anthrone oxidations observed in the shunt pathways to **4** and **5** since MtmOIII shows high similarities to anthrone oxygenases, such as AknX (40% amino acid identity, 55% similarity to MtmOIII), involved in aklavinone biosynthesis[40] or HedQ (36% amino acid identity, 51% similarity), the anthrone oxygenase of the hedamycin biosynthesis.[41]

In summary, the inactivation of the *mtmOII* gene resulted in an unexpected metabolite, premithramycinone G (**4**), which we assume to be a shunt product of the biosynthetic pathway. The structure of the accumulated product suggests that **4** is derived from 10 acetate units, with 3 extra carbon atoms that are introduced either in the form of two extra malonyl-CoA extender units at a later biosynthetic stage (which is no longer affected by the feeding experiments with $^{13}$C-labeled acetate) or from a different source, for example, 3-oxobutyrate from incomplete fatty acid degradation. These shunt reactions are probably only possible because in the absence of MtmOII, control over both the chain length and the fourth cyclization reaction is lacking, in addition to a possibly impaired 2-oxoacyl-ACP reductase MtmTII. It can be suggested that in the biosynthesis of mithramycin the oxygen atom at the 1′-position of **1** (= 4-position in **2** and **3**) is likely introduced by MtmOI, while MtmOII—when present in a multienyzme complex—may: 1) help to control the correct chain length, 2) protect positions of tricyclic aromatic intermediates, such as **6** (Scheme 3), from unwanted anthrone oxidations, and 3) ensure correct regiochemical control of the fourth cyclization, besides its main function, namely, the introduction of the oxygen atom which ends up in the 2-position of MTM (= 12a-position in **2** and **3**).

## Experimental Section

The inactivation of *mtmOII* was achieved through a frameshift mutation, see Ref. [13]. For the instruments/NMR methods used, see Ref. [42]. The labeled sodium [1,2-$^{13}C_2$]acetate used in the incorporation experiment was obtained from Isotec (Miamisburg, OH, USA).

Production and isolation of **4**: A seed culture was prepared by using tryptone soya broth media inoculated with spores of *S. argillaceus* M7OII and incubated in an orbital shaker (24 h, 30 °C, 250 rpm). This seed culture was used to inoculate 50 Erlenmeyer flasks each containing 100 mL of R5A medium and was cultivated for 6 days. The culture broth was centrifuged (4200 rpm for 30 min), and then the solution adjusted to pH 5.0 with acetic acid and extracted repeatedly with ethyl acetate. The mycelia were extracted with acetone (4 × 0.5 L), and the extract was concentrated under reduced pressure. The resulting aqueous solution was extracted with ethyl acetate. The combined ethyl acetate extracts from the supernatants and mycelia were analyzed by HPLC-MS and concentrated under reduced pressure. The resulting crude extract was subjected to purification on Sephadex LH-20 (MeOH) to afford three fractions. All attempts to purify **4** by column chromatography on silica gel and preparative TLC failed because it decomposed. The middle fraction containing **4** was purified by preparative HPLC (column: μBondapak $C_{18}$ radial compression cartridge, PrepPak cartridge, 19 × 150 mm, Waters; eluent: acetonitrile and water (gradient from 35 to 100% in 43 min); flow rate: 10 mL min$^{-1}$).

Feeding experiment: A seed culture was prepared using TSB inoculated with spores of *S. argillaecus* M7OII. The culture was incubated in an orbital shaker at 30 °C for 24 h and 250 rpm. The seed culture was used to inoculate (at 2.5% v/v) 16 250-mL Erlenmeyer flasks, each containing 100 mL of modified R5 medium. After 24 h, the pulse feeding of [1, 2-$^{13}$C]sodium acetate was started and continued for 48 h at 12 h intervals (4 feedings for a total of 1 g of sodium acetate per liter of culture). The culture was then left for an additional 72 h before extraction. $^{13}$C-Labeled **4** was isolated as described above for the unlabeled compound.

Received: February 7, 2006
Published online: July 20, 2006

**Keywords:** aureolic acids · enzyme complexes · mithramycin · oxidoreductases · polyketides

[1] R. C. Snyder, R. Ray, S. Blume, D. M. Miller, *Biochemistry* **1991**, *30*, 4290 – 4291.
[2] A. S. Jaiswal, R. Balusu, S. Narayan, *Carcinogenesis* **2006**, *27*, 252 – 261.
[3] L. L. Remsing, H. R. Bahadori, G. M. Carbone, E. M. McGuffie, C. V. Catapano, J. Rohr, *Biochemistry* **2003**, *42*, 8313 – 8324.
[4] P. D. King, M. C. Perry, *Oncologist* **2001**, *6*, 162 – 176.
[5] J. P. Dutcher, D. Coletti, E. Paietta, P. H. Wiernik, *Leuk. Res.* **1997**, *21*, 375 – 380.
[6] N. Zojer, A. V. Keck, M. Pecherstorfer, *Drug Saf.* **1999**, *21*, 389 – 406.
[7] J. Hurtado, P. Esbrit, *Expert Opin. Pharmacother.* **2002**, *3*, 521 – 527.
[8] A. G. Hadjipavlou, L. N. Gaitanis, P. G. Katonis, P. Lander, *Eur. Spine J.* **2001**, *10*, 370 – 384.
[9] S. Chatterjee, K. Zaman, H. Ryu, A. Conforto, R. R. Ratan, *Ann. Neurol.* **2001**, *49*, 345.
[10] R. J. Ferrante, H. Ryu, J. K. Kubilus, S. D'Mello, K. L. Sugars, J. Lee, P. Lu, K. Smith, S. Browne, M. F. Beal, B. S. Kristal, I. G. Stavrovskaya, S. Hewett, D. C. Rubinsztein, B. Langley, R. R. Ratan, *J. Neurosci.* **2004**, *24*, 10335 – 10342.
[11] A. Liacini, J. Sylvester, W. Li, M. Zafarullah, *Arthritis Res. Ther.* **2005**, *7*, R777 – R783.
[12] E. Fibach, N. Bianchi, M. Borgatti, E. Prus, R. Gambari, *Blood* **2003**, *102*, 1276 – 1281.
[13] L. Prado, F. Lombó, A. F. Brana, C. Méndez, J. Rohr, J. A. Salas, *Mol. Gen. Genet.* **1999**, *261*, 216 – 225.

 © 2006 Wiley-VCH Verlag GmbH & Co. KGaA, Weinheim 

[14] J. Rohr, C. Méndez, J. A. Salas, *Bioorg. Chem.* **1999**, *27*, 41 – 54.
[15] M. J. Fernandez-Lozano, L. L. Remsing, L. M. Quiros, A. F. Braña, E. Fernandez, C. Sanchez, C. Méndez, J. Rohr, J. A. Salas, *J. Biol. Chem.* **2000**, *275*, 3065 – 3074.
[16] J. Rohr, U. Weissbach, C. Beninga, E. Künzel, K. Siems, K. Bindseil, L. Prado, F. Lombó, A. F. Braña, C. Méndez, J. A. Salas, *Chem. Commun.* **1998**, 437 – 438.
[17] M. Nur-e-Alam, C. Méndez, J. A. Salas, J. Rohr, *Chembiochem* **2005**, *6*, 632 – 636.
[18] E. Fernandez, U. Weissbach, C. Sanchez Reillo, A. F. Braña, C. Méndez, J. Rohr, J. A. Salas, *J. Bacteriol.* **1998**, *180*, 4929 – 4937.
[19] L. L. Remsing, J. Garcia-Bernardo, A. M. Gonzalez, E. Künzel, U. Rix, A. F. Braña, D. W. Bearden, C. Méndez, J. A. Salas, J. Rohr, *J. Am. Chem. Soc.* **2002**, *124*, 1606 – 1614.
[20] L. L. Remsing, A. M. Gonzalez, M. Nur-e-Alam, M. J. Fernandez-Lozano, A. F. Braña, U. Rix, M. A. Oliveira, C. Méndez, J. A. Salas, J. Rohr, *J. Am. Chem. Soc.* **2003**, *125*, 5745 – 5753.
[21] V. Albertini, A. Jain, S. Vignati, S. Napoli, A. Rinaldi, I. Kwee, M. Nur-e-Alam, J. Bergant, F. Bertoni, G. M. Carbone, J. Rohr, C. V. Catapano, *Nucleic Acids Res.* **2006**, *34*, 1721 – 1734.
[22] L. Prado, E. Fernandez, U. Weissbach, G. Blanco, L. M. Quirós, A. F. Braña, C. Méndez, J. Rohr, J. A. Salas, *Chem. Biol.* **1999**, *6*, 19 – 30.
[23] M. Gibson, M. Nur-e-alam, F. Lipata, M. A. Oliveira, J. Rohr, *J. Am. Chem. Soc.* **2005**, *127*, 17594 – 17595.
[24] U. Rix, C. Fischer, L. L. Remsing, J. Rohr, *Nat. Prod. Rep.* **2002**, *19*, 542 – 580.
[25] F. Lombó, E. Künzel, L. Prado, A. F. Braña, K. U. Bindseil, J. Frevert, D. Bearden, C. Méndez, J. A. Salas, J. Rohr, *Angew. Chem.* **2000**, *112*, 808 – 811; *Angew. Chem. Int. Ed.* **2000**, *39*, 796 – 799.
[26] V. V. Krishnamurthy, D. J. Russell, C. E. Hadden, G. E. Martin, *J. Magn. Reson.* **2000**, *146*, 232 – 239.
[27] W. F. Reynolds, R. G. Enriquez, *J. Nat. Prod.* **2002**, *65*, 221 – 244.
[28] S. Gomi, M. Sezaki, M. Hamada, S. Kondo, T. Takeuchi, *J. Antibiot.* **1989**, *42*, 1145 – 1150.
[29] S. Kakinuma, K. Suzuki, M. Hatori, K. Saitoh, T. Hasegawa, T. Furumai, T. Oki, *J. Antibiot.* **1993**, *46*, 430 – 440.
[30] T. Tsuno, H. Yamamoto, Y. Narita, K. Suzuki, T. Hasegawa, S. Kakinuma, K. Saitoh, T. Furumai, T. Oki, *J. Antibiot.* **1993**, *46*, 420 – 429.
[31] T. Furumai, S. Kakinuma, H. Yamamoto, N. Komiyama, K. Suzuki, K. Saitoh, T. Oki, *J. Antibiot.* **1993**, *46*, 412 – 419.
[32] T. S. Lee, C. Khosla, Y. Tang, *J. Am. Chem. Soc.* **2005**, *127*, 12254 – 12262.
[33] F. Hiramoto, N. Nomura, T. Furumai, Y. Igarashi, T. Oki, *Biosci. Biotechnol. Biochem.* **2005**, *69*, 238 – 241.
[34] T. Oki, Y. Yamazaki, T. Furumai, Y. Igarashi, *Biosci. Biotechnol. Biochem.* **1997**, *61*, 1408 – 1410.
[35] C. Hertweck, L. Xiang, J. A. Kalaitzis, Q. Cheng, M. Palzer, B. S. Moore, *Chem. Biol.* **2004**, *11*, 461 – 468.
[36] N. Perić-Concha, B. Borovicka, P. F. Long, D. Hranueli, P. G. Waterman, I. S. Hunter, *J. Biol. Chem.* **2005**, *280*, 37455 – 37460.
[37] A. Li, J. Piel, *Chem. Biol.* **2002**, *9*, 1017 – 1026.
[38] E. R. Rafanan, Jr., C. R. Hutchinson, B. Shen, *Org. Lett.* **2000**, *2*, 3225 – 3227.
[39] I. S. Hunter, R. A. Hill in *Biotechnology of Antibiotics* (Ed.: W. R. Strohl), Marcel Decker, New York, **1997**, p. 659.
[40] J. Y. Chung, I. Fujii, S. Harada, U. Sankawa, Y. Ebizuka, *J. Bacteriol.* **2002**, *184*, 6115 – 6122.
[41] T. Bililign, C.-G. Hyun, J. S. Williams, A. M. Czisny, J. S. Thorson, *Chem. Biol.* **2004**, *11*, 959 – 969.
[42] L. Zhu, B. Ostash, U. Rix, E. A. M. Nur, A. Mayers, A. Luzhetskyy, C. Mendez, J. A. Salas, A. Bechthold, V. Fedorenko, J. Rohr, *J. Org. Chem.* **2005**, *70*, 631 – 638.

 © 2006 Wiley-VCH Verlag GmbH & Co. KGaA, Weinheim 

Coordination Polymers

DOI: 10.1002/anie.200601546

# Reversible Formation of Polymeric Chains by Coordination of Pentaphosphaferrocene with Silver(I) Cations**

*Manfred Scheer,* Laurence J. Gregoriades, Alexander V. Virovets, Werner Kunz, Roland Neueder, and Ingo Krossing*

One of the most exciting areas of contemporary chemical research involves the self-organization of discrete units to form supramolecular aggregates and networks.[1] Typically, N- and O-donor-containing ligands are used to connect different metal centers, but our strategy is to employ $P_n$- and $As_n$-ligand complexes as connecting moieties. We have already shown that the tetrahedrane complex $[\{CpMo(CO)_2\}_2(\mu,\eta^2\text{-}P_2)]$ ($Cp = C_5H_5$) is an efficient building block for the formation of oligomers and polymers with $Ag^I$[2] and $Cu^I$ salts[2,3] and that the solid-state structure of the product depends on the coordinating potential of the anion.[2] Furthermore, the pentaphosphaferrocenes $[Cp^xFe(\eta^5\text{-}P_5)]$ ($Cp^x = C_5Me_5$ (Cp*), $C_5Me_4Et$) form 1D and 2D polymers[4] as well as spherical fullerene-like aggregates[5,6] upon reaction with $Cu^I$ halides. More recently, we were able to demonstrate the capacity of $[Cp^*Mo(CO)_2(\eta^3\text{-}As_3)]$ to act as a supramolecular ligand.[7]

The coordinating potential of the halogen atoms in $Cu^I$ halides is crucial in determining the structure of the supramolecular aggregates resulting from reactions with $[Cp^*Fe(\eta^5\text{-}P_5)]$ (**1**). We therefore became interested in exploring the reactivity of **1** with salts of weakly coordinating anions, and first attempts with $CuPF_6$ and $Ag[O_3SCF_3]$ led to the immediate formation of amorphous solids. Use of the $Ag^I$ salt of the weakly coordinating anion $[Al\{OC(CF_3)_3\}_4]^-$,[8]

[*] Prof. Dr. M. Scheer, Dr. L. J. Gregoriades
Institut für Anorganische Chemie
Universität Regensburg
93040 Regensburg (Germany)
Fax: (+49) 941-943-4439
E-mail: mascheer@chemie.uni-regensburg.de
Dr. A. V. Virovets
Nikolaev Institute of Inorganic Chemistry
Siberian Division of RAS
Acad. Lavrentyev str. 3, Novosibirsk 630090 (Russia)
Prof. Dr. W. Kunz, Dr. R. Neueder
Institut für Physikalische und Theoretische Chemie
Universität Regensburg
93040 Regensburg (Germany)
Prof. Dr. I. Krossing
Institut für Anorganische und Analytische Chemie
Albert-Ludwigs Universität Freiburg
79104 Freiburg (Germany)

[**] This work was comprehensively supported by the Deutsche Forschungsgemeinschaft and the Fonds der Chemischen Industrie.

Supporting information for this article is available on the WWW under http://www.angewandte.org or from the author.

 © 2006 Wiley-VCH Verlag GmbH & Co. KGaA, Weinheim 

however, provided us with a breakthrough in this field. We report herein the synthesis and the structural features of an unprecedented silver complex, the 1D polymer $[Ag\{Cp^*Fe(\eta^5{:}\eta^2{:}\eta^1\text{-}P_5)\}_2]_n[Al\{OC(CF_3)_3\}_4]_n$ (**2**), which shows a novel 1,2,3-coordination mode of the *cyclo*-$P_5$ moiety in the solid state and unexpected dynamic behavior in solution.

Polymer **2** was prepared by the reaction of **1** with $Ag[Al\{OC(CF_3)_3\}_4]$ in $CH_2Cl_2$ and can be crystallized in the form of dark brown needles either from concentrated $CH_2Cl_2$ solutions or from a $CH_2Cl_2$/hexane mixture. The crystals were structurally characterized by X-ray diffraction analysis[9] and are indefinitely stable under an inert atmosphere at ambient conditions. Compound **2** is light-sensitive and is readily soluble in solvents like $CH_2Cl_2$ and THF, moderately soluble in toluene and acetone, sparingly soluble in $CH_3CN$, and insoluble in alkanes.

The structure of the linear polycationic chain of **2** (Figure 1) consists of $Ag^I$ cations that are doubly bridged by

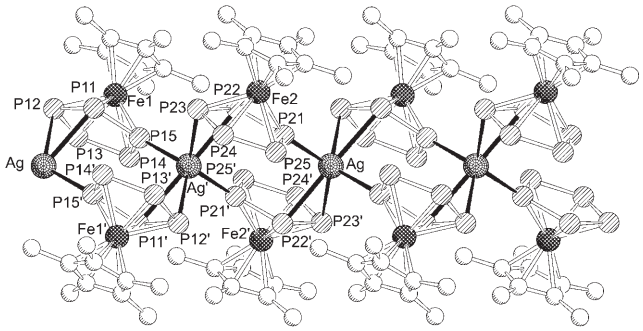


***Figure 1.*** Portion of the cationic chain of **2** in the solid state (hydrogen atoms are omitted for clarity). Selected bond lengths [Å] and angles [°]: P11-P12 2.156(4), P11-P15 2.124(4), P12-P13 2.141(4), P13-P14 2.112(4), P14-P15 2.111(4), P21-P22 2.118(4), P21-P25 2.110(4), P22-P23 2.155(4), P23-P24 2.129(4), P24-P25 2.107(5), Ag-P11 2.824(3), Ag-P12 2.758(2), Ag-P15′ 2.590(2), Ag-P21 2.615(3), Ag-P22′ 2.775(3), Ag-P23′ 2.809(3); P11-Ag-P12 45.41(8), P11-Ag-P15′ 83.05(8), P11′-Ag′-P21′ 97.96(8), P11′-Ag′-P22 171.86(8), P11′-Ag′-P23 127.11(9), P12-Ag-P15′ 125.75(8), P12′-Ag′-P21′ 98.76(8), P12′-Ag′-P22 128.29(8), P12′-Ag′-P23 99.78(9), P15-Ag′-P21′ 105.06(9), P15-Ag′-P22 100.89(8), P15-Ag′-P23 100.34(9), P21-Ag-P22′ 87.96(9), P21-Ag-P23′ 130.43(9), P22-Ag′-P23 45.39(8).

the *cyclo*-$P_5$ units of two molecules of **1** in a novel 1,2,3-coordination mode.[10] Until now, only NMR spectroscopic evidence of $\eta^2{:}\eta^1$ coordination of the *cyclo*-$P_5$ ligand was available.[11] Each $Ag^I$ cation in **2** is tetrahedrally coordinated to six phosphorus atoms of four *cyclo*-$P_5$ moieties through a side-on and an end-on coordination mode. To the best of our knowledge, such a homoleptic silver–phosphorus complex is the first of its kind to be observed. Owing to the unusual tetrahedral coordination, the polymer core may be formally viewed as being built up of a chain of six-membered $Ag_2P_4$ rings. Only alternate rings are identical, and each of these rings is fused to two three-membered $AgP_2$ rings through two opposite Ag–P edges. The lengths of the P–P bonds in the $Ag_2P_4$ rings (P11–P15 2.124(5) Å, P21–P22 2.118(4) Å) are essentially consistent with those of the uncoordinated complex **1**, as determined crystallographically in our group (2.116(2)–2.127(2) Å; further crystallographic details reported in reference [9]), and by electron diffraction (2.117(4) Å).[12] In contrast, the P–P bond lengths of the formal $AgP_2$ rings (P11–P12 2.156(4) Å, P22–P23 2.155(4) Å) are markedly larger, as would be expected owing to the π-coordination mode. The uncoordinated P–P edges directly adjacent to those of the $AgP_2$ rings are also somewhat elongated (P12–P13 2.141(4) Å, P23–P24 2.129(4) Å).

In view of the solid-state structure of **2**, we were surprised by the fact that in the $^{31}P$ NMR spectrum of **2** in $CD_2Cl_2$ at ambient temperature only one singlet at $\delta = 154.2$ ppm is detected. This signal is shifted slightly upfield relative to uncoordinated **1**, and no coupling to the $^{107/109}Ag$ nuclei is exhibited. As ESI-MS and vapor pressure osmometric (VPO) measurements have demonstrated, the polymer dissolves in $CH_2Cl_2$ by depolymerization to the monomer $[Ag\{Cp^*Fe(\eta^5\text{-}P_5)\}_2][Al\{OC(CF_3)_3\}_4]$ (**3**). Furthermore, dissolution in the more polar solvent $CH_3CN$ appears to lead to the formation of cationic species of even lower molecular mass, as indicated by the fragments $[Ag\{Cp^*Fe(\eta^5\text{-}P_5)\}(CH_3CN)_n]^+$ ($n = 0$, 1) observed by ESI-MS. Moreover, the simplicity of the $^{31}P$ NMR spectrum measured in $CD_2Cl_2$ at room temperature suggests dynamic behavior of the monomer **3**. At −90 °C the singlet splits into two broad signals at $\delta = 150.9$ and 123.2 ppm with an integration ratio of about 1:1 and no detectable $^{107/109}Ag$ satellites. In comparison to the $^{31}P$ NMR chemical shift of the free complex **1**, one would expect that the signals of the coordinated P atoms are shifted upfield. However, it is uncertain whether the monomeric species **3** is present exclusively in solution at this temperature, and whether higher aggregates such as the dimer $[Ag_2\{Cp^*Fe(\eta^5\text{-}P_5)\}_4][Al\{OC(CF_3)_3\}_4]_2$ (**4**) are already at hand.

To shed light on this dynamic behavior and the low-temperature $^{31}P$ NMR spectra, the structures of the monocation **I** in monomer **3** and the dication **II** in dimer **4** were calculated by density functional theory (DFT) methods. The calculations have shown that the structure of lowest energy for the cation **I** is a $\eta^2{:}\eta^2$-coordinated complex (Figure 2). At least four structures (**IIa**–**d**) that are within 16 kJ mol$^{-1}$ of each other could be localized on the potential energy surface (PES) of the dication, and only the two structures of lowest energy (**IIa** and **IIb**) are illustrated in Figure 2. Interestingly, the *cyclo*-$P_5$ moieties of the bridging units of **1** in the dication of lowest energy (**IIa**) are found in a 1,2,4- rather than the 1,2,3-coordination mode that was observed experimentally in the solid state. Furthermore, the energy difference between **I** and **IIa** is small (calculated enthalpy of dissociation of **IIa** to **I**: 2 kJ mol$^{-1}$ (25 °C), 10 kJ mol$^{-1}$ (−78 °C), 12 kJ mol$^{-1}$ (−90 °C)), and therefore one could predict that dynamic exchange should be facile in solution.

To test whether the results of the DFT calculations are reasonable, we assessed the thermodynamics of the formation of the cation **I** from $[Ag(CH_2Cl_2)_3]^+$ and complex **1** (Table 1). In agreement with the experiment one can conclude from Equation (1a) (Table 1) that the formation of **I** is favorable both in the gas phase and in solution. From Equation (1b) (Table 1) it also follows that **1** is a stronger ligand than $P_4$[13] (for comments on the importance of dispersive interactions, see the Supporting Information).

 © 2006 Wiley-VCH Verlag GmbH & Co. KGaA, Weinheim 

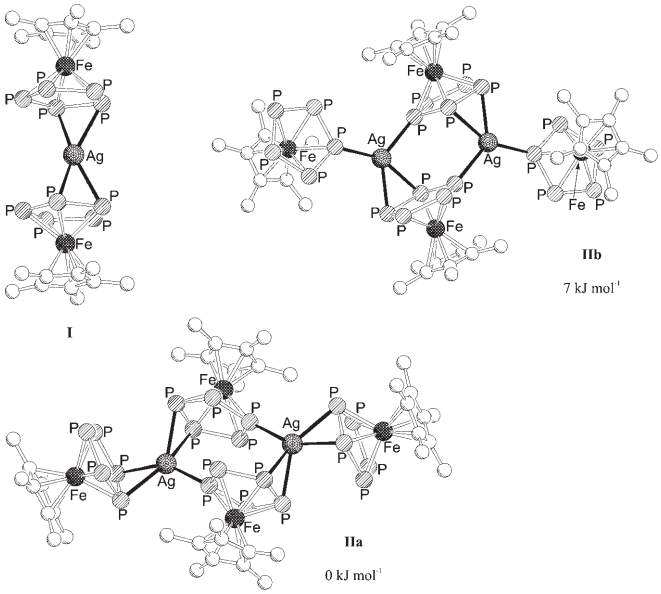


***Figure 2.*** Minimum structures of the monomeric cation in **3** (**I**) and the two most stable isomers of the dimeric dication in **4** (**IIa** and **IIb**).

***Table 1:*** Calculated energetics of the formation of $[Ag(L)_2]^+$.

| Reaction (1) $[Ag(CH_2Cl_2)_3]^+ + 2\,L \rightarrow [Ag(L)_2]^+ + 3\,CH_2Cl_2$ | $\Delta_r H(g)$ [kJ mol$^{-1}$] | $\Delta_r G°(g)$ [kJ mol$^{-1}$] | $\Delta_r G°(CH_2Cl_2)$ [kJ mol$^{-1}$] |
|---|---|---|---|
| a) L = {Cp*Fe($\eta^5$-$P_5$)}, (RI−)BP86/SV(P) | −121 | −153 | −103 |
| b) L = $P_4$; (RI−)BP86/SV(P) | 16 | −26 | −51 |

The variable-temperature $^{31}$P NMR spectra are best interpreted by considering the equilibria illustrated in Scheme 1. According to VPO data only the monomer **3**, and thus the monocation **I**, is present in $CH_2Cl_2$ solutions of the polymer **2** at room temperature, and the equilibrium can be seen as being entirely in favor of **I**. If, at room temperature, **I** existed in solution as depicted in Figure 2, one would expect at least two broad signals in the $^{31}$P NMR spectrum with an approximate integration ratio of 2:3, as four P atoms are coordinated and six are not, but only a sharp singlet is observed at this temperature. This observation is not surprising since the calculations have revealed that several structures of similar energy are possible for **I**. One would thus expect fast exchange between these structures in solution on the NMR time scale. This exchange may alternatively be viewed as fast rotation of the *cyclo*-$P_5$ moieties in **I**, which would render all P atoms equivalent. At low temperature, splitting of the signal is observed, but the new signals are in an approximate integration ratio of 1:1 and not 2:3.

The $^{31}$P NMR chemical shifts for **I**, **IIa**, and **IIb** have been calculated (see the Supporting Information), and the average chemical shifts for each species are listed in Table 2. This was deemed as a valid procedure since the aforementioned low energy differences for **I** and **II** would be expected to facilitate fast exchange processes, which would in turn render all P atoms within a species equivalent. These exchange processes are probably best viewed as fast rotation of the *cyclo*-$P_5$ moieties in the respective cations. For **I**, average $^{31}$P NMR chemical shifts of $\delta = 159/166$ ppm were calculated, which are comparable to that observed experimentally at room temperature (154.2 ppm). For **IIa** and **IIb**, values of $\delta = 149/157$ and 127/132 ppm, respectively, were calculated, and after consideration of the experimental spectra at −90 °C, which exhibit

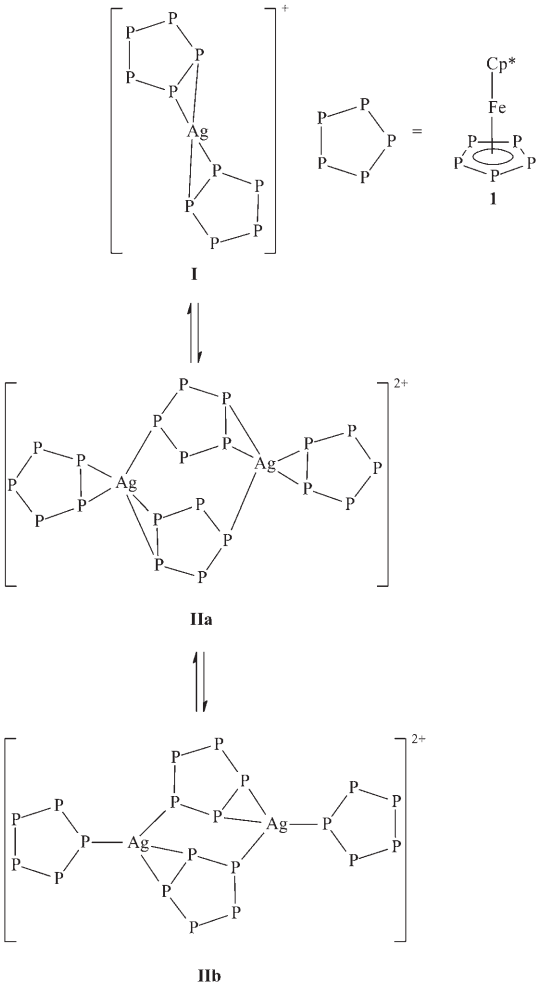


***Scheme 1.*** Proposed cation equilibria in solutions of **2**.

***Table 2:*** Average values of the DFT-calculated $^{31}$P NMR chemical shifts of **I**, **IIa**, and **IIb**.

| | I | | IIa | | IIb | |
|---|---|---|---|---|---|---|
| | SV(P)[a] | TZVPP[b] | SV(P)[a] | TZVPP[b] | SV(P)[a] | TZVPP[b] |
| all P atoms | 159 | 166 | 149 | 157 | 127 | 132 |
| coordinated P atoms | 125 | 133 | 128 | 139 | 88 | 97 |
| uncoordinated P atoms | 182 | 188 | 170 | 175 | 147 | 147 |

[a] BP86 with the SV(P) basis set for all atoms except Ag, for which the SVPalls2 all-electron basis set optimized for NMR calculations was used. [b] BP86 with the TZVPP basis set for all atoms except Ag, for which the TZVPPalls2 all-electron basis set optimized for NMR calculations was used.

 © 2006 Wiley-VCH Verlag GmbH & Co. KGaA, Weinheim 

two signals at $\delta = 150.9$ and 123.2 ppm in an approximate 1:1 integration ratio, one could postulate the existence of an equilibrium between **IIa** and **IIb** at this temperature. However, the presence of **I** at low temperature cannot be ruled out since its average chemical shift is essentially the same as that of **IIa** and the energy difference between **I** and **IIa** is small. The existence of all three of these cations, and perhaps even larger aggregates as well, is likely at low temperature. Moreover, the appearance of the spectra is most probably determined by rotational motion of the *cyclo*-$P_5$ units in the proposed cations, which is fast at room temperature and slow at low temperatures, rather than by monomer/dimer/oligomer equilibria.

To understand why the polymer **2**, rather than the monomer **3**, is formed in the solid state, it is useful to consider the Born–Haber cycle in Scheme 2. In solution, even

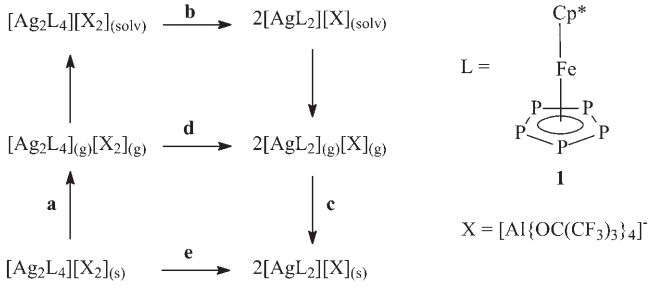


**a**: $-\Delta H_{Latt}$

**b**: $\Delta H_{Diss} = 2.0$ kJ mol$^{-1}$ (25 °C)
$= 10.0$ kJ mol$^{-1}$ (-78 °C)
$= 12.0$ kJ mol$^{-1}$ (-90 °C)
} (COSMO/BP86/SV(P))
$\Delta G_{Diss} < 0$ kJ mol$^{-1}$

**c**: $\Delta H_{Latt}$

**d**: $\Delta H_{Diss} = -108$ kJ mol$^{-1}$ (BP86/SV(P))

**e**: $\Delta G_{Diss} > 0$ kJ mol$^{-1}$

***Scheme 2.*** Born–Haber cycle for the oligomeric system.

though oligomerization is enthalpically slightly favored, particularly at lower temperatures,[14] the effect of entropy outweighs the enthalpic effect, and **2** thus dissolves by complete depolymerization. In the solid state, however, entropic effects are insignificant and lattice enthalpy gains the upper hand, which leads to crystallization of the polymer. This strange behavior is most likely a result of the low lattice energy of **2** which is induced by the large size of the $[Al\{OC(CF_3)_3\}_4]^-$ anion (diameter 1.25 nm, volume 0.758 nm$^3$).[15]

The results have shown that in combination with the $Ag^I$ salt of the weakly coordinating anion $[Al\{OC(CF_3)_3\}_4]^-$ the *cyclo*-$P_5$ ligand complex **1** is able to form the novel 1D polymer **2**. The backbone of this polymer consists of Ag cations and *cyclo*-$P_5$ rings in an unprecedented $\eta^2$:$\eta^1$-(1,2,3)-coordination mode of the *cyclo*-$P_5$ rings, whereby each Ag atom is tetrahedrally coordinated to six P atoms. Complex **2** dissolves by depolymerization to the monomer **3** in $CH_2Cl_2$, as demonstrated by ESI-MS and VPO measurements. Furthermore, solution $^{31}$P NMR measurements down to −90 °C have revealed dynamic behavior, such that a dynamic equilibrium exists between the monocation and polycation. This equilibrium is exclusively in favor of the monocation at room temperature and begins to shift in favor of the di/polycation at low temperature. The isolation of **2** further confirms the potential of **1** as a building block for novel self-assemblies.

## Experimental Section

All manipulations were performed in an atmosphere of dry nitrogen using standard glove-box and Schlenk techniques. All solvents were freshly distilled from appropriate drying agents immediately prior to use. Compound **1**[16] and $Ag[Al\{OC(CF_3)_3\}_4]$[8] were synthesized according to the literature procedures. IR spectra were recorded on a Varian FTS 800 spectrometer. Solution NMR spectra were acquired on a Bruker Avance spectrometer at either 400 or 600 MHz. ESI-MS spectra were measured on a Finnigan Thermoquest TSQ 7000 mass spectrometer. VPO measurements were performed on a Knauer K-7000 vapor pressure osmometer.

All theoretical calculations were performed with the TURBOMOLE program package.[17] The 28 electron cores of Ag were replaced by a quasirelativistic effective core potential.[18] All species were fully optimized at the BP86/SV(P) level.[19] Approximate solvation energies were calculated with the COSMO model[20] at the BP86/SV(P) level. Frequency calculations were performed for all species and structures (except for **II**, which is too large for the frequency calculation) to check that true minima without imaginary frequencies were found on the respective hypersurface.[21] NMR shifts at the BP86/TZVPP level (Ag: TZVPPalls2 all-electron basis set optimized for NMR calculations)[22] were calculated as single points on the BP86/SV(P)-optimized geometries. All calculated chemical shifts, together with machine-readable *xyz* orientations of the calculated structures and the calculated vibrational frequencies, are included in the Supporting Information.

**2**: A solution of **1** (100 mg, 0.29 mmol) and $Ag[Al\{OC(CF_3)_3\}_4]\cdot CH_2Cl_2$ (168 mg, 0.14 mmol) in $CH_2Cl_2$ (20 mL) was stirred at room temperature for 12 h in the dark. The solution was then filtered over diatomaceous earth, which was subsequently washed with $CH_2Cl_2$ (2 × 3 mL). The combined filtrate and washings were reduced in volume to about 5 mL under vacuum and stored at −30 °C. Crystals of $\mathbf{2}\cdot n\,CH_2Cl_2$ appeared within a week in the form of dark brown needles. The crystals were filtered, washed with pentane, and dried in vacuum to yield 128 mg of solvent-free **2**.[23] Addition of an equal volume of pentane to the mother liquor led to the isolation of a further crop of **2** (94 mg). Yield: 222 mg, 87 %; m.p. 196–204 °C (decomp); IR (KBr): $\tilde{\nu} = 2967$ (w), 2921 (w), 1617 (w), 1599 (w), 1480 (m), 1450 (m), 1429 (m), 1380 (m), 1354 (s), 1304 (s), 1278 (s), 1242 (s), 1219 (s), 1166 (s), 1101 (m), 1074 (m), 1021 (m), 974 (s), 862 (w), 828 (m), 820 (m), 756 (w), 727 (s), 560 (w), 537 (m), 443 (m) cm$^{-1}$; IR ($CH_2Cl_2$): $\tilde{\nu} = 1478$ (w), 1428 (w), 1377 (w), 1352 (w), 1300 (w), 1278 (m), 1272 (m), 1241 (m), 1224 (m), 1167 (w), 1022 (w), 976 (m), 730 (s), 561 (w), 537 (w), 445 (w) cm$^{-1}$; $^1$H NMR (600.13 MHz, $CD_2Cl_2$, 27 °C): $\delta = 1.38$ ppm (s, $CH_3$); $^{13}$C{$^1$H} NMR (150.90 MHz, $CD_2Cl_2$, 27 °C): $\delta = 121.64$ (q, $CF_3$, $^1J$(C,F) = 293 Hz), 95.41 (s, $C_5(CH_3)_5$), 79.37 (br, $OC(CF_3)_3$), 11.11 ppm (s, $CH_3$); $^{27}$Al{$^1$H}-NMR (104.26 MHz, $CD_2Cl_2$, 27 °C): $\delta = 33.63$ ppm (s, $[Al\{OC(CF_3)_3\}_4]^-$); $^{19}$F NMR (376.50 MHz, $CD_2Cl_2$, 27 °C): $\delta = -75.61$ ppm (s, $CF_3$); $^{31}$P{$^1$H} NMR (162.02 MHz, $CD_2Cl_2$, 27 °C): $\delta = 153.5$ ppm; ESI-MS ($CH_2Cl_2$): *m*/*z* (%): 798.8 (100) $[Ag\{Cp^*Fe(\eta^5\text{-}P_5)\}_2]^+$; ESI-MS ($CH_3CN$): *m*/*z* (%): 798.9 (100) $[Ag\{Cp^*Fe(\eta^5\text{-}P_5)\}_2]^+$, 493.9 (20) $[Ag\{Cp^*Fe(\eta^5\text{-}P_5)\}(CH_3CN)]^+$, 452.9 (15) $[Ag\{Cp^*Fe(\eta^5\text{-}P_5)\}]^+$;

 © 2006 Wiley-VCH Verlag GmbH & Co. KGaA, Weinheim 

molecular mass ($g\,mol^{-1}$) calcd for $[Ag\{Cp^*Fe(\eta^5\text{-}P_5)\}_2][Al\{OC(CF_3)_3\}_4]$: 1768, found (osmometric, $CH_2Cl_2$, 28 °C): 1725. Elemental analysis (%) calcd for $C_{36}H_{30}AgAlF_{36}Fe_2O_4P_{10}$: C 24.47, H 1.71; found: C 24.53, H 1.71.

Received: April 19, 2006
Published online: July 24, 2006

**Keywords:** coordination polymers · density functional calculations · phosphorus · silver · structure elucidation

[1] Recent review articles: a) N. C. Gianneschi, M. S. Masar III, C. A. Mirkin, *Acc. Chem. Res.* **2005**, *38*, 825 – 837; b) M. Ruben, J. Rojo, F. J. Romero-Salguero, L. H. Uppadine, J.-M. Lehn, *Angew. Chem.* **2004**, *116*, 3728 – 3747; *Angew. Chem. Int. Ed.* **2004**, *43*, 3644 – 3662; c) L. Carlucci, G. Ciani, D. M. Proserpio, *Coord. Chem. Rev.* **2003**, *246*, 247 – 289; d) G. F. Swiegers, T. J. Malefetse, *Coord. Chem. Rev.* **2002**, *225*, 91 – 121; e) B. J. Holliday, C. A. Mirkin, *Angew. Chem.* **2001**, *113*, 2076 – 2097; *Angew. Chem. Int. Ed.* **2001**, *40*, 2022 – 2043; f) S. Leininger, B. Olenyuk, P. J. Stang, *Chem. Rev.* **2000**, *100*, 853 – 908.

[2] J. Bai, E. Leiner, M. Scheer, *Angew. Chem.* **2002**, *114*, 820 – 823; *Angew. Chem. Int. Ed.* **2002**, *41*, 783 – 786.

[3] M. Scheer, L. Gregoriades, J. Bai, M. Sierka, G. Brunklaus, H. Eckert, *Chem. Eur. J.* **2005**, *11*, 2163 – 2169.

[4] J. Bai, A. V. Virovets, M. Scheer, *Angew. Chem.* **2002**, *114*, 1808 – 1811; *Angew. Chem. Int. Ed.* **2002**, *41*, 1737 – 1740.

[5] J. Bai, A. V. Virovets, M. Scheer, *Science* **2003**, *300*, 781 – 783.

[6] M. Scheer, J. Bai, B. P. Johnson, R. Merkle, A. V. Virovets, C. E. Anson, *Eur. J. Inorg. Chem.* **2005**, 4023 – 4026.

[7] L. J. Gregoriades, H. Krauss, J. Wachter, A. V. Virovets, M. Sierka, M. Scheer, *Angew. Chem.* **2006**, *118*, 4295 – 4298; *Angew. Chem. Int. Ed.* **2006**, *45*, 4189 – 4192.

[8] I. Krossing, *Chem. Eur. J.* **2001**, *7*, 490 – 502.

[9] The crystal structure analyses of **1** (crystallized from a concentrated $CH_2Cl_2$ solution at −30 °C) and **2** were performed on an STOE IPDS diffractometer with $Mo_{K\alpha}$ radiation ($\lambda$ = 0.71073 Å). The structures were solved by direct methods with the program SIR-97[24] (**1**) or SHELXS-97[25a] (**2**), and full-matrix least-squares refinement on $F^2$ in SHELXL-97[25b] was performed with anisotropic displacements for non-H atoms. Hydrogen atoms were located in idealized positions and refined isotropically according to the riding model. The $[Al(OC(CF_3)_3)_4]^-$ anion usually has a strong tendency to be rotationally disordered in two different ways: a) rotation of $CCF_3$ around the C–C bond, b) rotation of whole $OC(CF_3)_3$ group around the O–C bond. In the structure of **2** we observed both effects. Elongation of thermal ellipsoids of C11, C12, and C13 indicates the rotational disorder of type (b). At the same time, almost all of the ellipsoids of the fluorine atoms are elongated, thus showing disorder of type (a). As a result we had to constrain some C–F and C1–C13 distances to their normal values (1.35 and 1.45 Å, respectively) by using the DFIX option in the SHELXL-97 program. This led to a somewhat elevated $wR_2$ value. **1**: $C_{10}H_{15}FeP_5$, $M_r$ = 345.92, crystal dimensions 0.44 × 0.38 × 0.16 $mm^3$, monoclinic, space group $P2_1/n$ (No. 14), $a$ = 9.044(1), $b$ = 13.878(2), $c$ = 11.860(1) Å, $\beta$ = 97.07(1)°, $T$ = 123(1) K, $Z$ = 4, $V$ = 1477(1) $Å^3$, $\rho_{calcd}$ = 1.556 $Mg\,m^{-3}$, $\mu$ = 1.534 $mm^{-1}$, 20374 reflections collected, 2749 unique reflections ($R_{int}$ = 0.1628, $2\theta_{max}$ = 52°), 145 parameters, $R_1$ = 0.0556, $wR_2$ = 0.1540. **2**·$(CH_2Cl_2)_n$: $C_{37}H_{32}AgAlCl_2F_{36}Fe_2O_4P_{10}$, $M_r$ = 1851.78, crystal dimensions 0.20 × 0.14 × 0.04 $mm^3$, monoclinic, space group $P2_1/n$ (No. 14), $a$ = 10.524(2), $b$ = 32.471(7), $c$ = 18.221(4) Å, $\beta$ = 90.31(3)°, $T$ = 150(1) K, $Z$ = 4, $V$ = 6226(2) $Å^3$, $\rho_{calcd}$ = 1.975 $Mg\,m^{-3}$, $\mu$ = 1.275 $mm^{-1}$, 44498 reflections collected, 11596 unique reflections ($R_{int}$ = 0.1176, $2\theta_{max}$ = 52°), 839 parameters, $R_1$ = 0.0954, $wR_2$ = 0.2534. CCDC-604488 (**1**) and 604433 (**2**) contain the supplementary crystallographic data for this paper. These data can be obtained free of charge from The Cambridge Crystallographic Data Centre via www.ccdc.cam.ac.uk/data_request/cif.

[10] Previously, we were able to demonstrate 1,2-, 1,2,4-, and 1,2,3,4,5-coordination of the *cyclo*-$P_5$ ligand in the solid state (references [4–6]).

[11] a) G. Friedrich, Dissertation, University of Kaiserslautern, **1995**; b) M. Detzel, Dissertation, University of Kaiserslautern, **1995**.

[12] R. Blom, T. Brück, O. J. Scherer, *Acta Chem. Scand.* **1989**, *43*, 458 – 462.

[13] a) I. Krossing, *J. Am. Chem. Soc.* **2001**, *123*, 4603 – 4604; b) I. Krossing, L. van Wüllen, *Chem. Eur. J.* **2002**, *8*, 700 – 711.

[14] Higher-charged species are favored at low temperature in solution because the polarity of $CH_2Cl_2$ increases considerably with decreasing temperature (e.g., $\varepsilon_r$ = 8.93 at 25 °C, but 14.95 at −78 °C).

[15] I. Krossing, H. Brands, R. Feuerhake, S. Koenig, *J. Fluorine Chem.* **2001**, *112*, 83 – 90.

[16] M. Detzel, G. Friedrich, O. J. Scherer, G. Wolmershäuser, *Angew. Chem.* **1995**, *107*, 1454 – 1456; *Angew. Chem. Int. Ed. Engl* **1995**, *34*, 1321 – 1323.

[17] a) R. Ahlrichs, M. Bär, M. Häser, H. Horn, C. Kölmel, *Chem. Phys. Lett.* **1989**, *162*, 165 – 169; b) O. Treutler, R. Ahlrichs, *J. Chem. Phys.* **1995**, *102*, 346 – 354.

[18] W. Küchle, M. Dolg, H. Stoll, H. Preuss, *Mol. Phys.* **1991**, *74*, 1245 – 1263.

[19] a) J. C. Slater, *Phys. Rev. A* **1951**, *81*, 385 – 390; b) D. Becke, *Phys. Rev. A* **1988**, *38*, 3098 – 3100; c) S. H. Vosko, L. Wilk, M. Nusair, *Can. J. Phys.*, **1980**, *58*, 1200 – 1211; d) J. P. Perdew, *Phys. Rev. B* **1986**, *33*, 8822 – 8824; erratum: J. P. Perdew, *Phys. Rev. B* **1986**, *34*, 7406; e) K. Eichkorn, O. Treutler, H. Oehm, M. Haeser, R. Ahlrichs, *Chem. Phys. Lett.* **1995**, *242*, 652 – 660.

[20] A. Klamt, G. Schürmann, *J. Chem. Soc. Perkin Trans.* **1993**, *2*, 799 – 805.

[21] M. Bühl in *Encyclopedia of Computational Chemistry* (Eds.: P. von R. Schleyer, N. L. Allinger, T. Clark, J. Gasteiger, P. Kollman, H. F. Schaefer, P. R. Schreiner), Wiley, Chichester, **1998**, pp. 1835 – 1845.

[22] a) A. Schäfer, H. Horn, R. Ahlrichs, *J. Chem. Phys.* **1992**, *97*, 2571 – 2577; b) A. Schäfer, C. Huber, R. Ahlrichs, *J. Chem. Phys.* **1994**, *100*, 5829 – 5835.

[23] The $CH_2Cl_2$ molecule in the crystal lattice is easily lost upon drying.

[24] A. Altomare, G. Cascarano, C. Giacovazzo, A. Guagliardi, *J. Appl. Crystallogr.* **1993**, *26*, 343 – 350.

[25] a) G. M. Sheldrick, *SHELXS-97*, University of Göttingen, **1997**; b) G. M. Sheldrick, *SHELXL-97*, University of Göttingen, **1997**.

 © 2006 Wiley-VCH Verlag GmbH & Co. KGaA, Weinheim 

Asymmetric Rearrangement

DOI: 10.1002/anie.200601731

# Practical, Highly Active, and Enantioselective Ferrocenyl–Imidazoline Palladacycle Catalysts (FIPs) for the Aza-Claisen Rearrangement of *N*-*para*-Methoxyphenyl Trifluoroacetimidates**

*Matthias E. Weiss, Daniel F. Fischer, Zhuo-qun Xin, Sascha Jautze, W. Bernd Schweizer, and René Peters**

*Dedicated to Professor Dieter Enders on the occasion of his 60th birthday*

[3,3]-Sigmatropic rearrangements rank among the most fundamental reactions in organic chemistry.[1] Particularly attractive is the $Pd^{II}$-catalyzed aza-Claisen rearrangement, also known as the Overman rearrangement, which allows for the formation of chiral enantioenriched protected allylic amines starting from achiral allylic imidates, which are easily synthesized from allylic alcohols in a single high-yielding step.[2] The resulting allylic amine derivatives are valuable building blocks for the synthesis of important compound classes such as unnatural amino acids.[3] However, most of the catalytic asymmetric aza-Claisen rearrangements that have been investigated have been limited to *N*-aryl benzimidates, which are of little practical value since cleavage of the amide protecting group is typically very low-yielding. Notable exceptions are the use of allylic trichloroacetimidates[4] and *N*-*para*-methoxyphenyl trifluoroacetimidates[5] since the protecting groups can generally be removed in preparatively useful yields. Only a few studies have been devoted to these practical, but less reactive substrates, and the planar chiral oxazoline-based palladacycle complexes **1** (COP-X) and **2** (FOP-X) have emerged as the most versatile catalyst systems.[4,5] Their design is based upon the premise that steric bulk has to be projected above and below the Pd square plane in order to allow for a face-selective coordination of the substrate olefin to the $Pd^{II}$ complex.[2] FOP catalysts **2** are not accessible by direct cyclopalladation of the ferrocene moiety;

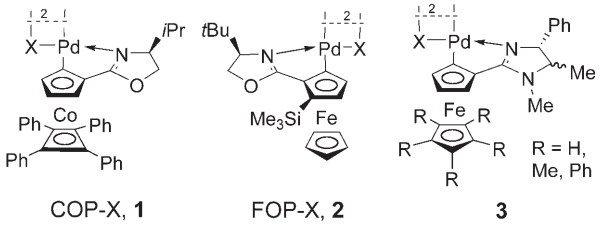


their preparation requires two *ortho* lithiations. Moreover, in the case of *N*-*para*-methoxyphenyl trifluoroacetimidates, the catalyst loading had to be as high as 5–7.5 mol% (that is, 10–15 mol% $Pd^{II}$) for both **1** and **2**, while long reaction times were still required in order to obtain preparatively useful conversions.

Our goal was to develop a practical, highly active catalyst for the asymmetric rearrangement of *N*-*para*-methoxyphenyl trifluoroacetimidates as a means to produce chiral primary allylic amines. Ideally the catalyst should be easily accessible without the necessity of low-temperature lithiations.

Recently, we described the first preparation of optically pure 2-ferrocenyl-1-alkyl imidazolines and their pentamethyl- as well as pentaphenylferrocenyl derivatives.[6,7] The direct cyclopalladations of these systems are diastereoselective only in the case of the pentaphenylferrocenyl derivative (R = Ph in **3**).[7] This Pd complex gave up to 88% *ee* for the aza-Claisen rearrangement of trifluoroacetimidates with 5 mol% catalyst loading at 40 °C after activation with $Ag^{I}$.[8] Based on these results, we have designed a less electron-rich catalyst system in which a bulky *N*-sulfonyl residue is the key constituent to permit a direct diastereoselective cyclopalladation of **4**. Steric

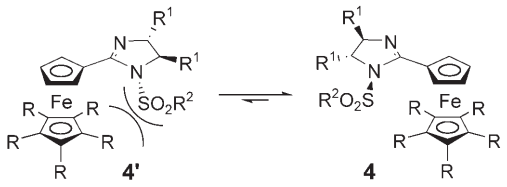


repulsion in **4** between the residue $R^1$ at the 5-position of the imidazoline and the sulfonyl group effects a transfer of chirality to the sulfonylated nitrogen atom, thus resulting in a preferred equilibrium conformation in which the sulfonyl group is oriented away from the ferrocenyl moiety, thereby allowing for a diastereoselective cyclopalladation.

The modular design allowed us to create catalysts **5** in which the steric demand and the electronic properties could be adjusted by each single module (Scheme 1), the modules

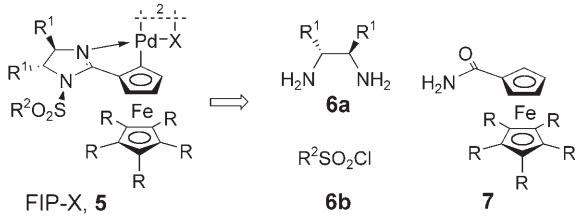


***Scheme 1.*** Modular design of catalysts **5**.

[*] M. E. Weiss, D. F. Fischer, Z.-q. Xin, S. Jautze, Dr. W. B. Schweizer, Prof. Dr. R. Peters
Laboratory of Organic Chemistry
ETH Zürich
Wolfgang-Pauli-Strasse 10, Hönggerberg HCI E 111
8093 Zürich (Switzerland)
Fax: (+41) 44-633-1226
E-mail: peters@org.chem.ethz.ch

[**] This work was financially supported by ETH Research Grant TH-30/04-2F, F. Hoffmann-La Roche, and Novartis (masters fellowship to M.E.W. and Ph.D. fellowship to Z.-q.X.). We thank Prof. B. Jaun and co-workers for performing nOesy experiments, Prof. E. M. Carreira for sharing laboratory equipment, and Dr. Martin Karpf and Dr. Paul Spurr (both F. Hoffmann-La Roche, Basel) for critically reading this manuscript.

Supporting information for this article is available on the WWW under http://www.angewandte.org or from the author.


InterScience
© 2006 Wiley-VCH Verlag GmbH & Co. KGaA, Weinheim

being a) a ferrocenyl,[9] pentamethylferrocenyl, or pentaphenylferrocenyl moiety, b) an imidazoline constituent that is synthesized from an enantiomerically pure $C_2$-symmetric diamine, and c) a sulfonyl residue.

The air-stable and crystalline imidazolines **4** were prepared in good yield from the amides **7**[6,7] by activation via the corresponding iminium ether intermediate and a subsequent sulfonylation (Scheme 2, Table 1).

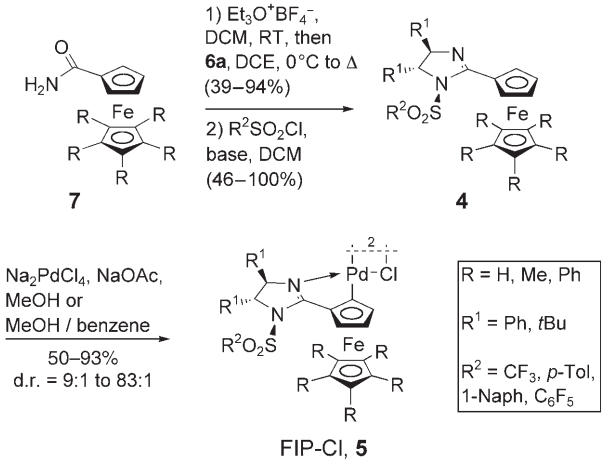


***Scheme 2.*** Synthesis of ferrocenyl–imidazoline palladacycles **5**. DCM = dichloromethane, DCE = 1,2-dichloroethane.

***Table 1:*** Preparation of imidazolines **4** and palladacycles **5**.

| Entry | Prod. | $C_5R_5$[a] | $R^1$ | $R^2$ | Yield[b] [%] | d.r.[d] | d.r.[e] |
|---|---|---|---|---|---|---|---|
| 1 | **4** | Cp | Ph | $CF_3$ | 72[c] | – | – |
| 2 | **4** | Cp | Ph | *p*-Tol | 73[c] | – | – |
| 3 | **4** | Cp | Ph | 1-Naph | 73[c] | – | – |
| 4 | **4** | Cp | *t*Bu | *p*-Tol | 18[c] | – | – |
| 5 | **4** | Cp* | Ph | $CF_3$ | 71[c] | – | – |
| 6 | **4** | Cp* | Ph | *p*-Tol | 81[c] | – | – |
| 7 | **4** | Cp* | Ph | $C_6F_5$ | 65[c] | – | – |
| 8 | **4** | $Cp^\Phi$ | Ph | *p*-Tol | 77[c] | – | – |
| 9 | **5** | Cp | Ph | $CF_3$ | 92 | 9:1 | 9:1 |
| 10 | **5** | Cp | Ph | *p*-Tol | 93 | 18:1 | 18:1 |
| 11 | **5** | Cp | Ph | 1-Naph | 91 | 12:1 | 12:1 |
| 12 | **5** | Cp | *t*Bu | *p*-Tol | 55 | 20:1 | 72:1 |
| 13 | **5** | Cp* | Ph | $CF_3$ | 69 | 15:1 | 83:1 |
| 14 | **5** | Cp* | Ph | *p*-Tol | 85 | 20:1 | 20:1 |
| 15 | **5** | Cp* | Ph | $C_6F_5$ | 60 | 7:1 | 14:1 |
| 16 | **5** | $Cp^\Phi$ | Ph | *p*-Tol | 50 | 20:1 | 38:1 |

[a] Cp* = $C_5Me_5$, $Cp^\Phi$ = $C_5Ph_5$. [b] Yield of isolated product after chromatography. [c] Yield over two steps from **7**. [d] Diastereomeric ratio of the crude product as determined by $^1$H NMR of complex **8** or **9**. [e] Diastereomeric ratio of the isolated product as determined by $^1$H NMR of complex **8** or **9**.

The hypothesis of chirality transfer to the *N*-sulfonyl group was confirmed by X-ray analysis of imidazoline **4**-Cp-*t*Bu-Ts (labeling system: **4**-$C_5R_5$-$R^1$-$R^2$),[10] in which the sulfonylated N atom is significantly pyramidalized, thus minimizing unfavorable steric interactions with the neighboring substituents (Figure 1).

Cyclopalladation under standard conditions at room temperature with $Na_2PdCl_4$/NaOAc in MeOH (with or without benzene) proved to be a very reliable method for preparing the air-stable dimeric complexes FIP-Cl (**5**) as geometrical isomers about the $Pd^{II}$ square planes in good yield and with moderate to high diastereoselectivity with regard to the planar chirality (d.r. = 7:1 to 20:1 and 9:1 to 83:1 before and after chromatography).[11] To determine the diastereoselectivity, the dimeric species **5** were treated with $PPh_3$ or Na(acac) to furnish the monomeric complexes **8** and **9** (Scheme 3).[12]

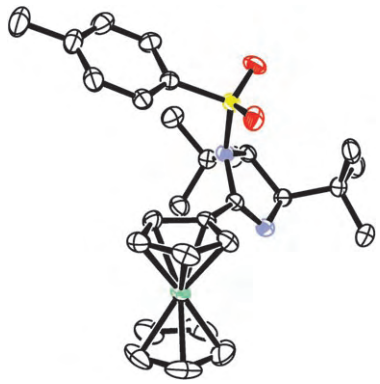

***Figure 1.*** ORTEP representation of **4**-Cp-*t*Bu-Ts with eclipsed Cp rings (the unit cell contains two different conformers). Ellipsoids are set at 50% probability (C black, N blue, O red, S yellow, Fe green); H atoms are omitted for clarity.

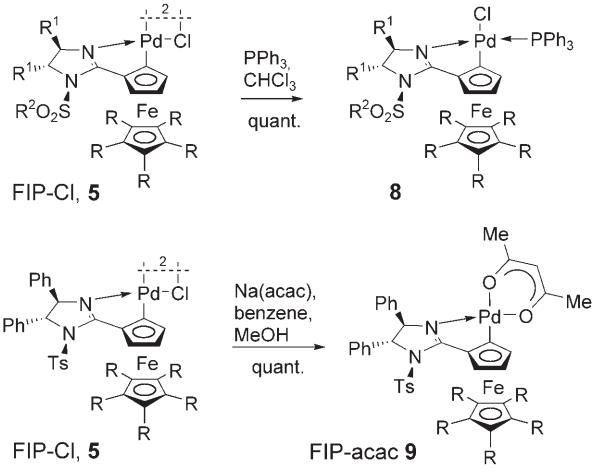


***Scheme 3.*** Synthesis of the monomeric complexes **8** and **9**. acac = acetylacetonate.

The crystal structures of **9**-$Cp^\Phi$-Ph-Ts (Figure 2)[13] and **8**-Cp*-Ph-Ts as well as nOesy experiments on **9**-Cp-Ph-Ts and **9**-$Cp^\Phi$-Ph-Ts (see the Supporting Information) confirmed the predicted $S_p$ configuration.[14,15]

The dimeric complexes **5** were then investigated in the aza-Claisen rearrangement of *N*-*para*-methoxyphenyl trifluoroacetimidates **10** (Scheme 4). With (*E*)- and (*Z*)-**10a** as model substrates, various silver salts AgX ($X = O_2CCF_3$ (TFA), OTf, OTs, $BF_4$) were evaluated for their catalyst-activating properties since the dimeric palladacycles **5** alone proved to be unreactive as catalysts. While silver trifluoroacetate is the most general activating reagent of those

 © 2006 Wiley-VCH Verlag GmbH & Co. KGaA, Weinheim 

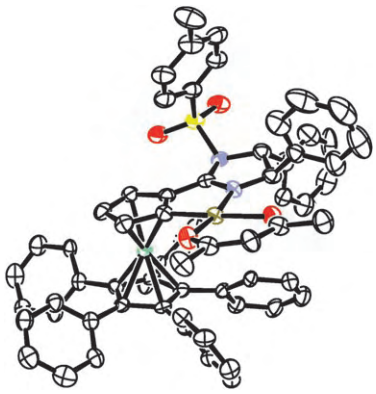

***Figure 2.*** ORTEP representation of **9**-Cp$^{\Phi}$-Ph-Ts with staggered conformation of the Cp rings (the unit cell contains two different conformers). Ellipsoids are set at 50% probability (C black, N blue, O red, S yellow, Fe green, Pd bronze); H atoms are omitted for clarity.

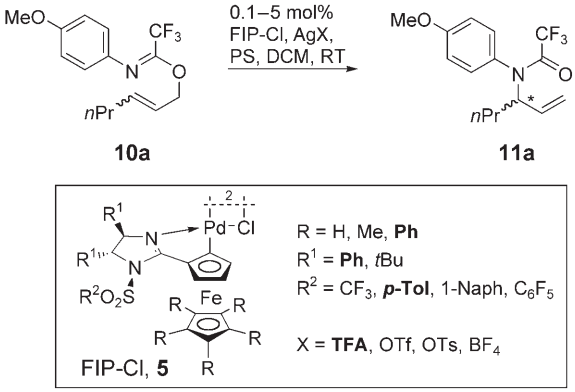


***Scheme 4.*** Screening of catalysts with model substrates (*E*)- and (*Z*)-**10a**.

investigated, AgOTf proved to be superior in the case of **5**-Cp catalyst precursors for *Z*-configured imidates **10**. The silver salts presumably not only lead to an exchange of Cl for X in the active catalyst species, but also oxidize the ferrocene moiety to provide a ferrocenium cation since the rearrangement proceeds extremely slowly with only two equivalents of AgX per dimer **5**. This assumption is supported by the fact that the $^1$H NMR spectrum of the catalyst disappears as a result of the formation of a paramagnetic species after addition of four equivalents of AgTFA, whereas with two equivalents the NMR signals are still sharp. In analogy to the work published by Overman et al., the rearrangements were performed in the presence of proton sponge (PS, two equivalents per dimer **5**), which resulted in higher *ee* values at the expense of somewhat decreased conversion rates, but led to significantly cleaner reactions. In all experiments described, only traces of side products were detected in the presence of PS.

After an extensive solvent screening,[16] $CH_2Cl_2$ was selected for further experiments, in which the influence of the different modules was investigated (Table 2). The comparison of different sulfonyl groups revealed that increasing the steric bulk of the sulfonyl group does not necessarily lead to higher enantioselectivities (Table 2, entries 1–6) but results

***Table 2:*** Catalyst screening with model substrates (*E*)- and (*Z*)-**10a**.

| Entry | (*E*/*Z*)-**10a** | mol% **5** | *T* [°C] | $C_5R_5$ | $R^1$ | $R^2$ | Yield[a] [%] | *ee*[b] [%] |
|---|---|---|---|---|---|---|---|---|
| 1 | ***E*** | 5 | 20 | Cp | Ph | $CF_3$ | 96[f] | 64 (*R*) |
| 2 | ***E*** | 5 | 20 | Cp | Ph | *p*-Tol | 88[f] | 67 (*R*) |
| 3 | ***E*** | 5 | 20 | Cp | Ph | 1-Naph | 54[f] | 65 (*R*) |
| 4[c] | ***Z*** | 5 | 20 | Cp | Ph | $CF_3$ | 90[e] | 91 (*S*) |
| 5[c] | ***Z*** | 5 | 20 | Cp | Ph | *p*-Tol | 75[f] | 89 (*S*) |
| 6[c] | ***Z*** | 5 | 20 | Cp | Ph | 1-Naph | 19[f] | 72 (*S*) |
| 7 | ***E*** | 5 | 20 | Cp | *t*Bu | *p*-Tol | 76[f] | 66 (*R*) |
| 8[h] | ***E*** | 5 | 40 | Cp* | Ph | $CF_3$ | 80[d] | 0 |
| 9[h] | ***E*** | 5 | 40 | Cp* | Ph | *p*-Tol | 91[e] | 89 (*R*) |
| 10[h] | ***E*** | 5 | 40 | Cp* | Ph | $C_6F_5$ | 88[e] | 74 (*R*) |
| 11 | ***Z*** | 5 | 40 | Cp* | Ph | *p*-Tol | 72[e] | 93 (*S*) |
| 12 | ***E*** | 1.0 | 20 | Cp$^{\Phi}$ | Ph | *p*-Tol | 96[e] | 97 (*R*) |
| 13 | ***E*** | 0.5 | 20 | Cp$^{\Phi}$ | Ph | *p*-Tol | 95[e] | 98 (*R*) |
| 14 | ***E*** | 0.1 | 20 | Cp$^{\Phi}$ | Ph | *p*-Tol | 94[e] | 97 (*R*) |
| 15 | ***E*** | 0.05 | 40 | Cp$^{\Phi}$ | Ph | *p*-Tol | 95[g] | 95 (*R*) |
| 16 | ***Z*** | 5 | 40 | Cp$^{\Phi}$ | Ph | *p*-Tol | 36[e] | 85 (*S*) |

[a] Yield determined by $^1$H NMR. [b] Enantiomeric excess determined by chiral HPLC (Daicel OD-H) after hydrolysis of **11a** to the secondary amine (see the Supporting Information). [c] AgOTf was used for activation. [d] Reaction time 5 h. [e] Reaction time 1 day. [f] Reaction time 2 days. [g] Reaction time 3 days. [h] Catalyst precursor **5** doped with 10% **4**-Cp*-Ph-Ts.

in prolonged reaction times. Since catalysts bearing the small and strongly electron-withdrawing trifluoromethylsulfonyl moiety led in some cases to catalyst decomposition (Table 2, entry 8), the tosyl group emerged as the sulfonyl moiety of choice.

With regard to the imidazoline backbone, no significant difference in enantioselectivity and yield of **11a** was found for $R^1$ = Ph or *t*Bu (Table 2, entries 2 and 7).[17] Since the imidazolines **4** with $R^1$ = Ph are prepared in much higher yields (Table 1), they were selected for the investigation of the influence of the ferrocenyl spectator ligand module, which has the highest impact on the rearrangement outcome. While catalysts possessing an unsubstituted Cp ring did not provide useful *ee* values for (*E*)-**10a** (Table 2, entries 1–3, 7), the rearrangement of (*Z*)-**10a** enabled amide **11a** to be prepared with 90% *ee* (Table 2, entries 4, 5). By contrast, with a bulkier yet electron-richer Cp* spectator ligand, both (*E*)- and (*Z*)-**10a** gave about 90% *ee* (Table 2, entries 9, 11) although the reaction mixtures had to be heated to 40°C to obtain useful conversion rates with a precatalyst loading of 5 mol%. Interestingly, in order to obtain these high levels of asymmetric induction for (*E*)-**10a**, the catalyst precursor **5**-Cp*-Ph-Ts had to be doped with 10% **4**-Cp*-Ph-Ts (that is, 0.5 mol% with regard to (*E*)-**10a**). In the absence of **4**-Cp*-Ph-Ts, the *ee* value decreased significantly to 73%. At present, we can only speculate about the origin of this effect and further studies will be required, but we hypothesize that the $R_p$-configured catalyst (the minor palladacycle isomer) is preferentially deactivated by the formation of a monomeric complex with the imidazoline N atom.[18]

Gratifyingly, the electron-poorer and even bulkier Cp$^{\Phi}$ spectator ligand (Cp$^{\Phi}$ = $C_5Ph_5$) resulted not only in significantly higher enantioselectivity for (*E*)-**10a** (97% *ee*, Table 2, entry 12) but also in a highly active catalyst, thus allowing the

 © 2006 Wiley-VCH Verlag GmbH & Co. KGaA, Weinheim 

amount of the precatalyst to be reduced to unprecedented levels of 0.05 to 1.0 mol% without largely affecting the enantioenrichment whilst still providing useful reaction rates (Table 2, entries 12–15).[19] Compound **5**-Cp$^{\Phi}$-Ph-Ts is however not a useful catalyst for (*Z*)-**10a** (Table 2, entry 16).

After the optimization of the reaction conditions, the scope of the rearrangement of imidates **10** was studied in detail by using **5**-Cp-Ph-Ts and **5**-Cp*-Ph-Ts for substrates (*Z*)-**10** and **5**-Cp$^{\Phi}$-Ph-Ts for substrates (*E*)-**10** (Table 3).

***Table 3:*** Screening of substrates **10** with different groups R$^1$ in the presence of **5**-Cp or **5**-Cp* [*Z* substrates] or **5**-Cp$^{\Phi}$ [*E* substrates].

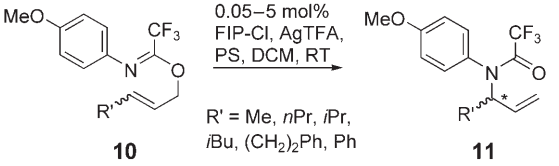


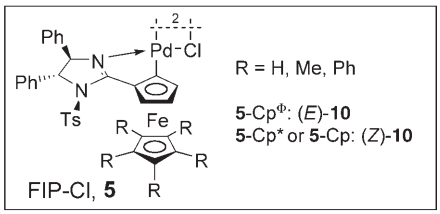


| Entry | (*E*/*Z*)-**10** | R′ | $C_5R_5$ | mol% **5** | *T* [°C] | Yield[a] [%] | *ee*[b] [%] |
|---|---|---|---|---|---|---|---|
| 1[c,e] | (*Z*)-**10a** | *n*Pr | Cp | 5 | 20 | 75 | 89 (*S*) |
| 2[c,e] | (*Z*)-**10b** | $(CH_2)_2$Ph | Cp | 5 | 20 | 70 | 90 (*S*) |
| 3[c,e] | (*Z*)-**10c** | *i*Bu | Cp | 5 | 20 | 69 | 96 (*S*) |
| 4[c] | (*Z*)-**10a** | *n*Pr | Cp* | 5 | 40 | 72 | 93 (*S*) |
| 5[c] | (*Z*)-**10b** | $(CH_2)_2$Ph | Cp* | 5 | 40 | 95 | 95 (*S*) |
| 6[c] | (*Z*)-**10c** | *i*Bu | Cp* | 5 | 40 | 82 | 96 (*S*) |
| 7[c] | (*E*)-**10a** | *n*Pr | Cp$^{\Phi}$ | 0.5 | 20 | 95 | 98 (*R*) |
| 8[c] | (*E*)-**10a** | *n*Pr | Cp$^{\Phi}$ | 0.1 | 40 | 89 | 97 (*R*) |
| 9[d] | (*E*)-**10a** | *n*Pr | Cp$^{\Phi}$ | 0.05 | 40 | 95 | 95 (*R*) |
| 10[d] | (*E*)-**10f** | Me | Cp$^{\Phi}$ | 0.1 | 20 | 91 | 95 (*R*) |
| 11[d] | (*E*)-**10f** | Me | Cp$^{\Phi}$ | 0.05 | 40 | 98 | 92 (*R*) |
| 12[c] | (*E*)-**10b** | $(CH_2)_2$Ph | Cp$^{\Phi}$ | 1.0 | 20 | 94 | 99.7 (*R*) |
| 13[d] | (*E*)-**10b** | $(CH_2)_2$Ph | Cp$^{\Phi}$ | 0.05 | 40 | 99 | 98 (*R*) |
| 14[c] | (*E*)-**10c** | *i*Bu | Cp$^{\Phi}$ | 0.2 | 40 | 96 | 98 (*R*) |
| 15[c] | (*E*)-**10c** | *i*Bu | Cp$^{\Phi}$ | 0.1 | 40 | 95 | 98 (*R*) |
| 16[c] | (*E*)-**10d** | *i*Pr | Cp$^{\Phi}$ | 0.5 | 40 | 75 | 96 (*R*) |
| 17[d] | (*E*)-**10d** | *i*Pr | Cp$^{\Phi}$ | 0.1 | 40 | 81 | 93 (*R*) |
| 18[c] | (*E*)-**10e** | Ph | Cp$^{\Phi}$ | 1.0 | 40 | 99 | 88 (*S*) |
| 19[c] | (*E*)-**10e** | Ph | Cp$^{\Phi}$ | 0.5 | 40 | 97 | 84 (*S*) |

[a] Yield of isolated product. [b] Enantiomeric excess determined by chiral HPLC (Daicel OD-H) after hydrolysis of **11** to the secondary amine (see the Supporting Information). [c] Reaction time 1 day. [d] Reaction time 3 days. [e] AgOTf was used for catalyst activation.

Whereas the former two catalyst precursors provide good conversions and yields only for α-unbranched allylic substrates (*Z*)-**10** and require a catalyst loading of 5 mol% (Table 3, entries 1–6), the Cp$^{\Phi}$ derivative has a broad applicability even at very low catalyst loadings. The rate of the rearrangement depends primarily on the steric bulk of the residue R′. With unbranched substituents (R′ = Me, *n*Pr, $(CH_2)_2$Ph, *i*Bu), (*R*)-**11** was formed in excellent yield with 0.05 to 0.1 mol% catalyst loading, and the highest enantioselectivities obtained so far for substrates **10** were exhibited (Table 3, entries 7–15; highest *ee* values previously reported: Me 88%, *n*Pr 95%, $(CH_2)_2$Ph 97%, *i*Bu 97%).[5a,7] The most difficult aliphatic substrate in terms of the enantioselectivity, prepared from crotonylic alcohol, furnished (*R*)-**11f** with 95% *ee* (Table 3, entry 10). Even in the case of the α-branched *i*Pr substituent, a case which has not been described so far, the rearrangement proceeded with acceptable rates with 0.1 to 0.5 mol% catalyst precursor (Table 3, entries 16 and 17). Also the aromatic Ph substituent, which has not provided useful yields and enantioselectivities so far (best reported results: 46% yield, 45% *ee*),[5c] is well-tolerated (Table 3, entries 18 and 19).

The opposite absolute configurations of the major enantiomers of rearrangement products **11** starting from either (*E*)- or (*Z*)-**10** may be accounted for by the working model depicted in Figure 3. Assuming that the olefin coordinates (in analogy to $PPh_3$) *trans* to the imidazoline N atom as a result of the *trans* effect,[20] the imidate N atom attacks the olefin at the face remote to the Pd atom. Increased steric interactions of the coordinated olefin with the Cp* and Cp$^{\Phi}$ ligands presumably results in a better face selectivity for the olefin coordination at the Pd$^{II}$ center, which thus explains the higher enantioselectivity as compared to derivatives that bear the unsubstituted Cp ligand. The very high activity of the catalyst derived from **5**-Cp$^{\Phi}$-Ph-Ts may be accounted for by the electron-withdrawing influence of the Cp$^{\Phi}$ ligand, but also by a higher tendency to form a monomeric, catalytically active species.

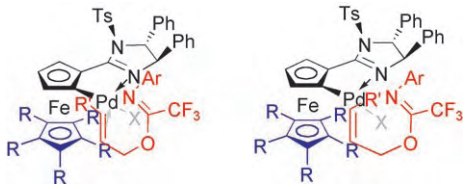


***Figure 3.*** Proposed explanation for the stereochemistry of the catalysis product.

In conclusion, we have developed practical, highly efficient ferrocenyl–imidazoline palladacycles (FIPs) as catalysts for the aza-Claisen rearrangement of *N*-*para*-methoxyphenyl trifluoroacetimidates, which are versatile substrates for the formation of protected chiral primary allylic amines. The catalysts are not only easily prepared but also exhibit unprecedented activity, enantioselectivity, and tolerance toward a broad spectrum of substrates. This methodology compares favorably to existing enantioselective approaches to protected chiral primary allylic amines.

Received: May 2, 2006
Published online: July 21, 2006

**Keywords:** aza-Claisen rearrangement · cyclopalladation · ferrocene · imidazoline · Overman rearrangement

 © 2006 Wiley-VCH Verlag GmbH & Co. KGaA, Weinheim 

[1] D. Enders, M. Knopp, R. Schiffers, *Tetrahedron: Asymmetry* **1996**, *7*, 1847.

[2] Review about enantioselective aza-Claisen rearrangements: T. K. Hollis, L. E. Overman, *J. Organomet. Chem.* **1999**, *576*, 290.

[3] C. E. Anderson, L. E. Overman, *J. Am. Chem. Soc.* **2003**, *125*, 12412.

[4] See reference [3] and S. F. Kirsch, L. E. Overman, M. P. Watson, *J. Org. Chem.* **2004**, *69*, 8101.

[5] a) L. E. Overman, C. E. Owen, M. M. Pavan, C. J. Richards, *Org. Lett.* **2003**, *5*, 1809; b) R. S. Prasad, C. E. Anderson, C. J. Richards, L. E. Overman, *Organometallics* **2005**, *24*, 77; c) C. E. Anderson, Y. Donde, C. J. Douglas, L. E. Overman, *J. Org. Chem.* **2005**, *70*, 648.

[6] R. Peters, D. F. Fischer, *Org. Lett.* **2005**, *7*, 4137.

[7] R. Peters, Z.-q. Xin, D. F. Fischer, W. B. Schweizer, *Organometallics* **2006**, *25*, 2917.

[8] For other applications of imidazolines in asymmetric catalysis, see for example: a) F. Menges, M. Neuburger, A. Pfaltz, *Org. Lett.* **2002**, *4*, 4713; b) C. A. Busacca, D. Grossbach, R. C. So, E. M. O'Brien, E. M. Spinelli, *Org. Lett.* **2003**, *5*, 595; c) S. Bhor, G. Anilkumar, M. K. Tse, M. Klawonn, C. Dobler, B. Bitterlich, A. Grotevendt, M. Beller, *Org. Lett.* **2005**, *7*, 3393.

[9] a) *Ferrocenes* (Eds.: T. Hayashi, A. Togni), VCH, Weinheim, **1995**; b) C. J. Richards, A. J. Locke, *Tetrahedron: Asymmetry* **1998**, *9*, 2377; c) R. C. J. Atkinson, V. C. Gibson, N. J. Long, *Chem. Soc. Rev.* **2004**, *33*, 313.

[10] CCDC-606393 (**4**-Cp-*t*Bu-Ts) contains the supplementary crystallographic data for this paper. These data can be obtained free of charge from The Cambridge Crystallographic Data Centre via www.ccdc.cam.ac.uk/data_request/cif.

[11] Only very few direct diastereoselective cyclopalladations of chiral ferrocene derivatives are known; see reference [7] and references therein.

[12] Note that six different dimeric isomers are possible for **5** and thus lead to complex NMR spectra.

[13] CCDC-604468 (**9**-$Cp^{\Phi}$-Ph-Ts) and CCDC-606392 (**8**-Cp*-Ph-Ts) contain the supplementary crystallographic data for this paper. These data can be obtained free of charge from The Cambridge Crystallographic Data Centre via www.ccdc.cam.ac.uk/data_request/cif.

[14] The stereodescriptors with regard to the planar chirality are used according to: K. Schlögl, *Top. Stereochem.* **1967**, *1*, 39.

[15] The crystal structures of **4**-Cp-*t*Bu-Ts and **9**-$Cp^{\Phi}$-Ph-Ts show two symmetrically independent molecules with different conformations of the Cp ring from almost eclipsed to staggered. Despite the different degree of bulkiness of the substituents on the Cp rings, the distance of the ring centers are nearly constant in all molecules (3.30–3.34 Å).

[16] General trends: a) catalyst activity: DCE > DCM > $CHCl_3$ > $C_6H_6$ > DCM/1% DMF > MeCN ≫ $Et_2O$ (catalyst not soluble); b) enantioselectivity: DCM ≈ DCM/1% DMF ≫ $C_6H_6$ > DCE ≈ MeCN > $CHCl_3$.

[17] The (1*R*,2*R*)-cyclohexyldiamine backbone resulted in much lower *ee* values.

[18] *N*-Methylimidazole is, for example, known to cleave palladacycle dimers: C. López, R. Bosque, X. Solans, M. Font-Bardía, D. Tramuns, G. Fern, J. Silver, *J. Chem. Soc. Dalton Trans.* **1994**, 3039.

[19] **5**-$Cp^{\Phi}$-Ph-Ts as well as **7**-$Cp^{\Phi}$ will soon be commercially available from Sigma–Aldrich.

[20] F. R. Hartley, *Chem. Soc. Rev.* **1973**, *2*, 163.


 © 2006 Wiley-VCH Verlag GmbH & Co. KGaA, Weinheim 

Molecular Knots

DOI: 10.1002/anie.200601111

# A Trefoil Knot Made of Amino Acids and Steroids**

*Martin Feigel,* Rüdiger Ladberg, Simon Engels, Regine Herbst-Irmer,* and Roland Fröhlich**

Linear oligoamides made from conformationally restricted non-natural amino acids can form helical or ribbonlike secondary structures.[1] Moreover, amide macrocycles have been shown to build knotted structures if concave structural elements are present in the monomeric units.[2] The concave surface of cholanic acids has often been used as a scaffold in supramolecular chemistry.[3] We have combined all three elements to prepare cyclopeptides from aminocholanic acids. We found that when the amine macrocycles consist of aminocholanic acids they form open cavities, while cyclopeptides composed of aminocholanic acids and natural dipeptides adopt closed-loop structures.[4] Here, we report the unexpected geometry of cyclic oligoamides built from alternating sequences of aminodeoxycholanic acid and a natural amino acid.

Linear sequences of alternating 3-α-aminodeoxycholanic acid and valine were made from the protected dipeptide **1** (Scheme 1). Condensation of fragments **1b** and **1c** yielded the tetrapeptide **2a**, and subsequently the hexapeptide **3**, by using standard EDC coupling procedures.

Deprotection and then activation of **3** as the pentafluorophenol ester gave the macrocycles cyclo(valine-3-α-aminodeoxycholic acid amide)$_3$ (**4**) and cyclo(valine-3-α-aminodeoxycholic acid amide)$_6$ (**5**). The compounds were isolated in moderate to high yields after column chromatography (Scheme 1). The $^1$H NMR spectrum of **4** in $CDCl_3$ reflects the expected average $C_3$ symmetry of the compound: only one set of partially broadened valine and aminocholanic acid signals was found (Figure 1). On cooling the solution, the lines broadened further and split into barely resolved signals at

[*] Prof. Dr. M. Feigel, Dr. R. Ladberg, S. Engels
Fakultät für Chemie
Ruhr-Universität Bochum
Universitätsstrasse 150, 44780 Bochum (Germany)
Fax: (+49) 234-321-4497
E-mail: feigel@indi-f.nsc.ruhr-uni-bochum.de
Dr. R. Herbst-Irmer[+]
Institut für Anorganische Chemie
Universität Göttingen
Tammannstrasse 4, 37077 Göttingen (Germany)
Dr. R. Fröhlich[+]
Organisch-chemisches Institut
Universität Münster
Corrensstrasse 40, 48149 Münster (Germany)
[+] X-ray structural analysis

[**] This work was supported by the Deutsche Forschungsgemeinschaft.
Supporting information for this article is available on the WWW under http://www.angewandte.org or from the author.


WILEY InterScience DISCOVER SOMETHING GREAT
© 2006 Wiley-VCH Verlag GmbH & Co. KGaA, Weinheim

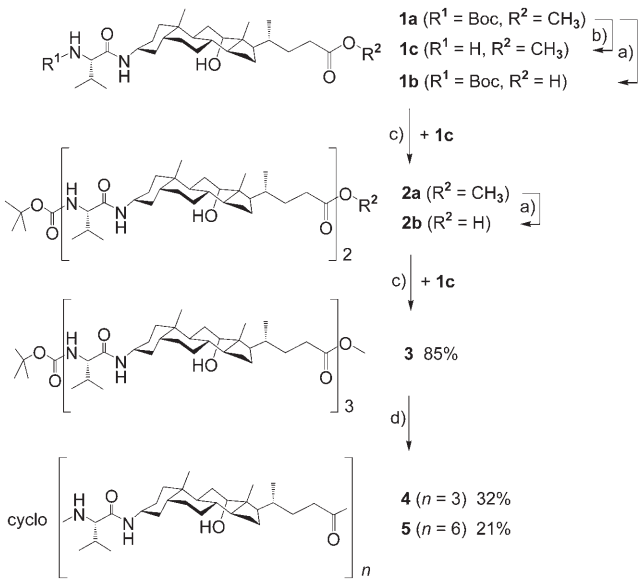


***Scheme 1.*** Synthesis of the macrolactams **4** and **5**. a) KOH, methanol, water; b) trifluoroacetic acid (TFA), dichloromethane; c) EDC, HOBt, dichloromethane; d) procedure (a) followed by: 1. dicyclohexylcarbodiimide, pentafluorophenol, 2. TFA, 3. sodium hydrogen carbonate, water, chloroform, dichloromethane. Boc = *tert*-butyloxycarbonyl, HOBt = 1-hydroxy-1*H*-benzotriazole, EDC = 1-(3-dimethylaminopropyl)-3-ethylcarbodiimide. Details of the synthesis are given in the Supporting Information.

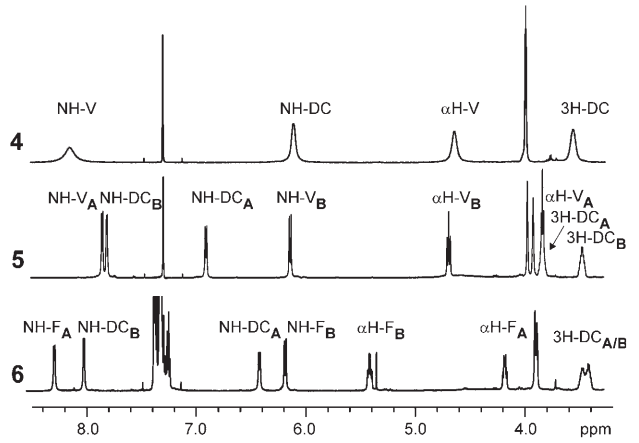


***Figure 1.*** $^1$H NMR spectra (600 MHz) of the macrolactams **4**, **5**, and **6** in chloroform. Abbreviations: V = valine, F = phenylalanine, DC = 3α-aminodeoxycholanic acid; the two different valine-aminocholanic units detected in **5** and **6** are denoted as **A** and **B**.

223 K, thus indicating three different valine-aminocholanic units. Intramolecular hydrogen bonds and/or aggregation in the solvent are probably responsible for the inequivalence of the groups.

The $^1$H NMR spectrum of **5** is completely different from that of **4** (Figure 1). Two well-resolved signals are observed for each proton of the six valine-aminocholanic units of **5**. The two sets of signals are denoted as **A** and **B** in Figure 1. NOE cross-peaks are found in the ROESY spectra between protons within each valine-aminocholanic acid unit, but some NOE contacts are also observed between valine protons of type **A** and valine protons of type **B**.[5] Clearly, the valine units of type **A** and **B** come into proximity, which is only possible if there is a constriction or crossing at these sites in the macrocyclic ring. Similar spectra and NOE data are found for macrocycle **6**, which contains phenylalanine instead of valine as the natural amino acid; the compound has also been synthesized by the route outlined in Scheme 1.[6] The splitting of the NMR signals in **5** and **6** persists in more-polar solvents (e.g. DMF) and at elevated temperatures (323 K). It is therefore unlikely that hydrogen bonds alone are the reason for the observed splitting of the signals, and a knot structure of **5** was postulated but could not be proved by NMR spectroscopy.[7]

Crystals of **5** suitable for X-ray structure determination were grown from *n*-propanol. The analysis shows unambiguously that **5** has the structure of a trefoil knot (Scheme 2, Figure 2).[8] The knot has almost $C_3$ symmetry. It consists of three equivalent loops made from three external steroid units, a chain-crossing region composed of valine amino acids, and a core built from three internal steroids.

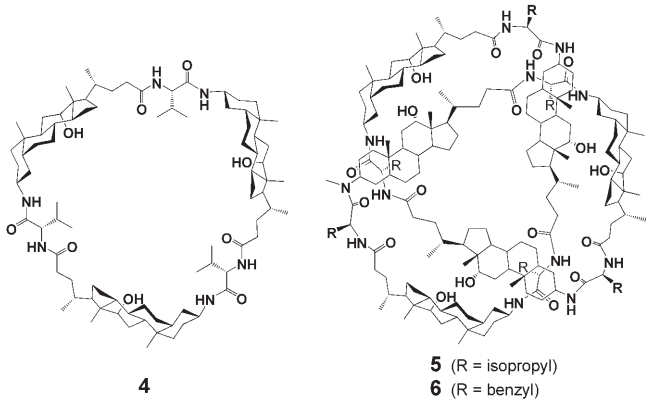


***Scheme 2.*** Structural formulas of **4**, **5**, and **6**.

Trefoil knots exist in two enantiomeric forms which are denoted $3_1^{ppp}$ and $3_1^{mmm}$ depending on the symmetry of the crossing of their chains.[9] The two knot forms of **5** are diastereomers because of the intrinsic chirality of L-valine and of the 3-α-aminocholanic acid unit. Only the $3_1^{ppp}$ diastereomer has been isolated; the isomer with $3_1^{mmm}$ symmetry could not be detected. It is apparent that the chirality of the ring elements favors the p-type crossing. A close inspection of the crossing region in the solid-state structure shows that hydrogen bonds are formed between valine units of **A** and **B** and that of an OH group of an aminodeoxycholanic unit is also involved in intramolecular hydrogen bonding to a valine moiety (Figure 2). In addition, one water molecule bridges OH groups of steroids of type **A** and **B** in the crossing region (a more detailed view is given in the Supporting Information).

The knots **5** and **6** are bowl shaped and have a nonpolar outer and a polar inner surface. The bowl is filled with two propanol and three water molecules in the solid-state structure of **5**. The different shape and polarity of the inner and outer surfaces of **5** are illustrated in Figure 3.

 © 2006 Wiley-VCH Verlag GmbH & Co. KGaA, Weinheim 

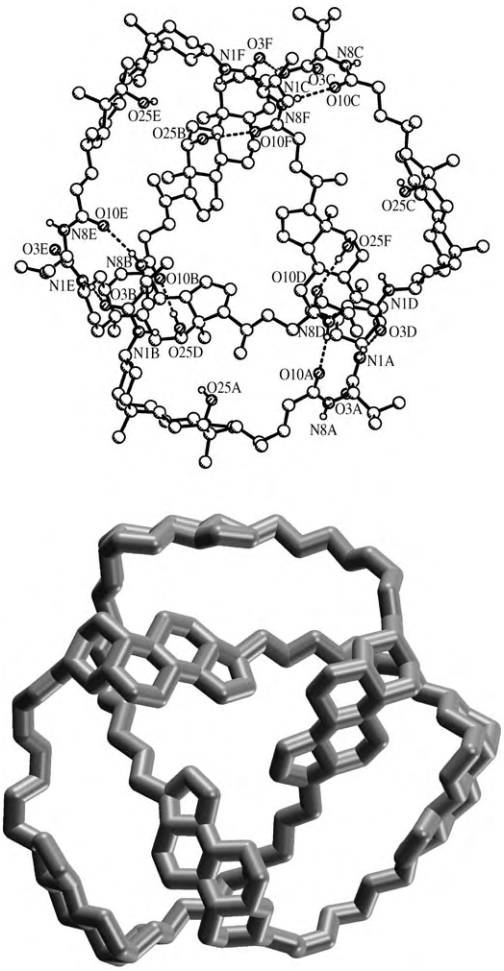




*Figure 2.* Structure of **5** in the solid state. Top: Schakal drawing with the intramolecular hydrogen-bonding scheme. Bottom: chain of backbone atoms illustrating the knot topology (view from the back side of the top figure).

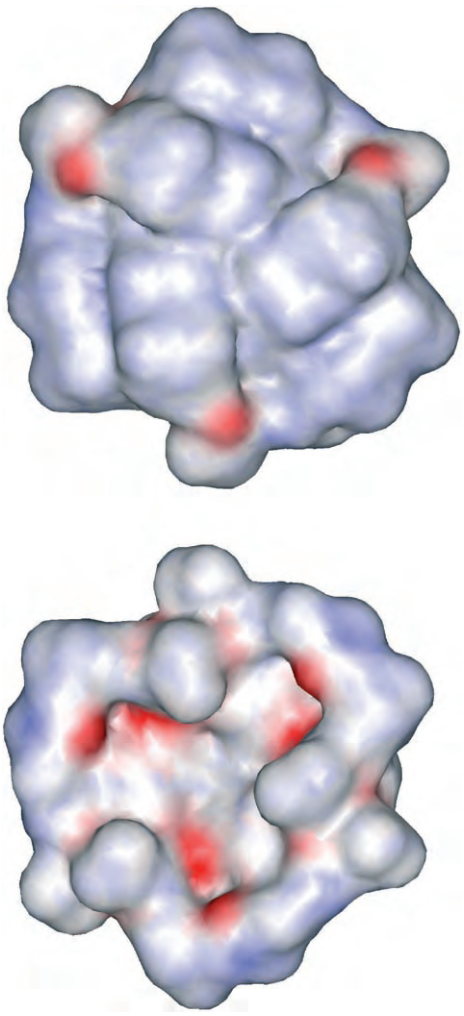

*Figure 3.* Surface drawings of the front and back sides of **5**.

It is difficult to rationalize why knot **5** is built in such high yields. Formation of an amide bond is an irreversible reaction, so the knot topology has to be preorganized prior to the final ring-closure step. The necessary crossing regions of the chain for the formation of knot **5** arise through intramolecular hydrogen bonding and bridging water molecules (see above). It is therefore possible that the two-phase system (chloroform/water) used in the cyclization procedure supports the correct type of chain crossing to give a knot. The CD spectra of the knot **5** and of its linear precursors **1a**, **2a**, and **3** were measured in trifluoroethanol. The CD curves of the cyclic and linear compounds have the same overall shape, with a minimum at 225 nm and a strong maximum near 200 nm (see the Supporting Information). The curvature of the linear precursors of the knot is therefore presumably similar to the curvature of the chain of the knot in that solvent—but of course, the conformations may differ in the solvent mixture used for the ring closure. The 2D-ROESY NMR spectra of the linear precursor **3** in chloroform do not contain the cross-signals which would be expected if distant valine units in **3** come into proximity; such an orientation should be expected during the dimerization of **3** prior to the final ring closure to form the knot.

The presence of amino acids in the chain of the knots **5** and **6** leads to the question as to whether helical conformations of the amino acids preorganize the linear precursor of the knot and induce the turns required to form a knot topology. The dihedral angles $\phi$ and $\psi$ at the valine residues of type **A** and **B** in the solid-state structure of **5** are **A**: $\phi = -91°$, $\psi = +145°$; **B**: $\phi = -111°$; $\psi = +134°$. Such values correspond to the upper left quadrant of the Ramachandran diagram of peptides where the parallel and antiparallel β sheets are located. In fact, the hydrogen-bonding pattern between the valine units **A** and **B** in **5** (see above) can be viewed as part of a heavily twisted parallel β sheet. The $^3J_{NH\text{-}C\alpha H}$ coupling constants of the amide protons of **5** and **6** in chloroform are consistent with the extended valine conformation found in the solid state. The values found in the linear precursor **3** are similar (see the Supporting Information). In conclusion, the turn geometry required to form the knot is not induced by a helical geometry of the amino acids. Hydrogen bonding (as well as the involvement of the OH groups of the cholanic acid), the chiral twisted pair of valine units, and the

 © 2006 Wiley-VCH Verlag GmbH & Co. KGaA, Weinheim 

concave shape of the steroid unit are the factors which together lead to the folding of the knot.

Only a few chemical systems are known in which cyclic molecules adopt the topology of a trefoil knot.[2,9–14] The first successful synthetic approach to this type of knotted cycles used copper-phenanthroline complexes to achieve the necessary chain crossing.[10] An alternative method is based on single-stranded DNA sequences designed to fold into twisted double-stranded DNA segments which produce a knotted cyclic DNA on enzymatic ligation of the free ends.[11]

The chain crossing of a third type of knot is based on the charge-transfer interaction between bipyridinium and 1,5-dioxynaphthalene units; this trefoil knot has been isolated in very low yields.[12]

The first amide knot was obtained in high yield by the condensation of 2,6-pyridinedicarboxylic acid chloride and *p*-diaminodiphenylmethane.[13] This compound was the starting point for a wealth of related knotane derivatives.[2,14] The structure **5** reported here is related to the amide knot but has some unique features: The chain of the knot **5** is directed since it is built from (natural and non-natural) amino acids. To our knowledge, it is the first example of a cyclic peptide having a knot structure in its backbone.[15] The compound has almost $C_3$ symmetry in the solid state and the solution NMR spectra confirm an averaged $C_3$ symmetry. Any intramolecular movement which interconverts the chain segments **A** and **B** in **5** is slow on the NMR time scale. The knot has a polar and a nonpolar surface; thus complexation, encapsulation, or catalytic transformation of molecular guests could be expected. Future investigations will show whether the knot is also formed when amino acids other than L-valine or L-phenylalanine are present. The position and type of amino acids in the sequence can be readily addressed by (solid-phase) peptide synthesis.

Received: March 21, 2006
Revised: May 11, 2006
Published online: July 20, 2006

**Keywords:** cyclopeptides · knots · lactams · macrocycles · steroids

[1] a) S. H. Gellman, *Acc. Chem. Res.* **1998**, *31*, 173–180; b) D. J. Hill, M. J. Mio, R. B. Prince, T. Hughes, J. Moore, *Chem. Rev.* **2001**, *101*, 3893–4011; c) L. H. Yuan, H. Q. Zeng, K. Yamato, A. R. Sanford, W. Feng, H. Atreya, D. K. Sukumaran, T. Szyperski, B. Gong, J. *Am. Chem. Soc.* **2004**, *126*, 16528–16537.

[2] For a recent review, see: O. Lukin, F. Vögtle, *Angew. Chem.* **2005**, *117*, 1480–1501; *Angew. Chem. Int. Ed.* **2005**, *44*, 1456–1477.

[3] For leading references, see: a) A. P. Davis, *Chem. Soc. Rev.* **1993**, *22*, 243–253; b) A. P. Davis, J.-B. Joos, *Coord. Chem. Rev.* **2003**, *240*, 143–156; c) E. Virtanen, E. Kolehmainen, *Eur. J. Org. Chem.* **2004**, 3385–3399.

[4] a) D. Albert, M. Feigel, *Helv. Chim. Acta* **1997**, *80*, 2168–2181; b) D. Albert, M. Feigel, K. Benet-Buchholz, R. Boese, *Angew. Chem.* **1998**, *110*, 2855–2857; *Angew. Chem. Int. Ed.* **1998**, *37*, 2727–2729; c) M. Feigel, R. Ladberg, M. Winter, D. Bläser, R. Boese, *Eur. J. Org. Chem.* **2006**, 371–377.

[5] Significant NOE cross-signals connect the α-hydrogen atom of valine type **B** (αH-$V_B$) and several hydrogen atoms of the valine unit of type **A** (e.g., NH-$V_A$, βH-$V_A$, and $CH_3$-$V_A$) in **5**. Similar data were found in the ROESY spectra of **6**, for example, αH-$F_B$–NH-$F_A$ and αH-$F_B$–βH-$F_A$; see the Supporting Information for more details.

[6] S. Engels, M. Feigel, unpublished results.

[7] R. Ladberg, Dissertation, University of Bochum **2001**.

[8] X-ray crystal structure analysis of **5**: $C_{174}H_{288}N_{12}O_{18}\cdot 12\,C_3H_7OH\cdot 4\,H_2O$, $M_r = 3629.36$, colorless crystal $0.45\times0.30\times0.20$ mm, $a = 23.825(1)$, $b = 25.642(1)$, $c = 37.758(1)$ Å, $V = 23067.1(15)$ Å$^3$, $\rho_{calcd} = 1.045$ g cm$^{-3}$, $\mu = 0.547$ mm$^{-1}$, empirical absorption correction ($0.791 \le T \le 0.899$), $Z = 4$, orthorhombic, space group $P2_12_12_1$ (No. 19), $\lambda = 1.54178$ Å, $T = 223$ K, $\omega$ and $\varphi$ scans, 196089 reflections collected ($\pm h$, $\pm k$, $\pm l$), $[(\sin\theta)/\lambda] = 0.60$ Å$^{-1}$, 40764 independent ($R_{int} = 0.079$) and 29891 observed reflections [$I \ge 2\sigma(I)$], 2306 refined parameters, 2850 geometrical and thermal restraints (SIMU, DELU, SAME, ISOR), $R = 0.099$, $wR^2 = 0.283$, Flack parameter 0.2(2), max./min. residual electron density 0.91/−0.44) e Å$^{-3}$, hydrogen atoms of water could not be located, all others were calculated and refined as riding atoms. The data set was collected on a Nonius KappaCCD diffractometer. Programs used: data collection COLLECT (Nonius **1998**), data reduction Denzo-SMN (Z. Otwinowski, W. Minor, *Methods Enzymol.* **1997**, *276*, 307–326), absorption correction Denzo (Z. Otwinowski, D. Borek, W. Majewski, W. Minor, *Acta Crystallogr. Sect. A* **2003**, *59*, 228–234), structure solution SHELXS-97 (G. M. Sheldrick, *Acta Crystallogr. Sect. A* **1990**, *46*, 467–473), structure refinement SHELXL-97 (G. M. Sheldrick, Universität Göttingen, **1997**), graphics SCHAKAL (E. Keller, Universität Freiburg, **1997**). CCDC-600890 contains the supplementary crystallographic data for this paper. These data can be obtained free of charge from The Cambridge Crystallographic Data Centre via www.ccdc.cam.ac.uk/data_request/cif.

[9] a) C. Dietrich-Buchecker, G. Rapenne, J.-P. Sauvage, A. De Cian, J. Fischer, *Chem. Eur. J.* **1999**, *5*, 1432–1439; b) F. Vögtle, A. Hünten, E. Vogel, S. Buschbeck, O. Safarowsky, J. Recker, A.-H. Parham, M. Knott, W. M. Müller, U. Müller, Y. Okamoto, T. Kubota, W. Lindner, E. Francotte, S. Grimme, *Angew. Chem.* **2001**, *113*, 2534–2537; *Angew. Chem. Int. Ed.* **2001**, *40*, 2468–2471.

[10] a) C. O. Dietrich-Buchecker, J.-P. Sauvage, *Angew. Chem.* **1989**, *101*, 192–194; *Angew. Chem. Int. Ed. Engl.* **1989**, *28*, 189–192; b) C. O. Dietrich-Buchecker, J. Guilhem, C. Pascard, J.-P. Sauvage, *Angew. Chem.* **1990**, *102*, 1202–1204; *Angew. Chem. Int. Ed. Engl.* **1990**, *29*, 1154–1156; c) for a review see: "Molecular Knots—From Early Attempts to High-Yield Template Synthesis": J.-P. Sauvage, C. Dietrich-Buchecker in *Molecular Catenanes, Rotaxanes and Knots* (Eds.: J.-P. Sauvage, C. Dietrich-Buchecker), Wiley-VCH, Weinheim, **1999**, pp. 107–142.

[11] a) J. E. Mueller, S. M. Du, N. C. Seeman, *J. Am. Chem. Soc.* **1991**, *113*, 6306–6308; b) N. C. Seeman, *Angew. Chem.* **1998**, *110*, 3408–3428; *Angew. Chem. Int. Ed.* **1998**, *37*, 3220–3238.

[12] P. R. Ashton, O. A. Matthews, S. Menzer, F. M. Raymo, N. Spencer, J. F. Stoddart, D. J. Williams, *Liebigs Ann.* **1997**, 2485–2494.

[13] O. Safarowsky, M. Nieger, R. Fröhlich, F. Vögtle, *Angew. Chem.* **2000**, *112*, 1699–1701; *Angew. Chem. Int. Ed.* **2000**, *39*, 1616–1618.

[14] a) O. Lukin, J. Recker, A. Böhmer, W. M. Müller, T. Kubota, Y. Okamoto, M. Nieger, F. Vögtle, *Angew. Chem.* **2003**, *115*, 458–461; *Angew. Chem. Int. Ed.* **2003**, *42*, 442–445; b) O. Lukin, W. M. Müller, U. Müller, A. Kaufmann, C. Schmidt, J. Leszczynski, F. Vögtle, *Chem. Eur. J.* **2003**, *9*, 3507–3517; c) O. Lukin, T. Kubota, Y. Okamoto, F. Schelhase, A. Yoneva, W. M. Müller,

 © 2006 Wiley-VCH Verlag GmbH & Co. KGaA, Weinheim 

U. Müller, F. Vögtle, *Angew. Chem.* **2003**, *115*, 4681 – 4684; *Angew. Chem. Int. Ed.* **2003**, *42*, 4542 – 4545; d) O. Lukin, T. Kubota, Y. Okamoto, A. Kaufmann, F. Vögtle, *Chem. Eur. J.* **2004**, *10*, 2804 – 2810.

[15] Cyclic peptides containing a knotted arrangement of disulfide bonds are known, for example: K. J. Rosengren, N. L. Daly, M. R. Plan, C. Waine, D. J. Craik, *J. Biol. Chem.* **2003**, *278*, 8606 – 8616.

 © 2006 Wiley-VCH Verlag GmbH & Co. KGaA, Weinheim 

Nanobiotechnology

DOI: 10.1002/anie.200600644

# Controlling the Activity of the 20S Proteasome Complex by Synthetic Gatekeepers**

*Katrin Schulze, Alart Mulder, Ali Tinazli, and Robert Tampé**

The 26S proteasome complex is the central degradation machinery in eukaryotic cells. It is composed of a proteolytically active core complex, the 20S proteasome, and the 19S or 11S regulatory particles (RPs). Within the ubiquitin–proteasome pathway, the proteasome complex is responsible for the degradation of unwanted and malfunctioning proteins.[1] It regulates a variety of key cellular processes, such as transcription, signal transduction, and apoptosis, and is involved in tumor development.

Four stacked heptameric rings ($\alpha_7\beta_7\beta_7\alpha_7$) enclosing three nanocompartments make up the 700-kDa barrel-shaped architecture of the 20S proteasome. The central degradation chamber is built up by two inner rings, each containing seven β subunits. The two outer rings consisting of seven closely packed α subunits give rise to two antechambers (Scheme 1a).[2] Substrate entry into this multicatalytic enzyme complex is suggested to be gated by the N-terminal tails of the α subunits. In the latent state, these N-terminal tails are anchored by an intricate lattice of interactions that restrict substrate entry through the orifices at both ends of the proteasome complex. The N-terminal tails are only a partial barrier to the passage of protein substrates as the restriction is not sufficient enough to hamper the entrance and degradation of short polypeptides.[3] These apertures open after association with RPs, like PA700, PA28, or PAN, that render the complex active and enable the processive degradation of proteins.[4,5]

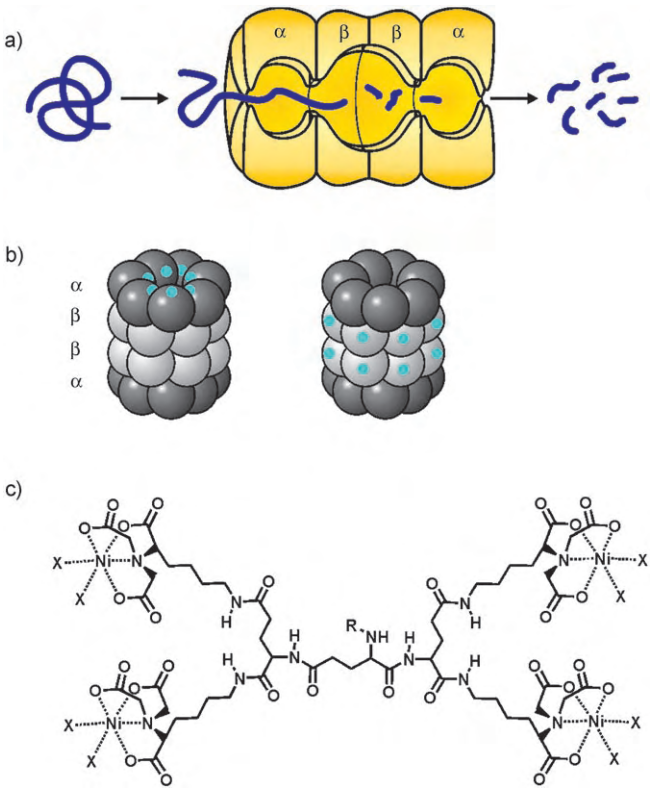


***Scheme 1.*** a) Substrate degradation by the 20S proteasome complex. Proteins are degraded inside the 20S proteasome complex and peptides are released. Substrate entry as well as product exit occur at both apertures of the proteasome. Access to the complex is controlled by the N-terminal tails of the α subunits. b) His tags (turquoise) were introduced either at the N termini of the α subunits (αN $His_6$–proteasome, left) or at the C termini of the β subunits (βC $His_6$–proteasome, right) of the 20S proteasome from *T. acidophilum*. c) Chemical structure of the nickel(II)-loaded tetrakisNTA. R = H, carboxyfluorescein, or ATTO565; X = free coordination site occupied by water or histidine.

The N-terminal tails of the archaeal α subunits are unstructured, allowing substrate access through ca. 13-Å large entrances even without special regulators.[6] The importance of each of these two orifices as both entry and exit gates has been demonstrated by breaking the $D_7$ symmetry of the 20S proteasome from *Thermoplasma acidophilum* by site-specific, uniformly oriented immobilization at nitrilotriacetic acid (NTA) interfaces.[7]

Herein, we present the use of a small synthetic gatekeeper to specifically and reversibly control the proteolytic activity of the 20S proteasome complex. A multivalent chelator head (MCH) with four NTA moieties (tetrakisNTA, Scheme 1c) is used to crosslink His tags introduced either at the N-terminal tails of the α subunits around the two openings (αN $His_6$–proteasome) or at the C-termini of the β subunits located at the side of the proteasome (βC $His_6$–proteasome, Scheme 1b).[8] The MCH is able to complex multiple histidine residues at its nickel(II) centers and forms strong, nanomolar-affinity complexes with histidine tags.[9]

[*] K. Schulze, Dr. A. Mulder, A. Tinazli, Prof. R. Tampé
Institute of Biochemistry, Biocenter
Johann Wolfgang Goethe-University
Max-von-Laue-Strasse 9, 60438 Frankfurt a. M. (Germany)
Fax: (+49) 69-798-29495
E-mail: tampe@em.uni-frankfurt.de

[**] We would like to thank Drs. Silke Hutschenreiter, Suman Lata and Jacob Piehler for useful discussions and support as well as Gerhard Spatz-Kümbel for excellent technical assistance. The Deutsche Forschungsgemeinschaft (DFG) and the Bundesministerium für Bildung und Forschung (BMBF) supported this research.


InterScience
© 2006 Wiley-VCH Verlag GmbH & Co. KGaA, Weinheim

We first analyzed the binding of fluorescent tetrakisNTA to the 20S proteasome from *T. acidophilum* by gel filtration chromatography. The αN $His_6$–proteasome was eluted with a retention volume ($V_R$) of 1.44 mL (≈700 kDa, Figure 1a).

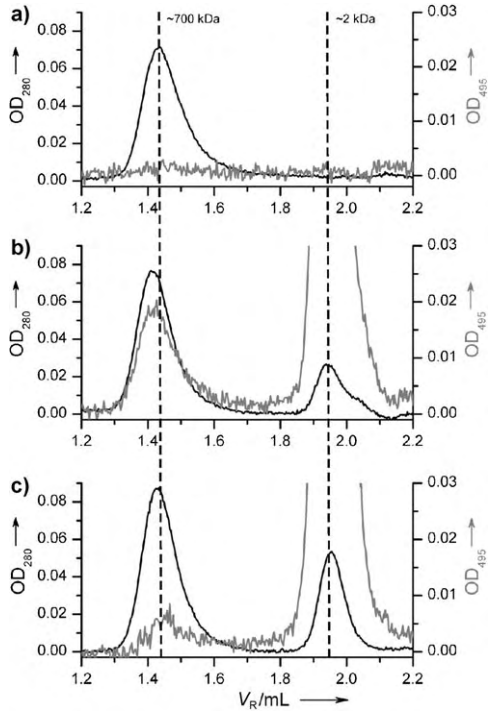


***Figure 1.*** Stable complex formation of tetrakisNTA(fluorescein) with the 20S proteasome from *T. acidophilum* analyzed by gel filtration. αN $His_6$–proteasome without a) and with b) 10-fold molar excess of tetrakisNTA(fluorescein). c) Isolation of the released 20S proteasome by addition of imidazole (50 mM) to the running buffer solution. The absorbance was monitored at 280 nm (black) and 495 nm (gray).

After incubation with a 10-fold molar excess of tetrakisNTA(fluorescein), the 20S proteasome elution peak at an optical density (OD) of 280 nm shows coinciding absorbance with 495 nm and a shift to a slightly lower $V_R$ (1.41 mL), indicating stable complex formation. Free tetrakisNTA(fluorescein) elutes at a $V_R$ of 1.94 mL (≈2 kDa, Figure 1b). No labeling was observed for proteins without histidine tags[10] or in the presence of ethylenediamine tetraacetate ($EDTA^{2-}$; 10 mM) or imidazole (100 mM), demonstrating that MCH binding is site specific. Near-complete dissociation (70–80%) of the MCHs–proteasome complex is achieved upon exposure to imidazole (50 mM), demonstrating the reversibility of the interaction (Figure 1c). Similar results were obtained for the βC $His_6$–proteasome (data not shown).

The number of MCHs bound to the isolated proteasome complexes was determined through the characteristic absorbance of the attached fluorophore and the protein concentration by using a bicinchoninic acid (BCA) assay.[11] As a result, two (±0.8) tetrakisNTA were bound to one αN $His_6$–proteasome complex, implying that one tetrakisNTA moiety is attached at each entrance of the proteasome. For the βC $His_6$–proteasome, stoichiometries of 1:3 (±0.2) were determined. This higher labeling ratio can be explained by less-densely clustered histidine tags on the βC $His_6$–proteasome.[8]

To provide evidence for the specificity of the MCH–His-tag interaction, *E. coli* cell lysates with ≈4300 different gene products[12] were incubated with tetrakisNTA(ATTO565) and analyzed by native-PAGE and fluorescence imaging (Figure 2). Comparison with isolated αN or βC $His_6$–proteasomes indicates that the fluorescent bands at ≈700 kDa (red arrow) correspond to labeled 20S proteasomes, which run slightly faster than unlabeled complexes (black arrow) because of the additional negative charges of the fluorescent MCHs. No labeling could be observed in cell lysates without expression of recombinant 20S proteasomes, demonstrating the high selectivity and specificity.

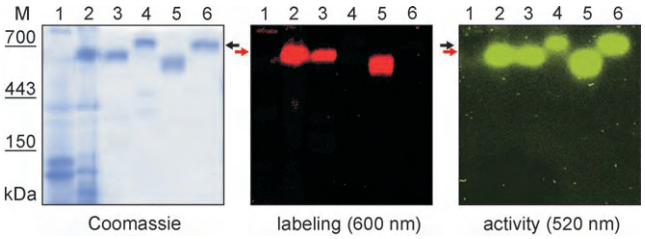


***Figure 2.*** Specific labeling of 20S proteasomes within a complete cell lysate analyzed by native-PAGE and fluorescence imaging. Cell lysates (140 μg *E. coli* proteins) or isolated 20S proteasomes (4 μg in buffer solution A, see the Experimental Section) were incubated with tetrakisNTA(ATTO565) (17.1 pmol in lanes 1, 2, 3, and 5). Cell lysate without (lane 1) and with expression (lane 2) of αN $His_6$–proteasome. Labeled and unlabeled αN (lanes 3 and 4) as well as βC $His_6$–proteasomes (lanes 5 and 6). Proteins were stained by coomassie brilliant blue G250 (left). TetrakisNTA(ATTO565) was detected at $\lambda_{em}$ 600 nm (middle). The activity of 20S proteasomes was monitored at $\lambda_{em}$ 520 nm by an overlay assay with Suc-LLVT-AMC (100 μM; right). Black arrow and red arrow: unlabeled and labeled 20S proteasomes, respectively. M = molecular-weight marker, Suc = succinyl.

To investigate the peptidase activity of the 20S proteasomes toward small fluorogenic substrates, an in-gel-substrate overlay assay was performed by using Suc-LLVT-AMC.[13] Proteolytic cleavage of this nonfluorescent peptide leads to the release of fluorescent amino-4-methylcoumarin (AMC).[14] Fluorescence imaging of the overlaid gel shows that both the free and the labeled complexed proteasomes are active, and that the association of the MCHs has no significant influence on the peptidase activity of the archaeal proteasomes toward peptidic substrates. These findings are in agreement with the observation that the packing of the N-terminal tails of the α subunits does not affect the entry of small peptides into the degradation chamber.[5]

The overlay assay only shows activity of single peptidase sites. Proteins have to be used as substrates to investigate the processive proteolytic activity of the proteosomes. Therefore, the influence of the MCHs on the degradation of fluorescein-labeled casein by the 20S proteasome was studied (Figure 3). Cleavage between fluorescein molecules attached to the casein leads to an increase in the fluorescence signal,[14] thus allowing the direct comparison of the activities of the free and complexed 20S proteasomes. Both recombinant 20S protea-

 © 2006 Wiley-VCH Verlag GmbH & Co. KGaA, Weinheim 

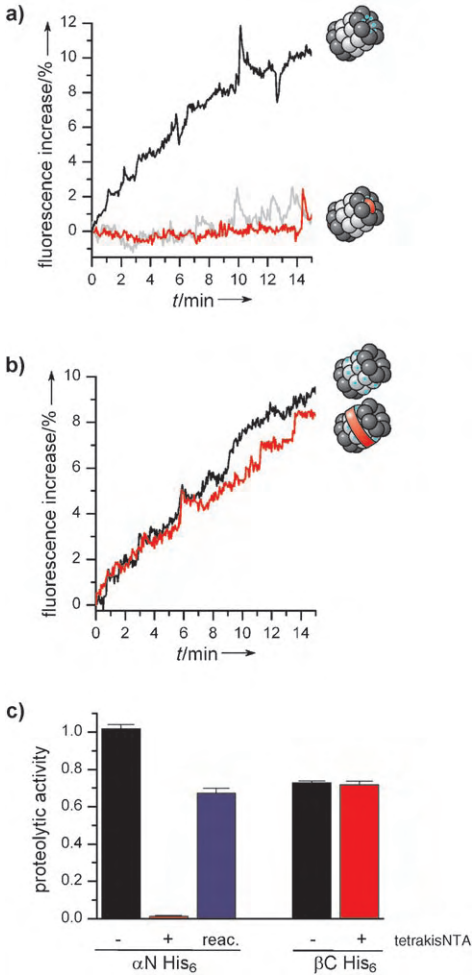


***Figure 3.*** Real-time degradation of fluorescein-labeled casein (100 nM) by 20S proteasomes (10 nM) in buffer solution A at 60 °C. a) Activity of the αN $His_6$–proteasome before (black trace) and after incubation with tetrakisNTA (140 nM; red trace) compared with the equilibrated fluorescein-labeled casein (gray trace). b) Activity of the βC $His_6$–proteasome before (black trace) and after incubation with tetrakisNTA (10 μM; red trace). c) Proteolytic activities of the recombinant 20S proteasomes with (red column) and without (black columns) tetrakisNTA, as well as activity of the reactivated αN $His_6$–proteasome after treatment with 50 mM imidazole (blue column).

somes have comparable activities (Figure 3, black traces and columns). However, after incubation with tetrakisNTA, the activity of the αN $His_6$–proteasomes is completely blocked, whereas the activity of the βC $His_6$–proteasomes is not even affected by a 1000-fold molar excess of tetrakisNTA (red traces and columns). These results indicate that binding of the MCHs to the histidine tags at the entrances leads to a specific and complete blockage of protein substrate entry into the degradation machinery.

Apparently, binding of the MCH leads to the organization of the His-tagged N-terminal tails near the entrances to the degradation chamber, thereby inhibiting processive protein degradation. In the absence of nickel (II) ions and/or the presence of $EDTA^{2-}$, the MCHs did not influence the proteolytic activity of the αN $His_6$–proteasome, demonstrating specific binding and full enzyme control. Imidazole competes in binding against the His tags and can be used to reactivate the blocked proteasomes. Removal of the synthetic gatekeeper and isolation of the free αN $His_6$–proteasomes were performed by gel filtration (Figure 1c). The isolated, reactivated αN $His_6$–proteasomes show 70–80% of the original proteolytic activity, which nicely corresponds to the amount of uncomplexed proteasome obtained after gel filtration (Figure 3c). Therefore, inactivation of the 20S proteasome by the MCH is completely reversible, and the inherent processive proteolytic activity of the 20S proteasome is not affected by the complexation/decomplexation processes.

In conclusion, based on the nanomolar and highly specific binding properties, tetrakisNTA is a versatile tool for specific protein labeling even within the entire cell lysate. The high stability of the MCH–His-tag interaction allows the visualization and straightforward quantification of recombinant proteins by native-PAGE and fluorescence imaging. The reversible inhibition of the αN $His_6$–proteasome by tetrakisNTA for proteinaceous substrates demonstrates that the MCH can also be applied for the specific control and designed manipulation of macromolecular machines. The high specificity and binding affinity would, in principle, allow for labeling in vivo and inactivation of the 20S proteasome, which, based on its central role in numerous cellular processes, would be of great and general interest.

## Experimental Section

Multivalent chelator head (MCH): The tetrakisNTA was synthesized as described.[9] Carboxyfluorescein- (Fluka) or ATTO565-*N*-hydroxysuccinimide ester (ATTO-TEC were coupled to the amino groups of the MCH in *N*,*N*-dimethylformamide (DMF). Purification of the fluorescent MCH was performed by reversed-phase $C_{18}$ HPLC, followed by loading the MCH with nickel(II) ions. The excess of nickel(II) ions was removed by anion-exchange chromatography (HiTrap Q, GE Healthcare). The tetrakisNTA concentration was determined by the absorption of the attached fluorophore.

20S proteasomes: The expression and purification of the recombinant 20S proteasomes was carried out as previously described.[7,8] For stable complex formation with the MCH, the 20S proteasome was incubated with a 10-fold molar excess of tetrakisNTA for 3 h on ice in buffer solution A (20 mM HEPES, 150 mM NaCl, pH 7.5). HEPES = *N*-2-hydroxyethylpiperazine-*N*′-2-ethanesulfonic acid.

Gel filtration studies: For the gel filtration, a Superose 6 PC 3.2 column (GE Healthcare) was equilibrated in buffer solution A with a flow rate of 50 μL $min^{-1}$ at 10 °C. A 50-μL portion of 20S proteasome (0.8 μM) in buffer solution A was added. To remove the tetrakisNTA from the 20S proteasome, the labeled proteasomes were incubated with imidazole (50 mM) in buffer solution A for 0.5 h on ice. The reactivated 20S proteasomes were isolated by gel filtration with imidazole (50 mM) in buffer solution A.

Native-PAGE: The native-PAGE as well as the substrate overlay assay were performed essentially as outlined by using a stacking gel with 3.5% polyacrylamide.[13] The $EDTA^{2-}$ concentration was reduced to 100 μM to prevent interference with the MCH–His-tag interaction. Cell lysates with 140 μg of *E. coli* proteins as well as 4 μg of purified αN and βC $His_6$–proteasomes with and without fluorescent tetrakisNTA (17.1 pmol) in buffer solution A were loaded to the gel. After electrophoresis, the gel was overlaid with Suc-LLVT-AMC (100 μM; Bachem) in Tris-HCl buffer solution (Tris (30 mM), $MgCl_2$ (5 mM), KCl (10 mM), DTT (0.5 mM); pH 7.8) for 20 min at 37 °C to

 © 2006 Wiley-VCH Verlag GmbH & Co. KGaA, Weinheim 

investigate the activities of the 20S proteasomes. Tris = tris(hydroxylmethyl)aminomethane, DTT = 1,4-dithiothreitol.

Degradation of fluorescein-labeled casein: The activities of the labeled and unlabeled 20S proteasomes were determined as published previously.[7,14] For labeling, a 14- or 1000-fold molar excess of the tetrakisNTA was used. The 20S proteasomes were added to a final concentration of 10 nM to a 100 nM solution of fluorescein-labeled casein in buffer solution A at 60 °C. The fluorescence increase was monitored over 15 min at 495 nm.

Received: February 17, 2006
Published online: July 21, 2006

**Keywords:** biotechnology · fluorescence · inhibitors · protein engineering · proteomics

[1] a) D. Voges, P. Zwickl, W. Baumeister, *Annu. Rev. Biochem.* **1999**, *68*, 1015; b) A. L. Goldberg, *Nature* **2003**, *426*, 895; c) M. Groll, M. Bochtler, H. Brandstetter, T. Clausen, R. Huber, *ChemBioChem* **2005**, *6*, 222; d) A. Ciechanover, *Angew. Chem.* **2005**, *117*, 6095; *Angew. Chem. Int. Ed.* **2005**, *44*, 5944; ; e) A. Hershko, *Angew. Chem.* 2005, 117, 6082; *Angew. Chem. Int. Ed.* **2005**, *44*, 5932.

[2] a) M. Groll, L. Ditzel, J. Löwe, D. Stock, M. Bochtler, H. D. Bartunik, R. Huber, *Nature* **1997**, *386*, 463; b) M. Groll, M. Bajorek, A. Kohler, L. Moroder, D. M. Rubin, R. Huber, M. H. Glickman, D. Finley, *Nat. Struct. Biol.* **2000**, *7*, 1062.

[3] A. Forster, F. G. Whitby, C. P. Hill, *EMBO J.* **2003**, *22*, 4356.

[4] a) M. Groll, H. Brandstetter, H. Bartunik, G. Bourenkow, R. Huber, *J. Mol. Biol.* **2003**, *327*, 75; b) F. G. Whitby, E. I. Masters, L. Kramer, J. R. Knowlton, Y. Yao, C. C. Wang, C. P. Hill, *Nature* **2000**, *408*, 115; c) M. Groll, R. Huber, *Int. J. Biochem. Cell Biol.* **2003**, *35*, 606.

[5] D. M. Smith, G. Kafri, Y. Cheng, D. Ng, T. Walz, A. L. Goldberg, *Mol. Cell* **2005**, *20*, 687.

[6] a) J. Löwe, D. Stock, B. Jap, P. Zwickl, W. Baumeister, R. Huber, *Science* **1995**, *268*, 533; b) W. Baumeister, A. Lupas, *Curr. Opin. Struct. Biol.* **1997**, *7*, 273.

[7] S. Hutschenreiter, A. Tinazli, K. Model, R. Tampé, *EMBO J.* **2004**, *23*, 2488.

[8] A. Thess, S. Hutschenreiter, M. Hofmann, R. Tampé, W. Baumeister, R. Guckenberger, *J. Biol. Chem.* **2002**, *277*, 36321.

[9] S. Lata, A. Reichel, R. Brock, R. Tampé, J. Piehler, *J. Am. Chem. Soc.* **2005**, *127*, 10205.

[10] C. van der Does, C. Presenti, K. Schulze, S. Dinkelaker, R. Tampé, *J. Biol. Chem.* **2006**, *281*, 5694.

[11] P. K. Smith, R. I. Krohn, G. T. Hermanson, A. K. Mallia, F. H. Gartner, E. K. Provenzano, E. K. Fujimoto, N. M. Goeke, B. J. Olson, D. C. Klenk, *Anal. Biochem.* **1985**, *150*, 76.

[12] F. R. Blattner, G. Plunkett, 3rd, C. A. Bloch, N. T. Perna, V. Burland, M. Riley, J. Collado-Vides, J. D. Glasner, C. K. Rode, G. F. Mayhew, J. Gregor, N. W. Davis, H. A. Kirkpatrick, M. A. Goeden, D. J. Rose, B. Mau, Y. Shao, *Science* **1997**, *277*, 1453.

[13] S. Hua, W. Y. To, T. T. Nguyen, M. L. Wong, C. C. Wang, *Mol. Biochem. Parasitol.* **1996**, *78*, 33.

[14] T. N. Akopian, A. F. Kisselev, A. L. Goldberg, *J. Biol. Chem.* **1997**, *272*, 1791.

 © 2006 Wiley-VCH Verlag GmbH & Co. KGaA, Weinheim 

Methane Activation

DOI: 10.1002/anie.200601273

# Low-Temperature Activation of Methane: It also Works Without a Transition Metal**

*Detlef Schröder* and Jana Roithová**

*Dedicated to Professor Antonín Holý on the occasion of his 70th birthday*

The activation of methane at ambient conditions and its conversion into more valuable feedstocks is a challenge for future, because it would permit a much more efficient use of methane from either geological deposits or biogenic sources.[1] Most low-temperature routes for the activation of methane are based on transition-metal catalysts, and particularly promising approaches involve the functionalization of methane with the aid of platinum complexes.[2] While these systems achieve the activation of methane under comparably mild conditions, they are far removed from possible future applications in large-scale processes because of the expensive catalysts or because of the nature of the products.[3]

A promising catalyst for the low-temperature activation of methane is $Li^+$ ion doped magnesium oxide, although this still needs considerable improvement before large-scale applications would be feasible.[1,4] This improvement is the point where basic research can complement applied science by means of providing a more detailed understanding of the underlying elementary steps at a molecular level. Accordingly, the reactions of diatomic MgO as well as several model clusters have been studied extensively by means of theory.[5–9] Theory strongly suggests that the cationic species $[MgO]^+$ should effectively activate methane,[10,11] and also for neutral MgO the computed activation barrier is rather low.[9] Accordingly, the elementary steps in the chemistry of magnesium and its oxides have received considerable attention in several experimental studies,[12–19] yet a decisive route for the generation of ionic species such as $[MgO]^+$ in amounts

[*] Dr. D. Schröder, Dr. J. Roithová
Institute of Organic Chemistry and Biochemistry
Academy of Science of the Czech Republic
Flemingovo nám. 2, 16610 Prague 6 (Czech Republic)
Fax: (+420) 220-183-583
E-mail: detlef.schroeder@uochb.cas.cz
jana.roithova@uochb.cas.cz
Dr. D. Schröder
Institut für Chemie
Technische Universität Berlin
Strase des 17. Juni 135, 10623 Berlin (Germany)
Fax: (+49) 303-142-1102

[**] This work was supported by the Grant Agency of the Academy of Sciences of the Czech Republic (Nr. KJB4040302) and the Deutsche Forschungsgemeinschaft (Sfb546). The authors thank Pavel Jungwirth for inspiring discussions. D.S. very much appreciates the continuous and grateful support of his research by Prof. Helmut Schwarz (TU-Berlin, Berlin (Germany)).


© 2006 Wiley-VCH Verlag GmbH & Co. KGaA, Weinheim

sufficient for subsequent reactivity studies has not been achieved to date.

Herein, we describe a new method for the generation of gaseous $[MgO]^+$ ions by means of electrospray ionization (ESI)[20] of aqueous magnesium(II) nitrate under enforced ionization conditions and address their gas-phase reactivity for the very first time.[21–23] Under mild conditions, ESI of $Mg(NO_3)_2$ affords cations of the type $[Mg(NO_3)(H_2O)_n]^+$ with $n$ up to 4 as the leading mononuclear species.[24] Increasingly harsher ionization conditions lead to consecutive losses of the water ligands to give bare $[Mg(NO_3)]^+$ ions, which—upon further activation—undergo subsequent fragmentation to afford $[MgO]^+$ concomitant with neutral $NO_2$ as the major products.[25,26] Thereby, ESI provides a straightforward route for the generation of gaseous $[MgO]^+$ in yields fully sufficient for reactivity studies.

When mass-selected $[MgO]^+$ is allowed to interact with methane (Figure 1), the reaction in Equation (1) occurs,

$$[MgO]^+ + CH_4 \rightarrow [MgOH]^+ + CH_3 \quad (1)$$

which proceeds with a rate constant of $k = (3.9 \pm 1.3) \times 10^{-10}\ cm^3\,s^{-1}$, corresponding to about 40% of the gas-kinetic collision rate. Likewise, $[MgOD]^+$ is formed in the presence of the deuterated methanes $CH_2D_2$ and $CD_4$, and a neutral-gain spectrum (Figure 1B)[27,28] reveals the expected isotope pattern for $[MgO]^+$ as the only ion present which is able to activate methane. From the ratio of the products $[MgOH]^+$ and $[MgOD]^+$ in the reaction with $CH_2D_2$, an intramolecular kinetic isotope effect (KIE) of $2.1 \pm 0.1$ can be derived. A value of similar magnitude has been observed in the reaction of $CH_2D_2$ with $[MoO_3]^+$ (KIE = 2.0),[29] whereas in the $[V_4O_{10}]^+/CH_2D_2$ system—which can be regarded as a prototype of a simple hydrogen-atom abstraction mechanism—the KIE amounts to only 1.35,[30] and is thus very similar to a KIE of about 1.3 for the H(D)-atom abstraction from methane by free OH radicals.[31] Not surprisingly, however, the intermolecular KIE in the reaction of $[MgO]^+$ with $CH_4$ or $CD_4$ is significantly lower (KIE = $1.3 \pm 0.2$).[32]

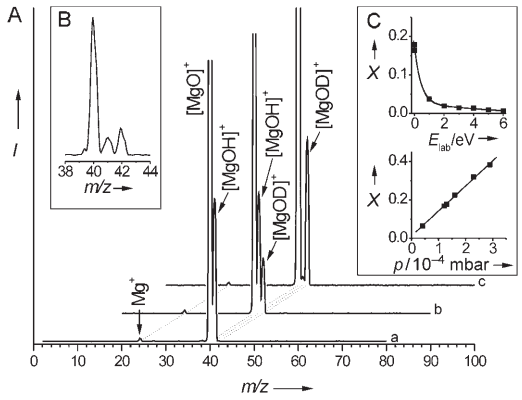


***Figure 1.*** A) Ion/molecule reactions of mass-selected $[MgO]^+$ with a) $CH_4$, b) $CH_2D_2$, and c) $CD_4$. The major reaction corresponds to H(D)-atom abstraction to afford $[MgOH]^+$ and $[MgOD]^+$, respectively. B) a neutral-gain spectrum with $\Delta m = 2$ in the presence of $CH_2D_2$, displaying the natural isotope pattern of $[MgO]^+$, as expected. C) The dependences of the $[MgO]^+$ conversion ($X$) on the interaction energy $E_{lab}$ (top) and the methane pressure (bottom). The small signal of $[MgOH]^+$ in the reaction with $CD_4$ (Figure 1Ac) is due to hydrogen-abstraction from water present in the background.

Additional mechanistic evidence concerns the rapid decrease of the conversion at elevated collision energies as well as the linear pressure dependence, which are both fully consistent with the occurrence of a thermal ion/molecule reaction (Figure 1C). In addition to hydrogen-atom abstraction from methane, a small amount of oxygen-atom transfer is observed [Eq. (2)] with a branching ratio below 2% for all

$$[MgO]^+ + CH_4 \rightarrow [Mg]^+ + CH_3OH \quad (2)$$

methane isotopologs. A trace amount of $[MgCH_2]^+ + H_2O$ is also observed, but this channel is close to the detection limit and therefore not pursued any further. Summarizing the experimental findings, it is clear that bare $[MgO]^+$ ions can efficiently activate methane with H-atom abstraction as the major pathway and O-atom transfer as only a minor route.

Further insight is gained by theoretical calculations of the $[MgCH_4O]^+$ system. While previous theoretical work exist,[10,11] the experimental findings reported herein, prompted us to reconsider the $[MgCH_4O]^+$ surface using still limited, but yet somewhat more elaborate theoretical methods. According to our theoretical calculations,[33] $[MgO]^+$ ion forms a remarkably strong encounter complex in which the methane is coordinated to the positively charged metal center. Note that the spin is almost exclusively located at the oxygen, such that the binding situation might be described as $CH_4\cdots Mg^{2+}\cdots O^{-\bullet}$, thereby mimicking the character of an oxygen-centered radical which is considered to be crucial in this type of methane activation.[1–4] The C–H bond activation of methane can then proceed via a transition structure (TS) which is energetically close to the entrance channel ($[MgO]^+ + CH_4$). Furthermore, this TS also is the highest point along the reaction coordinate of the reactions in Equations (1) as well as (2), and it thus represents the rate-determining step en route to product formation (Figure 2).

From the TS, the reaction proceeds to an intermediate, which is best described as the complex of a methyl radical with an $[MgOH]^+$ ion; fully consistent with this description, the spin is entirely located on the methyl group. The intermediate $CH_3\cdots[MgOH]^+$ also serves as the branch point for product formation in that either the methyl radical is lost directly or—in a long-range migration—the methyl group undergoes a rebound with the hydroxy group located at magnesium to afford the methanol/$Mg^+$ complex as the global minimum of the $[MgCH_4O]^+$ surface; this complex can eventually dissociate into $Mg^+ + CH_3OH$. Even though oxygen-atom transfer, Equation (2), is overall considerably more exothermic than hydrogen abstraction, Equation (1), the latter can compete very efficiently because the direct dissociation of intermediary $CH_3\cdots[MgOH]^+$ is entropically preferred, once the rate-determining TS is surpassed. The theoretical calculations thereby fully confirm present and previous experimental observations:

1) The occurrence of a thermal ion/molecule reaction with a rate on the order of magnitude of the gas-kinetic collision rate, but yet below unit efficiency, is in harmony with the

 © 2006 Wiley-VCH Verlag GmbH & Co. KGaA, Weinheim 

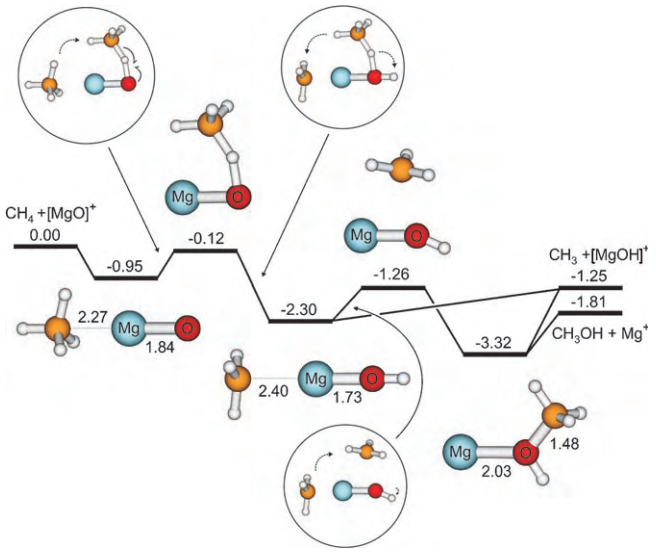


***Figure 2.*** Potential-energy surface (in eV) for the reaction of $[MgO]^+$ with $CH_4$ calculated at the MP2/6-311+G(2d,2p) level of theory; selected bond lengths [Å]. The encircled structures depict the rearrangements occurring along the reaction coordinate. Note that calculations using the B3LYP hybrid method lead to qualitatively similar results.

predicted rate-determining TS being situated only about 0.1 eV below the entrance channel of separated $[MgO]^+ + CH_4$.

2) The observed distribution between the reactions in Equations (1) and (2) is fully consistent with the computed surface.
3) Last but not least, the calculated exothermicities for the reactions in Equations (1) and (2) are in reasonable agreement with literature data.[12,13,17,34,35]

The most important result of the theoretical investigations is, however, that the C–H bond activation cannot just be described in terms of a simple hydrogen-atom abstraction process. Instead, throughout the entire reaction coordinate from the encounter complex to the $CH_3\cdots[MgOH]^+$ intermediate a significant interaction exists between the magnesium center and the carbon atom, which favorably assists C–H bond activation. In contrast, the transition structure for a hydrogen-atom abstraction by the oxygen atom in direct end-on attack of the C–H bond is only 0.01 eV below the entrance channel and thus cannot compete with the mechanism shown in Figure 2 in which the process is assisted by the Mg–C interaction. Consequently, the consideration of $Li^+$ ion doped magnesium oxide as a mere hydrogen-atom abstractor may be regarded as an oversimplification. The assisted mechanism proposed herein offers a strategy to eventually facilitate the activation of methane by deliberate incorporation of Lewis acidic sites.

In a more general perspective, the question arises as to whether the gas-phase studies of diatomic $[MgO]^+$ described herein can serve as models for the reactions occurring in methane activation by heterogeneous catalysts. Fortunately, the ESI conditions described above also permit the formation of the cluster ion $[Mg_2O_2]^+$, which can be regarded as the most simple cluster unit of $[MgO]^+$.[36] Herein, we thus report preliminary results about the gas-phase reactivity of this small cluster ion which will the basis of forthcoming studies. Not unexpectedly, $[Mg_2O_2]^+$ turns out to be less reactive than $[MgO]^+$ itself and does not activate methane. Nevertheless, $[Mg_2O_2]^+$ still is able to activate small hydrocarbons, such as propane and butane [Eq. (3) and (4) with $n=3$ and 4,

$$[Mg_2O_2]^+ + C_nH_{2n+2} \rightarrow [Mg_2O_2H]^+ + C_nH_{2n+1} \quad (3)$$

$$[Mg_2O_2]^+ + C_nH_{2n+2} \rightarrow [Mg_2O_2H_2]^+ + C_nH_{2n} \quad (4)$$

respectively], though with a rate about one order of magnitude lower than for diatomic $[MgO]^+$.

The ability of $[Mg_2O_2]^+$ to activate C–H bonds in general and the occurrence of hydrogen-atom abstraction in particular [Eq. (3)] suggest that the radical character of the oxygen atom also is maintained in the dinuclear cluster. While clustering is associated with some decrease of reactivity, the overall reactivity pattern is thus maintained. The cluster ion $[Mg_2O_2]^+$ is less reactive than the monomer, which can be ascribed to the lower positive charge of the magnesium centers in the cluster, resulting in a decreased energy gain upon coordination of methane and hence an increased barrier to C–H activation. Therefore, future strategies for the low-temperature activation of methane should not only focus on the generation of particularly reactive oxygen-centered radicals capable of hydrogen-atom abstraction, but also consider the additional energy benefit which can be gained by metal–carbon interactions.

Received: March 31, 2006
Published online: July 21, 2006

**Keywords:** ab initio calculations · hydrogen abstraction · magnesium · mass spectrometry · methane activation

[1] J. H. Lunsford, *Catal. Today* **2000**, *63*, 165.
[2] M. Lersch, M. Tilset, *Chem. Rev.* **2005**, *105*, 2471.
[3] J. A. Labinger, *J. Mol. Catal. A* **2004**, *220*, 27.
[4] J. H. Lunsford, *Angew. Chem.* **1995**, *107*, 1059; *Angew. Chem. Int. Ed. Engl.* **1995**, *34*, 970.
[5] K. J. Borve, L. G. M. Pettersson, *J. Phys. Chem.* **1991**, *95*, 7401.
[6] A. I. Boldyrev, J. Simons, *J. Phys. Chem.* **1996**, *100*, 8023.
[7] M. A. Johnson, E. V. Stefanovich, T. N. Truong, *J. Phys. Chem. B* **1997**, *101*, 3196.
[8] A. d'Ercole, C. Pisani, *J. Chem. Phys.* **1999**, *111*, 9743.
[9] C.-W. Hu, H.-Q. Yang, N.-B. Wong, Y.-Q. Chen, M.-C. Gong, A.-M. Tian, C. Li, W.-K. Lee, *J. Phys. Chem. A* **2003**, *107*, 2316.
[10] M.-A. D. Stiakki, A. C. Tsipis, C. A. Tsipis, C. E. Xanthopoulos, *New J. Chem.* **1994**, *18*, 203.
[11] D. Nachtigallová, M. Roeselová, R. Zahradník, *Chem. Phys. Lett.* **1997**, *270*, 357.
[12] M. M. Kappes, R. H. Staley, *J. Phys. Chem.* **1981**, *85*, 942.
[13] L. Operta, E. C. Tews, T. J. McMahon, B. S. Freiser, *J. Am. Chem. Soc.* **1989**, *111*, 9152.
[14] N. F. Dalleska, P. B. Armentrout, *Int. J. Mass Spectrom. Ion Processes* **1994**, *134*, 203.
[15] M. R. France, S. H. Pullins, M. A. Duncan, *Chem. Phys.* **1998**, *239*, 447.

 © 2006 Wiley-VCH Verlag GmbH & Co. KGaA, Weinheim 

[16] Q. Chen, R. K. Milburn, A. C. Hopkinson, D. K. Bohme, J. M. Goodings, *Int. J. Mass Spectrom.* **1999**, *184*, 153.
[17] A. Andersen, F. Muntean, D. Walter, C. Rue, P. B. Armentrout, *J. Phys. Chem. A* **2000**, *104*, 692.
[18] J. I. Lee, D. C. Sperry, J. M. Farrar, *J. Chem. Phys.* **2001**, *114*, 6180.
[19] Z. Huang, M. Chen, Q. Liu, M. Zhou, *J. Phys. Chem. A* **2003**, *107*, 11380.
[20] J. B. Fenn, M. Mann, C. K. Meng, S. F. Wong, C. M. Whitehouse, *Science* **1989**, *246*, 64.
[21] For a review also addressing the various conditions of electrospray ionization, see: N. B. Cech, C. G. Enke, *Mass Spectrom. Rev.* **2001**, *20*, 362.
[22] The experiments were performed with a tandem mass spectrometer with QHQ configuration (Q: quadrupole, H: hexapole) equipped with an electrospray-ionization (ESI) source as described elsewhere.[1] Briefly, the ions of interest were generated by ESI of an aqueous solution of $Mg(NO_3)_2$, mass-selected using Q1, allowed to interact with methane at a pressure of ca. $10^{-4}$ mbar, and the ionic products were then mass-analyzed using Q2. The interaction energy in the hexapole was varied between $E_{lab} = 0$–10 eV; all thermal reactivity studies refer to an interaction energy nominally set to 0 eV.
[23] D. Schröder, T. Weiske, H. Schwarz, *Int. J. Mass Spectrom.* **2002**, *219*, 729.
[24] Y.-H. Zhang, M. Y. Choi, C. K. Chan, *J. Phys. Chem. A* **2004**, *108*, 1712.
[25] Z. L. Cheng, K. W. M. Siu, R. Guevremont, S. S. Berman, *Org. Mass Spectrom.* **1992**, *27*, 1370.
[26] D. Schröder, M. C. Holthausen, H. Schwarz, *J. Phys. Chem. B* **2004**, *108*, 14407.
[27] In a neutral-gain spectrum, two mass analyzers are scanned independently with a fixed mass offset ($\Delta m$) between them, such that only ions which experience the respective mass increase in the intermediate collision region can reach the detector. In the present case with $\Delta m = 2$, only ions abstracting a deuterium atom from $CH_2D_2$ are detected, and any other reactive ions, for example, $[MgOH]^+$, would lead to deviations from the natural isotope pattern of $[MgO]^+$; also see ref. [28].
[28] D. Schröder, H. Schwarz, S. Schenk, E. Anders, *Angew. Chem.* **2003**, *115*, 5241; *Angew. Chem. Int. Ed.* **2003**, *42*, 5087.
[29] I. Kretzschmar, A. Fiedler, J. N. Harvey, D. Schröder, H. Schwarz, *J. Phys. Chem. A* **1997**, *101*, 6252.
[30] S. Feyel, J. Döbler, D. Schröder, J. Sauer, H. Schwarz, *Angew. Chem.* **2006**, *118*, 4797; *Angew. Chem. Int. Ed.* **2006**, *45*, 4681.
[31] G. Saueressig, J. N. Crowley, P. Bergamaschi, C. Bruhl, C. A. M. Brenninkmeijer, H. Fischer, *J. Geophys. Res. [Atmos.]* **2001**, *106*, 23127.
[32] See also: C. Shi, M. Xu, M. P. Rosynek, J. H. Lunsford, *J. Phys. Chem.* **1993**, *97*, 216.
[33] The calculations were performed using second-order Møller-Plesset perturbation theory with 6-311 + G(2d,2p) basis sets implemented in Gaussian 98 (Gaussian Inc., Pittsburgh, USA, 2002). All intermediates and transition structures were characterized by frequency analysis, and the energies include corrections for zero-point vibrations. Gaussian 98 (Revision A.7), M. J. Frisch, G. W. Trucks, H. B. Schlegel, G. E. Scuseria, M. A. Robb, J. R. Cheeseman, V. G. Zakrzewski, J. A. Montgomery, R. E. Stratmann, J. C. Burant, S. Dapprich, J. M. Millam, A. D. Daniels, K. N. Kudin, M. C. Strain, O. Farkas, J. Tomasi, V. Barone, M. Cossi, R. Cammi, B. Mennucci, C. Pomelli, C. Adamo, S. Clifford, J. Ochterski, G. A. Petersson, P. Y. Ayala, Q. Cui, K. Morokuma, D. K. Malick, A. D. Rabuck, K. Raghavachari, J. B. Foresman, J. Cioslowski, J. V. Ortiz, B. B. Stefanov, G. Liu, A. Liashenko, P. Piskorz, I. Komaromi, R. Gomperts, R. L. Martin, D. J. Fox, T. Keith, M. A. Al-Laham, C. Y. Peng, A. Nanayakkara, C. Gonzalez, M. Challacombe, P. M. W. Gill, B. G. Johnson, W. Chen, M. W. Wong, J. L. Andres, M. Head-Gordon, E. S. Replogle, J. A. Pople, Gaussian, Inc., Pittsburgh, PA, **1998**.
[34] M. Sodupe, C. W. Bauschlicher, Jr., *Chem. Phys. Lett.* **1992**, *195*, 494.
[35] C. W. Bauschlicher, Jr., S. R. Langhoff, H. Partridge, *J. Chem. Phys.* **1994**, *101*, 2644.
[36] J. M. Recio, R. Pandey, A. Ayuela, A. B. Kunz, *J. Chem. Phys.* **1993**, *98*, 4783.

 © 2006 Wiley-VCH Verlag GmbH & Co. KGaA, Weinheim 

# Cover Picture

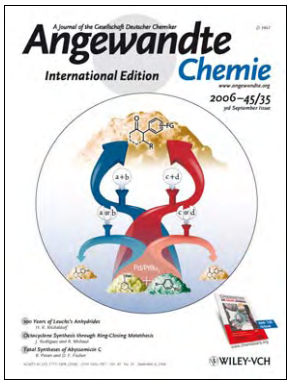


**Weiping Su, Steven Raders, John G. Verkade,* Xuebin Liao, and John F. Hartwig***

**A synergistic combination** of two metal fluoride additives is the key to the palladium-catalyzed coupling of aryl halides with silyl enol ethers. In their Communication on page 5852 ff., J. G. Verkade, J. F. Hartwig, and co-workers discuss the use of this approach to prepare α-aryl ketones from both cyclic and acyclic silyl enol ethers and a wide range of aryl bromides and chlorides. The cover picture depicts the difference in the yields from reactions with one and with two additives.

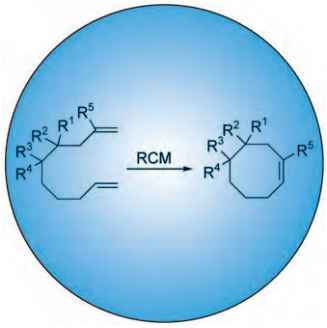


***Octacyclene Synthesis***
The construction of eight-membered rings is synthetically demanding. Ring-closing metathesis can be the key to success, as J. Rodriguez and A. Michaut describe in their Minireview on page 5740 ff. with its application to the synthesis of octacyclenes.

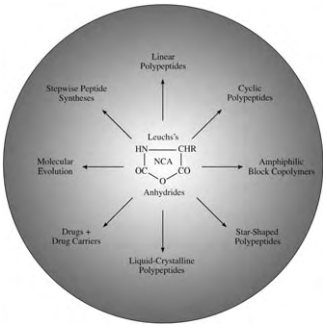


***Polypeptides***
Leuchs's anhydrides, α-amino acid *N*-carboxyanhydrides, have been used to synthesize peptide block copolymers and liquid-crystalline polypeptides through ring-opening polymerization. In the Review on page 5752 ff., H. R. Kricheldorf discusses new developments and the application of polypeptides as drug carriers.

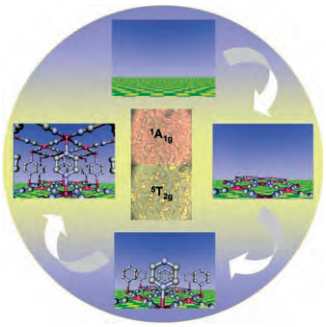


***Spin-Crossover Materials***
In their Communication on page 5786 ff., A. Bousseksou, G. Molnár et al. describe a successful multilayer assembly of [Fe(pyrazine){M(CN)$_4$}] (M = Ni, Pd, or Pt) thin films, which display spin-crossover phenomenon and provide a novel platform for the construction of devices.

# Contents

**The following Communications have been judged by at least two referees to be "very important papers" and will be published online at www.angewandte.org soon:**


*K. J. T. Noonan, D. P. Gates**
**Ambient-Temperature Living Anionic Polymerization of Phosphaalkenes: Homopolymers and Block Copolymers with Controlled Chain Lengths**

*J. Piera, K. Närhi, J.-E. Bäckvall**
**Palladium(II)-Catalyzed Aerobic Allylic Oxidative Carbocyclization of Allene-Substituted Olefins: Immobilization of an Oxygen-Activating Catalyst**

*T. J. Taylor, V. I. Bakhmutov, F. P. Gabbaï**
**Hydrocarbon Uptake in the Alkylated Micropores of a Columnar Supramolecular Solid**

*J.-P. Leclerc, K. Fagnou**
**Palladium-Catalyzed Cross-Coupling Reactions of Diazine *N*-Oxides with Aryl Chlorides, Bromides, and Iodides**

*J. W. Lee, J.-S. Lee, Y.-T. Chang**
**Colorimetric Identification of Carbohydrates by a pH Indicator/pH-Change-Inducer Ensemble**

*Z.-M. Cui, Q. Liu, W.-G. Song*, L.-J. Wan**
**Insights into the Mechanism of Methanol-to-Olefin Conversion from Zeolites with Systematically Selected Framework Structures**


## Books


| | | | |
|---|---|---|---|
| Aziridines and Epoxides in Organic Synthesis | Andrei K. Yudin | *reviewed by A. Gansäuer* | **5733** |
| Molecular Physics | Wolfgang Demtröder | *reviewed by C. v. Wüllen* | **5733** |


## Highlights

### Total Synthesis


R. Peters,* D. F. Fischer — **5736 – 5739**

Total Syntheses of the Antibacterial Natural Product Abyssomicin C


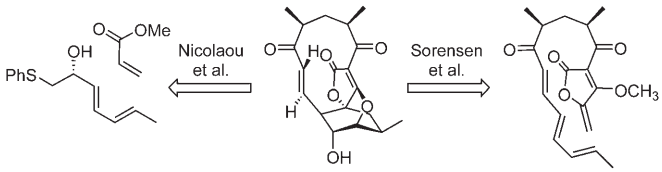


**Intra- or intermolecular**: Abyssomicin C, isolated from a marine bacterium, is a potent polyketide-type antibiotic and a synthetic target of prime importance because it inhibits pathogenic bacteria. In recent independent syntheses by the Sorensen and the Nicolaou groups, intra- and intermolecular Diels–Alder reactions featured as the respective key steps for the construction of the oxabicyclo-[2.2.2]octane core.


WILEY InterScience DISCOVER SOMETHING GREAT
© 2006 Wiley-VCH Verlag GmbH & Co. KGaA, Weinheim

# Minireviews

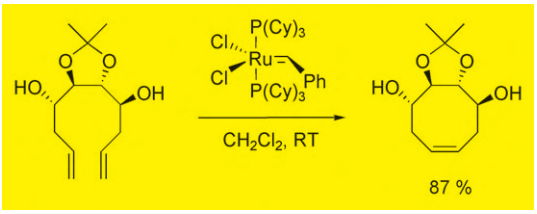


**The direct approach**: The direct synthesis of eight-membered carbocycles from acyclic precursors is a preparatively challenging task since entropic and enthalpic factors are unfavorable for the formation of rings of this size. Cyclooctanoids can be prepared successfully from acyclic precursors under mild reaction conditions with the help of ring-closing metathesis.


**Synthetic Methods**

A. Michaut, J. Rodriguez* — **5740 – 5750**

Selective Construction of Carbocyclic Eight-Membered Rings by Ring-Closing Metathesis of Acyclic Precursors


# Reviews

**100 years young**: In 2006 the chemistry of α-amino acid *N*-carboxyanhydrides (NCAs) marks a history of 100 years. The NCAs were used for syntheses of oligo- and polypeptides in numerous ways, and recently have played an important role in the hypothesis of molecular evolution. Peptide block copolymers, liquid-crystalline polypeptides, and the application of polypeptides as drugs or drug carriers are also discussed.

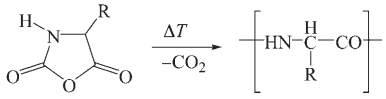



**Macromolecular Chemistry**

H. R. Kricheldorf* — **5752 – 5784**

Polypeptides and 100 Years of Chemistry of α-Amino Acid *N*-Carboxyanhydrides


# Communications

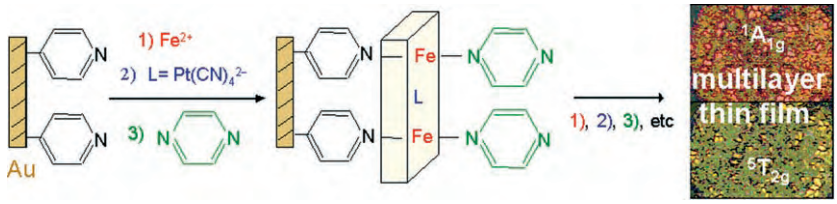


**Assembly time**: Thin films of [Fe(pyrazine){M(CN)$_4$}] (M = Ni, Pd, or Pt) coordination polymers were assembled sequentially through coordinate bonding on gold surfaces (see scheme). These multilayers exhibit spin-crossover phenomena with hysteresis at room temperature.


**Spin-Crossover Multilayers** VIP

S. Cobo, G. Molnár,* J. A. Real, A. Bousseksou* — **5786 – 5789**

Multilayer Sequential Assembly of Thin Films That Display Room-Temperature Spin Crossover with Hysteresis



**For the USA and Canada:**
ANGEWANDTE CHEMIE International Edition (ISSN 1433-7851) is published weekly by Wiley-VCH PO Box 191161, D 69451 Weinheim, Germany. Air freight and mailing in the USA by Publications Expediting Inc. 200 Meacham Ave., Elmont, NY 11003. Periodicals postage paid at Jamaica NY 11431. US POSTMASTER: send address changes to *Angewandte Chemie*, Wiley-VCH, 111 River Street, Hoboken, NJ 07030. Annual subscription price for institutions: US$ 5685/5168 (valid for print and electronic / print or electronic delivery); for individuals who are personal members of a national chemical society prices are available on request. Postage and handling charges included. All prices are subject to local VAT/sales tax.



© 2006 Wiley-VCH Verlag GmbH & Co. KGaA, Weinheim

# The best in chemistry –

## for more than a hundred years

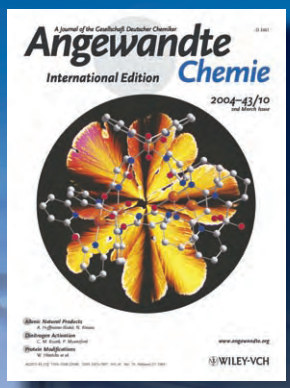


A Journal of the Gesellschaft Deutscher Chemiker

**Angewandte**
**International Edition** **Chemie**

**www.angewandte.org**

***1888:*** ***The beginning of a success story***

### Constant Innovations

***1962:*** *First issue of the International Edition*
***1976:*** *Graphical abstracts*
***1979:*** *Cover pictures*
***1988:*** *Centenary of Angewandte*
***1989:*** *Routine use of color*
***1991:*** *New section: Highlights*
***1992:*** *Computerized editorial tracking system*
***1995:*** *Internet service for readers*
***1998:*** *Regular press service; full-text online*
***2000:*** *New section: Essays; EarlyView: Communications available online ahead of the printed version*
***2001:*** *New section: Minireviews*
***2002:*** *Online submission of manuscripts*
***2003:*** *Weekly publication; new section: News; new layout*
***2004:*** *Backfiles (1962-1997); ManuscriptXpress: Online system for authors and referees*

### Angewandte's advisors...

***Robert Langer***
*Massachusetts Institute of Technology*

»***Angewandte Chemie*** *is one of the top chemistry journals in the world. As such, I try to publish there frequently and am honored to be a member of its International Advisory Board.*«

***Angewandte Chemie International Edition*** *is a journal of the German Chemical Society (GDCh)*

GDCh

WILEY InterScience® DISCOVER SOMETHING GREAT

WILEY-VCH

1841404_gu

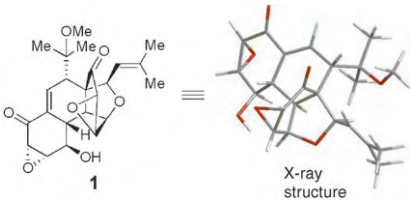


**Structure assigned**: The revised structure of (+)-hexacyclinol (**1**) proposed recently was confirmed following the total synthesis of the natural product. The synthesis was designed around the highly stereoselective Diels–Alder dimerization of an epoxyquinol monomer, followed by intramolecular acid-catalyzed cyclization.

## Hexacyclinol

J. A. Porco, Jr.,* S. Su, X. Lei, S. Bardhan, S. D. Rychnovsky ——— **5790 – 5792**

Total Synthesis and Structure Assignment of (+)-Hexacyclinol

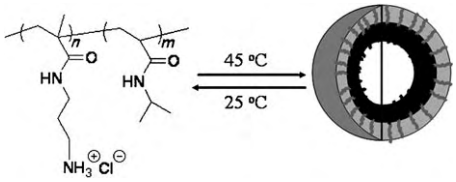


**Hot spots**: Thermally responsive AB diblock copolymers that self-assemble into vesicles at higher temperatures were prepared (see picture). These vesicles can be cross-linked by adding an oppositely charged polyelectrolyte.

## Block Copolymers

Y. Li, B. S. Lokitz, C. L. McCormick* ——— **5792 – 5795**

Thermally Responsive Vesicles and Their Structural "Locking" through Polyelectrolyte Complex Formation

**Green to the core**: $Cd_xZn_{1-x}Se$ alloy core nanocrystals are synthesized and overcoated with $Cd_yZn_{1-y}S$ to create core–shell nanocrystals with the ideal wavelength of emission for quantum dot light-emitting device (QD-LED) displays. These $(Cd_xZn_{1-x}Se)Cd_yZn_{1-y}S$ core–shell nanocrystals are used to fabricate color-saturated green-emitting QD-LEDs (see picture), which are suitable for display applications.

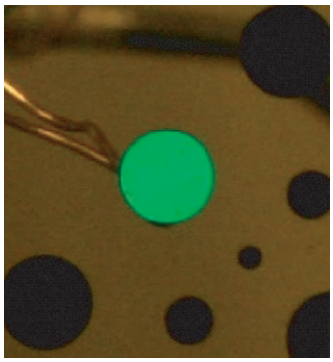

## Quantum Dots

J. S. Steckel, P. Snee, S. Coe-Sullivan, J. P. Zimmer, J. E. Halpert, P. Anikeeva, L.-A. Kim, V. Bulovic, M. G. Bawendi* ——— **5796 – 5799**

Color-Saturated Green-Emitting QD-LEDs

**Hold the mayo!** Sandwich complexes containing the arch-shaped $Pd_4$ chain (upper structure; C blue, Pd orange) or the V-shaped $Pd_5$ chain (lower) were synthesized and structurally characterized. The bending angles of the Pd chains reflect the p$\pi$-conjugated geometry of the template ligands.

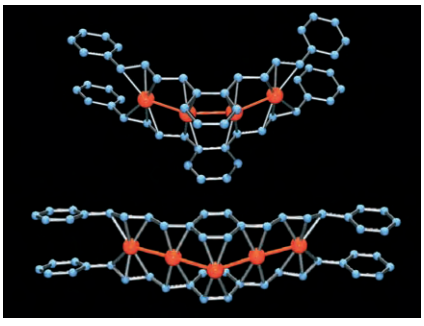

## Sandwich Compounds

Y. Tatsumi, K. Shirato, T. Murahashi,* S. Ogoshi, H. Kurosawa* ——— **5799 – 5803**

Sandwich Complexes Containing Bent Palladium Chains


© 2006 Wiley-VCH Verlag GmbH & Co. KGaA, Weinheim

# Contents


## Stereochemistry

M. S. Betson, J. Clayden,* C. P. Worrall, S. Peace ——— 5803 – 5807

Three Groups Good, Four Groups Bad? Atropisomerism in *ortho*-Substituted Diaryl Ethers

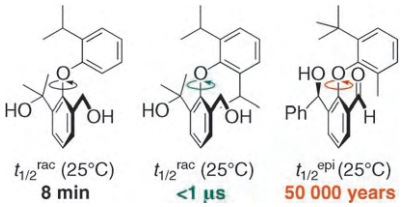


**Bring on the substitute**: Even outside of macrocyclic structures, such as vancomycin, appropriate substitution can give rise to atropisomerism in diaryl ethers. Stereochemical stability about the Ar–OAr axis at room temperature or above is possible when neither of the rings is symmetrically substituted and when at least one ring carries an *ortho tert*-butyl group or equivalent.

## Metal–Metal Bonding

Z. Zhu, R. J. Wright, M. M. Olmstead, E. Rivard, M. Brynda, P. P. Power* ——— 5807 – 5810

A Zinc–Zinc-Bonded Compound and Its Derivatives Bridged by One or Two Hydrogen Atoms: A New Type of Zn–Zn Bonding

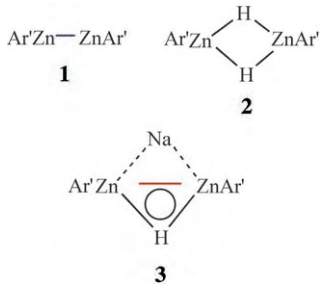


**Unique interactions**: Ar′ZnZnAr′ (**1**; Ar′ = $C_6H_3$-2,6-($C_6H_3$-2,6-*i*$Pr_2$)$_2$), the dimer Ar′Zn(μ-H)$_2$ZnAr′ (**2**), and the unprecedented species Ar′Zn(μ-H)(μ-Na)ZnAr′ (**3**) were synthesized and fully characterized. DFT calculations show that the Zn–Zn bonding interactions in **1** differ from those of other Zn–Zn compounds, and the calculations also indicate a new type of Zn–Zn bond in **3**.

## Diphosphite Ligands

D. Sémeril, C. Jeunesse, D. Matt,* L. Toupet ——— 5810 – 5814

Regioselectivity with Hemispherical Chelators: Increasing the Catalytic Efficiency of Complexes of Diphosphanes with Large Bite Angles

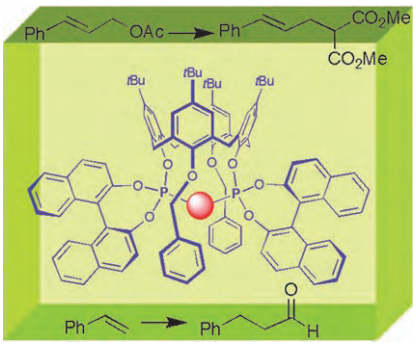


**Control through molecular pockets**: Calixarene-derived diphosphites provide effective hemispherical crowding about catalytic centers. When used in the palladium-catalyzed alkylation of cinnamyl acetate, regioselectivities higher than 98% in favor of the linear product are observed. In the rhodium-catalyzed hydroformylation of styrene, these diphosphites lead to phenylpropionaldehyde with selectivities as high as 76%.

## Metal–Metal Interactions

I-W. P. Chen, M.-D. Fu, W.-H. Tseng, J.-Y. Yu, S.-H. Wu, C.-J. Ku, C.-h. Chen,* S.-M. Peng* ——— 5814 – 5818

Conductance and Stochastic Switching of Ligand-Supported Linear Chains of Metal Atoms

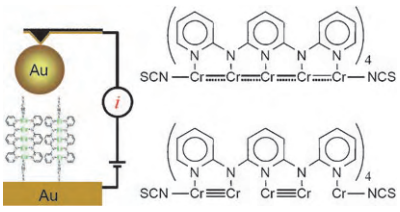


**An alternative string theory**: The current-versus-potential behavior of metal atom strings (Ni, Co, Cr) is dependent on the strength of the d-orbital coupling along the metal atom chain. Penta- and hepta-chromium strings each exhibit two sets of primary *I*–*V* curves, which depend on whether the Cr–Cr bonds alternate and are localized, or are delocalized (see picture).



© 2006 Wiley-VCH Verlag GmbH & Co. KGaA, Weinheim

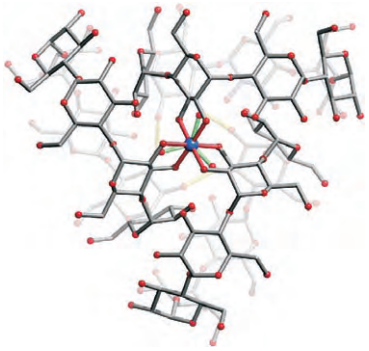

**Mining new assemblies**: A molecular bucket wheel consisting of three β-cyclodextrin units, three tetrahedral tetraaqualithium cations, and a tetravalent metal center has been prepared (see picture). The assembly, held together by a series of hydrogen bonds, is also stable in solution.


**Coordination Chemistry**

K. Benner, J. Ihringer, P. Klüfers,* D. Marinov ——— **5818 – 5822**

Cyclodextrin Bucket Wheels: An Oligosaccharide Assembly Accommodates Metal(IV) Centers


**Dyeing for sunlight**: A new dye **CYC-B1** (see picture), with the highest absorption coefficient known so far for Ru-based photosensitizers, was prepared. Solar cells sensitized with **CYC-B1** have a very high current density, and the conversion efficiency of **CYC-B1** is 10% higher than that of *cis*-di(thiocyanato)bis(2,2′-bipyridyl-4,4′-dicarboxylate)ruthenium(II) under AM 1.5 simulated sunlight.

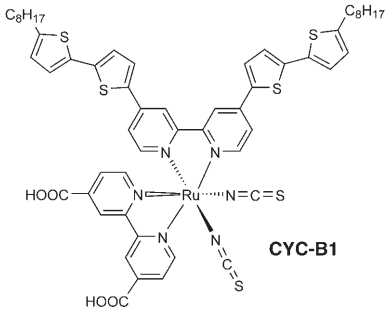



**Photosensitizers**

C.-Y. Chen, S.-J. Wu, C.-G. Wu,* J.-G. Chen, K.-C. Ho ——— **5822 – 5825**

A Ruthenium Complex with Superhigh Light-Harvesting Capacity for Dye-Sensitized Solar Cells


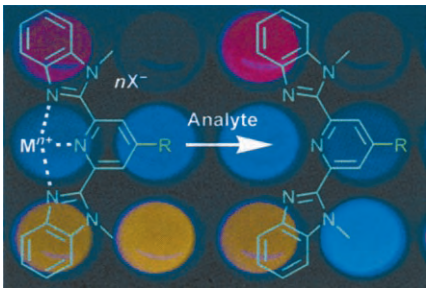


**Mixing and matching**: The highly selective detection of chemical-warfare-agent mimics can be achieved by judicious combination of carefully designed fluorescent ligands and metal ions. Designed sensor arrays of these multimetal/multiligand systems represent a modular and versatile approach for the detection of organophosphates and other analytes.


**Sensor Technology**

D. Knapton, M. Burnworth, S. J. Rowan,* C. Weder* ——— **5825 – 5829**

Fluorescent Organometallic Sensors for the Detection of Chemical-Warfare-Agent Mimics


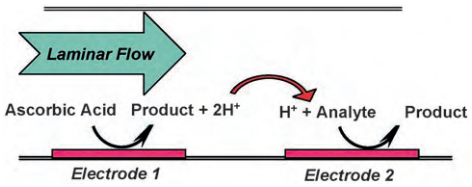


**One helps the other**: An upstream electrode (1) in a microfluidic channel drives a reaction that produces protons so that the reaction at the downstream electrode (2) becomes thermodynamically or kinetically viable. The shift in redox potential allows the analyte to be detected in conditions in which it would otherwise be undetectable.


**Electroanalysis**

I. M. Khalid, Q. Pu, J. C. Alvarez* ——— **5829 – 5832**

Thermodynamic and Kinetic Enhancement of Electrochemical Sensitivity by Chemical Coupling in Microfluidic Systems



© 2006 Wiley-VCH Verlag GmbH & Co. KGaA, Weinheim

# Contents


## Total Synthesis

A. Fürstner,* C. Aïssa, C. Chevrier, F. Teplý, C. Nevado, M. Tremblay —— **5832 – 5837**

Studies on Iejimalide B: Preparation of the Seco Acid and Identification of the Molecule's "Achilles Heel"

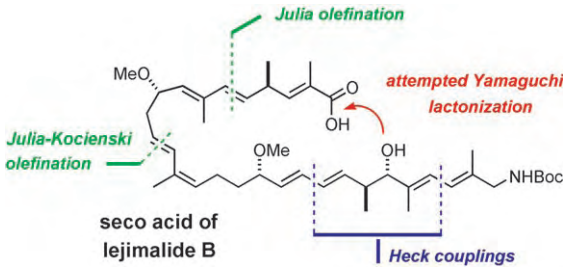


**Limitations of models** in total synthesis are illustrated by a study towards the potent cytotoxic macrolide iejimalide B. Although the Yamaguchi protocol allowed for the esterification of elaborate segments, attempted macrolactonization of the seco acid met with failure (see scheme, Boc = *tert*-butyloxycarbonyl). The assembly of the seco acid involves some of the most advanced applications of the Julia olefination known to date.

## Total Synthesis

A. Fürstner,* C. Nevado, M. Tremblay, C. Chevrier, F. Teplý, C. Aïssa, M. Waser —— **5837 – 5842**

Total Synthesis of Iejimalide B

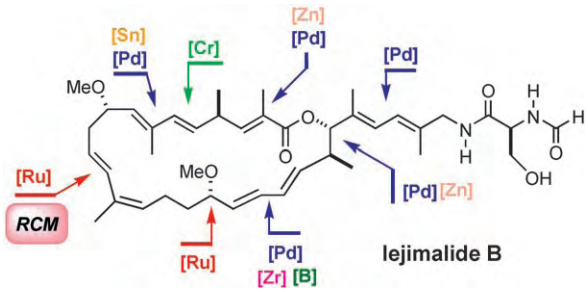


**Metathesis to the rescue**: Although counterintuitive at first sight, application of ring-closing metathesis (RCM) to a cyclization precursor containing 10 double bonds has led to the selective and high-yielding formation of the macrocyclic core of iejimalide B, a potent cytotoxic agent of marine origin. In contrast, a macrolactonization approach failed to afford this intricate target.

## Alkyne Oligomerization

T. B. Wen, Z. Y. Zhou, G. Jia* **5842 – 5846**

Osmium-Mediated Hexamerization of Phenylacetylene

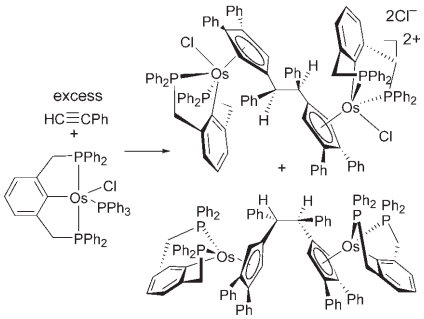


**A larger oligomer**: Although transition-metal-mediated reactions of alkynes to give dimers, trimers, tetramers, and polymers are well-known, reactions of alkynes to give well-defined oligomers of medium molecular weight (e.g. pentamers, hexamers) are very scarce. The selective hexamerization of HC≡CPh in the reaction with $[OsCl(PCP)(PPh_3)]$ (PCP = 2,6-$(Ph_2PCH_2)_2C_6H_3$; see scheme) is a rare example thereof.

## C–C Coupling

A.-P. Schaffner, V. Darmency, P. Renaud* —— **5847 – 5849**

Radical-Mediated Alkenylation, Alkynylation, Methanimination, and Cyanation of *B*-Alkylcatecholboranes

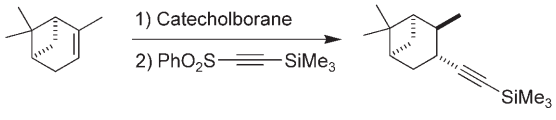


**Radical connection**: Organoboranes, prepared in situ from hydroboration of olefins with catecholborane, undergo efficient coupling reactions with vinyl and alkynyl sulfones through a radical mechanism. This procedure was also extended to the acylation and cyanation of organoboranes.



© 2006 Wiley-VCH Verlag GmbH & Co. KGaA, Weinheim

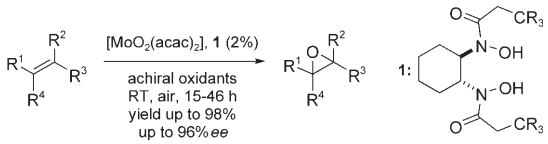


## Asymmetric Catalysis

A. U. Barlan, A. Basak, H. Yamamoto* ——— 5849 – 5852

Enantioselective Oxidation of Olefins Catalyzed by a Chiral Bishydroxamic Acid Complex of Molybdenum

**Excellent yields** and enantioselectivities can be achieved in the molybdenum–bishydroxamic acid catalyzed asymmetric oxidation of olefins in air at room temperature with an achiral oxidant (see scheme; acac = acetylacetonate). A range of terminal, *cis*-, and trisubstituted olefins can be used as the substrate. Furthermore, when there are multiple double bonds, the most electron-rich is oxidized.

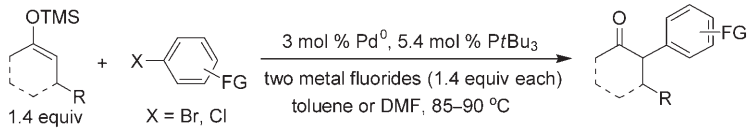


## Cross-Coupling

W. Su, S. Raders, J. G. Verkade,* X. Liao, J. F. Hartwig* ——— 5852 – 5855

Pd-Catalyzed α-Arylation of Trimethylsilyl Enol Ethers with Aryl Bromides and Chlorides: A Synergistic Effect of Two Metal Fluorides as Additives

**The long-sought-after** palladium-catalyzed coupling of silyl enol ethers, both cyclic and acyclic, with a wide range of aryl bromides and chlorides to form α-aryl ketones is realized. The key to effective activation of the silicon enolate was the use of two metal fluoride additives, which operate in a synergistic fashion.

**Without destruction of monocrystallinity**: The conformational switching of a dinuclear metal complex between four distinct states (see picture) occurs without destroying the single crystal. This observation implies a substantial degree of cooperativity between host molecules during guest uptake, release, or exchange.

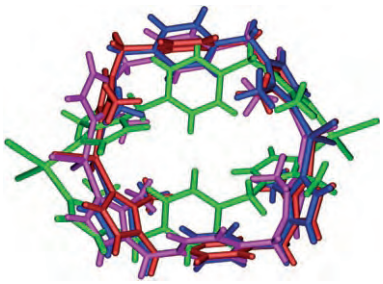

## Conformational Switching

L. Dobrzańska, G. O. Lloyd, C. Esterhuysen, L. J. Barbour* ——— 5856 – 5859

Guest-Induced Conformational Switching in a Single Crystal

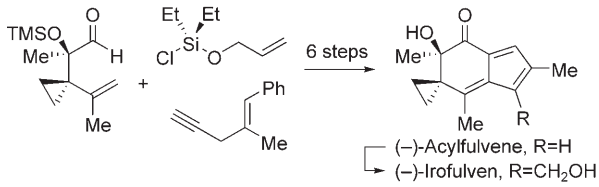


## Asymmetric Synthesis

M. Movassaghi,* G. Piizzi, D. S. Siegel, G. Piersanti ——— 5859 – 5863

Enantioselective Total Synthesis of (−)-Acylfulvene and (−)-Irofulven

**Antitumor agents** (−)-acylfulvene and (−)-irofulven are prepared in an approach that employs the powerful enyne ring-closing metathesis reaction to secure the spiro-bicyclic AB rings. Other key features of this synthesis include an efficient aldol-based introduction of the stereocenter at C2, a diazene-mediated reductive allylic transposition, and a ring-closing metathesis/oxidation sequence.

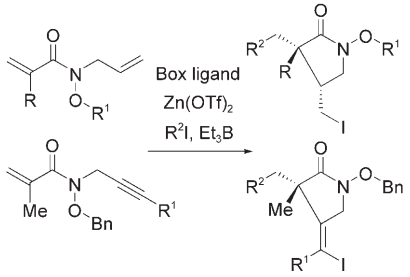


## Radical Reactions

H. Miyabe,* R. Asada, A. Toyoda, Y. Takemoto* ——— 5863 – 5866

Enantioselective Cascade Radical Addition–Cyclization–Trapping Reactions

**In addition**: The chiral Lewis acid mediated radical addition–cyclization–trapping reaction of a hydroxamate ester with two radical acceptors provides a cascade approach for the asymmetric synthesis of various γ-lactams (see scheme; Bn = benzyl, Box = bis(oxazoline), Tf = trifluoromethanesulfonyl).


© 2006 Wiley-VCH Verlag GmbH & Co. KGaA, Weinheim

# Contents


## Hybrid Compounds

Y. Zhang, Y. Shen, J. Yuan, D. Han, Z. Wang, Q. Zhang, L. Niu* **5867 – 5870**

Design and Synthesis of Multifunctional Materials Based on an Ionic-Liquid Backbone

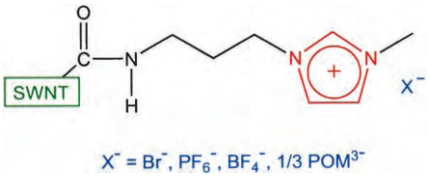


**No longer simply "green" solvents**, ionic liquids can be used as backbones to integrate independent components into a multifunctional compound. For example, single-walled carbon nanotubes (SWNTs) are coupled with various anions ($X^-$) by a simple anion-exchange reaction (see picture).

## Natural Product Synthesis

D. Amans, V. Bellosta, J. Cossy* **5870 – 5874**

Total Synthesis of Pseudotrienic Acid B: A Bioactive Metabolite from *Pseudomonas* sp. MF 381-IODS

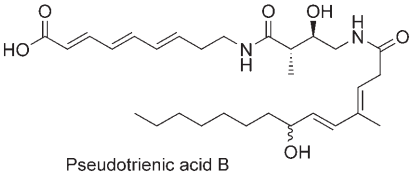


**Acid advancement**: An efficient and highly convergent stereoselective synthesis of pseudotrienic acid B (see structure) has been achieved. Synthetic highlights include a crotyltitanation reaction to control the stereogenic centers at C11 and C20, a cross-metathesis reaction to synthesize the triene moiety, and a Stille cross-coupling reaction to complete the assembly of the carbon framework of the natural product.

## G Quadruplexes

M. Wieland, J. S. Hartig* **5875 – 5878**

Turning Inhibitors into Activators: A Hammerhead Ribozyme Controlled by a Guanine Quadruplex

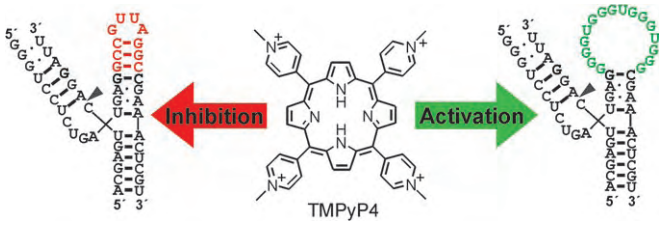


**Modular design** of functional RNAs can be used to tailor molecular properties. Guanosine-rich sequences were introduced as switching devices for functional nucleic acids. TMPyP4 (see picture) was identified as the strongest ribozyme inhibitor known to date. When quadruplex-forming, G-rich sequences were attached to the ribozyme, the TMPyP4-mediated response was inverted from inhibition to activation of the ribozyme reaction.

## Cyclization

S. F. Kirsch,* J. T. Binder, C. Liébert, H. Menz **5878 – 5880**

Gold(III)- and Platinum(II)-Catalyzed Domino Reaction Consisting of Heterocyclization and 1,2-Migration: Efficient Synthesis of Highly Substituted 3(2*H*)-Furanones

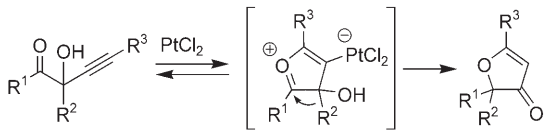


**$PtCl_2$-catalyzed alkyne activation** initiates a domino reaction, in which a heterocyclization is followed by a 1,2-alkyl migration, for the construction of a variety of substituted 3(2*H*)-furanones. This stereospecific reaction is proposed to proceed through an oxonium ion intermediate (see scheme).



© 2006 Wiley-VCH Verlag GmbH & Co. KGaA, Weinheim

**Improving on nature**: Azathilones **1a** and **1b** are "non-natural" natural products derived from epothilones through C→N exchange at position 12. They are highly potent inducers of tubulin polymerization (part of a microtubule is shown in the picture) and inhibit human cancer cell growth in vitro. These compounds present a new structural scaffold for microtubule stabilization and are promising lead structures for anticancer-drug discovery.

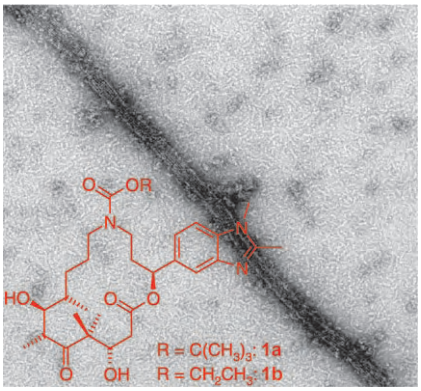


*Epothilones*

F. Feyen, J. Gertsch, M. Wartmann, K.-H. Altmann* ——— **5880 – 5885**

Design and Synthesis of 12-Aza-Epothilones (Azathilones)—"Non-Natural" Natural Products with Potent Anticancer Activity

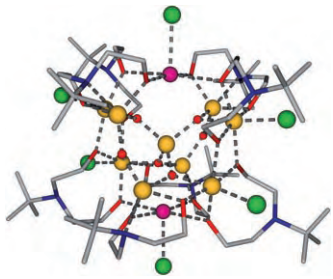

**Available in assorted shapes**: Three new oligonuclear complexes self-assemble from *t*Bu-*N*-diethanolamine and mixtures of iron(II) and iron(III) ions. Depending on the reaction conditions, a compact or linear defective hexacubane, or a body-centered six-sided iron(III) polyhedron (see structure; Fe gold, Ca purple, C gray, N blue, O red, Cl green) is formed.

*Iron Complexes*

R. Prakash,* R. W. Saalfrank,* H. Maid, A. Scheurer, F. W. Heinemann, A. X. Trautwein, L. H. Böttger ——— **5885 – 5889**

Synthesis and Redox Properties of Mixed-Valent Octanuclear Iron Defective Hexacubanes and a (CaCl)-Capped Body-Centered Six-Sided Iron(III) Polyhedron

**Looking for outstanding employees?**

**Do you need another expert for your excellent team?**
**... Chemists, PhD Students, Managers, Professors, Sales Representatives...**

Place an advert in the printed version and have it made available online for 1 month, free of charge!

***Angewandte Chemie International Edition***
**Advertising Sales Department: Marion Schulz**
**Phone: 0 62 01 - 60 65 65**
**Fax: 0 62 01 - 60 65 50**
**E-Mail: MSchulz@wiley-vch.de**

## Service

*Keywords* ——— *5890*

*Authors* ——— *5891*

*Vacancies* ——— *A49*

*Preview* ——— *6037*

# Retraction

After the publication of this Communication the authors have noticed that the scale bars on some of the TEM images are wrong. The particle size data extracted from these images is thus incorrect and the conclusions drawn from this data are therefore invalid. Accordingly, all the authors withdraw this Communication. They apologize for these mistakes and that the readership of *Angewandte Chemie* has been misled by the publication of this Communication.

Design and Size Control of Uniform Zeolite Nanocrystals Synthesized in Adjustable Confined Voids Formed by Recyclable Monodisperse Polymer Spheres

X. Yang, Y. Feng, G. Tian, Y. Du, X. Ge, Y. Di, Y. Zhang, B. Sun, F.-S. Xiao* **2563–2568**

*Angew. Chem. Int. Ed.* **2005**, *44*

DOI 10.1002/anie.200462187


© 2006 Wiley-VCH Verlag GmbH & Co. KGaA, Weinheim

Total Synthesis

DOI: 10.1002/anie.200602409

# Total Syntheses of the Antibacterial Natural Product Abyssomicin C

*René Peters* and Daniel F. Fischer*

**Keywords:**
abyssomicin · antibiotics · cycloaddition · total synthesis

In 2004 Süssmuth et al. reported the isolation of the polyketide-type antibiotic abyssomycin C (**1**), which inhibits

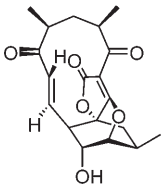

abyssomicin C (**1**)

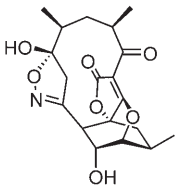

abyssomicin B (**2**)

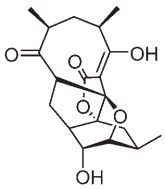

abyssomicin D (**3**)

Gram-positive bacteria, and of the two related non-antibiotic compounds abyssomicin B (**2**) and D (**3**) from the rare actinomycete *Verrucosispora* strain AB 18-032, which was found in a sediment sample collected in the Sea of Japan at a depth of almost 300 m.[1]

Compound **1** inhibits the bacterial biosynthetic pathway to tetrahydrofolate between chorismate and *p*-aminobenzoic acid (PABA), by mimicking chorismate and then presumably covalently binding the enzyme. The biosynthesis of PABA is a highly attractive target since it is essential for many microorganisms but absent in humans. Abyssomicin C has been reported to be the first known substance derived from a bacterial source that inhibits the biosynthesis of PABA. Süssmuth et al. suggested a possible mode of action based on the unique and intriguing structure, which was elucidated by NMR-spectroscopic studies and X-ray structure analysis. Abyssomicin C (**1**) contains a tetronic acid motif, an oxabicyclo[2.2.2]octane system, and an α,β-unsaturated ketone moiety. The oxabicyclo[2.2.2]octane system was proposed to be a mimic of chorismate (and is similar to transition-state analogues of chorismate mutase inhibitors). Presumably after noncovalent binding to the targeted enzyme, the enone part of **1** covalently traps a nucleophilic amino acid side chain from the enzyme by 1,4-addition. This would also explain why the related species **2** and **3** show no antibiotic activity: they lack the enone functionality.

Because abyssomicin C is a very attractive lead structure for the development of new inhibitors of pathogenic bacteria, compound **1** and analogues thereof are targets of prime importance. Indeed, two total syntheses have already been reported. This article highlights the syntheses by Sorensen et al. and Nicolaou et al. which both rely on a Diels–Alder reaction as the key step in the construction of the oxabicyclo[2.2.2]octane core.

In 2005 the Sorensen group reported the first synthesis of abyssomicin C based on an intramolecular, highly diastereoselective Diels–Alder reaction. The advanced diene intermediate **5**, containing all the carbon atoms of the natural product, was cyclized to form an 11-membered macrocycle (Scheme 1).[2,3] They speculated that the biosynthesis of **1** also proceeds by a Diels–Alder macrocyclization. Intermediate **5** was obtained by a convergent strategy from fragments **6**–**8**, which were coupled by two carbonyl addition reactions, namely, an aldol reaction of a synthetic equivalent of enolate **6** and commercially available *trans*,*trans*-2,4-hexadienal (**7**), followed by the addition of a lithiated tetronate **8** to an aldehyde carbonyl group.

The synthetic equivalent of **6**, ketone **10** (Scheme 2), was prepared in six steps (40% overall yield) from *meso*-2,4-di-

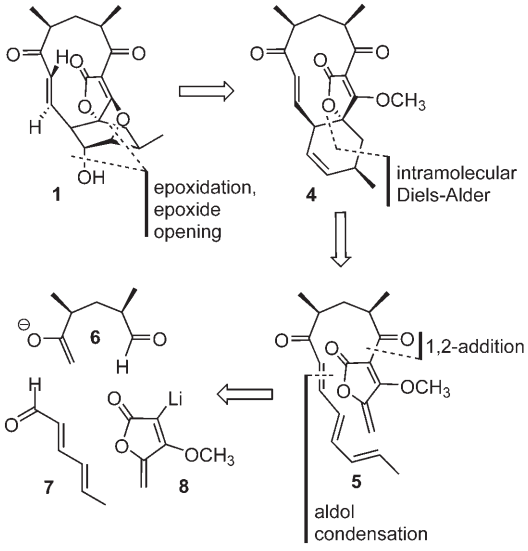


***Scheme 1.*** Sorensen's retrosynthetic analysis.

[*] Prof. Dr. R. Peters, D. F. Fischer
Laboratory of Organic Chemistry
ETH Zürich
Wolfgang-Pauli-Strasse 10
Hönggerberg HCI E 111
8093 Zürich (Switzerland)
Fax: (+41) 44-633-1226
E-mail: peters@org.chem.ethz.ch
Homepage: www.peters.ethz.ch


InterScience
© 2006 Wiley-VCH Verlag GmbH & Co. KGaA, Weinheim

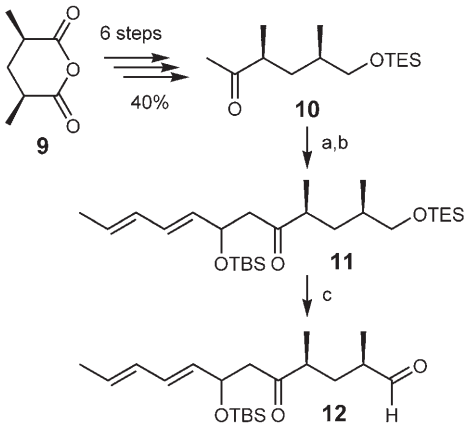


***Scheme 2.*** Synthesis of intermediate **12**. Reagents and conditions: a) LDA, THF, −78 °C; then ***7*** (94%, d.r. 1:1); b) TBSOTf, 2,6-lutidine, $CH_2Cl_2$, 0 °C (85%); c) $(COCl)_2$, DMSO, $Et_3N$, $CH_2Cl_2$, −40 to −78 °C (60–70%). DMSO = dimethylsulfoxide, LDA = lithium diisopropylamide, TBS = *tert*-butyldimethylsilyl, TES = triethylsilyl, Tf = trifluoromethanesulfonyl.

methylglutaric anhydride (**9**) using an efficient enzymatic desymmetrization described by Lautens et. al as a key step.[4] The kinetically formed enolate derived from **10** was joined with dienal **7** in excellent yield furnishing a diastereomeric mixture (1:1) of a secondary alcohol, which was protected as TBS ether to form the sensitive triene moiety during the cycloaddition by a β-elimination of the silyloxy group.

The known methyl tetronate **13** was subsequently lithiated using LDA (Scheme 3) and the resulting carbanion was reacted with aldehyde **12**, obtained by direct exposure of the primary TES ether **11** to Swern oxidation conditions. The yield for the coupling reaction was poor and variable (35–55%), which might be ascribed to chemoselectivity problems because of the presence of the unprotected keto group in **12**. However, the reaction could be performed on a gram scale giving access to the Diels–Alder substrate **14** by oxidation of the generated secondary alcohol. An impressive tandem β-elimination/diastereoselective cycloaddition to provide tricycle **4** was then accomplished in the presence of 10 mol% of $La(OTf)_3$ in toluene at 100 °C. No regioisomeric cycloadducts were detected. Alternatively, the β-elimination was performed in a separate step prior to the cycloaddition.

Oxidation of the generated cyclohexene with dimethyldioxirane gave regio- and diastereoselective access to epoxide **15**, which was opened by acid-catalyzed nucleophilic intramolecular attack of the vinylogous carboxylic acid moiety being released by nucleophilic demethylation of the tetronate subunit. Unfortunately, the epoxide opening was not regioselective. The resulting 1:1 mixture of the target molecule abyssomicin C (**1**) and isoabyssomicin C could be separated by column chromatography. The undesired isomer would be interesting for further elucidation of the structure–activity relationship (SAR). The target molecule has thus been synthesized by a convergent approach with a longest linear sequence of 15 steps (overall yield: 0.9–1.7%).

In 2006 Nicolaou and Harrison reported an alternative synthesis featuring an intermolecular Diels–Alder approach followed by an epoxidation and an epoxide-ring-opening sequence to form the oxabicyclo[2.2.2]octane core structure **18**; the strained 11-membered macrocycle in **1** was obtained by a ring-closing metathesis reaction (Scheme 4).[5,6] This approach led not only to the total synthesis of abyssomicin C (**1**) but also to the formation of atrop-abyssomicin C (**21**), a conformer

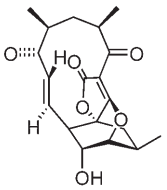


of the naturally occurring product **1** exhibiting even more potent antibiotic activity.

Like Sorensen's synthesis, Nicolaou's approach is characterized by its high convergency and diversity making it possible to synthesize new analogues for SAR studies. Hydroxydiene **20**, which was prepared in two steps from the known Weinreb amide **22**, underwent a remarkable Diels–Alder reaction with an excess of methyl acrylate in a protocol based on a procedure originally developed by Ward and Abaee[7]

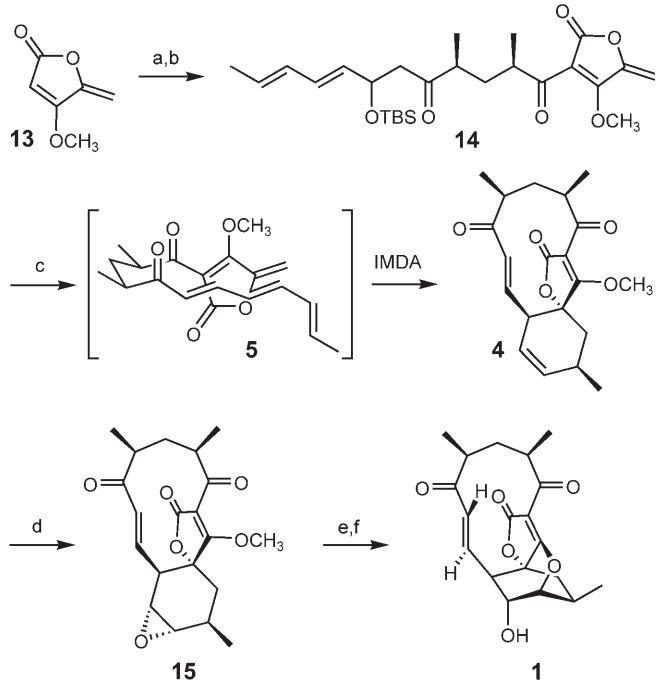


***Scheme 3.*** Synthesis of abyssomicin C (**1**) by Sorensen et al. Reagents and conditions: a) LDA, toluene, −78 °C, 6 min; then aldehyde **12**, (35–55%, d.r. 1:1); b) DMP, $CH_2Cl_2$, 0 to 23 °C (84%); c) $La(OTf)_3$ (10 mol%), toluene, 100 °C (50%); d) DMDO, acetone, 0→23 °C (67%); e) LiCl, DMSO, 50 °C (quant.); f) *p*-TsOH, LiCl, $CH_3CN$, 50 °C, (50%). DMDO = dimethyldioxirane, DMP = Dess–Martin periodinane, IMDA = intramolecular Diels–Alder reaction, *p*-TsOH = toluene-4-sulfonic acid.

 © 2006 Wiley-VCH Verlag GmbH & Co. KGaA, Weinheim 

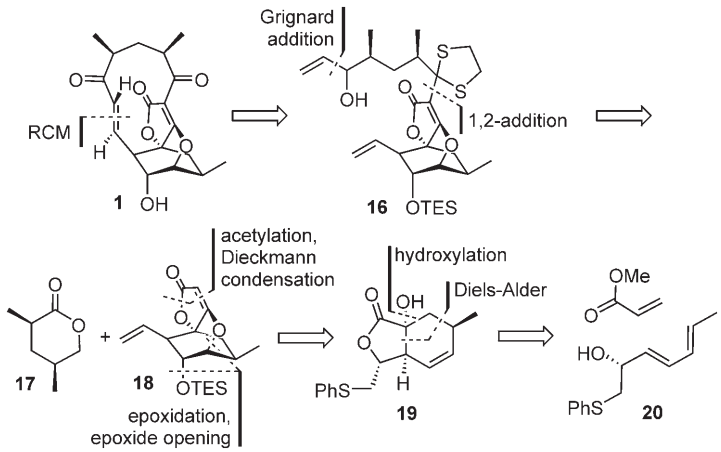


***Scheme 4.*** Nicolaou's retrosynthetic analysis. RCM = ring-closing metathesis.

(Scheme 5). Mixing 1 equivalent of **20** with 3 equivalents of the achiral ligand **23** and 4 equivalents of MeMgBr in toluene at 0 °C, followed by the addition of 10 equivalents of methyl acrylate and warming to 55 °C for 24 h provided cycloadduct **25** as a single diastereomer in 80 % yield, presumably via the Lewis acid templated transition state **24**. Further applications in catalytic asymmetric synthesis utilizing chiral enantiopure ligand motifs can be envisioned.

The resulting cycloaddition product was then hydroxylated diastereoselectively in the position α to the carbonyl group of the γ-lactone moiety (**25**→**19**). A reductive elimination of PhSH provided diene **26**, which subsequently underwent a [$VO(OEt)_3$]-promoted highly regio- and diastereoselective epoxidation utilizing *t*BuOOH. The reaction occurred exclusively at the bottom face of the molecule, and subsequently the tertiary hydroxy group was acetylated (**19**→**26**→**27**). In an elegant manner, deprotonation of the acetyl group followed by an intramolecular Claisen–Dieckmann cyclization and a subsequent regioselective epoxide opening directly furnished the tricyclic core structure in an almost quantitative yield. After silylation under standard conditions, the lithiation of **18** with *t*BuLi at −78 °C, followed by reaction with enantioenriched lactone **17** gave a lactol which was directly subjected to thioketalization with 1,2-ethanedithiol giving **28** in 75 % overall yield (Scheme 6).

Chemoselective oxidation of the primary hydroxy group with IBX (*o*-iodoxybenzoic acid), followed by nucleophilic addition of vinylmagnesium chloride to the generated aldehyde gave a diastereomeric mixture of allylic alcohols **16** (ca. 3:2). Formation of the macrocycle by ring-closing metathesis catalyzed by the Grubbs II catalyst (**29**) and a second chemoselective IBX oxidation converted the diastereomeric secondary allylic alcohols into a single hydroxy enone diastereomer **30**, which was *trans*-configured about the newly formed double bond.

Surprisingly, however, regeneration of the keto functionality protected as a thioketal with PIFA ($PhI(O_2CCF_3)_2$) did not give the expected target molecule **1** but the atropisomer **21** (structure determined by X-ray analysis); the overall yield was ca. 3.4 %, the longest linear sequence was 16 steps. Comparison of the X-ray crystal data of abyssomicin C (**1**) to those of atrop-abyssomicin C (**21**) reveals that the enone carbonyl group adopts a more transoid conformation in the natural product **1** (dihedral angle O=C–C=C 144.8°), whereas the conformation of this group in **21** is more cisoid (dihedral angle O=C–C=C 26.4°). Because **21** exhibits an increased degree of conjugation between the carbonyl group and the double-bond moiety, it is a better Michael acceptor than **1**, resulting in higher antibacterial activity [preliminary minimal inhibitory concentration (MIC) assays of **1**: 5.2 $mg\,mL^{-1}$; and of **21**: 3.5 $mg\,mL^{-1}$ for antibacterial activity against MRSA (methicillin-resistant *Staphylococcus aureus*)]. This finding supports the hypothesis by Süssmuth et al. on the origin of the bioactivity. Compound **21** was finally transformed into **1** under mild acidic conditions ($CDCl_3$ without a stabilizer) giving a 2:1 mixture of **1** and **21**, which can be separated by column chromatography.

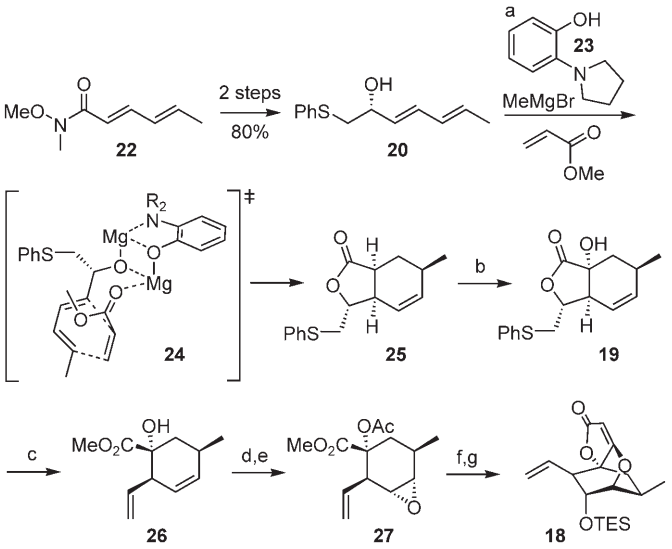


***Scheme 5.*** Synthesis of TES-protected oxabicyclo[2.2.2]octane intermediate **18**. Reagents and conditions: a) $PhCH_3$, 0 °C, then methyl acrylate (10 equiv), 55 °C, 24 h (80 %); b) LiHMDS, THF, −78 °C; then $(EtO)_3P$, $O_2$ (74 %); c) 4,4′-di-*tert*-butylbiphenyl, Li, THF, 0 °C, then −40 °C, **19**, then MeOH quenching, then DMF, $K_2CO_3$, MeI, 60 °C (97 %); d) [$VO(OEt)_3$], *t*BuOOH, $CH_2Cl_2$, 25 °C (90 %); e) $Ac_2O$, DMAP, $Et_3N$, 25 °C (93 %); f) LiHMDS, THF, −78 to 25 °C; then $NH_4Cl$, reflux; g) TESCl, imidazole, DMAP, DMF, 25 °C (97 %, two steps). DABCO = 1,4-diazabicyclo[2.2.2]octane, DMAP = 4-(dimethylamino)pyridine, DMF = *N*,*N*-dimethylformamide, LiHMDS = lithium bis(trimethylsilyl)amide.

 © 2006 Wiley-VCH Verlag GmbH & Co. KGaA, Weinheim 

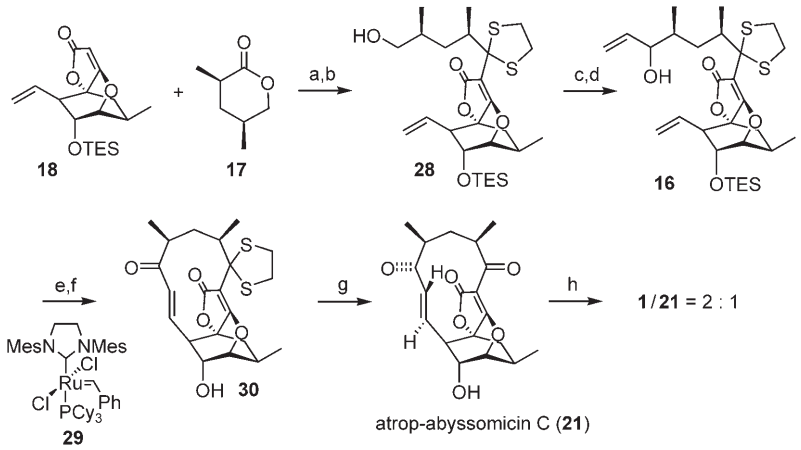


***Scheme 6.*** Completion of the total synthesis of atrop-abyssomicin C (**21**) and abyssomicin (**1**). Reagents and conditions: a) *t*BuLi, THF, −78 °C; then **17**, 10 min; b) 1,2-ethanedithiol, $CH_2Cl_2$, −78 °C; then TMSOTf; then 1 N aq. HCl, −78 to 25 °C, 75 %, two steps; c) IBX, DMSO, 25 °C; d) vinyl MgCl, THF, −78 °C, 65 %, two steps; e) **29**, $CH_2Cl_2$ (0.002 M), Δ, 85 %; f) IBX, DMSO, 25 °C, 50 %; g) $PhI(OTFA)_2$, $CH_3CN/H_2O$ (5:1), 50 %; h) $CDCl_3$. Cy = cyclohexyl, IBX = *o*-iodoxybenzoic acid, MES = trimethylphenyl, TFA = trifluoroacetyl.

Both synthetic approaches highlight impressively the power of the Diels–Alder reaction, either intramolecular to form a strained macrocyclic system, or intermolecular via a Lewis acid templated transition state. Both synthetic routes appear to be well suited to synthesize new analogues to enable further studies of the structure–activity relationship. It will be exciting to see if Süssmuth's hypothesis about the origin of the antibacterial activity of abyssomicin C will be proved right and if new antibacterial drugs will finally emerge based on these studies.

Published online: August 14, 2006

[1] a) B. Bister, D. Bischoff, M. Ströbele, J. Riedlinger, A. Reicke, F. Wolter, A. T. Bull, H. Zähner, H.-P. Fiedler, R. D. Süssmuth, *Angew. Chem.* **2004**, *116*, 2628; *Angew. Chem. Int. Ed.* **2004**, *43*, 2574; b) J. Riedlinger, A. Reicke, H. Zähner, B. Krismer, A. T. Bull, L. A. Maldonado, A. C. Ward, M. Goodfellow, B. Bister, D. Bischoff, R. D. Süssmuth, H.-P. Fiedler, *J. Antibiot.* **2004**, *57*, 271.

[2] C. W. Zapf, B. A. Harrison, C. Drahl, E. J. Sorensen, *Angew. Chem.* **2005**, *117*, 6691; *Angew. Chem. Int. Ed.* **2005**, *44*, 6533.

[3] For other Diels–Alder macrocyclizations, see: a) E. J. Corey, M. Petrzilka, *Tetrahedron Lett.* **1975**, *16*, 2537; b) G. Stork, E. Nakamura, *J. Am. Chem. Soc.* **1983**, *105*, 5510; c) H. Dyke, P. G. Steel, E. J. Thomas, *J. Chem. Soc. Perkin Trans. 1* **1989**, 525; d) K. Takeda, Y. Igarashi, K. Okazaki, E. Yoshii, K. Yamaguchi, *J. Org. Chem.* **1990**, *55*, 3431; e) J. A. McCauley, K. Nagasawa, P. A. Lander, S. G. Mischke, M. A. Semones, Y. Kishi, *J. Am. Chem. Soc.* **1998**, *120*, 7647; f) F. Matsuura, R. Peters, M. Anada, S. S. Harried, J. Hao, Y. Kishi, *J. Am. Chem. Soc.* **2006**, *128*, 7463.

[4] M. Lautens, J. T. Colucci, S. Hiebert, N. D. Smith, G. Bouchain, *Org. Lett.* **2002**, *4*, 1879.

[5] K. C. Nicolaou, S. T. Harrison, *Angew. Chem.* **2006**, *118*, 3334; *Angew. Chem. Int. Ed.* **2006**, *45*, 3256.

[6] For further synthetic studies see: a) J.-P. Rath, S. Kinast, M. E. Maier, *Org. Lett.* **2005**, *7*, 3089; b) B. B. Snider, Y. Zou, *Org. Lett.* **2005**, *7*, 4939; c) A. L. Zografos, A. Yiotakis, D. Georgiadis, *Org. Lett.* **2005**, *7*, 4515; d) J.-P. Rath, M. Eipert, S. Kinast, M. E. Maier, *Synlett* **2005**, 314; e) E. A. Couladouros, E. A. Bouzas, A. D. Magos, *Tetrahedron* **2006**, *62*, 5272.

[7] D. E. Ward, M. S. Abaee, *Org. Lett.* **2000**, *2*, 3937.

 © 2006 Wiley-VCH Verlag GmbH & Co. KGaA, Weinheim 

DOI: 10.1002/anie.200600787

Synthetic Methods

# Selective Construction of Carbocyclic Eight-Membered Rings by Ring-Closing Metathesis of Acyclic Precursors

*Antoine Michaut and Jean Rodriguez**

**Keywords:**
cyclic compounds · domino reactions · eight-membered rings · ring-closing metathesis · synthetic methods

*Dedicated to Professor Peter Vollhardt on the occasion of his 60th birthday*

*Although the efficient preparation of cyclooctanoids has remained a long-standing objective, a real breakthrough was possible only relatively recently with the development of more specific reagents and by the development of new reactions. The direct construction of carbocyclic eight-membered rings from acyclic precursors is still a challenge, mainly because of unfavorable entropic and enthalpic factors that preclude ring formation. This Minireview describes the utilization of ring-closing metathesis (RCM) as a new approach to synthesize cyclooctanoids.*

## 1. Introduction

Although eight-membered rings are less commonly encountered in nature than, for example, six-membered rings or smaller rings, they still occur widely in terrestrial plants, marine organisms, and fungi.[1] They have therefore attracted considerable interest from both theoretical and synthetic points of view.[2,3] Pioneering investigations and more recent structural studies based on spectroscopic methods, X-ray crystallography, and calculations dealt with conformational concerns, specific control of strain, and transannular interactions to provide a better understanding of the reactivity of this unique nucleus.[4,5] From a synthetic point of view, the efficient preparation of cyclooctanoid systems has remained a long-standing objective, since direct extrapolation of existing protocols for ring formation to this framework has proved difficult. The direct construction of carbocyclic eight-membered rings from acyclic precursors remains a challenging problem mainly because of the high degree of strain and transannular interactions which develop unfavorable entropic and enthalpic factors that preclude the formation of the ring.

[*] A. Michaut, Prof. J. Rodriguez
Université Paul Cézanne (Aix-Marseille III)
UMR-CNRS-6178-SYMBIO
Equipe RéSo, Réactivité en Synthèse Organique
Faculté des Sciences et Techniques de St Jérôme
boîte D12, 13397 Marseille cedex 20 (France)
Fax: (+33) 4-9128-8841
E-mail: jean.rodriguez@univ.u-3 mrs.fr

A real breakthrough was made relatively recently with the development of more specific reagents and new synthetic strategies. Most of this chemistry has already been covered comprehensively in two important reviews published in 1992[6] and 1997,[7] and the chemistry of eight-membered heterocycles series has also been reviewed.[8,9]

This Minireview presents an overview of the utilization of ring-closing metathesis (RCM) as a new approach to the synthesis of cyclooctanoids. Some specific examples are presented in an excellent and general review by Yet[10] on the metal-mediated synthesis of medium-sized rings and also in an interesting highlight by Maier[11] concerning the utilization of RCM for the formation of rings containing seven to ten atoms. This Minireview focuses only on the direct formation of carbocyclic eight-membered rings from functionalized acyclic dienes and enynes under metathesis conditions in which either Schrock's molybdenum carbene **1** or Grubbs-type ruthenium carbenes **2**–**6** were used as catalysts (Scheme 1).[12–18] Special attention is given to the different parameters influencing the cyclization, and some general trends useful for solving this tricky problem, such as the nature of the substituent, steric and conformational effects, the nature of the catalyst, and the reaction conditions have been compiled. A short review of some recent alternatives for the construction of eight-membered rings by RCM is given at the end of the Minireview.

## 2. Annulated Eight-Membered Rings

Since the beginning of the 1990s, RCM has emerged as one of the most powerful and versatile methods for the selective formation of a large variety of cyclic compounds,[19]


InterScience
© 2006 Wiley-VCH Verlag GmbH & Co. KGaA, Weinheim

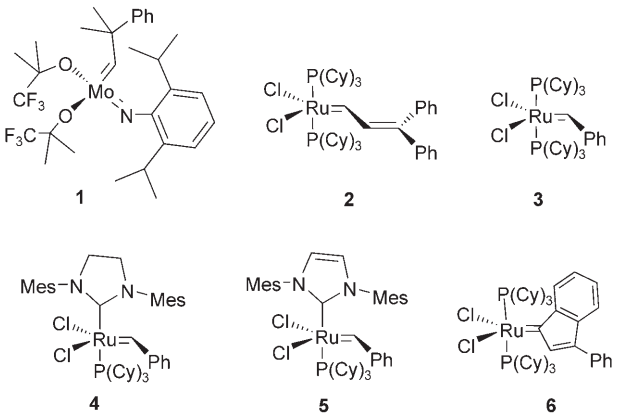


***Scheme 1.*** Mes = 2,4,6-trimethylphenyl, Cy = cyclohexyl.

including five- to seven-membered[20–24] rings as well as some complex macrocycles.[20,25–27] Extension of this approach to cyclooctanoids was addressed for the first time in 1995 by Grubbs and co-workers, and was found not to be trivial at all.[28] The initial study established that the direct cyclization of simple acyclic dienes with catalyst **2** did not take place, even at high dilution, and afforded only dimeric products resulting from intermolecular metathesis reactions (Scheme 2). Regardless of whether catalyst **1** or **3** was used, the presence of a geminal-disubstituted substrate[29] did not result in a RCM reaction that led to the expected eight-membered rings.[30]

Similar difficulties were reported a few years later by Mori et al.[31] for an enyne RCM that would lead to the formation of eight-membered rings bearing a synthetically valuable 1,3-

| $R^1$ | $R^2$ | $R^3$ | $R^4$ | $R^5$ | Catalyst | Yield [%] |
|---|---|---|---|---|---|---|
| Me | TESO | H | H | H | **2** | 0 |
| H | H | $CO_2Et$ | $CO_2Et$ | H | **1, 3** | 0 |
| H | H | $CO_2Et$ | $CO_2Et$ | Me | **1, 3** | 0 |

***Scheme 2.*** TES = triethylsilyl.

diene unit (Scheme 3). Even with the assistance of two quaternary carbon atoms in the acyclic chain (to take advantage of the geminal disubstituent effect),[29] only an incomplete transformation was found in the presence of

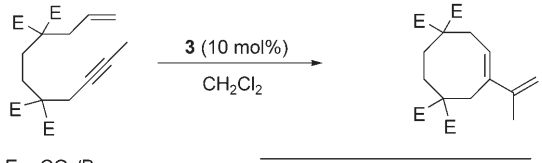


| Conditions | Time [h] | Yield [%] |
|---|---|---|
| reflux | 36 | 50 |
| RT | 22 | 0 |

***Scheme 3.***

10 mol% of catalyst **3** in refluxing $CH_2Cl_2$ after 36 h. The expected cyclic product was obtained in 50% yield along with starting material (45%); no reaction was evident after 22 h at room temperature.

The introduction of conformational constraints with substrates containing a preexisting ring to give fused bicycles appeared crucial for a successful cyclization. However, some of these transformations are still demanding in regard to the catalyst loading and the reaction conditions. A significant example involves a 1,2-*trans*-disubstituted cyclohexane, which presumably constrains the two olefin partners to be in proximity and results in the formation of the expected fused bicyclo[6.4.0]dodecene derivatives in 75% yield (Scheme 4).[28] In sharp contrast, the *cis* isomer was a poorer substrate and led to only a low yield of the ring-closed compound together with recovered starting material and significant amounts of side products.

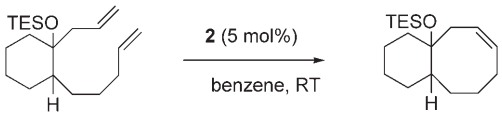


| Substrate | Time [h] | Yield [%] |
|---|---|---|
| *trans* | 4 | 75 |
| *cis* | 20 | 33 |

***Scheme 4.***

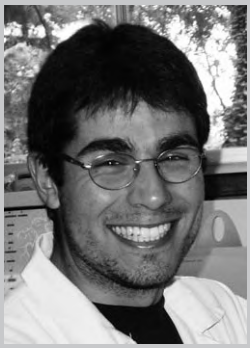

*Antoine Michaut was born in Reims, France, on 27 July 1979. After studying chemistry at the University of Paul Cézanne in Marseille, he went on two training courses at the research laboratory of Syngenta crop protection (2001–2002, Basel, Switzerland). In 2002, he started his PhD with Prof. Jean Rodriguez (completed 2005) at the University Paul Cézanne. He is currently a teacher and researcher within the same research group. His research interests concern the synthetic applications of the metathesis reaction and the development of domino reactions using 1,3-dicarbonyl compounds.*

*Jean Rodriguez was born in Cieza, Spain, on 25 June 1958, and in 1959 his family emigrated to France. After studying chemistry at the University Paul Cézanne in Marseille, France, he completed his PhD as a CNRS student with Prof. B. Waegell and Prof. P. Brun in 1987. He completed his Habilitation in 1992, also at Marseille, where he his currently Professor and Director of the UMR-CNRS-6178-SYMBIO. His research interests include the development of domino and multicomponent reactions, and their application in stereoselective synthesis. In 1998 he was awarded the Acros prize in Organic Chemistry from the French Chemical Society.*


© 2006 Wiley-VCH Verlag GmbH & Co. KGaA, Weinheim

Interestingly, it was shown that when the preexisting ring was a methyl-α-D-glucopyranoside derivative,[32] both *cis*- and *trans*-configured 5-hydroxy-1,9-diene precursors were cyclized with comparable moderate efficiency on treatment with 9 mol% of **3** for 31 and 41 h, respectively, in refluxing benzene (Scheme 5). In these cases, in addition to the conformational constraint, the presence of the unprotected tertiary alcohol probably played a crucial role in the transformation.[33–36]

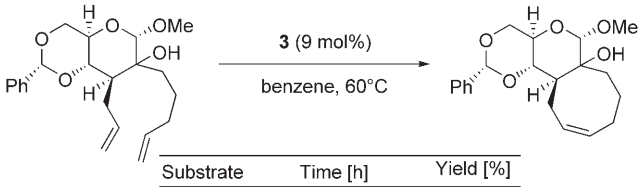


| Substrate | Time [h] | Yield [%] |
|---|---|---|
| *cis* | 31 | 44 |
| *trans* | 41 | 26 |

***Scheme 5.***

This RCM approach with conformational constraints was used for the construction of the B,C ring systems of taxol from appropriately functionalized cyclohexanes bearing a vinyl group in a sterically congested neopentylic position and a hexenyl chain in a 1,2 arrangement (Scheme 6).[37] However, it was clearly established with simple models having no

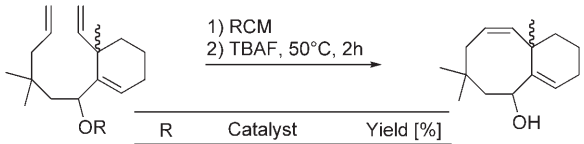


| R | Catalyst | Yield [%] |
|---|---|---|
| H | **1** | 0 |
| TES | **3** | 11[a] |
| TES | **1** | 85 |
| TES | **5** | 90 |

[a] Only β isomer.

***Scheme 6.***

specific conformational constraint that the presence of a free OH group inhibited the cyclization. The high enthalpic barrier could be overcome by protection as the corresponding triethylsilyl ether. With this transformation, the Schrock or the Nolan–Grubbs carbenes **1** and **5** were vastly superior to catalyst **3** (85 and 90% yields, respectively, after desilylation with TBAF).

The situation became more difficult with more-elaborate precursors. Besides competitive isomerization of the olefins,[38] the steric hindrance of the neopentylic vinyl substituent could also impair the reaction. In the case of a monosilylated 1,2-diol, only one isomer appeared to be reactive, and desilylated cyclized products were obtained in low yields after eight days when using 10 mol% of **3** or **5** as the catalyst; cyclooctenes in which the double bond had migrated were formed as by-products (Scheme 7).

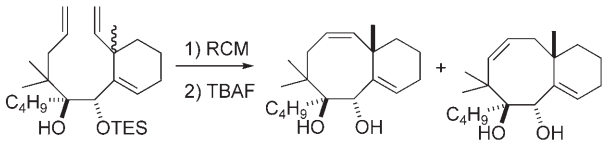


| Catalyst | Yield **a** [%] | Yield **b** [%] |
|---|---|---|
| **3** | 6[a] | 7[a] |
| **5** | 27[b] | 0 |

[a] Only β isomer. [b] Only α isomer.

***Scheme 7.***

Alternatively, both stereoisomers reacted smoothly when cyclic groups, such as silylene or acetonide, were used to protect the diol moiety (Scheme 8). The expected bicyclo-

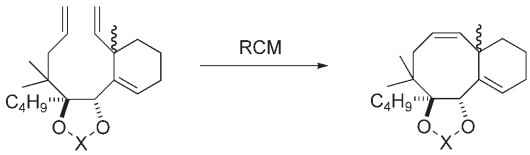


| X | Catalyst | Time | Yield [%] |
|---|---|---|---|
| $Si(tBu)_2$ | **1** | 3 d | 96 |
| $Si(tBu)_2$ | **3** | 8 d | 0 |
| $Si(tBu)_2$ | **5** | 20 h | 91 |
| $C(Me)_2$ | **1** | 3 d | 93 |
| $C(Me)_2$ | **3** | 8 d | 0 |
| $C(Me)_2$ | **5** | 15 h | 86 |

***Scheme 8.***

[6.4.0]dodecenes were isolated in very good yields when molybdenum carbene **1** or ruthenium carbene **5** were used. It is likely that the presence of the cyclic protecting group produces a favorable conformational control over the outcome of the RCM by bringing the two double bonds to a suitable distance for cyclization.

Quite unexpectedly, in the case of the corresponding cyclic carbonate, only one diastereomer cyclized in the presence of catalysts **1** and **3**. This reaction led to the selective formation of the *trans*-cyclooctene, which was isolated in yields of 34–41%, depending on the catalyst (Scheme 9).[39] A possible explanation for this result is that the reaction does

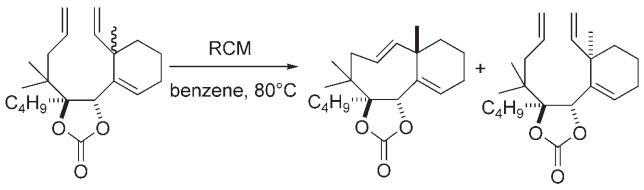


| Catalyst (10 mol%) | Time [d] | Yield **a** [%] | Yield **b** [%] |
|---|---|---|---|
| **1** | 3 | 34 | 46 |
| **3** | 8 | 41 | 34 |

***Scheme 9.***


© 2006 Wiley-VCH Verlag GmbH & Co. KGaA, Weinheim

not proceed to complete thermodynamic equilibrium under these conditions. A specific complexation of the catalyst to the carbonyl moiety was invoked on the basis of the exclusive formation of the *cis*-cyclooctene when the metathesis was performed in the presence of titanium isopropoxide.[40]

More recently, the high efficiency of catalyst **6** was clearly established by the quantitative formation of a functionalized bicyclo[6.4.0]dodecene framework starting from the corresponding monocyclic unsaturated ketone after only 17 h in refluxing $CH_2Cl_2$ (Scheme 10).[41] In this case, although the

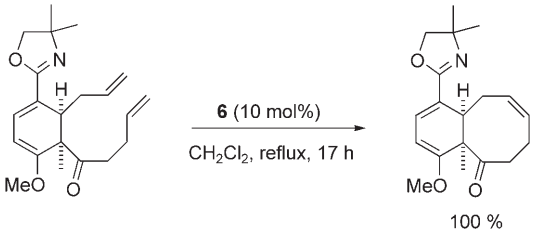


***Scheme 10.***

two olefinic groups are in an apparently unfavorable 1,2-*cis* relationship,[28] the presence of the intracyclic 1,3-diene unit allows the terminal olefins to be in proximity for the RCM (probably by flattening the molecule).

The synthesis of more-complex polycyclic skeletons including an eight-membered ring by RCM has not been the central focus of many studies; however, the pioneering contributions from Granja and co-workers are of prime importance.[42,43] In a study devoted to the design of carbocyclic analogues of the transition state in the isomerization of previtamin $D_3$ to vitamin $D_3$, the authors proposed the formation of tri- and tetracyclic systems incorporating a 6-8-6 core by direct RCM of 1,2-*cis*-difunctionalized cyclohexane substrates (Scheme 11). Although this stereochemistry was much less favorable than the 1,2-*trans* arrangement,[28] cyclization with 15 mol% of catalysts **3** or **4** was successful with various dienes and led to the expected tricyclic compounds in yields varying from 86 to 95%, regardless of whether the tertiary OH group was free or protected. As expected, the presence of a geminal disubstituted terminal olefin required the use of the more reactive carbene **4**. The introduction of a bulky substituent at the allylic position

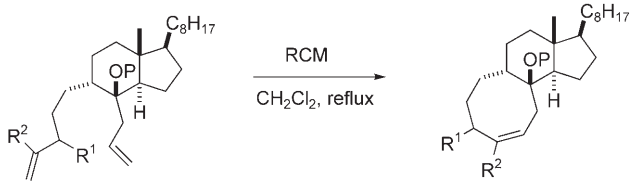


| $R^1$ | $R^2$ | P | Catalyst (15 mol%) | Yield [%] |
|---|---|---|---|---|
| H | H | H | **3** | 86 |
| H | Me | Me | **4** | 92 |
| H | Me | H | **4** | 89 |
| -$(CH_2)_4$- | | Me | **4** | 0 |

***Scheme 11.***

slowed the reaction down to six days, while a stereochemically demanding cyclohexyl derivative failed to give the corresponding tetracyclic compound.

1,3-Cyclohexenes were also considered as possible precursors for the construction of taxoidic A,B ring fragments. The RCM of appropriately functionalized substrates was reported as an efficient method for the formation of the central bridged bicyclo[5.3.1]undecene element found in some natural compounds (Scheme 12).[44] Interestingly, for

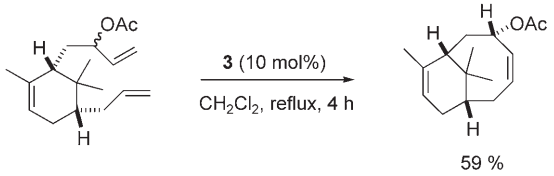


***Scheme 12.***

steric reasons, only the optically pure isomer leading to the naturally occurring configuration underwent a smooth cyclization in the presence of 10 mol% of carbene **3** in refluxing $CH_2Cl_2$. After 4 h the product was isolated in 59% yield.

Besides these efficient routes to 6-8 systems, a general strategy for the construction of fused bicyclic 5-8 skeletons found in ophiobolins and fusicoccin diterpenes was also developed starting from functionalized cyclopentenones.[45] The central unsaturated ketone most likely fixes the orientation of the two unsaturated alkyl chains, thereby favoring the cyclization. However, the reaction always remained incomplete with 8–10 mol% of catalyst **3**; even after three days at reflux in either $CH_2Cl_2$ or toluene the yield usually did not exceed 50% (Scheme 13).

| Conditions | **3** [mol%] | Time [days] | Yield [%] |
|---|---|---|---|
| $CH_2Cl_2$, 45°C | 10 | 3 | 48 |
| toluene, 65°C | 8 | 4 | 61 |

***Scheme 13.***

This approach found some very interesting synthetic applications, for example, in the very elegant and efficient total synthesis of dactylol and 3a-epidactylol in only six synthetic steps from two isomeric cyclopentenol derivatives (Scheme 14).[46] Although the Grubbs catalyst **3** did not effect the transformation, treatment with only 3 mol% of the Schrock molybdenum analogue **1** in hexane at 55°C for 3 h resulted in the formation, after desilylation with TBAF, ofthe expected natural product and its isomer in yields of 92 and 85%, respectively. Interestingly, although such a metathesis carbene catalyst was reported to be efficient in the presence of free OH groups, the direct cyclization of the corresponding cyclopentenols failed (quantitative recovery of the starting material). In sharp contrast, in a later study[47] of a related


© 2006 Wiley-VCH Verlag GmbH & Co. KGaA, Weinheim

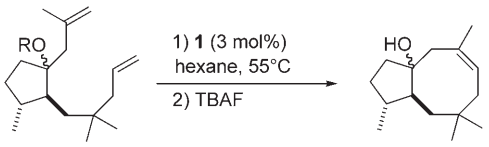


| R | OH | Yield [%] |
|---|---|---|
| $SiMe_3$ | β | 92[a] |
| $SiMe_3$ | α | 85[b] |
| H | α / β | 0 |

[a] Dactylol. [b] Epidactylol.

***Scheme 14.***

model transformation the presence of a tertiary hydroxy group was reported to be compatible with Grubbs catalyst **3** and led to the expected bicyclo[6.3.0]undecenol in 43–53% yield, depending on the reaction conditions (Scheme 15).

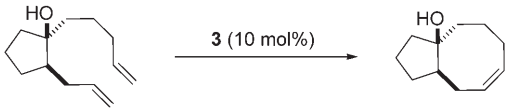


| Conditions | Time [h] | Yield [%] |
|---|---|---|
| $CH_2Cl_2$, reflux | 12 | 53 |
| $Et_2O$, reflux | 72 | 43 |

***Scheme 15.***

Following these pioneering examples, asteriscanolide, which bears a bridging butyrolactone group on a central "inside-outside" [6.3.0]carbocyclic skeleton, became a target compound that was studied independently by Paquette et al.[48] and Krafft et al.[49–51] The first strategic plan[48] involved a conformationally restricted oxabicyclo-[3.3.0]octane triene precursor, which gave rise to the expected tricyclic intermediate in 93% yield on reaction with 10 mol% of Grubbs carbene **3** in refluxing $CH_2Cl_2$ (Scheme 16). This very efficient transformation not only stressed the importance of conformational effects but also established the high

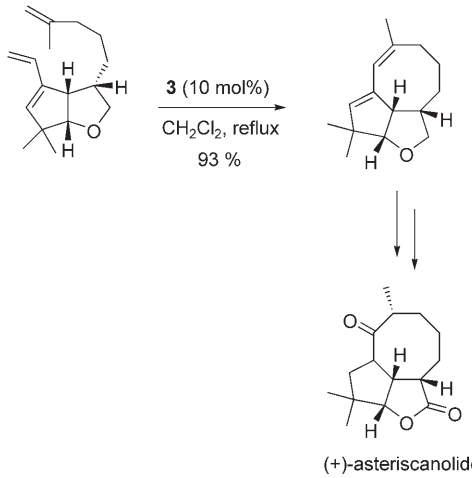


***Scheme 16.***

reactivity of a conjugated diene in the presence of the geminal disubstituted olefin.

In the alternative strategy,[50] the direct cyclization of a simple all-*cis*-configured oxabicyclo[3.3.0]octane model with 50 mol% of **3** led to the expected "outside-outside" tricycle in 65% yield (Scheme 17). More significantly, its epimer furnished the corresponding "inside-outside" derivative found in the natural compound in 80% yield.[49] The fully functionalized precursor of the tricyclic intermediate was similarly cyclized with the same efficiency in the presence of 50 mol% of **3** (Scheme 18). Despite the highly demanding experimental

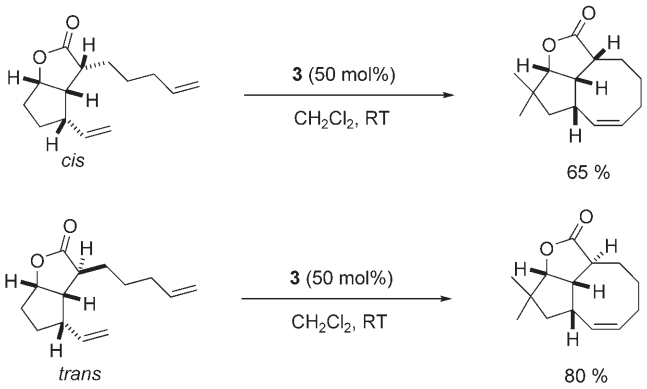


***Scheme 17.***

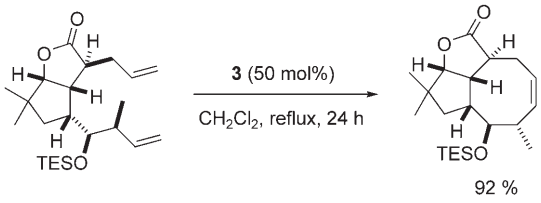


***Scheme 18.***

conditions, especially in terms of catalyst loading (up to 60 mol%) and the relatively long reaction time (8 h to 3 days), this RCM was proposed more recently[51] as a general approach to the construction of medium-sized ring systems with an intramolecular bridgehead. These results were rationalized by invoking the presence of the specific oxabicyclo[3.3.0]octane system that imposes a unique conformational constraint that allowed an efficient cyclization.

More-simple monocyclic butyrolactone precursors were utilized in the formation of fused oxabicyclo[6.3.0]undecene skeletons in $CH_2Cl_2$ at reflux with 30 mol% of **3** (Scheme 19).[52] Interestingly, the cyclization of the 1,2-*cis* isomer gave a poor result with the expected bicyclic methylene lactone formed in only 11% (along with 39% recovered starting material), while the 1,2-*trans* analogue allowed isolation of the corresponding lactone in 65% yield.

More recently, RCM of γ-lactones was proposed as a general route to enantiomerically enriched annulated γ-lactones fused to medium-sized rings, including a cyclooctene (Scheme 20).[53] The strategy involves the preparation of


© 2006 Wiley-VCH Verlag GmbH & Co. KGaA, Weinheim

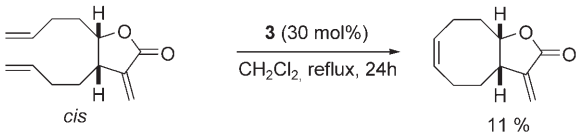


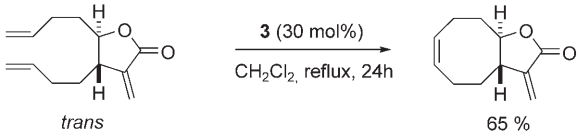


***Scheme 19.***

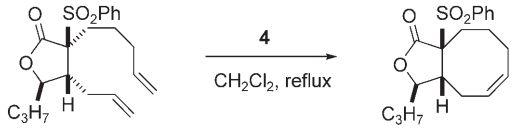


***Scheme 20.***

optically active α-phenylsulfonyl-γ-lactones flanked with two olefinic chains in a 1,2-*cis* relationship. The cyclization to the eight-membered ring proceeded smoothly by using 10 mol% of catalyst **4** in refluxing $CH_2Cl_2$ for 3 h to give the *cis*-fused bicyclic sulfone in 45% yield.

Another important synthetic challenge solved by involving RCM as a key step was addressed by Paquette and Efremov[54] during the total synthesis of teubrevins G and H (Scheme 21). The key step was the cyclization of a C3,C4

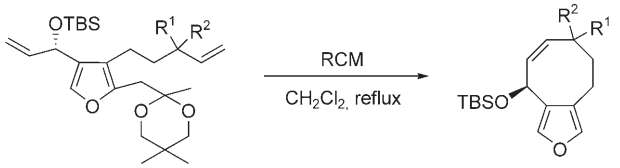


| $R^1$ | $R^2$ | Catalyst | Yield [%] |
|---|---|---|---|
| OH | H | **3** (30-35 mol%) | 0[a] |
| OH | H | **4** (8 mol%) | 88 |
| OTES | H | **3** (30-35 mol%) | 53 |
| =O | | **3** (30-35 mol%) | 35 |
| =O | | **4** (10 mol%) | 90 |

[a] Only isomerization to the corresponding unsatured ketones.

***Scheme 21.***

disubstituted furan ring, which imposed the steric constraint needed for an efficient cyclization between the two olefinic side arms. However, it was demonstrated that the ring closure with the allylic alcohol shown in Scheme 21 ($R^1$ = OH, $R^2$ = H), its triethylsilyl ether ($R^1$ = OTES, $R^2$ = H), or the corresponding unsaturated ketone was problematic, especially when catalyst **3** was used. Only very modest yields (20–53%) were obtained even with elevated catalyst loading (30–35 mol%) and extended reaction times (3–7 days). The best conditions consisted of the utilization of 8 to 10 mol% of Grubbs carbene **4** in refluxing $CH_2Cl_2$. Under these conditions, the presence of either a free allylic hydroxy group or the corresponding unsaturated ketone led to the expected bicyclic precursor of the natural product in yields of 88 and 90%, respectively.

## 3. Non-annulated Eight-Membered Rings

The preparation of non-annulated eight-membered rings is an even more challenging synthetic problem, and significant breakthroughs have been achieved only relatively recently by the utilization of various carbohydrates as precursors (Schemes 22 and 23). The pioneering approach was proposed

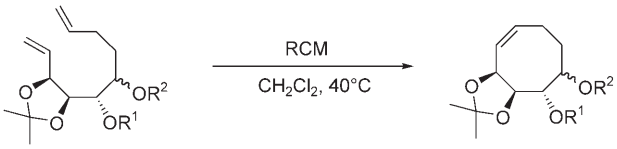


| $R^1$ | $R^2$ | Catalyst **3** (mol%) | Yield [%] |
|---|---|---|---|
| TBS | H | 5 | 0 |
| TBS | Ac | 5 | 94 |
| Ac | Ac | 7 | 93 |
| C=O | | 5 | 96 |

***Scheme 22.*** TBS = *tert*-butyldimethylsilyl, Ac = acetyl.

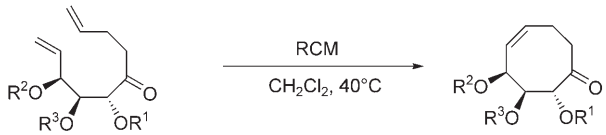


| $R^1$ | $R^2$ | $R^3$ | Catalyst | Yield [%] |
|---|---|---|---|---|
| TBS | $C(Me)_2$ | | **3** (13 mol%) | 68 |
| TBS | $C(Me)_2$ | | **5** (10 mol%) | 86 |
| Bn | Bn | Bn | **5** (10 mol%) | 66 |
| Bn | Bn | TES | **5** (10 mol%) | 68 |

***Scheme 23.*** Bn = benzyl.

by Hanna and co-workers,[55,56] who used galactose as the starting compound. The acyclic olefinic precursors were prepared efficiently by chemical modification of the protected sugar and were subjected to standard RCM conditions using 5–13 mol% of catalysts **3** or **5** in refluxing dichloromethane or benzene. Although in some cases the possible activating effect of allylic hydroxy groups in the substrate has been shown,[33–36] this study clearly established, in sharp contrast, that the presence of one free OH group on the polyhydroxylated chain prevented the cyclization. However, the introduction of diacetate or carbonate protecting groups (Scheme 22) or oxidation to the corresponding ketones (Scheme 23) allowed clean conversion into the highly functionalized and optically pure cyclooctenes in very good yields (ranging from 66 to 96%).

 © 2006 Wiley-VCH Verlag GmbH & Co. KGaA, Weinheim 

In a similar strategy, enantiomerically pure acyclic olefinic precursors obtained from D-glucose (Scheme 24) were submitted to RCM with catalyst **3**.[57] This study not only highlighted the problem of the free alcohol group at the

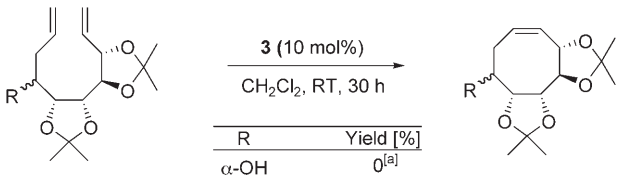


| R | Yield [%] |
|---|---|
| α-OH | 0[a] |
| β-OH | 17 |
| α-OAc | 99 |

[a] Only dimeric product.

*Scheme 24.*

homoallylic position but also showed the crucial importance of the absolute configuration at this stereocenter. The (*R*)-homoallylic alcohol gave only dimeric material in very poor yield, while the reaction of the *S* epimer was not much better (17% yield of the cyclooctene). However, the corresponding *R* acetate afforded an almost quantitative yield of the expected fully protected pentahydroxycyclooctene under the same conditions.

In a similar manner, metathesis precursors obtained from D-arabinose[58] and D-mannitol[59] were developed to form cyclooctanoic carbasugar analogues as carbohydrate mimetics (Schemes 25–28). In the case of D-arabinose, the presence of a

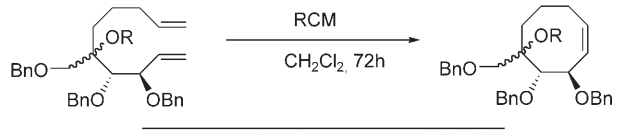


| R | Catalyst | Yield [%] |
|---|---|---|
| H | **3** (10 mol%) | 29 |
| H | **5** (10 mol%) | 0 |
| TBS | **3** (13 mol%) | 86 |
| TBS | **5** (10 mol%) | 0 |

*Scheme 25.*

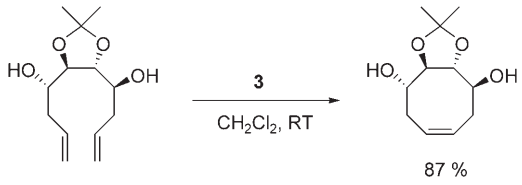


*Scheme 26.*

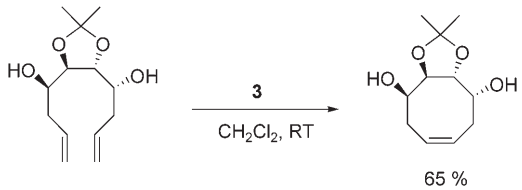


*Scheme 27.*

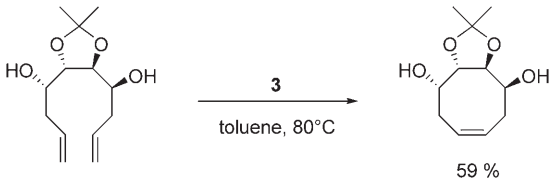


*Scheme 28.*

free hydroxy group once again proved to be a limiting factor when the reaction was performed in the presence of 10 mol% of either **3** or **5** (Scheme 25). However, the corresponding silyl ether was successfully cyclized in 86% yield after three days at 90°C when 13 mol% of **3** was used as the catalyst. Interestingly, and in sharp contrast, the isomeric diene acetonides prepared from D-mannitol could be cyclized in the presence of the simple ruthenium carbene **3** in $CH_2Cl_2$ at room temperature over 96 h. The presence of two secondary homoallylic free hydroxy groups caused no problems, and the expected eight-membered ring carbasugars were formed in yields of 65 to 87% (Schemes 26 and 27). A very similar result was reported starting from the enantiomeric acyclic precursor obtained by chemical modification of tartaric acid derivatives (Scheme 28).[60]

The crucial importance of a free alcohol group in RCM that leads to eight-membered rings was stressed again recently during a study directed towards the synthesis of *trans*-cyclooctene isomers with chair and twist conformations (Scheme 29).[61] The highly optically pure diolefinic diol

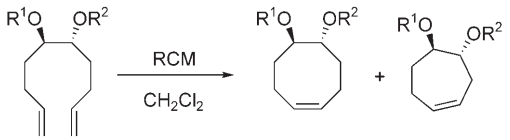


| $R^1$ | $R^2$ | Catalyst | Yield $C_8$ [%] | Yield $C_7$ [%] |
|---|---|---|---|---|
| H | H | **3** or **4** | 19 | 33 |
| $C(CH_3)_2$ | | **3** (2 mol%) | 89 | 0 |

*Scheme 29.*

precursor was obtained through Sharpless asymmetric dihydroxylation and submitted to RCM at room temperature in $CH_2Cl_2$ in the presence of only 2 mol% of catalysts **3** or **4**. Although the expected cyclooctene diol was formed in 19% yield, the major RCM product was the corresponding cycloheptene arising from loss of a methylene group after isomerization of one of the two double bonds. The corresponding acetonide smoothly and selectively evolved into the eight-membered ring in 89% yield.

In addition to carbohydrates, other compounds have been used as substrates for the synthesis of eight-membered rings. An interesting example is the rapid assembly of hydroxydifluorocyclooctenes (Scheme 30).[62] Neither the 1,3-diol nor the corresponding hydroxyketone precursors were reactive under the standard RCM conditions with **3** (refluxing $CH_2Cl_2$), and returned starting material only. However, pretreatment of the substrate with $Ti(OiPr)_4$ as co-catalyst[40] resulted in a quite efficient cyclization to form the expected


© 2006 Wiley-VCH Verlag GmbH & Co. KGaA, Weinheim

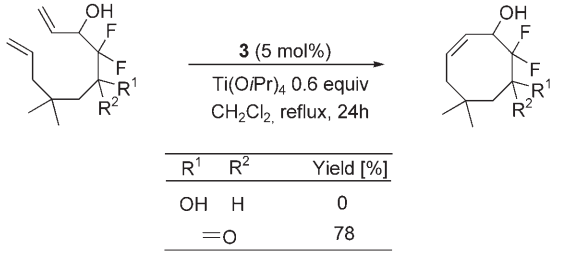


| $R^1$ | $R^2$ | Yield [%] |
|---|---|---|
| OH | H | 0 |
| =O | | 78 |

*Scheme 30.*

highly functionalized cyclooctenones in good yield. These results are in agreement with a possible inhibition of the active carbene catalyst through complexation with the polar groups of the substrate.

Also of interest is the quite general methodology involving simple substrates arising from a tandem radical addition/trapping sequence on unsaturated oxazolidinones (Scheme 31).[63] The cyclization using 10 mol% of **4** in

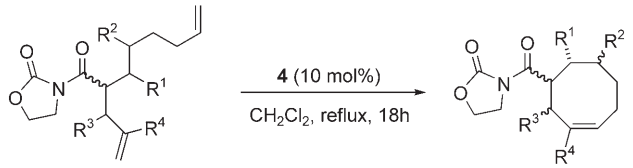


| $R^1$ | $R^2$ | $R^3$ | $R^4$ | Yield [%] |
|---|---|---|---|---|
| H | H | H | Me | 0[a] |
| $CO_2t$Bu | H | H | Me | 0[a] |
| H | H | H | H | 43 |
| H | Me | H | H | 88 |
| H | H | Me | H | 33 |
| $CO_2t$Bu | H | H | H | 70 |
| $CO_2t$Bu | Me | H | H | 70 |
| $CO_2t$Bu | H | Me | H | 19 |

[a] Only dimeric product.

*Scheme 31.*

refluxing $CH_2Cl_2$ for 18 h proceeded with various degrees of efficiency, depending on the nature of the substrate. Substrates with substituted double bonds ($R^4$ = Me) did not undergo RCM, regardless of the nature of the catalyst or of the reaction conditions. In general, successful transformations were observed with other substrates, but the presence of an allylic substituent ($R^3$) gave lower yields of the cyclized products as a result of steric hindrance.

Interestingly, this methodology could be extrapolated to the formation of the corresponding fused 5-8 and 6-8 bicyclic derivatives, and proved to be more efficient. Cyclizations of 1,2-*trans*-disubstituted cyclopentanes or cyclohexanes afforded yields of 96 and 95%, respectively (Scheme 32). Here also, the presence of a preexisting cycle imposes a favorable constraint to keep the two olefinic partners in proximity for the catalytic transformation.

More recently, chiral unsaturated cyanohydrins were used for the construction of diolefinic precursors that allowed the formation of cyclic 1,2-ethanolamines in good yields and with high enantiomeric excess by RCM.[64] A representative

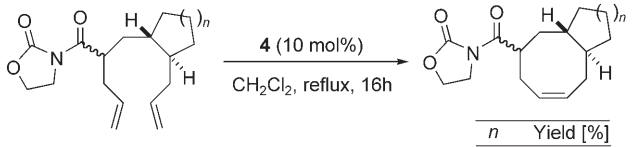


| *n* | Yield [%] |
|---|---|
| 1 | 96 |
| 2 | 95 |

*Scheme 32.*

example is the formation of a simple 1,2-difunctionalized cyclooctene in 68% yield by using only 4 mol% of catalyst **3** (Scheme 33).

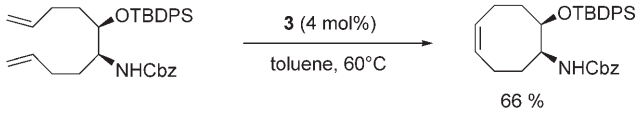


*Scheme 33.* TBDPS = *tert*-butyldiphenylsilyl, Cbz = benzyloxycarbonyl.

Functional group tolerance in RCM[22] is an important parameter, which has been addressed on many occasions. It was recently shown that the compatibility of ruthenium carbenes with other metallic centers present in the cyclization precursors allowed the elegant synthesis of large[65–68] and medium rings,[69,70] including cyclooctenes. An interesting example concerns the successful cyclization of an enantiopure $\eta^4$-(sulfinyldiene)irontricarbonyl complex with 8 mol% of **3** in toluene at room temperature to furnish very good yields of the corresponding cyclooctenedienylirontricarbonyl complex (Scheme 34).[71] The presence of the bulky irontricarbonyl unit was suspected to restrict the possible range of conformations for the olefin and thus had a positive effect on the cyclization.

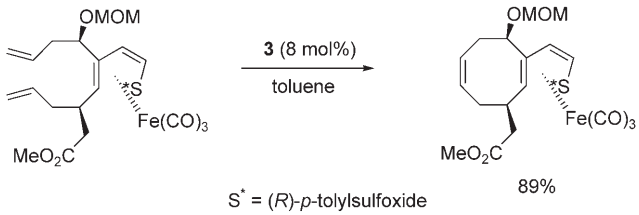


*Scheme 34.* MOM = methoxymethyl.

Similarly, a general approach to medium-sized-ring alkynes by RCM of dienes functionalized with two cobalthexacarbonyl complexes was reported more recently (Scheme 35).[72] It is notable that the complexed eight-membered rings were obtained in fair to good yields by using ruthenium complex **3** (15–44 mol%) at room temperature in $CH_2Cl_2$. The presence of a free OH group was again limiting; yields increased significantly with the corresponding acetate or ketone and reached up to 87% with the *tert*-butyldimethylsilyl ether.

 © 2006 Wiley-VCH Verlag GmbH & Co. KGaA, Weinheim 

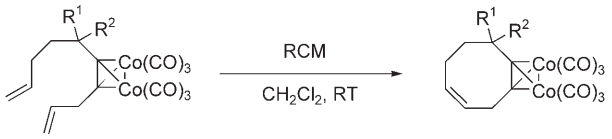


| $R^1$ | $R^2$ | **3** (mol%) | Yield [%] |
|---|---|---|---|
| OH | H | 30 | 29 |
| OAc | H | 25 | 55 |
| =O | | 44 | 58 |
| OTBS | H | 15 | 87 |

***Scheme 35.***

## 4. Domino Transformations

As an alternative to the direct cyclization of 1,9-dienes, Stragies and Blechert[73] introduced a domino strategy combining ring-opening, ring-closing, and cross-metathesis of functionalized norbornenes (Schemes 36 and 37). The synthesis of fused bicyclic systems was first studied by using ruthenium complex **3** in the presence of ethylene. This approach gave rise exclusively to the 1,2,4-trisubstituted cyclopentene through the selective ring opening of the strained bicyclo[2.2.1]alkene (Scheme 36). More gratifyingly, the use of 5 mol% of the Schrock carbene **1** in refluxing benzene resulted in completion of the domino process and the expected bicyclo[6.3.0]undecenes were isolated as single diastereomers in yields of 73 and 83% (depending on the functional group on the olefinic chain; Scheme 37).

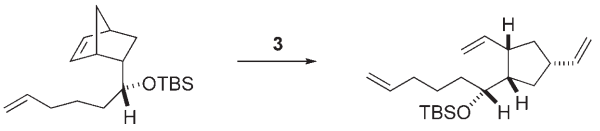


***Scheme 36.***

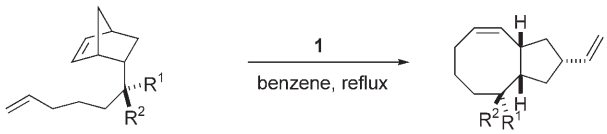


| $R^1$ | $R^2$ | **1** (mol%) | Yield [%] |
|---|---|---|---|
| $OCH_2CH_2O$ | | 8 | 73 |
| H | OTBS | 5 | 83 |

***Scheme 37.***

Functionalized enynes are also promising substrates for such one-pot transformations. An elegant domino sequence of a fully protected polyoxygenated dienyne was proposed by Hanna and co-workers[74] as a very efficient and quite general approach to polyoxygenated bicyclic systems containing a medium-sized ring. The optically pure dienynes were obtained by chemical modification of (+)-ribose and were subjected to RCM in refluxing dichloromethane or benzene (Scheme 38). Interestingly, the desired tandem process was only effective with 10 mol% of catalyst **4**, either with the free alcohol or with the corresponding triethylsilyl ethers, and led to the expected fused 5-8 and 6-8 bicycles in moderate to very good yields.

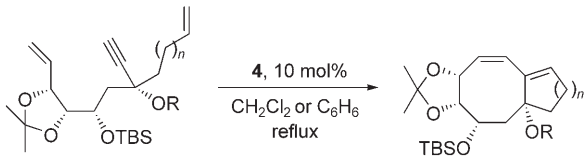


| *n* | R | Time | Yield [%] |
|---|---|---|---|
| 1 | H | 23 h | 79 |
| 1 | TES | 17 h | 96 |
| 2 | H | 2.5 days | 53 |
| 2 | TES | 5 h | 96 |

***Scheme 38.***

Finally, an alternative domino RCM of a functionalized dienyne was developed to circumvent the failure of the direct formation of the 6,8-fused bicyclic system found in vitamin D3 analogues.[42] This transformation with 15 mol% of Grubbs catalyst **3** in refluxing $CH_2Cl_2$ constituted the first example of the successful synthesis of a [6.4.0]bicycle by a domino RCM (Scheme 39).[43]

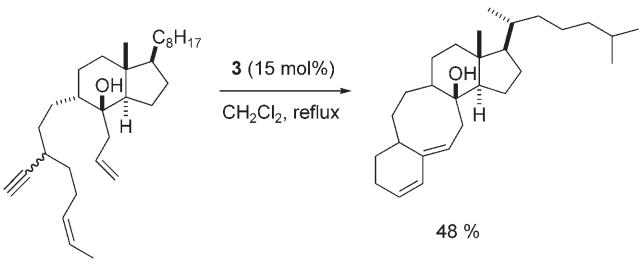


***Scheme 39.***

## 5. Miscellaneous Transformations

Two indirect approaches were proposed as alternative routes for the synthesis of eight-membered rings through RCM. The concept is based on the formation of a temporary bridge[75–77] in correctly functionalized bridged bicyclic derivatives followed by selective strategic bond fragmentations of these strained intermediates. Mascareñas and co-workers[78] introduced the selective formation/fragmentation of bicyclo-[3.3.1]nonanones with a hydroxy group at the bridgehead (Scheme 40). These intermediates were obtained in very good yields by RCM of an α-vinyl-α′-allyl- (shown in Scheme 40) or α-vinyl-α′propargylhydroxycyclohexanone using only

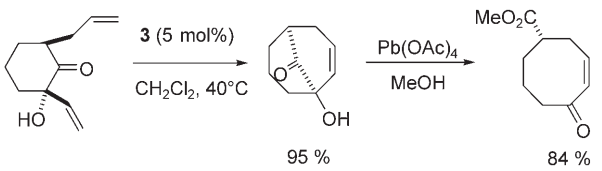


***Scheme 40.***


© 2006 Wiley-VCH Verlag GmbH & Co. KGaA, Weinheim

5 mol% of Grubbs carbene **3**. Subsequent $Pb(OAc)_4$-promoted ring cleavage of the bicyclo[3.3.1]nonan-9-ones with a hydroxy group at the bridgehead position afforded the corresponding monocyclic unsaturated ketones in good yields.

Finally, more recently we introduced a stereoselective RCM synthesis of bicyclo[4.2.1]nonane skeletons fused with a five-membered ring as a new versatile method for the efficient assembly of functionalized cyclooctanoids found in natural products (Scheme 41).[79] The required doubly unsaturated precursors were obtained through a domino process involving chemo-, regio-, and stereoselective α,γ-difunctionalization of a bicyclic β-ketoester. This crucial transformation takes advantage of the specific structure of the starting bicyclo[3.3.0]octane, which allows very good control over the required 1,3-*cis* arrangement of the two unsaturated chains. The RCM was highly catalyst-dependent. Only very low to moderate conversion was reached with **3**, even after refluxing in toluene for 36 h or after adding $Ti(OiPr)_4$ to prevent deactivation of the catalyst.[40] Alternatively, reproducible yields from 77 to 84% were achieved after refluxing in $CH_2Cl_2$ for only 3 h with only 2 mol% of the more active catalyst **4**.[80] The beneficial effect of a free hydroxy group in this reaction was evident. The corresponding alcohol and the 1,3-diol were successfully cyclized in very good yields using only 1 mol% of **4** in refluxing $CH_2Cl_2$ for 2 to 3 h. The functionalized bicyclo[4.2.1]nonanes thus formed were transformed either by retro-Dieckmann or Grob-type ring cleavages of the bridge to the corresponding functionalized cyclooctenes.

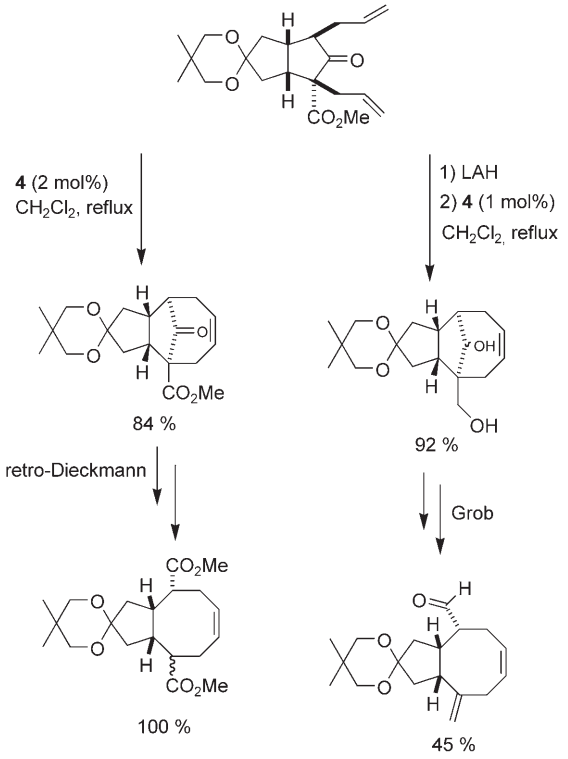


***Scheme 41.*** LAH = lithium aluminum hydride.

## 6. Conclusion

The studies presented here, which cover the last ten years, clearly show that RCM is an efficient methodology for addressing the challenging synthetic problem of functionalized eight-membered rings from acyclic precursors. Although it is not yet a completely general approach and often depends on the nature of both the catalyst and the substrate, it has become increasingly apparent that the formation of cyclooctenes by RCM requires a conformationally predisposed diene or an adequately oriented polar functional group that possibly acts as an internal ligand. Providing that an efficient steric effect (including stereoelectronic factors) or conformational control can be reached in the functionalized 1,9-diunsaturated precursors, this direct cyclization approach is successful for the formation of both monocyclic and fused polycyclic systems, usually under very mild experimental conditions. In cases where the direct approach is not successful, an elegant indirect metathesis can be used, including tandem processes or selective ring formation/ring fragmentation methodologies. There is no doubt that the wide interest in cyclooctanoids and the challenging structure of some important target compounds will result in other efficient applications of RCM.

*A.M. thanks the Ministère de l'Education Nationale de la Recherche et de la Technologie for a PhD grant. We are also particularly grateful to Prof. J. M. Pons, University Paul Cézanne, for his very careful proof-reading of the manuscript.*

Received: February 28, 2006
Published online: July 31, 2006

[1] *Studies in Natural Products Chemistry*, *Vol. 3* (Eds.: T. Oishi, Y. Ohtsuka, A. Rahman), **1989**, p. 73.
[2] F. A. L. Anet, R. Anet, *Top. Curr. Chem.* **1974**, *45*, 169.
[3] R. S. Glass, *Conformational Analysis of Medium Ring Heterocycles*, VCH, New York, **1988**.
[4] G. Illuminati, L. Mandolini, *Acc. Chem. Res.* **1981**, *14*, 95.
[5] G. Haufe, G. Mann, *Chemistry of Alicyclic Compounds*, Elsevier, Amsterdam, **1989**.
[6] N. A. Petasis, M. A. Patane, *Tetrahedron* **1992**, *48*, 5757.
[7] G. Mehta, V. Singh, *Chem. Rev.* **1999**, *99*, 881.
[8] A. Deiters, S. F. Martin, *Chem. Rev.* **2004**, *104*, 2199.
[9] M. D. McReynolds, J. M. Dougherty, P. R. Hanson, *Chem. Rev.* **2004**, *104*, 2239.
[10] L. Yet, *Chem. Rev.* **2000**, *100*, 2963.
[11] M. E. Maier, *Angew. Chem.* **2000**, *112*, 2153; *Angew. Chem. Int. Ed.* **2000**, *39*, 2073.
[12] R. R. Schrock, J. S. Murdzek, G. C. Bazan, J. Robbins, M. DiMare, M. O'Regan, *J. Am. Chem. Soc.* **1990**, *112*, 3875.
[13] S. T. Nguyen, R. H. Grubbs, J. W. Ziller, *J. Am. Chem. Soc.* **1993**, *115*, 9858.
[14] M. Scholl, S. Ding, C. W. Lee, R. H. Grubbs, *Org. Lett.* **1999**, *1*, 953.
[15] J. Huang, E. D. Stevens, S. P. Nolan, J. L. Petersen, *J. Am. Chem. Soc.* **1999**, *121*, 2674.
[16] M. Scholl, T. M. Trnka, J. P. Morgan, R. H. Grubbs, *Tetrahedron Lett.* **1999**, *40*, 2247.
[17] K. J. Harlow, A. F. Hill, J. D. E. T. Wilton-Ely, *J. Chem. Soc. Dalton Trans.* **1999**, 285.

 © 2006 Wiley-VCH Verlag GmbH & Co. KGaA, Weinheim 

[18] A. Fürstner, O. Guth, A. Düffels, G. Seidel, M. Liebl, B. Gabor, R. Mynott, *Chem. Eur. J.* **2001**, *7*, 4811.
[19] S. K. Armstrong, *J. Chem. Soc. Perkin Trans. 1* **1998**, 371.
[20] A. Fürstner, *Top. Catal.* **1997**, *4*, 285.
[21] A. Fürstner, *Angew. Chem.* **2000**, *112*, 3140; *Angew. Chem. Int. Ed.* **2000**, *39*, 3012.
[22] T. M. Trnka, R. H. Grubbs, *Acc. Chem. Res.* **2001**, *34*, 18.
[23] A. Fürstner, *Actual. Chim.* **2003**, 57.
[24] L. Hyldtoft, R. Madsen, *J. Am. Chem. Soc.* **2000**, *122*, 8444.
[25] C. W. Lee, T.-L. Choi, R. H. Grubbs, *J. Am. Chem. Soc.* **2002**, *124*, 3224.
[26] J. Prunet, *Angew. Chem.* **2003**, *115*, 2932; *Angew. Chem. Int. Ed.* **2003**, *42*, 2826.
[27] J. Prunet, *Angew. Chem.* **2003**, *115*, 3444; *Angew. Chem. Int. Ed.* **2003**, *42*, 3322.
[28] S. J. Miller, S.-H. Kim, Z.-R. Chen, R. H. Grubbs, *J. Am. Chem. Soc.* **1995**, *117*, 2108.
[29] M. E. Jung, G. Piizzi, *Chem. Rev.* **2005**, *105*, 1735.
[30] T. A. Kirkland, R. H. Grubbs, *J. Org. Chem.* **1997**, *62*, 7310.
[31] M. Mori, T. Kitamura, Y. Sato, *Synthesis* **2001**, 654.
[32] D. J. Holt, W. D. Barker, P. R. Jenkins, D. L. Davies, S. Garratt, J. Fawcett, D. Russell, R. S. Ghosh, *Angew. Chem.* **1998**, *110*, 3486; *Angew. Chem. Int. Ed.* **1998**, *37*, 3298.
[33] T. R. Hoye, H. Zhao, *Org. Lett.* **1999**, *1*, 1123.
[34] L. Ackermann, D. El Tom, A. Fürstner, *Tetrahedron* **2000**, *56*, 2195.
[35] T. K. Maishal, D. K. Sinha-Mahapatra, K. Paranjape, A. Sarkar, *Tetrahedron Lett.* **2002**, *43*, 2263.
[36] L. Caggiano, D. Castoldi, R. Beumer, P. Bayon, J. Telser, C. Gennari, *Tetrahedron Lett.* **2003**, *44*, 7913.
[37] D. Bourgeois, J. Mahuteau, A. Pancrazi, S. P. Nolan, J. Prunet, *Synthesis* **2000**, 869.
[38] D. Bourgeois, A. Pancrazi, S. P. Nolan, J. Prunet, *J. Organomet. Chem.* **2002**, *643–644*, 247.
[39] D. Bourgeois, A. Pancrazi, L. Ricard, J. Prunet, *Angew. Chem.* **2000**, *112*, 741; *Angew. Chem. Int. Ed.* **2000**, *39*, 725.
[40] A. Fürstner, K. Langemann, *J. Am. Chem. Soc.* **1997**, *119*, 9130.
[41] E. P. Kündig, A. Bellido, K. P. Kaliappan, A. R. Pape, S. Radix, *Synlett* **2003**, 2407.
[42] E. M. Codesido, L. Castedo, J. R. Granja, *Org. Lett.* **2001**, *3*, 1483.
[43] E. M. Codesido, J. R. Rodriguez, L. Castedo, J. R. Granja, *Org. Lett.* **2002**, *4*, 1651.
[44] M. Wenz, D. Grossbach, M. Beitzel, S. Blechert, *Synthesis* **1999**, 607.
[45] P. K. Ruprah, J.-P. Cros, J. E. Pease, W. G. Whittingham, J. M. J. Williams, *Eur. J. Org. Chem.* **2002**, 3145.
[46] A. Fürstner, K. Langemann, *J. Org. Chem.* **1996**, *61*, 8746.
[47] S. D. Edwards, T. Lewis, R. J. K. Taylor, *Tetrahedron Lett.* **1999**, *40*, 4267.
[48] L. A. Paquette, J. Tae, M. Arrington, A. H. Sadoun, *J. Am. Chem. Soc.* **2000**, *122*, 2742.
[49] M. E. Krafft, Y.-Y. Cheung, C. A. Juliano-Capucao, *Synthesis* **2000**, 1020.
[50] M. E. Krafft, Y. Y. Cheung, K. A. Abboud, *J. Org. Chem.* **2001**, *66*, 7443.
[51] M. E. Krafft, Y. Y. Cheung, S. A. Kerrigan, K. A. Abboud, *Tetrahedron Lett.* **2003**, *44*, 839.
[52] L. A. Paquette, S. Nakatani, T. M. Zydowsky, S. D. Edmondson, L.-Q. Sun, R. Skerlj, *J. Org. Chem.* **1999**, *64*, 3244.
[53] C. M. Rodriguez, J. L. Ravelo, V. S. Martin, *Org. Lett.* **2004**, *6*, 4787.
[54] L. A. Paquette, I. Efremov, *J. Am. Chem. Soc.* **2001**, *123*, 4492.
[55] I. Hanna, L. Ricard, *Org. Lett.* **2000**, *2*, 2651.
[56] F.-D. Boyer, I. Hanna, S. P. Nolan, *J. Org. Chem.* **2001**, *66*, 4094.
[57] J. Marco-Contelles, E. de Opazo, *J. Org. Chem.* **2002**, *67*, 3705.
[58] Y. Bleriot, A. Giroult, J.-M. Mallet, E. Rodriguez, P. Vogel, P. Sinay, *Tetrahedron: Asymmetry* **2002**, *13*, 2553.
[59] C. Gravier-Pelletier, O. Andriuzzi, Y. L. Merrer, *Tetrahedron Lett.* **2002**, *43*, 245.
[60] J. McNulty, V. Grunner, J. Mao, *Tetrahedron Lett.* **2001**, *42*, 5609.
[61] D. C. Braddock, G. Cansell, S. A. Hermitage, A. J. P. White, *Tetrahedron: Asymmetry* **2004**, *15*, 3123.
[62] B. M. Kariuki, W. M. Owton, J. M. Percy, S. Pintat, C. A. Smith, N. S. Spencer, A. C. Thomas, M. Watson, *Chem. Commun.* **2002**, 228.
[63] M. P. Sibi, M. Aasmul, H. Hasegawa, T. Subramanian, *Org. Lett.* **2003**, *5*, 2883.
[64] A. M. C. H. van den Nieuwendijk, A. B. T. Ghisaidoobe, H. S. Overkleeft, J. Brussee, A. van der Gen, *Tetrahedron* **2004**, *60*, 10385.
[65] M. J. Marsella, H. D. Maynard, R. H. Grubbs, *Angew. Chem.* **1997**, *109*, 1147; *Angew. Chem. Int. Ed. Engl.* **1997**, *36*, 1101.
[66] P. L. Ng, J. N. Lambert, *Synlett* **1999**, 1749.
[67] M. Weck, B. Mohr, J.-P. Sauvage, R. H. Grubbs, *J. Org. Chem.* **1999**, *64*, 5463.
[68] E. B. Bauer, J. Ruwwe, F. A. Hampel, S. Szafert, J. A. Gladysz, J. M. Martin-Alvarez, T. B. Peters, J. C. Bohling, T. Lis, *Chem. Commun.* **2000**, 2261.
[69] J. Renaud, S. G. Ouellet, *J. Am. Chem. Soc.* **1998**, *120*, 11836.
[70] E. Licandro, S. Maiorana, B. Vandoni, D. Perdicchia, P. Paravidino, C. Baldoli, *Synlett* **2001**, 757.
[71] R. S. Paley, L. A. Estroff, J.-M. Gauguet, D. K. Hunt, R. C. Newlin, *Org. Lett.* **2000**, *2*, 365.
[72] D. G. J. Young, J. A. Burlison, U. Peters, *J. Org. Chem.* **2003**, *68*, 3494.
[73] R. Stragies, S. Blechert, *Synlett* **1998**, 169.
[74] F.-D. Boyer, I. Hanna, L. Ricard, *Org. Lett.* **2001**, *3*, 3095.
[75] T. Lavoisier-Gallo, E. Charonnet, J. Rodriguez, *J. Org. Chem.* **1998**, *63*, 900.
[76] T. Lavoisier-Gallo, E. Charonnet, J.-M. Pons, M. Rajzman, R. Faure, J. Rodriguez, *Chem. Eur. J.* **2001**, *7*, 1056.
[77] C. Simon, J.-F. Peyronel, F. Clerc, J. Rodriguez, *Eur. J. Org. Chem.* **2002**, 3359.
[78] J. R. Rodriguez, L. Castedo, J. L. Mascarenas, *Chem. Eur. J.* **2002**, *8*, 2923.
[79] A. Michaut, S. Miranda-Garcia, J.-C. Menéndez, J. Rodriguez, *Org. Lett.* **2004**, *6*, 3075.
[80] J. A. Love, M. S. Sanford, M. W. Day, R. H. Grubbs, *J. Am. Chem. Soc.* **2003**, *125*, 10103.


© 2006 Wiley-VCH Verlag GmbH & Co. KGaA, Weinheim

H. R. Kricheldorf

DOI: 10.1002/anie.200600693

Macromolecular Chemistry

# Polypeptides and 100 Years of Chemistry of α-Amino Acid *N*-Carboxyanhydrides

*Hans R. Kricheldorf**

**Keywords:**
α-amino acids · Leuchs, Hermann · molecular evolution · polypeptides · ring-opening polymerization

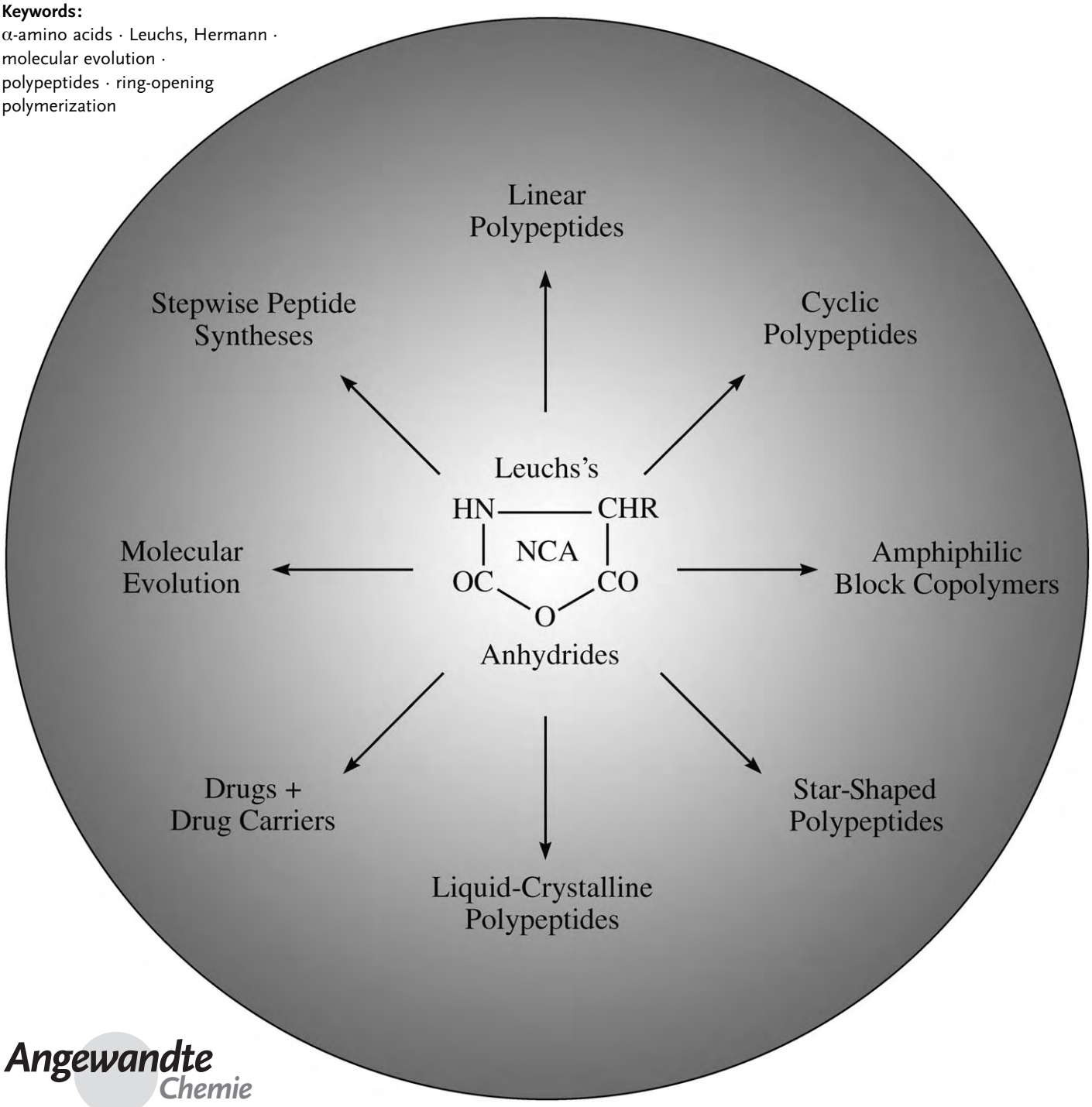




© 2006 Wiley-VCH Verlag GmbH & Co. KGaA, Weinheim

*Syntheses and polymerizations of α-amino acid* N*-carboxyanhydrides (NCAs) were reported for the first time by Hermann Leuchs in 1906. Since that time, these cyclic and highly reactive amino acid derivatives were used for stepwise peptide syntheses but mainly for the formation of polypeptides by ring-opening polymerizations. This review summarizes the literature after 1985 and reports on new aspects of the polymerization processes, such as the formation of cyclic polypeptides or novel organometal catalysts. Polypeptides with various architectures, such as diblock, triblock, and multiblock sequences, and star-shaped or dendritic structures are also mentioned. Furthermore, lyotropic and thermotropic liquid-crystalline polypeptides will be discussed and the role of polypeptides as drugs or drug carriers are reviewed. Finally, the hypothetical role of NCAs in molecular evolution on the prebiotic Earth is discussed.*

**From the Contents**

1. Introduction 5753
2. Stepwise Peptide Syntheses 5755
3. Living Polypeptides? 5756
4. New Organometallic Initiators 5758
5. Cyclic Polypeptides 5761
6. Block Copolymers 5764
7. Various Architectures 5768
8. Liquid-Crystalline Polypeptides 5772
9. Drugs and Drug Carriers 5774
10. NCAs and the Hypothesis of Molecular Evolution 5775
11. Various Aspects 5778

## 1. Introduction

In the years 1906, 1907, and 1908, three papers were published by Hermann Leuchs et al.[1–3] describing the syntheses and properties of α-amino acid *N*-carboxyanhydrides (NCAs, **1**; Scheme 1), which were for a long time also called Leuchs's anhydrides. Leuchs discovered the NCAs by coincidence when he attempted to purify *N*-ethoxycarbonyl or *N*-methoxycarbonyl amino acid chlorides by distillation. Leuchs was born on August 26, 1879 in Nürnberg and studied chemistry in München and Berlin.[4] He was a PhD student in the research group of Emil Fischer and completed his thesis in 1902. At that time Emil Fischer worked in the famous Kaiser-Wilhelm-Institut in Berlin, the forerunner of the first Max-Planck-Institut, which was founded after World War I. In the two decades before World War I, Emil Fischer was the most successful and most influential professor of organic chemistry in Germany. He was awarded the second Nobel Prize in Chemistry for his work on stepwise syntheses and the characterization of polypeptides and polysaccharides. After a short period in postdoctoral research, Leuchs was selected by Emil Fischer as his private assistant for research on the stepwise syntheses of peptides.[5]

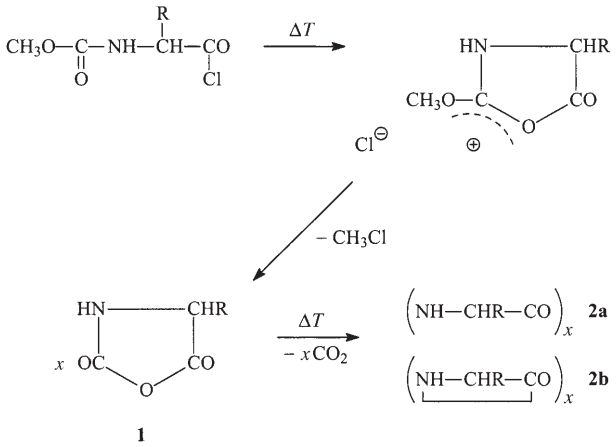


***Scheme 1.*** Synthesis and thermal polymerization of NCAs (**1**) by the Leuchs method.

In 1910, Leuchs received the status of assistant professor and became associate professor in 1914. It is remarkable that Leuchs was allowed to publish his work on NCAs without Emil Fischer as coauthor before he had reached the status of assistant professor. Nonetheless, Leuchs abandoned the work on NCAs after 1907 for the following reasons: First, peptide chemistry was the long-term research area of his former supervisor E. Fischer. Second, the polypeptides resulting from the water- or alcohol-initiated polymerizations of NCAs proved to be insoluble in common inert solvents and were difficult to characterize with the analytical methods available around 1910. Third, ring-opening polymerizations (ROPs) yielding high-molar-mass polymers were outside the experimental experience and mental scope of almost all chemists at that time. With the exception of H. Staudinger, almost no chemist believed in the existence of polymers with a covalent backbone and molecular weights around or above 10000 Da. E. Fischer denied the existence of biopolymers and synthetic polymers with molar masses above 6000 Da, and, until his death in 1915, was a fierce criticist of Staudinger's concept of

[*] Prof. Dr. H. R. Kricheldorf
Institut für Technische und Makromolekulare Chemie
Universität Hamburg
Bundesstrasse 45, 20146 Hamburg (Germany)
Fax: (+49) 40-42838-6008
E-mail: kricheld@chemie.uni-hamburg.de


© 2006 Wiley-VCH Verlag GmbH & Co. KGaA, Weinheim

covalent macromolecules. The characteristic properties of polymers known from biopolymers, such as polyisoprenes or cellulose derivatives, were ascribed to aggregates of oligomers. At first, (papers published in 1906 and 1907) Leuchs called the polymerization products of the NCAs "anhydrides of amino acids", meaning a dehydrated form of amino acids, and gave them the formula **2a** (Scheme 1). However, in his third paper,[3] Leuchs et al. concluded from the amorphous character and from the lack of a melting point (in contrast to the crystalline cyclic dipeptides) that his products were polymeric modifications of α-lactams and depicted the formula **2b**. As a consequence of this unsatisfactory situation, Leuchs changed his area of research completely and after 1907 worked mainly on the chemistry of strychnos alkaloids. His important contributions to this new research area were reported in 120 publications.

He was respected by his colleagues for his sharp analytical way of thinking and for his broad knowledge of chemistry. Yet, he was not a charismatic speaker, and he did not like to present his results at conferences. He spoke with perfect grammar but with a monotone voice. His co-workers respected him for his systematic teaching and for his careful and successful experimental work, but he did not raise enthusiasm in his research group. Leuchs was, for many years, editor of the "Berichte der Deutschen Chemischen Gesellschaft" together with "Liebigs Annalen", the leading journal of chemistry for German-speaking countries.

He received calls for full professor positions at the Universities of Graz (Austria) and Braunschweig (Germany).[5] However, he turned down these calls and preferred to continue his work in Berlin. This decision was apparently very much influenced by a great sympathy for Berlin and its numerous cultural and scientific activities. He traveled rarely and visited his hometown Nürnberg and his relatives in Bavaria only once or twice in forty years.[4]

Some years after the death of Emil Fischer, he was finally honored with the title of full professor and became vice director of the Chemical Institute of the University of Berlin. However, he was very disappointed that the ministry did not grant him the originally promised director post, but rather gave it to W. Schlenk. Furthermore, he was disappointed that neither he nor any other former co-workers or assistants of Emil Fischer succeeded this admired teacher and supervisor.

*Hans Rytger Kricheldorf studied chemistry at the University of Freiburg. After his PhD (1969), he continued his academic career in Freiburg and completed his Habilitation in 1975. He was appointed associate professor in 1980 and in 1982 he became a full professor for polymer science at the University of Hamburg. His research activities concern ring-opening polymerization and polycondensation, the synthesis of biodegradable polymers, thermostable engineering plastics, and liquid-crystalline polymers, and more recently the syntheses of cyclic and multicyclic polymers.*

His contacts with W. Schlenk were formal rather than warm despite the open-minded and friendly character of this colleague. These negative events in his professional career and factors embedded in his character had the consequence that he gradually developed a tendency towards depression. The political situation in Germany after 1933 and mainly after 1938 raised his skepticism about the future of Germany and of his private life. The gradual destruction of Berlin and the Chemical Institute by bomber raids of the Allied air forces beginning after 1941 deepened his depressions. There was nobody to help him out of his negative mood: he was not married, he did not have close relatives in Berlin, and he apparently did not have a close friend despite friendly contacts with several colleagues. The almost total destruction of Berlin in spring 1945 and the beginning of the occupation by Russian troops made him so desperate that he finally committed suicide on May 1 or May 2, 1945. In those chaotic days, nobody was there to organize an individual and honored burial ceremony, and he was buried along with numerous dead soldiers and citizens in a mass grave.[4]

The "career" of the NCAs as monomers for the preparation of (poly)peptides by ROP continued after 1921 with publications of Curtius et al.[6–8] and Wessely et al.,[9–16] who used water, alcohol, or primary amines as initiators and assumed for the first time that the reaction products of NCAs are high-molar-mass polypeptides. The time when the first publications of Curtius, Wessely, and co-workers appeared was not coincidental, but a consequence of two changes. First, World War I and the following economic depression in central Europe was over, and second, the attitude of most chemists towards the work of Staudinger had changed. In the years between 1920 and 1930, Staudinger's concept of covalent macromolecules became fully acknowledged by the international scientific community and this turnaround spurred systematic investigations of any kind of polymerization processes.[17] In the following five decades, the chemistry of NCAs together with synthesis and characterization of poly(α-amino acid)s derived from them were intensively studied by numerous research groups, and the results were reported in several hundred publications. Several aspects of this huge body of results deserve to be highlighted briefly.

Although NCAs were most widely used as monomers for the preparation of poly(amino acid)s through ROP, they also proved to be useful as synthons for the stepwise synthesis of oligopeptides and complex polypeptides. NCAs have the advantage that their ring structure combines activation of the CO group C5 with protection of the amino group. Their characteristic disadvantage is a high sensitivity to moisture and a low stability upon storage. Nonetheless, a team of the American Merck company headed by Denkewalter and Hirschmann had succeeded to prepare the enzyme ribonuclease-S exclusively by stepwise syntheses with NCAs.[18–24] In the years 1940–1980, homo- and copoly(amino acid)s obtained by ROP of NCAs played an important role as models of natural polypeptides and proteins with regard to relationships between primary and secondary structure. Systematic comparisons mainly by means of IR spectroscopy and wide-angle X-ray scattering (WAXS) or small-angle X-ray scattering (SAXS) measurements allowed for a subdivi-

 © 2006 Wiley-VCH Verlag GmbH & Co. KGaA, Weinheim 

sion of the poly(amino acid)s into the following three classes:[25,26]

1. Poly(amino acid)s exclusively forming β-sheet structures: glycine, valine, isoleucine, serine, threonine, and cysteine.
2. Poly(amino acid)s forming α-helical structures when the chains are sufficiently long: norleucine, leucine, β esters of aspartic acid, γ esters of glutamic acid, N-substituted lysine, phenylalanine, tyrosine, histidine, and tryptophane.
3. Polymers of N-substituted amino acids may form random coils such as polysarcosine or special helices such as proline and 4-hydroxyproline.

The systematic characterization of numerous homo- and copolypeptides also allowed several authors[27–32] to establish a group II order of increasing stability of the α helix of the individual amino acids. The availability of organosoluble and water-soluble α-helical poly(amino acid)s also had the consequence that kinetic and thermodynamic aspects of helix–coil transitions were studied in detail. Important for the proper understanding of ROPs of NCAs was the finding that the oligomers of all helicogenic amino acids adopt the β-sheet structure when the degree of polymerization ($P_n$) is below $10 \pm 1$ (depending on solvent and side chain).[33–36]

Synthetic polypeptides prepared from NCAs also played a key role in the elucidation of relationships between the primary structure of natural peptides and their immunogeneity.[37–40] It turned out that polymers of *N*-alkylamino acids possess negligible immunogenic properties. The presence of H-bond-forming peptide groups is important for an immunogenic reaction. Furthermore, aromatic side chains, above all those with functional groups, proved to be the most efficient haptens. Finally, it should be mentioned that poly(γ-benzyl-L-glutamate) (poly(γ-Bzl-L-Glu)) was the first polymer that was found to form a liquid-crystalline (LC) phase. Elliot and Ambrose[41] reported as early as 1950 that concentrating a solution of poly(γ-Bzl-L-Glu) in helicogenic solvents results in a birefringent phase with a high optical rotation. A few years later, Robinson[42] detected, by means of monochromatic light, that these birefringent phases possess a periodical supermolecular order corresponding to a cholesteric phase. In the following three decades, around 60 publications appeared dealing with syntheses and characterization of lyotropic phases based on polyglutamates. These papers were reviewed in a book by Block.[43] Other aspects of the chemistry of NCAs and numerous studies concerning the properties of poly(amino acid)s were summarized in several reviews and books up to the year 1985.[43–50] Therefore, we mainly concentrate here on the results published over the past twenty years. However, a more recent review by Daley et al. focuses on polyglutamates.[51]

## 2. Stepwise Peptide Syntheses

In principle the NCA ring renders these amino acid derivatives particularly suited for stepwise peptide syntheses. The CO group of the amino acid is strongly activated such that a rapid acylation of the amino groups can occur at room temperature (or below), and the amino group is protected such that no reaction with NCAs or other activated amino acid derivatives takes place. Although the synthesis of the enzyme ribonuclease-S has been achieved by means of N-unsubstituted NCAs, this approach has not attracted much interest for two reasons. First, NCAs are not stable upon storage over months or years, even in a refrigerator, apparently because traces of water fixed to the surface of the NCA crystals through H bonds slowly initiate polymerizations in the solid state. Second, the desired reaction steps may be accompanied by oligomerization reactions, the products of which are very difficult to separated from the desired oligopeptide. Both problems can be solved by NCAs with a protecting group attached to the nitrogen which can easily be removed after the coupling step.

N-protected NCAs can be prepared in two ways. One route (Scheme 2) is based on the cyclization of N-protected amino acids, whereas in the other route a protecting group is

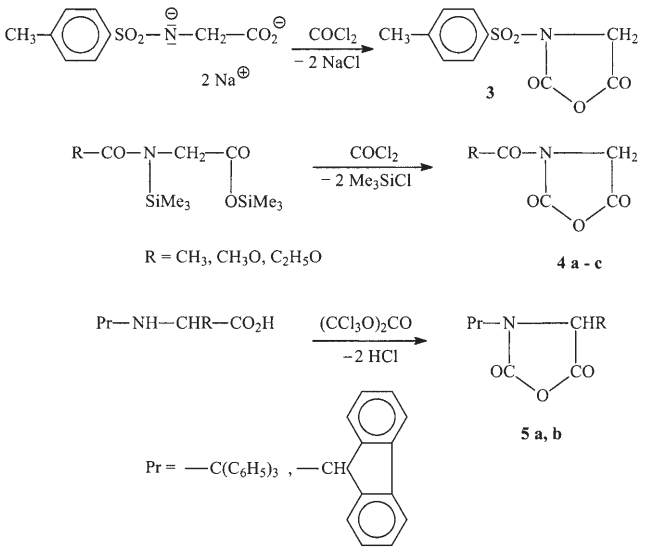


***Scheme 2.*** Synthesis of N-protected NCAs through cyclization.

attached to a preformed NCA (Scheme 3). When the amino group bears an electron-withdrawing substituent (typical for most protecting groups) on the nitrogen, it does not react with phosgene under mild conditions unless its nucleophilicity is activated. This aspect is illustrated by the first synthesis of a N-protected NCA, *N*-tosyl-Gly-NCA (**3**),[52] which was obtained by phosgenation of the disodium salt of *N*-tosyl glycine. Double silylation of glycine derivatives enabled the preparations of *N*-acetyl-, *N*-methoxycarbonyl-, and *N*-ethoxycarbonyl-Gly-NCA (**4a–c**).[53] In this way, the first urethane-protected NCAs (UNCAs) were obtained, but neither the methoxy- or ethoxycarbonyl groups nor the tosyl group are attractive protecting groups because selective removal without side reactions is difficult to achieve. NCAs with more-useful protecting groups were recently synthesized by phosgenation of *N*-trityl or *N*-phenylfluorenyl amino acids (**5a,b**).[54] All these syntheses by the first route are compiled in Scheme 2.


© 2006 Wiley-VCH Verlag GmbH & Co. KGaA, Weinheim

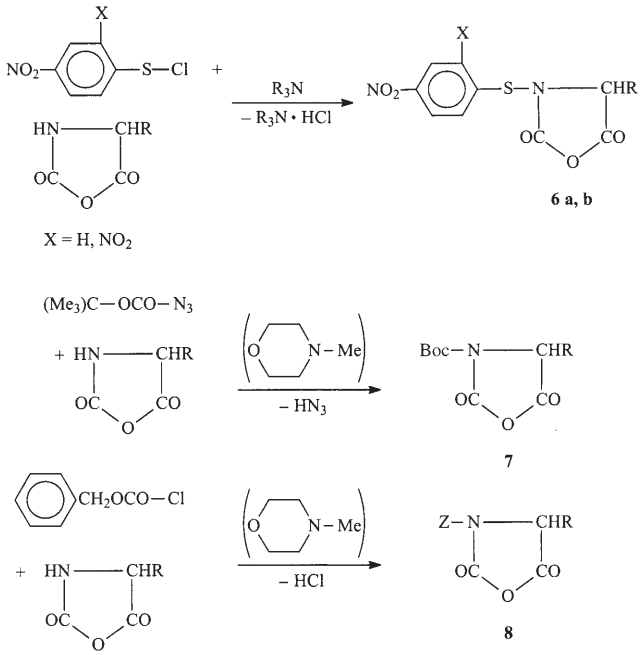


***Scheme 3.*** Synthesis of N-protected NCAs by "acylation" of preformed NCAs.

Examples of successful syntheses by the second route are outlined in Scheme 3. N substitution of NCAs in the presence of a strong base as the catalyst proceeds by an intermediate deprotonation and runs the risk of part of the NCA polymerizing. However, 4-nitrophenylsulfenyl chloride (Nps-Cl) and 2,4-dinitrophenylsulfenyl chloride proved so reactive that quantitative substitution was feasible with triethylamine as the base. Furthermore, most Nps-NCAs crystallize well, and thus several authors[55–59] used Nps-NCAs for syntheses of oligopeptides. However, these sulfenyl groups are less attractive as protecting groups than urethanes first because of side reactions with functional groups in the side chains of the amino acids and second because the purification of peptides from liberated Nps-Cl is more difficult. Therefore, it was a significant improvement that N substitution of NCAs with *tert*-butoxycarbonyl (Boc, **7**), benzyloxycarbonyl (Z), and fluorenylmethoxycarbonyl (Fmoc) groups became feasible.[60–62] The key to the successful acylation without polymerization was the use of *N*-methylmorpholine as the base. Owing to the extraordinary usefulness of the Boc protecting group, Boc-NCAs were commercialized. Boc-NCAs proved to be particularly useful in solid-phase peptide syntheses[60] as their steric demands are lower than those of other N-protected and CO-activated amino acids and because of their high reactivity. However, a fundamental problem of synthesis and application of both Nps-NCAs and UNCAs is their sensitivity to racemization;[56,61] even weak bases such as pyridine may cause deprotonation in the α position.

When NCAs are treated with strong bases in the absence of a nucleophilic reaction partner, the α deprotonation initiates a dimerization process after which decarboxylation yields substituted pyrrolidine-2,4-diones.[63,64] Compound **9** is such a dimerization product derived from Boc-Phe-NCA. Finally, it should be mentioned that N-protected β-amino acid NCAs such as **10** and **11** were also synthesized.[55,65]

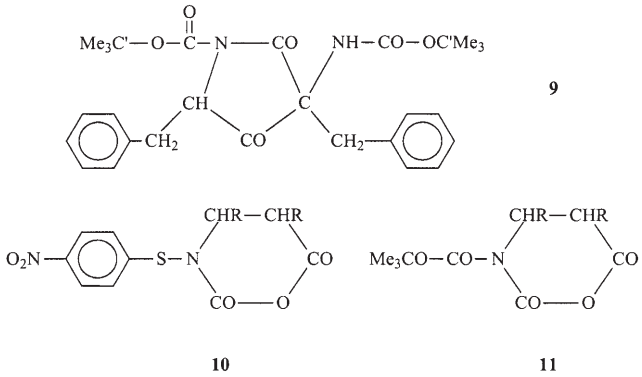


## 3. Living Polypeptides?

The expression "living polymers" was coined by M. Swarc in connection with the anionic polymerization of vinyl monomers. Its original definition combines two properties of polymers. First, the reactive end group responsible for the chain growth remains unchanged (alive) when the polymerization stops owing to either 100 % conversion of monomers, cooling, or precipitation. Second, the molecular weight distribution (MWD) is narrow with polydispersities (PDs) below 1.2, or better below 1.1 (the PD is defined as the quotient of weight-average molecular weight, $M_w$, and number average of the molecular weight, $M_n$). Polypeptides with a living end group such as a primary amino group may be expected to result from ROPs initiated by protic nucleophiles such as water, alcohol, or primary amines (Scheme 4). However, a low PD requires that the initiation step is faster than the growing step, and this requirement is only met by sterically unhindered primary aliphatic amines. This is one reason why primary-amine-initiated ROPs are the most widely used approach to the preparation of polypeptides from NCAs. The second reason is the easy control of the degree of polymerization ($P_n$; and thus $M_n$) by variation of the feed ratio NCA/amine (i.e. monomer/initiator ratio, M/I). Frequently used small amines are *n*-hexylamine and benzylamine[66–71] (see reference [49], Chapter 2). The third reason is introduction of functional end groups to the CO chain end of the polypeptides. Functional amines used by several authors are 2-hydroxyethylamine,[72] amines with vinyl groups,[73,74] and L-aspartic acid esters.[75] Furthermore, initiation with aliphatic $NH_2$ groups is the most frequently used synthetic method for the preparation of complex architectures such as block copolymers, dendritic copolymers, and star-shaped polymers, and for grafting of polypeptides on inorganic solid surfaces (see discussion below). In all of these cases preformed organic or inorganic polymers with two or more $NH_2$ groups served as "macroinitiators".

 © 2006 Wiley-VCH Verlag GmbH & Co. KGaA, Weinheim 

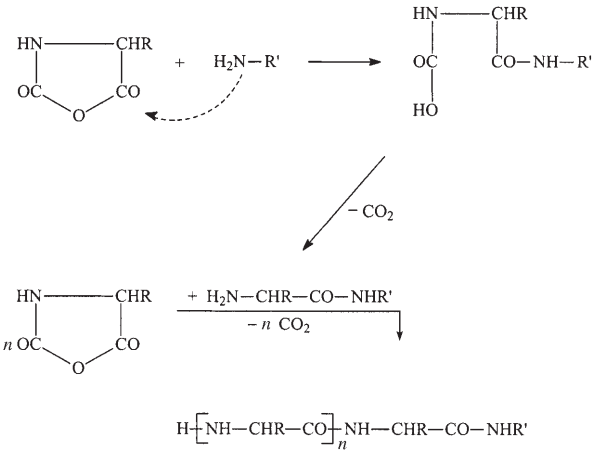


12

***Scheme 4.*** Initiation and growing steps of a primary-amine-initiated ROP of NCAs.

The answer to the question if and how a low PD can be achieved does not depend only on the reactivity of the initiator, the solubility and secondary structure of the growing peptide chains are also important. Low PDs can only be obtained for polypeptides soluble in inert reaction media such as poly(β-Bzl-L-Asp), poly(γ-Bzl-L-Glu), poly(γ-alkyl-L-Glu) (alkyl groups larger than ethyl), poly($N^{\varepsilon}$-Z-L-Lys), and polySar. For the vast majority of natural amino acids, the rapid precipitation of the oligo- and polypeptides from the reaction medium has the consequence of high PDs. This relationship is illustrated by the MALDI-TOF mass spectra of Figure 1. Figure 1a displays a narrow MWD for polySar (PD $\approx$1.15, through gel permeation chromatography),[68] and Figure 1b shows a broad distribution of poly(L-Ala) precipitated from the reaction medium (dioxane).[68] Broad frequency distributions were also reported for poly(L-Phe).[69] They resemble the frequency distributions of polycondensates, which typically have PDs $\geq$2.0.[76,77] At this point, it must be demonstrated that these MALDI-TOF spectra are not designed for the exact determination of the molecular weights or MWDs. However, the insolubility of most of the homopolypeptides in inert solvents prevents reliable characterization with gel permeation chromatography. At least mass spectroscopy allows determination of a qualitative picture of the frequency distribution.

Figure 2 illustrates what happens when growing oligopeptides are poorly soluble. Most of the oligomers precipitate in the form of β-sheet lamellae. A small fraction, however, stay in solution and these fully solvated chains continue chain growth in the α-helical structure when $P_n$ exceeds 10. Therefore, the reaction mixture contains three species with respect to conformation (secondary structure), all with somewhat different reactivities of the $NH_2$ end groups. Furthermore, the reactivities of the $NH_2$ groups on the surfaces of β-sheet lamellae vary owing to different steric environments resulting from a more or less pronounced backfolding (see reference [49], Chapter 3). A broad distribution of end-group reactivities has the consequence that the propagation rates scatter over a broad range and result in broad frequency

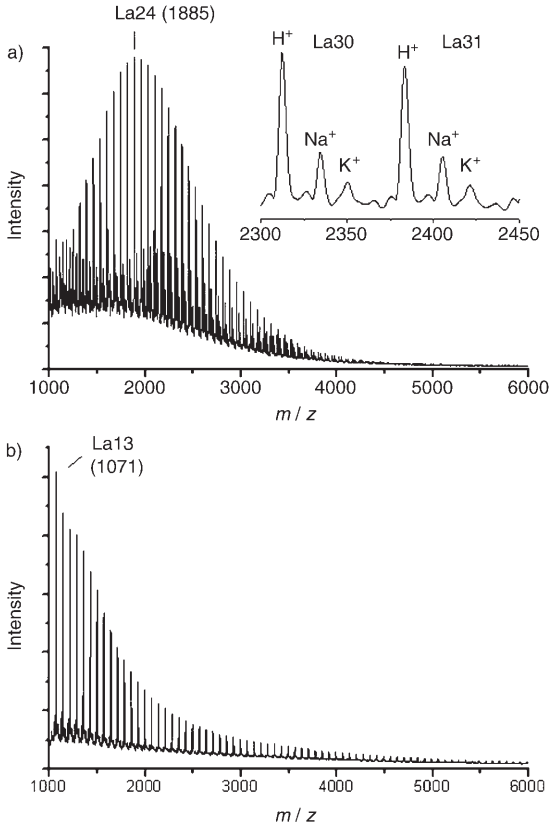


***Figure 1.*** MALDI-TOF mass spectra (dithranol + $K^+$ doping) of: a) polySar and b) poly(L-Ala), both initiated with benzylamine (M/I=80:1) in dioxane at 20 °C.[68] La: linear amine-terminated chain.

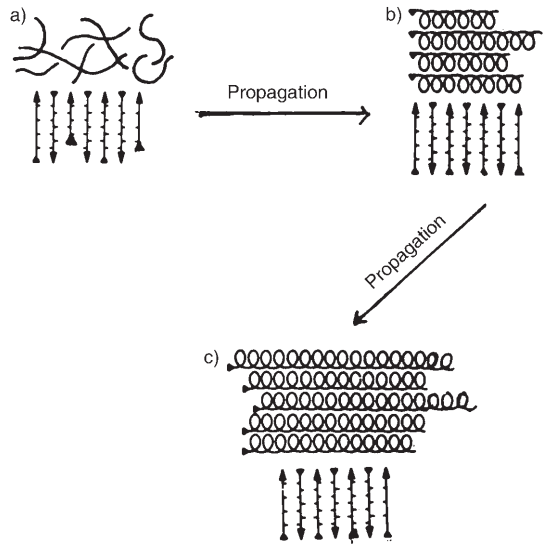


***Figure 2.*** Schematic illustration of the secondary structures formed in primary-amine-initiated polymerizations of L-Ala-NCA:[68] a) low conversion (the wormlike molecules represent soluble oligomers with $P_n < 10$, b) medium conversion, c) high conversion.

distributions. Narrow distributions require nearly identical propagation rates for all chains. The backfolding of growing chains on the surface of β-sheet lamellae also creates a serious problem for the preparation of high-molar-mass polypeptides.

 © 2006 Wiley-VCH Verlag GmbH & Co. KGaA, Weinheim 

Owing to steric hindrance, the chain growth will stop before all monomers are consumed (physical death of the polymerization). Therefore, high-molar-mass polymers ($M_n \geq$ 20000 Da) of exclusively β-sheet-forming amino acids have never been prepared. Long chains with low PDs can only be obtained from a handful of soluble and mostly helix-forming peptides. Therefore, more than 90% of all recent publications dealing with polypeptides derived from NCAs concentrate on poly(γ-alkyl-Glu)s and poly($N^{\varepsilon}$-Z-Lys).

In this context, the studies of primary-amine-initiated polymerizations of NCAs in the solid state reported by Kanazawa et al.[78–83] should be mentioned. NCA crystals suspended in *n*-hexane were polymerized by initiation with *n*-butylamine at 20–30 °C. The influence of the amino acids on the reactivity of the crystals, the change in the crystal lattice, and the secondary structure of the resulting polypeptides were examined by X-ray and IR methods, but no information on the MWDs were provided. However, for these solid-state polymerizations, low PDs should not be expected.

Both the $P_n$ and MWD of primary-amine-initiated polypeptides may also be affected by side reactions of the amino end group. An intramolecular termination step, which is characteristic for polyglutamates, is formulated in Scheme 5. Side reactions were also reported for $N^{\varepsilon}$-TFA-L-Lys-NCA (TFA = trifluoroacetyl);[71] lowering the temperature to 0 °C should result in a true living polymerization. When side reactions are absent and the polypeptides are isolated in the solid state, the reactive amino end groups can survive for decades. For instance, a benzylamine-initiated poly(L-Ala), analogous to that described in Figure 1b, was prepared by the author[68] 30 years before its MALDI-TOF mass spectrum was recorded, whereby an amino group per chain could be proved.

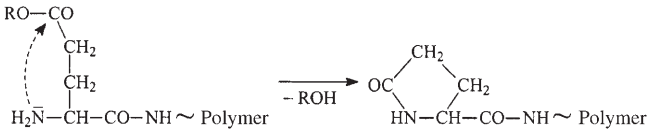


***Scheme 5.*** Intramolecular termination step that is typical for poly(γ-*O*-alkyl-L-glutamate)s.

## 4. New Organometallic Initiators

Numerous metal salts and covalent metal compounds were used as initiators or catalysts for the ROP of NCAs during the past decades. Among these initiators and catalysts used before 1985 are solutions of LiCl in dimethylformamide, sodium methoxide, and sodium benzyl carbamate, and the $Li^{\oplus}$, $Na^{\oplus}$, and $K^{\oplus}$ salts of pyrrolidone, hexabutyldistanoxane, tributyltinmethoxide, diethylcadmium, and tributylaluminum.[49] In the case of metal salts such as LiCl or $NaOCH_3$, intensive studies have clarified that the polymerization mechanism may be considered as a base-catalyzed polymerization beginning with the deprotonation of a NCA followed by the nucleophilic attack of the resulting NCA anion onto C5 of another NCA. However, in the case of covalent organometallic compounds, the complex reaction mechanisms have not yet been elucidated. All studies dealing with metal-based initiators and catalysts published before 1985 were summarized and discussed in Chapter 2.62 in reference [49].

More recently, polymerizations of γ-stearyl-L-Glu-NCA by means of two neodymium complexes, $[Nd(acac)_3]$ (acac=acetylacetanoate) and [$Nd^{III}$(2-ethylhexylphosphonate)], were described, and high-molar-mass polyglutamates with low PDs were obtained with the first catalyst.[84] The neat Nd complexes were not used but rather combinations with ethylalumoxanes, and as a result the mechanism of these polymerizations remain obscure.

Numerous metal complexes were studied by Deming and co-workers[85–113] with respect to their usefulness as catalysts/initiators. At first, *n*-hexylamine and phenetylamine complexes, such as those outlined in Scheme 6,[85] were examined

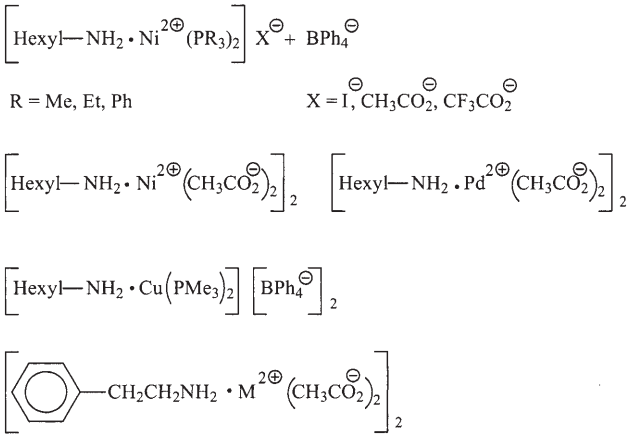


***Scheme 6.*** Primary-amine transition-metal complexes used as initiators for Bzl-L-Glu-NCA.[1,2]

in combination with γ-Bzl-L-Glu-NCA. It was hoped that the complexation of the initiator, and thus, of the amino end groups of the growing peptide chains would modify their reactivity so that side reactions would be suppressed and a better control of molecular weight and PD could be achieved. However, the results were disappointing either because the initiator complexes were not reactive enough or because the desired control of the polymerization process was not achieved. These studies were continued with salen-type complexes of various metals with the primary amine group covalently attached to the ligand (Scheme 7). With these initiators, high-molar-mass polyglutamates, including a control of the molar mass through the M/I ratio, and relatively low PDs (PD ≈ 1.25–1.55) were obtained. In contrast, neat phenethylamine gave poor control of the molar mass and a PD > 2.0. At first glance, these results look like success, but in fact they cannot be explained logically. If the complex is covalently fixed to the CO chain end of the polyglutamate, which forms a stiffened α helix (**13**, Scheme 7), it cannot influence the reactivity of the amino end group. Furthermore, the poor results obtained with phenethylamine are in contrast to results determined by other research groups[70] that have

 © 2006 Wiley-VCH Verlag GmbH & Co. KGaA, Weinheim 

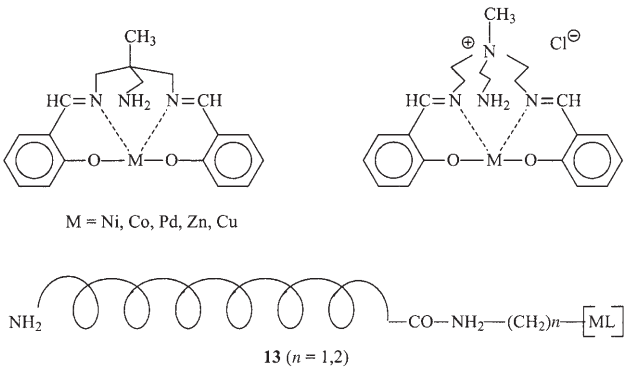


***Scheme 7.*** Metal complexes with covalently bound amine group and their fixation to the polyglutamate helix.

reported on primary-amine-initiated polymerizations of γ-Bzl-L-Glu-NCA.

An entirely new and more-successful approach was elaborated by Deming et al. on the basis of [$Ni^0$(cod)] (cod = cyclooctadiene) complexes (**14**, **15**, Scheme 8). It was known from other research groups that such nickel(0) complexes insert into cyclic dicarboxylic acid anhydrides (e.g. succinic anhydride) followed by elimination of CO. Yet, when these complexes are confronted with nonsymmetrical anhydrides, such as NCAs, the reaction may, in principle, follow two different pathways (I and II in Scheme 8). By using L-Leu-NCA that was selectively $^{13}C$ enriched either at C2 or at C5, Deming and co-workers could unambiguously demonstrate that reaction sequence I does not exist, and that only route II is correct.[88] The reaction product of route II is a nickel(0) amino acid amide complex (**16**) with low solubility in inert organic solvents. However, complexation with bipyridine (bipy) yields a soluble complex (**17**), which proved to be an excellent initiator for the ROP of NCAs yielding polypeptide chains of structure **18**[88–90] (Scheme 9). This polymerization process has the advantage that it may avoid side reactions, such as that formulated in Scheme 5 and the reaction of free amino end groups with *N*,*N*-dimethylformamide (DMF; yielding formamide end groups).

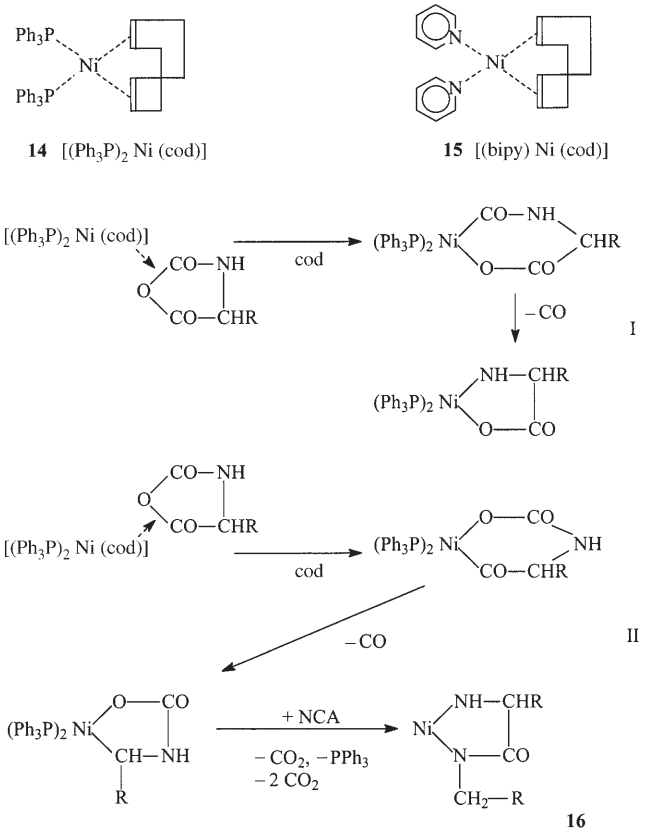


***Scheme 8.*** I and II) Potential reactions of nickel–cyclooctadiene complexes with NCAs: Route II was shown to be correct.

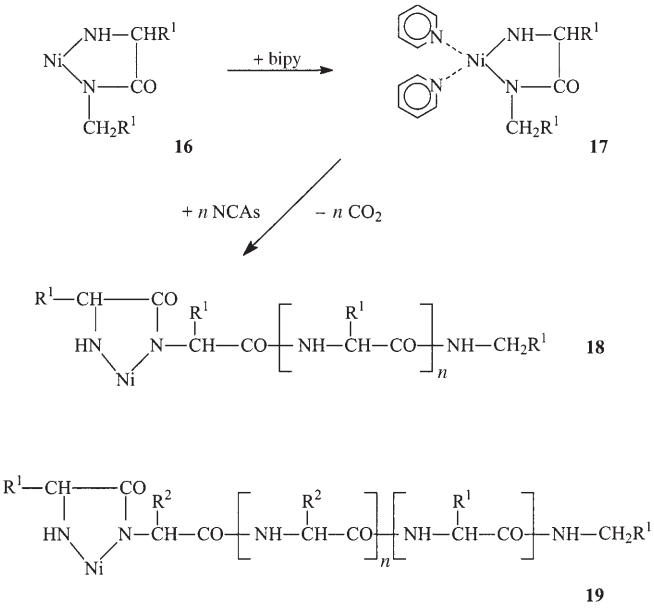


***Scheme 9.*** Polymerizations of NCAs initiated by a nickel(0) amino acid amide complex.

The $Ni^0$ complex allowed control of molecular weight and PD. Furthermore, it represents a living end group, which enables the preparation of diblock copolymers suh as **19** by sequential polymerization of two different NCAs.[89] The success of this approach in terms of high conversion of the second NCA and low PD of the second block requires that the first block (structure **18**) is soluble in the reaction medium and that it increases the solubility of the growing chain of the second block. Therefore, the macroinitiators **18** (Scheme 9) were typically prepared from γ-Bzl-L-Glu-NCA or $N^{\varepsilon}$-Z-L-Lys-NCA. However, the use of soluble macroinitiation for the preparation of block copolymers containing peptide blocks is a concept that allows for much broader variation as will be discussed in Section 6.

The scope and preparative usefulness of ROPs of NCAs that are initiated by $Ni^0$ complexes were explored by Curtin and Deming in several directions. To vary the structure of end groups attached to the CO end of the peptide chain and to introduce functional groups, new initiators (e.g. **20**–**22**) were prepared by a new synthetic method as outlined in Scheme 10.[91] The allyl end group, introduced through initiator **20** allows for a variety of addition and coupling reactions, whereas the naphthyl group of **22** allows detection

 © 2006 Wiley-VCH Verlag GmbH & Co. KGaA, Weinheim 

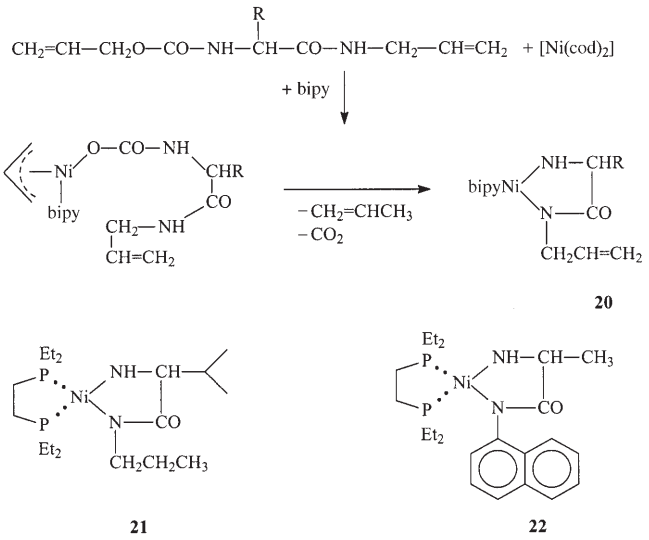


***Scheme 10.*** Synthesis and structures of Ni initiators allowing for broader variations of polypeptide end groups.

by UV spectroscopy and fluorescence measurements. Furthermore, chiral initiator complexes were synthesized from chiral and optically active ligands such as those displayed in Scheme 11.[92] By using optically active initiators, polymeri-

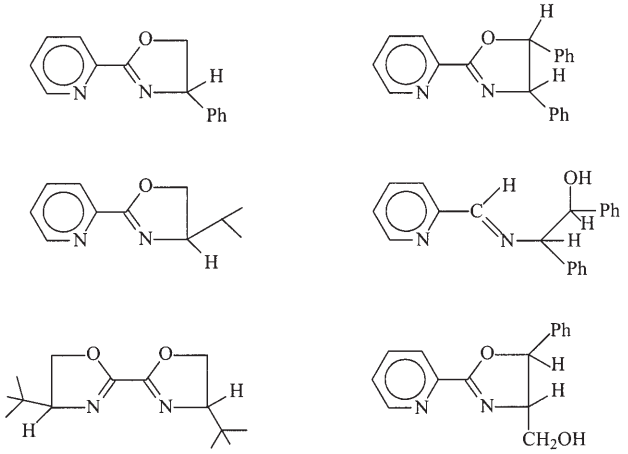

***Scheme 11.*** Examples of chiral ligands used for the complexation of {Ni(cod)} centers.

zations of γ-Bzl-D- and L-Glu NCA were performed separately and rate constants were determined and compared. Furthermore, racemic mixtures of γ-Bzl-D- and L-Glu-NCA were polymerized and stopped after moderate conversion to determine the selective incorporation of γ-Bzl-D- and L-Glu-NCAs. Depending on the ligand, low and high enantioselectivities were found.

A further extension of this area of research concerned variation of the metal. At first, the reactivity of the $[Pt(cod)_2]$ complex was studied in which the relatively stable *tert*-butyl-Gly-NCA was used as the model monomer.[93] However, when activated by two triethylphosphine ligands, the platinum underwent a redox insertion into the N–H bond of the *tert*-butyl-Gly-NCA and not, as hoped for, into the anhydride ring (Route I of Scheme 12). The N-metalated NCA **19** co-initiated oligomerization of NCAs but did not enable useful controlled polymerizations. An analogous insertion into the

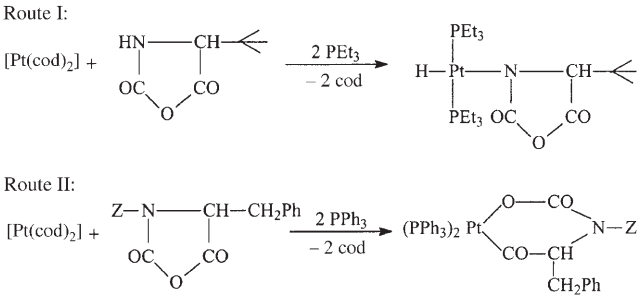


***Scheme 12.*** Reactions of $[Pt(cod)_2]$ with N-unsubstituted and N-substituted NCAs.

N–H bond was also observed for a palladium complex. After substitution of Phe-NCA with a protecting group, the Pt inserted into the anhydride ring, however, these N-protected NCAs cannot polymerize (Route II, Scheme 12) and as such did not result in any noteworthy advancements. Consequently, the investigation was directed towards more-successful proved syntheses and reactions of the chiral ruthenium and iridium complexes **23** and **24**. As illustrated in Scheme 13, these complexes can react with NCAs by inserting into the anhydride ring and forming an amino acid–amide complex that plays the role of initiator.[94] By using these optically active initiators, polymerizations of γ-Bzl-D- and γ-Bzl-L-Glu-NCA were performed separately and the enantioselectivities of the initiators were determined from the different polymerization rates.

Extension of these studies to iron and cobalt complexes gave the following results. $Fe^0$ and $Co^0$ complexes of dienes, such as cod, were not stable enough to serve as starting materials for the preparation of useful initiators, whereas the $Fe^0$–CO and $Co^0$–CO complexes were not reactive enough. Therefore, the $[(PMe_3)Fe]$, $[(PMe_3)_4Co]$, and $[(PMe_3)CoN_2]$ complexes were studied and found to be active as initiators.[95] The published reaction mechanisms are presented in Scheme 14 and Scheme 15. However, only low-molar-mass polyglutamates were obtained from the Fe complex, whereas the Co complexes proved to be even more reactive than the bipy–Ni complex. The Co complex $[(PMe_3)_4Co]$ allowed the preparation of high-molar-mass polyglutamates with full control of the molar mass and with low PD ($PD \leq 1.15$). They also enabled the preparation of diblock polypeptides by sequential copolymerization of two different NCAs.[95] In the course of these studies, it was also found that the reaction conditions have a strong influence on the success of Ni- and Co-initiated polymerizations.[96] Depending on the ligand, solvent, and temperature, the formation of the active species (such as **16** in Scheme 8) may not be quantitative, the initiator complex may dimerize, and side reactions may occur. A typical consequence of these effects is that the $M_n$ values are higher than expected from the M/I ratio. Therefore, the preparative usefulness of these new transition-metal complexes as initiators for NCA is strongly limited in several

 © 2006 Wiley-VCH Verlag GmbH & Co. KGaA, Weinheim 

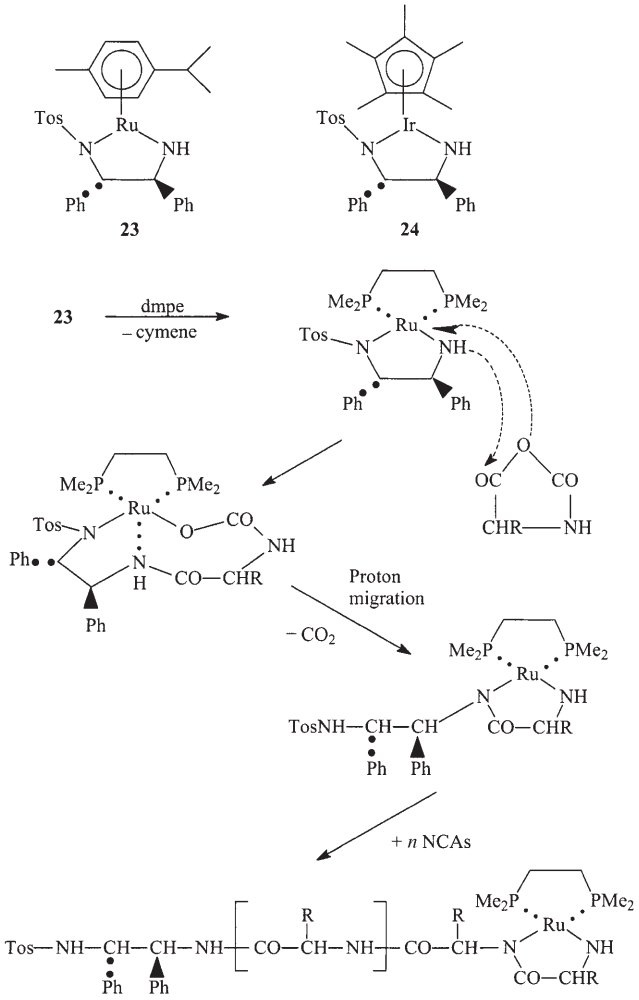

***Scheme 13.*** Chiral ruthenium and iridium complexes and their use as initiators. dmpe = $Me_2PCH_2CH_2PMe_2$, Tos = tosyl.

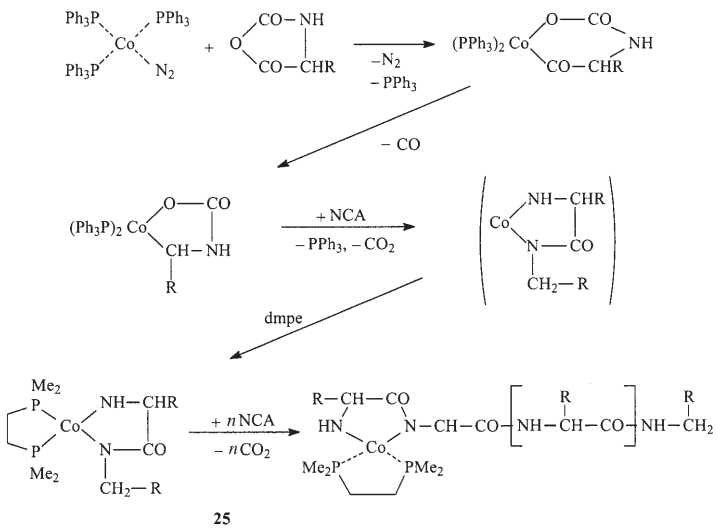

***Scheme 14.*** ROP of NCAs initiated by a cobalt complex.

directions. Only complexes of nickel and cobalt proved to be useable, and there is only a small selection of ligands.

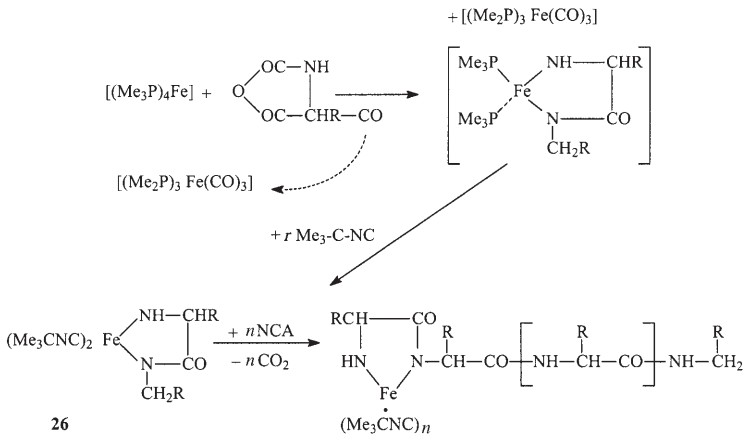

***Scheme 15.*** ROP of NCAs initiated by an iron complex.

Furthermore, the reaction medium allows little variation, with DMF being the optimum solvent, and only a handful of soluble polypeptides (i.e. Glu and Lys derivatives) may yield high molecular weights and allow control of $M_n$ and PD.

Despite these limitations Cheng and Deming have demonstrated a variety of interesting preparative applications. For instance, Ni-based complexes also allowed for polymerizations of β-amino acid NCAs[97] and even for polymerizations of β-lactams,[98] but only low-molar-mass polyamides were obtained. By using α-amino acid NCAs, a broad variety of homopolypeptides[99,100] and di-, tri-, or pentablock copolypeptides were synthesized.[101–113] The structure and properties of these block polypeptides will be discussed in Section 6.

From the viewpoint of synthetic methodology, the preparation of A–B–A triblock copolymers with a central poly(alkenamer) block needs to be highlighted (Scheme 16). The synthesis begins with metathesis polycondensation of α,ω-dienes that yield telechelic polymers with two phthalimide end groups (**27**). The then-liberated amino end groups (**28**) were acylated with the *N*-hydroxysuccinimide ester of an *N*-allyloxycarbonyl amino acid. The resulting telechelics of structure **29** were transformed into Ni complexes (**30**) capable of initiating the ROP of NCAs.[112]

Finally, a recent publication from another research group should be mentioned[114] that reports on aluminum Schiff base complexes (**31a**,**b**; Scheme 17) as initiators. $^1$H NMR spectra suggest that the NCAs insert into the Al–alkoxide bond such that polypeptides with ester end groups are formed. The further chain growth is assumed to proceed through the amino end group of the reactive intermediate **32**, but this mechanism has not been proven in all its details.

## 5. Cyclic Polypeptides

With one exception,[115] all publications dealing with ROP of NCAs before 2005 assumed that the resulting polypeptides have a linear structure, unless branching was intentionally initiated. Yet, as early as 1953, Wessely


© 2006 Wiley-VCH Verlag GmbH & Co. KGaA, Weinheim

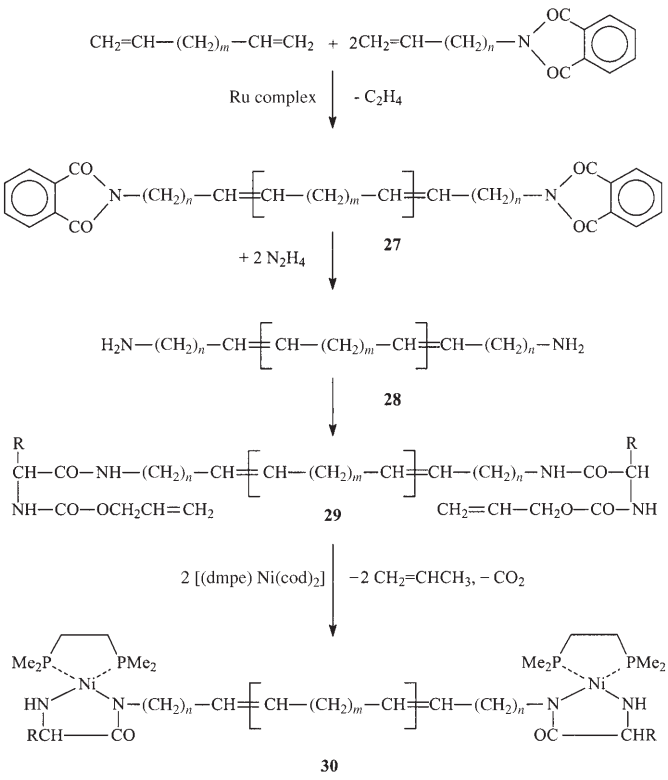

***Scheme 16.*** Syntheses of a macroinitiator from α,ω-dienes.

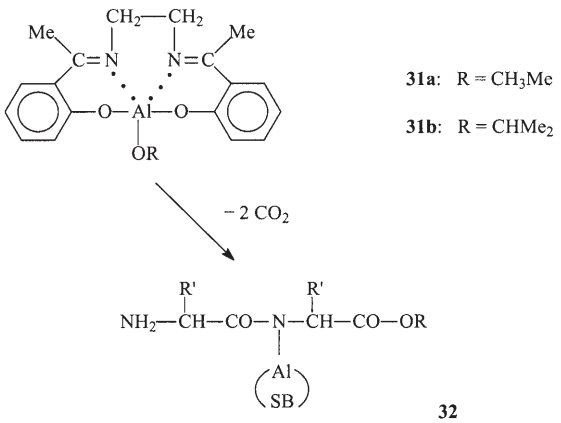

***Scheme 17.*** ROP of NCAs initiated by aluminum Schiff base (SB) complexes.

cyclic polypeptides is of interest for three reasons. First, in the case of high yields, such ROPs offer easy preparative access to a new architecture. Second, the formation of cyclic polypeptides contributes to a better understanding of the polymerization mechanism because it proved that bifunctional polypeptide chains with one nucleophilic and one electrophilic end group were present as reaction intermediates. Third, efficient cyclization hinders the chain growth and indicates that the given reaction conditions are not suited for the preparation of high-molar-mass polypeptides.

Initiation of NCAs with protic nucleophiles such as water, alcohols, and primary amines has the expected consequence that linear polypeptides are generated as outlined in Scheme 4. This course of the polymerization process has recently been confirmed by MALDI-TOF mass spectrometry.[68,69] However, secondary amines are more complicated and must be subdivided into three classes with regard to polymerization mechanisms and the role of cyclization: 1) Sterically nonhindered, highly nucleophilic amines, such as dimethylamine, piperidine, and morpholine, react like primary amines, 2) sterically hindered secondary amines, such as dicyclohexylamine, preferentially deprotonate NCAs and thus react like trialkylamines, and 3) heterocyclic secondary amines of low basicity like imidazole may react as nucleophiles but they produce an electrophilic amide end group that can react with the amino end group of the growing peptide chains (Scheme 18). When the growing oligo- and polypep-

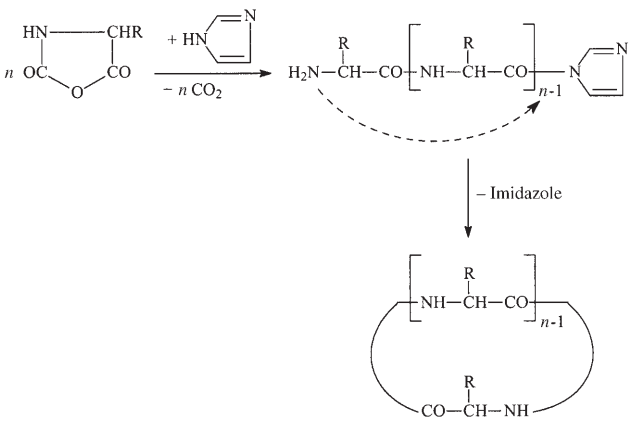

***Scheme 18.*** Mechanism of imidazole-initiated polymerizations.

and co-workers[115] conducted a careful study of pyridine-catalyzed polymerizations of several NCAs, but they did not succeed with the identification of the end groups. Furthermore, high yields of cyclic dipeptides (*N*,*N*-bisalkyl-2,5-dioxopiperazines) were isolated when *N*-alkyl-NCAs were treated with pyridine. Therefore, the authors concluded that the majority of their reaction products should have a cyclic structure. However, an analytical method allowing for a direct and routine detection of cyclic polypeptides in complex reaction mixtures did not exist before 1995. MALDI-TOF mass spectrometry closed this gap and allowed a reinvestigation of the classical polymerization methods and mechanisms with respect to the role of cyclization. The detection of

tides are soluble or mobile enough, as in the case of polySar, poly(D,L-Phe), and poly(D,L-Leu), cyclic polypeptides should be the main reaction products. This expectation was confirmed in a recent study;[116] however, rapid precipitation of growing oligomer in the β-sheet structure or as helices, as is typical for polymerizations of L-Ala-NCA, prevented cyclization by immobilization of the peptide chain.

As speculated by Wessely and co-workers,[115] ROPs catalyzed by pyridine yield cyclic polypeptides as the main products[117] (initiation by traces of water may also compete). At least in the case of Sar-NCA, a zwitterionic polycondensation reaction is the only plausible mechanism (Scheme 19). With N-unsubstituted NCAs, the charge separation step may

 © 2006 Wiley-VCH Verlag GmbH & Co. KGaA, Weinheim 

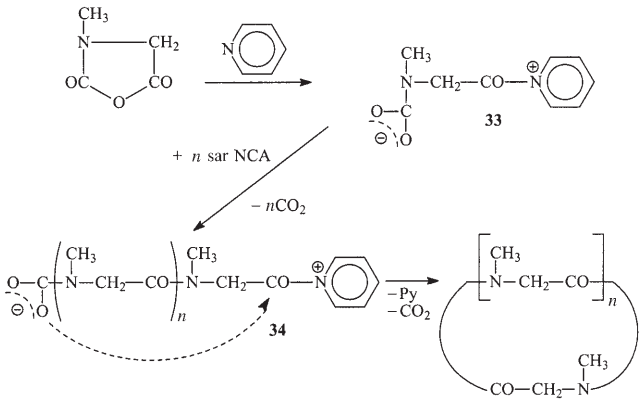

***Scheme 19.*** Mechanism of pyridine-catalyzed ROP of N-substituted NCAs via zwitterionic ionic intermediates.

be followed by the reaction of the acylium ion **33** with another NCA such that an *N*-aminoacyl NCA (**35**) is formed (Scheme 20). This difunctional dimer can continue chain

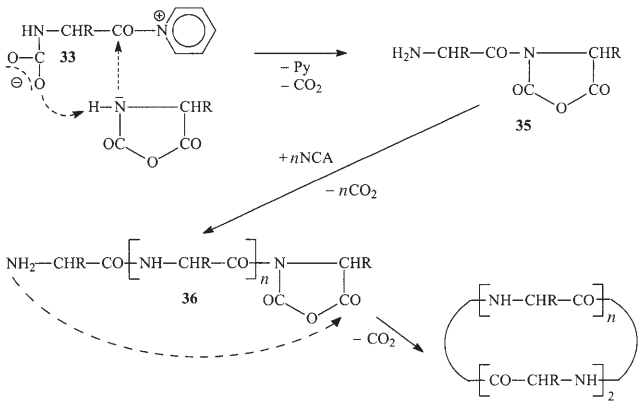

***Scheme 20.*** Alternative mechanism of pyridine-catalyzed N-unsubstituted NCAs.

growth through the primary-amine mechanism or by polycondensation, and cyclization of the difunctional chains (**36**) can compete with each growth step. Unexpectedly, it was found that solvents with high nucleophilicity and donor ability such as DMF, *N*-methylpyrrolidone (NMP), and dimethyl sulfoxide (DMSO) also catalyze zwitterionic polymerizations.[118] It is obvious that the polymerization mechanisms (Scheme 21 and Scheme 22) are, in principle, the same as those catalyzed by pyridine. Combinations of pyridine (or *N*,*N*-dimethylaminopyridine) and NMP seem to be particularly efficient for the preparation of cyclic polypeptides in high yields as illustrated in Figure 3 for poly(D,L-Ala). Furthermore, the short time needed for dissolution of NCAs in DMF may suffice to generate small amounts of cyclopeptides even when primary amines are added as initiators.[69] Over the past twenty years, most syntheses of homo- and copolypeptides were performed in DMF; therefore, numerous polypeptides that were assumed to be linear may in fact be "contaminated" with cyclic polypeptides.

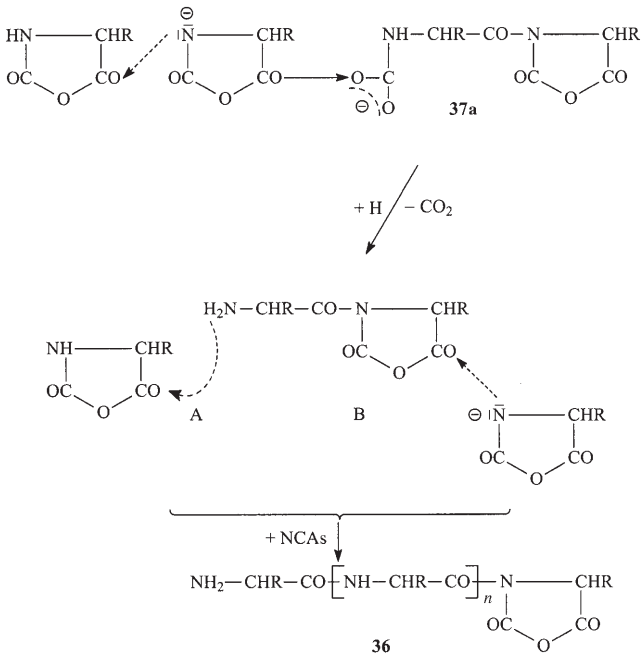

***Scheme 21.*** Mechanistic aspects of the base-catalyzed ROP.

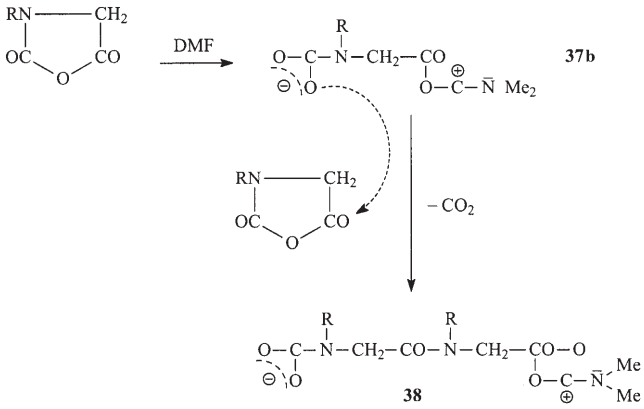

***Scheme 22.*** Initiation steps of a DMF(solvent)-induced zwitterionic polymerization of N-substituted NCAs.

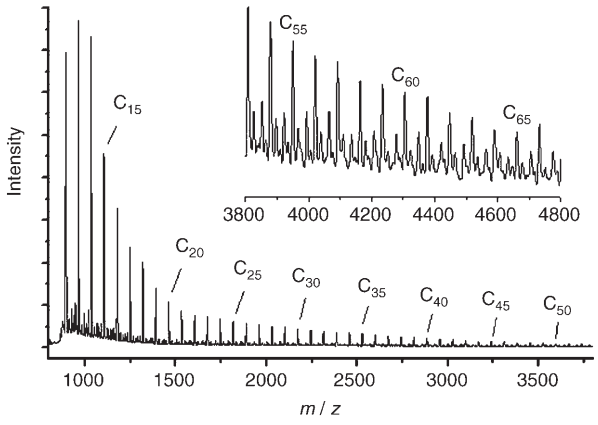


***Figure 3.*** MALDI-TOF mass spectrum (dithranol + $K^+$ doping) of cyclic poly(D,L-Ala) obtained by pyridine-catalyzed polymerization in NMP at 20 °C.

 © 2006 Wiley-VCH Verlag GmbH & Co. KGaA, Weinheim 

A sterically hindered basic trialkylamine, such as *N*-ethyldiisopropylamine, is not nucleophilic enough to catalyze a zwitterionic mechanism. Nonetheless, it was found[117] that *N*-ethyldiisopropylamine catalyzes the formation of cyclic polypeptides when added to solutions of N-unsubstituted NCAs in dioxane. In this case, N-deprotonation of the NCAs followed by a nucleophilic attack of the NCA anion onto C5 of another NCA is the most likely initiation mechanism (Scheme 23). It is known from various model reactions that

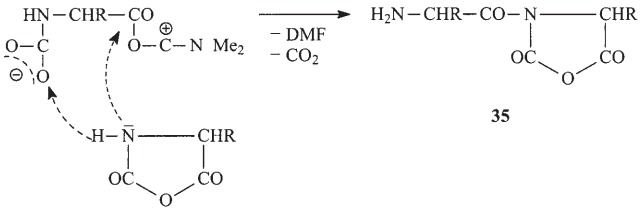


***Scheme 23.*** Initiation steps of a DMF(solvent)-induced ROP of N-unsubstituted NCAs.

strong bases such as trialkylamines can deprotonate NCAs (reference [49], Chapter 2.5). The difunctional dimer **37** can continue the chain growth through either route A (in Scheme 21) or by reaction of the *N*-acyl NCA chain with NCA anions (route B). The difunctional peptide chain **36**, which results from both routes, can in turn cyclize as outlined in Scheme 20. All the details of these base-initiated polymerization reactions have not been elucidated yet, but the formation of a large fraction of cyclic polypeptides proves the intermediate formation of difunctional chains such as **36**.

The thermal polymerization of NCAs should be discussed. Leuchs was the first to observe that NCAs polymerize rapidly in the molten state, but a detailed analysis of the reaction products has not been conducted since then. A recent investigation by means of MALDI-TOF mass spectrometry[119] showed that a significant fraction of the thermal reaction products, formed at 120 °C from a variety of NCAs, consists of cyclic polypeptides. It is obvious to assume that an NCA attacks another NCA in analogy to the nucleophilic attack (initiation) of imidazole (Scheme 18 and Scheme 22). An *N*-aminoacyl-NCA of structure **35** is formed (Scheme 24), which can grow and cyclize as illustrated in Scheme 20. In summary, cyclic polypeptides are formed under various reaction conditions, and the difunctional chains of structure **36** appear to play the key role in their formation. As

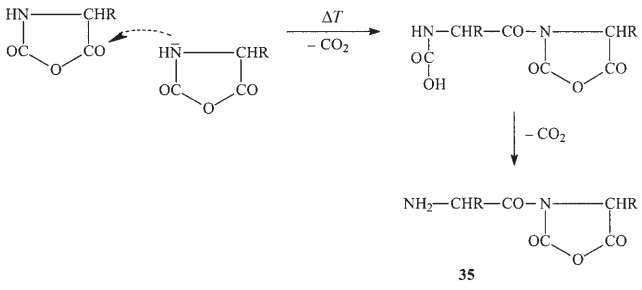


***Scheme 24.*** Initiation steps of the thermal (noncatalyzed) ROP of NCAs.

cyclization limits the chain growth, only those polypeptides that can rapidly form a stiff α helix preventing cyclization have a chance to reach high molecular weights.

Finally, it should be mentioned that the high cyclization tendency of soluble polypeptides that adopt a coil conformation became evident from chain-extension experiments with telechelic polysarcosines **39** (Scheme 25).[120] Regardless of

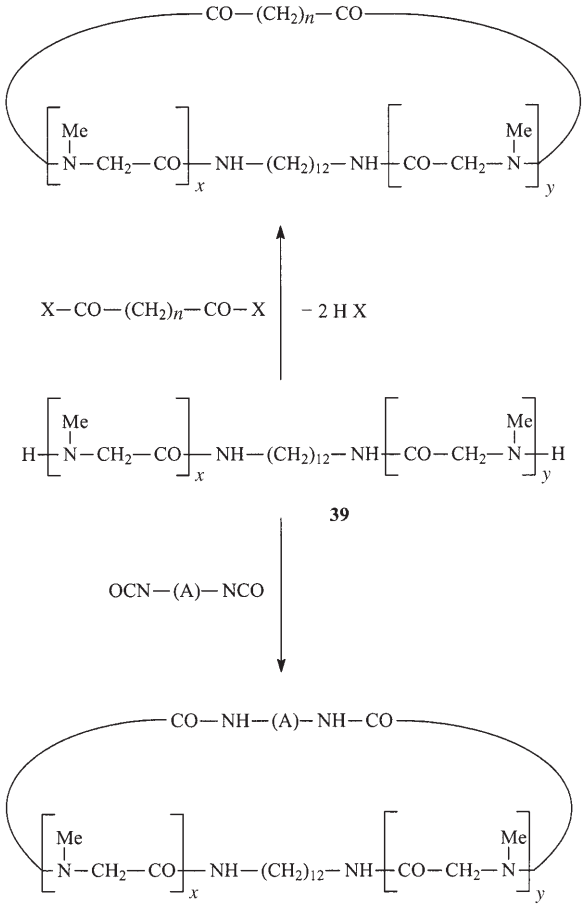


***Scheme 25.*** Cyclization of telechelic polysarcosines by means of difunctional coupling agents.

the coupling agent, a considerable fraction (almost all chains in the low-molar-mass range (less than 7000 Da)) formed a cyclic structure.

## 6. Block Copolymers

In this section, all the copolymers that combine two or more different monomers in a linear block structure will be reviewed. This group of copolymers will be subdivided according to two different aspects. First, taking into account the number of blocks, the copolymers will be called diblock, triblock, pentablock, or multiblock copolymers. Second, the term "block copolypeptide" will be reserved for copolymers exclusively built up by peptide blocks, whereas all other species will be called "block copolymers". The literature will be cited below according to the aforementioned classification.

 © 2006 Wiley-VCH Verlag GmbH & Co. KGaA, Weinheim 

The numerous publications dealing with syntheses and properties of diblock copolypeptides may be classified under two different aspects: from the viewpoint of the synthetic method, and from the viewpoint of properties and application. Two different initiation processes were applied to the stepwise (sequential) polymerization of two NCAs. Either amines such as *n*-propylamine, allylamine, *n*-hexylamine, and piperidine were used as initiators,[121–129] or a metal complex, most frequently $[Co(PMe_3)_4]$, was used.[89,102–109] Furthermore, two variants of the sequential copolymerization may be distinguished. In addition to the standard procedure, combining two different amino acids, NCAs of the same trifunctional amino acids carrying two different protecting groups for the third function may be copolymerized. Examples of this synthetic strategy are copolypeptides consisting of a poly(L-Glu) block combined with a poly(γ-Bzl-L-Glu) block (**40**).[121,122] In this case, the (L-Glu) block was prepared first

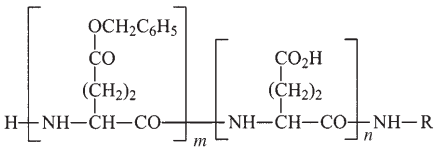

**40**

by deprotection of a poly(γ-Bzl-L-Glu) chain, which was then in turn used as a macroinitiator for the new γ-Bzl-L-Glu-NCA. Several diblock copolypeptides based on L-Lys were prepared by combining different substituents of the $N^{\varepsilon}$ protecting group[123,124] (structures **41** and **42**). These copolypeptides were of interest with respect to their layer structures and liquid-crystalline character. The parent LC homopolypeptides are discussed in Section 8.

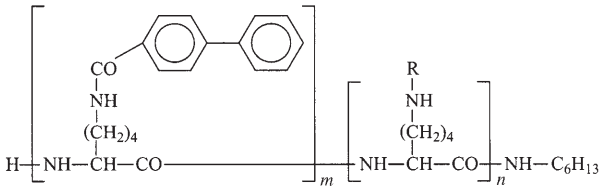

**41**

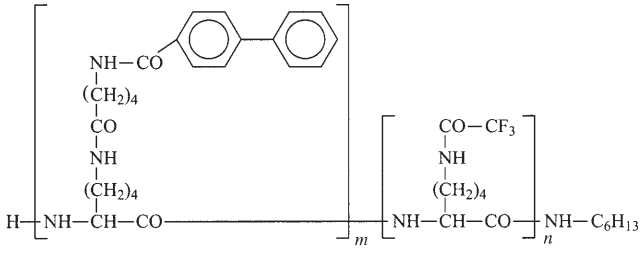

**42**

Diblock copolypeptides derived from unusual amino acids are summarized in formulas **43**–**45**. The copolypeptides **43** were studied for their optical properties.[125] The diblock

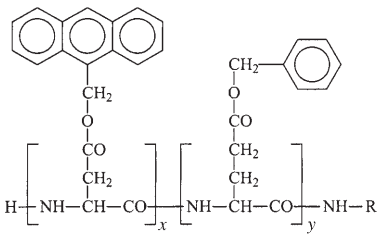

**43**

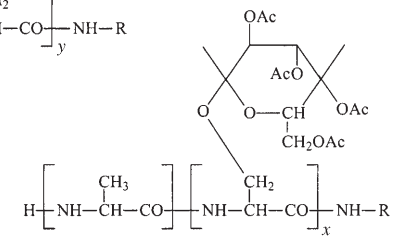

**44**

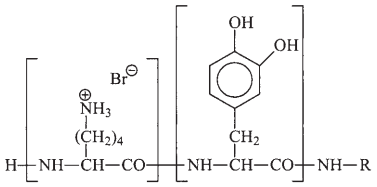

**45**

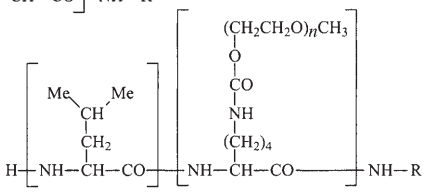

**46**

copolypeptides **44** together with the homopolypeptide of the glycosylated serine were part of a broader study on "glycopeptides".[126] Most diblock copolypeptides were prepared to obtain amphiphilic materials. Compounds **45** present an example containing a hydrophilic nonionic L-Lys unit in combination with the hydrophobic poly(L-Leu) block.[109] Other nonionic amphiphilic diblock copolypeptides were prepared from γ-Bzl-L-Glu-NCA in combination with Gly-NCA[128] or from $N^{\varepsilon}$-TFA-L-Lys-NCA in combination with Sar-NCA[129] (**46**). All other amphiphilic diblock copolypeptides contained poly(L-Lys-ε-HBr or poly(L-Glu) and its Na salt as the hydrophilic component. Poly(L-Val), forming β sheets, and poly(L-Leu), forming α helices, were the most widely used hydrophobic blocks. The secondary structure and morphology of these amphiphilic diblock materials were studied under various conditions. Particularly noteworthy is the formation of ordered silica structures by the hydrolysis of $Si(OEt)_4$ in the presence of diblock amphiphiles. This system can be used as a model of protein-controlled biomineralization, for example, bone growth.[102] Furthermore, the stabilization of magnetic γ-$Fe_2O_3$ nanoparticles in aqueous solution by amphiphilic block copolypeptides should be mentioned.[104] The controlled formation of $CaCO_3$ microspheres by a doubly hydrophilic diblock copolypeptide composed of L-Lys-ε-HBr-Na salt and L-Asp-β-Na salt units has also been observed.[107]

Most diblock copolymers consisting of a peptide block and another type of polymer chain may be subdivided into four classes (I–IV): I) amphiphilic copolymers containing a poly(ethylene oxide) (PEO) monomethyl ether block,[130–142]


© 2006 Wiley-VCH Verlag GmbH & Co. KGaA, Weinheim

II) amphiphilic copolymers based on a poly(oxazoline) as the hydrophilic block,[143,144] III) diblock copolymers based on macroinitiators that were prepared by polymerization of vinyl monomers,[111,145–150] and IV) copolymers combining a peptide block with a biodegradable polyester block.[151–157]

All diblock copolymers of classes I–III were prepared in such a way that a polymer with one primary amino end group was synthesized and served as macroinitiator for the ROP of NCAs. A typical example for a PEO-based diblock copolymer is presented in formula **47**. The influence of the

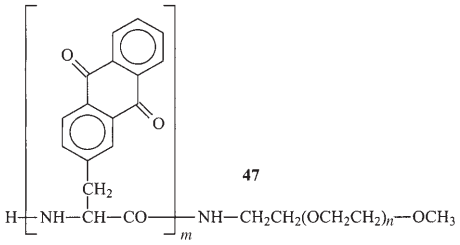

**47**

anthraquinoyl residue on the conformation and CD spectra of the polypeptide block was studied in more detail.[131] Most diblock copolymers of class I contained γ-alkyl esters of L-Glu as the peptide block, but in one paper the peptide block consisted of L-Ala units,[138] whereas in another publication the peptide blocks were prepared by copolymerization of D,L-Leu-NCA and D,L-Val-NCA.[141] Regardless of the amino acid, the PEO macroinitiator keeps the growing peptide chain in solution and prevents early aggregation and precipitation and thus, contributes to a low PD. The simultaneous presence of PEO-$NH_2$·HCl may also help to suppress side reactions of γ-Bzl-L-Glu chain ends (Scheme 5) so that particularly small MWD may be obtained.[136] This useful approach was first reported by another research group as discussed below for diblock copolymers of polystyrene. Diblock copolymers of PEO that contain a hydrophobic peptide block possess amphiphilic character and were studied with regard to secondary structure and morphology (e.g. formation of "core–shell particles").[132] Entirely hydrophilic diblock copolymers containing blocks of unprotected L-Lys, L-Glu, or L-Asp units showed interesting properties as components of drug-delivery systems.[140–142] Finally, the synthesis of poly(pseudo-rotaxane)s by threading α-cyclodextrin on a PEO-poly(γ-Bzl-L-Glu) diblock copolymer should be mentioned.[139]

Only two publications have reported on diblock copolymers that consist of polyoxazoline blocks.[143,144] The hydrophilic polyoxazoline blocks were prepared by cationic (e.g. methyl tosylate catalyzed) polymerizations of 2-methyl- or 2-phenyloxazoline (**4**; Scheme 26). Owing to the presence of an amino end group, the polyoxazolines served, in turn, as macroinitiators of L-Phe-, γ-Bzl-L-Glu-, or glycosylated L-Ser-NCA (**49**). The aggregation of the amphiphilic copolymers derived from L-Phe-NCA and the interaction of the aggregates with lipases in aqueous solution were studied in detail.[143]

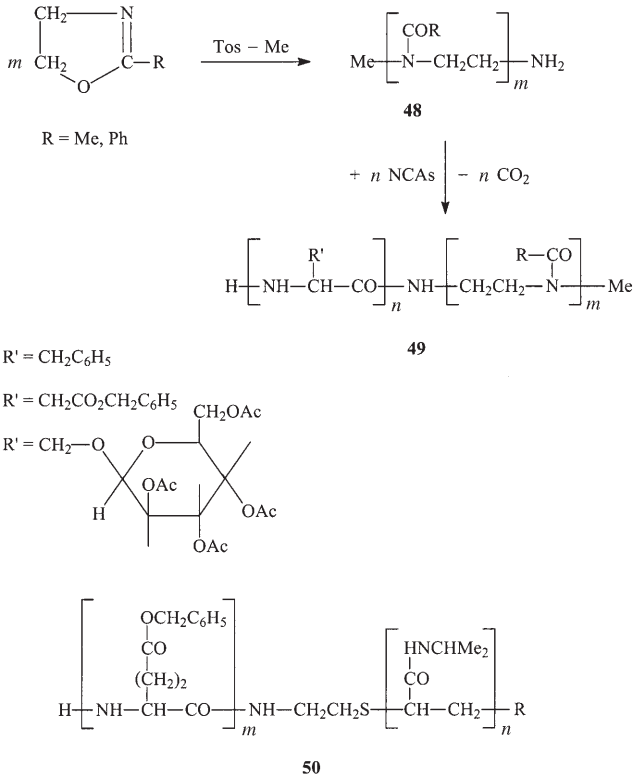

***Scheme 26.*** Preperation of hydrophilic polyoxazoline blocks

Class III diblock copolymers, again with amphiphilic character, were obtained when a hydrophilic macroinitiator derived from poly(*N*-isopropylacrylamide) was used. Such a macroinitiator was prepared by radical polymerization of *N*-isopropylacrylamide in which the addition of cysteamine yielded chain disruption and an amino end group that was capable of initiating the ROP of γ-Bzl-L-Glu-NCA (structure **50**; Scheme 26). The micelles formed by these diblock copolymers were compared to those formed by PEO-poly(γ-Bzl-L-Glu) amphiphiles.[145]

Diblock copolymers derived from polybutadiene belong to the earliest examples of block copolymers that contain peptide blocks.[146,147] The butadiene was polymerized by an anionic mechanism, and amino end groups were introduced in two different ways. The resulting macroinitiators produced diblock copolymers in combination with poly(γ-Bzl-L-Glu-NCA). Amphiphilic character was achieved by modification (aminolysis) of the benzyl ester side chain with 3-aminopropanol so that γ-3-hydroxypropyl-l-glutamine (**51**) is produced.[146] Diblock copolymers derived from styrene were prepared in two ways. The oldest approach[148] is based on a radical polymerization in the presence of cysteamine hydrochloride as the chain initiator and transfer reagent, so that the block copolymers of structure **52** were finally obtained (in analogy to the synthesis of **50**; Scheme 27). More recently, a BuLi-initiated anionic polymerization of styrene was performed and terminated with an N-silylated 3-chloropropylamine so that block copolymers of structure **53** were formed (Scheme 27). These structures were studied with regard to their self-assembly.[149] For initiation of $N^{\varepsilon}$-Z-Lys-NCA with

 © 2006 Wiley-VCH Verlag GmbH & Co. KGaA, Weinheim 

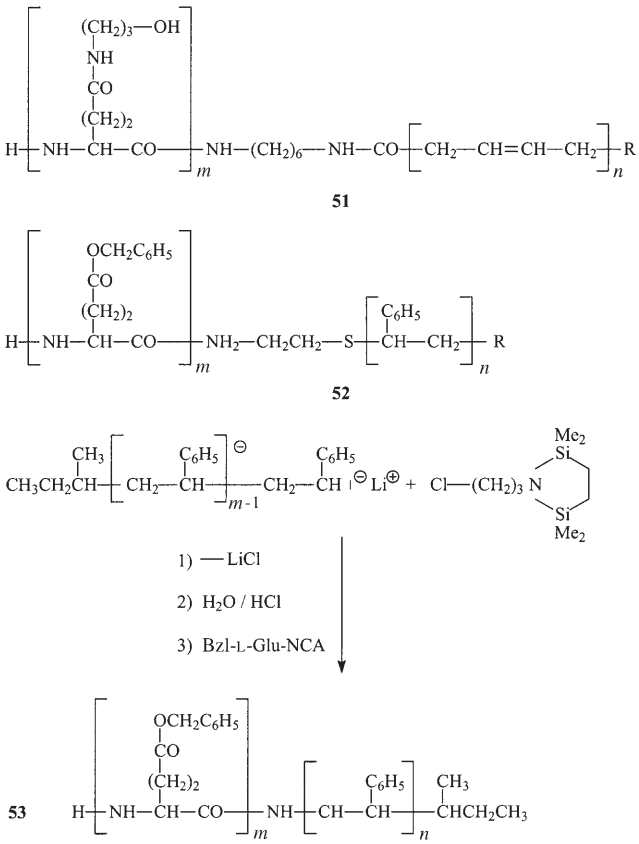

***Scheme 27.*** Synthesis of polystyrene-poly(Blz-L-Glu) diblock copolymers.

$NH_2$-terminated polystyrene, it was reported that the presence of $NH_2$·HCl end groups yields particularly low PDs of the polypeptide block.[150]

For diblock copolymers containing poly(methyl methacrylate)[148] or poly(methyl acrylate),[111] again two different synthetic methods were described. In the case of methyl methacrylate, classical free-radical polymerization in the presence of cysteamine successfully yielded an amine-terminated macroinitiator and block copolymers of structure **54** (Scheme 28). The atom-transfer-radical polymerization (ATRP) was used to prepare the block copolymers **55** according to Scheme 28.[111]

All syntheses of diblock copolymers derived from L-lactide (structure **56**, Scheme 29) followed the same strategy.[151–153] A Boc-protected amino alcohol served as an initiator in combination with a catalyst (e.g. $Et_2Zn$) for the ROP of L-lactide. The removal of the protecting group yielded an amino-terminated polylactides that served as macroinitiators for the NCAs of L-Ala, L-Phe, L-Leu, γ-Bzl-L-Glu, and β-Bzl-L-Asp. ABC triblock copolymers containing a polylactides block (**57**) were also reported.[154] A PEG monomethyl ether served as the initiator for the ROP of lactide, and the OH end group of the resulting polyester was transformed into an amino group by acylation with Boc-L-Phe-OH. The resulting diblock copolymers served in turn as macroinitiators for γ-Bzl-L-Glu-NCA.[155] Starting from ε-caprolactone (εCL), both diblock- (**58**, **59**) and ABA triblock

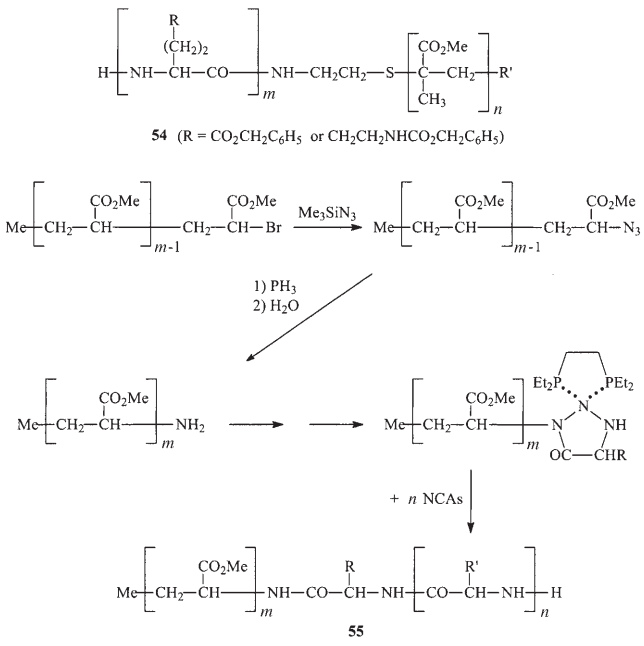

***Scheme 28.*** Synthesis of diblock copolymers through ATRP from methyl acrylate.

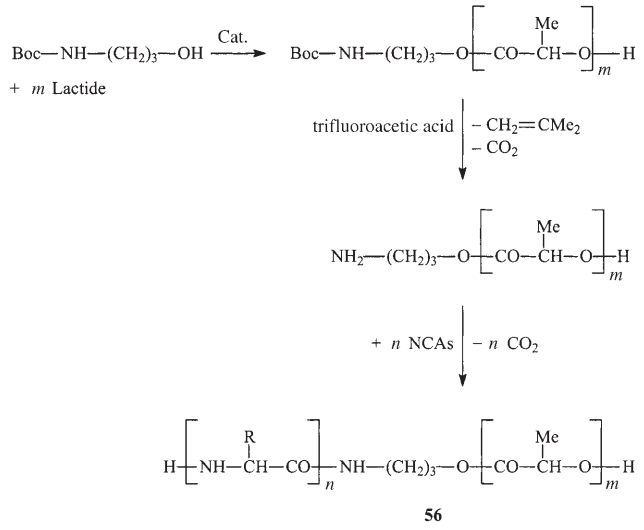

***Scheme 29.*** Synthesis of L-lactide-based diblock copolymers.

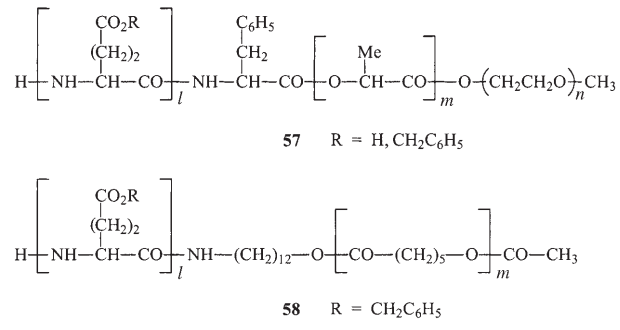


© 2006 Wiley-VCH Verlag GmbH & Co. KGaA, Weinheim

copolymers (**60**) were synthesized by three research groups.[155–157] Although all macroinitiators discussed above possessed primary aliphatic amino groups (or their metal complexes), the macroinitiator used for the block copolymers **59** and **60** had aromatic amino end groups (Scheme 30 and Scheme 31). Despite the lower nucleophilicity of the aromatic amino groups, complete conversion with Gly-NCA, L-Ala-NCA, L-Phe-NCA, and γ-Bzl-L-Glu-NCA was proved by $^1$H NMR spectroscopy.

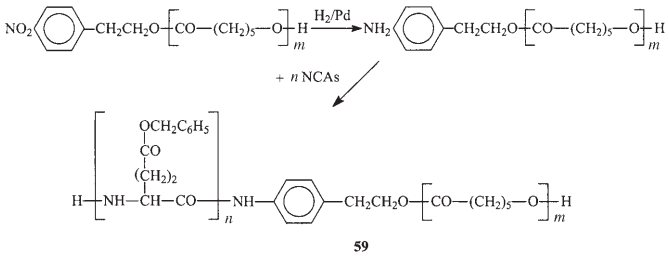


**59**

***Scheme 30.*** Synthesis of a diblock copolymer from ε-caprolactone.

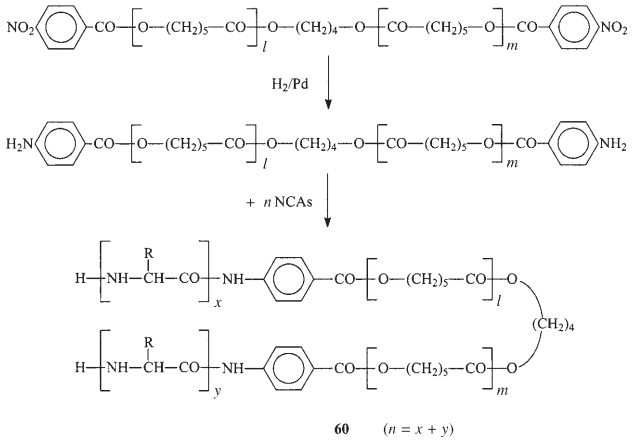


**60** $(n = x + y)$

***Scheme 31.*** Synthesis of ABA triblock copolymers from telechelic poly(ε-caprolactone).

Several ABA triblock copolypeptides exclusively built up by peptide chains were described by three research groups.[158–161] These triblocks were either composed of $N^{\varepsilon}$-Z-L-Lys and γ-Bzl-L-Glu units[159] or of L-Leu and γ-Bzl-L-Glu or L-Glu units.[160,161] All these copolypeptides were prepared by primary-amine-initiated polymerizations, and their characterization focused on their secondary structure and their properties as membranes. Further, triblock copolymers containing a hydrophobic segment were prepared from a telechelic $NH_2$-terminated polybutadiene that was rich in 1,4-*trans* units. This polymeric diamine served as macroinitiator for the ROP of γ-Bzl-L-Glu-NCA.[162,163] Characterization of the secondary structure and morphology were the main goals of those studies. In connection with ABA triblock copolymers containing a central hydrophobic block, the synthetic strategy outlined in Scheme 16 should be remembered.[112]

A broad variety of amphiphilic ABA triblock copolymers,[164–168] pentablock,[113] hexablock,[169] and multiblock copolymers[170,171] were built up from difunctional (telechelic) PEO blocks. As illustrated by formulas **61**–**63**, the PEO segments had primary amine end groups and served as

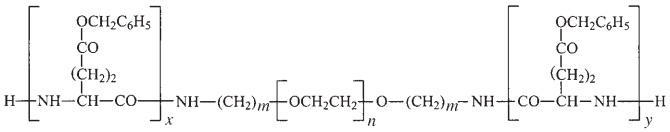

**61**

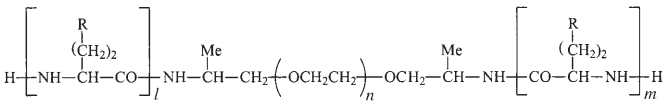

**62**

$R = CO_2CH_2C_6H_5$ or $CH_2CH_2NHCO_2CH_2C_6H_5$

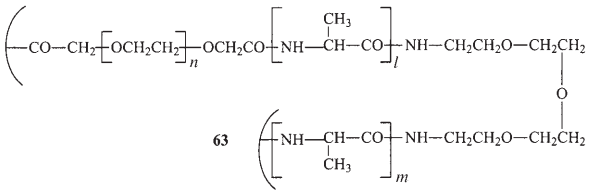

**63**

initiators for the NCAs, or they had $CO_2H$ end groups for chain extension (**63**). Typical properties of these amphiphilic block copolymers, which were studied by several research groups, are the self-assembly in aqueous solutions,[168] the formation of thermoplastic hydrogels,[169] and the release of albumine associated with multiblock copolymers.[170] Segmental copolymers containing short urethane blocks formed by 1,4-butanediol and 4,4′-diisocyanatodiphenylmethane (MDI) were mainly studied with regard to the secondary structure and aggregation and with respect to their mechanical properties and moisture uptake.[172,173] Finally, a review article focusing on amphiphilic copolypeptides should be mentioned.[174]

## 7. Various Architectures

The term "architecture" means variations in the primary structure without consideration of the end groups. Architectures of polypeptides derived from NCAs, which have already been discussed above, are the linear homopolypeptides, the cyclic polypeptides, and the di-, tri-, penta-, and multiblock copolymers. In this section, the following architectures will be summarized: linear copolypeptides with a (nearly) random sequence of two or more amino acid units, star-shaped polypeptides, copolymers with a (hyper)branched or dendritic structure, and polypeptides grafted on membranes or surfaces of inorganic materials.

Numerous papers dealing with syntheses and characterization of (nearly) random copolypeptides have been published since 1984.[124,127,132,160,175–186] Random copolypeptides can be prepared by two different methods. The standard method consists of copolymerizations of two or more differ-

 © 2006 Wiley-VCH Verlag GmbH & Co. KGaA, Weinheim 

ent NCAs. The second approach is based on the modification of a monopolypeptide of a trifunctional amino acid by a reagent attacking a part of the side chain in a statistical process. This second approach was used by one research group,[160] which prepared the copolypeptides **64** ($n=3$) by

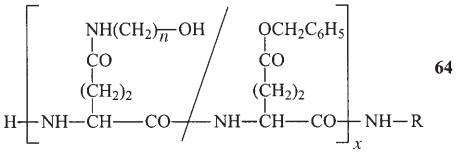

**64**

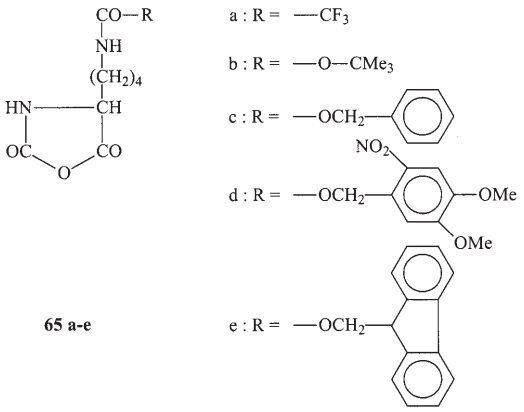

**65 a-e**

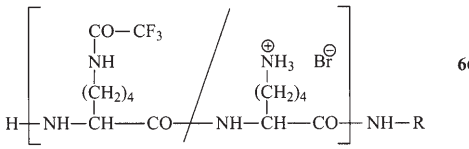

**66**

partial aminolysis of poly(γ-Bzl-L-Glu) with 3-aminopropanol. A similar approach was also used by two other groups.[175,176] Copolymerization of γ-methyl- and γ-Bzl-L-Glu-NCA yielded a random copolymer with regard to ester groups followed by hydrogenolytic removal of the benzyl group and aminolytic cleavage of the methyl ester groups by aminoethanol to give two different hydrophilic side groups.[175] Copolymerizations of two L-Lys-NCAs with different protecting groups in the $N^{\varepsilon}$-position (**65a–e**) followed by selective removal of one protecting group yielded copolypeptides such as **66**.[176]

Copolymerization of NCAs of various amino acids have the disadvantage that the NCAs possess different reactivities, mainly caused by different steric demands of their side chains.[127,177–179] The obvious consequences are different rates of incorporation and sequences that deviate from perfect randomness. Most spectroscopic methods (including IR spectroscopy, $^1$H NMR spectroscopy, and MALDI-TOF mass spectrometry) do not give information on the sequences of polypeptides. However, in three publications[177–179] dealing with L-Ala/L-Val, L-Leu/L-Val, and L-Ala/Gly/L-Val copolypeptides it was demonstrated that $^{15}$N NMR spectroscopy is sensitive enough to sequence effects and to calculate average block lengths. However, in all other publications, the sequences of the copolypeptides were considered to be random in nature without experimental evidence for this assumption.

Almost all publications on (nearly) random copolypeptides had the purpose to elucidate the correlation between composition and secondary structure (determined either in solution or in the solid state). However, in two papers[175,182] the usefulness of copolyglutamates as components of drug-delivery systems was examined, and in another publication "membrane-interactive copolypeptides" were described.[183] In a paper dealing with copolymers of β-ferrocenylalanine (**67**),[130] the electron-transport properties were investigated.

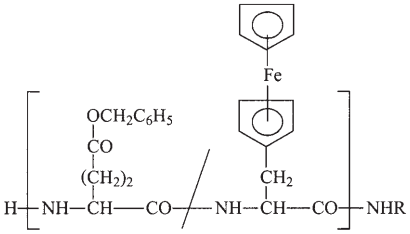

**67**

Another class of unusual nearly random copolypeptides was prepared by sodium *tert*-butoxide catalyzed copolymerization of $N^{\varepsilon}$-Z-L-Lys-NCA with *O*,*O*′-bis-Z-L-Dopa-NCA (Dopa = 3,4-dihydroxy-L-phenylalanine).[184–186] After removal of the Z protecting groups, the properties of the resulting copolypeptides as adhesives were evaluated. The influence of oxidation of the Dopa unit on the adhesion process was studied in detail. In other words, these copolypeptides were designed as models of the proteins allowing mussels and barnacles to adhere strongly to various rough surfaces in the presence of water. The ability to stick in the presence of sea water is of great interest to the development of synthetic glues.

Star-shaped polypeptides can be prepared in two ways: either the star center contains functional groups (e.g. $NH_2$) capable of initiating the ROP of NCAs and thus, the star arms are "grafted from" the core of the star, or linear polypeptides with one amino end group are "grafted on" a star center possessing electrophilic functional groups. This second approach has the advantage that a detailed characterization (length and PD) of the future star arms may be performed prior to the coupling with the star center; however, steric hindrance may prevent 100% conversion of the functional groups of the star center.

The first synthetic strategy was used by three research groups[187–190] that used the NCAs of β-Bzl-L-Asp or γ-Bzl-L-Glu for the grafting from the star center. In this way, nine-arm stars were obtained from the star center **68**, functionalized with nine aliphatic primary amine groups.[187] Two different phenoxy-substituted cyclophosphazenes with six primary amino groups were used as star centers by another research group.[188,189] Complete conversion of all six amino groups was proved by $^1$H NMR spectroscopy in the case of initiator **69a**. Yet, the less-reactive aromatic amino groups of **69b** did not completely react with γ-Bzl-L-Glu-NCA, and stars with less than six arms were obtained. Four-armed stars were prepared


© 2006 Wiley-VCH Verlag GmbH & Co. KGaA, Weinheim

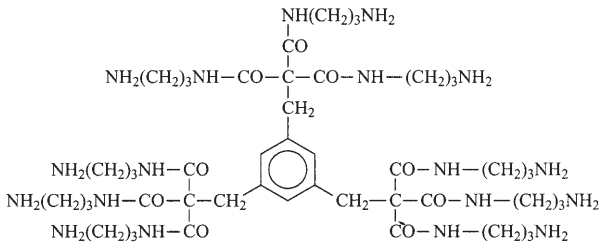

68

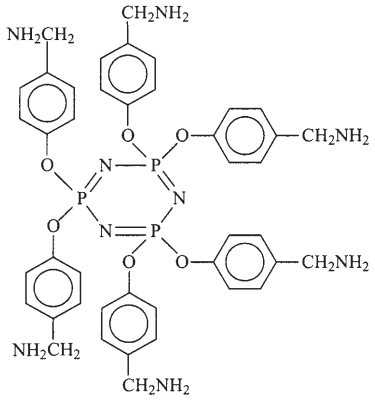

69a

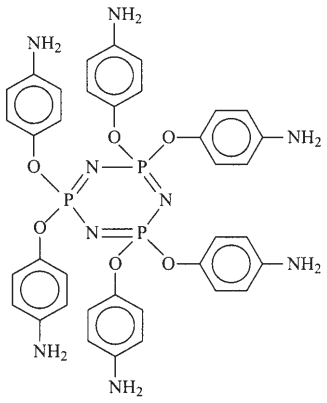

69b

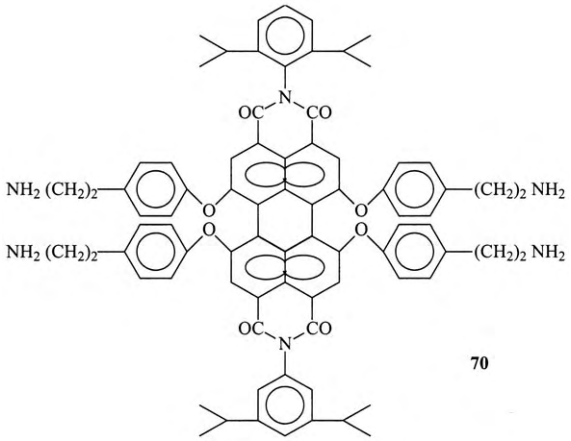

70

from the initiator **70** with the purpose of introducing a fluorescent star center.[186] Removal of the benzyl groups yielded water-soluble star-shaped polyglutamates, which allowed for changes in secondary structure and aggregation by variation in the pH value. One example of the second synthetic strategy was also reported.[191] Polypeptide chains of low PD were prepared by *n*-hexylamine-initiated ROP of γ-Bzl-L-Glu-NCA and grafted on tris(4-isocyanatophenyl)methane. All these star-shaped polypeptides have a commonality in that they possess rigid α-helical star arms in helix-supporting solvents.

The next architecture that should be discussed herein is (hyper)branched polypeptides. For a proper understanding, it is advisable to subdivide this group of polymers into two categories, with category I comprising polymers with the branching points in the peptide chain and category II including all polymers with linear peptide chains attached to branched or dendritic non-peptidic polymers. It is obvious that the two categories may overlap with each other and with the group of star-shaped polypeptides. Branched polypeptides were first synthesized in a stepwise manner by means of $N^{\varepsilon}$-protected L-Lys-NCAs.[192,193] A kind of hyperbranched poly-(L-lysine) was more recently obtained[194] by a combination of ROP of $N^{\varepsilon}$-Z-L-Lys-NCA or $N^{\varepsilon}$-TFA-L-Lys-NCA with a stepwise introduction of branching points through $N^{\alpha}$-, $N^{\varepsilon}$-bis-Fmoc-L-lysine. The Fmoc groups were selectively removed by means of piperidine so that $N^{\varepsilon}$-Z and $N^{\varepsilon}$-TFA groups of the linear segments remained unchanged. Both amino groups of the branching unit served, in turn, as initiators for a second batch of $N^{\varepsilon}$-Z-L-Lys-NCA or $N^{\varepsilon}$-TFA-L-Lys-NCA. Scheme 32 provides a brief illustration of this reaction sequence. The same group also described an alternative approach.[195] $N^{\varepsilon}$-Boc- or $N^{\varepsilon}$-TFA-L-Lys-NCA was grafted on linear poly(L-Lys) with free ε-amino groups. The ε-amino groups of the new side chains were deprotected, and the free ε-amino groups served again as initiators of $N^{\varepsilon}$-protected L-Lys-NCA.

Linear polypeptides attached to a polymer chain derived from vinyl monomers can be prepared in two ways. Either a vinyl-terminated polypeptide macromer such as **71**[196] or **72**[197] is synthesized in the first step and then in the second step subject to a homo- or copolymerization with other vinyl monomers, or a (co)polymer of vinyl monomers is prepared in the first step, followed by grafting of NCAs from the pendant primary amino groups.[197–200] In reference [192], both methods are compared—the synthesis and radical copolymerization of **72** with grafting of $N^{\varepsilon}$-Z-L-Lys-NCA from polymethacrylamide **73** (Scheme 33). It was found that the grafting process leaves many $NH_2$ groups of the poly(methacrylamide) **73** unreacted. In other words, densely packed "polypeptide brushes" were only obtained by the first approach. Owing to the extraordinary size of these "brushes", individual polymer molecules were visible by AFM imaging. The grafting of L-Ala-NCA on a copoly(methacrylamide) with pendant *n*-propylamino groups (analogous to **73**) was also described in an earlier publication.[198] Furthermore, γ-Bzl-L-Glu-NCA was grafted on liposomes synthesized from phospholipids with one amino and one vinyl end-group function.[199] Moreover, grafting of γ-Bzl-L-Glu-NCA on aminoethylated cellu-

 © 2006 Wiley-VCH Verlag GmbH & Co. KGaA, Weinheim 

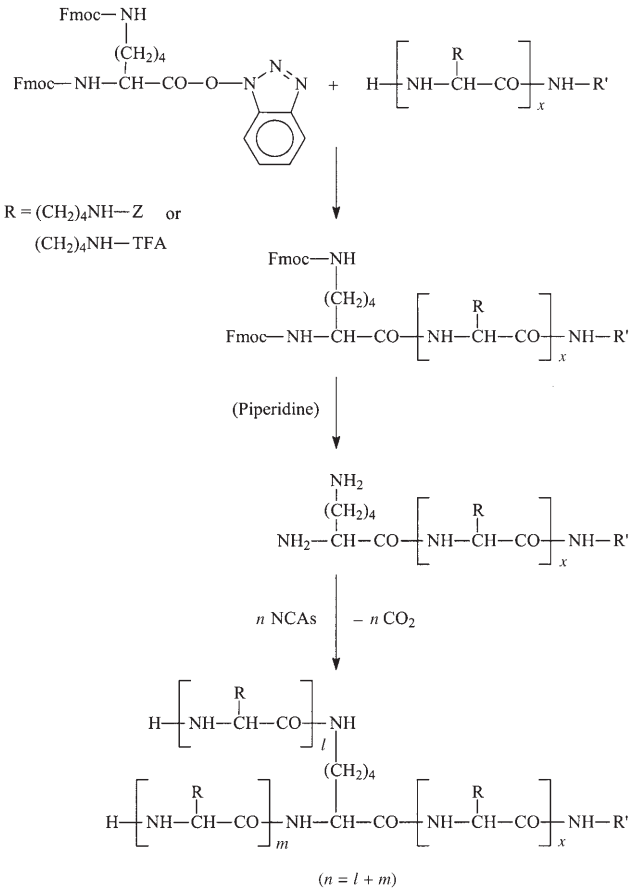

***Scheme 32.*** Synthesis of branched polylysine (first generation only).

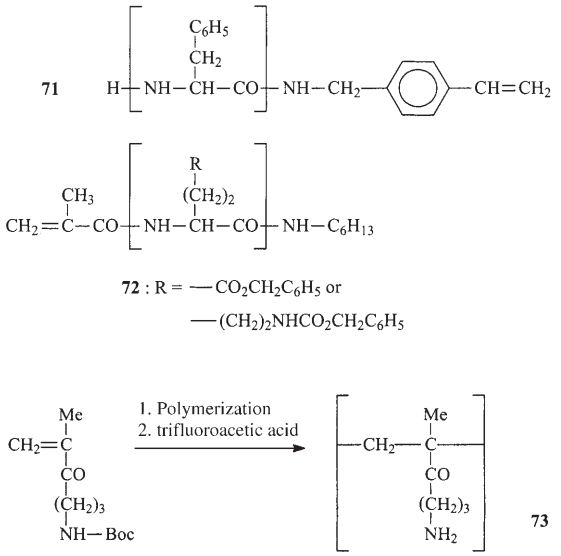

***Scheme 33.***

lose was described, and the blood compatibility of the blood copolymers was studied.[200] Six publications deal with grafting of NCAs on dendritic or hyperbranched "core polymers".[201–206] One research group used dendrimers of the poly(amide amine) type (PAMAM, **74**), third generation, as

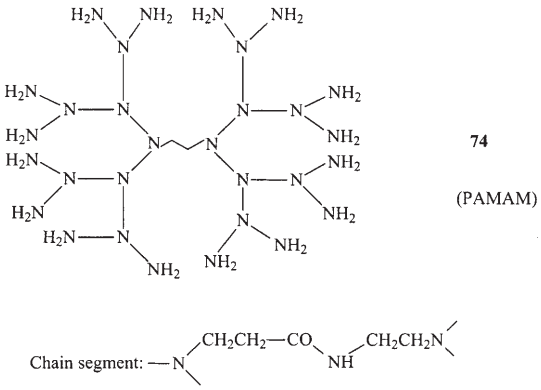

the initiator for *O*-(β-D-glucopyranosyl)-L-Ser-NCA. The feed ratio was selected so that, on the average, one NCA reacted with one amino group. In this way, ball-like oligomers with an outer sphere of tetraacetylglucose units was obtained, which were nicknamed "sugar balls".[201] The same type of dendrimers, but the fourth generation, was used for grafting γ-Bzl-L-Glu-NCA,[202] and the benzyl ester groups were reacted with an excess of 2-aminoethanol. The resulting water-soluble globular poly($N^{\varepsilon}$-hydroxyethyl-L-glutamine)s were claimed to be useful as drug carriers, and both blood compatibility and body distribution were studied. A completely water-soluble polymer was again obtained when Sar-NCA was grafted in a poly(trimethyleneimine) dendrimer.[203] In another publication,[204] a similar dendrimer served as microinitiator for the homopolymerization of γ-Bzl-L-Glu-NCA and for the copolymerization of γ-Bzl-L-Glu-NCA and L-Val-NCA (**75**). The resulting (co)polypeptides were found to complex $Cu^{2+}$ ions in organic solvents. Poly(γ-Bzl-L-Glu) grafted on commercial hyperbranched poly(ethyleneimine) yielded an amphiphilic multiarmed copolymer which was studied with regard to the formation of micelles.[205] Finally, a fluorescent and "shape-resistant" aromatic dendrimer (**76**), which was used as initiator for $N^{\varepsilon}$-Z-L-Lys-NCA, should be mentioned. After removal of the Z groups, a water-soluble graft or star copolymer was obtained, the secondary structure of which was characterized by various optical methods in water and trifluoroethanol.[206]

Grafting of γ-Bzl-L-Glu-NCA from polystyrene beads with pendant $CH_2$–$NH_2$ groups was reported to proceed best when catalyzed by a [$Ni^0$(cod)] complex.[207] Yet, the simple amine-initiated polymerization was successfully applied to a graft γ-stearyl-L-Glu-NCA on holofibers made from polypropylene.[208] γ-Bzl-L-Glu-NCA was grafted on poly(ethersulfone) membranes containing chain segments of structure **77**. These graft copolymers were designed as components of "molecularly imprinted sensor devices".[209] γ-Bzl-L-Glu-NCA was also grafted on a porous "omnipore" membrane.[210] This membrane consisted of an ethylene-tetrafluoroethylene copolymer modified with amino groups through a glow-discharge process. After hydrolysis of the γ-benzyl ester groups, the water permeation through the hydrophilic membrane was measured. Analogously, γ-Bzl-L-Glu-NCA was grafted on a microfiltration membrane based on $NH_2$-modified polypropylene.[211] The association of lipases to this

 © 2006 Wiley-VCH Verlag GmbH & Co. KGaA, Weinheim 

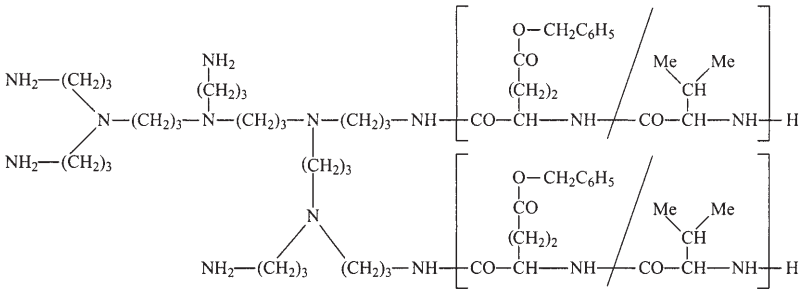

75

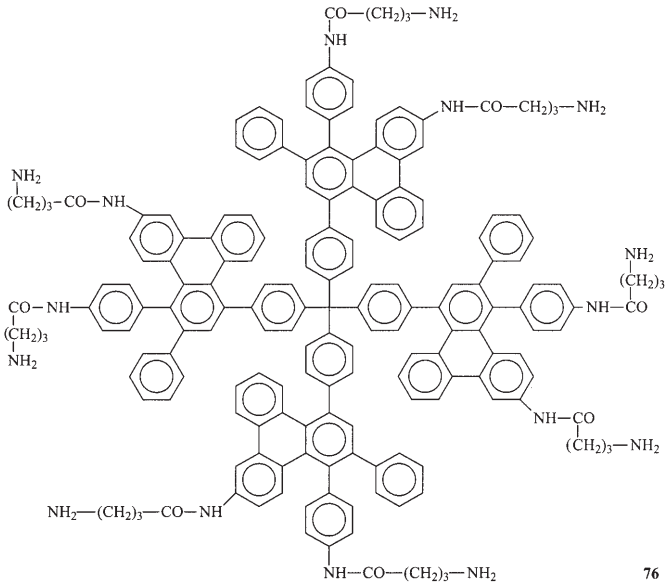

76

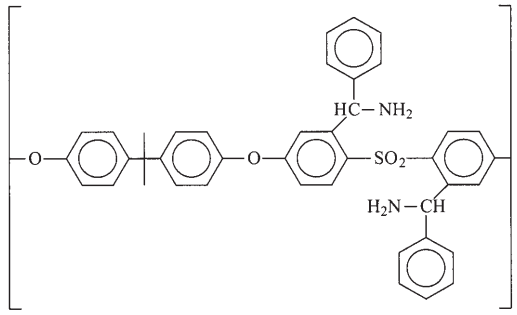

77

and similar membranes was studied in detail. Furthermore, grafting of γ-Me-L-Glu-NCA on carbon black[212] and grafting of γ-Bzl-L-Glu-NCA on amine-modified silica or quartz[213,214] were described. Finally, the deposition of thin polyglutamate films on neat gold was reported,[215] but it was not clarified if the binding was based on covalent bonds or through other electronic interactions.

## 8. Liquid-Crystalline Polypeptides

After the discovery that poly(γ-Bzl-L-Glu) can form a LC phase in concentrated solution in 1950,[41] systematic studies of LC polypeptides in general and polyglutamates in particular began in 1956.[42,216] There were 62 publications that dealt with this area of research and were mentioned and discussed by H. Block in his book on polyglutamates,[43] which appeared in 1983. Therefore, the short review presented below concentrates on publications that appeared after 1980. In this period not only original research reports but also several reviews were published[217–227] that either concentrated on LC polypeptides and eventually other LC biopolymers,[217–220,222,226] or dealt with a broad variety of LC polymers including LC polypeptides.[221,223–225,227] Almost all research activities concentrating on LC polypeptides before 1980 exclusively concerned formation and properties of lyotropic systems. When it was detected that helical polypeptides with suitable substituents may undergo thermotropic phase transition, intensive research on thermotropic systems set in. Consequently, an almost equal number of papers dealing with lyotropic phases, on the one hand, and thermotropic polypeptides, on the other, were published. Therefore, the following text is subdivided into the first part, which deals with lyotropic systems, and a second part, which reports on thermotropic materials. The third and last part concerns films and blends containing a partially ordered arrangement of polypeptide α helices.

Most papers dealing with the lyotropic phase of poly(glutamate ester)s concentrated on characterization of the cholesteric phase.[228] With classical optical rotatory dispersion (ORD) measurements of poly(γ-Bzl-L-Glu) and poly(γ-Bzl-D-Glu), the relationship between specific optical rotation and pitch of the cholesteric helix was elucidated.[228] In contrast to what was expected from the de Vries equation, it was found that the specific optical rotation is inversely proportional to the pitch of the cholesteric helix. Furthermore, an enhancement of the optical rotation was found in the regions of concentrations just below the critical point where extended cholesteric structures are formed. This enhancement was attributed to a short-range order of the long axes of the α helices. ORD measurements were again used to study the orientational effect (nematization effect) glass walls may have on polyglutamate α helices. Temperature, solvent, and polypeptide concentrations were varied.[229] Laser light scattering was used to check the perfection of the cholesteric structure of polyglutamates in various solvents.[230] The multiple-order scattering maxima of the laser light indicated that the axes of the cholesteric helices are not perfectly linear but contain displacements and deviation from linearity possibly owing to the PD of the poly(γ-Bzl-L-Glu).[231] A theory correlating this "inhomogeneous twisting of the directors" to the light-scattering pattern was also elaborated.

Poly(γ-Bzl-L-Glu) samples of different molar masses were compared in three different solvents. The temperature at which the cholesteric phase changes into a nematic phase depends on the chain length when 1,2-dichloroethane or dioxane were used as solvents. This was not the case for

 © 2006 Wiley-VCH Verlag GmbH & Co. KGaA, Weinheim 

DMF.[232] Owing to the high dipole moments of poly(glutamate) α helices, orientation in electric or magnetic fields is possible. In contrast to poly(ribonucleotide)s, the helix axes lies parallel to the external field.[233,234] Depending on the field strength, this parallelization may hinder more or less the formation of a cholesteric phase. Another interesting tool to influence the ordering of the α helices in lyotropic phases concerns the use or addition of special solvents and surfactants.[230,231] In one paper, the influence of chiral and racemic phenylethanol on the cholesteric structure of poly(γ-Bzl-L-Glu) and poly(γ-Bzl-D-Glu) was reported.[235] The pitch of the cholesteric helix of both polypeptides was enhanced when the L alcohol was added but reduced in the D alcohol relative to the racemic alcohol. A complete transformation of the cholesteric phase into a columnar hexagonal chain packing was observed when poly(octadecyl-L-Glu) was combined with amphiphilic solvents such as octadecylamine, octadecanol, and octadecanoic acid.[236] This higher-ordered mesophase changed into a cholesteric phase upon heating. Furthermore, it was studied[237] how the solvent-induced change of the helical sense of the cholesteric structure is related to conformal changes of the benzyl ester group of poly(γ-Bzl-L-Glu). Such a correlation was expected because the stacking of benzyl groups of neighboring poly(γ-Bzl-L-Glu) chains contributes to the stabilization of their lyotropic phases. However, $^1$H NMR spectroscopic studies of selectively deuterated poly(γ-Bzl-L-Glu) did not reveal significant changes in the side-chain conformations. The diffusion coefficients, and thus, the mobility of the entire poly(γ-octadecyl-L-Glu) helix were measured by means of the pulse-field-gradient spin–echo $^1$H NMR method (PFG SE).[238] These measurements were conducted in chloroform solution at 30 °C in the isotropic phase, in a biphasic region, and in the cholesteric phase. The diffusion coefficient considerably decreased in this order, and the diffusion parallel to the α-helix axis was significantly higher than perpendicular. In combination with a $^1$H NMR spectroscopic imaging technique, the PFG-SE measurements were extended to films and thus to the thermotropic situation at temperatures up to 80 °C.[239] The diffusion process was found to follow the Kirkwood theory. The macroscopic consequences of the molecular mobility were studied by means of rheological measurements.[240–242] These measurements included both poly(γ-Bzl-L-Glu) and poly($N^\varepsilon$-Z-L-Lys) but were restricted to solutions in *meta*-cresol. Temperatures, concentration, and molecular weights of the polypeptides were varied. Four papers were concerned with various theoretical aspects of mesophases based on rigid-rod polymers.[243–246] The titles of these papers indicate the direction of their content: "Molecular theory of solvent effects on cholesteric ordering in lyotropic polypeptide liquid crystals",[243] "On the origin of negative normal stresses in sheared or lyotropic liquid crystals",[244] "Phase equilibria in rod-like systems with flexible side chains",[245] and "Analytical description for the chiral nematic state in terms of molecular parameters".[246] A broader discussion of these papers is beyond the scope of this review.

Besides the properties of neat polyglutamates, the syntheses and LC properties of a handful of unusual polypeptides were reported.[247–250] Poly(γ-Bzl-L-Glu) was modified by covalent attachment to Fe, Co, Ni, or Cu complexes of 2,9,16,23-tetracarboxyphthalocyanines. These copolymers formed intensively colored mesophases.[242] Furthermore, the surfactant Triton X-100 was covalently bound to poly(γ-Bzl-L-Glu), and the LC phases were studied in different solvents.[243] A water-soluble polylysine was prepared by substitution with an oligoether side chain (**78**, Scheme 34).[249] The formation of

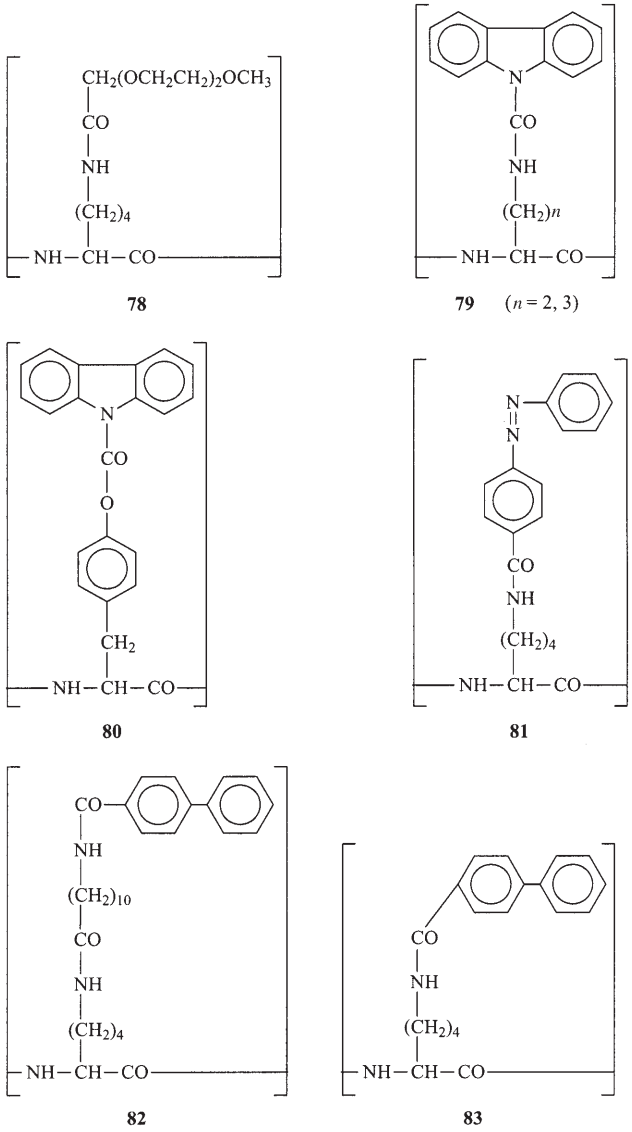


***Scheme 34.*** Unusual polypeptides forming lyotropic phases (**78**, **79**) or thermotropic phases (**81**–**83**).

a cholesteric phase in aqueous solution was determined by optical microscopy and X-ray scattering. A polyglutamate, a polylysine, and a polytyrosine all containing fluorescent carbazol groups were prepared (e.g. **79**, **80**)[250] and proposed as photoconducting materials. Fluorescence studies were also conducted with poly(γ-Bzl-L-Glu) that contained anthacene derivatives as additives.[251]

The first report on thermotropic LC polypeptides was published in 1978 by Thierry et al.,[252] who studied the X-ray patterns of poly(γ-lauryl-L-Glu) with variation in the temperature. However, those authors did not continue to work in this


© 2006 Wiley-VCH Verlag GmbH & Co. KGaA, Weinheim

field, and Watanabe and co-workers started an extensive elaboration of this new area of research at nearly the same time.[253–263] In contrast to Thierry et al., Watanabe and co-workers made their first observation of thermotropic phase transitions not in the case of homopolypeptides but with a random copolymer of γ-Me-L-Glu and γ-Bzl-L-Glu both with molar compositions between 30 and 70%.[253] An analogous thermotropic behavior was found for random copolymers of γ-Me-L-Glu and γ-hexyl-L-Glu[254] and for copolymers of γ-Bzl-L-Glu and γ-dodecyl-L-Glu.[256] The characterization included differential scanning calorimetry (DSC) and X-ray measurements, ORD and polarizing microscopy observations, and measurements of the viscoelastic properties. Depending on the composition and nature of the side chains, these (co)polypeptides formed a cholesteric melt upon heating to temperatures in the range of 100–150 °C. Watanabe and co-workers then concentrated their investigations on poly(γ-*n*-alkyl-L-Glu) homopolymers with systematic variation of the alkyl group up to the *n*-octadecyl residue. For *n*-alkyl groups with more than ten carbon atoms, formation of crystalline paraffin domains between the α helices was detected and the pitch of the cholesteric helices increased with the lengths of the alkyl chains and with the higher temperatures. For poly(γ-octadecyl-L-Glu), a solid columnar hexagonal mesophase was found at temperatures below the cholesteric phase.[261] Finally, polyglutamates with mesogenic groups in the side chain were included in these studies.[263]

Other research groups contributed to the characterization of thermotropic polyglutamates.[264–269] For instance, the segmental mobility and diffusion of the polypeptide helices in the LC phase were analyzed by means of NMR spectroscopic methods.[264–266] Furthermore, dielectric relaxation measurements were combined with DSC.[267] Mixtures of poly(γ-*n*-alkyl-L-Glu) and alkanes or polyglutamates with mesogenic ester groups were characterized by DSC, X-ray and electron spin resonance (ESR) measurements and also by polarizing microscopy.[269]

The detection of thermotropic polyglutamates prompted analogous studies of $N^{\varepsilon}$-substituted poly(L-lysine)s. Gallot et al. concentrated on lysine derivatives with mesogenic side chains such as azobenzene[270–272] and biphenyl moieties[123,124] (**81**–**83** in Scheme 34). Further to the properties of homopolymers, those of copolymers with $N^{\varepsilon}$-TFA-L-Lys were investigated.

Several publications dealt with the supramolecular order of polyglutamates in mobile monolayers[273,274] or in solid films.[275–277] Mono- or bilayers of polyglutamates were prepared at the air–water interface by using the Langmuir–Blodgett technique and were characterized by mechanical and FTIR spectroscopic measurements. Thin solid films of polyglutamate were also obtained by drying lyotropic cholesteric solutions on suitable surfaces. The dimensions of the fixed cholesteric structure were studied, whereby the optical properties and above all those of the Grand-Jean texture were of particular interest.

The optical properties were also in the focus of several studies with chromophores covalently bound to the polypeptide through L-Tyr[278] or dissolved and dispersed in polyglutamates.[279–281] The CD[279] and the nonlinear optical properties of these systems[279–281] were examined. Potential applications as "smart optical filters" were envisaged. Three-dimensional structure and morphology of blends containing cholesteric spherulites were the object of a further study.[282] Blends of poly(D,L-Phe), poly(γ-Me-L-Glu), and poly(γ-Bzl-L-Glu) with poly(ε-caprolactone) were investigated to elucidate if the polypeptides induce a mechanical reinforcement of biodegradable polyesters. However, the effect was poor, and rigid-rod types of aromatic polyesters bearing flexible compatibilizing substituents proved to be superior.[283]

## 9. Drugs and Drug Carriers

Homo- and copolypeptides prepared from NCAs have recently found increasing interest as drugs or drug carriers. Various block copolymers, mainly ABA triblock copolymers containing polypeptide A blocks, were synthesized and recommended as biodegradable components[284] of drug-delivery systems; however, clinical studies were not reported. Two types of copolypeptides based on *N*-(2-hydroxyethyl)-L-glutamine were studied with respect to their "biodistribution" in rats to find out if they allow for a targeting of drugs. One class of these copolypeptides is characterized by a random sequence of L-glutamic acid and *N*-(2-hydroxyethyl)-L-glutamine units,[285] whereas the second class was prepared by grafting (and modification) of γ-methyl-L-Glu-NCA on a $NH_2$-terminated dendrimer (fourth generation).[286]

Studies of blood compatibility as a prerequisite for pharmaceutical application were conducted with comblike polymers prepared by grafting γ-Bzl-L-Glu-NCA on cellulose.[287] Furthermore, a complex triblock copolymer was designed as "gene carrier" for the transport of DNA into the nucleus of a cell.[288] In this case, a $NH_2$-terminated PEO was again used as macroinitiator and central (B) block, and mixtures of $N^{\varepsilon}$-Z-L-Lys-NCA and L-Phe-NCA were copolymerized to yield the A blocks. After removal of the Z groups, the hydrophilic and lipophilic character was fine-tuned by the ratio of protonated ε-$NH_2$ groups of Lys and the hydrophobic benzyl groups of L-Phe.

Already in a promising stage of clinical tests are two anticancer agents, which both contain an established low-molar-mass drug that was covalently fixed to a polypeptide backbone. In the first case, an OH group of paclitaxel was esterified with γ-$CO_2H$ groups of poly(L-Glu).[289–292] In the second case, a vesicle-forming triblock copolymer was prepared from PEG and aspartic acid, the β-$CO_2H$ group of which was used to attach doxorubicin.[293,294]

Commercialized drug carriers based on poly(glutamic acid)s are available from Flamel Technologies.[295–298] These poly(amino acid)s were modified in such a way that hydrophobic groups (e.g. stearyl residues or α-tocopherol) were either attached to the chain ends or to the side chains of the repeat units (γ-$CO_2H$ functions). The purpose of these carriers is the stabilization and delayed delivery of peptide drugs and hormones, including interferons and interleukins.

Finally, the unique case of a polypeptide, which is itself a drug, should be mentioned. This drug is a nearly random copolymer of L-Ala, L-Glu, L-Lys, and L-Tyr (with a molar

 © 2006 Wiley-VCH Verlag GmbH & Co. KGaA, Weinheim 

ratio of 6.0:1.9:4.7:1.0).[299–302] Its efficiency was optimized by variation of composition and molecular weight. It is helpful in fighting multiple sclerosis and similar autoimmune diseases, and it has been commercialized by Tetra Pharmaceuticals (Israel) under the trademark copaxone. In summary, these comments demonstrate that drugs and drug carriers based on ROP of NCAs are still in their infancy but show promising results.

## 10. NCAs and the Hypothesis of Molecular Evolution

The speculation that NCAs might have played a role in molecular evolution on the early Earth is about thirty years old,[303–304] but experimental data supporting this speculation were lacking for a long time. However, three series of results meanwhile lend a certain credibility to the speculation that NCAs might have been involved in prebiotic evolution. First, several research groups observed[304–310] that the hydrolysis of CO-activated amino acid derivatives is catalyzed by $CO_2$ in buffered aqueous solution. The intermediate formation of carbamate anions and NCAs is the most obvious interpretation of these results (Scheme 35). This means that NCAs have played the role of reactive intermediates in many reactions of CO-activated derivatives when $CO_2$ was present.

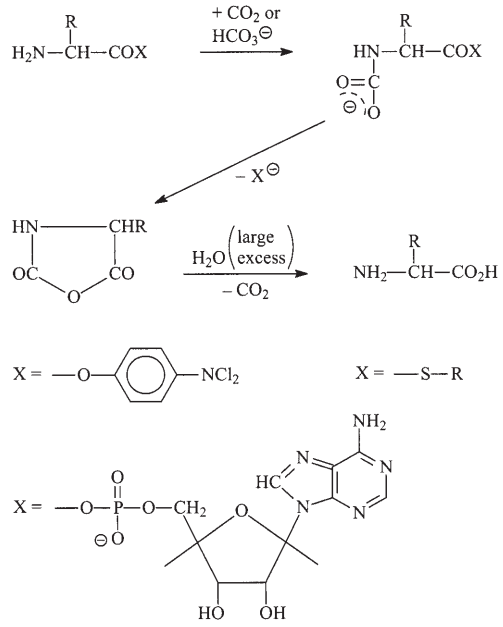


***Scheme 35.*** Hydrolysis of activated amino acids catalyzed by $CO_2$ or bicarbonate.

Second, the results of several research groups were particularly interesting and conclusive as they observed the formation of oligopeptides when amino acid esters[310–313] or aminoacyl adenylates[307,314] were treated with $CO_2$ or bicarbonate solutions. The first results in this direction were reported by Korshak et al.[311] as early as 1954. They observed an accelerated formation of oligopeptides when $CO_2$ was introduced into liquid alanine and glycine ethyl esters heated to temperatures above 50 °C. Under the same conditions, Gly-Gly-OEt did not yield oligoglycines, which indicates that $CO_2$-activated amino acid esters did not undergo a simple polycondensation reaction.[312] Analogous results were obtained by Brack with α-amino acid *p*-nitrophenyl esters.[307] When polycondensed in bicarbonate buffer, α-amino esters yielded oligopeptides, but the *p*-nitrophenylester of β-alanine did not. As the formation of β-amino acid NCAs from N-substituted β-amino acids is much more difficult to achieve than the synthesis of α-amino acid NCAs, these results suggest again that the polycondensations of α-amino acid *p*-nitrophenyl esters involved the intermediate formation of NCAs. Furthermore, bicarbonate-promoted polycondensations of thioethyl glutamate yielded oligomers, whereas the dipeptide ester (Glu-Glu-*S*-ethyl ester) mainly produced the cyclic dimer under identical conditions (Scheme 36).[310] It is

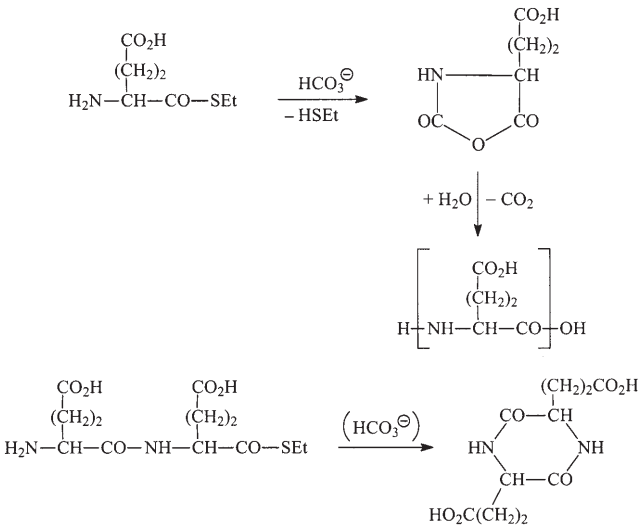


***Scheme 36.*** Oligomerizations of the thioethyl esters of glutamic acid and its dimer.

obvious that the bicarbonate-catalyzed polymerizations of α-aminoacyl adenylates also involved the formation of NCAs.[313,314] Finally, polycondensation of α-amino acids in aqueous buffered solution should be mentioned.[304,310,315] Under conditions where glutamic acid yielded oligopeptides, the preformed dimer Glu-Glu did not polymerize. Therefore, a reaction pathway involving intermediate formation of NCAs was proposed.[310]

A second series of experiments that contributed to the credibility that NCAs played an important role in the prebiotic evolution of oligo- and polypeptides was contributed by Orgel and co-workers.[304,316–322] These authors studied polymerizations of various α- and β-amino acids activated by carbonyl diimidazole (CDI). Several experimental findings suggest that the polymerization process involves the formation of NCAs that play the role of the true monomers (Scheme 37). Particularly informative is the observation that β-amino acids do not polymerize when treated with CDI under the same conditions as those for the polymerization of


© 2006 Wiley-VCH Verlag GmbH & Co. KGaA, Weinheim

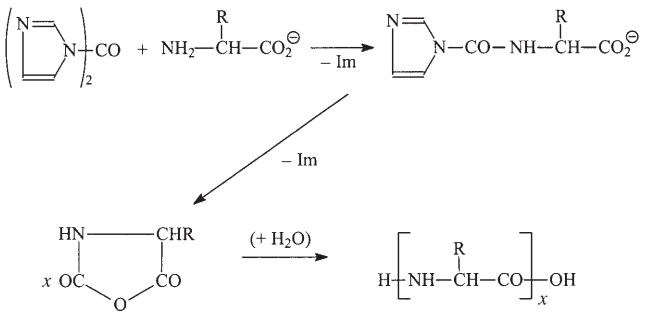

***Scheme 37.*** Formation of oligopeptides by carbonyl diimidazole promoted polymerizations of α-amino acids in alkaline aqueous solution. Im = imidazole.

α-amino acids. In contrast to α-amino acids, β-amino acids do not readily form (six-membered) NCAs but rather undergo a polycondensation process yielding oligoamides when activated at the $CO_2H$ group with 1-ethyl-3-(3-dimethylaminopropyl)carbodiimide.

Third, a new, interesting, and important contribution to this field was recently provided by Commeyras and coworkers.[323–330] These authors found that carbamoyl amino acids easily react with $NO/O_2$ gas mixtures to form NCAs in almost quantitative yields (Scheme 38). The carbamoyl amino

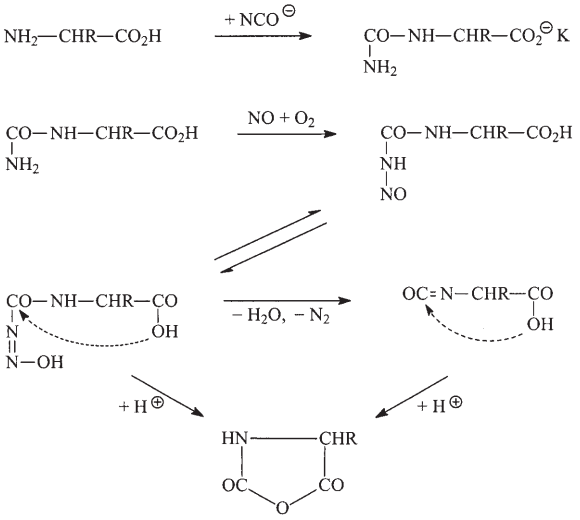

***Scheme 38.*** Formation of NCAs by nitrosation of *N*-carbamoyl amino acids.

acids (CAAs) result from the reaction of amino acids with cyanate ions, a prebiotic scenario that has been discussed in detail.[324] The treatment of CAAs with $NO/O_2$ may be conducted in water, whereby, depending on the pH value, hydrolysis and oligomerization of the resulting NCAs compete more or less efficiently with their formation. However, this novel synthesis of NCAs may also be performed in acetonitrile, a procedure that is advantageous for various preparative applications of NCAs. Owing to the quantitative conversion of CAAs, significant amounts of organic impurities are absent, and thus, the crude NCAs may be used for peptide syntheses. If mixed with equimolar amounts of amino acids in a basic buffered solution, dipeptides can be obtained in high yields. Such a stepwise peptide synthesis corresponds to the procedures elaborated for pure NCAs by the American Merck group. [18–24] However, in the absence of amino acids, the crude NCAs may be used to prepare polypeptides by ROP.

The formation of NCAs under prebiotic conditions may also have proceeded by a quite different pathway, namely through activation of amino acid by COS (Scheme 39). The role of COS in molecular evolution has been discussed in much detail.[330] The formation of NCAs according to Scheme 39 is still hypothetical and needs experimental verification.

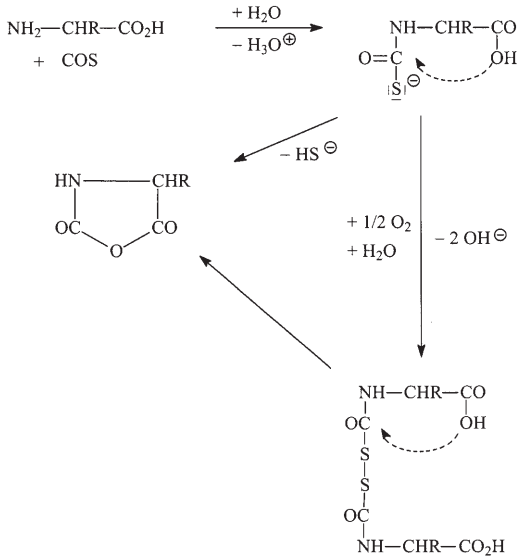

***Scheme 39.*** Formation of NCAs through activation of amino acids by COS.

Another interesting aspect of the role of NCAs in the prebiotic evolution concerns their interaction with phosphates. Formation of aminoacyl phosphates by reaction with inorganic phosphate ions has recently been demonstrated.[330] The formation of amino acyl adenylates from ATP (Scheme 40) is still speculative, but possible from a thermodynamic point of view. A detailed discussion of the role of activated amino acids, focusing on NCAs, in molecular evolution has quite recently been published.[328]

A completely different aspect of the role of NCAs in the current research on prebiotic evolution is the problem how oligo- and polypeptides based on L-amino acids have evolved. Studies of this problem focused on three questions, 1) how were long oligo- and polypeptides formed and stabilized in the presence of water? 2) which factors favored a homochiral coupling of α-amino acids? 3) why were oligopeptides containing D-amino acids finally eliminated?

First, comprehensive studies on the reactions of NCAs in water (mainly in buffered solutions)[331,332] revealed that hydrolysis is catalyzed by bases (i.e. at pH > 7) but not by acid. Under basic conditions, amino acid anions are formed

 © 2006 Wiley-VCH Verlag GmbH & Co. KGaA, Weinheim 

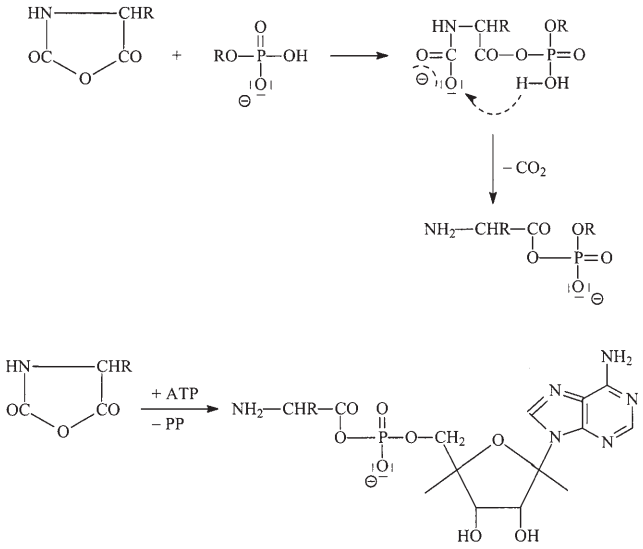

***Scheme 40.*** Interaction of NCAs with phosphate ions or adenosine 5′-triphosphate (ATP). PP = inorganic diphosphate.

and react with NCAs faster than hydroxide ions or water so that oligopeptides are formed (Scheme 41). To what extent hydrolysis can compete with oligomerization, and if the chain

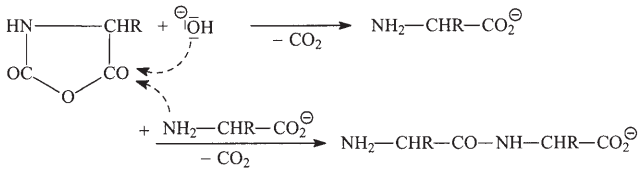

***Scheme 41.*** Competing reactions of NCAs in alkaline water.

growth can be stopped after one step (so that stepwise peptide syntheses can be achieved) depends on the NCA/$H_2O$ ratio, on the pH value, and temperature. Most studies on the formation of oligo- and polypeptides in an aqueous environment were conducted with amino acid CDI mixtures, which according to Scheme 37 form NCAs as reactive intermediates in buffered water.[304,307,316–322,333,334] It was found that the lengths of the oligopeptides ($P_n$) usually do not exceed 11 amino acid units. Higher concentrations of amino acids and CDI favor higher yields and $P_n$s. Furthermore, addition of positively charged surfactants, such as cetyl trimethylammonium bromide, also favor polymerization at the expense of hydrolysis when amino acids with negatively charged side chains are used as monomers.[317] Another research group recently reported[335] that anionic surfactants favor higher yields and higher molecular weights, when (isolated) NCAs are polymerized in water. A particularly interesting finding reported by Orgel and co-workers[318–322] concerns the adsorption of negatively charged oligopeptides (derived from Asp, Glu, or phosphorylated Ser) on minerals, such as ilite or hydroxy apatite. Batchwise addition of amino acids to CDI caused lengthening of these oligopeptides up to a $P_n$ value of around 55. These experiments are the first successful syntheses of medium-size polypeptides in aqueous solution.

The problem how of amplification of optical activity (or of an enantiomeric excess) can be explained was first studied by Bonner and co-workers[336–340] and the related problem, if and how homochiral sequences were favored, was first tackled by Brack et al.[307,310,315,333,334] The Bonner group polymerized D,L-Leu-NCA and D,L-Val-NCA in dioxane with a slight excess of one enantiomer. When the polymerizations were stopped at around 50% conversion, it was found that in the poly(Leu) chains the excess enantiomer was enriched, whereas in the Val-NCA statistical chains of D and L units were formed. Therefore, these experiments did not give a clear cut answer.[340] However, experiments of Japanese authors[341] with optically active hydantoins as initiators of NCA polymerizations demonstrated that formation of homochiral sequences was favored. When mixtures of D- and L-amino acids and CDI were polymerized in water, the resulting oligopeptides contained short homochiral blocks of either D- or L-units that can form a β-sheet structure.[310] Hydrolysis under normal conditions showed that the β sheets reduce the rate of hydrolysis, stabilizing the homochiral blocks relative to more-random sequences. This means that any heating–cooling cycles on the early Earth that combined permanent syntheses with partial hydrolytic degradation should have favored the survival of homochiral sequences.[310]

The influence of liposomes on the polymerization of L-Trp-NCA and D,L-Trp-NCA was studied in two directions. On the one hand, it was found that the presence of liposomes favors chain growth at the expense of hydrolysis, so that $P_n$ values up to 28 instead of a limit of $P_n = 7$ were found.[342] On the other hand, liposome were shown to favor the formation of homochiral sequences when racemic Trp-NCA (monomer) was polymerized.[343–345] Similar results were obtained with D,L-Leu-NCA or D,L-Ile-NCA.[343] Interestingly, homochiral blocks were even favored when the L-NCA of one amino acid (e.g. Trp) was copolymerized with the D-NCA of another amino acid (e.g. Leu).[344] The group of Luisi also investigated the influence of (±)-quartz (and to a lesser extent hydroxyapatite) on copolymerizations of D- and L-amino acid NCAs.[346–348] (±)-Quartz was found to favor the formation of homochiral blocks from various D,L-NCAs, but the effect was particularly pronounced for D,L-Leu-NCA. Furthermore, when nonracemic mixtures of D- and L-Leu-NCAs were polymerized and stopped prior to 100% conversion, the presence of quartz favored the incorporation of the enantiomer that was used in excess. In summary, all experiments with the addition of surfactants, liposomes, and minerals showed evidence that membranes and surfaces considerably favored enantioselectivity and homochirality, and thus, supports the hypothesis that such phase boundaries might have played an important role in the evolution of polypeptides that were exclusively composed of L-amino acids.

Recent results from Lahav and co-workers[349,350] fit in with the afore-mentioned studies. When the *S*-ethyl esters of $N^{\varepsilon}$-stearoyl-D,L-Lys or γ-stearyl-D,L-Glu were polymerized in the 2D lattices formed at the air–water interface, preferential formation of homochiral blocks was detected.[349] This polymerization process most likely involves the intermediate formation of NCAs as outlined for *S*-ethyl glutamate in Scheme 36. Predominantly homochiral oligopeptides were

 © 2006 Wiley-VCH Verlag GmbH & Co. KGaA, Weinheim 

also formed when the polymerization of crystalline D,L-Phe-NCA was performed in the solid state.[350]

### 11. Various Aspects

A few publications in the field of NCA chemistry that do not fit into one of the Sections presented above are summarized at the end of this Review article. Most of these publications deal with syntheses of NCAs and homopolypeptides. Although NCAs are sensitive to water and rapidly oligomerize at temperatures $\geq 20\,^{\circ}C$ in moist organic solvents, it was reported that washing NCA solutions at $0\,^{\circ}C$ with neutral water or sodium bicarbonate and subsequent rapid drying is an efficient purification method for crude NCAs.[351] After this washing, however, rapid and intensive drying of the organic phase is necessary. A disadvantage of this method is that many NCAs (e.g. Gly-NCA) are not very soluble in organic solutions that are not miscible with water.

Two NCAs with nitroxyl radicals in the side chain (**84** and **85**; Scheme 42) were prepared by phosgenation of the parent amino acids or their *N*,*O*-bistrimethylsilyl derivatives.[352,353] Although triethylamine was used as a polymerization catalyst to prepare high-molar-mass polypeptides for ESR spectroscopic studies, only oligomers were obtained even under optimized reaction conditions. In the case of NCA **85**, large amounts of the hydantoin **86** and of the cyclic dimer **87** were isolated as by-products in agreement with the mechanism discussed in Section 5. A new synthetic approach yielding NCAs directly from β-lactanes without intermediate isolation of α-amino acids was also reported.[354,355] For instance, the NCAs of structure **89** were obtained from the β-lactames **88** through the oxidative Bayer–Villiger rearrangement (Scheme 42). Analogously, the NCAs **91** were prepared from the β-lactams of structure **90** (Scheme 43). No polymerization experiments were described, but one of the new NCAs was used for the stepwise synthesis of the tripeptide **92**, which is a component of lysobactin.[355] Fmoc-protected NCAs were successfully used for acylation of so-called "Wang" and "Rink" resins with pendant OH groups.[356] This acylation served as a first step in a stepwise synthesis of oligopeptides through the Merrifield approach. Another paper[357] reported syntheses and conformational studies of poly(D-*p*-hydroxyphenyl glycine) **94** and its Z-protected precursor **93** (Scheme 43). A series of exclusively α-linked poly(L-aspartic acid)s and an analogous series of poly(D-aspartic acid)s were prepared by using α,β-dialkyl aspartates as initiators. The molecular weights were systematically varied according to the NCA/initiator ratio. These poly(aspartic acid)s were designed to serve for aminoglycoside-induced nephrotoxicity inhibition studies.[358] Another research group used poly(L-leucine) as the chiral component of a catalyst for the Julia–Colonna asymmetric epoxidation of benzal acetophenones.[359] The influence of the degree of polymerization on the stereoselectivity was studied. Furthermore, polymerizations of γ-Me-L-Glu-NCA in poly(acrylonitrile butadiene) rubber were performed.[360] The mechanical reinforcement effect of the relatively rigid polyglutamate helices on the soft rubber material was measured and compared to blends prepared from solutions of preformed polyglutamates and rubbers. In

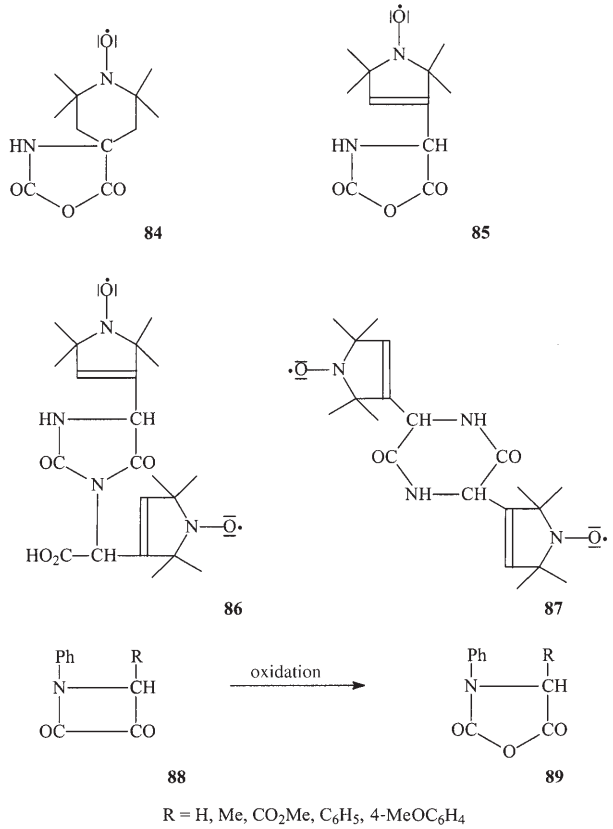


***Scheme 42.*** NCAs with nitroxyl radicals in the side chain.

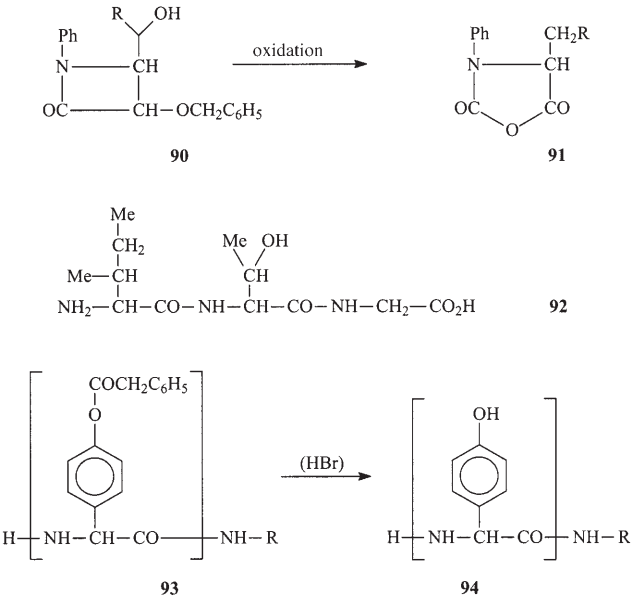


***Scheme 43.*** Preperation of NCAs **91** from the β-lactams of structure **90**. The preperation of **94** and the structure of **92**.

 © 2006 Wiley-VCH Verlag GmbH & Co. KGaA, Weinheim 

addition, a comparison with rigid aromatic polyesters was included in that work (a study which corresponds to the aforementioned work[283] on reinforced poly(ε-caprolactone).

Finally, it should be mentioned that all the numerous results presented above clearly demonstrate that the field of synthetic polypeptides and NCA chemistry is alive and has expanded into various areas of chemistry and material science. Therefore, it is no risk to predict that studies of oligo- and polypeptides derived from NCAs are an area of research that will survive the next hundred years.

*The author wishes to thank Dr. Gert Schwarz (Institut für Technische und Makromolekular Chemie, University of Hamburg) for his intensive investigation of the literature.*

Received: February 22, 2006

[1] H. Leuchs, *Ber. Dtsch. Chem. Ges.* **1906**, *39*, 857 – 861.
[2] H. Leuchs, W. Manasse, *Ber. Dtsch. Chem. Ges.* **1907**, *40*, 3235 – 3249.
[3] H. Leuchs, W. Geiger, *Ber. Dtsch. Chem. Ges.* **1908**, *41*, 1721 – 1726.
[4] F. Kröhnke *Chem. Ber.* **1952**, *85*, LV–LXXXIX.
[5] F. W. Lichtenthaler, *Eur. J. Org. Chem.* **2002**, *24*, 4095 – 4122.
[6] T. Curtius, W. Sieber, *Ber. Dtsch. Chem. Ges. B* **1921**, *54*, 1430 – 1437.
[7] T. Curtius, W. Sieber, *Ber. Dtsch. Chem. Ges. B* **1922**, *55*, 1543 – 1558.
[8] T. Curtius, K. Hochschwender, H. Meier, W. Lehmann, A. Benckiger, M. Schenk, W. Nirbatz, J. Gaier, W. Mühlhäuser, *J. Prakt. Chem.* **1930**, *125*, 211 – 302.
[9] F. Wessely, *Z. Physiol. Chem.* **1925**, *146*, 72 – 90.
[10] F. Wessely, F. Sigmund, *Z. Physiol. Chem.* **1926**, *159*, 102 – 119.
[11] F. Sigmund, F. Wessely, *Z. Physiol. Chem.* **1926**, *157*, 91 – 105.
[12] F. Wessely, M. John, *Z. Physiol. Chem.* **1927**, *170*, 38 – 43.
[13] F. Wessely, J. Mayer, *Monatsh. Chem.* **1928**, *50*, 439 – 448.
[14] F. Wessely, K. Riedel, H. Tuppy, *Monatsh. Chem.* **1950**, *81*, 861 – 872.
[15] F. Wessely, W. Swoboda, *Monatsh. Chem.* **1951**, *82*, 621 – 627.
[16] F. Wessely, K. Schlögl, G. Korgers, *Monatsh. Chem.* **1952**, *83*, 845 – 864.
[17] H. Staudinger, *Arbeitserinnerungen*, A. Hüthig, Heidelberg, **1961**.
[18] R. G. Denkewalter, H. Schwam, R. G. Strachan, F. E. Beesly, D. F. Veber, E. F. Schoenwaldt, H. Barkemeyer, W. J. Poleveda, Jr., T. A. Jacob, R. Hirschmann, *J. Am. Chem. Soc.* **1966**, *88*, 3163 – 3164.
[19] D. F. Veber, V. Pfeister, R. Hirschmann, *J. Med. Chem.* **1967**, *10*, 968 – 969.
[20] R. Hirschmann, H. Schwam, E. F. Schoenwaldt, H. Joshua, H. Barkemeyer, D. F. Veber, W. J. Poleveda, Jr., T. A. Jacob, F. E. Beesly, R. G. Denkewalter, *J. Org. Chem.* **1967**, *32*, 3415 – 3425.
[21] R. S. Devey, E. F. Schoenwaldt, H. Joshua, W. J. Poleveda, Jr., H. Schwam, H. Barkemeyer, B. H. Arison, D. F. Veber, R. G. Denkewalter, R. Hirschmann, *J. Am. Chem. Soc.* **1968**, *90*, 3254 – 3255.
[22] D. F. Veber, R. Hirschmann, R. G. Denkewalter, *J. Org. Chem.* **1969**, *34*, 753 – 755.
[23] R. G. Denkewalter, D. F. Veber, F. W. Holly, R. Hirschmann, *J. Am. Chem. Soc.* **1969**, *91*, 502 – 503.
[24] R. Hirschmann, H. Schwam, R. G. Strachan, E. F. Schoenwaldt, H. Barkemeyer, S. B. Möller, J. B. Conn, V. Garby, D. F. Veber, R. G. Denkewalter, *J. Am. Chem. Soc.* **1971**, *93*, 2746 – 2754.
[25] E. R. Blout, C. de Loué, S. M. Bloom, G. D. Fasmann, *J. Am. Chem. Soc.* **1960**, *82*, 3787 – 3789.
[26] S. M. Bloom, G. D. Fasmann, C. de Loué, E. R. Blout, *J. Am. Chem. Soc.* **1962**, *84*, 458 – 463.
[27] P. Doty, J. T. Jung, *J. Am. Chem. Soc.* **1956**, *78*, 498 – 500.
[28] E. R. Blout, P. Doty, J. T. Jung, *J. Am. Chem. Soc.* **1951**, *73*, 749 – 750.
[29] G. D. Fasmann in *Polyamino acids, Polypeptides and Proteins* (Ed.: M. H. Stahmann), Univ. of Wisconsin press, Madison, **1962**, chap. 19.
[30] Y. Konishi, J. W. van Nispen, G. Davenport, H. A. Scheraga, *Macromolecules* **1977**, *10*, 1264 – 1271 (and previous papers in this series).
[31] Y. Kobayashi, F. Cardinaux, B. O. Zweifel, H. A. Scheraga, *Macromolecules* **1977**, *10*, 1271 – 1283.
[32] D. J. Hill, F. Cardinaux, H. A. Schrager, *Biopolymers* **1977**, *16*, 2447 – 2467.
[33] E. R. Blout, A. Asradourian, *J. Am. Chem. Soc.* **1956**, *78*, 955 – 961.
[34] M. Idelson, E. R. Blout, *J. Am. Chem. Soc.* **1957**, *79*, 3948 – 3955.
[35] P. Doty, R. D. Lundberg, *J. Am. Chem. Soc.* **1956**, *78*, 4810 – 4812.
[36] J. C. Mitchell, A. E. Woodward, P. Doty, *J. Am. Chem. Soc.* **1957**, *79*, 3955 – 3960.
[37] P. H. Maurer in *Polyamino acids, Polypeptides and Proteins* (Ed.: M. A. Stahmann), University of Wisconsin Press, Madison, **1962**, chap. 35.
[38] T. J. Gill III, P. Doty in *Polyamino acids, Polypeptides and Proteins* (Ed.: M. A. Stahmann), University of Wisconsin Press, Madison, **1962**, chap. 35.
[39] M. Sela, *Adv. Immunol.* **1966**, 5, 29 – 129.
[40] E. Rüde, *Angew. Chem.* **1970**, *82*, 202 – 216; *Angew. Chem. Int. Ed. Engl.* **1970**, *9*, 206 – 219.
[41] A. Elliot, E. J. Ambrose, *Discuss. Faraday Soc.* **1950**, *9*, 46 – 51.
[42] C. Robinson, *Trans. Faraday Soc.* **1956**, *52*, 571 – 592.
[43] H. Block, *Poly(γ-benzyl-L-Glutamate) and other Glutamic Acid Containing Polymers*, Gordon and Breach, New York, **1983**.
[44] E. Katschalski, M. Sela, *Adv. Protein Chem.* **1958**, *11*, 475 – 492.
[45] *Poly-α-Amino Acids* (Ed.: G. P. Fasman), Marcel Dekker, New York, **1967**.
[46] M. Schwarz, *Adv. Polym. Sci.* **1965**, *4*, 1 – 65.
[47] C. H. Bamford, H. Block, *High Polym.* **1972**, *26*, 687 – 749.
[48] Y. Imanishi in *Ring-Opening Polymerization* (Eds.: K. J. Ivin, T. Saegusa), Elsevier, London, **1984**, chap. 8.
[49] H. R. Kricheldorf, *α -Amino Acid-N-Carboxyanhydrides and Related Heterocycles*, Springer, Berlin, **1987**.
[50] H. R. Kricheldorf in *Models of Biopolymers by Ring-Opening Polymerization* (Ed.: S. Penczek), CRC, Boca Raton, **1990**, chap. 1.
[51] W. H. Daly, D. Poché, I. Negulescu, *Prog. Polym. Sci.* **1994**, *19*, 79 – 135.
[52] M. Zaoral, J. Rudinger, *Collect. Czech. Chem. Commun.* **1961**, *26*, 2316 – 2332.
[53] H. R. Kricheldorf, *Makromol. Chem.* **1977**, *178*, 905 – 939.
[54] T. B. Sim, H. Rapoport, *J. Org. Chem.* **1999**, *64*, 2532 – 2536.
[55] H. R. Kricheldorf, *Angew. Chem.* **1973**, *85*, 86 – 87; *Angew. Chem. Int. Ed. Engl.* **1973**, *12*, 73 – 74.
[56] H. R. Kricheldorf, M. Fehrle, *Chem. Ber.* **1974**, *107*, 3533 – 3547.
[57] R. Katakai, *J. Org. Chem.* **1975**, *40*, 2697 – 2702.
[58] R. Katakai, Y. Nakayama, *Biopolymers* **1976**, *75*, 747 – 755.
[59] J. Halstrom, K. Brunfeldt, K. Kovacs, *Z. Physiol. Chem.* **1974**, *355*, 82 – 84.
[60] W. D. Fuller, M. P. Cohen, M. Shabankarch, R. K. Blair, M. Goodman, F. R. Naider, *J. Am. Chem. Soc.* **1990**, *112*, 7414 – 7416.
[61] C.-B. Xue, F. Naider, *J. Org. Chem.* **1993**, *58*, 350 – 355.

 © 2006 Wiley-VCH Verlag GmbH & Co. KGaA, Weinheim 

[62] T. T. Romoff, M. Goodman, *J. Pept. Res.* **1997**, *49*, 281 – 292.
[63] J. J. Leban, K. L. Colson, *J. Org. Chem.* **1996**, *61*, 228 – 231.
[64] L. Pothion, J.-A. Fehrentz, A. Aumelas, A. Loffet, J. Martinez, *Tetrahedron Lett.* **1996**, *37*, 1027 – 1030.
[65] M. McKiernan, J. Huck, J.-A. Fehrentz, M.-L. Roumestant, P. Villefront, J. Martinez, *J. Org. Chem.* **2001**, *66*, 6541 – 6544.
[66] W. N. E. Van Dijk-Wolthuis, L. van der Water, P. Van de Wetering, M. Van Steenbergen, J. J. Kettenes-Van den Bosch, W. Schuyl, W. E. Hennink, *Macromol. Chem. Phys.* **1997**, *198*, 3893 – 3906.
[67] F. Rypazek, M. Dvorak, T. Stefko, L. Machova, V. Skanlar, D. Kubics, *ACS Symp. Ser.* **2001**,*786*, 258 – 275.
[68] H. R. Kricheldorf, C. v. Lossow, G. Schwarz, *Macromol. Chem. Phys.* **2004**, *205*, 918 – 924.
[69] H. R. Kricheldorf, C. v. Lossow, G. Schwarz, *Macromol. Chem. Phys.* **2005**, *206*, 282 – 290.
[70] T. Aliferis, H. Tatrou, N. Hadjichristidis, *Biomacromolecules* **2004**, *5*, 1653 – 1656.
[71] W. Vayaboury, O. Giani, H. Coutet, A. Deratani, F. Schue, *Macromol. Rapid Commun.* **2004**, *25*, 1221 – 1224.
[72] J. W. Meng, Y.-B. Tan, *Gaofenzi Cailiao Kexue Yu Gongcheng* **2004**, *20*, 100 – 102.
[73] M. Tahaki, R. Asami, Y. Hanada, O. Yoichiro, N. Ochiao, *Polym. Bull.* **1987**, *18*, 105 – 110.
[74] Y. Ohkatsu, E. Suzuki, T. Kusano, *Yakagahu* **1992**, *41*, 465 – 471.
[75] V. S. Rao, P. Lapointe, D. N. McGregor, *Makromol. Chem.* **1993**, *194*, 1095 – 1104.
[76] P. Flory, *Chem. Rev.* **1946**, *46*, 137 – 197.
[77] H. R. Kricheldorf, G. Schwarz, *Macromol. Rapid Commun.* **2003**, *24*, 359 – 381.
[78] H. Kanazawa, Y. Ohashi, Y. Sasada, T. Kawac, *J. Polym. Sci. Polym. Phys. Ed.* **1982**, *20*, 1847 – 1862.
[79] H. Kanazawa, *Polymer* **1992**, *33*, 2557 – 2566.
[80] H. Kanazawa, Y. Ohashi, *Mol. Cryst. Liq. Cryst.* **1996**, *277*, 405 – 414.
[81] H. Kanazawa, *Fukushima Daigaku Kyoikugakubu Ronshu Rika Hokoku* **1994**, *53*, 7 – 12.
[82] H. Kanazawa, Y. Sato, *Fukushima Daigaku Kyoikugakubu Ronshu Rika Hokoku* **1996**, *59*, 13 – 17.
[83] H. Kanazawa, *Mol. Cryst. Liq. Cryst.* **1998**, *313*, 205 – 210.
[84] X. P. Hu, J. Wu, Z.-K. Xu, L.-X. Deng, *Chin. J. Polym. Sci.* **2000**, *18*, 369 – 372.
[85] T. J. Deming, *Polym. Prepr. Am. Chem. Soc. Div. Polym. Chem.* **1996**, *37*, 435 – 436.
[86] T. J. Deming, *J. Am. Chem. Soc.* **1997**, *119*, 2759 – 2760.
[87] T. J. Deming, *Adv. Mater.* **1997**, *9*, 299 – 311.
[88] T. J. Deming, *J. Am. Chem. Soc.* **1998**, *120*, 4240 – 4241.
[89] T. J. Deming, *Nature* **1997**, *390*, 386 – 389.
[90] T. J. Deming, *Macromolecules* 1999, 32, 4500 – 4502.
[91] S. A. Curtin, T. J. Deming, *J. Am. Chem. Soc.* **1999**, *121*, 7427 – 7428.
[92] J. Cheng, T. J. Deming, *Macromolecules* **1999**, *32*, 4745 – 4747.
[93] A. A. Goodwin, X. Bu, T. J. Deming, *J. Organomet. Chem.* **1999**, *589*, 111 – 114.
[94] S. W. Seidel, T. J. Deming, *Macromolecules* **2003**, *36*, 969 – 972.
[95] T. J. Deming, *Macromolecules* **1999**, *32*, 4500 – 4502.
[96] T. J. Deming, S. A. Curtin, *J. Am. Chem. Soc.* **2000**, *122*, 5710 – 5717.
[97] J. Cheng, T. J. Deming, *J. Am. Chem. Soc.* **2001**, *123*, 9457 – 9458.
[98] J. Cheng, T. J. Deming, *Macromolecules* **2001**, *34*, 5169 – 5174.
[99] M. Yu, A. P. Nowak, T. J. Deming, *J. Am. Chem. Soc.* **1999**, *121*, 12210 – 12211.
[100] H. Cui, V. Krikorian, J. Thompson, A. P. Nowak, T. J. Deming, D. J. Pochan, *Macromolecules* **2005**, *38*, 7371 – 7377.
[101] J. N. Cha, H. Birkedal, L. E. Euliss, M. H. Bartl, M. S. Wong, T. J. Deming, G. D. Stucky, *J. Am. Chem. Soc.* **2003**, *125*, 8285 – 8289.
[102] J. R. Cha, G. D. Stucky, D. E. Morse, T. J. Deming, *Nature* **2000**, *403*, 289 – 292.
[103] A. P. Nowak, V. Breedeveld, L. Pakstis, B. Ozbas, D. J. Pine, D. Pochan, T. J. Deming, *Nature* **2002**, *417*, 424 – 428.
[104] L. E. Euliss, S. G. Granckarov, S. O'Brien, T. J. Deming, G. D. Stucky, G. B. Murray, G. A. Held, *Nano Lett.* **2003**, *3*, 1489 – 1493.
[105] L. M. Pakstis, B. Ozbas, K. D. Hales, A. P. Nowak, T. J. Deming, D. Pochan, *Biomacromolecules* **2004**, *5*, 312 – 318.
[106] A. P. Nowak, V. Breedeveld, D. J. Pine, T. J. Deming, *J. Am. Chem. Soc.* **2003**, *125*, 15666 – 15670.
[107] L. E. Euliss, R. M. Trnka, T. J. Deming, G. D. Stucky, *Chem. Commun.* **2004**, *15*, 1736 – 1737.
[108] V. Breedeveld, A. P. Nowak, J. Sato, T. J. Deming, D. J. Pine, *Macromolecules* **2004**, *37*, 3943 – 3952.
[109] E. G. Bellomo, M. D. Wyrsta, L. Pakstis, D. J. Pochan, T. J. Deming, *Nat. Mater.* **2004**, *3*, 244 – 248.
[110] T. J. Deming, *Phys. Rev. E* **2005**, *1*, 28 – 35.
[111] K. R. Brzezinska, T. J. Deming, *Macromol. Biosci.* **2004**, *4*, 566 – 569.
[112] K. R. Brzezinska, T. J. Deming, *Macromolecules* **2001**, *34*, 4348 – 4354.
[113] K. R. Brzezinska, S. A. Curtin, T. J. Deming, *Macromolecules* **2002**, *35*, 2970 – 2976.
[114] A.-B. Luximon, S. Jhurry, J. Belleney, V. Grury, *Macromolecules* **2003**, *36*, 977 – 982.
[115] L. Bilek, J. Darkosch, H. Michl, F. Wessely, *Monatsh. Chem.* **1953**, *84*, 718.
[116] H. R. Kricheldorf, C. von Lossow, G. Schwarz, *J. Polym. Sci. Part A* **2005**, *43*, 5690 – 5698.
[117] H. R. Kricheldorf, C. von Lossow, G. Schwarz, *J. Polym. Sci. Part A*, *Polym Chem.* **2006**, *44*, 4680 – 4695.
[118] H. R. Kricheldorf, C. von Lossow, G. Schwarz, *Macromolecules* **2005**, *38*, 5513.
[119] H. R. Kricheldorf, C. von Lossow, G. Schwarz, *Pure Appl. Chem.*, in press
[120] H. R. Kricheldorf, C. von Lossow, G. Schwarz, *Macromol. Chem. Phys.* **2005**, *206*, 1165 – 1170.
[121] F. Rypacek, M. Dvorak, I. Stefko, L. Machova, V. Sharda, D. Kubics, *ACS Symp. Ser.* **2001**, *265*–275 – 278.
[122] N. Higashi, T. Koga, M. Niwa, *Langmuir* **2000**, *16*, 3482 – 3486.
[123] G. Guillemain, B. Gallot, *Macromol. Chem. Phys.* **2002**, *203*, 1346 – 1356.
[124] G. Guillemain, B. Gallot, *Liq. Cryst.* **2002**, *29*, 141 – 153.
[125] M. Sisido, A. Okamoto, S. Eguro, Y. Imanishi, *Polym. J.* **1985**, *17*, 1253 – 1261.
[126] K. Aoi, K. Tsutsumichi, M. Okada, *Macromolecules* **1994**, *27*, 875 – 877.
[127] V. Goury, D. Jhurry, A. Bhaw-Luximon, B. M. Novak, J. Bellemy, *Biomacromolecules* **2005**, *6*, 1987 – 1991.
[128] P. Papadopoulos, G. Floudas, *Biomacromolecules* **2005**, *6*, 2352 – 2361.
[129] A. Douvy, B. Gallot, *Polymer* **1987**, *28*, 147 – 154.
[130] M. Sisido, T. Matsubara, H. Shinohara, *Pept. Chem.* **1996**, *34*, 473 – 476.
[131] T. Matsubara, H. Shinohara, M. Sisido, *Macromolecules* **1997**, *30*, 2651 – 2656.
[132] C.-S. Cho, J.-W. Nah, Y.-I. Jeong, J.-B. Cheon, S. Asayama, H, Use, T. Akaik, *Polymer* **1999**, *40*, 6769 – 6775.
[133] G. Kim, D. Sohn, Y. C. Myoung, E. R. Kim, 220th ACS National Meeting, Book of Abstracts, **2000**.
[134] C. S. Cho, Y.-I. Jeong, S.-H. Kim, J.-W. Nah, M. Kubota, T. Komoto, *Polymer* **2000**, *41*, 5185 – 5193.


 © 2006 Wiley-VCH Verlag GmbH & Co. KGaA, Weinheim 

[135] G. Kim, J.-Y. Kim, D. Sohn, Y. Lee, *Macromol. Res.* **2002**, *10*, 49 – 52.
[136] J. F. Lutz, D. Schütt, S. Kubowicz, *Macromol. Rapid Commun.* **2005**, *26*, 23 – 28.
[137] H. F. Lee, H.-S. Sheu, V.-S. Jeng, C.-F. Huang, F.-C. Chang, *Macromolecules* **2005**, *38*, 6551 – 6558.
[138] G. Zhang, J. Ma, Y. Li, Y. Wang, *J. Biosci. J. Biomat. Sci. Polym. Ed.* **2003**, *14*, 1389 – 1400.
[139] I. Cho, J.-B. Kim, H.-J. Jung, *Polymer* **2003**, *44*, 5497 – 5500.
[140] A. Larasanifar, J. Samuel, G. S. Kwon, *Adv. Drug Delivery Rev.* **2002**, *54*, 169 – 173.
[141] C. Li, *Adv. Drug Delivery Rev.* **2002**, *54*, 695.
[142] Y. Kabizawa, K. Kataoka, *Adv. Drug Delivery Rev.* **2002**, *54*, 203.
[143] K. Tsutsumiuchi, K. Aoi, M. Okada, *Macromolecules* **1997**, *30*, 4013 – 4017.
[144] K. Naka, R. Yamashita, T. Nakamura, A. Okki, S. Macda, *Macromol. Chem. Phys.* **1997**, *198*, 89 – 100.
[145] J. B. Cheon, Y. I. Jeong, C.-S. Cho, *Polymer* **1999**, *40*, 2041 – 2050.
[146] B. Perly, A. Douy, B. Gallot, *Makromol. Chem.* **1976**, *177*, 2569 – 2589.
[147] B. Perly, A. Douy, B. Gallot, *C. R. Seances Acad. Sci. Ser. C* **1974**, *279*, 1109.
[148] M. Tanaka, A. Mon, Y. Imanishi, C. H. Bamford, *J. Biol. Macromol.* **1985**, *7*, 173 – 181.
[149] H. A. Klok, J. F. Langewalter, S. Lecomandoux, *Macromolecules* **2000**, *33*, 7819 – 7826.
[150] I. Dimitrov, H. Schlaad, *Chem. Commun.* **2003**, 2944 – 2945.
[151] M. Gotsche, H. Keul, H. Höcker, *Macromol. Chem.* **1995**, *196*, 3891 – 3903.
[152] H. Hrimuro, Y. Ohija, T. Ouchi, *Macromol. Rapid Commun.* **2004**, *25*, 743 – 747.
[153] S. Caillol, S. Lecomandoux, A.-F. Mingotand, M. Schappacher, A. Soum, N. Bryson, R. Meyrueix, *Macromolecules* **2003**, *36*, 1118 – 1124.
[154] C. Deng, G. Rong, H. Tian, Z. Fang, X. Claen, X. Jing, *Polymer* **2005**, *46*, 653 – 659.
[155] P. Degee, P. Dubois, R. Jerôme, P. Teyssié, *J. Polym. Sci. Part A* **1993**, *31*, 275 – 278.
[156] G. Rong, M. Deng, C. Deng, Z. Fang, L. Riao, X. Chen, X. Jing, *Biomacromolecules* **2003**, *4*, 1800 – 1804.
[157] H. R. Kricheldorf, K. Hauser, *Biomacromolecules* **2001**, *2*, 1110 – 1115.
[158] N. Nishioka, A. Teramoto, *Polym. J.* **1979**, *11*, 71 – 79.
[159] N. Minoura, S. Alba, Y. Fujiwara, *J. Am. Chem. Soc.* **1993**, *115*, 5902 – 5906.
[160] N. Minoura, M. Higuchi, *Macromolecules* **1997**, *30*, 1023 – 1027.
[161] H. Yokoi, S. Mizutani, T. Kinoshita, *Trans. Mater. Res. Soc. Jpn.* **2002**, *27*, 551 – 554.
[162] A. Nakajima, T. Hayashi, K. Kugo, K. Shinoda, *Macromolecules* **1979**, *12*, 840 – 843.
[163] A. Nakajima, K. Kugo, T. Kayashi, *Macromolecules* **1979**, *12*, 844 – 848.
[164] T. Nishimura, Y. Sato, M. Yokoyama, M. Okuya, K. Kataoka, T. Okano, Y. Sakurai, *Makromol. Chem.* **1984**, *185*, 2109 – 2116.
[165] C.-S. Cho, S.-W. Kim, *Makromol. Chem.* **1990**, *191*, 981 – 991.
[166] C.-S. Cho, B.-W. Jo, J.-K. Kwon, T. Kamoto, *Macromol. Chem. Phys.* **1994**, *198*, 2195 – 2206.
[167] G. Floudas, P. Papadopoulos, H. A. Klok, G. W. M. Vandermeulen, J. Rodriguez-Hernandez, *Macromolecules* **2003**, *36*, 3673 – 3683.
[168] Z. Yang, J. Yuan, S. Cheng, *Eur. Polym. J.* **2005**, *41*, 267 – 274.
[169] C.-S. Cho, Y.-I. Jeong, S.-H. Kim, J.-W. Nah, M. Kubote, T. Konoto, *Polymer* **2000**, *41*, 5185 – 5193.
[170] C.-S. Cho, Y.-I. Jeong, S.-H. Kim, J. W. Nah, Y.-M. Lee, I.-K. Kang, Y.-K. Sung, *Korea Polym. J.* **1999**, *7*, 203 – 207.
[171] D. Sogah, O. Rathore, *Polym. Prepr. Am. Chem. Soc. Div. Polym. Chem.* **2002**, *43*, 640 – 641.
[172] S. Uchida, T. Oohori, M. Suzuki, H. Shirai, *J. Polym. Sci. Part A* **1999**, *37*, 383 – 389.
[173] S. Uchida, T. Oohori, T. Tanaka, M. Suzuki, H. Shirai, *Macromol. Chem. Phys.* **1999**, *200*, 2645 – 2650.
[174] T. Niwa, H. Yokoi, T. Kinishita, S. Zhang, *Polym. J.* **2004**, *36*, 665 – 673.
[175] D. Bayley, M. R. Sancho, J. Brown, L. Brockman, K. Petrak, P. Goddard, A. Steward, *J. Bioact. Compat. Polym.* **1993**, *8*, 51 – 68.
[176] J. R. Hernandez, H.-A. Klok, *J. Polym. Sci. Part A* **2003**, *41*, 1167 – 1187.
[177] H. R. Kricheldorf, D. Müller, W. E. Hull, *Biopolymers* **1985**, *24*, 2113 – 2129.
[178] H. R. Kricheldorf, W. E. Hull, D. Müller, *Macromolecules* **1985**, *18*, 2135 – 2140.
[179] H. R. Kricheldorf, D. Müller, W. E. Hull, *Int. J. Biol. Macromol.* **1986**, *8*, 20 – 26.
[180] C. Uchida, Y. Iizuka, E. Ohta, K. Wakamatsu, M. Oya, *Bull. Acad. Vet. Fr. Bull. Soc. Chim. Soc. Jpn.* **1996**, *69*, 791 – 796.
[181] Y. Ohatsu, T. Watanabe, T. Goto, M. Wakita, *Bull. Chem. Soc. Jpn.* **1994**, *67*, 742 – 747.
[182] J. R. Hernandez, H.-A. Klok, *J. Polym. Sci. Part A* **2003**, *41*, 1167 – 1187.
[183] M. D. Wyrsta, A. L. Cogen, T. J. Deming, *J. Am. Chem. Soc.* **2001**, *123*, 12919 – 12920.
[184] M. Yu, J. Hwang, T. J. Deming, *J. Am. Chem. Soc.* **1999**, *21*, 5825 – 5826.
[185] M. Yu, T. J. Deming, *Macromolecules* **1998**, *31*, 4739 – 4745.
[186] M. Yu, T. J. Deming, *Polym. Mater. Sci. Eng.* **1998**, *79*, 248 – 249.
[187] D. S. Poché, W. H. Daly, F. S. Russo, *Polym. Prepr. Am. Chem. Soc. Div. Polym. Chem.* **1990**, *31*, 418 – 419; D. S. Poché, W. H. Daly, F. S. Russo, *Polym. Prepr. Am. Chem. Soc. Div. Polym. Chem.* **1990**, *31*, 639 – 640.
[188] K. Inoue, H. Sakai, S. Ochi, T. Itaya, T. Tanigaki, *J. Am. Chem. Soc.* **1994**, *116*, 10783 – 10784.
[189] K. Inoue, S. Honbe, M. Fukae, T. Muraki, E. Ihara, H. Kayame, *Macromol. Biosci.* **2003**, *3*, 26 – 33.
[190] H. A. Klok, J. R. Hernandez, S. Becker, K. Müllen, *J. Polym. Sci. Part A* **2001**, *39*, 1572 – 1583.
[191] T. Aliferis, H. Iatrou, N. Hadjichristidis, *J. Polym. Sci. Part A* **2005**, 43, 4670 – 4673.
[192] R. G. Denkewalter, J. Kole, W. J. Luckasavage, U.S. 4.289.872, **1981**.
[193] S. M. Aharoni, C. R. Crosby III, E. K. Walsh, *Macromolecules* **1982**, *15*, 1093.
[194] J. R. Hernandez, M. Gatti, H.-A. Klok, *Biomacromolecules* **2003**, *4*, 249 – 258.
[195] H. A. Klok, J. Rodriguez-Hernandez, *Macromolecules* **2002**, *35*, 8718 – 8723.
[196] M. Takaki, R. Asami, Y. Hunada, N. Ochiai, *Polym. Bull.* **1987**, *18*, 105 – 110.
[197] B. Zhong, K. Fischer, M. Schmidt, *Macromol. Chem. Phys.* **2005**, *206*, 157 – 162.
[198] J. Boulahia, F. Carrcese, H. Sekuguchi, *Makromol. Chem.* **1989**, *190*, 1975 – 1986.
[199] Y. Ohkatsu, E. Suzuki, T. Kusano, *Bunseki Kagaku Yakagaku* **1992**, *41*, 465 – 471.
[200] T. Migamoto, S. Takahashi, S. Tsuji, H. Ito, H. Inagaki, Y. Noishiki, *J. Appl. Polym. Sci.* **1986**, *31*, 2303 – 2314.
[201] K. Aoi, T. Hatanaka, K. Tsutsumiuchi, M. Okada, T. Imae, *Macromol. Rapid Commun.* **1999**, *20*, 378 – 382.
[202] K. D. Winne, S. Vanderkerken, K. Hoste, P. Dubruel, E. Schacht, *Polymer* **2004**, *19*, 367 – 382.
[203] K. Aoi, T. Hatanaka, K. Tsutsumiuchi, M. Okada, T. Imae, *Macromol. Rapid Commun.* **1999**, *20*, 378 – 382.

 © 2006 Wiley-VCH Verlag GmbH & Co. KGaA, Weinheim 

[204] D. Appelhaus, K. Kumber, R. Kirchner, J. Seidel, C. E. Huand, D. Voigt, D. Kucklong, E. C. Chang, B. Voit, *Macromol. Rapid Commun.* **2005**, *26*, 586 – 591.
[205] H.-Y. Tian, C. Deng, H. Lin, J. Sun, M. Deng, X. Chen, Y. Jing, *Biomaterials* **2005**, *26*, 4209 – 4217.
[206] G. Milov, D. Grekel-Kochler, A. Lübbert, W. M. Vandermeulen, A. Herrmann, H.-A. Klok, K. Müllen, *Bioconjugate Chem.* **2005**, *16*, 283 – 293.
[207] P. Witte, H. Menzel, *Macromol. Chem. Phys.* **2004**, *205*, 1735 – 1743.
[208] Z.-M. Liu, Z. K. Xu, J.-Q. Wang, Q. Yang, J. Wu, P. Seta, *Eur. Polym. J.* **2003**, *39*, 2291 – 2299.
[209] G. P. Robertson, M. D. Guiver, E. Bilodeau, M. Yoshikawa, *J. Polym. Sci. Part A* **2003**, *41*, 1316 – 1329.
[210] Y. Ito, Y. Ochiai, Y. S. Park, Y. Imanishi, *J. Am. Chem. Soc.* **1997**, *119*, 1619 – 1623.
[211] H.-T. Deng, Z.-K. Xu, J. Wu, P. Ye, Z.-M. Liu, P. Seta, *J. Mol. Catal. B* **2004**, *10*, 95 – 100.
[212] N. Tsubukawa, K. Kobayashi, Y. Sone, *Polym. J.* **1987**, *19*, 1147 – 1155.
[213] R.-H. Wiennga, E. A. Sierling, P. F. M. Geurts, P. J. Werkmann, E. J. Vorenkamp, V. Erb, M. Stamm, A. J. Shouten, *Langmuir* **2001**, *17*, 6477 – 6484.
[214] Y.-C. Chang, C. W. Frank, *Langmuir* **1998**, *14*, 326 – 334.
[215] V. K. Gupta, A. J. Williams, *Polym. Mater. Sci. Eng.* **2001**, *84*, 25 – 26.
[216] C. Robinson, J. C. Ward, R. B. Beevers, *Discuss. Faraday Soc.* **1958**, *25*, 29 – 31.
[217] D. B. DuPre, E. T. Samulski, *Liq. Cryst.: Fourth State Matter* (Conference Report), Marcel Dekker, New York, **1979**, pp. 203–247.
[218] E. T. Samulski, *Liq. Cryst. Order Polym.* (Conference Report), Academic Press, New York, **1978**, pp. 167–190.
[219] E. T. Samulski, *J. Chim. Phys. Phys.-Chim. Biol.* **1983**, *80*, 25 – 30.
[220] I. Uematsu, Y. Uematsu, *Adv. Polym. Sci.* **1984**, *59*, 37 – 73.
[221] C. Noel, *Makromol. Chem. Macromol. Symp.* **1988**, *22*, 95 – 139.
[222] C. Viney, *Protein Based Materials* (Conference Report), Birkhäuser, Boston, **1997**, pp. 281–311.
[223] S. H. Chen, H. Shi, J. C. Mastrangelo, J. J. Ou, *Prog. Polym. Sci.* **1996**, *21*, 1211 – 1233.
[224] G. Xue, *Prog. Polym. Sci.* **1997**, *22*, 313 – 406.
[225] E. Lizuka, *Int. J. Polym. Mater.* **2000**, *45*, 191 – 238.
[226] J. Lin, *Recent Progress in Polycondensation* (Conference Report), Research Signpost, Trivandrum, **2000**, pp. 209–226.
[227] G. Floudas, *Prog. Polym. Sci.* **2004**, *29*, 1143 – 1171.
[228] D. L. Patel, D. B. Pupre, *J. Chem. Phys.* **1980**, *72*, 2515.
[229] Y. Uematsu, I. Uematsu, *Polym. Prepr. Am. Chem. Soc. Div. Polym. Chem.* **1979**, *20*, 66 – 69.
[230] T. Hashimoto, S. Ebisu, N. Inaba, H. Kawai, *Polym. J.* **1981**, *13*, 701 – 713.
[231] T. Hashimoto, N. Inaba, S. Ebisu, H. Kawai, *Polym. J.* **1981**, *13*, 897 – 910.
[232] S. Itou, *Mol. Cryst. Liq. Cryst.* **1989**, *172*, 201 – 210.
[233] E. Iizuka, *Polym. Prepr. Am. Chem. Soc. Div. Polym. Chem.* **1979**, *20*, 78 – 81.
[234] E. Iizuka, *J. Appl. Polym. Sci. Appl. Polym. Symp.* **1985**, *41*, 131 – 147.
[235] C. L. Shiau, M. M. Labes, *Mol. Cryst. Liq. Cryst.* **1985**, *124*, 125 – 130.
[236] J. Watanabe, K. Sakajiri, K. Okoshi, S. Kawauchi, J. Mayoshi, *Macromol. Chem. Phys.* **2001**, *202*, 1004 – 1009.
[237] M. V. R. Rao, M. Atreyi, A. V. Pantar, *Liq. Cryst.* **1987**, *2*, 889 – 893.
[238] Y. Yin, C. Zhao, A. Sasaki, H. Kimura, K. Hideaki, S. Kuroki, I. Ando, *Macromolecules* **2002**, *35*, 5910 – 5915.
[239] I. Ando, Y. Yin, C. Zhao, S. Kuroki, *Polym. Prepr. Am. Chem. Soc. Div. Polym. Chem.* **2003**, *44*, 323 – 324.
[240] G. Kiss, R. S. Porter, *Mol. Cryst. Liq. Cryst.* **1980**, *60*, 267 – 280.
[241] G. Kiss, R. S. Porter, *J. Polym. Sci. Polym. Phys. Ed.* **1980**, *18*, 361 – 388.
[242] T. Asada, T. Tanaka, S. Onogi, *J. Appl. Polym. Sci. Appl. Polym. Symp.* **1985**, *41*, 229 – 239.
[243] M. A. Osipov, *Chem. Phys.* **1985**, *86*, 259 – 270.
[244] C. E. Chaffey, R. S. Porter, *J. Rheol.* **1985**, *29*, 281 – 305.
[245] M. Ballauf, *Macromolecules* **1986**, *19*, 1366 – 1374.
[246] A. V. Emelyanenko, *Phys. Rev. E* **2003**, *67*, 031704.
[247] K. Hanabasa, C. Kobayashi, T. Koyama, E. Masuda, H. Shirai, Y. Kondo, K. Takemoto, E. Iizuka, N. Hojo, *Makromol. Chem.* **1986**, *18*, 753 – 761.
[248] M. V. R. Rao, M. Atreyi, A. V. Pantar, *Liq. Cryst.* **1987**, *2*, 889 – 893.
[249] E. G. Bellomo, P. Davidson, M. Imperor-Clerc, T. J. Deming, *J. Am. Chem. Soc.* **2004**, *126*, 9101 – 9105.
[250] J. Halstroem, L. L. Chapoy, K. Kovacs, K. Brunfeldt, M. A. Quasim, *Proc. Eur. Pept. Symp.* **1981**, 759 – 767.
[251] T. Torii, T. Yamashita, H. Ushiki, K. Horie, *Eur. Polym. J.* **1993**, *29*, 465 – 467.
[252] A. Thierry, A. Skoulios, G. Lang, S. Forestier, *Mol. Cryst. Liq. Cryst.* **1978**, *41*, 125 – 128.
[253] R. Gehani, J. Watanabe, S. Kasuya, I. Uematsu, *Polym. J.* **1980**, *12*, 871 – 882.
[254] J. Watanabe, Y. Fukuda, R. Gehani, I. Uematsu, *Macromolecules* **1984**, *17*, 1004 – 1009.
[255] J. Watanabe, H. Ono, I. Uematsu, A. Abe, *Macromolecules* **1985**, *18*, 2141 – 2148.
[256] J. Watanabe, M. Goto, T. Nagase, *Macromolecules* **1987**, *20*, 284 – 304.
[257] J. Watanabe, T. Nagase, *Polym. J.* **1987**, *19*, 781 – 784.
[258] J. Watanabe, T. Nagase, *Macromolecules* **1988**, *21*, 171 – 175.
[259] J. Watanabe, T. Nagase, H. Ito, T. Ishii, T. Sato, *Mol. Cryst. Liq. Cryst.* **1988**, *164*, 135 – 143.
[260] J. Watanabe, T. Nagase, T. Ichizuka, *Polym. J.* **1990**, *22*, 1029 – 1033.
[261] J. Watanabe, Y. Takashina, *Macromolecules* **1991**, *24*, 3423 – 3426.
[262] J. Watanabe, Y. Takashina, *Polym. J.* **1992**, *24*, 709 – 713.
[263] J. Watanabe, T. Tominaga, *Macromolecules* **1993**, *26*, 4032.
[264] Y. Yin, C. Zhao, S. Kuroki, I. Ando, *J. Chem. Phys.* **2000**, *113*, 7635 – 7639.
[265] Y. Yin, C. Zhao, S. Kuroki, I. Ando, *Macromolecules* **2002**, *35*, 2335 – 2338.
[266] I. Ando, Y. Yige, C. Zhao, S. Kaneraka, S. Kuroki, *Macromol. Symp.* **2005**, *220*, 61 – 73.
[267] E. Neagu, R. Neagu, W. H. Daly, I. I. Nequlescu, *Trans. SAEST Trans. El. Insul.* **1993**, *28*, 122 – 127.
[268] E. Iizuka, S. Inoue, K. Hanabusa, H. Shirai, *Mol. Cryst. Liq. Cryst.* **1987**, *149*, 61 – 77.
[269] K. Hanabusa, K. Yanagisawa, J. Higashi, H. Shirai, T. Hayakawa, N. Hojo, *J. Polym. Sci. Part A* **1990**, *28*, 825 – 835.
[270] B. Gallot, M. Fafiotte, A. Fissi, O. Pieroni, *Macromol. Rapid Commun.* **1996**, *17*, 493 – 501.
[271] B. Gallot, M. Fafiotte, A. Fissi, O. Pieroni, *Liq. Cryst.* **1997**, *23*, 137 – 146.
[272] B. Gallot, C. Guillermain, A. Fissi, O. Pieroni, *Mol. Cryst. Liq. Cryst. Sci. Technol. Sect. A* **1999**, *330*, 1309 – 1317.
[273] R. Tredgold, R. Jones, *Langmuir* **1989**, *5*, 531 – 533.
[274] A. Shibata, Y. Bekku, S. Ueno, T. Yamashitu, *Langmuir* **1994**, *10*, 3723 – 3726.
[275] S. Ishihara, F. Yokotani, Y. Matsuo, K. Morimoto, *Polymer* **1988**, *29*, 2141 – 2145.
[276] S. Sasaki, M. Painaku, *Macromolecules* **1990**, *23*, 4939 – 4943.

 © 2006 Wiley-VCH Verlag GmbH & Co. KGaA, Weinheim 

[277] C.-C. Yen, F. Araoka, M. Tokita, S. Kawauchi, B. Park, T. Byoungchoo, H. Takezoe, J. Watanabe, *Jpn. J. Appl. Phys. Part 1* **2004**, *43*, 7026 – 7031.
[278] Y. Sato, M. Hatano, *Makromol. Chem.* **1982**, *183*, 997 – 1005.
[279] R. Pachter, S. S. Patnaik, R. L. Crane, W. W. Adams, *Proc. SPIE-Int. Soc. Opt. Eng.* **1993**, *1916*, 2 – 13.
[280] H. Wang, M. Jin, R. C. Jarnagen, E. T. Samulski, *Proc. SPIE-Int. Soc. Opt. Eng.* **1993**, *1853*, 89 – 98.
[281] Z. Tobarski, B. L. Epling, E. T. Samulski, T. M. Grinstead, T. M. Cooper, R. L. Crane, *Proc. SPIE-Int. Soc. Opt. Eng.* **1993**, *1853*, 68 – 73.
[282] Y. Bouligand, F. Livolant, *J. Phys.* **1984**, *45*, 1899 – 1923.
[283] H. R. Kricheldorf, L. Wahlen, K. Chen, *Macromol. Rapid Commun.* **1997**, *18*, 569 – 574.
[284] T. J. Deming, *Adv. Drug Delivery Rev.* **2002**, *54*, 1145 – 1155.
[285] D. Bayley, M. R. Sancho, J. Brown, L. Brookman, K. Petrak, P. Goddard, A. Steward, *J. Bioact. Compat. Polym.* **1993**, *8*, 51 – 68.
[286] K. de Winne, S. Vanderkerken, K. Hoste, P. Dubruel, E. Schacht, M. Jelinkova, B. Rihova, *J. Bioact. Compat. Polym.* **2004**, *19*, 367 – 382.
[287] T. Miyamoto, S. Takahashi, H. Ito, H. Inagaki, Y. Noishiki, *J. Appl. Polym. Sci.* **1986**, *31*, 2303 – 2314.
[288] J.-K. Hong, Y.-R. Choi, M.-H. Lee, C.-H. Ahn, 229th ACS Nat. Meeting, March 13 – 17, **2005**, Book of Abstracts.
[289] C. Li, D. F. Yu, R. A. Newman, F. Chabral, L. C. Stephens, N. Honter, L. Milas, S. Wallace, *Cancer Res.* **1998**, *58*, 2404 – 2409.
[290] V. A. Studden, *Proc. Am. Assoc. Cancer Res.* **2001**, *42*, 2883.
[291] P. Sabbatini, *Proc. Am. Soc. Clin. Oncol.* **2002**, 871.
[292] S. Schaffer, *Proc. Am. Assoc. Cancer Res.* **2002**, *43*, 2067.
[293] K. Kataoka, G. S. Kwon, M. Yokoyama, T. Okano, Y. Sakorai, *J. Controlled Release* **1993**, *24*, 119 – 132.
[294] T. Nakanishi, S. Fukushima, K. Okamoto, M. Suzuki, Y. Matsumara, M. Yokoyama, T. Okano, Y. Sakurai, K. Kataoka, *J. Controlled Release* **2001**, *74*, 295 – 302.
[295] G. Poliliquen, R. Meyrueix, O. Soula (Flamel Technol), Fr, Dem. 2862541, **2005**.
[296] R. Soula, P. Y. Chan, O. Soula, O. Breyne (Flamel Technol), Fr. Dem. 2860516, **2005**.
[297] S. Angot, O. Breyne, Y. P. Chan (Flamel Technol), Fr. Dem. 2855521, **2004**.
[298] S. Angot, Y. P. Chan, G. Soula (Flamel Technol), Fr. Dem. PfO 2004060968, **2004**.
[299] M. Selu, *Int. Rev. Immunol.* **1999**, *18*, 201 – 216.
[300] R. Aharoni, D. Teitelbaum, R. Arnon, M. Sela, *Proc. Natl. Acad. Sci. USA* **1999**, *96*, 634 – 639.
[301] D. Teitelbaum, R. Arnon, M. Sela, *Proc. Natl. Acad. Sci. USA* **1999**, *96*, 3842 – 3847.
[302] K. P. Johnson, *J. Neurol.* **1996**, *243*(Suppl. 1), 3 – 7.
[303] K. W. Ehler, *J. Org. Chem.* ***1976***, *41*, 3041 – 3042.
[304] K. W. Ehler, L. E. Orgel, *Biochim. Biophys. Acta* **1976**, *434*, 233 – 243.
[305] T. Wieland, F. Jaenicke, *Justus Liebigs Ann. Chem.* **1956**, *599*, 125 – 130.
[306] R. W. Hay, L. Main, *Aust. J. Chem.* **1968**, *21*, 155 – 169.
[307] A. Brack, *Biosystems* **1982**, *15*, 201 – 207.
[308] J. C. Lacey, N. Senaratne, D. W. Mullins, *Origins Life* **1984**, *15*, 45 – 54.
[309] D. W. Mullins, N. Senaratne, J. C. Lacey, *Origins Life* **1984**, *14*, 597 – 604.
[310] A. Brack, *Origins Life* **1987**, *17*, 367 – 379.
[311] V. V. Korshak, K. T. Poroshin, T. D. Kuzarenko, *Izv. Akad. Nauk. USSR Otdel Khim. Nautz.* **1954**, 663 – 669.
[312] T. D. Kozarenko, K. T. Poroshin, Yu. I. Khuryin, *Izv. Akad. Nauk* **1957**, 640 – 642.
[313] M. Paecht-Horowitz, J. Berger, A. Kutchalsi, *Nature* **1970**, *228*, 636 – 639.
[314] D. W. Armstrong, R. Segain, C. J. McNeal, R. D. Farlane, J. H. Fendler, *J. Am. Chem. Soc.* **1978**, *100*, 4605 – 4606.
[315] A. Brack, *Origins Life* **1984**, *14*, 229 – 236.
[316] G. Zieboll, L. E. Orgel, *J. Mol. Evol.* **1994**, *38*, 561 – 565.
[317] C. Böhler, A. R. Hill, Jr., L. E. Orgel, *Origins Life Evol. Biosphere* **1996**, *26*, 1 – 5.
[318] A. R. Hill, Jr., L. E. Orgel, *Origins Life Evol. Biosphere* **1996**, *26*, 539 – 545.
[319] A. R. Hill, Jr., C. Böhler, L. E. Orgel, *Origins Life Evol. Biosphere* **1998**, *28*, 235 – 243.
[320] R. Liu, L. E. Orgel, *Origins Life Evol. Biosphere* **1998**, *28*, 47 – 60.
[321] R. Liu, L. E. Orgel, *Origins Life Evol. Biosphere* **1998**, *28*, 245 – 257.
[322] J. P. Ferris, A. R. Hill, Jr., R. Liu, L. E. Orgel, *Nature*, **1996**, *381*, 59 – 61.
[323] H. Collet, C. Bied, L. Mion, J. Taillades, A. Commeyras, *Tetrahedron Lett.* **1996**, *37*, 9043 – 9046.
[324] J. Taillades, I. Beuzelin, L. Garrel, V. Tobaciky, C. Bied, A. Commeyras, *Origins Life Evol. Biosphere* **1998**, *28*, 61 – 77.
[325] J. Taillades, H. Collet, L. Garrel, I. Beuzelin, L. Boiteau, H. Choukroun, A. Commeyras, *J. Mol. Evol.* **1999**, *48*, 638 – 645.
[326] A. Commeyras, H. Collet, L. Boiteau, J. Taillades, O. Vandenabeele-Trambouze, H. Cottet, J. P. Biron, R. Plasson, L. Miron, O. Lagrille, H. Martin, F. Seilsis, M. Dobrijevic, *Polym. Int.* **2002**, *51*, 661 – 665.
[327] R. Plasson, J.-P. Biron, H. Cottet, A. Commeyras, J. Taillades, *J. Chromatogr. A* **2002**, *952*, 239 – 248.
[328] R. Pascal, L. Boiteau, A. Commeyras, *Top. Curr. Chem.* **2005**, *259*, 69 – 122.
[329] J.-P. Biron, R. Pascal, *J. Am. Chem. Soc.* **2004**, *126*, 9198 – 9199.
[330] L. Leman, L. E. Orgel, M. R. Ghadiri, *Science* **2004**, *306*, 283 – 286.
[331] P. D. Bartlett, R. H. Jones, *J. Am. Chem. Soc.* **1957**, *79*, 2153 – 2159.
[332] P. D. Bartlett, D. C. Dittmer, *J. Am. Chem. Soc.* **1957**, *79*, 2159 – 2160.
[333] A. Brack, G. Spach, *J. Mol. Evol.* **1979**, *13*, 47 – 56.
[334] G. Spach, A. Brack, *J. Mol. Evol.* **1980**, *15*, 231 – 238.
[335] K. Goto, Y. Yamakawa, Y. Yoshida, T. Hayashi, *Seitai Zairyo* **1998**, *16*, 315 – 322.
[336] W. A. Bonner, N. E. Blair, *Z. Chem.* **1972**, *7*, 409.
[337] W. A. Bonner, M. A. van Dort, M. R. Yearion, H. D. Zeman, G. C. Li, *Isr. J. Chem.* **1977**, *15*, 89 – 95.
[338] J. J. Flores, W. A. Bonner, G. A. Massey, *J. Am. Chem. Soc.* **1977**, *99*, 3622 – 3625.
[339] P. R. Kavasmaneck, W. A. Bonner, *J. Am. Chem. Soc.* **1977**, *99*, 44 – 50.
[340] N. E. Blair, W. A. Bonner, *Origins Life* **1980**, *10*, 255 – 263.
[341] Y. Hashimoto, Y. Imanishi, *Biopolymers* **1981**, *20*, 489 – 505.
[342] M. Blocher, D. Liu, P. Walde, P. L. Luisi, *Macromolecules* **1999**, *32*, 7332 – 7334.
[343] M. Blocher, D. Liu, P. L. Luisi, *Macromolecules* **2000**, *33*, 5787 – 5796.
[344] M. Blocher, T. Hitz, P. L. Luisi, *Helv. Chim. Acta* **2001**, *84*, 842 – 848.
[345] T. Hitz, M. Blocher, P. Walde, P. L. Luisi, *Macromolecules* **2001**, *34*, 2443 – 2449.
[346] T. Hitz, P. L. Luisi, *Helv. Chim. Acta* **2002**, *85*, 3975 – 3983.
[347] T. Hitz, P. L. Luisi, *Helv. Chim. Acta* **2003**, *86*, 1423 – 1434.
[348] T. Hitz, P. L. Luisi, *Origins Life Evol. Biosphere* **2004**, *34*, 93 – 110.
[349] I. Weissbuch, H. Zepik, G. Bolbach, E. Shavit, M. Tang, T. R. Jensen, K. Kjaer, L. Leiserowitz, M. Lahav, *Chem. Eur. J.* **2004**, *10*, 1782 – 1994.
[350] J. G. Nery, G. Bolbach, I. Weissbuch, M. Lahav, *Chem. Eur. J.* **2005**, *11*, 3039 – 3048.


© 2006 Wiley-VCH Verlag GmbH & Co. KGaA, Weinheim

[351] D. S. Poché, M. J. Moore, J. L. Bowles, *Synth. Commun.* **1999**, *29*, 843 – 854.
[352] R. Seidemann, L. Dulog, *Makromol. Chem.* **1986**, *187*, 2545 – 2551.
[353] R. Seidemann, *Makromol. Chem.* **1989**, *190*, 1891 – 1902.
[354] C. Palomo, J. M. Aizpura, I. Ganoba, E. Maneiro, B. Odriozola, *J. Chem. Soc. Chem. Commun.* **1994**, 1505 – 1507.
[355] C. Palomo, M. Oiarbide, G. Mikel, I. Ganoba, J. I. Miranda, *Tetrahedron Lett.* **2001**, *42*, 8955 – 8957.
[356] P. A. Swain, B. L. Anderson, W. D. Fuller, F. Naider, M. Goodman, *React. Polym.* **1994**, *22*, 155 – 163.
[357] T. Hayakawa, K. Inouye, M. Katsuhito, A. Matsuzaki, H. Yamamoto, *Polym. J.* **1985**, *17*, 529 – 531.
[358] K. S. Rao, P. Lopointe, D. N. Mc Gregor, *Makromol. Chem.* **1993**, *194*, 1095 – 1104.
[359] R. Takago, S. Begum, A. Siraki, A. Yoneshige, K. Koyama, K. Ohkata, *Heterocycles* **2004**, *64*, 129 – 131.
[360] N. Ogata, *Macromol. Symp.* **1994**, *83*, 1 – 11.

 © 2006 Wiley-VCH Verlag GmbH & Co. KGaA, Weinheim 

Spin-Crossover Multilayers

DOI: 10.1002/anie.200601885

# Multilayer Sequential Assembly of Thin Films That Display Room-Temperature Spin Crossover with Hysteresis**

*Saioa Cobo, Gábor Molnár,* José Antonio Real, and Azzedine Bousseksou**

*Dedicated to Professor Jean-Jacques Bonnet*

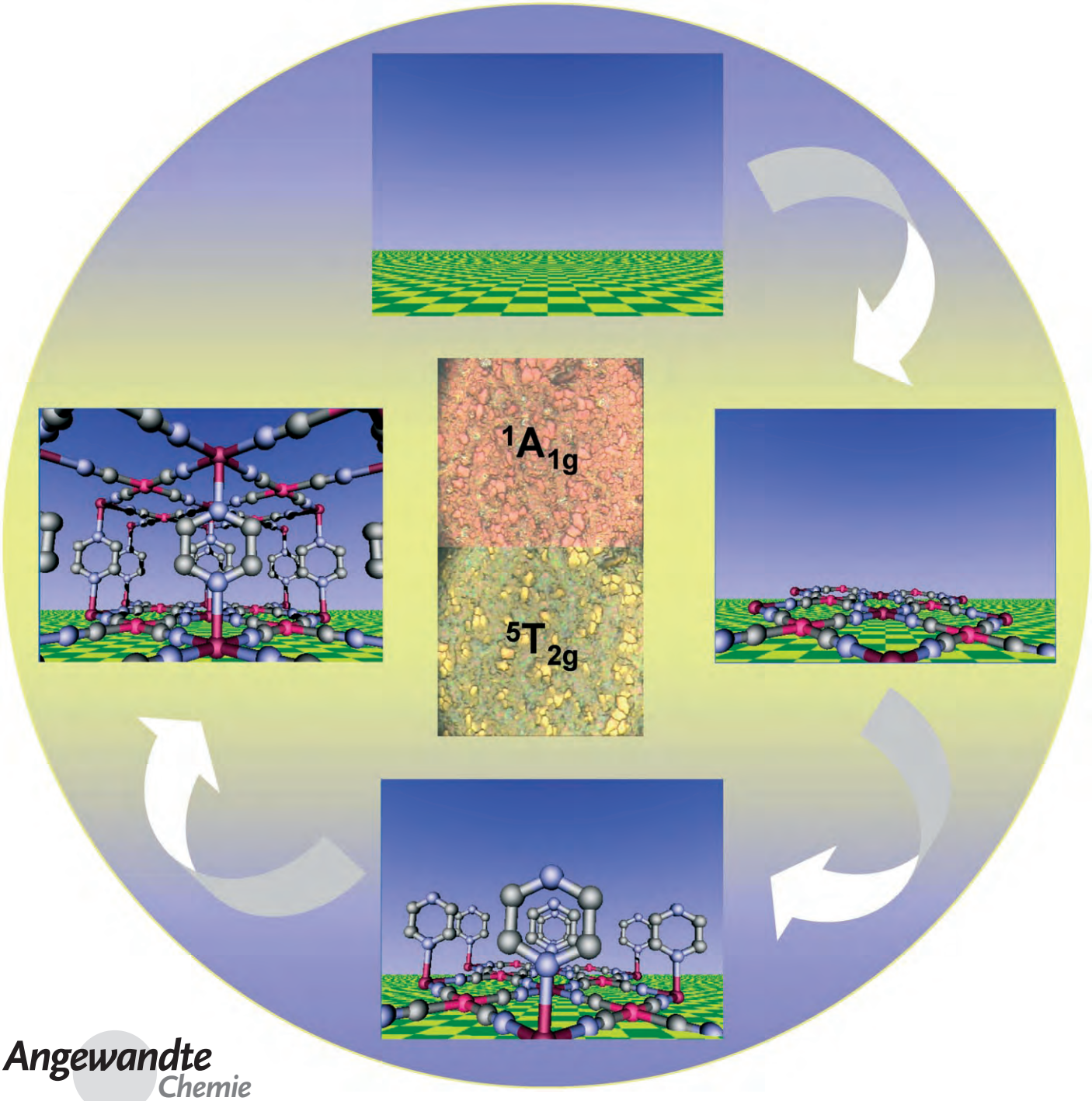




InterScience

© 2006 Wiley-VCH Verlag GmbH & Co. KGaA, Weinheim

The phenomenon of spin crossover between high-spin (HS) and low-spin (LS) states of $3d^4$–$3d^7$ transition-metal ions represents an important area of coordination chemistry.[1] Beside its theoretical aspects, the potential applications of this phenomenon also continue to draw attention.[2] In this context, we have recently shown that the change in spin state is accompanied also by a variation in the dielectric constant ($\varepsilon$) of the material and we could even observe room-temperature hysteresis of $\varepsilon$.[3] We suggested that this dielectric hysteresis property may be useful to build memory devices that can store information by high and low capacitance states. Further work by Freysz et al. and also by ourselves demonstrated that switching between the two spin states may be accomplished by using short (8-ns) laser pulses within the hysteresis region[4] and even at room temperature.[5]

These appealing properties cannot be exploited in bulk materials, but only if thin films of the compounds are prepared. However, up to now, very few examples for thin films of spin-crossover complexes have been reported.[6] These studies employed the Langmuir–Blodgett technique or a simple mixing of the complexes with polymers, which can be spin- or dip-coated onto surfaces. In any case, the resulting films were not purely composed of the spin-crossover complex but consisted of a mixture of the complex and a polymer or an amphiphile, which alters strongly the spin crossover as well as the dielectric and optical properties of the films.

In our quest to achieve thin layers of spin-crossover materials, our attention was drawn to an approach in which polymer multilayers were assembled on surfaces by using alternate adsorption of cations and anions.[7] This layer-by-layer assembly method has been extended to a variety of materials and allowed the deposition of dense, ultrathin films on diverse substrates, with precise control over the molecular arrangement and thicknesses on the nanometer scale. Though the assembly of films through transition-metal coordination reactions met more difficulties than the ionic route, a number of examples for successful multilayer assembly through coordination bonding have been reported.[8] Inspired by these studies, especially those of Mallouk and co-workers,[8a,b] we report herein our successful deposition of the three-dimensional (3D) spin-crossover coordination polymers, [Fe(pyrazine){M(CN)$_4$}] (M = Ni, Pd, or Pt).

The multilayer thin films consist of planar polymeric sheets formed of square-planar tetracyanometalate ions connected by six-coordinate $Fe^{II}$ ions. Normal to these sheets, the iron ions are bridged by bidentate pyrazine ligands to form a 3D network (Figure 1). The assembly of the film

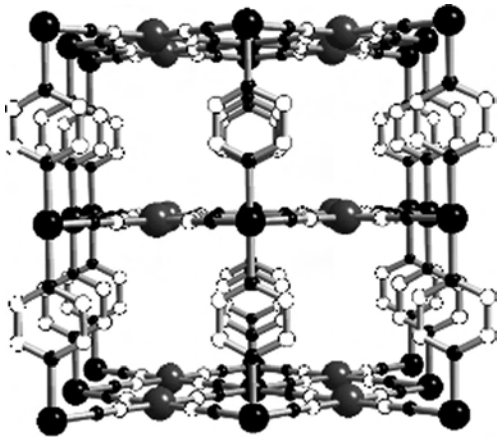

***Figure 1.*** Schematic drawing of the 3D coordination polymers [Fe(pyrazine){M(CN)$_4$}] (M = Ni, Pd, or Pt). M gray; Fe black (large); N black (small); C white.

involved the sequential dipping of the substrate into solutions of $Fe(BF_4)_2 \cdot 6H_2O$, $(TBA)_2M(CN)_4$ (M = Ni, Pd, or Pt; TBA = tetrabutylammonium), and pyrazine in ethanol (Scheme 1). To reduce the desorption rate of the coordinated species, the reactions were conducted at low temperature (−60 °C).

For the efficient adsorption of iron ions in the first adsorption cycle, the substrate surface must be modified by a monolayer of anchoring groups. We initially used mercapto-

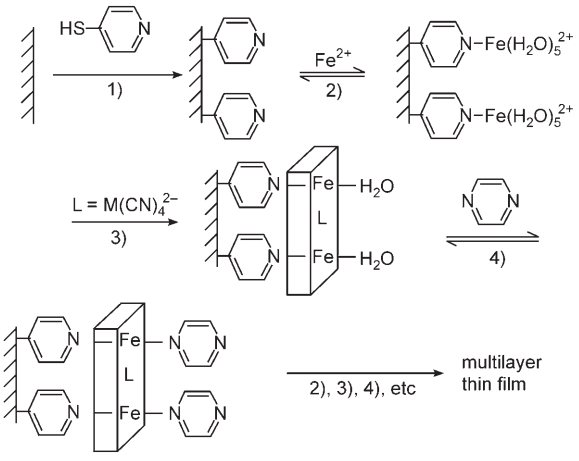


***Scheme 1.*** Sequential assembly of [Fe(pyrazine){M(CN)$_4$}] (M = Ni, Pd, or Pt) films.

[*] S. Cobo, Dr. G. Molnár, Dr. A. Bousseksou
Laboratoire de Chimie de Coordination, UPR8241
Centre National de la Recherche Scientifique
205, route de Narbonne, 31077 Toulouse (France)
Fax: (+33) 5-6155-3003
E-mail: molnar@lcc-toulouse.fr
boussek@lcc-toulouse.fr
Homepage: http://www.lcc-toulouse.fr
Prof. J. A. Real
Instituto de Ciencia Molecular/Departamento de Química Inorgánica
Universidad de Valencia
Edificio de Institutos de Paterna
P.O. Box 22085, 46071 Valencia (Spain)

[**] The authors are grateful to L. Rechignat (LCC-CNRS) and G. L. Agusti (ICMol) for experimental help. This work was supported by the Plateforme Technologique du LAAS CNRS (Toulouse, France). J.A.R. is grateful to the Spanish Ministerio de Educatión y Ciencia (MEC; CTQ 2004-03456/BQU).

Supporting information for this article is available on the WWW under http://www.angewandte.org or from the author.

 © 2006 Wiley-VCH Verlag GmbH & Co. KGaA, Weinheim 

pyridine or cystamine monolayers on gold, but the obtained films were rather discontinuous. Therefore, we introduced a templating film on the mercaptopyridine layer. This film was constructed on the substrate by dipping it into a solution of 4,4′-azopyridine instead of pyrazine (step 4 in Scheme 1). The 4,4′-azopyridine ligand assembles in the same way as the pyrazine analogue, but it was found to anchor more efficiently on the surface even at room temperature. The subsequent steps were performed as previously but using pyrazine in step 4. This strategy provides a surface layer whose chemistry and structure closely match that of the target compound [Fe(pyrazine){M(CN)$_4$}], allowing the "epitaxial" growth of continuous films of the latter (see Supporting Information).

To identify the compounds assembled in the thin films and to probe the spin state, we carried out Raman microscopy measurements. We have extensively employed this technique in the past to investigate the bulk form of these complexes.[9] The Raman spectra of these compounds exhibit CN stretching modes around 2200 cm$^{-1}$ and pyrazine internal modes between 600 and 1600 cm$^{-1}$. The lower frequency modes can be attributed primarily to metal–ligand vibrations and lattice phonons. Several vibrational modes may be followed to probe the change in spin state, but the most useful is probably the intense pyrazine in-plane bending mode, which exhibits a shift from 645 to 675 cm$^{-1}$ when going from the high-spin to the low-spin state.

Figure 2 shows Raman spectra of powder and film samples of [Fe(pyrazine){Pt(CN)$_4$}] recorded at 295 and 120 K. Spectra of the powder and film samples are virtually identical. Moreover, in the films we can easily recognize the frequency shifts that accompany the thermally induced spin crossover, in agreement with our previous assignments on bulk samples.[9b] The strong intensity enhancement of the pyrazine modes at 1230 and 1605 cm$^{-1}$ in the LS state is also confirmed in the multilayers. This phenomenon is probably related to the observed color change of the sample (yellow in the HS state; red in the LS state). Note that similar spectral changes were also observed in the Ni and Pd samples (see Supporting Information).

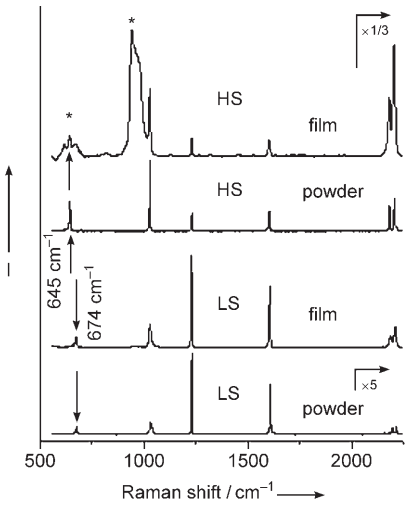


***Figure 2.*** Raman spectra of [Fe(pyrazine){Pt(CN)$_4$}] powder and film samples recorded in high-spin (HS; 295 K) and low-spin states (LS; 120 K). Asterisks indicate Raman scattering from the Si substrate.

Figure 3 shows the temperature dependence of the Raman intensity in the cooling and heating cycles for the powder and multilayer samples. (We chose the modes at 1025 and 1230 cm$^{-1}$ for their high intensity, but other Raman markers provided comparable results.) The powder sample reveals a hysteresis loop with a width of 25 K centered around 290 K. This hysteresis corresponds closely to the magnetic susceptibility measurements (Figure 3a). The multilayers display a hysteresis loop centered around 310 K also with a width of 25 K. The spin transition in the multilayers, however, is less abrupt and the square shape of the hysteresis is lost (Figure 3b). Similar observations were made for the Ni and Pd samples as well (see Supporting Information), which we can attribute to solvent effects. In fact, we have previously demonstrated that the spin-crossover behavior of powder samples depends in a dramatic fashion on the water content, and a heat treatment at 420 K is necessary to remove the water of crystallization.[5] Only the dehydrated powders exhibit wide, square-shaped hysteresis behavior. Annealing the film samples (which are prepared in ethanol, contrary to the powders) to 420 K influenced also the spin crossover in the multilayers, but we could not obtain abrupt spin transitions either as a result of residual solvent content or for other reasons, such as the extent of crystallinity of the films.

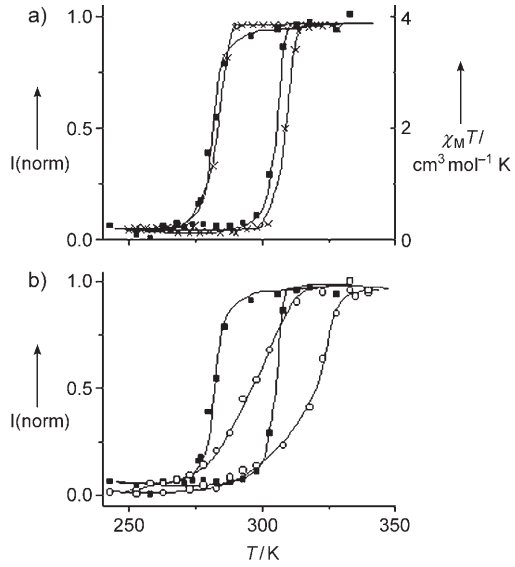


***Figure 3.*** a) Temperature dependence of the $\chi_M T$ product (×; $\chi_M$ is the molar magnetic susceptibility) and the normalized Raman intensity ratio (■; I(norm) = I(1025 cm$^{-1}$)/I(1230 cm$^{-1}$)) for [Fe(pyrazine){Pt(CN)$_4$}] powder upon cooling and heating. b) Temperature dependence of the normalized Raman intensity ratio (I(norm) = I(1025 cm$^{-1}$)/ I(1230 cm$^{-1}$)) for [Fe(pyrazine){Pt(CN)$_4$}] powder (■) and film samples (○) upon cooling and heating.

In summary, we have demonstrated a successful multilayer assembly of [Fe(pyrazine){M(CN)$_4$}] polymers through coordinate covalent bonding. To our knowledge, these

 © 2006 Wiley-VCH Verlag GmbH & Co. KGaA, Weinheim 

samples represent the first example of unmixed, multilayer thin films that display spin-crossover phenomenon. Of additional importance is the fact that this spin crossover occurs with hysteresis and around room temperature. We believe this result provides thus not only an alternative for exploring optical and dielectric properties of spin-crossover materials but also a novel platform for the construction of devices, which is the supreme goal of our research. Studies continue to optimize the growth and physical properties of these systems and also to extend this method for other compounds.

## Experimental Section

Powder samples were synthesized as described in Ref. [9a]. Thin films were assembled on 50-mm$^2$ gold surfaces (15-nm Au/2-nm Ti evaporated on polished Si wafers) as follows: The substrates were first functionalized by submersing them overnight into a solution of 1 mM mercaptopyridine (or cystamine) in ethanol. These wafers were soaked alternately (total of 5 cycles) in 100 mM $Fe(BF_4)_2$, 100 mM $(TBA)_2Ni(CN)_4$, and 100 mM 4,4′-azopyridine (synthesized according to Ref. [10]) in ethanol solutions (1 min) at room temperature, with rinsing in pure ethanol between steps (30 s). Then, the wafers were soaked alternately (total of 20 cycles) in 100 mM $Fe(BF_4)_2$, 100 mM $(TBA)_2M(CN)_4$ (where M = Ni, Pd, or Pt), and 100 mM pyrazine in ethanol solutions (1 min) at −60 °C, with rinsing in pure ethanol between steps (30 s). Finally, they were dried under Ar flow.

Variable-temperature magnetic susceptibility measurements were carried out at 325–225 K on the powder samples using an MPMS magnetometer (Quantum Design) operated at 1 T. Experimental susceptibilities were corrected for the diamagnetism of the constituent atoms by the use of Pascal's constants.

Variable-temperature Raman spectra were collected in the 150–2300 cm$^{-1}$ frequency range. Samples were enclosed under nitrogen atmosphere on the cold finger of a THMS600 (Linkam) liquid nitrogen cryostage. Before the measurements were taken, the samples were heated to 423 K during 30 min to eliminate residues of solvents. The LabRAM-HR (Jobin Yvon) Raman spectrometer used in these experiments consists of a BXFM (Olympus) optical microscope, a single-grating spectrograph (1800 grooves mm$^{-1}$, $f$ = 800 mm), and a DU420-OE (Andor) CCD detector. The entrance slit was kept at 100 mm, and a spectral resolution of ca. 1 cm$^{-1}$ was obtained. The 632.8 nm line of a 17-mW He/Ne laser was used as the excitation source, and plasma lines were removed by using a narrow-band interference filter. The exciting radiation was directed through a neutral density filter (OD = 2) to avoid sample heating and was focused on the sample through a ×50, 10.6-mm working-distance objective (NA = 0.5). The scattered light was collected in a back-scattering configuration using the same microscope objective, and the Rayleigh scattering was removed by means of a holographic notch filter.

Received: May 12, 2006
Published online: July 26, 2006

**Keywords:** coordination polymers · multilayer assemblies · Raman microscopy · spin crossover · thin films

[1] a) P. Gütlich, A. Hauser, H. Spiering, *Angew. Chem.* **1994**, *106*, 2109; *Angew. Chem. Int. Ed. Engl.* **1994**, *33*, 2024; b) "Spin Crossover in Transition Metal Compounds I–III": *Topics in Current Chemistry* (Eds.: P. Gütlich, H. A. Goodwin), *Vol. 233–235*, Springer, Heidelberg, **2004**; c) A. Bousseksou, G. Molnár, G. Matouzenko, *Eur. J. Inorg. Chem.* **2004**, 4353; d) J. A. Real, A. B. Gaspar, M. Carmen Munoz, *Dalton Trans.* **2005**, 2062.

[2] a) O. Kahn, J. Kröber, C. O. Jay, *Adv. Mater.* **1992**, *4*, 718; b) O. Kahn, C. J. Martinez, *Science* **1998**, *279*, 44; c) J.-F. Létard, P. Guionneau, L. Goux-Capes, *Top. Curr. Chem.* **2004**, *235*, 221.

[3] a) A. Bousseksou, G. Molnár, P. Demont, J. Menegotto, *J. Mater. Chem.* **2003**, *13*, 2069; b) "Molecular Memory and Method for Making Same": A. Bousseksou, C. Vieu, J.-F. Létard, P. Demont, J.-P. Tuchagues, L. Malaquin, J. Menegotto, L. Salmon, EP1430552, **2004**; c) S. Bonhommeau, T. Guillon, L. M. Lawson Daku, P. Demont, J. S. Costa, J.-F. Létard, G. Molnár, A. Bousseksou, *Angew. Chem.* **2006**, *118*, 1655; *Angew. Chem. Int. Ed.* **2006**, *45*, 1625.

[4] E. Freysz, S. Montant, S. Létard and J.-F. Létard, *Chem. Phys. Lett.* **2004**, *394*, 318.

[5] S. Bonhommeau, G. Molnár, A. Galet, A. Zwick, J.-A. Real, J. J. McGarvey, A. Bousseksou, *Angew. Chem.* **2005**, *117*, 4137; *Angew. Chem. Int. Ed.* **2005**, *44*, 4069.

[6] a) H. Soyer, C. Mingotaud, M.-L. Boillot, P. Delhaes, *Langmuir* **1998**, *14*, 5890; b) J.-F. Létard, O. Nguyen, H. Soyer, C. Mingotaud, P. Delhaès, O. Kahn, *Inorg. Chem.* **1999**, *38*, 3020; c) S.-W. Lee, J.-W. Lee, S.-H. Jeong, I.-W. Park, Y.-M. Kim, J.-I. Jin, *Synth. Met.* **2004**, *142*, 243; d) A. Nakamoto, Y. Ono, N. Kojima, D. Matsumura, T. Yokoyama, *Chem. Lett.* **2003**, *32*, 476.

[7] a) G. Decher, *Science* **1997**, *277*, 1232; b) *Multilayer Thin Films* (Eds.: G. Decher, J. B. Schlenoff), Wiley-VCH, Weinheim, **2003**.

[8] a) C. M. Bell, M. F. Arendt, L. Gomez, R. H. Schmeh, T. E. Mallouk, *J. Am. Chem. Soc.* **1994**, *116*, 8314; b) C. M. Bell, S. W. Keller, V. M. Lynch, T. E. Mallouk, *Mater. Chem. Phys.* **1993**, *35*, 225; c) C. Lin, C. R. Kagan, *J. Am. Chem. Soc.* **2003**, *125*, 336; d) M. A. Ansell, A. C. Zeppenfeld, K. Yoshimoto, E. B. Cogan, C. J. Page, *Chem. Mater.* **1996**, *8*, 591.

[9] a) V. Niel, J. M. Martínez-Agudo, M. C. Muñoz, A. B. Gaspar, J.-A. Real, *Inorg. Chem.* **2001**, *40*, 3838; b) G. Molnár, V. Niel, A. B. Gaspar, J.-A. Real, A. Zwick, A. Bousseksou, J. J. McGarvey, *J. Phys. Chem. B* **2002**, *106*, 9701; c) G. Molnár, V. Niel, J.-A. Real, L. Dubrovinsky, A. Bousseksou, J. J. McGarvey, *J. Phys. Chem. B* **2003**, *107*, 3149; d) T. Tayagaki, A. Galet, G. Molnár, M. Carmen Muñoz, A. Zwick, K. Tanaka, J. A. Real, A. Bousseksou, *J. Phys. Chem. B* **2005**, *109*, 14859; e) G. Molnar, A. Zwick, A. Bousseksou, J. J. McGarvey, *Chem. Phys. Lett.* **2003**, *367*, 593.

[10] J.-P. Launay, M. Tourrel-Pagis, J.-F. Lipskier, V. Marvaud, C. Joachim, *Inorg. Chem.* **1991**, *30*, 1033.

 © 2006 Wiley-VCH Verlag GmbH & Co. KGaA, Weinheim 

Hexacyclinol

DOI: 10.1002/anie.200602854

# Total Synthesis and Structure Assignment of (+)-Hexacyclinol**

*John A. Porco, Jr.,* Shun Su, Xiaoguang Lei, Sujata Bardhan, and Scott D. Rychnovsky*

The structurally novel antiproliferative metabolite, hexacyclinol (**1**; Scheme 1) was isolated in 2002 by Gräfe and co-workers from *Panus rudis* strain HKI 0254.[1] The proposed structure contains both reactive epoxyketone and highly strained endoperoxide moieties. A synthesis of the structure proposed by Gräfe and co-workers, as well as preliminary evaluation of non-peroxide-containing precursors as antimalarial agents, was recently reported by La Clair.[2] Recently, one of us[3] proposed an alternative structure of hexacyclinol (**2**; Scheme 1) based on calculated $^{13}C$ NMR chemical shift correlations. This structure was proposed to arise from acid-catalyzed rearrangement of the ubiquitin-activating enzyme inhibitor, panepophenanthrin (**3**), also isolated from the mushroom strain *Panus rudis* Fr. IFO8994.[4] In light of our prior synthesis of **3** and access to the natural product as well as chiral, nonracemic epoxyquinol monomer precursors,[5] we initiated studies to prepare proposed structure **2**. Herein, we report the total synthesis of the revised (+)-hexacyclinol structure **2** and confirmation of the proposed reassignment of the natural product. The synthesis is designed around the highly stereoselective Diels–Alder dimerization of an epoxyquinol monomer, followed by an intramolecular acid-catalyzed cyclization.

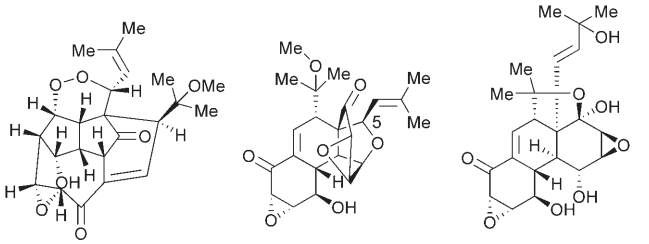


***Scheme 1.*** Structures of hexacyclinol and panepophenanthrin (**3**).

Our initial studies involved treatment of synthetic **3** with methanol under acidic conditions to determine the feasibility of further transformation to **2**. As noted previously,[3] this tactic was based on the proposal that hexacyclinol may arise from panepophenanthrin as an isolation artifact formed by the use of silica gel and methanol during the isolation of the natural product. However, treatment of synthetic (+)-**3** under a variety of acidic conditions (e.g., $SiO_2$ or K10 clay in MeOH or $CHCl_3$/MeOH mixtures at room temperature) did not lead to observable conversion into **2** or other products. As we have noted earlier,[5] the hemiacetal structure of **3** "locks" the dimeric framework, thus preventing further ring opening to the corresponding hydroxyketone under acidic conditions.

We thus revised our synthetic route as depicted in Scheme 2. Structure **2** may be derived from dimeric precursor **4** by intramolecular acid-catalyzed demethoxylation.[6] "Pre-hexacyclinol" (**4**) may be derived from highly selective *exo*-Diels–Alder dimerization[5] of epoxyquinol monomer **5**, a rearranged allylic ether formally derived from the natural product panepoxydon (**6**).[7]

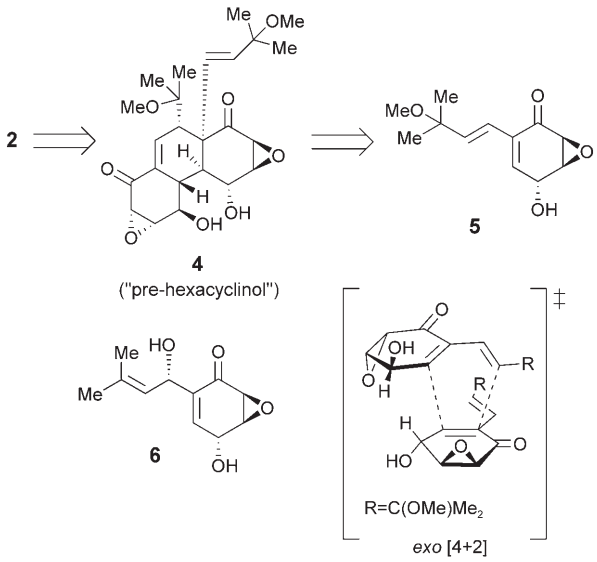


***Scheme 2.*** Revised retrosynthetic analysis for hexacyclinol (**2**).

The synthesis of epoxyquinol diene monomer **5** was initiated from the readily available *anti*-epoxy alcohol **7**[5] (Scheme 3). For initial studies, we employed (±)-**7** to develop the synthetic route. Ketal deprotection of **7** with Montmorillonite K10 clay in $CH_2Cl_2$[8] cleanly afforded an intermediate

[*] Prof. Dr. J. A. Porco, Jr., S. Su, X. Lei, S. Bardhan
Department of Chemistry and
Center for Chemical Methodology and Library Development
Boston University
590 Commonwealth Avenue, Boston, MA 02215 (USA)
Fax: (+1) 617-358-2847
E-mail: porco@bu.edu
Prof. Dr. S. D. Rychnovsky
Department of Chemistry
University of California—Irvine
Irvine, CA 92697-2025 (USA)

[**] We thank Mr. Andrew Germain (Boston University) for helpful discussions, Dr. Friedrich A. Gollmick (Leibniz Institute for Natural Products Research and Infection Biology—Hans-Knöll-Institute, Jena, Germany) for providing spectra of natural hexacyclinol, and Dr. Emil Lobkovsky (Cornell University) for X-ray crystal structure analysis. Financial support from the NIH (GM62842 and P50 GM067041), Bristol-Myers Squibb, Merck, and Novartis is gratefully acknowledged.

Supporting information for this article is available on the WWW under http://www.angewandte.org or from the author.


InterScience
© 2006 Wiley-VCH Verlag GmbH & Co. KGaA, Weinheim

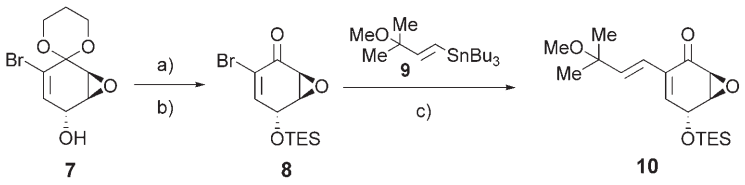


***Scheme 3.*** a) K10 clay, $CH_2Cl_2$, 6 h, 98%; b) $Et_3SiCl$, 2,6-lutidine, DMAP (cat.), $CH_2Cl_2$, 83%; c) $[Pd_2(dba)_3]$, $AsPh_3$, toluene, 110°C, 1 h, 96%. dba = dibenzylideneacetone; DMAP = 4-dimethylaminopyridine; TES = triethylsilyl.

epoxyketone (bromoxone),[9] which was protected[10] to afford triethylsilyl ether **8**.[11] In line with a report by Baldwin and coworkers in their synthesis of panepophenanthrin,[10] we elected to utilize Stille coupling for installation of the allylic ether side chain. The requisite vinyl stannane coupling partner **9** was prepared by hydrostannylation of 3-methoxy-3-methyl-1-butyne[12] using Guibé's conditions.[13] Cross-coupling of **8** with **9** was cleanly effected using our previously reported conditions for coupling of related epoxyketone substrates[14] ($[Pd_2(dba)_3]$, $AsPh_3$) to afford the silyl-protected monomer **10** (96%).

As anticipated, monomer **10** partially dimerized upon standing without solvent (25°C). Accordingly, after chromatography **10** was immediately deprotected with $Et_3N{\cdot}3HF$ (TREAT-HF)[7b,15] in $CH_3CN$ to give a mixture of monomer **5**

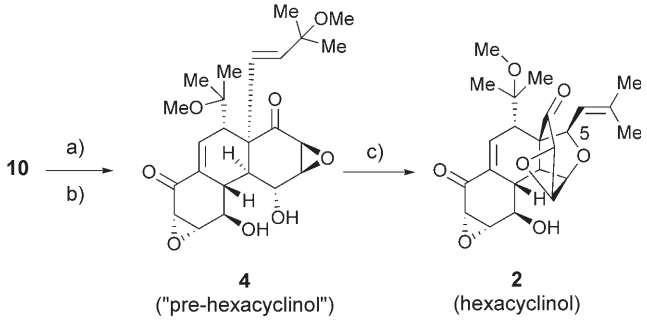


***Scheme 4.*** a) $Et_3N{\cdot}3HF$, $CH_3CN$, 0°C→RT, 15 min; b) neat, room temperature, 72 h, 87% (two steps); c) K10 clay, EtOAc, room temperature, 99%.

and a trace amount of dimer **4**, which was allowed to further stand at room temperature (neat, 72 h; Scheme 4). Under these conditions, "pre-hexacyclinol" (**4**) was cleanly obtained in 87% yield as a single diastereomer.[5,10] To assess the transformation[7] of panepoxydon (**6**) to monomeric precursor **5**, we treated commercially available[16] **6** with K10 clay in $CD_3OD$ (40°C, 10 h) which afforded epoxyquinol diene monomer **5** (60% conversion according to $^1H$ NMR spectroscopy).[11]

After considerable experimentation, we found that the final $S_N2'$ substitution/cyclization of **4** to hexacyclinol (**2**) was efficiently mediated by K10 clay[17] (EtOAc, room temperature, 3 min, 99%). Synthetic **2** was confirmed to be identical to spectral data ($^1H$, $^{13}C$ NMR) reported by Gräfe and co-workers.[1] X-ray crystal structure analysis fully confirmed the structural framework, including the configuration at the newly created C-5 stereocenter (Figure 1).[11] Interestingly, ±-**2** crystallized as a centrosymmetric racemate ($P\bar{1}$ space group) in a similar fashion to an "open" dimer prepared during our panepophenanthrin synthesis.[5] Examination of the X-ray crystal structure of **2** shows that the $S_N2'$

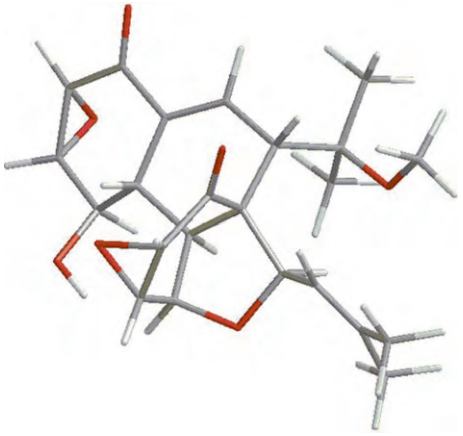

***Figure 1.*** X-ray crystal structure analysis of synthetic **2** (O red, C dark gray, H pale gray).

cyclization places the prenyl substituent at C-5 in a pseudo equatorial orientation, which minimizes steric interactions on the envelope conformation of the tetrahydrofuran ring.

Beginning with chiral, nonracemic (+)-**7** (93% *ee*)[11] we prepared (+)-hexacyclinol (**2**), for which analytical data were confirmed to be identical to those reported for natural (+)-hexacyclinol by $^1H$ and $^{13}C$ NMR spectroscopy and optical-rotation studies (synthetic **2**: $[\alpha]_D = +133.3°$, $c = 0.40$, $CH_3OH$).[11] Our synthesis thus confirms the absolute configuration of (+)-**2** and its relationship to (+)-panepophenanthrin (**3**).

Finally, we performed comparative thermolysis experiments on "pre-hexacyclinol" (**4**) and hexacyclinol (**2**; Scheme 5). Heating of dimer **4** ($[D_8]$toluene, 100°C, 12 h) led to quantitative production of a solution of monomer **5** ($^1H$ NMR spectroscopy). In contrast, thermolysis of **2** ($[D_8]$toluene, 100°C, 12 h) led to recovered starting material, indicating that the additional tetrahydrofuran ring of **2** serves to stabilize the pseudodimeric structure towards retro-[4+2] cycloaddition.

In summary, the first enantioselective total synthesis of the reassigned (+)-hexacyclinol structure **2** has been accomplished. Racemic **2** was found to crystallize as a centrosymmetric racemate ($P\bar{1}$ space group), which was crucial for unambiguous structural confirmation of the natural product. Our studies reinforce that hexacyclinol is likely an isolation artifact arising from acid-catalyzed rearrangement of panepoxydon, dimerization, and $S_N2'$ cyclization. Additional synthetic studies related to hexacyclinol, as well as biological

 © 2006 Wiley-VCH Verlag GmbH & Co. KGaA, Weinheim 

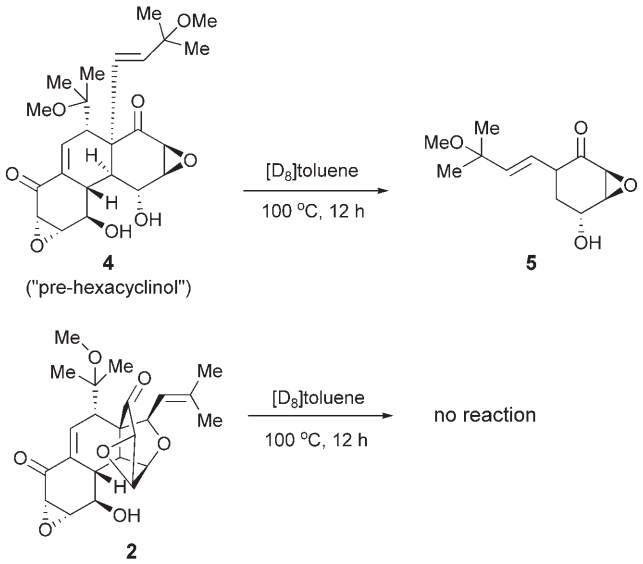


***Scheme 5.*** Comparative thermolysis experiments.

evaluation of **2** and derivatives, are in progress and will be reported in due course.

Received: July 18, 2006
Published online: July 27, 2006

**Keywords:** antiproliferative agents · cyclization · natural products · terpenoids · total synthesis

[1] B. Schlegel, A. Härtl, H.-M. Dahse, F. A. Gollmick, U. Gräfe, H. Dörfelt, B. Kappes, *J. Antibiot.* **2002**, *55*, 814.
[2] J. J. La Clair, *Angew. Chem.* **2006**, *118*, 2835; *Angew. Chem. Int. Ed.* **2006**, *45*, 2769.
[3] S. D. Rychnovsky, *Org. Lett.* **2006**, *8*, 2895.
[4] R. Sekizawa, S. Ikeno, H. Nakamura, H. Naganawa, S. Matsui, H. Iinuma, T. Takeuchi, *J. Nat. Prod.* **2002**, *65*, 1491.
[5] X. Lei, R. P. Johnson, J. A. Porco, Jr., *Angew. Chem.* **2003**, *115*, 4043; *Angew. Chem. Int. Ed.* **2003**, *42*, 3913.
[6] S. Taneja, V. Sethi, S. Andotra, K. Samar, S. Koul, G. Qazi, *Synth. Commun.* **2005**, *35*, 2297.
[7] a) Z. Kis, A. Closse, H. P. Sigg, L. Hruban, G. Snatzke, *Helv. Chim. Acta* **1970**, *53*, 1577; for the synthesis of (±)-panepoxydon and allylic alcohol transposition under mildly acidic conditions, see: b) J. B. Shotwell, S. Hu, E. Medina, M. Abe, R. Cole, C. M. Crews, J. L. Wood, *Tetrahedron Lett.* **2000**, *41*, 9639.
[8] E. C. L. Gautier, A. E. Graham, A. McKillop, S. P. Standen, R. J. K. Taylor, *Tetrahedron Lett.* **1997**, *38*, 1881.
[9] a) C. R. Johnson, M. W. Miller, *J. Org. Chem.* **1995**, *60*, 6674; b) O. Block, G. Klein, H.-J. Altenbach, D. J. Brauer, *J. Org. Chem.* **2000**, *65*, 716.
[10] J. E. Moses, L. Commeiras, J. E. Baldwin, R. M. Adlington, *Org. Lett.* **2003**, *5*, 2987.
[11] See Supporting Information for complete experimental details.
[12] L. T. Scott, G. J. DeCicco, J. L. Hyun, G. Reinhardt, *J. Am. Chem. Soc.* **1985**, *107*, 6546.
[13] H. X. Zhang, F. Guibé, G. Balavoine, *J. Org. Chem.* **1990**, *55*, 1857.
[14] C. Li, S. Bardhan, E. A. Pace, M.-C. Liang, T. D. Gilmore, J. A. Porco, Jr., *Org. Lett.* **2002**, *4*, 3267.
[15] M. A. Tius, H. Hu, J. K. Kawakami, J. Busch-Petersen, *J. Org. Chem.* **1998**, *63*, 5971.
[16] Panepoxydon (**6**) was obtained from Boston Biochem, Inc. (Cambridge, MA).
[17] a) For Montmorillonite K10 clay-catalyzed reactions of prenyl phenyl ethers, see: M. R. Dintzner, K. M. Morse, K. M. McClelland, D. M. Coligado, *Tetrahedron Lett.* **2004**, *45*, 79; b) for a review of clay-catalyzed organic transformations, see: M. D. Nikalje, P. Phukan, A. Sudalai, *Org. Prep. Proced. Int.* **2000**, *32*, 1–40.

 © 2006 Wiley-VCH Verlag GmbH & Co. KGaA, Weinheim 

Block Copolymers

DOI: 10.1002/anie.200602168

# Thermally Responsive Vesicles and Their Structural "Locking" through Polyelectrolyte Complex Formation**

*Yuting Li, Brad S. Lokitz, and Charles L. McCormick**

Vesicles composed of lipid molecules play an important role in several biological functions including the storage and transportation of small molecules.[1] Vesicles formed from the self-assembly of amphiphilic block copolymers are often more durable than conventional liposomes and have recently been the focus of research.[2–4] Among them, the chemically cross-linked vesicles reported by Du et al. are quite stable under extreme conditions.[5] Methods for vesicle formation from amphiphilic block copolymers typically involve the use of an organic solvent such as tetrahydrofuran, *N*,*N*-dimethylformamide (DMF), or dioxane[2,3,6] and require further purification, which can be time-consuming and problematic. Furthermore, the self-assembly is highly dependent on the rate of dialysis or the addition of another solvent, which is difficult to control. Recently, stimuli-responsive (pH-sensitive) block copolymers that self-assemble into vesicles without the addition of organic solvents have been reported.[7,8] Compared with pH-responsive materials, thermally responsive materials are advantageous for biological applications because of the stringent pH requirements in mammalian

[*] Dr. Y. Li, B. S. Lokitz, Prof. C. L. McCormick
Department of Polymer Science
University of Southern Mississippi
Hattiesburg, MS 39406-0076 (USA)
Fax: (+1) 601-266-5635
E-mail: charles.mccormick@usm.edu
Homepage: http://www.psrc.usm.edu/Mccormic.html

[**] Paper 123 in a series entitled "Water-Soluble Polymers". We gratefully acknowledge financial support provided by the Department of Energy (DE-FC26-01BC15317) and the MRSEC program of the National Science Foundation (DMR-0213883).

Supporting information for this article is available on the WWW under http://www.angewandte.org or from the author.


© 2006 Wiley-VCH Verlag GmbH & Co. KGaA, Weinheim

systems. Our group has a long-standing interest in the controlled polymerization of hydrophilic (meth)acrylamido monomers[9] and the self-assembly behavior of block copolymers in aqueous solutions.[10] Herein we report the first example of vesicle formation from the self-assembly of hydrophilic–hydrophilic block copolymers directly in water by variation of the solution temperature. The shells of the resultant vesicles were then cross-linked by polyelectrolyte complexation (Scheme 1).

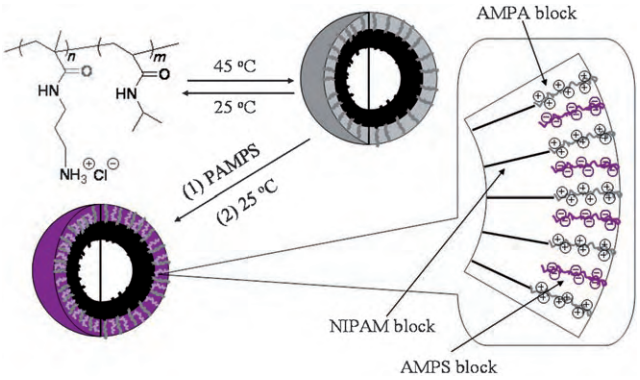


***Scheme 1.*** Schematic illustration of the formation of vesicles from PAMPA-PNIPAM diblock copolymers and their subsequent ionic cross-linking. PAMPS: poly(*N*-(3-aminopropyl)methacrylamide hydrochloride).

***Table 1:*** Block copolymers composition, molecular weight, and molecular-weight distribution.

| Entry | Structure | $M_n$ | $M_w/M_n$ |
|---|---|---|---|
| 1 | $AMPA_{40}$ | 7280[a] | 1.04 |
| 2 | $AMPA_{88}$ | 15700[a] | 1.06 |
| 3 | $AMPA_{40}$-$NIPAM_{34}$ | 11300[b] | 1.11 |
| 4 | $AMPA_{88}$-$NIPAM_{40}$ | 21200[b] | 1.13 |
| 5 | $AMPA_{88}$-$NIPAM_{50}$ | 22500[b] | 1.16 |
| 6 | $AMPA_{88}$-$NIPAM_{74}$ | 24100[b] | 1.19 |

[a] Measured by SEC in aqueous solution. [b] Measured by SEC in DMF (the AMPA block was first converted to the primary amine form).

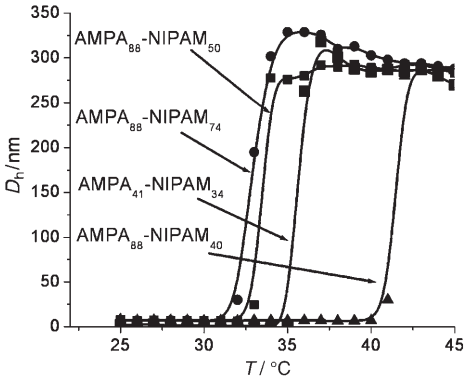


***Figure 1.*** Variation of hydrodynamic diameter with temperature for a 0.5% (w/w) aqueous solution of the diblock copolymers (heating rate = 0.1 °C min$^{-1}$).

The diblock copolymer poly(*N*-(3-aminopropyl)methacrylamide hydrochloride)-*block*-(*N*-isopropylacrylamide) (PAMPA-*b*-PNIPAM) was synthesized by the reversible addition–fragmentation chain-transfer (RAFT) polymerization technique (see the Supporting Information). AMPA was first polymerized in a dioxane/water mixture by employing 4-cyanopentanoic acid dithiobenzoate (CTP) as the chain-transfer agent (CTA) and 4,4′-azobis(4-cyanopentanoic acid) (V-501) as the free-radical source. The pH value of the solution was maintained between 4 and 5 to avoid hydrolysis and/or aminolysis of the CTA.[11] Under these conditions, the RAFT polymerization of AMPA is controlled (see the Supporting Information). The PAMPA homopolymer was then used as macroCTA for the block polymerization of NIPAM. Adjustment of the dioxane/water ratio allows the reaction to proceed under homogeneous conditions throughout the polymerization. Well-defined PAMPA-*b*-PNIPAM diblock copolymers were obtained (Table 1, see also the Supporting Information). The composition of the copolymer was calculated on the basis of size-exclusion chromatography (SEC) and $^1$H NMR data (Table 1).

The diblock copolymers were dissolved in aqueous solution at room temperature. Increasing the solution temperature led to the formation of uniform aggregates with diameters of approximately 280 nm (Figure 1). Since the contour length of the diblock copolymers is approximately 35 nm, vesicular rather than micellar structures were found. The phase-transition temperature was shown to be dependent on the composition of the block copolymer; polymers with longer NIPAM block lengths had lower phase-transition temperatures. If the NIPAM block length is kept constant, increasing the AMPA block length results in an increase in the phase-transition temperature. This is in agreement with recent results by Stover and co-workers[12] which showed that the lower critical solution temperature of NIPAM homopolymers is dependent on both the molecular weight of the polymer and hydrophilicity of the end group.

The heating rate near the phase-transition temperature is an important factor for vesicle formation. To obtain a uniform size distribution, the heating rate should be kept around 0.1 °C min$^{-1}$. This was found to be especially important at higher solution concentrations (5 mg mL$^{-1}$). For example, at 5 mg mL$^{-1}$, an increase in the solution temperature from 25 to 45 °C over 5 min leads to a broad size distribution. If the solution concentration is kept relatively low (< 0.5 mg mL$^{-1}$), faster heating rates can lead to uniform vesicles; however, the vesicles are smaller than those formed by a slow increase in the solution temperature (see the Supporting Information). The vesicles were shown to be stable, as their size remains constant above the phase-transition temperature. Thus, the vesicle self-assembly process seems to be kinetically controlled.

Figure 2 shows a TEM image of the vesicles formed from the $AMPA_{88}$-*b*-$NIPAM_{50}$ diblock copolymer. The number-average particle diameter of the vesicles in Figure 2 (left) is approximately 145 nm, which is slightly larger than the intensity-average diameter reported by dynamic light scattering (DLS; 118 nm) and suggests flattening of the vesicles adsorbed onto the TEM grid. The vesicle wall is estimated to

 © 2006 Wiley-VCH Verlag GmbH & Co. KGaA, Weinheim 

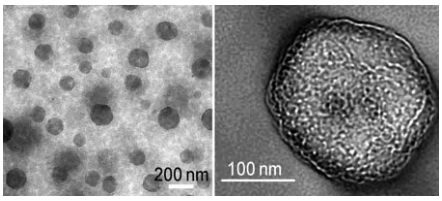


***Figure 2.*** TEM images of vesicles prepared from $PAMPA_{88}$-$PNIPAM_{50}$ from the fast increase of the solution temperature from 25 to 45 °C (left) and a single vesicle (right).

be 7 nm thick and is somewhat thinner than the contour length (12.5 nm) that was calculated for the hydrophobic $PNIPAM_{50}$ block.

The vesicles are stable between pH 0 and 11. However, the particle size was shown to vary with the pH of the solution (see the Supporting Information). At lower pH values, the vesicle was largest (310 nm at pH 3.0), and increasing the pH value of the solution decreased the size of the vesicles (e.g., 220 nm at pH 10.8). This is most likely caused by deprotonation of the AMPA block above its $pK_a$ value. The solution concentration was also shown to influence the size distribution of the vesicles (see the Supporting Information). The vesicles were larger at higher solution concentrations (283 nm, 0.5 %, 50 °C) than at lower solution concentrations (192 nm, 0.005 %, 50 °C).

The complexation of oppositely charged polyelectrolytes has been used extensively for layer-by-layer deposition and DNA condensation. Recently, Armes and co-workers successfully applied this technology to form shell cross-linked micelles.[13] The group used a block polyelectrolyte (anionically charged) to cross-link a cationically charged micelle and concluded that a homopolyelectrolyte cross-linker led only to the formation of flocculated micelles. Herein, we found that the anionic homopolymer poly(sodium 2-acrylamido-2-methylpropanesulfonate) (PAMPS, $M_n = 17000$, $M_w/M_n = 1.18$), synthesized by RAFT, can be used efficiently to cross-link cationicaly charged vesicles. The rapid mixing of the vesicle solution with the PAMPS solution at 45 °C leads to the formation of ionically cross-linked vesicles owing to the interpolyelectrolyte complexation of the PAMPA and PAMPS block (The AMPA/AMPS molar ratio was kept at 1:1). The vesicle size changes from 270 to 140 nm (Figure 3), which may be attributed to a decrease in the hydrophilicity of the APMA/AMPS block upon complexation; the vesicle morphologies remain the same.

After cross-linking, the solution was cooled to 25 °C. DLS indicated that the vesicles did not dissociate (Figure 3), which confirmed that the vesicle structure had been successfully "locked" by polyelectrolyte complexation. This conclusion was also confirmed by $^1$H NMR analysis (Figure 4). At 25 °C, the diblock copolymers are fully solvated and signals associated with each block are visible. An increase in the solution temperature to 45 °C causes the NIPAM signal to become broadened, which indicates the formation of vesicles (this is also confirmed by DLS; Figure 1). After cross-linking at 45 °C, the solution was cooled to 25 °C upon which the NIPAM signal regained its intensity as the NIPAM block

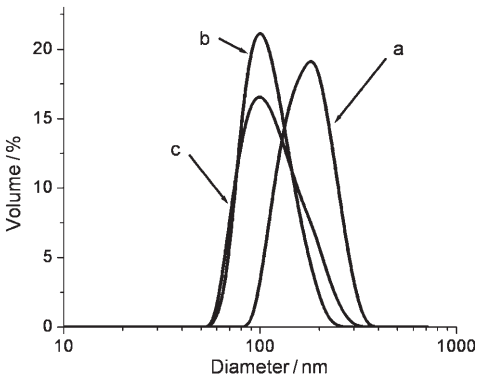


***Figure 3.*** The size distribution (measured by dynamic light scattering) of the $PAMPA_{88}$-$PNIPAM_{50}$ diblock copolymer under specific conditions: a) 0.05 % aqueous solution at 45 °C; b) 0.05 % aqueous solution with PAMPS at 45 °C; c) 0.05 % aqueous solution with PAMPS at 25 °C.

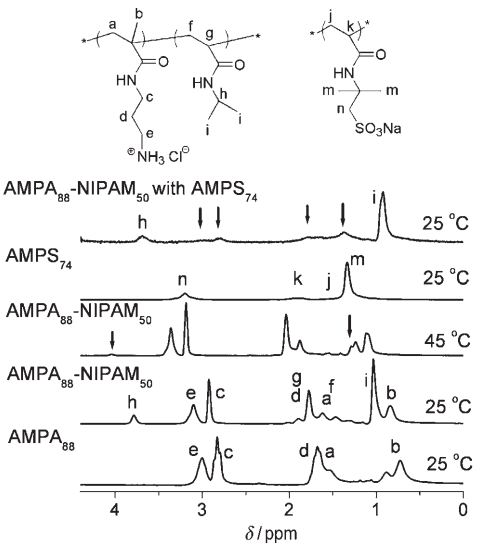


***Figure 4.*** The $^1$H NMR spectra of the homo and block copolymers at selected temperatures.

becomes hydrophilic whereas the AMPA and AMPS peaks broaden owing to their reduced mobility as a result of poleyelectrolyte complexation. The cross-linking process should be carried out at low concentrations ($< 0.5\ mg\,mL^{-1}$) to prevent flocculation.

The ionically cross-linked vesicles are stable over a wide pH range (0–10.5). (DLS studies indicate these particles dissociate above pH 11, possibly because of hydrolytic instability.) Furthermore, the cross-linked vesicles retain their structural integrity in the presence of 0.8 M NaCl. Raising the salt concentration above 1.0 M causes the vesicles to dissociate.

Ionically cross-linked systems have advantages over chemically cross-linked vesicles in that the cross-linking reaction is facile (the process can be completed within a few minutes) and reversible (the cross-links can be removed by adding electrolyte), which will facilitate the removal of the vesicles after bioapplication.

 © 2006 Wiley-VCH Verlag GmbH & Co. KGaA, Weinheim 

In summary, thermally responsive AB diblock copolymers were successfully prepared by RAFT polymerization. At room temperature, these block copolymers exist as unimers in aqueous solution and self-assemble into vesicles when the solution temperature is increased. It has been shown that both the solution concentration and the heating rate influence the size and size distribution of the vesicles. These vesicles can be cross-linked (structurally "locked") by adding an oppositely charged polyelectrolyte.

## Experimental Section

All chemicals were purchased from Aldrich at the highest available purity and used as received unless otherwise noted. *N*-(3-Aminopropyl)methacrylamide hydrochloride (AMPA) was purchased from Polysciences Inc. and used directly. *N*-Isopropylacrylamide (NIPAM; 97%, Aldrich) was recrystallized twice from a benzene/hexane mixture. 4,4′-Azobis(4-cyanopentanoic acid) (V-501) was donated by Wako Chemicals and used directly. 4-Cyanopentanoic acid dithiobenzoate (CTP) was synthesized and purified as previously reported.[14] $^1$H NMR spectra were recorded in $D_2O$ on a temperature-controlled Mercury Innova 500 MHz spectrometer. Size-exclusion chromatography (SEC) of aqueous solutions was performed with SynChropak CATSEC columns (100, 300, and 1000 Å; Eichrom Technologies Inc.), a Knauer K-2301 RI detector ($\lambda = 950$ nm), a Wyatt DAWN DSP multiangle laser light scattering detector ($\lambda =$ 633 nm), and 1 wt% acetic acid/0.1 M $Na_2SO_4$(aq) as the eluent at a flow rate of 0.3 mL min$^{-1}$. The d*n*/d*c* of poly(AMPA) (0.181 mL g$^{-1}$) in the above eluent was determined at 25 °C with a Knauer K-2301 RI detector ($\lambda = 950$ nm). SEC in *N*,*N*-dimethylformamide was performed with a Viscotek-TDA (302 RI (633 nm), 7-mW 90° and 7° true low-angle light scattering detectors, $\lambda = 670$ nm) equipped with two Polymer Labs PLgel Mixed "C" columns (5 μm (30 cm), 200–2 000 000 g mol$^{-1}$) at 60 °C (flow rate 0.5 mL min$^{-1}$). Dynamic light scattering (DLS) studies of the block copolymer vesicles in aqueous solution were conducted with a Malvern Instruments Zetasizer Nano series instrument equipped with a 4-mW He–Ne laser operating at $\lambda =$ 632.8 nm, an avalanche photodiode detector with high quantum efficiency, and an ALV/LSE-5003 multiple tau digital correlator electronics system. Transmission electron microscopy (TEM) measurements were conducted on a JEOL JEM-2100 electron microscope at an acceleration voltage of 200 kV. The specimens were prepared by placing a drop of the vesicle solution on a carbon-coated copper grid followed by water evaporation at 45 °C.

General procedure for the RAFT polymerization of AMPA: CTP (0.0078 g, 0.028 mmol) and AMPA (1.00 g, 5.6 mmol) were added along with deionized (DI) water (2.0 mL) to an ampoule. V-501 (0.00156 g, 0.0056 mmol) dissolved in dioxane (1.0 mL) was then added. The solution was stirred until all the CTP was dissolved. The ampoule was sparged with nitrogen for approximately 30 min and then placed in a preheated oil bath at 70 °C. The reaction was terminated after a specified time by cooling the reaction tube in an ice bath followed by exposure to air. The product was purified by dialysis against water (pH 4–5) and isolated by lyophilization.

Block copolymer synthesis: NIPAM (0.272 g, 2.4 mmol), $PAMPA_{88}$ (0.20 g), and V-501 (0.8 mg, 0.0024 mmol, dissolved in 0.6 g dioxane) were added along with DI water (0.8 mL) to an ampoule. After sparging with nitrogen for 30 min, the reaction was allowed to proceed at 70 °C for 2 h. The reaction was quenched by cooling the reaction vessel in an ice bath and exposure to air. The product was purified by dialysis against deionized water and isolated by lyophilization.

Received: May 31, 2006
Published online: July 31, 2006

**Keywords:** block copolymers · chain-transfer polymerization · self-assembly · vesicles · water-soluble polymers

[1] H. R. Petty, *Molecular Biology of Membranes, Structure and Function*, Plenum, New York, **1993**.
[2] a) L. Zhang, A. Eisenberg, *Science* **1995**, *268*, 1728; b) D. E. Discher, A. Eisenberg, *Science* **2002**, *297*, 967; c) L. Zhang, A. Eisenberg, *Macromolecules* **1996**, *29*, 8805; d) L. Luo, A. Eisenberg, *Langmuir* **2001**, *17*, 6804; e) L. Luo, A. Eisenberg, *Angew. Chem.* **2002**, *114*, 1043; *Angew. Chem. Int. Ed.* **2002**, *41*, 1001; f) J. Wu, A. Eisenberg, *J. Am. Chem. Soc.* **2006**, *128*, 2880.
[3] B. M. Discher, Y. Won, D. S. Ege, J. C. M. Lee, F. S. Bates, D. E. Discher, D. A. Hammer, *Science* **1999**, *284*, 1143.
[4] a) P. P. Ghoroghchian, G. Li, D. H. Levine, K. P. Davis, F. S. Bates, D. A. Hammer, M. J. Therien, *Macromolecules* **2006**, *39*, 1673; b) Y. He, Z. Li, P. Simone, T. P. Lodge, *J. Am. Chem. Soc.* **2006**, *128*, 2745.
[5] a) J. Z. Du, Y. M. Chen, Y. H. Zhang, C. C. Han, K. Fischer, M. Schmidt, *J. Am. Chem. Soc.* **2003**, *125*, 14710; b) J. Z. Du, Y. M. Chen, *Macromolecules* **2004**, *37*, 5710; c) J. Z. Du, Y. M. Chen, *Angew. Chem.* **2004**, *116*, 5194; *Angew. Chem. Int. Ed.* **2004**, *43*, 5084; d) J. Z. Du, Y. M. Chen, *Macromolecules* **2004**, *37*, 6322.
[6] P. L. Soo, A. Eisenberg, *J. Polym. Sci. Part B* **2004**, *42*, 923.
[7] a) F. Chécot, S. Lecommandoux, Y. Gnanou, H. A. Klok, *Angew. Chem.* **2002**, *114*, 1395; *Angew. Chem. Int. Ed.* **2002**, *41*, 1339; b) J. Rodriguez-Hernandez, S. Lecommandoux, *J. Am. Chem. Soc.* **2005**, *127*, 2026.
[8] a) J. Du, S. P. Armes, *J. Am. Chem. Soc.* **2005**, *127*, 12800; b) J. Du, Y. Tang, A. L. Lewis, S. P. Armes, *J. Am. Chem. Soc.* **2005**, *127*, 17982.
[9] C. L. McCormick, A. B. Lowe, *Acc. Chem. Res.* **2004**, *37*, 312.
[10] a) Y. Li, B. S. Lokitz, C. L. McCormick, *Macromolecules* **2006**, *39* 81–89; b) Y. Li, B. S. Lokitz, S. P. Armes, C. L. McCormick, *Macromolecules* **2006**, *39*, 2726.
[11] D. B. Thomas, A. J. Convertine, R. D. Hester, A. B. Lowe, C. L. McCormick, *Macromolecules* **2004**, *37*, 1735.
[12] a) Y. Xia, X. Yin, N. A. D. Burke, H. D. H. Stover, *Macromolecules* **2005**, *38*, 5937; b) Y. Xia, N. A. D. Burke, H. D. H. Stover, *Macromolecules* **2006**, *39*, 2275.
[13] J. V. M. Weaver, Y. Q. Tang, S. Liu, P. D. Iddon, R. Grigg, S. P. Armes, N. C. Billingham, R. Hunter, S. P. Rannard, *Angew. Chem.* **2004**, *116*, 1413; *Angew. Chem. Int. Ed.* **2004**, *43*, 1389.
[14] Y. Mitsukami, M. S. Donovan, A. B. Lowe, C. L. McCormick, *Macromolecules* **2001**, *34*, 2248.

 © 2006 Wiley-VCH Verlag GmbH & Co. KGaA, Weinheim 

Quantum Dots

DOI: 10.1002/anie.200600317

# Color-Saturated Green-Emitting QD-LEDs**

*Jonathan S. Steckel, Preston Snee, Seth Coe-Sullivan, John P. Zimmer, Jonathan E. Halpert, Polina Anikeeva, Lee-Ann Kim, Vladimir Bulovic, and Moungi G. Bawendi**

Semiconductor nanocrystals (NCs) or quantum dots (QDs) show great promise for use in QD-LED (quantum dot light-emitting device) displays, owing to their unique optical properties and the continual development of new core and core–shell structures to meet specific color needs.[1–10] This in combination with the recent development of more efficient and saturated QD-LEDs as well as new QD-LED fabrication techniques,[11,12] suggests that QD-LEDs have the potential to become an alternative flat-panel display technology. The ideal red, green, and blue emission spectrum of an LED for a display application should have a narrow bandwidth and a wavelength such that its color coordinates on the Commission Internationale de l'Eclairage (CIE) chromaticity diagram lie outside the current National Television System Committee (NTSC) standard color triangle (see Figure 2). For a Gaussian emission spectrum with a full width at half maximum (FWHM) of 30 nm and a maximized perceived power, the optimal peak wavelength for display applications is $\lambda = 610$–620 nm for red, $\lambda = 525$–530 nm for green, and $\lambda = 460$–470 nm for blue. For the red pixels, wavelengths longer than $\lambda = 620$ nm become difficult for the human eye to perceive, while those shorter than $\lambda = 610$ nm have coordinates that lie inside the standard NTSC color triangle. Optimization of wavelength for the blue pixels follows the same arguments as for the red pixel, but at the other extreme of the visible spectrum. For green pixels, $\lambda = 525$–530 nm provides a color triangle with the largest area on the CIE chromaticity diagram (and therefore the largest number of colors accessible by a display). Wavelengths longer than $\lambda = 530$ nm make some of the blue/green area of the triangle inaccessible. Wavelengths shorter than $\lambda = 525$ nm compromise the yellow display emissions.

To date, efficient red-emitting QD-LEDs with a peak emission wavelength optimized for display applications have been realized using (CdSe)ZnS core–shell NCs,[11,13] while blue QD-LEDs with a peak wavelength of emission optimized for display applications have been realized with a (CdS)ZnS core–shell material.[10] To date, although efficient green-emitting core–shell semiconductor NCs that emit at $\lambda = 525$ nm have been synthesized, they have not been successfully incorporated into a QD-LED suitable for display applications. Previous work using (CdSe)ZnS core–shell NCs gave QD-LEDs that emit at wavelengths no shorter than $\lambda = 540$–560 nm.[13,14] Using (CdSe)ZnS core–shell NCs to achieve $\lambda = 525$ nm emission requires making small CdSe cores ($\approx 2.5$ nm in diameter).[15,16] Such small CdSe semiconductor NCs can be difficult to synthesize with narrow size distributions and high quantum efficiencies, and are also more difficult to process and overcoat with a higher-band-gap inorganic semiconductor, which is necessary for incorporation into solid-state structures. A core–shell composite, rather than an organically passivated NC, is desirable in a solid-state QD-LED device owing to the enhanced photoluminescence and electroluminescence (EL) quantum efficiencies of core–shell NCs and their greater tolerance to the processing conditions necessary for device fabrication.[13,15–20] Larger NCs are also more desirable for use in QD-LEDs because the absorption cross section of NCs scales with size. Larger NCs with larger absorption cross sections lead to an increase in the efficiency of Förster energy transfer from electroluminescing organic molecules to NCs in a working QD-LED, which in turn leads to more efficient devices.

Herein, we report the synthesis of a $Cd_xZn_{1-x}Se$ alloy core on which we then grew a $Cd_yZn_{1-y}S$ shell to create a core–shell NC material with the ideal spectral characteristics for green emission in a QD-LED display and with a size large enough for fabricating a working QD-LED. Our $Cd_xZn_{1-x}Se$ core synthesis was based on work recently published, in which Cd and Se precursors were slowly introduced into a growth solution of ZnSe NCs.[1,2] A three-step synthetic route was employed to prepare the $(Cd_xZn_{1-x}Se)Cd_yZn_{1-y}S$ core–shell NCs. In the first step, ZnSe NCs were prepared by rapidly injecting 0.7 mmol of diethylzinc (Strem) and 1 mL of tri-*n*-octylphosphine selenide (TOPSe; 1M) dispersed in 5 mL of tri-*n*-octylphosphine (TOP; 97% Strem) into a round-bottom flask containing 7 grams of degassed hexadecylamine (distilled from 90% Sigma–Aldrich) at 310°C and by then growing the NCs at 270°C for 90 min. The second step consisted of transferring 8 mL of the above ZnSe NC growth solution, at 160°C, into a degassed solution of 16 grams of tri-*n*-octylphosphine oxide (TOPO; distilled from 90% Sigma–Aldrich) and 4 mmol of hexylphosphonic acid (HPA; Alfa Aesar), also at 160°C. A solution of 1.1 mmol of dimethylcadmium (Strem) and 1.2 mL of TOPSe (1M) dispersed in 8 mL of TOP (97% Strem) was then introduced dropwise

[*] Dr. J. S. Steckel,[+] Dr. P. Snee,[+] Dr. J. P. Zimmer, J. E. Halpert, Prof. M. G. Bawendi
Massachusetts Institute of Technology
Department of Chemistry
Center for Materials Science and Engineering
and The Institute for Soldier Nanotechnologies
77 Massachusetts Avenue, Room 6-221
Cambridge, MA 02139 (USA)
Fax: (+1) 617-253-7030
E-mail: mgb@mit.edu
Dr. S. Coe-Sullivan,[+] P. Anikeeva, L.-A. Kim, Prof. V. Bulovic
Massachusetts Institute of Technology
Laboratory of Organic Optics and Electronics
Department of Electrical Engineering and Computer Science
Cambridge, MA 02139 (USA)
[+] These authors contributed equally to this work.

[**] This work was funded in part by the NSF-MRSEC program (DMR 0213282), by the US Army through the Institute for Soldier Nanotechnologies, under Contract DAAD-19-02-0002 with the US Army Research Office, by the Presidential Early Career Award for Scientists and Engineers (PECASE). QD-LED = quantum dot light-emitting device.

 InterScience DISCOVER SOMETHING GREAT © 2006 Wiley-VCH Verlag GmbH & Co. KGaA, Weinheim 

(1 drop/ ≈ 2 s) into the ZnSe NC growth solution/TOPO/HPA mixture at 150 °C. The solution was then stirred at 150 °C for 46 h. Before overcoating the $Cd_xZn_{1-x}Se$ cores with $Cd_yZn_{1-y}S$, the $Cd_xZn_{1-x}Se$ cores were isolated by precipitation out of solution twice with a miscible non-solvent. In the third step, the $Cd_yZn_{1-y}S$ shell was grown by introducing dropwise a solution of dimethylcadmium (20% of total required moles of cation; Strem), diethylzinc (Strem), and hexamethyldisilathiane (Fluka) in 8 mL of TOP into a degassed solution of 10 grams of TOPO (distilled from 90% Sigma–Aldrich) and 2.4 mmol of HPA (Alfa Aesar), which contained the core $Cd_xZn_{1-x}Se$ NCs, at 150 °C (the $Cd_xZn_{1-x}Se$ cores dispersed in hexane were added to the degassed TOPO/HPA solution and the hexane was removed at 70 °C under vacuum prior to the addition of the shell precursors).

To fully characterize our $Cd_xZn_{1-x}Se$ core material, aliquots were sampled from the growth solution at time $t =$ 7, 60, and 2760 min (46 h) and analyzed with transmission electron microscopy (TEM), wavelength dispersive spectroscopy (WDS), and absorption and fluorescence spectrophotometry. Figure 1 a shows the absorption and emission spectra of these three aliquots as well as the absorption spectrum of the starting ZnSe NCs ($2.6 \pm 0.5$ nm in diameter, as determined by TEM). Over time the absorption and emission spectra shift to the red and the broad trap emission diminishes after 46 h of growth (Figure 1 a, spectrum 4), yielding particles approximately 3 nm in diameter. Upon overcoating the cores of $Cd_xZn_{1-x}Se$ with $Cd_yZn_{1-y}S$, the trap emission was completely suppressed, yielding an efficient (quantum yields of 50–60%),[21] saturated (FWHM = 30 nm), green-emitting core–shell material ( ≈ 4 nm in diameter) suitable for QD-LED display applications (Figure 1 b). An alloyed material for the shell was used to minimize lattice mismatch with the $Cd_xZn_{1-x}Se$ core.

Table 1 shows the growth time ($t = 0$, 7, 60, and 2760 min) of each aliquot, the average outer diameter determined by TEM, the Zn to Cd ratio determined by WDS, the measured first absorption peak, and calculated alloy ($Cd_xZn_{1-x}Se$) and core–shell ((ZnSe)CdSe core-shell) wavelengths based on the observed Zn to Cd ratios. We see from the raw data that as the reaction proceeds, the first absorption peak shifts to the red, the Zn to Cd ratio decreases, and the diameter of the particles increases. It is important to note that there is a relatively large increase in particle diameter from $t = 7$ to $t = 60$ min of growth, followed by a negligible increase in diameter from $t = 60$ to $t = 2760$ min (46 h). This small change in diameter is accompanied by a relatively large change in the Zn to Cd ratio as well as a relatively large shift of the first absorption peak to the red. This situation suggests that at $t = 7$ min the structure is most likely a (ZnSe)CdSe core–shell structure and that for $t > 7$ min the structure becomes a $Cd_xZn_{1-x}Se$ alloy, as a result of the migration of cations in the material.[3] It is of note that a decrease in particle diameter is initially observed following the introduction of neat hexadecylamine ZnSe growth solution ($2.6 \pm 0.5$ nm in diameter) into TOPO/phosphonic acid solution at 160 °C after about 2/3 of the Cd and Se precursors have been added (7 min aliquot, $1.9 \pm 0.3$ nm in diameter). This particle etching is plausible based on the large excess of acid present in the solution.

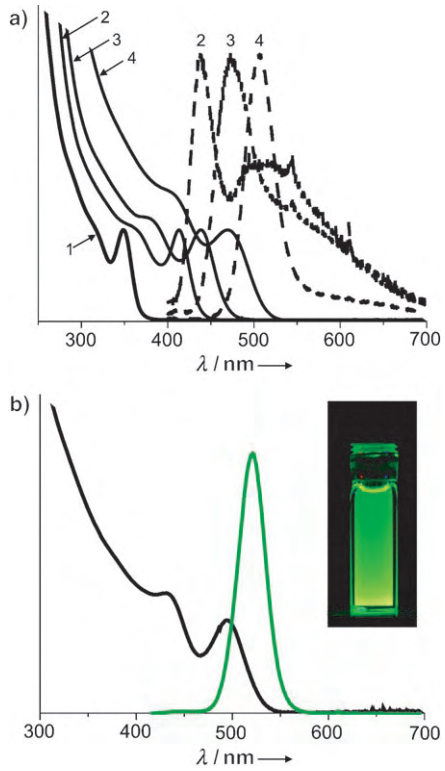


***Figure 1.*** a) Normalized absorption (solid) and emission (dashed) spectra of the core NCs over time: 1) Starting ZnSe NCs (first absorption peak at 350 nm); 2) Aliquot taken out after 7 min of growth (first absorption peak at 413 nm; emission peak at 439 nm); 3) Aliquot taken out after 60 min of growth (438 nm; 475 nm); 4) Aliquot taken out after 46 h of growth (470 nm; 506 nm (FWHM = 34 nm)). b) Absorption (black) and emission (green) spectra of $(Cd_xZn_{1-x}Se)Cd_yZn_{1-y}S$ core–shell NCs. The emission peaks at 520 nm with a FWHM of 30 nm, and the first absorption feature is at 495 nm. The inset shows the bright, color saturated, green emission from the NCs upon excitation with a UV lamp.

***Table 1:*** Experimental data and the results of effective-mass-approximation calculations of the first transition energy of alloyed ($Cd_xZn_{1-x}Se$) versus core–shell (ZnSe)CdSe NCs.

| Growth time [min][a] | Outer diameter [nm][b] | Zn/Cd[c] | Absorption wavelength [nm][d] | Calculated alloy wavelength [nm] | Calculated core–shell wavelength [nm] | Inner diameter [nm][e] |
|---|---|---|---|---|---|---|
| 0 | $2.6 \pm 0.5$ | | 350 | | | |
| 7 | $1.9 \pm 0.3$ | 0.33 | 413 | 324 | 416 | 0.65 |
| 60 | $3.1 \pm 0.5$ | 0.18 | 438 | 477 | 509 | 1.64 |
| 2760 | $3.2 \pm 0.5$ | 0.08 | 470 | 505 | 534 | 1.35 |

[a] Time from when the Cd and Se precursors were introduced into the flask containing the ZnSe NCs to when the aliquot was removed from the flask (complete addition of the Cd and Se precursors occurred at 9.5 min). [b] Measured from TEM. [c] Measured from WDS. [d] First absorption feature from absorption spectra shown in Figure 1 a. [e] Calculated from the Zn/Cd ratio and the known outer NC diameter from TEM measurements. This parameter is relevant only for the core–shell calculations, while the alloy results depend only on the outer diameter.


© 2006 Wiley-VCH Verlag GmbH & Co. KGaA, Weinheim

To help confirm our analysis of the NC morphology ($Cd_xZn_{1-x}Se$ alloy versus (ZnSe)CdSe core–shell) we performed calculations whose results are summarized in Table 1. The energies of an electron and hole within an alloyed or a core–shell semiconductor NC were calculated using the effective-mass approximation.[22,23] These calculations used electron and hole effective masses and band gaps optimized to match reported experimental results for both pure CdSe and ZnSe NCs.[24–26] We performed two sets of calculations using these optimized parameters to represent an alloyed material or a strict core–shell structure. To model an alloyed NC we adjusted the optimized band gap and electron/hole effective masses by a linear interpolation of the parameters for the pure materials based upon the experimentally determined stoichiometry (i.e., Zn to Cd ratio determined by WDS, shown in Table 1). To model a core–shell structure, we used the measured stoichiometry to determine the core radius and calculated the lowest electron and hole energies of a material with a ZnSe core, CdSe shell, and organic capping layer which has a high band offset (5 eV) for the electron and hole. The lowest transition energy is then determined by adding the electron and hole energies to the optimized band gap[26] along with the Coulombic binding energy of the electron and hole as determined from perturbation theory.[27] It can be seen that the calculated first transition energy for a core–shell structure is a good match for the NC material after the initial (7 min aliquot) exposure to the Cd and Se precursors. After prolonged ($>1$ h) exposure, the trends in our calculations suggest that an alloyed structure better matches the experimental results, while a core–shell material has a first absorption that is too low in energy. These results suggest that an alloy better represents the electronic structure of our materials.

The $(Cd_xZn_{1-x}Se)Cd_yZn_{1-y}S$ core–shell NCs were isolated by precipitation out of solution twice with a miscible nonsolvent and then filtered through a 0.2 μm syringe filter before use in device fabrication. QD-LED fabrication consisted of first thermally evaporating 4,4′-*N*,*N*′-dicarbazolyl-biphenyl (CBP) (hole transport layer (HTL)) onto an indium tin oxide (ITO) coated glass substrate at $<5\times10^{-6}$ torr. The QD monolayer, under air-free conditions, was then deposited onto the organic thin film of CBP using micro-contact printing. The substrate was then transported back into the thermal evaporator without exposure to air, where the hole blocking layer (HBL), 3-(4-biphenyllyl)-4-phenyl-5-*tert*-butylphenyl-1,2,4-triazole (TAZ), and then the electron transporting layer (ETL), tris(8-hydroxyquinoline)aluminum ($Alq_3$), were deposited. Finally the metal cathode (50 nm thick Mg:Ag, 50:1 by weight, 50 nm Ag cap) was thermally evaporated through a shadow mask to define devices of 1 mm in diameter (see Figure 2a for a diagram of the assembled device structure).

Figure 2a shows the EL spectrum of a typical green-emitting QD-LED. The small peak in the EL spectrum at $\lambda=380$ nm is CBP emission, which is only 2.6% of the total emission from the device, the rest being QD emission. When the EL spectrum shown in Figure 2a is transformed into its corresponding CIE chromaticity diagram color coordinates ($CIE_x=0.21$ and $CIE_y=0.70$) we see that it lies far outside of the standard NTSC color triangle (Figure 2b). This shows that using these saturated green-emitting QD-LEDs for a display would provide a significantly larger color triangle on the CIE chromaticity diagram. Figure 3 shows a plot of the external quantum efficiency (EQE) for the device versus current density ($J$) as well as the current–voltage plot. These devices show low operating voltages ($<10$ V) and peak EQEs of 0.5%.

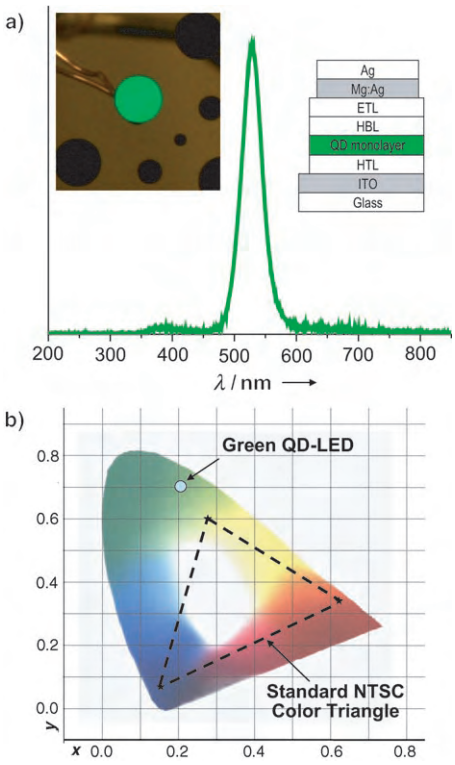


***Figure 2.*** a) The electroluminescence (EL) spectrum for the device: ITO/HTL/$(Cd_xZn_{1-x}Se)Cd_yZn_{1-y}S$ QD monolayer/HBL/ETL/Mg:Ag/Ag (assembled device structure is shown in the inset on the right; see text for details). The emission of the QD-LED peaks at 527 nm with a FWHM of 35 nm. The inset on the left is a photograph of the working green QD-LED. b) The EL spectrum shown in (a), transformed into its CIE chromaticity diagram color coordinates. The standard NTSC color triangle is shown for comparison.

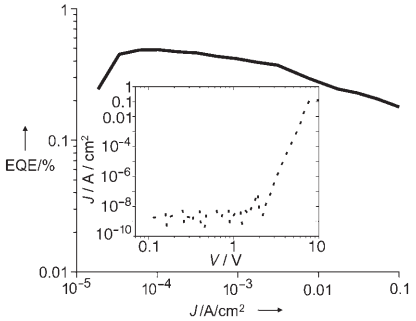


***Figure 3.*** External quantum efficiency (EQE) versus current density ($J$) for the device (assembled device structure is shown in the inset on the right of Figure 2a). The inset shows the current–voltage curve.

 © 2006 Wiley-VCH Verlag GmbH & Co. KGaA, Weinheim 

In summary, we have synthesized $Cd_xZn_{1-x}Se$ alloy core nanocrystals and overcoated these nanocrystals with $Cd_yZn_{1-y}S$ to create core–shell nanocrystals with the ideal wavelength of emission for QD-LED displays. We have used these $(Cd_xZn_{1-x}Se)Cd_yZn_{1-y}S$ core–shell nanocrystals to fabricate color-saturated green-emitting QD-LEDs, suitable for display applications.

Received: January 24, 2006
Published online: July 28, 2006

**Keywords:** light-emitting devices · nanocrystals · quantum dots · semiconductors

[1] S. A. Ivanov, J. Nanda, A. Piryatinski, M. Achermann, L. P. Balet, I. V. Bezel, P. O. Anikeeva, S. Tretiak, V. I. Klimov, *J. Phys. Chem. B* **2004**, *108*, 10625.
[2] X. Zhong, R. Xie, Y. Zhang, T. Basche, W. Knoll, *Chem. Mater.* **2005**, *17*, 4038.
[3] X. Zhong, M. Han, Z. Dong, T. J. White, W. Knoll, *J. Am. Chem. Soc.* **2003**, *125*, 8589.
[4] R. E. Bailey, S. Nie, *J. Am. Chem. Soc.* **2003**, *125*, 7100.
[5] X. Zhong, Y. Feng, W. Knoll, M. Han, *J. Am. Chem. Soc.* **2003**, *125*, 13559.
[6] R. Xie, X. Zhong, T. Basche, *Adv. Mater.* **2005**, *17*, 2741.
[7] J. J. Li, Y. A. Wang, W. Guo, J. C. Keay, T. D. Mishima, M. B. Johnson, X. Peng, *J. Am. Chem. Soc.* **2003**, *125*, 12567.
[8] D. V. Talapin, R. Koeppe, S. Gotzinger, A. Kornowski, J. M. Lupton, A. L. Rogach, O. Benson, J. Feldmann, H. Weller, *Nano Lett.* **2003**, *3*, 1677.
[9] P. Reiss, J. Bleuse, A. Pron, *Nano Lett.* **2002**, *2*, 781.
[10] J. S. Steckel, J. P. Zimmer, S. Coe-Sullivan, N. E. Stott, V. Bulovic, M. G. Bawendi, *Angew. Chem.* **2004**, *116*, 2206; *Angew. Chem. Int. Ed.* **2004**, *43*, 2154.
[11] S. Coe-Sullivan, J. S. Steckel, W.-K. Woo, M. G. Bawendi, V. Bulovic, *Adv. Funct. Mater.* **2005**, *15*, 1117.
[12] S. Coe-Sullivan, J. S. Steckel, L. A. Kim, M. G. Bawendi, V. Bulovic, *Proc. SPIE-Int. Soc. Opt. Eng.* **2005**, *5739*, 108.
[13] S. Coe-Sullivan, W.-K. Woo, J. S. Steckel, M. G. Bawendi, V. Bulović, *Org. Electron.* **2003**, *4*, 123.
[14] S. Coe, W.-K. Woo, M. Bawendi, V. Bulović, *Nature* **2002**, *420*, 800.
[15] M. A. Hines, P. Guyot-Sionnest, *J. Phys. Chem.* **1996**, *100*, 468.
[16] B. O. Dabbousi, J. Rodriguez-Viejo, F. V. Mikulec, J. R. Heine, H. Mattoussi, R. Ober, K. Jensen, M. G. Bawendi, *J. Phys. Chem. B* **1997**, *101*, 9463.
[17] B. O. Dabbousi, O. Onitsuka, M. G. Bawendi, M. F. Rubner, *Appl. Phys. Lett.* **1995**, *66*, 1316.
[18] V. L. Colvin, M. C. Schlamp, A. P. Alivisatos, *Nature* **1994**, *370*, 354.
[19] M. C. Schlamp, X. Peng, A. P. Alivisatos, *J. Appl. Phys.* **1997**, *82*, 5837.
[20] H. Mattoussi, L. H. Radzilowski, B. O. Dabbousi, E. L. Thomas, M. G. Bawendi, M. F. Rubner, *J. Appl. Phys.* **1998**, *83*, 7965.
[21] The $(Cd_xZn_{1-x}Se)Cd_yZn_{1-y}S$ core–shell NC photoluminescence quantum efficiencies were determined by comparing the integrated emission of a given NC sample in dilute hexane solution with an optical density of 0.1 with that of the appropriate laser dye.
[22] A. R. Kortan, R. Hull, R. L. Opila, M. G. Bawendi, M. L. Steigerwald, P. J. Carroll, L. E. Brus, *J. Am. Chem. Soc.* **1990**, *112*, 1327.
[23] W. R. Frensley, H. Kroemer, *Phys. Rev. B* **1977**, *16*, 2642.
[24] C. B. Murray, D. J. Norris, M. G. Bawendi, *J. Am. Chem. Soc.* **1993**, *115*, 8706.
[25] M. A. Hines, P. Guyot-Sionnest, *J. Phys. Chem. B* **1998**, *102*, 3655.
[26] The optimized electron effective masses used were 0.3727 for CdSe and 0.345 for ZnSe. The optimized band gaps were 1.9433 for CdSe and 2.9437 for ZnSe. The deviation between the calculated first transition energies versus experiment was on the order of $\pm 2$ nm using these parameters. Band offsets for CdSe relative to ZnSe (−1.20 eV for the electron and 0.22 eV for the hole) were obtained from "Subvolume b, Physics of II–VI and I–VII Compounds, Semimagnetic Semiconductors": *Landolt-Börnstein, New Series, Group III: Crystal and Solid State Physics, Vol. 17* (Ed.: K.-H. Hellwege, O. Madelung, M. Schule, H. Weiss), Springer, Berlin, **1982**.
[27] L. E. Brus, *J. Chem. Phys.* **1984**, *80*, 4403.

 © 2006 Wiley-VCH Verlag GmbH & Co. KGaA, Weinheim 

*Sandwich Compounds*

DOI: 10.1002/anie.200601641

# Sandwich Complexes Containing Bent Palladium Chains**

*Yasuki Tatsumi, Katsunori Shirato, Tetsuro Murahashi,* Sensuke Ogoshi, and Hideo Kurosawa**

Since the landmark discovery of ferrocene in 1951–52,[1] organometallic sandwich compounds have been the subject of extensive research owing to the wide utility of these as molecular materials and catalysts.[2] Recently, we developed one-dimensional sandwich chain complexes as a new class of extended organometallic sandwich compounds.[3,4] It has been proven that all-*trans*,all-s-*trans* conjugated polyenes serve as template ligands for a linear palladium chain (for example,

[*] Y. Tatsumi, K. Shirato, Prof. T. Murahashi, Prof. S. Ogoshi, Prof. H. Kurosawa
Department of Applied Chemistry
Graduate School of Engineering
Osaka University
Suita, Osaka, 565-0871 (Japan)
Fax: (+81) 6-6879-7394
E-mail: tetsu@chem.eng.osaka-u.ac.jp
Prof. T. Murahashi
PRESTO, Japan Science and Technology Agency
Suita, Osaka, 565-0871 (Japan)

[**] This work was supported by PRESTO, Japan Science and Technology Agency (JST) and Grants-in-aid for Scientific Research, Ministry of Education, Culture, Sports, Science and Technology of Japan. Y.T. thanks the research fellowships for young scientists from the Japan Society for the Promotion of Science.

Supporting information for this article is available on the WWW under http://www.angewandte.org or from the author.

 © 2006 Wiley-VCH Verlag GmbH & Co. KGaA, Weinheim InterScience 

compound **1**).[3a,5] It is of continued interest to know how other pπ-conjugated ligands which have different conjugation geometries from the linear ones can accommodate a multi-

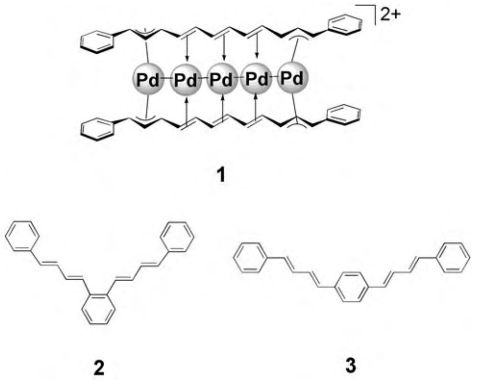


nuclear metal moiety in a sandwich framework.[6] A simple way to attain a nonlinear pπ-conjugation geometry is the incorporation of a *cis* or s-*cis* segment into the *trans*,s-*trans* polyene sequence. Herein, we report the unique coordination behavior of the *o*- or *p*-phenylene-inserted polyenes 1,2-bis(4-phenyl-1,3-butadienyl)benzene (*o*-BPBB) (**2**)[7] and 1,4-bis(4-phenyl-1,3-butadienyl)benzene (*p*-BPBB) (**3**),[8] which leads to the formation of the remarkable sandwich complexes containing bent polypalladium chains.

Treatment of the bis(perylene)tetrapalladium complex $[Pd_4(perylene)_2L_2][BAr^F]_2$ (**4**; $L = CH_3CN$, $BAr^F = B\{3,5\text{-}(CF_3)_2C_6H_3\}_4$)[6] with *o*-BPBB (**2**, 5 equiv) resulted in the quantitative formation of the bis(*o*-bpbb)-tetrapalladium complex $[Pd_4(o\text{-bpbb})_2][BAr^F]_2$ (**5**, Scheme 1). Complex **5** was alternatively isolated in 69% yield by the

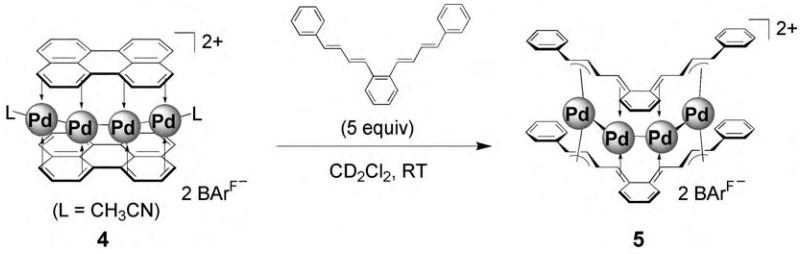


***Scheme 1.*** Synthesis of $[Pd_4(o\text{-bpbb})_2][BAr^F]_2$ (**5**).

reaction of $[Pd_2(CH_3CN)_6][BF_4]_2$[3b] and $[Pd_2(dba)_3]$ (1 equiv; dba=dibenzylideneacetone) with an excess of *o*-BPBB and subsequent anion exchange from $BF_4$ to $BAr^F$. Complex **5** was stable in $CD_2Cl_2$ for one week at ambient temperature.

The molecular structure of **5** was determined by X-ray crystallographic analysis (Figure 1).[9] In the structure, a $Pd_4$ chain is sandwiched between two *o*-bpbb ligands through $\mu_4$-$\eta^3$:$\eta^2$:$\eta^2$:$\eta^3$ coordination. The $Pd_4$ chain is bent at Pd2 and Pd2* (Pd1-Pd2-Pd2* 149.93(3)°) along the *cisoid* pπ-conjugation framework of C10-C11-C24*-C23*. This arch-shaped

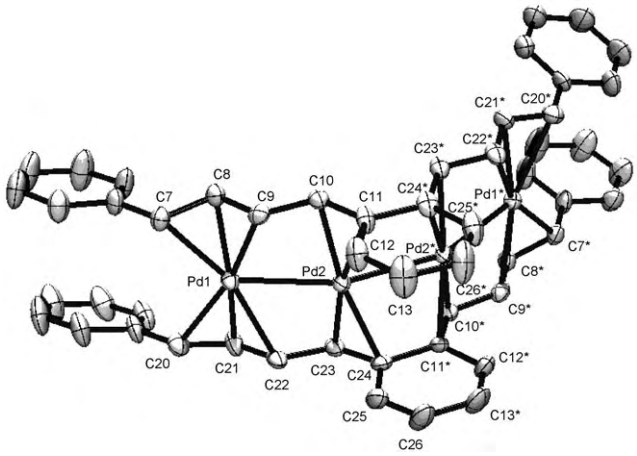


***Figure 1.*** ORTEP drawing of **5** (30% probability thermal ellipsoids; counterions, solvent molecules, and hydrogen atoms are omitted for clarity). Selected bond lengths [Å] and angles [deg]: Pd1-Pd2 2.701(1), Pd2-Pd2* 2.584(1), C9-C10 1.44(1), C10-C11 1.42(1), C11-C24* 1.51(1), C11-C12 1.42(1), C12-C13 1.37(1), C13-C26* 1.40(2), C25-C26 1.32(2), C24-C25 1.44(1), C23-C24 1.43(1), C22-C23 1.45(1); Pd1-Pd2-Pd2* 149.93(3).

geometry of the $Pd_4$ chain is in sharp contrast to the linear $Pd_4$ chain in $[Pd_4(dpdp)_2]^{2+}$.[5] In **5**, each Pd–Pd bond length (Pd1–Pd2 2.701(1) Å, Pd2–Pd2* 2.584(1) Å) is in the range of normal Pd–Pd bonds.[10] The internal Pd2–Pd2* bond (2.584(1) Å) is somewhat shorter than the corresponding bond in $[Pd_4(dpdp)_2]^{2+}$ (2.676(1) Å).[5] The CH(*o*-$C_6H_4$)CH units of the *o*-bpbb ligands in **5** may be regarded as an *o*-xylylene moieties in view of the $\eta^2$(C10,C11):$\eta^2$(C23*,C24*) coordination mode and the single-bond character of the C11–C24* bond (1.51(1) Å).[11,12]

We then carried out the reaction of *p*-BPBB (**3**) with complex **4** (Scheme 2). The reaction proceeded smoothly in $CH_2Cl_2$ at ambient temperature to afford the bis(*p*-bpbb)tetrapalladium complex $[Pd_4(p\text{-bpbb})_2][BAr^F]_2$ (**6**) as a brown precipitate (81% yield of isolated product). The structure of **6** was deciphered on the basis of $^1$H, $^{13}C\{^1H\}$ NMR, H–H COSY, HMQC, HMBC, and NOE analyses in [D$_6$]acetone. The upfield shift of the $^{13}C\{^1H\}$ NMR signals for C1–C10 in **6** ($\delta = 115$–82 ppm) relative to those of free *p*-BPBB indicated that the carbon atoms C1–C10 are involved in the coordination to the $Pd_4$ chain (Scheme 2).[13] The conformation of the *p*-bpbb ligands in **6** was determined by difference NOE experiments.[14]

Complex **6** transformed spontaneously into the bis(*p*-bpbb)pentapalladium complex $[Pd_5(p\text{-bpbb})_2][BAr^F]_2$ (**7**) in $CD_2Cl_2/CD_3CN$ (v/v = 1:1; 41% yield after two days). During the transformation, partial decomposition of **6** might generate $Pd^0$ species, a part of which is trapped by the remaining $Pd_4$ complex **6** to form the $Pd_5$ complex **7**.[15] The yield of complex **7** was not greatly improved when 0.5 equivalents of $[Pd_2(dba)_3]$ was added to a solution of **6** (49% yield). Isolated **7** underwent no decomposition or isomerization over one week in $CD_2Cl_2$ at ambient temperature.

 © 2006 Wiley-VCH Verlag GmbH & Co. KGaA, Weinheim 

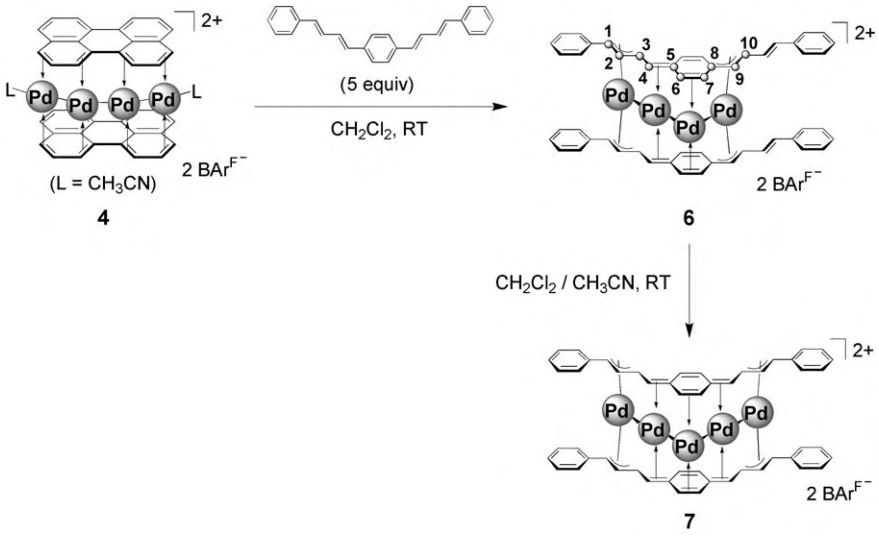


***Scheme 2.*** Synthesis of $[Pd_4(p\text{-bpbb})_2][BAr^F]_2$ (**6**) and $[Pd_5(p\text{-bpbb})_2][BAr^F]_2$ (**7**).

The structure of **7** was determined by X-ray structure analysis (Figure 2).[16] A unique V-shaped $Pd_5$ chain is sandwiched between *p*-bpbb ligands through $\mu_5$-$\eta^3$:$\eta^2$:$\eta^2$:$\eta^2$:$\eta^3$ coordination. The $Pd_5$ chain is bent at the central Pd3 atom (Pd2-Pd3-Pd4 121.81(4)°), which is coordinated by the *p*-phenylene moieties. This bent arrangement is in stark contrast to the linear $Pd_5$ chain in complex **1**. As a consequence of bending, the apex Pd atom (Pd3) in complex **7** has a unique four-coordinate "butterfly-type" geometry (**A**, Scheme 3).[17] In the known bent M-M-M chain complexes of Group 10 transition metals, one or two ligands interact with the apex M atom from the in-plane direction with respect to the M-M-M plane (**B** and **C**, Scheme 3).[18] Complex **7** was found to be inert toward MeCN and pyridine. Each Pd–Pd bond length in **7** (Pd1–Pd2 2.722(1) Å, Pd2–Pd3 2.713(1) Å, Pd3–Pd4 2.721(1) Å, Pd4–Pd5 2.733(1) Å) is in the range of normal Pd–Pd bonds.[10]

A formal quinoid character of the CH(*p*-$C_6H_4$)CH moieties of the *p*-bpbb ligands in **7** may be suggested by the $\eta^2$(C10,C11):$\eta^2$(C12,C13):$\eta^2$(C16,17) and $\eta^2$(C36,C37):$\eta^2$(C38,C39):$\eta^2$-(C42,43) coordination modes, as well as by the alternation in C–C bond lengths in the sequences C11-C14-C15-C16 (1.43(1), 1.34(1), 1.45(1) Å) and C37-C40-C41-C42 (1.42(1), 1.36(1), 1.44(1) Å).[19,20]

The bent sandwich chain complexes **8** and **9** were also prepared from 1,4-bis(2-phenylethenyl)benzene (*p*-BPEB),[21] according to Scheme 4.

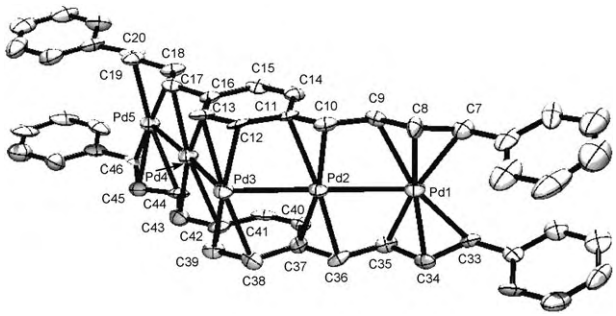


***Figure 2.*** ORTEP drawing of **7** (50% probability thermal ellipsoids; counterions, solvent molecules, and hydrogen atoms are omitted for clarity). Selected bond lengths [Å] and angles [deg]: Pd1-Pd2 2.722(1), Pd2-Pd3 2.713(1), Pd3-Pd4 2.721(1), Pd4-Pd5 2.733(1), C10-C11 1.42(1), C11-C12 1.45(1), C11-C14 1.43(1), C12-C13 1.37(1), C13-C16 1.42(1), C14-C15 1.34(1), C15-C16 1.45(1), C16-C17 1.42(1), C36-C37 1.44(1), C37-C38 1.46(1), C37-C40 1.42(1), C38-C39 1.38(1), C39-C42 1.44(1), C40-C41 1.36(1), C41-C42 1.44(1), C42-C43 1.45(1); Pd1-Pd2-Pd3 177.34(4), Pd2-Pd3-Pd4 121.81(4), Pd3-Pd4-Pd5 176.45(4).

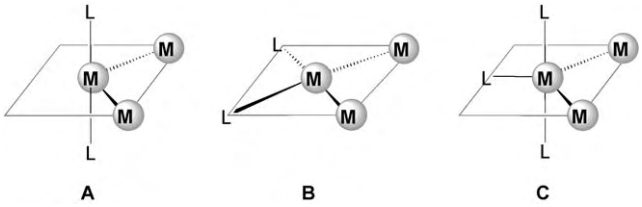


***Scheme 3.*** Schematic representation of the coordination geometry at the apex metal atom in bent M-M-M chains of Group 10 metals.

The bending of polypalladium chains in **5** and **7** occurred along the *cisoid* $C_4$ moieties (shown in purple, Scheme 5) at the phenylene units of the ligands. It is noticeable that the bending angles of the polypalladium chains (149.93(3)° (**5**) and 121.81(4)° (**7**)) reflect the angles of the p$\pi$-conjugated skeleton (150° in *o*-bpbb, 120° in *p*-bpbb; Scheme 5).[22]

Thus, it is reasonably concluded that the bending of the polypalladium chains in **5** or **7** is caused by the template effect of p$\pi$-conjugated $sp^2$-carbon frameworks. This result suggests

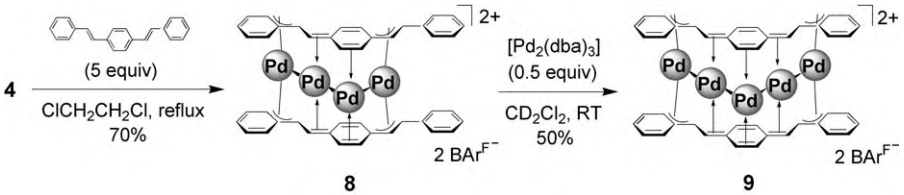


***Scheme 4.*** Synthesis of $[Pd_4(p\text{-bpeb})_2][BAr^F]_2$ (**8**) and $[Pd_5(p\text{-bpeb})_2][BAr^F]_2$ (**9**).

 © 2006 Wiley-VCH Verlag GmbH & Co. KGaA, Weinheim 

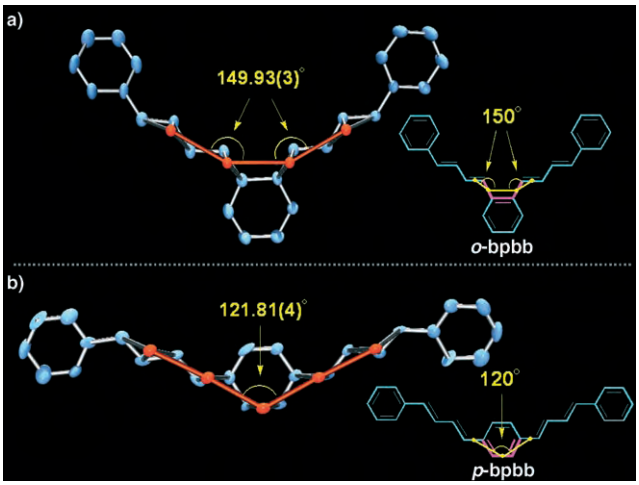


***Scheme 5.*** Template roles of p$\pi$-conjugated sp$^2$-carbon frameworks for shaping the Pd chains. a) The arch-shaped $Pd_4$ chain on *o*-bpbb; b) the V-shaped $Pd_5$ chain on *p*-bpbb.

the potential utility of *carbon π templates* in controlling the shape of the metal assembly. Further studies on the construction of different shapes of polypalladium assemblies, such as zigzag and ring shapes, by using appropriate unsaturated hydrocarbons as carbon π templates are currently in progress.

Received: April 26, 2006
Published online: July 25, 2006

**Keywords:** chain structures · palladium · pi interactions · sandwich complexes · structure elucidation

[1] a) T. J. Kealy, P. L. Pauson, *Nature* **1951**, *168*, 1039; b) S. A. Miller, J. A. Tebboth, J. F. Tremaine, *J. Chem. Soc.* **1952**, 632; c) G. Wilkinson, M. Rosenblum, M. C. Whiting, R. B. Woodward, *J. Am. Chem. Soc.* **1952**, *74*, 2125; d) E. O. Fischer, W. Z. Pfab, *Z. Naturforsch. B* **1952**, *7*, 377.

[2] a) *Metallocenes: Synthesis-Reactivity-Applications* (Eds.: A. Togni, R. L. Halterman), Wiley-VCH, New York, **2000**; b) N. J. Long, *Metallocenes*, Blackwell Science, Oxford, **1998**.

[3] a) T. Murahashi, E. Mochizuki, Y. Kai, H. Kurosawa, *J. Am. Chem. Soc.* **1999**, *121*, 10660; b) T. Murahashi, T Nagai, T. Okuno, T. Matsutani, H. Kurosawa, *Chem. Commun.* **2000**, 1689; c) T. Murahashi, T. Nagai, Y. Mino, E. Mochizuki, Y. Kai, H. Kurosawa, *J. Am. Chem. Soc.* **2001**, *123*, 6927; d) T. Murahashi, Y. Higuchi, T. Katoh, H. Kurosawa, *J. Am. Chem. Soc.* **2002**, *124*, 14288; e) Y. Tatsumi, T. Nagai, H. Nakashima, T. Murahashi, H. Kurosawa, *Chem. Commun.* **2004**, 1430; f) T. Murahashi, H. Nakashima, T. Nagai, Y. Mino, T. Okuno, M. A. Jalil, H. Kurosawa, *J. Am. Chem. Soc.* **2006**, *128*, 4377.

[4] A review on metal–metal chain compounds: J. K. Bera, K. R. Dunbar, *Angew. Chem.* **2002**, *114*, 4633; *Angew. Chem. Int. Ed.* **2002**, *41*, 4453.

[5] X-ray crystallographic analysis revealed the presence of linear $Pd_4$ and $Pd_5$ chains in $[Pd_4(dpdp)_2]^{2+}$ (dpdp = all-*trans*,s-*trans*-1,10-diphenyl-1,3,5,7,9-decapentaene) and **1**, respectively. T. Murahashi, H. Kurosawa et al., unpublished results.

[6] T. Murahashi, T. Uemura, H. Kurosawa, *J. Am. Chem. Soc.* **2003**, *125*, 8436.

[7] *o*-BPBB was prepared by the Wittig reaction; the experimental details are given in the Supporting Information.

[8] R. N. McDonald, T. W. Champbell, *J. Org. Chem.* **1959**, *24*, 1969.

[9] Crystal data for **5**: $C_{122}H_{80}B_2F_{48}Cl_{12}Pd_4$, $M_r = 3330.55$, monoclinic, space group $C2/c$ (no. 15), $a = 23.060(1)$, $b = 25.619(2)$, $c = 25.149(2)$ Å, $\beta = 116.352(3)°$, $V = 13313(1)$ Å$^3$, $Z = 4$, $F(000) = 6568$, $\rho_{calcd} = 1.661$ g cm$^{-3}$, $\mu(Mo_{K\alpha}) = 8.87$ cm$^{-1}$, $T = 133$ K, 835 variables refined with 24034 reflections with $I > 3\sigma(I)$ to $R1 = 0.091$. CCDC-604663 contains the supplementary crystallographic data for this paper. These data can be obtained free of charge from The Cambridge Crystallographic Data Centre via www.ccdc.cam.ac.uk/data_request/cif.

[10] T. Murahashi, H. Kurosawa, *Coord. Chem. Rev.* **2002**, *231*, 207.

[11] The C–C bond lengths of the *o*-phenylene moiety in Ph(CH=CH)(*o*-$C_6H_4$)(CH=CH)Ph range from 1.378 to 1.412 Å: A. Böhm, M. Adam, H. Mauermann, S. Stein, K. Müllen, *Tetrahedron Lett.* **1992**, *33*, 2795.

[12] *o*-Xylylene is known to form stable complexes with transition metals. For several examples of π-bonded *o*-xylylene complexes, see: a) W. R. Roth, J. D. Meier, *Tetrahedron Lett.* **1967**, *8*, 2053; b) R. Victor, R. Ben-Shoshan, *J. Organomet. Chem.* **1974**, *80*, C1; c) S. D. Chappell, D. J. Cole-Hamilton, *J. Chem. Soc. Chem. Commun.* **1981**, 319; d) J. W. Hull Jr., W. L. Gladfelter, *Organometallics* **1982**, *1*, 1716; e) A. M. Madonilc, D. Asruc, *J. Am. Chem. Soc.* **1984**, *106*, 2437; f) J. M. Grosselin, H. L. Bozec, C. Moinet, L. Toupet, P. H. Dixneuf, *J. Am. Chem. Soc.* **1985**, *107*, 2809; g) J.-M. Grosselin, H. L. Bozec, C. Moinet, L. Toupet, F. H. Köhler, P. H. Dixneuf, *Organometallics* **1988**, *7*, 88; h) M. A. Bennett, M. Bown, L. Y. Goh, D. C. R. Hockless, T. R. B. Mitchell, *Organometallics* **1995**, *14*, 1000.

[13] A possible coordination mode of *p*-bpbb in **6** is $\mu_4$-$\eta^3$:$\eta^2$:$\eta^2$:$\eta^3$. The same coordination mode was found in the analogous $Pd_4$ complex $[Pd_4\{Ph\{all\text{-}trans,s\text{-}trans\text{-}(CH=CH)_4\}Ph\}_2][BAr^F]_2$.[3a]

[14] The NOE signals were observed between H4 and H6 and between H7 and H9 in **6**.

[15] During the reaction, a yellow precipitate of *p*-BPBB was generated.

[16] Crystal data for **7**: $C_{124}H_{83}B_2NF_{48}Cl_6Pd_5$, $M_r = 3265.29$, monoclinic, space group $P2_1/n$ (no. 14), $a = 16.9054(3)$, $b = 24.2244(4)$, $c = 29.8064(4)$ Å, $\beta = 90.8575(6)°$, $V = 12205.0(3)$ Å$^3$, $Z = 4$, $F(000) = 6432$, $\rho_{calcd} = 1.777$ g cm$^{-3}$, $\mu(Mo_{K\alpha}) = 9.79$ cm$^{-1}$, $T = 133$ K, 1668 variables refined with 35196 reflections with $I > 3\sigma(I)$ to $R1 = 0.077$. CCDC-604664 contains the supplementary crystallographic data for this paper. These data can be obtained free of charge from The Cambridge Crystallographic Data Centre via www.ccdc.cam.ac.uk/data_request/cif.

[17] A four-coordinate $Pd^{II}$ complex in which the Pd center is largely distorted from the square-planar geometry was recently reported: C. M. Frech, L. J. W. Shimon, D. Milstein, *Angew. Chem.* **2005**, *117*, 1737; *Angew. Chem. Int. Ed.* **2005**, *44*, 1709, and references therein.

[18] a) Y. Yamamoto, K. Takahashi, H. Yamazaki, *J. Am. Chem. Soc.* **1986**, *108*, 2458; b) P. Braunstein, M. A. Luke, *New J. Chem.* **1988**, *12*, 429; c) Y. Yamamoto, H. Yamazaki, *Organometallics* **1993**, *12*, 933; d) M. Rashidi, J. J. Vittal, R. J. Puddephatt, *J. Chem. Soc. Dalton Trans.* **1994**, 1283; e) T. Tanase, H. Takahata, H. Ukaji, M. Hasegawa, Y. Yamamoto, *J. Organomet. Chem.* **1997**, *538*, 247; f) T. Tanase, H. Toda, Y. Yamamoto, *Inorg. Chem.* **1997**, *36*, 1571; g) T. Tanase, H. Ukaji, H. Takahata, H. Toda, T. Igoshi, Y. Yamamoto, *Organometallics* **1998**, *17*, 196.

[19] The C–C bond lengths of the *p*-phenylene moiety in oligo-*p*-phenylene vinylenes Ph(CH=CH){$C_6H_4$(CH=CH)}$_n$Ph range from 1.373 to 1.406 Å for $n = 1$, and 1.331 to 1.421 Å for $n = 3$: a) G. P. Bartholomew, X. Bu, G. C. Bazan, *Chem. Mater.* **2000**, *12*, 2311; b) P. F. van Hutten, J. Wildeman, A. Meetsma, G. Hadziioannou, *J. Am. Chem. Soc.* **1999**, *121*, 5910.

 © 2006 Wiley-VCH Verlag GmbH & Co. KGaA, Weinheim 

[20] A similar bond alternation was found in the X-ray structure of [{Fe(CO)$_3$}$_2${$\mu_2$-$\eta^4$:$\eta^4$-(*p*-divinylbenzene)}], in which the four carbon atoms in the *p*-phenylene moiety participate in the coordination to two Fe centers. R. E. Davis, R. Pettit, *J. Am. Chem. Soc.* **1970**, *92*, 716.
[21] T. W. Campbell, R. N. McDonald, *J. Org. Chem.* **1959**, *24*, 1246.
[22] The angles 150° and 120° in Scheme 5 are defined by the midpoints of the C–C bonds, such that all C–C bond lengths and C-C-C angles are fixed as being equivalent.

 © 2006 Wiley-VCH Verlag GmbH & Co. KGaA, Weinheim 

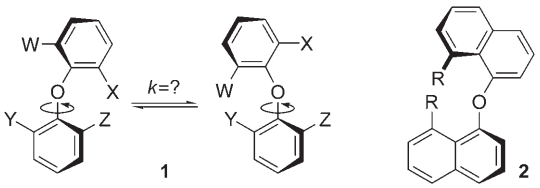


***Scheme 1.*** Atropisomerism in diaryl ethers.

Stereochemistry

DOI: 10.1002/anie.200601866

# Three Groups Good, Four Groups Bad? Atropisomerism in *ortho*-Substituted Diaryl Ethers**

*Mark S. Betson, Jonathan Clayden,* Christopher P. Worrall, and Simon Peace*

The vancomycin family of antibiotics[1] contains a cyclic peptide aglycone that features three unusual stereogenic features—an atropisomeric biaryl and two atropisomeric diaryl ether units—all incorporated into three fused macrocyclic rings. Atropisomerism is associated principally with single bonds that join a pair of hindered planar groups,[2] and the *ortho*-substituted biaryl atropisomers (of the type present in vancomycin and its acyclic congener actinoidic acid,[3] for example, but also many other compounds) are of course by far the most well known. By contrast, the structural requirements for atropisomerism in diaryl ethers **1** outside of a cyclic framework remain unclear (Scheme 1), despite the presence of diaryl ether units in a range of natural products, including the bastadins for example.[4] McRae et al. in 1954[5a] commented that compounds of type **1** "show, in wooden models, an unusually great degree of steric hindrance about the diphenyl ether linkage". Dahlgard and Brewster[5b] proposed in 1958 that diaryl ethers might exist as separable atropisomers, and some sub-atropisomeric barriers to bond rotations were measured in a small range of compounds **1**,[6,7] but it was not until 1998 that Fuji and co-workers[8] resolved three examples of **2**, the only non-macrocyclic diaryl ethers that have yet proved to be atropisomeric. Herein, we report the synthesis, stereochemistry, stereodynamics, and stereoisomeric separation of a set of simple diaryl ethers and deduce some empirical rules to describe the requirements for chirality in this class of molecule.

Two complementary methods provided the hindered diaryl ethers. Nucleophilic aromatic substitution is generally less sensitive to steric hindrance than the metal-catalyzed coupling reactions commonly used to make diaryl ethers,[9] and we found that the potassium salts of even rather hindered phenols **5** readily displaced the chloride group from **4** (made by lithiation of nitrile **3**[10]) to obtain ethers **6a**–**11a** in good yield. A sequence of addition, protection,[11] oxidation, and reduction reactions yielded the further series of compounds **6**–**11** shown in Scheme 2. Directed *ortho*-metalation is a powerful way of building sterically congested aromatic substitution in a regiocontrolled manner,[12] and the reported[13] sequence of lithiation and oxidation reactions shown in Scheme 3 gave further ethers **14**–**16**. Compounds **7e**, **9e**, **10e**, and **17** were additionally made from 3-bromobenzonitrile by a modification of Scheme 2 (the full experimental details are provided in the Supporting Information).

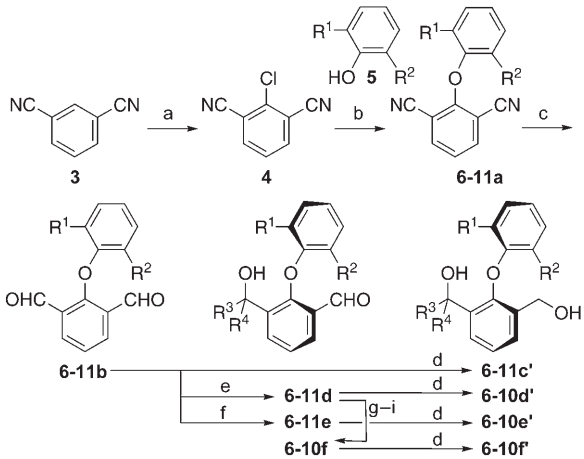


***Scheme 2.*** Synthesis of diaryl ethers by nucleophilic aromatic substitution. Reagents and conditions: a) 1. LDA, −95 °C, THF; 2. $C_2Cl_6$; b) **5**, KOH, toluene, Δ, 2 h, then **4**, DMF, 150 °C, 16 h; c) 1. DIBAL, −78→20 °C, 16 h; 2. HCl, $H_2O$, 1 h; d) $NaBH_4$, THF; e) MeLi, $Et_2O$, −78 °C, 16 h; f) PhLi, $Et_2O$, −78 °C, 16 h; g) $(COCl)_2$, $Me_2SO$, $Et_3N$, −78 °C, $CH_2Cl_2$; h) (1*R*,2*S*)-(−)-ephedrine, toluene, Δ, 16 h; i) 1. MeMgI, THF, 0→20 °C, 16 h; 2. HCl, $H_2O$. DIBAL = diisobutylaluminum hydride, DMF = *N*,*N*-dimethylformamide, LDA = lithium diisopropylamide.

[*] Dr. M. S. Betson, Prof. J. Clayden, C. P. Worrall
School of Chemistry
University of Manchester
Oxford Road, Manchester M13 9PL (UK)
Fax: (+44) 161-275-4939
E-mail: clayden@man.ac.uk

Dr. S. Peace
GlaxoSmithKline Medicines Research Centre
Gunnels Wood Road
Stevenage, Herts SG1 2NY (UK)

[**] We are grateful to the Leverhulme Trust, GlaxoSmithKline, and the EPSRC for funding this study.

Supporting information for this article is available on the WWW under http://www.angewandte.org or from the author.

 © 2006 Wiley-VCH Verlag GmbH & Co. KGaA, Weinheim 

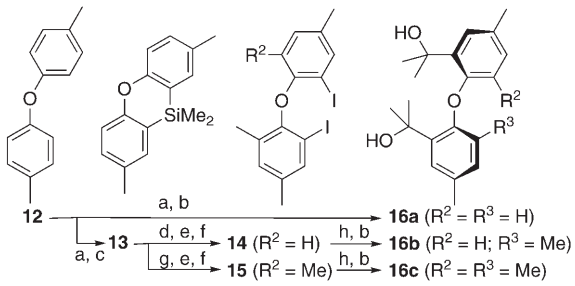


***Scheme 3.*** Synthesis of diaryl ethers by sequential lithiation of di-*para*-tolyl ether.[13] Reagents and conditions: a) *n*BuLi, TMEDA, 20 °C; b) acetone; c) $Me_2SiCl_2$; d) *sec*-BuLi (×2), TMEDA, $Et_2O$, 0 °C, 2 h; e) MeI; f) ICl, $CH_2Cl_2$; g) *s*-BuLi (×3.5), TMEDA, $Et_2O$, 0 °C, 2 h; h) *n*BuLi, THF, −78 °C. TMEDA = *N*,*N*,*N*′,*N*′-tetramethyl-1,2-ethanediamine.

Activation parameters for bond rotation were estimated by using dynamic NMR spectroscopy at low and high temperature, following broadening or coalescence of diastereotopic H or Me signals or diastereoisomeric C*H*OH signals, and using an Eyring plot of the corresponding rates of interconversion $k$ obtained by lineshape simulation.[14] Table 1 summarizes the results of these investigations (entries 1–15) and gives $t_{1/2}$ values (the half-life for racemization or epimerization[15] of **6**–**8**, estimated at 25 °C) and the $\Delta G^{\neq}$ value (the free energy of activation for the interconversion of stereoisomers) where appropriate. As expected, the barriers increased with increasing sizes of $R^2$ and $R^3$ for each type of substituent $R^1$ and were higher when the trisubstituted ring bore a tetrahedral $CH_2OH$ group in the place of a trigonal CHO group or a digonal CN group.[16] The half-life for epimerization of **7d** displayed negligible solvent dependence in $CDCl_3$, [$D_8$]toluene, $CD_3OD$, and [$D_6$]DMSO (DMSO = dimethyl sulfoxide). The iodo- and isopropyl-substituted ethers **6** and **7** had broadly similar barriers to rotation (with **6** slightly higher) and in the case of **6f′** (Table 1, entry 4) variable temperature (VT) NMR spectroscopic

***Table 1:*** Rates of isomerization in *ortho*-substituted diaryl ethers.[a]

| Entry | $R^1$ | $R^2$ | $R^3$ | $R^4$ | Ether | Aldehydes **6**–**11** | | Alcohols **6′**–**11′** | |
|---|---|---|---|---|---|---|---|---|---|
| | | | | | | $\Delta G^{\neq}$[b] [kJ mol$^{-1}$] | $t_{1/2}$[b] | $\Delta G^{\neq}$[b] [kJ mol$^{-1}$] | $t_{1/2}$[b] |
| 1 | I | H | H | H | **6c** | – | – | 78.8[c] | 4 s[c] |
| 2 | I | H | Me | H | **6d** | [d] | 0.02 s[e] | [d] | 7 s |
| 3 | I | H | Ph | H | **6e** | [d] | 0.06 s[e] | [d] | 7 s |
| 4 | I | H | Me | Me | **6f** | 76.8 | 3 s | 95.7 | 1 h |
| 5 | *i*Pr | H | H | H | **7c** | – | – | 71.5[c] | 0.2 s[c] |
| 6 | *i*Pr | H | Me | H | **7d** | [d] | 0.02 s[e] | [d] | 2 s |
| 7 | *i*Pr | H | Ph | H | **7e** | [d] | 0.02 s[e]<br>0.006 s[e,f] | [d] | 0.4 s |
| 8 | *i*Pr | H | Me | Me | **7f** | 78.5 | 3 s | 90.9 | 8 min |
| 9 | *t*Bu | H | H | H | **8c** | – | – | 88.0[c] | 2 min[c] |
| 10 | *t*Bu | H | Me | H | **8d** | [d] | 30 s | 105.0<br>102.0[g] | 20 h |
| 11 | *t*Bu | H | Ph | H | **8e** | [d] | 2 min | [d] | > 10 h[h] |
| 12 | *t*Bu | H | Me | Me | **8f** | > 97[h] | > 2 h | 113.5[i,j] | 50 days[k] |
| 13 | $CMe_2OH$[l] | H | H | – | **16a** | – | – | 71.0 | 0.1 s |
| 14 | $CMe_2OH$[l] | H | Me | – | **16b** | – | – | 114.0[m] | 40 days[k] |
| 15 | $CMe_2OH$[l] | H | $CH_2OMe$ | – | **17** | – | – | 108.7[j] | 7 days |
| 16 | Me | Me[n] | H | H | **9c** | – | – | < 36[o] | < 1 μs |
| 17 | Me | Me[n] | Me | H | **9d** | < 36[o] | < 1 μs | < 36[o] | < 1 μs |
| 18 | Me | Me[n] | Me | Me | **9f** | < 38[o] | < 1 μs | < 38[o] | < 1 μs |
| 19 | *i*Pr | *i*Pr | H | H | **10c** | – | – | < 37[o] | < 1 μs |
| 20 | *i*Pr | *i*Pr | Me | H | **10d** | < 36[o] | < 1 μs | < 37[o] | < 1 μs |
| 21 | *i*Pr | *i*Pr | Me | Me | **10f** | < 38[o] | < 1 μs | < 38[o] | < 1 μs |
| 22 | *t*Bu | Me | H | H | **11c** | – | – | 86.8[p] | – |
| 23 | *t*Bu | Me | Me | H | **11d** | [d] | 6000 years[q,r] | – | – |
| 24 | *t*Bu | Me | Ph | H | **11e** | [d] | 50000 years[q,r] | – | – |
| 25 | $CMe_2OH$[s] | Me | Me | – | **16c** | – | – | > 128[t] | > 50 years[r] |

[a] Barriers to bond rotation determined by VT-NMR spectroscopic analysis at > 25 °C in [$D_6$]DMSO unless otherwise indicated. [b] Free energy of activation (±0.5–1.0 kJ mol$^{-1}$) for bond rotation and half-life for interconversion of rotamers (generally racemization or epimerization to equilibrium mixture) calculated at 25 °C.[15] [c] Rotamers are not stereoisomers in this case. [d] Bond rotation leads to epimerization. [e] Determined by VT-NMR spectroscopic analysis at < 25 °C in $CDCl_3$ (**6d**, **e**), [$D_8$]toluene (**7e**), $CD_3OD$ (**7e**-CN), and in each of $CDCl_3$, [$D_8$]toluene, $CD_3OD$, and [$D_6$]DMSO (**7d**). [f] Half-life for the corresponding nitrile. [g] Barriers for two diastereoisomers determined by separation (HPLC) and equilibration at 40 °C in hexane/*i*PrOH (98:2). [h] No coalescence up to 150 °C. [i] Determined by resolution (HPLC, β-GEM, hexane/*i*PrOH (98:2)) followed by racemization in hexane/*i*PrOH (98:2) at 70 (**8f′**), 40 (**16b**), 60, and 80 °C (**17**). [j] Barrier at 70 °C. [k] Half-life estimated by assuming $\Delta S^{\neq} = 0$. [l] For comparison with **8**; $R^{2,3}$ refer to structure **16**. [m] Barrier at 40 °C. [n] Carries a *p*-Me substituent as well. [o] VT-NMR spectroscopic analysis in $CD_3OD$ at −90–+20 °C.[20] [p] Determined by VT-NMR spectroscopic analysis in [$D_6$]DMSO at 25–150 °C; barrier probably corresponds to bond rotation that does not lead to racemization.[21] [q] Determined by flash column chromatography of diastereoisomers (**11d**: $R_f$ = 0.58, 0.71 petrol/EtOAc (5:1)) and equilibration at 90 °C in [$D_8$]toluene (**11d**) or 115 °C in [$D_6$]DMSO (**11e**). [r] Half-life estimated by assuming $\Delta S^{\neq} = 0$. [s] For comparison with **11**; $R^{2,3}$ refer to structure **16**. [t] Determined by resolution (HPLC, β-GEM, hexane/*i*PrOH (98:2)) followed by attempted racemization in hexane/*i*PrOH (98:2) at 60 °C.

 © 2006 Wiley-VCH Verlag GmbH & Co. KGaA, Weinheim 

analysis indicated that the separation of atropisomeric stereoisomers might be possible at ambient temperature.[17] The results confirm that acyclic diaryl ethers have much lower barriers to rotation than those constrained within a macrocyclic ring.[18]

Nonetheless, many of the *tert*-butyl-substituted ethers **8** and related compounds **16b** and **17** showed no coalescence, even at 150 °C in [$D_6$]DMSO (Table 1, entries 9–15), which is indicative of barriers to rotation beyond those required for atropisomerism. Indeed, atropisomeric diastereoisomers **8d′** and atropisomeric enantiomers **8f′**, **16b**, and **17** were separable by HPLC. Each isomer showed a first-order decay to an equilibrium mixture when incubated in hexane/*i*PrOH between 40 and 70 °C, and we derived the half-lives reported in entries 10, 12, 14, and 15 (Table 1) from the rate of this decay.

Simplistically, we expected that—as with biaryl compounds[2,19]—two 2,6-disubstituted rings (namely, four *ortho* substituents) would provide much higher barriers to rotation for a variety of substitution patterns. However, dynamic NMR studies of the tetrasubstituted ethers **9** and **10**, in which $R^1 = R^2$, painted a very different picture (Table 1, entries 16–21). For all of these compounds, diastereotopic or diastereoisomeric signals of groups carried by the unsymmetrical ring remained unresolved even at −90 °C in $CD_3OD$, thus suggesting[20] barriers to racemization or epimerization at least as low as 36–38 kJ mol$^{-1}$.[21] The corresponding half-life for racemization or epimerization for these compounds is probably[20] less than $10^{-6}$ s, a factor of 100 000 shorter than for even the fastest racemization of the comparable ethers **7** bearing only one isopropyl group at $R^1$ and comparable with the rate of Ar–OAr rotation in thyroxine,[7] a di-*ortho*-substituted diaryl ether.

Molecular mechanics studies of some simplified analogues allow us to propose a reason for this huge discrepancy. Figure 1a,b shows two-dimensional plots generated by a macromodel (MM2*)[22] of the energy of simple tri- and tetrasubstituted model compounds **18** and **19**. The calculated

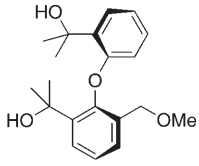

**17**

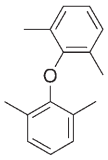

**18**

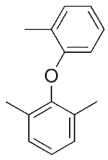

**19**

ground-state conformations of **18** and **19** are consistent with previous proposals:[23] the two rings are more or less perpendicular in **19** (conformations C and D in Figure 1), with the H atom "*endo*", whereas the two rings lie skew to one another in **18** to avoid steric interactions with the *ortho* substituents (conformations A and B in Figure 1).[24]

The "valleys" in Figure 1a,b run diagonally, which indicates that the lowest energy pathways for conformational interconversion in both **18** and **19** involve concerted (geared) rotation[25] of the two O–Ar bonds. For ethers **18** and any simple tetrasubstituted diaryl ether with at least one symmetrically substituted ring, such a process allows transition from one global minimum A to a mirror-image global minimum B. Ether **18** is symmetrical, but interconversion between mirror-image structures can take place along the dotted line in Figure 1a via transition state *x*.

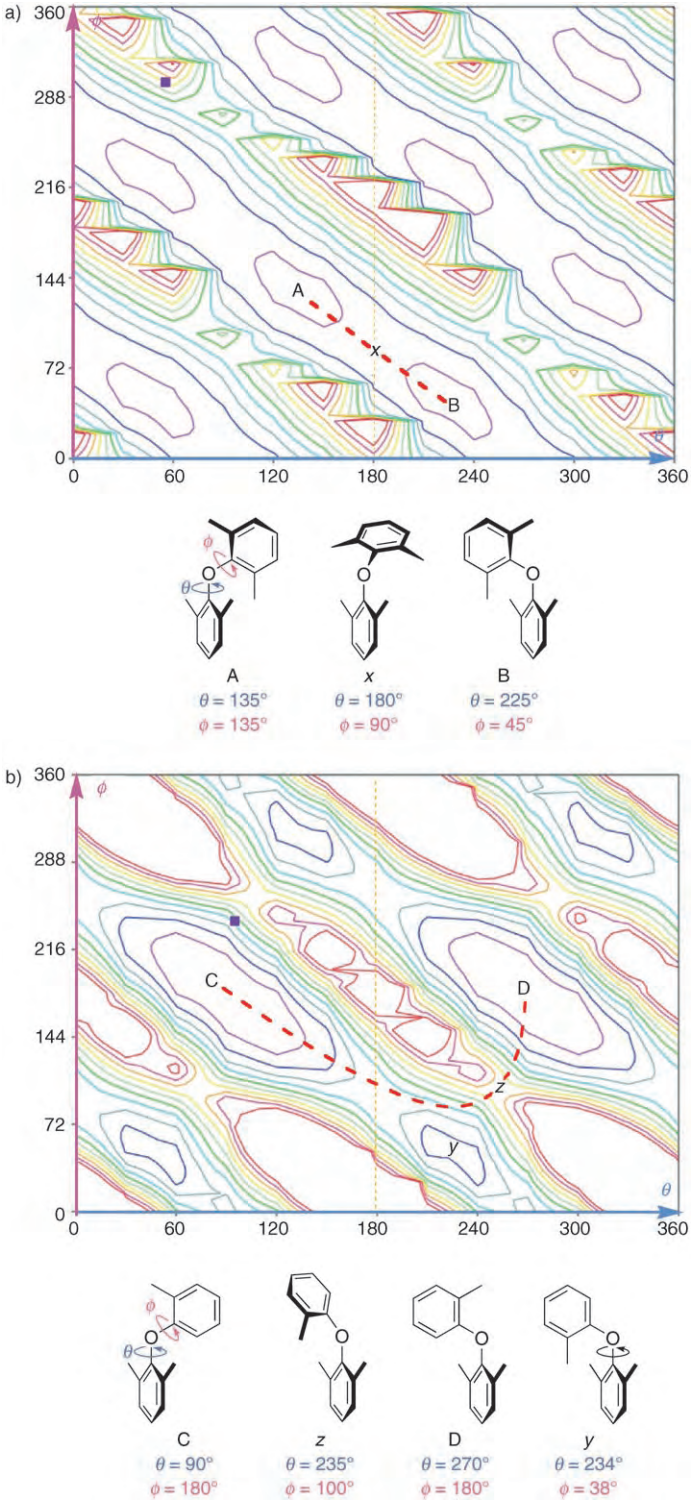


***Figure 1.*** Potential-energy plots for bond rotation in **18** and **19**. a) Concerted bond rotation in **18.** b) Decoupled bond rotation in **19**.


© 2006 Wiley-VCH Verlag GmbH & Co. KGaA, Weinheim

Concerted rotation cannot interconvert the global minimum of one stereoisomer with that of its mirror image for the trisubstituted ether **19** (Figure 1b); concerted rotation from C instead passes through local minimum *y*, with the methyl group "*endo*". One of the two rings must decouple and undergo an independent rotation to racemize and yield D via transition state *z*. Mirror-image minima lie separated by the ridges on the potential-energy surface illustrated in Figure 1b, and their interconversion must follow the pathway represented by the dotted line.

If the proposal that the huge difference in rates of racemization between **6–8** and **9** and **10** arises from a change in mechanism of isomerization is correct, then any diaryl ether, whether trisubstituted or tetrasubstituted, that cannot isomerize by a low-energy concerted pathway (namely, in which both rings are unsymmetrically substituted) has the potential to display atropisomerism. We tested this hypothesis with the unsymmetrically tetrasubstituted ethers **11** and **16c** (Table 1, entries 22–25). Chromatographic separation of atropisomers was achieved for **11d**, **11e**, and **16c**, and incubation of the diastereoisomers of **11d**, **11e**, and **16c** at raised temperatures in toluene showed only slow isomerization, even over a period of weeks. We estimate that the half-lives for epimerization of **11d** and **11e** at room temperature reach well into millennia. Hindered 2,6,2′,6′-tetrasubstituted diaryl ethers with two unsymmetrically substituted rings are stable chiral compounds.

From this data, we draw the following conclusions about the potential for atropisomerism in acyclic diaryl ethers:

a) Atropisomerism in diaryl ethers depends less on the total number of substituents than the substitution pattern.
b) Diaryl ethers in which one of the rings is symmetrically substituted do not exhibit atropisomerism because their stereoisomers may interconvert by concerted bond rotation. This behavior means that even diaryl ethers with four *ortho* substituents may racemize rapidly.
c) Diaryl ethers in which both rings are unsymmetrically substituted may exhibit atropisomerism, as long as at least one of the substituents is as large as a *tert*-butyl group. This condition can hold even for diaryl ethers with only three *ortho* substituents.

In summary, the feature most favorable to high rotational barriers in diaryl ethers **1** is heavy, but unsymmetrical, substitution: for stable chirality **1** requires $(W, X, Y, Z \neq H)$, $(W \neq X)$, $(Y \neq Z)$, $(W \geq t\text{Bu})$, and $(Y \geq t\text{Bu})$.

Received: May 11, 2006
Published online: July 28, 2006

**Keywords:** atropisomerism · diaryl ethers · NMR spectroscopy · rotational barriers · stereochemistry

[1] K. C. Nicolaou, C. N. C. Boddy, S. Bräse, N. Winssinger, *Angew. Chem.* **1999**, *111*, 2230; *Angew. Chem. Int. Ed.* **1999**, *38*, 2096; B. M. Crowley, D. L. Boger, *J. Am. Chem. Soc.* **2006**, *128*, 2885, and references therein.
[2] E. L. Eliel, S. H. Wilen, *Stereochemistry of Organic Compounds*, Wiley, New York, **1994**.
[3] S. Boidnard, L. Neuville, M. Bois-Choussy, J. Zhu, *Org. Lett.* **2000**, *2*, 2459.
[4] E. A. Couladouros, E. N. Pitsinos, V. I. Moutsos, G. Sarakinos, *Chem. Eur. J.* **2005**, *11*, 406.
[5] a) J. A. McRae, R. Y. Moir, J. J. Ursprung, H. H. Gibbs, *J. Org. Chem.* **1954**, *19*, 1500; b) M. Dahlgard, R. Q. Brewster, *J. Am. Chem. Soc.* **1958**, *80*, 5861.
[6] H. Kessler, A. Rieker, W. Rundel, *J. Chem. Soc. Chem. Commun.* **1968**, 475; J. J. Bergman, W. D. Chandlwe, *Can. J. Chem.* **1972**, *50*, 353; P. A. Lehman, *Org. Magn. Reson.* **1970**, *2*, 467.
[7] B. M. Duggan, D. J. Craik, *J. Med. Chem.* **1997**, *40*, 2259.
[8] K. Fuji, T. Oka, T. Kawabata, T. Kinoshita, *Tetrahedron Lett.* **1998**, *39*, 1373.
[9] F. Theil, *Angew. Chem.* **1999**, *111*, 2493; *Angew. Chem. Int. Ed.* **1999**, *38*, 2345; J. S. Sawyer, *Tetrahedron* **2000**, *56*, 5045; Z. Liu, R. C. Larock, *Org. Lett.* **2004**, *6*, 99; D. A. Evans, J. L. Katz, T. R. West, *Tetrahedron Lett.* **1998**, *39*, 2937; D. M. T. Chan, K. L. Monaco, R. Wang, M. P. Winters, *Tetrahedron Lett.* **1998**, *39*, 2933; G. Mann, J. F. Hartwig, *Tetrahedron Lett.* **1997**, *38*, 8005.
[10] T. D. Krizan, J. C. Martin, *J. Org. Chem.* **1982**, *47*, 2681.
[11] For the use of (−)-ephedrine-derived oxazolidines as protecting groups for aldehydes during lithiation, see: J. Clayden, Y. J. Y. Foricher, M. Helliwell, P. Johnson, D. Mitjans, V. Vinader, *Org. Biomol. Chem.* **2006**, *4*, 444.
[12] J. Clayden in *Chemistry of Organolithium Compounds*, *Vol. 1* (Eds.: Z. Rappoport, I. Marek), Wiley, Chichester, **2004**, p. 495; H. W. Gschwend, H. R. Rodriguez, *Org. React.* **1979**, *26*, 1.
[13] M. S. Betson, J. Clayden, *Synlett* **2006**, 745.
[14] Lineshapes at a range of temperatures close to, above, and below the $T_c$ value were simulated by using gNMR software (Adept Scientific).
[15] The half-lives are for the approach to the equilibrium mixture, not half-lives for bond rotation. The bond rotation monitored in **6c**, **7c**, and **8c** does not in fact lead to interconversion of stereoisomers, but the half-life value is calculated in the same way for consistency.
[16] For examples in which trigonal substituents provide low barriers to bond rotation, see: A. I. Meyers, J. R. Flisak, R. A. Aitken, *J. Am. Chem. Soc.* **1987**, *109*, 5446; A. Ahmed, R. A. Bragg, J. Clayden, L. W. Lai, C. McCarthy, J. H. Pink, N. Westlund, S. A. Yasin, *Tetrahedron* **1998**, *54*, 13277; K. Kamikawa, M. Uemura, *Synlett* **2000**, 938.
[17] Oki has suggested that atropisomers be defined as conformers that interconvert with a half-life of more than $1000\ s^{-1}$: M. Oki, *Top. Stereochem.* **1983**, *14*, 1.
[18] D. L. Boger, J.-H. Weng, S. Miyazaki, J. J. McAtee, S. L. Castle, S. H. Kim, Y. Mori, O. Rogel, H. Strittmatter, Q. Jin, *J. Am. Chem. Soc.* **2000**, *122*, 10047.
[19] R. Adams, H. C. Yuan, *Chem. Rev.* **1933**, *33*, 261.
[20] This estimation is made on the assumption that at least one pair of diastereotopic or more or less equally populated diastereoisomeric peaks would have a peak separation of $> 0.1$ ppm at the slow exchange limit.
[21] Substituents attached to the symmetrical ring may show coalescences at higher temperatures, which is indicative of much higher barriers, but these must be barriers to nonconcerted bond rotations; a full discussion will follow in a later report.
[22] F. Mohmadi, N. G. J. Richards, W. C. Guida, R. Liskamp, M. Lipton, C. Caufield, G. Chang, T. Hendrickson, W. C. Still, *J. Comput. Chem.* **1990**, *11*, 440.
[23] P. A. Lehman, E. C. Jorgensen, *Tetrahedron* **1965**, *21*, 363; G. Montaudo, P. Finocchiaro, E. Trivellone, F. Bottino, P. Maravigna, *Tetrahedron* **1971**, *27*, 2125; J. C. Emmett, E. S. Pepper, *Nature* **1975**, *257*, 334.
[24] Ground-state destabilization of tetra-*ortho*-substituted relative to tri-*ortho*-substituted diaryl ethers may also play a role in

 © 2006 Wiley-VCH Verlag GmbH & Co. KGaA, Weinheim 

lowering the barrier, but the results presented in Table 1, entries 22–25 suggest that it is not an important one.

[25] For a discussion of geared rotation in related compounds, see: J. Clayden, J. H. Pink, *Angew. Chem.* **1998**, *110*, 2040; *Angew. Chem. Int. Ed.* **1998**, *37*, 1937; R. A. Bragg, J. Clayden, *Org. Lett.* **2000**, *2*, 3351; R. A. Bragg, J. Clayden, G. A. Morris, J. H. Pink, *Chem. Eur. J.* **2002**, *8*, 1279; for a more general discussion of gearing effects, see: G. S. Kottas, L. I. Clarke, D. Horinek, J. Michl, *Chem. Rev.* **2005**, *105*, 1281; H. Iwamura, K. Mislow, *Acc. Chem. Res.* **1988**, *21*, 175.

 © 2006 Wiley-VCH Verlag GmbH & Co. KGaA, Weinheim 

*Metal–Metal Bonding*

DOI: 10.1002/anie.200601926

# A Zinc–Zinc-Bonded Compound and Its Derivatives Bridged by One or Two Hydrogen Atoms: A New Type of Zn–Zn Bonding**

*Zhongliang Zhu, Robert J. Wright, Marilyn M. Olmstead, Eric Rivard, Marcin Brynda, and Philip P. Power**

Recently, the synthesis and structural characterization of decamethyldizincocene [Cp*ZnZnCp*] (**1**; Cp* = $\eta^5$-$C_5Me_5$, Zn–Zn 2.305(3) Å) was reported by Carmona and co-workers.[1] It was the first stable compound that contained a Zn–Zn bond.[2] This landmark development was confirmed by calculations which showed that the Zn–Zn bond is formed mainly by the overlap of the Zn 4s orbitals while the Zn 4p orbitals interact with the $\eta^5$-$C_5Me_5$ ligand.[1b,3] A further example of a compound with a Zn–Zn bond, [{HC(CMeNAr)$_2$}ZnZn{HC(CMeNAr)$_2$}] (Ar = 2,6-*i*Pr$_2$C$_6$H$_3$) (**2**), was reported by Robinson and co-workers,[4] and this species has a Zn–Zn bond length of 2.3586(7) Å. The zinc atoms are three-coordinate, and the metal–metal bond has 95% s character. The Zn–Zn bond in **2** is about 0.05 Å longer than that in **1** despite its lower metal coordination number. Clearly, the type of ligand exerts a large influence on the Zn–Zn bond length. It is therefore desirable to have zinc–zinc-bonded species in which the Zn atoms are bound to only one ligand atom to provide the simplest possible bonding arrangement and also to show that Zn–Zn bonds can in fact be stabilized by monodentate ligands. Furthermore, the synthesis of the singly or doubly bridged hydride derivatives of such a species would provide further information on the nature of the Zn–Zn bonding. We now describe the synthesis and characterization of the zinc–zinc-bonded species Ar′ZnZnAr′ (**4**) (Ar′ = $C_6H_3$-2,6-($C_6H_3$-2,6-*i*Pr$_2$)$_2$), the hydride-bridged dimer Ar′Zn(μ-H)$_2$ZnAr′ (**5**), which has a Zn···Zn separation very similar to that in **4**, and the unique compound Ar′Zn(μ-H)(μ-Na)ZnAr′ (**6**), in which the Zn atoms are connected by a new type of Zn–Zn interaction.

Dinuclear **4** was synthesized by the reduction of Ar′ZnI (**3**) with Na. The hydride, Ar′Zn(μ-H)$_2$ZnAr′ (**5**), was prepared by the treatment of **3** with NaH. Rather than forming zinc–zinc-bonded compound **4** (as indicated in the indirect route for **1** whereby KH was used to reduce the [Zn(Cp*)$_2$] species in situ[1b] or whereby [Cp*ZnZnCp*] was obtained by the unforeseen ligand exchange between [ZnCp*$_2$] and ZnEt$_2$[1a] (Scheme 1)), further reduction of **5** by NaH provided the unprecedented sodium hydride-bridged species Ar′Zn(μ-H)(μ-Na)ZnAr′ (**6**, Scheme 2).

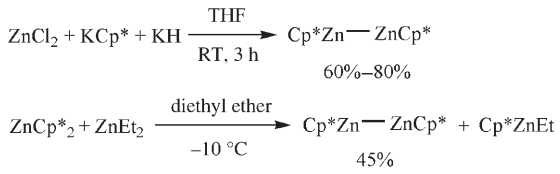


***Scheme 1.*** Synthetic routes to the zinc–zinc-bonded dimer [Cp*ZnZnCp*] (**1**).[1]

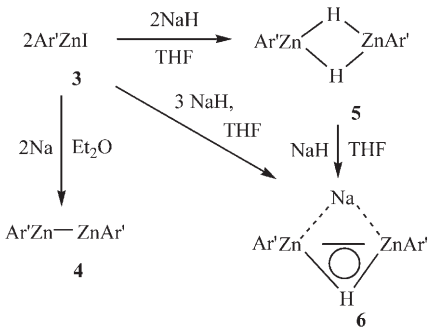


***Scheme 2.*** Synthetic routes to **4**, **5**, and **6**.

The crystal structure of **4** (Figure 1)[5] confirms the presence of a Zn–Zn bond. The observed Zn–Zn bond length in **4** (2.3591(9) Å) is about 0.05 Å larger than that in **1** (2.305(3) Å) and is essentially the same as that in **2** (2.3586(7) Å). The two Ar′ ligands are arranged in a nearly orthogonal orientation to each other, which provides effective steric protection of the Zn–Zn moiety. An almost linear arrangement is observed for the {C(*ipso*)-Zn-Zn-C(*ipso*)} interior, which is in contrast to the other known metal–metal-bonded dimers ArMMAr, (M = Cr,[6a] Ga,[6b] Ge,[6c] As,[6d] or Se[6e]) which for numerous reasons display strongly *trans*-bent geometries.

[*] Z. Zhu, Dr. R. J. Wright, Prof. M. M. Olmstead, Dr. E. Rivard, Dr. M. Brynda, Prof. P. P. Power
Department of Chemistry
University of California
One Shields Avenue, Davis, CA 95616 (USA)
Fax: (+1) 530-752-8995
E-mail: pppower@ucdavis.edu

[**] The authors thank the National Science Foundation for financial support. E.R. thanks NSERC of Canada for a postdoctoral fellowship.

Supporting information for this article is available on the WWW under http://www.angewandte.org or from the author.

 © 2006 Wiley-VCH Verlag GmbH & Co. KGaA, Weinheim 

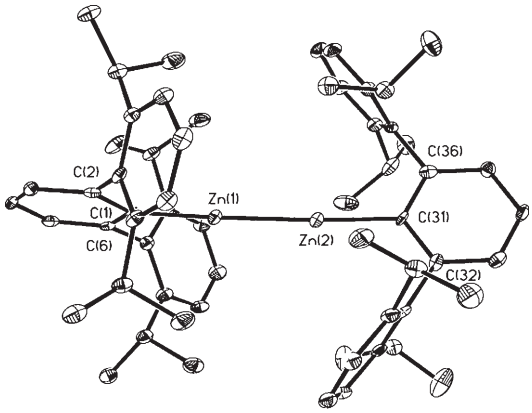


***Figure 1.*** Thermal-ellipsoid plot (ellipsoids set at 30% probability) of **4** without hydrogen atoms. Selected bond lengths [Å] and angles [°]: Zn(1)-Zn(2) 2.3591(9), Zn(1)-C(1) 1.965(6), Zn(2)-C(31) 1.974(5); C(31)-Zn(2)-Zn(1) 177.28(18), Zn(2)-Zn(1)-C(1) 177.57(18), C(32)-C(31)-Zn(2) 120.5(4), C(36)-C(31)-Zn(2) 119.1(4).

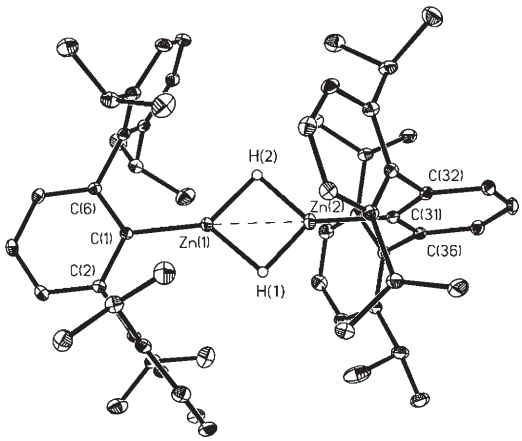


***Figure 2.*** Thermal-ellipsoid plot (ellipsoids set at 30% probability) of **5** without hydrogen atoms. Selected bond lengths [Å] and angles [°]: Zn(1)···Zn(2) 2.4084(3), Zn(1)-H(1) 1.67(2), Zn(1)-H(2) 1.79(3), Zn(1)-C(1) 1.9301(16); C(1)-Zn(1)-Zn(2) 175.14(5), Zn(1)-Zn(2)-C(31) 175.60(5), C(1)-Zn(1)-H(1) 138.3(9), Zn(2)-Zn(1)-H(1) 45.2(8), C(6)-C(1)-Zn(1) 121.21(11), C(2)-C(1)-Zn(1) 120.00(12).

Well-characterized, stable Zn–H species are relatively rare because of the high tendency of these species to oligomerize or polymerize.[7] Nonetheless, the synthesis of **5**[5] proceeded smoothly and in moderate yield. The bridging hydrogen atoms in **5** were located in the electron difference map. The overall appearance of the molecular structure of **5** (Figure 2) and perpendicular orientation of the ligands are very similar to those of **4** (crystals of **4** and **5** are isomorphous), and the Zn···Zn separation in **5** (2.4084(3) Å) is lengthened by only about 0.05 Å in comparison with that in **4**. In the $^1$H NMR spectrum a signal corresponding to the bridging hydride in **5** was located at $\delta = 4.84$ ppm, in a 1:1 intensity ratio with the signals of the aryl ligand. A similar chemical shift was observed at $\delta = 4.59$ ppm in the zinc hydride [RZn(μ-H)$_2$ZnR] (R = [{(2,6-*i*Pr$_2$C$_6$H$_3$)N(Me)C}$_2$-CH]; Zn···Zn 2.4513(9) Å).[7e] It is notable that the Zn···Zn separation in this hydride species is about 0.1 Å longer than that seen in the zinc–zinc-bonded β-diketiminate derivative **2**.[4]

DFT calculations[8,9] for **4** (Figure 3) were performed at the B3LYP/6-31g* level and indicate that the HOMO is localized mainly in the Zn–Zn σ-bonding region with some additional Zn–C(*ipso*) σ-bonding character. The LUMO and LUMO + 1 consist of two almost degenerate orbitals of π symmetry, which are localized mostly on the central {Zn–Zn}$^{2+}$ unit. These calculations show that the Zn–Zn bond is formed from the overlap of mainly 4p$_z$ orbitals in the HOMO, thus leaving two empty orthogonal p$_x$ and p$_y$ orbitals to form the π-symmetric LUMOs. The 4s orbitals of the zinc centers are mainly involved in bonding to the *ipso* carbon atoms of the ligands. In contrast to **4**, the Zn 4s orbitals form the Zn–Zn bond in **1**, and this Zn–Zn bonding orbital is the HOMO−4. The orbitals HOMO to HOMO−3 of **1** are mostly ligand-based π levels of the η$^5$-C$_5$Me$_5$ ring. In **2**, the Zn–Zn bond is the HOMO, and the LUMO is a ligand orbital of π symmetry.

The sodium hydride bridged compound **6**[5] could be obtained from **3** or **5** by the reaction with the appropriate number of equivalents of NaH (Scheme 2). The Zn–Zn bond length in **6** is 2.352(2) Å (Figure 4), which is essentially the same as that in **4** (2.3591(9) Å). In contrast to **4** and **5**, the two central aryl rings on the Ar′ ligand are nearly coplanar in **6**, and the bridging sodium and hydride centers also lie near this plane. The Na$^+$ counterion is sequestered by strong η$^6$ interactions involving the flanking aryl rings on the Ar′ ligand. The Na$^+$···C(aryl) separations range from 2.843 to 3.108 Å, and the Na$^+$–centroid distances of the two flanking aryl rings are 2.658 Å and 2.670 Å, respectively. In addition, the two sets of Zn···Na$^+$ and Zn···H$^-$ distances are 3.113(4)/3.130(4) Å and 1.75(6)/1.74(6) Å, respectively. The $^1$H NMR spectrum of **6** displays a broad signal at $\delta =$ 2.04 ppm, which was assigned to the bridging hydride.

The metal–metal bonding in **6** differs considerably from that observed in **4**. The DFT calculations indicate that there is a delocalized orbital formed by the bridging hydrogen atom and two zinc atoms, as illustrated in HOMO−17 (Figure 5). In contrast to **4**, 4s orbitals of zinc atoms participate in the

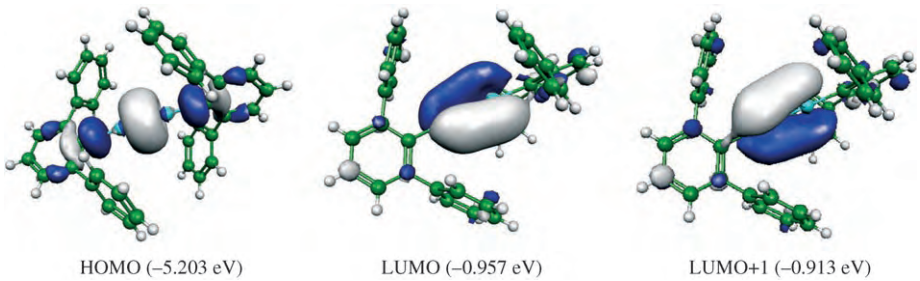


***Figure 3.*** Representation of the key molecular orbitals of **4** from DFT calculations.

 © 2006 Wiley-VCH Verlag GmbH & Co. KGaA, Weinheim 

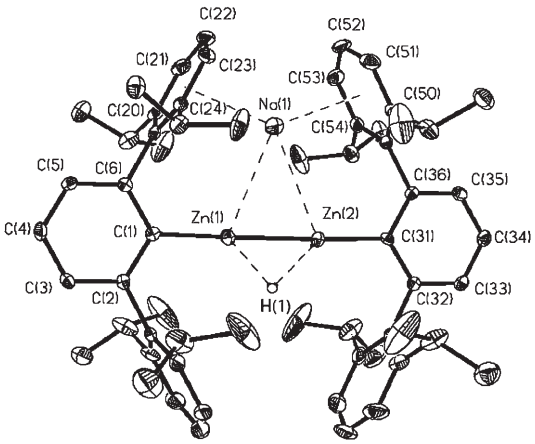


***Figure 4.*** Thermal-ellipsoid plot (ellipsoids set at 30% probability) of **6** without hydrogen atoms. Selected bond lengths [Å] and angles [°]: Zn(1)-Zn(2) 2.352(2), Zn(1)-H(1) 1.75(6), Zn(1)-Na(1) 3.113(4), Zn(1)-C(1) 1.977(5); C(1)-Zn(1)-Zn(2) 170.38(15), Zn(2)-Zn(1)-Na(1) 68.25(5), Zn(2)-Zn(1)-H(1) 47.6(18), Zn(1)-Na(1)-Zn(2) 44.26(7), C(6)-C(1)-Zn(1) 121.21(11), C(2)-C(1)-Zn(1) 120.00(12); dihedral angles: between the C1–C6 and C31–C36 planes 1.9°, between the C1–C6 and $Zn_2HNa$ planes 8.9°, between the C31–C36 and $Zn_2HNa$ planes 9.3°.

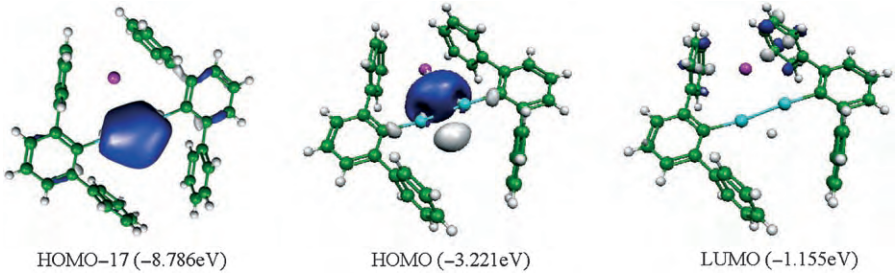


***Figure 5.*** Representation of the key molecular orbitals of **6** from DFT calculations.

HOMO−17 bonding interaction to yield an orbital that has both Zn−Zn and Zn−H bonding character. The HOMO of **6** has considerable electron density in the region between the $Na^+$ ion and the zinc atoms, and between the zinc centers. There is also a smaller region of electron density of opposite phase near the bridging hydrogen atom such that the orbital resembles a distorted Zn−Zn bonding interaction of π symmetry. However, the Wiberg bond order[9] calculations indicate that the Zn−Zn bond order (0.81) in **6** is slightly less than that (0.95) in **4** with a considerable bonding interaction between the zinc centers and sodium atom (bond order 0.68).

In conclusion, a new zinc–zinc-bonded compound supported by monodentate ligands has been synthesized by a straightforward procedure. The related hydrogen-bridged dimer shows that, although it has no Zn−Zn bond, the metal–metal separation is only about 0.05 Å longer. In contrast to the zinc–zinc-bonded compounds **1** and **2**,[1,4] the Zn−Zn bond in Ar′ZnZnAr′ (**4**) is formed by using mainly $4p_z$ orbitals. DFT calculations and the structure parameters indicate a new type of Zn−Zn bond in **6**. Future work will focus on investigations of the reactivity of the Zn−Zn bond in compounds **4**, **6**, and related species.

## *Experimental Section*

All manipulations were carried out under anaerobic and anhydrous conditions. $^1H$ and $^{13}C$ NMR spectra were recorded on a Varian 300 spectrometer and referenced to known standards.

**4**: A solution of **3** (0.93 g, 1.58 mmol) in diethyl ether (50 mL) was added to a Schlenk tube containing finely cut Na (0.036 g, 1.58 mmol) at about 25 °C. After stirring for 2 days, some Zn metal was precipitated. The solution was filtered, and the solvent was removed in a dynamic vacuum. The residue was redissolved in hexane (5 mL), and storage for 2 days in a freezer (ca. −40 °C) afforded large colorless X-ray quality crystals of **4**. Yield: 0.174 g, 23.9%; m.p. > 360 °C (when the temperature was kept at ca. 360 °C for several minutes, **4** decomposed, and a black solid was deposited); $^1H$ NMR (300 MHz, $C_6D_6$, 25 °C): $\delta = 1.00$ (d, 12H, *o*-CH($CH_3$)$_2$, $^3J_{HH} = 6.9$ Hz), 1.12 (d, 12H, *o*-CH($CH_3$)$_2$, $^3J_{HH} = 6.9$ Hz), 2.86 (sept, 4H, $CH(CH_3)_2$, $^3J_{HH} = 6.9$ Hz), 7.06–7.24 ppm (m, 9H, *m*-$C_6H_3$, *p*-$C_6H_3$, *m*-Dipp, and *p*-Dipp; Dipp = 2,6-*i*$Pr_2C_5H_3$); $^{13}C\{^1H\}$ NMR ($C_6D_6$, 100.6 MHz, 25 °C): $\delta = 24.7$ ($CH(CH_3)_2$), 24.8 ($CH(CH_3)_2$), 30.4 ($CH(CH_3)_2$), 123.0 (*m*-Dipp), 125.7 (*p*-$C_6H_3$), 127.6 (*p*-Dipp), 128.3 (*m*-$C_6H_3$), 142.3 (*i*-Dipp), 146.9 (*o*-$C_6H_3$), 147.4 (*o*-Dipp), 162.4 ppm (*i*-$C_6H_3$).

**5**: The iodide derivative **3** (1.00 g, 1.70 mmol) and NaH (0.060 g, 2.50 mmol) were combined with THF (50 mL) under an inert atmosphere of dry argon at ambient temperature. The mixture was stirred for 2 days, the solvent was then removed in a dynamic vacuum, and the residue was extracted with hexane (50 mL). The slurry was allowed to settle, and the mother liquor was separated from the precipitate (NaI and excess NaH). The volume was concentrated to about 10 mL, and storage for 2 days in a freezer (ca. −40 °C) afforded colorless X-ray quality crystals of **5**. Yield: 0.81 g, 89.1% (based on **3**); decomposed before melting (loss of crystallinity started at 210 °C, and decomposition of **5** to a black solid was observed at 290°); $^1H$ NMR (300 MHz, $C_6D_6$, 25 °C): $\delta = 1.01$ (d, 12H, *o*-CH($CH_3$)$_2$, $^3J_{HH} = 6.9$ Hz), 1.11 (d, 12H, *o*-CH($CH_3$)$_2$, $^3J_{HH} = 6.9$ Hz), 2.91 (sept, 4H, $CH(CH_3)_2$, $^3J_{HH} = 6.9$ Hz), 4.84 (s, 1H, ZnH), 7.04–7.25 ppm (m, 9H, *m*-$C_6H_3$, *p*-$C_6H_3$, *m*-Dipp, and *p*-Dipp); $^{13}C\{^1H\}$ NMR ($C_6D_6$, 100.6 MHz, 25 °C): $\delta = 24.3$ ($CH(CH_3)_2$), 25.1 ($CH(CH_3)_2$), 30.6 ($CH(CH_3)_2$), 123.2 (*m*-Dipp), 126.0 (*p*-$C_6H_3$), 127.8 (*p*-Dipp), 128.5 (*m*-$C_6H_3$), 143.4 (*i*-Dipp), 146.7 (*o*-$C_6H_3$), 148.7 (*o*-Dipp), 155.7 ppm (*i*-$C_6H_3$); IR (nujol): $\tilde{\nu}_{(Zn\text{-}H)}$ bands are likely obscured by overlapping of ligand vibrations.

**6**: Compound **5** (0.50 g, 1.08 mmol) and NaH (0.039 g, 1.62 mmol) were combined in THF (50 mL). The mixture was stirred for 2 days, the solvent was then removed in a dynamic vacuum, and the residue was extracted with PhMe (50 mL). The slurry was allowed to settle, and the mother liquor was separated from the precipitate (NaH) by a filter cannula. The solvent volume was concentrated to about 10 mL, and storage for 2 days in a freezer (ca. −18 °C) afforded colorless X-ray quality crystals of **6**. Yield: 1.03 g, 87.3% (based on **5**); decomposed before melting (loss of crystallinity started at 235 °C, and decomposition of **6** to a black solid was seen at 268 °C); $^1H$ NMR (300 MHz, $C_6D_6$, 25 °C): $\delta = 1.09$ (d, 12H, *o*-CH($CH_3$)$_2$, $^3J_{HH} = 6.9$ Hz), 1.15 (d, 12H, *o*-CH($CH_3$)$_2$, $^3J_{HH} = 6.9$ Hz), 2.04 (br, 1H, $Zn_2NaH$), 2.99 (sept, 4H, $CH(CH_3)_2$, $^3J_{HH} = 6.6$ Hz), 7.01–7.27 ppm (m, 9H, *m*-$C_6H_3$, *p*-$C_6H_3$, *m*-Dipp, and *p*-Dipp); $^{13}C\{^1H\}$ NMR ($C_6D_6$, 100.6 MHz, 25 °C): $\delta = 23.6$ ($CH(CH_3)_2$), 25.2 ($CH(CH_3)_2$), 30.7 ($CH(CH_3)_2$), 122.4 (*m*-Dipp), 127.3 (*p*-$C_6H_3$), 146.8 (*i*-Dipp), 148.1 (*o*-$C_6H_3$), 148.8 (*o*-Dipp), 158.7 ppm (*i*-$C_6H_3$), *m*-$C_6H_3$ and *p*-Dipp

 © 2006 Wiley-VCH Verlag GmbH & Co. KGaA, Weinheim 

resonances are likely obscured by the $C_6H_6$ signal; IR (nujol): $\tilde{\nu}_{(Zn\text{-}H)}$ bands are likely obscured by overlapping of ligand vibrations.

Received: May 16, 2006
Published online: August 14, 2006

**Keywords:** density functional calculations · hydride ligands · steric hindrance · structure elucidation · zinc

[1] a) I. Resa, E. Carmona, E. Gutierrez-Puebla, A. Monge, *Science* **2004**, *305*, 1136 – 1138; b) D. del Río, A. Galindo, I. Resa, E. Carmona, *Angew. Chem.* **2005**, *117*, 1270 – 1273; *Angew. Chem. Int. Ed.* **2005**, *44*, 1244 – 1247.

[2] Some examples of Hg–Hg bonds and Cd–Cd bonds have been reported: a) D. Brwvo-Zhivotovskii, M. Yozefovich, M. Bendikov, Y. Apeloig, *Angew. Chem.* **1999**, *111*, 1169 – 1171; *Angew. Chem. Int. Ed.* **1999**, *38*, 1100 – 110; b) R. Faggiani, R. J. Gillespie, J. E. Vekris, *J. Chem. Soc. Chem. Commun.* **1986**, 517; c) D. L. Reger, S. S. Mason, A. L. Rheingold, *J. Am. Chem. Soc.* **1993**, *115*, 10406 – 10407.

[3] a) Y. Xie, H. F. Schaefer III, R. B. King, *J. Am. Chem. Soc.* **2005**, *127*, 2818 – 2819; b) H. S. Kang, *J. Phys. Chem. A* **2005**, *109*, 4342 – 4351; c) J. W. Kress, *J. Phys. Chem. A* **2005**, *109*, 7757 – 7763; d) Z.-Z. Xie, W. H. Fang, *Chem. Phys. Lett.* **2005**, *404*, 212 – 216; e) Z.-Z. Liu, W. Q. Tian, J.-K. Feng, G. Zhang, W.-Q. Li, *J. Mol. Struct.* **2006**, *758*, 127 – 138.

[4] Y. Wang, B. Quillian, P. Wei, H. Wang, X.-J. Yang, Y. Xie, R. B. King, P. von R. Schleyer, H. F. Schaefer III, G. H. Robinson, *J. Am. Chem. Soc.* **2005**, *127*, 11944 – 11945.

[5] Crystallographic data for **4**, **5**, and **6** were recorded at 90 K with $Mo_{K\alpha}$ radiation ($\lambda = 0.71073$ Å). **4**: $a = 12.2630(15)$, $b = 16.883(2)$, $c = 12.6996(16)$ Å, $\beta = 92.419(2)°$, monoclinic, space group $P2_1$, $Z = 2$, $R1 = 0.0650$ for 9529 ($I > 2\sigma(I)$) data, w$R2$ (all data) = 0.1481. **5**: $a = 12.3101(8)$, $b = 16.8622(10)$, $c = 12.6693(8)$ Å, $\beta = 92.9500(10)°$, monoclinic, space group $P2_1$, $Z = 2$, $R1 = 0.0316$ for 15989 ($I > 2\sigma(I)$) data, w$R2$ (all data) = 0.0722. **6**: $a = 16.641(17)$, $b = 16.656(17)$, $c = 28.38(3)$ Å, $\beta = 109.722(19)°$, monoclinic, space group $P2_1/c$, $Z = 4$, $R1 = 0.0642$ for 10647 ($I > 2\sigma(I)$) data, w$R2$ (all data) = 0.1557. CCDC-606921 (**4**), CCDC-606920 (**5**), and CCDC-606922 (**6**) contain the supplementary crystallographic data for this paper. These data can be obtained free of charge from The Cambridge Crystallographic Data Centre via www.ccdc.cam.ac.uk/data_request/cif.

[6] a) T. Nguyen, A. D. Sutton, M. Brynda, J. C. Fettinger, G. J. Long, P. P. Power, *Science* **2005**, *310*, 844 – 847; b) N. J. Hardman, R. J. Wright, A. D. Phillips, P. P. Power, *J. Am. Chem. Soc.* **2003**, *125*, 2667 – 2679; c) M. Stender, A. D. Phillips, R. J. Wright, P. P. Power, *Angew. Chem.* **2002**, *114*, 1863 – 1865; *Angew. Chem. Int. Ed.* **2002**, *41*, 1785 – 1787; d) B. Twamley, C. D. Sofield, M. M. Olmstead, P. P. Power, *J. Am. Chem. Soc.* **1999**, *121*, 3357 – 3367; e) J. J. Ellison, K. Ruhlandt-Senge, H. H. Hope, P. P. Power, *Inorg. Chem.* **1995**, *34*, 49 – 54.

[7] a) N. A. Bell, P. T. Moseley, H. M. M. Shearer, C. B. Spencer, *J. Chem. Soc. Chem. Commun.* **1980**, 359; b) A. Looney, R. Han, I. B. Gorrell, M. Cornebise, K. Yoon, G. Parkin, A. L. Rheingold, *Organometallics* **1995**, *14*, 274 – 284; c) W. Kläui, U. Schilde, M. Schmidt, *Inorg. Chem.* **1997**, *36*, 1598; d) M. Krieger, B. Neumüller, K. Dehnicke, *Z. Anorg. Allg. Chem.* **1998**, *624*, 1563; e) H. Hao, C. Cui, H. W. Roesky, G. Bai, H.-G. Schmidt, M. Noltemeyer, *Chem. Commun.* **2001**, 1118 – 1119.

[8] F. Weinhold, C. R. Landis, *Valency and Bonding. A Natural Bond Orbital Donor-Acceptor Perspective*, Cambridge University Press, Cambridge, **2005**, p. 556.

[9] DFT calculations were performed at the B3LYP/6-31g* level by using simplified models based on the X-ray diffraction structures of **4** and **6** on which isopropyl groups of the flanking aryls were replaced with protons. The single point (SP) calculations were performed by using Gaussian 03 software (Gaussian 03 (Revision B.03): M. J. Frisch et al. (see the Supporting Information). The representations of Kohn–Sham orbitals were generated using the MOLEKEL package (MOLEKEL, P. Flukiger, H. P. Luthi, S. Portmann, J. Weber, MOLEKEL 4.3, Swiss Center for Scientific Computing, Manno, Switzerland, **2000–2002**), and the Wiberg bond orders were computed from SP B3LYP/6-31g* calculations using the AOMix program (AOMIX, S. I. Gorelsky, AOMix program, Rev. 5.44, http://www.obbligato.com/software/aomix/).

 © 2006 Wiley-VCH Verlag GmbH & Co. KGaA, Weinheim 

*Diphosphite Ligands*

DOI: 10.1002/anie.200601978

# Regioselectivity with Hemispherical Chelators: Increasing the Catalytic Efficiency of Complexes of Diphosphanes with Large Bite Angles**

*David Sémeril, Catherine Jeunesse, Dominique Matt,* and Loïc Toupet*

The entrapment of substrates in molecular pockets that incorporate a metal ion constitutes an exciting approach to catalytic transformations displaying shape-, regio-, and enantioselectivity.[1–3] The environment of a bound substrate can be closely controlled by confinement of the metal center, in particular enabling a catalytic reaction to be driven towards the product that best adapts to the steric restraints imposed by the confining structure. Although these and other effects of coordination are seen to operate ubiquitously in biology, their transposition to catalytic systems of industrial relevance still remains limited.[4–8]

Calix[4]arenes are molecules readily fixed in various conformations that provide very different relative orientations of substituent groups. These substituent groups may contain donor atoms and the commonly encountered *cone* conformer thus provides not only a particularly useful plat-

[*] Dr. D. Sémeril, Dr. C. Jeunesse, Dr. D. Matt
Laboratoire de Chimie Inorganique Moléculaire
LC3 CNRS
Université Louis Pasteur
67008 Strasbourg Cedex (France)
Fax: (+33) 390-241-749
E-mail: dmatt@chimie.u-strasbg.fr
Dr. L. Toupet
Groupe Matière Condensée et Matériaux
UMR 6626 CNRS
Université de Rennes 1
35042 Rennes Cedex (France)

[**] Financial support from the Agence Nationale de la Recherche is gratefully acknowledged.

Supporting information for this article is available on the WWW under http://www.angewandte.org or from the author.


InterScience
© 2006 Wiley-VCH Verlag GmbH & Co. KGaA, Weinheim

form for the construction of chelators with a constrained bite angle,[10] but also a convenient means of generating secondary coordination spheres.[9] We now report the synthesis and characterization of pocket-shaped, calixarene-based diphosphites that combine the advantage of an effective bite-angle control with that of steric pressure exerted, in the present case, by lateral pendent groups, anchored to two distal oxygen atoms of the macrocyclic skeleton. The catalytic activity of $Pd^{II}$ and $Rh^{I}$ complexes of these diphosphites has been evaluated in the allylic alkylation of unsymmetrical allyl acetates and in the hydroformylation of olefins.

Diphosphites **3** and **4** were prepared by double deprotonation of the corresponding dialkylated precursors **1** and **2**, respectively, followed by reaction with [(*S*)-(1,1′-binaphthalene-2,2′-diyl)]chlorophosphite (Scheme 1). The conical structure of the resulting calixarenes was unambiguously inferred from the $^{13}C$ NMR spectra, which both display $ArCH_2Ar$ signals near 32 ppm ($\delta = 31.96/33.30$ (**3**), 31.78/33.54 ppm (**4**)), that is, in a range typical for this conformation. In keeping with $C_2$ symmetry, the $ArCH_2$ protons of each ligand appear as two distinct AB patterns in the $^1H$ NMR spectrum, while the corresponding $^{31}P$ NMR spectra exhibit a single signal in the phosphite region ($\delta = 133.76$ (**3**), 123.59 ppm (**4**)). The rather large separation between the distal phenoxy rings of the calixarene moiety, combined with the steric bulk created by the "binaphthyl" moieties, makes these ligands, a priori, suitable for the synthesis of chelate complexes in which the P–M–P bite angle should significantly surpass 90°.

Complex **5** was obtained quantitatively by addition of one equivalent of **3** to a $[\{Pd(\eta^3\text{-allyl})Cl\}_2]/NH_4PF_6$ suspension in acetone. The formation of a chelate complex was inferred from the corresponding mass spectrum, which shows an intense peak at 1507.57, corresponding to the $[Pd(allyl)\cdot\mathbf{3}]^+$ cation. Owing to the presence of a $\eta^3$-bonded allyl ligand, the whole complex is no longer $C_2$ symmetrical. This is best seen in the $^1H$ NMR spectrum, which exhibits four AB systems for the $ArCH_2$ protons. The same features were observed for the related complex **6**, obtained in a similar way from **4**. As revealed by a single crystal X-ray diffraction study, diphosphite **3** displays a bite angle of ca. 107.5° in complex **5**. Obviously, the steric encumbrance of the binaphthyl units largely contributes to such a large bite angle (Figure 1), as in a related calixarene bearing significantly smaller $P(OR)_2$ moieties the P–M–P angle was found to be only 101°.[11] The molecular structure further shows that the metal–allyl moiety sits deep in a pocket generated by two nearly symmetrically sited naphthyl moieties and the two propoxy groups. We note also that, owing to the presence of a typically flattened cone conformation (Figure 1), the *O*-propyl groups are pushed towards the palladium center, and are therefore significantly involved in an effective embrace of the allyl group.

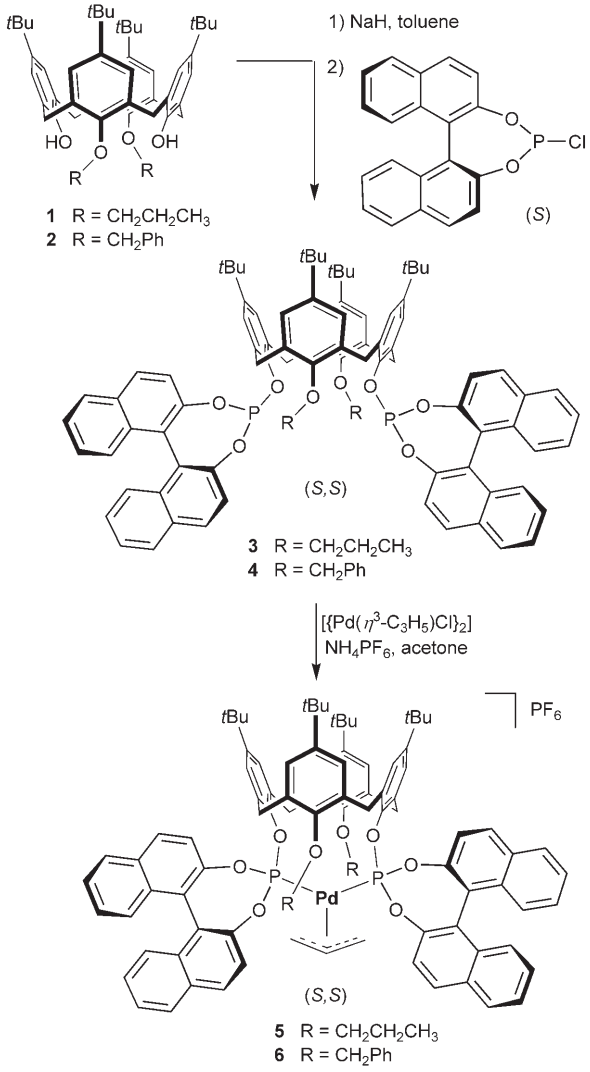


***Scheme 1.*** Synthesis of the diphosphites and their cationic allyl–palladium complexes.

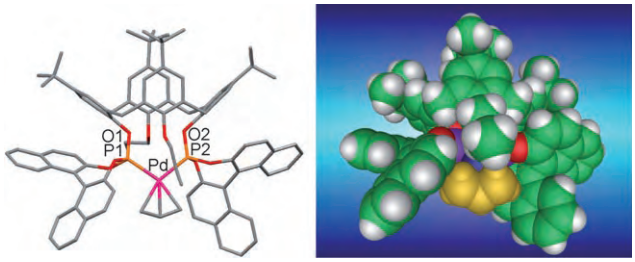


***Figure 1.*** Molecular structure of **5**. In the CPK representation (right), the allyl group is in yellow. Selected bond lengths [Å] and angles [°]: Pd–P1 2.292(2), Pd–P2 2.294(2); P1–Pd–P2 107.50(8), O1–P1–Pd 119.6(2), O2–P2–Pd 119.3(2); interplanar angle between the two naphthyl moieties embracing the allyl group: 49.6°; dihedral angles between facing phenoxy rings: 81.1° (O1/O2), 2.0° (O3/O4). The $PF_6$ anion and the six $CH_2Cl_2$ solvent molecules are omitted for clarity.

The ligands **3** and **4** were assessed in the Pd-catalyzed alkylation of 3-phenylallyl acetate **7** with dimethyl malonate (Scheme 2). With both ligands, the linear product **9** was formed with over 98% selectivity (98.1% for **3**; 98.3% for **4**). This remarkably high regioselectivity sharply contrasts with that obtained for the same substrate using other diphosphanes.[12–16] Diphenylphosphanylethane (dppe), for example, led under similar conditions to a **9**:**8** ratio of 91.8:8.2. The highest linear:branched ratio obtained with a diphosphite,

 © 2006 Wiley-VCH Verlag GmbH & Co. KGaA, Weinheim 

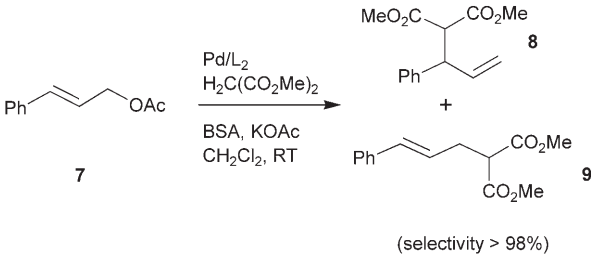


***Scheme 2.*** Palladium-catalyzed allylic substitution of the unsymmetrical substrate **7**. BSA = *N*,*O*-Bis(trimethylsilyl)acetamide.

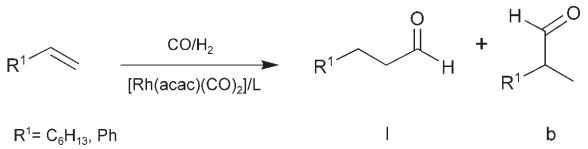


***Scheme 3.*** Rhodium-catalyzed hydroformylation of 1-octene and styrene. acac = acetylacetone.

93:7, was reported by Claver et al. for a furanoside diphosphite.[16] The unusual selectivities obtained with **3** and **4** might be explained by the presence of pockets created around the metal center. Molecular models clearly show that in the allyl complex formed with **7**, the unsubstituted allylic carbon atom is the one for which the incoming nucleophile interferes least with the naphthyl and *O*-alkyl groups, whatever the orientation of the phenylallyl group, *syn* or *anti*. It should be recalled here that steric parameters become particularly important in alkylation reactions that involve a late transition state. It is further interesting to note that, unlike the situation found in related Pd–allyl–Xantphos complexes,[17] the allyl embrace by the calixarene–diphosphites involves not only P substituents, but also auxiliary side groups axially positioned with respect to the metal center, hence resulting in an increased steric protection of the allyl moiety.

The homogeneous hydroformylation of olefins is the favorite application for diphosphanes with large bite angles.[5,18–23] The ligands **3** and **4** were therefore tested in the rhodium-catalyzed hydroformylation of *n*-octenes (Scheme 3). A large excess of phosphite was required to obtain high regioselectivities (compare entries 1 and 2 and 4 and 5 in Table 1), indicating relatively inefficient complexation and the possible involvement of a Rh catalyst species with only one or even no phosphite coordinated through its P atom.

Diphosphite **3**, bearing two pendant propoxy groups, turned out to be very effective for the hydroformylation of 1-octene. TOF values up to 1440 (Table 1, entry 2) were observed, for a l:b ratio as high as 58.0. We observed that the high preference for the linear product was maintained until the end of the reaction. Nevertheless, an important proportion of isomeric products was produced (ca. 50% of the amount of octene converted). This is possibly due to the steric encumbrance created about transient "Rh(isoalkyl)" moieties, which favors β elimination in these intermediates (and hence isomerization) over a carbonylation step. The ability of the Rh/**3** system to isomerize 1-octene led us to test **3** in the hydroformylation of the less reactive *trans*-2-octene. Here the TOF value droped to 170, but the selectivity towards the linear aldehyde remained good, the l:b ratio being kept in the range 4.3–4.6 (Table 1, entry 3). For comparison, using $PPh_3$[24] or van Leeuwen's most bulky Xantphite[25] gave l:b ratios of only 0.9 and 2.8, respectively.

The relevance of the pendent side groups for the regioselectivity was shown by replacing the propoxy substituents by the bulkier benzyloxy groups. Thus, in the hydroformylation of 1-octene with **4** at 80°C, the l:b ratio rose to 80 without loss of activity (Table 1, entry 5) and with little isomerization. When used in the hydroformylation of *trans*-2-octene at 120°C, **4** resulted in a high selectivity towards the linear aldehyde, the l:b ratio in this case reaching 24.9 (Table 1, entry 6). The latter result implies that under these conditions, isomerization towards 1-octene occurs.

Finally, the two diphosphites were assessed in the hydroformylation of styrene (Table 2, entries 1 and 3). In all catalytic runs, the linear aldehyde was the major product, whereas conventional mono- and diphosphanes usually give more branched product.[26] For example, at 20 bar, and after 20% conversion, the selectivity towards the linear aldehyde was 58.8% with **3** and 73.6% with the bulkier diphosphite **4**. Decreasing the pressure of $CO/H_2$ from 20 to 10 bar increased the selectivity to 67.4 (**3**) and 76.1% (**4**), respectively, without reducing significantly the activity (Table 2, entries 2 and 4). This unusual regioselectivity can, in line with van Leeuwen's findings made for ligands with large bite angles, be assigned to a pocket effect. The fact that the selectivity of **4** towards the linear aldehyde is higher than that of the propoxy-substituted ligand **3** is of course a clear indication that the degree of steric

***Table 1:*** Rhodium-catalyzed hydroformylation of *n*-octenes using diphosphites **3** and **4**.

| Entry | Olefin | Ligand | L/Rh | *t* [h] | Conversion [%][a] | TOF[b] | l:b[c] | Isomerization [%][d] |
|---|---|---|---|---|---|---|---|---|
| 1[e] | 1-octene | **3** | 1 | 3.75 | 32.1 | 430 | 3.2 | 9.6 |
| 2[e] | 1-octene | **3** | 10 | 1.2 | 34.5 | 1440 | 58.0 | 17.0 |
| | | | | 8 | 98.5 | 620 | 56.3 | 46.7 |
| 3[f] | *trans*-2-octene | **3** | 10 | 2 | 41.6 | 170 | 4.3 | 1.9 |
| | | | | 8 | 70.0 | 70 | 4.6 | 3.4 |
| 4[e] | 1-octene | **4** | 1 | 1 | 23.1 | 1150 | 7.2 | 2.6 |
| 5[e] | 1-octene | **4** | 10 | 1 | 23.9 | 1190 | n.d.[g] | 3.0 |
| | | | | 24 | 87.3 | 180 | 80.1 | 12.1 |
| 6[f] | *trans*-2-octene | **4** | 10 | 8 | 44.6 | 50 | 24.9 | 3.3 |

[a] Determined by GC; calibration based on decane. [b] mol(converted octene) per mol(Rh) and hour. [c] Ratio, percent of linear (l) aldehyde to percent of branched (b) aldehyde. [d] Isomerized 1-octene/all octenes or 2-octene/all octenes. [e] Reaction conditions: 1-octene (10 mmol), 1-octene/Rh = 5000, initial pressure (at 80°C): 20 bar $CO/H_2$ (1/1), $T$ = 80°C, toluene/*n*-decane (15 mL/0.5 mL), incubation overnight at 80°C. [f] Reaction conditions: *trans*-2-octene (3.2 mmol), *trans*-2-octene/Rh = 800, initial pressure (at 120°C): 20 bar $CO/H_2$ (1/1), $T$ = 120°C, toluene/*n*-decane (15 mL/0.5 mL), incubation overnight at 80°C. [g] Not determined, because of a very low amount of branched aldehyde.

 © 2006 Wiley-VCH Verlag GmbH & Co. KGaA, Weinheim 

***Table 2:*** Rhodium-catalyzed hydroformylation of styrene using diphosphites **3** and **4**.[a]

| Entry | Ligand | $p(CO/H_2)$ [bar] | $t$ [h] | Conversion [%][b] | TOF[c] | Branched [%] | Linear [%] |
|---|---|---|---|---|---|---|---|
| 1 | **3** | 20 | 5 | 18.3 | 180 | 41.2 | 58.8 |
| 2 | **3** | 10 | 5 | 21.7 | 220 | 34.8 | 65.2 |
| | | | 24 | 58.7 | 120 | 32.6 | 67.4 |
| 3 | **4** | 20 | 4.5 | 19.1 | 210 | 26.4 | 73.6 |
| 4 | **4** | 10 | 5.5 | 21.4 | 200 | 23.9 | 76.1 |
| | | | 24 | 64.4 | 134 | 23.4 | 76.6 |

[a] Reaction conditions: styrene (10 mmol), styrene/Rh = 5000, L/Rh = 10, $CO/H_2$ (1/1) initial pressure (at 80 °C), $T$ = 80 °C, toluene/*n*-decane (15 mL/0.5 mL), incubation overnight. [b] Determined by GC, calibration based on decane. [c] mol(converted styrene) per mol(Rh) and h.

protection about the metal center plays a key role for the catalytic outcome. This is also in keeping with the observation that the selectivity obtained with **4** is somewhat better than that reported for the Xantphites, which have similar large bite angles, but which are deprived of any side group able to exert an additional steric pressure on the first coordination sphere of the metal.[25]

Overall, calixarenes **3** and **4** provide unprecedented examples of hemispherical chelators able to drive allylic alkylation as well as olefin hydroformylation reactions towards the formation of "linear" products. With these ligands, the metal embrace is particularly effective, the large bite angles being associated with a conformation of the calixarene which produces a steric protection by the *O*-alkyl substituents of the apical positions on the metal, already encumbered by the substituents on the bound P atoms. These steric effects are cooperative consequences of the known fact that flattening of the orientation of two opposed phenyl rings of a calix[4]arene to the mean macrocyclic plane results in a steeper orientation of the other pair.

## *Experimental Section*

Full experimental details for all products are given in the Supporting Information.

**3**: $^1$H NMR (300 MHz, $C_6D_6$): $\delta$ = 7.69–7.27 (15 H, $CH_{arom}$), 7.18–6.98 (10 H, $CH_{arom}$), 6.95–6.75 (7 H, $CH_{arom}$), 5.10 and 3.52 (AB system, 4 H, $ArCH_2Ar$, $^2J$ = 13.0 Hz), 5.00 and 3.00 (AB system, 4 H, $ArCH_2Ar$, $^2J$ = 13.0 Hz), 4.00–3.79 (m, 4 H, $OCH_2$), 2.06–1.85 (m, 4 H, $CH_2CH_3$), 1.26 (s, 18 H, $C(CH_3)_3$), 1.23 (s, 18 H, $C(CH_3)_3$), 0.39 ppm (t, 6 H, $CH_2CH_3$, $^3J$ = 7.4 Hz). $^{13}$C{$^1$H} NMR (75 MHz, $C_6D_6$): $\delta$ = 154.10–121.98 ($C_{arom}$), 77.34 (s, $OCH_2$), 33.81 (s, $C(CH_3)_3$), 33.79 (s, $C(CH_3)_3$), 33.30 (s, $ArCH_2Ar$), 31.96 (s, $ArCH_2Ar$), 31.43 (s, $C(CH_3)_3$), 31.40 (s, $C(CH_3)_3$), 22.96 (s, $CH_2CH_3$), 9.44 ppm (s, $CH_2CH_3$). $^{31}$P{$^1$H} NMR (121 MHz, $C_6D_6$): $\delta$ = 133.76 ppm (s, $OP(OAr)_2$).

Crystal structure of **5**·6 $CH_2Cl_2$: $M_r$ = 2163.56, monoclinic, $P2_1$, $a$ = 13.4071(7), $b$ = 23.4689(8), $c$ = 17.0844(8) Å, $\beta$ = 102.469(4)°, $V$ = 5248.8(4) Å$^3$, $Z$ = 2, $D_x$ = 1.369 mg m$^{-3}$, $\lambda(Mo_{K\alpha})$ = 0.71073 Å, $\mu$ = 5.91 cm$^{-1}$, $F(000)$ = 2228, $T$ = 100(1) K. Data were collected on an Oxford Diffraction Xcalibur Saphir 3 diffractometer (graphite $Mo_{K\alpha}$ radiation, $\lambda$ = 0.71073 Å). The structure was solved with SIR-97[27] which revealed the non-hydrogen atoms of the molecule. After anisotropic refinement, many hydrogen atoms were found with a Fourier difference analysis. The whole structure was refined with SHELX-97[28] and full-matrix least-square techniques (use of $F^2$; $x$, $y$, $z$, $\beta_{ij}$ for Pd, P, F, Cl, C and O atoms, $x$, $y$, $z$ in riding mode for H atoms; 1163 variables and 11795 observations with $I > 2.0\,\sigma(I)$; calc $w = 1/[\sigma^2(F_o^2) + (0.18P)^2 + 28.7P]$ where $P = (F_o^2 + 2F_c^2)/3$. $R$ = 0.088, $R_w$ = 0.248, $S_w$ = 0.938, $\Delta\rho < 2.9$ e Å$^{-3}$. CCDC 297616 contains the supplementary crystallographic data for this paper. These data can be obtained free of charge from The Cambridge Crystallographic Data Centre via www.ccdc.cam.ac.uk/data_request/cif.

Received: May 18, 2006
Published online: August 3, 2006

**Keywords:** allylic alkylation · calixarenes · diphosphites · hydroformylation · regioselectivity

[1] B. Kersting, *Z. Anorg. Allg. Chem.* **2004**, *630*, 765.
[2] C. Jeunesse, D. Armspach, D. Matt, *Chem. Commun.* **2005**, 5603.
[3] T. S. Koblenz, H. L. Dekker, C. G. de Koster, P. W. N. M. van Leeuwen, J. N. H. Reek, *Chem. Commun.* **2006**, 1700.
[4] M. T. Reetz, S. R. Waldvogel, *Angew. Chem.* **1997**, *109*, 870; *Angew. Chem. Int. Ed. Engl.* **1997**, *36*, 865.
[5] R. Paciello, L. Siggel, M. Röper, *Angew. Chem.* **1999**, *111*, 2045; *Angew. Chem. Int. Ed.* **1999**, *38*, 1920.
[6] V. F. Slagt, J. N. H. Reek, P. C. J. Kamer, P. W. N. M. van Leeuwen, *Angew. Chem.* **2001**, *113*, 4401; *Angew. Chem. Int. Ed.* **2001**, *40*, 4271.
[7] D. Armspach, D. Matt, F. Peruch, P. Lutz, *Eur. J. Inorg. Chem.* **2003**, 805.
[8] S. Steyer, C. Jeunesse, J. Harrowfield, D. Matt, *Dalton Trans.* **2005**, 1301.
[9] *Calixarenes 2001* (Eds.: Z. Asfari, V. Böhmer, J. M. Harrowfield, J. Vicens), Kluwer Academic Publishers, Dordrecht, **2001**.
[10] P. Kuhn, C. Jeunesse, D. Sémeril, D. Matt, P. Lutz, R. Welter, *Eur. J. Inorg. Chem.* **2004**, 4602.
[11] C. Kunze, D. Selent, I. Neda, M. Freytag, P. G. Jones, R. Schmutzler, W. Baumann, A. Börner, *Z. Anorg. Allg. Chem.* **2002**, *628*, 779.
[12] R. Prétôt, A. Pfaltz, *Angew. Chem.* **1998**, *110*, 337; *Angew. Chem. Int. Ed.* **1998**, *37*, 323.
[13] S.-L. You, X.-Z. Zhu, Y.-M. Luo, X.-L. Hou, L.-X. Dai, *J. Am. Chem. Soc.* **2001**, *123*, 7471.
[14] D. Laurenti, M. Feuerstein, G. Pèpe, H. Doucet, M. Santelli, *J. Org. Chem.* **2001**, *66*, 1633.
[15] M. Diéguez, O. Pàmies, C. Claver, *J. Org. Chem.* **2005**, *70*, 3363.
[16] M. Diéguez, O. Pàmies, C. Claver, *Adv. Synth. Catal.* **2005**, *347*, 1257.
[17] M. Kranenburg, P. C. J. Kamer, P. W. N. M. van Leeuwen, *Eur. J. Inorg. Chem.* **1998**, 25; Xantphos: 9,9-dimethyl-4,5-bis(diphenylphosphanyl)xanthene.
[18] C. P. Casey, G. T. Whiteker, M. G. Melville, L. M. Petrovich, J. A. Gavney, Jr., D. R. Powell, *J. Am. Chem. Soc.* **1992**, *114*, 5535.
[19] L. A. van der Veen, P. H. Keeven, G. C. Schoemaker, J. N. H. Reek, P. C. J. Kamer, P. W. N. M. van Leeuwen, M. Lutz, A. L. Spek, *Organometallics* **2000**, *19*, 872.
[20] P. W. N. M. van Leeuwen, P. C. J. Kamer, J. N. H. Reek, P. Dierkes, *Chem. Rev.* **2000**, *100*, 2741.
[21] W. Ahlers, M. Röper, P. Hofmann, D. C. M. Warth, R. Paciello, WO 01/58589 (BASF), **2001**.
[22] J. R. Briggs, G. T. Whiteker, *Chem. Commun.* **2001**, 2174.
[23] R. P. J. Bronger, P. C. J. Kamer, P. W. N. M. van Leeuwen, *Organometallics* **2003**, *22*, 5358.
[24] L. A. van der Veen, P. C. J. Kamer, P. W. N. M. van Leeuwen, *Angew. Chem.* **1999**, *111*, 349; *Angew. Chem. Int. Ed.* **1999**, *38*, 336.

 © 2006 Wiley-VCH Verlag GmbH & Co. KGaA, Weinheim 

[25] C. B. Dieleman, P. C. J. Kamer, J. N. H. Reek, P. W. N. M. van Leeuwen, *Helv. Chim. Acta* **2001**, *84*, 3269; Xantphite ligands are derived from the 2,7,9,9-tetramethyl-9*H*-xanthen-4,5-diol skeleton and the appropriate phosphorochloridite.
[26] C. K. Brown, G. Wilkinson, *J. Chem. Soc. A* **1970**, 2753.
[27] "SIR97: a new tool for crystal structure determination and refinement": A. Altomare, M. C. Burla, M. Camalli, G. Cascarano, C. Giacovazzo, A. Guagliardi, A. G. G. Moliterni, G. Polidori, R. Spagna, *J. Appl. Crystallogr.* **1998**, *31*, 74 – 77.
[28] G. M. Sheldrick, SHELX-97, Program for the refinement of Crystal Structures, University of Göttingen, Germany, **1997**.

 © 2006 Wiley-VCH Verlag GmbH & Co. KGaA, Weinheim 

Metal–Metal Interactions

DOI: 10.1002/anie.200600800

# Conductance and Stochastic Switching of Ligand-Supported Linear Chains of Metal Atoms**

*I-Wen Peter Chen, Ming-Dung Fu, Wei-Hsiang Tseng, Jian-Yuan Yu, Sung-Hsun Wu, Chia-Jui Ku, Chun-hsien Chen,* and Shie-Ming Peng**

Molecular wires and switches are forecast to be the elemental building blocks for future electronic applications. Synthesizing 1D molecules and comprehensively understanding their electric characteristics has become one of the major focus areas of materials science. The growth of this research field has been encouraged by the discovery of a strong dependence of electron transport on the length, conjugation, conformation, and substituents of tailored molecules.[1,2] While remarkable progress has been achieved during the past decade, most of the knowledge learned has been from conjugated organic molecules whose counterpart, organometallic molecular wires,[3–17] has been rarely explored.

Herein we present quantitative measurements of single-molecule conductance of 1D multinuclear metal strings ($[M_nL_4(NCS)_2]$, $M_n = Cr_3$, $Co_3$, $Ni_3$, $Cr_5$, $Co_5$, $Ni_5$, and $Cr_7$; L = oligo-α-pyridylamine; Scheme 1).[3] The conductance

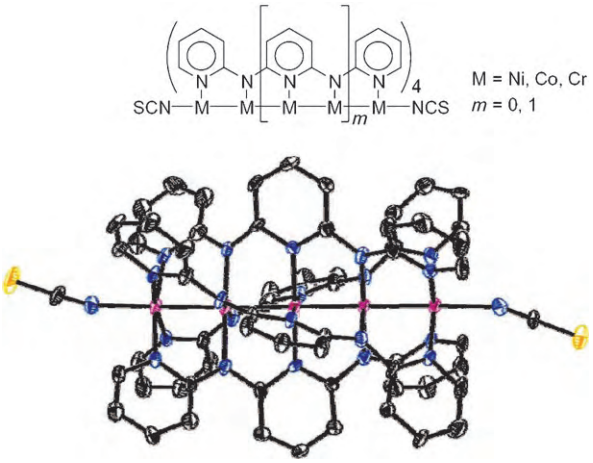


***Scheme 1.*** Top: The metal atom chain is supported by four oligo-α-pyridylamine ligands.[3] Bottom: ORTEP view of the pentacobalt complex;[19] in general the metal atoms are collinear and wrapped helically by four ligands. Co purple, N blue, S yellow, C gray.

values correlate well with the d-orbital electronic coupling between adjoining metal atoms. Among the strings, penta- and heptachromium complexes exhibit stochastic switching events. Such multinuclear strings are important in setting up a perfect platform for the study of metal–metal interactions beyond dinuclear complexes.[18] Complexes up to nonanickel (i.e., M = Ni, $m = 3$ in Scheme 1, but with Cl axial ligands) have been characterized crystallographically[3] and the length of the ligand extended up to 12 repetitive pyridylamine units ($m = 11$). While purification and crystallization become increasingly challenging owing to poorer solubility for longer oligomers, preliminary MALDI-MS spectra show that a string of 17 nickel ions ($m = 7$ in Scheme 1) is obtainable. An understanding of the conduction propagating along the metal chains will further advance progress towards molecular wires for nanodevices.

Figure 1 shows the results of STM (scanning tunneling microscopy) break junction for the trinuclear and pentanuclear string complexes.[20,21] Experimental procedures were documented in detail by the groups of Tao and Lindsay.[20,21]

[*] I-W. P. Chen, M.-D. Fu, W.-H. Tseng, J.-Y. Yu, S.-H. Wu, C.-J. Ku, Prof. C.-h. Chen[+]
Department of Chemistry
National Tsing Hua University
Hsinchu, Taiwan 30013 (Republic of China)
Fax: (+886) 3-571-1082
E-mail: chhchen@mx.nthu.edu.tw

Prof. S.-M. Peng
Department of Chemistry
National Taiwan University
Taipei, Taiwan 106 (Republic of China)
and
Institute of Chemistry
Academia Sinica
Taipei, Taiwan 115 (Republic of China)
Fax: (+886) 2-2363-6359
E-mail: smpeng@ntu.edu.tw

[+] Current Address:
Department of Chemistry
National Taiwan University
Taipei, Taiwan 106 (Republic of China)
Fax: (+886) 2-2363-6359

[**] Thanks to Professor I-C. Chen (NTHU) for fruitful discussions, to Dr. Andy H. Kung (IAMS, Academia Sinica, Taipei) for comments on the manuscript and to collaborators of S.-M.P. for the routine supply of metal string complexes. C.-h.C. acknowledges Professor T.-Y. Luh (NTU) for use of a NanoScope IIIa and the Department of Chemistry (NTHU) for the strong research support. This work was funded by the National Science Council and the Ministry of Education of the Republic of China.

Supporting information for this article is available on the WWW under http://www.angewandte.org or from the author.


InterScience
© 2006 Wiley-VCH Verlag GmbH & Co. KGaA, Weinheim

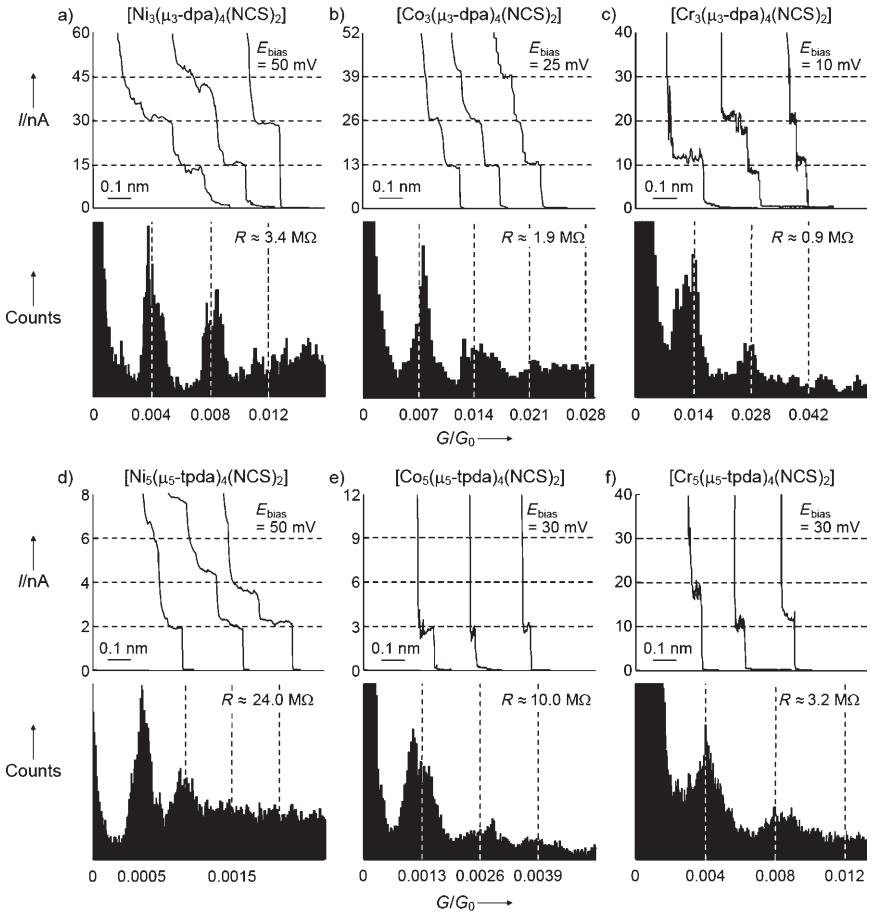


***Figure 1.*** a)–f) Single-molecule conductance of metal strings measured by STM break junction. Top panels: typical current curves acquired by stretching the molecular junctions are presented with arbitrary *x*-axis offsets. Currents and conductance of the metal string complexes decrease in quantized steps. Bottom panels: the conductance histograms are obtained from more than 2000 measurements. The resistance of a single heptachromium string is 6.9 MΩ (see Supporting Information). In the absence of molecules, no such steps or peaks are observed within the same conductance range.

Briefly, housed in a nitrogen-filled chamber, a gold STM tip is brought into and out of contact with a gold substrate in toluene, which also contains the metal strings. Upon repeated formation of the tip–substrate gap, the isothiocyanate axial ligands at the termini of the metal strings bind to the gold electrodes and complete a molecular junction. At a fixed bias voltage across the electrodes ($E_{bias}$, top panels of Figure 1), the STM tip is pulled away from the substrate, which results in the currents monitored having a stepped profile. The current values are scaled with $E_{bias}$. Controlled experiments in toluene gave exponential tunneling decay,[20,21] thus confirming that the "staircase" waveforms arise from the metal strings.

The histograms (bottom panels of Figure 1) plotted against $G/G_0$ ($G_0$ = conductance quantum for the cross section of a metallic contact being only that of a single atom; $G_0 = 2e^2/h$, $\approx (12.9\ \mathrm{k\Omega})^{-1}$).[20–23] summarize thousands of measurements. The local maxima are distributed at integer multiples of the fundamental $G_0$ values of each molecule, which suggests that the number of molecules in the junctions is one, two, three, etc.[20,21] The top-right corner of each histogram states the single-molecular resistance, $R$, which is calculated by dividing $E_{bias}$ by the fundamental current.

Although the conjugated oligopyridylamido ligand and tunneling events along the metal chains might be involved in the conduction mechanism, given that each chain has identical ligands, analogous crystallographic structures, and similar physical dimensions,[3,19,24–29] the discrepancy between the molecular resistances of the chains most likely lies in the extent of coupling of the d-orbital electrons between adjoining metal atoms. In ascending order of conductance the sequence is nickel, cobalt, and chromium for strings with the same number of metal centers. This trend correlates well with the results of extended Hückel (EH) MO calculations in which the d-electron configurations for pentanickel,[25] pentacobalt,[25] and pentachromium[26] strings are $\sigma_1^2\pi_1^4\sigma_2^2\pi_2^4\delta_{n1}^2\delta_{n2}^2\pi_{n3}^4\delta_{n3}^2\pi^{*4}_4\delta_{n4}^2\pi^{*4}_5\delta_{n5}^2\sigma_{n3}^2\sigma^{*2}_4\sigma^{*2}_5$, $\sigma_1^2\pi_1^4\sigma_2^2\pi_2^4\delta_{n1}^2\delta_{n2}^2\pi_{n3}^4\delta_{n3}^2\pi^{*4}_4\delta_{n4}^2\pi^{*4}_5\delta_{n5}^2\sigma_{n3}^1$, and $\sigma_1^2\sigma_2^2\pi_1^4\pi_2^4\delta_{n1}^2\delta_{n2}^2\delta_{n3}^2\pi_{n(dxy)}^1\pi_{n(dyz)}^1$, respectively (where the subscript n denotes nonbonding). The metal–metal bond orders for strings of nickel, cobalt, and chromium cores are 0, 0.5, and 1.5, respectively; these values indicate the degree of electron delocalization and thus the efficiency of electrons conducting through the metal centers.

The resistance of single molecules is also described by a tunneling decay constant, $\beta$, approximately given by $I \propto \exp(-\beta x)$, in which $x$ is either the number of repetitive units or the molecular dimensions and $I$ is the current. $\beta$ represents the electronic-coupling strength of the molecule along the electron pathway. A small $\beta$ value indicates a less significant impedance in electron transport through the molecule. By taking the natural logarithm of the reciprocal of resistance values against the molecular length, we obtain a small tunneling decay constant of 0.50 per Cr atom or approximately 0.21 $\mathrm{Å}^{-1}$ (see Supporting Information), which makes the Cr strings among the most conductive molecular wires reported.[2,30]

In addition to their extraordinary conductive properties, the metal strings of penta- and heptachromium complexes show an electric switching phenomenon that is not readily discernible by STM break junction. The on/off states of the two chromium strings are revealed by the conductive atomic force microscopy (CAFM) developed by Lindsay and coworkers.[31] The metal strings are attached to a gold surface and isolated within an *n*-alkanethiol matrix. The films are then incubated for 1–3 h in dichloromethane containing

 © 2006 Wiley-VCH Verlag GmbH & Co. KGaA, Weinheim 

triphenylphosphine-stabilized gold clusters (nominally 2 nm in diameter).[31,32] A metal–molecule–nanocluster junction is configured through the isothiocyanate axial ligands. The gold clusters improve the electrical contact with the gold-coated cantilever of the CAFM and enable highly reproducible current-versus-potential ($I$–$V$) measurements for single molecules.[31,32] Figure 2a demonstrates that more than 2500 $I$–$V$

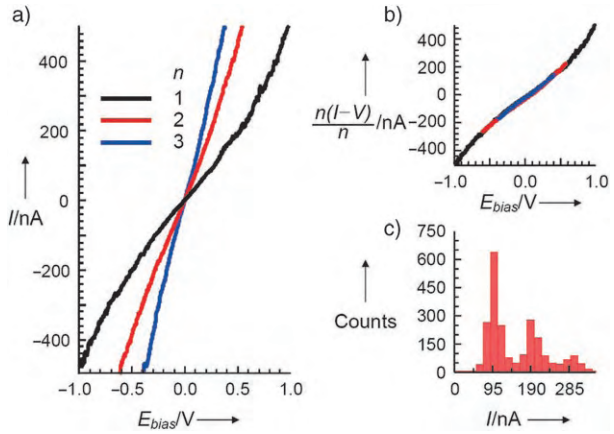


***Figure 2.*** *I–V* data of $[Cr_3(\mu_3\text{-dpa})_4(NCS)_2]$ in an *n*-octanethiol matrix measured by CAFM, see text for details. a) *I–V* curves of groups centered at integral multiples *n* of a single-molecule conductance. b) Overlap of the curves in (a) after being divided by *n* at each point. c) Histogram plot of the currents measured at 0.25 V bias. The CAFM experiments were carried out in toluene under nitrogen. The force was constantly monitored and set at 2.5 nN.

measurements of the trichromium complex can be grouped into three curves, which converge into one after the values of the curves are divided by $n$ (Figure 2b; $n = 2$ and 3, for the red and blue curves, respectively). Figure 2c is a histogram of the currents measured at a bias of 0.25 V. The strong correlation of an integral multiplicity between the three groups suggests that the one centered at 95 nA corresponds to the primary case of a single trichromium metal string sandwiched between a gold nanocluster and the substrate.

The $I$–$V$ curves and histograms for all the metal strings show a similar quantized behavior, which is consistent with the findings revealed by STM break junction, although this CAFM approach is complicated by Coulomb blockade charged at the attached gold cluster and thus the essence of the $I$–$V$ curves is not straightforward.[32] The fundamental curves of the single trinuclear and pentanuclear strings are summarized in Figures 3a and b. Note that the pentachromium string shows two fundamental curves with current values of about 410 and 66 nA at a bias of 1.0 V (blue curves in Figure 3b). The heptachromium string complex also has two sets of $I$–$V$ curves with 252 and 56 nA at a bias of 1.0 V (see Supporting Information).

Readily discernible from their histograms at a bias of 0.25 V are two sets of fundamental current values centered at 74 and 17 nA (Figure 3c) for the pentachromium string, and at 50 and 10 nA (Figure 3d) for the heptachromium string. The dataset of the more conductive complex has a $\beta$ value of 0.16 per Cr atom, thus indicating a stronger electronic

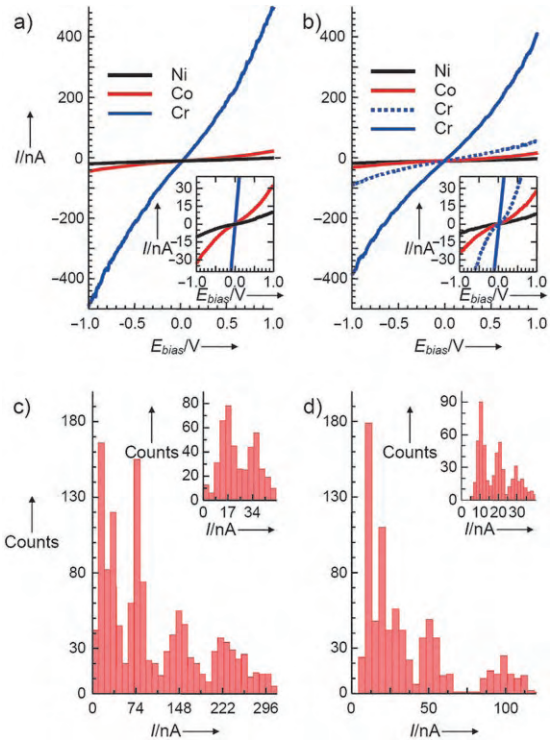


***Figure 3.*** *I–V* characteristics of metal strings measured by CAFM. Fundamental *I–V* curves of a) the trinuclear and b) the pentanuclear complexes and magnified view of the traces between ±40 nA (insets). Histograms of the currents measured at a bias of 0.25 V for c) the pentachromium and d) the heptachromium complexes; insets show the same histograms plotted with a narrower bin size (that is, the width of the histogram bars is smaller) to magnify the current range for the less conductive groups. Tri-, penta-, and heptanuclear complexes were isolated in matrices of *n*-octanethiol, *n*-tetradecanethiol, and *n*-octadecanethiol monolayers, respectively.

coupling than the $\beta$ value of 0.29 per Cr atom derived from dataset of the less conductive complex. Although the $\beta$ values are not quantitative owing to Coulomb blockade,[32] the substantial difference between the two values suggests that the two sets of conductance peaks are not due to the S–Au contacts at atop and hollow sites.[21] The ratio of the occurrence of the smaller-current dataset to that of the larger-current dataset is 345:1251 and 970:200 for penta- and heptachromium strings, respectively. The fraction of the smaller-current dataset increases with the number of chromium cores. Note that the trichromium metal string does not show two sets of primary $I$–$V$ curves, which suggests that the less-conductive set is either absent or very rare.

The imaging frames of conducting-current mode in Figure 4 display the electric switching of the pentachromium molecule. Figure 4a shows the current toggling between a low value of 17 nA and a high value of about 75 nA. In Figures 4b and c, the current switches between twice that of the less conductive mode and twice that of the more conductive mode, which suggests the presence of two pentachromium strings underneath the gold nanocluster (Figure 4d). Stochastic on/off switching has been observed in π-electron conjugated systems and alkanethiols. Recent findings narrow down the switching mechanisms to conformation effects[33] on through-

 © 2006 Wiley-VCH Verlag GmbH & Co. KGaA, Weinheim 

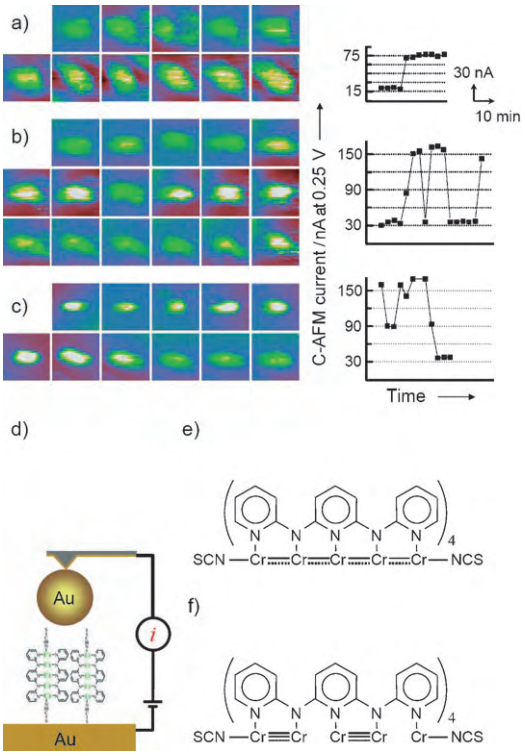


***Figure 4.*** Electric on/off switching of pentachromium strings within an *n*-tetradecanethiol matrix. a)–c) Sequential images and the plots of conducting current versus time were acquired by CAFM at a bias of 0.25 V. The time interval between each frame (30×30 nm) was about 3 min. The corresponding current magnitudes indicate that underneath each gold nanocluster (≈2 nm in diameter) there is one molecule for (a) and two molecules for (b) and (c). d) Circuit diagram of the apparatus used to take the CAFM measurements showing two sting molecules under the gold nanocluster. e),f) Structures of the pentachromium metal string with delocalized (on state) and alternating (off state) Cr—Cr bonds, respectively.

bond or through-space tunneling[34] and to sulfur–substrate fluctuations through bond breaking or molecular tilt angles associated with the sp or $sp^3$ hybridization of the sulfur atom.[35–37]

For the molecular wires studied herein, the stochastic switching cannot be entirely explained by sulfur–substrate fluctuations because all the complexes have the same axial ligand, isothiocyanate, yet only penta- and heptachromium strings clearly exhibit two sets of fundamental curves. In addition, the difference in $\beta$ values and the strong correlation of the number of chromium cores with the occurrence frequency suggest a significant effect of metal–metal interactions on the molecular conductance. The aforementioned EHMO calculations were based on delocalized conformations (or symmetric metal–metal bond lengths) and are unequivocal for nickel[4,25] and cobalt[4,19,27] strings with isothiocyanate axial ligands. For chromium strings, treatment to refine crystallographically disordered chromium centers found alternative bond lengths with a difference ($\Delta d_{Cr-Cr}$) of 0.25 Å and 0.65 Å for tri-[28] and pentachromium[29] strings, respectively.

The crystal structures of trichromium strings are sensitive to subtle factors such as solvent and temperature during crystallization, and to different axial ligands.[24,28,29] Density functional theory (DFT) calculations of a trichromium analogue, $[Cr_3(dpa)_4Cl_2]$, by Rohmer and Benard gave a symmetric (i.e., delocalized) structure at the shallow ground state and a conformation with alternating bond lengths at slightly higher states.[24,28] The calculated energies relative to the symmetric conformation are 0.97 kcal mol$^{-1}$ and 4.25 kcal mol$^{-1}$ for a slightly unsymmetrical ($\Delta d_{Cr-Cr} = 0.106$ Å) and a localized state ($\Delta d_{Cr-Cr} = 0.679$ Å), respectively. Thus, it is possible that penta- and heptachromium strings with delocalized and alternating Cr—Cr bonds are present simultaneously and that these delocalized and alternating states are interchangeable in the *n*-alkanethiol matrix (Figures 4e and f). However, as there is an energy difference of less than 5 kcal mol$^{-1}$ between the delocalized and localized states of the trichromium complex, the switching rate observed for the pentachromium string is slow. Theoretical studies and variable-temperature experiments will be carried out to elicit the activation energy and switching mechanism.

We have demonstrated that conductance in metal string complexes correlates well with the metal–metal bond order. Penta- and heptachromium strings each exhibit two sets of primary *I–V* curves, ascribed to conformations of delocalized and alternating Cr—Cr bond lengths; electrons in the latter are localized, which results in a molecular conductance inferior to that of the delocalized conformation. The molecules are stable under ambient conditions and can offer stringent tests of our understanding of interatomic interactions.

Received: March 1, 2006
Revised: May 5, 2006
Published online: July 27, 2006

**Keywords:** electron transport · metal–metal interactions · molecular electronics · scanning probe microscopy · single-molecule studies

[1] *Molecular Nanoelectronics* (Eds.: M. A. Reed, T. Lee), American Scientific Publishers, Stevenson Ranch, CA, **2003**.
[2] D. M. Adams, L. Brus, C. E. D. Chidsey, S. Creager, C. Creutz, C. R. Kagan, P. V. Kamat, M. Lieberman, S. Lindsay, R. A. Marcus, R. M. Metzger, M. E. Michel-Beyerle, J. R. Miller, M. D. Newton, D. R. Rolison, O. Sankey, K. S. Schanze, J. Yardley, X. Zhu, *J. Phys. Chem. B* **2003**, *107*, 6668–6697.
[3] C.-Y. Yeh, C.-C. Wang, C.-h. Chen, S.-M. Peng in *Nano Redox Sites: Nano-Space Control and its Applications* (Ed.: T. Hirao), Springer, Berlin, **2006**, chap. 5, pp. 85–117.
[4] S.-Y. Lin, I.-W. P. Chen, C.-h. Chen, M.-H. Hsieh, C.-Y. Yeh, T.-W. Lin, Y.-H. Chen, S.-M. Peng, *J. Phys. Chem. B* **2004**, *108*, 959–964.
[5] P. Braunstein, C. Frison, N. Oberbeckmann-Winter, X. Morise, A. Messaoudi, M. Benard, M.-M. Rohmer, R. Welter, *Angew. Chem.* **2004**, *116*, 6246–6251; *Angew. Chem. Int. Ed.* **2004**, *43*, 6120–6125.
[6] E. Goto, R. A. Begum, S. Zhan, T. Tanase, K. Tanigaki, K. Sakai, *Angew. Chem.* **2004**, *116*, 5139–5142; *Angew. Chem. Int. Ed.* **2004**, *43*, 5029–5032.
[7] J. F. Berry, F. A. Cotton, C. A. Murillo, *Organometallics* **2004**, *23*, 2503–2506.

 © 2006 Wiley-VCH Verlag GmbH & Co. KGaA, Weinheim 

[8] A. S. Blum, T. Ren, D. A. Parish, S. A. Trammell, M. H. Moore, J. G. Kushmerick, G.-L. Xu, J. R. Deschamps, S. K. Pollack, R. Shashidhar, *J. Am. Chem. Soc.* **2005**, *127*, 10010 – 10011.
[9] G.-L. Xu, R. J. Crutchley, M. C. DeRosa, Q.-J. Pan, H.-X. Zhang, X. Wang, T. Ren, *J. Am. Chem. Soc.* **2005**, *127*, 13354 – 13363.
[10] J. Park, A. N. Pasupathy, J. I. Goldsmith, C. Chang, Y. Yaish, J. R. Petta, M. Rinkoski, J. P. Sethna, H. D. Abruna, P. L. McEuen, D. C. Ralph, *Nature* **2002**, *417*, 722 – 725.
[11] C. Tejel, M. A. Ciriano, B. E. Villarroya, J. A. Lopez, F. J. Lahoz, L. A. Oro, *Angew. Chem.* **2003**, *115*, 547 – 550; *Angew. Chem. Int. Ed.* **2003**, *42*, 529 – 532.
[12] W. Liang, M. P. Shores, M. Bockrath, J. R. Long, H. Park, *Nature* **2002**, *417*, 725 – 729.
[13] X. Lu, K. W. Hipps, X. D. Wang, U. Mazur, *J. Am. Chem. Soc.* **1996**, *118*, 7197 – 7202.
[14] T. L. Schull, J. G. Kushmerick, C. H. Patterson, C. George, M. H. Moore, S. K. Pollack, R. Shashidhar, *J. Am. Chem. Soc.* **2003**, *125*, 3202 – 3203.
[15] J. G. Kushmerick, D. B. Holt, S. K. Pollack, M. A. Ratner, J. C. Yang, T. L. Schull, J. Naciri, M. H. Moore, R. Shashidhar, *J. Am. Chem. Soc.* **2002**, *124*, 10654 – 10655.
[16] J. K. Bera, K. R. Dunbar, *Angew. Chem.* **2002**, *114*, 4633 – 4637; *Angew. Chem. Int. Ed.* **2002**, *41*, 4453 – 4457, and references therein.
[17] H. Vahrenkamp, A. Geiß, G. N. Richardson, *J. Chem. Soc. Dalton Trans.* **1997**, 3643 – 3651.
[18] F. A. Cotton, R. A. Walton, *Multiple Bonds between Metal Atoms*, Oxford University Press, New York, **1993**.
[19] S.-J. Shieh, C.-C. Chou, G.-H. Lee, C.-C. Wang, S.-M. Peng, *Angew. Chem.* **1997**, *109*, 57 – 59; *Angew. Chem. Int. Ed. Engl.* **1997**, *36*, 56 – 59.
[20] B. Xu, N. J. Tao, *Science* **2003**, *301*, 1221 – 1223.
[21] X. Li, J. He, J. Hihath, B. Xu, S. M. Lindsay, N. J. Tao, *J. Am. Chem. Soc.* **2006**, *128*, 2135 – 2141.
[22] H. Ohnishi, Y. Kondo, K. Takayanagi, *Nature* **1998**, *395*, 780 – 783.
[23] A. I. Yanson, G. Rubio-Bollinger, H. E. van den Brom, N. Agrait, J. M. van Ruitenbeek, *Nature* **1998**, *395*, 783 – 785.
[24] M.-M. Rohmer, M. Benard, *J. Cluster Sci.* **2002**, *13*, 333 – 353, and references therein.
[25] C.-C. Wang, W.-C. Lo, C.-C. Chou, G.-H. Lee, J.-M. Chen, S.-M. Peng, *Inorg. Chem.* **1998**, *37*, 4059 – 4065.
[26] H.-C. Chang, J.-T. Li, C.-C. Wang, T.-W. Lin, H.-C. Lee, G.-H. Lee, S.-M. Peng, *Eur. J. Inorg. Chem.* **1999**, 1243 – 1251.
[27] R. Clerac, F. A. Cotton, S. P. Jeffery, C. A. Murillo, X. Wang, *Inorg. Chem.* **2001**, *40*, 1265 – 1270.
[28] J. F. Berry, F. A. Cotton, T. Lu, C. A. Murillo, B. K. Roberts, X. Wang, *J. Am. Chem. Soc.* **2004**, *126*, 7082 – 7096, and references therein.
[29] J. F. Berry, F. A. Cotton, C. S. Fewox, T. Lu, C. A. Murillo, X. Wang, *Dalton Trans.* **2004**, 2297 – 2302.
[30] K. Moth-Poulsen, L. Patrone, N. Stuhr-Hansen, J. B. Christensen, J.-P. Bourgoin, T. Bjornholm, *Nano Lett.* **2005**, *5*, 783 – 785.
[31] X. D. Cui, A. Primak, X. Zarate, J. Tomfohr, O. F. Sankey, A. L. Moore, T. A. Moore, D. Gust, G. Harris, S. M. Lindsay, *Science* **2001**, *294*, 571 – 574.
[32] J. Tomfohr, G. Ramachandran, O. F. Sankey, S. M. Lindsay in *Introducing Molecular Electronics*, *Vol. 680* (Eds.: G. Cuniberti, G. Fagas, K. Richter), Springer, Berlin, **2005**, pp. 301 – 312.
[33] R. Ochs, D. Secker, M. Elbing, M. Mayor, H. B. Weber, *Faraday Discuss.* **2006**, *131*, 281 – 289.
[34] W. Haiss, H. van Zalinge, D. Bethell, J. Ulstrup, D. J. Schiffrin, R. J. Nichols, *Faraday Discuss.* **2006**, *131*, 253 – 264.
[35] G. K. Ramachandran, T. J. Hopson, A. M. Rawlett, L. A. Nagahara, A. Primak, S. M. Lindsay, *Science* **2003**, *300*, 1413 – 1416.
[36] A. M. Moore, A. A. Dameron, B. A. Mantooth, R. K. Smith, D. J. Fuchs, J. W. Ciszek, F. Maya, Y. Yao, J. M. Tour, P. S. Weiss, *J. Am. Chem. Soc.* **2006**, *128*, 1959 – 1967.
[37] H. Basch, R. Cohen, M. A. Ratner, *Nano Lett.* **2005**, *5*, 1668 – 1675.

 © 2006 Wiley-VCH Verlag GmbH & Co. KGaA, Weinheim 

Coordination Chemistry

DOI: 10.1002/anie.200601162

# Cyclodextrin Bucket Wheels: An Oligosaccharide Assembly Accommodates Metal(IV) Centers**

*Klaus Benner, Johannes Ihringer, Peter Klüfers,* and Danira Marinov*

Mononuclear metal complexes in aqueous solution lie at the heart of coordination chemistry. Their significance is evident in areas ranging from simple textbook chemistry to sophisticated applications in fields of current interest. Water as a solvent is the most important medium in biochemistry and environmental chemistry. When the challenges that it poses have been met, water could be an especially advantageous solvent for technical catalysis, particularly in green chemistry. The chemistry of mononuclear coordination complexes in water, as characterized by the variety of multidentate organic chelators that may bind to a metal center, is most extensive for the medium oxidation states of a metal, typically +II and +III. This statement also holds for metalloenzymes, in which protein side chains act as ligands. The chemistry of higher metal oxidation states in water is, however, usually severely restricted. Hydrolytic reactions lead to replacement of the mononuclear metal/chelator core with mono- and polynuclear (hydr)oxido metal species and, finally, (hydrated) oxide phases. This is the case for main-group-metal as well as transition-metal centers, examples being tin(IV) and manganese(IV). The latter shows another property of high-oxidation-state centers that may prohibit the formation of stable mononuclear coordination compounds with organic ligands, namely, its reactivity as an oxidant. The combination of these properties results in decidedly restricted chemistry in water. A good example is lead(IV), whose coordination chemistry in

[*] Dr. K. Benner, J. Ihringer, Prof. Dr. P. Klüfers, Dr. D. Marinov
Department Chemie und Biochemie
Ludwig-Maximilians-Universität
Butenandtstrasse 5–13, 81377 München (Germany)
Fax: (+49) 89-2180-77407
E-mail: kluef@cup.uni-muenchen.de

[**] Polyol metal complexes, Part 53. This work was supported by the Deutsche Forschungsgemeinschaft and the Fachagentur Nachwachsende Rohstoffe. Part 52: M. Hinrichs, F. R. Hofbauer, P. Klüfers, *Chem. Eur. J.* **2006**, *12*, 4675–4683.


WILEY InterScience DISCOVER SOMETHING GREAT
© 2006 Wiley-VCH Verlag GmbH & Co. KGaA, Weinheim

water is restricted to a couple of halogeno plumbates(IV) in acidic solution, and the hexahydroxidoplumbate(IV) ion at high pH values. In line with this experience, the lead(IV) compounds used in synthetic organic chemistry, lead tetraacetate and its derivatives, rapidly decompose on contact with moisture to form black lead dioxide.[1] Attempts to prepare chelates by adding potential chelators such as oxalate, catecholate, or glycosides to hexahydroxidoplumbate(IV) solutions result in the formation of mostly brownish suspensions of decomposition products.

In our efforts to develop the coordination chemistry of carbohydrates,[2] which form the most abundant class of biomolecules, we found that the functional groups of the oligosaccharide β-cyclodextrin are able to assemble into a nanoscaled trimer that provides a mononucleating binding site for high-valent metal centers. β-Cyclodextrin (β-CD) is a cyclic glucose heptamer that is composed of seven α-1,4-linked D-glucopyranose residues. The outer diameter of a single, torus-shaped β-CD unit is about 1.5 nm.[3] The size of the metal–counterion–cyclodextrin assemblies described herein approach those of small proteins such as a ferredoxin. Most data were collected for tin(IV), because not only could X-ray crystal structures be determined, but the $^{119}$Sn nucleus also allows NMR spectroscopic analysis of the complexes in the solution state. As a result, the assembly described below was shown not to be a loose aggregate in the solid state, but rather a formation that is so stable that it was the only solution species present.

The hexahydroxidostannate(IV) ion $[Sn(OH)_6]^{2-}$ was used as a precursor. At pH values higher than about 11, a single signal was observed in the $^{119}$Sn NMR spectrum, which proved that this ion is the only Sn-containing solution species. Hydrated tin oxide precipitated when the pH value was adjusted close to neutrality (ca. pH 8). The addition of a chelator such as oxalate to an alkaline hydroxidostannate(IV) solution did not alter the $^{119}$Sn NMR spectrum at higher pH values nor affect the formation of hydrated tin oxide at pH values close to neutrality.[4] Ligands such as catecholate(2−) and ethanediolate(2−) were better competitors with the hydroxido/oxido ligand. In a typical experiment, the $^{119}$Sn NMR spectrum of hydroxidostannate and a threefold molar amount of ethanediol showed a mixture of the heteroleptic mono- and bis(ethanediolato)hydroxidostannates and the homoleptic tris(ethanediolato)stannate, the first two species being the major ones. Such observations make it plausible that well-defined homoleptic stannates(IV) with organic chelators are not usually accessible from aqueous solution equilibria.

In contrast to these observations, the $^{119}$Sn NMR spectrum of a threefold molar amount of β-cyclodextrin with hexahydroxidostannate(IV) showed a single signal, whose chemical shift indicated a new, hexacoordinate, tin-containing species in solution. Lowering the pH value to about 8 did not change the signal, but the solution started to become cloudy (e.g., pH 8.8 clear solution, pH 7.8 slightly cloudy solution, pH 7 $SnO_2$ precipitate). The tentative coordination compound was obviously destroyed at pH 7. This behavior indicated that deprotonated β-CD species were the actual tin-binding entities. When lithium was used as the counterion, crystals suitable for X-ray diffraction grew over the course of one week following controlled ethanol addition. The results from the structural analysis were consistent with the spectroscopic results. The most conspicuous building unit of the crystals is a bucket-wheel-shaped assembly with threefold rotational symmetry that consists of three components: three β-CD dianions, three tetrahedral tetraaqualithium cations, and a tetravalent metal center. An ethanol guest molecule inside each β-cyclodextrin ring may be regarded as a fourth kind of building unit whose presence is responsible for the necessary decrease of the solubility of the assembly at the onset of crystallization. Figure 1 (top) gives an overview of the $C_3$-symmetric complex. The three β-cyclodextrin rings are

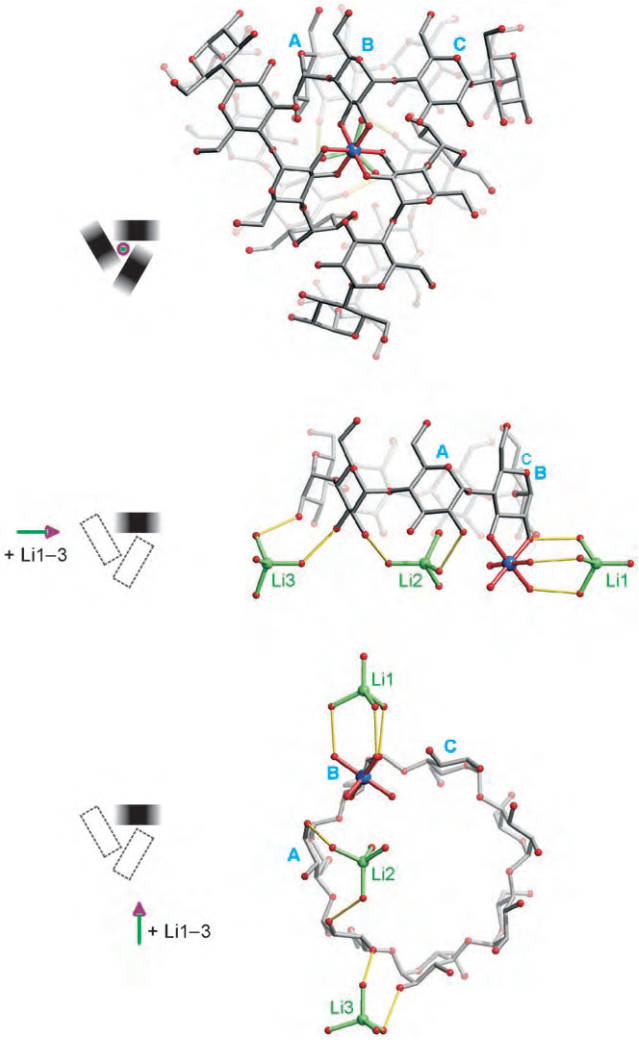


***Figure 1.*** Top: The $M^{IV}(β\text{-CD})_3$ bucket-wheel motif together with the innermost $Li(H_2O)_4$ counterion (Li2 in the middle and bottom illustrations) viewed along the threefold symmetry axis. The metal-binding site is located in the center at the front of the picture. Middle and bottom: sections of the structure as detailed in the cartoons on the left, together with the hydrated Li1 and Li3 counterions; $M^{IV}$ blue, Li green, O red, hydrogen bonds: yellow. Ethanol guest molecules inside each β-CD torus are omitted. The threefold symmetry axis runs through the lithium atoms and the tetravalent central metal. The blue letters A–C correspond to the glucose units shown in Scheme 1. The data for the germanium structure were used to draw the structure.

 © 2006 Wiley-VCH Verlag GmbH & Co. KGaA, Weinheim 

nested. Close inter-cyclodextrin contacts are established between the diol functions along the O2/3 rim of the cyclodextrin (see Scheme 1 for atom numbering) in the coordination sphere of the tetravalent metal center (shown in

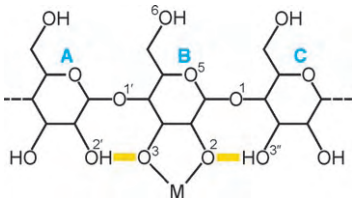


***Scheme 1.*** The section of the tris(diolato) metal-binding site near the $M^{IV}$ center. The diolato ligand shown is hydrogen-bonded (yellow bars) to the hydroxy functions of the neighboring glucose units. The blue letters A–C correspond to the glucose units shown in Figure 1. Mean O···O and M—O distances (in pm): O2′···O3: Mn 283.6(8), Ge 282.2(5), Sn 274.0(7), Pb 273.8(5); O3″···O2: Mn 275.9(9), Ge 280.4(5), Sn 277.7(6), Pb 276.4(5); M—O2: Mn 196.7(5), Ge 193.6(3), Sn 208.7(4), Pb 217.4(3); M—O3: Mn 189.4(6), Ge 189.2(3), Sn 204.3(4), Pb 214.4(3).

blue) as well as between the CD rings at the rear of Figure 1. In the latter, three short hydrogen-bonded contacts between diol-O atoms establish a direct link between the cyclodextrin rings (O···O 257 pm). Other contacts that contribute to the stability of the trimer are shown by viewing perpendicular to the threefold axis (Figure 1, middle and bottom). The projections show hydrogen bonds between the aqua ligands of the lithium counterions and diol-O atoms of the cyclodextrin. Fifteen such hydrogen bonds between counterion and cyclodextrin may be counted when symmetry is taken into account, which makes the three $[Li(H_2O)_4]^+$ ions well-matching connectors: two of them are inside the assembly and one is peripherally bonded (this latter counterion may be substituted by a hydrated sodium ion). The interaction between the nested cyclodextrin rings and the connectors contributes to the stability of the most important feature of the assembly, namely, the metal-binding site. This site consists of six ligating O atoms derived from the β-CD diol groups and is embedded in a hydrogen-bond environment. The hydrogen bonds between the cyclodextrin oxygen atoms are omitted from Figure 1 for clarity, but are shown in Scheme 1 (three of the seven glucose units are shown). The O2 atom of the metal-binding site is hydrogen-bonded to the O3″H hydroxy function of the anhydroglucose unit, and the ligating O3 alkoxido O atom is hydrogen-bonded to the O2′H anhydroglucose hydroxy function. In total, the $O_6$ metal-binding site is supported by nine hydrogen bonds: six intra-cyclodextrin bonds and three from the peripherically bound counterion.

The absence of mixed cyclodextrin–hydroxidostannate species is understandable, because only the complete trimer benefits from the stabilization by the hydrogen bonds between CD units and with the hydrated counterions. Accordingly, the overall stability of the bucket-wheel-shaped stannate is higher than the stability of stannates of related glycosides. Thus, the $^{119}$Sn NMR spectrum of a mixture of 1 mol $[Sn(OH)_6]^{2-}$, 3 mol β-CD, and 3 mol of the methylated cyclodextrin building block methyl-α-D-glucopyranoside showed only the bucket-wheel complex and no Sn-bound methylglucoside.

Both the high tendency for formation of the bucket-wheel motif and its robustness were demonstrated by its formation with a strongly oxidizing central metal: lead(IV). The reactant used was hexahydroxidoplumbate(IV).[5] The unsuccessful attempts to coordinate well-established chelators to lead(IV) are described above. The addition of β-cyclodextrin, however, did not result in decomposition reactions; crystals were formed from the yellowish solutions. X-ray analysis revealed an isotypic structure with the typical bucket-wheel motif (see caption of Scheme 1 for atomic distances). Both the crystals and the solutions are stable over prolonged periods of time. It should be recalled at this point that the above-mentioned use of lead(IV) acetate in organic synthesis includes the oxidative cleavage of diols. Taken together with the NMR investigation of the stannate, the cyclodextrin bucket-wheel motifs prove to be stable against dissociative decay as well as resistant to oxidative degradation to a much larger extent than related chelators that lack supramolecular support.

A specific restriction of carbohydrate chelation remains to be investigated. Diol functions attached to a furanose ring are most suited to chelate small central atoms, whereas diol functions attached to a pyranose ring in the *trans* configuration are much less suited.[6] The latter is the situation for β-cyclodextrin, so a lower limit for the atomic radius of the $M^{IV}$ center has to be expected. To clarify whether the β-CD bucket-wheel motif provides a binding site for the particularly important first-row transition metals and post-transition-metal elements, the reactions of silicate and germanate with β-cyclodextrin were investigated. No six-coordinate silicon was detected by $^{29}$Si NMR spectroscopy, but germanium was found to occupy the metal-binding site of the bucket-wheel motif (see caption of Scheme 1 for atomic distances). This result indicates that transition metals could also bind, since the size of the germanium(IV) center is almost the same as that of a tetravalent first-row transition metal (compare the crystal radii of the octahedrally coordinated tetravalent ions: Pb 92, Sn 83, Ge 67, Mn 67 pm, Si 54 pm).[7] The synthesis of a mononuclear manganese complex in an aqueous environment is a challenge because of the strong tendency of manganese(IV) to form oxido-, hydroxido-, carboxylato-, and alkoxido-bridged polynuclear species. We attempted to synthesize a bucket-wheel-type manganese(IV) compound by starting from a manganese(II) salt. Oxidation with either air, hydrogen peroxide, or hexacyanidoferrate(III) yielded deep red solutions of a tentative manganese(IV) complex. Crystallization succeeded, and the structure determination again revealed the bucket-wheel motif. The metrical properties of the manganese and the germanium coordination octahedra are very similar, which is expected given that the crystal radii of Ge and $Mn^{IV}$ are the same and there is no Jahn–Teller distortion for the central $d^3$ $Mn^{IV}$ ion (mean M–O bond lengths: Ge 191, Mn 190 pm; as the ionic radius of high-spin $Mn^{III}$ is 12 pm larger than that of $Mn^{IV}$,[7] a mean Mn–O bond length of more than 200 pm is expected for an $Mn^{III}O_6$ coordination sphere). The assignment of the oxidation state

 © 2006 Wiley-VCH Verlag GmbH & Co. KGaA, Weinheim 

+IV to the manganese center is in accord with the typical red color of the $Mn^{IV}O_6$ chromophore.

The coordination chemistry of carbohydrates encompasses a broad scope of central metals and their oxidation states. This work has now expanded this field of knowledge to strongly oxidizing and potentially dioxide-forming metal centers. The oxophilic metal centers investigated herein mark one end of the range of metals with affinity to carbohydrates; the other end includes soft metal centers such as rhenium(I) and palladium(II).[8,9] The molecular origin of this unusual versatility is the polyfunctionality of carbohydrates. Aside from the functions that are involved in the metal-binding site, the remaining functional groups are able to arrange themselves, following the rules of supramolecular chemistry, into molecular patterns that support the metal-binding site. Carbohydrates thus patently represent an efficient and versatile class of ligands whose coordination chemistry follows the same supramolecular principles that shape a metalloenzyme.

## Experimental Section

The general formula of the hexagonal β-cyclodextrin bucket-wheel structures is close to $[\{Li(H_2O)_4\}_3\{\Lambda\text{-}M^{IV}(\beta\text{-}CDH_{-2})_3\}]H_{-1}\cdot 25\,H_2O$.[10] There are a two possible sites of deprotonation: A close hydrogen-bonded contact between diol O atoms at the rear of the bucket wheel suggests that, in line with the acidity constants, a diol hydroxy group is deprotonated rather than a water molecule. However, the presence of hydroxide can not be excluded. There are large, empty channels along [00*z*] which contain weakly defined electron density. The cavity inside of each cyclodextrin torus is filled with the precipitating agent in an ordered way in the case of ethanol; the channels, however, contain disordered precipitating agent (note the small deviations between the idealized formulae given in this section and the deposited data that take disorder into account).

Tin: Sodium hexahydroxidostannate(IV) (0.117 g, 0.44 mmol) was dissolved in water (24 mL). β-Cyclodextrin (1.498 g, 1.32 mmol) was added to the solution. Lithium hydroxide monohydrate (0.055 g, 1.32 mmol) was added, the solution was stirred for 60 minutes, and then the mixture was saturated with ethanol (12 mL). After the slow diffusion of ethanol vapor into the solution over the course of three weeks at 12 °C, colorless crystals of $[\{Na(H_2O)_4\}\{Li(H_2O)_4\}_2\{\Lambda\text{-}Sn(\beta\text{-}CDH_{-2})_3\}]H_{-1}\cdot 27\,H_2O\cdot 3\,EtOH$ (**1**) were formed. The Li1 position (Figure 1, bottom) is occupied by sodium in terms of electron density and atomic distances. $^{119}Sn$ NMR spectroscopy ($H_2O$, 23 °C): $\delta = -493.3$ ppm (sodium hexahydroxidostannate(IV): −593.5 ppm).

Lead: β-Cyclodextrin (0.749 g, 0.66 mmol) and lithium hydroxide monohydrate (0.028 g, 0.66 mmol) were dissolved in water (10 mL). Sodium hexahydroxidoplumbate(IV) (0.078 g, 0.22 mmol) was added with stirring. The solution was stirred for 60 minutes and then saturated with ethanol. The solution was kept at 12 °C under the diffusion of ethanol vapors. Crystals of $[\{Li(H_2O)_4\}_3\{\Lambda\text{-}Pb(\beta\text{-}CDH_{-2})_3\}]H_{-1}\cdot 34\,H_2O\cdot 5\,MeOH$ (**2**) formed within one week. Small amounts of sodium (ca. 0.15 per formula unit) were refined close to the Li1 position.

Germanium: β-Cyclodextrin (1.317 g, 1.16 mmol) and lithium hydroxide monohydrate (0.340 g, 8.10 mmol) were dissolved in water (10 mL). Tetramethoxygermanium (0.791 g, 4.02 mmol) was added with stirring. Heating the solution for 30 min caused the formation of a colorless precipitate. After filtration of the mixture, ethanol vapors were allowed to diffuse into the filtrate. Crystals of $[\{Li(H_2O)_4\}_3\{\Lambda\text{-}Ge(\beta\text{-}CDH_{-2})_3\}]H_{-1}\cdot 24\,H_2O\cdot 3\,EtOH$ (**3**) grew over the course of half a year.

Manganese: β-Cyclodextrin (1.362 g, 1.20 mmol) and lithium hydroxide monohydrate (0.504 g, 12.0 mmol) were dissolved in water (13 mL). Manganese(II) nitrate tetrahydrate (0.201 g, 0.80 mmol) and β-cyclodextrin (1.362 g, 1.20 mmol), dissolved in water (7 mL), were added. A yellow solution formed which gradually turned dark red upon stepwise addition of potassium hexacyanidoferrate(III) (0.527 g, 1.60 mmol) in water (10 mL). Finally, the reaction mixture was filtered and layered with methanol. Red crystals of $K_2[\{Li(H_2O)_4\}_3\{\Lambda\text{-}Mn(\beta\text{-}CDH_{-2})_3\}]H_{-3}\cdot 23\,H_2O\cdot MeOH$ (**4**) were obtained over the course of six weeks.

Received: March 23, 2006
Published online: July 26, 2006

**Keywords:** cyclodextrins · germanium · lead · manganese · tin

[1] J. E. H. Buston, T. D. W. Claridge, S. J. Heyes, M. A. Leech, M. G. Moloney, K. Prout, M. Stevenson, *Dalton Trans.* **2005**, 3195–3203.
[2] A. Geißelmann, P. Klüfers, C. Kropfgans, P. Mayer, H. Piotrowski, *Angew. Chem.* **2005**, *117*, 946–949; *Angew. Chem. Int. Ed.* **2005**, *44*, 924–927, and references therein.
[3] G. A. Jeffrey, W. Saenger, *Hydrogen Bonding in Biological Structures*, Springer, Berlin, **1991**.
[4] The crystallization of a tris(oxalato)stannate(IV) complex from strongly acidic solution is reported in: G. J. Kruger, E. L. J. Breet, R. van Eldik, *Inorg. Chim. Acta* **1976**, *19*, 151–157.
[5] H. Zocher, *Z. Anorg. Allg. Chem.* **1920**, *112*, 1–66.
[6] X. Kästele, P. Klüfers, F. Kopp, J. Schuhmacher, M. Vogt, *Chem. Eur. J.* **2005**, *11*, 6326–6346.
[7] R. D. Shannon in *Encyclopedia of Inorganic Chemistry*, *Vol. 2* (Ed.: R. B. King), Wiley, Chichester, **1994**, pp. 929–942.
[8] M. Hinrichs, F. R. Hofbauer, P. Klüfers, *Chem. Eur. J.*, **2006**, *12*, 4675–4683.
[9] P. Klüfers, T. Kunte, *Chem. Eur. J.* **2003**, *9*, 2013–2018.
[10] Crystal structure analysis: common details for all structures: hexagonal, $P6_3$, $Z = 2$, $T = 200(3)$ K, $Mo_{K\alpha}$, $\lambda = 0.71073$ Å, max. shift/error: 0.001, programs used: SHELX, SCHAKAL. **1**: $C_{132}H_{299}Li_2NaO_{147}Sn$, $M_r = 4394.280$, colorless prism, $0.14 \times 0.09 \times 0.07$ mm$^3$, $a = 21.1929(2)$, $c = 26.7008(3)$ Å, $V = 10385.7(2)$ Å$^3$, $\rho = 1.40520(2)$ g cm$^{-3}$, $\mu(Mo_{K\alpha}) = 0.222$ mm$^{-1}$, no absorption correction, KappaCCD, $\theta$ range: 3.19–22.79, 109926 reflections, 9359 independent and used in refinement, 8395 with $I \geq 2\sigma(I)$, $R_{int} = 0.1233$, mean $\sigma(I)/I = 0.0419$, 831 parameters, $R(F_{obs}) = 0.0612$, $R_w(F^2) = 0.1739$, $S = 1.076$, Flack parameter: −0.03(2), min. and max. residual electron density: −0.398, 1.029 e Å$^{-3}$. **2**: $C_{131}H_{315}Li_3O_{156}Pb$, $M_r = 4614.8$, colorless prism, $0.23 \times 0.07 \times 0.06$ mm$^3$, $a = 21.3205(1)$, $c = 26.5876(2)$ Å, $V = 10466.6(1)$ Å$^3$, $\rho = 1.46432(2)$ g cm$^{-3}$, $\mu(Mo_{K\alpha}) = 0.933$ mm$^{-1}$, no absorption correction, KappaCCD, $\theta$ range: 3.19–27.48, 106587 reflections, 15995 independent and used in refinement, 13957 with $I \geq 2\sigma(I)$, $R_{int} = 0.0764$, mean $\sigma(I)/I = 0.0590$, 792 parameters, $R(F_{obs}) = 0.0464$, $R_w(F^2) = 0.1196$, $S = 1.048$, Flack parameter: −0.009(3), min. and max. residual electron density: −0.760, 0.843 e Å$^{-3}$. **3**: $C_{132}H_{290}GeLi_3O_{144}$, $M_r = 4275.062$, colorless prism, $0.23 \times 0.17 \times 0.15$ mm$^3$, $a = 21.084(1)$, $c = 26.686(2)$ Å, $V = 10274(1)$ Å$^3$, $\rho = 1.3820(1)$ g cm$^{-3}$, $\mu(Mo_{K\alpha}) = 0.270$ mm$^{-1}$, no absorption correction, Stoe IPDS, $\theta$ range: 1.53–24.01, 83759 reflections, 10712 independent and used in refinement, 8774 with $I \geq 2\sigma(I)$, $R_{int} = 0.0661$, mean $\sigma(I)/I = 0.0510$, 775 parameters, $R(F_{obs}) = 0.0542$, $R_w(F^2) = 0.1455$, $S = 0.978$, Flack parameter: 0.006(13), min. and max. residual electron density: −0.573, 0.792 e Å$^{-3}$. **4**: $C_{127}H_{281}K_2Li_3MnO_{141}$, $M_r = 4218.463$, red brick, $0.25 \times 0.19 \times 0.17$ mm$^3$, $a = 20.968(2)$, $c = 26.654(2)$ Å, $V = 10149(1)$ Å$^3$, $\rho = 1.3805(2)$ g cm$^{-3}$, $\mu(Mo_{K\alpha}) = 0.242$ mm$^{-1}$, numerical absorption correction, Stoe IPDS, $\theta$ range: 1.36–

 © 2006 Wiley-VCH Verlag GmbH & Co. KGaA, Weinheim 

20.85, 28834 reflections, 7065 independent and used in refinement, 6001 with $I \geq 2\sigma(I)$, $R_{int} = 0.0610$, mean $\sigma(I)/I = 0.0534$, 766 parameters, $R(F_{obs}) = 0.0752$, $R_w(F^2) = 0.2140$, $S = 1.053$, Flack parameter: 0.00(6), min. and max. residual electron density: $-0.688$, 1.083 e $\text{Å}^{-3}$. CCDC-600809 (**1**), -600808 (**2**), -600806 (**3**), -600807 (**4**) contain the supplementary crystallographic data for this paper. These data can be obtained free of charge from The Cambridge Crystallographic Data Center via www.ccdc.cam.ac.uk/data_request/cif.

 © 2006 Wiley-VCH Verlag GmbH & Co. KGaA, Weinheim 

Photosensitizers

DOI: 10.1002/anie.200601463

# A Ruthenium Complex with Superhigh Light-Harvesting Capacity for Dye-Sensitized Solar Cells**

*Chia-Yuan Chen, Shi-Jhang Wu, Chun-Guey Wu,* Jian-Ging Chen, and Kuo-Chuan Ho*

A dye-sensitized solar cell (DSSC) using Ru complexes as a photosensitizer was first reported by O'Regan and Grätzel in 1991.[1] The low-cost, easy preparation make DSSC one of the most promising photovoltaic cells for conversion of sunlight to electricity. Numerous sensitizers have been prepared, and their performance has been tested.[2–10] A conversion efficiency of up to 11% was achieved by using *cis*-di(thiocyanato)bis(2,2′-bipyridyl-4,4′-dicarboxylate)ruthenium(II) (**N3**) as a photosensitizer.[11–12] However, the conversion efficiency of DSSCs is still lower than that of the silicon-based photovoltaic cells. To obtain a high conversion efficiency, optimization of the short-circuit photocurrent ($I_{sc}$) and open-circuit potential ($V_{oc}$) of the cell is essential. The value of $V_{oc}$ depends on the edge of conduction band in $TiO_2$ and the redox potential of $I^-/I_3^-$, otherwise $I_{sc}$ is related to the interaction between $TiO_2$ and the sensitizer as well as the absorption coefficient of the sensitizer. The conduction band of $TiO_2$ was known to have a Nernstian dependence on pH.[13–14] Thus, the molecular engineering of the ruthenium complexes for achieving the highest efficiency was attempted to increase the molar absorption coefficient and reduce the number of protons on the complexes. 4,4′-Dicarboxylic acid-2,2′-bipyridine (dcbpy) has been considered as the best anchoring ligand in Ru sensitizers.[15] Finding new metal-complex sensitizers with higher conversion efficiency was achieved by modifying one of the anchoring ligands. Replacement of one of the dcbpy anchoring ligands with a highly conjugated ancillary ligand represents a molecular engineering approach for increasing the absorption coefficient and therefore the photocurrent density of the sensitizers as reported by Grätzel and coworkers.[16–20] Herein, we report a new ruthenium photosensitizer **CYC-B1** in which one of the dcbpy ligands in **N3** was replaced with abtpy, a bipyridine ligand substituted with alkyl bithiophene groups. **CYC-B1** has the highest absorption coefficient among the Ru-based photosensitizers used in DSSCs, and its power-conversion efficiency is 10% higher than that of **N3** under the same cell fabrication and measuring procedures carried out in our laboratory.

**CYC-B1** was prepared in a typical one-pot synthesis,[20] and its structure (Scheme 1) was identified from NMR spectroscopy, mass spectrometry, and elemental analysis. The electronic absorption spectra of the free dcbpy and abtpy ligands, **CYC-B1**, and **N3** in DMF are displayed in Figure 1, and the optical data are summarized in Table 1. The absorption maximum ($\lambda_{max}$) assigned to the π–π* transition for dcbpy and abtpy are 299 nm and 375 nm, respectively. The absorption maximum of abtpy is red-shifted by 76 nm, which is attributed to its longer conjugation length, compared to that of dcbpy. The absorption spectrum of **CYC-B1** shows three bands centered at 553 nm, 400 nm, and 312 nm. Based on comparison with the free abtpy ligand and the homoleptic complex **N3**, the absorption band at 312 nm for **CYC-B1** is assigned to the intraligand π–π* transitions of dcbpy. The band centered at 400 nm contains two components: the π–π* transition of the abtpy ligand and one of the metal-to-ligand charge transfer (MLCT) transitions for **CYC-B1**. The π–π* transition of abtpy has a higher contribution since this band has a much stronger absorption coefficient than the corresponding band observed in **N3**. The absorption band at 553 nm is the characteristic MLCT transition for determining

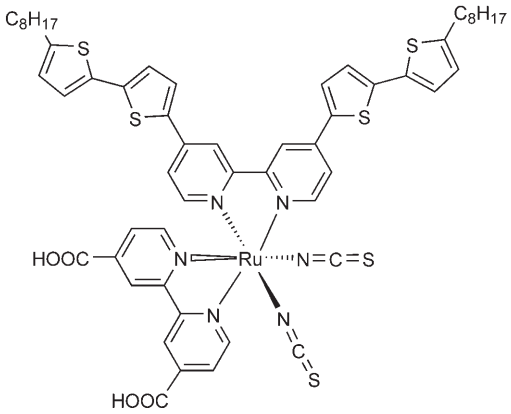


***Scheme 1.*** The structure of **CYC-B1**.

[*] C.-Y. Chen, S.-J. Wu, Prof. C.-G. Wu
Department of Chemistry
National Central University
Jung-Li, Taiwan 32054 (Republic of China)
Fax: (+886) 3-422-7664
E-mail: t610002@cc.ncu.edu.tw
J.-G. Chen, Prof. K.-C. Ho
Department of Chemical Engineering
National Taiwan University
Taipei, 10617, Taiwan (Republic of China)

[**] This work was financially supported by the National Science Council, Taiwan.

Supporting information for this article is available on the WWW under http://www.angewandte.org or from the author.


InterScience
© 2006 Wiley-VCH Verlag GmbH & Co. KGaA, Weinheim

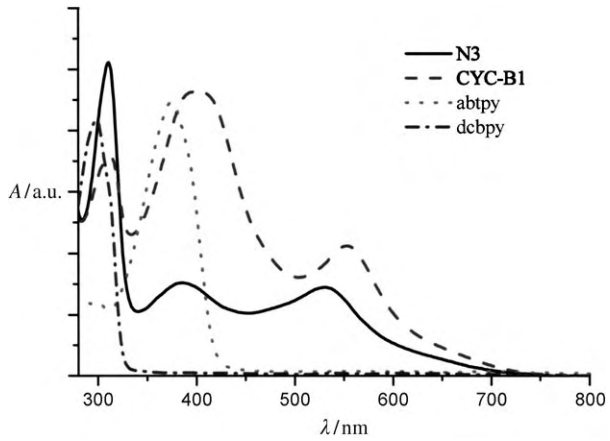


***Figure 1.*** UV/Vis absorption spectra of dcbpy, abtpy, **N3**, and **CYC-B1** in DMF.

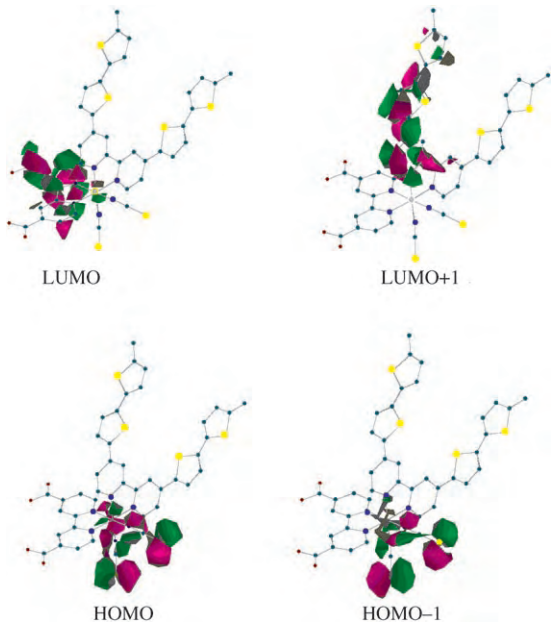


***Figure 2.*** Graphical representation of the frontier orbitals of **CYC-B1** (O red, S yellow, C green, N blue, Ru gray).

the conversion efficiency of **CYC-B1**. This MLCT band may come from one of the two different conjugated ligands in **CYC-B1**. However, the COOH substituents on the dcbpy anchoring ligand have a higher electron-withdrawing ability than the alkyl bithiophene substituents of the abtpy ancillary ligand. The LUMO of the dcbpy ligand has a lower energy than that of abtpy.[21] Therefore, the lower-energy MLCT band in **CYC-B1** corresponds to the charge transfer between the metal center and the dcbpy anchoring ligand. The absorption maxima of both MLCT bands in **CYC-B1** are larger than those of **N3**, thus suggesting that the abtpy ligand has lifted the energy level of the metal center. Encouragingly, the molar absorption coefficient of the lower-energy MLCT band of **CYC-B1** is very high, higher than all Ru-based dyes used in solar cells.

To confirm the identity of the lower-energy MLCT band in **CYC-B1**, the location of the HOMOs and LUMOs in **CYC-B1** were calculated with a semiempirical computational method (ZINDO/1),[22–25] and the results are displayed in Figure 2. It is known[26] that the HOMO and HOMO−1 of **N3** have amplitudes on the ruthenium center and the NCS ligands whereas its LUMO and LUMO+1 are localized homogeneously on the two dcbpy ligands, thus facilitating the injection of electrons from the excited Ru complex to $TiO_2$. The locations of HOMO and HOMO−1 in **CYC-B1** are similar to those of **N3**, mainly on the metal center and NCS ligands. However, the LUMO is located only on the dcbpy anchoring ligand through which the excited electrons are directly transferred to $TiO_2$. These results suggest that **CYC-B1** is better than **N3** as a photosensitizer for DSSCs, since both dcbpy ligands on **N3** cannot bind to $TiO_2$ particles simultaneously and the excited electron in the moiety that is not directly connected to $TiO_2$ provides a very small contribution to the conversion efficiency of the DSSCs. Furthermore, for a high-efficiency sensitizer in DSSCs, the energy level of its LUMO should be well-matched with the lower limit of the conduction band in $TiO_2$, and its HOMO should be sufficiently low in energy to accept electrons from the redox electrolyte such as $I^-/I_3^-$. The energy level of the frontier orbitals for **CYC-B1** that was established from the electrochemical and absorption data is also listed in Table 1. It was found that the energy levels of the HOMO and LUMO for **CYC-B1** match well with the redox potential of $I^-/I_3^-$ and the LUMO of $TiO_2$. Therefore, the higher molar absorption coefficient of **CYC-B1** can be expected to have a better conversion efficiency than **N3**.

The monochromatic incident photon-to-current conversion efficiency (IPCE) and characteristic photocurrent density versus voltage curves for **CYC-B1**- and **N3**-based cells are illustrated in Figure 3, and the detailed parameters of the devices are also included in Table 1. The broad IPCE curve for **CYC-B1** covers almost the entire visible spectrum from

***Table 1:*** Physical data and performance of **CYC-B1**- and **N3**-sensitized cells.

| Complex | $\varepsilon$ [$\times 10^4$ M$^{-1}$ cm$^{-1}$] ($\lambda_{max}$ [nm]) | | | $E_{ox}$[a] of $Ru^{III/II}$ | $E_{HOMO}$[b] | $E_{LUMO}$ | Cell performance | | | |
|---|---|---|---|---|---|---|---|---|---|---|
| | π–π* | π–π* or 4d–π* | 4d–π* | [V vs. $Fc/Fc^+$] | [eV] | [eV] | $I_{sc}$ [mA cm$^{-2}$] | $V_{oc}$ [V] | *FF* | $\eta$ [%] |
| **CYC-B1** | 3.58 (312) | 4.64 (400) | 2.12 (553) | 0.30 | 5.10 | 3.52 | 23.92 | 0.65 | 0.55 | 8.54 |
| **N3** | 5.11 (311) | 1.52 (385) | 1.45 (530) | 0.40 | 5.20 | 3.52 | 21.32 | 0.66 | 0.54 | 7.70 |

[a] The $Ag/AgNO_3$ reference electrode was calibrated with a ferrocene/ferrocinium ($Fc/Fc^+$) redox couple. The electrochemical experiments were carried out in 0.1 M [$n$Bu$_4$N]$BF_4$/DMF solution. [b] The absorption onset of each complex was used to calculate the energy gap and the frontier orbitals. The energy levels of the HOMO and LUMO were calculated with the following formulas: $E_{HOMO} = E_{ox} - E_{Fc/Fc+} + 4.8$ eV; $E_{LUMO} = E_{HOMO} - E_g$; $E_g$ = absorption threshold of the Ru complexes.

 © 2006 Wiley-VCH Verlag GmbH & Co. KGaA, Weinheim 

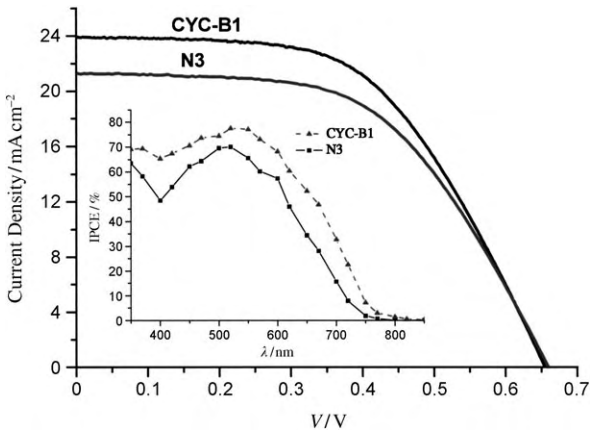


***Figure 3.*** Current density vs. voltage characteristic of photovoltaic devices with **N3** and **CYC-B1** as sensitizers under AM 1.5 simulated sunlight (100 mW cm$^{-2}$) illumination; inset: the typical photocurrent-action spectra of the photovoltaic devices (thickness of $TiO_2$: 20 μm; cell active area: 0.25 cm$^2$).

350 to 700 nm with a maximum of 77.5 %. Unlike the **N3** cell, the IPCE curves for the **CYC-B1** cell are not consistent with its absorption spectrum in DMF. The band centered at 400 nm, which mainly comes from the abtpy intraligand π–π* transitions, has a smaller contribution to the photon-to-current conversion efficiency. Under AM 1.5 sunlight illumination (100 mW cm$^{-2}$), the **CYC-B1**-sensitized solar cell gave a power-conversion efficiency ($\eta$) of 8.54 %, which is 10 % higher than that of the **N3**-sensitized cell under the same cell fabrication and measuring procedures. Both the $V_{oc}$ and *FF* values of the **CYC-B1**-sensitized cell are close to those of the **N3**-sensitized cell. The higher $\eta$ value of the **CYC-B1** cell (compared to the **N3** cell) comes from the higher $I_{sc}$ value, which is mainly attributed to the high absorption coefficient of the MLCT band for dcbpy. Furthermore, the objective of this work is to find the best photosensitizer for DSSCs. The alkyl group on the abtpy ancillary ligand can prevent the complexes from water-induced desorption of the dye molecules from the $TiO_2$ surface.[27] We could anticipate that DSSCs sensitized with **CYC-B1** may also exhibit good stability.

Enhancing the absorption coefficient of the MLCT band by increasing the conjugation length of the ancillary ligand is a known strategy.[16–20] What is so special about the alkyl bithiophene group compared to other substituents (such as phenylenevinylene) that have already been reported?[18,19] It is known[28] that a polythiophene moiety can be regarded as a *cis*-polyacetylene chain bridged with sulfur atoms. The "bridging sulfur atoms" could effectively provide aromatic stability to the polyacetylene chain while preserving the desirable physical properties such as high charge transport. The facile functionalization of thiophene groups also offers relatively efficient synthetic solutions to solubility, polarity, and band-gap tuning. Furthermore, sulfur has greater radial extension in its bonding than the second-row elements such as carbon. Therefore, thiophene is a more electron-rich moiety; incorporation of thiophene onto bipyridine ligands can raise the energy levels of the metal center and the LUMO of the ligands.[29] As a consequence, the band resulting from charge transfer from the metal center to the anchoring ligand is red-shifted, and upon illumination of the sample the electrons on the metal center are transferred to the anchoring dcdpy ligand where electrons can move to the outer circuit through the $TiO_2$ particles more efficiently. These results account for the high current density of the **CYC-B1**-sensitized cell.

In this study we found a way to improve the power-conversion efficiency of DSSCs by molecular engineering of an Ru-based photosensitizer. The **CYC-B1** compound reported herein is a representative ruthenium complex with high current density and conversion efficiency. We believe that ruthenium-based DSSCs with even higher efficiency can be obtained by fine-tuning the structure of the ruthenium complexes.

## Experimental Section

**CYC-B1** was prepared in a typical one-pot synthesis[20,30] by using the new ligand abtpy, which was devised and prepared in our laboratory. LRMS (FAB): calcd *m/z*: 1170.17; found: 1170.2 (m) $[M]^+$, 1112.2 (s) $[M-NCS]^+$; $^1$H NMR (500 MHz, [D$_6$]DMSO, atom-numbering scheme is provided in the Supporting Information): $\delta = 9.49$ (d, H$^6$, $J = 5.7$ Hz), 9.15 (d, H$^{6'}$, $J = 5.7$ Hz), 9.10 (s, H$^3$), 8.96 (s, H$^{3'}$), 8.94 (s, H$^{3''}$), 8.80 (s, H$^{3'''}$), 8.32 (d, H$^5$, $J = 5.7$ Hz), 8.19 (d, H$^{6''}$, $J = 3.8$ Hz), 8.11 (d, H$^{5'}$, $J = 5.7$ Hz), 7.99 (d, H$^{5''}$, $J = 3.8$ Hz), 7.95 (d, H$^{6'''}$, $J = 5.9$ Hz), 7.64 (d, H$^{5'''}$, $J = 5.9$ Hz), 7.47 (d, H$^{9''}$, $J = 3.7$ Hz), 7.37 (d, H$^{9'''}$, $J = 6.8$ Hz), 7.35 (d, H$^{10''}$, $J = 3.7$ Hz), 7.31 (d, H$^{14''}$, $J = 3.4$ Hz), 7.28 (d, H$^{10'''}$, $J = 6.8$ Hz), 7.21 (d, H$^{15''}$, $J = 3.4$ Hz), 6.86 (d, H$^{14'''}$, $J = 3.4$ Hz), 6.80 (d, H$^{15'''}$, $J = 3.4$ Hz), 2.79 (t, 2H), 2.74 (t, 2H), 1.61 (t, 2H), 1.57 (t, 2H), 1.23 (m, 20H), 0.85 (t, 3H), 0.83 ppm (t, 3H). Elemental analysis (%) calcd for $C_{56}H_{56}N_6O_4S_6Ru$: C 57.46, H 4.82, N 7.18, S 16.44; found: C 55.14, H 5.05, N 6.81, S 15.44. The detailed procedures for synthesis and characterization of the ligand and complex as well as the DSSC fabrication and measuring conditions can be found in the Supporting Information.

Received: April 13, 2006
Revised: June 7, 2006
Published online: July 25, 2006

**Keywords:** charge transfer · conjugation · dyes/pigments · photosensitizers · ruthenium

[1] B. O'Regan, M. Grätzel, *Nature* **1991**, *353*, 737.
[2] M. K. Nazeeruddin, P. Péchy, T. Renouard, S. M. Zakeeruddin, R. Humphry-Baker, P. Comte, P. Liska, L. Cevey, E. Costa, V. Shklover, L. Spiccia, G. B. Deacon, C. A. Bignozzi, M. Grätzel, *J. Am. Chem. Soc.* **2001**, *123*, 1613.
[3] A. Islam, H. Sugihara, M. Yanagida, K. Hara, G. Fujihashi, Y. Tachibana, R. Katoh, S. Murata, H. Arakawa, *New J. Chem.* **2002**, *26*, 966.
[4] P. Wang, R. H. Baker, J. E. Moser, S. M. Zakeeruddin, M. Grätzel, *Chem. Mater.* **2004**, *16*, 3246.
[5] S. Altobello, R. Argazzi, S. Caramori, C. Contado, S. Da Fré, P. Rubino, C. Choné, G. Larramona, C. A. Bignozzi, *J. Am. Chem. Soc.* **2005**, *127*, 15342.
[6] K. Hara, M. Kurashige, Y. Dan-oh, C. Kasada, A. Shinpo, S. Suga, K. Sayama, H. Arakawa, *New J. Chem.* **2003**, *27*, 783.
[7] T. Horiuchi, H. Miura, K. Sumioka, S. Uchida, *J. Am. Chem. Soc.* **2004**, *126*, 12218.
[8] T. Kitamura, M. Ikeda, K. Shigaki, T. Inoue, N. A. Anderson, X. Ai, T. Lian, S. Yanagida, *Chem. Mater.* **2004**, *16*, 1806.

 © 2006 Wiley-VCH Verlag GmbH & Co. KGaA, Weinheim 

[9] M. K. Nazeeruddin, R. Humphry-Baker, D. L. Officer, W. M. Campbell, A. K. Burrell, M. Grätzel, *Langmuir* **2004**, *20*, 6514.
[10] Q. Wang, W. M. Campbell, E. E. Bonfantani, K. W. Jolley, D. L. Officer, P. J. Walsh, K. Gordon, R. Humphry-Baker, M. K. Nazeeruddin, M. Grätzel, *J. Phys. Chem. B* **2005**, *109*, 15397.
[11] M. K. Nazeeruddin, A. Kay, L. Rodicio, R. Humphry-Baker, E. Müller, P. Liska, N. Vlachopoulos, M. Grätzel, *J. Am. Chem. Soc.* **1993**, *115*, 6382.
[12] M. Grätzel, *J. Photochem. Photobiol. A* **2004**, *164*, 3.
[13] S. Yan, J. T. Hupp, *J. Phys. Chem.* **1996**, *100*, 6867.
[14] T. Watanabe, A. Fujishima, O. Tatsuoki, K. Honda, *Bull. Chem. Soc. Jpn.* **1976**, *49*, 8.
[15] M. Yanagida, L. P. Singh, K. Sayama, K. Hara, R. Katoh, A. Islam, H. Sugihara, H. Arakawa, M. K. Nazeeruddin, M. Grätzel, *J. Chem. Soc. Dalton Trans.* **2000**, 2817.
[16] H. Sugihara, L. P. Singh, K. Sayama, H. Arakawa, Md. K. Nazeeruddin, M. Grätzel, *Chem. Lett.* **1998**, *10*, 1005.
[17] T. Renouard, R.-A. Fallahpour, Md. K. Nazeeruddin, R. Humphry-Baker, S. I. Gorelsky, A. B. P. Lever, M. Grätzel, *Inorg. Chem.* **2002**, *41*, 367.
[18] P. Wang, S. M. Zakeeruddin, J.-E. Moser, R. Humphry-Baker, P. Comte, V. Aranyos, A. Hagfeldt, M. K. Nazeeruddin, M. Grätzel, *Adv. Mater.* **2004**, *16*, 1806.
[19] P. Wang, C. Klein, R. Humphry-Baker, S. M. Zakeeruddin, M. Grätzel, *J. Am. Chem. Soc.* **2005**, *127*, 808.
[20] C. Klein, Md. K. Nazeeruddin, P. Liska, D. Di Censo, N. Hirata, E. Palomares, J. R. Durrant, M. Grätzel, *Inorg. Chem.* **2005**, *44*, 178.
[21] Z. Yang, I. Sokolik, F. E. Karasz, *Macromolecules* **1993**, *26*, 1188.
[22] H. Rensmo, S. Södergren, L. Patthey, K. Westmark, L. Vayssieres, O. Khole, P. A. Brühwiler, A. Hagfeldt, H. Siegbahn, *Chem. Phys. Lett.* **1997**, *274*, 51.
[23] M. K. Nazeeruddin, S. M. Zakeeruddin, R. Humphry-Baker, S. I. Goreslky, A. B. P. Lever, M. Grätzel, *Coord. Chem. Rev.* **2000**, *208*, 213.
[24] T. Renouard, R. A. Fallahpour, M. K. Nazeeruddin, R. Humphry-Baker, S. I. Gorelsky, A. B. P. Lever, M. Grätzel, *Inorg. Chem.* **2002**, *41*, 367.
[25] E. Figgemeier, V. Aranyos, E. C. Constable, R. W. Handel, C. E. Housecroft, C. Risinger, A. Hagfeldt, E. Mukhtar, *Inorg. Chem. Commun.* **2004**, *7*, 117.
[26] N. Hirata, J.-J. Lagref, E. J. Palomares, J. R. Durrant, M. K. Nazeeruddin, M. Grätzel, D. Di Censo, *Chem. Eur. J.* **2004**, *10*, 595.
[27] P. Wang, S. M. Zakeeruddin, J.-E. Moser, M. K. Nazeeruddin, T. Sekiguchi, M. Grätzel, *Nat. Mater.* **2003**, *2*, 402.
[28] J. D. Tovar, A. Rose, T. M. Swager, *J. Am. Chem. Soc.* **2002**, *124*, 7762.
[29] S. S. Zhu, R. P. Kingsborough, T. M. Swager, *J. Mater. Chem.* **1999**, *9*, 2123.
[30] C.-Y. Chen, H.-C. Lu, C.-G. Wu, J.-G. Chen, K.-C. Ho, *Adv. Funct. Mater.* **2006**, in press.

 © 2006 Wiley-VCH Verlag GmbH & Co. KGaA, Weinheim 

Sensor Technology

DOI: 10.1002/anie.200601634

# Fluorescent Organometallic Sensors for the Detection of Chemical-Warfare-Agent Mimics**

*Daniel Knapton, Mark Burnworth, Stuart J. Rowan,* and Christoph Weder**

Organophosphates are toxic species commonly found in both pesticides and chemical-warfare agents whose rapid and severe effects on human and animal health lie in their ability to block the action of acetylcholinesterase, a critical central-nervous-system enzyme.[1] As a consequence, intense research efforts have been directed to develop sensitive and selective schemes for the detection of these compounds.[2] A variety of approaches has been investigated for sensors, including the use of enzymatic assays,[3] molecular imprinting and lanthanide luminescence,[4] colorimetric methods,[5] surface acoustic waves,[6] organic fluorescent compounds,[7] gas chromatography–mass spectrometry,[8] and interferometry.[9] In general, each of these methods suffers from at least one undesirable limitation, such as limited selectivity, low sensitivity, operational complexity, lack of portability, and/or the difficulties of real-time monitoring.[4b,7a]

One of the most convenient and simplest means of chemical detection is the generation of an optical event, such as a change in absorption or fluorescence color, in the presence of an analyte of interest.[10] It was previously shown that lanthanide complexes, with characteristically narrow excitation and emission bands, intense fluorescence, and long excited-state lifetimes, are well suited to be used as fluorescence-based chemical sensors.[11] For example, $Eu^{3+}$ complexes can exhibit intense luminescence in the presence of an appropriate UV-light-absorbing ligand through the so-called "antenna effect".[12] This process involves optical absorption by the ligand, followed by ligand-to-metal energy transfer and results in metal-ion-based fluorescence. Any analyte, which can act as a competitive binder for the $Eu^{3+}$ center, can "switch off" the $Eu^{3+}$-based emission and potentially restore the emission of the "free" ligand. On the other hand, many metal ions do not lend themselves to metal-based emission,

[*] Dr. D. Knapton, M. Burnworth, Prof. Dr. S. J. Rowan, Prof. Dr. C. Weder
Department of Macromolecular Science and Engineering
Case Western Reserve University
2100 Adelbert Road, Cleveland OH 44106-7202 (USA)
Fax: (+1) 216-368-4202
E-mail: stuart.rowan@case.edu
christoph.weder@case.edu

[**] The material reported herein is based on work supported by the US army research office (Grant No. DAAD19-03-1-0208), the National Science Foundation (Grant No. CAREER-CHE 0133164), and the Case School of Engineering. The authors also thank Eric Giles, Casey Johnson, and Dr. Parameswar K. Iyer for their assistance.

Supporting information for this article is available on the WWW under http://www.angewandte.org or from the author.

 © 2006 Wiley-VCH Verlag GmbH & Co. KGaA, Weinheim 

for example $Zn^{2+}$ or $La^{3+}$; in these cases, the ligand-based fluorescence may be quenched or shifted to a different wavelength upon complexation. Taking advantage of these processes and exploiting the known binding affinity of organophosphates to lanthanide ions,[4,6a,12c] we present herein a most versatile sensor platform (Figure 1) that

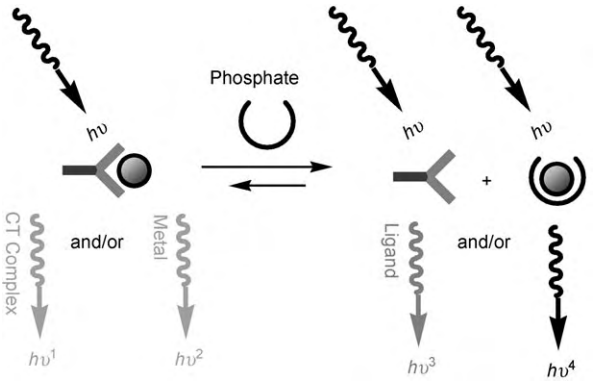


***Figure 1.*** Schematic representation of the mechanism utilized for the detection of metal-ion-coordinating analytes.

combines high selectivity and sensitivity with ease of signal transduction. The approach relies on the fact that 2,6-bis(1′-methylbenzimidazolyl)pyridine (Mebip) ligands are highly fluorescent and have been shown[13] to act as "antenna" for $Eu^{3+}$ ions. Furthermore, we have developed Mebip ligands and complexes in which ligand–metal energy transfer is absent. We show herein that such ligand-based emission can be designed to occur at different wavelengths upon metal ion (de-)complexation. Mixing and matching consciously designed ligands and carefully selected metal ions allows the formation of sensor complexes which can exhibit different selectivity and optical response.

In our ongoing efforts to develop metallo-supramolecular materials,[14] we previously reported the synthesis of the ditopic Mebip-functionalized ethynylene **1** and its self-assembly with $Zn(ClO_4)_2$. The metal-ion coordination results in large bathochromic shifts of both the absorption and fluorescence spectra.[14b] We now show that the addition of one equivalent of $[La(NO_3)_3]\cdot 6H_2O$ to ethynylene **1** produces a similar effect: the maximum of the emission band $\lambda_{max}$ is shifted by 97 nm upon complexation (Table 1; all experiments

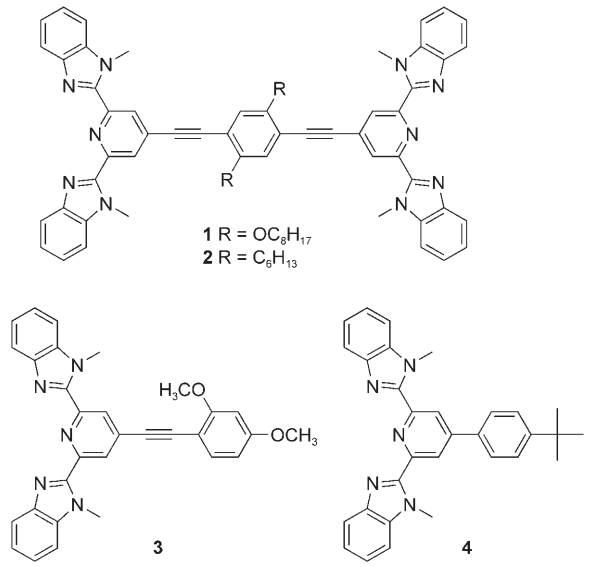


***Table 1:*** Emission and UV/Vis absorption data for solutions of the free ligands **1**–**4** and their corresponding complexes (compound/$M^{n+}$ = 1:1).

| Ligand/ complex[a] | Ligand emission $\lambda_{max}$ [nm][b] | Complex emission $\lambda_{max}$ [nm][b] | Ligand absorbance $\lambda_{max}$ [nm][d] | Complex absorbance $\lambda_{max}$ [nm][d] |
|---|---|---|---|---|
| **1**/[**1**·$La^{3+}$] | 448 | 545 | 395 | 427 |
| **2**/[**2**·$La^{3+}$] | 397 | 428 | 347 | 365 |
| **3**/[**3**·$La^{3+}$] | 420[c] | 493[c] | 341 | 378 |
| **3**/[**3**·$Zn^{2+}$] | 420[c] | 570[c] | 341 | 391 |
| **3**/[**3**·$Eu^{3+}$] | 420[c] | 578, 593, 614[c] | 341 | 383 |
| **4**/[**4**·$La^{3+}$] | 375 | 413 | 337 | 356 |

[a] All measurements were made in $CHCl_3/CH_3CN$ (9:1, v/v) solutions at concentrations of 0.025 mM. [b] Excitation at 320 nm. [c] Excitation at 360 nm. [d] Lowest-energy transition.

were conducted in $CHCl_3/CH_3CN$ (9:1, v/v)).[15] The large red-shift of the ligand emission upon $La^{3+}$ binding is consistent with either an intraligand charge transfer (CT), which results from the electron-rich arylethynylene core to the electron-poor metal-bound Mebip moieties,[14b,16] or a narrowing of the π–π* transition upon metal binding, on account of stabilization of the π* molecular orbital.[17] In both mechanisms, the electron density on the ligand is a key factor in the large bathochromic shift. This behavior is evident by comparison of the **1**/[**1**·$La^{3+}$] system with **2**/[**2**·$La^{3+}$]: In ligand **2**, the electron density of the core component was decreased by replacing the alkoxy functionality with alkyl substituents, thus resulting in a significantly smaller red shift (31 nm) upon binding to $La^{3+}$ (Table 1).

Having demonstrated the ability to readily control the extent to which the fluorescence of the Mebip ligands changes upon metal binding, we refined our sensory system for the detection of competitive coordinating organophosphates. To avoid any potential complications associated with multiple metal–ligand interactions and self-assembly/polymerization, we designed and synthesized fluorescent Mebip ligands with only one binding site. Different ligands (**3** and **4**) were prepared with the objective of investigating the influence of the electron density of the ligand on the fluorescence color change that occurs upon binding to $La^{3+}$ or $Zn^{2+}$ ions and on the sensing abilities of these complexes. In addition, these ligands were complexed to $Eu^{3+}$ ions to study sensor complexes that utilize well-defined lanthanide-based emission. Dialkoxyarylethynylene **3** contains an electron-rich aromatic group, whereas the electron-donating nature of the *tert*-butyl aryl moiety in **4** can be expected to be significantly less. Compounds **3** and **4** were prepared through Sonogashira and Suzuki coupling reactions, respectively. The ligands were complexed to the $La^{3+}$ center in a 1:1 ligand/$M^{n+}$ ratio, and the resulting emission and absorption spectra were recorded. Figure 2a shows that upon binding with $La^{3+}$ the emission spectrum of ligand **3** experiences a significant bathochromic

 © 2006 Wiley-VCH Verlag GmbH & Co. KGaA, Weinheim 

shift ($\Delta\lambda_{max} = 73$ nm, Table 1), which is manifested in a pronounced change of the emission color (blue to green), and the fluorescence intensity is significantly decreased. At the same time, a large change of the lowest-energy UV/Vis absorption band ($\Delta\lambda_{max} = 37$ nm, Table 1) is observed. As expected, much smaller changes are observed in the emission ($\Delta\lambda_{max} = 38$ nm, Table 1) and UV/Vis absorption spectra ($\Delta\lambda_{max} = 19$ nm, Table 1) for ligand **4**.

The readily available triethyl phosphate was used as a mimic for phosphate-based chemical-warfare agents to determine the organophosphate-sensing capability of the 1:1 [**3**·$La^{3+}$] and [**4**·$La^{3+}$] complexes.[7b,18] In addition, tri-*o*-tolyl phosphate (TOTP) was employed to investigate the selectivity of the phosphate sensing. The phosphates were titrated into dilute solutions of each complex in $CHCl_3/CH_3CN$ (9:1, v/v; 25 μM). In the case of the aliphatic phosphate, an instantaneous blue shift of the emission spectra and increase of the fluorescence intensities are observed, thus indicating the release of "free" ligand (Figure 2), which is consistent with the phosphate binding to the $La^{3+}$ ions. As expected, the largest spectral changes are observed at low analyte concentrations, with the effect leveling off at a concentration of approximately 10 mM phosphate for both complexes. Plotting the relative fluorescence intensity, defined as the (intensity at a given analyte concentration − intensity of the initial 1:1 complex)/intensity of the free ligand × 100, at the $\lambda_{max}$ value of the free ligand as a function of analyte concentration yields a sensory response for each complex (Figure 2, insets). The importance of bestowing the ligand with electron-donating substituents is readily evident as a visible color change was observed for [**3**·$La^{3+}$] at a concentration of 1.8 mM phosphate, whereas the sensory response of [**4**·$La^{3+}$] could only be monitored spectrophotometrically at a similar concentration of phosphate. Interestingly, the addition of the aromatic phosphate TOTP yielded only very small fluorescent responses when added to [**3**·$La^{3+}$] (Figure 2a). Even at a very large concentration of TOTP (17.5 mM), only a very small intensity increase and blue shift of the emission can be detected (Figure 2a, inset), thus indicating the virtual absence of the free ligand and pointing to very weak competitive binding. A very similar response was observed for water at comparably high concentrations (Figure 2a, inset), thus demonstrating that this sensor system shows excellent selectivity for the detection of alkyl phosphates over bulky aromatic phosphates and water.

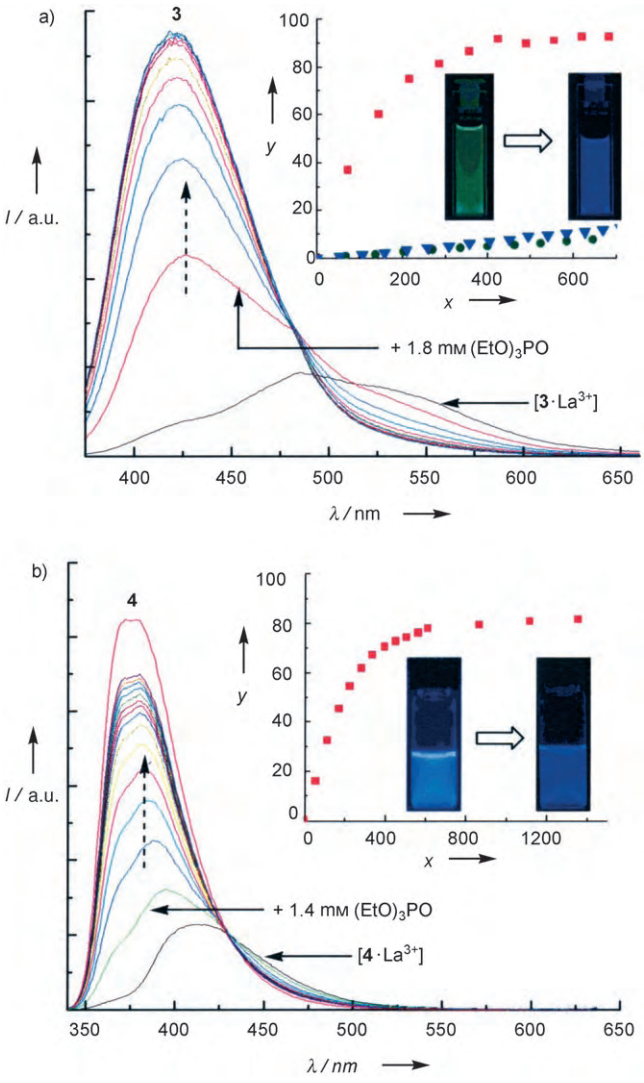


***Figure 2.*** Photoluminescence (PL) spectra acquired upon titration of a) [**3**·$La(NO_3)_3$] and b) [**4**·$La(NO_3)_3$] (0.025 mM) in $CHCl_3/CH_3CN$ (9:1, v/v) with $(EtO)_3PO$. The inset (a) shows the relative emission at 420 nm (*y*) as a function of the ratio of analyte ($(EtO)_3PO$, red square; TOTP, blue triangle; and $H_2O$, green circle) to [**3**·$La(NO_3)_3$] (*x*). The inset (b) shows the relative emission at 375 nm (*y*) as a function of the ratio of $(EtO)_3PO$/[**4**·$La(NO_3)_3$] (*x*). The pictures illustrate the fluorescence color of the initial sensor complex solutions, as well as those after adding $(EtO)_3PO$ to the saturation point.

Having established the high selectivity of these Me bip·$La^{3+}$ complexes for trialkyl phosphate over triaryl phosphate moieties and water, $La^{3+}$ was replaced with $Eu^{3+}$ and $Zn^{2+}$ to further explore the influence of different metal ions on the sensory capacity of the resulting complexes. The [**3**·$Zn^{2+}$] complex fluoresces yellow and displays an even larger bathochromic shift of the emission band ($\Delta\lambda_{max} =$ 150 nm, Table 1) than [**3**·$La^{3+}$]. By contrast, the [**3**·$Eu^{3+}$] complex displays emission characteristics that are dominated by a red, metal-based fluorescence, whereas the ligand-based emission is fully suppressed. Both complexes were exposed to increasing amounts of $(EtO)_3PO$. Again the relative fluorescence intensity at a wavelength of 420 nm was plotted as a function of analyte concentration to yield the sensory response for each complex (Figure 3a). The sensory response of [**3**·$Eu^{3+}$] was observed to behave in a similar manner to that of [**3**·$La^{3+}$], thus indicating that the binding of $La^{3+}$ and $Eu^{3+}$ to **3** is comparable. However, we should point out that the visual effect is much more pronounced in the case of the [**3**·$Eu^{3+}$] complex on account of the suppression of the intense $Eu^{3+}$-based emission.

With the objective of determining the sensitivity of these new sensor complexes, triethyl phosphate titrations were conducted with [**4**·$Eu^{3+}$] in a fashion similar to those reported above but with the addition of smaller aliquots of the analyte. The experiments yielded a spectroscopically observable increase of the fluorescence intensity (corresponding to free ligand) at analyte concentrations of as low as 20 μM—a level

 © 2006 Wiley-VCH Verlag GmbH & Co. KGaA, Weinheim 

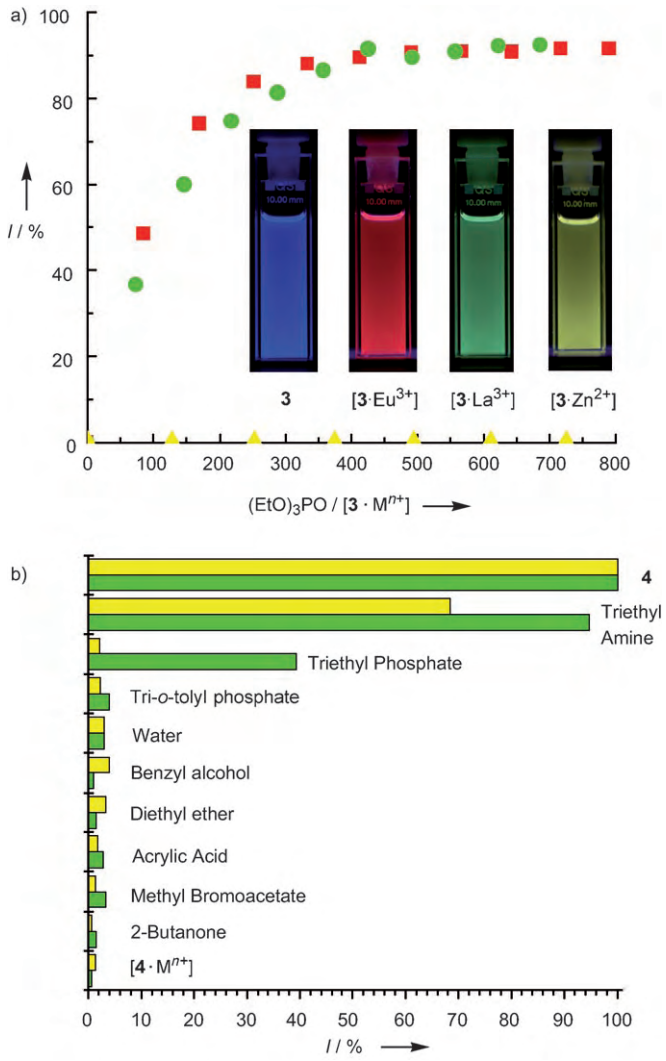


***Figure 3.*** a) Relative emission at 420 nm as a function of the ratio of $(EtO)_3PO$ to the 1:1 metal/ligand complexes [**3**·$MX_n$] (0.025 mM, M = $Eu^{3+}$, $La^{3+}$, and $Zn^{2+}$) in $CHCl_3/CH_3CN$ (9:1, v/v). b) Relative fluorescence intensity (% relative to the intensity of the free ligand) of solutions of [**4**·$La(NO_3)_3$] and [**4**·$Zn(ClO_4)_2$] upon exposure to common organic compounds. Experiments were performed at a complex concentration of 0.025 mM and analyte concentrations of 2.5 mM in $CHCl_3/CH_3CN$ (9:1, v/v).

commensurate with current organophosphate biosensors.[18] In contrast to its lanthanide counterparts, [**3**·$Zn^{2+}$] showed no increase of "free"-ligand fluorescence intensity upon addition of even large amounts (19 mM) of $(EtO)_3PO$ (Figure 3a). The absence of a response for [**3**·$Zn^{2+}$] illustrates the stronger binding of Mebip to $Zn^{2+}$ ions relative to $Ln^{3+}$ ions and/or a preference of the phosphate for interaction with $Ln^{3+}$ ions, thus clearly demonstrating the importance of carefully tailoring the strength of the metal–ligand interaction to an appropriate level.

One important aspect in the design of effective organophosphate sensors is to impart a high degree of analyte specificity, which is necessary to avoid false positive readings.[7a,b,20] To determine the extent to which our complexes would respond to various common organic species, 25 μM solutions of [**4**·$La^{3+}$] and [**4**·$Zn^{2+}$] were exposed to a variety of compounds (2.5 mM). As can be seen from the data compiled in Figure 3b, under these conditions both complexes show effectively no response to ketones, esters, organic acids, ethers, alcohols, water, and bulky aromatic phosphates, thus imparting a great degree of selectivity to these sensors. Apart from the trialkyl phosphate, the only other investigated compound that elicited a response was triethylamine. Importantly, although [**4**·$La^{3+}$] shows a response to both of these analytes, [**3**·$Zn^{2+}$], as discussed above, and equally [**4**·$Zn^{2+}$], do not show the presence of aliphatic phosphates but do respond to amines. Thus, using different combinations of metal ions and Mebip ligands, one is allowed to readily differentiate between aliphatic phosphates and amines. This point is illustrated clearly by the sensor array shown in Figure 4a. The array demonstrates the ability to detect the presence of aliphatic over aromatic phosphates, which is dictated by the nature of the binding of the lanthanide and Mebip ligand. In addition, the use of $Zn^{2+}$ complexes, such as [**1**·$Zn^{2+}$] for example, which detect only amines, provides the ability to single out the latter and prevent amine-driven false positive readings.

To facilitate practical devices, the vapor-phase detection of organophosphates is desirably accomplished by the use of a solid-state sensor.[20,21] The first experiments to address this need involved hydrophobic silica particles treated with a solution of [**4**·$Eu^{3+}$] to yield (after drying) a pink fluorescent powder (Figure 4b). The fluorescence color of the powder

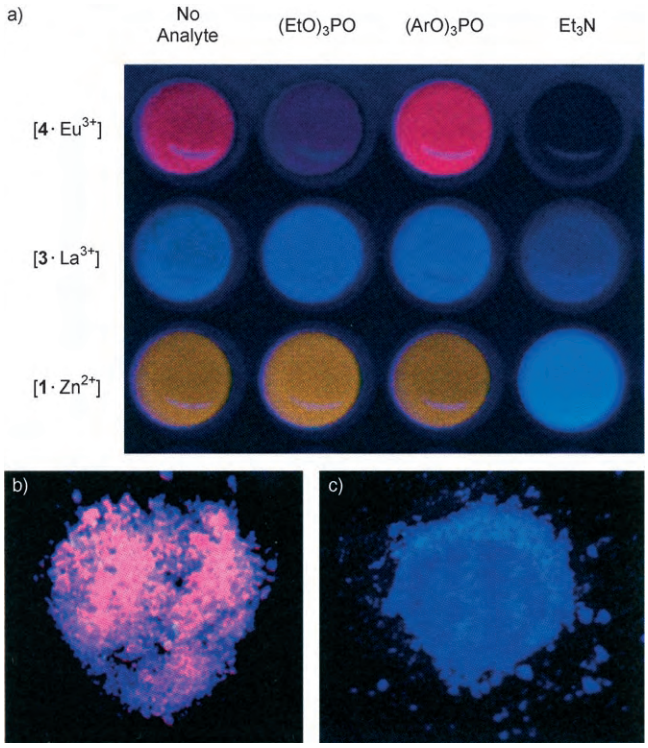


***Figure 4.*** Pictures taken under excitation at 365 nm of a) a sensor array, which illustrates the selective detection of $(EtO)_3PO$ and $Et_3N$ by 1:1 metal ion complexes (experiments were carried out in $CHCl_3/CH_3CN$ (9:1, v/v) with a complex concentration of 0.025 mM and analyte concentrations of 2.5 mM); b) hydrophobic silica particles coated with [**4**·$Eu^{3+}$]; c) hydrophobic silica particles coated with [**4**·$Eu^{3+}$] after exposure to $(EtO)_3PO$ vapor for 2 h at 60 °C.

 © 2006 Wiley-VCH Verlag GmbH & Co. KGaA, Weinheim 

changed slowly upon exposure to $(EtO)_3PO$ vapor (on account of the low vapor pressure of this analyte, as confirmed by the instantaneous response from exposure of the solid-state sensor to $(EtO)_3PO$ in liquid form) from pink to blue (Figure 4c), which is indicative of the decomplexation of [**4**·$Eu^{3+}$] and the formation of "free" ligand **4**.

In summary, we have developed a modular sensory system that utilizes a multimetal/multiligand-based approach. The judicious design of fluorescent ligands and the careful selection of metal/ligand combinations allowed us to create a very simple system that allows the selective detection of aliphatic organophosphates with good sensitivity. By tailoring the nature of the metal–ligand interactions, it should be possible to further enhance the sensitivity of these systems on the one hand and tailor their selectivity towards different analytes on the other.

Received: April 25, 2006
Published online: July 28, 2006

**Keywords:** fluorescence · lanthanides · organophosphates · sensors · supramolecular chemistry

[1] a) S. M. Somani, *Chemical Warfare Agent*, Academic Press, San Diego, **1992**; b) C. H. Gunderson, C. R. Lehmann, F. R. Sidell, B. Jabbari, *Neurology* **1992**, *42*, 946; c) S. U. Khan, *Pesticides in the Soil Environment*, Elsevier, Amsterdam, **1980**.

[2] a) J. A. Ashley, C.-H. Lin, K. D. Wirsching, K. D. Janda, *Angew. Chem.* **1999**, *111*, 1909; *Angew. Chem. Int. Ed.* **1999**, *38*, 1793; b) S. D. Richardson, *Chem. Rev.* **2001**, *101*, 211; c) D. Prosnitz, *Science* **2005**, *310*, 978; d) T. Dale, J. Rebek, *J. Am. Chem. Soc.* **2006**, *128*, 4500.

[3] A. J. Russell, J. A. Berberich, G. F. Drevon, R. R. Koepsel, *Annu. Rev. Biomed. Eng.* **2003**, *5*, 1.

[4] a) A. L. Jenkins, O. M. Uy, *Anal. Commun.* **1997**, *34*, 221; b) A. L. Jenkins, O. M. Uy, G. M. Murray, *Anal. Chem.* **1999**, *71*, 373; c) A. L. Jenkins, R. Yin, J. L. Jensen, *Analyst* **2001**, *126*, 798; d) C. M. Rudzinski, A. M. Young, D. G. Norcera, *J. Am. Chem. Soc.* **2002**, *124*, 1723.

[5] a) H. O. Michel, E. C. Gordon, J. Epstein, *Environ. Sci. Technol.* **1973**, *7*, 1045; b) T. J. Novak, L. W. Daasch, J. Epstein, *Anal. Chem.* **1979**, *51*, 1271.

[6] a) M. S. Nieuwenhuizen, J. L. N. Harteveld, *Sens. Actuators B* **1997**, *40*, 167; b) J. Negeh-Ngwainbi, P. H. Foley, S. S. Kuan, G. G. Guilbault, *J. Am. Chem. Soc.* **1986**, *108*, 5444.

[7] a) K. A. Van Houten, D. C. Heath, R. Pilato, *J. Am. Chem. Soc.* **1998**, *120*, 12359; b) S.-W. Zhang, T. M. Swager, *J. Am. Chem. Soc.* **2003**, *125*, 3420; c) S. Yamaguchi, I. Yoshimura, T. Kohira, S.-I Tamaru, I. Hamachi, *J. Am. Chem. Soc.* **2005**, *127*, 11835.

[8] W. E. Steiner, S. J. Klopsch, W. A. English, B. H. Clowers, H. H. Hill, *Anal. Chem.* **2005**, *77*, 4792.

[9] H. Sohn, S. Letant, M. J. Sailor, W. C. Trogler, *J. Am. Chem. Soc.* **2000**, *122*, 5399.

[10] a) N. A. Rakow, K. S. Suslick, *Nature* **2000**, *406*, 710; b) N. A. Rakow, A. Sen, M. C. Janzen, J. B. Ponder, K. S. Suslick, *Angew. Chem.* **2005**, *117*, 4604; *Angew. Chem. Int. Ed.* **2005**, *44*, 4528; c) R. C. Smith, A. G. Tennyson, M. H. Lim, S. J. Lippard, Org. Lett. **2005**, *7*, 3573.

[11] a) J.-C. G. Bünzli, C. Piguet, *Chem. Soc. Rev.* **2005**, *34*, 1048; b) B. Zhao, X. Y. Chen, P. Cheng, D.-Z. Liao, S.-P. Yan, Z. H. Jiang, *J. Am. Chem. Soc.* **2004**, *126*, 15394; c) D. Parker, *Coord. Chem. Rev.* **2004**, *205*, 109.

[12] a) S. Lis, *J. Alloys Comp.* **2002**, *341*, 45; b) N. Sabbatini, M. Guardigli, J.-M. Lehn, *Coord. Chem. Rev.* **1993**, *123*, 201; c) S. W. Magennis, S. Parsons, Z. Pikramenou *Chem. Eur. J.* **2002**, *8*, 5761.

[13] S. Petoud, J.-C. G. Bünzli, T. Glanzman, C. Piguet, Q. Xiang, P. Thummel, *J. Lumin.* **1999**, *82*, 69.

[14] a) J. B. Beck, S. J. Rowan, *J. Am. Chem. Soc.* **2003**, *125*, 13922; b) P. K. Iyer, J. B. Beck, C. Weder, S. J. Rowan, *Chem. Commun.* **2005**, 319; c) D. Knapton, S. J. Rowan, C. Weder, *Macromolecules* **2006**, *39*, 651; d) J. B. Beck, J. M. Ineman, S. J. Rowan *Macromolecules* **2005**, *38*, 5060.

[15] It should be noted that ethynylene **1** does not undergo a large degree of self-assembly in solution with the addition of [La-$(NO_3)_3$]; see the Supporting Information and S. Petoud, J.-C. G. Bünzli, K. J. Schenk, C. Piguet, *Inorg. Chem.* **1997**, *36*, 1345.

[16] J. N. Wilson, U. H. F. Bunz, *J. Am. Chem. Soc.* **2005**, *127*, 4124.

[17] C. Piguet, J.-C. G. Bünzli, G. Bernardinelli, C. G. Bochet, P. Froidevaux, *J. Chem. Soc. Dalton Trans.* **1995**, 83–96.

[18] A. R. Hopkins, N. S. Lewis, *Anal. Chem.* **2001**, *73*, 884.

[19] M. Janotta, M. Karlowatz, F. Vogt, B. Mizaikoff, *Anal. Chim. Acta* **2003**, *496*, 339.

[20] A. L. Simonian, T. A. Good, S.-S. Wang, J. R. Wild, *Anal. Chim. Acta.* **2005**, *534*, 69.

[21] L. Rotiroti, L. De Stefano, I. Rendina, L. Moretti, A. M. Rossi, A. Piccolo, *Biosens. Bioelectron.* **2005**, *20*, 2136.

 © 2006 Wiley-VCH Verlag GmbH & Co. KGaA, Weinheim 

*Electroanalysis*

DOI: 10.1002/anie.200601640

# Thermodynamic and Kinetic Enhancement of Electrochemical Sensitivity by Chemical Coupling in Microfluidic Systems**

*Imtiaz M. Khalid, Qiaosheng Pu, and Julio C. Alvarez**

Herein, we report the enhancement of electrochemical sensitivity by chemical coupling of two independent reactions in a microfluidic channel. Scheme 1 illustrates the general concept of this approach: an upstream electrode ($E_1$) drives a reaction that produces protons while a downstream electrode ($E_2$) conducts a second reaction that consumes protons. The reactions are chemically coupled by the electrogenerated protons, which are used to harness thermodynamically or kinetically the reaction at $E_2$. Herein, we show two examples of a positive shift in the redox potential ($E^{\circ\prime}$) of an analyte in

[*] I. M. Khalid, Dr. Q. Pu, Prof. J. C. Alvarez
Department of Chemistry
Virginia Commonwealth University
Richmond, VA, 23284–2006 (USA)
Fax: (+1) 804-828-8599
E-mail: jcalvarez2@vcu.edu

[**] This work is supported by Virginia Commonwealth University and the Jeffress Memorial Trust of Virginia.

Supporting information for this article is available on the WWW under http://www.angewandte.org or from the author.


© 2006 Wiley-VCH Verlag GmbH & Co. KGaA, Weinheim

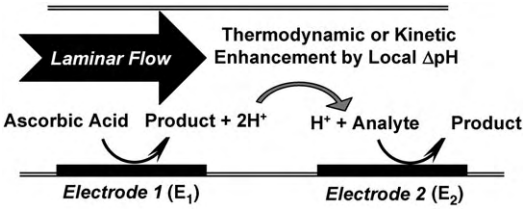


***Scheme 1.*** Chemical coupling of electrochemical reactions.

response to electrogeneration of protons at $E_1$. As a result of this shift, two effects with analytical value arise: first, the analyte is now fully detectable at potentials more positive than $E^{\circ\prime}$, where the analyte is undetectable; and second, two redox analytes with overlapping $E^{\circ\prime}$ values can be discriminated if one of them is not sensitive to protonation. The most significant aspect of this approach is that the effects reported herein are observable as a result of using a microfluidic cell instead of a traditional electrochemical cell. Prior work in the area of hydrodynamic voltammetry[1–7] and the generation of chemical gradients in flow systems is directly related to the present work.[8–12]

The advantage of chemically coupled reactions as depicted in Scheme 1 can be realized by considering a biochemical process such as the conversion of phospho-(enol)pyruvate (PEP) into pyruvate in the glycolisis cycle.[13] The phosphorylation of adenosine diphosphate (ADP) to form adenosine triphosphate (ATP) is an energetically unfavorable process. However, when this reaction is coupled to the exergonic hydrolysis of PEP that produces pyruvate and inorganic phosphate, the net reaction becomes energetically favorable with an overall negative $\Delta G^{\circ}$.[13] We used this principle to enhance the current response for the reduction of model analytes [Eq. (1)] by using the oxidation of ascorbic

$$\mathrm{DMBQ} + 2\,\mathrm{H^+} + 2\,\mathrm{e^-} \rightarrow \mathrm{H_2DMBQ} \qquad \Delta G^{\circ\prime} = +42.8\ \mathrm{kJ\,mol^{-1}}\ (\mathrm{pH}\ 7.0) \tag{1}$$

acid (AA) that produces dehydroascorbic acid (DAA) and protons [Eq. (2)].[14] The only requirement to observe the

$$\mathrm{AA} \rightarrow \mathrm{DAA} + 2\,\mathrm{H^+} + 2\,\mathrm{e^-} \quad \Delta G^{\circ\prime} = -57.1\ \mathrm{kJ\,mol^{-1}}\ (\mathrm{pH}\ 7.0) \tag{2}$$

effect is that the analyte reaction must involve the consumption of protons so that the overall $\Delta G^{\circ\prime}$ value [Eq. (3)] can be made more negative than that of the analyte reaction alone.

$$\mathrm{AA} + \mathrm{DMBQ} \rightarrow \mathrm{H_2DMBQ{+}DAA} \qquad \text{Total } \Delta G^{\circ\prime} = -14.3\ \mathrm{kJ\,mol^{-1}} \tag{3}$$

Figure 1 shows the reduction of dimethyl benzoquinone (DMBQ) at two different pH values under buffer conditions. An overall decrease of 4.4 units in pH produced a positive shift in $E^{\circ\prime}$ from −0.310 to −0.089 V,[15] which translates into an average of around 50.3 mV/pH unit, which is similar to the shift observed for other quinones.[16] Figure 2 shows a series of data points obtained for coupling experiments in nonbuffered solution mixtures of AA and DMBQ with the initial pH adjusted to 7.0. The reduction of DMBQ was monitored at $E_2$ while the potential of $E_1$ (and hence rate of oxidation of AA)

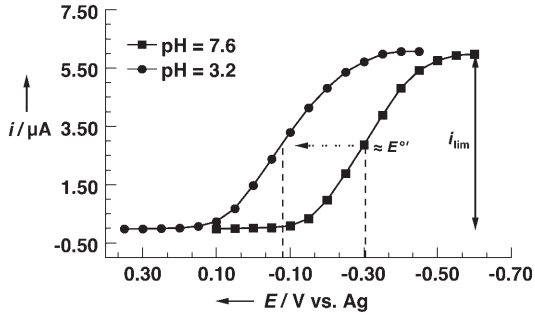


***Figure 1.*** Voltammetry of 5.0 mM DMBQ in a microfluidic channel with 0.1 M phosphate buffer and 0.1 M KCl.

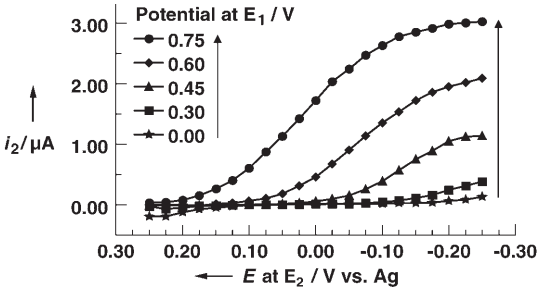


***Figure 2.*** Voltammetry under coupling conditions of 5.0 mM DMBQ, 10 mM AA, and 0.1 M KCl; initial pH = 7.0 (no buffer).

was increased; no oxidation of AA was observed at 0.00 V and a maximum rate was observed at 0.75 V (see the Supporting Information). As the oxidation of AA is a two-electron process that generates two protons and the electroinactive species DAA,[14] AA can not be redox recycled at $E_2$.

The production of protons at $E_1$ induces an increase of the current at $E_2$ in a potential window in which quinone is not reduced at neutral pH (Figure 1). At the maximum rate of proton production on $E_1$ (0.75 V), the final $E^{\circ\prime}$ value observed for the quinone was 0.016 V with an overall positive shift of 0.422 V. A similar trend with somewhat diminished shift was observed when the experiment was conducted under buffered conditions at pH 7.0 (see the Supporting Information). Table 1 summarizes the $E^{\circ\prime}$ and limiting current $i_{lim}$ values at different buffer concentrations. The $E^{\circ\prime}$ value obtained for DMBQ under coupling conditions was always less positive as the ionic strength of the buffer increased. Likewise, the $i_{lim}$ values for the reduction of DMBQ in 1.0 M buffer was about 50% lower than that obtained in 0.05 M buffer.

To verify the local pH decrease upon AA oxidation, we monitored this reaction in the presence of a pH indicator with a fluorescence microscope.[17,18] The fluorescence of the dye

***Table 1:*** Effect of buffer strength on $E^{\circ\prime}$ DMBQ at $E_2$.

| Buffer concentration [M][a] | $E^{\circ\prime}$ [V][b] | $i_{lim}$ [μA] |
|---|---|---|
| 0.05 | −0.087 | 4.24 |
| 0.10 | −0.106 | 4.06 |
| 0.50 | −0.158 | 3.10 |
| 1.0 | −0.172 | 2.31 |

[a] pH 7.0. [b] $E_1$ kept at 0.75 V.

 © 2006 Wiley-VCH Verlag GmbH & Co. KGaA, Weinheim 

was negligible at the initial pH 7.0 (see the Supporting Information), but there was a local increase in fluorescence around the transparent electrode after the electrode potential was stepped to 0.900 V for 3 s (Figure 3).

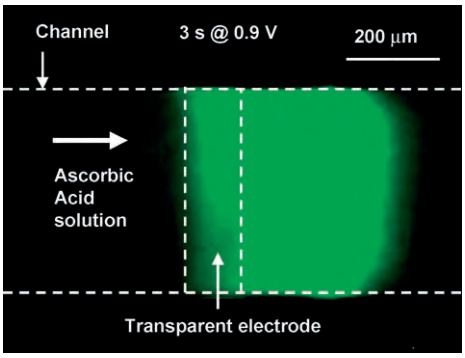


***Figure 3.*** Fluorescence monitoring of proton release upon electrooxidation of 36 mM AA and 0.1 M NaCl with an initial pH of 7.0 and 10 μM Lyzosensor DND-160; excitation wavelength = 365 nm, emission wavelength > 515 nm.

The effect of the protons on DMBQ can be understood by considering Equation (1) and the coupling principle described above. We detected a redox wave about 0.3 V more positive than the quinone reduction wave when HCl was added to pure DMBQ (see the Supporting Information). The same wave was observed for mixtures of AA and DMBQ when the voltammetric scan included the oxidation of AA. These results are consistent with previous reports[15] and support the presence of an intermediate that is stabilized by protonation and is responsible for the positive thermodynamic shifts observed above.

To illustrate how the proton coupling enhances the detection sensitivity for DMBQ in a microfluidic cell, we performed calibration curves with mixtures of AA and DMBQ at different concentrations of DMBQ. Figure 4 shows a series of data points obtained under three different conditions: a mixture AA and DMBQ with proton coupling (A); the same mixture measured without proton coupling (B); and a pure DMBQ solution under the conditions of proton coupling (C). The slope of the fitted line for data set A

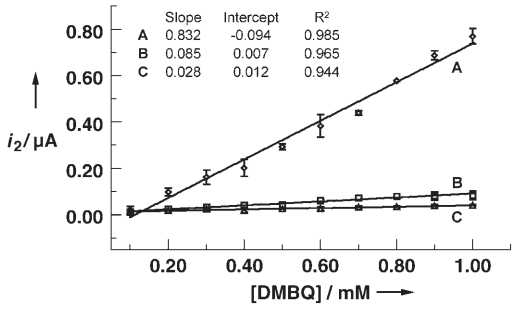


***Figure 4.*** Calibration curve for a 1:4 mixture of DMBQ and AA in 0.1 M KCl; initial pH = 7.3, $E_1$ was kept at 0.750 V while $E_2$ was pulsed at −0.225 V vs. Ag. A) DMBQ coupled signal; B, C) controls (see text).

is about 10 times higher than that for the control experiment B and approximately 30 times that for C.

The reduction of $[Ru(NH_3)_6]^{3+}$ [Eq. (4)] at $E_2$ was investigated because the ammonia ligand is basic. However, the

$$[Ru(NH_3)_6]^{3+} + e^- \rightarrow [Ru(NH_3)_6]^{2+}\ (E_2) \qquad (4)$$

ligand exchange kinetics of $[Ru(NH_3)_6]^{3+}$ is so slow[19] relative to the time scale of conventional voltammetric experiments that in neutral or weakly acidic conditions the voltammetry of $[Ru(NH_3)_6]^{3+}$ appears relatively insensitive to pH. Taube and co-workers[19] found that the slow aquation rate for $[Ru(NH_3)_6]^{2+}$ [Eq. (5), $k \approx 1.24 \times 10^{-3}\,M^{-1}s^{-1}$] can be accelerated significantly in acidic conditions.[19]

$$H_2O + [Ru(NH_3)_6]^{2+} + H^+ \rightarrow [Ru(NH_3)_5H_2O]^{2+} + NH_4^+ \qquad (5)$$

Since Equation (5) involves the product of Equation (4), the addition of protons promotes Equation (4) with a concomitant positive shift in $E^{\circ\prime}$. Figure 5 shows the effect

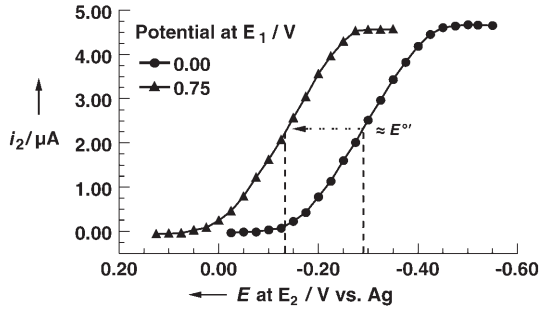


***Figure 5.*** Voltammetry under coupling conditions for 5.0 mM $[Ru(NH_3)_6]^{3+}$, 4.0 mM AA, and 0.1 M KCl; initial pH 3.1 (no buffer).

of changing the potential of $E_1$ from 0.00 to 0.75 V while reducing $[Ru(NH_3)_6]^{3+}$ at $E_2$ in a solution mixture with AA initially at pH 3.1. A positive shift from −0.293 to −0.137 V was observed when $E_1$ was set to obtain the maximum rate of proton generation. Although the overall effect is thermodynamic, we consider it kinetically induced because under neutral and weakly acidic conditions the ligand exchange is so slow that the pH dependence disappears.

In summary, by taking advantage of the flow control and the presence of multiple electrodes in a microfluidic channel, we have implemented a principle of chemical coupling that biological systems extensively utilize to overcome the severe thermodynamic constraints in life-sustaining processes.[13] As a proof of concept, we used this principle to enhance the electrochemical sensitivity of a pH-dependent reaction and showed that is not necessary to change the pH of the whole solution to attain advantageous effects in detection. This could be beneficial in integrated bioanalysis in which the pH prior to the detection stage needs to be restricted. Furthermore, since this approach can be applied to any pair of reactions sharing a common reactant or product (including electrochemical, photonic, and chemical reactions), we are currently investigating coupling schemes that could lead to

 © 2006 Wiley-VCH Verlag GmbH & Co. KGaA, Weinheim 

signal amplification. Finally, the coupling can be modulated easily by simply changing the flow rate or interelectrode gap.

## Experimental Section

The microfluidic cells made of poly(dimethylsiloxane) (PDMS) and gold- or indium-tin-oxide-coated glass were fabricated following photolithographic procedures.[20,21] A typical microelectrochemical cell consisted of a rectangular PDMS channel (500 μm wide and 25 μm high) glued onto the glass surface (see the Supporting Information). The patterned electrodes (200 μm wide and 150 μm apart) were located close to a big circular reservoir in which a Pt and an Ag wire were used as counter and quasi-reference electrodes, respectively. All experiments were conducted with a bipotentiostat (CH Instruments, Austin, TX) by pulsing the potential of $E_2$ (0.1 s) while keeping the potential of $E_1$ at the desired value. The uncompensated resistance was always about 20 kΩ and $E_{1/2} \approx E^{\circ\prime}$ when $D_{ox} = D_{red}$ is assumed.[22] The flow rate (1 μL min$^{-1}$) was controlled with a precision syringe pump (Harvard Apparatus, Holliston, MA).

Received: April 26, 2006
Published online: July 31, 2006

**Keywords:** electrochemistry · microfluidics · sensors · signal transduction

[1] C. Amatore, A. Oleinick, O. V. Klymenko, I. Svir, *ChemPhysChem* **2005**, *6*, 1581 – 1589.
[2] A. C. Fisher, R. G. Compton, *J. Appl. Electrochem.* **1991**, *21*, 208 – 212.
[3] M. Thompson, O. V. Klymenko, R. G. Compton, *J. Electroanal. Chem.* **2005**, *576*, 333 – 338.
[4] M. Zhong, J. Zhou, S. M. Lunte, G. Zhao, D. M. Giolando, J. R. Kirchhoff, *Anal. Chem.* **1996**, *68*, 203 – 207.
[5] I. E. Henley, K. Yunus, A. C. Fisher, *J. Phys. Chem. B* **2003**, *107*, 3878 – 3884.
[6] R. G. Compton, R. A. W. Dryfe, J. A. Alden, N. V. Rees, P. J. Dobson, P. A. Leigh, *J. Phys. Chem.* **1994**, *98*, 1270 – 1275.
[7] R. G. Compton, J. J. Gooding, A. Sokirko, *J. Appl. Electrochem.* **1996**, *26*, 463 – 469.
[8] M. E. Robbins, E. D. Hopper, M. H. Schoenfisch, *Langmuir* **2004**, *20*, 10296 – 10302.
[9] C. R. Cabrera, B. Finlayson, P. Yager, *Anal. Chem.* **2001**, *73*, 658 – 666.
[10] S. M. Mitrovski, R. G. Nuzzo, *Lab Chip* **2005**, *5*, 634 – 645.
[11] J. Pihl, J. Sinclair, E. Sahlin, M. Karlsson, F. Petterson, J. Olofsson, O. Orwar, *Anal. Chem.* **2005**, *77*, 3897 – 3903.
[12] C. A. Paddon, G. J. Pritchard, T. Thiemann, F. Marken, *Electrochem. Commun.* **2002**, *4*, 825 – 831.
[13] R. H. Garrett, C. M. Grisham, *Biochemistry*, 3rd ed., Thomson Brooks/Cole, Belmont, **2005**, p. 1086.
[14] P. Karabinas, D. Jannakoudakis, *J. Electroanal. Chem.* **1984**, *160*, 159 – 167.
[15] J. Q. Chambers in *The Chemistry of the Quinonoid Compounds*, *Vol. 2* (Eds.: S. Patai, Z. Rappoport), Wiley, New York, **1988**, pp. 719 – 757, and references therein.
[16] M. M. Walczak, D. A. Dryer, D. D. Jacobson, M. G. Foss, N. T. Flynn, *J. Chem. Educ.* **1997**, *74*, 1195 – 1197.
[17] S. Fledler, R. Hagedorn, T. Schnelle, E. Richter, B. Wagner, G. Fuhr, *Anal. Chem.* **1995**, *67*, 820 – 828.
[18] K. P. McNamara, T. Nguyen, G. Dumitrascu, J. Ji, N. Rosenzweig, Z. Rosenzweig, *Anal. Chem.* **2001**, *73*, 3240 – 3246.
[19] P. C. Ford, J. R. Kuempel, H. Taube, *Inorg. Chem.* **1968**, *7*, 1976 – 1983.
[20] Y. N. Xia, G. M. Whitesides, *Angew. Chem.* **1998**, *110*, 568 – 594; *Angew. Chem. Int. Ed.* **1998**, *37*, 550 – 575.
[21] W. Zhan, J. Alvarez, R. M. Crooks, *J. Am. Chem. Soc.* **2002**, *124*, 13265 – 13270.
[22] A. J. Bard, L. R. Faulkner, *Electrochemical Methods Fundamentals and Applications*, 2nd ed., Wiley, New York, **2001**, p. 344.

 © 2006 Wiley-VCH Verlag GmbH & Co. KGaA, Weinheim 

Total Synthesis

DOI: 10.1002/anie.200601859

# Studies on Iejimalide B: Preparation of the Seco Acid and Identification of the Molecule's "Achilles Heel"**

*Alois Fürstner,* Christophe Aïssa, Carine Chevrier, Filip Teplý, Cristina Nevado, and Martin Tremblay*

Extraction of the tunicate *Eudistoma* cf. *rigida* collected off Ie island, Okinawa province, Japan, led to the isolation of a family of novel 24-membered polyene macrolides designated iejimalides A–D (**1**–**4**).[1] Although the structure of these

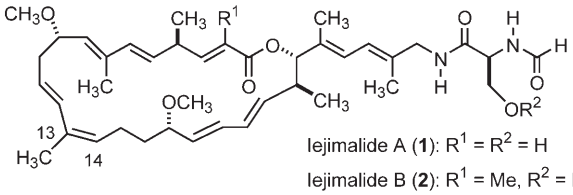

Iejimalide A (**1**): $R^1 = R^2 = H$
Iejimalide B (**2**): $R^1 = Me$, $R^2 = H$
Iejimalide C (**3**): $R^1 = H$, $R^2 = SO_3Na$
Iejimalide D (**4**): $R^1 = Me$, $R^2 = SO_3Na$

extremely scarce cytotoxic metabolites (0.0003–0.0006 % of the tunicates wet weight) could be established, it was only after a reextraction from a *Cystodytes* sp. that enough

[*] Prof. A. Fürstner, Dr. C. Aïssa, Dr. C. Chevrier, Dr. F. Teplý, Dr. C. Nevado, Dr. M. Tremblay
Max-Planck-Institut für Kohlenforschung
45470 Mülheim/Ruhr (Germany)
Fax: (+49) 208-306-2994
E-mail: fuerstner@mpi-muelheim.mpg.de

[**] Generous financial support from the MPG, the Fonds der Chemischen Industrie, the Alexander-von-Humboldt Foundation (fellowship to C.N.), and the NSERC, Canada (fellowship to M.T.) is gratefully acknowledged. We thank Dr. R. Riveiros for assistance in the initial phase of this project, and Dr. R. Mynott, B. Gabor, and C. Wirtz for their invaluable help with the structure assignment of several key compounds.

Supporting information for this article is available on the WWW under http://www.angewandte.org or from the author.


© 2006 Wiley-VCH Verlag GmbH & Co. KGaA, Weinheim

material was accumulated to allow for the establishment of their relative and absolute stereochemistry; at the same time, the configuration of the C13–C14 double bond was corrected to *Z* (rather than *E* as originally assigned).[2]

The scarcity of the iejimalides also delayed in-depth studies of their physiological properties; details reported recently, however, are very encouraging. Specifically, the data for iejimalide A, disclosed in 2005 by the National Cancer Institute (NCI), illustrates the truly remarkable potency of **1** against the panel of 60 standard human cancer cell lines, with the concentrations required to inhibit growth by 50% ($GI_{50}$) and tumor gene index (TGI) values in the low nanomolar range.[3,4] Equally remarkable is the report by Kobayashi and co-workers that the activity profile of **1**–**4** does not correlate with those of other anticancer drugs, which might indicate an unprecedented mode of action.[2] The same authors also demonstrated the potent in vivo activity of **3** and **4** against P388 leukemia.[2a]

Collectively, these data suggest that the iejimalides may be candidates for further development in a (pre)clinical setting. Spurred on by this prospect, we ventured into a synthesis-driven investigation of these enticing targets.[5] Therefore, it was necessary to prepare sufficient amounts for further testing. Presented in this and the following Communication is a preliminary report on our endeavors in the field, which not only led to the first total synthesis of iejimalide B (**2**) as the most active member of the series, but also unraveled many of the peculiar chemical characteristics of these delicate lead compounds.[6,7]

A cursory inspection of **1**–**4** shows that five of the six chiral centers reside at allylic or even doubly allylic sites. Apprehensive that this feature likely potentiates the lability of their polyunsaturated backbones, our first approach to **2** gravitated toward methodology that is believed to cope with such potentially fragile structural elements.

Specifically, it was planned to incorporate the peptide residue at the very end of the synthesis, because of the proclivity of *N*-formylserine derivatives toward racemization, formyl cleavage, and oxazoline formation. The success of the venerable Yamaguchi macrolactonization in complex settings[8,9] and our excellent experiences with the Julia olefination for the elaboration of sensitive, and even enolizable compounds, suggested the use of these transformations in the present context.[10,11] Complemented by Pd-catalyzed C–C bond formations,[12] this ensemble of reliable and mild chemical reactions promised a flexible access route to **2** starting from five synthons of similar size and moderate complexity (Scheme 1).

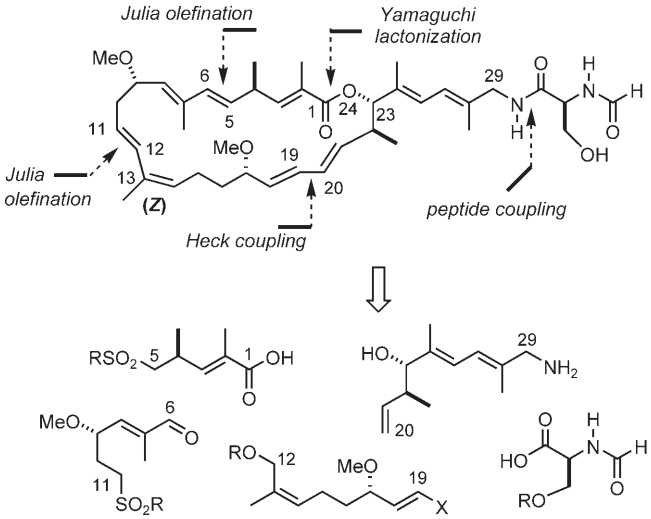


***Scheme 1.*** "First generation" retrosynthetic analysis and Kobayashi's numbering scheme of iejimalide B (**2**).

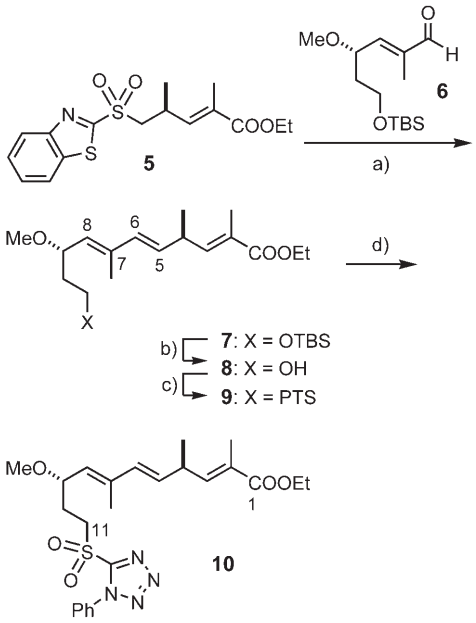


***Scheme 2.*** a) NaHMDS, THF, −78 °C→RT ("Barbier conditions"), 89% (*E*/*Z* = 4:1); b) HCl (5% in EtOH), EtOH, 0 °C, 60%; c) 1-phenyl-1*H*-tetrazol-5-thiol, DEAD, $PPh_3$, THF, 82%; d) cat. $[Mo_7O_{24}(NH_4)_6]\cdot 4H_2O$, aq $H_2O_2$, EtOH, 75%. HMDS = 1,1,1,3,3,3-hexamethyldisilazane, DEAD = diethylazodicarboxylate, PTS = 1-phenyl-1*H*-tetrazol-5-thiyl.

The required building block **10** (Scheme 2) was prepared by a Julia olefination of sulfone **5** (derived from the commercial Roche ester)[13] and aldehyde **6** (derived from commercial (*S*)-2-hydroxybutyrolactone)[13] to give alkene **7** in almost quantitative yield in a diastereomeric ratio of *E*/*Z* = 4:1. Since attempted isomerization with PhSSPh/azobisisobutyronitrile (AIBN) led to a complex mixture, (*E*)-**7** and (*Z*)-**7** were separated by preparative HPLC prior to removal of the terminal *tert*-butyldimethylsilyl (TBS) ether and installation of a phenyltetrazolyl sulfone terminus in **10** by the standard two-step protocol. It is notable that the cleavage of the silyl ether in **7** worked only with dilute HCl in EtOH; the use of tetra-*n*-butylammonium fluoride (TBAF)/HOAc affected the integrity of the conjugated diene. Although this finding forecasted there would be subtle stability issues, it was not until the late stages of the synthesis that this aspect was fully appreciated.

The complementary hemisphere of **2** was accessible by adaptation of a literature route,[7a] involving an effective Heck reaction of **11** and **12** as the key step,[14] delivering multigram

 © 2006 Wiley-VCH Verlag GmbH & Co. KGaA, Weinheim 

amounts of aldehyde **15** (Scheme 3). This compound was then subjected to Brown crotylation[15] to install the *anti*-configured homoallylic motif of **16** in excellent chemical yield and remarkable optical purity (*anti*/*syn* 98:2, 95 % *ee*).

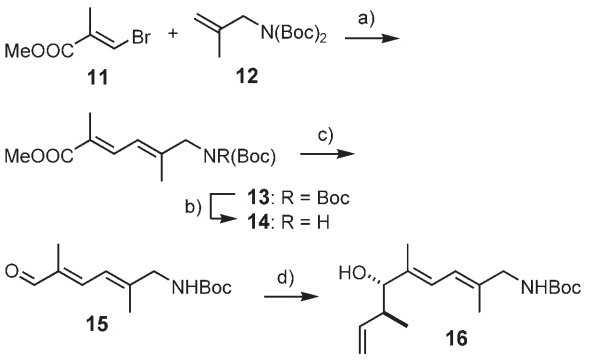


***Scheme 3.*** a) $Pd(OAc)_2$ (3 mol%), P(*o*-tol)$_3$ (6 mol%), $Et_3N$, 100°C, 84%; b) trifluoroacetic acid, $CH_2Cl_2$, 87%; c) 1. DIBAL-H, $CH_2Cl_2$, −78°C, 97%; 2. DMSO, $(COCl)_2$, $Et_3N$, $CH_2Cl_2$, −78°C→RT, 79%; d) (+)-((*E*)-crotyl)-B(Ipc)$_2$, THF, −78°C, 82% (95% *ee*). Boc = *tert*-butyloxycarbonyl, tol = tolyl, DIBAL-H = diisobutylaluminum hydride, Ipc = isopinocampheyl.

The coupling partner **24** was prepared by asymmetric transfer hydrogenation of ketone **17**[13] following conditions developed by Noyori and co-workers and furnished propargyl alcohol **19** in 98% yield and 98.8% *ee*, without affecting the olefinic and the acetylenic sites in the vicinity (Scheme 4).[16] In contrast, however, the seemingly trivial conversion of **19** into methyl ether **20** was surprisingly troublesome. After considerable experimentation, it was found that the use of DMSO as a dipolar cosolvent gave satisfactory and reproducible results on fairly large scale reactions.[17] Oxidative cleavage of the double bond followed by a modified Still–Gennari olefination of the resulting aldehyde **21** afforded the required *Z*-configured enoate **22** as a single isomer.[18,19] Cleavage of the silyl group with $K_2CO_3$ in MeOH,[20] exhaustive reduction/carbometalation of the resulting product **23** with an excess of $[Cp_2Zr(H)Cl]$,[21] and an iodolytic workup completed the synthesis of alkenyl iodide **24**, which was obtained in 34% yield over seven readily scalable operations.

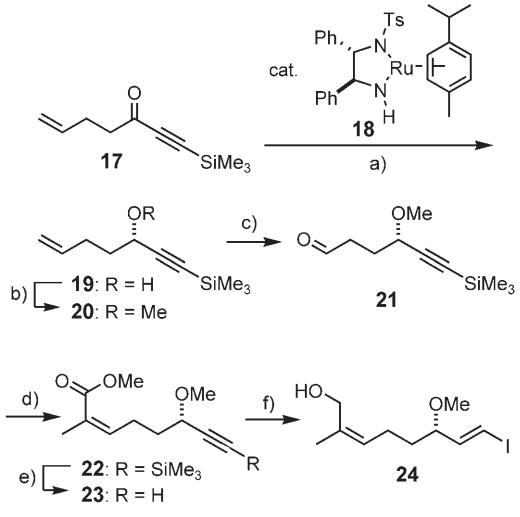


***Scheme 4.*** a) **18** (0.6 mol%), *i*PrOH, 98% (98.8% *ee*); b) 1. *n*BuLi, MeI, THF, −78°C; 2. DMSO, −25°C→RT; c) cat. $OsO_4$, $NaIO_4$, 2,6-lutidine, aq 1,4-dioxane, 74% (over two steps); d) $(CF_3CH_2O)_2P(O)CH(Me)COOMe$, KHMDS, [18]crown-6 (0.7 equiv), toluene, −20°C, 87%; e) $K_2CO_3$, MeOH, 80%; f) $[Cp_2Zr(H)Cl]$ (3.1 equiv), THF, then $I_2$, 80%. Cp = cyclopentadienyl, Ts = toluene-4-sulfonyl.

Since the homoallylic terminus renders **16** directly amenable to cross-coupling under Heck conditions, this particular C–C bond formation was preferred over other conceivable reactions. Despite its impressive track record,[14] attempted fusion of iodide **24** with alkene **16** under various experimental conditions led to a morass of isomers. A successful coupling of these components was only possible after switching to the "cationic manifold", which is operative upon addition of AgOAc (1.2 equiv)[22] (Scheme 5). The desired *E*,*E*-configured diene **25** could be separated from the *E*,*Z* isomer by careful chromatography.

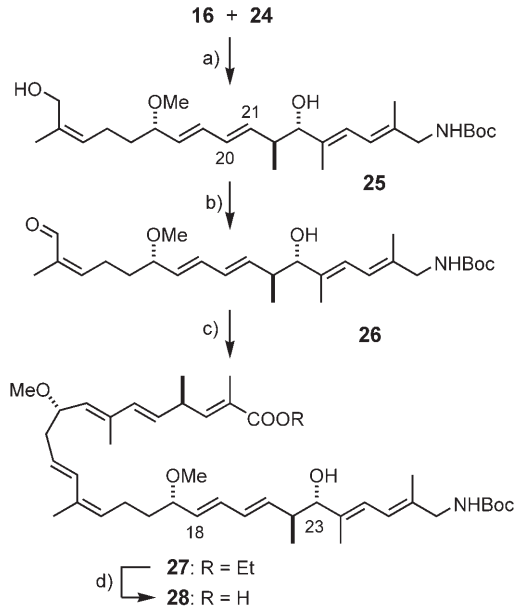


***Scheme 5.*** a) $Pd(OAc)_2$ (10 mol%), AgOAc, DMF, RT, 46% (**25**) + 13% ($\Delta^{[20,21]}$ isomer); b) cat. *t*BuOK, cat. $CuBr_2$, cat. 2,2′-bipyridine, cat. TEMPO, $O_2$ (1 atm), $MeCN/H_2O$ (2:1), 94%; c) **10**, NaHMDS, THF, −78°C→RT, 57% (*E*/*Z* > 10:1); d) $Me_3SnOH$ (40 equiv), 1,2-dichloroethane, 80°C, 94%. TEMPO = 2,2,6,6-tetramethyl-1-piperidinoxyl (free radical), TES = triethylsilyl, PMB = *para*-methoxybenzyl.

Although both alcohol groups in **25** are allylic, the selective oxidation of the primary one was accomplished with the aid of a procedure co-catalyzed by copper and TEMPO, using $O_2$ as the ultimate oxidant.[23] The resulting aldehyde **26** was amenable to Julia–Kocienski olefination[10,24] with tetrazolylsulfone **10**, provided that this reagent was deprotonated with an excess of NaHMDS in the presence of the aldehyde ("Barbier conditions").

 © 2006 Wiley-VCH Verlag GmbH & Co. KGaA, Weinheim 

The success of this transformation attests to the maturity of the Kocienski methodology, especially if one considers that an unprotected OH group,[25] a carbamate, and potentially acidic C–H sites are present in the reaction partners. The desired alkene **27**, which represents the C1–C28 carbon backbone of **2** in a fully functional form, was obtained in a reproducible yield of 57% with excellent selectivity for the required *E* isomer ($E/Z > 10{:}1$, NMR).

At this stage, iejimalide B seemed to be just a few standard manipulations away; the most important lessons, however, had yet to be learned. First, attempted conversion of ester **27** into the required seco acid **28** turned out to be very difficult. While saponification of the north segment **9**, naively considered as a valid model, worked as expected (Scheme 6),

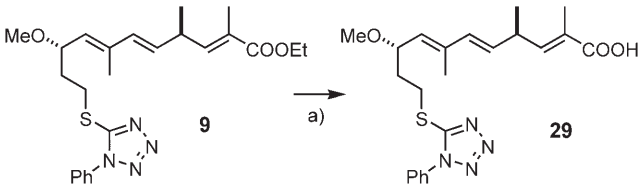


***Scheme 6.*** a) aq LiOH (1 M), THF/MeOH (1:1), RT, 91%.

attempted saponification of **27** compromised the seemingly remote C18–C23 region of the molecule without touching the ester function at all; other standard conditions were equally unsuitable. Only the procedure recently outlined by Nicolaou et al. afforded the desired product **28**,[26,27] although a large excess of $Me_3SnOH$ and prolonged ($\geq 5$ days) heating were necessary to obtain satisfactory results.

Prior to subjecting this valuable material to macrocyclization, the arsenal of feasible methods[8b] was validated in various model reactions. By far the best results over the entire series were obtained with the Yonemitsu variant of the Yamaguchi method.[8,28] The most advanced and instructive case is the successful esterification of the northern domain **29** with the elaborate south-eastern hemisphere **25b** (R = TBS), which afforded product **30** in a respectable 72% yield (Scheme 7).

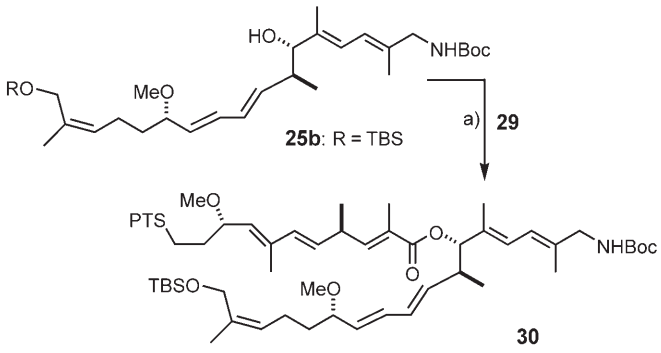


***Scheme 7.*** An intermolecular esterification serving as a model for the projected macrocyclization: a) 2,4,6-trichlorobenzoyl chloride, $Et_3N$, cat. DMAP, toluene, 72%. DMAP = 4-dimethylaminopyridine.

Despite this encouraging precedent, attempted lactonization of seco acid **28** failed to afford the desired macrocycle (Scheme 8). Rather, the C1–C6 unit of the substrate was

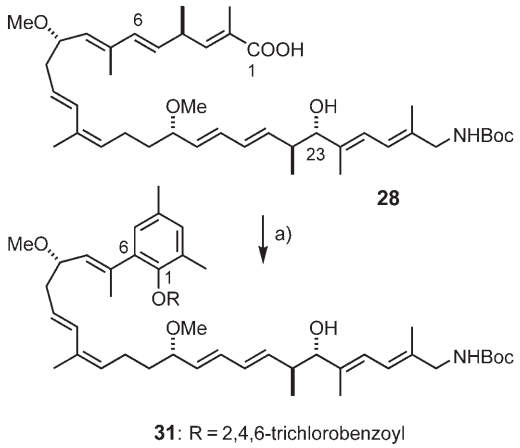


***Scheme 8.*** Attempted macrocyclization under Yamaguchi conditions: a) 1. 2,4,6-trichlorobenzoyl chloride, $Et_3N$, THF; 2. cat. DMAP, toluene, see text.

aromatized to a phenol ring, as shown by extensive 2D NMR spectroscopic investigations. The contrast between this outcome and the intermolecular esterification depicted in Scheme 7 is striking. Although phenol **31** was isolated in rather low yields (25–40%), it was the only distinct product that was reproducibly formed under the standard Yamaguchi, as well as the "one-pot" Yonemitsu conditions. Unaware of any precedent, we propose the mechanism depicted in Scheme 9 to explain this unusual result. Attack of the base (most likely DMAP)[29] on the α,β-unsaturated mixed anhydride **32** initially formed may outperform the attack by the hindered alcohol at C23. Collapse of the resulting intermediate **33** is thought to release ketene **34**, which eliminates the dimethylpyridinium moiety to give the polyunsaturated

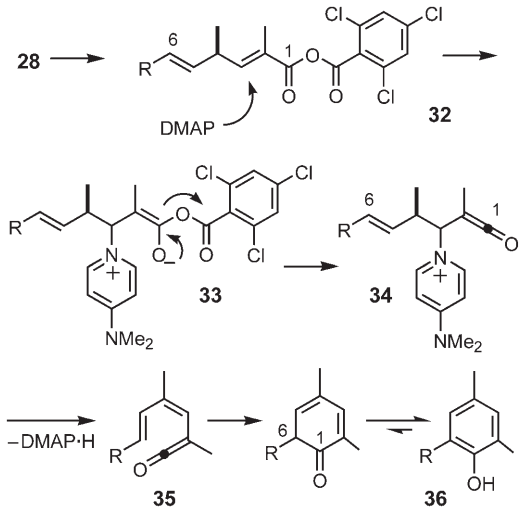


***Scheme 9.*** Proposed mechanism for the observed phenol formation under Yamaguchi conditions.

 © 2006 Wiley-VCH Verlag GmbH & Co. KGaA, Weinheim 

ketene **35**, which is set-up for a subsequent 6π-electrocyclization with formation of phenol **36**.[30] This compound is finally acylated to give the observed product **31**.

Despite considerable experimentation, this unfavorable reaction channel could not be avoided.[29] Gentle warming of the mixture with the hope of rendering the attack by the tethered alcohol competitive, only led to the rapid destruction of the starting material. Similarly, applications of other standard macrolactonization strategies[8b] failed.

At this point, we had to conclude that the lactone entity of **2** constitutes a highly vulnerable "Achilles heel" of this unusually sensitive marine natural product in a synthetic context. Even though the required seco acid **28** could be secured by a convergent approach involving one of the most advanced applications of the Julia–Kocienski olefination known to date,[10] our inability to lactonize the seco acid enforced a relaunch of the entire project. Since the crucial ester clearly must be installed intermolecularly, only a macrocyclization by C–C-bond formation can forge the 24-membered ring of **2**. Among the various conceivable options, ring-closing metathesis (RCM) ultimately proved viable,[31] even though application of this method may seem counter-intuitive in view of the necessity to activate a polyunsaturated and likely very fragile cyclization precursor by the catalyst in a strictly regio- and chemoselective fashion. The following Communication reports how this ambitious plan was achieved in practice, although success came only after experiencing yet another "Achilles heel" of the iejimalides that went undetected in the studies summarized above.[6]

Received: May 11, 2006
Published online: August 4, 2006

**Keywords:** Heck reaction · lactones · macrolides · olefination · total synthesis

[1] a) J. Kobayashi, J. Cheng, T. Ohta, H. Nakamura, S. Nozoe, Y. Hirata, Y. Ohizumi, T. Sasaki, *J. Org. Chem.* **1988**, *53*, 6147–6150; b) Y. Kikuchi, M. Ishibashi, T. Sasaki, J. Kobayashi, *Tetrahedron Lett.* **1991**, *32*, 797–798.

[2] a) K. Nozawa, M. Tsuda, H. Ishiyama, T. Sasaki, T. Tsuruo, J. Kobayashi, *Bioorg. Med. Chem.* **2006**, *14*, 1063–1067; b) M. Tsuda, K. Nozawa, K. Shimbo, H. Ishiyama, E. Fukushi, J. Kawabata, J. Kobayashi, *Tetrahedron Lett.* **2003**, *44*, 1395–1399.

[3] The activity data are available from the NCI homepage (http://www.dtp.nci.nih.gov/docs/dtp_search.html).

[4] Although the NCI data show no particular selectivity, a preliminary report from the Walther Cancer Research Center (http://www.nd.edu/≈science/documents/waltherbrochure.pdf) claims spectacular effects against colon cancer and stunning morphological changes upon injection of iejimalides into solid tumors.

[5] For a related endeavor see: A. Fürstner, D. Kirk, M. D. B. Fenster, C. Aïssa, D. De Souza, O. Müller, *Proc. Natl. Acad. Sci. USA* **2005**, *102*, 8103–8108.

[6] A. Fürstner, C. Nevado, M. Tremblay, C. Chevrier, F. Teplý, C. Aïssa, M. Waser, *Angew. Chem.* **2006**, *118*, 5969–5974; *Angew. Chem. Int. Ed.* **2006**, *45*, 5837–5842.

[7] For fragment syntheses see: a) M. Cottard, N. Kann, T. Rein, B. Åkermark, P. Helquist, *Tetrahedron Lett.* **1995**, *36*, 3115–3118; b) M. T. Mendlik, M. Cottard, T. Rein, P. Helquist, *Tetrahedron Lett.* **1997**, *38*, 6375–6378; c) T. M. Pedersen, E. L. Hansen, J. Kane, T. Rein, P. Helquist, P.-O. Norrby, D. Tanner, *J. Am. Chem. Soc.* **2001**, *123*, 9738–9742.

[8] a) J. Inanaga, K. Hirata, H. Saeki, T. Katsuki, M. Yamaguchi, *Bull. Chem. Soc. Jpn.* **1979**, *52*, 1989–1993; b) review: A. Parenty, X. Moreau, J.-M. Campagne, *Chem. Rev.* **2006**, *106*, 911–939.

[9] For advanced applications from our research group see: a) O. Lepage, E. Kattnig, A. Fürstner, *J. Am. Chem. Soc.* **2004**, *126*, 15970–15971; b) J. Mlynarski, J. Ruiz-Caro, A. Fürstner, *Chem. Eur. J.* **2004**, *10*, 2214–2222.

[10] Review: P. R. Blakemore, *J. Chem. Soc. Perkin Trans. 1* **2002**, 2563–2585.

[11] a) A. Fürstner, M. Albert, J. Mlynarski, M. Matheu, E. DeClercq, *J. Am. Chem. Soc.* **2003**, *125*, 13132–13142; b) A. Fürstner, J. Mlynarski, M. Albert, *J. Am. Chem. Soc.* **2002**, *124*, 10274–10275; c) A. Fürstner, F. Feyen, H. Prinz, H. Waldmann, *Tetrahedron* **2004**, *60*, 9543–9558.

[12] K. C. Nicolaou, P. G. Bulger, D. Sarlah, *Angew. Chem.* **2005**, *117*, 4516–4563; *Angew. Chem. Int. Ed.* **2005**, *44*, 4442–4489.

[13] For details see the Supporting Information.

[14] S. Bräse, A. de Meijere in *Metal-Catalyzed Cross-Coupling Reactions*, *Vol. 1* (Eds.: A. de Meijere, F. Diederich), Wiley-VCH, Weinheim, **2004**, pp. 217–315.

[15] H. C. Brown, K. S. Bhat, *J. Am. Chem. Soc.* **1986**, *108*, 293–294.

[16] a) K. Matsumura, S. Hashiguchi, T. Ikariya, R. Noyori, *J. Am. Chem. Soc.* **1997**, *119*, 8738–8739; b) R. Noyori, S. Hashiguchi, *Acc. Chem. Res.* **1997**, *30*, 97–102; c) for a recent application from this research group see: A. Fürstner, P. Hannen, *Chem. Eur. J.* **2006**, *12*, 3006–3019.

[17] R. Suzuki, H. Tsukuda, N. Watanabe, Y. Kuwatani, I. Ueda, *Tetrahedron* **1998**, *54*, 2477–2496.

[18] W. C. Still, C. Gennari, *Tetrahedron Lett.* **1983**, *24*, 4405–4408.

[19] S. J. Mickel, G. H. Sedelmeier, D. Niederer, F. Schuerch, M. Seger, K. Schreiner, R. Daeffler, A. Osmani, D. Bixel, O. Loiseleur, J. Cercus, H. Stettler, K. Schaer, R. Gamboni, A. Bach, G.-P. Chen, W. Chen, P. Geng, G. T. Lee, E. Loeser, J. McKenna, F. R. Kinder, Jr., K. Konigsberger, K. Prasad, T. M. Ramsey, N. Reel, O. Repiè, L. Rogers, W.-C. Shieh, R.-M. Wang, L. Waykole, S. Xue, G. Florence, I. Paterson, *Org. Process Res. Dev.* **2004**, *8*, 113–121.

[20] The use of TBAF and other fluoride sources scrambled the trisubstituted olefin of the enoate.

[21] D. W. Hart, J. Schwartz, *J. Am. Chem. Soc.* **1974**, *96*, 8115–8116.

[22] M. Kalesse, K. P. Chary, M. Quitschalle, A. Burzlaff, C. Kasper, T. Scheper, *Chem. Eur. J.* **2003**, *9*, 1129–1136.

[23] P. Gamez, I. W. C. E. Arends, R. A. Sheldon, J. Reedijk, *Adv. Synth. Catal.* **2004**, *346*, 805–811.

[24] P. R. Blakemore, W. J. Cole, P. J. Kocienski, A. Morley, *Synlett* **1998**, 26–28.

[25] Note that an alcohol might interfere with the Smiles rearrangement, which constitutes the crucial second step of the Kocienski variant of the Julia olefination, see. Ref. [24].

[26] K. C. Nicolaou, A. A. Estrada, M. Zak, S. H. Lee, B. S. Safina, *Angew. Chem.* **2005**, *117*, 1402–1406; *Angew. Chem. Int. Ed.* **2005**, *44*, 1378–1382.

[27] Attempts to form the macrocycle by intramolecular transesterification following a closely related method (cat. $Bu_2SnO$, toluene, reflux) were unsuccessful; compare: P. Baumhof, R. Mazitschek, A. Giannis, *Angew. Chem.* **2001**, *113*, 3784–3786; *Angew. Chem. Int. Ed.* **2001**, *40*, 3672–3674.

[28] M. Hikota, Y. Sakurai, K. Horita, O. Yonemitsu, *Tetrahedron Lett.* **1990**, *31*, 6367–6370.

[29] Attempts to suppress this pathway by replacement of DMAP with 2,6-di-*tert*-butylpyridine as a more bulky base were unsuccessful.

 © 2006 Wiley-VCH Verlag GmbH & Co. KGaA, Weinheim 

[30] Formation of phenols by electrocyclizations of polyunsaturated ketenes: a) M. J. Heileman, H. W. Moore, *Tetrahedron Lett.* **1998**, *39*, 3643 – 3646; b) W. F. Austin, Y. Zhang, R. L. Danheiser, *Org. Lett.* **2005**, *7*, 3905 – 3908.
[31] a) T. M. Trnka, R. H. Grubbs, *Acc. Chem. Res.* **2001**, *34*, 18 – 29; b) A. Fürstner, *Angew. Chem.* **2000**, *112*, 3140 – 3172; *Angew. Chem. Int. Ed.* **2000**, *39*, 3012 – 3043.

 © 2006 Wiley-VCH Verlag GmbH & Co. KGaA, Weinheim 

*Total Synthesis*

DOI: 10.1002/anie.200601860

# Total Synthesis of Iejimalide B**

*Alois Fürstner,* Cristina Nevado, Martin Tremblay, Carine Chevrier, Filip Teplý, Christophe Aïssa, and Mario Waser*

Recent disclosures of the potent cytotoxicity and in vivo anticancer activity of the iejimalides are expected to revitalize the interest in these polyene macrolides, which were reported by Kobayashi and co-workers as early as 1988.[1–3] Extracted in minute amounts from tunicates harvested off the south Japanese coast, the limited availability of these natural products constitutes the prime obstacle for more detailed preclinical investigations. Intrigued by the prospect of contributing to an in-depth evaluation and challenged by the notably fragile structures of these polyunsaturated compounds, we embarked on a synthesis-driven investigation at the chemistry/biology interface. As the initial step of this endeavor, we now present the first total synthesis of iejimalide B (**1**), the most active member of this family.

This project would not have been successful without the intelligence gathered in a parallel approach in which a macrolactonization was envisaged for the formation of the 24-membered ring.[4] This key step, however, failed to afford the desired lactone but engaged the seco acid (**A**, Scheme 1) in a previously unknown aromatization process. Therefore, we concluded that the ester bond in **1** should be formed intermolecularly and hence the macrocyclization must occur at a C–C bond. Although counterintuitive at first sight, we opted for metathesis,[5] not least because of our excellent experiences with this catalytic transformation in a variety of complex settings.[6]

Nonetheless, this strategic decision bore considerable risk because application of RCM to the present case demands for no less than the selective activation of two out of ten double bonds in the cyclization precursor **B** (Scheme 1).[7] Moreover,

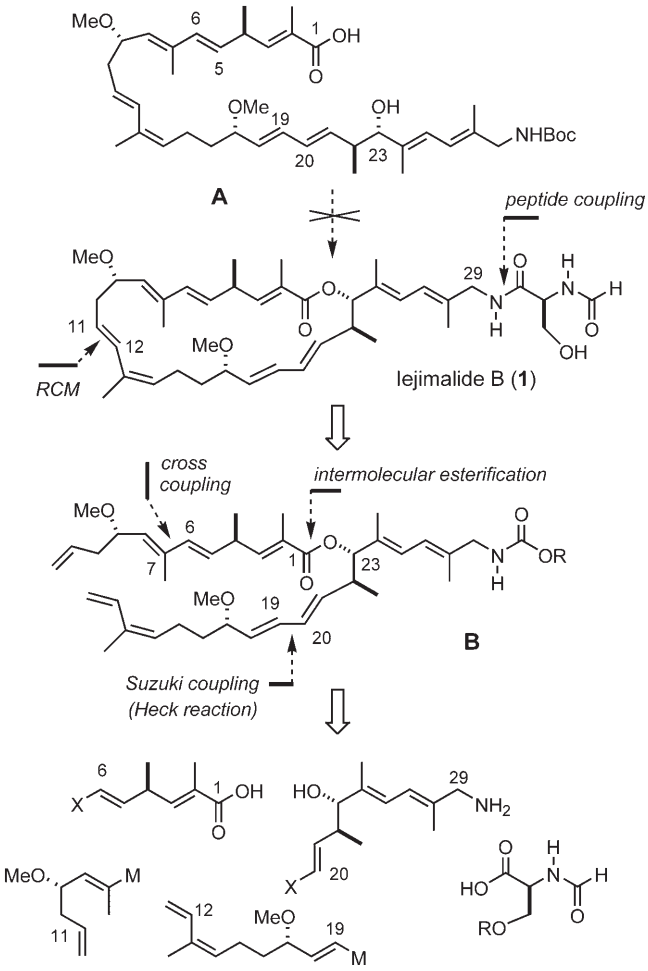


***Scheme 1.*** Refined retrosynthetic analysis of iejimalide B. RCM = ring-closing metathesis, Boc = *tert*-butyloxycarbonyl.

conjugated dienes in general are known to be problematic substrates for metathesis. It is well precedented that Grubbs-type catalysts may attack either double bond; in a cyclization process, this lack of regioselectivity engenders problems with ring contraction, not to mention the still missing control over the stereochemical outcome of the reaction.[7,8] With this analysis and the known influence of chelating groups on the effectiveness of RCM in mind,[9] the C11–C12 double bond in **1** seemed to be the only promising site for an RCM-based macrocyclization approach.

Although the assembly of the required precursor **B** could certainly be achieved merely by adapting the route leading to the seco acid **A**,[4] we took the relaunch of the project as an

[*] Prof. A. Fürstner, Dr. C. Nevado, Dr. M. Tremblay, Dr. C. Chevrier, Dr. F. Teplý, Dr. C. Aïssa, Dr. M. Waser
Max-Planck-Institut für Kohlenforschung
45470 Mülheim/Ruhr (Germany)
Fax: (+49) 208-306-2994
E-mail: fuerstner@mpi-muelheim.mpg.de

[**] Generous financial support from the MPG, the Fonds der Chemischen Industrie, the Alexander-von-Humboldt Foundation (fellowship to C.N.), the NSERC Canada (fellowship to M.T.), and the Austrian Fonds zur Förderung der Wissenschaftlichen Forschung (fellowship to M.W.) is gratefully acknowledged. We thank Dr. R. Mynott, B. Gabor, and C. Wirtz for their invaluable help with the structure assignment of several key compounds, and R. Leichtweiß for HPLC assistance.

 © 2006 Wiley-VCH Verlag GmbH & Co. KGaA, Weinheim 

opportunity to address some of the encountered shortcomings. Highest priority on our agenda was given to the fragment coupling at C19-C20 by a Heck reaction, which afforded only 46% yield of the product and required a tedious chromatographic purification. Therefore we opted for a Suzuki coupling as an alternative, which is known to be highly effective even in demanding cases.[10] Likewise, the entire assembly process might be streamlined if the stereo-unselective Julia olefination forging the C5–C6 alkene in **A** could be replaced by a stereochemically unambiguous step; again, a palladium-catalyzed cross coupling at the adjacent C6–C7 bond might qualify for this purpose.

The implementation of this refined analysis started with the readily available ester **2**,[4] which was converted by a sequence of routine operations into diene **4** (Scheme 2).

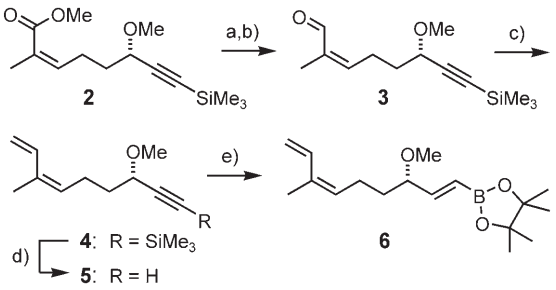


***Scheme 2.*** a) DIBAL-H, $CH_2Cl_2$, −78 °C; b) $MnO_2$, $CH_2Cl_2$, 96% (over two steps); c) $Ph_3PCH_3Br$, *n*BuLi, THF, −78 °C→RT, quant.; d) $K_2CO_3$, MeOH, 83%; e) pinacolborane, 9-BBN (10 mol%), THF, 45 °C, 56%. DIBAL-H = diisobutylaluminum hydride, 9-BBN = 9-borabicyclo-[3.3.1]nonane.

Subsequent cleavage of the silyl group afforded the terminal alkyne **5** (>97% *ee*), which underwent a chemoselective hydroboration with pinacolborane without damaging the tethered 1,3-diene entity, provided that catalytic amounts of 9-BBN were added to the reaction mixture.[11]

A suitable coupling partner for this Suzuki donor was prepared by a palladium-catalyzed, $Et_2Zn$-mediated addition of the enantiopure propargyl mesylate **8**[12] to aldehyde **7** (Scheme 3).[4] The best *anti* selectivity was obtained with **8a**, which bears a triisopropylsilyl (TIPS) group at the acetylene moiety (7.5:1 d.r.), whereas the use of the terminal alkyne **8b** ($R^1 = H$) was less satisfactory (3.5:1 d.r.). After chromatographic purification, the major isomer **9** was obtained in 72% yield. Subsequent cleavage of the silyl group gave **10** which was temporarily protected as the corresponding pivalate **11**. Hydrozirconation/iodination[13] followed by the chemoselective cleavage of the pivalate with DIBAL-H readily afforded the required alkenyl iodide **13**.

At this juncture, we were facing the challenge to join fragments **6** and **13** by a Suzuki coupling.[10] Having previously experienced the sensitivity of advanced iejimalide subunits towards basic conditions,[4] much care was taken to optimize the reaction conditions. Following a lead from the recent literature in which $Ba(OH)_2{\cdot}8H_2O$ was shown to be a particularly suitable promoter for the formation of products embodying fragile diene units,[14] these conditions were

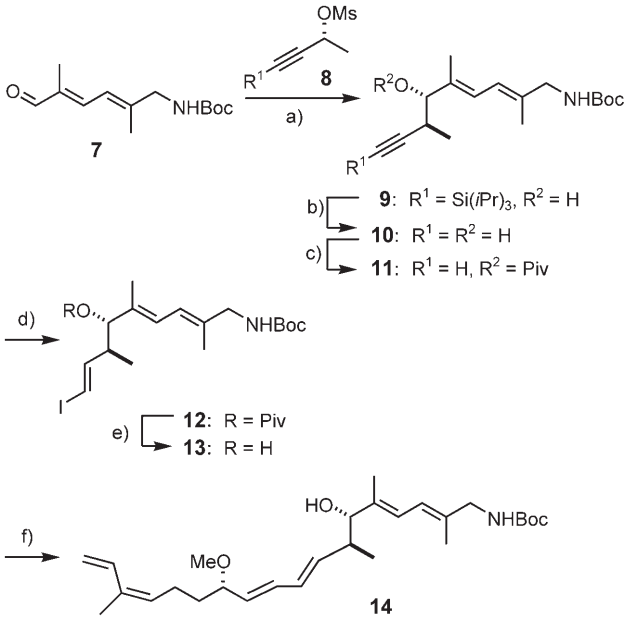


***Scheme 3.*** a) $[Pd(OAc)_2]$ (5 mol%), $PPh_3$ (5 mol%), $Et_2Zn$ (3 equiv), THF, −78 °C→−20 °C, 72%; b) TBAF, THF, 94%; c) pivaloyl chloride, pyridine, 0 °C→RT, 76%; d) $[Cp_2Zr(H)Cl]$, THF, then $I_2$, 0 °C→RT, 85%; e) DIBAL-H, $CH_2Cl_2$, −78 °C, 87%; f) boronate **6**, $[PdCl_2(dppf)]$ (15 mol%), $Ba(OH)_2{\cdot}8H_2O$ (1.2 equiv), DMF, 40 °C, 70%. Ms = methanesulfonyl, TBAF = tetra-*n*-butylammonium fluoride, Piv = pivaloyl, dppf = 1,1′-bis(diphenylphosphanyl)ferrocene.

adapted to the present case and found to be highly suitable. In fact, the amount of base could be reduced to 1.2 equivalents and the reaction was found to proceed at, or slightly above, room temperature at acceptable rates. Product **14**, as a suitably functionalized surrogate of the entire south-eastern domain of **1**, was thus obtained in 70% yield.

The revised approach to the northern segment of iejimalide B (Scheme 4) commenced with commercial lactone **15**, which was converted on a large scale into alkyne **17** by three

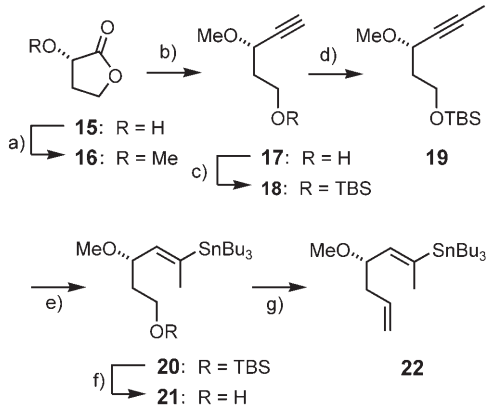


***Scheme 4.*** a) MeI, $Ag_2O$, MeCN, 92%; b) 1. DIBAL-H, $CH_2Cl_2$, −78 °C; 2. $MeOC(=N_2)P(O)(OMe)_2$, $K_2CO_3$, MeOH, 70% (over two steps); c) TBSCl, $Et_3N$, cat. DMAP, $CH_2Cl_2$, 90%; d) *n*BuLi, MeI, THF, 98%; e) $Bu_3SnH$, $[PdCl_2(PPh_3)_2]$ (5 mol%), THF, 65%; f) TBAF, THF, 93%; g) 1. Dess–Martin periodinane, $CH_2Cl_2$, 84%; 2. $[Ph_3P{=}CH_2]$, THF, −78 °C→RT, 93%. DMAP = 4-dimethylaminopyridine.

 © 2006 Wiley-VCH Verlag GmbH & Co. KGaA, Weinheim 

routine operations. Subsequent O-silylation and end-capping of the alkyne unit with a methyl group set the stage for a palladium-catalyzed hydrostannation which afforded product **20** in 65% yield.[15] Conventional management of protecting groups and oxidation states, followed by a Wittig reaction, finally delivered compound **22** in pure form.

Reduction of the Roche ester derivative **23** with DIBAL-H and chain extension with the functionalized phosphonate **24**[16] gave enol silane **25** as a single isomer (Scheme 5). This

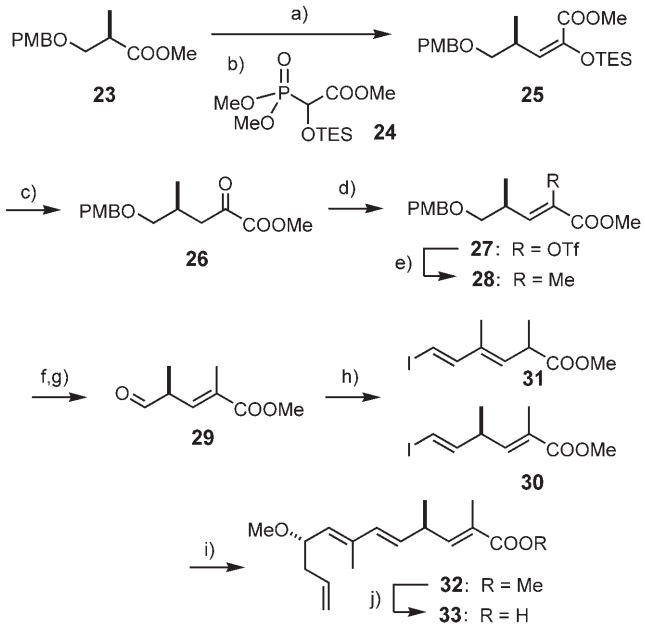


***Scheme 5.*** a) DIBAL-H, $CH_2Cl_2$, −78 °C; b) **24**, LiHMDS, THF, −78 °C→−40 °C, 75% (over both steps); c) aq HCl, THF, 91%; d) *N*-(5-chloro-2-pyridyl)-bis(trifluoromethansulfonimide), KHMDS, THF, −78 °C→−40 °C, 65%; e) MeZnCl, $[Pd(PPh_3)_4]$ (5 mol%), THF, 50 °C, 91%; f) DDQ, $CH_2Cl_2/H_2O$, 91%; g) Dess–Martin periodinane, $CH_2Cl_2$; h) $CHI_3$, $CrCl_2$, THF/1,4-dioxane (1:6), 62% (over two steps); i) stannane **22**, $[Pd(PPh_3)_4]$ (5 mol%), CuTC, $Ph_2PO_2NBu_4$, DMF, RT, 82%; j) aq LiOH, THF/MeOH, 87%. HMDS = 1,1,1,3,3,3-hexamethyldisilazane, TES = triethylsilyl, PMB = *p*-methoxybenzyl, DDQ = 2,3-dichloro-5,6-dicyano-1,4-benzoquinone, Tf = triflate.

compound afforded the corresponding enol triflate **27** of opposite double-bond configuration by acid-catalyzed hydrolysis, followed by treatment of **26** with Comins reagent[17] in the presence of KHMDS as the optimal base. Triflate **27** could be cross-coupled with MeZnCl in the presence of catalytic amounts of $[Pd(PPh_3)_4]$.[18,19] The PMB ether in the resulting enoate **28** was cleaved with DDQ and the liberated alcohol was oxidized to the corresponding aldehyde **29**, which underwent a Takai olefination[20] to give the desired alkenyl iodide **30** and its double bond isomer **31**.[21] Since these compounds could not be separated, the mixture was subjected to Stille cross-coupling[22] with stannane **22**. This transformation required careful optimization but proceeded nicely under notably mild conditions in the presence of $[Pd(PPh_3)_4]$, copper-2-thiophenecarboxylate (CuTC), and $Ph_2PO_2NBu_4$ in DMF.[23] Since the by-product derived from the cross-coupling of the isomeric iodide **31** could be easily removed after saponification of the ester group, a productive entry into the required acid **33** was secured.

With all the necessary components in hand, the stage was set to probe the envisaged end game of the synthesis. In line with our previous experiences,[4] the intermolecular esterification of **14** and **33** could be effected under Yonemitsu conditions (Scheme 6).[24] We were delighted to see that the

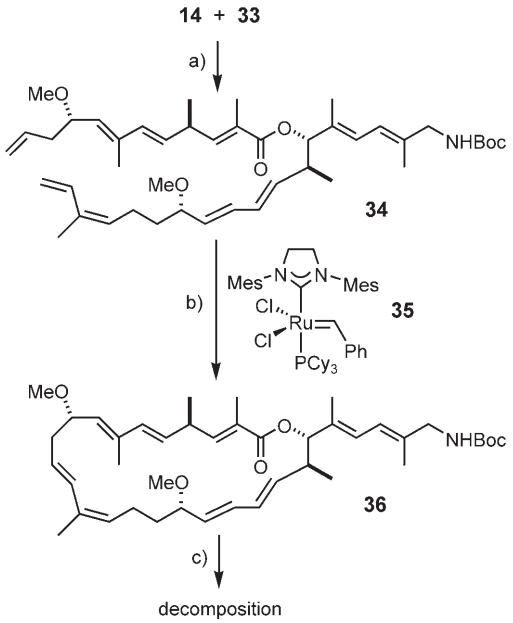


***Scheme 6.*** a) 2,4,6-trichlorobenzoyl chloride, $Et_3N$, cat. DMAP, toluene, 73%; b) complex **35**, (2×10 mol%), $CH_2Cl_2$, RT, 2 d, 96%; c) TMSOTf, 2,6-lutidine, $CH_2Cl_2$, 0 °C, see text for further details. TMS = trimethylsilyl, Cy = cyclohexyl, Mes = mesityl.

projected ring closure of the polyunsaturated compound **34** with the aid of the "second generation" ruthenium alkenylidene complex **35**[25] gave the desired macrocycle in almost quantitative yield as the required *E* isomer only.

With this gratifying result, the completion of the total synthesis of iejimalide B seemed to be just a matter of two routine operations, that is, cleavage of the Boc group followed by attachment of the serine residue. However, our hopes were dashed by the inability to remove the *N*-Boc group of **36** under a variety of experimental conditions. Even the use of TMSOTf buffered with 2,6-lutidine, reported to be a particularly mild method,[26] failed completely and decomposed the valuable product virtually instantaneously.

Although the degradation pathway of **36** remains unknown, model experiments explain, at least in part, this unexpected behavior (Scheme 7). Thus, treatment of **37a**,**b** (R = Ac and tigelate respectively) with TBSOTf/2,6-lutidine converted these compounds into a common product **40**. It is believed that the conjugated diene efficiently communicates activation of the Boc moiety by the Lewis acid to the remote substituent residing at C23. Rearrangement of the π system extrudes the ester and engenders formation of the heterocyclic motif.

 © 2006 Wiley-VCH Verlag GmbH & Co. KGaA, Weinheim 

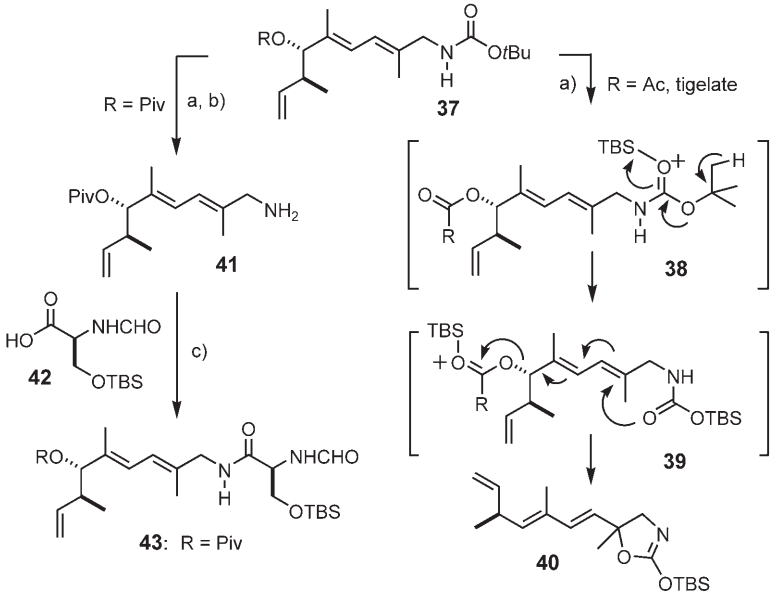


***Scheme 7.*** a) TBSOTf, 2,6-lutidine, $CH_2Cl_2$, 40 °C, 91 % (R = Ac, 1:1 d.r.); 85 % (R = −C(O)C(Me)=CHMe); b) HOAc, THF, 50 °C; c) compound **42**, EDC, HOBt, NMM, $CH_2Cl_2$, 0 °C → RT, 95 % (over steps (a)–(c)). EDC = 3-(3-dimethylaminopropyl)-1-ethylcarbodiimide, HOBT = 1-hydroxy-1*H*-benzotriazole, NMM = *N*-methylmorpholine.

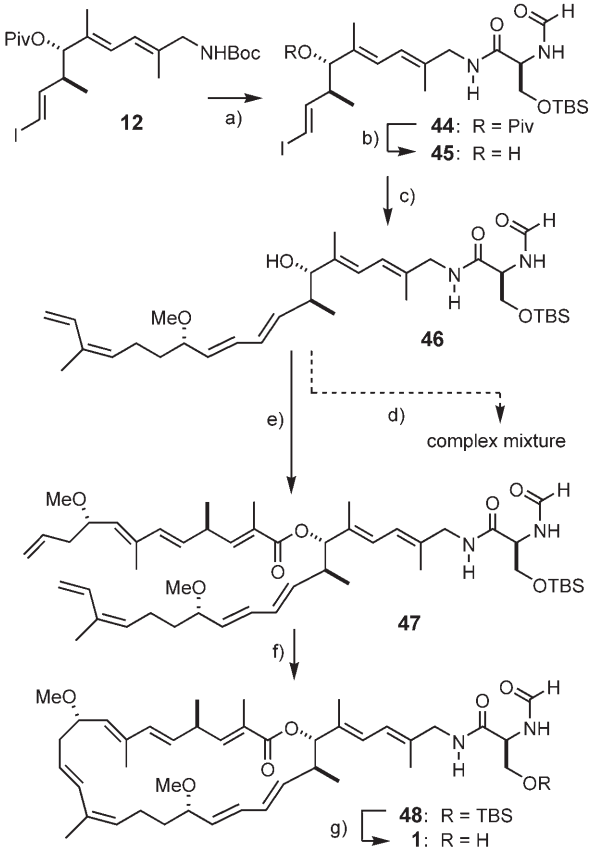


***Scheme 8.*** a) 1. TMSOTf, 2,6-lutidine, $CH_2Cl_2$, then CsF, 0 °C; 2. **42**, EDC, HOBt, NMM, $CH_2Cl_2$, 85 % (over two steps); b) $LiBEt_3H$, THF, 0 °C, 70 %; c) boronate **6**, [$PdCl_2$(dppf)] (15 mol %), $Ba(OH)_2 \cdot 8H_2O$ (1.2 equiv), DMF, RT, 70 %; d) 2,4,6-trichlorobenzoyl chloride, $Et_3N$, cat. DMAP, toluene; e) **33**, DCC, 4-pyrrolidinylpyridine (30 mol %), $CH_2Cl_2$, 0 °C → RT, 84 %; f) complex **35** (15 mol %), $CH_2Cl_2$ ($5 \times 10^{-3}$ M), RT, 69 %; g) TBAF, THF, 0 °C, 80 %. DCC = *N*,*N*′-dicyclohexylcarbodiimide.

The subtleties in the behavior of iejimalide and the limited analogy between seemingly closely related cases previously encountered on several occasions,[4] re-appeared in this series. Thus, in striking contrast to acetate **37a**, the corresponding pivalate **37c** (R = Piv) allowed for the clean removal of the Boc substituent under otherwise identical conditions; the bulky ester most likely forces **37c** to adopt a conformation in which orbital overlap between the C–O bond and the π system of the diene is minimized, thus blocking the decomposition pathway. The resulting amine **41** was coupled to the L-serine derivative **42**[27] to give product **43** in excellent overall yield.

This dichotomy in the reactivity pattern enforced a final adjustment of our synthetic plan. The crucial role of the protecting group on the lateral amine invalidated the original idea to introduce the peptide moiety last. Since the preparation of **43** provided a way to attach this entity to a readily accessible and validated segment, it was decided to repeat the assembly process with the L-serine already in place, even though the presence of yet another labile structural motif was daunting.

In fact, the method for the introduction of the serine moiety could be translated from the model compound **37c** to alkenyl iodide **12**; the pivalate in the resulting compound **44** was removed with the aid of $LiBEt_3H$ without affecting the formamide entity (Scheme 8). The previous careful optimization of the Suzuki reaction also paid off, since the use of $Ba(OH)_2 \cdot 8H_2O$ allowed for the coupling of **45** and boronate **6** at ambient temperature, which was absolutely crucial for the success of this particular transformation.[28] Although the Yonemitsu method had worked well in several advanced models,[4] most notably in the closely related case depicted in Scheme 6, the seemingly remote serine terminus clearly interfered and did not allow for proper esterification of acid **33** and alcohol **46**; only small amounts (≤ 20 %) of product **47** were formed at 20 °C,[29] while even a moderate increase of the temperature to 35–45 °C destroyed the compound. Gratifyingly, however, the use of DCC/4-pyrrolidinylpyridine worked exceptionally well in this case, and gave ester **47** in 84 % yield.

Cyclization of this polyene with the aid of the ruthenium catalyst **35**[25] delivered the 24-membered macrocycle **48** in 69 % yield as a single *E* isomer. In view of the exceptional thermal lability of the iejimalide precursors in the Suzuki and the esterification steps, it was instrumental that this key operation proceeded at ambient temperature. The outcome of the reaction is truly remarkable if interpreted in light of the implicit selectivity and stability issues. Although the strategic advantages of RCM have been illustrated many times and need no further confirmation,[5,6] we believe that this specific case is particularly instructive, and highlights the superb application profile of Grubbs-type catalysts in general. The first total synthesis of iejimalide B was then completed by cleavage of the remaining TBS ether from the serine residue in **48**. The analytical and spectroscopic data of the synthetic

 © 2006 Wiley-VCH Verlag GmbH & Co. KGaA, Weinheim 

samples of **1** matched those of the natural product in every detail.[1,2]

In summary, a synthetic route to the potent cytotoxic macrolide iejimalide B (**1**) has been established which provides this valuable marine natural product in sufficient quantity for further testing. As evident from this and the preceding Communication,[4] the development of the successful route required several rounds of adjustment and fine tuning. This struggle largely originated from the exceptionally low level of homology in the behavior of seemingly closely related compounds that differed only in remote and ostensibly innocent substituents. The gathered intelligence, however, should provide a sound basis for the next round of exploration of this promising lead structure. We are currently extending our studies to the other members of this family and translating the acquired knowledge to the design of potential analogues with optimized application profiles.

Received: May 11, 2006
Published online: July 28, 2006

**Keywords:** anticancer agents · cross-coupling · macrolides · metathesis · natural products

[1] a) K. Nozawa, M. Tsuda, H. Ishiyama, T. Sasaki, T. Tsuruo, J. Kobayashi, *Bioorg. Med. Chem.* **2006**, *14*, 1063 – 1067; b) the cytotoxicity data are available from the NCI homepage (http://www.dtp.nci.nih.gov/docs/dtp search.html).

[2] a) J. Kobayashi, J. Cheng, T. Ohta, H. Nakamura, S. Nozoe, Y. Hirata, Y. Ohizumi, T. Sasaki, *J. Org. Chem.* **1988**, *53*, 6147 – 6150; b) Y. Kikuchi, M. Ishibashi, T. Sasaki, J. Kobayashi, *Tetrahedron Lett.* **1991**, *32*, 797 – 798; c) M. Tsuda, K. Nozawa, K. Shimbo, H. Ishiyama, E. Fukushi, J. Kawabata, J. Kobayashi, *Tetrahedron Lett.* **2003**, *44*, 1395 – 1399.

[3] For previous synthetic efforts see: a) M. Cottard, N. Kann, T. Rein, B. Åkermark, P. Helquist, *Tetrahedron Lett.* **1995**, *36*, 3115 – 3118; b) M. T. Mendlik, M. Cottard, T. Rein, P. Helquist, *Tetrahedron Lett.* **1997**, *38*, 6375 – 6378; c) T. M. Pedersen, E. L. Hansen, J. Kane, T. Rein, P. Helquist, P.-O. Norrby, D. Tanner, *J. Am. Chem. Soc.* **2001**, *123*, 9738 – 9742.

[4] A. Fürstner, C. Aïssa, C. Chevrier, F. Teplý, C. Nevado, M. Tremblay, *Angew. Chem.* **2006**, *118*, 5964 – 5969; *Angew. Chem. Int. Ed.* **2006**, *45*, 5832 – 5837.

[5] a) T. M. Trnka, R. H. Grubbs, *Acc. Chem. Res.* **2001**, *34*, 18 – 29; b) A. Fürstner, *Angew. Chem.* **2000**, *112*, 3140 – 3172; *Angew. Chem. Int. Ed.* **2000**, *39*, 3012 – 3043; c) R. R. Schrock, A. H. Hoveyda, *Angew. Chem.* **2003**, *115*, 4740 – 4782; *Angew. Chem. Int. Ed.* **2003**, *42*, 4592 – 4633; d) A. Deiters, S. F. Martin, *Chem. Rev.* **2004**, *104*, 2199 – 2238; e) K. C. Nicolaou, P. G. Bulger, D. Sarlah, *Angew. Chem.* **2005**, *117*, 4564 – 4601; *Angew. Chem. Int. Ed.* **2005**, *44*, 4490 – 4527; f) M. Schuster, B. Blechert, *Angew. Chem.* **1997**, *109*, 2124 – 2144; *Angew. Chem. Int. Ed. Engl.* **1997**, *36*, 2036 – 2056.

[6] Selected examples: a) C. Aïssa, R. Riveiros, J. Ragot, A. Fürstner, *J. Am. Chem. Soc.* **2003**, *125*, 15512 – 15520; b) A. Fürstner, F. Jeanjean, P. Razon, C. Wirtz, R. Mynott, *Chem. Eur. J.* **2003**, *9*, 320 – 326; c) A. Fürstner, K. Radkowski, C. Wirtz, R. Goddard, C. W. Lehmann, R. Mynott, *J. Am. Chem. Soc.* **2002**, *124*, 7061 – 7069; d) A. Fürstner, T. Dierkes, O. R. Thiel, G. Blanda, *Chem. Eur. J.* **2001**, *7*, 5286 – 5298; e) A. Fürstner, T. Müller, *J. Am. Chem. Soc.* **1999**, *121*, 7814 – 7821; f) B. Scheiper, F. Glorius, A. Leitner, A. Fürstner, *Proc. Natl. Acad. Sci. USA* **2004**, *101*, 11960 – 11965; g) A. Fürstner, C. Müller, *Chem. Commun.* **2005**, 5583 – 5585.

[7] For a pertinent example of an attempted RCM prohibited by intervention of a 1,3-diene unit see: a) A. K. Ghosh, G. Gong, *J. Org. Chem.* **2006**, *71*, 1085 – 1093. For recent total syntheses involving metathesis in the presence of 1,3-dienes that remain untouched see: b) T. Yoshimura, F. Yakushiji, S. Kondo, X. Wu, M. Shindo, K. Shishido, *Org. Lett.* **2006**, *8*, 475 – 478; c) B. Wu, Q. Liu, G. A. Sulikowski, *Angew. Chem.* **2004**, *116*, 6841 – 6843; *Angew. Chem. Int. Ed.* **2004**, *43*, 6673 – 6675; d) D. J. Kerr, A. C. Willis, B. L. Flynn, *Org. Lett.* **2004**, *6*, 457 – 460; e) R. E. Maleczka, Jr., L. R. Terrell, F. Geng, J. S. Ward, *Org. Lett.* **2002**, *4*, 2841 – 2844.

[8] a) For a particularly instructive case see: K. Biswas, H. Lin, J. T. Njardarson, M. D. Chappell, T.-C. Chou, Y. Guan, W. P. Tong, L. He, S. B. Horwitz, S. J. Danishefsky, *J. Am. Chem. Soc.* **2002**, *124*, 9825 – 9832; b) a discussion and a comprehensive literature coverage of metathetic diene–ene cyclizations is found in: F. Lacombe, K. Radkowski, G. Seidel, A. Fürstner, *Tetrahedron* **2004**, *60*, 7315 – 7324.

[9] a) A. Fürstner, K. Langemann, *J. Org. Chem.* **1996**, *61*, 3942 – 3943; b) A. Fürstner, K. Langemann, *Synthesis* **1997**, 792 – 803; c) A. Fürstner, K. Langemann, *J. Am. Chem. Soc.* **1997**, *119*, 9130 – 9136.

[10] A. Suzuki, *J. Organomet. Chem.* **1999**, *576*, 147 – 168.

[11] a) A. Arase, H. Hoshi, A. Mijin, K. Nishi, *Synth. Commun.* **1995**, *25*, 1957 – 1962; b) K. C. Nicolaou, K. C. Fylaktakidou, H. Monenschein, Y. Li, B. Weyershausen, H. J. Mitchell, H. Wei, P. Guntupalli, D. Hepworth, K. Sugita, *J. Am. Chem. Soc.* **2003**, *125*, 15433 – 15442.

[12] a) J. A. Marshall, *Chem. Rev.* **2000**, *100*, 3163 – 3185; b) J. A. Marshall, N. D. Adams, *J. Org. Chem.* **1999**, *64*, 5201 – 5204; c) recent application: O. Lepage, E. Kattnig, A. Fürstner, *J. Am. Chem. Soc.* **2004**, *126*, 15970 – 15971.

[13] D. W. Hart, J. Schwartz, *J. Am. Chem. Soc.* **1974**, *96*, 8115 – 8116.

[14] A. Gopalarathnam, S. G. Nelson, *Org. Lett.* **2006**, *8*, 7 – 10.

[15] Small amounts (10–15%) of the regioisomeric alkenylstannane could be separated by flash chromatography. The corresponding pinacolborane was also prepared but failed to undergo productive cross-coupling with iodide **30**.

[16] a) S. M. Ceccarelli, U. Piarulli, J. Tesler, C. Gennari, *Tetrahedron Lett.* **2001**, *42*, 7421 – 7425; b) D. Horne, J. Gaudino, W. J. Thompson, *Tetrahedron Lett.* **1984**, *25*, 3529 – 3532.

[17] D. L. Comins, A. Dehghani, *Tetrahedron Lett.* **1992**, *33*, 6299 – 6302.

[18] E. Negishi, X. Zheng, Z. Tan, M. Qian, Q. Hu, Z. Huang in *Metal-Catalyzed Cross-Coupling Reactions*, *Vol. 2*, 2nd ed. (Eds.: A. de Meijere, F. Diederich), Wiley-VCH, Weinheim, **2004**, pp. 815 – 889.

[19] This route to **27** was chosen for two reasons: first, problems with partial racemization were encountered when the aldehyde derived from **23** was treated with Wittig reagents in an attempt to form **28** directly; secondly, it is known that iejimalide B bearing a methyl group at C2 is more active than iejimalide A which features a proton at this position, see Ref. [2]; the chosen route via triflate **27** allows for systematic variations at this position.

[20] a) K. Takai, K. Nitta, K. Utimoto, *J. Am. Chem. Soc.* **1986**, *108*, 7408 – 7410; b) D. A. Evans, W. C. Black, *J. Am. Chem. Soc.* **1993**, *115*, 4497 – 4513; c) review: A. Fürstner, *Chem. Rev.* **1999**, *99*, 991 – 1045.

[21] Worried that reversible double-bond isomerizations at the aldehyde stage or an equilibrium between **30** and **31** would racemize the chiral center at C4, the *ee* value of compound **30** was carefully checked and found to be $\geq 90\%$.

[22] P. Espinet, A. M. Echavarren, *Angew. Chem.* **2004**, *116*, 4808 – 4839; *Angew. Chem. Int. Ed.* **2004**, *43*, 4704 – 4734.

 © 2006 Wiley-VCH Verlag GmbH & Co. KGaA, Weinheim 

[23] a) H. Fuwa, N. Kainuma, K. Tachibana, M. Sasaki, *J. Am. Chem. Soc.* **2002**, *124*, 14983 – 14992; b) for the use of CuTC in Pd-free Stille reactions see: G. D. Allred, L. S. Liebeskind, *J. Am. Chem. Soc.* **1996**, *118*, 2748 – 2749; c) T. B. Durham, N. Blanchard, B. M. Savall, N. A. Powell, W. R. Roush, *J. Am. Chem. Soc.* **2004**, *126*, 9307 – 9317.
[24] M. Hikota, Y. Sakurai, K. Horita, O. Yonemitsu, *Tetrahedron Lett.* **1990**, *31*, 6367 – 6370.
[25] a) M. Scholl, S. Ding, C. W. Lee, R. H. Grubbs, *Org. Lett.* **1999**, *1*, 953 – 956; b) see also: J. Huang, E. D. Stevens, S. P. Nolan, J. L. Pedersen, *J. Am. Chem. Soc.* **1999**, *121*, 2674 – 2678; c) L. Ackermann, A. Fürstner, T. Weskamp, F. J. Kohl, W. A. Herrmann, *Tetrahedron Lett.* **1999**, *40*, 4787 – 4790.
[26] a) M. Sakaitani, Y. Ohfune, *J. Org. Chem.* **1990**, *55*, 870 – 876; b) M. Nazaré, H. Waldmann, *Chem. Eur. J.* **2001**, *7*, 3363 – 3376; c) B. M. Trost, D. R. Fandrick, *Org. Lett.* **2005**, *7*, 823 – 826.
[27] D. R. Hill, C.-N. Hsiao, R. Kurukulasuriya, S. J. Wittenberger, *Org. Lett.* **2002**, *4*, 111 – 113.
[28] Uncontrolled isomerizations were observed even at 35 °C.
[29] Significant amounts of the symmetrical anhydride derived from acid **33** could even be isolated from the mixture; for precedents and a mechanistic discussion see: I. Dhimitruka, J. SantaLucia, Jr., *Org. Lett.* **2006**, *8*, 47 – 50.

 © 2006 Wiley-VCH Verlag GmbH & Co. KGaA, Weinheim 

Alkyne Oligomerization

DOI: 10.1002/anie.200601542

# Osmium-Mediated Hexamerization of Phenylacetylene**

*Ting Bin Wen, Zhong Yuan Zhou, and Guochen Jia**

Transition-metal-mediated oligomerization and polymerization reactions of alkynes are attractive atom-economical C–C bond-formation reactions for organic and organometallic synthesis. Previous studies have led to the discovery of catalysts that can mediate selective dimerization,[1] trimerization,[2–4] tetramerization,[5,6] and polymerization[7] of alkynes. Parallel to this development, a number of organometallic complexes derived from dimerization, trimerization, and tetramerization of alkynes have been isolated, including interesting metallacycles,[8] complexes with cyclobutadiene,[9a–c] vinylvinylidene,[9d–e] benzene,[10] fulvene,[11–13] hexadienyne,[14] and unusual ligands derived from the tetramerization of alkynes.[15] In contrast, reactions of alkynes to give selectively well-defined oligomers of medium molecular weight (for example, pentamers, hexamers) of alkynes, either stoichiometric or catalytic in nature, are very scarce.[16] Herein we report a rare example of selective hexamerization of HC≡CPh to give bimetallic osmium complexes with bridging μ-1,2-bis($\eta^5$-cyclopentadienyl)-1,2-diphenyl-ethane ligands from the reaction of [OsCl(PCP)-($PPh_3$)] (PCP = 2,6-$(Ph_2PCH_2)_2C_6H_3$) with HC≡CPh.

Treatment of [OsCl(PCP)($PPh_3$)] (**1**) with excess HC≡CPh in benzene rapidly produced a brownish solution of the vinylidene complex [OsCl(=C=CHPh)(PCP)($PPh_3$)] (**2**).[17] When the solution was left standing, complex **2** was consumed gradually. After four days, the reaction produced an orange-red precipitate and a dark brown solution. The orange-red precipitate was identified to be the racemic mixture of the (*R*,*R*) and (*S*,*S*) isomers of the dicationic bimetallic complex **4** (Scheme 1). From the filtrate, the neutral bimetallic complex **5** and a small amount of the cationic monomeric complex **3** could be isolated (Scheme 1). The reaction of isolated vinylidene complex **2** with excess HC≡CPh gave the same result.

Complex **3** has been characterized by elemental analysis, FAB-MS, and multinuclear NMR spectroscopy. The structure has also been confirmed by an X-ray diffraction study.[18] The molecular structure of the complex cation of **3**, shown in Figure 1, clearly reveals that the complex is a four-legged piano stool cyclopentadienyl osmium(IV) complex with a facially bound PCP ligand and a chloride ligand. The solution NMR spectroscopic data are consistent with the solid-state structure. The facial arrangement of the PCP ligand in **3** is worth noting. Numerous complexes with PCP and related ligands have been reported in recent years.[19] In most of these reported complexes, the PCP and related ligands usually adopt a meridional geometry. Complex **3** represents a rare example of a PCP complex with a facially arranged PCP ligand.[20]

The most interesting result from the reaction of **1** with HC≡CPh is the formation of the bimetallic complexes **4** and **5**, which contain a μ-1,2-bis($\eta^5$-cyclopentadienyl)-1,2-diphenyl-ethane bridging ligand (Scheme 1). The bridging ligand is formally derived from selective hexamerization of HC≡CPh. As a result of the different configurations (*R* or *S*) of the CHPh carbon atoms, both the neutral and dicationic complexes are expected to have (*R*,*R*), (*S*,*S*), and *meso* stereoisomers. Experimentally, all three isomers of the neutral complex **5** have been isolated and identified: the *meso* isomer **5c** was obtained as a yellow solid, and the (*R*,*R*) isomer **5a** and (*S*,*S*) isomer **5b** were obtained in the form of a racemic mixture. For the cationic complex, we have isolated the (*R*,*R*) and (*S*,*S*) isomers (**4a** and **4b**) as a racemic mixture.

The structures of all these bimetallic complexes have been determined by X-ray diffraction. As an illustration, the molecular structures of cationic complex **4a** ((*R*,*R*) isomer), neutral complexes **5a** ((*R*,*R*) isomer), and **5c** (*meso* isomer) are shown in Figures 2, 3, and 4, respectively. Complex **4a** has crystallographic $C_2$ symmetry with the twofold axis passing

[*] Dr. T. B. Wen, Prof. Dr. G. Jia
Department of Chemistry
The Hong Kong University of Science and Technology
Clear Water Bay
Kowloon, Hong Kong (P.R. China)
Fax: (+852) 2358-7361
E-mail: chjiag@ust.hk
Prof. Z. Y. Zhou
Department of Applied Biology and Chemical Technology
Hong Kong Polytechnic University
Hung Hum, Hong Kong (P.R. China)

[**] This work was supported by the Hong Kong Research Grant Council (HKUST6090/02P).

 InterScience © 2006 Wiley-VCH Verlag GmbH & Co. KGaA, Weinheim 

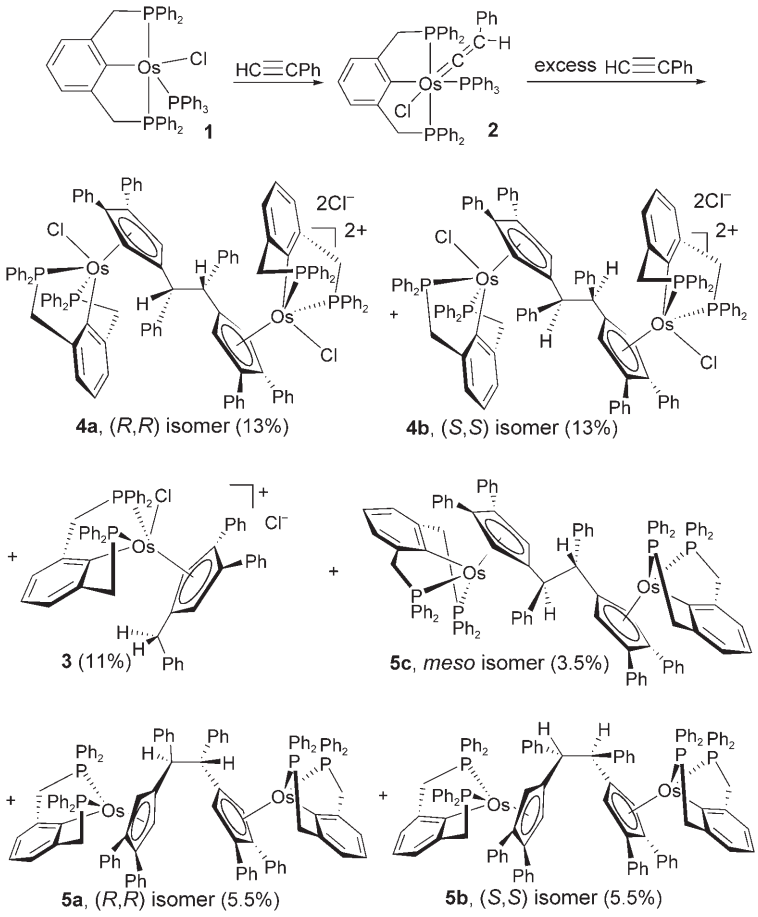


***Scheme 1.*** Synthesis of complexes **3**–**5**.

As indicated by the plausible mechanism shown in Scheme 2, complexes **3**, **4**, and **5** could all be formed through the fulvene intermediate **D** derived from a formal [2+2+1] cyclotrimerization of HC≡CPh. Thus, reaction of **1** with HC≡CPh produces the vinylidene complex [OsCl(=C=CHPh)($PPh_3$)(PCP)] (**2**), which has been confirmed experimentally. Complex **2** could dissociate the $PPh_3$ ligand in solution to give the unsaturated vinylidene **A**. Complex **A** undergoes a cycloaddition reaction with HC≡CPh to give first the metallacyclobutene complex **B** and then the metallacyclohexadiene complex **C**, which could undergo a reductive elimination to give the $\eta^4$-fulvene complex **D**. Protonation of **D** at the exocyclic CHPh carbon atom would give **3**. Couplings of vinylidenes at M=C bonds with alkynes are known reactions.[21] Although relatively rare, formation of fulvene metal complexes from formal [2+2+1] cyclotrimerizations of terminal alkynes has been reported in the stoichiometric reactions of rhodium,[11] iridium,[12] and palladium[13] complexes with alkynes. It is interesting to note that HC≡CR is dimerized on related metal fragments such as {Cp*Ru} (or {CpRu}; $Cp^* = C_5Me_5$, $Cp = C_5H_5$) and {TpRu} (Tp = hydrotris(pyrazolyl)borate) to give metallacyclopentadienes by oxidative coupling,[8b,c] or vinylvinylidenes by coupling of vinylidenes at C=C bonds with alkynes.[9d,e]

The fulvene intermediate **D** could undergo an intramolecular electron transfer (or "electron tautomerism") to generate the transient cyclopentadienyl osmium complex **E**, featuring an $Os^{III}$ center

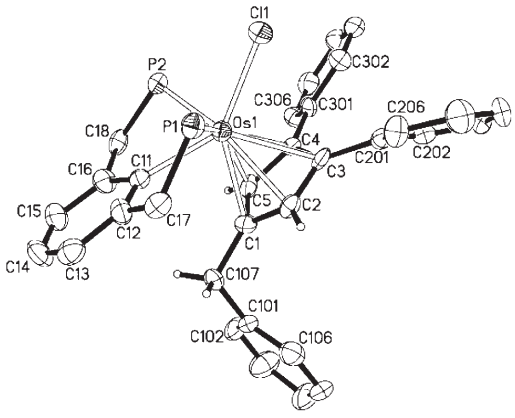


***Figure 1.*** Molecular structure for the cation of **3**. The $PPh_2$ phenyl rings of the PCP ligands are omitted for clarity.

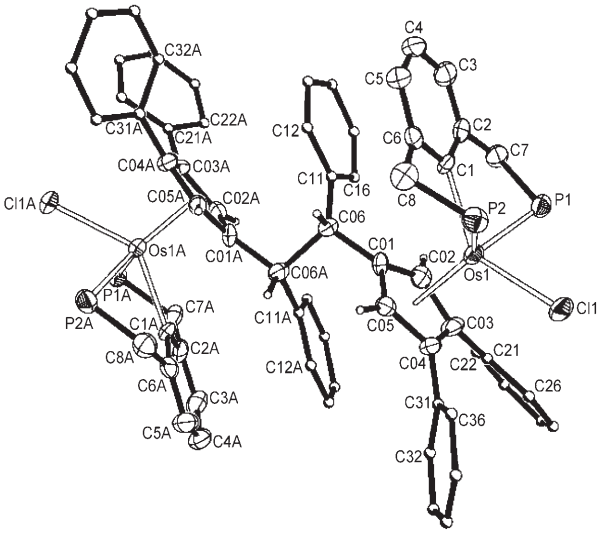


***Figure 2.*** Molecular structure for the cation of **4a** ((*R*,*R*) isomer). The $PPh_2$ phenyl rings of the PCP ligands are omitted for clarity.

through the midpoint of C06 and C06A. The *meso* complex **5c** has idealized $C_i$ symmetry with the crystallographic inversion center at the midpoint of C06 and C06A. All the complexes contain a facially bound PCP ligand. The solid-state structures are supported by their solution NMR spectroscopic data.

and a carbon-centered radical, which then undergoes intermolecular radical coupling to produce the paramagnetic $Os^{III}$ complex **F**. The 19-electron $Os^{III}$ species **F** may undergo

 © 2006 Wiley-VCH Verlag GmbH & Co. KGaA, Weinheim 

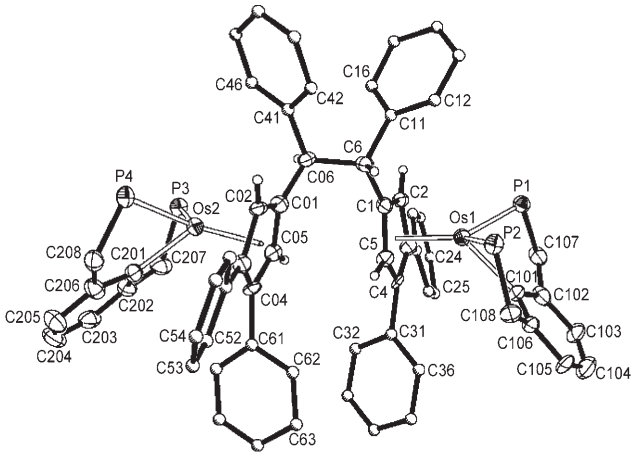


***Figure 3.*** Molecular structure for **5a** ((*R*,*R*) isomer). The $PPh_2$ phenyl rings of the PCP ligands are omitted for clarity.

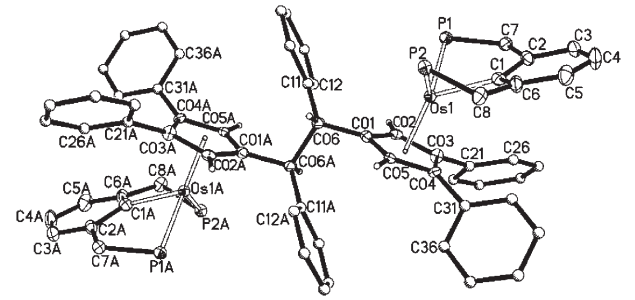


***Figure 4.*** Molecular structure for **5c** (*meso* isomer). The $PPh_2$ phenyl rings of the PCP ligands are omitted for clarity.

disproportionation to give the neutral $Os^{II}$ complex **5** and the dicationic $Os^{IV}$ complex **4** with $Cl^-$ as the counteranion. Radical dimerization involving coordinated fulvene has been proposed previously, for example, in the reaction of $[CpCo(C_2H_4)_2]$ with 6,6-dimethylpentafulvene to give paramagnetic (1,1,2,2-tetramethyl-1,2-ethanediyl)biscobaltocene,[22] and in the dimerization of ferrocenylmethyl carbocations to give the paramagetic iron(III) 1,2-bis(ferroceniumyl)ethane complexes.[23]

Consistent with this proposition, treatment of vinylidene complex **2** with HC≡CPh in benzene in the presence of added $HEt_3NCl$ produced **3** as the major product [Eq. (1)]. Isolated **3** readily undergoes H/D exchange with $D_2O$ to give $CD_2Ph$-deuterated [$D_2$]-**3**, thus suggesting that the transient intermediate **D** can be generated by deprotonation of **3**. Treatment of **3** with $NEt_3$ can also produce the bimetallic complexes **4** and **5**, presumably via the fulvene intermediate **D** that is generated by deprotonation of **3** with $NEt_3$. Following the proposed mechanism, one would expect that the reaction of **1** with PhC≡CH would lead to the formation of a mixture of (*R*,*R*), (*S*,*S*), and *meso* stereoisomers for both neutral and cationic complexes. Experimentally, we have isolated and identified all three isomers of the neutral complex **5**, though *meso* isomer **5c** was obtained in a relatively low yield. For the cationic complexes, we have been able to isolate and characterize the (*R*,*R*) and (*S*,*S*) isomers **4a** and **4b**. In line with the low yield of **5c**, isolation of the dicationic meso isomer **4c** was not successful. It is noted that only racemic isomers of bis(ferroceniumyl)ethane were obtained in the dimerization reaction of $[Cp^*Fe(C_5H_4CHPh)]^+$.[23b]

In summary, reaction of $[OsCl(PPh_3)(PCP)]$ with excess HC≡CPh led to the unprecedented formation of bimetallic osmium complexes containing a μ-1,2-bis($\eta^5$-cyclopentadienyl)-1,2-diphenyl-ethane bridging ligand, which are presumably formed through a fulvene intermediate which is generated from a formal [2+2+1] cylotrimerization of HC≡CPh.

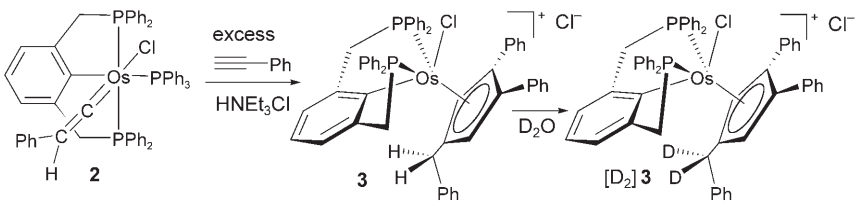


(1)

## *Experimental Section*

A mixture of $[OsCl(PPh_3)(PCP)]$ (0.80 g, 0.83 mmol) and phenylacetylene (1.40 mL, 12.7 mmol) in benzene (12 mL) was stirred at room temperature for 4 days to give an orange-red precipitate and a dark brown solution. The orange-red solid was collected by filtration, washed with benzene (2 mL) and diethyl ether (2 × 5 mL), dried in a vacuum overnight, and was identified to be a racemic mixture of **4a** and **4b**. Yield: 221 mg, 26%. The benzene washings and the mother liquid were collected and combined. The solution was concentrated to about 1 mL to give **3** as an orange-yellow crystalline solid, which was collected by filtration, washed with benzene (1 mL) and diethyl ether (2 × 2 mL), and dried in a vacuum overnight. Yield: 95 mg, 11%. The filtrate and the benzene washings were again combined and reduced to about 0.5 mL. Addition of diethyl ether (20 mL) to the residue provided a brownish-yellow solid, which was isolated by filtration and dried in a vacuum. The solid was then recrystallized from a small amount of benzene to give a racemic mixture of **5a** and **5b** as a yellow microcrystalline solid. Yield: 88 mg, 11%. The solvent of the final filtrate obtained above was removed in a vacuum. The residue was washed with hexane (2 × 20 mL) to give a brown solid, which was dried under vacuum and recrystallized from a small amount of benzene to give **5c** as a yellow microcrystalline solid. Yield: 29 mg, 3.5%.

**3**: $^{31}P\{^1H\}$ NMR (121.5 MHz, $CD_2Cl_2$): $\delta = 7.6$ ppm (s); $^1H$ NMR (300.13 MHz, $CD_2Cl_2$): $\delta = 2.71$ (s, 2H, C$H_2$Ph), 4.42 (dd, $J$(PH) = 14.2 Hz, $J$(HH) = 16.2 Hz, 2H, PCP-C$H_2$), 4.57 (d, $J$(HH) = 16.2 Hz, 2H, PCP-C$H_2$), 6.66 (s, 2H, Cp-C*H*), 6.78–7.84 ppm (m, 38H, $PPh_2$, $C_6H_3$, $C_6H_5$); $^{13}C\{^1H\}$ NMR (100.4 MHz, $CD_2Cl_2$): $\delta = 147.9$ (t, $J$(PC) = 6.6 Hz, Os-*C*(aryl)), 137.5–124.5 (m, other aromatic carbon atoms), 114.1 (s, Cp-*C*$CH_2$Ph), 108.4 (s, 2Cp-*C*Ph), 90.6 (s, 2 Cp-*C*H), 43.9 (dd, $J$(PC) = 23.1, 19.8 Hz, PCP-*C*$H_2$), 32.8 ppm (s, *C*$H_2$Ph); FAB-MS (*m*-nitrobenzyl alcohol (NBA)): *m*/*z*: 1007.8 ([*M*−Cl]$^+$, calcd 1007.2). Elemental analysis (%) calcd for $C_{56}H_{46}Cl_2P_2Os$: C 64.55, H 4.45; found: C 64.29, H 4.67.

Racemic isomers **4a and 4b**: $^{31}P\{^1H\}$ NMR (121.5 MHz, $CD_2Cl_2$): $\delta = 9.1$ (d), 5.2 (d), $J$(PP) = 18.4 Hz; $^1H$ NMR (300.13 MHz, $CD_2Cl_2$): $\delta = 2.97$ (dd, $J$(HH) = 15.3 Hz, $J$(PH) = 3.1 Hz, 1H, PCP-C$H_2$), 3.63 (t, $J$(PH) = 15.3 Hz, $J$(HH) = 15.3 Hz, 1H, PCP-C$H_2$), 3.79 (s, 1H, C*H*Ph), 4.45 (t, $J$(PH) =

 © 2006 Wiley-VCH Verlag GmbH & Co. KGaA, Weinheim 

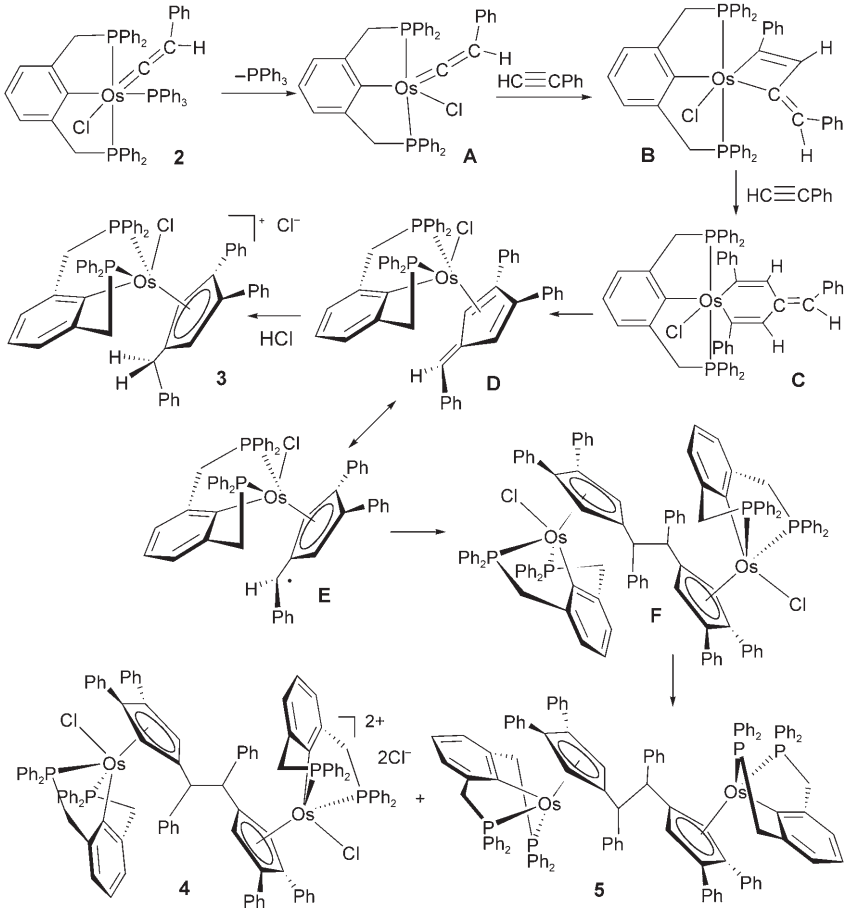

***Scheme 2.*** Proposed mechanism for the formation of **3**–**5**.

15.8 Hz, $J$(HH) = 15.8 Hz, 1H, PCP-C$H_2$), 5.54 (s, 1H, Cp-C*H*), 6.08–7.88 (m, 39H, $PPh_2$, $C_6H_3$, $C_6H_5$, 1H of PCP-C$H_2$ at ca. 7.1 ppm (obscured by aromatic proton resonances, assigned by $^1$H,$^1$H COSY and $^1$H,$^{13}$C COSY NMR experiments)), 8.98 (s, 1H, Cp-C*H*); $^{13}$C{$^1$H} NMR (100.4 MHz, $CD_2Cl_2$): $\delta$ = 149.0 (dd, $J$(PC) = 35.7, 10.4 Hz, Os-*C*(aryl)), 134.0–122.9 (m, other aromatic carbon atoms), 116.3 (s, Cp), 110.9 (d, $J$(PC) = 5.9 Hz, Cp), 107.1 (d, $J$(PC) = 7.4 Hz, Cp), 89.9 (d, $J$(PC) = 4.5 Hz, Cp-*C*H), 87.2 (d, $J$(PC) = 5.9 Hz, Cp-*C*H), 54.3 (s, *C*HPh, hidden under $CD_2Cl_2$ resonance, confirmed by DEPT-135, $^1$H,$^{13}$C COSY experiments), 45.9 (d, $J$(PC) = 41.6 Hz, PCP-*C*$H_2$), 45.0 ppm (d, $J$(PC) = 41.7 Hz, PCP-*C*$H_2$); FAB-MS (NBA): $m/z$: 2012.0 ([$M$−2Cl]$^+$, calcd 2012.5), 1006.3 ([$M$−2Cl]$^{2+}$, calcd 1006.2). Elemental analysis (%) calcd for $C_{112}H_{90}Cl_4P_4Os_2$: C 64.61, H 4.36; found: C 64.76, H 4.50.

Racemic isomers **5a** and **5b**: $^{31}$P{$^1$H} NMR (121.5 MHz, $CD_2Cl_2$): $\delta$ = 30.7 (d), 15.8 ppm (d), $J$(PP) = 13.9 Hz; $^1$H NMR (300.13 MHz, $CD_2Cl_2$): $\delta$ = 3.04 (s, 1H, C*H*Ph), 3.07 (dd, $J$(HH) = 14.6 Hz, $J$(PH) = 5.8 Hz, 1H, PCP-C$H_2$), 3.48 (dd, $J$(HH) = 13.8 Hz, $J$(PH) = 5.6 Hz, 1H, PCP-C$H_2$), 3.78 (t, $J$(HH) = 13.8 Hz, $J$(PH) = 13.3 Hz, 1H, PCP-C$H_2$), 4.01 (dd, $J$(HH) = 14.6, $J$(PH) = 12.8 Hz, 1H, PCP-C$H_2$), 4.32 (br s, 1H, Cp-C*H*), 4.59 (br s, 1H, Cp-C*H*), 5.62–7.47 ppm (m, 38H, $PPh_2$, $C_6H_3$, $C_6H_5$); $^{13}$C {$^1$H} NMR (100.4 MHz, $CD_2Cl_2$): $\delta$ = 167.0 (t, $J$(PC) = 6.6 Hz, Os-*C*(aryl)), 147.1–119.7 (m, other aromatic carbon atoms), 96.4 (s, Cp), 91.2 (d, $J$(PC) = 6.5 Hz, Cp), 88.1 (s, Cp-*C*H), 85.4 (d, $J$(PC) = 8.2 Hz, Cp-*C*H), 78.9 (d, $J$(PC) = 13.2 Hz, Cp), 50.1 (d, $J$(PC) = 44.5 Hz, PCP-*C*$H_2$), 49.0 (s, *C*HPh), 48.4 ppm (d, $J$(PC) = 42.9 Hz, PCP-*C*$H_2$); FAB-MS (NBA, $m/z$): 1942.3 ($M^+$, calcd 1942.5). Elemental analysis (%) calcd for $C_{112}H_{90}P_4Os_2$: C 69.33, H 4.68; found: C 69.50, H 4.69.

**5c:** $^{31}$P{$^1$H} NMR (121.5 MHz, $CD_2Cl_2$, 298 K): $\delta$ = 29.2 (br), 22.9 ppm (d (unresolved), $J$(PP) = 13.2 Hz); $^1$H NMR (300.13 MHz, $CD_2Cl_2$, 298 K): $\delta$ = 3.29 (br s, 1H, C*H*Ph), 3.41–3.55 (m, 3H, PCP-C$H_2$), 3.94 (br s, 1H, Cp-C*H*), 4.19 (t, $J$(HH) = 14.4 Hz, $J$(PH) = 13.4 Hz, 1H, PCP-C$H_2$), 4.32 (br s, 1H, Cp-C*H*), 5.81–7.37 ppm (m, 38H, $PPh_2$, $C_6H_3$, $C_6H_5$); $^{13}$C{$^1$H} NMR (100.4 MHz, $CD_2Cl_2$): $\delta$ = 165.7 (br, Os-*C*(aryl)), 147.6–120.0 (m, other aromatic carbon atoms), 96.7 (br s, Cp), 95.0 (s, Cp), 85.5 (s, Cp-*C*H), 80.5 (br s, Cp-*C*H), 79.0 (br s, Cp), 51.2 (d, $J$(PC) = 48.5 Hz, PCP-*C*$H_2$), 51.0 (s, *C*HPh), 48.4 ppm (d, $J$(PC) = 42.3 Hz, PCP-*C*$H_2$); FAB-MS (NBA): $m/z$: 1941.0 ($M^+$, calcd 1942.5). Elemental analysis (%) calcd for $C_{112}H_{90}P_4Os_2$: C 69.33, H 4.68; found: C 69.27, H 5.15.

Received: April 19, 2006
Published online: July 31, 2006

**Keywords:** alkynes · fulvene · oligomerization · osmium · vinylidene ligands

[1] See, for example: a) W. Weng, C. Guo, R. Celenligil-Cetin, B. M. Foxman, O. V. Ozerov, *Chem. Commun.* **2006**, 197; b) M. V. Jimenez, E. Sola, F. J. Lahoz, L. A. Oro, *Organometallics* **2005**, *24*, 2722; c) J. Le Paih, S. Derien, B. Demerseman, C. Bruneau, P. H. Dixneuf, L. Toupet, G. Dazinger, K. Kirchner, *Chem. Eur. J.* **2005**, *11*, 1312; d) X. Chen, P. Xue, H. H. Y. Sung, I. D. Williams, M. Peruzzini, C. Bianchini, G. Jia, *Organometallics* **2005**, *24*, 4330; e) H. Katayama, H. Yari, M. Tanaka, F. Ozawa, *Chem. Commun.* **2005**, 4336; f) C. C. Lee, Y. C. Lin, Y. H. Liu, Y. Wang, *Organometallics* **2005**, *24*, 136; g) M. Schafer, J. Wolf, H. Werner, *Organometallics* **2004**, *23*, 5173; h) C. Bianchini, M. Peruzzini, F. Zanobini, P. Frediani, A. Albinati, *J. Am. Chem. Soc.* **1991**, *113*, 5443.

[2] Formation of benzenes: S. Saito, Y. Yamamoto, *Chem. Rev.* **2000**, *100*, 2901, and references therein.

[3] Formation of fulvenes: a) E. S. Johnson, G. J. Balaich, P. E. Fanwick, I. P. Rothwell, *J. Am. Chem. Soc.* **1997**, *119*, 11086; b) U. Radhakrishnan, V. Gevorgyan, Y. Yamamoto, *Tetrahedron Lett.* **2000**, *41*, 1971.

[4] Formation of linear trimers: a) H. F. Klein, M. Mager, S. Isringhausen-Bley, U. Florker, H. J. Haupt, *Organometallics* **1992**, *11*, 3174; b) A. Haskel, J. Q. Wang, T. Straub, T. G. Neyroud, M. S. Eisen, *J. Am. Chem. Soc.* **1999**, *121*, 3025; c) J. Wang, A. K. Dash, M. Kapon, J. C. Berthet, M. Ephritikhine, M. S. Eisen, *Chem. Eur. J.* **2002**, *8*, 5384.

[5] Cyclotetramerization: B. E. Straub, C. Gollub, *Chem. Eur. J.* **2004**, *10*, 3081, and reference therein.

[6] Catalytic linear tetramerization: a) A. D. Burrows, M. Green, J. C. Jeffery, J. M. Lynam, M. F. Mahon, *Angew. Chem.* **1999**, *111*, 3228; *Angew. Chem. Int. Ed.* **1999**, *38*, 3043; b) A. Haskel, T. Straub, A. K. Dash, M. S. Eisen, *J. Am. Chem. Soc.* **1999**, *121*, 3104.

[7] J. P. Claverie, R. Soula, *Prog. Polym. Sci.* **2003**, *28*, 619, and references therein.

 © 2006 Wiley-VCH Verlag GmbH & Co. KGaA, Weinheim 

[8] Metallacyclopentadienes: a) E. A. Ison, K. A. Abboud, J. M. Boncella, *Organometallics* **2006**, *25*, 1557; b) Y. Yamamoto, T. Arakawa, K. Itoh, *Organometallics* **2004**, *23*, 3610; c) J. Le Paih, F. Monnier, S. Derien, P. H. Dixneuf, E. Clot, O. Eisenstein, *J. Am. Chem. Soc.* **2003**, *125*, 11964; d) M. Martin, E. Sola, O. Torres, P. Plou, L. A. Oro, *Organometallics* **2003**, *22*, 5406; e) U. Rosenthal, V. V. Burlakov, P. Arndt, W. Baumann, A. Spannenberg, *Organometallics* **2003**, *22*, 884; f) C. Bianchini, A. Meli, M. Peruzzini, V. Vacca, F. Vizza, *Organometallics* **1991**, *10*, 645; metallacyclohexadienes or metallabenzofuran: g) G. R. Clark, P. M. Johns, W. R. Roper, L. J. Wright, *Organometallics* **2006**, *25*, 1771; metallacycloheptatrienes: h) M. Paneque, M. L. Poveda, N. Rendon, K. Mereiter, *J. Am. Chem. Soc.* **2004**, *126*, 1610; i) E. Alvarez, M. Gomez, M. Paneque, C. M. Posadas, M. L. Poveda, N. Rendon, L. L. Santos, S. Rojas-Lima, V. Salazar, K. Mereiter, C. Ruiz, *J. Am. Chem. Soc.* **2003**, *125*, 1478; metallabenzynes: j) T. B. Wen, Z. Zhou, G. Jia, *Angew. Chem.* **2001**, *113*, 2005; *Angew. Chem. Int. Ed.* **2001**, *40*, 1951; .

[9] See, for example: a) R. Gleiter, D. B. Weiz, *Organometallics* **2005**, *24*, 4316; b) C. Schaefer, D. B. Werz, T. H. Staeb, R. Gleiter, F. Rominger, *Organometallics* **2005**, *24*, 2106; c) B. Hellbach, F. Rominger, R. Gleiter, *Angew. Chem.* **2004**, *116*, 5970; *Angew. Chem. Int. Ed.* **2004**, *43*, 5486; d) Y. Sun, H. S. Chan, P. H. Dixneuf, Z. Xie, *Organometallics* **2006**, *25*, 2719; e) M. A. Jimenez-Tenorio, M. J. Tenorio, M. C. Puerta, P. Valerga, *Organometallics* **2000**, *19*, 1333.

[10] See, for example: a) Y. Yamamoto, T. Arakawa, R. Ogawa, K. Itoh, *J. Am. Chem. Soc.* **2003**, *125*, 12143; b) C. Bianchini, K. G. Caulton, C. Chardon, M. L. Doublet, O. Eisenstein, S. A. Jackson, T. J. Johnson, A. Meli, M. Peruzzini, W. E. Streib, A. Vacca, F. Vizza, *Organometallics* **1994**, *13*, 2010.

[11] a) W. S. Han, S. W. Lee, *Organometallics* **2005**, *24*, 997; b) G. Moran, M. Green, A. G. Orpen, *J. Organomet. Chem.* **1983**, *250*, C15; c) J. Moreto, K. Maruya, P. M. Bailey, P. M. Maitlis, *J. Chem. Soc. Dalton Trans.* **1982**, 134.

[12] J. M. O'Connor, K. Hiibner, R. Merwin, P. K. Gantzel, B. S. Fong, *J. Am. Chem. Soc.* **1997**, *119*, 3631.

[13] H. J. Kim, N. S. Choi, S. W. Lee, *J. Organomet. Chem.* **2000**, *616*, 67.

[14] H. Werner, M. Schafer, J. Wolf, K. Peters, H. G. von Schnering, *Angew. Chem.* **1995**, *107*, 213; *Angew. Chem. Int. Ed. Engl.* **1995**, *34*, 191.

[15] a) M. I. Bruce, B. C, Hall, B. W. Skelton, A. H. White, N. N. Zaitseva, *J. Chem. Soc. Dalton Trans.* **2000**, 2279; b) H. Komatsu, H. Yamazaki, *Chem. Lett.* **2001**, 998.

[16] Pentamers, hexamers, and octamers of 1-alkynes were formed together with lower oligomers in organoactinide- and ruthenium-catalyzed reactions: Y. Gao, R. J. Puddephatt, *Inorg. Chim. Acta* **2003**, *350*, 101; reference [6b].

[17] T. B. Wen, Y. K. Cheung, J. Z. Yao, W. T. Wong, Z. Y. Zhou, G. Jia, *Organometallics* **2000**, *19*, 3803.

[18] Crystal data for **3**: $C_{56}H_{46}ClOsP_2 \cdot 0.5\,CH_2Cl_2$ (from $CH_2Cl_2$/hexane), $M_r = 1084.43$, monoclinic, space group $P2_1/n$, $a = 15.626(2)$, $b = 38.941(5)$, $c = 15.771(2)$ Å, $\beta = 104.365(4)°$, $V = 9296(2)$ Å$^3$, $Z = 8$, $\rho_{calcd} = 1.550$ g cm$^{-3}$, $\mu(Mo_{K\alpha}) = 3.023$ mm$^{-1}$, $F(000) = 4344$, $\theta_{max} = 26.00°$, 55082 reflections, 18265 independent ($R_{int} = 0.1267$), $R_1 = 0.0520$, $wR_2 = 0.0742$ for 1119 parameters and 6519 reflections with $I > 2\sigma(I)$. Crystal data for **4a**: $C_{112}H_{90}Cl_4Os_2P_4 \cdot 1.5\,CH_2Cl_2$ (from $CH_2Cl_2$/hexane), $M_r = 2209.30$, monoclinic, space group $C2/c$, $a = 30.714(4)$, $b = 22.381(3)$, $c = 14.4277(18)$ Å, $\beta = 92.770(3)°$, $V = 9906(2)$ Å$^3$, $Z = 4$, $\rho_{calcd} = 1.481$ g cm$^{-3}$, $\mu(Mo_{K\alpha}) = 2.865$ mm$^{-1}$, $F(000) = 4420$, $\theta_{max} = 27.57°$, 33649 reflections, 11418 independent ($R_{int} = 0.1004$), $R_1 = 0.0617$, $wR_2 = 0.1560$ for 573 parameters and 4689 reflections with $I > 2\sigma(I)$. Crystal data for **5a**: $C_{112}H_{90}Os_2P_4 \cdot CH_2Cl_2$ (from $CH_2Cl_2$/hexane), $M_r = 2025.05$, triclinic, space group $P\bar{1}$, $a = 13.1359(16)$, $b = 17.841(2)$, $c = 21.203(3)$ Å, $\alpha = 113.654(3)$, $\beta = 91.597(3)$, $\gamma = 95.632(3)°$, $V = 4517.1(9)$ Å$^3$, $Z = 2$, $\rho_{calcd} = 1.489$ g cm$^{-3}$, $\mu(Mo_{K\alpha}) = 2.991$ mm$^{-1}$, $F(000) = 2032$, $\theta_{max} = 25.00°$, 20231 reflections, 14998 independent ($R_{int} = 0.0847$), $R_1 = 0.0416$, $wR_2 = 0.0615$ for 1090 parameters and 7745 reflections with $I > 2\sigma(I)$. Crystal data for **5c**: $C_{112}H_{90}Os_2P_4 \cdot C_6H_6$ (from saturated benzene solution), $M_r = 2018.23$, triclinic, space group $P\bar{1}$, $a = 11.290(5)$, $b = 12.564(6)$, $c = 19.052(9)$ Å, $\alpha = 92.669(12)$, $\beta = 96.504(11)$, $\gamma = 114.198(10)°$, $V = 2436(2)$ Å$^3$, $Z = 1$, $\rho_{calcd} = 1.376$ g cm$^{-3}$, $\mu(Mo_{K\alpha}) = 2.720$ mm$^{-1}$, $F(000) = 1016$, $\theta_{max} = 27.72°$, 16710 reflections, 11080 independent ($R_{int} = 0.0713$), $R_1 = 0.0587$, $wR_2 = 0.1266$ for 556 parameters and 6682 reflections with $I > 2\sigma(I)$. Single-crystal X-ray diffraction data were collected on a Bruker SMART CCD area detector with graphite-monochromated $Mo_{K\alpha}$ radiation at 293 K. All of the data sets were corrected for absorption with the SADABS program (G. M. Sheldrick, SADABS). All structures were solved by direct methods, expanded by difference Fourier syntheses, and refined by full-matrix least squares on $F^2$ using the Bruker SHELXTL (Version 5.10) program package. Non-H atoms were refined anisotropically, except for the disordered $CH_2Cl_2$ solvent molecule, which was refined isotropically with fixed C–Cl distance restraints. Hydrogen atoms were introduced at their geometric positions and refined as riding atoms. CCDC-604120 (**3**), CCDC-604121 (**4a**), CCDC-604122 (**5a**), and CCDC-604123 (**5c**) contain the supplementary crystallographic data for this paper. These data can be obtained free of charge from The Cambridge Crystallographic Data Centre via www.ccdc.cam.ac.uk/data_request/cif.

[19] a) M. Albrecht, G. van Koten, *Angew. Chem.* **2001**, *113*, 3866; *Angew. Chem. Int. Ed.* **2001**, *40*, 3750; b) M. E. van der Boom, D. Milstein, *Chem. Rev.* **2003**, *103*, 1759; c) J. T. Singleton, *Tetrahedron* **2003**, *59*, 1837.

[20] J. Takaya, J. F. Hartwig, *J. Am. Chem. Soc.* **2005**, *127*, 5756.

[21] a) C. Bruneau, P. H. Dixneuf, *Angew. Chem.* **2006**, *118*, 2232; *Angew. Chem. Int. Ed.* **2006**, *45*, 2176; b) C. Bruneau, P. H. Dixneuf, *Acc. Chem. Res.* **1999**, *32*, 311.

[22] H. Wadepohl, C. W. von der Lieth, F. J. Paffen, H. Pritzkow, *Chem. Ber.* **1995**, *128*, 317.

[23] a) C. Zou, M. S. Wrighton, *J. Am. Chem. Soc.* **1990**, *112*, 7578, and references therein; b) B. Bildstein, A. Hradsky, H. Kopacka, R. Malleier, K. H. Ongania, *J. Organomet. Chem.* **1997**, *540*, 127.

 © 2006 Wiley-VCH Verlag GmbH & Co. KGaA, Weinheim 

C–C Coupling

DOI: 10.1002/anie.200601206

# Radical-Mediated Alkenylation, Alkynylation, Methanimination, and Cyanation of *B*-Alkylcatecholboranes**

*Arnaud-Pierre Schaffner, Vincent Darmency, and Philippe Renaud**

Organoboranes are very valuable synthetic intermediates that are used in numerous synthetic processes.[1–6] For example, the Suzuki–Miyaura reaction continually proves to be one of the most efficient methods for the formation of carbon–carbon bonds through cross-coupling reactions between organoboron derivatives and organic electrophiles.[7–9] From the earliest investigations by Brown, organoboranes have been identified as a source of radicals.[10–12] Recently, we have become interested in developing novel synthetic methods based on the use of organoboranes, and more particularly of *B*-alkylcatecholborane, as a source of radicals.[12–14] For example, we reported an efficient allylation procedure based on the use of readily available allyl sulfones.[15–18] Herein, we report alkenylations, acylations, cyanations, and alkynylations of alkylcatecholboranes, mediated by free-radicals. All of these reactions are based on a common process: radical addition to the carbon atom of a multiple (double or triple) bond bearing an arene sulfonyl group [Eqs. (1) and (2)].[19]

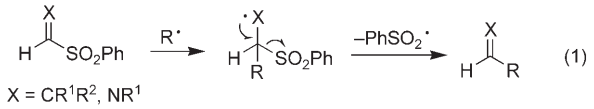


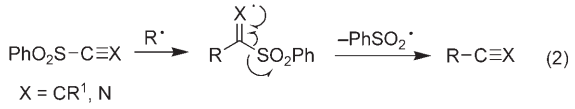


Russell et al.,[20,21] Ono et al.,[22] and others[23] have demonstrated the feasibility of radical alkenylation reactions.[24–27] Secondary and tertiary alkyl radicals, generated either by hydrogen atom abstraction as reported by Fuchs and co-workers[28,29] or from iodides and xanthates as reported by Zard and co-workers,[30] were alkenylated through α addition to vinyl sulfones. Intramolecular reactions involving sulfoxides, sulfoximines, and phosphine oxides have also been reported.[31–33] Interestingly, Nozaki and co-workers[34] reported the vinylation of trialkylboranes with styryl sulfoxides and sulfones. The mechanism proposed at that time involves the formation of vinyl radicals. More recently, Yao and co-workers[35,36] reported the alkenylation of trialkylboranes with β-nitrostyrene, but this nonchain reaction requires the use of a threefold excess of the trialkylborane. Therefore, we decided to investigate the reaction of *B*-alkylcatecholboranes with alkenyl sulfones. Hydroboration of the alkenes such as 1-octene (**1**, Table 1, entry 1), β-pinene (**2**, entry 2), cyclohexene (**3**, entry 3), α-pinene (**4**, entries 4 and 5), and tetramethylethylene (**5**, entry 6) with catecholborane was achieved by taking advantage of the very mild, efficient, and cost-effective hydroboration conditions developed by Garett and Fu[37] in which *N*,*N*-dimethylacetamide (10 mol%) was used as a catalyst in refluxing dichloromethane. In situ treatment of the *B*-alkylcatecholborane with vinyl sulfone **6** or **7** (1.2–3 equivalents) in the presence of di-*tert*-butylhyponitrite (3 mol%) as the initiator, afforded the expected alkenylated products **8**–**13** in reasonable yields (Table 1, entries 1–6). The bissulfone **6** proved to be a convenient reagent for the vinylation reaction and afforded alkenyl sulfones that are interesting starting materials for further functionalization.[38] Furthermore, the product resulting from the bissubstitution of the two sulfonyl groups was not detected. The use of phenyl 2-phenylvinyl sulfone (**7**) allows the introduction of a styryl group (Table 1, entry 5).

***Table 1:*** Alkenylation of *B*-alkylcatecholboranes with vinyl sulfones.

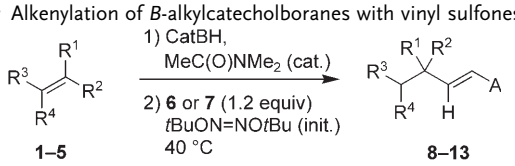


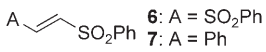


| Entry | | Alkene | Sulfone | | Product | Yield [%] |
|---|---|---|---|---|---|---|
| 1 | **1** | | **6** | **8** | 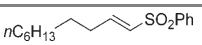 | 55 |
| 2 | **2** | | **6** | **9** | 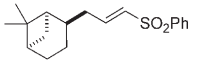 | 58 |
| 3 | **3** | | **6** | **10** | 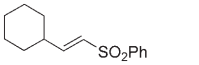 | 72 |
| 4 | **4** | | **6** | **11** | 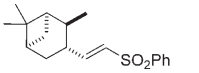 | 64 |
| 5 | **4** | | **7** | **12** | 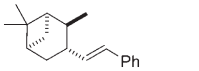 | 66[a] |
| 6 | **5** | | **6** | **13** | 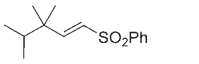 | 60 |

[a] Using 3 equiv of **7**. CatBH = Catecholborane.

[*] A.-P. Schaffner, V. Darmency, Prof. P. Renaud
Universität Bern
Departement für Chemie und Biochemie
Freiestrasse 3, 3000 Bern 9 (Switzerland)
Fax: (+41) 31-631-3426
E-mail: philippe.renaud@ioc.unibe.ch

[**] This work was supported by the Swiss National Science Foundation (project 21-103627). We thank BASF Corporation for the generous gift of catecholborane.

Supporting information for this article (experimental procedures and characterizations of compounds **3**–**8**, **15**–**18**, and **22**–**27**) is available on the WWW under http://www.angewandte.org or from the author.


© 2006 Wiley-VCH Verlag GmbH & Co. KGaA, Weinheim

An acylation protocol was then tested using *N*-benzyloxy-1-(phenylsulfonyl)methanimine, as reported by Kim and co-workers.[39] Primary (Table 2, entry 1) and secondary alkyl radicals (Table 2, entries 2–4) react well to afford the stable oxime ethers. This transformation corresponds formally to a formylation of the *B*-alkylcatecholborane.

***Table 2:*** Formylation of *B*-alkylcatecholboranes.

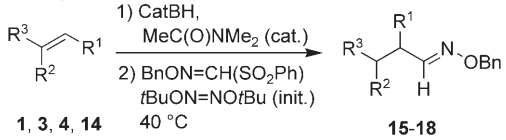


| Entry | Alkene | | Product | | Yield [%] |
|---|---|---|---|---|---|
| 1 | **1** | | **15** | | 73 |
| 2 | **3** | | **16** | 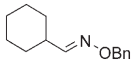 | 74 |
| 3 | **4** | | **17** | 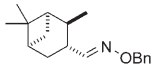 | 74 |
| 4 | **14** | | **18** | 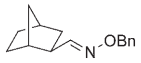 | 53 |

Bn = benzyl.

The reaction with alkynyl sulfones was investigated next. Following the seminal work of Russell and co-workers[20,21,40] as well as of Fuchs and co-workers,[28,41] we decided to investigate the alkynylation process (Table 3). This reaction is particularly interesting because, to the best of our knowledge, no palladium-catalyzed cross-coupling between alkylboranes and acetylene derivatives has been reported.[42,43] The reaction with phenyl phenylethynyl sulfone (**20**)[44] proved to be efficient with primary to tertiary alkyl radicals (Table 3, entries 1, 2, and 4). Interestingly, similar results were obtained with the phenyl trimethylsilylethynyl sulfone (**21**, Table 3, entry 3).[24] This result is best explained by the steric interaction of the $Me_3Si$ group that favors an addition at the α-position to the sulfonyl group. The trimethylsilylacetylene derivative **25**, obtained in 72% yield, undergoes a facile desilylation[43] through treatment with aqueous sodium hydroxide to afford the desired terminal alkyne **26** in near quantitative yield.[45]

Finally, a related cyanation process was attempted using the commercially available *p*-toluenesulfonyl cyanide (**22**, Table 3).[46–48] Good yields were obtained with primary and secondary radicals (Table 3, entries 5 and 6). Reaction with (+)-carene (**19**) afforded monocyclic cyanide **30**, which results from the isomerization of the cyclopropylmethyl radical to a homoallyl radical. The cyanation of organoboranes also has no precedent in the literature, to the best of our knowledge.

We demonstrate here that hydroboration with commercially available catecholborane, followed by treatment with easily available reagents such as alkenyl or alkynyl phenyl sulfones in the presence of a radical initiator (di-*tert*-butylhyponitrite or oxygen), represents an effective and simple one-pot procedure for performing direct vinylation, formylation, alkynylation, and cyanation of *B*-alkylcatecholboranes. These radical transformations of alkylboranes represent powerful reactions that should find applications in the total syntheses of natural products. Furthermore, these transformations demonstrate the generality of the use of organoboranes for the generation of primary, secondary, and tertiary alkyl radicals. The use of nontoxic *B*-alkylcatecholboranes, which are easily prepared from alkenes and may contain additional functionality,[13,49] in addition to the mild reaction conditions, make this metal-free procedure very attractive for the formation of C–C bonds.

***Table 3:*** Alkynylation and cyanation of *B*-alkylcatecholboranes.

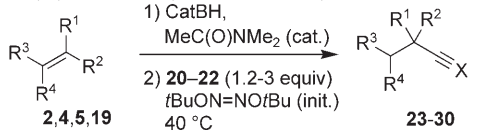


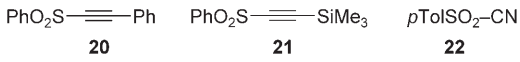


| Entry | Alkene | | Sulfone | Product | | Yield [%] |
|---|---|---|---|---|---|---|
| 1 | **2** | | **20** | **23** | 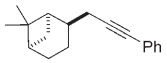 | 89[a] |
| 2 | **4** | | **20** | **24** | 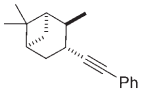 | 84[b] |
| 3 | **4** | | **21** | **25** (R = $SiMe_3$)<br>**26** (R = H)[43] | 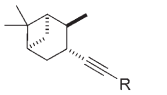 | 72[b]<br>72[c] |
| 4 | **5** | | **20** | **27** | 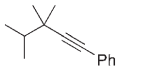 | 83 |
| 5 | **2** | | **22** | **28** | 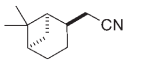 | 75[a] |
| 6 | **4** | | **22** | **29** | 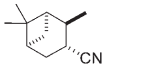 | 88[b] |
| 7 | **19** | 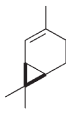 | **22** | **30** | 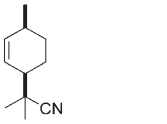 | 90 |

[a] Diastereomeric ratio ≥97:3. [b] Diastereomeric ratio ≥95:5. [c] After treatment of the crude cyanide **25** with aqueous NaOH. Tol = tolyl.

## *Experimental Section*

General procedure: Catecholborane (0.468 mL, 4.4 mmol) was added dropwise at 0 °C to a solution of olefin (2.0 mmol) and *N*,*N*-dimethylacetamide (0.019 mL, 0.20 mmol) in $CH_2Cl_2$ (2 mL) under nitrogen. The reaction mixture was heated to reflux for 5 h. *t*BuOH (0.234 mL, 2.5 mmol) was added at 0 °C and the solution was stirred for 15 min at RT. The sulfone (6 mmol) was then added and the solution was warmed to reflux and di-*tert*-butylhyponitrite (3 mol%) was added every 1 h. The reaction was monitored by GC-MS. By the end of the reaction, the solution had turned black. The crude product was purified by flash chromatography over silica gel.

Received: March 27, 2006
Revised: June 22, 2006
Published online: August 4, 2006

 © 2006 Wiley-VCH Verlag GmbH & Co. KGaA, Weinheim 

**Keywords:** C–C coupling · hydroboration · olefination · radical reactions · sulfones


[1] H. C. Brown, *Angew. Chem.* **1980**, *92*, 675.
[2] H. C. Brown, *Boranes in Organic Chemistry*, Cornell University Press, Ithaca, **1972**.
[3] H. C. Brown, G. W. Kramer, A. B. Levy, M. M. Midland, *Organic Synthesis via Boranes*, Wiley, New York, **1975**.
[4] H. C. Brown, *Hydroboration*, Benjamin-Cumming, Reading, **1980**.
[5] A. Pelter, K. Smith, H. C. Brown, *Borane Reagents*, Academic Press, London, **1988**.
[6] D. S. Matteson, *Stereodirected Synthesis with Organoboranes*, Springer, Berlin, **1995**.
[7] N. Miyaura, A. Suzuki, *Chem. Rev.* **1995**, *95*, 2457.
[8] For reviews on organoboron compounds, see: N. Miyaura, *Cross-Coupling Reactions: A Practical Guide*, *Vol. 219*, Springer, Berlin, **2002**.
[9] F. Bellina, R. Rossi, *Synthesis* **2004**, 2419.
[10] H. C. Brown, M. M. Midland, *Angew. Chem.* **1972**, *84*, 702; *Angew. Chem. Int. Ed. Engl.* **1972**, *11*, 692.
[11] B. Giese, *Radicals in Organic Syntheses: Formation of Carbon-Carbon Bonds*, Pergamon, Oxford, **1986**.
[12] C. Ollivier, P. Renaud, *Chem. Rev.* **2001**, *101*, 3415.
[13] A.-P. Schaffner, P. Renaud, *Eur. J. Org. Chem.* **2004**, 2291.
[14] V. Darmency, P. Renaud in *Topics in Current Chemistry*, *Vol. 263* (Ed.: A. Gansaeuer), Springer, Berlin, **2006**, p. 71.
[15] A.-P. Schaffner, P. Renaud, *Angew. Chem.* **2003**, *115*, 2762; *Angew. Chem. Int. Ed.* **2003**, *42*, 2658.
[16] A.-P. Schaffner, B. Becattini, C. Ollivier, V. Weber, P. Renaud, *Synthesis* **2003**, 2740.
[17] V. Darmency, E. M. Scanlan, A.-P. Schaffner, P. Renaud, *Org. Synth.* **2005**, *83*, 24.
[18] V. Darmency, P. Renaud, *Chimia* **2005**, *59*, 109.
[19] F. Bertrand, F. Le Guyader, L. Liguori, G. Ouvry, B. Quiclet-Sire, S. Seguin, S. Z. Zard, *C. R. Acad. Sci. Ser. II C* **2001**, *4*, 547.
[20] G. A. Russell, P. Ngoviwatchai, H. I. Tashtoush, A. Pladalmau, R. K. Khanna, *J. Am. Chem. Soc.* **1988**, *110*, 3530.
[21] G. A. Russell, P. Ngoviwatchai, *J. Org. Chem.* **1989**, *54*, 1836.
[22] N. Ono, A. Kamimura, A. Kaji, *J. Org. Chem.* **1987**, *52*, 5111.
[23] A. J. Clark, S. Rooke, T. J. Sparey, P. C. Taylor, *Tetrahedron Lett.* **1996**, *37*, 909.
[24] Recently, the first example of the introducion of a trimethylsilylethynyl group was reported: S. Usugi, H. Yorimitsu, H. Shinokubo, K. Oshima, *Bull. Chem. Soc. Jpn.* **2002**, *75*, 2687.
[25] K. Takami, S. I. Usugi, H. Yorimitsu, K. Oshima, *Synthesis* **2005**, 824.
[26] K. Takami, H. Yorimitsu, K. Oshima, *Org. Lett.* **2004**, *6*, 4555.
[27] For a review on radical fragmentation processes, see: I. J. Rosenstein in *Radicals in Organic Synthesis*, *Vol. 1* (Eds.: P. Renaud, M. P. Sibi), Wiley-VCH, Weinheim, **2001**, p. 50.
[28] J. Xiang, P. L. Fuchs, *J. Am. Chem. Soc.* **1996**, *118*, 11986.
[29] J. Xiang, W. Jiang, J. Gong, P. L. Fuchs, *J. Am. Chem. Soc.* **1997**, *119*, 4123.
[30] F. Bertrand, B. Quiclet-Sire, S. Z. Zard, *Angew. Chem.* **1999**, *111*, 2135; *Angew. Chem. Int. Ed.* **1999**, *38*, 1943.
[31] D. Leca, L. Fensterbank, E. Lacôte, M. Malacria, *Angew. Chem.* **2004**, *116*, 4316; *Angew. Chem. Int. Ed.* **2004**, *43*, 4220.
[32] D. Leca, K. Song, M. Albert, M. G. Goncalves, L. Fensterbank, E. Lacôte, M. Malacria, *Synthesis* **2005**, 1405.
[33] B. Delouvrié, L. Fensterbank, E. Lacôte, M. Malacria, *J. Am. Chem. Soc.* **1999**, *121*, 11395.
[34] N. Miyamoto, D. Fukuoka, K. Utimoto, H. Nozaki, *Bull. Soc. Chem. Jpn.* **1974**, *47*, 503.
[35] J.-T. Liu, Y.-J. Jang, Y.-K. Shih, S.-R. Hu, C.-M. Chu, C.-F. Yao, *J. Org. Chem.* **2001**, *66*, 6021.
[36] C.-F. Yao, C.-M. Chu, J.-T. Liu, *J. Org. Chem.* **1998**, *63*, 719.
[37] C. E. Garett, G. C. Fu, *J. Org. Chem.* **1996**, *61*, 3224.
[38] R. F. W. Jackson, S. P. Standen, W. Clegg, A. McCamley, *J. Chem. Soc. Perkin Trans. 1* **1995**, 141.
[39] a) S. Kim, I. Y. Lee, J.-Y. Yoon, D. H. Oh, *J. Am. Chem. Soc.* **1996**, 5138;b) S. Kim, C. J. Lim, *Bull. Korean Chem. Soc.* **2003**, *24*, 1219.
[40] G. A. Russell, P. Ngoviwatchai, *Tetrahedron Lett.* **1986**, *27*, 3479.
[41] J. C. Gong, P. L. Fuchs, *J. Am. Chem. Soc.* **1996**, *118*, 4486.
[42] Coupling with a reverse polarity of the reagents (Sonogashira and Kumada–Corriu reactions), involving electrophilic alkyl halides with alkynyl nucleophiles are known: M. Eckhardt, G. C. Fu, *J. Am. Chem. Soc.* **2003**, *125*, 13642; L. M. Yang, L.-F. Huang, T.-Y. Luh, *Org. Lett.* **2004**, *6*, 1461.
[43] A procedure for the preparation of acetylene derivatives from organoboranes through iodine-mediated rearrangement of ate complexes has been reported: H. C. Brown, V. K. Mahindroo, N. G. Bhat, B. Singaram, *J. Org. Chem.* **1991**, *56*, 1500.
[44] For a review on acetylenic sulfones, see: T. G. Back, *Tetrahedron* **2001**, *57*, 5263.
[45] Alkynylation with alkynyl phenyl sulfones such as non-1-ynyl phenyl sulfone and 3-methylbut-1-ynyl phenyl sulfone do not afford the desired products, because simple aliphatic chains are not able to orient the radical addition at the α-position of the sulfonyl group. However, such products are available from the reaction with the $Me_3Si$-substituted reagent **21**, followed by desilylation and by alkylation of the terminal acetylene derivative.
[46] Radical-mediated decarboxylative cyanation using tosyl cyanide has been reported: D. H. R. Barton, J. C. Jaszberenyi, E. A. Theodorakis, *Tetrahedron* **1992**, *48*, 2613.
[47] J.-M. Fang, M.-Y. Chen, *Tetrahedron Lett.* **1987**, *28*, 2853.
[48] S. Kim, H.-J. Song, *Synlett* **2002**, 2110.
[49] B. Becattini, C. Ollivier, P. Renaud, *Synlett* **2003**, 1485.


 © 2006 Wiley-VCH Verlag GmbH & Co. KGaA, Weinheim 

*Asymmetric Catalysis*

DOI: 10.1002/anie.200601742

# Enantioselective Oxidation of Olefins Catalyzed by a Chiral Bishydroxamic Acid Complex of Molybdenum**

*Allan U. Barlan, Arindrajit Basak, and Hisashi Yamamoto**

Since the first report of Sharpless's titanium tartrate catalyst,[1] a number of useful methods for asymmetric oxidation

[*] A. U. Barlan, Dr. A. Basak, Prof. Dr. H. Yamamoto
Department of Chemistry
University of Chicago
5735 South Ellis Avenue, Chicago, Illinois 60637 (USA)
Fax: (+1) 773-702-0805
E-mail: yamamoto@uchicago.edu

[**] Support for this research was provided by the SORST project of the Japan Science and Technology Agency (JST) and GAANN.

Supporting information for this article is available on the WWW under http://www.angewandte.org or from the author.


© 2006 Wiley-VCH Verlag GmbH & Co. KGaA, Weinheim
WILEY InterScience DISCOVER SOMETHING GREAT

have been developed. Among these, the most practical method utilizes manganese–*N*,*N*'-bis(salicylidene)ethylenediamine dianion (Mn–salen) mediated epoxidation of alkenes (Jacobsen–Katsuki epoxidation). However, the application of the manganese–salen catalyst is limited by the requirement of a low reaction temperature and the lack of selectivity observed during the epoxidation of *Z* olefins.[2] More recently, a metal-free oxidation of alkenes has also been reported, mediated by a fructose-derived, chiral dioxirane.[3] Although this method complements the selectivity for *trans*-alkene oxidation, it often requires high catalyst loading to obtain good yield.

Our continuing efforts to develop a simple method for asymmetric oxidation revealed that a chiral vanadium–hydroxamic acid complex with an achiral oxidant induced high enantioselectivity in the epoxidation of allylic alcohols.[4] The recently discovered bishydroxamic acid (BHA; **2**) was utilized as a ligand for the vanadium-catalyzed asymmetric epoxidation of *cis*-allylic alcohols and for the molybdenum-catalyzed asymmetric oxidation of sulfides and disulfides (Scheme 1).[5] In these previous studies, it was found that the

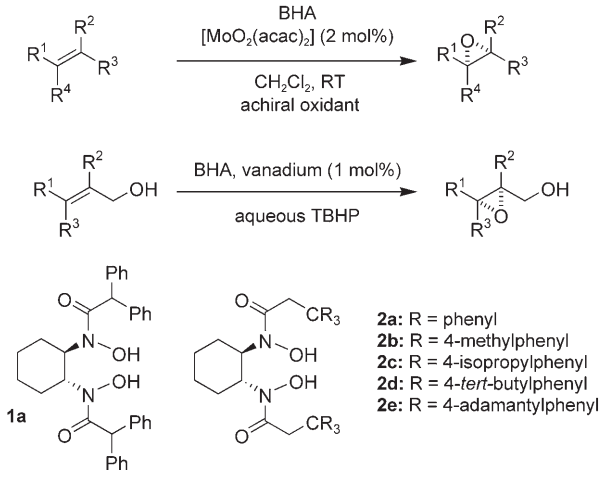


***Scheme 1.*** acac = acetylacetone.

epoxidation of geraniol with the molybdenum complex of **2a** in the presence of *tert*-butyl hydroperoxide (TBHP) provided a 1:1 mixture of 2,3-epoxygeraniol and 6,7-epoxygeraniol.[5a,6] These results suggested that a $Mo^{VI}$ complex of BHA in the presence of an organic hydroperoxide is a stronger oxidizing agent than the $V^{V}$ complex, and that the former does not require substrate metal coordination during the catalytic cycle.[7] This prompted us to explore the enantioselective oxidation of olefins with the Mo–BHA catalyst.

The use of molybdenum-peroxo complexes for the industrial-scale epoxidation of alkenes has been extensively explored over the last 40 years, beginning with homogeneous $Mo^{VI}$ catalysts in the Halcon and Arco processes.[8] Early reports of asymmetric epoxidation with a chiral molybdenum complex include the use of a stoichiometric molybdenum–(*S*)-lactic acid piperidineamide system by Schurig, Kagan and co-workers.[9] Consequently, considerable effort has been directed towards the development of enantioselective epoxidation protocols in which chiral molybdenum catalysts are used.[10,11] However, weak coordination of ligands with the molybdenum has resulted in very little success having been achieved. To this end, the Mo–BHA system has several advantages: 1) molybdenum is less toxic than manganese,[12] 2) in the ease of preparation of the Mo–BHA complex relative to other catalysts, (3) the ambient reaction temperature and the high stability of our catalyst system in air, and 4) the simple aqueous work-up needed to remove any metal residues as BHA acts as a metal scavenger.[13] Herein, we report a successful Mo–BHA catalyzed asymmetric oxidation of mono-, di-, and trisubstituted olefins under mild conditions to give epoxides in high yields and excellent selectivity.

In early experiments of the epoxidation of olefin **3a**, we found that ligand **2a** provided a higher selectivity than ligand **1a** in the presence of aqueous TBHP (Table 1, entries 1 and

***Table 1:*** Effect of the achiral oxidant and ligand.[a]

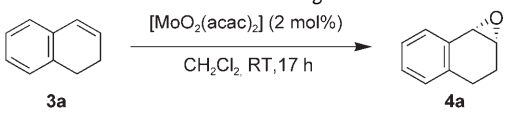


**3a** **4a**

| Entry | Oxidant | Ligand | Yield [%][b] | *ee* [%][c] |
|---|---|---|---|---|
| 1 | TBHP(aq) | **1a** | 20 | 28 |
| 2 | TBHP(aq) | **2a** | 15 | 42 |
| 3 | CHP | **2a** | 72 | 66 |
| 4 | THP | **2a** | 27 | 96 |
| 5 | CHP | **2c** | 92 | 80 |
| 6 | CHP | **2d** | 82 | 87 |

[a] All reactions were carried out in $CH_2Cl_2$ in the presence of 1.5 equiv of oxidant and 2 mol% of molybdenum catalyst at RT in air unless otherwise indicated. [b] Yield of isolated product after chromatographic purification. [c] Determined by chiral HPLC or GC.

2). Changing the oxidant to cumene hydroperoxide (CHP) or tritylhydroperoxide (THP) did improve the selectivity, but reactivity was lower when bulkier THP was utilized. Furthermore, oxidation of **3a** with bulkier ligands (**2b**–**2d**) or a bulkier oxidant provided good to excellent selectivity (entries 4–6). It is noteworthy that oxidation of **3a** with vanadium complex of **2a** under similar reaction conditions was very slow, and only a small amount of epoxide (< 5%) was detected.

We examined the scope of the reaction under optimized conditions. In all cases, epoxidation with the Mo–BHA catalyst in the presence of a cooxidant proceeded smoothly in air at room temperature. More notably, the size of ligands and the number of alkene substituents play a crucial role in determining the rate of the oxidation. As illustrated in Table 2, all the *cis*-substituted olefins gave excellent selectivity during oxidation (entries 1–4). It is noteworthy that the epoxidation of **3c** generated only *cis* product; no *trans* product was detected (entry 3). Trisubstituted and terminal alkenes also provided good selectivity (entries 6–8, 10 and 11). Another important aspect of this Mo–BHA catalyst is that it selectively oxidizes the most electron-rich alkene in the presence of multiple double bonds (entries 12 and 13).

 © 2006 Wiley-VCH Verlag GmbH & Co. KGaA, Weinheim 

***Table 2:*** Oxidation of olefins with different substitution patterns.[a]

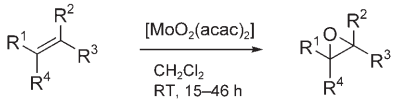


**3a–n** **4a–n**

| Entry | Epoxide | Ligand | Oxidant | *t* [h] | Yield [%][b] | *ee* [%][c] (Config)[d] |
|---|---|---|---|---|---|---|
| 1 | 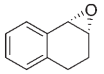 | **2c** | THP | 18 | 98 | 95 (*S*,*R*) |
| 2 | 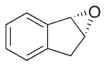 | **2b** | THP | 20 | 94 | 92 (*S*,*R*) |
| 3 | 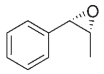 | **2c** | THP | 20 | 60 | 90 (*S*,*R*) |
| 4 | 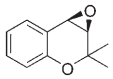 | **2d** | TBHP | 20 | 92 | 96 (*R*,*R*) |
| 5 | | **2d** | CHP | 22 | 77 | 64 (*R*,*S*) |
| 6 | 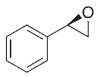 | **2d** | CHP | 40 | 95 | 85 (*R*) |
| 7 | 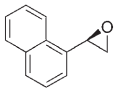 | **2d** | CHP | 36 | 84 | 82 (*R*) |
| 8 | 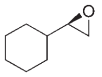 | **2d** | CHP | 40 | 95 | 85 (*R*) |
| 9 | | **2d** | CHP | 40 | 92 | 50 (*R*) |
| 10 | 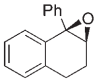 | **2d** | TBHP | 36 | 44 | 62 (*R*,*S*) |
| 11 | | **2d** | CHP | 36 | 92 | 85 (*S*,*S*) |
| 12 | 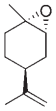 | **2d** | CHP | 46 | 94 | 66% *de* *trans*/*cis* |
| 13 | 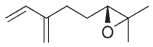 | **2e** | CHP | 42 | 82 | 76 (*R*) |

[a] All reactions were carried out in $CH_2Cl_2$ in the presence of 1.5 equiv of oxidant and 2 mol% of molybdenum catalyst at RT unless otherwise indicated. [b] Yield of isolated product after chromatographic purification. [c] Determined by chiral HPLC or GC. [d] Configurations determined by comparison of the specific rotation to literature values.

Encouraged by the selectivity observed during the oxidation of myrcene (**3m**), squalene (**3n**), an important biogenetic precursor of steroids and polycyclic terpenoids, was subjected to similar reaction conditions (Scheme 2).[14] To our delight, the use of the Mo complex of **2e** in the presence of one equivalent of CHP selectively provided 2,3-epoxysqualene with good enantioselectivity (76% *ee*). It is noteworthy that the synthesis of **4n** often requires multiple steps.

We believe that the mechanism follows the concerted metal alkylperoxide mechanism supported by Sharpless.[15] The Mo–BHA complex combines with the achiral oxidant to oxidize the olefin in a concerted fashion by transfer of oxygen from the metal peroxide to the olefin. We are currently trying to elucidate the mechanism.

In conclusion, we have developed a catalytic asymmetric oxidation of mono-, di-, and trisubstituted olefins using chiral molybdenum catalysts in air at room temperature to obtain good to excellent selectivity. This method advances the use and application of molybdenum-catalyzed asymmetric oxidation of olefins.

## *Experimental Section*

Representative experimental procedure: $[MoO_2(acac)_2]$ (6.5 mg, 0.02 mmol) was added to a solution of BHA (0.022 mmol) in $CH_2Cl_2$ (1 mL), and the mixture stirred for 1 h at RT. Olefin **3a** (1.0 mmol) and alkyl hydroperoxide (1.5 mmol) were added to the resulting solution and stirring continued at the same temperature for 18 h. The oxidation was monitored by TLC. Saturated aqueous $Na_2SO_3$ was then added and the mixture stirred for 30 min at RT. The mixture was extracted with $CH_2Cl_2$, dried over $Na_2SO_4$, and concentrated under reduced pressure. The remaining residue was purified by flash column chromatography on silica gel to provide epoxide **4a**. Determination of the *ee* values of the epoxides is provided in the Supporting Information.

Received: May 3, 2006
Published online: July 28, 2006

**Keywords:** alkenes · asymmetric catalysis · enantioselectivity · epoxidation · molybdenum

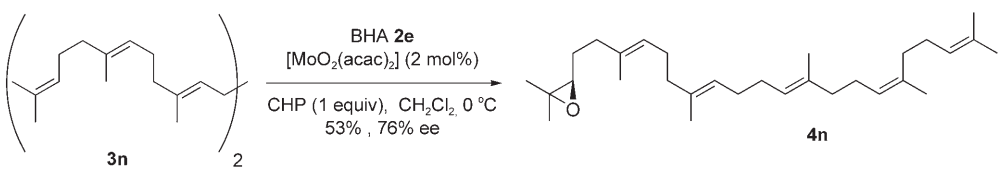


***Scheme 2.*** Regio- and enantioselective oxidation of squalene.

 © 2006 Wiley-VCH Verlag GmbH & Co. KGaA, Weinheim 

[1] a) K. Jorgensen, *Chem. Rev.* **1989**, *89*, 431; b) C. Bonini, R. Giuliana, *Tetrahedron* **2002**, *58*, 4981; c) T. Katsuki, E. N. Jacobsen, M. H. Wu in *Comprehensive Asymmetric Catalysis I–III* (Eds.: E. N. Jacobsen, A. Pfaltz, H. Yamamoto), Springer, Berlin, **1999**, pp. 621–678; d) I. Ojima, *Catal. Asymmetric Synthesis*, Wiley-VCH, New York, **2000**, pp. 231–325; e) H. Adolfsson in *Modern Oxidation Methods* (Eds.: J. E. Backvall), Wiley-VCH, Weinheim, **2004**, pp. 21–49; f) T. Katsuki, *J. Am. Chem. Soc.* **1980**, *102*, 5974.

[2] a) R. Irie, K. Noda, Y. Ito, N. Matsumoto, T. Katsuki, *Tetrahedron Lett.* **1990**, *31*, 7345; b) W. Zhang, J. L. Loebach, S. R. Wilson, E. N. Jacobsen, *J. Am. Chem. Soc.* **1990**, *112*, 2801.

[3] a) Y. Shi, *Acc. Chem. Res.* **2004**, *37*, 3435; b) M. Hickey, D. Goeddel, Z. Crane, Y. Shi, *Proc. Natl. Acad. Sci. USA* **2004**, *101*, 5794.

[4] a) Y. Hoshino, H. Yamamoto, *J. Org. Chem.* **1999**, *64*, 338; b) Y. Hoshino, N. Murase, M. Oishi, H. Yamamoto, *Bull. Chem. Soc. Jpn.* **2000**, *73*, 1653; c) Y. Hoshino, H. Yamamoto, *J. Am. Chem. Soc.* **2000**, *122*, 10452.

[5] a) W. Zhang, A. Basak, Y. Kosugi, Y. Hoshino, H. Yamamoto, *Angew. Chem.* **2005**, *117*, 4463; *Angew. Chem. Int. Ed.* **2005**, *44*, 4389; b) A. Basak, A. Barlan, H. Yamamoto, *Tetrahedron: Asymmetry* **2006**, *17*, 508.

[6] The vanadium–**2a** complex in the presence of TBHP selectively oxidized geraniol to generate 2,3-epoxygeraniol.

[7] O. Bortolini, S. Campestrini, E. Furia, G. Modena, *J. Org. Chem.* **1987**, *52*, 5093.

[8] a) M. N. Sheng, G. J. Zajaczek (ARCO), GB 1.136.923, **1968**; b) J. Kolar (Halcon), US 3.350.422, US 3.351.635, **1967**.

[9] V. Schurig, K. Hintzer, U. Leyrer, C. Mark, P. Pitchen, H. Kagan, *J. Organomet. Chem.* **1989**, *370*, 81.

[10] a) S. Yamada, T. Mashiko, S. Tershima, *J. Am. Chem. Soc.* **1977**, *99*, 1988; b) R. C. Michaelson, R. E. Palermo, K. B. Sharpless, *J. Am. Chem. Soc.* **1977**, *99*, 1990; c) F. Kuhn, J. Zhao, W. A. Herrmann, *Tetrahedron: Asymmetry* **2005**, *16*, 3469, and references therein.

[11] a) K. Ambroziak, R. Peloch, E. Milchert, T. Dziemboska, Z. Rozwadowski, *J. Mol. Catal. A* **2004**, *211*, 9; b) M. Masteri-Farahani, F. Farzaneh, M. Ghandhi, *J. Mol. Catal. A* **2003**, *192*, 103; c) S. Kotov, T. Kolev, M. Georgrieva, *J. Mol. Catal. A* **2003**, *195*, 83; d) I. Gonclaves, A. Santos, C. Romao, A. Lopes, J. Rodriguez-Borges, M. Pillinger, P. Ferriera, J. Rocha, R. Kuhn, *J. Organomet. Chem.* **2001**, *626*, 1; e) X. Wang, H. Shi, C. Sun, Z. Zhang, *Tetrahedron* **2004**, *60*, 10993; f) J. Fridgen, W. A. Herrmann, G. Eickerling, A. Santos, F. Kuhn, *J. Organomet. Chem.* **2004**, *689*, 2752.

[12] OSHA recommends exposure to Mo to be 15 $mg\,m^{-3}$ versus 5 $mg\,m^{-3}$ of Mn.

[13] H. Yale, *Chem. Rev.* **1943**, *43*, 209.

[14] a) S. Raina, V. Singh, *Tetrahedron* **1995**, *51*, 2467; b) E. J. Corey, M. Noe, W. Shieh, *Tetrahedron Lett.* **1993**, *34*, 5995.

[15] a) D. Deubal, J. Sundermeyer, G. Frenking, *J. Am. Chem. Soc.* **2000**, *122*, 10101; b) D. Deubal, J. Sundermeyer, G. Frenking, *Eur. J. Inorg. Chem.* **2001**, 1819; c) I. Yadanov, C. Valentin, P. Gisdakis, N. Rosch, *J. Mol. Catal. A* **2000**, *158*, 189; d) H. Mimoun, *Angew. Chem.* **1982**, *94*, 750; *Angew. Chem. Int. Ed. Engl.* **1982**, *21*, 734; e) D. Deubal, G. Frenking, P. Gisdakis, W. A. Herrmann, N. Rosch, J. Sundermeyer, *Acc. Chem. Res.* **2004**, *37*, 645; f) K. B. Sharpless, J. M. Townsend, D. R. Williams, *J. Am. Chem. Soc.* **1972**, *94*, 295.


 © 2006 Wiley-VCH Verlag GmbH & Co. KGaA, Weinheim 

Cross-Coupling

DOI: 10.1002/anie.200601887

# Pd-Catalyzed α-Arylation of Trimethylsilyl Enol Ethers with Aryl Bromides and Chlorides: A Synergistic Effect of Two Metal Fluorides as Additives**

*Weiping Su, Steven Raders, John G. Verkade,* Xuebin Liao, and John F. Hartwig**

Ketone enolates are among the most common nucleophiles in organic chemistry, and transition-metal-catalyzed cross-coup ling reactions are among the most commonly used catalytic processes.[1] However, the combination of these two chemistries—cross-coupling of enolate nucleophiles—has been developed only recently.[2–6] Moreover, coupling of silyl enol ethers, which temper the high basicity and nucleophilicity of alkali metal enolates,[7] is undeveloped.[8–11] The first example of the cross-coupling of silyl enol ethers was reported in 1982 by Kuwajima and Urabe, and the reactions of related tin enolates were reported by Kosugi and co-workers in 1984.[9] The reactions of silyl enol ethers were limited to the enolates of methyl ketones, and the activation of the silyl enol ether was conducted with stoichiometric tributyltin fluoride. Over the next twenty years, the scope and utility of the coupling of silyl or stannyl enol ethers has advanced only slightly.[10–12]

The cross-coupling of silyl enol ethers offers several advantages over the coupling of alkali-metal enolates of ketones. The reduced basicity should improve functional-group compatibility; the defined structure of the main-group enolate could allow coupling at the more hindered site of a ketone with two enolizable positions; and conditions for the coupling of silyl enol ethers could ultimately allow the development of enantioselective processes to form acidic tertiary stereocenters.

[*] Dr. W. Su,[+] S. Raders, Prof. Dr. J. G. Verkade
Department of Chemistry
Gilman Hall, Iowa State University
Ames, IA 50011 (USA)
Fax: (+1) 515-294-0105
E-mail: jverkade@iastate.edu

Dr. X. Liao, Prof. Dr. J. F. Hartwig
Department of Chemistry
Yale University, P.O. Box 208107
New Haven, CT 06520-8107 (USA)
Fax: (+1) 203-432-6144
E-mail: john.hartwig@yale.edu

[+] Current address:
Fujian Institute of Research on the Structure of Matter
Chinese Academy of Sciences
Fujian 350002 (P.R. China)

[**] J.G.V. gratefully acknowledges the National Science Foundation for financial support of this investigation, and J.F.H. thanks the NIH (NIGMS GM-58108). The authors thank Professor Robert Angelici for helpful discussions.

Supporting information for this article is available on the WWW under http://www.angewandte.org or from the author.


WILEY InterScience DISCOVER SOMETHING GREAT
© 2006 Wiley-VCH Verlag GmbH & Co. KGaA, Weinheim

We report two protocols for the coupling of several classes of ketones with aryl bromides catalyzed by palladium and P*t*Bu$_3$. These reactions are conducted in toluene as the solvent with a combination of tributyltin fluoride and cesium fluoride as additives, or in *N*,*N*-dimethylformamide (DMF) with a combination of cesium fluoride and zinc fluoride as additives. The success of these procedures, which tolerate a variety of electrophilic functionalities and allow arylations at the more hindered position of dialkyl ketones, results from a synergistic effect[13] of two fluoride activators.

One set of studies focused on the arylation of silyl enol ethers formed by the addition of Grignard regents to α,β-unsaturated ketones in the presence of CuBr·Me$_2$S, chlorotrimethylsilane, and hexamethylphosphoramide (HMPA; Scheme 1).[14] Studies of the model reaction of 2-trimethylsiloxy-4-phenyl-2-butene (**1**) with 1-bromo-4-*tert*-butylbenzene (**2**) were examined with a variety of additives, ligands, solvents, and palladium sources (Table 1). In the presence of catalytic amounts of Pd(OAc)$_2$ and P*t*Bu$_3$, the reaction between 1.2 equivalents of **1** with limiting **2** in toluene in the absence of an additive did not afford the desired product in appreciable amounts (entry 1). The same reactions conducted with added Bu$_3$SnF formed some arylated product, but the yields were poor (entry 2). These reactions with added CsF or ZnF$_2$ (entries 3 and 4) formed the product in low yield, and reactions conducted with the more soluble Me$_4$NF apparently caused only decomposition of silyl enol ether **1** (entry 6).

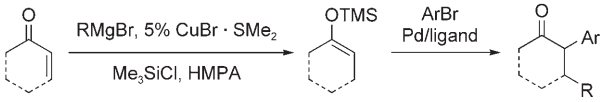


***Scheme 1.*** Two approaches to α-arylated carbonyl compounds.

***Table 1:*** Coupling of **1** with **2**.[a]

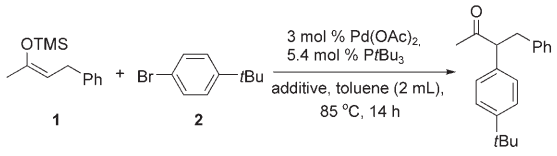


| Entry | Additive (equiv) | Ratio of **1**/**2** | Yield [%][b] |
|---|---|---|---|
| 1 | | 1.2:1 | 0 |
| 2 | Bu$_3$SnF (1.2) | 1.2:1 | 34 |
| 3 | CsF (1.2) | 1.2:1 | 18 |
| 4 | Bu$_3$SnF (1.2), CsF (1.2) | 1.2:1 | 81 |
| 5 | ZnF$_2$ (1.2) | 1.2:1 | 38[c] |
| 6 | Me$_4$NF (1.2) | 1.2:1 | 0 |
| 7 | Bu$_3$SnF (1.2), CsF (1.2) | 1:1.2 | 65 |
| 8 | Bu$_3$SnF (1.4), CsF (1.4) | 1.4:1 | 98 |
| 9 | Bu$_3$SnF (0.14), CsF (1.4) | 1.4:1 | 67 |
| 10 | CsF (1.4) | 1.4:1 | 81[d] |
| 11 | Bu$_3$SnF (1.4), CsF (1.4) | 1.4:1 | 93[d] |

[a] Reactions were run at 85 °C with 0.5 mmol **2** (0.25 M). [b] Yield of the isolated product (average of two runs). [c] DMF was used as the solvent. [d] THF was used as the solvent.

The reaction of 1.4 equivalents of **1** with **2** in THF containing CsF as the additive afforded the desired product in a high yield of 81% (entry 10), but the functional-group tolerance of reactions with CsF alone was similar to that of reactions of alkali-metal enolates. For example, reactions of **1** with 1-bromo-4-nitrobenzene and 4′-bromoacetophenone in THF afforded only 40 and 10% yields, respectively [Eq. (1)].

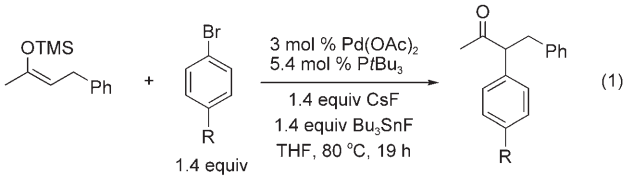


Values in parentheses are yields obtained without Bu$_3$SnF

R = NO$_2$; yield: 78% (40%)

R = COMe; yield 60% (10%)

In contrast, reactions conducted with a combination of Bu$_3$SnF and CsF as additives occurred in high yields (entry 4) and with a broad scope (see below). Reactions conducted with a catalytic amount of Bu$_3$SnF (10 mol% based on the silyl enol ether) and 1 equivalent of CsF afforded the desired product in 67% yield (entry 9). Altering the ligand, palladium precursor, and solvent did not further improve the reaction (reactions in toluene and THF occurred in comparable yields), but increasing the amount of the silyl enol ether and additive (1.4:1.4:1.4:1 ratio of the two additives, enol **1**, and aryl halide **2**) led to formation of the coupled product in 98% yield (entry 8).

Table 2 illustrates the scope of the reactions under the conditions of entry 8 in Table 1 with Bu$_3$SnF and CsF as the additives. Both acyclic and cyclic silyl enol ethers smoothly underwent coupling at 85–90 °C with a wide variety of aryl bromides and chlorides to form α-arylated ketones in good-to-excellent yields. These weakly basic conditions were compatible with ester, nitro, cyano, and keto substituents. Both sterically hindered aryl bromides and heterocyclic aryl bromides, such as 3-bromothiophene, served as coupling partners.

The coupling between a vinyl bromide and a silyl enol ether under these conditions was tested briefly [Eq. (2)].[15] The combination of 3 mol% Pd(OAc)$_2$ and 5.4 mol% P*t*Bu$_3$ catalyzed the coupling of α-bromostyrene with **1** in THF in the presence of 1.4 equivalents of CsF and 0.7 equivalents of Bu$_3$SnF (based on the amount of silyl enol ether) in 66% yield.

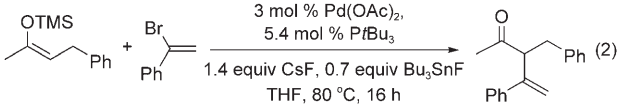


Considering the stoichiometric amounts of tin reagent in the couplings of Table 2 and the toxicity of tin, other combinations of metal fluorides were examined to promote the couplings of silyl enol ethers. One of us recently reported

 © 2006 Wiley-VCH Verlag GmbH & Co. KGaA, Weinheim 

***Table 2:*** Scope of the arylation of a trimethylsilyl enol ether.[a]

| Entry | Silyl enol ether | Halide | Products | Yield [%][b] |
|---|---|---|---|---|
| 1 | 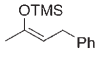 | 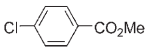 | 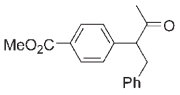 | 89[c] |
| 2 | 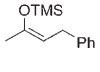 | 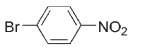 | 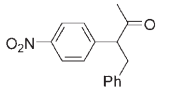 | 84 |
| 3 | 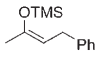 | 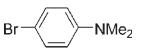 | 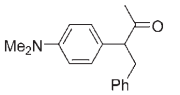 | 96 |
| 4 | 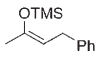 | 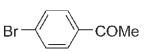 | 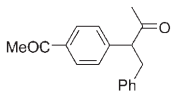 | 97 |
| 5 | 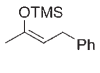 | | 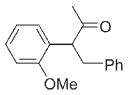 | 97 |
| 6 | 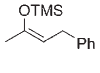 | | 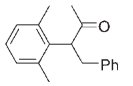 | 93 |
| 7 | 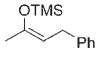 | 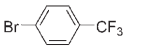 | 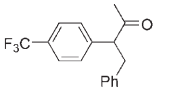 | 91 |
| 8 | 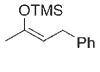 | 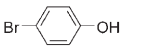 | 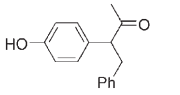 | 55 |
| 9 | 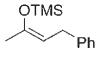 | 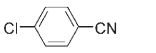 | 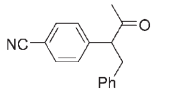 | 80[c] |
| 10 | 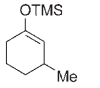 | 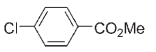 | 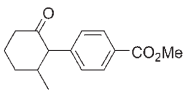 | 80[c] |
| 11 | 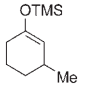 | 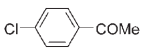 | 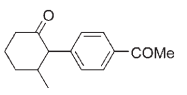 | 70[c] |
| 12 | 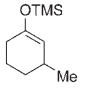 | 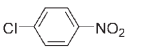 | 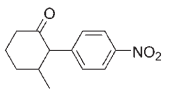 | 84 |
| 13 | 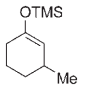 | 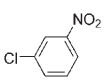 | 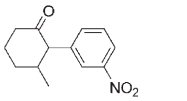 | 77[c] |
| 14 | 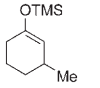 | | 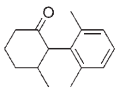 | 85 |
| 15 | 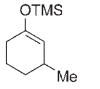 | | 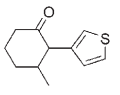 | 78 |

[a] Reactions were run under the conditions of entry 8 in Table 1 for 12–20 h. [b] Yield of the isolated product (average of two runs). [c] Reaction run at 90 °C.

that the combination of CsF and $ZnF_2$ promotes the asymmetric iridium-catalyzed allylation of silyl enol ethers with allylic carbonates.[16] Thus, we investigated the combination of $ZnF_2$ with other metal fluorides as promoters for the palladium-catalyzed coupling of silyl enol ethers with bromoarenes.

The results of experiments to develop reaction conditions with the metal fluoride additives are provided in the Supporting Information. Experiments on the coupling of **1** with 4-bromoacetophenone showed that conditions could be developed for the coupling of silyl enol ethers with aryl bromides in high yield and in the presence of the combination of stoichiometric amounts of $ZnF_2$ and either CsF or $MnF_2$ as additives. These reactions occurred in much higher yield in the polar DMF than the less polar toluene and with $[Pd(dba)_2]$ (dba = dibenzylideneacetone) as the precursor than $Pd(OAc)_2$. Reactions carried out in DMF with $[Pd(dba)_2]$ and $PtBu_3$ as the catalyst with stoichiometric amounts of $ZnF_2$ and CsF occurred in lower yields than reactions with stoichiometric amounts of $ZnF_2$ and 0.4 equivalents of CsF. Reactions with stoichiometric $ZnF_2$ and substoichiometric CsF as additives occurred with high functional-group tolerance (see below). However, this combination of metal fluorides led to diarylation of the silyl enol ethers of methyl ketones. Selective monoarylation of silyl enol ethers of ketones was achieved instead when the reactions were carried out with the combination of $ZnF_2$ and $MnF_2$ as additives.

Several examples of the $[Pd(dba)_2]/PtBu_3$-catalyzed reactions of silyl enol ethers promoted by catalytic CsF or $MnF_2$ and stoichiometric $ZnF_2$ are shown in Table 3. Most generally, these data illustrate the same two beneficial effects of conducting the coupling of silyl enol ethers in the presence of these fluoride activators, as was observed from the use of $Bu_3SnF$ and CsF as additives: The product from the reaction of the silyl enol ether 2-siloxy-1-butene was formed by monoarylation of the methyl group with aryl halides that contained functionalities intolerant of the basic conditions of the couplings of alkali-metal enolates, and reactions of the more substituted silyl enol ethers of an alkyl ketone regioselectively formed the product from arylation at the more hindered enolizable position.

The first two examples (Table 3, entries 1 and 2) show that similar yields for reactions of electron-neutral and *ortho*-substituted bromoarenes are obtained for reactions containing tin fluoride as an additive. Entries 3 and 4 show that these conditions allow the coupling of bromoarenes with functionalities that are not tolerated by the basic alkali-metal enolates. Hydrolysis of the silyl enol ether during the reaction of bromophenol did limit the yield of entry 4, but substantial quantities of coupled product were formed. Entries 5–7 show examples of the selective monoarylation of the silyl enol ether of 4-phenyl-2-butanone with bromoarenes that are intolerant of alkali-metal enolates. Finally, entry 8 (Table 3) shows the first coupling of an enolate of acetone without tin reagents. Diarylation to form 1,1-diphenylacetone competed with the monoarylation in this case, but the use of excess silyl enol ether led to the formation of α-aryl acetone in good yield.

In summary, the combination of two metal fluorides synergistically promotes the coupling of silyl enol ethers with aryl bromides and chlorides. Two procedures are presented, each with certain advantages: reactions containing CsF and tributyltin fluoride occur in nonpolar solvents, whereas the reactions containing either $ZnF_2/MnF_2$ or $ZnF_2$/CsF occur

 © 2006 Wiley-VCH Verlag GmbH & Co. KGaA, Weinheim 

***Table 3:*** Scope of the palladium-catalyzed arylation of trimethylsilyl enol ethers in the presence of $ZnF_2$ and CsF or $MnF_2$.

| Entry | Silyl enol ether | Halide | Product | Yield [%] |
|---|---|---|---|---|
| 1 | | 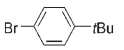 | 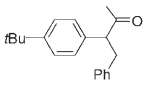 | 89[a] |
| 2 | | | 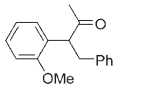 | 87[a] |
| 3 | | 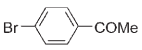 | 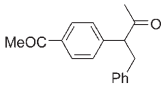 | 90[a] |
| 4 | | 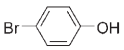 | 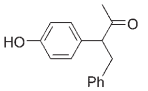 | 53[a] |
| 5 | | 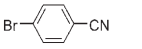 | 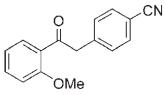 | 78[b] |
| 6 | | 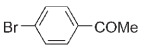 | 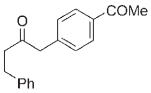 | 71[b,c] |
| 7 | | 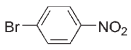 | 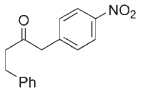 | 64[d,e] |
| 8 | | | | 68[f,g] |

[a] Reaction conditions: aryl halide (1.0 equiv), silyl enol ether (1.4 equiv), zinc fluoride (1.4 equiv), cesium fluoride (0.4 equiv), [Pd(dba)$_2$] (3 mol%), and P*t*Bu$_3$ (5.4 mol%), 85°C; DMF (1 mL) was added per 0.2 mmol of aryl halide. [b] Reaction conditions: aryl halide (1.0 equiv), silyl enol ether (1.5 equiv), zinc fluoride (1.0 equiv), manganese fluoride (0.4 equiv), [Pd(dba)$_2$] (2 mol%), and P*t*Bu$_3$ (4 mol%), 70°C; DMF (1 mL) was added per 0.2 mmol of aryl halide. [c] The ratio of mono/diarylation was 5.5:1. [d] Reaction conditions: aryl halide (1.0 equiv), silyl enol ether (1.5 equiv), zinc fluoride (1.4 equiv), manganese fluoride (1.4 equiv), [Pd(dba)$_2$] (3 mol%), and P*t*Bu$_3$ (5.4 mol%), 60°C; DMF (1 mL) was added per 0.2 mmol of aryl halide. [e] The ratio of mono/diarylation was 4:1. [f] Reaction conditions: aryl halide (1.0 equiv), silyl enol ether (5.0 equiv), zinc fluoride (1.4 equiv), manganese fluoride (1.4 equiv), [Pd(dba)$_2$] (3 mol%), and P*t*Bu$_3$ (5.4 mol%), 70°C; DMF (2 mL) was added per 0.2 mmol of aryl halide. [g] The ratio of mono/diarylation was 5.5:1.

without tin. All the reactions appear to occur without cleavage to form alkali-metal enolates, thus providing a mild and selective methodology for the preparation of α-aryl ketones. Studies to determine the origin of the synergistic effect, which remains unclear at this time, will be the subject of future studies.

Received: May 12, 2006
Published online: July 17, 2006

[1] a) A. de Meijere, F. Diederich, *Metal-Catalyzed Cross-Coupling Reactions*, Wiley-VCH, Weinheim, **2004**; b) E. Negishi, *Handbook of Organopalladium Chemistry for Organic Synthesis*, Wiley, Hoboken, **2002**.
[2] a) D. Culkin, J. F. Hartwig, *Acc. Chem. Res.* **2003**, *36*, 234; b) M. Miura, M. Nomura, *Top. Curr. Chem.* **2002**, *219*, 211.
[3] a) M. Palucki, S. L. Buchwald, *J. Am. Chem. Soc.* **1997**, *119*, 11108; b) B. C. Hamann, J. F. Hartwig, *J. Am. Chem. Soc.* **1997**, *119*, 12382; c) M. Kawatsura, J. F. Hartwig, *J. Am. Chem. Soc.* **1999**, *121*, 1473; d) J. M. Fox, X. H. Huang, A. Chieffi, S. L. Buchwald, *J. Am. Chem. Soc.* **2000**, *122*, 1360; e) T. Satoh, Y. Kawamura, M. Miura, M. Nomura, *Angew. Chem.* **1997**, *109*, 1820; *Angew. Chem. Int. Ed. Engl.* **1997**, *36*, 1740; f) J. L. Rutherford, M. P. Rainka, S. L. Buchwald, *J. Am. Chem. Soc.* **2002**, *124*, 15168; g) M. S. Viciu, R. F. Germaneau, S. P. Nolan, *Org. Lett.* **2002**, *4*, 4053; h) D. Solé, L. Vallverdú, X. Solans, M. Font-Bardia, J. Bonjoch, *J. Am. Chem. Soc.* **2003**, *125*, 1587; i) A. Ehrentraut, A. Zapf, M. Beller, *Adv. Synth. Catal.* **2002**, *344*, 209; j) T. Satoh, Y. Kametani, Y. Terao, M. Miura, M Nomura, *Tetrahedron Lett.* **1999**, *40*, 5345; k) Y. Terao, Y. Kametani, H. Wahui, T. Satoh, M. Miura, M Momura, *Tetrahedron* **2001**, *57*, 5967.
[4] a) M. Jørgensen, S. Lee, X. Liu, J. P. Wolkowski, J. F. Hartwig, *J. Am. Chem. Soc.* **2002**, *124*, 12557; b) W. A. Moradi, S. L. Buchwald, *J. Am. Chem. Soc.* **2001**, *123*, 7996; c) S. Lee, N. A. Beare, J. F. Hartwig, *J. Am. Chem. Soc.* **2001**, *123*, 8410.
[5] a) N. A. Beare, J. F. Hartwig, *J. Org. Chem.* **2002**, *67*, 541; b) S. Lee, J. F. Hartwig, *J. Org. Chem.* **2001**, *66*, 3402; c) J. Cossy, A. Filippis, D. G. Pardo, *Org. Lett.* **2003**, *5*, 3037.
[6] T. Hamada, A. Chieffi, J. Ahman, S. L. Buchwald, *J. Am. Chem. Soc.* **2002**, *124*, 1261.
[7] I. Fleming, A. Barbero, D. Walter, *Chem. Rev.* **1997**, *97*, 2063.
[8] I. Kuwajima, H. Urabe, *J. Am. Chem. Soc.* **1982**, *104*, 6831.
[9] M. Kosugi, I. Hagiwara, T. Sumiya, T. Migita, *Bull. Chem. Soc. Jpn.* **1984**, *57*, 242.
[10] For a recent coupling of a diphenyl bisenol ether, see: J. Chae, J. Yun, S. L. Buchwald, *Org. Lett.* **2004**, *6*, 4809.
[11] For coupling of silyl ketene acetals, see: a) T. Hama, X. Liu, D. A. Culkin, J. F. Hartwig, *J. Am. Chem. Soc.* **2003**, *125*, 11176; b) X. Liu, J. F. Hartwig, *J. Am. Chem. Soc.* **2004**, *126*, 5182.
[12] For activation of silyl ketene acetals of an acetate, see: F. Agnelli, G. A. Sulikowski, *Tetrahedron Lett.* **1998**, *39*, 8807.
[13] A synergistic effect of the combination of CsF and CuI as additives has been observed in the promotion of Stille coupling reactions; see: S. P. H. Mee, V. Lee, J. E. Baldwin, *Angew. Chem.* **2004**, *116*, 1152; *Angew. Chem. Int. Ed.* **2004**, *43*, 1132.
[14] S. Matsuzawa, Y. Horiguchi, E. Nakamura, I. Kuwajima, *Tetrahedron* **1989**, *45*, 349.
[15] For the palladium-catalyzed intermolecular vinylation of ketones, see: Ref. [6]; A. Chieffi, K. Kamikawa, J. Ahman, J. M. Fox, S. L. Buchwald, *Org. Lett.* **2001**, *3*, 1897; for the palladium-catalyzed intramolecular vinylation of ketones, see: a) T. Wang, J. M. Cook, *Org Lett.* **2000**, 2057; b) D. Solé, E. Peidró, J. Bonjoch, *Org. Lett.* **2000**, *2*, 2225; c) D. Solé, F. Diaba, J. Bonjoch, *J. Org. Chem.* **2003**, *68*, 5746; d) D. Solé, X. Urbaneja, J. Bonjoch, *Adv. Synth. Catal.* **2004**, *346*, 1646.
[16] T. Graening, J. F. Hartwig, *J. Am. Chem. Soc.* **2005**, *127*, 17192.

**Keywords:** additives · cross-coupling · enolates · fluorine · palladium

 © 2006 Wiley-VCH Verlag GmbH & Co. KGaA, Weinheim 

Conformational Switching

DOI: 10.1002/anie.200602057

# Guest-Induced Conformational Switching in a Single Crystal**

*Liliana Dobrzańska, Gareth O. Lloyd, Catharine Esterhuysen, and Leonard J. Barbour**

One of the defining characteristics of the crystalline state is that atoms are generally considered to be frozen in place, each with only a modest ability to vibrate about its well-defined equilibrium position. Although solid-to-solid phase transformations as a result of a variety of physical or chemical factors are well known, it is rare for individual crystals to survive such processes by retaining their mosaicity.[1] Considerable mechanical stress is thought to occur at the boundary of two interconverting phases,[1a] particularly if the two phases are incompatible in packing periodicity. Therefore, in order for a crystal to maintain its monocrystallinity during transformation, it seems reasonable either that the structural changes to the principal framework must be insignificant, or that the molecules must cooperate[1d,2] in a concerted fashion as they undergo positional and/or topological reorganization. In this regard, a number of recent reports have advocated the phenomenon of cooperativity in order to account for the apparent fluidity of crystalline building blocks during the uptake or release of solvent molecules, with concomitant rearrangement of the host lattice as a single-crystal transformation.[1d,2,3] These studies have involved relatively small changes of molecular conformation in systems possessing conceptually infinite rigid assemblies.[1b–g,2–4] Furthermore, these reports describe structural switching between only two states.

Crystal engineering[5] encompasses both the "synthesis" and modification of structures. In recent years, the principles of this burgeoning field have been applied vigorously to the design of new porous functional materials[6] with a view to mimicking and even surpassing the important properties of zeolites.[7] Targeted applications include catalysis,[8] as well as the storage,[9] separation,[10] and sensing[1a,11] of molecules. To date, most studies have focused on so-called "soft materials" (that is, organic[1d,10b,12] or metal–organic[1b,c,g,2,3,4b–e] systems), owing to their vast potential for structural diversity.

A common strategy for engineering porous crystals is to first prepare a solvent-templated structure and then to extract the solvent molecules without causing collapse of the resulting metastable apohost framework. Desolvation of molecular (that is, 0D) solids generally results in reorganization of the host molecules into a densely packed nonporous phase,[13] whereas metal–organic frameworks (MOFs) have been shown to maintain structural integrity because of their intrinsic long-range rigidity.[6a] Nevertheless, some MOFs undergo structural modifications in one or more of the following forms: 1) lateral sliding of neighboring layers relative to one another,[3,4d] 2) adjustment of the interlayer spacing,[1b] 3) distortion of 2D or 3D grids,[1b,14] and 4) conformational changes of their components.[4b] In several recently reported cases where such structural changes have been observed, MOF crystals have been shown to retain their macroscopic integrity.[1b,c,g,3,4c,d]

Although useful for characterization of the different phases by means of powerful diffraction techniques, single crystals are generally not required for applications such as catalysis, storage, and separation. On the other hand, if an engineered crystal is to be incorporated into a device such as a substrate-triggered sensor, fully reversible phase transformations with retention of monocrystallinity would be essential for repeated operation. It is therefore of considerable importance to study the processes that govern cooperative fluidity in dynamic crystals with a view to gaining better insight into the fascinating phenomenon of single-crystal transformations.

Our approach to producing porous crystals involves the use of discrete "donut-shaped" dinuclear metal–organic complexes[15] that cannot pack efficiently owing to their lack of self-complementarity in shape.[16] When crystallized from a suitable solvent, these complexes usually enclose appropriate solvent molecules into their apertures. Desolvation necessarily results in the formation of voids or channels if the host complexes retain their shape. As part of our ongoing studies, crystals composed of neutral molecular rectangles were obtained by slow evaporation of an equimolar solution of 1,4-bis[(2-methylimidazol-1-yl)methyl]benzene (L) and $CuCl_2 \cdot 2H_2O$ in acetone (Scheme 1). A single-crystal X-ray diffraction analysis revealed that the coordination geometry about each copper ion is tetrahedrally distorted square-planar. Discrete metallacyclic complexes are eclipsed and stacked parallel to the crystallographic *a* axis to form

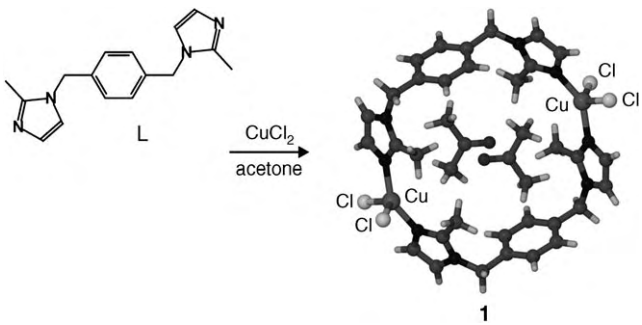


***Scheme 1.*** Formation of $[Cu_2Cl_4L_2] \cdot 2(CH_3)_2CO$ (**1**); N black.

[*] Dr. L. Dobrzańska, G. O. Lloyd, Dr. C. Esterhuysen, Prof. L. J. Barbour
Department of Chemistry
University of Stellenbosch
7602 Matieland (South Africa)
Fax: (+27) 21-808-3849
E-mail: ljb@sun.ac.za

[**] We acknowledge financial support from the National Research Foundation (South Africa) and L.D. thanks the Claude Harris Leon Foundation for a postdoctoral fellowship.

Supporting Information for this article is available on the WWW under http://www.angewandte.org or from the author.


InterScience
© 2006 Wiley-VCH Verlag GmbH & Co. KGaA, Weinheim

conceptually infinite tubules (see Supporting Information). The resulting channels are occupied by occluded acetone molecules, such that each dinuclear complex enshrouds two molecules (see **1** in Figure 1) to form an efficiently packed binary structure. The acetone templating effect in **1** is inferred from the presence of weak C–H···O hydrogen bonds between the ligand methyl groups and the solvent carbonyl oxygen atoms.

Thermogravimetric analysis shows that desolvation (that is, loss of acetone) occurs at room temperature. Our attempts to obtain a porous material by desolvation involved either heating crystals at 70 °C for approximately one hour or exposing them to high vacuum for three hours. During desolvation of **1** by either method, the crystals remained transparent, although their color transformed from light brown to light green. No fracturing was evident and it was therefore possible to determine the structure of the desolvated phase (**2**) by single-crystal X-ray diffraction analysis. In contrast to our previous findings involving analogous dinuclear complexes,[16] the host molecules in **2** undergo significant conformational changes as a result of desolvation and reorganization. The molecular rectangles collapse to assume an "imploded" conformation (Figure 1) with loss of the guest-templated aperture. Implosion of the complex occurs by means of elongation of the intramolecular Cu···Cu distance from 10.2 Å in **1** to 13.3 Å in **2**, with corresponding adjustment of the N-Cu-N angles from 147.2 to 90.1°. Loss of the molecular aperture, in conjunction with spatial rearrangement of the conformationally altered host molecules, results in shrinkage of the crystal volume by approximately 17 %.

Upon exposure of **2** to acetone vapor for 2.5 h, the crystals reversibly transformed back to phase **1** with stoichiometric uptake of the solvent. Once again the bulk integrity of each individual crystal was maintained (as confirmed by successful single-crystal X-ray diffraction analysis) and the color reverted back to light brown. In a subsequent experiment, exposure of **2** to acetonitrile vapor for several minutes resulted in a change in color to red, again with no apparent fracturing of the individual crystals. Single-crystal X-ray diffraction analysis revealed that a third phase (**3**, Figure 1) is formed upon stoichiometric uptake of acetonitrile. The host complex reconforms to once again yield a rectangular complex that enshrouds two molecules of acetonitrile. The packing mode is similar to that observed for **1**. However, examination of the complex in **3** reveals that, although metrically similar to that in **1**, the conformation of the bridging ligands is quite different, especially with regard to the relative positions of the methyl substituents of the imidazole groups (Figure 2).

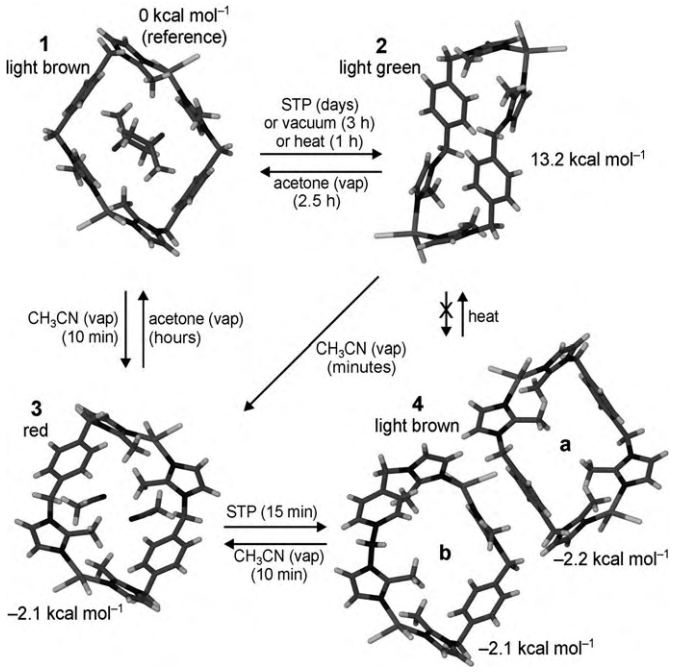


***Figure 1.*** Capped-stick projections of the molecules in phases **1** to **4** viewed along [100]. Conditions for interconversion of the various structures are indicated (vap: vapor, STP: ambient conditions). Calculations were performed at the nonlocal DFT level of theory with the B3LYP/LANL2DZ basis set. Computational details are included in the Supporting Information.

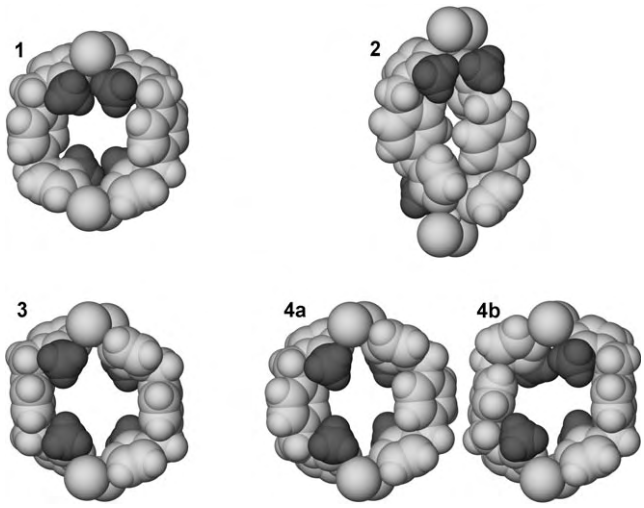


***Figure 2.*** Space-filling projections of the metal complexes in phases **1** to **4**. The methyl groups on the imidazole moieties are darkened to highlight the most significant conformational differences.

In phases **1**–**3**, the metal complexes are all situated on crystallographic inversion centers with half of the complex unique in each case. In all three cases, two methyl substituents on the imidazole moieties are situated on one side of the mean plane of the dinuclear complex, while the remaining two methyl groups are situated on the opposite side of this plane. With reference to the projections in Figure 2, we can refer to the methyl groups as "U" or "D" if they are directed up or down, respectively. Starting with the upper-left methyl group and proceeding in a clockwise direction, the conformation of **1** with respect to the orientations of the methyl groups can be expressed as UUDD. Although the ligand conformation changes significantly during the transformation from **1** to **2**, the positions of the methyl groups relative to the metallacyclic complex are retained as UUDD. However, the

 © 2006 Wiley-VCH Verlag GmbH & Co. KGaA, Weinheim 

conformation in **3** is UDDU, and comparison of the relative positions of the methyl substituents of the complexes in **1** and **3** shows the most notable difference to be rotation of two of the imidazole groups by approximately 120° about their Cu–N vectors.

Phase **3** can be also be obtained directly from phase **1** by exposure of the latter to acetonitrile vapor for approximately 10 min. The single-crystal integrity is maintained and X-ray diffraction analysis showed that acetone is exchanged for acetonitrile. This process can be reversed, although not as readily as the transformation from **1** to **3**; that is, exposure of **3** to acetone vapor requires several hours for reversion to phase **1** as a single-crystal transformation. When crystals of **3** are exposed to atmospheric conditions for approximately 15 min, transformation to yet a fourth phase (**4**, Figure 1) occurs, again with maintenance of the macroscopic integrity of the crystals.

Single-crystal X-ray diffraction analysis revealed the presence of two different conformations of the metallacyclic complex in **4**. Although one of these conformations (**4a**) is similar to that of **3** with regard to the relative positions of its methyl substituents (UDDU), the angle of the phenylene ring of the ligand with respect to the mean plane of the coordinated nitrogen atoms is significantly different (70.3° in **3** and 114.9° in **4a**). The second conformation (**4b**) of the complex present in **4** is unlike any of the conformations observed in **1** to **3**. This new conformation is DUDU and does not possess inversion symmetry. In an attempt to rationalize the transformation from **3** to **4**, it is interesting to consider the two distinct complexes in **4** in relation to two corresponding molecules in **3**. A projection of two neighboring molecules in **3**, related to one another by a crystallographic $2_1$ screw axis, is shown in Figure 3, and it seems reasonable to suggest that these molecules correspond to the two crystallographically distinct molecules in **4**, which are also shown in Figure 3. Apart from rotation of the phenylene group of the ligand, as described above, there is little change in the conformation or the relative position of the molecule at the upper left. However, the second molecule undergoes a transition from its original conformation, but only by rotation of its imidazole groups at one end (its upper left-hand side, as shown in Figure 3). Energetically, the DUDU conformation of **4b** and the UDDU conformation of **3** differ by less than 0.01 kcal $mol^{-1}$.

The orientations of the methyl groups on the two imidazole moieties represent the most dramatic conformational attributes of the ligand, while the angle of the phenylene spacer group is a comparatively minor structural characteristic. The series of interconvertible structures described herein encompasses all the possible permutations of major conformational features that the dinuclear complexes can possess, with the exception of UUUU. The near completeness of a set of mutable structures is an important consideration for further study of monocrystalline conformational switching aimed at understanding why only a small number of crystals appear to have this remarkable ability.

Chromatic changes in single crystals are potentially important phenomena that can be implemented in gas- or vapor-sensing devices.[1a] A single-crystal transformation accompanied by a vapochromic response can easily be rationalized when changes in the composition of the coordination sphere occur.[1a,f] However, Lee and Suh have recently demonstrated that alteration of only the geometry of the coordination sphere can also result in vapochromism, although a simple explanation for this has not yet been postulated.[1c] To date, conformational switching of a structure between only two states has been reported for several systems possessing long-range rigidity (extensively hydrogen-bonded networks, 2D layers, or infinite 1D, 2D, and 3D frameworks that allow rows or sheets of molecules to move in unison).[1b–f,2–4] However, monocrystalline switching between four (and possibly even more) states, as described herein, is unprecedented, as is the magnitude of the conformational changes that we have described. It seems self-evident that a significant level of cooperation must occur between the contorting molecules within the crystal in order for such large conformational changes to be accommodated without catastrophic disruption of the packing continuity.

In summary, we have described the single-crystal to single-crystal interconversion of four distinct molecular crystal forms consisting of neutral, dinuclear metal complexes. During uptake and release of solvent vapors, the host molecules undergo significant conformational, positional, and topological changes, each of which is accompanied by a vapochromic response. Moreover, these monocrystalline transformations are reversible and meet the requirements for the development of functional devices based upon structural modification of "soft" crystalline materials as an extension of the field of crystal engineering.

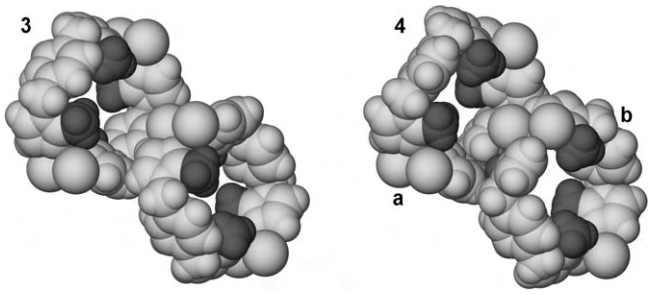


***Figure 3.*** Space-filling projections of the metal complexes in phases **3** and **4**, showing the positional relationships of **4a** and **4b** with respect to their counterparts in **3**. The methyl groups on the imidazole moieties are darkened to highlight the most significant conformational differences.

## *Experimental Section*

1,4-Bis[(2-methylimidazol-1-yl)methyl]benzene was synthesized by the $S_N2$ reaction of 2-methylimidazole with α,α′-dichloro-*p*-xylene. Crystal data can be found in the Supporting Information. CCDC-602877, CCDC-602878, CCDC-602879, and CCDC-602880 contain the supplementary crystallographic data for this paper. These data can be obtained free of charge from The Cambridge Crystallographic Data Centre via www.ccdc.cam.ac.uk/data_request/cif.

Received: May 23, 2006
Published online: July 27, 2006

 © 2006 Wiley-VCH Verlag GmbH & Co. KGaA, Weinheim 

**Keywords:** cooperative phenomena · crystal engineering · host–guest systems · phase transitions · solvatochromism


[1] a) M. Albrecht, M. Lutz, A. L. Spek, G. van Koten, *Nature* **2000**, *406*, 970 – 974; b) G. J. Halder, C. J. Kepert, *J. Am. Chem. Soc.* **2005**, *127*, 7891 – 7900; c) E. Y. Lee, M. P. Suh, *Angew. Chem.* **2004**, *116*, 2858 – 2861; *Angew. Chem. Int. Ed.* **2004**, *43*, 2798 – 2801; d) J. L. Atwood, L. J. Barbour, A. Jerga, B. L. Schottel, *Science* **2002**, *298*, 1000 – 1002; e) J. W. Steed, *Science* **2002**, *298*, 976 – 977; f) K. Takaoka, M. Kawano, M. Tominaga, M. Fujita, *Angew. Chem.* **2005**, *117*, 2189 – 2192; *Angew. Chem. Int. Ed.* **2005**, *44*, 2151 – 2154; g) S. Kitagawa, R. Kitaura, S.-I. Noro, *Angew. Chem.* **2004**, *116*, 2388 – 2430; *Angew. Chem. Int. Ed.* **2004**, *43*, 2334 – 2375.

[2] S. Kitagawa, K. Uemura, *Chem. Soc. Rev.* **2005**, *34*, 109 – 119.

[3] K. Uemura, S. Kitagawa, K. Fukui, K. Saito, *J. Am. Chem. Soc.* **2004**, *126*, 3817 – 3828.

[4] a) C. J. Kepert, D. Hesek, P. D. Beer, M. J. Rosseinsky, *Angew. Chem.* **1998**, *110*, 3335 – 3337; *Angew. Chem. Int. Ed.* **1998**, *37*, 3158 – 3160; b) E. Y. Lee, S. Y. Jang, M. P. Suh, *J. Am. Chem. Soc.* **2005**, *127*, 6374 – 6381; c) K. Biradha, M. Fujita, *Angew. Chem.* **2002**, *114*, 3542 – 3545; *Angew. Chem. Int. Ed.* **2002**, *41*, 3392 – 3395; d) K. Biradha, Y. Hongo, M. Fujita, *Angew. Chem.* **2002**, *114*, 3545 – 3548; *Angew. Chem. Int. Ed.* **2002**, *41*, 3395 – 3398; e) E. J. Cussen, J. B. Claridge, M. J. Rosseinsky, C. J. Kepert, *J. Am. Chem. Soc.* **2002**, *124*, 9574 – 9581.

[5] *Frontiers in Crystal Engineering* (Eds.: E. R. T. Tiekink, J. J. Vittal), Wiley, Chichester, **2006**.

[6] a) O. M. Yaghi, M. O'Keefe, N. W. Ockwig, H. K. Chae, M. Eddaoudi, J. Kim, *Nature* **2003**, *423*, 705 – 714; b) G. Férey, C. Mellot-Dranznieks, C. Serre, F. Millange, J. Dutour, S. Surble, I. Margiolaki, *Science* **2005**, *309*, 2040 – 2042.

[7] M. A. Zwijnenburg, S. T. Bromley, J. C. Jansen, T. Maschmeyer, *Chem. Mater.* **2004**, *16*, 12 – 20.

[8] J. S. Seo, D. Whang, H. Lee, S. I. Jun, J. Oh, Y. J. Jeon, K. Kim, *Nature* **2000**, *404*, 982 – 986.

[9] H. K. Chae, D. Y. Siberio-Perez, J. Kim, Y. Go, M. Eddaoudi, A. J. Matzger, M. O'Keefe, O. M. Yaghi, *Nature* **2004**, *427*, 523 – 527.

[10] a) B. Chen, C. Leng, J. Yang, D. S. Contreras, Y. L. Clancy, E. B. Lobkovsky, O. M. Yaghi, S. Dai, *Angew. Chem.* ***2006***, *118*, 1418 – 1421; *Angew. Chem. Int. Ed.* ***2006***, *45*, 1390 – 1393; b) J. L. Atwood, L. J. Barbour, A. Jerga, *Angew. Chem.* **2004**, *116*, 3008 – 3010; *Angew. Chem. Int. Ed.* **2004**, *43*, 2948 – 2950.

[11] O. Ohmori, M. Kawano, M. Fujita, *J. Am. Chem. Soc.* **2004**, *126*, 16292 – 16293.

[12] P. Sozzani, S. Bracco, A. Comotti, L. Ferretti, R. Simonutti, *Angew. Chem.* **2005**, *117*, 1850 – 1854; *Angew. Chem. Int. Ed.* **2005**, *44*, 1816 – 1820.

[13] M. R. Caira, L. R. Nassimbeni, *Comprehensive Supramolecular Chemistry*, *Vol. 6* (Eds.: J. L. Atwood, J. E. D. Davies, D. D. MacNicol, F. Vögtle), Elsevier Science, Oxford, **1996**, pp. 825 – 850.

[14] C. Serre, F. Millange, C. Thouvenot, M. Nogues, G. Marsolier, D. Louer, G. Férey, *J. Am. Chem. Soc.* **2002**, *124*, 13519 – 13526.

[15] L. Applegarth, N. Clark, A. C. Richardson, A. D. M. Parker, I. Radosavljevic-Evans, A. E. Goeta, J. A. K. Howard, J. W. Steed, *Chem. Commun.* **2005**, 5423 – 5425.

[16] a) L. Dobrzańska, G. O. Lloyd, H. G. Raubenheimer, L. J. Barbour, *J. Am. Chem. Soc.* **2005**, *127*, 13134 – 13135; b) L. Dobrzańska, G. O. Lloyd, H. G. Raubenheimer, L. J. Barbour, *J. Am. Chem. Soc.* **2006**, *128*, 698 – 699.


 © 2006 Wiley-VCH Verlag GmbH & Co. KGaA, Weinheim 

Asymmetric Synthesis

DOI: 10.1002/anie.200602011

# Enantioselective Total Synthesis of (−)-Acylfulvene and (−)-Irofulven**

*Mohammad Movassaghi,* Grazia Piizzi, Dustin S. Siegel, and Giovanni Piersanti*

While sesquiterpene illudins M and S (**1** and **2**, respectively) are highly cytotoxic compounds isolated from *Omphalotus illudens*, a semisynthetic derivative, (−)-irofulven (**4**; hydroxymethyl acylfulvene (HMAF)), has recently demonstrated far superior efficacy as an antitumor agent.[1,2] (−)-Irofulven (**4**) is currently in phase II clinical trials for the treatment of ovarian, prostate, and thyroid cancers both as monotherapy and combination therapy.[2] Significantly, it has demonstrated activity against a variety of solid tumors. Prior syntheses of irofulven using the Padwa carbonyl ylide 1,3-dipolar cycloaddition reaction and the Pauson–Khand reaction have been reported.[3] Herein, we describe a convergent enantioselective total synthesis of (−)-acylfulvene (**3**) and (−)-irofulven (**4**).

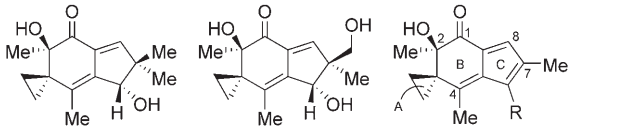


Illudin M (**1**) Illudin S (**2**) (−)-Acylfulvene (**3**), R=H (−)-Irofulven (**4**), R=$CH_2OH$

The inhibition of DNA synthesis and S-phase arrest in cells treated with these compounds stems from sequential nucleophilic addition at C8 and cyclopropyl ring opening, thus

[*] Prof. Dr. M. Movassaghi, Dr. G. Piizzi, D. S. Siegel, Dr. G. Piersanti[+]
Department of Chemistry
Massachusetts Institute of Technology
Cambridge, MA 02139 (USA)
Fax: (+1) 617-254-1504
E-mail: movassag@mit.edu
Homepage: http://web.mit.edu/movassag/www/index.htm

[+] Current address:
Universitá degli Studi di Urbino "Carlo Bo"
Istituto di Chimica Farmaceutica
Piazza Rinascimento 6, 61029 Urbino (Italy)

[**] M.M. is a Dale F. and Betty Ann Frey Damon Runyon Scholar supported by the Damon Runyon Cancer Research Foundation (DRS-39-04). M.M. is a Firmenich Assistant Professor of Chemistry. G.P. acknowledges partial support for a postdoctoral fellowship from Universitá degli Studi di Urbino "Carlo Bo". We are grateful to Professors A. H. Hoveyda and E. N. Jacobsen for generous samples of their silylcyanation catalysts. We acknowledge financial support by MIT, Paul M. Cook Fund, and Boehringer Ingelheim Pharmaceutical Inc.

Supporting information for this article is available on the WWW under http://www.angewandte.org or from the author.

 © 2006 Wiley-VCH Verlag GmbH & Co. KGaA, Weinheim 

leading to B-ring aromatization.[3a] In light of their potent antitumor activity, we sought to develop a general solution to the synthesis of the fully functional spirocyclic AB-ring system common to these antitumor agents by employing a versatile enyne ring-closing metathesis reaction (EYRCM; Scheme 1).[4] A convergent assembly of trienyne **8** by addition

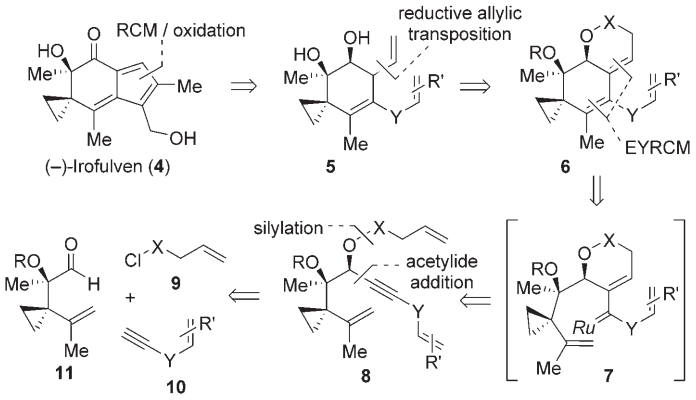


***Scheme 1.*** Retrosynthetic analysis of (−)-irofulven (**4**). *Ru* = 1,3-dimesityl-4,5-dihydroimidazol-2-ylidene ruthenium dichloride, X = $SiR_2$ or $Si(O)R_2$.

of a lithium acetylide to a suitable α-alkoxy aldehyde **11** followed by temporary introduction of an allyl group was envisioned. The planned EYRCM cascade of trienyne **8** would provide rapid access to the fully functional tricycle **6**, which contains the core structure of compounds **1**–**4**, via the ruthenium alkylidene **7**. Deconjugation of the newly formed diene **6** would set the stage for the final ring-closing metathesis (RCM)/oxidation sequence to complete the synthesis of the target compounds.[4,5]

An enantioselective route to aldehyde **11** (R = TMS) was developed based on the Evans copper-catalyzed aldol addition reaction (Scheme 2).[6] The addition of the strained ketene hemithioacetal **12**[7] to a solution of methyl pyruvate **13** and (*R*,*R*)-2,2′-isopropylidene-bis(4-*tert*-butyl-2-oxazoline)-copper(II) triflate (10 mol%) in THF at −78°C gave the desired *O*-trimethylsilyl diester **14** (95%, 92% *ee*; Scheme 2). The stereochemistry at C2 of **14** was secured by X-ray analysis (a related salt with (−)-brucine)[7] and was found to be consistent with the predicted sense of carbonyl addition.[6a]

Under optimal conditions, the methyl ketone **15** was efficiently prepared by the cross-coupling of thiol ester **14** with methylzinc iodide using SPhos as a supporting ligand.[8] Methods employing more nucleophilic reagents were plagued by significant decomposition of the reactive cyclopropyl ketone **15**. Methylenation of the sensitive and sterically hindered ketone **15** was achieved using $CH_2I_2/Zn/TiCl_4$ in the presence of catalytic $PbCl_4$[9] to provide multigram batches of the methyl ester **16**. The conversion of ester **16** into the corresponding aldehyde (+)-**11** afforded the key building block for the synthesis of the spirocyclic AB-ring system of **1**–**4**. Given the presence of this substructure in a number of natural illudins, the efficiency of this aldol-based approach in securing the 2*R* stereochemistry of the intermediates in large quantities is noteworthy.[10]

The proposed EYRCM cascade (**8**→**6**; Scheme 1) would require the formation of a tetrasubstituted alkene on a sterically congested and fully substituted B ring.[11] We examined the EYRCM of dienynes **17a**–**f** (Table 1) to quickly

***Table 1:*** Evaluation of the EYRCM strategy.[a]

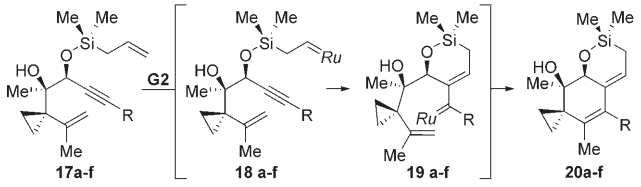


| Entry | Substrate | R | Yield [%][b] |
|---|---|---|---|
| 1 | **a** | $CH_2CHMe_2$ | 76[c] |
| 2 | **b** | $(CH_2)_2CH{=}CMe_2$ | 64 |
| 3 | **c** | $CH_2OPiv$ | 66 |
| 4 | **d** | $(CH_2)_4OPiv$ | 66 |
| 5 | **e** | $(CH_2)_2CHO$ | 59 |
| 6 | **f** | $(CH_2)_4I$ | 52[d] |

[a] Uniform reaction conditions (unless noted): **G2** (10 mol%), benzene, 65°C, [**17**] = 0.02 M, 1 h. [b] Yield of the isolated product **20** after purification. [c] Toluene, 80°C, 40 min. [d] *t* = 6 h.

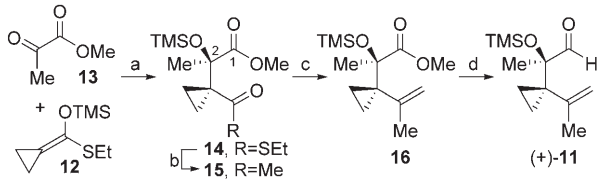


***Scheme 2.*** Enantioselective synthesis of (+)-aldehyde **11**. Reagents and conditions: a) (*R*,*R*)-2,2′-isopropylidene-bis(4-*tert*-butyl-2-oxazoline), $Cu(OTf)_2$, THF, −78°C, 12 h (95%, 92% *ee*); b) MeZnI, $[Pd_2dba_3]$, SPhos, THF, NMP, 65°C, 2 h (83%); c) $CH_2I_2$, $TiCl_4$, Zn, $PbCl_4$, $CH_2Cl_2$, THF, 23°C, 4 h (89%); d) DIBAl-H, $Et_2O$, −78°C; Dess–Martin periodinane, $CH_2Cl_2$, 23°C (91%). dba = dibenzylideneacetone, Dess–Martin periodinane = 1,1,1-triacetoxy-1,1-dihydro-1,2-benziodoxol-3-(1*H*)-one, DIBAl-H = diisobutylaluminumhydride, NMP = *N*-methylpyrrolidinone, OTf = trifluoromethane sulfonate, SPhos = 2-dicyclohexylphosphino-2′,6′-dimethoxy-1,1′-biphenyl, TMS = trimethylsilyl.

probe the potential generality of this approach in the synthesis of the B ring. The dienyne substrates **17** were prepared by allyldimethylsilylation of the corresponding diol obtained by addition of the lithium acetylide of an appropriate alkyne to the key aldehyde **11**.[12] Gratifyingly, treatment of the dienynes **17** with the Grubbs second generation catalyst (**G2**)[13] afforded the desired corresponding tricyclic dienes **20** (Table 1).[14]

Interestingly, this strategy not only provides the fully functional and substituted AB-ring system of many illudins,[15] but it also tolerates sensitive functional groups, such as an aldehyde or a primary iodide (Table 1, entries 5 and 6, respectively). Monitoring these reactions by $^1H$ NMR spectroscopic analysis in situ ([$D_6$]benzene) revealed excellent conversion of the starting dienynes into the EYRCM

 © 2006 Wiley-VCH Verlag GmbH & Co. KGaA, Weinheim 

products. The yield of the isolated dienes **20** (Table 1) is diminished as a result of their sensitivity to chromatography on silica and alumina gel. Attempted protodesilylative transposition of the dienes **20** (namely, **6**→**5** in Scheme 1) to provide the vinyl group necessary for the final RCM was plagued by extensive decomposition. Additionally, tricycles **20** were found to be sensitive toward oxidative breakdown; for example, Tamao oxidation of product **20a** (Table 1, entry 1) gave the corresponding triol in poor yield (27%).[16] We reasoned that the use of an allyloxydialkylsilyl tether in the EYRCM cascade (**8**→**6**; Scheme 1) would not only obviate the need for the isolation of dienes **20**, but also permit alternative methods for the synthesis of the key triene **5** (Scheme 1).[17,18]

The successful synthesis of (−)-acylfulven and (−)-irofulven by using the above EYRCM strategy began with the rapid assembly of the key trienyne **23a** through the multigram scale coupling of the readily available aldehyde (+)-**11**, enyne **21**, and allyloxydiethylchlorosilane (Scheme 3).

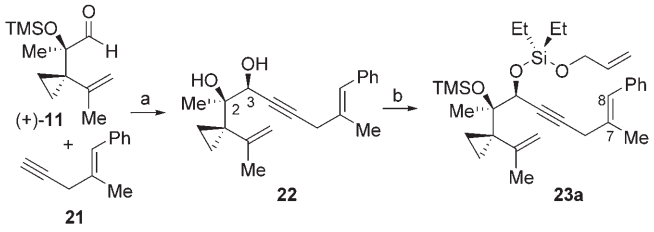


***Scheme 3.*** Synthesis of the trienyne **23a**. For clarity, the major diastereomer of the intermediates is shown. Reagents and conditions: a) **21**, LHMDS, THF, −78→−40°C; (+)-**11**; TBAF, AcOH (75%); b) $(Et)_2Si(Cl)OCH_2CH{=}CH_2$, 2,6-lutidine, $CH_2Cl_2$; TMSOTf, −78°C (83%). LHMDS = lithium hexamethyldisilazide, TBAF = tetrabutylammonium fluoride, TMSOTf = trimethylsilyltrifluoromethane sulfonate.

Addition of the corresponding lithium acetylide of enyne **21** (two steps from α-methylcinnamyl alcohol)[7] to (+)-**11** provided the diol **22** in 75% yield after desilylation of the immediate product from silyl migration (C2→C3) as a mixture of C3 diastereomers (3*S*/3*R* ≈ 6:1), thus favoring the Felkin–Ahn mode of carbonyl addition (Scheme 3). Given the final stage oxidation of the hydroxy group at C3 to the corresponding carbonyl group of the target compounds, both diastereomers were moved forward in the optimized synthetic sequence without chromatographic separation. The diastereomeric mixture of diol **22** was subjected to sequential secondary alcohol allyloxydiethylsilylation followed by trimethylsilylation of the tertiary alcohol at C2 to give trienyne **23a** (3*S*/3*R* = 6:1) in 83% yield in a single step (Scheme 3).[7] Protection of the tertiary hydroxy group of **22** was found to increase the stability of these trienynes during purification.

We were delighted to find that the treatment of **23a** with the Grubbs **G2** catalyst (15 mol%) in toluene (0.01M) at 90°C afforded the desired dihydrodioxasilepine **24a** (≥90%; Table 2, entry 1) in 30 min, which was directly converted into the key triol **25a** (3*S*/3*R* = 6:1) in 74–79% yield of the isolated product. Thus, use of the allyloxysilyl tether in the key EYRCM cascade not only removed the need for the isolation of sensitive intermediates, but also led to a marked increase in the overall efficiency of the process.[19] The key triol **25a** contained all the necessary functional groups and the carbon skeleton needed for completion of the synthesis.

***Table 2:*** Implementation of the EYRCM cascade.[a]

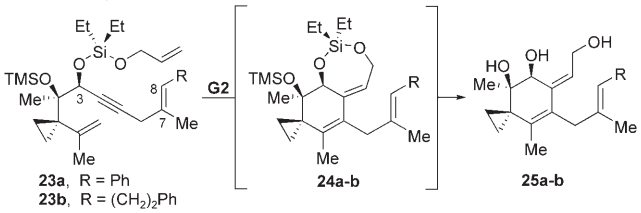


| Entry | Substrate | Product | | Yield [%] |
|---|---|---|---|---|
| 1 | **23a** | 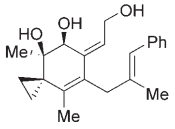 | **25a** | 74–79 |
| 2 | **23b** | 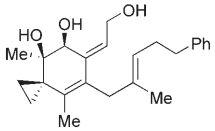 | **25b** | 52 |
| | | 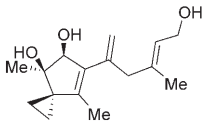 | **26** | < 20 |

[a] Reaction conditions: **G2** (15 mol%), toluene, 90°C, [**23**] = 0.01M, 30 min, then TBAF, AcOH, THF, 23°C, 10 min.

Importantly, both C3 diastereomers of **23a** were equally effective substrates for this key EYRCM cascade. While this EYRCM cascade provided the desired triol with a range of dienyne substrates, a minor EYRCM by-product (**26**, Table 2, entry 2) was observed when employing trienyne **23b**.[20] Careful inspection of this transformation revealed that triol **26** was formed by sequential RCM involving the C7 alkene of **23b**, EYRCM, and C7 olefin isomerization.[7] Significantly, the by-product **26** is not observed when the C7–C8 segment is appropriately masked as in trienyne **23a** (also see Table 1, entry 2). Guided by this insight and using **23a**, multigram quantities of the desired triol **25a** (Table 2, entry 1) were prepared.

Sequential exposure of the key triol **25a** to TBSOTf (1 equiv) followed by triphosgene (1.5 equiv) and tetrabutylammonium fluoride (TBAF) afforded the desired alcohol **27** (Scheme 4), thus setting the stage for the planned reductive allylic transposition and RCM steps. The Mitsunobu displacement of alcohol **27** with 2-nitrobenzene-sulfonylhydrazide (NBSH) in *N*-methylmorpholine (−30→23°C) gave the triene **30** (6*S*/6*R* = 3:1) through a sigmatropic loss of dinitrogen from the intermediate monoalkyldiazene **29**.[21] The poor solubility of **27** in optimal solvents for this transformation and the required high concentration of reagents (≈0.3M) led to variable yields of product **30** (35–54%). We found that use of the more stable acetone hydrazone of NBSH gave the (isolable) hydrazone **28** through an efficient Mitsunobu reaction at a more dilute concentration (≈0.1M in

 © 2006 Wiley-VCH Verlag GmbH & Co. KGaA, Weinheim 

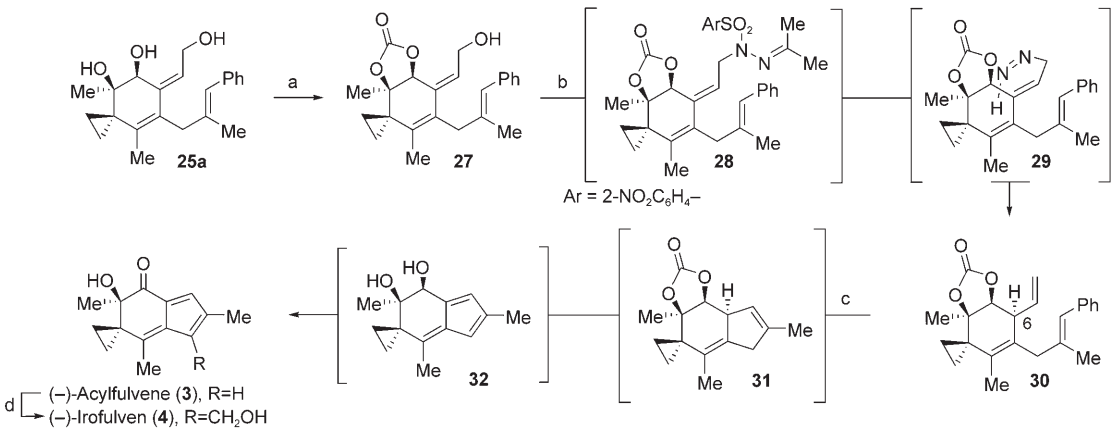


***Scheme 4.*** Synthesis of **3** and **4**. For clarity, the major diastereomer of the compounds **25a**–**32** is shown. Reagents and conditions: a) TBSOTf, 2,6-lutidine, $CH_2Cl_2$, −78 °C; triphosgene; TBAF (67%); b) 2-$NO_2C_6H_4SO_2NHN{=}CMe_2$, DEAD, $Ph_3P$, THF, 0→23 °C; TFE, $H_2O$ (71%); c) Grubbs **G2** catalyst (15 mol%), PhH, 78 °C; NaOMe; AcOH; DDQ (**30**→**3**, 30%)—or use chloranil to isolate **32** (70% from **30**) then IBX, DMSO (83%); d) $H_2SO_4$, $CH_2O_{aq}$ (63%). DDQ = 2,3-dichloro-5,6-dicyano-1,4-benzoquinone, DEAD = diethylazadicarboxylate, DMSO = dimethyl sulfoxide, IBX = *ortho*-iodoxybenzoic acid, TBSOTf = *tert*-butyldimethysilyltrifluormethane sulfonate, TFE = 2,2,2-trifluoroethanol.

THF) and without requiring sub-zero reaction temperatures or additives. Importantly, the addition of trifluoroethanol and water following the Mitsunobu displacement step led to in situ hydrolysis and fragmentation of **28** to give the desired triene **30** in 71% yield of the isolated product (6*S*/6*R* = 3:1) from **27** (Scheme 4).

The **G2**-catalyzed RCM reaction of triene **30** afforded the sensitive tricyclic diene carbonate **31** (70%, 6*S*/6*R* = 3:1). Initially, **31** was isolated and converted into the stable diol fulvene **32** by sequential dehydrogenation with DDQ followed by hydrolysis of the cyclic carbonate. We later discovered that addition of sodium methoxide upon completion of the RCM reaction, followed by treatment with chloranil gave the desired diol **32** with greater overall efficiency (70%). Treatment of **32** with IBX in DMSO provided the target compound (−)-acylfulvene (**3**) in 83% yield.[3a] Importantly, simple exchange of chloranil with DDQ provided **3** from **30** without isolation of the intermediates in 30% yield in a sequence that involved RCM, methanolysis, and two consecutive dehydrogenation reactions. (−)-Acylfulvene (**3**) was converted into (−)-irofulven (**4**) based on conditions described by McMorris and co-workers.[3a] Spectroscopic data of our synthetic (−)-**3** and (−)-**4** matched those in the literature.[7]

The powerful EYRCM and RCM reactions play key roles in our enantioselective total synthesis of **3** and **4**. Only five intermediates (**22**, **23a**, **25a**, **27**, and **30**) need to be isolated in the conversion of the readily available aldehyde (+)-**11** and alkyne **21** to (−)-acylfulvene (**3**), the direct precursor to the potent anticancer agent (−)-irofulven (**4**). Noteworthy features of this chemistry include an aldol addition strategy that uses new reagent **12** to secure the stereochemistry at C2, a general EYRCM cascade to introduce the AB-ring system of these compounds, and the development of new conditions for the generation of a transient monoalkyldiazene species for reductive allylic transposition. The application of this chemistry to the synthesis of other cytotoxic illudins is underway. This synthetic route is expected to provide ready access to derivatives of **3** and **4** not available through semisynthesis.

Received: May 21, 2006
Published online: August 4, 2006

**Keywords:** aldol reaction · antitumor agents · asymmetric catalysis · metathesis · total synthesis

[1] a) M. Anchel, A. Hervey, W. J. Robbins, *Proc. Natl. Acad. Sci. USA* **1952**, *38*, 927; b) T. C. McMorris, M. J. Kelner, W. Wang, J. Yu, L. A. Estes, R. Taetle, *J. Nat. Prod.* **1996**, *59*, 896.

[2] a) J. Alexandre, E. Raymond, M. O. Kaci, E. C. Brian, F. Lokiec, C. Kahatt, S. Faivre, A. Yovine, F. Golwasser, S. L. Smith, J. R. MacDonald, J.-L. Misset, E. Cvitkovic, *Clin. Cancer Res.* **2004**, *10*, 3377; b) J. Gong, J. F. Neels, X. Yu, T. W. Kensler, L. A. Peterson, S. J. Sturla, *J. Med. Chem.* **2006**, *49*, 2593; c) M. Serova, F. Calvo, F. Lokiec, F. Koeppel, V. Poindessous, A. K. Larsen, E. S. Van Laar, S. J. Waters, E. Cvitkovic, E. Raymond, *Cancer Chemother. Pharmacol.* **2006**, *57*, 491; d) http://cancernet.nci.nih.gov/clinicaltrials.

[3] Enantioselective synthesis of (−)-**4**: a) T. C. McMorris, M. D. Staake, M. J. Kelner, *J. Org. Chem.* **2004**, *69*, 619; formal enantioselective synthesis of (−)-**4**: b) K. M. Brummond, J. Lu, J. Peterson, *J. Am. Chem. Soc.* **2000**, *122*, 4915; also, see: K. M. Brummond, J. Lu, *J. Am. Chem. Soc.* **1999**, *121*, 5087.

[4] For recent reviews, see: a) K. C. Nicolaou, P. G. Bulger, D. Sarlah, *Angew. Chem.* **2005**, *117*, 4564; *Angew. Chem. Int. Ed.* **2005**, *44*, 4490; ; b) S. T. Diver, A. Giessert, *Chem. Rev.* **2004**, *104*, 1317; for representative examples, see: c) S.-H. Kim, N. Bowden, R. H. Grubbs, *J. Am. Chem. Soc.* **1994**, *116*, 10801; d) W. J. Zuercher, M. Scholl, R. H. Grubbs, *J. Org. Chem.* **1998**, *63*, 4291; e) M. E. Layton, C. A. Morales, M. D. Shair, *J. Am. Chem. Soc.* **2002**, *124*, 773; f) H. Fukumoto, K. Takanishi, J. Ishihara, S. Hatakeyama, *Angew. Chem.* **2006**, *118*, 2797; *Angew. Chem. Int. Ed.* **2006**, *45*, 2731.

[5] a) R. H. Grubbs, *Tetrahedron* **2004**, *60*, 7117; b) R. R. Schrock, A. H. Hoveyda, *Angew. Chem.* **2003**, *115*, 4740; *Angew. Chem. Int. Ed.* **2003**, *42*, 4592; c) A. Fürstner, *Angew. Chem.* **2000**, *112*, 3140; *Angew. Chem. Int. Ed.* **2000**, *39*, 3012.

 © 2006 Wiley-VCH Verlag GmbH & Co. KGaA, Weinheim 

[6] a) D. A. Evans, C. S. Burgey, M. C. Kozlowski, S. W. Treay, *J. Am. Chem. Soc.* **1999**, *121*, 686; b) several other catalytic asymmetric routes to **11** (namely, cyanation of the corresponding methyl ketone or dihydroxylation of a related diene) were explored and ultimately the most efficient route was selected.
[7] Please see the Supporting Information for details.
[8] a) H. Tokuyama, S. Yokoshima, T. Fukuyama, *Tetrahedron Lett.* **1998**, *39*, 3189; b) J. E. Milne, S. L. Buchwald, *J. Am. Chem. Soc.* **2004**, *126*, 13028.
[9] K. Takai, T. Kakiuchi, Y. Kataoka, K. Utimoto, *J. Org. Chem.* **1994**, *59*, 2668.
[10] For reports on other natural illudins, see: a) A. Arnone, R. Cardillo, G. Nasini, O. V. De Pava, *J. Chem. Soc. Perkin Trans. 1* **1991**, 733; b) A. Arnone, R. Cardillo, V. di Modugno, G. Nasini, *Gazz. Chim. Ital.* **1991**, *121*, 345; c) I.-K. Lee, C.-Y. Jeong, S.-M. Cho, B.-S. Yun, Y.-S. Kim, S.-H. Yu, H. Koshino, I.-D. Yoo, *J. Antibiot.* **1996**, *49*, 821; d) C. Dufresne, K. Young, F. Pelaez, A. González del Val, D. Valentino, A. Graham, G. Platas, A. Bernard, D. Zink, *J. Nat. Prod.* **1997**, *60*, 188; e) M. L. Burgess, Y. L. Zhang, K. D. Barrow, *J. Nat. Prod.* **1999**, *62*, 1542; f) M. Reina, J. C. Orihuela, A. Gonzáles-Coloma, C. de Inés, M. de la Crus, A. González del Val, J. R. Torno, B. M. Fraga, *Phytochemistry* **2004**, *65*, 381.
[11] For representative syntheses of cyclohexenes containing a tetrasubstituted olefin through enyne metathesis, see: a) T. Kitamura, Y. Sato, M. Mori, *Chem. Commun.* **2001**, *14*, 1258; b) T. Kitamura, Y. Sato, M. Mori, *Adv. Synth. Catal.* **2002**, *344*, 678.
[12] The experimental procedure for the preparation of diol **22** is given in the Supporting Information.
[13] M. Scholl, S. Ding, C. W. Lee, R. H. Grubbs, *Org. Lett.* **1999**, *1*, 953.
[14] For a review on silicon-tether reactions, see: a) L. Festerbank, M. Malacria, S. M. Sieburth, *Synthesis* **1997**, 813; for representative examples of olefin metathesis mediated by an allyldialkylsilicon tether, see: b) S. Chang, R. H. Grubbs, *Tetrahedron Lett.* **1997**, *38*, 4757; c) Q. Yao, *Org. Lett.* **2001**, *3*, 2069.
[15] For other synthetic studies, see: a) T. Matsumoto, H. Shirahama, A. Ichihara, H. Shin, S. Kagawa, F. Sakan, S. Matsumoto, S. Nishida, *J. Am. Chem. Soc.* **1968**, *90*, 3280; b) F. R. Kinder, K. W. Bair, *J. Org. Chem.* **1994**, *59*, 6965; c) A. Padwa, V. P. Sandanayaka, E. A. Curtis, *J. Am. Chem. Soc.* **1994**, *116*, 2667; d) H. Primke, G. S. Sarin, S. Kohlstruk, G. Adiwidjaja, A. de Meijere, *Chem. Ber.* **1994**, *127*, 1051; e) T. C. McMorris, J. Yu, Y. Hu, *J. Org. Chem.* **1997**, *62*, 3015; f) F. R. Kinder, R. M. Wang, W. E. Bauta, K. W. Bair, *Synth. Commun.* **1997**, *62*, 521; g) T. C. McMorris, Q. Cong, M. J. Kelner, *J. Org. Chem.* **2003**, *68*, 9648; h) M. C. Pirrung, H. Liu, *Org. Lett.* **2003**, *5*, 1983.
[16] K. Tamao, N. Ishida, M. Kumada, *Org. Synth.* **1990**, *69*, 96; for examples of a Tamao oxidation of silicon-tethered metathesis products, see Ref. [14b–c].
[17] For examples of metathesis reactions using allyloxysilicon tethers, see: a) T. R. Hoye, M. A. Promo, *Tetrahedron Lett.* **1999**, *40*, 1429; b) S. S. Zhu, D. R. Cefalo, D. S. La, J. Y. Jamieson, W. M. Davis, A. H. Hoveyda, R. R. Schrock, *J. Am. Chem. Soc.* **1999**, *121*, 8251; c) A. Briot, M. Bujard, V. Gouverneur, S. P. Nolan, C. Mioskowski, *Org. Lett.* **2000**, *2*, 1517; d) P. Van de Weghe, D. Aoun, J.-G. Boiteau, J. Eustache, *Org. Lett.* **2002**, *4*, 4105; e) M. H. Postema J. L. Piper, *Tetrahedron Lett.* **2002**, *43*, 7095; f) P. E. Evans, J. Cui, S. J. Gharpure, A. Polosukhin, H.-R. Zhang, *J. Am. Chem. Soc.* **2003**, *125*, 14702.
[18] Initial EYRCM reactions to test the new allyloxydiethylsilyl tether were successfully carried out on dienynes related to those described in Table 1.
[19] The EYRCM reaction of the C2 hydroxy variants of trienynes **23a–b** exclusively gave the desired triols **25a–b**, respectively, in approximately 50% yield of the isolated product, but required a longer reaction time and higher catalyst loadings.
[20] The trienyne **23b** was prepared according to the procedure described for the trienyne **23a**.
[21] a) A. G. Myers, B. Zheng, *Tetrahedron Lett.* **1996**, *37*, 4841; b) A. G. Myers, M. Movassaghi, B. Zheng, *J. Am. Chem. Soc.* **1997**, *119*, 8572.

 © 2006 Wiley-VCH Verlag GmbH & Co. KGaA, Weinheim 

*Radical Reactions*

DOI: 10.1002/anie.200602042

# Enantioselective Cascade Radical Addition–Cyclization–Trapping Reactions**

*Hideto Miyabe,* Ryuta Asada, Akira Toyoda, and Yoshiji Takemoto**

In recent years, studies on enantioselective radical reactions have achieved some remarkable success,[1] particularly in intermolecular addition reactions, allylations, and H-atom transfer reactions.[2,3] In contrast, only a handful of reports describe enantioselective radical cyclizations, which can be classified into three types by the nature of the coordination with a Lewis acid (**I–III**, Scheme 1).[4–7] A high degree of stereocontrol was achieved in type **II** cyclizations using α-radical species generated from a β-keto ester as a coordination site and was applied to cascade cyclization by Yang and co-workers.[7] However, there are no reports on enantioselective cascade reactions involving both inter- and intramolecular C–C bond-forming processes. Herein, we report a cascade type **IV** strategy that takes advantage of the hydroxamate ester.[5,8]

As most radical reactions proceed through early transition states, the structure of the substrate plays an important role;[9] thus, the control of the rotamer population would be crucial for achieving high selectivity in cascade reactions. We consider that the predominant formation of a single reactive

[*] Dr. H. Miyabe, R. Asada, A. Toyoda, Prof. Y. Takemoto
Graduate School of Pharmaceutical Sciences
Kyoto University
Yoshida, Sakyo-ku, Kyoto 606-8501 (Japan)
Fax: (+81) 75-753-4569
E-mail: hmiyabe@pharm.kyoto-u.ac.jp
takemoto@pharm.kyoto-u.ac.jp

[**] This work was supported in part by a Grant-in-Aid for Young Scientists (B) (H.M.) and Scientific Research on Priority Areas 17035043 (Y.T. and H.M.) from the Ministry of Education, Culture, Sports, Science, and Technology of Japan, 21st Century COE Program "Knowledge Information Infrastructure for Genome Science".

Supporting information for this article is available on the WWW under http://www.angewandte.org or from the author.

 © 2006 Wiley-VCH Verlag GmbH & Co. KGaA, Weinheim InterScience 

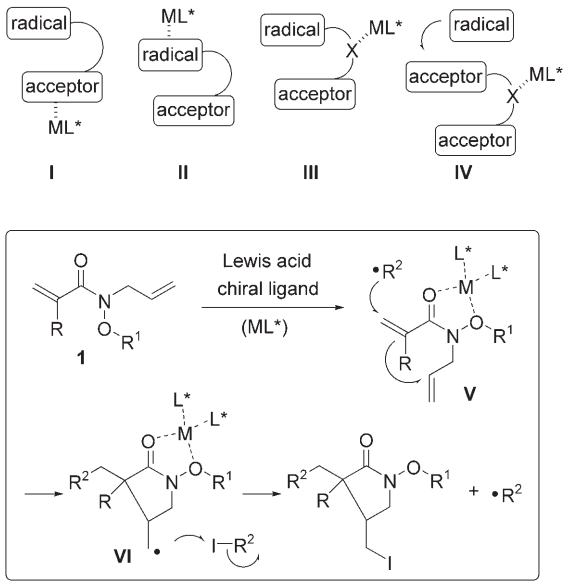


***Scheme 1.*** Chiral Lewis acid mediated radical cyclization. ML* = chiral Lewis acid.

rotamer must be achieved by the type **IV** approach, which contains a coordination tether (X) inbetween two acceptors. Therefore, we selected a hydroxamate ester **1**, because rotamer **V** will prevail through a stable five-membered chelation.[10] We were also interested in probing the effect of the fluxional substituent of **1** ($R^1$) on the stereochemistry.[11]

A suitable combination of a chiral Lewis acid and hydroxamate ester would lead to the highly diastereo- and enantioselective reaction of **1A** (Scheme 2).[12] The radical reactions were initiated by triethylborane.[13] No reaction occurred in the absence of a Lewis acid (LA; Table 1, entry 1). In contrast, the addition of a Lewis acid promoted the reaction at 20 °C to give the 5-*exo* cyclization product **2Aa** along with recovered starting material **1A** (Table 1, entries 2 and 3), although the reaction did not proceed at −78 °C even with a Lewis acid (Table 1, entry 4). With a stoichiometric amount of the chiral Lewis acid prepared from $Zn(OTf)_2$ (Tf = trifluoromethanesulfonyl) and ligand **3**, the adduct **2Aa** was formed even at −78 °C with 71 % *ee* and high *cis*

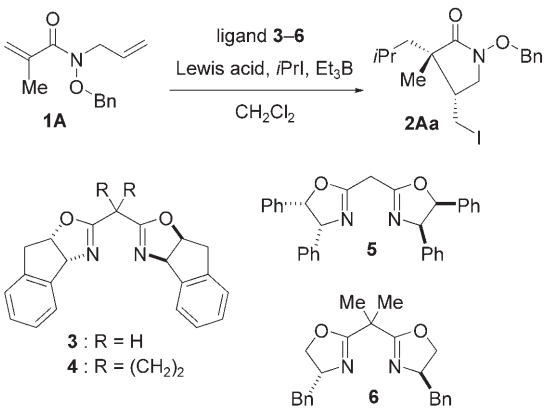


***Scheme 2.*** Radical addition–cyclization–trapping reaction of **1A**.

***Table 1:*** Cascade radical reaction of **1A** with isopropyl iodide.[a]

| Entry | LA | Ligand | *T* [°C] | Yield [%][b] | d.r.[c] | *ee* [%][d] |
|---|---|---|---|---|---|---|
| 1[e] | – | – | 20 | – | – | – |
| 2[e] | $Zn(OTf)_2$ | – | 20 | 41 (42) | >98:2 | – |
| 3[e] | $Mg(OTf)_2$ | – | 20 | 23 (69) | >98:2 | – |
| 4[e] | $Zn(OTf)_2$ | – | −78 | – | – | – |
| 5[e] | $Zn(OTf)_2$ | **3** | −78 | 76 | >98:2 | 71 |
| 6[e] | $Zn(OTf)_2$ | **4** | −78 | 81 | >98:2 | 76 |
| 7[f] | $Zn(OTf)_2$ | **4** | −78 | 71 | >98:2 | 77 |
| 8[e] | $Zn(OTf)_2$ | **5** | −78 | 81 | >98:2 | −69 |
| 9[e] | $Mg(OTf)_2$ | **6** | −78 | 16 (79) | >98:2 | racemic |

[a] Reactions were carried out with **1A** (1 equiv), isopropyl iodide (30 equiv), and $Et_3B$ in hexane (1.0 M, 2.5 equiv) with a Lewis acid (1 equiv) and ligand **3**–**6** (1 equiv). [b] Yield of the isolated product; the yield in parentheses is for the recovered starting material **1A**. [c] Determined by $^1H$ NMR spectroscopic analysis. [d] Determined by HPLC analysis. [e] In $CH_2Cl_2$. [f] In toluene/$CH_2Cl_2$ (4:1, v/v).

diastereoselectivity (Table 1, entry 5). These results suggest that the chelation with chiral Lewis acid led to decreased conformational flexibility and the expected rotamer **V** was present to a significant extent.[14] Somewhat better enantioselectivities were obtained by using ligand **4**, whereas the reaction with ligand **5** attenuated the enantiomeric excess, thus surprisingly resulting in the enantiomer of adduct **2Aa** (Table 1, entries 6–8).[15] In contrast, the combination of $Mg(OTf)_2$ and ligand **6** decreased the cyclization rate and gave the nearly racemic product (Table 1, entry 9).[16] A remarkable feature of this reaction is the construction of three bonds and tertiary and quaternary stereogenic centers through cascade inter- and intramolecular C−C bond-forming processes.

We next evaluated the effect of the substituent $R^1$ of **1B**–**E** on yield and selectivity (Scheme 3 and Table 2). The size of the substituent had an impact on enantioselectivity, with

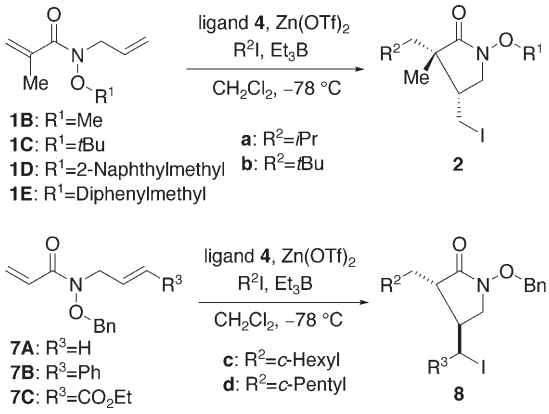


***Scheme 3.*** Radical reactions of **1B–E** and **7A–C**.

larger groups leading to lower *ee* values. Reaction of **1B**, which has a small methoxy group, lead to high enantio- and diastereoselectivity (Table 2, entry 1). More interestingly, the use of substrate **1E** with a diphenylmethyl group gave the nearly racemic product **2Ea**, probably as a result of dissonance between the chiral Lewis acid and bulky substituent

 © 2006 Wiley-VCH Verlag GmbH & Co. KGaA, Weinheim 

***Table 2:*** Cascade reaction of **1B–E** and **7A–C** with alkyl iodides.[a]

| Entry | Substrate | $R^2$ | Product | Yield [%][b] | d.r.[c] | *ee* [%][d] |
|---|---|---|---|---|---|---|
| 1 | **1B** | *i*Pr | **2Ba** | 75 | >98:2 | 82 |
| 2 | **1C** | *i*Pr | **2Ca** | 71 | >98:2 | 75 |
| 3 | **1D** | *i*Pr | **2Da** | 75 | >98:2 | 73 |
| 4 | **1E** | *i*Pr | **2Ea** | 52 | >98:2 | racemic |
| 5 | **1B** | *t*Bu | **2Bb** | 78 | >98:2 | 88 |
| 6 | **7A** | *i*Pr | **8Aa** | 52 | 92:8 | 92 |
| 7 | **7A** | cHex | **8Ac** | 57 | 94:6 | 92 |
| 8 | **7A** | *c*Pent | **8Ad** | 35 | 94:6 | 91 |
| 9 | **7B** | *i*Pr | – | – | – | – |
| 10 | **7C** | *i*Pr | complex mixture | | | |

[a] Reactions were carried out with **1B–E** or **7A–C** (1 equiv), $R^2I$ (30 equiv), and $Et_3B$ in hexane (1.0 M, 2.5 equiv) with $Zn(OTf)_2$ (1 equiv) and ligand **4** (1 equiv). [b] Yield of the isolated product. [c] Determined by $^1H$ NMR spectroscopic analysis. [d] Determined by HPLC analysis.

(Table 2, entry 4). These observations clearly indicate that rigid conformation of the ternary complex formed from **1A**, $Zn(OTf)_2$, and ligand **4** is required for a good yield and high selectivity. Similarly, the reaction of **1B** with the *tert*-butyl radical gave **2Bb** with higher enantioselectivity (Table 2, entry 5). Outstanding levels of enantioselectivity were obtained in the reaction of acrylate substrate **7A** (Table 2, entries 6–8).[17] The reaction of **7A** with an isopropyl radical source gave 52% yield of the cyclic product **8Aa** with 92% *ee* and good *trans* diastereoselectivity (Table 2, entry 6). The moderate chemical yields of products **8** were attributed to competitive polymerization of **7A** through the acrylamide moiety.

The success of these reactions reflects the overall difference in the stability of the $R^2$ radical and a cyclic radical intermediate **VI**. Thus, the iodine atom-transfer process from secondary or tertiary alkyl iodide ($R^2I$) to unstable primary intermediate radical **VI** is a key step.[18] Indeed, the formation of cyclic products was not observed in the reaction of substrates **7B** and **7C**, which involves less effective iodine atom transfer to stable secondary radicals **VI** (Table 2, entries 9 and 10).

The cyclization of **1A–E** that leads to the major *cis* diastereomer occurs via the conformer **VII** (Scheme 4), in which two olefin units adopt a *cis* configuration, probably as a result of the effect of the orbital symmetry reported by Beckwith and Houk.[19] In marked contrast, the *trans* selectivity in the reaction of **7A** was regarded as being through the conformer **VIII** and the result of steric repulsion.

We next investigated the chiral substrate (*R*)-**9** (Scheme 5).[20] In the presence of ligand **4**, the reaction of (*R*)-**9** (81% *ee*) gave a 63% yield of (*S*)-*cis*-**10** with 99% *ee*,

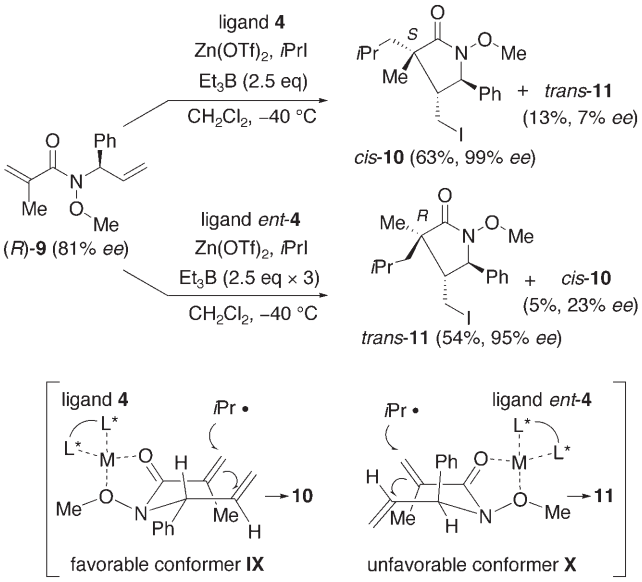


***Scheme 5.*** Cascade radical reaction of chiral substrate (*R*)-**9**.

accompanied by a small amount of *trans*-**11** with low enantiomeric excess. The major cyclization proceeded via favorable conformer **IX**, thus minimizing the allylic 1,3-strain effect. The enhanced enantioselectivity of *cis*-**10** can be explained by kinetic resolution of an intermediate chiral radical. To substantiate this explanation, the enantiomer of ligand **4** (*ent*-**4**) was employed. Although the reaction using ligand *ent*-**4** required a large amount of $Et_3B$ ($3 \times 2.5$ equiv), the expected *R*-enriched *trans*-**11** (95% *ee*) was obtained via unfavorable conformer **X**, which carried an axial Ph group to avoid steric interaction with the allylic substituent. The absolute configuration was deduced from NOESY experiments of *cis*-**10** and *trans*-**11** with three chiral centers that assume an *R* configuration for the phenyl-substituted stereogenic carbon center.[21] Therefore, the absolute configuration at the quaternary carbon atom derived from substrates **1A–E** was also determined to be the *S* configuration.

We finally investigated the reaction of alkynes **12A** and **12B** (Scheme 6). The reactions gave high enantioselectivities

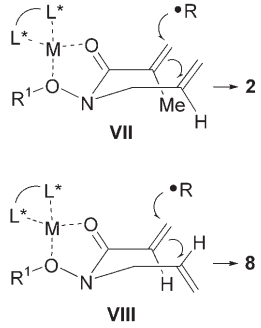


***Scheme 4.*** Possible cyclic transition states **VII** and **VIII**.

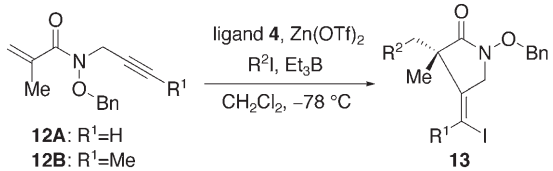


***Scheme 6.*** Cascade radical reaction of **12A** and **12B**.

 © 2006 Wiley-VCH Verlag GmbH & Co. KGaA, Weinheim 

(Table 3) and proceeded equally well with 30 mol% of chiral Lewis acid as with stoichiometric amounts. Further reduction of the catalyst load to 10 mol% resulted in a decrease of the chemical yield and enantioselectivity (Table 3, entry 4). The high *Z*/*E* selectivity of products **13** clearly indicates that the iodine atom transfer from $R^2I$ to an intermediate radical proceeded efficiently.

***Table 3:*** Cascade radical reaction of **12A** and **12B** with alkyl iodides.[a]

| Entry | Substrate | $R^2$ | LA [equiv] | Product | Yield [%][b] | d.r.[c] | *ee* [%][d] |
|---|---|---|---|---|---|---|---|
| 1 | **12A** | *i*Pr | 1.0 | **13Aa** | 87 | >98:2 | 80 |
| 2 | **12A** | *i*Pr | 0.5 | **13Aa** | 85 | >98:2 | 81 |
| 3 | **12A** | *i*Pr | 0.3 | **13Aa** | 82 | >98:2 | 81 |
| 4 | **12A** | *i*Pr | 0.1 | **13Aa** | 49[e] | >98:2 | 47 |
| 5 | **12A** | *t*Bu | 1.0 | **13Ab** | 85 | >98:2 | 92 |
| 6 | **12A** | *c*Hex | 1.0 | **13Ac** | 82 | >98:2 | 81 |
| 7 | **12B** | *i*Pr | 1.0 | **13Ba** | 86 | >98:2 | 83 |
| 8 | **12B** | *i*Pr | 0.3 | **13Ba** | 74 | >98:2 | 81 |
| 9 | **12B** | *t*Bu | 1.0 | **13Bb** | 94 | >98:2 | 90 |
| 10 | **12B** | *c*Hex | 1.0 | **13Bc** | 87 | >98:2 | 85 |

[a] Reactions were carried out using **12A** or **12B** (1 equiv), $R^2I$ (30 equiv), and $Et_3B$ in hexane (1.0 M, 2.5 equiv) with $Zn(OTf)_2$ and ligand **4**. [b] Yield of the isolated product. [c] Determined by $^1H$ NMR spectroscopic analysis. [d] Determined by HPLC analysis. [e] Compound **12A** was recovered in 29% yield.

In conclusion, we have succeeded in performing the enantioselective radical addition–cyclization–trapping reaction that provides a powerful synthetic approach to chiral γ-lactams.

Received: May 23, 2006
Published online: July 28, 2006

**Keywords:** asymmetric synthesis · enantioselectivity · lactams · lewis acids · radical reactions

[1] For general information on enantioselective radical reactions, see: a) P. Renaud, M. Gerster, *Angew. Chem.* **1998**, *110*, 2704; *Angew. Chem. Int. Ed.* **1998**, *37*, 2562; b) M. P. Sibi, N. A. Porter, *Acc. Chem. Res.* **1999**, *32*, 163; c) G. Bar, A. F. Parsons, *Chem. Soc. Rev.* **2003**, *32*, 251; d) M. P. Sibi, S. Manyem, J. Zimmerman, *Chem. Rev.* **2003**, *103*, 3263.

[2] For selected examples of enantioselective radical addition reactions and allylations, see: a) M. P. Sibi, G. Petrovic, J. Zimmerman, *J. Am. Chem. Soc.* **2005**, *127*, 2390; b) G. K. Friestad, Y. Shen, E. L. Ruggles, *Angew. Chem.* **2003**, *115*, 5215; *Angew. Chem. Int. Ed.* **2003**, *42*, 5061; c) M. P. Sibi, J. Zimmerman, T. Rheault, *Angew. Chem.* **2003**, *115*, 4659; *Angew. Chem. Int. Ed.* **2003**, *42*, 4521; d) Y. Watanabe, N. Mase, R. Furue, T. Toru, *Tetrahedron Lett.* **2001**, *42*, 2981; e) U. Iserloh, D. P. Curran, S. Kanemasa, *Tetrahedron: Asymmetry* **1999**, *10*, 2417; f) M. Murakata, T. Jono, Y. Mizuno, O. Hoshino, *J. Am. Chem. Soc.* **1997**, *119*, 11713; g) M. P. Sibi, J. Ji, *J. Am. Chem. Soc.* **1996**, *118*, 9200; h) J. H. Wu, R. Radinov, N. A. Porter, *J. Am. Chem. Soc.* **1995**, *117*, 11029.

[3] For selected examples of enantioselective hydrogen-atom transfer reactions, see: a) M. P. Sibi, K. Patil, *Angew. Chem.* **2004**, *116*, 1255; *Angew. Chem. Int. Ed.* **2004**, *43*, 1235; b) M. P. Sibi, Y. Asano, J. B. Sausker, *Angew. Chem.* **2001**, *113*, 1333; *Angew. Chem. Int. Ed.* **2001**, *40*, 1293; c) M. Murakata, H. Tsutsui, N. Takeuchi, O. Hoshino, *Tetrahedron* **1999**, *55*, 10295; for selected examples of enantioselective reductions using chiral hydrogen-atom transfer reagents, see: d) Y. Cai, B. P. Roberts, D. A. Tocher, *J. Chem. Soc. Perkin Trans. 1* **2002**, 1376; e) D. Dakternieks, C. H. Schiesser, *Aust. J. Chem.* **2001**, *54*, 89; f) M. Blumenstein, K. Schwarzkopf, J. O. Metzger, *Angew. Chem.* **1997**, *109*, 245; *Angew. Chem. Int. Ed. Engl.* **1997**, *36*, 235; g) D. Nanni, D. P. Curran, *Tetrahedron: Asymmetry* **1996**, *7*, 2417.

[4] For a report on the transfer of chirality in radical cyclization, see: D. P. Curran, W. Liu, C. H.-T. Chen, *J. Am. Chem. Soc.* **1999**, *121*, 11012.

[5] M. Nishida, H. Hayashi, A. Nishida, N. Kawahara, *Chem. Commun.* **1996**, 579.

[6] K. Hiroi, M. Ishii, *Tetrahedron Lett.* **2000**, *41*, 7071.

[7] a) D. Yang, S. Gu, Y.-L. Yan, N.-Y. Zhu, K.-K. Cheung, *J. Am. Chem. Soc.* **2001**, *123*, 8612; b) D. Yang, S. Gu, Y.-L. Yan, H.-W. Zhao, N.-Y. Zhu, *Angew. Chem.* **2002**, *114*, 3143; *Angew. Chem. Int. Ed.* **2002**, *41*, 3014; c) D. Yang, B.-F. Zheng, Q. Gao, S. Gu, N.-Y. Zhu, *Angew. Chem.* **2006**, *118*, 261; *Angew. Chem. Int. Ed.* **2006**, *45*, 255.

[8] For hydroxamic acid derivatives explored as achiral templates in the Diels–Alder reaction, see: a) O. Corminboeuf, P. Renaud, *Org. Lett.* **2002**, *4*, 1731; b) O. Corminboeuf, P. Renaud, *Org. Lett.* **2002**, *4*, 1735.

[9] M. P. Sibi, J. Ji, *J. Am. Chem. Soc.* **1996**, *118*, 3063.

[10] The principal function of a Lewis acid is to control the rotamer populations of substrates; see: a) P. Renaud, T. Bourquard, M. Gerster, N. Moufid, *Angew. Chem.* **1994**, *106*, 1680; *Angew. Chem. Int. Ed. Engl.* **1994**, *33*, 1601; b) M. P. Sibi, J. Ji, *Angew. Chem.* **1996**, *108*, 198; *Angew. Chem. Int. Ed. Engl* **1996**, *35*, 190; see also reference [1a].

[11] O. Corminboeuf, L. Quaranta, P. Renaud, M. Liu, C. P. Jasperse, M. P. Sibi, *Chem. Eur. J.* **2003**, *9*, 28.

[12] M. Ueda, H. Miyabe, A. Nishimura, O. Miyata, Y. Takemoto, T. Naito, *Org. Lett.* **2003**, *5*, 3835.

[13] For reviews, see: a) H. Yorimitsu, H. Shinokubo, K. Oshima, *Synlett* **2002**, 674; b) C. Ollivier, P. Renaud, *Chem. Rev.* **2001**, *101*, 3415.

[14] A $^1H$ NMR study of **1a** in the presence of a chiral Lewis acid is provided in the Supporting Information; a downfield shift in the chemical shifts of hydrogen atoms around the hydroxamate ester moiety was observed.

[15] For a report on a similar inversion in configuration, see: M. P. Sibi, J. Ji, *J. Org. Chem.* **1997**, *62*, 3800.

[16] In general, the combination of phenyl-substituted bis(oxazoline) (box) ligand and zinc Lewis acid gives high selectivity, whereas the aliphatic-substituted box ligands give high selectivity in combination with magnesium Lewis acids; see: a) M. P. Sibi, J. Ji, *J. Am. Chem. Soc.* **1996**, *118*, 9200; b) N. A. Porter, J. H. L. Wu, G. R. Zhang, A. D. Reed, *J. Org. Chem.* **1997**, *62*, 6702; c) M. P. Sibi, J. Zimmerman, T. Rheault, *Angew. Chem.* **2003**, *115*, 4659; *Angew. Chem. Int. Ed.* **2003**, *42*, 4521.

[17] The absolute configuration at the newly formed stereocenter of **8** could not be determined. The relative configuration of *trans* and *cis* diastereomers **8Aa** was determined by NOESY experiments (see the Supporting Information).

[18] For discussions on atom-transfer cyclization, see: a) D. P. Curran, J. Tamine, *J. Org. Chem.* **1991**, *56*, 2746; b) D. P. Curran, W. Shen, J. Zhang, T. A. Heffner, *J. Am. Chem. Soc.* **1990**, *112*, 6738.

[19] a) A. L. J. Beckwith, *Tetrahedron* **1981**, *37*, 3073; b) D. C. Spellmeyer, K. N. Houk, *J. Org. Chem.* **1987**, *52*, 959.

[20] The chiral substrate of (*R*)-**9** (81% *ee*) was prepared by our method using an iridium catalyst and the pyridinebis(oxazoline)-(pybox) ligand; see: a) H. Miyabe, K. Yoshida, M. Yamauchi, Y. Takemoto, *J. Org. Chem.* **2005**, *70*, 2148; b) H. Miyabe, A. Matsumura, K. Moriyama, Y. Takemoto, *Org. Lett.* **2004**, *6*, 4631.

[21] Details are provided in the Supporting Information.

 © 2006 Wiley-VCH Verlag GmbH & Co. KGaA, Weinheim 

*Hybrid Compounds*

DOI: 10.1002/anie.200600120

# Design and Synthesis of Multifunctional Materials Based on an Ionic-Liquid Backbone**

*Yuanjian Zhang, Yanfei Shen, Junhua Yuan, Dongxue Han, Zhijuan Wang, Qixian Zhang, and Li Niu**

Ionic liquids (ILs) have attracted an increasing amount of interest, owing to their low volatility, non-flammability, high chemical and thermal stabilities, high ionic conductivity, and broad electrochemical windows.[1] Initial investigations concerning ILs focused on employing them as "green" solvents in chemical synthesis, catalysis, separation, and electrochemistry, for example.[1a,2] Recently, ILs have emerged as templates or stabilizers for nanostructures,[3] and as supported catalysts for organic and electrochemical reactions.[4] Some task-specific ILs have also been designed,[5] because the structures and properties of ILs can be easily tuned by selecting the appropriate combination of organic cations and anions (Scheme 1 a).[1] It is also possible to utilize one ionic component to deliver a unique function and the other to deliver a different and independent function. This concept would provide a facile and promising method to prepare multifunctional compounds. In contrast, to achieve this combination with a molecular compound would provide all sorts of synthetic challenges. However, to our knowledge, this type of flexibility of ILs has hardly been realized, as the majority of the applications of ILs are limited to employing them as novel solvents, catalysts, or surfactants.[1–4]

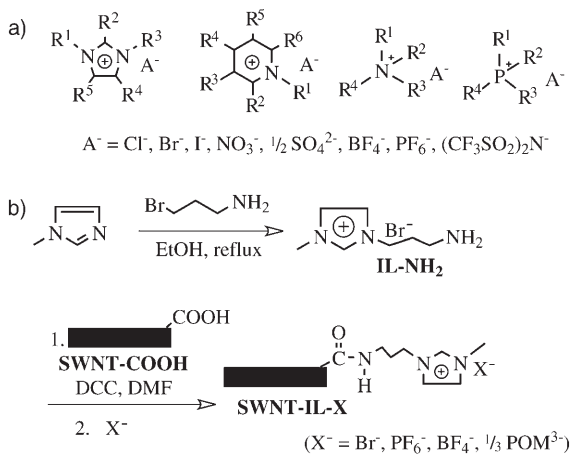


***Scheme 1.*** a) Cations and anions commonly used in ILs. b) The preparation of SWNT-IL-X.

Herein, we report a new concept for the preparation of multifunctional compounds by using an IL backbone. Single-walled carbon nanotubes (SWNTs) and counteranions such as $Br^-$, $PF_6^-$, $BF_4^-$, and polyoxometalates (POMs) can be deliberately coupled by using the imidazolium group, which is a common cation in ILs, as the backbone (Scheme 1). Preliminary results indicate that the individual properties of the SWNTs and the various counteranions are easily and successfully delivered into the resulting compounds.

Owing to their unique thermal, electronic, and mechanical properties, SWNTs have attracted a great deal of attention.[6] It has been envisioned that the integration of SWNTs and other functional components would not only highlight the unique physical properties of SWNTs but would also lead to multifunctional materials.[6b–k] Nevertheless, there are still many synthetic challenges.[6f] As illustrated below with ILs, efficient coupling of SWNTs with other components is achieved in a simple anion-exchange reaction.

The preparation of SWNT-substituted imidazolium salts bearing various anions X (SWNT-IL-X) is illustrated in Scheme 1 b. The characteristic G band and radical breathing mode (RBM) of the SWNT were observed by Raman spectroscopy after coupling (see Supporting Information), which indicates that the original properties of the SWNT are preserved in the final SWNT-IL-X, as reported previously.[6] To determine whether the functions of the other components were also preserved in the SWNT-IL-X products, the properties of the X counteranions were investigated further.

The wettability of ILs is unique. It has been reported that the $Br^-$ anions of imidazolium salts can easily be exchanged with $BF_4^-$ or $PF_6^-$, thereby modulating the wettability.[1b,4e,5b] In order to investigate whether the tunable wettability derived from these anions could be delivered into SWNT-IL-X, SWNT-IL-Br was first assembled on a hydrophilic glass substrate as the outmost layer with the aid of polyethyleneimine (PEI) and poly(styrene-4-sulfonate) (PSS) by a typical layer-by-layer (LbL) process (glass/PEI/PSS/SWNT-IL-Br).[4e] The anion was exchanged by submerging this film in 10 mM $NaBF_4$ or $NaPF_6$ for 4 hours and then rinsing thoroughly with water.[5b] It was found that the water contact angle of the glass/PEI/PSS/SWNT-IL-Br multilayer could be tuned by this anion exchange, while for the glass/PEI/PSS multilayer in the control experiments no changes were observed (Figure 1). Because the wettability of an LbL multilayer is dominated by the outmost layer, the change in contact angle observed should be due only to anion exchange of the SWNT-IL-X.[4e] In agreement with previous reports,[4e,5b] the contact angle of SWNT-IL-$PF_6$ ($49.7 \pm 2.3°$) is higher than that of SWNT-IL-$BF_4$ ($45.8 \pm 0.9°$) and much higher than that of SWNT-IL-Br ($39.8 \pm 1.3°$). Therefore, tunable wettability can also be successfully delivered into

[*] Y. Zhang, Y. Shen, J. Yuan, D. Han, Z. Wang, Q. Zhang, Prof. Dr. L. Niu
State Key Laboratory of Electroanalytical Chemistry
Changchun Institute of Applied Chemistry
and Graduate School of the Chinese Academy of Sciences
Chinese Academy of Sciences
Changchun 130022 (P.R. China)
Fax: (+86) 431-526-2800
E-mail: lniu@ciac.jl.cn

[**] The authors are grateful to the NSFC, China (grant no. 20475053) and to the Department of Science and Technology of Jilin Province (grant no. 20050102) for financial support.

Supporting Information for this article is available on the WWW under http://www.angewandte.org or from the author.

 © 2006 Wiley-VCH Verlag GmbH & Co. KGaA, Weinheim 

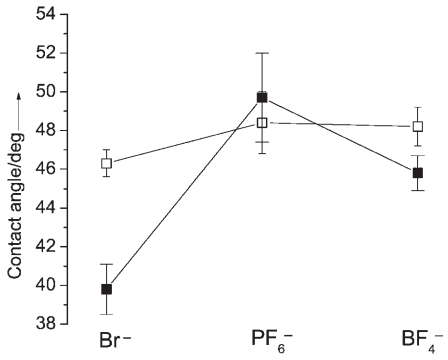


***Figure 1.*** Effects of counteranions on the water contact angle of SWNT-IL-X (solid squares) and the control sample (hollow squares).

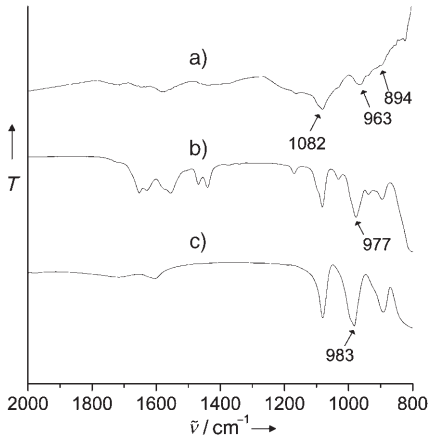


***Figure 2.*** FTIR spectra of SWNT-IL-POM (a), IL-POM (b), and $H_3$POM (c).

SWNT-IL-X (X = $Br^-$, $PF_6^-$, and $BF_4^-$) merely by exchanging the anion.

In this initial investigation, the ionic character of the IL is utilized to couple the SWNT to the other components. The ionic functionalization of SWNTs allows the counterion to be readily exchanged. Therefore, such an ionic feature might allow electrostatic interactions between SWNT-ILs and biological molecules, and could serve as the basis for developing biocompatible SWNT compounds. In general, the ionic functionalization of SWNTs in previous reports[6i] was based on an acid–base reaction. Herein, the advantage of the IL is that its ionic character is not dependent on the pH, so its reactivity should be more general. Another advantage is the diversity of anions (organic/inorganic) and cations available (with various R groups, see Scheme 1), which makes it possible to integrate multiple functional components into one compound. For example, it should be possible to combine optical, electronic, and magnetic components in a single compound. Additionally, some IL properties are also unique. For instance, as discussed above, the wettability of SWNT-IL-X can be controlled merely by exchanging the $Br^-$ anion with $BF_4^-$ or $PF_6^-$, which is rarely seen for common SWNT composites and could be very useful for the phase-transfer of SWNTs in various solvents and their self-assembly at interfaces.[6l]

To further illustrate this concept, the anion of phosphotungstic acid, $H_3[PW_{12}O_{40}]$ ($H_3$POM), a typical Keggin-type polyoxometalate (POM), was also coupled with an SWNT to construct a multifunctional compound for charge transfer. POMs have recently been extensively investigated in catalysis, electro- and photochromism, and medicine.[7] They also undergo multiple consecutive and reversible multi-electron reductions into mixed-valence species (so-called heteropolyblues, HPBs), without decomposition. Therefore, their anion derivatives have been widely integrated into composite compounds by covalent[7b,c] or ionic bonding.[7d,e]

The integration of the POM and the SWNT is evident from the FTIR spectrum (Figure 2). The characteristic bands of the POM near 1082 (P–O), 963 (W=$O_{ter}$), and 894 $cm^{-1}$ (W–O–W) are clearly observed in the spectrum of SWNT-IL-POM. Energy-dispersive X-ray (EDX) microanalysis further confirmed the complete exchange of $Br^-$ for $POM^{3-}$ in the resulting SWNT-IL-POM (see Supporting Information). Interestingly, a red-shift of approximately 20 $cm^{-1}$ with respect to the W=$O_{ter}$ vibration in $H_3$POM is observed for the SWNT-IL-POM, while a red-shift of only 6 $cm^{-1}$ is observed for the IL-bearing POM (IL-POM). As SWNTs readily accept electrons,[6g] electron delocalization between the SWNT and the POM might occur, which would decrease the electron density of W=$O_{ter}$ and result in the distinct red-shift. On the basis of this unique interaction between the SWNT and the POM, and considering their individual properties, SWNT-IL-POM might find applications in electron donor–acceptor systems.

Cyclic voltammetry (CV) was further used to investigate the redox/charge activity of SWNT-IL-POM. The surface-confined SWNT-IL-POM shows three couples of sharp and well-defined redox waves due to the POM cluster (Figure 3a). A plot of the cathodic peak current ($I$) as a function of the scan rate ($\nu$) is linear up to 2 $V s^{-1}$, while the peak potentials remain nearly constant (Figure 3b). The small difference in the anodic and cathodic peak potentials ($\Delta E_p < 60$ mV) implies that the redox response remains practically reversible. It is therefore reasonable to assume that the rich redox activity of the POM has been successfully transferred to SWNT-IL-POM by a simple anion-exchange reaction.

It has been reported that the characteristics of the cyclic voltammograms of POM microparticles attached to electrode surfaces depend on the conductivity, solubility, and dissolution kinetics of the adhered solid and the electrogenerated products.[7f] In order to illustrate the unusual redox/charge-transfer activity of SWNT-IL-POM, a set of control CV experiments with a POM-modified SWNT, a POM-modified SWNT-COOH, and IL-POM in 0.5 M $H_2SO_4$ were also performed (see Supporting Information). Owing to the synergistic effect of each component, only the cyclic voltammogram of SWNT-IL-POM gave sharp and well-defined redox waves. The cyclic voltammograms of the POM-modified SWNT and the POM-modified SWNT-COOH are dominated by the charging current of the SWNT, as only a small amount of the POM is absorbed physically on the SWNT. This indicates that the IL on the SWNT plays an important role in effectively immobilizing the POM through

 © 2006 Wiley-VCH Verlag GmbH & Co. KGaA, Weinheim 

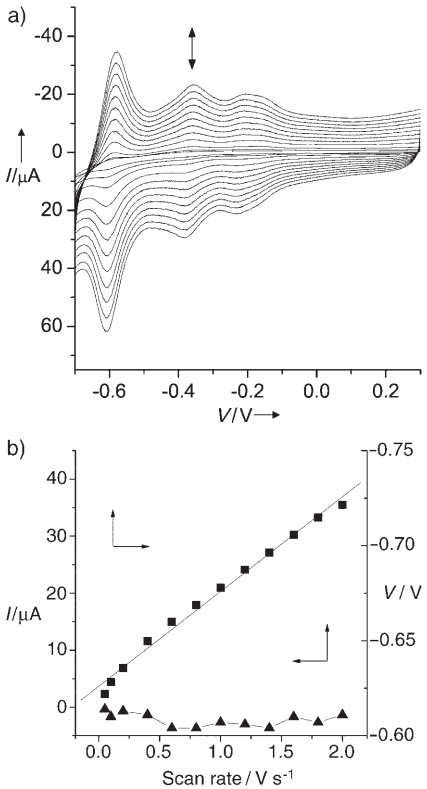


***Figure 3.*** a) Cyclic voltammograms of an SWNT-IL-POM-modified glassy carbon (GC) electrode ($d = 3$ mm) in 0.5 M $H_2SO_4$ at scan rates of 0.05, 0.1, 0.2, 0.4, 0.6, 0.8, 1.0, 1.2, 1.4, 1.6, 1.8, and 2.0 $V s^{-1}$ (from inner to outer). b) Plot of the peak current (squares) and peak potential (triangles) of the third reduction wave as a function of scan rate. Reference electrode: Ag/AgCl (saturated KCl); counter electrode: Pt.

ionic bonding. Only two weak redox waves were observed in the cyclic voltammograms of IL-POM. Hence, it can be concluded that the SWNT is also important for this unusual redox/charge-transfer activity, because of its unique electronic properties. In fact, there are three possible causes for this unusual charge-transfer activity in SWNT-IL-POM: the high electron conductivity of the SWNT, the ionic conductivity of the IL, and the redox conductivity of the POM. Furthermore, in conjunction with the electron delocalization between the SWNT and the POM, SWNT-IL-POM might be considered for future applications in ionic devices (for example, photoelectrochemical cells, fuel cells, and double-layer capacitors).[1c,6g] Therefore, a multifunctional architecture for charge transfer has been prepared by deliberately combining the useful functions of SWNTs, ILs, and POMs into one compound.

In summary, an SWNT and species such as $Br^-$, $PF_6^-$, $BF_4^-$, and POMs have been successfully coupled onto an IL backbone. The resulting compounds retain the original properties of each component and display unusual tunable wettability and charge-transfer activity. Moreover, this principle could also be extended to the deliberate combination of other independent components into multifunctional compounds. No longer simply "green" solvents, the full exploitation of this feature of ILs will shed light on the design and synthesis of multifunctional compounds.

## Experimental Section

Pristine SWNTs (single-walled volume content >50%, length 5–15 μm, diameter <2 nm) were produced by a chemical vapor deposition (CVD) process and were obtained from Shenzhen Nanotech Port Co. Ltd., China, in purified form. Unless otherwise stated, reagents were of analytical grade and were used as received.

SWNT-IL-X was synthesized by an amidation reaction between the carboxylic-acid functionalized SWNT (SWNT-COOH) and the amine-terminated IL (IL-$NH_2$).[6h,j,k] IL-$NH_2$ was prepared by treating 1-methylimidazole (0.02 mol) with 2-bromopropylamine hydrobromide (0.02 mol) by refluxing in ethanol (50 mL) under nitrogen for 24 h and then purified by recrystallization.[5a] ESI-MS ($H_2O$): $m/z$ 140 [$M^+$]; $^1$H NMR ($D_2O$): $\delta = 8.74$ (s, 1H), 7.48 (s, 1H), 7.42 (s, 1H), 4.29 (t, $J$(H,H) = 7.2 Hz, 2H), 3.02 (t, $J$(H,H) = 7.8 Hz, 2H), 2.23 ppm (m, 2H). IL-$NH_2$ is soluble in ethanol, DMF, and DMSO, very soluble in water, and stable in air. SWNT-COOH was prepared by refluxing the pristine SWNTs in 3 M $HNO_3$. SWNT-IL was prepared by ultrasonicating a solution of SWNT-COOH (5 mg), IL-$NH_2$ (10 mg), and dicyclohexylcarbodiimide (DCC, 10 mg) in DMF (10 mL) for 15 min and then vigorously stirring at 50 °C for 24 h. Unreacted SWNTs were removed by centrifugation. SWNT-IL-Br was subsequently filtered through a nylon membrane with 0.22-μm pores and thoroughly washed with DMF, ethanol, and water. The covalent bonding between SWNT-COOH and IL-$NH_2$ was demonstrated by FTIR spectroscopy (see Supporting Information). EDX microanalysis showed that the molar ratio of carbon atoms in the SWNTs to the imidazolium salt was approximately 15:1, which is similar to that reported previously.[6f] SWNT-IL-POM was prepared by vigorously stirring an aqueous solution of SWNT-IL-Br and excess $H_3$POM overnight; SWNT-IL-POM was collected by centrifugation and thoroughly washed with water. It is insoluble in water, and its stability depends on the POM cluster. POM-modified SWNT and SWNT-COOH were prepared similarly by stirring the SWNT or SWNT-COOH in $H_3$POM aqueous solution.

Received: January 11, 2006
Revised: March 29, 2006
Published online: July 28, 2006

**Keywords:** carbon nanotubes · charge transfer · ionic liquids · polyoxometalates · tunable wettability

[1] a) *Ionic Liquids as Green Solvents* (Eds.: R. D. Rogers, K. R. Seddon), American Chemical Society, Washington, DC, **2003**; b) *Ionic Liquids in Synthesis* (Eds.: P. Wasserscheid, T. Welton), Wiley-VCH, Weinheim, **2002**; c) *Electrochemical Aspects of Ionic Liquids* (Ed.: H. Ohno), Wiley, Hoboken, New Jersey, **2005**.

[2] a) J. Zhang, A. M. Bond, *Anal. Chem.* **2003**, *75*, 2694; b) F. van Rantwijk, R. M. Lau, R. A. Sheldon, *Trends Biotechnol.* **2003**, *21*, 131; c) C. F. Weber, R. Puchta, N. J. R. van Eikema Hommes, P. Wasserscheid, R. van Eldik, *Angew. Chem.* **2005**, *117*, 6187; *Angew. Chem. Int. Ed.* **2005**, *44*, 6033; d) W. Qian, E. Jin, W. Bao, Y. Zhang, *Angew. Chem.* **2005**, *117*, 974; *Angew. Chem. Int. Ed.* **2005**, *44*, 952; e) D. S. Jacob, A. Joseph, S. P. Mallenahalli, S. Shanmugam, S. Makhluf, J. Calderon-Moreno, Y. Koltypin, A. Gedanken, *Angew. Chem.* **2005**, *117*, 6718; *Angew. Chem. Int. Ed.* **2005**, *44*, 6560; f) J. H. Li, Y. F. Shen, Y. J. Zhang, Y. Liu, *Chem. Commun.* **2005**, 360; g) Y. J. Zhang, Y. F. Shen, J. H. Li, L. Niu, S. J. Dong, A. Ivaska, *Langmuir* **2005**, *21*, 4797.

[3] a) M. Antonietti, D. B. Kuang, B. Smarsly, Z. Yong, *Angew. Chem.* **2004**, *116*, 5096; *Angew. Chem. Int. Ed.* **2004**, *43*, 4988, and

 © 2006 Wiley-VCH Verlag GmbH & Co. KGaA, Weinheim 

references therein; b) J. Huang, T. Jiang, H. X. Gao, B. X. Han, Z. M. Liu, W. Z. Wu, Y. H. Chang, G. Y. Zhao, *Angew. Chem.* **2004**, *116*, 1421; *Angew. Chem. Int. Ed.* **2004**, *43*, 1397; c) S. Miao, Z. Liu, B. Han, J. Huang, Z. Sun, J. Zhang, T. Jiang, *Angew. Chem.* **2006**, *118*, 272; *Angew. Chem. Int. Ed.* **2006**, *45*, 266.

[4] a) C. P. Mehnert, *Chem. Eur. J.* **2004**, *10*, 50, and references therein; b) T. Sasaki, C. M. Zhong, M. Tada, Y. Iwasawa, *Chem. Commun.* **2005**, 2506; c) A. Riisager, R. Fehrmann, S. Flicker, R. van Hal, M. Haumann, P. Wasserscheid, *Angew. Chem.* **2005**, *117*, 826; *Angew. Chem. Int. Ed.* **2005**, *44*, 815; d) D. W. Kim, D. Y. Chi, *Angew. Chem.* **2004**, *116*, 489; *Angew. Chem. Int. Ed.* **2004**, *43*, 483; e) Y. Shen, Y. Zhang, Q. Zhang, L. Niu, T. You, A. Ivaska, *Chem. Commun.* **2005**, 4193.

[5] a) E. Bates, R. Mayton, I. Ntai, J. Davis, *J. Am. Chem. Soc.* **2002**, *124*, 926; b) B. S. Lee, Y. S. Chi, J. K. Lee, I. S. Choi, C. E. Song, S. K. Namgoong, S.-G. Lee, *J. Am. Chem. Soc.* **2004**, *126*, 480.

[6] a) E. Katz, I. Willner, *ChemPhysChem* **2004**, *5*, 1085; b) A. Bianco, M. Prato, *Adv. Mater.* **2003**, *15*, 1765; c) Y. P. Sun, K. Fu, Y. Lin, W. Huang, *Acc. Chem. Res.* **2002**, *35*, 1096; d) S. Niyogi, M. A. Hamon, H. Hu, B. Zhao, P. Bhowmik, R. Sen, M. E. Itkis, R. C. Haddon, *Acc. Chem. Res.* **2002**, *35*, 1105; e) S. Banerjee, T. Hemraj-Benny, S. S. Wong, *Adv. Mater.* **2005**, *17*, 17; f) J. L. Bahr, J. M. Tour, *J. Mater. Chem.* **2002**, *12*, 1952; g) D. M. Guldi, G. M. A. Rahman, F. Zerbetto, M. Prato, *Acc. Chem. Res.* **2005**, *38*, 871; h) Y. J. Zhang, J. Li, Y. F. Shen, M. J. Wang, J. H. Li, *J. Phys. Chem. B* **2004**, *108*, 15343; i) M. A. Hamon, J. Chen, H. Hu, Y. S. Chen, M. E. Itkis, A. M. Rao, P. C. Eklund, R. C. Haddon, *Adv. Mater.* **1999**, *11*, 834; j) T. Ramanathan, F. T. Fisher, R. S. Ruoff, L. C. Brinson, *Chem. Mater.* **2005**, *17*, 1290; k) J. Gao, M. E. Itkis, A. Yu, E. Bekyarova, B. Zhao, R. C. Haddon, *J. Am. Chem. Soc.* **2005**, *127*, 3847; l) Y. Wang, D. Maspoch, S. Zou, G. C. Schatz, R. E. Smalley, C. A. Mirkin, *Proc. Natl. Acad. Sci. USA* **2006**, *103*, 2026.

[7] a) Special issue on polyoxometalates: *Chem. Rev.* **1998**, *98*, 1; b) C. Cannizzo, C. R. Mayer, F. Seheresse, C. Larpent, *Adv. Mater.* **2005**, *17*, 2888; c) J. Kang, B. B. Xu, Z. H. Peng, X. D. Zhu, Y. G. Wei, D. R. Powell, *Angew. Chem.* **2005**, *117*, 7062; *Angew. Chem. Int. Ed.* **2005**, *44*, 6902; d) L. Plault, A. Hauseler, S. Nlate, D. Astruc, J. Ruiz, S. Gatard, R. Neumann, *Angew. Chem.* **2004**, *116*, 2984; *Angew. Chem. Int. Ed.* **2004**, *43*, 2924; e) D. G. Kurth, P. Lehmann, D. Volkmer, H. Cölfen, M. J. Koop, A. Müller, A. Du Chesne, *Chem. Eur. J.* **2000**, *6*, 385; f) J. Zhang, A. I. Bhatt, A. M. Bond, A. G. Wedd, J. L. Scott, C. R. Strauss, *Electrochem. Commun.* **2005**, *7*, 1283.

 © 2006 Wiley-VCH Verlag GmbH & Co. KGaA, Weinheim 

Natural Product Synthesis

DOI: 10.1002/anie.200601114

# Total Synthesis of Pseudotrienic Acid B: A Bioactive Metabolite from *Pseudomonas* sp. MF 381-IODS**

*Dominique Amans, Véronique Bellosta, and Janine Cossy**

*In memory of Pierre Potier*

Pseudotrienic acids A and B are two bioactive metabolites with antimicrobial activity that have been recently isolated from *Pseudomonas* sp. MF 381-IODS.[1] Their structures were established by $^{1}H$ NMR (600 MHz) and $^{13}C$ NMR (150 MHz) spectroscopy and by ESI mass spectrometry. Each of the pseudotrienic acids A and B was isolated as a 1:1 mixture of epimers at C20, but the absolute configurations at C11 and C12 were well defined as *S* and *R*, respectively. The molecular architecture of these compounds is further characterized by a *E*,*E*,*E* trienic conjugated acid (C1–C7), two amide bonds, and a trisubstituted conjugated *E*,*E* diene (C16–C19).

Both pseudotrienic acids A and B inhibit growth of *Staphylococcus aureus* (minimum inhibitory concentration (MIC) of 70 $\mu g\,mL^{-1}$) and *Pseudomonas syringae* pv. *syringae* (MIC of 70 $\mu g\,mL^{-1}$). Moreover, Pohanka et al.[1] observed that pseudotrienic acids A and B were prone to macrolactonization in an acidic environment and, therefore, could be transformed into two naturally occurring 19-membered-ring lactones, FR252922 and FR252921, respectively, by treatment with trifluoroacetic acid (TFA) (Scheme 1). These two macrolactones, isolated in 2003 by Fujine et al.[2] from the culture broth of *Pseudomonas fluorescens* no. 408813, showed immunosuppressive activity against murine splenocyte proliferation stimulated with a lipopolysaccharide (LPS) or anti-CD3 in vitro.[2] Interestingly, their site and mechanism of action seem to be distinct from those of FK-506 and cyclosporin A (CsA).[2] To date, the configuration of the three stereocenters in FR252922 and FR252921 has not been established. However, it was suggested that the pseudotrienic acids A and B are derived from ring opening of the two macrolactones FR252922 and FR252921, respectively, by a nucleophilic attack of $H_2O$ at C20 according to a nonstereospecific $S_N''$ substitution, thus leading to a mixture of epimers at C20 (Scheme 1).[1] However, since the biosynthesis of polyketides of this type is usually stereospecific, the possi-

[*] D. Amans, Dr. V. Bellosta, Prof. J. Cossy
Laboratoire de Chimie Organique associé au CNRS
ESPCI, 10 rue Vauquelin, 75231 Paris Cedex 05 (France)
Fax: (+33) 1-40-79-46-60
E-mail: janine.cossy@espci.fr

[**] We wish to thank the Société de Chimie Thérapeutique/SERVIER for financial support of this work and Dr. D.-H. Caignard for scientific discussions. We also wish to acknowledge Dr. Fisher and Dr. Trimmer from Materia, USA, for a generous gift of the Grubbs–Hoveyda catalyst.

 WILEY InterScience DISCOVER SOMETHING GREAT © 2006 Wiley-VCH Verlag GmbH & Co. KGaA, Weinheim 

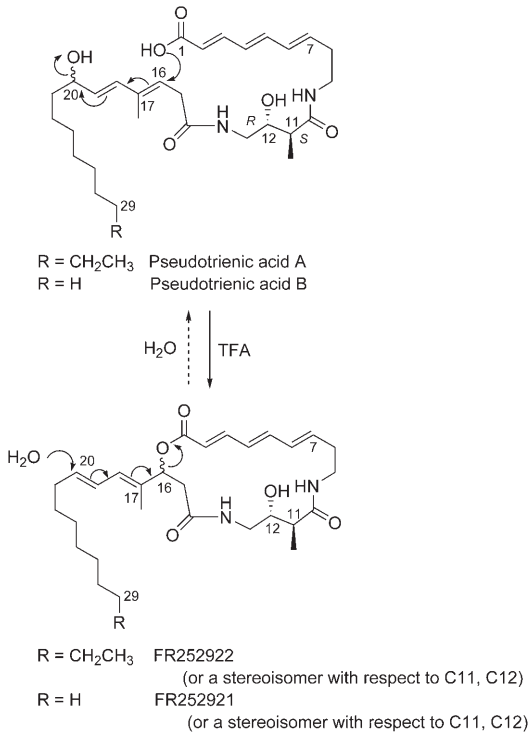


***Scheme 1.*** Lactone formation of FR252921 and FR252922 under acidic conditions.

bility that an epimerization took place during the isolation process of the natural product cannot be ruled out.

Based on these observations, it seems reasonable to assume that FR252922 and FR252921 possess the absolute configuration *S* at C11 and *R* at C12, but the configuration at C16 in the two latter compounds remains to be established. One can suggest that if both epimers at C20 of pseudotrienic acid B were prepared, an $S_N2''$ reaction carried out in an *anti* stereospecific fashion could transfer the configuration from C20 in pseudotrienic acid B to C16 in FR252921. This should then lead to a correct assignment of this stereogenic center in FR252921. The inherent structure of pseudotrienic acids A and B, as well as the biomimetic transformation, makes these antimicrobial agents interesting targets for total synthesis. Herein, we report the first highly convergent total synthesis of pseudotrienic acid B as a mixture of epimers at C20.

The strategy employed to synthesize pseudotrienic acid B is depicted in Scheme 2. It relied on a Stille coupling between the vinyl iodide **20** and the vinyl stannane **17** to generate the *E*,*E* diene. The alkenyl iodide **20** could be obtained by combining two key fragments, carboxylic acid **13** and trienic protected amine **18**, through amide formation. A previous amide formation between the carboxylic acid **8** and the trienic amine **5** would install the second amide bond. Finally, a cross-metathesis/HWE sequence was envisaged for the initial synthesis of the trienic ester **5** from commercially available methyl sorbate (**1**).

Scheme 3 delineates the synthesis of the amino trienoate **5**, which commenced with methyl sorbate (**1**) and proceeded through cross-metathesis and a Horner–Wadsworth–Emmons reaction as the key steps. Thus, methyl sorbate (**1**) was first

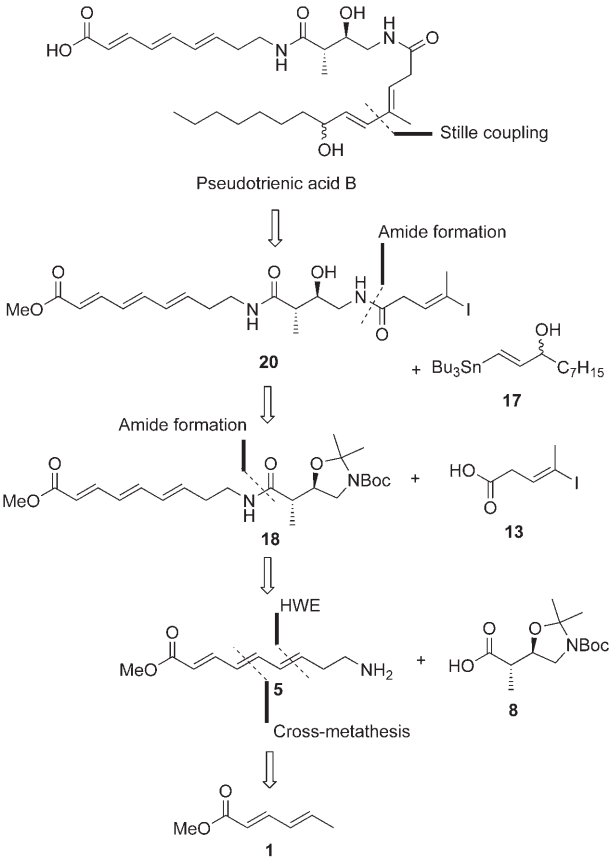


***Scheme 2.*** Retrosynthetic analysis of pseudotrienic acid B. Boc = *tert*-butyloxycarbonyl, HWE = Horner–Wadsworth–Emmons reaction.

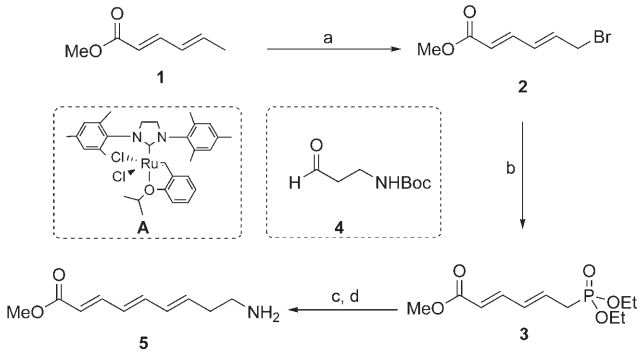


***Scheme 3.*** Synthesis of amino trienoate **5**. Reagents and conditions: a) allyl bromide (5 equiv), **A** (2 mol%), $CH_2Cl_2$, RT, 48 h, 48%; b) $P(OEt)_3$, toluene, reflux, 1 h, 99%; c) LDA (1.4 equiv), aldehyde **4**, THF, −78°C for 15 min then 0°C for 30 min; d) TFA/$CH_2Cl_2$ (1:5), 0°C→RT, then $Na_2CO_3$, 52% (2 steps). LDA = lithium diisopropylamide, THF = tetrahydrofuran.

treated with allyl bromide (5 equiv) in $CH_2Cl_2$ at room temperature for 48 h, in the presence of the Grubbs–Hoveyda catalyst[3] (**A**, 2 mol%), to produce **2** in 48% yield with good stereoselectivity ($E,E/E,Z > 95:5$).[4] Subsequent phosphonation of the dienic allylic bromide **2** under Michaelis–Arbuzov conditions led to the formation of diethylphosphonate **3** in 99% yield.[5] It is worth noting that a cross-metathesis

 © 2006 Wiley-VCH Verlag GmbH & Co. KGaA, Weinheim 

reaction between methyl sorbate and diethyl allylphosphonate also furnishes **3** with a similar yield but, with this procedure, the purification of **3** was complicated by difficulties in the removal of ruthenium byproducts from this highly polar compound. Horner–Wadsworth–Emmons olefination between phosphonate **3** and the *N*-Boc-protected amino aldehyde **4** was accomplished in the presence of LDA[6] and resulted, after TFA-mediated deprotection, in the formation of the free trienic amine **5** in 52% yield. Thus, the trienic ester **5** was synthesized efficiently in four steps from methyl sorbate (**1**) in approximately 25% overall yield.

The synthesis of the amino acid **8**, which was to be coupled with **5** to produce the C1–C14 fragment of pseudotrienic acid B, was achieved by starting from the *N*-Boc-protected glycine methyl ester **6** (Scheme 4). In order to control the

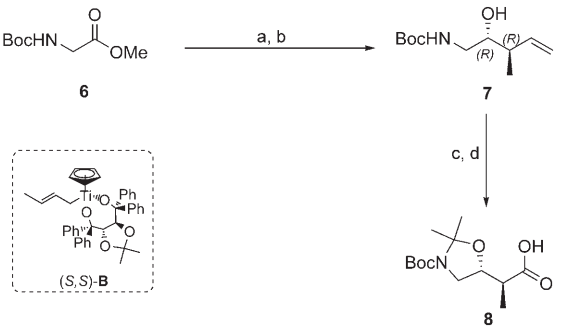


***Scheme 4.*** Synthesis of carboxylic acid **8**. Reagents and conditions: a) DIBAL-H in toluene (1.1 equiv), $CH_2Cl_2$, −78 °C, 2 h; b) (*S*,*S*)-**B** (1.3 equiv), $Et_2O$, −78 °C, 12 h, 57% (2 steps); c) 2,2-DMP, *p*TsOH (0.1 equiv), acetone, RT, 5 min; d) $RuCl_3$ (0.05 equiv), $NaIO_4$ (4.0 equiv), $CCl_4/CH_3CN/H_2O$ (2:2:3), RT, 12 h, 75% (2 steps). DIBAL-H = diisobutylaluminum hydride, 2,2-DMP = 2,2-dimethoxypropane, *p*TsOH = toluene-4-sulfonic acid.

configuration of the two stereogenic centers C11 and C12 in pseudotrienic acid B, the amino ester **6** was transformed into the corresponding aldehyde by reduction with DIBAL-H,[7] and then treated directly with the highly face-selective crotyltitanium complex (*S*,*S*)-**B**,[8] which gave rise to the homoallylic amino alcohol **7** in 57% yield with high diastereoselectivity (d.r. > 95:5) and enantioselectivity (> 95% *ee*).[9] Subsequent protection of the obtained amino alcohol as the *N*,*O*-acetonide by using 2,2-DMP followed by ruthenium-catalyzed oxidative cleavage of the terminal olefin under Sharpless conditions[10] led to the desired carboxylic acid **8** with an overall yield of 75% for the two steps (Scheme 4).

The *E* vinyl iodide **13**, which corresponds to the C16–C19 fragment of pseudotrienic acid B, was synthesized in three steps from the commercially available pent-3-yn-1-ol (**9**) as outlined in Scheme 5. Regio- and stereoselective stannylcupration with the mixed higher-order cuprate reagent $[(Bu_3Sn)BuCu(CN)Li_2]$[11] in the presence of MeOH afforded the two known vinyl stannanes **10** and **11** in a 9:1 ratio with a combined yield of 74%. These two regioisomers were separated by flash chromatography on silica gel and the desired *E* vinyl stannane **10** was subjected to iododestannylation to give the known vinyl iodide **12** in very high yield

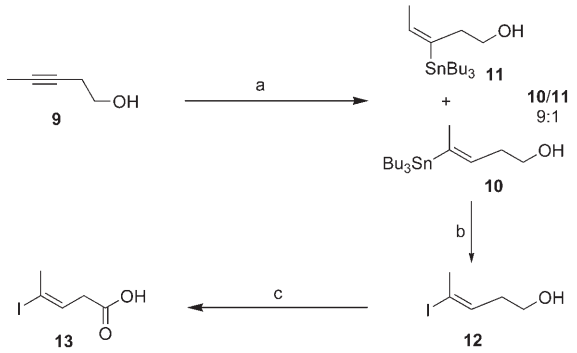


***Scheme 5.*** Synthesis of vinyl iodide **13**. Reagents and conditions: a) CuCN (4.0 equiv), *n*BuLi (8.0 equiv), $nBu_3SnH$ (8.0 equiv), MeOH (0.2 equiv), THF, −40 °C, 12 h, 74%; b) $I_2$, $Et_2O$, 0 °C → RT, 94%; c) $CrO_3$–$H_2SO_4$ (3.1 equiv), acetone, 0 °C, 30 min, 92%.

(94%).[12] Oxidation with Jones' reagent afforded the desired carboxylic acid **13** in 92% yield.

The last fragment, the vinyl stannane **17** (C20–C29 fragment), was prepared from the commercially available octanal (**14**) (Scheme 6). After addition of ethynyl magnesium bromide, the resulting propargylic alcohol **15** (81% yield)[13,14] was treated with NBS in the presence of $AgNO_3$, thus leading to the bromoalkyne **16** in 93% yield. Regio- and stereocontrolled (> 95% *E* isomer) Pd-mediated hydrostannylation[15] of bromoalkyne **16** with $nBu_3SnH$ in the presence of 5 mol% of $[PdCl_2(PPh_3)_2]$ afforded the desired alkenyl stannane **17** in 70% yield (Scheme 6).

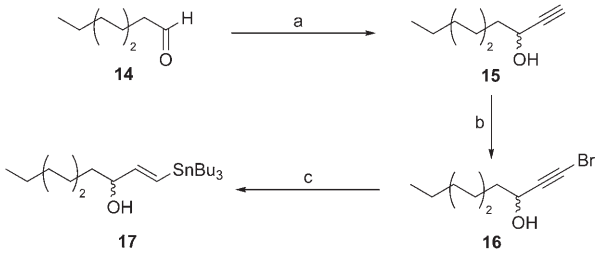


***Scheme 6.*** Synthesis of vinyl stannane **17**. Reagents and conditions: a) HC≡CMgBr (2.0 equiv), THF, 0 °C → RT, 12 h, 81%; b) NBS (1.1 equiv), $AgNO_3$ (0.1 equiv), acetone, 12 h, RT, 93%; c) $nBu_3SnH$ (4.0 equiv), $[PdCl_2(PPh_3)_2]$ (0.05 equiv), THF, 0 °C, 4 h, 70%. NBS = *N*-bromosuccinimide.

With the four fragments in hand, the coupling reactions were performed as shown in Scheme 7. First, the carboxylic acid **8** was coupled with the amino trienic ester **5** by using HOBt, HBTU, and NMM in acetonitrile and amide **18** was isolated in 96% yield (Table 1). In order to obtain the C1–C19 fragment of pseudotrienic acid B, compound **18** was treated with *p*TsOH in MeOH to afford the *N*-Boc-protected amino alcohol **19** in 82% yield.[16] After removal of the *tert*-butyloxycarbonyl group, the resulting amino alcohol was coupled with the carboxylic acid **13** to produce compound **20**, the C1–C19 fragment of pseudotrienic acid B (Table 1).

 © 2006 Wiley-VCH Verlag GmbH & Co. KGaA, Weinheim 

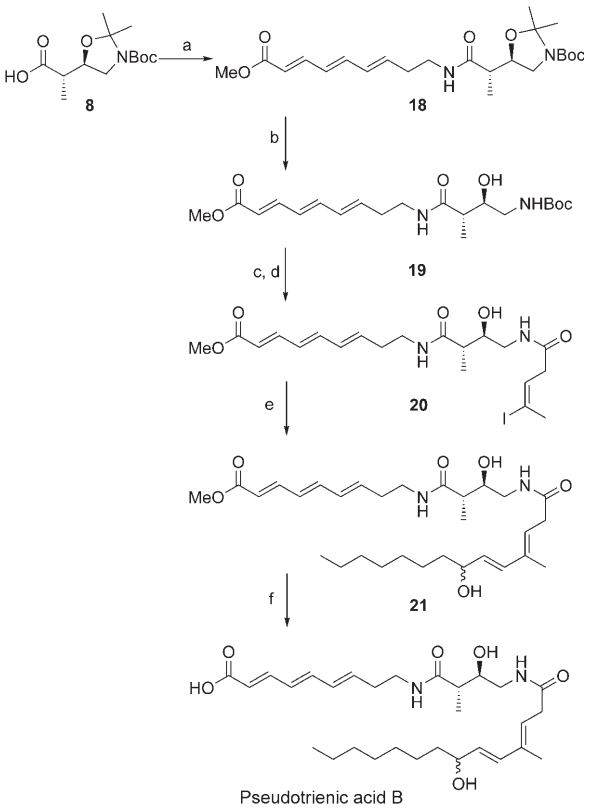


***Scheme 7.*** Completion of the total synthesis of pseudotrienic acid B. Reagents and conditions: a) **5** (1.2 equiv), HOBT (1.2 equiv), HBTU (1.2 equiv), NMM (3.0 equiv), $CH_3CN$, 0 °C→RT, 6 h, 96%; b) *p*TsOH (0.5 equiv), MeOH, 4 h, RT, 82%; c) TFA/$CH_2Cl_2$ (1:5), 0 °C→RT, 45 min; d) **13** (1.1 equiv), HOBT (1.1 equiv), HBTU (1.1 equiv), NMM (3.0 equiv), $CH_3CN$, 0 °C→RT, 12 h, 78% (2 steps); e) **17** (1.5 equiv), $[PdCl_2(MeCN)_2]$ (0.05 equiv), DMF degassed with Ar, RT, 12 h, 51%; f) LiOH (30 equiv), MeOH/THF/$H_2O$ (2:2:1), RT, 12 h, 75%. HOBT = *N*-hydroxybenzotriazole, HBTU = *O*-(1*H*-benzotriazol-1-yl)-*N*,*N*,*N*′,*N*′-tetramethyluronium hexafluorophosphate, NMM = *N*-methylmorpholine, DMF = *N*,*N*-dimethylformamide, TFA = trifluoroacetic acid.

***Table 1:*** Selected analytical data for compounds **18**, **20**, and **21**.

**18**: $[\alpha]_D^{20} = -4.50$ ($c = 1.36$, MeOH); IR (film): $\tilde{\nu}_{max} = 3424, 3338, 2978, 2938, 1693, 1658, 1616, 1542, 1392, 1367, 1253, 1140, 1007, 839\ cm^{-1}$; $^1H$ NMR (400 MHz, $CDCl_3$): $\delta = 7.29$ (dd, $J = 15.2, 11.2$ Hz, 1H), 6.51 (dd, $J = 14.8, 10.8$ Hz, 1H), 6.30–6.15 (m, 2H and NH), 5.87 (m, 1H), 5.87 (d, $J = 15.2$ Hz, 1H), 4.09 (m, 1H), 3.75 (s, 3H), 3.64 (brs, 1H), 3.37 (m, 2H), 3.11 (t, $J = 9.9$ Hz, 1H), 2.37 (m, 3H), 1.56 (brs, 3H), 1.51 (brs, 3H), 1.47 (s, 9H), 1.14 ppm (brs, 3H); $^{13}C$ NMR (75 MHz, $CDCl_3$): $\delta = 173.2$ (s), 167.5 (s), 152.2 and 151.8 (s), 144.6 (d), 140.4 (d), 136.1 (d), 131.9 (d), 128.8 (d), 120.4 (d), 94.0 and 93.5 (s), 80.4 and 79.8 (s), 75.0 (d), 51.5 (q), 49.6 and 49.5 (t), 44.2 and 44.0 (d), 38.5 (t), 33.1 (t), 28.3 (3q), 27.3, 26.2, 25.2, and 24.4 (2q), 13.4 ppm (q); HRMS ($CI^+$, $NH_3$): calcd for $C_{23}H_{37}O_6N_2$ [$M$+$H^+$]: 437.2652; found: 437.2643.

**20**: $[\alpha]_D^{20} = +6.93$ ($c = 0.88$, $CHCl_3$); IR (film): $\tilde{\nu}_{max} = 3293, 2930, 1711, 1639, 1616, 1541, 1433, 1263, 1233, 1136, 1004, 732, 618\ cm^{-1}$; $^1H$ NMR (400 MHz, $CDCl_3$): $\delta = 7.28$ (dd, $J = 15.3, 11.3$ Hz, 1H), 6.78 (brm, NH, 1H), 6.57 (brm, NH, 1H), 6.52 (dd, $J = 14.9, 10.8$ Hz, 1H), 6.31 (brt, $J = 7.5$ Hz, 1H), 6.25 (dd, $J = 14.9, 11.3$ Hz, 1H), 6.20 (dd, $J = 15.4, 10.8$ Hz, 1H), 5.87 (d, $J = 15.3$ Hz, 1H), 5.87 (m, 1H), 4.61 (m, 1H), 3.74 (s, 3H), 3.66 (brm, OH, 1H), 3.51 (ddd, $J = 11.5, 6.6, 4.2$ Hz, 1H), 3.34 (m, 2H), 3.12 (ddd, $J = 11.5, 7.5, 4.9$ Hz, 1H), 2.97 (d, $J = 7.5$ Hz, 2H), 2.40 (s, 3H), 2.40–2.31 (m, 3H), 1.24 ppm (d, $J = 7.0$ Hz, 3H); $^{13}C$ NMR (75 MHz, $CDCl_3$): $\delta = 175.8$ (s), 170.2 (s), 167.5 (s), 144.7 (d) 140.4 (d), 135.7 (d), 132.8 (d), 132.1 (d), 128.9 (d), 120.3 (d), 97.8 (s), 73.2 (d), 51.6 (q), 44.4 (t), 43.2 (d), 38.5 (t), 37.7 (t), 33.0 (t), 27.9 (q), 15.7 ppm (q); HRMS ($CI^+$, $NH_3$): calcd for $C_{20}H_{30}O_5N_2I$ [$M$+$H^+$]: 505.1199; found: 505.1195.

**21**: $[\alpha]_D^{20} = +7.37$ ($c = 0.38$, $CHCl_3$); IR (film): $\tilde{\nu}_{max} = 3308, 2956, 2927, 2856, 1720, 1646, 1619, 1546, 1459, 1435, 1271, 1137, 1074, 1007, 739\ cm^{-1}$; $^1H$ NMR (400 MHz, $CDCl_3$): $\delta = 7.22$ (dd, $J = 15.2, 11.2$ Hz, 1H), 6.45 (dd, $J = 14.7, 10.7$ Hz, 1H), 6.29 (m, NH, 1H), 6.20 (d, $J = 15.7$ Hz, 1H), 6.20–6.04 (m, 2H and NH), 5.81 (m, 1H), 5.80 (d, $J = 15.2$ Hz, 1H), 5.62 (dd, $J = 15.6, 6.8$ Hz, 1H), 5.53 (t, $J = 7.6$ Hz, 1H), 4.33 (d, $J = 5.9$ Hz, OH, 1H), 4.09 (m, 1H), 3.68 (s, 3H), 3.55 (brm, 1H), 3.45 (m, 1H), 3.29 (m, 2H), 3.03 (m, 3H), 2.31 (q, $J = 6.8$ Hz, 2H), 2.22 (m, 1H), 1.70 (s, 3H), 1.55–1.40 (m, 2H), 1.30–1.15 (m, 10H and OH), 1.18 (d, $J = 7.6$ Hz, 3H), 0.81 ppm (t, $J = 6.7$ Hz, 3H); $^3C$ NMR (75 MHz, $CDCl_3$): $\delta = 175.6$ (s), 172.0 (s), 167.6 (s), 144.7 (d), 140.4 (d), 137.6 (s), 135.7 (d), 133.9 (d), 132.2 (d), 132.0 (d), 128.9 (d), 123.2 (d), 120.4 (d), 73.5 (d), 72.9 (d), 51.6 (q), 44.4 (t), 43.2 (d), 38.5 (t), 37.5 (t), 36.2 (t), 33.0 (t), 31.8 (t), 29.6 (t), 29.3 (t), 25.5 (t), 22.7 (t), 15.7 (q), 14.1 (q), 12.8 ppm (q); HRMS ($CI^+$, $NH_3$): calcd for $C_{30}H_{49}O_6N_2$ [$M$+$H^+$]: 533.3591; found: 533.3597.

The synthesis of pseudotrienic acid B was completed by performing a $[PdCl_2(MeCN)_2]$-catalyzed Stille cross-coupling reaction in DMF[17] between vinyl iodide **20** and vinyl stannane **17** with a nonprotected allylic alcohol, thus producing the core structure of pseudotrienic acid B in 51% yield as a mixture of two diastereoisomers, epimeric at C20 (compound **21**) (Table 1). It is noteworthy that only one set of NMR signals is observed, a fact suggesting that these two diastereoisomers cannot be distinguished by NMR spectroscopy since they give an identical spectrum. Finally, a simple saponification of the methyl ester **21** with LiOH afforded the expected pseudotrienic acid B in 75% yield.[18] The spectroscopic data for synthetic pseudotrienic acid B were in agreement with those reported in the literature for the natural product.[1]

In conclusion, a concise, efficient, and highly convergent stereoselective synthesis of the bioactive natural product pseudotrienic acid B has been achieved, with a longest linear sequence of 10 steps from methyl sorbate (**1**) (5.8% overall yield). Synthetic highlights include a crotyltitanation reaction to control the stereogenic centers at C11 and C20, a cross-metathesis reaction to synthesize the triene moiety, and a palladium-catalyzed Stille cross-coupling reaction to complete the assembly of the carbon framework of pseudotrienic acid B. This rapid and flexible synthetic approach will allow access to a wide variety of analogues for biological evaluation. The possibility of assigning the configuration at C16 in FR252921 by the stereoselective synthesis of each of the two epimers of pseudotrienic acid B is currently under investigation.

Received: March 21, 2006
Revised: May 10, 2006
Published online: July 31, 2006

**Keywords:** cross-coupling · crotyltitanation · metathesis · natural products · total synthesis

 © 2006 Wiley-VCH Verlag GmbH & Co. KGaA, Weinheim 

[1] A. Pohanka, A. Broberg, M. Johansson, L. Kenne, J. Levenfors, *J. Nat. Prod.* **2005**, *68*, 1380 – 1385.

[2] a) K. Fujine, M. Tanaka, K. Ohsumi, M. Hashimoto, S. Takase, H. Ueda, M. Hino, T. Fujii, *J. Antibiot.* **2003**, *56*, 55 – 61; b) K. Fujine, F. Abe, N. Seki, H. Ueda, M. Hino, T. Fujii, *J. Antibiot.* **2003**, *56*, 62 – 67; c) K. Fujine, H. Ueda, M. Hino, T. Fujii, *J. Antibiot.* **2003**, *56*, 68 – 71.

[3] J. S. Kingsbury, J. P. A. Harrity, P. J. Bonitatebus, Jr., A. H. Hoveyda, *J. Am. Chem. Soc.* **1999**, *121*, 791 – 799.

[4] Bromodiene **2** was contaminated by traces of mono- and polyunsaturated ω-bromoester byproducts, which could not be separated by flash chromatography on silica gel.

[5] K.-U. Schöning, R. Wittenberg, A. Kirschning, *Synlett* **1999**, 1624 – 1626.

[6] K. C. Nicolaou, R. A. Daines, T. K. Chakraborty, Y. Ogawa, *J. Am. Chem. Soc.* **1988**, *110*, 4685 – 4696.

[7] D. A. Powell, R. A. Batey, *Org. Lett.* **2002**, *4*, 2913 – 2916.

[8] A. Hafner, R. O. Duthaler, R. Marti, J. Rihs, P. Rhote-Streit, F. Schwarzenbach, *J. Am. Chem. Soc.* **1992**, *114*, 2321 – 2336.

[9] The 2*R*,3*R* absolute configuration of **7** was confirmed by the $^{1}$H NMR spectra of the two corresponding mandelates, according to the procedure described in J. M. Seco, E. Quiñoa, R. Riguera, *Tetrahedron: Asymmetry* **2001**, *12*, 2915 – 2925.

[10] a) A. V. Statsuk, D. Liu, S. A. Kozmin, *J. Am. Chem. Soc.* **2004**, *126*, 9546 – 9547; b) P. H. J. Carlsen, T. Katsuki, V. S. Martin, K. B. Sharpless, *J. Org. Chem.* **1981**, *46*, 3936 – 3938.

[11] a) B. H. Lipshutz, E. L. Ellsworth, S. H. Dimock, D. C. Reuter, *Tetrahedron Lett.* **1989**, *30*, 2065 – 2068; b) I. Beaudet, J.-L. Parrain, J.-P. Quintard, *Tetrahedron Lett.* **1991**, *32*, 6333 – 6336; c) J.-F. Betzer, F. Delaloge, B. Muller, A. Pancrazi, J. Prunet, *J. Org. Chem.* **1997**, *62*, 7768 – 7780.

[12] L. Commeiras, M. Santelli, J.-L. Parrain, *Org. Lett.* **2001**, *3*, 1713 – 1715.

[13] L. Skattebøl, E. R. H. Jones, M. C. Whiting, *Organic Syntheses, Vol IV*, Wiley, New York, **1967**, p. 792.

[14] P. L. Rinaldi, G. C. Levy, *J. Org. Chem.* **1980**, *45*, 4348 – 4351.

[15] H. X. Zhang, F. Guibé, G. Balavoine, *J. Org. Chem.* **1990**, *55*, 1857 – 1867.

[16] A. Dondoni, P. P. Giovannini, A. Massi, *Org. Lett.* **2004**, *6*, 2929 – 2932.

[17] a) J. K. Stille, *Angew. Chem.* **1986**, *98*, 504 – 519; *Angew. Chem. Int. Ed. Engl.* **1986**, *25*, 508 – 524; b) J.-F. Betzer, J.-L. Lallemand, A. Pancrazi, *Synthesis* **1998**, 522 – 534; c) K. C. Nicolaou, Y. Li, K. Sugita, H. Monenschein, P. Guntupalli, H. J. Mitchell, K. C. Fylaktakidou, D. Vourloumis, P. Giannakakou, A. O'Brate, *J. Am. Chem. Soc.* **2003**, *125*, 15443 – 15454.

[18] Only one set of NMR signals is observed for the mixture of epimers at C20.


 © 2006 Wiley-VCH Verlag GmbH & Co. KGaA, Weinheim 

G Quadruplexes

DOI: 10.1002/anie.200600909

# Turning Inhibitors into Activators: A Hammerhead Ribozyme Controlled by a Guanine Quadruplex**

*Markus Wieland and Jörg S. Hartig**

Guanosine-rich nucleic acid sequences are prone to adopt quadruplex structures consisting of stacked planes of four base-paired guanine nucleobases.[1,2] Inside cells, such four-stranded complexes are thought to play important regulatory roles.[3,4] For example, the G-rich strand of the telomeric DNA repeat has been demonstrated to fold into a G quadruplex under certain conditions, potentially regulating the function of these "genomic caps" during the cell cycle.[5,6] In addition, many promoter elements within the human genome contain G-rich sequences that are thought to be involved in controlling gene expression.[7–9] Also, some examples are known where quadruplexes within messenger RNAs act as regulatory elements.[10,11] Furthermore, several compounds have been characterized that interact with DNA quadruplex structures.[12] Some of these substances display strong and specific affinity towards quadruplex strands. For example, compounds have been identified that are able to induce quadruplex folding of a G-rich DNA strand even when the latter is hybridized to the complementary, cytosine-rich strand.[13]

Although interactions between DNA quadruplexes and their respective ligands have been characterized in great detail over the last decade, compounds binding to RNA quadruplexes have so far received much less attention, even though G-rich RNA is known to fold into quadruplexes as well.[14,15] We are interested in developing nucleic acid modules that enable the regulation of attached functional nucleic acid sequences. In our opinion, quadruplex structures are well suited as switching devices since a global conformational change takes places upon traversing from the unfolded to the highly compact, four-stranded state. Moreover, it should be possible to find suitable substances that specifically induce the folding of such rigid structures.

In order to search for compounds that are able to trigger an RNA quadruplex switch, we have fused G-rich RNA sequences to the hammerhead ribozyme (HHR). Within this setup, the cleavage reaction of the ribozyme should be placed under control of a quadruplex-inducing compound, rendering the catalytic property of the ribozyme accessible to external regulation. Initially, we set out to generate two differently regulated variants of the hammerhead ribozyme, one that is activated and one that is inhibited by a G-quadruplex-inducing ligand. When testing a series of compounds for their effects on unmodified ribozymes, we surprisingly found that one of the compounds exhibited the most potent inhibition of a nonaltered hammerhead ribozyme known to date. Subsequently, by fusing G-rich sequences to the hammerhead sequence, we succeeded in generating a ribozyme variant that is activated instead of inhibited by the very same compound.

The hammerhead ribozyme (HHR) is a well characterized, small RNA motif that exhibits phosphodiesterase activity.[16] Minimum requirements for cleavage activity are folding of the conserved catalytic core and stems I–III and the presence of divalent metal ions such as $Mg^{2+}$. For our studies, we chose a catalytically well-behaved hammerhead sequence that is able to undergo multiple substrate turnovers, referred to as wild-type HHR (wt-HHR, Figure 1a).[17,18] In order to search for compounds that interfere with ribozyme cleavage, we screened a series of compounds previously known to bind to DNA quadruplexes. Among these substances, the porphyrin derivative TMPyP4 (*meso*-5,10,15,20-tetrakis-(*N*-methyl-4-pyridinio)porphine)[19] exhibited very potent inhibition of the unmodified, wt-HHR with half-maximum activity (i.e. rate of cleavage) at a concentration of $(105 \pm 5)$ nM (Figure 1b). For better comparison, we reevaluated the inhibitory potential at conditions similar to those used in a previous study of hammerhead ribozyme inhibitors (i.e. in the absence of potassium ions).[18] When monovalent ions were depleted, the inhibitory potency even increased with an $IC_{50}$ of $(46 \pm 10)$ nM (see the Supporting Information). To our knowledge, the porphyrin TMPyP4 represents the most powerful inhibitor of a ribozyme cleavage reaction known to date.

Our initial goal was to evaluate the suitability of G-rich sequences as switching devices for catalytic activity. A powerful demonstration of such a regulatory module would be the realization of a ribozyme that is activated by the strongly inhibitory compound TMPyP4, hence reversing the compound's action towards the RNA functionality. Starting from wt-HHR, we generated several ribozyme variants by exchanging stem II for G-rich sequence stretches. Alteration of stem II has been utilized previously for enabling regulation of the hammerhead ribozyme.[20–23] Formation of stem-loop II is necessary for correct folding of the catalytic core, and hence cleavage activity.[24] In the present study we exploited a destabilization of the catalytic core by introducing the G-rich loop that diminishes the base pairs found in stem II of the wild-type ribozyme wt-HHR. This results in a catalytically impaired ribozyme GQP-HHR (Figure 1c). Indeed, the resulting sequence exhibited only low cleavage activity ($k_{obs} = 0.00012\ min^{-1}$, column "GQP-HHR alone", Figure 1d). However, when the formerly inhibitory compound TMPyP4 was added, activation of the cleavage reaction was observed. At 200 nM concentration of the quadruplex binder,

[*] M. Wieland, Prof. Dr. J. S. Hartig
University of Konstanz
Department of Chemistry
Universitätsstrasse 10, 78457 Konstanz (Germany)
Fax: (+49) 7531-885-140
E-mail: joerg.hartig@uni-konstanz.de

[**] J.S.H. gratefully acknowledges the Volkswagen Foundation for funding a Lichtenberg Professorship. We thank the Department of Chemistry at the University of Konstanz for support.

Supporting information for this article, including description of RNA preparation, ribozyme reactions, nuclease digestions, and additional ribozyme cleavage data, is available on the WWW under http://www.angewandte.org or from the author.

 © 2006 Wiley-VCH Verlag GmbH & Co. KGaA, Weinheim 

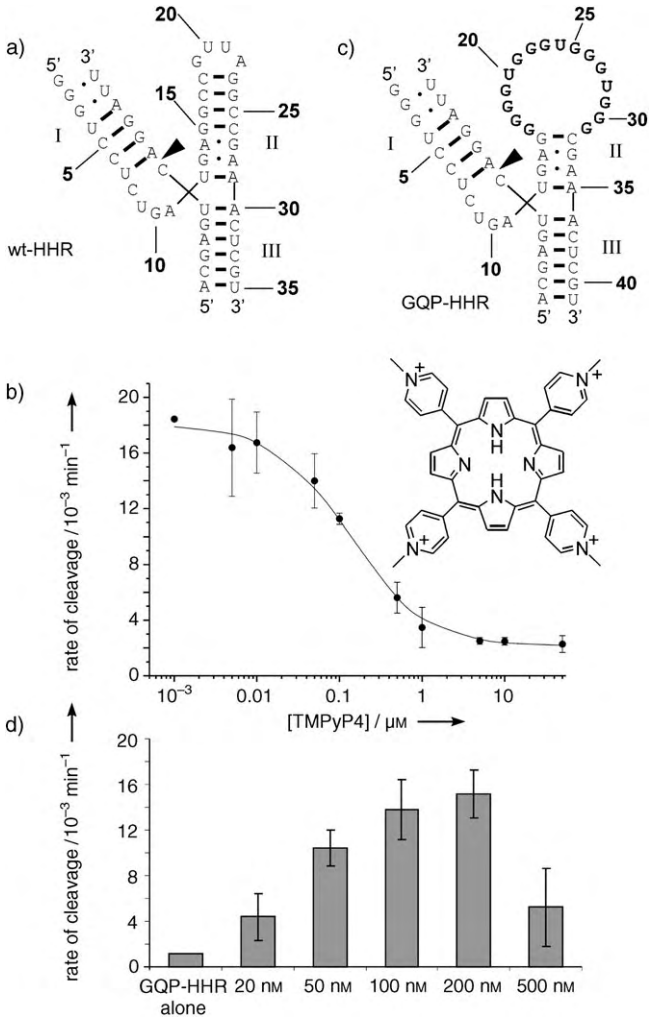


***Figure 1.*** Secondary structures and activity of hammerhead ribozymes (HHRs) in response to TMPyP4. a) Structure of the wild-type ribozyme (wt-HHR) in complex with the substrate strand. The arrow indicates the substrate cleavage site. b) Inhibition of wt-HHR by the porphyrin TMPyP4 (insert). The initial cleavage activity is shown. Half-maximal inhibition ($IC_{50}$) occurs at a concentration of 105 nM. c) Structure of the HHR variant GQP-HHR containing a G-rich loop in stem II. d) Activation of the G-rich ribozyme variant GQP-HHR by TMPyP4. Ribozyme reactions were carried out in 50 mM tris(hydroxymethyl)-aminomethane (Tris), pH 7.5, containing 100 mM KCl, 10 mM $MgCl_2$, 500 nM substrate, 10 nM wt-HHR or 50 nM GQP-HHR at 25 °C. For details see the Supporting Information.

more than tenfold activation could be induced. In contrast, pronounced inhibition of catalytic activity is already observed at this concentration for the wt-HHR. Nevertheless, only approximately one-tenth of the wt-HHR cleavage rate is achieved by TMPyP4-mediated induction of GQP-HHR. Higher concentrations ($\geq$ 500 nM) of TMPyP4 inhibited the GQP-HHR as well (see Figure 1 d).

With respect to the applied design for generation of the activated ribozyme GQP-HHR, the TMPyP4-dependence of the cleavage reaction suggests that folding of the G-rich loop is induced upon addition of the G-quadruplex binder. A stabilization of stem II and the catalytic core would result in enhanced cleavage activity. To validate this hypothesis, we probed the structures of both ribozymes by digesting the RNA sequences with ribonuclease T1. The endonuclease cleaves preferentially single-stranded RNA after guanosine residues. This specificity is best suited for detecting the hypothesized compound-induced folding of the G-rich loop of the GQP-HHR ribozyme since quadruplex structures are less accessible than unstructured sequences for nuclease digestion.[25] The nuclease digestions were carried out in analogy to the ribozyme cleavage reactions, except that an RNA substrate lacking the 2′-hydroxy function at the cleavage site was used to prevent ribozyme-catalyzed cleavage.

First, the wt-HHR was probed at various concentrations of TmPyP4 (Figure 2). The strongest nuclease-mediated cleavage was observed at position G13 (for numbering see Figure 1, the position corresponds to G8 following the general numbering system for hammerhead ribozymes, see reference [26]), a nucleoside that is part of the catalytic core of the ribozyme. Interestingly, the T1-cleavage intensity increases with increasing porphyrin concentrations for the wt-HHR. This is in accordance with inhibition of catalytic activity of wt-HHR in response to increasing TmPyP4 concentrations. For efficient ribozyme activity, the catalytic core must be folded as depicted in Figure 1 a. With increasing concentrations of the porphyrin, the catalytic core is destabilized and hence more accessible to nuclease digestion. Minor cleavage sites such as position G16 as well as guanosines within stem-loop II show similar behavior.

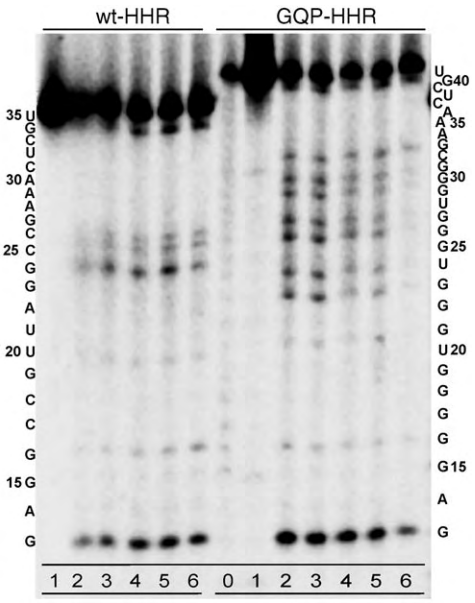


***Figure 2.*** Probing of ribozyme structures in response to TMPyP4 by means of ribonuclease T1 digestion. Ribonuclease T1 digest of wt-HHR (left) and GQP-HHR (right). The ribozymes were labeled at the 5′-end using γ-$^{32}$P-ATP and polynucleotide kinase. 1) Undigested ribozymes, 2) T1-digested ribozymes; ribozymes digested in the presence of 3) 1 nM TMPyP4, 4) 10 nM TMPyP4, 5) 100 nM TmPyP4, 6) 1 μM TMPyP4; 0) $OH^-$ ladder of GQP-HHR. Significant cleavage fragments shorter than the shown 13nt were not observed. For secondary structures and numbering of wt-HHR and GQP-HHR see Figure 1.

 © 2006 Wiley-VCH Verlag GmbH & Co. KGaA, Weinheim 

A possible explanation for the inhibitory mechanism could be that the porphyrin derivative binds next to the three-helix junction within the catalytic core. This part contains G–A as well as three-base pairs that would allow extended π-stacking interactions.[27,28] Binding directly to the catalytic core would explain the pronounced effects of TMPyP4. Although the mechanism of inhibition cannot be extracted from the T1 digestions, formation of G quadruplexes is very unlikely in the wt-HHR, since no G-rich stretches are present in the ribozyme. An intermolecular G quadruplex composed of four ribozymes could in principle form from the 5′-GGG trinucleotide but is unlikely to occur at a ribozyme concentration as low as 10 nM. Moreover, such a structure would have to compete with binding of the RNA substrate; the latter is present in 50-fold excess. When we subsequently probed the GQP-HHR by T1 nuclease digestion, the observed behavior with respect to increasing TMPyP4 concentrations was opposite. G13 again showed strongest T1 cleavage, followed by several residues in the introduced G-rich loop. At all sites, nuclease-mediated cleavage diminishes with increasing porphyrin concentrations. This is in contrast to the digestion of wt-HHR and in accordance with the initial activation mediated by TMPyP4. Since the formation of the catalytically active structure was destabilized by exchanging stem-loop II for the G-rich loop, nuclease cleavage is strongest in absence of TMPyP4. With increasing compound concentrations the G-rich loop folds, supporting cleavage activity by formation of the catalytic core.

About ten years ago, the discovery of ribozyme inhibitors stimulated interest in RNA as a drug target.[29–31] Over the past decade, RNA binders such as aminoglycosides and tetracyclines have been characterized in great detail as inhibitors of ribozyme cleavage. In contrast, substances that interact with DNA quadruplexes have not yet been tested for interference with ribozymes. Here, we have presented the *N*-methyl-pyridyl-substituted porphyrin TMPyP4 as a novel RNA binder that exhibits two to three orders of magnitude more potent inhibition of the unmodified, wt-HHR than that of previously known HHR inhibitors.[18,29–31] Furthermore, we were able to demonstrate that G-rich sequences are well suited as regulatory motifs for RNA cleavage activity. By exclusively employing rational design of the functional nucleic acid sequence, we were able to turn the strongly inhibitory effect of TMPyP4 into an activating one by adding G-rich sequences that apparently create a further binding site for TMPyP4. The example demonstrates that the response of a biologically functional macromolecule to a certain stimulus can strongly depend on, and hence be influenced by, modular design.[32] The concept of modular RNA switches is essentially supported by the fascinating architectures of recently discovered riboswitches.[33]

Although TMPyP4 strongly inhibits ribozyme cleavage in the absence of the designed G-quadruplex module, the compound is well tolerated in vivo, suggesting a specific interaction. For example, TMPyP4 shows efficient uptake in yeast and is nontoxic in human cell culture as well as in mice.[34–36] Moreover, TMPyP4 is considered as a potential antiproliferative therapeutic given that inhibition of tumor xenograft growth was demonstrated in mice.[36,37] Future work in our lab will focus on the regulation of other functional RNAs by G-quadruplex modules as well as exploring the possibility to employ such mechanisms for switching nucleic acid functions in vivo.

Received: March 8, 2006
Published online: July 27, 2006

**Keywords:** inhibitors · nucleic acids · porphyrinoids · riboswitches · ribozymes

[1] M. A. Keniry, *Biopolymers* **2000**, *56*, 123.
[2] T. Simonsson, *Biol. Chem.* **2001**, *382*, 621.
[3] R. H. Shafer, I. Smirnov, *Biopolymers* **2000**, *56*, 209.
[4] H. Arthanari, P. H. Bolton, *Chem. Biol.* **2001**, *8*, 221.
[5] S. Neidle, G. N. Parkinson, *Curr. Opin. Struct. Biol.* **2003**, *13*, 275.
[6] T. R. Cech, *Angew. Chem.* **2000**, *112*, 34; *Angew. Chem. Int. Ed.* **2000**, *39*, 34.
[7] A. Siddiqui-Jain, C. L. Grand, D. J. Bearss, L. H. Hurley, *Proc. Natl. Acad. Sci. USA* **2002**, *99*, 11593.
[8] J. Dai, T. S. Dexheimer, D. Chen, M. Carver, A. Ambrus, R. A. Jones, D. Yang, *J. Am. Chem. Soc.* **2006**, *128*, 1096.
[9] S. Rankin, A. P. Reszka, J. Huppert, M. Zloh, G. N. Parkinson, A. K. Todd, S. Ladame, S. Balasubramanian, S. Neidle, *J. Am. Chem. Soc.* **2005**, *127*, 10584.
[10] J. C. Darnell, K. B. Jensen, P. Jin, V. Brown, S. T. Warren, R. B. Darnell, *Cell* **2001**, *107*, 489.
[11] S. Bonnal, C. Schaeffer, L. Creancier, S. Clamens, H. Moine, A. C. Prats, S. Vagner, *J. Biol. Chem.* **2003**, *278*, 39330.
[12] S. M. Kerwin, *Curr. Pharm. Des.* **2000**, *6*, 441.
[13] A. Rangan, O. Y. Fedoroff, L. H. Hurley, *J. Biol. Chem.* **2001**, *276*, 4640.
[14] B. Pan, Y. Xiong, K. Shi, M. Sundaralingam, *Structure* **2003**, *11*, 1423.
[15] H. Liu, A. Matsugami, M. Katahira, S. Uesugi, *J. Mol. Biol.* **2002**, *322*, 955.
[16] S. Verma, N. K. Vaish, F. Eckstein, *Curr. Opin. Chem. Biol.* **1997**, *1*, 532.
[17] T. K. Stage-Zimmermann, O. C. Uhlenbeck, *RNA* **1998**, *4*, 875.
[18] A. Jenne, J. S. Hartig, N. Piganeau, A. Tauer, D. A. Samarsky, M. R. Green, J. Davies, M. Famulok, *Nat. Biotechnol.* **2001**, *19*, 56.
[19] R. J. Fiel, J. C. Howard, E. H. Mark, N. Datta Gupta, *Nucleic Acids Res.* **1979**, *6*, 3093.
[20] M. Koizumi, G. A. Soukup, J. N. Kerr, R. R. Breaker, *Nat. Struct. Biol* **1999**, *6*, 1062.
[21] J. Tang, R. R. Breaker, *Chem. Biol.* **1997**, *4*, 453.
[22] J. S. Hartig, M. Famulok, *Angew. Chem.* **2002**, *114*, 4440; *Angew. Chem. Int. Ed.* **2002**, *41*, 4263.
[23] J. S. Hartig, S. H. Najafi-Shoushtari, I. Grune, A. Yan, A. D. Ellington, M. Famulok, *Nat. Biotechnol.* **2002**, *20*, 717.
[24] T. Tuschl, F. Eckstein, *Proc. Natl. Acad. Sci. USA* **1993**, *90*, 6991.
[25] V. Dapic, P. J. Bates, J. O. Trent, A. Rodger, S. D. Thomas, D. M. Miller, *Biochemistry* **2002**, *41*, 3676.
[26] K. J. Hertel, A. Pardi, O. C. Uhlenbeck, M. Koizumi, E. Ohtsuka, S. Uesugi, R. Cedergren, F. Eckstein, W. L. Gerlach, R. Hodgson, et al., *Nucleic Acids Res.* **1992**, *20*, 3252.
[27] H. W. Pley, K. M. Flaherty, D. B. McKay, *Nature* **1994**, *372*, 68.
[28] W. G. Scott, J. T. Finch, A. Klug, *Cell* **1995**, *81*, 991.
[29] T. K. Stage, K. J. Hertel, O. C. Uhlenbeck, *RNA* **1995**, *1*, 95.
[30] J. B. Murray, J. R. Arnold, *Biochem. J.* **1996**, *317*, 855.
[31] Q. Vicens, E. Westhof, *ChemBioChem* **2003**, *4*, 1018.
[32] R. Penchovsky, R. R. Breaker, *Nat. Biotechnol.* **2005**, *23*, 1424.
[33] W. C. Winkler, R. R. Breaker, *Annu. Rev. Microbiol.* **2005**, *59*, 487.

 © 2006 Wiley-VCH Verlag GmbH & Co. KGaA, Weinheim 

[34] E. Izbicka, L. D. Barnes, A. K. Robinson, K. K. Davidson, R. A. Lawrence, G. T. Hannibal, *Anticancer Res.* **2001**, *21*, 1899.
[35] S. Y. Rha, E. Izbicka, R. Lawrence, K. Davidson, D. Sun, M. P. Moyer, G. D. Roodman, L. Hurley, D. Von Hoff, *Clin. Cancer Res.* **2000**, *6*, 987.
[36] C. L. Grand, H. Han, R. M. Munoz, S. Weitman, D. D. Von Hoff, L. H. Hurley, D. J. Bearss, *Mol. Cancer Ther.* **2002**, *1*, 565.
[37] L. R. Kelland, *Eur. J. Cancer* **2005**, *41*, 971.

 © 2006 Wiley-VCH Verlag GmbH & Co. KGaA, Weinheim 

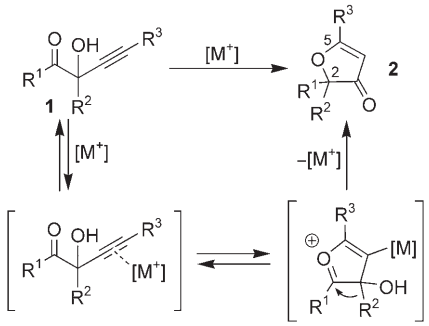

***Scheme 1.*** Projected synthesis of 3(2*H*)-furanones **2** by a catalyzed domino reaction consisting of heterocyclization and α-ketol rearrangement.

*Cyclization*

DOI: 10.1002/anie.200601836

# Gold(III)- and Platinum(II)-Catalyzed Domino Reaction Consisting of Heterocyclization and 1,2-Migration: Efficient Synthesis of Highly Substituted 3(2*H*)-Furanones**

*Stefan F. Kirsch,* Jörg T. Binder, Clémence Liébert, and Helge Menz*

Transition-metal-catalyzed rearrangements of unsaturated frameworks provide rapid access to complex structures. Owing to their exceptional ability to activate alkynes toward nucleophilic attack, gold[1,2] and platinum[3] complexes have found increased use as catalysts.[4] In the context of our ongoing efforts to develop cascade reactions initiated by transition-metal-catalyzed π-activation,[5] we now report a novel approach to 3(2*H*)-furanones by a catalyzed heterocyclization/1,2-migration cascade.

Recently, a $AuCl_3$-catalyzed cyclization of 2-(1-alkynyl)-2-alken-1-ones was reported leading to substituted furans.[6,7] This reaction is believed to proceed via oxonium ions. Based on this, we envisaged that alkynyl carbonyl compound **1** bearing a hydroxy group at the propargylic position might undergo a previously unknown transformation (Scheme 1). The intermediate oxonium ion is expected to trigger an irreversible 1,2-shift analoguous to a formal α-ketol rearrangement.[8] In contrast to the related pinacol rearrangements,[9] oxonium ion rearrangements have not been used to terminate cationic cyclizations. The overall sequence provides an efficient and flexible access to 3(2*H*)-furanones **2**, which are structural elements in many natural products[10] and pharmaceutically active substances.[11] Moreover, the reaction represents a significant departure from the conventional strategy for constructing 3(2*H*)-furanones, as bond formations between C5 and O1 typically are used in a cyclization step, and the hydroxy function at C2 is usually installed at an earlier stage.[12]

To probe the feasibility of this concept, we initially focused on the conversion of the alkynyl carbonyl compound **1a** into the spirocyclic compound **2a** (Table 1). Whereas the use of cationic gold(I) and silver(I) complexes was accompanied by a significant amount of decomposition, treatment of the starting alkyne **1a** with $PtCl_2$ or $AuCl_3$ resulted in the clean formation of 3(2*H*)-furanone **2a**. Depending on the reaction temperature, $AuCl_3$ provided the desired compound **2a** after 90 min in $CH_2Cl_2$ in yields of 83% or 95% (Table 1, entries 1 and 2). In the presence of catalytic amounts of $PtCl_2$, isomerization was observed at an impractical rate at 23 °C in $CH_2Cl_2$. Nevertheless, increasing the reaction temperature to 80 °C (in toluene) led to the anticipated increase in reaction rate (Table 1, entry 8).

***Table 1:*** Efficiency of transition-metal catalysts for the conversion of **1a** into **2a**.[a]

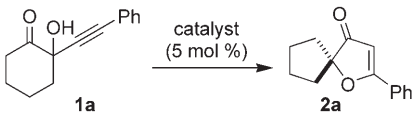

| Entry | Cat. | Conditions | Yield [%] | |
|---|---|---|---|---|
| | | | **2a**[b] | **1a**[b,c] |
| 1 | $AuCl_3$ | 23 °C, $CH_2Cl_2$, 90 min | 83 | 0 |
| 2 | $AuCl_3$ | 38 °C, $CH_2Cl_2$, 90 min | 95 | 0 |
| 3 | $(Ph_3P)AuBF_4$ | 23 °C, $CH_2Cl_2$, 90 min | 0 | 10 |
| 4 | $AgSbF_6$ | 23 °C, $CH_2Cl_2$, 90 min | 50 | 12 |
| 5 | $Pd(OAc)_2$ | 23 °C, $CH_2Cl_2$, 90 min | 0 | 98 |
| 6[d] | CuI | 80 °C, DMF, 120 min | 22 | 67 |
| 7 | $PtCl_2$ | 23 °C, $CH_2Cl_2$, 240 min | 15 | 81 |
| 8 | $PtCl_2$ | 80 °C, toluene, 90 min | 93 | 0 |

[a] Conditions: **1a** (0.03 M), 5 mol% catalyst, solvent. [b] Yield of pure product after column chromatography. [c] Recovered starting material **1a**. [d] 10 mol% CuI, 0.08 M.

[*] Dr. S. F. Kirsch, J. T. Binder, C. Liébert, H. Menz
Department Chemie
Technische Universität München
Lichtenbergstrasse 4, 85747 Garching (Germany)
Fax: (+49) 89-2891-3315
E-mail: stefan.kirsch@ch.tum.de

[**] This project was supported by the Deutsche Forschungsgemeinschaft (DFG) and the Fonds der Chemischen Industrie. We thank Andrea Rothballer and Markus Scheerer for excellent technical assistance.

Supporting information for this article is available on the WWW under http://www.angewandte.org or from the author.


InterScience
© 2006 Wiley-VCH Verlag GmbH & Co. KGaA, Weinheim

The scope of this transition-metal-catalyzed domino approach to substituted 3(2*H*)-furanones is summarized in Table 2. When $AuCl_3$ was used as the catalyst, spirocyclic

***Table 2:*** Transition-metal-catalyzed synthesis of 3(2*H*)-furanones **2b–k** by cycloisomerization of **1b–k**.[a]

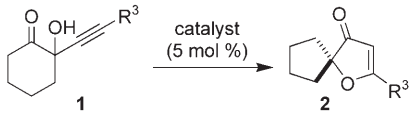


**1** **2**

| Entry | Substr. | $R^3$ | Product | Yield [%][b] |
|---|---|---|---|---|
| 1 | **1b** | 2-MeO-$C_6H_4$ | **2b** | 91 (18 h)<br>81 (5 h)[c] |
| 2 | **1c** | 4-F-$C_6H_4$ | **2c** | 90 (15 h)<br>70 (4 h)[c] |
| 3 | **1d** | 4-*t*Bu-$C_6H_4$ | **2d** | 87 (18 h) |
| 4 | **1e** | 3-thienyl | **2e** | 65 (18 h) |
| 5 | **1f** | *n*Pent | **2f** | 65 (2 h) |
| 6 | **1g** | $(CH_2)_3$OTHP | **2g** | 82 (4 h)<br>11 (6 h)[c] |
| 7 | **1h** | $CH_2$(*c*-$C_6H_{11}$) | **2h** | 75 (12 h) |
| 8 | **1i** | *c*-$C_6H_{11}$ | **2i** | 78 (3 h) |
| 9 | **1j** | 1-cyclohexenyl | **2j** | 68 (3 h) |
| 10[d] | **1k** | TMS | **2k** | 57 (19 h) |

[a] Conditions: **1** (0.03 M), 5 mol% $PtCl_2$, 80 °C, toluene. [b] Yield of pure product after column chromatography. [c] Conditions: **1** (0.03 M), 5 mol% $AuCl_3$, 23 °C, $CH_2Cl_2$. [d] 10 mol% $PtCl_2$, 90 °C.

compounds **2** were formed in high yields and $R^3$ was restricted to aryl substituents (Table 2, entries 1 and 2). Furanones having an alkyl substituent as $R^3$ were obtained in low yields with concomitant decomposition of the starting material (Table 2, entry 6). Gratifyingly, the $PtCl_2$-catalyzed reaction proceeds without this limitation, thus expanding the scope of the method markedly [5 mol% $PtCl_2$, 80 °C, toluene (0.03 M)]. In the presence of $PtCl_2$, a broad variety of alkynes **1** with different $R^3$ groups were effectively converted into the corresponding furanones (Table 2). Notably, the reaction of aromatic and heteroaromatic substrates was as clean as the reaction of substrates containing silyl, alkyl, and alkenyl substituents.

This approach to spirocyclic compounds is of particular synthetic value since alkyl migration is not limited to forming five-membered ring systems. For example, substrates **1l** and **1m** derived from cycloheptanone and cyclooctanone, respectively, undergo ring contraction to give the corresponding spirocycles (Table 3, entries 1 and 2). Furthermore, acyclic systems also reacted by migration of alkyl and aryl groups, although the yields were modest (Table 3, entries 3 and 4). Trialkylsilyl ethers such as **3** (V = $SiMe_3$) and **4** (V = $SiEt_3$) also underwent $PtCl_2$-initiated ring-contracting cyclization providing 3(2*H*)-furanone **2a** in good yields (Scheme 2).

Although we have not yet conducted detailed mechanistic studies, the results listed in Table 4 indicate that the rearrangement is stereospecific. In each case, product formation is consistent with the rearrangement proceeding via the cyclic oxonium ion intermediate **A**. Accordingly, the alkynyl carbonyl compound **5a** provided 3(2*H*)-furanone **7a** exclusively, whereas formation of diastereomer **7b** was not

***Table 3:*** Transition-metal-catalyzed synthesis of 3(2*H*)-furanones **2l–o** by cycloisomerization of **1l–o**.[a]

| Entry | Substrate | Product | Yield [%][b] |
|---|---|---|---|
| 1 | **1l** | **2l** | 85[c] (4 h) |
| 2 | **1m** | **2m** | 50 (24 h) |
| 3 | **1n** | **2n** | 51 (48 h) |
| 4 | **1o** | **2o** | 56 (18 h) |

[a] Conditions: **1** (0.03 M), 5 mol% $PtCl_2$, 80 °C, toluene. [b] Yield of pure product after column chromatography. [c] Determined by $^1$H NMR spectroscopy.

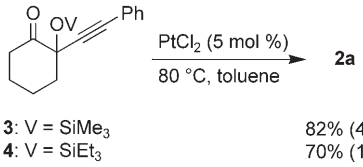


**3**: V = $SiMe_3$ 82% (4 h)
**4**: V = $SiEt_3$ 70% (12 h)

***Scheme 2.*** $PtCl_2$-catalyzed reaction of silyl ethers **3** and **4**.

observed. In the case of **5b**, the spirocyclic compound **7b** was obtained as the sole product. When the alkynyl carbonyl compound **6** was employed as a mixture of diastereomers, the diastereomeric products **7a** (from **6a**) and **7b** (from **6b**) were obtained in ratios identical to those of the starting material.

In summary, a novel approach to 3(2*H*)-furanones is described that combines a transition-metal-catalyzed activation of alkynes with a heterocyclization and subsequent 1,2-

***Table 4:*** Stereospecific course of the domino reactions of **5** and **6**.

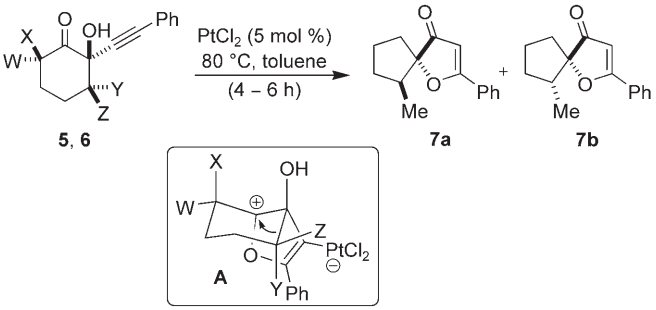


**5, 6** **7a** **7b**

| Substr. | W | X | Y | Z | **a**/**b**[a] | Yield [%] | **7a**/**7b** |
|---|---|---|---|---|---|---|---|
| **5a** | H | Me | H | H | >95:5 | 74 | >95:5 |
| **5b** | Me | H | H | H | <5:95 | 76 | <5:95 |
| **6a** | H | H | H | Me | 80:20 | 88 | 80:20 |
| **6b** | H | H | Me | H | 25:75 | 85 | 25:75 |

[a] Ratio of starting compounds **5a**/**5b** or **6a**/**6b**.

 © 2006 Wiley-VCH Verlag GmbH & Co. KGaA, Weinheim 

alkyl shift. The use of 2-hydroxy-2-alkynylcarbonyl compounds as starting materials is particularly convenient as these substrates can be prepared by simple oxygenation of α-alkynyl carbonyl compounds using 2-iodoxybenzoic acid (IBX).[13] We are currently working to expand this concept for the synthesis of related heterocycles.

## Experimental Section

General procedure: Synthesis of **2a**: $PtCl_2$ (5 mol%, 6.3 mg) was added to a solution of **1a** (100 mg, 0.46 mmol) in toluene (16 mL), and the reaction vial was sealed. The resulting pale yellow solution was stirred at 80°C for 90 min (until TLC analysis indicated complete conversion). The mixture was concentrated under reduced pressure. Purification of the residue by flash chromatography on silica (pentanes/EtOAc 85:15) gave furanone **2a** as a colorless solid (93 mg, 0.43 mmol, 93%). $R_f = 0.42$ (pentanes/EtOAc 80:20); $^1$H NMR (360 MHz, $CDCl_3$): $\delta = 1.95$–$2.10$ (m, 8H), 6.01 (s, 1H), 7.50 (tt, $J = 7.0$, 1.5 Hz, 2H), 7.57 (tt, $J = 7.0$, 1.5 Hz, 1H), 7.84 ppm (dt, $J = 7.0$, 1.5 Hz, 2H); $^{13}$C NMR (90.6 MHz, $CDCl_3$): $\delta = 25.7$ (t), 37.2 (t), 98.9 (s), 99.9 (d), 127.1 (d), 128.8 (d), 129.4 (s), 132.5 (d), 183.7 (s), 206.1 ppm (s); MS (70 eV): $m/z$ (%): 214 (42) [$M^+$], 173 (90), 102 (100), 77 (12). HRMS calcd for $C_{14}H_{14}O_2$: 214.0994, found: 214.0991.

Received: May 10, 2006
Published online: July 26, 2006

**Keywords:** cyclization · domino reactions · heterocycles · platinum · rearrangement

[1] For reviews on gold catalysis, see: a) S. Ma, S. Yu, Z. Gu, *Angew. Chem.* **2006**, *118*, 206; *Angew. Chem. Int. Ed.* **2006**, *45*, 200; b) A. S. K. Hashmi, *Angew. Chem.* **2005**, *117*, 7150; *Angew. Chem. Int. Ed.* **2005**, *44*, 6990; c) A. Hoffmann-Röder, N. Krause, *Org. Biomol. Chem.* **2005**, *3*, 387; d) A. S. K. Hashmi, *Gold Bull.* **2004**, *37*, 51; e) A. S. K. Hashmi, *Gold Bull.* **2003**, *36*, 3.

[2] For selected recent examples of gold-catalyzed alkyne activation, see: a) E. Genin, P. Y. Toullec, S. Antoniotti, C. Brancour, J.-P. Genêt, V. Michelet, *J. Am. Chem. Soc.* **2006**, *128*, 3112; b) M. J. Johansson, D. G. Gorin, S. T. Staben, F. D. Toste, *J. Am. Chem. Soc.* **2005**, *127*, 18002; c) L. Zhang, S. A. Kozmin, *J. Am. Chem. Soc.* **2005**, *127*, 6962; d) A. S. K. Hashmi, M. Rudolph, J. P. Weyrauch, M. Wölfle, W. Frey, J. W. Bats, *Angew. Chem.* **2005**, *117*, 2858; *Angew. Chem. Int. Ed.* **2005**, *44*, 2798; e) X. Shi, D. J. Gorin, F. D. Toste, *J. Am. Chem. Soc.* **2005**, *127*, 5802.

[3] For selected recent examples of platinum-catalyzed alkyne activation, see: a) A. Fürstner, P. Hannen, *Chem. Eur. J.* **2006**, *12*, 3006; b) A. Fürstner, P. W. Davies, *J. Am. Chem. Soc.* **2005**, *127*, 15024; c) A. Fürstner, P. W. Davies, T. Gress, *J. Am. Chem. Soc.* **2005**, *127*, 8244; d) B. A. B. Prasad, F. K. Yoshimoto, R. Sarpong, *J. Am. Chem. Soc.* **2005**, *127*, 12468; e) T. J. Harrison, G. R. Dake, *Org. Lett.* **2004**, *6*, 5023.

[4] For reviews, see: a) C. Bruneau, *Angew. Chem.* **2005**, *117*, 2380; *Angew. Chem. Int. Ed.* **2005**, *44*, 2328; b) A. M. Echavarren, C. Nevado, *Chem. Soc. Rev.* **2004**, *33*, 431; c) M. Méndez, V. Mamane, A. Fürstner, *Chemtracts: Org. Chem.* **2003**, *16*, 397.

[5] M. H. Suhre, M. Reif, S. F. Kirsch, *Org. Lett.* **2005**, *7*, 3925.

[6] a) N. T. Patil, H. Wu, Y. Yamamoto, *J. Org. Chem.* **2005**, *70*, 4531; b) T. Yao, X. Zhang, R. C. Larock, *J. Org. Chem.* **2005**, *70*, 7679; c) T. Yao, X. Zhang, R. C. Larock, *J. Am. Chem. Soc.* **2004**, *126*, 11164.

[7] For related cyclizations, see: a) A. S. K. Hashmi, L. Schwarz, J.-H. Choi, T. M. Frost, *Angew. Chem.* **2000**, *112*, 2382; *Angew. Chem. Int. Ed.* **2000**, *39*, 2285; b) J. A. Marshall, C. A. Sehon, *J. Org. Chem.* **1995**, *60*, 5966.

[8] a) L. A. Paquette, J. E. Hofferberth, *Org. React.* **2003**, *62*, 477; b) Y. Nagao, S. Tanaka, A. Ueki, M. Kumazawa, S. Goto, T. Ooi, S. Sano, M. Shiro, *Org. Lett.* **2004**, *6*, 2133; c) H. Brunner, F. Stöhr, *Eur. J. Org. Chem.* **2000**, 2777.

[9] a) L. E. Overman, L. D. Pennington, *J. Org. Chem.* **2003**, *68*, 7143; b) J. P. Markham, S. T. Staben, F. D. Toste, *J. Am. Chem. Soc.* **2005**, *127*, 9708.

[10] a) P. J. Jerris, A. B. Smith, III, *J. Org. Chem.* **1981**, *46*, 577; b) A. B. Smith III, M. A. Guaciaro, S. R. Schow, P. M. Wovkulich, B. H. Toder, T. W. Hall, *J. Am. Chem. Soc.* **1981**, *103*, 219.

[11] a) S. S. Shin, Y. Byun, K. M. Lim, J. K. Choi, K.-W. Lee, J. H. Moh, J. K. Kim, Y. S. Jeong, J. Y. Kim, Y. H. Choi, H.-J. Koh, Y.-H. Park, Y. I. Oh, M.-S. Noh, S. Chung, *J. Med. Chem.* **2004**, *47*, 792; b) S. W. Felman, I. Jirkovsky, K. A. Memoli, L. Borella, C. Wells, J. Russell, J. Ward, *J. Med. Chem.* **1992**, *35*, 1183.

[12] a) K. Kato, H. Nouchi, K. Ishikura, S. Takaishi, S. Motodate, H. Tanaka, K. Okudaira, T. Mochida, R. Nishigaki, K. Shigenobu, H. Akita, *Tetrahedron* **2006**, *62*, 2545; b) M. Reiter, H. Turner, R. Mills-Webb, V. Gouverneur, *J. Org. Chem.* **2005**, *70*, 8478; c) A. B. Smith, III, P. A. Levenberg, P. J. Jerris, R. M. Scarborough, Jr., P. M. Wovkulich, *J. Am. Chem. Soc.* **1981**, *103*, 1501.

[13] S. F. Kirsch, *J. Org. Chem.* **2005**, *70*, 10210.

 © 2006 Wiley-VCH Verlag GmbH & Co. KGaA, Weinheim 

*Epothilones*

DOI: 10.1002/anie.200601359

# Design and Synthesis of 12-Aza-Epothilones (Azathilones)—"Non-Natural" Natural Products with Potent Anticancer Activity**

*Fabian Feyen, Jürg Gertsch, Markus Wartmann, and Karl-Heinz Altmann**

Natural products provide an immeasurable pool of lead structures for drug discovery, and more than 50% of today's

[*] Dr. F. Feyen, Dr. J. Gertsch, Prof. Dr. K.-H. Altmann
ETH Zürich
Department of Chemistry and Applied Biosciences
Institute of Pharmaceutical Sciences
ETH Hönggerberg, HCI H 405
Wolfgang-Pauli-Strasse 10, 8093 Zürich (Switzerland)
Fax: (+41) 44-633-1360
E-mail: karl-heinz.altmann@pharma.ethz.ch
Dr. M. Wartmann
Oncology DA
Novartis Institute for Biomedical Research
4002 Basel (Switzerland)

[**] We thank Bettina Sager, Jacqueline Loretan, and Robert Reuter for their excellent technical assistance. The Electron Microscopy Centre (EMEZ) of ETH Zürich is acknowledged for excellent technical support.

Supporting information for this article is available on the WWW under http://www.angewandte.org or from the author.

 WILEY InterScience DISCOVER SOMETHING GREAT © 2006 Wiley-VCH Verlag GmbH & Co. KGaA, Weinheim 

prescription drugs are ultimately derived from compounds first obtained from natural sources.[1] While the screening of large collections of natural products will continue to be an important strategy for the identification of new drug leads or compounds of biochemical and pharmacological interest,[2] various approaches have been developed in the more recent past that aim at expanding the structural scope of natural-products-based drug discovery. In particular, this includes the de novo construction of libraries of "natural-products-like" compounds through diversity-oriented synthesis (DOS),[3] as pioneered by Schreiber et al., and the design of natural-products-based libraries, a concept that was introduced by Waldmann et al. in 2002[4] and has been continuously refined over the last few years.[5]

Our own research in the area of natural-products-based drug discovery has been directed towards the development of new biologically active scaffolds (or chemotypes) through the extensive structural modification (rather than simple peripheral derivatization) of existing natural product leads.[6] In this context we have also investigated the biological activity of 12-aza-epothilones, which are characterized by the replacement of a backbone carbon atom by nitrogen in the epothilone macrocycle.[6c,d,7] The resulting analogues may best be described as "non-natural" natural products,[8] as they still retain most of the (two-dimensional) structural features of the natural product lead; at the same time they are structurally unique, as they are outside of the general scope of nature's biosynthetic machinery for polyketide biosynthesis, which is not programmed for the incorporation of single nitrogen atoms in a regular polyketide backbone.[9] As a result of these studies we discovered that 12-aza-epothilones **1** (termed

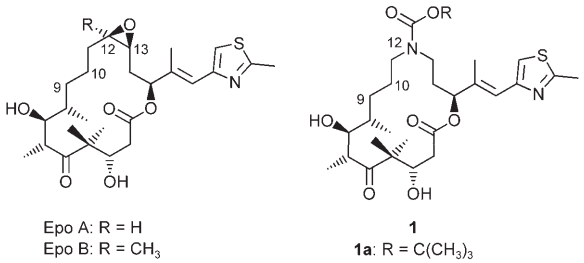


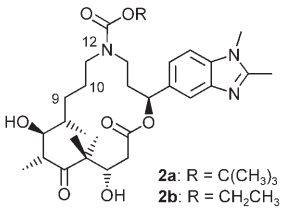


"azathilones") can retain much of the antiproliferative activity of natural epothilones, depending on the nature of the acyl substituent attached to the backbone nitrogen atom.[6d,10]

Unfortunately, our first-generation synthesis of these compounds proved to be relatively inefficient and tedious.[6d] At the same time, the activity of azathilones **1** even in the best case, i.e. with R = *tert*-butyl (**1a**), was ca. 15–50 times lower than that of Epo A. These shortcomings led us to investigate alternative synthetic routes to this class of compounds, with the concurrent incorporation of additional structural modifications designed to enhance biological activity. Apart from available data on the structure–activity relationships (SARs) for azathilones **1** with regard to the nature of the acyl substituent attached to N12 (vide supra),[6d] the design of these analogues was additionally guided by the results of previous studies in our laboratory, which had revealed a general activity-enhancing effect of a dimethylbenzimidazole side chain in combination with the natural epothilone macrocycle.[6a,b,11] These considerations resulted in compounds **2a** and **2b** as initial targets for total synthesis and biological investigation, both of which eventually proved to be highly potent inhibitors of human tumor growth in vitro. In this communication we now wish to report on the total synthesis of azamacrolides **2a** and **2b**,[10] either through ring-closing olefin metathesis (RCM) or by a macrolactonization approach, and the preliminary biological characterization of these compounds.

Macrocycle formation through RCM featured as a particularly attractive approach to the target azathilones, as it offered simultaneous access to specific unsaturated analogues (as the immediate cyclization products), which could be interesting new antiproliferative agents in their own right.[12] Our RCM-based synthesis of target structure **2a** and its 9,10-didehydro derivative **9** (Scheme 1) involved three key strategic steps, namely, 1) the stereoselective aldol reaction between aldehyde **3**[13] and ketone **4**[14] (d.r. 8:1), 2) esterification of carboxylic acid **7** with the unsaturated alcohol **10**,[15] and 3) RCM of bisolefin **8**.

Initial attempts to cyclize **8** employing the first-generation Grubbs catalyst[16] met with complete failure and no conversion was observed. In contrast, the use of the dihydroimidazol-2-ylidene-based second-generation catalyst[16] produced the cyclic olefin in excellent yield (85%) and with exclusive *E* selectivity. No trace of the corresponding *Z* product could be isolated, and similar observations have been made for the RCM-based cyclization of the analogue of **8** containing the natural epothilone side chain.[24]

Unfortunately, the efficiency of the cyclization reaction was thwarted by serious difficulties encountered in the subsequent reduction of the C9–C10 double bond, which proved to be extremely sluggish under all experimental conditions investigated (thus leading to low yields and also side reactions such as reductive ester cleavage with $H_2$/Pd-C without reduction of the double bond). The only viable approach for the transformation of **9** into **2a** involved the use of in situ generated diimide, which had been successfully employed in the transformation of 9,10- and 10,11-didehydroEpo D, respectively, into Epo D (= 12,13-deoxyEpoB),[17] and which produced **2a** in 31% yield from **9** after purification by preparative HPLC.

While this approach provided sufficient material for initial biological testing, it was clear that an alternative strategy would have to be developed for more extensive profiling and eventual in vivo studies, should those appear to be warranted. In light of the highly promising biological data obtained for

 © 2006 Wiley-VCH Verlag GmbH & Co. KGaA, Weinheim 

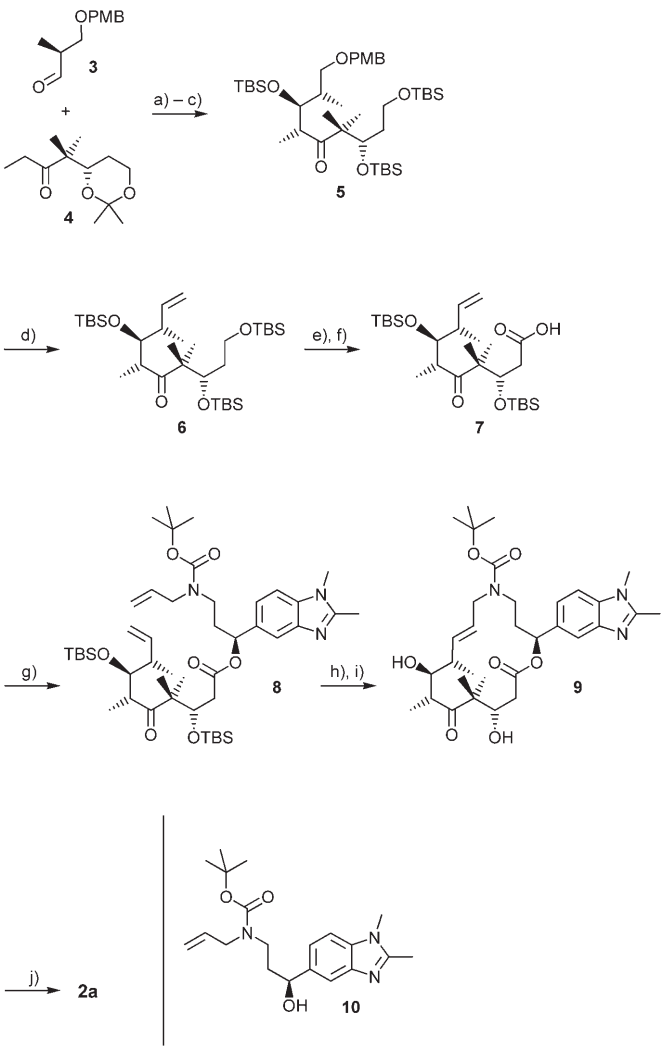

***Scheme 1.*** Reaction conditions: a) **4**, LDA, −78 °C, 5 h, then addition of **3**, −90 °C, 75 min, 76%, d.r. 8:1; b) PPTS, MeOH, RT, 20 h, 86%; c) 1. TBSOTf, 2,6-lutidine, −78 °C → RT, 1.5 h; 2. flash chromatography; 76%; d) 1. $H_2$/Pd-C, MeOH, RT, 20 h; 2. TPAP, NMO, 4-Å MS, $CH_2Cl_2$, RT, 1 h; 3. $MePPh_3Br$, LiHMDS, THF, 0 °C, 1.5 h, 79% (three steps); e) CSA (1.0 equiv), $CH_2Cl_2$/MeOH 1:1, 0 °C, 1 h, 87%; f) PDC (11 equiv), DMF, RT, 64 h, 85%; g) **10**, DCC (1.2 equiv), DMAP (0.3 equiv), $CH_2Cl_2$, 0 °C, 15 min, RT, 15 h, 60%; h) 2nd-generation Grubbs catalyst (0.15 equiv, incremental addition), $CH_2Cl_2$, reflux, 8 h, 85%; i) HF·pyridine, pyridine, THF, RT, 4 h, 70%; j) $KO_2C$-N=N-$CO_2K$ (excess), AcOH, $CH_2Cl_2$, 31%, pure **1** obtained through purification by preparative HPLC. CSA = (+)-camphorsulfonic acid, DCC = *N*,*N*′-dicyclohexylcarbodiimide, DMAP = 4-dimethylaminopyridine, LDA = lithium diisopropylamide, LiHMDS = lithium 1,1,1,3,3,3-hexamethyldisilazide, NMO = 4-methylmorpholine-*N*-oxide, PDC = pyridinium dichromate, PMB = *para*-methoxybenzyl, PPTS = pyridinium *p*-toluenesulfonate, TBS = *tert*-butyldimethylsilyl, TPAP = tetrapropylammonium perruthenate.

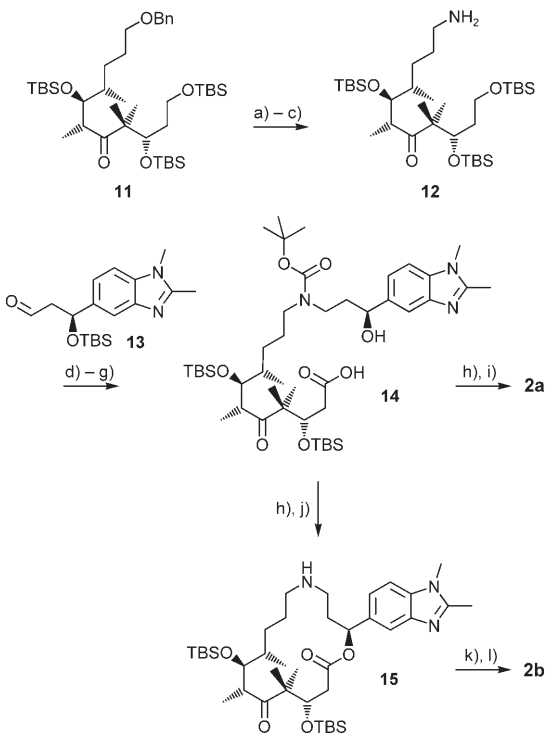

***Scheme 2.*** Reaction conditions: a) $H_2$/Pd-C, EtOAc, RT, 62 h, 86%; b) $HN_3$, DEAD, $PPh_3$, THF, 0 °C, 25 min, RT, 30 min, 96%; c) $H_2$/Pd-C, MeOH, RT, 3 h, 92%; d) 1. **13** (1.1 equiv), $NaBH(OAc)_3$ (1.6 equiv), AcOH (2.0 equiv), 4-Å MS, RT, 2.5 h; 2. $Boc_2O$, $Et_3N$, THF, 0 °C, 45 min, 60% (two steps); e) CSA (1.1 equiv), $CH_2Cl_2$/MeOH 1:1, 0 °C, 3 h, 80%; f) PDC (15 equiv), DMF, RT, 24 h, 50%; g) TBAF (6 equiv), THF, RT, 24 h; h) 2,4,6-$Cl_3C_6H_2C(O)Cl$, $Et_3N$, THF, 0 °C, 20 min, then diluted with toluene and added to a solution of DMAP in toluene, 75 °C, 1 h, 44% (two steps); i) HF·pyridine, pyridine, THF, RT, 2.5 h, then preparative HPLC, 40%. j) $ZnBr_2$ (4.0 equiv), $CH_2Cl_2$, RT, 2.5 h, quant.; k) $CH_3CH_2OC(O)Cl$, $Et_3N$, THF, 0 °C, 30 min; l) HF·pyridine, pyridine, THF, RT, 3.5 h, then preparative HPLC, 32% (two steps). Bn = benzyl, Boc = *tert*-butyloxycarbonyl, DEAD = diethylazodicarboxylate, TBAF = tetrabutylammonium fluoride.

**2a** (vide infra), we thus embarked on the elaboration of an alternative route to **2a** that would be based on macrolactonization rather than RCM.

This approach employed the reductive amination of aldehyde **13** with amine **12** (obtained in three steps from the known protected tetrol **11**[14a]) to assemble the heteroaliphatic skeleton of **2a** (Scheme 2). The reaction was best conducted with a slight excess of aldehyde **13** (1.1 equiv) and $NaBH(OAc)_3$ as the reducing agent in the presence of AcOH (2 equiv) and 4-Å molecular sieves. Owing to its pronounced polarity (arising from the presence of the secondary amino group as well as the benzimidazole moiety) the reductive-amination product was not purified but directly converted into the corresponding *N*-*tert*-butyloxycarbonyl derivative, which was obtained in 60% yield (based on amine **12**). Selective cleavage of the primary *tert*-butyldimethylsilyl (TBS) ether with CSA followed by oxidation of the resulting free alcohol with PDC and removal of the TBS protecting group from C15–O with TBAF then led to seco acid **14**, which was cyclized under Yamaguchi conditions[18] to produce fully protected **2a** (44% based on C15-O-TBS-protected **14**). Subsequent selective removal of the TBS protecting groups with HF·pyridine gave target structure **2a** in 40% yield (after HPLC purification).

In a preliminary attempt to assess the importance of the *tert*-butyl moiety of **2a** for biological potency (vide infra), we also prepared the closely related azathilone **2b**, which

 © 2006 Wiley-VCH Verlag GmbH & Co. KGaA, Weinheim 

incorporates a N12-ethoxycarbonyl substituent in place of the *tert*-butyloxycarbonyl moiety present in **2a**.[19] Azathilone **2b** was obtained from bis-TBS-protected **2a** through highly selective cleavage of the *tert*-butyloxycarbonyl group from N12 ($ZnBr_2$, $CH_2Cl_2$, RT)[20] followed by acylation of the resulting free amine **15** with ethyl chloroformate and subsequent removal of the TBS protecting groups with HF·pyridine (Scheme 2).

The data summarized in Table 1 indicate that azathilone **2a** is a highly potent antiproliferative agent, which inhibits the growth of different types of drug-sensitive human cancer cell lines (A549, HCT-116, PC-3M, KB-31) with $IC_{50}$ values in the low nanomolar range.

***Table 1:*** αβ-Tubulin-polymerizing and antiproliferative activity of azathilones **2a**, **2b**, and **9**.

| Cmpd | $EC_{50}$ (Tubulin polym.) [μM][a] | $IC_{50}$ [nM][b] | | | | |
|---|---|---|---|---|---|---|
| | | A549 | HCT-116 | PC-3M | KB-31 | KB-8511 |
| **2a** | 3.9 ± 0.6 | 1.9 ± 0.4 | 1.6 ± 0.5 | 2.3 ± 0.6 | 0.34 ± 0.15 | 222 ± 48 |
| **2b** | 5.4 ± 0.4 | 18.0 ± 3.1 | 23.9 ± 2.9 | 12.3 ± 1.1 | 12.6 ± 1.0 | > 1000 |
| **9** | 9.1 ± 0.7 | 920 ± 85 | 1009 ± 71 | 973 ± 64 | n.d.[e] | n.d.[e] |
| **1a** | 5.6 ± 0.4 | 130 ± 24 | 110 ± 19 | 126 ± 22 | 31[c] | 105[c] |
| Epo A | 4.6 ± 0.5 | 3.2 ± 0.5 | 2.2 ± 0.3 | 3.4 ± 0.4 | 2.15[d] | 1.91[d] |

[a] Concentration required to induce 50% of the maximum αβ-tubulin polymerization achievable with the respective compound (10 μM of porcine brain tubulin). Tubulin polymerization was determined by turbidity measurements at 340 nm ($A_{340}$).[22] For a given compound concentration, the achievement of an equilibrium state between soluble and polymerized tubulin is indicated by a stable plateau in $A_{340}$. Maximum tubulin polymerization is reached when increases in compound concentration no longer result in an increase of the plateau value for $A_{340}$. Similar maximum values for $A_{340}$ were observed for all compounds investigated in this study. [b] $IC_{50}$ values for inhibition of human cancer cell growth. KB-31, KB-8511: cervix; A549: lung; HCT-116: colon; PC-3M: prostate. KB-8511 is a P-glycoprotein 170 (P-gp170)-overexpressing multidrug-resistant subline of the KB-31 parental line. Cells were exposed to compounds for 72 h. Cell numbers were determined by quantification of protein content of fixed cells by staining with methylene blue.[23a] For further experimental details see reference [23b]. Values represent the means of at least three independent experiments (± standard deviation). [c] Data from reference [6d]. [d] Data from reference [6a]. [e] Not determined.

The antiproliferative activity of **2a** is thus comparable to that of Epo A, with the exception of the multidrug-resistant KB-8511 line, where **2a** is significantly less potent (vide infra). Likewise, **2a** induces tubulin polymerization in vitro with potency similar to that of Epo A (Table 1, Figure 1A), which strongly suggests that inhibition of human cancer cell proliferation by **2a**, as for natural epothilones, is a consequence of interference with microtubule functionality. This view is further corroborated by the fact that treatment of cancer cells with **2a** results in cell cycle arrest at $G_2$/M, which mirrors the effects on the cell cycle observed upon treatment with Epo A or B[7] (Figure 1B).

Upon analysis of the data presented in Table 1 in more detail, it also becomes apparent that **2a** is > 60 times more potent against drug-sensitive human cancer cells than the corresponding parent (natural-side-chain-containing) azathilone **1a**. Although the molecular origin of this activity difference is unclear, it should be noted that the potency increase observed for **2a** over **1a** dramatically exceeds the potency-enhancing effects previously observed for the dimethylbenzimidazole side chain in combination with polyketide-based macrocycles (2–15-fold).[6a,b,11] Equally intriguing is the observation that compound **9**, which incorporates a *trans* double bond between C9 and C10, is significantly less potent than the fully saturated azathilone **2a** (both at the levels of tubulin polymerization as well as cellular activity). A similar potency difference also exists between **1a** and its *trans* 9,10-didehydro derivative.[25] These findings are in marked contrast to the effects observed for Epo B and D, where the introduction of a *trans* double bond between C9 and C10 results in enhanced cellular potency,[12b,17a] and they may be indicative of differences in the bioactive conformation between azathilone-type analogues and natural epothilones.

Compared to azathilone **2a**, analogue **2b** exhibits somewhat reduced cellular activity (Table 1), but the compound still remains a very potent antiproliferative agent against all drug-sensitive cancer cell lines investigated. In addition, as **2b** can safely be assumed to be more acid-stable than **2a**, the former could in fact offer some advantage over the latter in vivo (for oral administration). Based on the tubulin-polymerization data shown in Table 1, **2a** is a more potent inducer of tubulin polymerization than **2b**, which indicates that hydrophobic interactions between the protein and the N12-carbamate substituent play an inportant role in the binding of these compounds to α/β-tubulin.[19] Whether the difference in tubulin-polymerizing activity between **2a** and **2b** can fully account for the difference in cellular potency is unknown at this

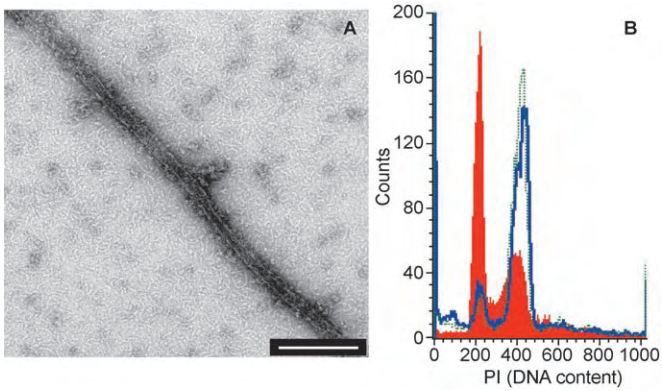


***Figure 1.*** A: Compound **2a** induces the formation of microtubules in vitro. [20 μM of purified porcine αβ-tubulin was incubated with 20 μM of **2a** for 30 min in BRB80 buffer at RT]. Electron micrograph shows part of a single long microtubule. Scale bar: 100 nm. B: Cell-cycle effects of **2a** in PC-3M cells ($G_1$ vs. $G_2$/M). **2a** (250 nM) was incubated for 1 h with $2\times10^5$ cells and then removed. Cells were subsequently grown for 24 h prior to analysis of DNA content with propidium iodide. Vehicle control (red) shows cells in the $G_1$ phase of the cell cycle. In the presence of compound **2a** (blue line) or Epo A (250 nM; dotted green line) cells accumulate in $G_2$/M. PI = propidium iodide.

 © 2006 Wiley-VCH Verlag GmbH & Co. KGaA, Weinheim 

point; the latter may also be affected by differences in non-target-related parameters such as cellular uptake or intracellular distribution.

Compared to their effects on drug-sensitive cancer cell lines, both **2a** and **2b** exhibit reduced antiproliferative activity against the P-gp-overexpressing human cervix carcinoma line KB-8511, which indicates that both compounds are substrates for the P-gp efflux pump. However, we have recently shown that the susceptibiliy of polyketide-based epothilone analogues to P-gp-mediated drug efflux can be modulated through adjustments in compound lipophilicity; this strategy will also be explored for lead structures **2a** and **2b**.[21]

In summary, we have achieved the total synthesis of two representative examples of a new class of highly potent microtubule-stabilizing agents, which are based on an azamacrolide backbone and which we have termed azathilones. While the conception of these compounds is closely connected to the structure of natural epothilones (hence the name "azathilones"), given the degree of structural divergence from the natural epothilone template, they may be considered as members of a distinct group of "non-natural" natural products with unique structural features and, as indicated by some preliminary SAR data, a unique SAR profile. Both compounds investigated in this study are potent growth inhibitors of drug-sensitive human cancer cells in vitro and, thus, should be attractive new lead structures for anticancer-drug discovery.

Received: April 6, 2006
Published online: July 27, 2006

**Keywords:** antitumor agents · epothilones · microtubule stabilizers · natural products · total synthesis

[1] G. M. Cragg, D. J. Newman, *Pure Appl. Chem.* **2005**, *77*, 7–24.
[2] B. A. Posner, *Curr. Opin. Drug Discovery Dev.* **2005**, *8*, 487–494.
[3] M. D. Burke, S. L. Schreiber, *Angew. Chem.* **2004**, *116*, 48–60; *Angew. Chem. Int. Ed.* **2004**, *43*, 46–58.
[4] R. Breinbauer, I. R. Vetter, H. Waldmann, *Angew. Chem.* **2002**, *114*, 3002–3015; *Angew. Chem. Int. Ed.* **2002**, *41*, 2878–2890.
[5] a) M. A. Koch, H. Waldmann, *Drug Discovery Today* **2005**, *10*, 471–483; b) M. A. Koch, A. Schuffenhauer, M. Scheck, S. Wetzel, M. Casaulta, A. Odermatt, P. Ertl, H. Waldmann, *Proc. Natl. Acad. Sci. USA* **2005**, *102*, 17272–17277; c) M. A. Koch, L.-O. Wittenberg, S. Basu, D. A. Jeyaraj, E. Gourzoulidou, K. Reinecke, A. Odermatt, H. Waldmann, *Proc. Natl. Acad. Sci. USA* **2004**, *101*, 16721–16726.
[6] a) F. Cachoux, T. Isarno, M. Wartmann, K.-H. Altmann, *ChemBioChem* **2006**, *7*, 54–57; b) F. Cachoux, T. Isarno, M. Wartmann, K.-H. Altmann, *Angew. Chem.* **2005**, *117*, 7636–7640; *Angew. Chem. Int. Ed.* **2005**, *44*, 7469–7473; c) F. Cachoux, F. Schaal, A. Teichert, T. Wagner, K.-H. Altmann, *Synlett* **2004**, 2709–2712; d) K.-H. Altmann, A. Flörsheimer, G. Bold, G. Caravatti, M. Wartmann, *Chimia* **2004**, *58*, 686–690.
[7] For reviews on epothilones cf., e.g.: a) G. Höfle, H. Reichenbach in *Anticancer Agents from Natural Products* (Eds.: G. M. Cragg, D. G. I. Kingston, D. J. Newman), CRC, Boca Raton, **2005**, pp. 413–450; b) K.-H. Altmann, *Curr. Pharm. Des.* **2005**, *11*, 1595–1613; c) K.-H. Altmann, *Org. Biomol. Chem.* **2004**, *2*, 2137–2152; d) C. R. Harris, S. J. Danishefsky, *J. Org. Chem.* **1999**, *64*, 8434–8456; e) K. C. Nicolaou, F. Roschangar, D. Vourloumis, *Angew. Chem.* **1998**, *110*, 2120–2153; *Angew. Chem. Int. Ed.* **1998**, *37*, 2014–2045.
[8] For a previous use of the term "non-natural natural product" see: L. F. Tietze, H. P. Bell, S. Chandrasekar, *Angew. Chem.* **2003**, *115*, 4128–4160; *Angew. Chem. Int. Ed.* **2003**, *42*, 3996–4028.
[9] For a review, cf., e.g.: C. A. Walsh, *Curr. Opin. Chem. Biol.* **1999**, *3*, 598–606.
[10] The term "azathilones" is meant to reflect removal of the *epo*xide oxygen in natural epothilones with concomitant replacement of C12 by nitrogen. However, the term is used herein rather loosely, as the benzimidazole-containing analogues **2a** and **2b** strictly speaking should not be named azathilones, because of the absence of a thiazole moiety, from which the "thil" in epothilone is derived (cf. K. Gerth, N. Bedorf, G. Höfle, H. Irschik, H. Reichenbach, *J. Antibiot.* **1996**, *49*, 560–564).
[11] K.-H. Altmann, G. Bold, G. Caravatti, A. Flörsheimer, V. Guagnano, M. Wartmann, *Bioorg. Med. Chem. Lett.* **2000**, *10*, 2765–2768: The magnitude of the activity-enhancing effect of the dimethylbenzimidazole side chain strongly depends on the exact nature of the polyketide macrocycle. It is significantly more pronounced in the deoxyepothilone series (Epo C and D) than for the corresponding analogues of Epo A and B. (Cf. also references [6a, b]).
[12] a) A. Rivkin, T.-C. Chou, S. J. Danishefsky, *Angew. Chem.* **2005**, *117*, 2898–2910; *Angew. Chem. Int. Ed.* **2005**, *44*, 2838–2850; b) A. Rivkin, F. Yoshimura, G. Fumihiko, A. E. Gabarda, Y. S. Cho, T.-C. Chou, H. Dong, S. J. Danishefsky, *J. Am. Chem. Soc.* **2004**, *126*, 10913–10922; c) R. L. Arslanian, L. Tang, S. Blough, W. Ma, R.-G. Qiu, L. Katz, J. R. Carney, *J. Nat. Prod.* **2002**, *65*, 1061–1064; d) I. H. Hardt, H. Steinmetz, K. Gerth, F. Sasse, H. Reichenbach, G. Höfle, *J. Nat. Prod.* **2001**, *64*, 847–856.
[13] J. D. White, R. G. Carter, K. F. Sundermann, M. Wartmann, *J. Am. Chem. Soc.* **2001**, *123*, 5407–5413. Aldehyde **3** was obtained by Swern oxidation of the corresponding primary alcohol and directly used in step (a) of Scheme 2 without purification. The yield reported for this step is based on the assumption that the oxidation was quantitative.
[14] a) K.-H. Altmann, G. Bold, G. Caravatti, D. Denni, A. Flörsheimer, A. Schmidt, G. Rihs, M. Wartmann, *Helv. Chim. Acta* **2002**, *85*, 4086–4110; b) D. Schinzer, A. Bauer, O. M. Böhm, A. Limberg, M. Cordes, *Chem. Eur. J.* **1999**, *5*, 2483–2491.
[15] Olefin **10** was obtained in three steps from the acylsultam precursor of aldehyde **13** (cf. Ref. [11]). Details of the synthesis will be described elsewhere. For carboxylic acid **7** alternative synthetic approaches have been described; cf., e.g., Ref. [12b].
[16] For recent reviews on olefin metathesis cf., e.g.: a) R. H. Grubbs, *Tetrahedron* **2004**, *60*, 7117–7140; b) T. M. Trnka, R. H. Grubbs, *Acc. Chem. Res.* **2001**, *34*, 18–29.
[17] a) F. Yoshimura, A. Rivkin, A. E. Gabarda, T.-C. Chou, H. Dong, G. Sukenick, F. F. Morel, R. E. Taylor, S. J. Danishefsky, *Angew. Chem.* **2003**, *115*, 2622–2625; *Angew. Chem. Int. Ed.* **2003**, *42*, 2518–2521; b) K. Biswas, H. Lin, J. T. Njardson, M. D. Chappell, T.-C. Chou, Y. Guan, W. P. Tong, L. He, S. B. Horwitz, S. J. Danishefsky, *J. Am. Chem. Soc.* **2002**, *124*, 9825–9832.
[18] J. Inanaga, K. Hirata, H. Saeki, T. Katsuki, M. Yamaguchi, *Bull. Chem. Soc. Jpn.* **1979**, *52*, 1989–1993.
[19] SAR studies on azathilones **1** had also included the N-unsubstituted version of these compounds, which proved to be completely inactive. For this reason the free amine corresponding to **2a** and **2b** (N12-unsubstituted) was not investigated in the current study.
[20] R. M. Williams, J. Cao, H. Tsujishima, *Angew. Chem.* **2000**, *112*, 2640–2644; *Angew. Chem. Int. Ed.* **2000**, *39*, 2540–2544.
[21] F. Cachoux, T. Isarno, M. Wartmann, K.-H. Altmann, *Synlett* **2006**, 1384–1388.

 © 2006 Wiley-VCH Verlag GmbH & Co. KGaA, Weinheim 

[22] E. Hamel, A. A. del Campo, J. Lustbader, C. M. Lin, *Biochemistry* **1983**, *22*, 1271 – 1279.
[23] a) T. Meyer, U. Regenass, D. Fabbro, E. Alteri, J. Rösel, M. Müller, G. Caravatti, A. Matter, *Int. J. Cancer* **1989**, *43*, 851 – 856; b) K. C. Nicolaou, R. Scarpelli, B. Bollbuck, B. Werschkun, M. M. Pereira, M. Wartmann, K.-H. Altmann, D. Zaharevitz, R. Gussio, P. Giannakakou, *Chem. Biol.* **2000**, *7*, 593 – 599.
[24] F. Feyen, K.-H. Altmann, unpublished results.
[25] J. Gertsch, F. Feyen, K.-H. Altmann, unpublished results.

 © 2006 Wiley-VCH Verlag GmbH & Co. KGaA, Weinheim 

Iron Complexes

DOI: 10.1002/anie.200601478

# Synthesis and Redox Properties of Mixed-Valent Octanuclear Iron Defective Hexacubanes and a (CaCl)-Capped Body-Centered Six-Sided Iron(III) Polyhedron**

*Raju Prakash,* Rolf W. Saalfrank,* Harald Maid, Andreas Scheurer, Frank W. Heinemann, Alfred X. Trautwein, and Lars H. Böttger*

*Dedicated to Professor Robert Weiss on the occasion of his 65th birthday*

Recently, we reported the template syntheses of the six- and eight-membered iron coronates $\{M\subset[Fe_n(L^1)_n]\}^+$ $\{M = Na, n = 6;\ M = Cs, n = 8;\ (L^1)^{3-} = N[(CH_2)_2O^-]_3\}$ from iron(III) chloride and triethanolamine.[1] In contrast, the six-membered iron coronands $[Fe_6(L^2)_6Cl_6]$ $\{(L^2)^{2-} = RCH_2N[(CH_2)_2O^-]_2\}$,[2] the mixed-valent manganese coronates $[NEt_4]\{Mn^{II}\subset[Mn^{II}_3Mn^{III}_3(L^2)_6Cl_6]\}$,[3] the heteronuclear iron–manganese coronate $[PPh_4]\{Fe^{III}\subset[Fe^{III}_2Mn^{II}_4(L^{2a})_6Cl_6]\}$ $\{(L^{2a})^{2-} = BnN[(CH_2)_2O^-]_2\}$,[4] and the ferric star $\{Fe[Fe(L^{2b})_2]_3\}$ $\{(L^{2b})^{2-} = MeN[(CH_2)_2O^-]_2\}$[5] were obtained with α-methylene N-substituted diethanolamines.[2] These oligonuclear complexes have attracted much attention, in view of their unusual structures and properties (for example, magnetic cooling[6] and single-molecule magnetism[7]), as well as their multistep one-electron redox reactions.[3,4] These exciting results prompted us to study the behavior of α-branched diethanolamines in the assembly of supramolecular mixed-valent iron complexes.

Herein, we describe the synthesis of two unprecedented mixed-valent octanuclear iron defective hexacubane complexes and a (CaCl)-capped nonanuclear body-centered six-sided iron(III) polyhedron through the use of α-branched *t*Bu-*N*-diethanolamine ($H_2L^3$) instead of an α-methylene N-substituted diethanolamine. There have been several reports on complexes with a defective double-cubane core,[8] but only a few on related more complex systems.[9] The development of routes for the synthesis of such species is of great importance, because these systems have potential fields of applications, such as bioinorganic chemistry, magnetochemistry, materials science, and solid-state physics.[8–10]

The mixed-valent octanuclear defective hexacubanes $[Fe^{II}_4Fe^{III}_4(L^3)_6Cl_4O_2]$ (**1**) and $[Fe^{II}_2Fe^{III}_6(L^3)_6Cl_6O_2]$ (**2**) were formed through the self-assembly of tridentate $H_2L^3$, mixtures of iron(II) and iron(III) chlorides ($Fe^{II}/Fe^{III} = 1{:}1$ for **1**; $Fe^{II}/Fe^{III} = 1{:}3$ for **2**), and cesium carbonate in MeCN (Scheme 1). After recrystallization from $CH_2Cl_2/Et_2O$, **1** and **2** were

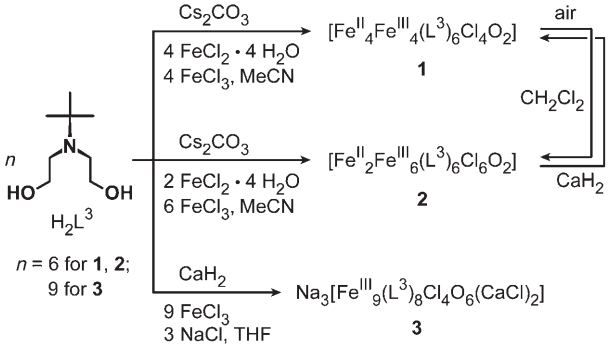


***Scheme 1.*** Synthesis of complexes **1**, **2**, and **3**.

isolated as highly air-sensitive green or green-yellow microcrystals, in yields of 58 or 65%, respectively. In contrast, the reaction of $H_2L^3$ with iron(III) chloride and calcium hydride in THF afforded the (CaCl)-capped body-centered six-sided iron(III) polyhedron $Na_3[Fe^{III}_9(L^3)_8Cl_4O_6(CaCl)_2]$ (**3**) in 70% yield.

The structure of **1** was determined by a low-temperature single-crystal X-ray structure analysis (Figure 1).[11] Complex **1** is a compact defective hexacubane and is the first iron

[*] Dr. R. Prakash, Prof. Dr. R. W. Saalfrank, Dr. H. Maid, Dr. A. Scheurer
Institut für Organische Chemie
Universität Erlangen-Nürnberg
Henkestrasse 42, 91054 Erlangen (Germany)
Fax: (+49) 9131-852-1165
E-mail: raju.prakash@chemie.uni-erlangen.de
saalfrank@chemie.uni-erlangen.de
Homepage: http://www.organik.uni-erlangen.de/saalfrank/
Dr. F. W. Heinemann
Institut für Anorganische Chemie
Universität Erlangen-Nürnberg
91058 Erlangen (Germany)
Prof. Dr. A. X. Trautwein, Dipl.-Phys. L. H. Böttger
Institut für Physik
Universität zu Lübeck
23538 Lübeck (Germany)

[**] Chelate Complexes, Part 34. This work was supported by the Deutsche Forschungsgemeinschaft (SFB 583, GK 312, SPP 1137), the Bayerisches Langzeitprogramm Neue Werkstoffe, and the Fonds der Chemischen Industrie. The generous allocation of cyclic voltammetric facilities by Dr. M. Moll, Institut für Anorganische Chemie, Universität Erlangen-Nürnberg, is gratefully acknowledged. We thank Prof. Dr. H. Burzlaff for assistance in assigning complex **3**. Part 33: Ref. [7].

Supporting information for this article (syntheses, characterizations, X-ray structure determinations) is available on the WWW under http://www.angewandte.org or from the author.

 © 2006 Wiley-VCH Verlag GmbH & Co. KGaA, Weinheim 

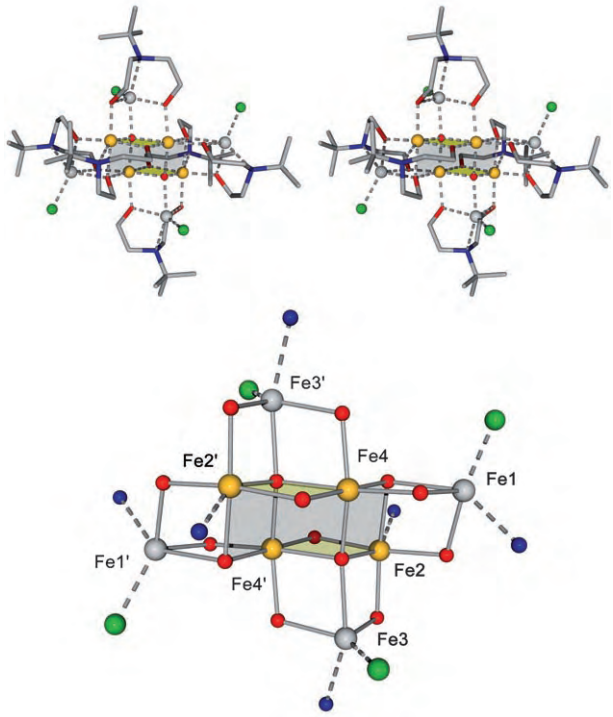


***Figure 1.*** Compact defective hexacubane **1**. Top: stereo representation. Bottom: the hexacubane framework. $Fe^{II}$ silver, $Fe^{III}$ gold, C gray, N blue, O red, Cl green; the shared faces of the $[Fe_3O_4]$ partial cubanes are highlighted.

complex of this type.[12] The complex crystallizes in the centrosymmetric space group *C*2/*c* and has crystallographically imposed inversion symmetry ($C_i$).

The six tridentate $(L^3)^{2-}$ ligands exhibit two different types of bonding modes: four are tritopic, and two are tetratopic. The complex contains four distinct pairs of iron centers: two pairs of five-coordinate iron(II) ions and two pairs of six-coordinate iron(III) ions. The four peripheral iron(II) ions (Fe1, Fe1′, Fe3, and Fe3′) occupy trigonal bipyramidal coordination environments. The Fe1 and Fe1′ ions are each coordinated by one nitrogen donor and two $\mu_2$-$O^-$ donors from one ligand, one $\mu_3$-$O^-$ donor from a neighboring ligand, and one $Cl^-$ ion. The Fe3 and Fe3′ ions are each surrounded by one nitrogen donor and two $\mu_2$-$O^-$ donors from the same ligand, one $\mu_4$-$O^{2-}$ ion, and one $Cl^-$ ion. In contrast, the four central iron(III) ions (Fe2, Fe2′, Fe4, and Fe4′) have octahedral coordination environments. The Fe2 and Fe2′ ions are each coordinated by one nitrogen donor, three $\mu_2$-$O^-$ donors, one $\mu_3$-$O^-$ donor, and one $\mu_4$-$O^{2-}$ ion. The Fe4 and Fe4′ ions are each coordinated by three $\mu_2$-$O^-$ donors, one $\mu_3$-$O^-$ donor, and two $\mu_4$-$O^{2-}$ ions.

In **1**, six $[Fe_3O_4]$ cubane fragments are arranged in a cross-shaped manner. The two central partial cubane units share a common face, and each shares two faces with two peripheral partial cubane units. The mean Fe–O distance in the peripheral units (2.08 Å) is marginally longer than that in the inner units (1.98 Å). The nitrogen atoms and the chloride ions are not incorporated in the compact defective hexacubane framework, but rather, complete the coordination spheres around the iron ions.

The cyclic voltammogram of **1** exhibits four quasireversible waves at potentials of $E_{1/2} = 42, 429, 599, 816$ mV relative to the normal hydrogen electrode (NHE; Figure 2, top, red line), which are assigned to the successive one-electron oxidations ($\Delta E = 95$–$110$ mV; $E_p - E_{p/2} \approx 90$–$95$ mV) of the four iron(II) ions. The first redox wave is well separated from the three other waves, and the small positive $E_{1/2}$ value indicates the pronounced oxidation affinity of **1**. All four redox processes are diffusion-controlled (the peak currents are linearly proportional to the square root of the scan speeds) and are completely reversible over several successive cycles. However, no redox waves were observed in the negative potential region down to −1200 mV, which implies

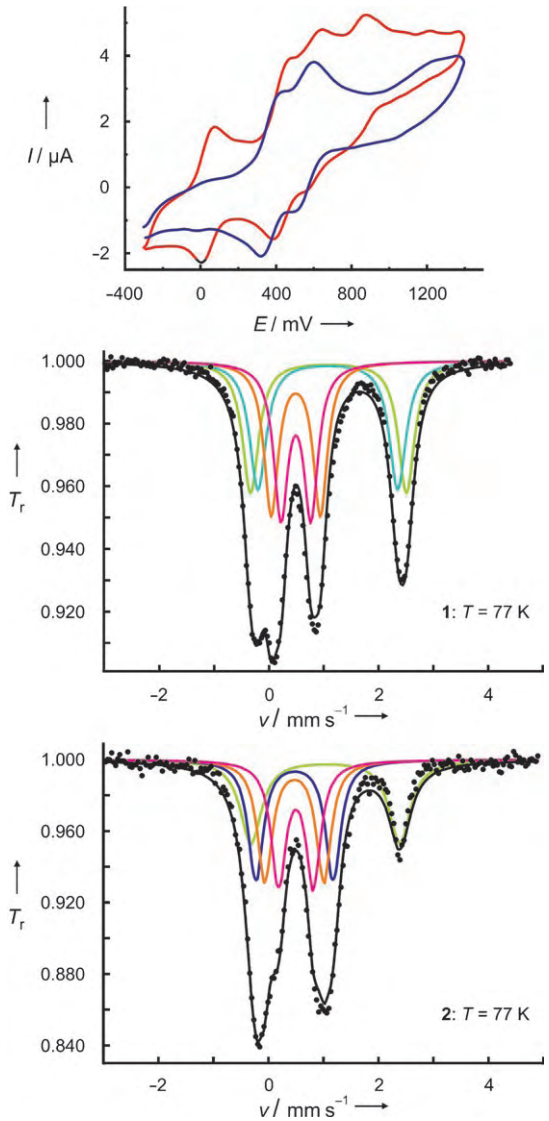


***Figure 2.*** Top: cyclic voltammograms of **1** (red line) and **2** (blue line) in $CH_2Cl_2$ (0.1 M $Bu_4NPF_6$, $T = 293$ K, scan rate $\nu = 100$ mV s$^{-1}$). Center: Mössbauer spectrum of **1** ($T = 77$ K). Experiment: black dots; simulation: black line; peripheral $Fe^{II}$ ions: turquoise and green lines; central $Fe^{III}$ ions: magenta and orange lines. Bottom: Mössbauer spectrum of **2** ($T = 77$ K). Experiment: black dots; simulation: black line; peripheral $Fe^{II}$ ions: green line; central $Fe^{III}$ ions: magenta, orange, and blue lines. $T_r$ = relative transmission.

 © 2006 Wiley-VCH Verlag GmbH & Co. KGaA, Weinheim 

that no further iron(III) to iron(II) reduction occurs in this potential range.

The Mössbauer spectrum of **1** at 77 K in the absence of an applied magnetic field consists of four quadrupole doublets with relative intensities of 1:1:1:1 (Figure 2, center), indicating four different pairs of iron ions. The two doublets with larger quadrupole splittings (turquoise line: quadrupole splitting $\Delta E_Q = 2.55\ mm\,s^{-1}$, isomer shift $\delta = 1.09\ mm\,s^{-1}$, line width $\Gamma = 0.37\ mm\,s^{-1}$; green line: $\Delta E_Q = 2.84\ mm\,s^{-1}$, $\delta = 1.10\ mm\,s^{-1}$, $\Gamma = 0.36\ mm\,s^{-1}$) each correspond to a pair of high-spin iron(II) ($S = 2$) species. The two doublets with smaller quadrupole splittings (magenta line: $\Delta E_Q = 0.54\ mm\,s^{-1}$, $\delta = 0.51\ mm\,s^{-1}$, $\Gamma = 0.31\ mm\,s^{-1}$; orange line: $\Delta E_Q = 0.89\ mm\,s^{-1}$, $\delta = 0.51\ mm\,s^{-1}$, $\Gamma = 0.31\ mm\,s^{-1}$) each correspond to a pair of high-spin iron(III) ($S = 5/2$) species. The relative intensity of each quadrupole doublet is 25 %. The isomer shifts of the iron(II) ions of **1** are significantly lower than those reported for six-coordinate iron(II) systems;[13] however, they are similar to the values reported for five-coordinate iron(II) systems.[14] Therefore, the four peripheral five-coordinate iron ions in **1** can be assigned as iron(II).

The structure of **2** was also determined by a low-temperature single-crystal X-ray structure analysis (Figure 3).[15]

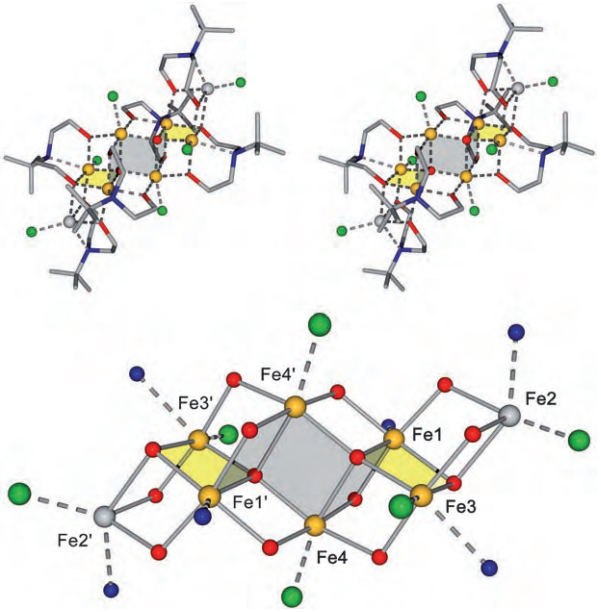


***Figure 3.*** Linear defective hexacubane **2**. Top: stereo representation. Bottom: the hexacubane framework. $Fe^{II}$ silver, $Fe^{III}$ gold, C gray, N blue, O red, Cl green; the shared faces of the $[Fe_3O_4]$ partial cubanes are highlighted.

Complex **2** is a linear defective hexacubane and is the first iron complex of this type.[12] In the crystal structure, the complex is located on an inversion center of the space group $P2_1/n$ and has $C_i$ point symmetry.

In analogy to **1**, the six tridentate $(L^3)^{2-}$ ligands in **2** participate in two different bonding modes: four are tritopic, and two are tetratopic. Of four discrete pairs of metal centers, one pair of iron(II) ions is five-coordinate, and three pairs of iron(III) ions are six-coordinate. The two peripheral iron(II) ions (Fe2 and Fe2′) occupy trigonal bipyramidal coordination environments consisting of two ethanolate $\mu_2$-$O^-$ donors, one ethanolate $\mu_3$-$O^-$ donor, one nitrogen donor, and one $Cl^-$ ion. In contrast, the six iron(III) ions (Fe1, Fe1′, Fe3, Fe3′, Fe4, and Fe4′) have octahedral coordination environments. The Fe1 and Fe1′ ions are each coordinated by three ethanolate $\mu_2$-$O^-$ donors, one ethanolate $\mu_3$-$O^-$ donor, one $\mu_4$-$O^{2-}$ ion, and one nitrogen donor. The Fe3 and Fe3′ ions are each coordinated by two ethanolate $\mu_2$-$O^-$ donors, one ethanolate $\mu_3$-$O^-$ donor, one $\mu_4$-$O^{2-}$ ion, one nitrogen donor, and one $Cl^-$ ion. The Fe4 and Fe4′ ions are each coordinated by three ethanolate $\mu_2$-$O^-$ donors, two $\mu_4$-$O^{2-}$ ions, and one $Cl^-$ ion.

The core of **2** is composed of a chain of six $[Fe_3O_4]$ defective cubane units in a zigzag arrangement. The four inner defective cubane units share two faces each and the two terminal units only one. As in **1**, the nitrogen donors and $Cl^-$ ions are not incorporated in the defective hexacubane framework, but rather, complete the coordination spheres around the iron ions.

The cyclic voltammogram of **2** exhibits two quasireversible waves at $E_{1/2} = 374$ and 549 mV relative to the NHE (Figure 2, top, blue line), which are each assigned to a one-electron transfer process ($\Delta E \approx 100$ mV; $E_p - E_{p/2} \approx 90$ mV) and correspond to reversible oxidation steps of two iron(II)/iron(III) redox couples. In addition, two distinct quasireversible one-electron waves ($\Delta E \approx 285$–$300$ mV) occur at $E_{1/2} = -362$ and $-526$ mV in the negative potential region (not shown in Figure 2), which can be assigned to $\mathbf{2}^{0/-1}$ and $\mathbf{2}^{-1/-2}$ reductions, respectively.

The Mössbauer spectrum of **2** at 77 K in the absence of an applied magnetic field consists of four quadrupole doublets with relative intensities of 1:1:1:1 (Figure 2, bottom), indicating four different pairs of iron ions. The doublet with the largest quadrupole splitting (green line: $\Delta E_Q = 2.70\ mm\,s^{-1}$, $\delta = 1.04\ mm\,s^{-1}$, $\Gamma = 0.47\ mm\,s^{-1}$) corresponds to the high-spin iron(II) ($S = 2$) species, and the three other quadrupole doublets (magenta line: $\Delta E_Q = 0.63\ mm\,s^{-1}$, $\delta = 0.50\ mm\,s^{-1}$, $\Gamma = 0.32\ mm\,s^{-1}$; orange line: $\Delta E_Q = 1.07\ mm\,s^{-1}$, $\delta = 0.47\ mm\,s^{-1}$, $\Gamma = 0.32\ mm\,s^{-1}$; blue line: $\Delta E_Q = 1.41\ mm\,s^{-1}$, $\delta = 0.47\ mm\,s^{-1}$, $\Gamma = 0.32\ mm\,s^{-1}$) correspond to high-spin iron(III) ($S = 5/2$) species. The relative area of each quadrupole doublet is 25 %. The two five-coordinate iron ions at the periphery of **2** can be assigned as iron(II).

Complex **1** can be converted into **2** by a controlled oxidation reaction. Treatment of a solution of **1** in $CH_2Cl_2$ with an equimolar amount of air over 3 days afforded **2** in a moderate yield.[16] In contrast, **2** can be reduced to **1** with an excess of calcium hydride.

When $H_2L^3$ was treated with calcium hydride, instead of cesium carbonate (as for **1** and **2**), and subsequently with iron(III) chloride, the novel heterometallic complex $Na_3[Fe^{III}{}_9(L^3)_8Cl_4O_6(CaCl)_2]$ (**3**) was formed (Scheme 1).[17] The molecular structure of **3** was determined by a low-temperature single-crystal X-ray structure analysis (Figure 4).[18] Complex **3** crystallizes in the achiral space group $P\bar{1}$, and the unit cell includes both enantiomers. The complex contains four octahedrally and four pseudotetragonal pyramidally coordinated homochiral iron centers,[19] and has nearly ideal $D_2$ symmetry.

 © 2006 Wiley-VCH Verlag GmbH & Co. KGaA, Weinheim 

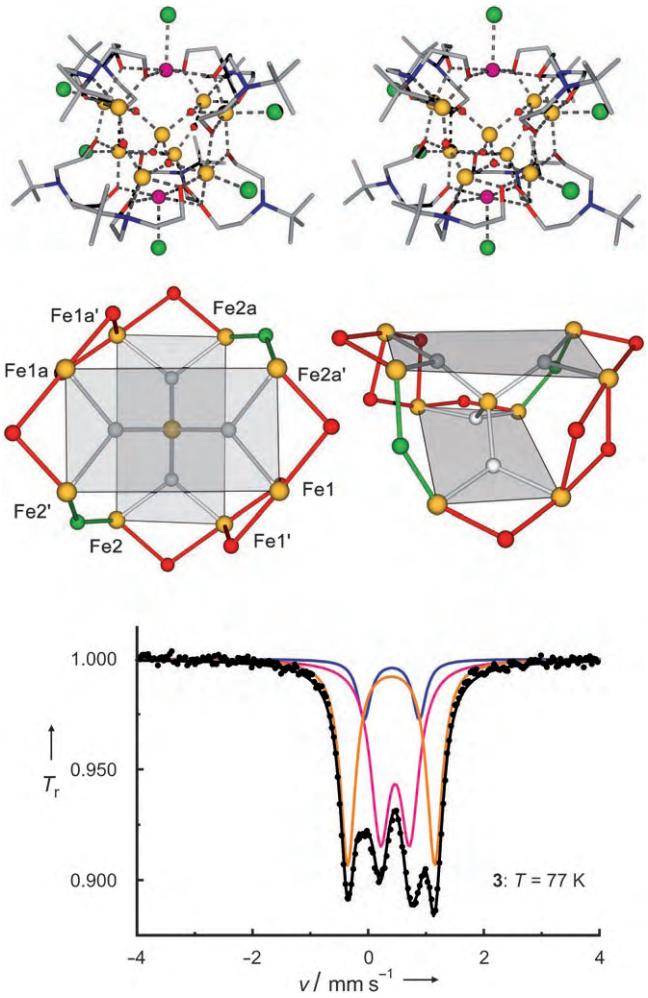


***Figure 4.*** (CaCl)-capped body-centered six-sided iron(III) polyhedron **3**. Top: stereo representation. Fe gold, Ca purple, N blue, O red, Cl green. Center: top view (left) and side view (right) of the disphenoid framework. Fe gold, $\mu_2$-$O^-$ red, $\mu_2$-$O^{2-}$ green, $\mu_3$-$O^{2-}$ gray. Bottom: Mössbauer spectrum of **3** ($T = 77$ K). Experiment: black dots; simulation: black line; four-coordinate $Fe^{III}$ ions: blue line; five-coordinate $Fe^{III}$ ions: orange line; six-coordinate $Fe^{III}$ ions: magenta line.

Four of the eight potentially tridentate $(L^3)^{2-}$ ligands function as such, whereas the remaining four act as bidentate ligands. In the bidentate cases, the nitrogen atoms of the $(L^3)^{2-}$ ligands do not coordinate, which is unprecedented for diethanolamine ligands.[2–4] All eight ligands are tritopic, each linking two iron centers and one calcium ion. There are two sets of four nearly equivalent iron centers (related by the well approximated noncrystallographic $D_2$ symmetry; Fe1, Fe1′, Fe1a, Fe1a′, and Fe2, Fe2′, Fe2a, Fe2a′).[20] The Fe1, Fe1′, Fe1a, and Fe1a′ ions have octahedral environments and are coordinated by four ethanolate $\mu_2$-$O^-$ donors, one $\mu_3$-$O^{2-}$ ion, and one $Cl^-$ ion. The Fe2, Fe2′, Fe2a, and Fe2a′ ions have pseudotetragonal pyramidal environments and are coordinated by two ethanolate $\mu_2$-$O^-$ donors, one $\mu_3$-$O^{2-}$ ion, one $\mu_2$-$O^{2-}$ ion, and one nitrogen donor. The central iron(III) ion is tetrahedrally coordinated by four $\mu_3$-$O^{2-}$ ions. The square pyramidal coordination spheres of each of the two $Ca^{2+}$ ions consist of four ethanolate $\mu_2$-$O^-$ donors and one $Cl^-$ ion. Note that the iron ions in **3** occupy three different types of coordination environments, including a tetrahedral environment, which is uncommon for iron(III).

The eight outer iron ions can be considered as the corners of a six-sided polyhedron.[21] Two orthogonal rectangles are linked through their corners by four ethanolate $\mu_2$-$O^-$ donors and two $\mu_2$-$O^{2-}$ ions, and through the central iron(III) ion by four $\mu_3$-$O^{2-}$ ions. The entire framework is fixed by the two (CaCl) caps.

Compound **3** does not display any redox waves at positive potentials. However, two quasireversible one-electron waves are observed at $E_{1/2} = -335$ and $-532$ mV relative to the NHE ($\Delta E = 285$ and 295 mV; not shown), which correspond to the redox couples $\mathbf{3}^{0/-1}$ and $\mathbf{3}^{-1/-2}$.

The Mössbauer spectrum of **3** at 77 K in the absence of an applied field consists of three quadrupole doublets with relative intensities of 4:4:1 (Figure 4). The doublet with $\Delta E_Q = 1.50$ mm s$^{-1}$, $\delta = 0.40$ mm s$^{-1}$, $\Gamma = 0.32$ mm s$^{-1}$, and a relative area of 44.4(3)% (orange line) corresponds to the four five-coordinate high-spin iron(III) ($S = 5/2$) species, whereas the doublet with $\Delta E_Q = 0.51$ mm s$^{-1}$, $\delta = 0.47$ mm s$^{-1}$, $\Gamma = 0.40$ mm s$^{-1}$, and a relative area of 44.4(3)% (magenta line) is assigned to the four six-coordinate high-spin iron(III) ions. The quadrupole doublet with $\Delta E_Q = 0.95$ mm s$^{-1}$, $\delta = 0.41$ mm s$^{-1}$, $\Gamma = 0.27$ mm s$^{-1}$, and a relative area of 11.1(3)% (blue line) is ascribed to the central tetrahedrally coordinated high-spin iron(III) ion.

In conclusion, we have demonstrated that the α-branched ligand $H_2L^3$ and mixtures of iron(II) and iron(III) salts readily self-assemble to yield the mixed-valent octanuclear iron defective hexacubanes **1** and **2**, as well as the homovalent (CaCl)-capped nonanuclear body-centered six-sided iron(III) polyhedron **3**. Complexes **1** and **2** can be interconverted by controlled oxidation and reduction. The structures of the three novel compounds were characterized by X-ray diffraction and Mössbauer spectroscopy, and their multistep one-electron redox reactions were studied by cyclic voltammetry.

Received: April 13, 2006
Published online: July 28, 2006

**Keywords:** cage compounds · cubanes · iron complexes · Mössbauer spectroscopy · structure elucidation

[1] R. W. Saalfrank, I. Bernt, E. Uller, F. Hampel, *Angew. Chem.* **1997**, *109*, 2596–2599; *Angew. Chem. Int. Ed. Engl.* **1997**, *36*, 2482–2485.
[2] a) R. W. Saalfrank, I. Bernt, F. Hampel, *Angew. Chem.* **2001**, *113*, 1745–1748; *Angew. Chem. Int. Ed.* **2001**, *40*, 1700–1703; b) R. W. Saalfrank, C. Deutscher, H. Maid, A. M. Ako, S. Sperner, T. Nakajima, W. Bauer, F. Hampel, B. A. Heß, N. J. R. van Eikema Hommes, R. Puchta, F. W. Heinemann, *Chem. Eur. J.* **2004**, *10*, 1899–1905; c) R. W. Saalfrank, C. Deutscher, S. Sperner, T. Nakajima, A. M. Ako, E. Uller, F. Hampel, F. W. Heinemann, *Inorg. Chem.* **2004**, *43*, 4372–4382.
[3] R. W. Saalfrank, T. Nakajima, N. Mooren, A. Scheurer, H. Maid, F. Hampel, C. Trieflinger, J. Daub, *Eur. J. Inorg. Chem.* **2005**, 1149–1153.

 © 2006 Wiley-VCH Verlag GmbH & Co. KGaA, Weinheim 

[4] R. W. Saalfrank, R. Prakash, H. Maid, F. Hampel, F. W. Heinemann, A. X. Trautwein, L. Böttger, *Chem. Eur. J.* **2006**, *12*, 2428 – 2433.

[5] R. W. Saalfrank, I. Bernt, M. M. Chowdhry, F. Hampel, G. B. M. Vaughan, *Chem. Eur. J.* **2001**, *7*, 2765 – 2769.

[6] a) O. Waldmann, R. Koch, S. Schromm, P. Müller, I. Bernt, R. W. Saalfrank, *Phys. Rev. Lett.* **2002**, *89*, 246401/1 – 4; b) O. Waldmann, R. Koch, S. Schromm, J. Schülein, P. Müller, I. Bernt, R. W. Saalfrank, F. Hampel, E. Balthes, *Inorg. Chem.* **2001**, *40*, 2986 – 2995.

[7] R. W. Saalfrank, A. Scheurer, I. Bernt, F. W. Heinemann, A. V. Postnikov, V. Schünemann, A. X. Trautwein, M. S. Alam, H. Rupp, P. Müller, *Dalton Trans.* **2006**, 2865 – 2874.

[8] a) P. King, R. Clérac, W. Wernsdorfer, C. E. Anson, A. K. Powell, *Dalton Trans.* **2004**, 2670 – 2676; b) M. Koikawa, H. Yamashita, T. Tokii, *Inorg. Chim. Acta* **2004**, *357*, 2635 – 2642; c) G. S. Papaefstathiou, A. Escuer, M. Font-Bardía, S. P. Perlepes, X. Solans, R. Vicente, *Polyhedron* **2002**, *21*, 2027 – 2032; d) Y. Nakamura, M. Yonemura, K. Arimura, N. Usuki, M. Ohba, H. Ōkawa, *Inorg. Chem.* **2001**, *40*, 3739 – 3744; e) R. Villanneau, R. Delmont, A. Proust, P. Gouzerh, *Chem. Eur. J.* **2000**, *6*, 1184 – 1192; f) M. Mikuriya, Y. Hashimoto, S. Nakashima, *Chem. Commun.* **1996**, 295 – 296.

[9] a) S. Triki, J. Sala-Pala, F. Thétiot, C. J. Gómez-García, J.-C. Daran, *Eur. J. Inorg. Chem.* **2006**, 185 – 199; b) D. Foguet-Albiol, K. A. Abboud, G. Christou, *Chem. Commun.* **2005**, 4282 – 4284; c) L. Zhang, L.-F. Tang, Z.-H. Wang, M. Du, M. Julve, F. Lloret, J.-T. Wang, *Inorg. Chem.* **2001**, *40*, 3619 – 3622; d) C. Goh, A. Nivorozhkin, S. J. Yoo, E. L. Bominaar, E. Münck, R. H. Holm, *Inorg. Chem.* **1998**, *37*, 2926 – 2932; e) K. L. Taft, G. C. Papaefthymiou, S. J. Lippard, *Inorg. Chem.* **1994**, *33*, 1510 – 1520; f) C. Boskovic, H. U. Güdel, G. Labat, A. Neels, W. Wernsdorfer, B. Moubaraki, K. S. Murray, *Inorg. Chem.* **2005**, *44*, 3181 – 3189; g) L. F. Jones, E. K. Brechin, D. Collison, M. Helliwell, T. Mallah, S. Piligkos, G. Rajaraman, W. Wernsdorfer, *Inorg. Chem.* **2003**, *42*, 6601 – 6603; h) J. C. Goodwin, R. Sessoli, D. Gatteschi, W. Wernsdorfer, A. K. Powell, S. L. Heath, *J. Chem. Soc. Dalton Trans.* **2000**, 1835 – 1840.

[10] a) R. E. P. Winpenny, *J. Chem. Soc. Dalton Trans.* **2002**, 1 – 10; b) G. Christou, D. Gatteschi, D. N. Hendrickson, R. Sessoli, *MRS Bull.* **2000**, *25*, 66 – 71; c) D. Gatteschi, R. Sessoli, A. Cornia, *Chem. Commun.* **2000**, 725 – 732; d) R. M. Cinco, A. Rompel, H. Visser, G. Aromí, G. Christou, K. Sauer, M. P. Klein, V. K. Yachandra, *Inorg. Chem.* **1999**, *38*, 5988 – 5998.

[11] Crystallographic data for **1**·0.5 THF·0.5 $Et_2O$: $C_{52}H_{111}Cl_4Fe_8N_6O_{15}$, $M_r = 1649.07\ g\,mol^{-1}$, monoclinic, space group $C2/c$, $a = 29.200(3)$, $b = 14.389(2)$, $c = 16.962(1)$ Å, $\beta = 97.060(2)°$, $V = 7072.7(13)$ Å$^3$, $Z = 4$, $\rho_{calcd} = 1.549\ g\,cm^{-3}$, $T = 100(2)$ K, $\mu = 1.804\ mm^{-1}$, $F(000) = 3444$, $6.64 < 2\theta < 55.74°$, $T_{max/min} = 0.780/0.633$, 70699 collected reflections, 8417 unique ($R_{int} = 0.0306$), 6981 observed ($I > 2\sigma(I)$), 425 parameters, $R_1 = 0.0259$ ($I > 2\sigma(I)$), $wR_2 = 0.0657$ (all data), GOF = 1.127, max/min residual electron density = 0.866/−0.430 e Å$^{-3}$. CCDC-602908 (**1**), CCDC-602909 (**2**), and CCDC-602910 (**3**) contain the supplementary crystallographic data for this paper. These data can be obtained free of charge from The Cambridge Crystallographic Data Centre via www.ccdc.cam.ac.uk/data_request/cif.

[12] Compact defective cubanes: a) M. D. Godbole, O. Roubeau, R. Clérac, H. Kooijman, A. L. Spek, E. Bouwman, *Chem. Commun.* **2005**, 3715 – 3717; b) S. Tanase, G. Aromí, E. Bouwman, H. Kooijman, A. L. Spek, J. Reedijk, *Chem. Commun.* **2005**, 3147 – 3149; linear defective cubanes: c) S. N. Shaikh, J. Zubieta, *Inorg. Chem.* **1986**, *25*, 4615 – 4616; d) C. J. Milios, F. P. A. Fabbiani, S. Parsons, M. Murugesu, C. Christou, E. K. Brechin, *Dalton Trans.* **2006**, 351 – 356.

[13] N. N. Greenwood, T. C. Gibb, *Mössbauer Spectroscopy*, Chapmann & Hall, London, **1971**.

[14] A. X. Trautwein, *J. Mol. Struct.* **1978**, *45*, 199 – 216.

[15] Crystallographic data for **2**·2 $CH_2Cl_2$: $C_{50}H_{106}Cl_{10}Fe_8N_6O_{14}$, $M_r = 1816.71\ g\,mol^{-1}$, monoclinic, space group $P2_1/n$, $a = 11.175(1)$, $b = 28.055(2)$, $c = 11.726(2)$ Å, $\beta = 103.89(1)°$, $V = 3568.8(7)$ Å$^3$, $Z = 2$, $\rho_{calcd} = 1.691\ g\,cm^{-3}$, $T = 100(2)$ K, $\mu = 2.013\ mm^{-1}$, $F(000) = 1876$, $6.46 < 2\theta < 55.02°$, $T_{max/min} = 0.820/0.667$, 73245 collected reflections, 8112 unique ($R_{int} = 0.0593$), 6242 observed ($I > 2\sigma(I)$), 434 parameters, $R_1 = 0.0344$ ($I > 2\sigma(I)$), $wR_2 = 0.0692$ (all data), GOF = 1.007, max/min residual electron density = 0.543/−0.421 e Å$^{-3}$.

[16] The formation of **2** through a mild oxidation of **1** was confirmed by its mass spectrum and cyclic voltammogram. Note that the reaction of **1** with excess air/oxygen yielded a yellow solid, which could not yet be characterized.

[17] See: a) W. Schmitt, C. E. Anson, W. Wernsdorfer, A. K. Powell, *Chem. Commun.* **2005**, 2098 – 2100; b) A. K. Boudalis, B. Donnadieu, V. Nastopoulos, J. M. Clemente-Juan, A. Mari, Y. Sanakis, J.-P. Tuchagues, S. P. Perlepes, *Angew. Chem.* **2004**, *116*, 2316 – 2320; *Angew. Chem. Int. Ed.* **2004**, *43*, 2266 – 2270; c) G. W. Powell, H. N. Lancashire, E. K. Brechin, D. Collison, S. L. Heath, T. Mallah, W. Wernsdorfer, *Angew. Chem.* **2004**, *116*, 5896 – 5899; *Angew. Chem. Int. Ed.* **2004**, *43*, 5772 – 5775.

[18] Crystallographic data for **3**·$H_2L^3$·4 $CH_2Cl_2$·2.61 $H_2O$: $C_{76}H_{168.22}Ca_2Cl_{14}Fe_9N_9Na_3O_{26.61}$, $M_r = 2782.26\ g\,mol^{-1}$, triclinic, space group $P\bar{1}$, $a = 17.197(2)$, $b = 17.425(2)$, $c = 23.628(4)$ Å, $\alpha = 80.27(2)$, $\beta = 75.98(2)$, $\gamma = 63.45(1)°$, $V = 6129.9(16)$ Å$^3$, $Z = 2$, $\rho_{calcd} = 1.507\ g\,cm^{-3}$, $T = 100(2)$ K, $\mu = 1.496\ mm^{-1}$, $F(000) = 2890$, $6.42 < 2\theta < 54.20°$, $T_{max/min} = 1.000/0.905$, 116603 collected reflections, 26959 unique ($R_{int} = 0.0631$), 18331 observed ($I > 2\sigma(I)$), 1339 parameters, $R_1 = 0.0534$ ($I > 2\sigma(I)$), $wR_2 = 0.1559$ (all data), GOF = 1.049, max/min residual electron density = 1.694/−1.104 e Å$^{-3}$.

[19] For the determination of the chirality of **3** see: a) M. F. Brown, B. R. Cook, T. E. Sloan, *Inorg. Chem.* **1975**, *14*, 1273 – 1278; b) T. Damhus, C. E. Schäffer, *Inorg. Chem.* **1983**, *22*, 2406 – 2412; c) A. von Zelewsky, *Stereochemistry of Coordination Compounds*, Wiley, Chichester, **1996**, p. 70.

[20] For clarity, this simplified labeling is used instead of that used in the crystallographic data (Fe1–Fe9).

[21] Six-sided polyhedron: Generated from an orthorhombic disphenoid (four-sided polyhedron, similar to a tetrahedron, but with unequal edges) cut by a basic pinacoid (two parallel planes).


 © 2006 Wiley-VCH Verlag GmbH & Co. KGaA, Weinheim 

# Cover Picture

**Michael Göbel, Konstantin Karaghiosoff, and Thomas M. Klapötke***

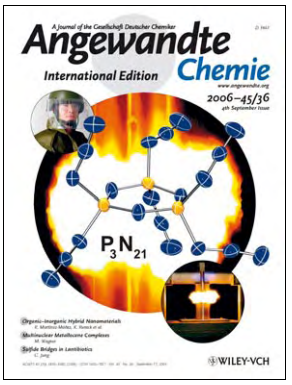


***A binary P–N molecule***
was unambiguously characterized for the first time. The cover shows the molecular structure of $P_3N_{21}$ determined by X-ray diffraction. The explosive decomposition of a sample in a drop-hammer experiment and the protective clothing that must be worn during such an experiment are also depicted. Further details on the balancing act between the formation and decomposition of this molecule are provided by T. M. Klapötke and co-workers in their Communication on page 6037 ff.

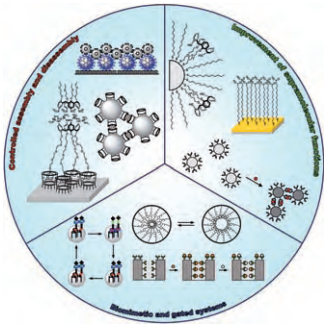

***Hybrid Materials***
The combination of supramolecular chemistry and nanomaterials has yielded its first successes. In their Review on page 5924 ff., R. Martínez-Máñez, K. Rurack, and co-workers describe a selection of these functional systems.

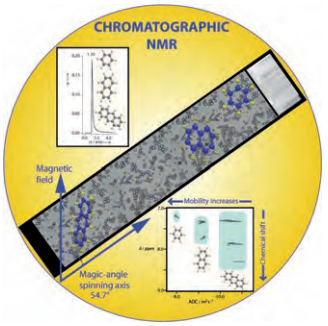


***Spectroscopic Methods***
In their Communication on page 5950 ff., G. Pages et al. use solid-enhanced DOSY NMR spectroscopy to achieve a spectral separation of aromatic molecules on silica gel, which is not possible by HPLC.

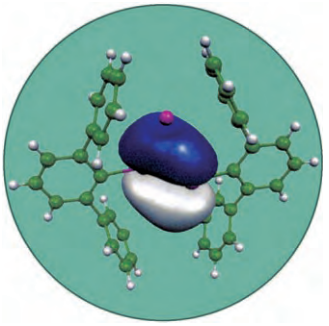

***Dialuminyne***
The aluminum alkyne analogue $Na_2[Ar'AlAlAr']$ ($Ar' = C_6H_3$-2,6-$(C_6H_3$-2,6-$iPr_2)_2$) has a planar trans-bent C–Al–Al–C array. P. P. Power and co-workers report its synthesis and characterization in their Communication on page 5953 ff.

# Contents

**VIP** *The following Communications have been judged by at least two referees to be "very important papers" and will be published online at www.angewandte.org soon:*


*K. J. T. Noonan, D. P. Gates**
**Ambient-Temperature Living Anionic Polymerization of Phosphaalkenes: Homopolymers and Block Copolymers with Controlled Chain Lengths**

*J. Piera, K. Närhi, J.-E. Bäckvall**
**Palladium(II)-Catalyzed Aerobic Allylic Oxidative Carbocyclization of Allene-Substituted Olefins: Immobilization of an Oxygen-Activating Catalyst**

*T. J. Taylor, V. I. Bakhmutov, F. P. Gabbaï**
**Hydrocarbon Uptake in the Alkylated Micropores of a Columnar Supramolecular Solid**

*J.-P. Leclerc, K. Fagnou**
**Palladium-Catalyzed Cross-Coupling Reactions of Diazine N-Oxides with Aryl Chlorides, Bromides, and Iodides**

*J. W. Lee, J.-S. Lee, Y.-T. Chang**
**Colorimetric Identification of Carbohydrates by a pH Indicator/pH-Change-Inducer Ensemble**

*Z.-M. Cui, Q. Liu, W.-G. Song*, L.-J. Wan**
**Insights into the Mechanism of Methanol-to-Olefin Conversion from Zeolites with Systematically Selected Framework Structures**


## Web Sites


www.lipidbank.jp
www.lipidmaps.org — Lipids and Lipidomics — *T. Kolter* — **5910**


## Books


Encyclopedia of Inorganic Chemistry — R. Bruce King — *reviewed by D. Scheschkewitz* — **5912**


## Highlights

### Molecular Electronics


M. Wagner* — **5916 – 5918**

A New Dimension in Multinuclear Metallocene Complexes


**Radial oligocyclopentadienyl metal complexes** were synthesized for the first time by a highly efficient Negishi coupling. Such compounds open fascinating possibilities for applications on the threshold between homogeneous and heterogeneous catalysis as well as in molecular electronics.

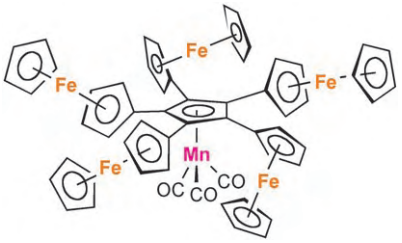


### Lantibiotic Biosynthesis


G. Jung* — **5919 – 5921**

Enzyme-Catalyzed Sulfide Ring Formation in Lantibiotics


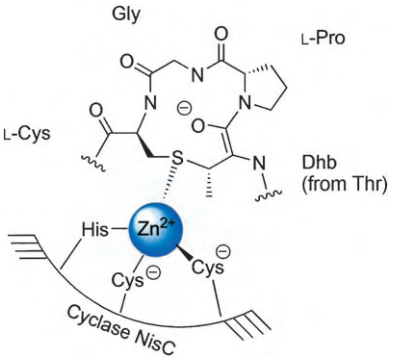


**Building bridges**: The crystal structure of the zinc enzyme NisC was solved recently by X-ray diffraction. This cyclase single-handedly catalyzes the formation of several sulfide bridges in the dehydrated precursor protein NisA of the lantibiotic nisin. The Highlight discusses the impact of these results on the field of lantibiotic research.



© 2006 Wiley-VCH Verlag GmbH & Co. KGaA, Weinheim

# Reviews

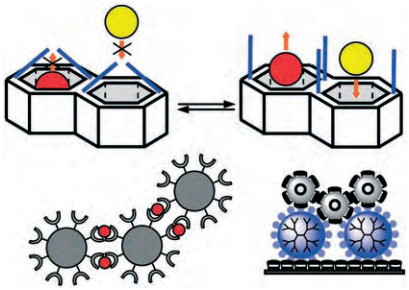

**Taking chemical functionality to a new level**: Blending 2D and 3D nanoscopic structures with supramolecular concepts can be used to generate systems for enhanced recognition and sensing, to control assembly and disassembly processes, and give the possibility for biomimetic reactions within nanoscopic scaffolds.


**Mesoporous Materials**

A. B. Descalzo, R. Martínez-Máñez,* F. Sancenón, K. Hoffmann, K. Rurack* ——— **5924 – 5948**

The Supramolecular Chemistry of Inorganic–Organic Hybrid Materials


# Communications

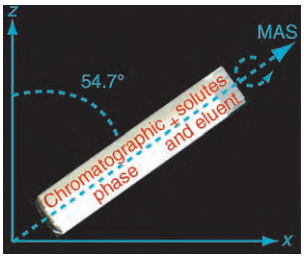


**Break it up**: Ordinarily, silica gel produces no separation in a mixture of aromatic molecules by HPLC; however, solid-enhanced DOSY NMR spectroscopy succeeds in this task, although its separation capabilities concern just the spectral components. Chromatographic NMR spectroscopy may thus prove a simple complement to HPLC in favorable cases. MAS = magic-angle spinning.


**NMR Spectroscopy**

G. Pages,* C. Delaurent, S. Caldarelli ——— **5950 – 5953**

Simplified Analysis of Mixtures of Small Molecules by Chromatographic NMR Spectroscopy


**An alkyne analogue with Al**: The first "dialuminyne" of formula $Na_2[Ar'AlAlAr']$ (see picture; $Ar' = C_6H_3$-2,6-$(C_6H_3$-2,6-$iPr_2)_2$) was synthesized and characterized by X-ray crystallography. The structure contains a planar *trans*-bent C–Al–Al–C array with an Al–Al bond length of 2.428(1) Å and a bending angle of 131.71(7)° at Al.

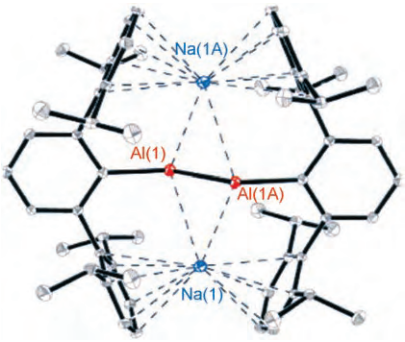



**Al–Al Multiple Bonds** VIP

R. J. Wright, M. Brynda, P. P. Power* ——— **5953 – 5956**

Synthesis and Structure of the "Dialuminyne" $Na_2[Ar'AlAlAr']$ and $Na_2[(Ar''Al)_3]$: Al–Al Bonding in $Al_2Na_2$ and $Al_3Na_2$ Clusters



**For the USA and Canada:**
ANGEWANDTE CHEMIE International Edition (ISSN 1433-7851) is published weekly by Wiley-VCH PO Box 191161, D 69451 Weinheim, Germany. Air freight and mailing in the USA by Publications Expediting Inc. 200 Meacham Ave., Elmont, NY 11003. Periodicals postage paid at Jamaica NY 11431. US POSTMASTER: send address changes to *Angewandte Chemie*, Wiley-VCH, 111 River Street, Hoboken, NJ 07030. Annual subscription price for institutions: US$ 5685/5168 (valid for print and electronic / print or electronic delivery); for individuals who are personal members of a national chemical society prices are available on request. Postage and handling charges included. All prices are subject to local VAT/sales tax.



© 2006 Wiley-VCH Verlag GmbH & Co. KGaA, Weinheim

# The best in chemistry –

## for more than a hundred years

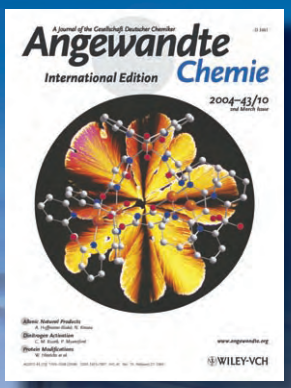


A Journal of the Gesellschaft Deutscher Chemiker

**Angewandte**
**International Edition** **Chemie**

**www.angewandte.org**

**1888:** ***The beginning of a success story***

### Constant Innovations

**1962:** *First issue of the International Edition*
**1976:** *Graphical abstracts*
**1979:** *Cover pictures*
**1988:** *Centenary of Angewandte*
**1989:** *Routine use of color*
**1991:** *New section: Highlights*
**1992:** *Computerized editorial tracking system*
**1995:** *Internet service for readers*
**1998:** *Regular press service; full-text online*
**2000:** *New section: Essays; EarlyView: Communications available online ahead of the printed version*
**2001:** *New section: Minireviews*
**2002:** *Online submission of manuscripts*
**2003:** *Weekly publication; new section: News; new layout*
**2004:** *Backfiles (1962-1997); ManuscriptXpress: Online system for authors and referees*

### Angewandte's advisors...

**Martin Quack**
*Physical Chemistry,*
*ETH Zürich*

»**Angewandte Chemie** *is my favourite journal covering all aspects of chemistry, from theoretical and physical chemistry to inorganic, organic, and biochemistry. It is by far the best journal worldwide for an overview of current research in chemistry as a whole. Beyond just publishing the best research in chemistry, it also helps us to fight the trend of too narrow specialization.*«

***Angewandte Chemie International Edition*** *is a journal of the German Chemical Society (GDCh)*

GDCh

WILEY InterScience® DISCOVER SOMETHING GREAT

WILEY-VCH

1197404_gu

**Double up**: Photochemical upconversion by MLCT-sensitized triplet–triplet annihilation is demonstrated (MLCT = metal-to-ligand charge transfer). Selective visible excitation of $[Ru(dmb)_3]^{2+}$ (dmb = 4,4′-dimethyl-2,2′-bipyridine) in the presence of anthracene efficiently produces the [4+4] cycloaddition product. This transformation traditionally requires ultraviolet light.

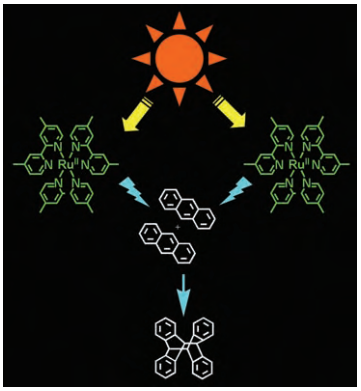

## Photochemistry

R. R. Islangulov, F. N. Castellano* ——— 5957 – 5959

Photochemical Upconversion: Anthracene Dimerization Sensitized to Visible Light by a $Ru^{II}$ Chromophore

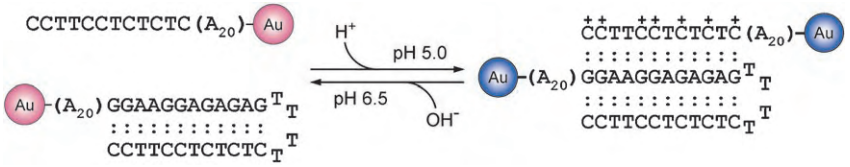


**Fueled up**: The protonation of the imino group of cytosines in double-stranded DNA, which is required for the formation of a triplex, can be used to guide the assembly/disassembly of DNA-conjugated gold nanoparticles. The reversible switching of the nanoparticles is demonstrated by repeated cycling of pH between 5.0 and 6.5 with the proton as a fuel (see picture).

## Nanobiotechnology

Y. H. Jung, K.-B. Lee, Y.-G. Kim,* I. S. Choi* ——— 5960 – 5963

Proton-Fueled, Reversible Assembly of Gold Nanoparticles by Controlled Triplex Formation

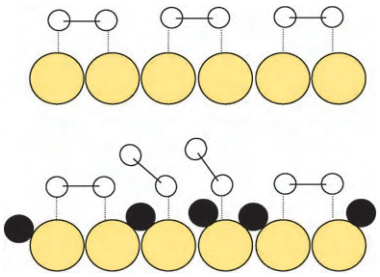

**A change in orientation** of adsorbed oxygen molecules from parallel (top) at the bare Pt electrode to a mixture of parallel and end-on modes at a Pt surface modified by the electrodeposition of manganese oxide nanoparticles (nano-MnOx/Pt) causes a higher population of oxygen molecules at the MnOx/Pt surface (bottom). The modified electrode is thus a superior electrocatalyst for the reduction of oxygen (Pt yellow, O white, MnOx black).

## Surface Chemistry

M. S. El-Deab, T. Ohsaka* — 5963 – 5966

Manganese Oxide Nanoparticles Electrodeposited on Platinum Are Superior to Platinum for Oxygen Reduction

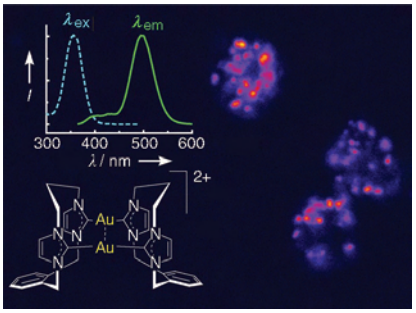


**Gold lights the way**: A bidentate cyclophane N-heterocyclic carbene ligand has been used to synthesize a new dinuclear $Au^{I}$ complex of the formula $[Au_2L_2]^{2+}$. The short Au···Au distance imposed by the rigid cyclophane ligand leads to a red-shifted luminescence profile that enables the complex to be used as a luminescent probe for distribution studies in single living cancer cells.

## Gold Luminescent Probes

P. J. Barnard, L. E. Wedlock, M. V. Baker,* S. J. Berners-Price,* D. A. Joyce, B. W. Skelton, J. H. Steer — 5966 – 5970

Luminescence Studies of the Intracellular Distribution of a Dinuclear Gold(I) N-Heterocyclic Carbene Complex


© 2006 Wiley-VCH Verlag GmbH & Co. KGaA, Weinheim

# Contents


## Materials Science

X. Zhang, D. Li* ——— **5971 – 5974**

Metal-Compound-Induced Vesicles as Efficient Directors for Rapid Synthesis of Hollow Alloy Spheres

**Hollow alloy**: Vesicles formed from tetrabutylammonium bromide and metal compounds act as efficient directors for the rapid synthesis of a variety of binary, ternary, and quaternary intermetallic materials with hollow structures. In this way, different metals were co-alloyed on the vesicle surface to produce hollow alloy spheres containing more than two kinds of metals.

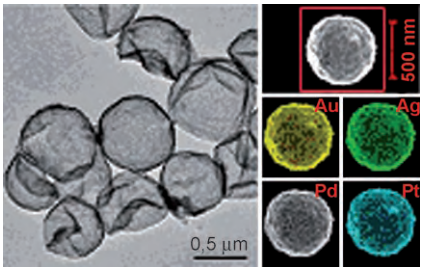


## Hybrid Materials

P. Horcajada, C. Serre,* M. Vallet-Regí, M. Sebban, F. Taulelle, G. Férey* ——— **5974 – 5978**

Metal–Organic Frameworks as Efficient Materials for Drug Delivery

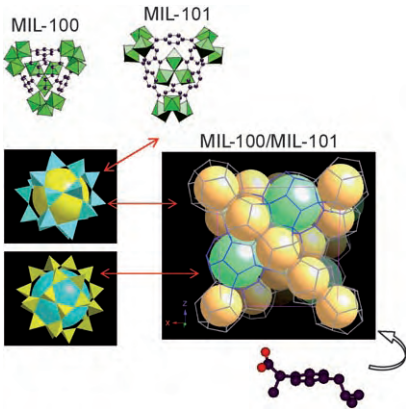


**Fill 'em up**: The metal carboxylates MIL-100 and MIL-101 act as porous matrices (see picture; MIL = Materials of Institut Lavoisier) for drug-delivery systems using Ibuprofen as a model substrate. Very large amounts of the drug could be incorporated, up to an unprecedented capacity of 1.4 g of drug per gram of porous solid for MIL-101, and the total release of Ibuprofen was achieved under physiological conditions in 3 (MIL-100) and 6 days (MIL-101).

## Combinatorial Chemistry

T. Arai,* M. Watanabe, A. Fujiwara, N. Yokoyama, A. Yanagisawa **5978 – 5981**

Direct Monitoring of the Asymmetric Induction of Solid-Phase Catalysis Using Circular Dichroism: Diamine–$Cu^{I}$-Catalyzed Asymmetric Henry Reaction

**The direct approach**: A new high-throughput screening system for analyzing the asymmetric induction in catalytic enantioselective synthesis couples solid-phase reactions with a circular dichroism detection system (see picture). Thus, direct monitoring of asymmetric induction without the need for purification or chromatographic analysis is obtained.

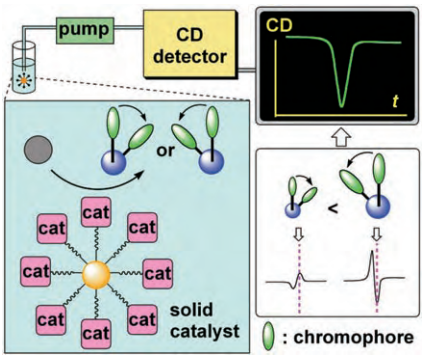


## Molecular Mechanics

N. Pour, L. Itzhaki, B. Hoz, E. Altus, H. Basch, S. Hoz* ——— **5981 – 5983**

Auxetics at the Molecular Level: A Negative Poisson's Ratio in Molecular Rods

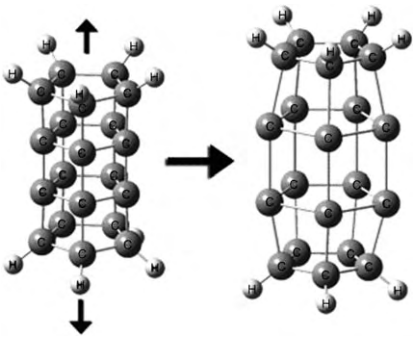

**Negative feedback**: Auxetic materials are materials that, counterintuitively, become thicker when stretched and thinner when compressed (negative Poisson's ratio). Quantum mechanical computations were used to identify poly[*n*]prismanes ($n = 3$–6), the first nanomolecular systems that manifest auxetic behavior at the molecular level. The magnitude of the negative Poisson's ratio in these prismanes ranges from 7 to 15%.



© 2006 Wiley-VCH Verlag GmbH & Co. KGaA, Weinheim

**Discriminating reactions**: While no self-aldol reaction is observed in the reaction shown, catalyst **1** promotes the Michael addition of aldehydes to nitroalkenes with the lowest catalyst loading and lowest stoichiometric ratio of reactant aldehyde that have been reported so far for this type of reaction.

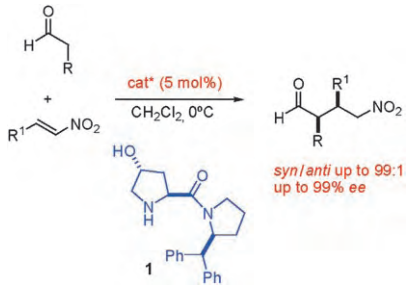


## Organocatalysis

C. Palomo,* S. Vera, A. Mielgo, E. Gómez-Bengoa ——— **5984 – 5987**

Highly Efficient Asymmetric Michael Addition of Aldehydes to Nitroalkenes Catalyzed by a Simple *trans*-4-Hydroxyprolylamide

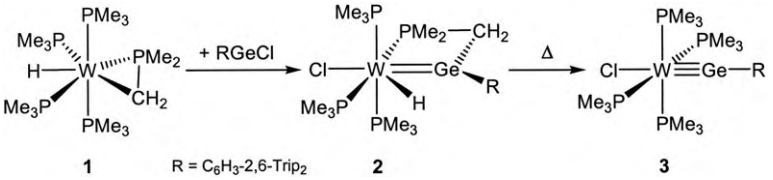


**A new activation mode** of aryl germanium(II) chlorides at electron-rich metal centers leads to compounds featuring metal–germanium triple bonds. Reaction of **1** with RGeCl affords the hydrido–germylidene complex **2**, which rearranges thermally to give the germylidyne complex **3** (see scheme; Trip = $C_6H_2$-2,4,6-$iPr_3$). In contrast, the reaction of $[Mo(PMe_3)_6]$ with RGeCl yields directly the germylidyne complex *trans*-$[Cl(PMe_3)_4Mo{\equiv}GeR]$.

## Germylidyne Complexes

A. C. Filippou,* N. Weidemann, A. I. Philippopoulos, G. Schnakenburg ——— **5987 – 5991**

Activation of Aryl Germanium(II) Chlorides by $[Mo(PMe_3)_6]$ and $[W(\eta^2\text{-}CH_2PMe_2)H(PMe_3)_4]$: A New Route to Metal–Germanium Triple Bonds

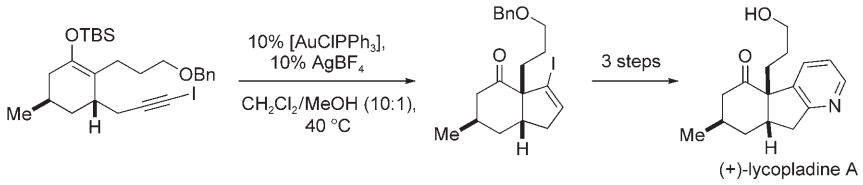


**In control**: Gold(I)-catalyzed intramolecular addition of silyl enol ethers to alkynes and allenes allows for the diastereoselective synthesis of cyclopentenes with control of the position of the double bond. The utility of these reactions is demonstrated by an efficient total synthesis of (+)-lycopladine A that takes advantage of the orthogonal reactivity of $Au^I$ and $Pd^0$ towards unsaturated iodides (see scheme).

## Carbocyclization

S. T. Staben, J. J. Kennedy-Smith, D. Huang, B. K. Corkey, R. L. LaLonde, F. D. Toste* ——— **5991 – 5994**

Gold(I)-Catalyzed Cyclizations of Silyl Enol Ethers: Application to the Synthesis of (+)-Lycopladine A

**Scope broadened**: A previously developed asymmetric Cu-catalyzed allylic substitution can be applied to more substituted allylic patterns. Two classes of β-disubstituted substrates, cinnamyl derivatives and aliphatic endocyclic allylic chlorides, afford excellent regio- and enantioselectivities (see schemes; L* = phosphoramidite ligand).

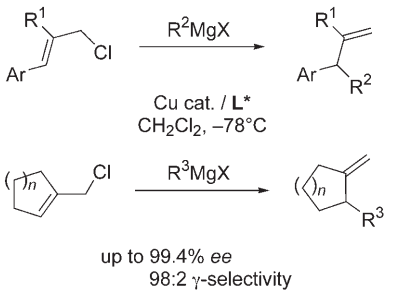


## Asymmetric Catalysis

C. A. Falciola, K. Tissot-Croset, A. Alexakis* ——— **5995 – 5998**

β-Disubstituted Allylic Chlorides: Substrates for the Cu-Catalyzed Asymmetric $S_N2'$ Reaction


© 2006 Wiley-VCH Verlag GmbH & Co. KGaA, Weinheim

# Contents


## Emission-Control Catalysts

H. Tanaka,* M. Taniguchi, M. Uenishi, N. Kajita, I. Tan, Y. Nishihata, J. Mizuki, K. Narita, M. Kimura, K. Kaneko _____ **5998 – 6002**

Self-Regenerating Rh- and Pt-Based Perovskite Catalysts for Automotive-Emissions Control

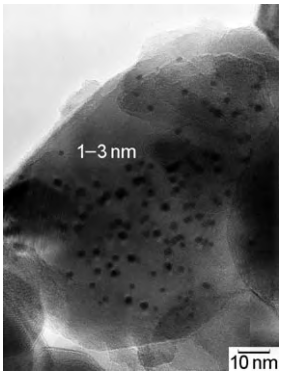


**As good as new**: Perovskite-based catalysts containing Rh and Pt for use in exhaust-emissions control systems are developed. These catalysts are found to be self-regenerating and could thus lead to the use of lower amounts of precious metals. The picture shows the TEM image of Pt grains of catalyst $CaTi_{0.95}Pt_{0.05}O_3$ aged in an engine exhaust at 900 °C for 100 h.

## Synthetic Methods

Z. Gu, S. Ma* _____ **6002 – 6005**

$Pd(OAc)_2$-Catalyzed Coupling/Cyclization of 2,3-Allenoic Acids and Methyl Propiolate: Observation of Double 1,7-Hydrogen Shifts

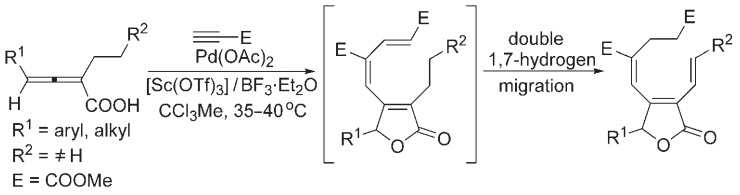


**On the move**: A $Pd(OAc)_2$-catalyzed coupling/cyclization reaction of 2,3-allenoic acids with methyl propiolate in the presence of $[Sc(OTf)_3]/BF_3{\cdot}Et_2O$ (OTf = triflate) leads to a "π-bond migration" in the 1:2 adducts, which may proceed through double 1,7-hydrogen migrations.

## Hydrogen Storage

S. K. Brayshaw, J. C. Green, N. Hazari, J. S. McIndoe, F. Marken, P. R. Raithby, A. S. Weller* _____ **6005 – 6008**

Storing and Releasing Hydrogen with a Redox Switch

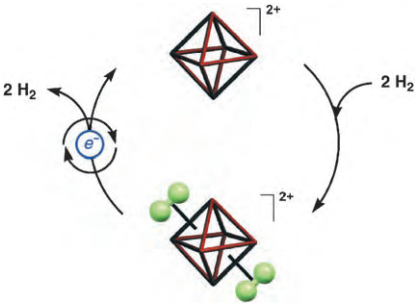


**Give and take**: A molecular cluster that readily takes up and stores two molecules of $H_2$ also rapidly releases (milliseconds) the stored $H_2$ by a simple redox process. This process represents a new method of hydrogen storage and release from a well-defined molecular material.

## Mg/Air Battery Materials

W. Li, C. Li, C. Zhou, H. Ma, J. Chen* _____ **6009 – 6012**

Metallic Magnesium Nano/Mesoscale Structures: Their Shape-Controlled Preparation and Mg/Air Battery Applications

**Magnesium nano/mesostructures** with spherical, platelike, rodlike, and sea-urchin-like shapes are prepared by a simple and efficient vapor-transport method. They exhibit excellent electrochemical properties in Mg/air batteries. The figure shows discharge curves of the Mg/air batteries made from two samples, at a constant current of 0.5 mA and a temperature of 25 °C.

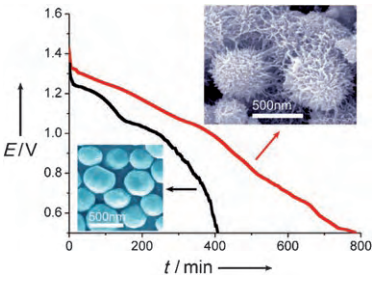




© 2006 Wiley-VCH Verlag GmbH & Co. KGaA, Weinheim

**Changed in a flash**: A photochemically unreactive crystal of 5-methyl-2-pyridone with a trimesic acid host is transformed in the solid state into a reactive phase by heating or by contact with solvent vapor. The mechanism was revealed to involve desolvation and a 180° turn of one molecule with respect to the other.

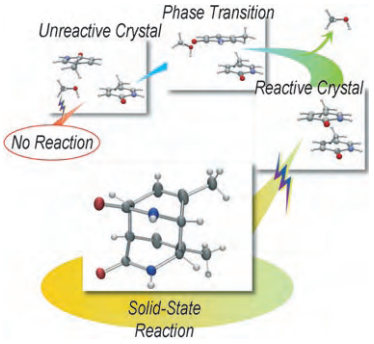


## Solid-State Reactions

S. Hirano, S. Toyota, F. Toda,* K. Fujii, H. Uekuasa* ——— **6013 – 6016**

Solid-State Phase Transition of an Inclusion Complex of 5-Methyl-2-pyridone with 1,3,5-Benzenetricarboxylic Acid

---

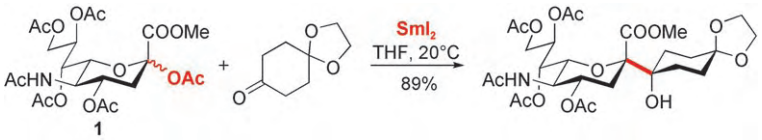


**Teaching an old molecule new tricks**: A new solution for an expeditious C-sialylation from *N*-acetylneuraminic acid involves the use of the peracetylated derivative **1**, a very common starting material prepared 40 years ago in Heidelberg, through an anomeric umpolung by samarium diiodide without an additive, in the presence of a carbonyl compound. Excellent yields are obtained for the coupling with cyclic ketones (see scheme).

## C-Sialylation

A. Malapelle, Z. Abdallah, G. Doisneau, J.-M. Beau* ——— **6016 – 6020**

Anomeric Acetates of *N*-Acetylneuraminic Acid are Useful *C*-Sialyl Donors in Samarium-Mediated Reformatsky Coupling Reactions

---

**A clean break**: An N-heterocyclic carbene catalyzes the ring-opening of chiral non-racemic formylcyclopropanes, with simultaneous oxidation of the aldehyde function and without the need for stoichiometric reagents. The activated carboxylate intermediate is trapped by a variety of nucleophiles, thus leading to chiral esters, thioesters, or carboxylic acids (see scheme; DBU = 1,8-diazabicyclo-[5.4.0]undec-7-ene, EWG = electron-withdrawing group, Nu = nucleophile.)

## Organocatalysis

S. S. Sohn, J. W. Bode* ——— **6021 – 6024**

N-Heterocyclic Carbene Catalyzed C–C Bond Cleavage in Redox Esterifications of Chiral Formylcyclopropanes

---

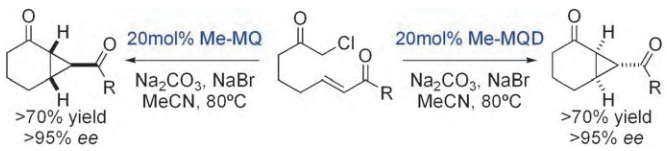


**A mechanism-guided design process** was used to develop cinchona alkaloids that are substituted at the C2′ position of the quinoline moiety. These compounds prove to be excellent organocatalysts for an enantioselective intramolecular cyclopropanation reaction (see scheme).

## Asymmetric Synthesis

C. C. C. Johansson, N. Bremeyer, S. V. Ley, D. R. Owen, S. C. Smith, M. J. Gaunt* ——— **6024 – 6028**

Enantioselective Catalytic Intramolecular Cyclopropanation using Modified Cinchona Alkaloid Organocatalysts


© 2006 Wiley-VCH Verlag GmbH & Co. KGaA, Weinheim

# Contents


## Intermolecular Cyclization

S. López, E. Herrero-Gómez, P. Pérez-Galán, C. Nieto-Oberhuber, A. M. Echavarren* _____ **6029 – 6032**

Gold(I)-Catalyzed Intermolecular Cyclopropanation of Enynes with Alkenes: Trapping of Two Different Gold Carbenes

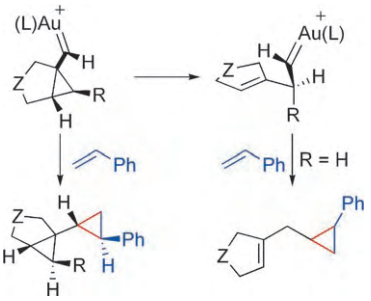


**Caught in a trap**: Intermolecular cyclopropanation reactions of enynes with alkenes allows the synthesis of complex cyclic systems with gold(I) catalysts under mild conditions. Furthermore, gold carbenes are trapped intermolecularly with alkenes (see scheme; L = ligand), thereby providing experimental evidence for the involvement of two different types of metal carbenes in the skeletal rearrangement of enynes.

## Single-Molecule Magnets

T. Glaser,* M. Heidemeier, T. Weyhermüller, R.-D. Hoffmann, H. Rupp, P. Müller _____ **6033 – 6037**

Property-Oriented Rational Design of Single-Molecule Magnets: A $C_3$-Symmetric $Mn_6Cr$ Complex based on Three Molecular Building Blocks with a Spin Ground State of $S_t = 21/2$

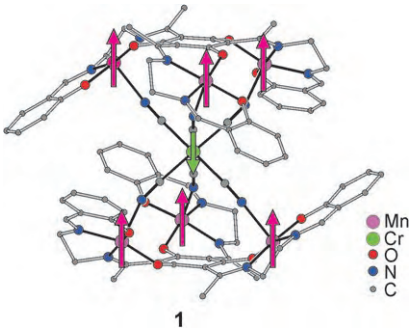


**1**

**Forced to comply**: The $Mn^{III}_6Cr^{III}$ complex **1** is constructed from two trinuclear manganese triplesalen complexes and one $[Cr(CN_6)]^{3-}$ ion, and possesses a spin ground state of $S_t = 21/2$. The threefold symmetry enforced by the triplesalen ligand precludes a complete cancellation of the single-site magnetic anisotropies and minimizes quantum tunneling of the magnetization. The analysis of the magnetic properties reveals that this complex is indeed a single-molecule magnet.

## Phosphorus Nitrides

M. Göbel, K. Karaghiosoff, T. M. Klapötke* _____ **6037 – 6040**

The First Structural Characterization of a Binary P–N Molecule: The Highly Energetic Compound $P_3N_{21}$

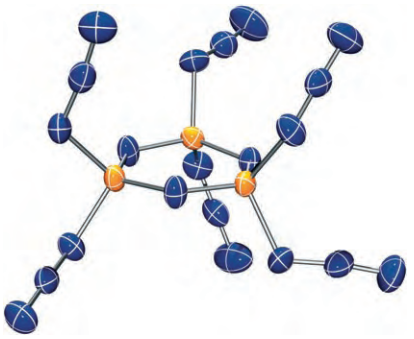

**An explosive mixture**: The first structural characterization of a binary molecule of phosphorus and nitrogen is described. With the help of a new synthetic strategy, the phosphorus azide $P_3N_{21}$ is prepared in pure form, and single crystals are isolated, enabling a structure determination by X-ray diffraction (see structure; P orange, N blue).

## Organozinc Compounds

A. Krasovskiy, V. Malakhov, A. Gavryushin, P. Knochel* _____ **6040 – 6044**

Efficient Synthesis of Functionalized Organozinc Compounds by the Direct Insertion of Zinc into Organic Iodides and Bromides

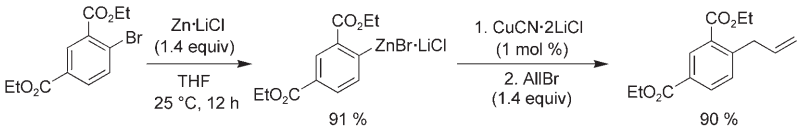


**Insider dealing**: A wide range of polyfunctional (hetero)aromatic and aliphatic zinc reagents can be easily prepared in THF. The compounds are formed by a Zn insertion reaction mediated by the addition of LiCl (see scheme; All = allyl).



© 2006 Wiley-VCH Verlag GmbH & Co. KGaA, Weinheim

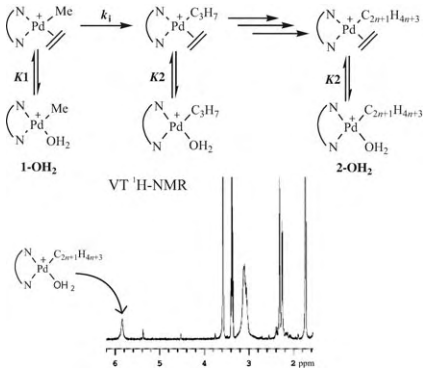


**Position blocked?** Quantitative studies of polyethylene chain growth in the presence of water by variable-temperature (VT) $^1$H NMR spectroscopy show, unexpectedly, that water can compete with monomer binding at the vacant coordination site in cationic diimine palladium(II) methyl as well as higher alkyl complexes (see scheme); the latter are prepared cleanly as water complexes at $T < 0\,^\circ C$.

## Polymerization

A. Berkefeld, S. Mecking* — **6044 – 6046**

Mechanistic Studies of Catalytic Polyethylene Chain Growth in the Presence of Water

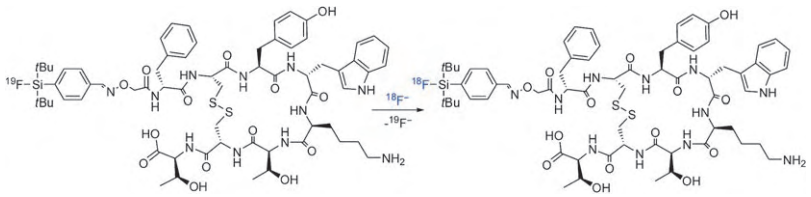

**F on**: Fluorotriorganosilyl-derivatized Tyr$^3$-octreotate was labeled with $^{18}F^-$ providing the first practical formulation in $^{18}F$-radiochemistry for the labeling of a peptide (see scheme). The very mild reaction conditions and the fast labeling make this strategy a valuable tool for the synthesis of $^{18}F$-radiopharmaceuticals.

## Radioactive Peptides

R. Schirrmacher,* G. Bradtmöller, E. Schirrmacher, O. Thews, J. Tillmanns, T. Siessmeier, H. G. Buchholz, P. Bartenstein, B. Wängler, C. M. Niemeyer, K. Jurkschat* — **6047 – 6050**

$^{18}F$-Labeling of Peptides by means of an Organosilicon-Based Fluoride Acceptor

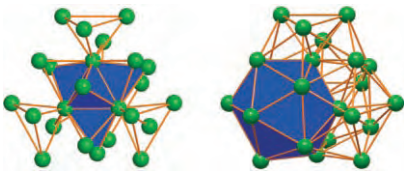

**A star is born**: The $Li_{26}$ cluster in the new intermetallic phase $Li_{13}Na_{29}Ba_{19}$ can be described on the basis of a tetrahedral star (left) or four interpenetrating centered icosahedra (right). The $M_{26}$ cluster is known from γ-brass and was predicted to be stable for Li in the gas phase. $Li_{13}Na_{29}Ba_{19}$ contains the first example of a homoatomic $M_{26}$ cluster in the solid state.

## Icosahedral Clusters

V. Smetana, V. Babizhetskyy, G. V. Vajenine, A. Simon* — **6051 – 6053**

$Li_{26}$ Clusters in the Compound $Li_{13}Na_{29}Ba_{19}$

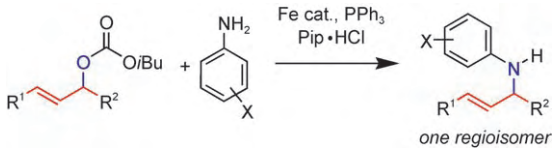


**Iron age**: An air- and water-resistant iron(−II) catalyst, in the presence of triphenylphosphane under buffered conditions, allows for the highly regioselective and stereoselective allylation of primary aromatic amines. A broad substrate range both in the aniline and in the allyl carbonate moiety is tolerated.

## Homogeneous Catalysis

B. Plietker* — **6053 – 6056**

Regioselective Iron-Catalyzed Allylic Amination


© 2006 Wiley-VCH Verlag GmbH & Co. KGaA, Weinheim

# Contents

WILEY InterScience®
DISCOVER SOMETHING GREAT

"**Hot Papers**" are chosen by the Editors for their importance in a rapidly evolving field of high current interest. A preview with the graphical abstracts of these articles can be found on the *Angewandte Chemie* homepage in Wiley InterScience at www.angewandte.org.

All articles in *Angewandte Chemie* are published online several weeks ahead of print. They are found under the "**EarlyView**" link on the journal's homepage in Wiley InterScience.

## Service

*Keywords* ——— *6058*

*Authors* ——— *6059*

*Preview* ——— *6061*

*For more information on Chemistry—An Asian Journal see www.chemasianj.org*


© 2006 Wiley-VCH Verlag GmbH & Co. KGaA, Weinheim

## Lipids and Lipidomics

Lipidomics? Who cares about lipids, except those who want to or have to undertake a diet? We know that lipids are not only body fuels, but are essentially involved in the maintenance and regulation of cell function. Alterations in lipid metabolism are associated with human diseases like atherosclerosis, cancer, diabetes, and neurodegenerative and infectious diseases. Despite the rapid advances in the biochemistry of lipids, fundamental questions about the role of lipids in health and disease remain unanswered. A eukaryotic cell contains more than 1000 different lipid species, many of them bilayer-forming lipids, which are differentially distributed within the membranes of a cell. We still do not know the detailed lipid composition of a certain organelle membrane, of its two bilayer leaflets, and their lateral organization within a leaflet. We do not really know how the local lipid concentration is regulated in time, and not too much about the identity of the interacting proteins.[1]. Owing to the importance of lipids for cell function, more and more attempts have been made towards the system-level analysis of lipids and their interacting partners ("lipidomics").[2] Within this area, the reader is referred to two websites: *Lipidbank*, which is primarily focused on the structure and properties of lipids, and *Lipidmaps*, which contains also information on genes and proteins involved in lipid metabolism and function. Several other internet resources about lipids and lipidomics are available, such as *The Lipid Library* by William W. Christie (www.lipidlibrary.co.uk), Al Merrill's *SphinGOMAP*, which contains metabolic maps of sphingolipid metabolism (www.sphingomap.org), or the website of the recently established *European Lipidomics Initiative* (www.lipidomics.net).

*Lipidbank* is a database initiated in 1996 by the International Medical Center of Japan and the Japan Science and Technology Corporation. It provides information on more than 6000 different lipid species, which are organized in 17 lipid groups and 28 lipid classes. Among the groups are fatty acids and their derivatives, including long-chain bases and ceramides. Other groups are fat-soluble vitamins, phospholipids, and glycolipids. On entering the name of the lipid, the user gets information about chemical and physical properties, metabolism, and biological activities (Figure 1). Structural formulas are given, which can be downloaded in ChemDraw format. Analytical data such as chromatographic behavior and spectral data (UV, IR, NMR, MS) can be retrieved. References are included, also older ones, but the information is not comprehensive. Database records can be found by keyword or structural feature searches, or by browsing the entries within the classification. The website can be recommended if one needs data about lipids or to get a quick overview on a certain lipid class.

*Lipidmaps* (Figure 2) is derived from "lipid metabolites and pathways strategy". It is the name of a consortium led by the University of California in San Diego and sponsored by the US National Institute of General Medicine. It was founded in 2003 with the aim to characterize lipid metabolites and to quantify changes in their level and localization within a cell. Initially, the lipid metabolites in one cell type are analyzed to identify networks of interactions amongst lipid metabolites and to make this information available to other researchers. The consortium selected macrophages from mice as the cell type to begin with, as mouse cells with specific genetic mutations are available and allow analysis of genetic defects on the levels of lipid molecular species. Macrophages play a central role in important physiological processes such as inflammation and immunity, and exert some of their actions through

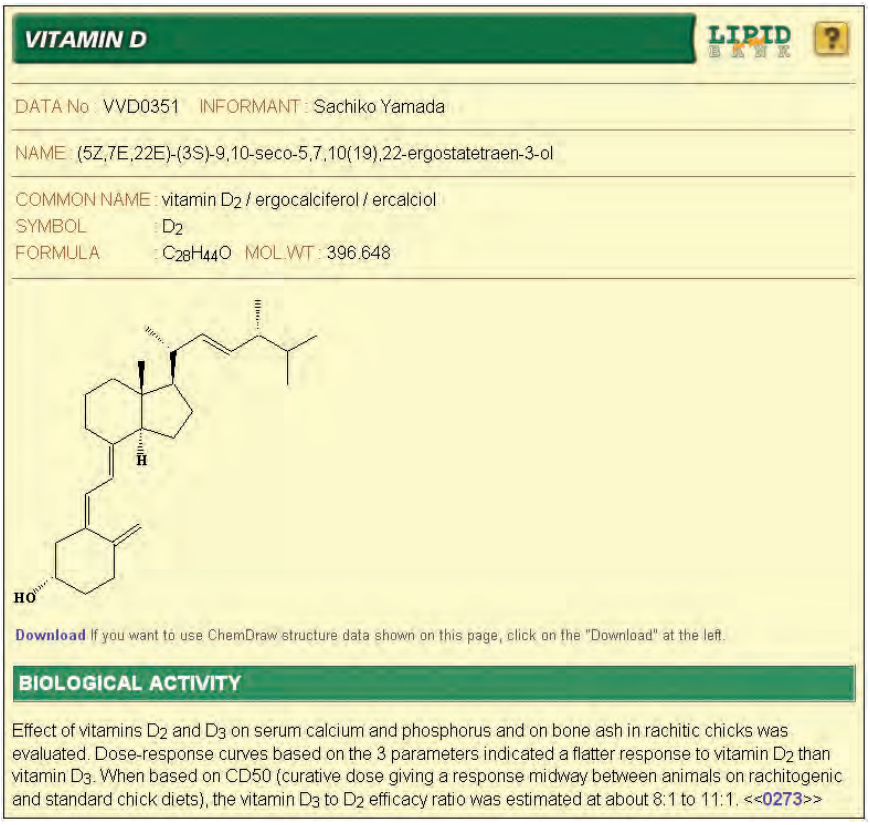


***Figure 1.*** Vitamin D2 entry in *Lipidbank* ...


WILEY InterScience DISCOVER SOMETHING GREAT
© 2006 Wiley-VCH Verlag GmbH & Co. KGaA, Weinheim

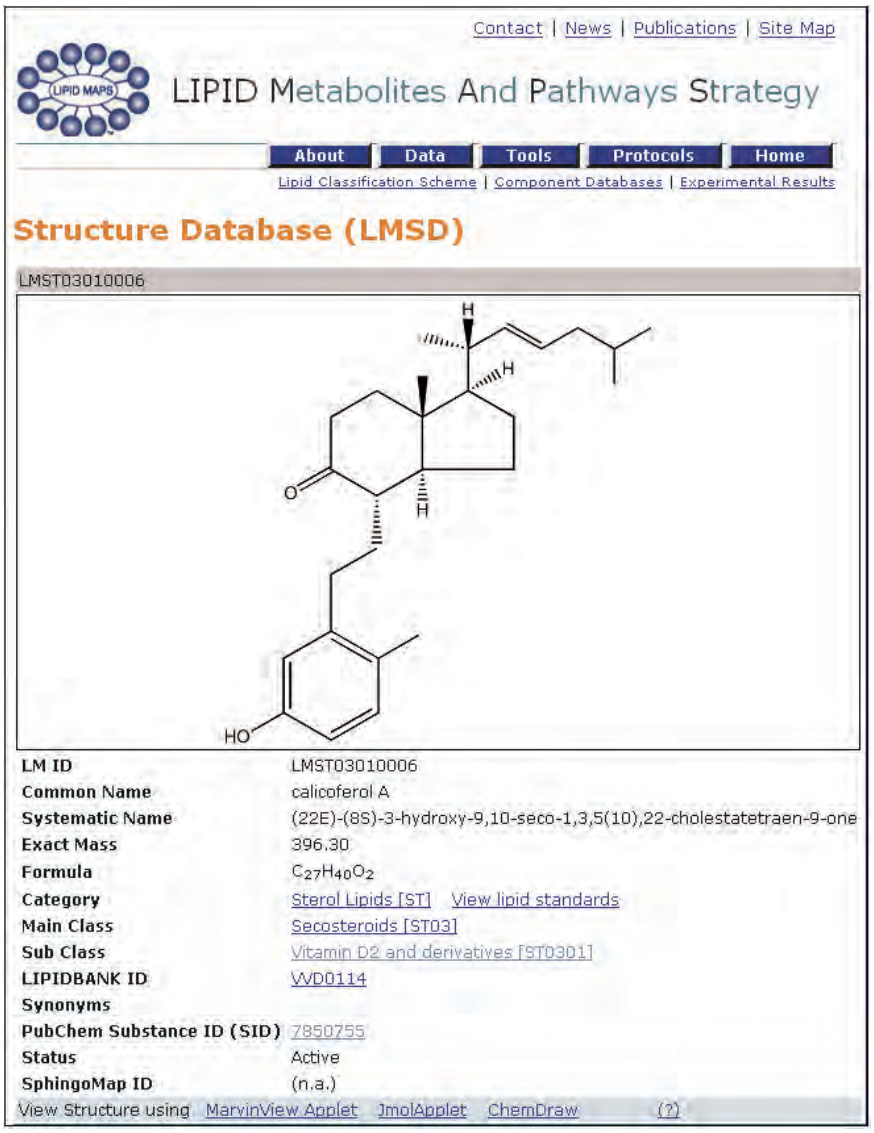


***Figure 2.*** ... and its derivative calicoferol A in *Lipidmaps*.

eicosanoid lipids. Protocols, standards, and tools with the focus on murine macrophages are available from the website.

Features of more general interest are a searchable lipid structure database of more than 7500 records, and a database of lipid-associated protein sequences with annotations from UniProt, EntrezGene, ENZYME, Gene Ontology, and KEGG.[3] Other useful utilities are mass spectrometry tools, information on commercially available lipid standards for mass spectrometry, and a drawing tool for lipid structures that allows the export of graphics in different formats. Of general importance is that *Lipidmaps* uses a recently suggested nomenclature and assignment system for lipids,[4] consisting of a 12-digit code for each molecular lipid species. It classifies lipids into eight categories: fatty acyls, glycerolipids, glycerophospholipids, sphingolipids, sterol lipids, prenol lipids, saccharolipids, and polyketides. This classification will facilitate lipid research in the coming years. *Lipidmaps* also uses a unified scheme for representing the chemical structures of individual lipids and their derivatives. This is a website recommended for the specialist who tries to determine lipid levels by mass spectrometry and for the scientist who has to collect information on a certain lipid. The website is far from being complete, but it promises to become a key resource in this part of metabolomics.

*Thomas Kolter*
Rheinische Friedrich-Wilhelms-Universität Bonn (Germany)

[1] G. van Meer, *EMBO J.* **2005**, *24*, 3159.
[2] M. R. Wenk, *Nat. Rev. Drug Discovery* **2005**, *4*, 594.
[3] D. Cotter, A. Maer, C. Guda, B. Saunders, S. Subramaniam, *Nucleic Acids Res.* **2006**, *34*, D507 – D510.
[4] E. Fahy, S. Subramaniam, H. A. Brown, C. K. Glass, A. H. Merrill, Jr., R. C. Murphy, C. R. Raetz, D. W. Russell, Y. Seyama, W. Shaw, T. Shimizu, F. Spener, G. van Meer, M. S. VanNieuwenhze, S. H. White, J. L. Witztum, E. A. Dennis, *J. Lipid Res.* **2005**, *46*, 839.

**DOI: 10.1002/anie.200603313**

**For more information, visit:**
www.lipidbank.jp
www.lipidmaps.org


© 2006 Wiley-VCH Verlag GmbH & Co. KGaA, Weinheim

Molecular Electronics

DOI: 10.1002/anie.200601787

# A New Dimension in Multinuclear Metallocene Complexes

*Matthias Wagner**

**Keywords:**
metallocenes · metal–metal interactions · molecular electronics · nanostructures · radialenes

From molecular electronics to homogeneous catalysis, multinuclear metallocene complexes have considerable potential.[1] For example, oligomeric ferrocene derivatives have found application as multielectron redox catalysts, electron-storage devices, and in the surface modification of electrodes.[2,3]

Among the large variety of possible structures, linear poly(ferrocenylenes) are here considered first since their development is currently the most advanced. The decisive synthetic breakthrough was realized with the ring-opening polymerization of strained [1]ferrocenophanes, which leads to the well-characterized and easily processible macromolecules **1** (Scheme 1).[4] Recently, boranediyl-bridged derivatives **2** were also prepared from 1,1′-bis(dibromoboryl)ferrocene by a novel condensation reaction (Scheme 1).[5] After appropriate substitution of the bromine atoms, the resulting materials display pronounced electronic communication between the iron centers, which is a result of efficient charge delocalization through the empty p orbitals of the boron atoms.

Maximization of electronic interaction along the main polymer chain is an important factor for the development of nanoscale wires for molecular electronics. In this respect, it is likely that poly(ferrocenylenes) **3** (Scheme 1) with directly connected cyclopentadienyl rings will display a number of promising properties. To date, attempts to synthesize polymers of type **3** have concentrated on the stepwise coupling of 1,1′-diiodoferrocene with 1,1′-dilithioferrocene·tmeda.[6] This approach, however, resulted primarily in oligomeric species with short chains. Furthermore, purification and characterization were not straightforward owing to poor solubility. More recently, these problems could partially be circumvented by introducing solubilizing alkyl substituents. Especially noteworthy are the methods for preparing poly(ferrocenylenes) $[-(C_5H_3R)Fe(C_5H_3R)-]_n$ by reaction of the di(hexyl)fulvalene dianion with $[FeCl_2(thf)_2]$ (R = hexyl)[7] and through the CuCl-mediated coupling of 1,1′-bis(tri-*n*-butylstannyl)-3,3′-bis(trimethylsilyl)ferrocene (R = $SiMe_3$).[8]

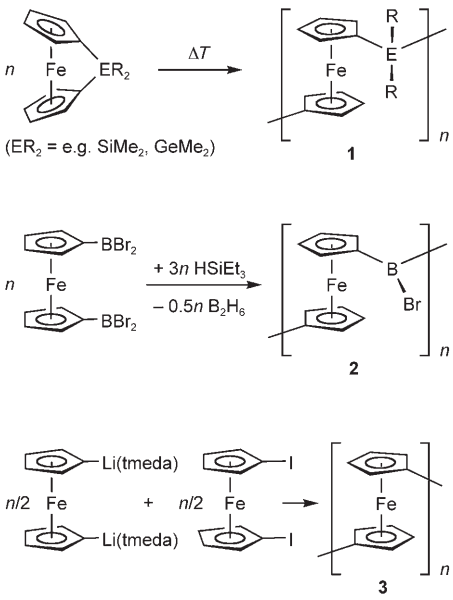


***Scheme 1.*** Synthetic strategies for poly(ferrocenylenes) **1**–**3**.

Going from one-dimensional polymers to two-dimensional, star-shaped or dendritic oligo(metallocene) structures remains a challenge, but at the same time bears great potential. For preparative reasons, the molecules which were first synthesized were those in which individual metallocene moieties were connected through saturated bridging units. Important early examples of such multinuclear two-dimensional metallocene aggregates include the tentacle complexes **4** and **5** (Figure 1). The synthesis of **4** makes use of the increased acidity of the methyl protons in $[(C_5H_5)Fe(C_6Me_6)]^+$ to introduce six ferrocenylbutyl residues in a sequence of nucleophilic substitution reactions with 4-ferrocenylbutyliodide.[9] The undecanuclear ferrocene species **5** can be synthesized from deca(allyl)ferrocene by tenfold hydrosilylation with dimethylsilylferrocene.[10] The cyclic voltammogram of **5** shows that the terminal ferrocenyl substituents are all oxidized simultaneously in a single ten-electron transition. The degree of any possible intramolecular electronic interaction permitted by the molecular scaffold is therefore quite small.

It would be desirable here, too, to replace the essentially isolating alkyl chains with alternative bridging units which could promote electronic communication between the separate redox-active moieties. Initial investigations in this area have already been undertaken, for example in the construction of star-shaped organometallic compounds in which a central tricarbonyl(cyclobutadiene)iron fragment is connected to $\{(C_4H_3)Fe(CO)_3\}$ (**6**, Figure 1) or

[*] Prof. Dr. M. Wagner
Institut für Anorganische Chemie
Johann Wolfgang Goethe-Universität
Frankfurt
Max-von-Laue-Strasse 7
60438 Frankfurt/Main (Germany)
Fax: (+49) 69-798-29260
E-mail: matthias.wagner@chemie.uni-frankfurt.de


InterScience
© 2006 Wiley-VCH Verlag GmbH & Co. KGaA, Weinheim

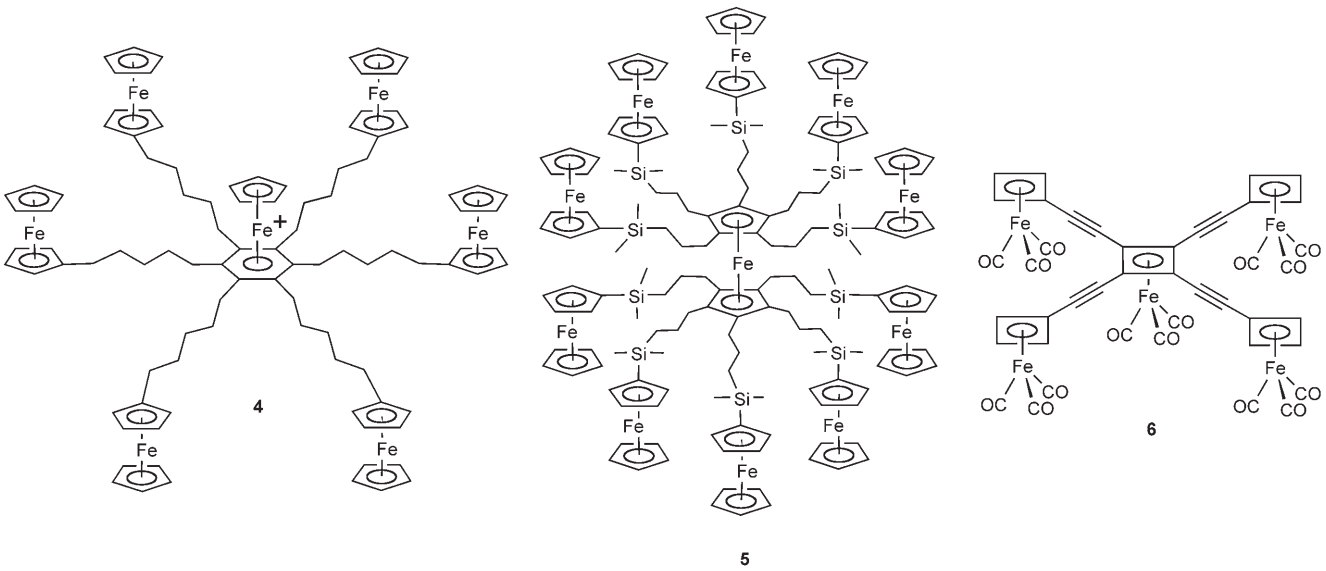


***Figure 1.*** Two-dimensional oligonuclear iron complexes **4**–**6**.

$\{(C_5H_4)Mn(CO)_3\}$ substituents through alkynediyl bridges.[11] The key step in this synthesis is the quadruple palladium-catalyzed Stille coupling of the corresponding organometallic stannylacetylenes with $[(C_4I_4)Fe(CO)_3]$.

As with linear poly(ferrocenylenes), optimal electronic properties can be expected for two-dimensional aggregates with directly connected metallocene fragments. Vollhardt and co-workers are now one large step closer to achieving this goal.[12] Using a Negishi coupling of $[(C_5I_5)Mn(CO)_3]$[13] and Zn-$[(C_5H_4)Mn(CO)_3]_2$ or $Zn[(C_5H_4)Fe(C_5H_5)]_2$, they were able to synthesize the radial oligocyclopentadienyl metal complexes **7** and **8** in good yield (Scheme 2).

In 1996, the same group reported the synthesis of the penta(cyclopentadienyl)cyclopentadienyl complex $[(C_5H_5)_5C_5Mn(CO)_3]$ and its deprotonation to the corresponding pentaanion $[(C_5H_4)_5C_5Mn(CO)_3]^{5-}$. This compound should then be able to act as a bridging ligand in a hexanuclear star-shaped metal complex.[14] Surprisingly, the permetallation of this compound has yet to be achieved, thus leaving the coupling reaction described above as the first viable route to compounds of type **7** and **8**.

Electrochemical investigation of the ferrocene derivative **8** resulted in three separate redox waves corresponding to a single one-electron transition and a pair

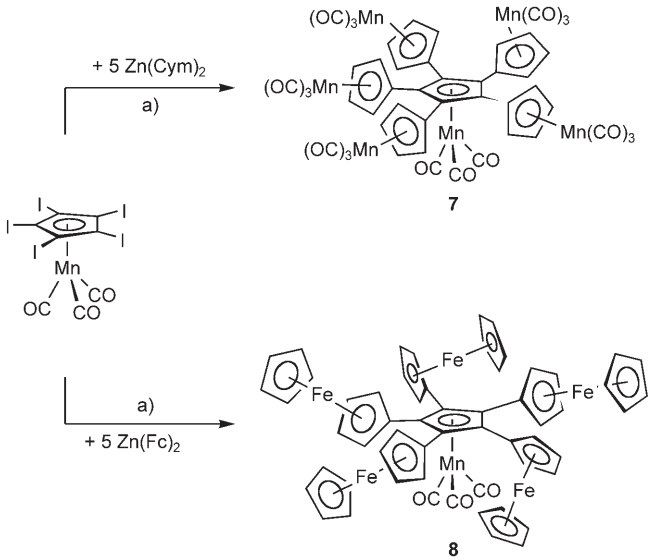


***Scheme 2.*** Synthesis of penta(cymantrenyl)cymantrene **7** and penta(ferrocenyl)cymantrene **8**. a) $[Pd_2(dba)_3]$ (25%), THF, 65°C, dba = dibenzylideneacetone; Cym = $(C_5H_4)Mn(CO)_3$, Fc = $(C_5H_4)Fe(C_5H_5)$.

of two-electron transitions. In contrast to **5** (Figure 1), the architecture of compound **8** apparently allows for considerable electronic interaction within the molecule. An increased degree of charge delocalization should be achievable by two routes: 1) formation of clusters by connecting six metal ions through direct metal–metal bonds in addition to the bridging $[(C_5H_4)_5C_5]^{6-}$ ligand or 2) intramolecular cross-linking of the cyclopentadienyl substituents, thus leading to inhibition of their freedom of rotation and an orientation parallel to the π-electron system of the central five-membered ring.

The known photolability of carbonyl complexes makes the hexamanganese complex **7** a promising starting material for cluster formation. In fact, photolysis of **7** in THF (450 W mercury lamp, $t$ = 130 s) and consequent liberation of one equivalent of carbon monoxide leads to a compound in which the central complex and three unchanged $\{(C_5H_4)Mn(CO)_3\}$ substituents remain

 © 2006 Wiley-VCH Verlag GmbH & Co. KGaA, Weinheim 

alongside a $\{(C_5H_4)(CO)_2Mn(\mu\text{-}CO)\text{-}Mn(CO)_2(C_5H_4)\}$ moiety with a Mn–Mn bond. Higher-order clusters have not yet been identified. First attempts at annealing cyclopentadienyl side groups were undertaken with ferrocene derivative **8**. Combination of **8** with aqueous *p*-toluene sulfonic acid resulted in the expulsion of a $\{(C_5H_5)Fe\}$ unit and formation of a C–C bond between the free cyclopentadienyl group and a neighboring ferrocenyl substituent (**9**, Figure 2). Under oxidative-coupling conditions after addition of $Cu^{II}$ trifluoromethylsulfonate to **8**, two $\{(C_5H_5)Fe\}$ fragments are eliminated and two C–C bonds are formed. One of these bonds forms in the desired fashion, whereas the other involves the $C_5H_5$ ring of one of the remaining ferrocenyl substituents (**10**, Figure 2).

Vollhardt's system can be significantly expanded by decomplexation of the central cyclopentadienyl ring in **8**, which can be achieved by irradiation of the complex in THF to give free penta(ferrocenyl)cyclopentadiene. The addition of 100 equivalents of 1-heptyne is essential for the success of this decomplexation, although the exact role of the alkyne in the reaction is not yet clear. Considering the fact that cyclopentadienides are among the most important ligands in organometallic chemistry, the accessibility of a derivative which is extremely sterically hindered while at the same time displays properties that can be influenced electrochemically opens fascinating possibilities.

The work of Vollhardt and co-workers discussed here represents an important advancement in the area of organometallic materials since it overcomes the hurdles that have constrained related research to linearly bound poly(metallocenes) and provides a route to the synthesis of two-dimensional structures. Apart from the elegant synthesis, it is important to note that even sterically overloaded penta(cyclopentadienyl)cyclopentadienyl complexes still adopt molecular conformations which allow for pronounced electronic interaction between connected metal centers. We can thus continue to look forward to interesting developments in the field of organometallic nanostructures.

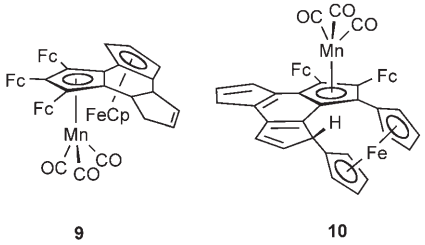


9 10

***Figure 2.*** Reaction products of **8** after addition of *p*-toluene sulfonic acid (**9**) or $Cu^{II}$ trifluoromethylsulfonate (**10**).

Note added in proof: Recently, Vollhardt and co-workers succeeded in the synthesis of the long-sought-after hexaferrocenylbenzene by sixfold Negishi-type ferrocenylation of hexabromo- or hexaiodoferrocene.[15]

Published online: August 14, 2006

[1] *Metallocenes: Synthesis, Reactivity, Applications* (Eds.: A. Togni, R. L. Halterman), Wiley-VCH, Weinheim, **2006**.

[2] D. Astruc, *Electron Transfer and Radical Processes in Transition-Metal Chemistry*, Wiley-VCH, Weinheim, **1995**.

[3] D. Astruc, *Acc. Chem. Res.* **1997**, *30*, 383–391.

[4] I. Manners, *Adv. Organomet. Chem.* **1995**, *37*, 131–168.

[5] J. B. Heilmann, M. Scheibitz, Y. Qin, A. Sundararaman, F. Jäkle, T. Kretz, M. Bolte, H.-W. Lerner, M. C. Holthausen, M. Wagner, *Angew. Chem.* **2006**, *118*, 934–939; *Angew. Chem. Int. Ed.* **2006**, *45*, 920–925.

[6] E. W. Neuse, L. Bednarik, *Macromolecules* **1979**, *12*, 187–195.

[7] T. Hirao, M. Kurashina, K. Aramaki, H. Nishihara, *J. Chem. Soc. Dalton Trans.* **1996**, 2929–2933.

[8] P. Park, A. J. Lough, D. A. Foucher, *Macromolecules* **2002**, *35*, 3810–3818.

[9] J.-L. Fillaut, J. Linares, D. Astruc, *Angew. Chem.* **1994**, *106*, 2540–2542; *Angew. Chem. Int. Ed. Engl.* **1994**, *33*, 2460–2462.

[10] P. Jutzi, C. Batz, B. Neumann, H.-G. Stammler, *Angew. Chem.* **1996**, *108*, 2272–2274; *Angew. Chem. Int. Ed. Engl.* **1996**, *35*, 2118–2121.

[11] U. H. F. Bunz, V. Enkelmann, *Organometallics* **1994**, *13*, 3823–3833.

[12] Y. Yu, A. D. Bond, P. W. Leonard, K. P. C. Vollhardt, G. D. Whitener, *Angew. Chem.* **2006**, *118*, 1826–1831; *Angew. Chem. Int. Ed.* **2006**, *45*, 1794–1799.

[13] U. H. F. Bunz, V. Enkelmann, J. Räder, *Organometallics* **1993**, *12*, 4745–4747.

[14] R. Boese, G. Bräunlich, J.-P. Gotteland, J.-T. Hwang, C. Troll, K. P. C. Vollhardt, *Angew. Chem.* **1996**, *108*, 1100–1102; *Angew. Chem. Int. Ed. Engl.* **1996**, *35*, 995–998.

[15] Y. Yu, A. D. Bond, P. W. Leonard, U. J. Lorenz, T. V. Timofeeva, K. P. C. Vollhardt, G. D. Whitener, A. A. Yakovenko, *Chem. Commun.* **2006**, 2572–2574.

 © 2006 Wiley-VCH Verlag GmbH & Co. KGaA, Weinheim 

Lantibiotic Biosynthesis

DOI: 10.1002/anie.200601850

# Enzyme-Catalyzed Sulfide Ring Formation in Lantibiotics

*Günther Jung**

**Keywords:**
biosynthesis · cyclization · enzyme catalysis · metalloenzymes · zinc

Polycyclic peptide antibiotics that contain thioether amino acids, such as lanthionine, are called lantibiotics.[1] In contrast to most other peptide antibiotics, lantibiotics are synthesized ribosomally and modified post-translationally by enzymes. Biologically active polypeptides may contain several sulfide bridges, as well as other modified residues, for example, 2,3-didehydroamino acids.[2] Previous studies showed that lantibiotic biosynthesis proceeds through precursors on which a variety of enzymes act to modify the polypeptides at specific serine, threonine, and cysteine residues.[3–6] On the basis of these studies, gene technology (e.g. site-directed mutagenesis) has allowed the construction and elaboration of various lantibiotic analogues. For example, many analogues of epidermin (a highly active drug against acne) and nisin (an important food preservative) have already been engineered.[7–9]

Type A lantibiotics such as epidermin and nisin are elongated amphiphiles that act on Gram-positive bacteria by binding to the cell wall precursor lipid II, which simultaneously enables the formation of a target-specific, ion-permeable, transmembrane pore as well as the inhibition of bacterial cell wall biosynthesis.[10,11] On the other hand, type B lantibiotics are compact globular polypeptides with highly constrained sulfide rings and they interfere with specific enzyme functions.[12]

In 1988, the first structural gene of a lantibiotic was discovered and the main principles of the biosynthesis of lantibiotics through post-translational modifications of precursor proteins were outlined using the example of epidermin.[1] Studies of the biosynthetic gene cluster of nisin followed in 1989 (see Refs. [3,4,12]).

A further highlight in lantibiotic research was the first isolation, sequencing, and mass spectrometric characterization of the different biosynthetic intermediate prepeptides of the lantibiotic Pep5.[13] The precursor pre-Pep5 was sixfold dehydrated at four threonine and two serine residues. Completely unmodified pre-Pep5 as well as pre-Pep5 with three sulfide rings and two α,β-didehydroamino acids were also isolated.

Recently, the crystal structure of the metalloenzyme NisC was solved by X-ray diffraction.[14] This cyclase catalyzes the formation of several sulfide bridges in the dehydrated 57 amino acid containing precursor protein NisA of the lantibiotic nisin (Figure 1). The characterization of the dehydrated nisin precursor protein by van der Donk and co-workers[14] confirmed earlier findings about this intermediate of lantibiotic biosynthesis by Kuipers et al.[15]

During the last 15 years of lantibiotic research, most of the biosynthetic puzzles have been unraveled for epidermin, Pep5, and nisin, among others. For example, both the icosapeptide epidermin and mersacidin have an additional unusual modification, namely an enzymatic oxidative decarboxylation of the C-terminal cysteine, which takes place one step prior to the enzymatic sulfide ring formation. The yellow oxidizing flavoenzyme EpiD[16] was the first of all the enzymes involved in lantibiotic biosynthesis to be expressed and isolated in pure form. EpiD has been tested extensively in vitro for specificity with peptidylcysteine libraries using HPLC-MS.[17] Interestingly, EpiD oxidizes even short dipeptidylcysteines, allowing the preparation of peptides that carry unusually amidated C termini and rings with *S*-(2-aminovinyl)-cysteines which were previously inaccessible by synthesis. Furthermore, this special area of lantibiotic research has led to the discovery of related flavoenzymes for which the X-ray crystal structure and in vitro activities have been determined.[18,19]

In 1991, it was written in the outlook of a review on lantibiotics:[2] "*We still do not know how the stereospecific addition of the cysteinyl SH groups to the double bonds of the α,β-didehydroamino acids is catalyzed.*" Since then, several groups of peptide chemists have shown that biomimetic thioether cyclizations can be carried out to give lanthionines with the correct stereochemistry from synthetic peptides containing α,β-didehydroamino acids and cysteines.[12,20] Thus, non-enzymatic spontaneous cyclizations have been reported to be involved in the natural steps of lantibiotic biosynthesis.

In their recent report on the structure and mechanism of lantibiotic cyclase involved in nisin biosynthesis, van der Donk and co-workers[14] gave a detailed description of an enzymatic cyclization catalyzed by NisC. First, the enzyme catalyzes the formation of *all* five sulfide rings of nisin, even though

[*] Prof. Dr. G. Jung
Institute of Organic Chemistry
University of Tübingen
Auf der Morgenstelle 18
72075 Tübingen (Germany)
Fax: (+49) 7071-29-5560
E-mail: guenther.jung@uni-tuebingen.de


© 2006 Wiley-VCH Verlag GmbH & Co. KGaA, Weinheim

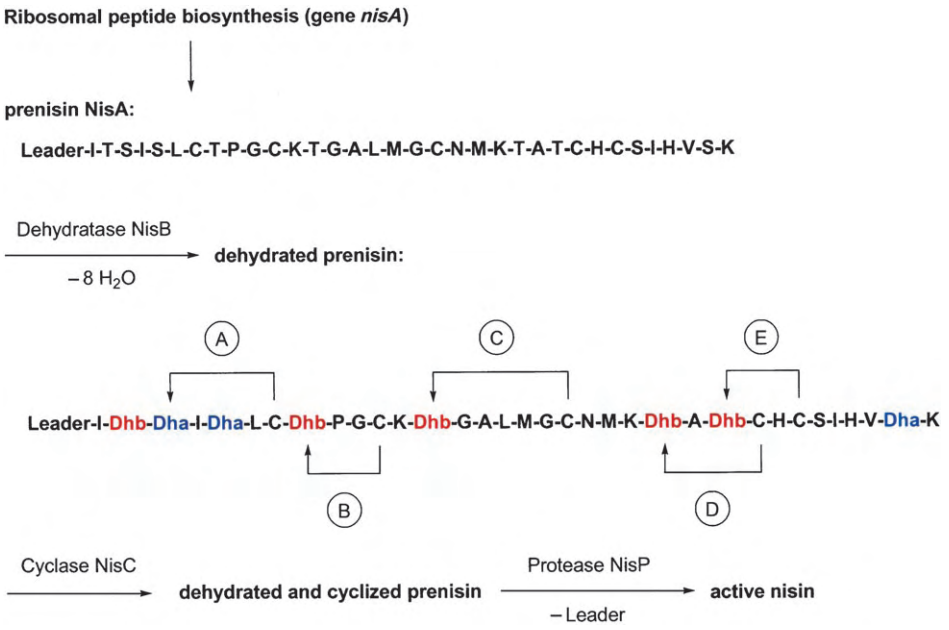


***Figure 1.*** Biosynthesis of nisin: Sequence of prenisin (NisA) and the dehydrated prepeptide of nisin (Dha = 2,3-didehydroalanine, Dhb = 2,3-didehydrobutyrine) illustrating the formation of thioether rings A to E catalyzed by cyclase NisC. After ring formation, the leader peptide (MSTKDFNLDLVSVSKKDSGASPR) is cleaved by processing peptidase NisP to yield the active lantibiotic nisin.

they differ in ring sizes and electrophiles (2,3-didehydroalanine (Dha) or 2,3-didehydrobutyrine (Dhb)). This observation is particularly remarkable in view of the in vitro cyclization process of dehydrated prenisin demonstrated therein.[14] It was confirmed that the leader peptide of NisA is required for substrate recognition of the dehydrated prenisin by NisC. The first experimental evidence for the involvement of such LanC proteins for the control of cyclizations was given by Sahl and co-workers with the Pep5 biosynthetic system in 1995.[21] Pronounced effects of leader peptide mutations on the biosynthesis of lantibiotic Pep5 were reported later.[22] Similar experiments followed using NisC. Interestingly, SpaC, the lantibiotic cyclase of subtilin, also produced nisin from dehydrated prenisin, thus further proving the independence of the dehydration and cyclization steps for type A lantibiotics (in contrast to type B lantibiotics; see below).

The crystal structure of the zinc enzyme NisC shows a protein composed of a total of 14 α helices, of which seven form the inner layer of a toroid structure (α/α barrel). The zinc ion is located in the center of the toroid and is tetrahedrally coordinated by two cysteines, one histidine, and a molecule of water (Figure 2).[14]

Similarities of NisC to farnesyl transferase and other zinc proteins that catalyze thiol alkylations were discussed. However, the enzymes referred to by van der Donk and co-workers therein[23] differ topologically from the α/α-barrel folds of NisC and other enzymes that they discussed themselves.[14] (For clarification, see the Review by Wendt and Schulz.[24]) The authors also pointed to the interesting homology of LanC-like proteins in mammals which have 20–25 % sequence identity, conserved Zn ligands, an active-site base, and extended domains. These proteins are suggested to catalyze a post-translational cysteine modification of a currently unknown protein.

To act as a cyclizing catalyst at neutral pH values, NisC must deprotonate the cysteine thiol group to accelerate nucleophilic addition of the activated thiolate to the α,β-unsaturated amino acids. Interestingly, an enolate intermediate is formed during the cyclizing *anti* addition of the cysteine thiolate

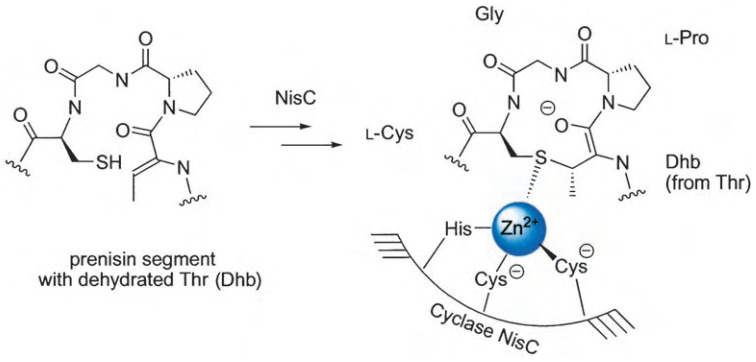


***Figure 2.*** Formation of thioether ring B from prenisin segments Thr-Pro-Gly-Cys of NisA (see Figure 1) through the substrate dehydrated prenisin while the sulfur atom of L-cysteine ((*R*)-cysteine) is still coordinated to $Zn^{2+}$ complexed by His331, Cys330, and Cys284 residues of the cyclase NisC (hydrogen atoms are omitted). Adapted from Reference [14].

 © 2006 Wiley-VCH Verlag GmbH & Co. KGaA, Weinheim 

to the β-carbon atom of Dha or *Z*-Dhb (Figure 2). This enolate is protonated at the α-carbon atom, resulting in an inversed configuration of the α-carbon atom of the original L-threonine residue, whereas the original L-cysteine residue maintains its *R* configuration within the formed (2*S*,3*S*,6*R*)-β-methyllanthionine (MeLan).[25]

Besides regio- and stereoselectivity of sulfide ring formation, LanC enzymes are also responsible for the directionality of ring formation, which is always N-terminal to C-terminal for type A lantibiotics (that is, C-terminal cysteine adds to N-terminal dehydroamino acids Dha or Dhb). However, some sulfide bridges in type B lantibiotics are formed from N-terminal cysteine to C-terminal dehydroamino acids. As shown experimentally and discussed by van der Donk and co-workers, the major difference between the two directionalities of ring formation is due to the generation of an endocyclic (type A) or exocyclic enolate (type B).[12,14] Furthermore, LanC enzymes are also responsible for similar rates of natural cyclization of lanthionines compared to those of β-methyllanthionines, which were shown to differ by several orders of magnitude in biomimetic chemical model studies.[20]

Large bifunctional enzymes LanM of unknown structure are involved in the dehydration and cyclization processes of compact globular lantibiotics type B. LanM enzymes differ from the LanB and LanC enzymes for biosynthesis of type A lantibiotics (see Ref. [12]). These single enzymes require adenosine triphosphate (ATP) and $Mg^{2+}$, and they display no homology to LanB dehydratase and 20–27% sequence identity to LanC proteins.

The proposed mechanism for NisC (Figure 2) is not based on the crystal structure of a substrate–enzyme complex but instead is derived from a docking experiment using the 13-membered B ring of nisin composed of Pro9, Gly10, and MeLan, which together form a β turn according to NMR spectroscopic analysis. Nevertheless, the modeling study provides a first hint for the mechanism of cyclization to yield sulfide rings containing between four (ring B) and seven amino acids in the shallow substrate cavity of NisC. The positively charged leader peptide of dehydrated prenisin seems to be bound to a specific negatively charged binding groove of NisC. However, the specific role of the leader peptide remains to be shown in more detail as well as the order of ring formation in the biosynthesis of nisin. As the prepeptides of lantibiotics and their derivatives are readily accessible by chemical peptide synthesis,[26] a chemical and biochemical research study could answer this question and open new strategies for the production of cyclic peptides that have been difficult to synthesize or even inaccessible until now. Research on lantibiotics remains a challenging field for discoveries in biosynthetic mechanisms and continues to attract chemists and biochemists as well as microbiologists and protein engineers.

Published online: August 17, 2006


[1] N. Schnell, K.-D. Entian, U. Schneider, F. Götz, H. Zähner, R. Kellner, G. Jung, *Nature*, **1988**, *333*, 276–278.

[2] G. Jung, *Angew. Chem.* **1991**, *103*, 1067–1084; *Angew. Chem. Int. Ed. Engl.* **1991**, *30*, 1051–1068.

[3] *Nisin and Novel Lantibiotics* (Eds.: G. Jung, H.-G. Sahl), Escom, Leiden, **1991**.

[4] R. W. Jack, G. Bierbaum, H.-G. Sahl, *Lantibiotics and Related Peptides*, Springer, Berlin, **1998**.

[5] R. Jack, F. Götz, G. Jung in *Lantibiotics, Vol. 7* (Eds.: H.-J. Rehm, G. Reed), VCH, Weinheim, **1997**, chap. 8, pp. 323–368.

[6] R. W. Jack, G. Jung, *Curr. Opin. Chem. Biol.* **2000**, *4*, 310–317.

[7] G. Bierbaum, C. Szekat, M. Josten, C. Heidrich, C. Kempter, G. Jung, H.-G. Sahl, *Appl. Environ. Microbiol.* **1996**, *62*, 385–392.

[8] B. Ottenwälder, T. Kupke, S. Brecht, V. Gnau, J. Metzger, G. Jung, F. Götz, *Appl. Environ. Microbiol.* **1995**, *61*, 3894–3903.

[9] O. P. Kuipers, G. Bierbaum, B. Ottenwälder, H. M. Dodd, N. Horn, J. Metzger, T. Kupke, V. Gnau, R. Bongers, P. van den Bogaard, K. Kosters, H. S. Rollema, W. M. de Vos, R. J. Siezen, G. Jung, F. Götz, H.-G. Sahl, M. J. Gasson, A. van Leeuwenhoek, *J. Microbiol.* **1996**, *69*, 161–170.

[10] H. Brötz, M. Josten, I. Wiedemann, U. Schneider, F. Götz, G. Bierbaum, H.-G. Sahl, *Mol. Microbiol.* **1998**, *30*, 317–327.

[11] E. Breukink, I. Wiedemann, C. van Kraaij, O. P. Kuipers, H.-G. Sahl, B. de Kruijff, *Science* **1999**, *286*, 2361–2364.

[12] For a comprehensive review on lantibiotics covering the recent literature on genetics, biosynthesis, structure, and mode of action, see: C. Chatterjee, M. Paul, L. Xie, W. A. van der Donk, *Chem. Rev.* **2005**, *105*, 633–683.

[13] H.-P. Weil, A. G. Beck-Sickinger, J. Metzger, S. Stevanovic, G. Jung, M. Josten, H.-G. Sahl, *Eur. J. Biochem.* **1990**, *194*, 217–223.

[14] B. Li, J. P. J. Yu, J. S. Brunzelle, G. N. Moll, W. A. van der Donk, S. K. Nair, *Science* **2006**, *311*, 1464–1467.

[15] A. Kuipers, E. de Boef, R. Rink, S. Fekken, L. D. Kluskens, A. J. M. Driessen, K. Leenhouts, O. P. Kuipers, G. N. Moll, *J. Biol. Chem.* **2004**, *279*, 22176–22182.

[16] T. Kupke, C. Kempter, G. Jung, F. Götz, *J. Biol. Chem.* **1995**, *270*, 11282–11289.

[17] C. Kempter, T. Kupke, D. Kaiser, J. W. Metzger, G. Jung, *Angew. Chem.* **1996**, *108*, 2235–2238; *Angew. Chem. Int. Ed. Engl.* **1996**, *35*, 2104–2107.

[18] P. Hernández-Acosta, D. G. Schmid, G. Jung, F. A. Culiánez-Macià, T. Kupke, *J. Biol. Chem.* **2002**, *277*, 20490–20498.

[19] T. Kupke, M. Uebele, D. Schmid, G. Jung, M. Blaessel, S. Steinbacher, *J. Biol. Chem.* **2000**, *275*, 31838–31846.

[20] Y. Zhu, M. D. Gieselman, H. Zhou, O. Averin, W. A. van der Donk, *Org. Biomol. Chem.*, **2003**, *1*, 3304–3315.

[21] S. Neis, G. Bierbaum, M. Josten, C. Kempter, G. Jung, H.-G. Sahl, *FEMS Lett.* **1997**, *149*, 249–255.

[22] C. Meyer, G. Bierbaum, C. Heidrich, M. Reis, J. Süling, M. I. Iglesias-Wind, C. Kempter, E. Molitor, H.-G. Sahl, *Eur. J. Biochem.* **1995**, *232*, 478–489.

[23] See Ref. [14] and Refs. [16] and [17] cited therein.

[24] K. U. Wendt, G. E. Schulz, *Structure*, **1998**, *6*, 127–133.

[25] Note: The authors used the confusing conventional D assignment to the original L-cysteine ((*R*)-cysteine) moiety of MeLan in Ref. [14] (Figure 4 therein).

[26] A. G. Beck-Sickinger, G. Jung in *Nisin and Novel Lantibiotics* (Eds.: G. Jung, H.-G. Sahl), Escom, Leiden, **1991**, pp. 218–230.


 © 2006 Wiley-VCH Verlag GmbH & Co. KGaA, Weinheim 

Mesoporous Materials

DOI: 10.1002/anie.200600734

# The Supramolecular Chemistry of Organic–Inorganic Hybrid Materials

*Ana B. Descalzo, Ramón Martínez-Máñez,* Félix Sancenón, Katrin Hoffmann, and Knut Rurack**

**Keywords:**
aggregation · mesoporous materials · molecular recognition · nanoparticles · sensors

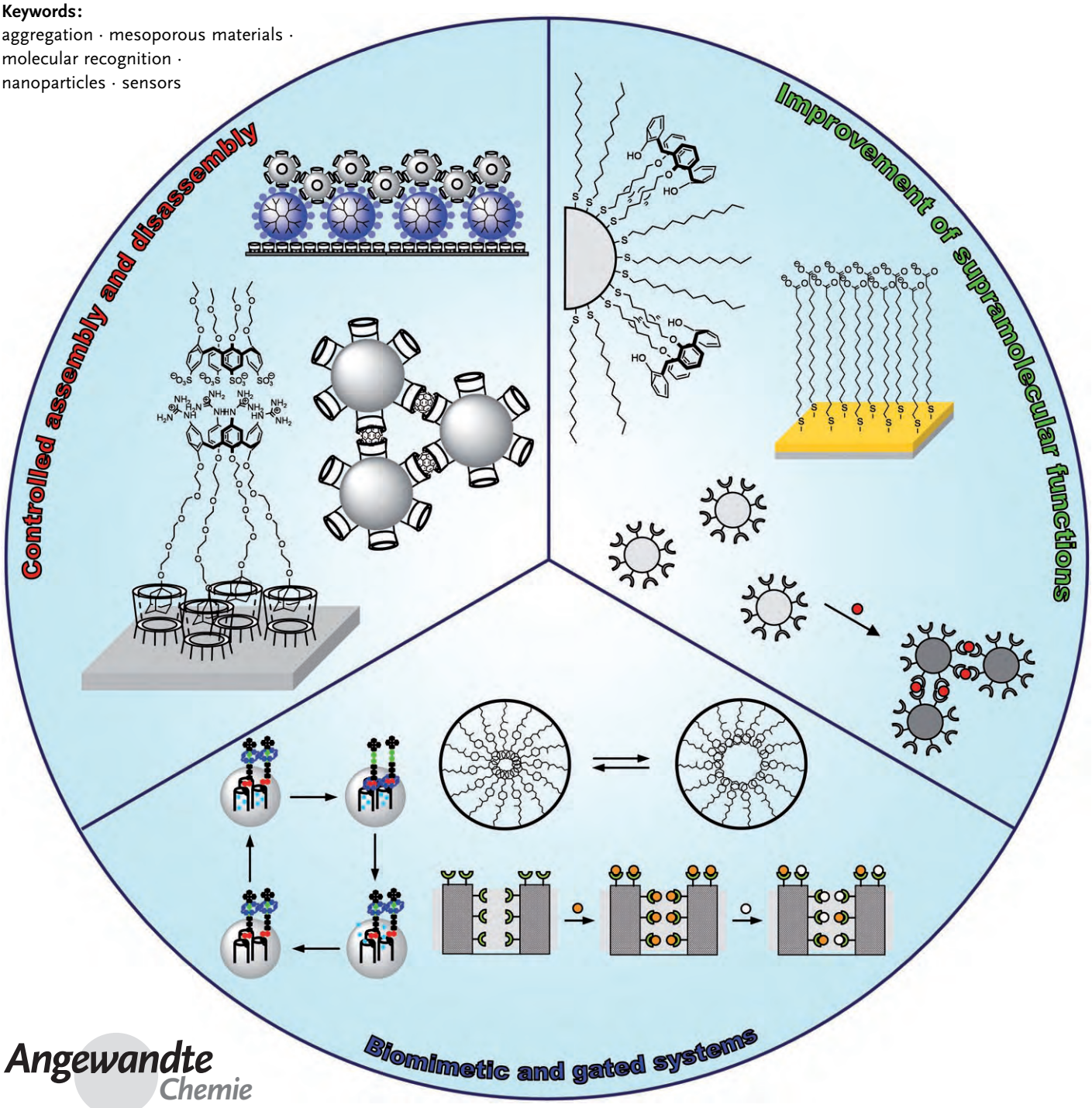




© 2006 Wiley-VCH Verlag GmbH & Co. KGaA, Weinheim

*The combination of nanomaterials as solid supports and supramolecular concepts has led to the development of hybrid materials with improved functionalities. These "hetero-supramolecular" ideas provide a means of bridging the gap between molecular chemistry, materials sciences, and nanotechnology. In recent years, relevant examples have been reported on functional aspects, such as enhanced recognition and sensing by using molecules on preorganized surfaces, the reversible building of nanometer-sized networks and 3D architectures, as well as biomimetic and gated chemistry in hybrid nanomaterials for the development of advanced functional protocols in three-dimensional frameworks. This approach allows the fine-tuning of the properties of nanomaterials and offers new perspectives for the application of supramolecular concepts.*

**From the Contents**

1. Introduction—Fusing Supramolecular Chemistry and Nanotechnology 5925
2. Improvement of Supramolecular Functions by Preorganization on Surfaces 5926
3. Controlled Assembly and Disassembly 5932
4. Biomimetic and Gated Supramolecular Chemistry in Hybrid Nanomaterials 5937
5. Conclusions and Outlook 5945

## 1. Introduction—Fusing Supramolecular Chemistry and Nanotechnology

Chemistry began when man started to use and transform natural inorganic and organic materials such as rock, wood, and pigments for specific purposes. Since then, the development of new materials from atoms or molecules has strongly influenced our life. Very recently, two major research areas have transformed our vision of the chemistry of molecules as well as materials sciences: supramolecular chemistry was established in the 1980s and is concerned with the study of the interaction between molecules, and nanotechnology emerged in the 1990s and involves the research and development of technology at the nanometer level (1–100 nm).[1]

In many respects, supramolecular chemistry still largely utilizes molecular organic components, so that it has traditionally had little connection with the chemical concepts of—mainly inorganic—nanoscopic solids. However different these two chemistries might seem, their combination at the nanoscopic level was anticipated in two keynote reports. In 1959 Richard P. Feynman's classic lecture on the "top-down" approach included the famous sentence "*there is plenty of room at the bottom*",[2] while more recently Jean-Marie Lehn gave the imaginative reply that "*there is even more room at the top*", when refering to the "bottom-up" approach.[3,4]

Successful supramolecular systems based on molecular architectures have to date been synthesized mainly by the successive formation of covalent bonds.[5] Alternative routes for the generation of supramolecular structures utilize the self-assembly of (supra)molecular components.[6] Besides the design of completely organic superstructures for various purposes,[5] recent years have witnessed the development of larger networks from metal–organic frameworks[7] and coordination polymers[8] derived from inorganic and organic building blocks.

An alternative route to generate organized hybrid systems, for example, inorganic–organic supramolecular ensembles for special applications, is to use inorganic solids with preorganized nanostructures and attach, arrange, or assemble functional molecules of different complexity on the inner and/or outer surface of the inorganic scaffold. Recent examples suggest that the combination of supramolecular principles and such solid structures leads to materials with variable properties and opens up new perspectives for the application of supramolecular concepts. There are excellent reviews on both nanostructures[9] and supramolecular chemistry.[10] There are also recent reports of functional hybrid materials which mainly emphasize the synthetic procedures and applications in catalysis or physisorption but also review the physical properties.[11] Moreover, there is a subdiscipline within hybrid materials chemistry that deals with the interaction of nanoparticles and bio(macro)molecules[12] as well as the biomimetic approaches in nanotechnology.[13]

In contrast to many of these publications, the majority of which deal with the hybrid materials themselves, we describe the supramolecular functions of hybrid scaffolds. This is an area that we find particularly intriguing, but reports are scattered throughout the literature.[14] Thus, this Review will

[*] Dr. A. B. Descalzo,[+] Prof. R. Martínez-Máñez, Dr. F. Sancenón
Instituto de Química Molecular Aplicada
Departamento de Química
Universidad Politécnica de Valencia
Camino de Vera s/n, 46071 Valencia (Spain)
Fax: (+34) 96-387-9349
E-mail: rmaez@qim.upv.es
Dr. K. Hoffmann, Dr. K. Rurack
Div. I.5
Bundesanstalt für Materialforschung und -prüfung (BAM)
Richard-Willstätter-Strasse 11, 12489 Berlin (Germany)
Fax: (+49) 30-8104-5005
E-mail: knut.rurack@bam.de
[+] present address:
Div. I.5
Bundesanstalt für Materialforschung und -prüfung (BAM)
Richard-Willstätter-Strasse 11, 12489 Berlin (Germany)

 © 2006 Wiley-VCH Verlag GmbH & Co. KGaA, Weinheim 

not describe synthetic details of hybrid systems or review the simple interaction of molecules with those materials. Instead, it will highlight new functional chemical properties and new approaches that improve on the already existing concepts. It is the appearance of synergistic effects that are hardly achievable in molecular-based systems or in nanoscopic solids alone that makes these "hetero-supramolecular" functionalities so unique. We have classified the functional aspects according to the complexity and dimensionality.

## 2. Improvement of Supramolecular Functions by Preorganization on Surfaces

Functional two-dimensional hybrid systems are based on the attachment of a larger number of a single or several different chemical units on the surface of nanoparticles or nanostructured solids. Traditionally, the functionalization of surfaces was used to modulate adhesion characteristics or to improve the dispersion of particles in liquids. From a supramolecular chemistry viewpoint, however, the functionalization of nanostructured solids with specific groups to enhance active functions, such as the recognition of guests or to switch surface properties, is particularly interesting. Such materials with a high and readily accessible specific surface can amplify certain functional chemical processes. The amplification processes can be principally divided into two classes. One class commonly shows an enhancement of classical recognition features as a consequence of entropic factors associated with the restriction of movement and the proximity of molecular entities on the surface. The second class, often more advanced, does not necessarily recognize a guest much better, but usually provides an amplified output signal that arises from collective phenomena between the preorganized functional units. The step from a one-dimensional molecule to a two-dimensional arrangement—the hetero-supramolecular ensemble—leads to unique properties which are not simply an extrapolation of the solution conduct to the surface.

### 2.1. Enhancement of Molecular Recognition by Preorganization

The enhancement of recognition through the influence of the surface has been reported mainly for gold nanoparticles (AuNPs) that carry suitable ligands that are generally linked to the surface through an alkane-1-thiol spacer. The simplest systems contain a mixture of "active" and "passive" chemical groups, depending on the synthetic strategies employed.

*Ramón Martínez-Máñez received his degree in chemistry from the University of Valencia in 1986 and completed his PhD in organometallic chemistry under the supervision of Professor P. Lahuerta in 1990. After a postdoctoral stay at Cambridge (UK) to conduct research in redox-active helicands with E. C. Constable, he moved back to the Polytechnic University of Valencia where he became professor of Inorganic Chemistry in 2002. His research interests cover supramolecular chemistry and hybrid materials, particularly of redox-active and photoresponsive receptors for guest recognition.*

*Félix Sancenón graduated in chemistry in Valencia in 1991 and carried out research at the University of Valencia and later at the Polytechnic University of Valencia where he was working in the field of colorimetric chemosensors with Professor R. Martínez-Máñez. He received a PhD in 2003, and in 2004 received a Marie Curie grant to join Professor L. Fabbrizzi at the University of Pavia, where he worked on ditopic receptors. In 2005 he moved back to the Polytechnic University of Valencia on a Ramón y Cajal contract. His research interest is focused on supramolecular applications of chemosensors.*

*Katrin Hoffmann studied chemistry at the Humboldt University Berlin and completed her PhD on ordered porous solids as hosts for functional optical materials at the Technical University Berlin. After research at the Academy of Sciences of the GDR (1980–1991), the Federal Institute for Materials Research and Testing (BAM), and the Institute for Applied Chemistry Berlin-Adlershof (1992–1997), she moved to Div. I.3 at BAM. Since 2006, she has been a research scientist in Div. I.5 "Bioanalytics" at BAM. Her current research is focused on fluorescence spectroscopy and microscopy.*

*Knut Rurack studied chemistry/food chemistry at Kiel and Münster Universities and obtained his "Staatsexamen" at CVUA (Chemisches Landes- und Staatliches Veterinäruntersuchungsamt) Münster. From 1993 to 1998, he worked with Siegfried Dähne at the BAM laboratory for time-resolved spectroscopy and with Wolfgang Rettig at the Humboldt University, Berlin, where he completed his PhD in 1999. He returned to Div. I.3 "Structural Analysis" at BAM in 1999 and moved to Div. I.5 "Bioanalytics" in 2006. His research interests encompass functional dyes and optical materials, supramolecular chemistry, and optical spectroscopy.*

*Ana B. Descalzo studied chemistry at the University of Valencia. She then joined the group of Professor R. Martínez-Máñez at the Polytechnic University of Valencia, where she obtained her PhD in 2004, working in the field of optical chemosensors and silica-based hybrid materials. Currently, she is an Alexander-von-Humboldt postdoctoral fellow with Knut Rurack at Div. I.5 "Bioanalytics" of BAM. Her research interests are centered around fluorescent near-infrared dyes and chemosensors.*


© 2006 Wiley-VCH Verlag GmbH & Co. KGaA, Weinheim

These procedures are often adapted from the Brust–Schiffrin method,[15] in which simple "passive" dodecanethiol residues in a monolayer protecting the AuNPs are partly or fully replaced in a controlled way with the "active" unit. This approach allows a discrete number of receptors to be arranged on the surface of the NPs. Typical functionalized AuNPs consist of 200–300 gold atoms covered with 70–90 alkanethiolate chains, have a core diameter of about 2 nm, and a surface area of approximately 20 $nm^2$.[16] Besides the target-directed selection of the organic ligands employed, another prerequisite for such hetero-supramolecular chemistry lies with signal expression. AuNPs display size- and shape-dependent plasmon absorption bands. Furthermore, the aggregation of NPs in solution can generate further color changes because of the mutual induction of dipoles which varies with the aggregate size and interparticle distance.[17]

Before describing some representative examples of such functionalized nanoparticles, we will briefly introduce the underlying principle of recognition enhancement through preorganization by the simple case of a self-assembled monolayer (SAM) of ligands on a "flat" substrate (Figure 1).[18] Major and Zhu reported the enhancement of the complexation constant for the binding of $Cu^{2+}$ ions to carboxylic acid functions over bidentate or monodentate carboxylates in aqueous solution when using SAMs of 16-mercaptohexadecanoic acid on gold surfaces.[19] The authors interpret the results in terms of a statistical advantage of the multidentate coordination environment that arises from the preorganized ligands on the surface (surface chelate effect). Dicarboxylates are known to bind metal cations stronger than can monocarboxylates because the second chelating site operates initially in a unimolecular reaction. A dense, two-dimensional array of ligands on the surface leads to an even higher statistical probability of the complexation of $Cu^{2+}$ ions. This effect is manifested in binding constants that are more than two orders of magnitude higher for the hybrid material than the corresponding free carboxylate ligands. Similar effects have been reported for completely organic scaffolds such as coordinating dendrimers, where a "positive dendritic effect" is ascribed to the ability of dendrimers to achieve a better recognition of target guests as the generation of the dendrimer increases.[20]

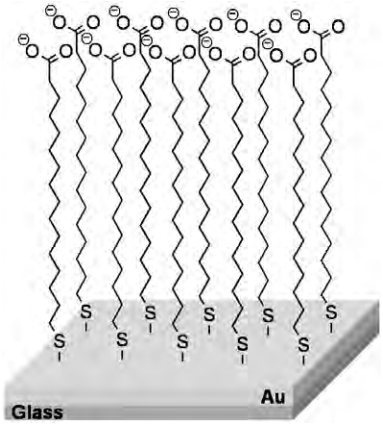


***Figure 1.*** SAM of 15-mercaptohexadecanoate on gold.

Recent representative examples of hybrid frameworks that involve the use of gold nanoparticles cofunctionalized with simple as well as guest-responsive alkanethiols have been reported mainly for anion sensing. Astruc and co-workers described the electrochemical sensing of anions (Figure 2) by amidoferrocenyl moieties attached in various amounts to AuNPs through simple alkanethiols[21] or dendritic structures.[22] The simpler systems were several thousand times more sensitive than amidoferrocenylalkanethiol monomers or trimers for the detection of tetraalkylammonium salts of $H_2PO_4^-$ and $HSO_4^-$.[23] Moreover, anion-induced hydrogen bonding, electrostatic interactions, and topological changes in the periphery of the alkanethiol–gold nanoparticles in dichloromethane led to two- or fivefold displacements of the reversible oxidation wave of the ferrocene groups with respect to the modulations observed for the tri- and monomeric molecular analogues, respectively.[21] Interestingly, in these materials up to 38 amidoferrocenyl units bound on a AuNP respond collectively on the electrochemical time scale and show only a single redox wave in the cyclic voltammogram (see Section 2.2.2).

The research groups of Beer and Pochini increased the sensitivity for anion, organic cation, and ion-pair detection by

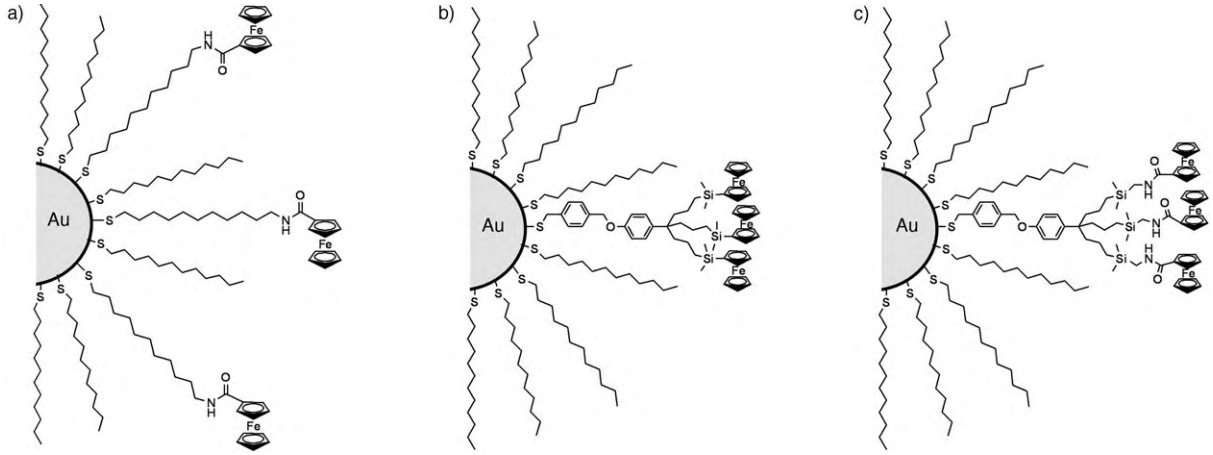


***Figure 2.*** AuNPs containing redox-active ferrocenyl units.


© 2006 Wiley-VCH Verlag GmbH & Co. KGaA, Weinheim

assembling metalloporphyrins[24] or calix[4]arenes[25,26] (Figure 3) on the surface of AuNPs. In both cases, preorganization of the binding sites resulted in a significant enhancement of guest coordination at the surface of the nanoparticle

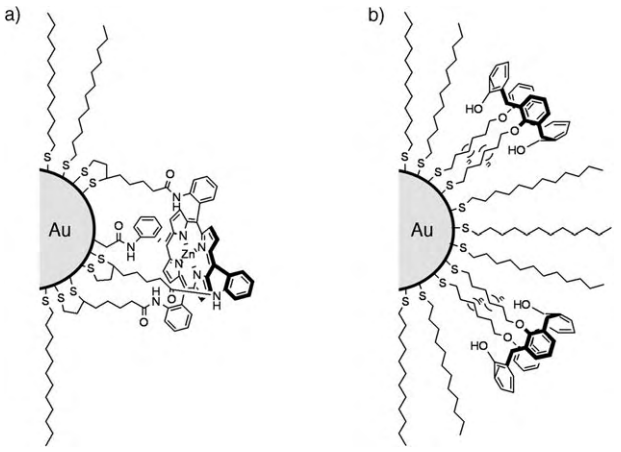


***Figure 3.*** AuNPs functionalized with metalloporphyrin (a) and calix[4]arene groups (b).

relative to the free receptor in solution. The preorganization of the receptors on the surface reduced their conformational flexibility (entropic contributions) and increased their effective concentration at the surface, thus creating a dominantly hydrophobic SAM-like environment in the boundary layer at the surface that leads to the drastically improved recognition characteristics.

The chemical amplification of the coordination can be deduced from the binding constants of the functionalized hybrid systems and the respective molecular-based model receptors. Studies in DMSO revealed that the surface-confined porphyrin-functionalized nanoparticles (Figure 3a) bind chloride ions ($\log K = 4.3$) two orders of magnitude more strongly than the free zinc porphyrin ($\log K < 2$). A similar effect was also found for $H_2PO_4^-$ ($\log K = 4.1$ versus 2.5) even in aqueous solvent mixtures.

In the second example, the calix[4]arene-modified AuNPs were funtionalized with alkanethiol chains of two different lengths (six or eleven carbon atoms), and two sets of nanoparticles with different amounts of appended calixarene were prepared (Figure 3b). The 1,3-dialkoxycalixarenes were used for the formation of inclusion complexes with quaternary ammonium cations. Pochini and co-workers found from $^1$H NMR titrations in $CDCl_3$ that these host structures showed stronger binding than the free calixarene in solution and that the efficiency of binding was enhanced as the number of calixarene units on the gold nanoparticle increased. Interestingly, an increase in the length of the spacer between the particle surface and the calix[4]arene also led to dramatically enhanced recognition in a solvent of medium polarity such as chloroform. This is an interesting case of radial coordination amplification that appears to be an exclusive feature of nanoparticles. Pochini and co-workers also demonstrated that certain molecular-recognition properties of the molecular host, such as a counterion effect, are preserved in the hybrid superstructures. Recently, modification of the ligands led to systems that were able to recognize cationic pyridinium moieties even in an aqueous environment.[26]

Improved coordination has also been reported for other nanostructured supports such as mesoporous silica functionalized with a single type of chemosensor molecule for the fluorogenic sensing of anions.[37] The strategy followed by Martínez-Máñez and co-workers involved the grafting of alkyl aminoanthracene groups onto MCM-41 as shown in Figure 4. The solid contains a secondary amino group as the

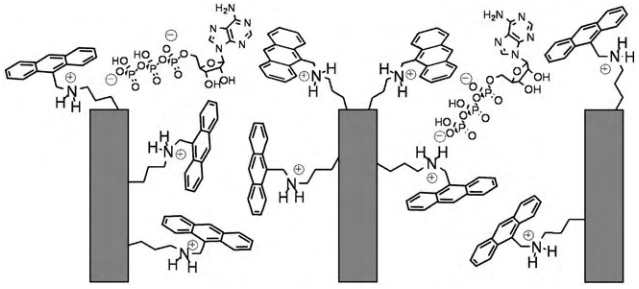

***Figure 4.*** Mesoporous MCM-41 materials functionalized with protonated aminoanthracene units for enhanced recognition of ATP (schematic).

anion coordinating site in the linear spacer and an anthracene unit fused to the remote end for both signaling and provision of additional π-stacking interactions with the target anion ATP. The addition of ATP to acidic aqueous suspensions of the solid resulted in remarkable fluorescence quenching; the association constants for anion–host interactions were two orders of magnitude larger than those obtained for a similar molecular-based system in solution. The enhanced response of the mesoporous solid to ATP reveals a cooperative effect related to an effective enhancement of the concentration because of the regular mesoporosity of the MCM-41 solid.

The influence of the density of the reporter molecules on the fluorometric detection, which is prone to autoinduced modulations, could also be demonstrated with this system. An increase in the number of alkyl aminoanthracene units on the MCM-41—and thus a reduction in the mean distance between two anthracenes (from 33 or 23 to 10 nm)—leads to the appearance of a significant amount of excimer fluorescence generated from an excited anthracene and a neighboring one in the ground state, even in the absence of an analyte.[27b,28,29]

A similar, amplified response toward $H_2PO_4^-$ ion, as noted by Astruc and co-workers, has been reported by Paolucci and Prato for single-walled carbon nanotubes functionalized with amidoferrocenyl receptor/reporter groups by using voltammetric detection (Figure 5).[30] Solutions of the ferrocene-functionalized carbon nanotubes in dichloromethane displayed a single anodic peak centered at 760 mV for the oxidation of the ferrocenyl groups. Addition of $H_2PO_4^-$ ions, to these solutions resulted in the appearance of a new oxidation peak at 530 mV as a result of hydrogen-bonding interactions between the anion and the amido groups conjugated to the ferrocene unit. The presence of a large number of amidoferrocenyl groups on the surface of the

 © 2006 Wiley-VCH Verlag GmbH & Co. KGaA, Weinheim 

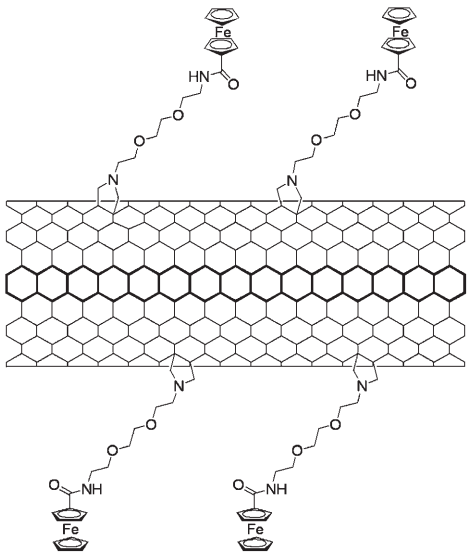


***Figure 5.*** Ferrocene-functionalized single-walled carbon nanotubes for electrochemical sensing of $H_2PO_4^-$ ions (schematic).

nanotube accounts for the larger shift in the oxidation potential (230 mV) obtained upon capture of the anions, which is comparable to the guest-induced modulations observed for the gold nanoparticle ensembles.

A nice example of the use of functionalized surfaces employs gold nanoparticles with di(acylamino)pyridine hydrogen-bonding moieties and pyrene aromatic stacking elements linked through linear alkanethiol spacers.[31] In this hybrid material the chemical detection of flavins is facilitated by the synergistic effects of multiple noncovalent interactions—hydrogen bonding and $\pi$ stacking. The association constant $K$ of the colloid in Figure 6a with flavin ($K = 323\,M^{-1}$) is distinctly higher than that observed for the system in Figure 6b ($K = 196\,M^{-1}$) where only hydrogen-bonding interactions can occur.[32] Boal and Rotello later found that the multitopic binding of flavin also has a strong radial dependence.[33] Hybrid systems with shorter spacers between the receptor units and the nanoparticle bind flavin stronger than longer chain counterparts. For example, recognition was enhanced threefold when the pyrene and pyridine units were located closer to the nanoparticle surface. Boal and Rotello attributed this radial coordination amplification to increased organization in the short-chain systems. Interestingly, this effect is reversed upon reduction of flavin. Nanoparticles with longer spacers bind flavin approximately seven times stronger because of unfavorable dipolar interactions between the electron-rich aromatic units and the anionic flavin.

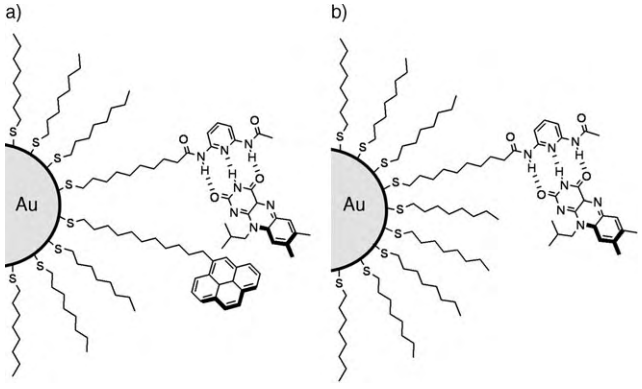


***Figure 6.*** AuNPs containing linear alkanethiol spacers and diacyldiaminopyridine hydrogen-bonding moieties. The pyrene units in (a) enhance flavin recognition through arene–$\pi$ stacking.

### 2.2. Improved Signaling by Preorganization

Supramolecular sensors are based on the transmission of a recognition event to a measurable signal. Signaling of the presence of analytes can be accomplished in a number of ways, but is commonly based on a change in color, fluorescence, or a redox potential. A number of chemosensors based on this concept have been reported for anionic,[34] cationic,[35] and neutral species.[36] In molecular chemosensors, the signaling process usually comprises two steps: 1) selective coordination of the guest by a binding site and 2) transduction of that event by modulation of a photophysical or electrochemical process within the probe. One of the key tasks in this field is to seek out new and effective chemical sensors that show enhanced performance with respect to selectivity and sensitivity, for example, by signal amplification and a reduction in the detection limit.

For a hybrid system consisting of an inorganic nanoparticle and one or more organic functional groups at the surface, signal expression can principally contain a contribution from the support material (for example, the plasmon band of AuNPs) as well as a contribution from the attached units (for example, the characteristic absorption of an appended porphyrin chromophore).[24] The possibility to independently influence a single signal or both signals offers a multitude of possibilities for the design of advanced signaling systems.[37]

This section is thus divided into two parts. The first deals with the effect of a recognition event on the signaling properties, specifically the optical properties, of the inorganic core. The second part gives an overview of signal amplification that arises from the preorganization of the reporter units on the surface.

#### 2.2.1. Signal Induction by Aggregation

Although two types of inorganic nanoparticles with distinct optical properties—gold nanoparticles and semiconductor nanocrystals or quantum dots (QDs)[38]—have received ever-increasing attention in the last few years, only gold nanoparticles have been employed to a significant degree in supramolecular inorganic–organic hybrid materials to date. Quantum dots have found wide-spread application as "passive" labels in imaging, diagnostics, and bioanalytics,[39] but examples of functional ensembles in the sense discussed in this Review are very rare.[40]

The unique sensing protocol discussed in this section is almost exclusively applicable to metal nanoparticles. It is

 © 2006 Wiley-VCH Verlag GmbH & Co. KGaA, Weinheim 

based on the ability of functionalized nanoparticles (for example, AuNPs) to show strong optical changes upon guest-induced aggregation processes (Figure 7). The color change observed upon aggregation is due to a coupling of the dipoles

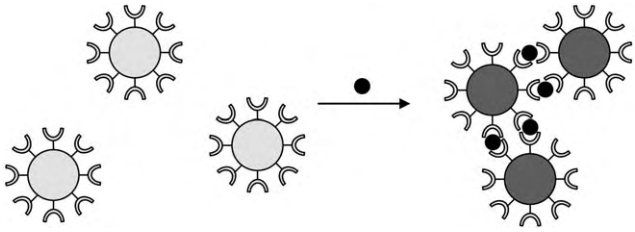

***Figure 7.*** Aggregation of AuNPs induced by coordination.

which results in a significant red-shift of the plasmon band when the interparticle distances in the aggregates decrease to less than the average particle radius. The concomitant decrease in the extinction coefficient observed, for example, upon DNA-induced aggregation of AuNPs (in colorimetric DNA analysis) is attributed to a screening of the nanoparticles embedded deeply within the aggregate interior.[41,42]

The color change based on analyte-induced aggregation/deaggregation protocols has been used for the colorimetric sensing of metal ions and anions. A simple colorimetric technique based on this principle for the detection of low concentrations of heavy metal ions ($Pb^{2+}$, $Cd^{2+}$, $Hg^{2+}$) in aqueous solution has been reported by Hupp and co-workers.[43] The ensemble in this case consists of AuNPs functionalized with alkanethiol chains carrying carboxylate functions at the distal terminal end. Aggregation of the particles upon addition of metal ions leads to both a shift in the plasmon band and a substantial increase in long-wavelength Rayleigh scattering, as evidenced by a color change from red to blue. The selectivity of this early example was rather low and alternative strategies were developed to improve the metal-ion recognition. One such strategy was developed as a sensitive colorimetric biosensor for $Pb^{2+}$ ions and takes advantage of the catalytic DNA ("DNAzyme") directed assembly of DNA-functionalized gold nanoparticles.[44] In the presence of $Pb^{2+}$ ions, the DNAzyme cleaves the substrate strand that ensured aggregation of the DNA–AuNPs and the ensuing deaggregation is indicated by a color change from blue to red.

Other representative examples describe the detection of poorly coordinating metal cations such a $Li^+$[45] or $K^+$[46] in water. Murphy and co-workers functionalized 4-nm gold particles with 1,10-phenanthroline for the detection of $Li^+$ ions. The anchored ligand binds selectively to $Li^+$ ions through formation of a ligand–metal (2:1) species which causes the gold nanoparticles to aggregate and results in a concomitant color shift. Chen and co-workers reported an efficient recognition of $K^+$ ions by colloidal gold nanoparticles functionalized with [15]crown-5 in aqueous solution through formation of 2:1 sandwich-type complexes; again a color change from red to blue was observed (Figure 8). Interestingly, interference from $Na^+$ ions is avoided as this cation does not induce any aggregation. Very recently, these authors improved their system by co-attaching 1,2-dithiolane-3-pentanoic acid (thioctic acid) and alkanethiol-appended [15]crown-5 (for sensing $K^+$ ions) or [12]crown-4 (for targeting $Na^+$ ions) onto AuNPs.[47] The difunctionalized hybrid material shows a rate constant for $K^+$ complexation that is four orders of magnitude faster than that of the crown ether material of reference [46]. Only if the spacer lengths of both receptor types are matched with one another will the introduction of the carboxylate functions greatly enhance the binding of the cation through cooperative electrostatic forces.[47] Both materials were also successfully employed for the detection of $K^+$ and $Na^+$ ions in urine samples.

Aggregation-amplified colorimetric sensing with gold nanoparticles has also been realized for anions. In a recent example by Watanabe et al. the sensory properties of amide-functionalized gold nanoparticles in the presence of anions such as $H_2PO_4^-$, $HSO_4^-$, $AcO^-$, $NO_3^-$, $Cl^-$, $Br^-$, and $I^-$ in $CH_2Cl_2$ were investigated by monitoring the changes in the UV/Vis spectra (Figure 9).[48] The addition of certain anions caused dramatic changes in the plasmon band (red-shift and intensity decrease), while control tests with hexanethiolate-protected gold nanoparticles which lacked the amide ligand did not show a significant change. The marked decrease in the absorption arose from anion-induced aggregation through formation of a hydrogen bond between the anions and the amide ligands on the particles. The surface-modified gold nanoparticles resulted in a decrease in the detection limit of anions by about three orders of magnitude over that of the

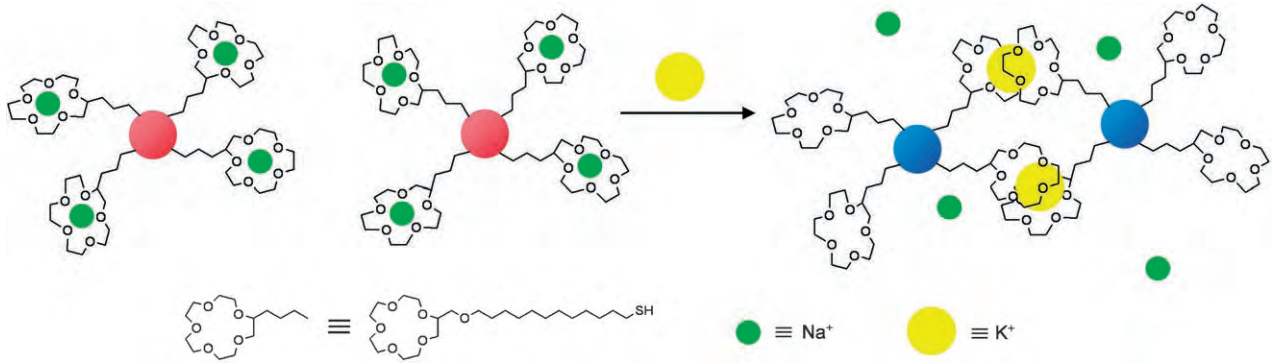


***Figure 8.*** Potassium-induced aggregation of AuNPs modified with crown ether/thiol groups through formation of sandwich complexes.

 © 2006 Wiley-VCH Verlag GmbH & Co. KGaA, Weinheim 

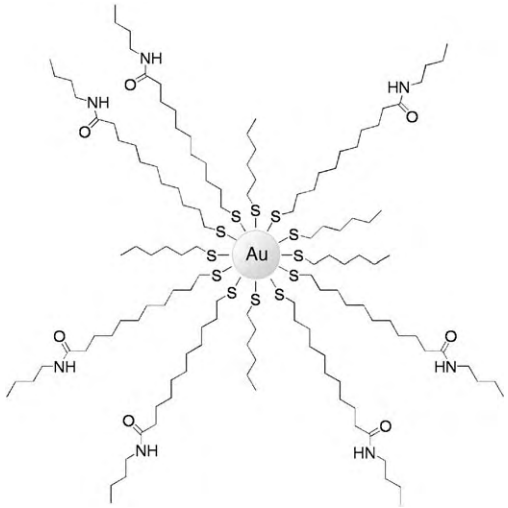


***Figure 9.*** Amide-functionalized AuNPs.

free receptor. In a similar example, Kubo et al. used (isothiouronium)alkanethiol-capped AuNPs to selectively detect micromolar concentrations of acetate and $HPO_4^{2-}$ in aqueous methanol.[49]

One of the very few examples of analyte-induced aggregation of hybrid nanoparticles not containing gold is the specific case of functionalized CdS quantum dots.[50] Chen and Rosenzweig synthesized several QDs modified with different organic groups and found in part very different behaviors. One such system fits nicely into the series of examples discussed here. Capping the CdS QDs with L-cysteine generated a hybrid material that selectively responds to the presence of $Zn^{2+}$ ions with a twofold increase in the luminescence; common strongly competing metal ions such as $Cu^{2+}$, $Ca^{2+}$, and $Mg^{2+}$ had no effect. Since the system was studied in neutral buffer solution, the formation of a passivating $Zn(OH)_2$ layer around the CdS particles is not responsible for the increase in emission; microfluorometry showed that the formation of QD clusters in the presence of $Zn^{2+}$ ions is the cause.

Two further QD systems are described in this section where the optical properties of the inorganic core are changed through recognition of an analyte, without any particle aggregation being involved. Besides the L-cysteine-modified QDs described above, Chen and Rosenzweig also tested thioglycerol-capped QDs as metal-ion sensors.[50] It was found that these quantum dots showed a strong quenching and a red-shift of their emission band upon addition of $Cu^{2+}$ ions in water. This time, $Zn^{2+}$ and other metal ions did not cause any modulation of the optical signal. The authors interpreted these findings in terms of an electron transfer from thioglycerol to the $Cu^{2+}$ ions. Reduction of $Cu^{2+}$ to $Cu^{+}$ results in the formation of $CdS^{+}$–$Cu^{+}$ species on the surface of the QDs which have a lower energy level than pure CdS QDs.[51]

In the second example, Gattás-Asfura and Leblanc studied the effect of metal ions on CdS QDs coated with thioglycolic acid and 2-mercaptoethylamine in aqueous solution.[52] They found that the luminescence of the first type of QDs was quenched to different extents by $Cu^{2+}$, $Ni^{2+}$, $Fe^{3+}$, and $Ag^{+}$, while all the other metal ions ($K^{+}$, $Mg^{2+}$, $Ca^{2+}$, $Co^{2+}$, $Zn^{2+}$, $Cd^{2+}$) enhanced the emission intensity. The 2-mercaptoethylamine-capped QDs, on the other hand, showed emission quenching in the presence of all the metal ions except for $Zn^{2+}$. To improve the performance of the system, the authors coated the CdS QDs with a custom-designed pentapeptide. This system demonstrated the desired high selectivity toward $Cu^{2+}$ and $Ag^{+}$ in the presence of other biologically important metal ions. The studies further revealed that complexation of only one of the surface peptides was required to quench the luminescence significantly, thus showing clear features of signal amplification.

#### 2.2.2. *Signal Amplification by Preorganization of Surface + nFunctionalities*

A first elegant example of a remarkable signaling enhancement by preorganization of organic fluorophores on an inorganic support has been described by Montalti et al. for silica nanoparticles covered with covalently linked dansyl moieties (Figure 10).[53] Protonation of some of the dansyl groups resulted in a dramatic quenching of the fluorescence of

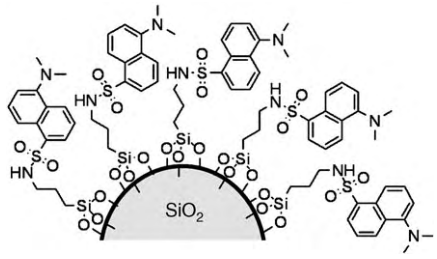


***Figure 10.*** Silica nanoparticles functionalized with dansyl groups.

both the protonated units and the surrounding unprotonated ones. As the signal modulation involves a larger number of units than those actually protonated, the chemical input is translated into an amplified fluorescence response. This collective effect has also been observed for the dansylated nanoparticles upon addition of metal ions such as $Cu^{2+}$, $Co^{2+}$, and $Ni^{2+}$ that commonly quench the emission of organic fluorophores.[54] Montalti et al. estimated that a single $Cu^{2+}$ ion caused a fluorescence decrease which corresponds to the total quenching of 13 dansyl moieties. Communication between photoactive units is thus not restricted only to functionalized dendrimers,[55] but is also highly efficient in nanoparticles. Whereas the quenching between the paramagnetic ions and the excited dye most probably proceeds through electronic energy transfer to a low-lying metal-centered state,[56] the efficient interchromophoric mechanisms leading to the collective quenching can have several causes that result from the design and composition of the system.[57]

Besides functionalization with one type of chemical group that can act at the same time as a binding and reporting unit, another approach of sensory amplification exists that takes advantage of cooperative effects associated with the independent anchoring of binding sites and signaling groups in proximity to the surface of a support. This close arrangement allows intercommunication between both subunits without the need for a direct covalent chemical link between them, as shown schematically for a difunctionalized fluorogenic sensor

 © 2006 Wiley-VCH Verlag GmbH & Co. KGaA, Weinheim 

in Figure 11. Coordination of a guest by the receptor induces energy or electron transfer to the fluorophore which results in fluorescence quenching. The organization of the ligands on the surface and the ligand-to-fluorophore ratio permits the

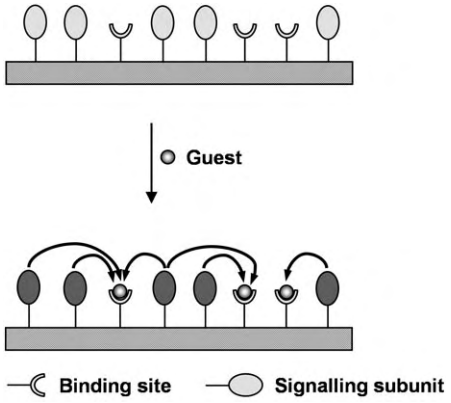


***Figure 11.*** A difunctionalized surface ensures the required spatial proximity for communication between the binding sites and signaling subunits. The black arrows denote quenching induced by the guest.

performance of a system to be tuned. An excess of reporter units around a few binding sites should equip a system with the ability to show signal amplification similar to that described above for the dansyl groups on silica NPs. On the other hand, an approximate 1:1 ratio between the two types of units should generate an ensemble with a larger dynamic sensing range; in this case the signal expression would be more comparable with analogous molecular systems in solution. Grafting the receptor and the dye subunits to the surface of the nanoparticles does not only ensure communication between the two components, but can also induce cooperative processes in the binding of the substrate. This is an attractive approach where such a preorganization on the surface may avoid tedious synthetic routes to obtain complicated receptors and makes it possible to achieve the desired selectivity by using combinatorial approaches and commercially available or simple small molecules.

This strategy has been used by Tecilla, Tonellato, and co-workers for the development of a fluorescent sensor for $Cu^{2+}$ ions based on silica nanoparticles functionalized on the surface with trialkoxysilane derivatives of picolinamide as the ligand and dansylamide as the fluorescent dye.[58] The picolinamide ligand complexes the $Cu^{2+}$ ions strongly, and the bound ion still quenches the dansyl emission substantially in DMSO. The sensitivity of the hybrids additionally depends on the ligand-to-dye ratio on the surface of the nanoparticles. The use of bidentate ligands and the preference of $Cu^{2+}$ ions for four- or sixfold coordination results in the sensitivity of the system increasing as a function of the molar fraction of picolinamide residues, thus yielding a detection limit below the micromolar range. In further studies, the authors used a combinatorial approach to functionalize silica nanoparticles with other ligands and dyes in various ratios.[59] The cooperative and collective effects are achieved by the organization of the organic components on the particle surface to form multivalent binding sites with an increased affinity for $Cu^{2+}$ ions. Alternatively, binding of a single metal ion can lead to the quenching of up to 10 fluorescent groups surrounding a receptor unit, thus producing an amplification of the signal.

Improved signaling by independent preorganization of ligands and signaling units has also been observed for polymeric nanoparticles,[60] micellar systems,[61] and in extended surfaces such as in difunctionalized self-assembled monolayers[62] and Langmuir–Blodgett films.[63] SAMs on gold or glass are interesting examples of difunctionalized surfaces where directional preorganization facilitates communication between the binding group and signaling subunit in a similar way as described above. The collaboration of Crego-Calama, Reinhoudt, and co-workers has created chemosensor materials for both cations and anions by using a combinatorial approach where glass monolayers were functionalized with fluorescent groups (rhodamine derivatives) and independent coordinating units (amino, aryl urea, alkyl urea, aryl amide, alkyl amide, sulphonamide, urea, and thiourea).

### 2.3. Control of Recognition

As a link between Sections 2.1 and 2.2 and the next chapter that deals with the controlled assembly and disassembly of larger objects, one of the few examples that allows control over the state of the activity of a hybrid host material toward a guest by an entirely different means will be discussed. For this purpose, Thomas and co-workers attached photoswitchable spiropyran units through alkanethiol spacers to the surface of AuNPs.[64] The spiropyran (SP)/merocyanine (MC) couple was chosen such that the typically higher fluorescent and longer-wave-absorbing MC form is also capable of binding certain amino acids in methanol. In the closed spiro form, the system of approximately 130 SP units attached to the AuNPs displays only the typical plasmon band of the nanoparticles in the visible range and the presence of amino acids does not result in any spectroscopic changes. Irradiation at 360 nm results in SP being converted into MC, which is visible by the appearance of an absorption band centered at about 520 nm. Excitation of the system at 520 nm in highly polar solvents leads to a broad and strongly Stokes-shifted fluorescence band at 640 nm, which is typical for MC derivatives. An increase in the fluorescence lifetime of the MC–AuNP conjugates was observed in the presence of amino acids. The considerable high number of photochromic units on the particle surface enabled high loadings of amino acids to be achieved. Since the switching process can be controlled in both directions by irradiation with light of the correct wavelength, the amino acids could also be collectively liberated upon inducing the back reaction from the MC to the SP form. A perfection of such hybrids thus might lead to potent drug-delivery systems in the future.

## 3. Controlled Assembly and Disassembly

Synthetic chemistry requires powerful tools for building at will complex chemical structures in a modular fashion from

 © 2006 Wiley-VCH Verlag GmbH & Co. KGaA, Weinheim 

simple blocks.[65] This goal has been partially achieved at the molecular level through formation of covalent bonds by templated self-assembly.[66] However, despite the fact that there are also some interesting examples of large self-assembled structures,[67] there is still a general lack of understanding of standardized procedures for the step-by-step synthesis of nanoscopic structures.[68] A better understanding of such processes however would facilitate the design of molecular building blocks for the construction of complex functional architectures and "smart" materials for applications in molecular electronics and mechanics. Functionalized surfaces could in principle be used as shape-persistent supports for the reversible assembly of two-dimensional architectures. If layer-by-layer techniques were used, even the construction of three-dimensional nanoscale objects should be feasible. A key factor in such directed nanochemistry is the availability of a suitable casting mould or, in other words, the placing of preferably noncovalent binding or "trapping" sites such as calixarenes or cyclodextrins in a predefined manner on the surface of a support. The function of these trapping sites is to assemble either a number of single guests, for example, for further layer-by-layer growth or the assembly of network aggregates, or to allow larger objects with several binding sites to dock to the surface at various sites. The latter approach is much like placing an EPROM at its designated position on a circuit board of an electronic device. Especially attractive are those examples where the assembly/disassembly processes are coupled with switching protocols that allow reversible control over the building process.

### 3.1. Network Aggregates

In an early example of the assembly of network aggregates, Kaifer and co-workers used fullerenes as the small noncovalent linking units to bridge γ-cyclodextrin (CD) capped gold nanoparticles of 3.2 nm diameter in a three-dimensional fashion and create large assemblies of hybrid nanoparticles with diameters of about 300 nm (Figure 12).[69] The motivation here was the induction of aggregation by supramolecular recognition to create nanoparticle assemblies for electronic circuit components with extraordinarily high degrees of integration.[70] Kaifer and co-workers showed that various sized assemblies could be obtained by simple adjustment of the temperature during the association process. The advantages of their strategy are that the aggregates are stable in water, the process is entirely reversible by a change of the solvent (for extraction of the $C_{60}$ linkers), and the plasmon bands of the isolated AuNPs and the aggregates are virtually identical (because of the small diameter of the AuNPs).

Liu et al. studied the capture of fullerenes by network aggregates consisting of cyclodextrin polypseudorotaxanes (PPR) threaded with amino-functionalized polypropylene glycol (PPG) and AuNPs of about 20 nm in diameter for biochemical purposes (Figure 13).[71] The choice of the larger

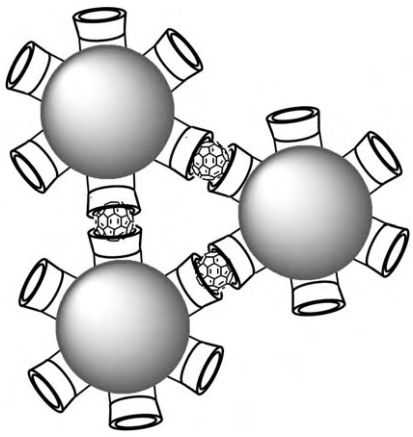

*Figure 12.* Fullerene-induced aggregation of γ-CD-capped gold nanoparticles.

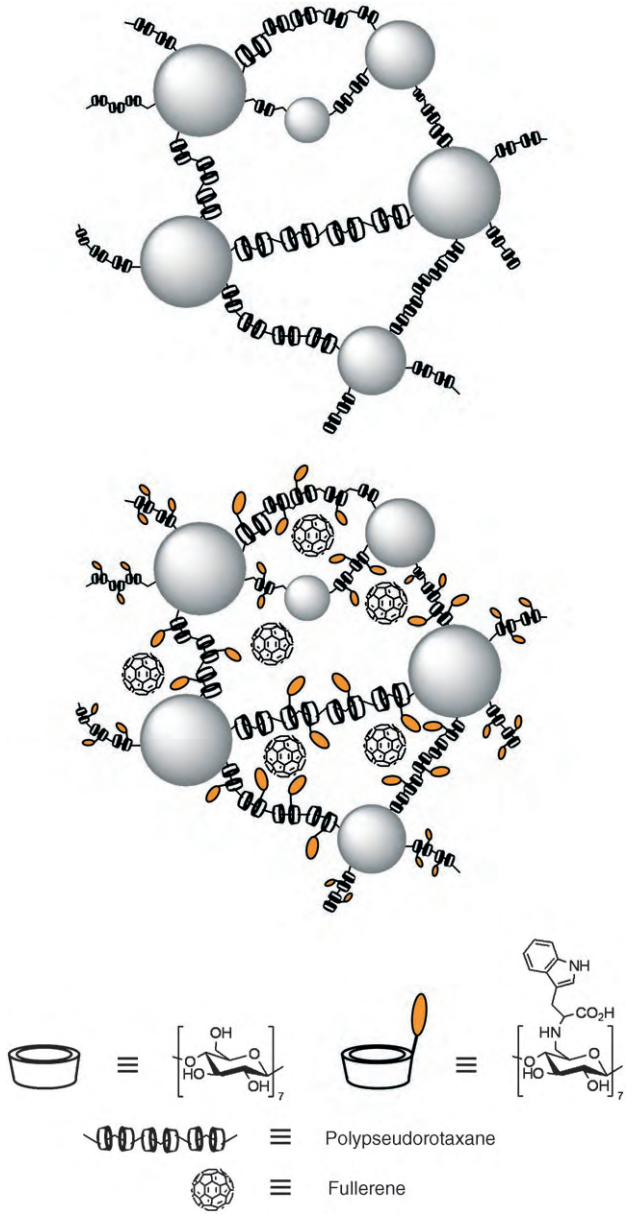


*Figure 13.* Supramolecular networks constructed from AuNPs and PPG-cyclodextrin polypseudorotaxanes.

 © 2006 Wiley-VCH Verlag GmbH & Co. KGaA, Weinheim 

AuNPs meant that the formation of the higher-generation aggregates could be traced by the color change from red to bluish-violet (see Chapter 2.2.1). The average diameter of the larger, water-soluble superparticles amounted to about 450 nm. When the CD moieties threaded on the PPG chain were additionally functionalized with L-tryptophan groups, the network aggregates exhibited typical tryptophan fluorescence. The capture of fullerenes and the formation of ternary aggregates were then signaled by the quenching of the fluorescence, which was ascribed to electron transfer between the amino acid moieties and the $C_{60}$ guests. Preliminary experiments showed that these ternary hybrid aggregates are potent agents for light-induced cleavage of DNA.

Reinhoudt and co-workers explored the possibilities of creating a multitude of network aggregates or three-dimensional layer-by-layer architectures based on the AuNP-CD system (see Section 3.2). In a recent study, they investigated the structural requirements for the formation of stable network aggregates when using CD–adamantane host–guest interactions as the supramolecular driving force for aggregation.[72] They probed the influence of multivalency[73] and cooperativity on the assembly of network aggregates from β-CD-capped AuNPs and adamantyl carboxylate, a linear bis(adamantyl) guest molecule, and fully adamantyl-terminated dendrimers of various generations (Figure 14). The key finding was that if the degree of favorable host–guest interactions–-as exhibited by CD–AuNPs and the dendrimer linkers–-is too high, precipitation of the aggregates results. The linear bis(adamantly) spacer showed better performance in generating more-soluble aggregates, although a signifcant number of the spacers are "passivated" by docking to two binding sites on the same nanoparticle. When used on both types of combinations (linear linkers/AuNPs and dendrimers/AUNPs), the monomeric adamantyl carboxylate can only compete successfully with the linear difunctionalized linker for the binding sites on the AuNPs. These results demonstrated that a directed assembly of superstructures can be obtained by controlling the geometry and valency of the guest or linker.

A reversible assembly/disassembly process can also be controlled thermally through appropriate choice of the components. For such a purpose, Naka, Roh, and Chujo functionalized 2.3-nm AuNPs with pyrene-appended alkanethiol units and assembled these nanoparticles with linear bis(dinitrophenyl) linkers of various chain length into network-type superstructures (Figure 15).[74] The small size of the AuNPs prevented UV/Vis experiments from giving clear evidence of the formation of aggregates. Optical control of the nanofabrication process is possible, however, as the charge-transfer interactions between the pyrene units of the particles and the dinitrophenyl units of the linkers do not only induce the assembly of the network but also quench the fluorescence of the fluorophore-functionalized AuNPs. The authors could further show the possibilities of temperature

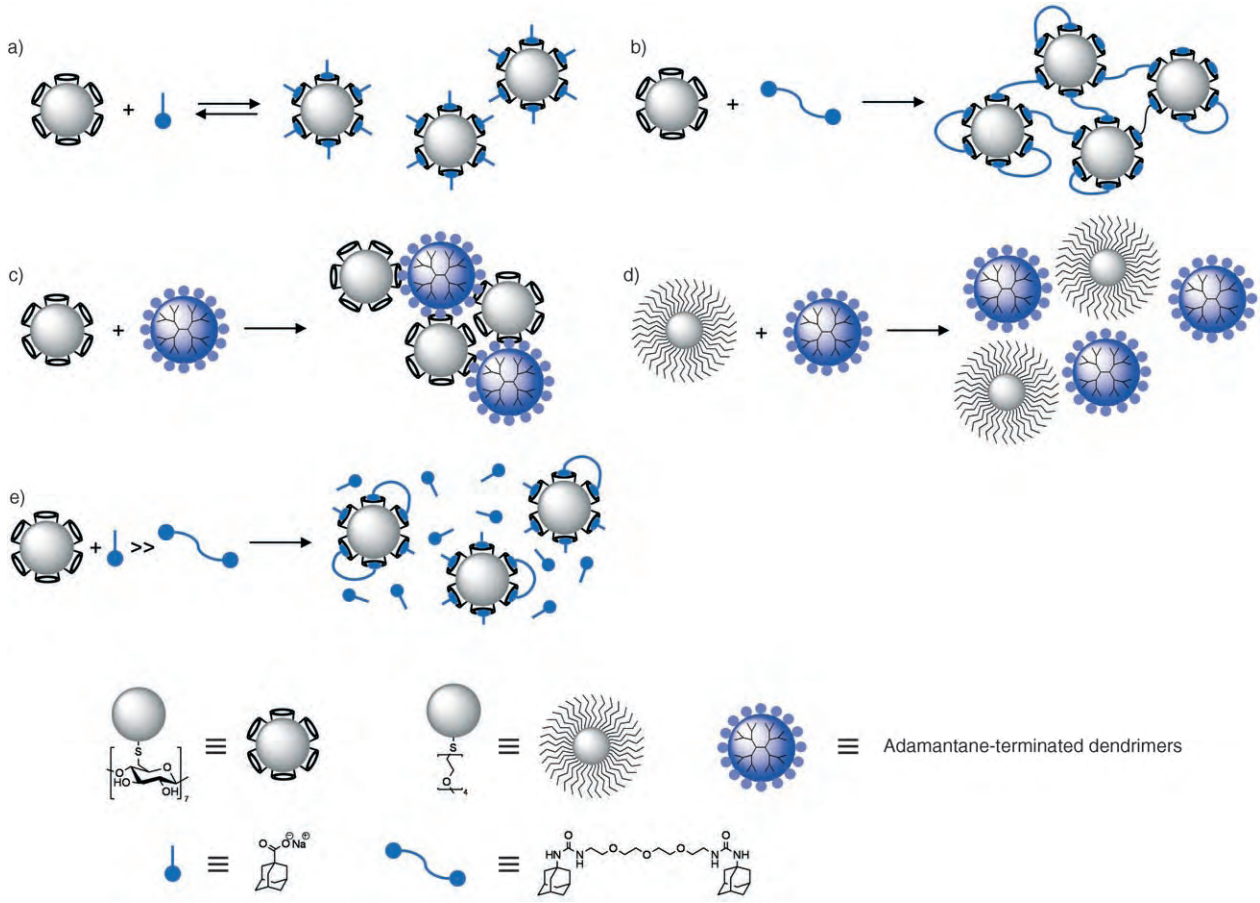


***Figure 14.*** Different aggregation protocols of CD-functionalized AuNPs with adamantyl-containing guest molecules.

 © 2006 Wiley-VCH Verlag GmbH & Co. KGaA, Weinheim 

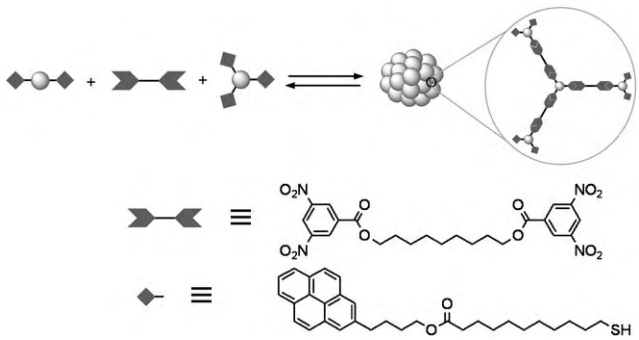

*Figure 15.* Thermally reversible self-assembly of metal nanoparticles by charge-transfer interactions.

control in such nanochemical processes. Not only did the size of the aggregates depend on the synthesis temperature (for example, whereas room temperature led to 1-μm aggregates, 0 °C led to 5-μm objects), but the assembly/disassembly process was reversible over several cycles when switching between two temperatures (for example, 25 and 50 °C).

### 3.2. Stepwise and Controlled Assembly/Disassembly

A further step toward control and directionality was achieved by Reinhoudt and co-workers. They fixed tetraguanidinium calix[4]arenes functionalized with four adamantyl units onto a β-CD monolayer on gold through formation of strong inclusion complexes between the adamantane and the hydrophobic cavity of the β-cyclodextrins (Figure 16).[75] This approach allowed the positively charged guanidinium subunits of the calixarenes to be exposed on the outer face of the surface. In a second step, tetrasulfonate calix[4]arenes were assembled onto the modified surface through electrostatic interactions. The binding process takes advantage of the improved coordination by preorganization, and the association constant for the assembly at the surface is larger than for the same assembly in solution, thus indicating positive cooperativity. The molecular ensemble could be disassembled chemically by rinsing with 1M KCl solution (dissociation of the tetrasulfonate calix[4]arene) and then with 2-propanol (desorption of the tetraguanidinium derivative).

The strong cyclodextrin–adamantane interaction was also the driving force for the formation of more complex structures by layer-by-layer techniques.[76] CD-functionalized gold or silicon oxide surfaces, adamantyl-terminated dendrimers (5th generation, 64 adamatyl end groups), and gold nanoparticles functionalized with cyclodextrins were the three components used for this multilayer device (Figure 17). Since small AuNPs (2.8 nm diameter) were again employed that show negligible shifts of the plasmon band upon aggregation, UV/Vis spectroscopy could be used to monitor the growth of the layers by the increase in the intensity of the plasmon band at 525 nm as a function of the number of bilayers deposited on the surface. Well-defined multilayer thin films with up to 18 nanometer-thick layers were thus created in a controlled manner. Another interesting example of layer-by-layer assembly based on supramolecular

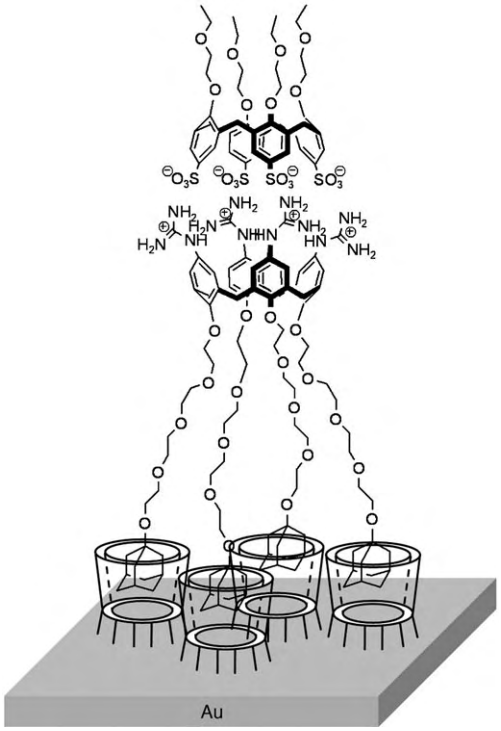


*Figure 16.* Adsorption of tetraguanidinium calix[4]arene functionalized with four adamantyl units on β-CD monolayers and their subsequent assembly with tetrasulfonate calix[4]arene.

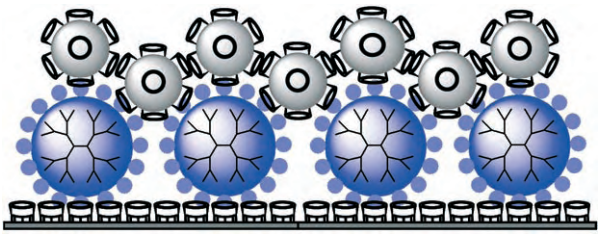

*Figure 17.* Representation of layer-by-layer assembly of adamantyl-terminated dendrimers and AuNPs functionalized with cyclodextrins on a CD SAM.

interactions was developed by Rubinstein and co-workers: they deposited gold nanoparticles onto gold through coordinative interactions with $Zr^{4+}$ ions to achieve a regular increase in thickness of 4.8 nm.[77]

Coordinative forces also play a key role in the first example of a hybrid layer structure that shows an explicit function, the enhanced generation of photocurrent (Figure 18).[78] Besides this function, the construction of the system is also particularly interesting. First, the imidazolyl-substituted zinc porphyrin rings carry 10,10′-(3,5-phenylene)bis(oxy)bis(decane-1-thiol) groups which are attached to the supporting gold surface. The next layers consisting of *meso*,*meso*-linked bis(imidazolylporphyrinato-zinc) (bIPZ) complexes are prepared in two steps. In the first step, the terminal imidazolyl units of bIPZ coordinate to the axial positions of the zinc ions. Since the bIPZ structures also have allyl butyrate side chains, the assembled units could be covalently cross-linked pairwise by a metathesis reaction

 © 2006 Wiley-VCH Verlag GmbH & Co. KGaA, Weinheim 

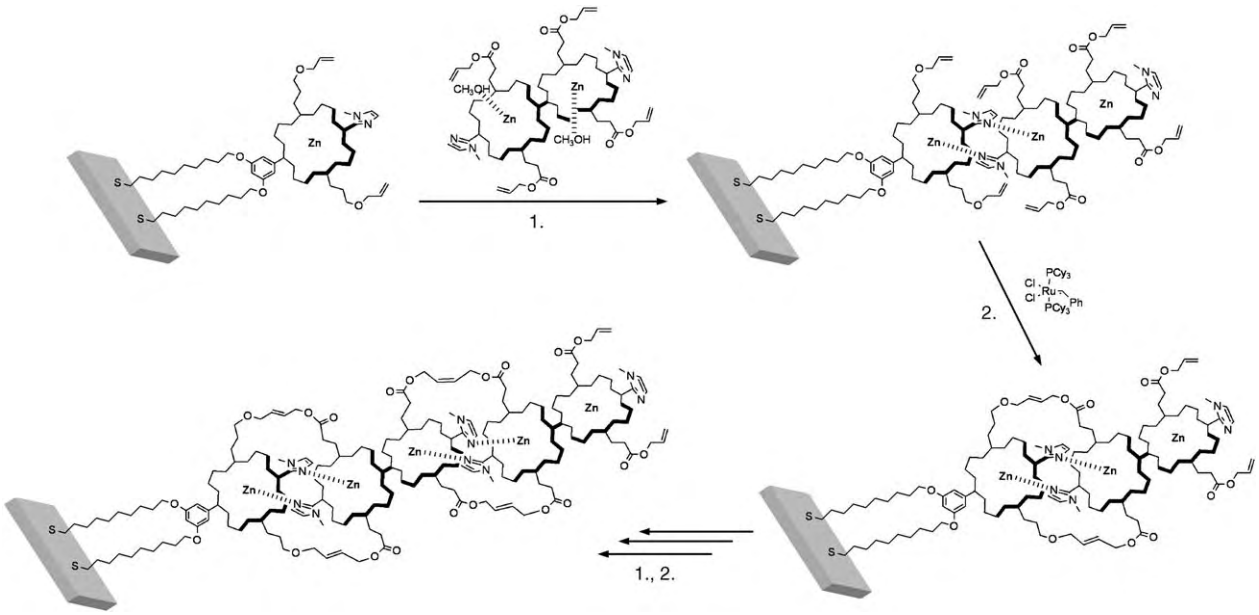


***Figure 18.*** Layer-by-layer assembly of imidazolyl-substituted porphyrinatozinc complexes onto a gold surface.

(step 2). Repetition of these two steps yielded rigidly fixed multiporphyrin arrays with up to six layers; the growth per accumulation cycle was about 1.0 nm. The resulting ensemble resembles the head of a brush, with the bristles (the porphyrin stacks) sticking out into the third dimension. In the presence of viologen as an electron carrier this nanomaterial revealed outstanding "light-harvesting" properties, with the photocurrent being amplified with each layer.

Another advantage of the multilayer ensembles concerns emission output: Whereas the emission of the zinc porphyrins is strongly quenched for the mono- and bilayer systems because of the vicinity of the gold surface and energy-transfer quenching by surface plasmons, the tri- and higher layer systems show considerable emission. The inner porphyrin rings thus act more like "active" transmitter masts than antennae. The light-harvesting efficiency of the higher layer arrays was improved as photosensitization is strongly enhanced with increasing numbers of layers. The authors also synthesized a porphyrin-based system composed of four layers with a fullerene covalently bound at the terminal layer. The efficient photoinduced charge separation that takes place at such terminal moieties resulted in the photocurrent in the $C_{60}$-terminated antennae being threefold higher than in the respective unmodified antenna. The work by Kobuke and co-workers impressively demonstrates how hetero-supramolecular strategies can yield highly ordered hybrid materials with three-dimensional architectures that conserve the photoexcitation energy through suppression of deactivation pathways that commonly dissipate the excitation energy at structural defects of conventional disordered multichromophoric assemblies.

The application of layered functional hybrid materials constructed by assembly techniques for the incorporation of chemical compounds has also been reported recently. For example, Reinhoudt and co-workers deposited adamantyl-terminated fifth-generation dendrimers onto β-CD-functionalized glass supports and loaded the dendrimers with organic dyes (Figure 19).[79] The advantages of the dendritic layer compared to a system[80] in which the fluorophore was

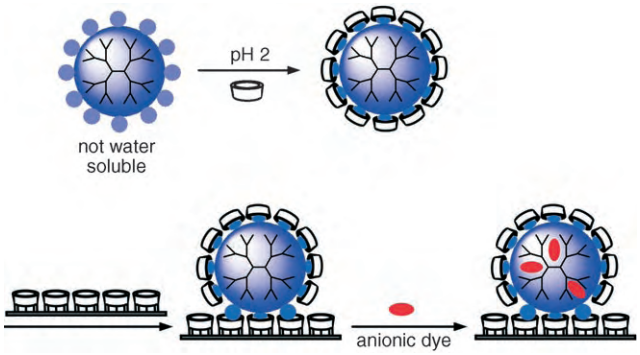


***Figure 19.*** Solubilization of adamantyl-terminated dendrimers with β-CD, subsequent microcontact printing on a β-CD-functionalized glass support, and filling of the inmmobilized dendrimer with anionic dyes.

functionalized with only two or four adamantyl units and situated directly on the surface are the significantly improved stability in aqueous solution and the possibility to load the dendrimers with a larger number of dyes. Microcontact printing techniques[81] can be used to load dendritic "molecular boxes" with different dyes, thereby creating color patterns. The versatility of this approach was illustrated by rinsing/refilling experiments, in which the same pattern, for example, could be switched from green fluorescent (loaded with fluorescein) via nonfluorescent (empty material) to reddish fluorescent (loaded with Bengal rose).

In a second example, Samitsu et al. created a first prototype of a hybrid layered material that might serve as a device to recognize polymer chains by their diameter.[82] They

 © 2006 Wiley-VCH Verlag GmbH & Co. KGaA, Weinheim 

assembled β-cyclodextrin–dodecanethiol inclusion complexes on a gold-covered silica wafer (CDT–Au), while gold surfaces capped only with unfunctionalized dodecanethiol (T–Au) were used as the reference system. After deposition of the respective supramolecular layers on the surfaces, both types of samples were treated with "molecular tubes" (MTs) consisting of one-dimensional, covalently linked oligomers of four to five α-CDs. Whereas the MTs immediately reacted with the CDT–Au surface and changed the material's character from hydrophobic to hydrophilic, T–Au did not bind a significant number of the tubular supramolecules. Preliminary STM and AFM measurements suggested that the MTs are uniformly layered on the functionalized surface. However, evidence that the system can be used for the intended recognition of polymer chains has still to be provided.

Besides light-harvesting, chemical incorporation, and possible recognition, switching functions have also been introduced into hybrid systems, primarily to control the assembly/disassembly step by an external stimulus. The photochemically reversible building of nanoarchitectures has been realized by using peptide nanotubes functionalized with hydroxyazobenzene carboxylic acid units (Figure 20).[83] In the absence of light, these nanotubes were immobilized on a gold surface carrying self-assembled monolayers of α-cyclodextrins (Figure 20) through formation of inclusion complexes between the terminal phenyl group of the azo derivatives in the *trans* configuration and the α-CDs. When this system was irradiated with UV light (360 nm) the azo derivatives photoisomerized to the *cis* configuration and the nanotubes were released from the α-cyclodextrin. The azobenzene nanotubes could be reattached onto the α-cyclodextrin surface by keeping the solution in the dark. By using a similar approach, peptide nanotubes functionalized with ferrocenecarboxylic acid were used to form a supramolecular ensemble with β-CD-functionalized gold surfaces through inclusion of the ferrocene moieties.[84] In this case, the detachment of ferrocene nanotubes was achieved by electrochemical oxidation to ferrocinium, which was not effectively bound by the β-CDs.

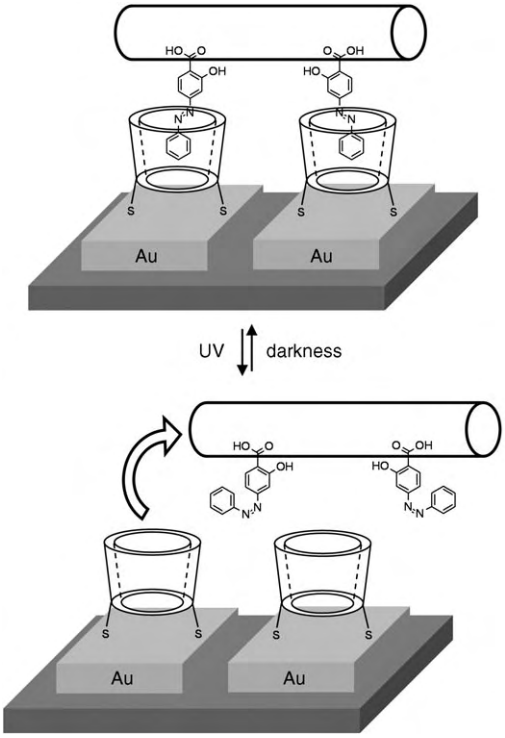


***Figure 20.*** Light-induced nanotube detachment/attachment of azobenzene-functionalized nanotubes on complementary α-CD/Au surfaces.

In a comparable way, but using tetrathiafulvalene (TTF) paraquat/cyclophane chemistry, Cooke and co-workers were able to control the complexation properties of a functional surface toward different electron-poor macrocycles.[85] TTF functionalized with thioctic acid was immobilized on a 0.5-mm gold wire and the competitive binding experiments were carried out in acetonitrile/dichloromethane mixtures by cyclovoltammetric techniques. In its neutral state, the TTF units on the surface readily bind cyclobis(paraquat-*p*-phenylene) in a pseudorotaxane-type of fashion, while electrochemical oxidation of the TTF moiety results in a dethreading of the electron-deficient macrocycle from the TTF host. Correspondingly, the more electron-rich macrocyclic bis(1,5-dioxynaphthalene) cyclophane shows a better pseudorotaxane-type interaction with the oxidized TTF SAMs, thus indicating that the complexation features should be controllable. However, the reversibility of the electrochemically controlled architectures formed by the sequential oxidation of the TTF moieties was poor. This problem first has to be addressed before a device that can discriminate between different guests by simple electrochemical Umpolung will become available for exciting new applications in chemical sensing technology.

Reversible control of the assembly and disassembly of a supramolecular ensemble should also have promising applications in the construction of molecular devices and nanomachines. A recent example suggests that surfaces functionalized with bistable [3]rotaxanes can act as a "molecular muscle" and generate nanoscale movements when attached to gold surfaces.[86] Future studies will show if cyclodextrin-capped substructures on gold surfaces might in future act as "parking lots" for "nanocars"[87] by utilizing, for example, the forces reported by Kaifer and co-workers to be active in certain network aggregates.[69]

## 4. Biomimetic and Gated Supramolecular Chemistry in Hybrid Nanomaterials

From the previously described examples of hetero-supramolecular chemistry, several general observations on the binding of molecules at the surfaces of nanostructures can be derived. Each system involves suitably functionalized particles that are able to bind in a supramolecular sense by cooperative forces. Their host–guest interactions amplify either the recognition event alone or recognition and signal expression which are not found in the unfunctionalized host molecule itself (1D system). The last examples also showed how nanostructures can be built and disassembled by using functional surfaces and reversible supramolecular forces.


© 2006 Wiley-VCH Verlag GmbH & Co. KGaA, Weinheim

Again, this approach relies on cooperative effects mediated by the surface and the interaction of the appended groups. The supramolecular event is already encoded in the functionalized particle irrespective of whether coordination, signaling, or reactivity is the amplified process.

The question thus arises, how to go beyond these observed effects? How do we assemble molecules such as receptors or reporters so that the ensemble has a higher functional complexity? A possible starting point is dimensionality: If specific molecular entities are not anchored on "flat" 2D surfaces but in 3D nanoscopic scaffolds, new supramolecular concepts can be explored. Although this particular field is still in its infancy, prominent examples have already emerged—for example, new directions in gated nanochemistry, the switching of morphology, and biomimetic signaling. Most of these examples took advantage of 3D nanoscopic architectures such as those found in MCM-41-type silicates and certain nanotubes.

### 4.1. Gated Nanochemical Processes

Supramolecular nanoarchitectures that incorporate chemical entities which can act as a gate and allow controlled access to a certain site are described in this section. Relevant examples have been reported for the entry/release of chemical species into or from mesoporous silica hosts. A graphical representation of the method of operation is shown in Figure 21. The outer surface of the mesoporous silica is functionalized with switchable molecules, and either chemical species are entrapped in the inner pores or the latter are empty. The gate opens upon application of an external stimulus and the hybrid material either releases the confined guests or permits the entrance of molecular species from the bulk solution. Hybrid structures with gatelike entry/release mechanisms can be controlled by photochemical, electrochemical, and ionic methods. This approach is assumed to have high potential for novel nanomachines or complex delivery systems.

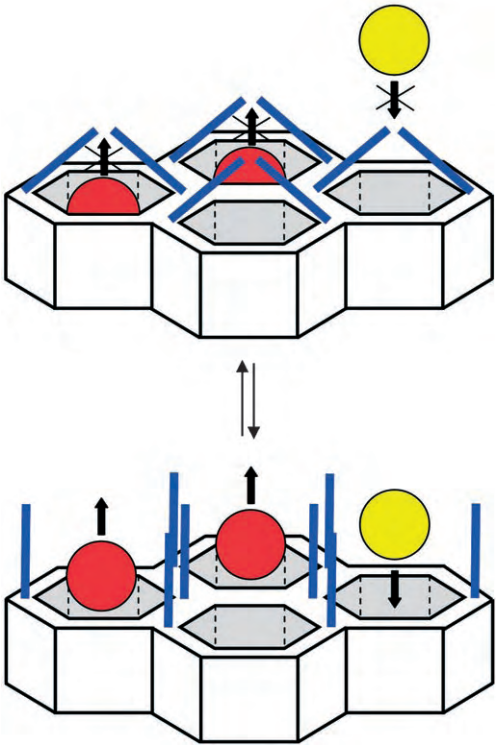

*Figure 21.* A nanoscopic molecular gate on the pore outlets of mesoporous materials (schematic).

An early report of gated nanochemical processes in 3D hybrid scaffolds was developed by Fujiwara and co-workers. Photoresponsive coumarin derivatives were grafted onto the pore outlets of mesoporous (MCM-41-type) solids with a pore diameter of approximately 2.5 nm and a specific surface area of about 850 $m^2 g^{-1}$.[88] Irradiation at $>350$ nm resulted in the photodimerization of the coumarin core and formation of the cyclobutane dimer, which closed the pores. The coumarin monomer could be regenerated and the pores reopened by photocleavage of the dimer by using higher energy irradiation (250 nm, Figure 22). This example shows how the use of a simple process (photodimerization) in combination with 3D architectures (for example, mesoporous solids) allows regulation of a supramolecular function such as the release or uptake of a chemical species in a controlled way.

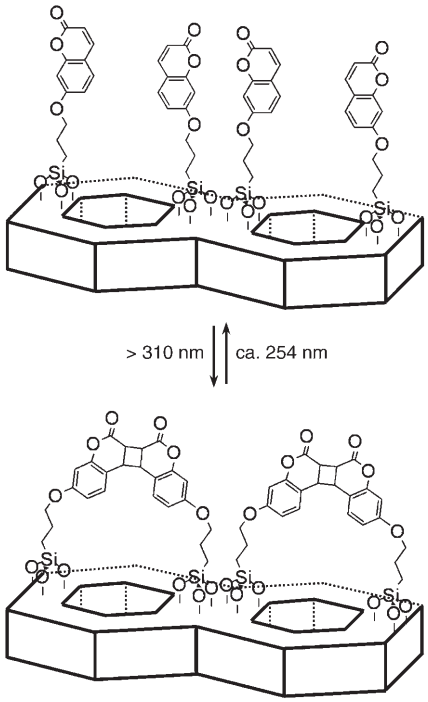


*Figure 22.* Opening and closing of coumarin-functionalized mesoporous materials.

Martínez-Máñez and co-workers reported the first gated hybrid system that operates in aqueous solution and can be controlled ionically by pH modulation. Figure 23 shows a mesoporous silica scaffold with open pores that is functionalized with polyamines on the external surface.[89] In this study UVM-7 was used, which is an MCM-41-type material with a

 © 2006 Wiley-VCH Verlag GmbH & Co. KGaA, Weinheim 

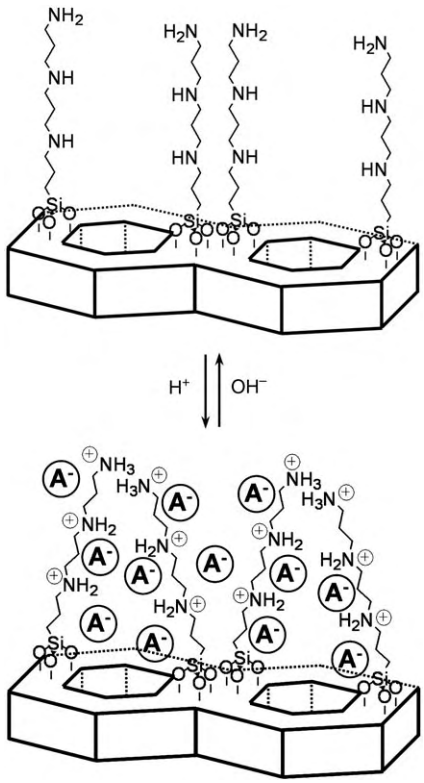


***Figure 23.*** An ion-gated hybrid nanosystem in aqueous solution.

characteristic bimodal pore system of MCM-41 particles (2.6 nm diameter) and larger pores between the particles (45.2 nm diameter textural porosity) and a specific surface area of about 630 $m^2 g^{-1}$. From calculations based on chemical analysis and surface measurements, a total of 22 $Å^2$ per polyamine moiety is found, which corresponds to about 30 molecules per pore opening. In this system, the opening/closing protocol arises from hydrogen-bonding interactions between less or unprotonated amines (open pores) and coulombic repulsions between protonated amino groups (closed pores). The inner pores of the material were funtionalized with thiol groups, which are known to react with a blue squaraine (SQ) dye to give a colorless derivative, to enable the opening and closing to be monitored.[90] The operation of the gate was studied by measuring the uptake of SQ into the pores from bulk solution. At acidic pH values the amines are fully protonated, the gate is closed, and access to the inner pores is denied; thus the solution remains blue. In contrast, in the neutral pH region the amines are only partially protonated, the gate is open, and the dye can enter the pores, thus leading to a bleaching of the SQ solution. An anion-controlled effect was also observed. In the neutral pH region the gate is only open in the presence of small anions such as $Cl^-$, while bulky anions such as ATP close the gate through formation of strong complexes with the amines at the pore outlets. Very recently, Xiao and co-workers reported a complementary system, formed by anchoring carboxylates in porous SBA-15 silica rods.[91] In this case, the pores are closed at neutral and basic pH values (the carboxylate state), whereas the pores remain open at acidic pH values (the carboxylic acid state).

An electrochemically controlled system has been developed by using a pseudorotaxane consisting of a 1,5-dioxynaphthalene (DON) derivative and cyclobis(paraquat-*p*-phenylene) (CBP) that recognizes the DON groups through noncovalent interactions, and acts as the "gatekeeper".[92] The inorganic host material is comprised of mesostructured thin films of silica with cylindrical pores of about 2 nm diameter. An external reducing agent was used to break up the pseudorotaxane; reduction of DON results in spontaneous dethreading of the CBP ring and allows the release of the guest from inside the pores (Figure 24). This gating effect is related to the electrochemical removal of a "cap". This system was further elaborated by attaching a second redox-active site

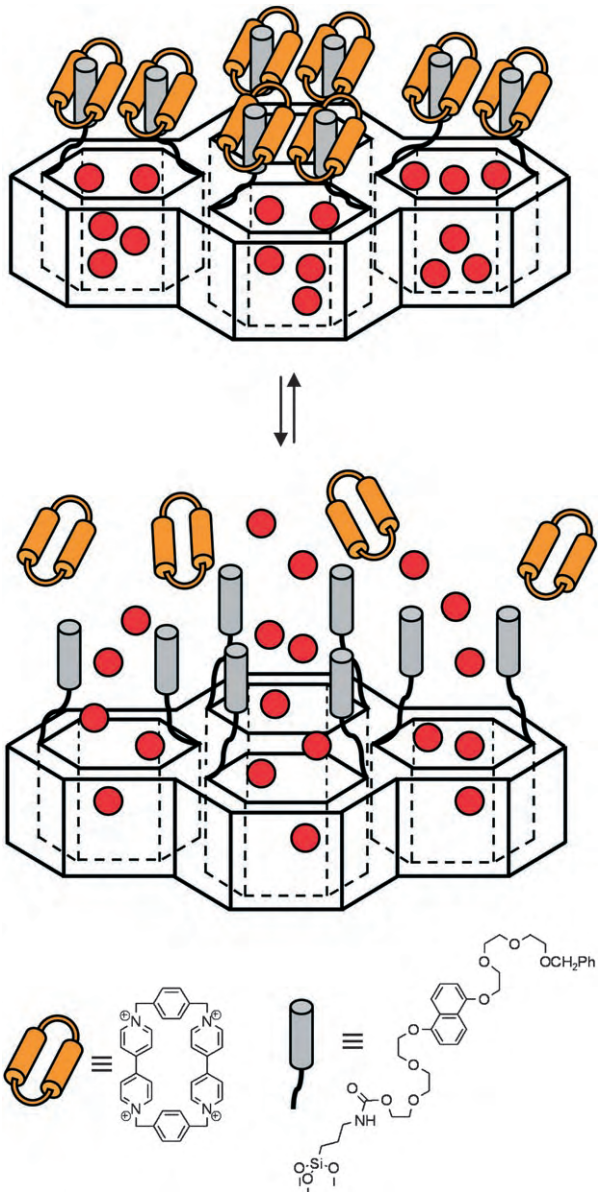


***Figure 24.*** Electrochemically controlled pseudorotaxane consisting of a 1,5-dioxynaphthalene derivative as the "gatekeeper" and cyclobis-(paraquat-*p*-phenylene) as the "lock".

 © 2006 Wiley-VCH Verlag GmbH & Co. KGaA, Weinheim 

on to the distal end of the DON gatepost (Figure 25).[93] In this case, an oligoethyleneglycol-benzyl-3-(trioxysilyl)propylcarbamate linker covalently attaches the DON unit to the pore outlets. A bis(diethyleneglycol)terphenyl spacer then bridges and connects the redox-active DON and TTF sites, and a bulky 4,4′-[(4-ethylphenyl)(phenyl)methylene]bis(*tert*-butylbenzene) group acts as the outer stopper.

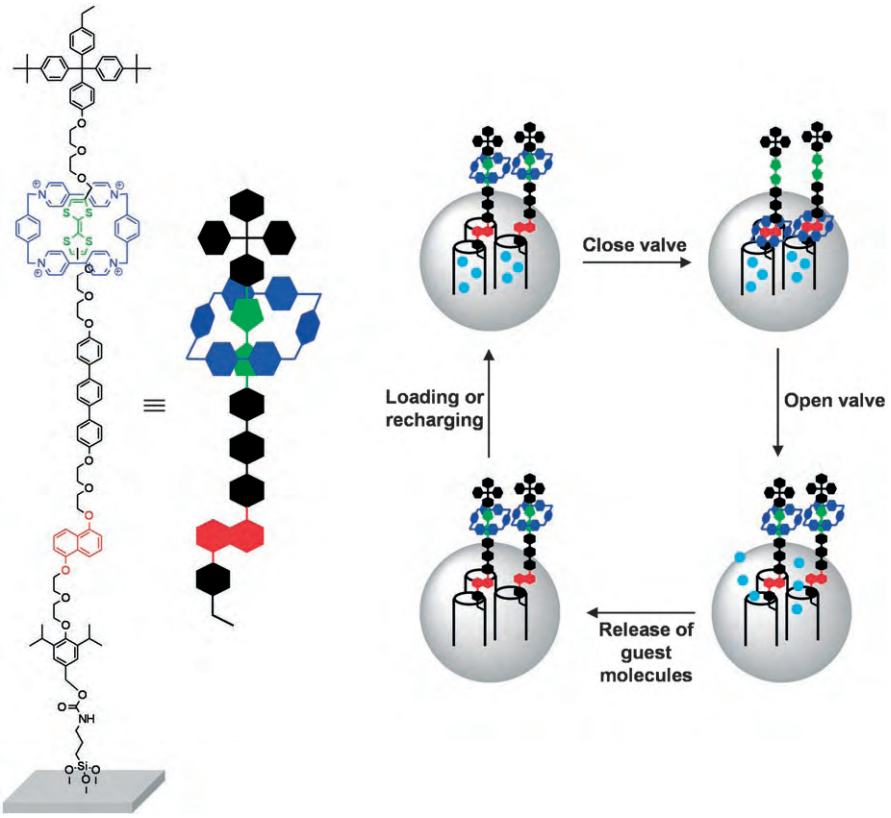


***Figure 25.*** A bistable rotaxane on the surface of mesoporous silica particles. The right-hand side of the Figure shows the cycle for the loading and release of guest molecules.

In the ground state, the CBP tetracation cap prefers to encircle the TTF moiety in a rotaxane-type manner ("open" position). The pores can be closed by two-electron oxidation of the TTF unit to $TTF^{2+}$. The resulting Coulomb repulsion results in the tetracation shuttling over to the DON station ("closed" state). Reduction of $TTF^{2+}$ back to neutral TTF results in the return of the cationic CBP macrocycle to the TTF station. The loading (by soaking) and unloading of the nanopores of the spherical MCM41 particles by diffusion was tested in organic solvents with both a neutral (tris(2,2′-phenylpyridyl)iridium(III), $[Ir(ppy)_3]$) and a cationic compound (rhodamine B). These fluorescent guests enabled Stoddart, Zink, and co-workers to follow the operation of the valve indirectly—by the increase of the emission in bulk solution after release of the guest—and directly—by monitoring the DON luminescence, since the CBP ring quenches the DON fluorescence when the valve is closed. After reduction of the TTF unit and subsequent return of the CBP to its outer position, the intensity of the naphthalene emission increases fourfold. Similar performance was found for the neutral and the cationic dye; thus charged molecules do not seem to disrupt the operation of the nanovalve. This example of reversible motion in hybrid nanosystems controlled by redox chemistry is an exciting proof-of-principle for future nanomechanical devices that might be able to perform a multitude of complex functions.

The removal of a cap is also at the heart of a gated system that consists of mesoporous silica nanospheres with an average particle size of 200 nm and an average pore diameter of 2.3 nm as the porous host and CdS nanoparticles of about 2.0 nm diameter as the stoppers at the pore outlets.[94] Cap removal is triggered here by the rupture of a disulfide bridge that anchors the CdS nanoparticles to the siliceous framework by using specific disulfide-reducing agents. In this case, the mesopores were filled with various pharmaceutical drug molecules and neurotransmitters, such as vancomycin and ATP, and the delivery efficiency was demonstrated with astrocytes in vivo.

Lin and co-workers recently showed in two publications the versatility of the concept of closing the pores of mesoporous silica nanospheres with particulate objects. In analogy to the CdS stoppers, they also used poly(amidoamine) dendrimers (PAMAM) and established again a thiol–disulfide gating mechanism.[95] As a proof-of-principle for drug-delivery applications, they studied the release of ATP from the pores of the nanospheres by ATP-induced luciferase chemiluminescence imaging in real time. ATP release in the subsecond time regime was monitored down to a concentration of $10^{-8}$ M with an iCCD-equipped microscope in real time. Comparative studies of the CdS- and the PAMAM-capped systems allowed further conclusions to be drawn on the design of such ensembles. Whereas only 57% of the pores could be closed in the case of the inorganic stopper, the dendritic cap allowed almost complete sealing. In a second study, Lin and co-workers demonstrated that nanochemical processes can aso be controlled by magnetism.[96] In this study, mesoporous silica rods with an average particle size of $200 \times 80$ nm and an average pore diameter of 3.0 nm were used as the inorganic 3D host. The host scaffold was functionalized through amidation of the 3-(propyldisulfanyl)propionic acid groups bound at the pore surface with 3-aminopropyltriethoxysilyl-appended superparamagnetic iron oxide nanoparticles with an average diameter of 10 nm (Figure 26). These nanoparticles do not act as "corks in bottlenecks", but instead the larger magnetic NPs close the pores as "a lid on a pot" does, fully covering the entrance.

As shown in the above cases, the disulfide linkages between the nanorods and the $Fe_3O_4$ NPs can be cleaved with reducing agents such as dihydrolipoic acid or dithiothreitol. A unique feature of this hybrid material is the fact that the entire $Fe_3O_4$-capped nanorod carrier system is magnetic so

 © 2006 Wiley-VCH Verlag GmbH & Co. KGaA, Weinheim 

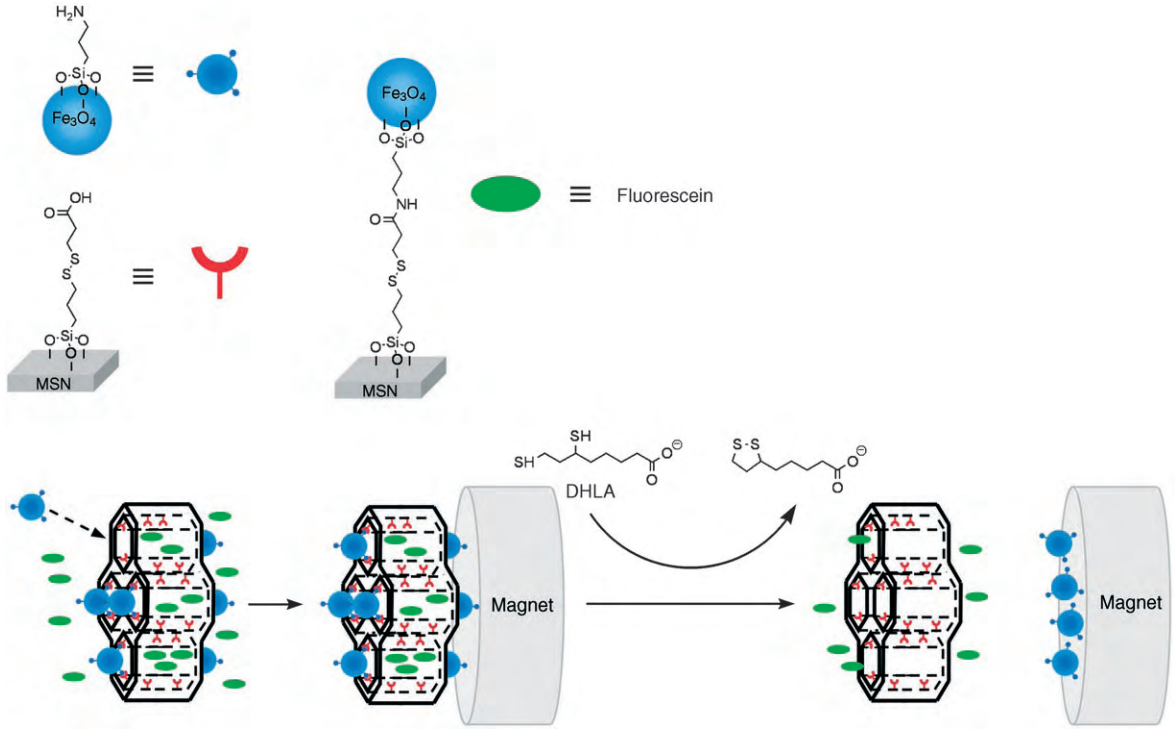


***Figure 26.*** A delivery system based on mesoporous silica capped with superparamagnetic iron oxide nanoparticles. The release mechanism utilizes the reduction of a disulfide linkage.

that the system can be first magnetically directed to a site of interest where the cargo can then be released. Lin and co-workers demonstrated the performance of the system by using fluorescein-loaded nanorods in aqueous buffer solution. When two cuvettes were loaded with the dye-containing magnetic material and an external magnetic field was applied to one side, the carrier particles moved to that side of the cuvette. One of the cuvettes was then incubated with a disulfide-reducing agent. Whereas the fluorescein-loaded magnetic nanorods remained nonfluorescent in the absence of the reducing agent, because of the quenching of the fluorescein emission by the $Fe_3O_4$ nanoparticles, the other solution showed the fast increase in the typical green fluorescence after release of the dye. These results impressively show that site-selective delivery and controlled release can be achieved by a sophisticated, yet not too difficult to prepare, hybrid supramolecular ensemble.

The above mentioned examples share the common feature that they are based on silica host scaffolds with nanopores for which the accessibility—either by release from the inside or by entering from the outside—is controlled by a gate. Mesoporous silica has been chosen because of its unique properties, such as uniform-sized nanopores with a very narrow pore distribution, and the widely known methods for its functionalization. However, other 3D scaffolds have also been used for the design of gates. An elegant example by Bachas, Hinds, and co-workers employed functional membranes of polystyrene fitted with multiwalled carbon nanotubes (MWNTs) with diameters of about 7.5 nm that mimic ligand-gated ion channels.[97] The open ends of the carbon nanotubes were first activated with carboxylic acid groups, which were functionalized in a second step with a desthiobiotin derivative that shows reversible binding to streptavidin. The large pore diameter of the MWNTs meant that small molecules such as coumarins, polyamines, or pseudorotaxanes are no longer sufficient to close the pores. Thus, larger biomolecules, such as biotin, had to be used instead. The opening/closing cycle operated as follows: Host–guest interactions between streptavidin and the membrane containing the carbon nanotubes leads to the closing of the pores. The opening was then achieved by dissociation of the desthiobiotin–streptavidin conjugate after addition of an aqueous solution of biotin, since the affinity of streptavidin to biotin is much higher than to desthiobiotin. The opening and closing of the pores was monitored by the transport of methyl viologen and $[Ru(bipy)_3]^{2+}$ through the MWNT membrane, which was more than 20-times slower after binding of streptavidin.

### *4.2. Switching of Morphological Properties*

Opening and closing the pores of a 3D architecture is an important function for the delivery of substances upon application of external stimuli, the capture or sensing of compounds, and the regulation of the access of chemical species to channels or cavities. However, the simple opening and closing of a gate is often not exclusively a sufficient means of control in directed and selective mass transport. In analogy to ion channels in biological membranes, the operation can be twofold, such that complexation of a protein to ligands at the outlet of a channel triggers the gating function, but then the

 © 2006 Wiley-VCH Verlag GmbH & Co. KGaA, Weinheim 

chemical texture of the inner surfaces of the channels determines additional features such as size-, hydrophilicity-, or charge-selective transport and co-transport. Several artificial ion channels have been created in recent years by employing different strategies such as SAMs on electrodes or the synthesis or assembly of solely organic supramolecules.[98] The examples of mesoporous hybrids with switchable inner morphology reviewed here can give valuable inspiration to this field of research.

In one of the first examples, Brinker and co-workers elucidated the possibility of photochemically controlling the pore size with photoisomerizable molecules such as azobenzene anchored to the inner surface of mesoporous MCM-41 structures. The effective size of the pores could be controlled in a valvelike manner through light-induced changes in the molecular dimensions resulting from reversible *trans–cis* photoisomerization, with a putative change in the pore size of approximately 6.8 Å (Figure 27).[99]

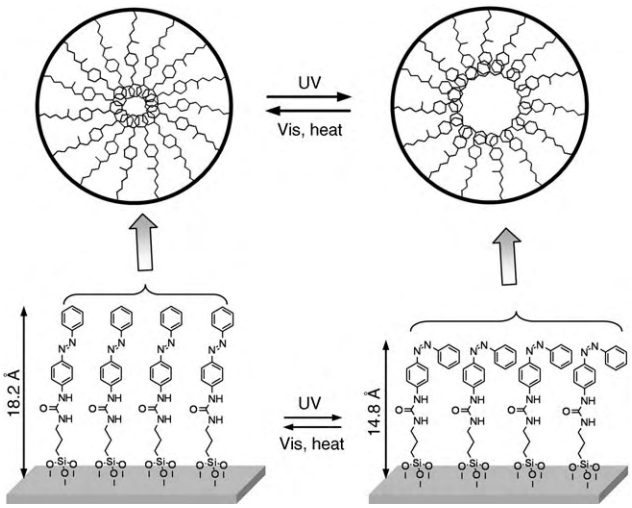


***Figure 27.*** Modulation of the effective size of mesopores through the dimensional changes of azobenzene resulting from reversible *trans–cis* photoisomerization.

In later experiments, Brinker and co-workers used ferrocenedimethanol and ferrocenedimethanol diethylene glycol as redox probes to test the transport behavior.[100] For these studies the photoresponsive nanocomposite membranes were spin-coated onto an ITO substrate and the steady-state oxidative currents at constant potential for the reactions taking place at the electrode were monitored. At constant potential, the increase or decay of the signal until steady-state conditions are reached is a measure of the accessibility of the surface and thus the transport through the pores. Brinker and co-workers could cycle the system many times by switching between 360 and 435 nm; in this way the time (ca. 300 s) required by the system to reach the respective steady-state under particular illumination conditions could be reproduced. Consequently, a change in the illumination intensity accelerated or decelerated the process.

In a second example, López and co-workers prepared monodisperse spherical mesoporous particles with diameters of 10 μm by a sol–gel process.[101] Atom-transfer radical polymerization, which allows the attachment of polymers exclusively to surfaces and avoids the formation of unspecific polymer objects in bulk solution or in the cavities and channels of porous frameworks, was used to graft polymer brushes of *N*-isopropylacrylamide (IPAA) onto the (inner and outer) surfaces of the particles and their pores. IPAA is hydrated at room temperature and inhibits the transport of solutes in water, whereas at temperatures over 50 °C, it is hydrophobic, dehydrates, and thus collapses at the pore wall, thus making the pores permeable to solutes. By employing fluorescein as the tracer and flow cytometry as the detection method, the researchers were able to show how the transport of the fluorescent guest could be controlled by a variation in the temperature.

Zhong and co-workers combined the basic principles of network aggregates (see Section 3.1) with the idea of biomimetic ion gating.[102] They developed core–shell gold nanoparticles capped with thiolates and alkanethiols, the latter functionalized with carboxylic groups that could form networks by hydrogen-bonding linkages through an exchange, cross-linking, and precipitation reaction pathway. In contrast to the mesoporous silica hosts, such network assemblies are open frameworks in which void space appears in the form of a channel or chamber. The nanometer-sized cores and their geometric arrangement define the size and shape of the network, while the shell structures define the chemical specificity. The network is formed through multiple hydrogen bonds between the terminal carboxylic acid groups, and can thus be reversibly opened (high pH, carboxylate form) or closed (low pH, carboxylic acid form). Thin films of the network aggregates were cast on various supports such as metals, glass, and glassy carbon to enable their properties to be studied by electrochemistry and IR reflectance spectroscopy. The biomimetic ion-gating properties were demonstrated by measuring the response of the pH-tuned network to two redox probes, $[Fe(CN)]_6^{3-/4-}$ and $[Ru(NH_3)_6]^{3+/2+}$, in both states. The studies of Zhong and co-workers showed that the response is a function of the degree of protonation/deprotonation of the acid groups at the interparticle linkages, the core sizes of the AuNPs (NPs with diameters of 2 and 5 nm were used), and the charges of the redox probes. At low pH values, in the closed state, neither $[Fe(CN)]_6^{3-/4-}$ nor $[Ru(NH_3)_6]^{3+/2+}$ can enter the network. At high pH values, $[Fe(CN)_6]^{3-/4-}$ is still efficiently blocked, because of electrostatic effects, but the positively charged probe is readily taken up. Moreover, the smaller AuNPs show generally better performance both in blocking and admitting these small analytes. These findings clearly demonstrate that alternative pathways to biomimetic molecular recognition harbor a wealth of possibilities for future sensing at the nanoscopic scale.

### 4.3. Biomimetic Signaling with Nanometer-Sized Binding Pockets

The third main area of functional 3D hybrid frameworks is biomimetic signaling through the formation of nanometer-

 © 2006 Wiley-VCH Verlag GmbH & Co. KGaA, Weinheim 

sized binding pockets by anchoring suitable binding sites to the surface of preorganized solids. The motivation is to create, in as simple a way as possible, sensing ensembles that can indicate the presence of analytes for which: 1) no functional receptor group is available, 2) selectivity is hard to achieve with conventional synthetic methods, or 3) the tremendous synthetic effort for the development of a receptor would be unreasonably high and time consuming. The idea of utilizing hybrid frameworks is related to the ways used by nature for dealing with such issues. Many proteins, whether highly specific or processing a whole class of substrates, succeed in tightly binding a designated chemical species with rather weak forces (hydrogen bonds, $\pi$ stacking, etc.) in aqueous media because they extract the substrate into a hydrophobic pocket where the complex formed between the active site and the substrate is shielded against competing water molecules. These active sites of proteins are usually embedded in a flexible (super)structure and upon entry of the substrate, the latter "induces the fit": the binding site is reoriented, the pocket is closed, and any remaining water is squeezed out. Chemists have strived to mimic such behavior for a long time by employing the strategies discussed in this Review, and only recently have the first examples been realized (mainly based on mesoporous silica materials). In general, the solid 3D support is polyfunctionalized: After loading the "recognition" centers onto the surface, a second functionalization of the inner pore walls is performed to fine-tune the polarity of the pores. Such systems are clearly more selective as molecular probes, because in addition to the recognition at the binding site there is a further supramolecular control, governed by the size and polarity of the nanopore.

In one of the first examples, Lin et al. functionalized the inner pores of MCM-41 with an amine-sensitive *o*-phthalic hemithioacetal group that reacts with amines to produce a highly fluorescent isoindole. The pores were cofunctionalized with different groups such as propyl, phenyl, and pentafluorophenyl to further enhance the selectivity of the system, (Figure 28a).[103] Some of these solids could differentiate between dopamine and glucosamine. Interestingly, this selectivity was not observed when using amorphous silica (a 2D system) functionalized with the same organic groups. An alternative method for regulating the penetration of molecules into the nanopores was realized by coating the mesoporous particles with a poly(lactic acid).[104] The neurotransmitter dopamine diffused much more quickly than tyrosine and glutamic acid into the pores. The discrimination is based on coulombic forces, since at the neutral pH value employed dopamine is positively charged, whereas tyrosine and glutamic acid are negatively charged and are thus repelled by the negatively charged poly(lactic acid) coating.

Another example of cooperativity has recently been developed by Rurack, Martínez-Máñez, and co-workers. Two functional entities were anchored to the inner walls of a porous 3D MCM-41 host material. Besides the anchoring of a chromo- and fluorogenic urea–phenoxazinone derivative as the anion receptor, the inner surface was further functionalized with trimethylsilyl groups. The hydrophilic inner walls of the silica skeleton were thereby transformed into hydro-

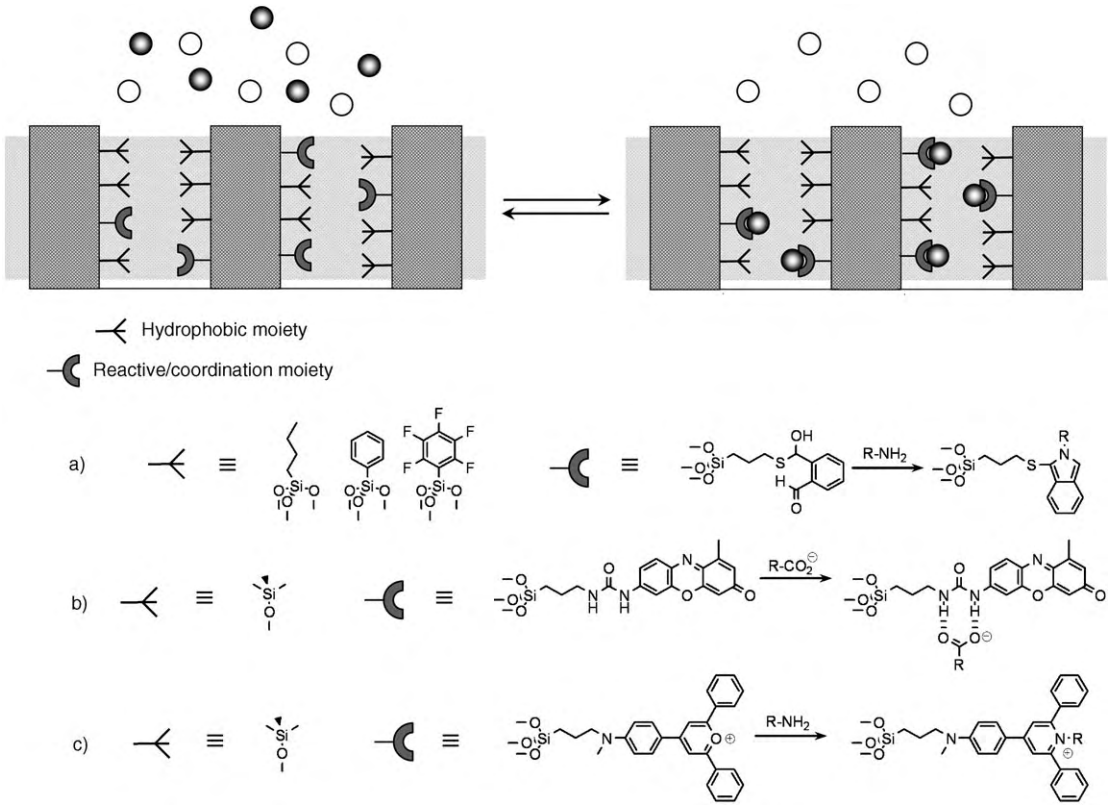


***Figure 28.*** Mesoporous silica functionalized with hydrophobic groups and coordination or reactive sites for the enhanced sensing of amines (a and c) and fatty acids (b).


© 2006 Wiley-VCH Verlag GmbH & Co. KGaA, Weinheim

phobic pockets which also contained the probes for carboxylate recognition (Figure 28b).[105] The system showed a selective response to long-chain (fatty) carboxylates in water, whereas short-chain carboxylates, inorganic cations, anions, and biological species such as triglycerides, cholesterol, bile acids, and organic phosphates gave no significant response. Apparently, only sufficiently hydrophobic analytes could enter the pores of the highly hydrophobic material, and only if the analytes also contained an ionic head group could they bind to the urea receptor and trigger the fluorescence signal. Glycerophospholipids, for example, could enter the pores but were unable to induce the fluorescent signal. The exclusivity of the enhancement of the response is evident if one compares the reactivity of the difunctionalized hybrid material with those of the molecular urea–phenoxazinone probe and the hybrid material that was only monofunctionalized with the probe but not yet passivated. The two latter systems do not respond to any of the above mentioned guests in water and the probe responds only unspecifically to carboxylates and $H_2PO_4^-$ ions in polar organic solvents. The performance of the hydrophobic hybrid material suggests that after extraction of the fatty carboxylates into the pores, the water content in the hydrophobic layer at the inner wall is presumably reduced so that hydrogen bonding between the carboxylate and urea groups can occur.

A related approach has recently been reported for discrimination within a class of amines by siliceous solids that contain an amine-sensitive pyrylium derivative attached to lipophilic trimethylsilylated nanopores.[106] Pyrylium derivatives are known to react with primary amines to give the corresponding pyridinium salt (Figure 28c), with a color change from magenta to yellow. In solution, the chromogenic pyrylium dye reacts unspecifically with primary amines but gives a selective response when placed in the hydrophobic nanopockets. Among the various linear primary aliphatic amines tested, only relatively short but sufficiently hydrophobic medium-chain amines (for example, *n*-octylamine) induced a chromogenic reaction in water, whereas hydrophilic (for example, *n*-propylamine) or long-chain amines (for example, *n*-dodecylamine) remained silent. The latter result was attributed to a closing of the pores after initial reaction of fatty amines with the dyes close to the opening. The orientation of the long chain of the reaction product such that it points into the free volume of the pore results in the diffusion of following analytes being hampered because of steric crowding.

These interesting results demonstrate that selective molecular recognition can be achieved not only by synthesizing complex hosts and attempting recognition in the traditional supramolecular sense, but also by creating multifunctional nanometer-sized binding pockets through a combination of covalent and/or noncovalent interactions. The fine-tuning of the inner polarity of such structures is a key step toward improved responses. In this respect, Inumaru et al. reported interesting results on the adsorption behavior of alkyl phenols and alkyl anilines by MCM-41 solids.[107] They prepared a series of solids and grafted not only alkyl chains of different length onto the surface, but also doped the host material with different concentrations of $Al^{3+}$ ions. It was found that lipophilic guests were preferably taken up as the chain length of the anchored functional group increased. Moreover, besides hydrophobicity, a discrimination of the guest molecules based on their hydrophilic head groups was found. For example, alkyl anilines with a more hydrophilic group were better adsorbed than alkyl phenols, because of stronger hydrogen-bonding interactions (and/or weak acid–base interactions) with the inorganic walls.

Artificial binding pockets with receptors can also be used in selective colorimetric displacement assays (Figure 29). After functionalization of the porous host with adequate binding sites, the latter can be loaded with a dye that coordinates to these anchored sites. In the presence of a target anion that forms a stronger complex with those inner binding sites, a displacement of the dye and diffusion into the bulk solution takes place, thus resulting in the colorimetric detection of the guest.[108] The system was tested with mesoporous MCM-41 solids containing guanidinium groups as the binding sites and methylthymol blue as the dye. A

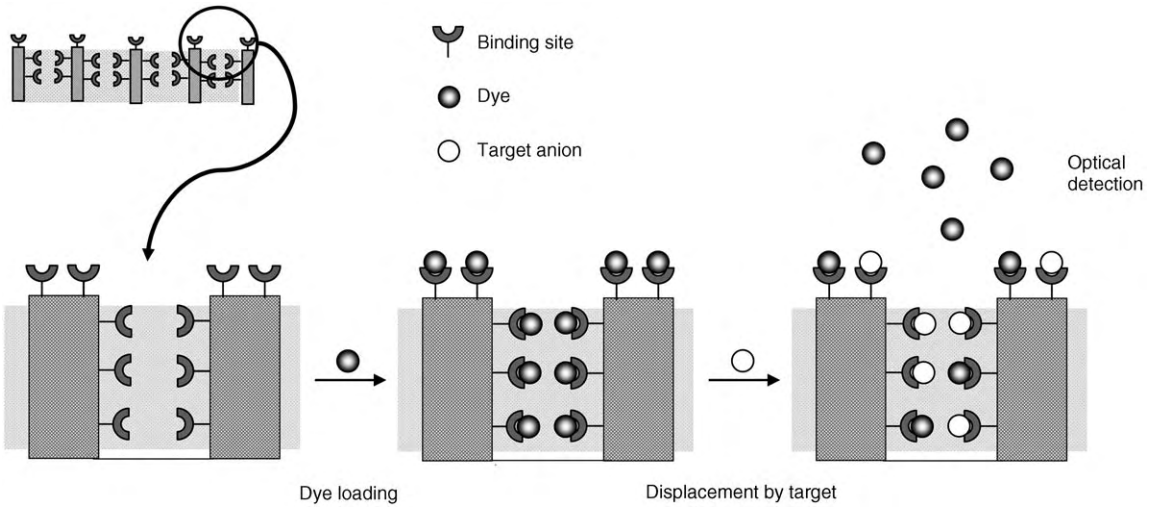


***Figure 29.*** The principle of a colorimetric displacement assay with functionalized mesoporous materials.

 © 2006 Wiley-VCH Verlag GmbH & Co. KGaA, Weinheim 

citrate-selective response was found, thus indicating that the binding pockets are capable of recognizing this anion relative to other carboxylates through favorable coordination. Interestingly, a similarly functionalized 2D material that lacks the homogeneous porosity of mesoporous solids showed a very poor response. A solid containing mannose as the binding site and a boronic acid dye as the indicator was also prepared by similar protocols for the chromogenic sensing of borate in water.

Having presented several examples of sensing ensembles that utilize 3D hybrid materials, we will conclude with a related yet somewhat unique system that shows that there is still plenty of room for the design of novel hetero-supramolecular ensembles for specific applications. The system is based on silica nanotubes which are able to recognize estrone, with imprinting methodologies used to tailor both the shape and size of specific recognition sites (Figure 30).[109] Com-

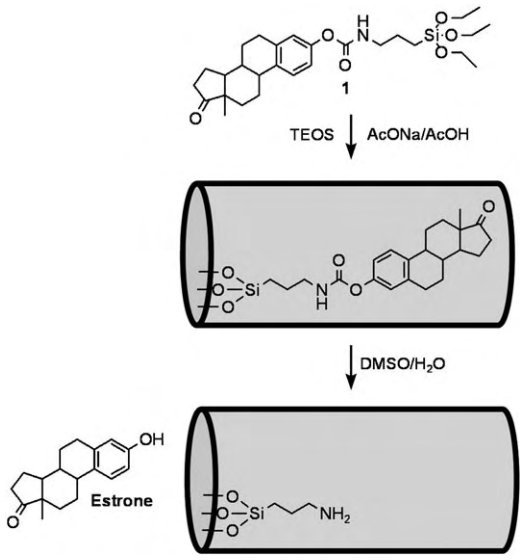


***Figure 30.*** Molecular imprinting of silica nanotubes for the recognition of estrone.

pound **1** was synthesized and used to generate imprinted silica nanotubes within the pores of alumina membranes by using sol–gel methodologies. The estrone template could be easily removed from the nanotubes by heating in $DMSO/H_2O$ solution, thereby leaving pockets with optimum selectivity for estrone binding. The imprinted membranes of silica nanotube showed selective estrone extraction in the presence of testosterone propionate (a structural analogue of estrone). The porosity and the wall size of the nanotubes also have a favorable effect on the diffusion times of the estrone into the imprinted binding pockets.

## 5. Conclusions and Outlook

In this Review, we have described and discussed selected examples of novel supramolecular functions that arise from a combination of suitable organic molecules and preorganized or preexisting nanoscopic supports, linked in a covalent manner. The 2D systems presented in the first sections are basically distinguished by improved features of classical supramolecular functions (such as molecular recognition or signaling). Besides application in catalysis (not discussed here), such hybrid materials will in future be mainly developed for the field of (bio)chemical analysis,[110] especially for anions, organic molecules, or other analytes with weak binding forces. The potential for systems based on gold nanoparticles as well as quantum dots for sensing purposes lies in the adjustment of the optical properties of the inorganic particles and the attached dye units as well as the exploitation of guest-modulated photonic or energetic interaction between the two components. Moreover, it remains to be investigated whether the collective enhancement of a signal can also be achieved with ensembles consisting of fluorophores attached to optically silent matrices. Up to now, all of these examples only show cooperative quenching phenomena. Enhanced signals, however, would be more advantageous in terms of specificity and sensitivity. It is envisaged that strategies adopted from light-harvesting or energy-transfer arrays or cascades might bring new advances here. From another perspective, the first example of luminol-cofunctionalized gold nanoparticles has recently introduced electrochemiluminescence as a further signaling mode for hybrid functional materials.[111]

Despite the multitude of chemical functionalities available from traditional host–guest chemistry and the modularity of their construction, nanomechanical devices and nanofabrication strategies are still only in their infancy. We have introduced various concepts for the controlled assembly and disassembly of hybrid materials. Future developments will show if integration of these chemical concepts with nanoelectronics, chip technology, microarrays, or microanalytical systems will open up new and exciting prospects for miniaturization.[112]

Moving from 2D blueprints and layer-by-layer techniques to 3D preorganized solid frameworks offers further possibilities in exploring new functional hetero-supramolecular concepts for hybrid systems. Gated supramolecular chemistry with such materials will strongly influence work in the area of programmed and targeted delivery. Similar advances in the field of biochemical analysis is expected with biomimetic sensory materials. Moreover, whereas most of the examples reported up to now have utilized mesoporous silica as support, further research in the multifunctionalization of carbon nanotubes[113] should shift those materials more into focus.

The elements of control discussed in this Review are a particularly exciting and promising direction of further research. As we have shown, control is possible by optical, electrochemical, chemical, thermal, and magnetic means and can induce a variety of functions from directed switching to changes in size. We anticipate that progress in the functional control of hybrid ensembles will stimulate scientists to reach new degrees of sophistication for processes such as fabrication, mechanics, directed transport, sensing, and delivery at the nanometric level. Finally, what distinguishes all these described functionalities and renders them attractive is the

 © 2006 Wiley-VCH Verlag GmbH & Co. KGaA, Weinheim 

appearance of specifically improved synergistic functional effects that are difficult to achieve using molecular-based systems or nanostructured solids alone.

*This work was supported by the Ministerio de Ciencia y Tecnología (MAT2003-08568-C03-02), the Ministerio de Educación y Ciencia (Ramón y Cajal contract to F.S.), the Alexander-von-Humboldt Stiftung (Research Fellowship to A.B.D.), and the Bundesministerium für Wirtschaft und Arbeit (K.H., within BMWA VI A2-17/03).*

Received: February 24, 2006

[1] K. E. Drexler, *Engines of Creation*, Anchor Books/Doubleday, **1986**; electronic version: http://www.foresight.org/EOC/.
[2] R. P. Feynman, *Eng. Sci.* **1960**, *23*, 22–26, 30, 34, and 36; electronic version: http://www.zyvex.com/nanotech/feynman.html.
[3] J.-M. Lehn, *Supramolecular Chemistry: Concepts and Perspectives*, VCH, Weinheim, **1995**.
[4] For a comprehensive introduction to the "bottom-up" and "top-down" approaches of nanochemistry and nanophysics, see G. A. Ozin, *Adv. Mater.* **1992**, *4*, 612–649. This report also provides a comprehensive review of the early work in the field.
[5] *Top. Curr. Chem.* **2005**, *262*, 1–277 (Ed.: T. R. Kelly); B. W. Purse, J. Rebek, Jr., *Proc. Natl. Acad. Sci. USA* **2005**, *102*, 10777–10782; A. C. Grimsdale, K. Müllen, *Angew. Chem.* **2005**, *117*, 5732–5772; *Angew. Chem. Int. Ed.* **2005**, *44*, 5592–5629.
[6] S. Uppuluri, L. T. Piehler, J. Li, D. R. Swanson, G. L. Hagnauer, D. A. Tomalia, *Adv. Mater.* **2000**, *12*, 796–800; K. Haupt, *Chem. Commun.* **2003**, 171–178.
[7] *Microporous Mesoporous Mater.* **2004**, *73*, 1–108 (Eds.: S. Kaskel, F. Schüth, M. Stöcker).
[8] S. Kitagawa, R. Kitaura, S. Noro, *Angew. Chem.* **2004**, *116*, 2388–2430; *Angew. Chem. Int. Ed.* **2004**, *43*, 2334–2375.
[9] M. Antonietti, G. A. Ozin, *Chem. Eur. J.* **2004**, *10*, 28–41.
[10] *Encyclopedia of Supramolecular Chemistry*, *Vols. 1, 2* (Ed.: J. L. Atwood, J. W. Steed), Taylor & Francis Group, New York, **2004**, **2005**.
[11] S. Onclin, B. J. Ravoo, D. N. Reinhoudt, *Angew. Chem.* **2005**, *117*, 6438–6462; *Angew. Chem. Int. Ed.* **2005**, *44*, 6282–6304; A. Vinu, K. Z. Hossain, K. Ariga, *J. Nanosci. Nanotechnol.* **2005**, *5*, 347–371; D. M. Ford, E. E. Simanek, D. F. Shantz, *Nanotechnology* **2005**, *16*, S458–S475; D. Brühwiler, G. Calzaferri, *Microporous Mesoporous Mater.* **2004**, *72*, 1–23; S. Banerjee, M. G. C. Kahn, S. S. Wong, *Chem. Eur. J.* **2003**, *9*, 1898–1908.
[12] N. L. Rosi, C. A. Mirkin, *Chem. Rev.* **2005**, *105*, 1547–1562; E. Katz, I. Willner, *Angew. Chem.* **2004**, *116*, 6166–6235; *Angew. Chem. Int. Ed.* **2004**, *43*, 6042–6108.
[13] M. Sarikaya, C. Tamerler, A. K.-Y. Jen, K. Schulten, F. Baneyx, *Nat. Mater.* **2003**, *2*, 577–585; J. Wengel, *Org. Biomol. Chem.* **2004**, *2*, 277–280.
[14] Selected recent examples of functional hybrid nanoscopic materials: A. Verma, V. M. Rotello, *Chem. Commun.* **2005**, 303–312; U. Drechsler, B. Erdogan, V. M. Rotello, *Chem. Eur. J.* **2004**, *10*, 5570–5579; G. Cooke, *Angew. Chem.* **2003**, *115*, 5008–5018; *Angew. Chem. Int. Ed.* **2003**, *42*, 4860–4870.
[15] M. Brust, M. Walker, D. Bethell, D. J. Schiffrin, R. Whyman, *J. Chem. Soc. Chem. Commun.* **1994**, 801–802.
[16] M. J. Hostetler, J. E. Wingate, C.-J. Zhong, J. E. Harris, R. W. Vachet, M. R. Clark, J. D. Londono, S. J. Green, J. J. Stokes, G. D. Wignall, G. L. Glish, M. D. Porter, N. D. Evans, R. W. Murray, *Langmuir* **1998**, *14*, 17–30.
[17] U. Kreibig, M. Vollmer, *Optical Properties of Metal Clusters*, Springer, Berlin, **1998**; M.-C. Daniel, D. Astruc, *Chem. Rev.* **2004**, *104*, 293–346.
[18] Recent advances in sensor functionalization of SAMs or thin-film objects: F. Schreiber, *J. Phys. Condens. Matter* **2004**, *16*, R881-R900; J. J. Gooding, F. Mearns, W. Yang, J. Liu, *Electroanalysis* **2003**, *15*, 81–96; S. Flink, F. C. J. M. van Veggel, D. N. Reinhoudt, *Adv. Mater.* **2000**, *12*, 1315–1328.
[19] R. C. Major, X.-Y. Zhu, *J. Am. Chem. Soc.* **2003**, *125*, 8454–8455.
[20] D. Astruc, M.-C. Daniel, J. Ruiz, *Chem. Commun.* **2004**, 2637–2649.
[21] A. Labande, D. Astruc, *Chem. Commun.* **2000**, 1007–1008; A. Labande, J. Ruiz, D. Astruc, *J. Am. Chem. Soc.* **2002**, *124*, 1782–1789.
[22] a) M.-C. Daniel, J. Ruiz, S. Nlate, J. Palumbo, D. Astruc, J.-C. Blais, *Chem. Commun.* **2001**, 2000–2001; b) M.-C. Daniel, J. Ruiz, S. Nlate, J.-C. Blais, D. Astruc, *J. Am. Chem. Soc.* **2003**, *125*, 2617–2628.
[23] Introducing the dendritic structures to the AuNPs did not increase these figures significantly, which indicates that a further degree of complexity does not necessarily improve the performance of such hybrid systems. Sufficient proximity of the amidoferrocenyl moieties seems to be the decisive key parameter.
[24] P. D. Beer, D. P. Cormode, J. J. Davis, *Chem. Commun.* **2004**, 414–415.
[25] A. Arduini, D. Demuru, A. Pochini, A. Secchi, *Chem. Commun.* **2005**, 645–647.
[26] T. R. Tshikhudo, D. Demuru, Z. Wang, M. Brust, A. Secchi, A. Arduini, A. Pochini, *Angew. Chem.* **2005**, *117*, 2973–2976; *Angew. Chem. Int. Ed.* **2005**, *44*, 2913–2916.
[27] a) A. B. Descalzo, D. Jiménez, M. D. Marcos, R. Martínez-Máñez, J. Soto, J. El Haskouri, C. Guillem, D. Beltrán, P. Amorós, M. V. Borrachero, *Adv. Mater.* **2002**, *14*, 966–969; b) A. B. Descalzo, M. D. Marcos, R. Martínez-Máñez, J. Soto, D. Beltrán, P. Amorós, *J. Mater. Chem.* **2005**, *15*, 2721–2731.
[28] A dependence of the measured signal on the binding/signaling units in the presence of analytes has also been found in part for several amidoferrocenyl–AuNP combinations and certain target anions. Since this problem is nontrivial and nongeneral, the reader is referred to the original publications for further details.[21] However, according to Astruc and co-workers, such difficulties can be circumvented when using the dendronized systems.[22b]
[29] Similar observations have been made for hybrid optical materials that contain fluorophores but do not exhibit any other explicit function, see M. Ganschow, M. Wark, D. Wöhrle, G. Schulz-Ekloff, *Angew. Chem.* **2000**, *112*, 167–170; *Angew. Chem. Int. Ed.* **2000**, *39*, 160–163.
[30] A. Callegari, M. Marcaccio, D. Paolucci, F. Paolucci, N. Tagmatarchis, D. Tasis, E. Vázquez, M. Prato, *Chem. Commun.* **2003**, 2576–2577.
[31] A. K. Boal, V. M. Rotello, *J. Am. Chem. Soc.* **2000**, *122*, 734–735.
[32] A. K. Boal, V. M. Rotello, *J. Am. Chem. Soc.* **1999**, *121*, 4914–4915.
[33] A. K. Boal, V. M. Rotello, *J. Am. Chem. Soc.* **2002**, *124*, 5019–5024.
[34] R. Martínez-Máñez, F. Sancenón, *Chem. Rev.* **2003**, *103*, 4419–4476; P. D. Beer, P. A. Gale, *Angew. Chem.* **2001**, *113*, 502–532; *Angew. Chem. Int. Ed.* **2001**, *40*, 486–516.
[35] J. F. Callan, A. P. de Silva, D. C. Magri, *Tetrahedron* **2005**, *61*, 8551–8588; B. Valeur, I. Leray, *Coord. Chem. Rev.* **2000**, 205, 3–40.
[36] G. J. Mohr, *Sens. Actuators B* **2005**, *107*, 2–13; G. J. Mohr, *Chem. Eur. J.* **2004**, *10*, 1082–1090.

 © 2006 Wiley-VCH Verlag GmbH & Co. KGaA, Weinheim 

[37] To our knowledge, no report has yet appeared where the modulation of both signals occurs upon the supramolecular event or has been exploited for sensing or signaling purposes. For a more detailed account on the photophysics of AuNP–chromophore conjugates, see: K. G. Thomas, P. V. Kamat, *Acc. Chem. Res.* **2003**, *36*, 888 – 898.

[38] C. Burda, X. Chen, R. Narayanan, M. A. El-Sayed, *Chem. Rev.* **2005**, *105*, 1025 – 1102; J. Stangl, V. Holý, G. Bauer, *Rev. Mod. Phys.* **2004**, *76*, 725 – 783.

[39] X. Michalet, F. F. Pinaud, L. A. Bentolila, J. M. Tsay, S. Doose, J. J. Li, G. Sundaresan, A. M. Wu, S. S. Gambhir, S. Weiss, *Science* **2005**, *307*, 538 – 544; I. L. Mednitz, H. T. Uyeda, E. R. Goldman, H. Mattoussi, *Nat. Mater.* **2005**, *4*, 435 – 446.

[40] For a comprehensive introduction to the underlying mechanistics, see A. N. Shipway, E. Katz, I. Willner, *ChemPhysChem* **2000**, *1*, 18 – 52.

[41] A. A. Lazarides, G. C. Schatz, *J. Phys. Chem. B* **2000**, *104*, 460 – 467; A. A. Lazarides, G. C. Schatz, *J. Chem. Phys.* **2000**, *112*, 2987 – 2993; J. J. Storhoff, A. A. Lazarides, R. C. Mucic, C. A. Mirkin, R. L. Letsinger, G. C. Schatz, *J. Am. Chem. Soc.* **2000**, *122*, 4640 – 4650.

[42] AuNPs possess extremely high molar absorptivities in the visible region (for example, $7.5 \times 10^7\,\text{M}^{-1}\,\text{cm}^{-1}$ at 520 nm and $4.7 \times 10^9\,\text{M}^{-1}\,\text{cm}^{-1}$ at 524 nm for 8- and 13-nm-diameter particles), see R. C. Mucic, J. J. Storhoff, C. A. Mirkin, R. L. Letsinger, *J. Am. Chem. Soc.* **1998**, *120*, 12674 – 12675.

[43] Y. Kim, R. C. Johnson, J. T. Hupp, *Nano Lett.* **2001**, *1*, 165 – 167.

[44] J. Liu, Y. Lu, *J. Am. Chem. Soc.* **2003**, *125*, 6642 – 6643.

[45] S. O. Obare, R. E. Hollowell, C. J. Murphy, *Langmuir* **2002**, *18*, 10407 – 10410.

[46] S.-Y. Lin, S.-W. Liu, C.-M. Lin, C.-H. Chen, *Anal. Chem.* **2002**, *74*, 330 – 335.

[47] S. Y. Lin, C. H. Chen, M. C. Lin, H. F. Hsu, *Anal. Chem.* **2005**, *77*, 4821 – 4828.

[48] S. Watanabe, M. Sonobe, M. Arai, Y. Tazume, T. Matsuo, T. Nakamura, K. Yoshida, *Chem. Commun.* **2002**, 2866 – 2867.

[49] Y. Kubo, S. Uchida, Y. Kemmochi, T. Okubo, *Tetrahedron Lett.* **2005**, *46*, 4369 – 4372.

[50] Y. Chen, Z. Rosenzweig, *Anal. Chem.* **2002**, *74*, 5132 – 5138.

[51] A. V. Isarov, J. Chrysochoos, *Langmuir* **1997**, *13*, 3142 – 3149.

[52] K. M. Gattás-Asfura, R. M. Leblanc, *Chem. Commun.* **2003**, 2684 – 2685.

[53] M. Montalti, L. Prodi, N. Zacheronni, G. Falini, *J. Am. Chem. Soc.* **2002**, *124*, 13540 – 13546.

[54] M. Montalti, L. Prodi, N. Zaccheroni, *J. Mater. Chem.* **2005**, *15*, 2810 – 2814.

[55] V. Balzani, P. Ceroni, S. Gestermann, C. Kauffmann, M. Gorka, F. Vögtle, *Chem. Commun.* **2000**, 853 – 854; F. Vötgle, S. Gestermann, C. Kauffmann, P. Ceroni, V. Vicinelli, V. Balzani, *J. Am. Chem. Soc.* **2000**, *122*, 10398 – 10404.

[56] K. Rurack, *Spectrochim. Acta Part A* **2001**, *57*, 2161 – 2195.

[57] V. Balzani, P. Ceroni, M. Maestri, V. Vicinelli, *Curr. Opin. Chem. Biol.* **2003**, *7*, 657 – 665.

[58] E. Brasola, F. Mancin, E. Rampazzo, P. Tecilla, U. Tonellato, *Chem. Commun.* **2003**, 3026 – 3027.

[59] E. Rampazzo, E. Brasola, S. Marcuz, F. Mancin, P. Tecilla, U. Tonellato, *J. Mater. Chem.* **2005**, *15*, 2687 – 2696.

[60] R. Méallet-Renault, R. Pansu, S. Amigoni-Gerbier, C. Larpent, *Chem. Commun.* **2004**, 2344 – 2345; J. M. Kürner, O. S. Wolfbeis, I. Klimant, *Anal. Chem.* **2002**, *74*, 2151 – 2156.

[61] E. L. Doyle, C. A. Hunter, H. C. Philips, S. J. Webb, N. H. Williams, *J. Am. Chem. Soc.* **2003**, *125*, 4593 – 4599; P. Grandini, F. Mancin, P. Tecilla, P. Scrimin, U. Tonellato, *Angew. Chem.* **1999**, *111*, 3247 – 3250; *Angew. Chem. Int. Ed.* **1999**, *38*, 3061 – 3064.

[62] L. Basabe-Desmonts, J. Beld, R. S. Zimmerman, J. Hernando, P. Mela, M. F. García Parajó, N. F. van Hulst, A. van den Berg, D. N. Reinhoudt, M. Crego-Calama, *J. Am. Chem. Soc.* **2004**, *126*, 7293 – 7299; M. Crego-Calama, D. N. Reinhoudt, *Adv. Mater.* **2001**, *13*, 1171 – 1174.

[63] Y. Zheng, J. Orbulescu, X. Ji, F. M. Andreopoulos, S. M. Pham, R. M. Leblanc, *J. Am. Chem. Soc.* **2003**, *125*, 2680 – 2686.

[64] B. I. Ipe, S. Mahima, K. G. Thomas, *J. Am. Chem. Soc.* **2003**, *125*, 7174 – 7175.

[65] C. J. Hawker, K. L. Wooley, *Science* **2005**, *309*, 1200 – 1205; U. Hahn, M. Elhabiri, A. Trabolsi, H. Herschbach, E. Leize, A. van Dorsselaer, A.-M. Albrecht-Gary, J.-F. Nierengarten, *Angew. Chem.* **2005**, *117*, 5472 – 5475; *Angew. Chem. Int. Ed.* **2005**, *44*, 5338 – 5341; H. C. Kolb, M. G. Finn, K. B. Sharpless, *Angew. Chem.* **2001**, *113*, 2056 – 2075; *Angew. Chem. Int. Ed.* **2001**, *40*, 2004 – 2021.

[66] R. Vilar, *Struct. Bonding (Berlin)* **2004**, *111*, 85 – 137.

[67] D. N. Reinhoudt, M. Crego-Calama, *Science* **2002**, *295*, 2403 – 2407.

[68] Only recently, Ercolani raised new doubts that cooperative effects are one of the main driving forces in classical supramolecular self-assembled structures, see G. Ercolani, *J. Am. Chem. Soc.* **2003**, *125*, 16097 – 16103.

[69] J. Liu, J. Alvarez, W. Ong, A. E. Kaifer, *Nano Lett.* **2001**, *1*, 57 – 60.

[70] D. L. Feldheim, C. D. Keating, *Chem. Soc. Rev.* **1998**, *27*, 1 – 12.

[71] Y. Liu, H. Wang, Y. Chen, C. F. Ke, M. Liu, *J. Am. Chem. Soc.* **2005**, *127*, 657 – 666.

[72] O. Crespo-Biel, A. Jukovic, M. Karlsson, D. N. Reinhoudt, J. Huskens, *Isr. J. Chem.* **2005**, *45*, 353 – 362.

[73] A. Mulder, J. Huskens, D. N. Reinhoudt, *Org. Biomol. Chem.* **2004**, *2*, 3409 – 3424.

[74] K. Naka, H. Roh, Y. Chujo, *Langmuir* **2003**, *19*, 5496 – 5501.

[75] F. Corbellini, A. Mulder, A. Sartori, M. J. W. Ludden, A. Casnati, R. Ungaro, J. Huskens, M. Crego-Calama, D. N. Reinhoudt, *J. Am. Chem. Soc.* **2004**, *126*, 17050 – 17058.

[76] O. Crespo-Biel, B. Dordi, D. N. Reinhoudt, J. Huskens, *J. Am. Chem. Soc.* **2005**, *127*, 7594 – 7600.

[77] M. Wanunu, R. Popovitz-Biro, H. Cohen, A. Vaskevich, I. Rubinstein, *J. Am. Chem. Soc.* **2005**, *127*, 9207 – 9215.

[78] M. Morisue, S. Yamatsu, N. Haruta, Y. Kobuke, *Chem. Eur. J.* **2005**, *11*, 5563 – 5574.

[79] S. Onclin, J. Huskens, B. J. Ravoo, D. N. Reinhoudt, *Small* **2005**, *1*, 852 – 857.

[80] T. Auletta, B. Dordi, A. Mulder, A. Sartori, S. Onclin, C. M. Bruinink, M. Péter, C. A. Nijhuis, H. Beijleveld, H. Schönherr, G. J. Vancso, A. Casnati, R. Ungaro, B. J. Ravoo, J. Huskens, D. N. Reinhoudt, *Angew. Chem.* **2004**, *116*, 373 – 377; *Angew. Chem. Int. Ed.* **2004**, *43*, 369 – 373; A. Mulder, S. Onclin, M. Péter, J. P. Hoogenboom, H. Beijleveld, J. ter Maat, M. F. García-Parajó, B. J. Ravoo, J. Huskens, N. F. van Hulst, D. N. Reinhoudt, *Small* **2005**, *1*, 242 – 253.

[81] Y. Xia, G. M. Whitesides, *Angew. Chem.* **1998**, *110*, 568 – 594; *Angew. Chem. Int. Ed.* **1998**, *37*, 550 – 575.

[82] S. Samitsu, T. Shimomura, K. Ito, M. Hara, *Appl. Phys. Lett.* **2004**, *85*, 3875 – 3877.

[83] I. A. Banerjee, L. Yu, H. Matsui, *J. Am. Chem. Soc.* **2003**, *125*, 9542 – 9543.

[84] Y.-F. Chen, I. A. Banerjee, L. Yu, R. Djalali, H. Matsui, *Langmuir* **2004**, *20*, 8409 – 8413.

[85] M. R. Bryce, G. Cooke, F. M. A. Duclairoir, P. John, D. F. Perepichka, N. Polwart, V. M. Rotello, J. F. Stoddart, H. R. Tseng, *J. Mater. Chem.* **2003**, *13*, 2111 – 2117.

[86] T. J. Huang, B. Brough, C.-M. Ho, Y. Liu, A. H. Flood, P. A. Bonvallet, H.-R. Tseng, J. F. Stoddart, M. Baller, S. Magonov, *Appl. Phys. Lett.* **2004**, 85, 5391 – 5393; Y. Liu, A. H. Flood, P. A. Bonvallet, S. A. Vignon, B. H. Northrop, H.-R. Tseng, J. O. Jeppesen, T. J. Huang, B. Brough, M. Baller, S. Magonov,

 © 2006 Wiley-VCH Verlag GmbH & Co. KGaA, Weinheim 

S. D. Solares, W. A. Goddard, C.-M. Ho, J. F. Stoddart, *J. Am. Chem. Soc.* **2005**, *127*, 9745 – 9759.
[87] Y. Shirai, A. J. Osgood, Y. Zhao, K. F. Kelly, J. M. Tour, *Nano Lett.* **2005**, *5*, 2330 – 2334.
[88] N. K. Mal, M. Fujiwara, Y. Tanaka, *Nature* **2003**, *421*, 350 – 353; N. K. Mal, M. Fujiwara, Y. Tanaka, T. Taguchi, M. Matsukata, *Chem. Mater.* **2003**, *15*, 3385 – 3394.
[89] R. Casasús, M. D. Marcos, R. Martínez-Máñez, J. V. Ros-Lis, J. Soto, L. A. Villaescusa, P. Amorós, D. Beltrán, C. Guillem, J. Latorre, *J. Am. Chem. Soc.* **2004**, *126*, 8612 – 8613.
[90] J. V. Ros-Lis, B. García-Acosta, D. Jiménez, R. Martínez-Máñez, F. Sancenón, J. Soto, F. Gonzalvo, M. C. Valldecabres, *J. Am. Chem. Soc.* **2004**, *126*, 4064 – 4065.
[91] Q. Yang, S. Wang, P. Fan, L. Wang, Y. Di, K. Lin, F.-S. Xiao, *Chem. Mater.* **2005**, *17*, 5999 – 6003.
[92] R. Hernandez, H.-R. Tseng, J. W. Wong, J. F. Stoddart, J. I. Zink, *J. Am. Chem. Soc.* **2004**, *126*, 3370 – 3371.
[93] T. D. Nguyen, H. R. Tseng, P. C. Celestre, A. H. Flood, Y. Liu, J. F. Stoddart, J. I. Zink, *Proc. Natl. Acad. Sci. USA* **2005**, *102*, 10029 – 10034.
[94] C.-Y. Lai, B. G. Trewyn, D. M. Jeftinija, K. Jeftinija, S. Xu, S. Jeftinija, V. S.-Y. Lin, *J. Am. Chem. Soc.* **2003**, *125*, 4451 – 4459.
[95] J. A. Gruenhagen, C. Y. Lai, D. R. Radu, V. S.-Y. Lin, E. S. Yeung, *Appl. Spectrosc.* **2005**, *59*, 424 – 431.
[96] S. Giri, B. G. Trewyn, M. P. Stellmaker, V. S.-Y. Lin, *Angew. Chem.* **2005**, *117*, 5166 – 5172; *Angew. Chem. Int. Ed.* **2005**, *44*, 5038 – 5044.
[97] P. Nednoor, N. Chopra, V. Gavalas, L. G. Bachas, B. J. Hinds, *Chem. Mater.* **2005**, *17*, 3595 – 3599.
[98] N. Sakai, J. Mareda, S. Matile, *Acc. Chem. Res.* **2005**, *38*, 79 – 87; Y. Umezawa, H. Aoki, *Anal. Chem.* **2004**, *76*, 320 A – 326 A; G. W. Gokel, A. Mukhopadhyay, *Chem. Soc. Rev.* **2001**, *30*, 274 – 286.
[99] N. Liu, Z. Chen, D. R. Dunphy, Y.-B. Jiang, R. A. Assink, C. J. Brinker, *Angew. Chem.* **2003**, *115*, 1773 – 1776; *Angew. Chem. Int. Ed.* **2003**, *42*, 1731 – 1734.
[100] N. G. Liu, D. R. Dunphy, P. Atanassov, S. D. Bunge, Z. Chen, G. P. Lopez, T. J. Boyle, C. J. Brinker, *Nano Lett.* **2004**, *4*, 551 – 554.
[101] Q. Fu, G. V. R. Rao, L. K. Ista, Y. Wu, B. P. Andrzejewski, L. A. Sklar, T. L. Ward, G. P. López, *Adv. Mater.* **2003**, *15*, 1262 – 1266.
[102] W. X. Zheng, M. M. Maye, F. L. Leibowitz, C. J. Zhong, *Analyst* **2000**, *125*, 17 – 20; W. X. Zheng, M. M. Maye, F. L. Leibowitz, C. J. Zhong, *Anal. Chem.* **2000**, *72*, 2190 – 2199.
[103] V. S.-Y. Lin, C.-Y. Lai, J. Huang, S.-A Song, S. Xu, *J. Am. Chem. Soc.* **2001**, *123*, 11510 – 11511.
[104] D. R. Radu, C.-Y. Lai, J. W. Wiench, M. Pruski, V. S.-Y. Lin, *J. Am. Chem. Soc.* **2004**, *126*, 1640 – 1641.
[105] A. B. Descalzo, K. Rurack, H. Weisshoff, R. Martínez-Máñez, M. D. Marcos, P. Amorós, K. Hoffmann, J. Soto, *J. Am. Chem. Soc.* **2005**, *127*, 184 – 200.
[106] M. Comes, M. D. Marcos, R. Martínez-Máñez, F. Sancenón, J. Soto, L. A. Villaescusa, P. Amorós, D. Beltrán, *Adv. Mater.* **2004**, *16*, 1783 – 1786.
[107] K. Inumaru, Y. Inoue, S. Kakii, T. Nakano, S. Yamanaka, *Chem. Lett.* **2003**, *32*, 1110 – 1111; K. Inumaru, Y. Inoue, S. Kakii, T. Nakano, S. Yamanaka, *Phys. Chem. Chem. Phys.* **2004**, *6*, 3133 – 3139.
[108] M. Comes, G. Rodríguez-López, M. D. Marcos, R. Martínez-Máñez, F. Sancenón, J. Soto, L. A. Villaescusa, P. Amorós, D. Beltrán, *Angew. Chem.* **2005**, *117*, 2978 – 2982; *Angew. Chem. Int. Ed.* **2005**, *44*, 2918 – 2922.
[109] H.-H. Yang, S.-Q. Zhang, W. Yang, X.-L. Chen, Z.-X. Zhuang, J.-G. Xu, X.-R. Wang, *J. Am. Chem. Soc.* **2004**, *126*, 4054 – 4055.
[110] A. P. R. Johnston, B. J. Battersby, G. A. Lawrie, M. Trau, *Chem. Commun.* **2005**, 848 – 850.
[111] S. Roux, B. Garcia, J.-L. Bridot, M. Salomé, C. Marquette, L. Lemelle, P. Gillet, L. Blum, P. Perriat, O. Tillement, *Langmuir* **2005**, *21*, 2526 – 2536.
[112] D. Diamond, *Anal. Chem.* **2004**, *76*, 279A – 286A; P. M. Mendes, A. H. Flood, J. F. Stoddart, *Appl. Phys. A* **2005**, *80*, 1197 – 1209.
[113] W. Wu, S. Wieckowski, G. Pastorin, M. Benincasa, C. Klumpp, J.-P. Briand, R. Gennaro, M. Prato, A. Bianco, *Angew. Chem.* **2005**, *117*, 6516 – 6520; *Angew. Chem. Int. Ed.* **2005**, *44*, 6358 – 6362.

 © 2006 Wiley-VCH Verlag GmbH & Co. KGaA, Weinheim 

NMR Spectroscopy

DOI: 10.1002/anie.200601622

# Simplified Analysis of Mixtures of Small Molecules by Chromatographic NMR Spectroscopy**

*Guilhem Pages,* Corinne Delaurent, and Stefano Caldarelli*

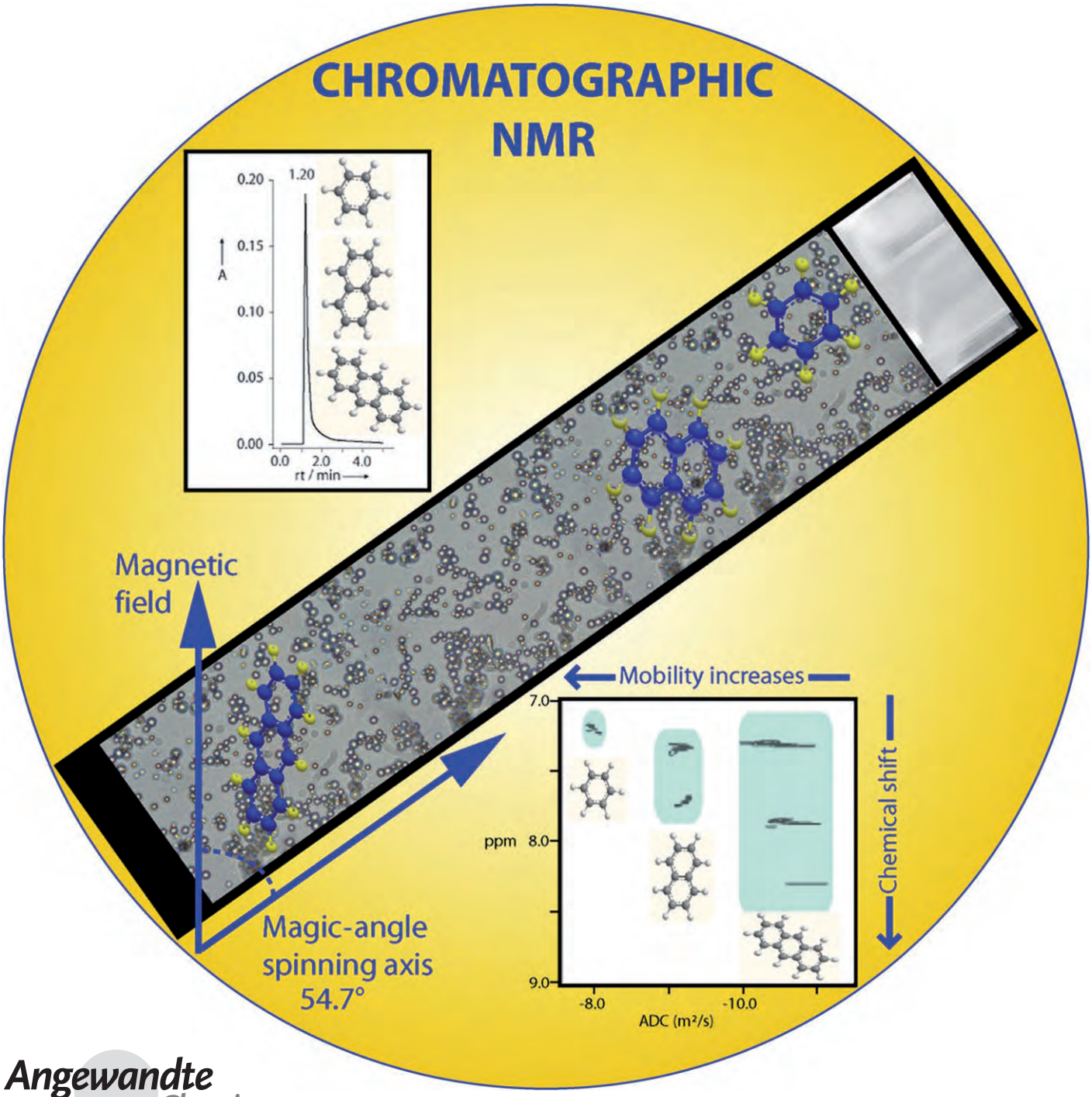




WILEY InterScience DISCOVER SOMETHING GREAT

© 2006 Wiley-VCH Verlag GmbH & Co. KGaA, Weinheim

The determination of the components of assemblies of small molecules is an extremely common task in chemical laboratories, and HPLC is the preferred technique for separation and analysis of complex mixtures. A wide variety of sophisticated functionalized chromatographic solid supports has been developed (octadecylsilyl (ODS), cyano, amino) and adapted to different analytical problems. Recently, we introduced an alternative for the identification of the components in a mixture, without any chromatography involved, by using solid-enhanced diffusion-based NMR spectroscopy.[1,2] The method mimics a part of the chromatographic process in that the molecular average mobilities in the mixture are modified according to the individual affinities for the stationary phase. This enhances the spectral-separation capabilities of diffusion-based pulsed field gradient (PFG) experiments, such as DOSY.[3] Herein we show that, at least in favorable cases, this technique can provide a simpler approach to mixture analysis, yielding separation of the spectral components by using simple solid supports, such as regular porous silica gels.

A homologous series of aromatic compounds (benzene, naphthalene, and anthracene) was used as the test mixture. The usual procedure for chromatographic separation for this kind of compound requires reversed-phase (RP) partition chromatography, using ODS-functionalized silica and an organic/water mixture as the mobile phase (Figure 1a). Aromatic moieties are also known to interact with untreated silica gels because they are electron donor moieties and bare silica is an electron acceptor moiety.[4] However, on silica gel and using the same eluent conditions as for RPLC, namely an acetonitrile/water mixture, no solute separation is recorded on the chromatogram (Figure 1b). Direct-phase liquid chromatography also does not separate aromatic molecules.

Molecular diffusion coefficients can be measured by NMR spectroscopy by using PFG.[5–7] In fact, the molecular mobility has long been exploited in NMR spectroscopy as an independent dimension, as exemplified by the DOSY approach, which correlates the NMR spectrum on one dimension and the associated self-diffusion rates on a second dimension. The resulting layout is reminiscent of TLC. The enhanced performance of this application of high-resolution magic-angle spinning (HRMAS)–DOSY NMR spectroscopy[1] descends from the addition of a solid chromatographic support to the mixture. Selective affinity for the solids varies according to the molecular mobility and results in improvement in the resolution. Experiments were performed under HRMAS[8] conditions in which the $^1$H NMR spectrum is recorded while spinning the sample oriented at the so-called magic angle with respect to the magnetic field. Relatively fast spinning rates are easily achieved by current technology and induces averaging of magnetic susceptibility broadening and other sources of decreased resolution of the spectrum.[9] Consequently, the NMR proton spectrum of the mixture thus obtained has a spectral quality close, although still reduced, to the one recorded without the solid phase. In Figure 2, we analyze the performance of this method in terms of separation of the spectral components. ODS-substituted silica (Figure 2a) provides a satisfactory separation of the peaks. An increase in the apparent-diffusion-coefficient (ADC) logarithm is equivalent to a decrease in the HPLC

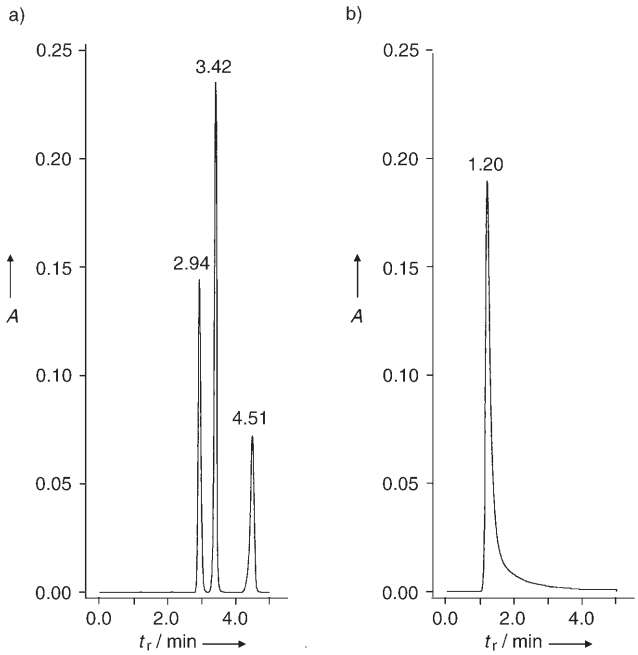


***Figure 1.*** Aromatic homologous mixture chromatogram on a) an ODS column and b) a silica gel stationary phase. Eluent: acetonitrile/water, (90/10, v/v). Length of columns 250×4 mm. Flow rate 1.0 mL min$^{-1}$. Detection wavelength: 254 nm. $t_r$ = retention time.

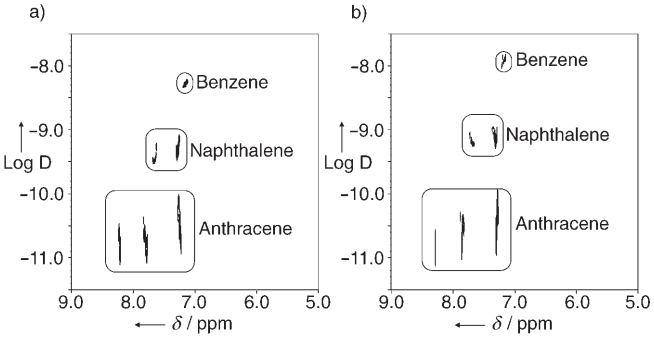


***Figure 2.*** $^1$H DOSY NMR spectra of an aromatic homologous series in acetonitrile/water (90/10, v/v) a) with an ODS chromatographic stationary phase and b) with a bare silica gel. D = apparent diffusion coefficient.

[*] G. Pages, Dr. C. Delaurent, Prof. S. Caldarelli
JE 2421 TRACES
Universités de Provence et Paul Cézanne Aix-Marseille I et III
Site de Saint Jérôme, Case 512
Avenue Escadrille Normandie-Niemen
13397 Marseille Cedex 20 (France)
Fax: (+33) 491-282-897
E-mail: guilhem.pages@univ-cezanne.fr

[**] This study was supported in part by a grant from the French Conseil Régional Provence-Alpes-Côte-d'Azur and the Pharmaceutical Laboratory DistriB3 (Marseille, France). We thank VWR International France for providing all chromatographic stationary phases used herein.

 © 2006 Wiley-VCH Verlag GmbH & Co. KGaA, Weinheim 

retention time. The NMR spectroscopy retention scale obtained is therefore consistent with RPLC: benzene is "eluted" first then naphthalene and, finally, anthracene with a good resolution in both HPLC and NMR spectroscopy methods. The surprising outcome of a similar analysis performed by using bare silica gel (Figure 2b) is that a separative quality that is comparable to RP conditions is achieved. Indeed, about the same ADCs were measured and the diffusion resolution is in the same order of magnitude as with ODS chromatographic stationary phase, whereas in LC no separation was observed between these molecules on bare silica.

The NMR spectroscopy result is all the more surprising as the acetonitrile/water mixture is in competition with the aromatic molecules for adsorption on the silica gel. The differences between HPLC and the HRMAS–DOSY results must stem from the absence of flow and the higher solid-to-liquid ratio used in the NMR spectroscopy experiment. Experiments are underway to investigate further the mechanistic aspects.

This promising NMR spectroscopy method has some significant limits. The first is a technological one: only molecules that diffuse on timescales accessible with the available gradient strength (about $10^{-8}$ to $10^{-11}$ $m^2 s^{-1}$) on a conventional HRMAS probe can be observed. A first amelioration of this aspect can be achieved by using a special setup with a microimaging gradient system.[10] The necessity of good resolution in both the NMR and diffusion dimension is another limiting factor. Even under the beneficial effects of HRMAS, the line width remains broader than in solution-state NMR spectroscopy, and spectral overlap in frequency dimension may introduce artifacts in the processing. In fact, the diffusion-dimension layout is calculated by measuring an exponential decay[11] for which current day algorithms are still prone to misinterpret the results and so to produce a meaningless DOSY diagram. This blockage can surely be progressed upon as hinted by recent advances on the achievable precision of more-adapted processing methods for DOSY processing.[12,13] Moreover, it should be noted here that diffusion in the presence of porous solids may be more complex than the simple monoexponential model suggests as this behavior corresponds to a rather limited case.[14] This may partly explain the significantly worse resolution observed in our HRMAS-DOSY experiment when compared with the corresponding free liquid.

Although conceptually similar, chromatographic NMR spectroscopy and LC do not share all elementary steps, notably because of the absence of the flow of the mobile phase. The solid-induced deceleration of the tested molecules appears to be very similar in both bonded and bare silica gels. Consequently, good separation is achieved with very basic chromatographic materials, which may result in a simplification in the analysis of mixtures. As stated previously, a hint for the physical basis of this result could be provided by the affinity of aromatic molecules for silica gels. The full potential of the approach remains to be probed, but the illustration provided herein already points out a strong correspondence between chromatographic NMR spectroscopy and LC.

## Experimental Section

The chromatographic phases used were Lichrospher100 Si (5 μm) and Lichrospher100 C18 (5 μm). For the NMR spectroscopy analysis, the test mixture was benzene (90.0 $g L^{-1}$), naphthalene (9.0 $g L^{-1}$), and anthracene (1.6 $g L^{-1}$) dissolved in $CH_3CN/H_2O$ (90/10 v/v). The HRMAS rotor contained about 30 mg of chromatographic stationary phase and 10 μL of the test mixture. Roughly half of the stationary phase was introduced inside the rotor, then the solution was added and finally, the rotor was filled with the remaining part of the solid. All NMR spectroscopic experiments were performed at 400 MHz on a Bruker Avance spectrometer equipped with a $^1H$ HRMAS probe head producing magic-angle gradients with a maximum strength of 55 $G cm^{-1}$. Samples were prepared in 4 mm $ZrO_2$ rotors with a detection volume of 50 μL. The spectra were recorded at a spinning rate of 4000 Hz, at 303 K with a free induction decay containing 2 or 4 K data points. The pulse sequence used was based on the stimulated echo and incorporated bipolar gradient pulses and a longitudinal eddy current delay (BPP–LED).[15] The shape of all gradient pulses was sinusoidal. The gradients were generated through a built-in coil, which was aligned to the magic angle. No rotor synchronization was necessary. The spoil gradient pulses were 1 ms and the LED was 5 ms. The 2D diagram was realized with a gradient pulse of 2000 or 2200 μs and a diffusion time of 500 or 800 ms for the silica gel and for the bonded chromatographic stationary phase, respectively. A BPP–LED experiment was realized by using 16 different gradient values with longitudinal spacing, varying from 2 to 95% of the maximum gradient strength; for each of them 16 scans were recorded. For the processing, 128 points were represented in the diffusion dimension.

Chromatograms were recorded by using a L-6000 pump (Merck), a Jasco UV-975 detector, and a D-2500 integrator (Merck). The columns used were Lichrospher100 C18 250 × 4 mm (5 μm) and Lichrochart60 Si 250 × 4 mm (5 μm). The eluent was $CH_3CN/H_2O$ (90/10 v/v) with a flow rate of 1.0 $mL min^{-1}$. The detection wavelength was 254 nm. The test mixture was benzene (770 $mg L^{-1}$), naphthalene (90 $mg L^{-1}$), and anthracene (5 $mg L^{-1}$) dissolved in the eluent.

Received: April 25, 2006
Revised: June 20, 2006
Published online: July 26, 2006

**Keywords:** analytical methods · chromatography · diffusion · magic-angle spinning · NMR spectroscopy

[1] S. Viel, F. Ziarelli, S. Caldarelli, *Proc. Natl. Acad. Sci. USA* **2003**, *100*, 9696 – 9698.
[2] G. Pages, C. Delaurent, S. Caldarelli, *Anal. Chem.* **2006**, *78*, 561 – 566.
[3] C. S. Johnson, *Prog. Nucl. Magn. Reson. Spectrosc.* **1999**, *34*, 203 – 256.
[4] L. R. Snyder, *Principles of adsorption chromatography*, Chromatographic science series ed., Marcel Dekker, New-York, **1968**.
[5] E. O. Stejskal, J. E. Tanner, *J. Chem. Phys.* **1965**, *42*, 288 – 292.
[6] P. Stilbs, *Anal. Chem.* **1981**, *53*, 2135 – 2137.
[7] P. Stilbs, *Prog. Nucl. Magn. Reson. Spectrosc.* **1987**, *19*, 1 – 45.
[8] W. L. Fitch, G. Detre, C. P. Holmes, J. N. Shoolery, P. A. Keifer, *J. Org. Chem.* **1994**, *59*, 7955 – 7956.
[9] P. A. Keifer, L. Baltusis, D. M. Rice, A. A. Tymiak, J. N. Shoolery, *J. Magn. Reson. Ser. A* **1996**, *119*, 65 – 75.
[10] A. Pampel, K. Zick, H. Glauner, F. Engelke, *J. Am. Chem. Soc.* **2004**, *126*, 9534 – 9535.
[11] A. A. Istratov, O. F. Vyvenko, *Rev. Sci. Instrum.* **1999**, *70*, 1233 – 1257.
[12] B. Antalek, W. Windig, *J. Am. Chem. Soc.* **1996**, *118*, 10331 – 10332.

 © 2006 Wiley-VCH Verlag GmbH & Co. KGaA, Weinheim 

[13] P. Thureau, A. Thevand, B. Ancian, P. Escavabaja, G. S. Armstrong, V. A. Mandelshtam, *ChemPhysChem* **2005**, *6*, 1510 – 1513.
[14] P. T. Callaghan in *Principles of Nuclear Magnetic Resonance Microscopy*, 1st ed. (Ed.: C. Press), Oxford Science, Oxford, **1991**, pp. 344 – 350.
[15] D. H. Wu, A. D. Chen, C. S. Johnson, *J. Magn. Reson. Ser. A* **1995**, *115*, 260 – 264.

 © 2006 Wiley-VCH Verlag GmbH & Co. KGaA, Weinheim 

Al–Al Multiple Bonds

DOI: 10.1002/anie.200601925

# Synthesis and Structure of the "Dialuminyne" $Na_2[Ar'AlAlAr']$ and $Na_2[(Ar''Al)_3]$: Al–Al Bonding in $Al_2Na_2$ and $Al_3Na_2$ Clusters**

*Robert J. Wright, Marcin Brynda, and Philip P. Power**

The synthesis of $R_2AlAlR_2$ ($R = CH(SiMe_3)_2$) by Uhl in 1988 marked a key development for compounds with Group 13 metal–metal bonds because it was the first example of a stable molecule with an Al–Al bond to be structurally characterized.[1] In the early 1990s it was shown that this compound and its gallium congeners, as well as related aryl-substituted derivatives, could be reduced to afford anions of the type $[R_2MMR_2]^-$ (M = Al or Ga, $R = CH(SiMe_3)_2$[2–4] or $C_6H_2$-2,4,6-$i$Pr$_3$[5,6]), which had M–M bonds of formal order 1.5 owing to occupation of a π orbital by a single electron. Later work expanded these initial results to several other classes of Group 13 compounds with metal–metal multiple bonds,[7] including most notably the "digallyne" $Na_2[Ar^*GaGaAr^*]$ (**1**; $Ar^* = C_6H_3$-2,6-($C_6H_2$-2,4,6-$i$Pr$_3$)$_2$)[8] of Robinson and coworkers, the bonding of which has attracted considerable debate.[9] This compound has a *trans*-bent, planar C-Ga-Ga-C array, a short Ga–Ga bond length of about 2.32 Å, and a formal Ga–Ga triple bond (by analogy with alkynes). The only related Group 13 element derivative of this type is the closely related compound $Na_2[Ar'GaGaAr']$ (**2**; $Ar' = C_6H_3$-2,6-($C_6H_3$-2,6-$i$Pr$_2$)$_2$), which has very similar structural parameters to those of **1** but whose flanking aryl rings do not carry a *para*-$i$Pr substituent.[10,11]

[*] Dr. R. J. Wright, Dr. M. Brynda, Prof. P. P. Power
Department of Chemistry
University of California
One Shields Avenue, Davis, CA 95616 (USA)
Fax: (+1) 530-752-8995
E-mail: pppower@ucdavis.edu

[**] We thank the National Science Foundation for financial support. We also thank Dr. J. C. Fettinger and Dr. R. Fischer for assistance with crystallographic and NMR studies. $Ar' = C_6H_3$-2,6-($C_6H_3$-2,6-$i$Pr$_2$)$_2$; $Ar'' = C_6H_3$-2,6-($C_6H_2$-2,4,6-Me$_3$)$_2$.

Supporting information for this article is available on the WWW under http://www.angewandte.org or from the author.

Since 2000, however, work on the isoelectronic neutral Group 14 element derivatives RM′M′R (M′ = Si,[12–14] Ge,[15,16] Sn,[17] Pb;[18] R = bulky organic or silyl group) has progressed to the extent that stable homonuclear species for each member of the series have now been isolated and structurally characterized. In addition, a series of related neutral Group 13 metal Ar′MMAr′ derivatives (M = Ga,[10,11] In,[19] Tl[20]) has been reported. These results prompted us to attempt a similar advance for the heavier Group 13 element alkyne analogues, especially in the case of aluminum, which is of key importance as the first metal of the p-block elements.[21] We now describe the synthesis and characterization of the first "dialuminyne" species $Na_2[Ar'AlAlAr']$ (**3**) and the "cyclotrialuminene" $Na_2[(AlAr'')_3]$ (**4**; $Ar'' = C_6H_3$-2,6-($C_6H_2$-2,4,6-Me$_3$)$_2$).

Compounds **3** and **4** were synthesized by reduction of solutions of $Ar'AlI_2$ (**5**) and $Ar''AlI_2$ (**8**) in diethyl ether with excess sodium [Eq. (1)]. The reduction of **5** initially leads to **6**,

$$\underset{\mathbf{5}}{2\,Ar'AlI_2} \xrightarrow[-2\,NaI]{2\,Na} \underset{\mathbf{6}}{I(Ar')AlAl(Ar')I} \xrightarrow[-2\,NaI]{2\,Na} \underset{\mathbf{7}}{Ar'AlAlAr'} \xrightarrow{2\,Na} \underset{\mathbf{3}}{Na_2[Ar'AlAlAr']} \qquad (1)$$

$$\underset{\mathbf{8}}{3\,Ar''AlI_2} \xrightarrow[-6\,NaI]{8\,Na} \underset{\mathbf{4}}{Na_2[(AlAr'')_3]}$$

thence to **7**,[22] which affords **3** upon further reduction. Compound **3** was isolated in about 20% yield as deep red, almost black crystals, while **4** was isolated in about 25% yield as red-orange crystals. The clusters were characterized by $^1$H and $^{13}$C NMR spectroscopy, UV/Vis spectroscopy, and X-ray crystallography.[23]

X-ray crystallographic analysis of **3** (Figure 1) revealed a centrosymmetric $Al_2Na_2$ core with Al–Al and Al–Na separations of 2.428(1) and 3.152(1) Å, respectively. The aluminum atoms are bound to the Ar′ substituents through the *ipso* carbon atoms (C(1) and C(1A)) of the central aryl ring, as well as to the sodium atoms (Na(1) and Na(1A)), which are further complexed in an $\eta^6$ fashion to the flanking aryl rings of Ar′ (centroid–Na 2.656(2) and 2.637(2) Å; C–Na 2.881(2)–3.084(2) Å). The C(1)-Al(1)-Al(1A)-C(1A) array has a *trans*-bent structure (C(1)-Al(1)-Al(1A) dihedral: 131.71(7)°) with local $C_{2h}$ symmetry.

The structure of **4** is characterized by a triangular $Al_3$ core (Figure 2, Al–Al 2.5202(2) Å) with a crystallographically required three-fold axis of symmetry. Each aluminum atom has distorted trigonal-planar geometry and is bound to two aluminum atoms and to an Ar″ ligand through the *ipso* carbon atom of the central aryl ring. This ring is orientated perpendicularly to the $Al_3C_3$ core array. The two Na atoms are located above and below the centroid of the $Al_3$ core, and are also coordinated to the flanking mesityl rings of the terphenyl ligand (centroid–Na 3.177(2) Å, Na–Al 3.285(2) Å). The Al-Al-C bond angles differ by about 15°, such that the extension of the C–Al vector does not pass through the centroid of the $Al_3$ triangle.

 © 2006 Wiley-VCH Verlag GmbH & Co. KGaA, Weinheim 

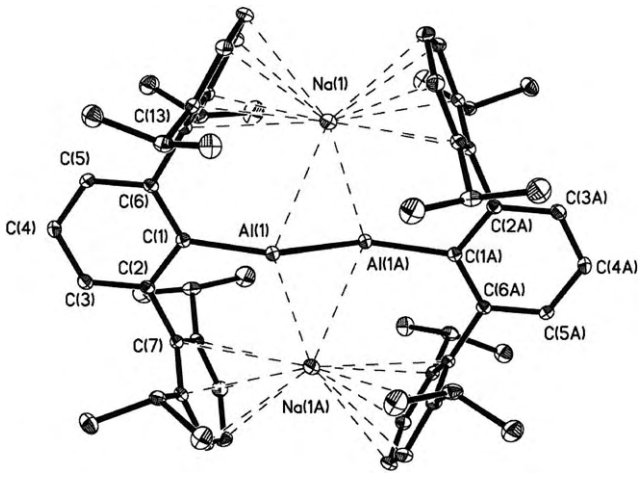


***Figure 1.*** Thermal ellipsoid plot (30% probability) of **3** without H atoms. Selected bond lengths [Å] and angles [deg]: Al(1)-Al(1A) 2.428(1), Al(1)-C(1) 2.043(2), Al(1)-Na(1A) 3.152(1), Na-$C_{ring}$ 2.881(2)–3.084(2) [av. 2.991(2)], Dipp(centroid)-Na(1) 2.656(2), Dipp(centroid)-Na(1A) 2.637(2); C(1)-Al(1)-Al(1A) 131.71(7), Na(1)-Al(1)-Na(1A) 134.58(2), Al(1A)-Al(1)-Na(1) 67.65(3), Al(1A)-Al(1)-Na(1A) 66.93(3), C(1)-Al(1)-Na(1) 104.71(6), C(1)-Al(1)-Na(1A) 105.07(6), Al(1)-C(1)-C(2) 121.9(1), Al(1)-C(1)-C(6) 122.2(1), C(1)-C(2)-C(7) 120.7(2), C(1)-C(6)-C(13) 120.8(2). Dipp = $C_6H_3$-2,6-$iPr_2$.

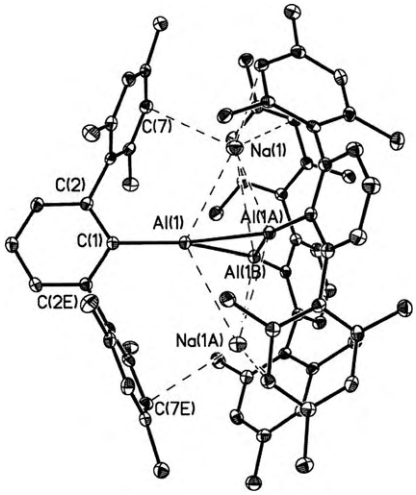


***Figure 2.*** Thermal ellipsoid plot (30% probability) of **4** without H atoms. Selected bond lengths [Å] and angles [deg]: Al(1)-Al(1A) 2.520(2), Al(1)-C(1) 2.021(3), Al(1)-Na(1) 3.285(2), Na(1)-C(7) 3.066(2), Na-$C_{ring}$ 3.066(2)–3.808(2) [av. 3.459(2)], Mes(centroid)-Na(1A) 3.177(2); A1(1)-Al(1A)-Al(1B) 60.0, Al(1A)-Na(1)-Al(1B) 45.12(3), C(1)-Al(1)-Al(1A) 142.8(1), C(1)-Al(1)-Al(1B) 157.2(1). Dihedral angle between $Al_3$ plane and Na(1)-$Al_3$(centroid)-Na(1 A) plane: 90.0. Mes = $C_6H_2$-2,4,6-$Me_3$.

The structure of **3** may be compared with those of the recently reported "disilyne" R′SiSiR′[14] (R′ = Si{CH-($SiMe_3$)$_2$}$_2$*i*Pr; Si–Si 2.319(2) Å, Si-Si-Si 137.44(4)°) and the "digallynes" **1** (Ga–Ga 2.319(2) Å, C-Ga-Ga ca. 131°) and **2** (Ga–Ga 2.347(1) Å, C-Ga-Ga 130.7(1)°). The Al–Al bond length in **3** (2.428(1) Å) is considerably longer than the Si–Si or Ga–Ga bond lengths although the bending angle at Al is within 1° of those in **1** and **2** and is only 5.7° smaller than that of the "disilyne". The longer Al–Al bond length is a result of the larger radius of Al (1.3 Å) versus that of Si (1.17 Å) or Ga (1.25 Å). The dianionic nature of $[Ar'AlAlAr']^{2-}$ versus the neutral "disilyne" is also a factor in the large disparity in bond length. Nonetheless, the Al–Al bond length in **3** is much shorter than those in the Al–Al single-bonded compounds $R_2AlAlR_2$ (R = $CH(SiMe_3)_2$; Al–Al 2.660(3) Å)[1] and $R'_2AlAlR'_2$ (R′ = $C_6H_2$-2,4,6-*i*$Pr_3$; Al–Al 2.647(3) Å)[6] although it is only about 0.04 Å shorter than the Al–Al bond length in the one-electron-reduction product Li(tmeda)$_2$[$R'_2AlAlR'_2$] (2.470(2) Å), which has a formal bond order of 1.5.[6]

The Al–Al bond lengths in **3** may also be affected by sodium–aryl interactions. Calculations by the groups of Nagase,[24] Cotton and Cowley have suggested that this is the case for the "digallynes".[25] More recent high-level calculations by Frenking and co-workers have demonstrated the importance of the Na–Ga interactions.[26] This work has shown that the Ga–Ga bond order in the model species $Na_2$[PhGaGaPh] is about half that of $[PhGaGaPh]^{2-}$. Unfortunately, computational data on model compounds for **3** feature only separated anions with simple ligands such as H[27,28] or Me[28] and do not take Na–aryl interactions into consideration. The calculated geometries of the organosubstituted (Me or Ph) model compounds all afforded planar *trans*-bent structures similar to that found experimentally with Al–Al bond lengths in the range 2.50–2.52 Å and Al-Al-C bond angles in the range 120–127°.[28] The longer calculated Al–Al distances support the view that some of the shortening (0.07–0.09 Å) of the Al–Al bond is indeed a result of the effect of the sodium atoms. The Al–Al bond order, calculated by the method of Mayer,[29] for the simplest planar *trans*-bent model $[HAlAlH]^{2-}$ is 2.51.[28] DFT calculations at the B3LYP/6-31g* level[30] on the model species $Li_2$[HAlAlH], followed by Wiberg bond-order calculations,[31] resulted in an Al–Al bond order of 1.35. Calculations at the same level of theory on the entire molecule of **3** afforded an Al–Al bond order of 1.13, while the same calculations on the gallium analogue **2** afforded a value of 1.39. Finally, we note that the Al–Al bond length in **3** is about 0.20 Å larger than that recently predicted from the sum of the triple-bond radii of aluminum (2.22 Å).[32]

Kohn–Sham frontier-orbital surfaces for the model compound $Na_2$[ArAlAlAr] (Ar = $C_6H_3$-2,6-$Ph_2$) were generated from the DFT calculations by using crystallographic coordinates of **3** (Figure 3).[33] The HOMO is clearly the out-of-plane π bond, and the HOMO−1 can be designated as n_[34] (this type of orbital has also been called a slipped π bond),[35] although calculations on related gallium and germanium species indicate that such an orbital is essentially nonbonding in its effect.[36] The HOMO−2 features σ bonding between the metal centers and from the metal centers to the ligand carbon atoms. These calculations also shed light on the UV/Vis spectrum of **3**, which features three orbitally allowed absorbances at 354, 456, and 600 nm. Two of these absorbances are likely attributable to transitions from the HOMO ($a_u$) and the HOMO−1 ($b_u$) to the LUMO ($a_g$) while the highest-energy transition may involve the HOMO and the LUMO + 1 ($a_g$) levels.

 © 2006 Wiley-VCH Verlag GmbH & Co. KGaA, Weinheim 

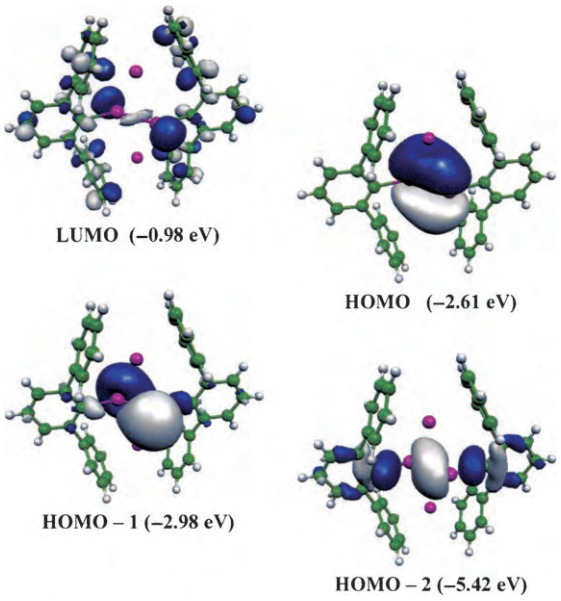


***Figure 3.*** Selected Kohn–Sham orbital representations for the model species $Na_2[ArAlAlAr]$ ($Ar = C_6H_3$-2,6-$Ph_2$).

Compound **4**, the "cycloaluminene", is isoelectronic to the recently reported cyclotrisilenylium ion $[Si_3R_2R']^+$ ($R = Si\mathit{t}Bu_3$, $R' = SiMe_2\mathit{t}Bu$) published by Sekiguchi and co-workers[37] and the previously described gallium salts $M_2[(GaAr'')_3]$ (**9**, M = Na[38]; **10**, M = K[39]) of Robinson and co-workers. The structure of **4** bears a resemblance to that of **9** except that the Al–Al bond length exceeds that of its gallium analogue **9** by about 0.08 Å and is about 0.30 Å larger than the Si–Si bond lengths in the cyclotrisilenylium ion $[Si_3R_2R']^+$. Kohn–Sham orbital representations were also generated for $Na_2[(AlAr)_3]$ (Figure 4; $Ar = C_6H_3$-2,6-$Ph_2$) and showed that the HOMO−2 is a π orbital delocalized over the three metal centers while the HOMO and HOMO−1 are Al–Al σ-bonding orbitals.

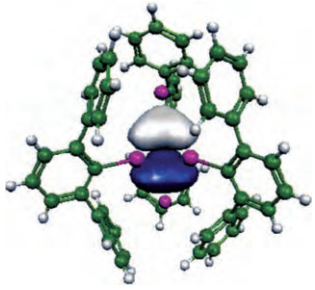

***Figure 4.*** Kohn–Sham orbital representation for the delocalized HOMO−2 of $Na_2[(AlAr)_3]$ ($Ar = C_6H_3$-2,6-$Ph_2$).

The presence of a delocalized 2π orbital suggests that **4** is aromatic. Work on the related gallium species **9** and **10** has shown that they possess delocalized π systems, and nucleus-independent chemical shift (NICS) calculations confirmed their metalloaromaticity.[40] NICS calculations have not been undertaken on **4**, and attempts to obtain a $^{27}Al$ NMR spectrum which might provide further insight into the aromaticity of **4** failed.

The formal M–M bond order in **4** is 1.33; however, the calculated Wiberg bond order in the geometry-optimized model species $Na_2[(AlMe)_3]$ is 0.72 while a value of 0.88 was obtained for calculations (B3LYP/6-31g*) on the entire molecule of **4**. The lower bond orders are likely a result of the distorted localized geometry ($C_{3h}$ instead of $D_{3h}$) caused by lone-pair character at the Al centers and polar–covalent Na–Al interactions. The Na–Al bond orders in $Na_2[(AlMe)_3]$ are calculated to be 0.34 and are indicative of incomplete electron transfer to the $Al_3$ ring. Clearly, the sodium atoms play an important role in the structure of the complex, and, like **3**, it should be viewed not as a separated dianion but as a Na/Al cluster.

In conclusion, the first "dialuminyne" $Na_2[Ar'AlAlAr']$ (**3**) and the "cycloaluminene" $Na_2[(AlAr'')_3]$ (**4**) have been synthesized. Compound **3** features an Al–Al bond with multiple-bond character (Wiberg bond order of 1.13). However, this value is substantially lower than the formal value of three, as a result of the *trans*-bent C-Al-Al-C core, which implies the presence of nonbonding lone-pair density at the Al centers (see HOMO−1). Theoretical calculations on the cyclic compound **4** showed that the HOMO−2 is a delocalized π bond. However, the Al–Al σ bonding is somewhat weakened by the lone-pair character at the metal centers, which results in a lower Al–Al bond order. Apparently, the Al–Al bonds in **3** and **4** are also weakened by Na–aryl interactions. Future work will be focused on the isolation of the neutral $Ar'AlAlAr'$ and $(Ar''Al)_3$ species and other heavier element analogues of **3** and **4**.

## *Experimental Section*

All manipulations were carried out under anhydrous and anaerobic conditions.

**3**: $Ar'AlI_2$ (2.20 g, 3.25 mmol), Na (0.299 g, 13.0 mmol), and $Et_2O$ (125 mL) were added to a Schlenk vessel (150 mL). The mixture was stirred for five days and gave a deep red-black solution. The solution was filtered by filter cannula, and concentration under reduced pressure to about 15 mL afforded dark red, almost black crystals of **3**. The mother liquor was carefully removed, and **3** was dried in a vacuum. Yield: 0.298 g, 20%; m.p. 275–278 °C. X-ray quality crystals ($0.1 \times 0.1 \times 0.1\ mm^3$) of **3** were obtained upon slow cooling of solutions of **3** in $Et_2O$. $^1H$ NMR (300.1 MHz, $C_6D_6$, 25 °C): $\delta = 1.029$ (d, 24H, $o$-$CH(CH_3)_2$, $^3J_{HH} = 6.9$ Hz), 1.470 (d, 24H, $o$-$CH(CH_3)_2$, $^3J_{HH} = 6.9$ Hz), 2.964 (sept, 8H, $o$-$CH(CH_3)_2$, $^3J_{HH} = 6.9$ Hz), 6.960 (d, 6H, $m$-$C_6H_3$), 7.124 (s, 12H, $m$-Dipp), 7.189 ppm (t, 3H, $p$-$C_6H_3$); $^{13}C\{^1H\}$ NMR (75.5 MHz, $C_6D_6$, 25 °C): $\delta = 23.66$ ($CH(CH_3)_2$), 25.66 ($CH(CH_3)_2$), 30.92 ($CH(CH_3)_2$), 123.75 ($m$-Dipp), 127.48 ($p$-$C_6H_3$), 128.97 ($m$-$C_6H_3$), 129.21 ($p$-Dipp), 141.93 ($i$-Dipp), 147.04 ($o$-Dipp), 147.14 ppm ($o$-$C_6H_3$); UV/Vis (hexanes): $\lambda_{max}$ [nm] ($\varepsilon$ in $mol^{-1}\,L\,cm^{-1}$): 354 (25600), 456 (16800), 600 (12400).

**4**: $Ar''AlI_2$ (3.2 g, 5.39 mmol), Na (0.51 g, 22 mmol), and $Et_2O$ (70 mL) were added to a Schlenk vessel (150 mL). The mixture was stirred for three days to give a red solution. The solution was filtered by filter cannula and concentrated to about 30 mL. Upon addition of dry degassed hexane (ca. 15 mL) and overnight storage at about −20 °C, **4** precipitated as a red solid. The powder (0.486 g, 25% yield) was isolated and dissolved in benzene (300 mL), and storage at about 10 °C resulted in small, red hexagonal crystals of X-ray quality. M.p.

 © 2006 Wiley-VCH Verlag GmbH & Co. KGaA, Weinheim 

183–185 °C; $^1$H NMR (300.1 MHz, $C_6D_6$, 25 °C): $\delta = 2.255$ (s, 36 H, *o*-Me), 2.372 (s, 18 H, *p*-Me), 6.695 (d, 6 H, *m*-$C_6H_3$), 7.124 ppm (t, 3 H, *p*-$C_6H_3$); $^{13}$C{$^1$H} NMR: (75.5 MHz, $C_6D_6$, 25 °C): $\delta = 21.92$ (*p*-Me), 22.12 (*o*-Me), 100.30, 125.91, 127.40, 134.39, 138.17 ppm; UV/Vis (hexanes) $\lambda_{max}$ [nm] ($\varepsilon$ in $mol^{-1}\,L\,cm^{-1}$): 280 (9000), 296 (10000), 330 (13000), 380 (16000).

Received: May 16, 2006
Published online: August 9, 2006

**Keywords:** aluminum · aromaticity · density functional calculations · multiple bonds · structure elucidation

[1] W. Uhl, *Z. Naturforsch. B* **1988**, *43*, 1113.
[2] C. Pluta, K. R. Pörschke, C. Krueger, K. Hildenbrand, *Angew. Chem.* **1993**, *105*, 451; *Angew. Chem. Int. Ed. Engl.* **1993**, *32*, 388.
[3] W. Uhl, A. Vester, W. Kaim, J. Poppe, *J. Organomet. Chem.* **1993**, *454*, 9.
[4] W. Uhl, U. Schütz, W. Kaim, E. Waldhör, *J. Organomet. Chem.* **1995**, *501*, 79.
[5] X. He, R. A. Bartlett, M. M. Olmstead, K. Ruhlandt-Senge, B. E. Sturgeon, P. P. Power, *Angew. Chem.* **1993**, *105*, 761; *Angew. Chem. Int. Ed. Engl.* **1993**, *32*, 717.
[6] R. J. Wehmschulte, K. Ruhlandt-Senge, M. M. Olmstead, H. Hope, B. E. Sturgeon, P. P. Power, *Inorg. Chem.* **1993**, *32*, 2983.
[7] a) P. P. Power, *Struct. Bonding (Berlin)* **2002**, *103*, 57; b) A. Schnepf, H. Schnöckel, *Angew. Chem.* **2002**, *114*, 3682; *Angew. Chem. Int. Ed.* **2002**, *41*, 3532; c) H. W. Roesky, *Inorg. Chem.* **2004**, *43*, 7284; d) H. W. Roesky, S. S. Kumar, *Chem. Commun.* **2005**, *32*, 4027.
[8] J. Su, X.-W. Li, R. C. Crittendon, G. H. Robinson, *J. Am. Chem. Soc.* **1997**, *119*, 5471.
[9] R. A. Dagani, *Chem. Eng. News* **1998**, *76*(11), 31.
[10] N. J. Hardman, R. J. Wright, A. D. Phillips, P. P. Power, *J. Am. Chem. Soc.* **2003**, *125*, 2667.
[11] N. J. Hardman, R. J. Wright, A. D. Phillips, P. P. Power, *Angew. Chem.* **2002**, *114*, 2966; *Angew. Chem. Int. Ed.* **2002**, *41*, 2842.
[12] N. Wiberg, T. Blank, K. Amelunxen, H. Nöth, H. Schnöckel, E. Baum, A. Purath, D. Fenske, *Eur. J. Inorg. Chem.* **2002**, 341.
[13] N. Wiberg, S. K. Vasisht, G. Fischer, P. Mayer, *Z. Anorg. Allg. Chem.* **2004**, *630*, 1823.
[14] A. Sekiguchi, R. Kinjo, M. Ichinohe, *Science* **2004**, *305*, 1755.
[15] M. Stender, A. D. Phillips, R. J. Wright, P. P. Power, *Angew. Chem.* **2002**, *114*, 1863; *Angew. Chem. Int. Ed.* **2002**, *41*, 1785.
[16] Y. Sugiyama, T. Sasamori, Y. Hosoi, Y. Furukawa, N. Takagi, S. Nagase, N. Tokitoh, *J. Am. Chem. Soc.* **2006**, *128*, 1023.
[17] A. D. Phillips, R. J. Wright, M. M. Olmstead, P. P. Power, *J. Am. Chem. Soc.* **2002**, *124*, 5930.
[18] L. Pu, B. Twamley, P. P. Power, *J. Am. Chem. Soc.* **2000**, *122*, 3524.
[19] R. J. Wright, A. D. Phillips, N. J. Hardman, P. P. Power, *J. Am. Chem. Soc.* **2002**, *124*, 8538.
[20] R. J. Wright, A. D. Phillips, S. Hino, P. P. Power, *J. Am. Chem. Soc.* **2005**, *127*, 4794.
[21] The first stable low-valent organo-Al(I) compounds (or lower-oxidation-state species) $K_2[Al_{12}iBu_{12}]$ and $[\{Al(\eta^5\text{-}C_5Me_5)\}_4]$ were characterized in 1991: W. Hiller, K. W. Klinkhammer, W. Uhl, J. Wagner, *Angew. Chem.* **1991**, *103*, 182; *Angew. Chem. Int. Ed. Engl.* **1991**, *30*, 179; C. Dohmeier, C. Robl, M. Tacke, H. Schnöckel, *Angew. Chem.* **1991**, *103*, 594; *Angew. Chem. Int. Ed. Engl.* **1991**, *30*, 564.
[22] R. J. Wright, A. D. Phillips, P. Power, *J. Am. Chem. Soc.* **2003**, *125*, 11626.
[23] Crystallographic data for **3** and **4** ($T = 90$ K with $Mo_{K\alpha}$ ($\lambda = 0.71073$ Å) radiation): **3**: monoclinic, space group $P2_1/n$, $a = 11.493(1)$, $b = 18.148(1)$, $c = 13.478(1)$ Å, $\beta = 100.167(1)°$, $Z = 2$, $R1 = 0.0518$ for 6554 ($I > 2\sigma(I)$) data; **4**: hexagonal, space group $P6_3/m$, $a = 13.9787(4)$, $b = 13.9787(4)$, $c = 20.266(1)$, $Z = 2$, $R1 = 0.0494$ for 2140 ($I > 2\sigma(I)$) data. CCDC-606648 (**3**) and CCDC-606647 (**4**) contain the supplementary crystallographic data for this paper. These data can be obtained free of charge from The Cambridge Crystallographic Data Centre via www.ccdc.cam.ac.uk/data_request/cif.
[24] N. Takagi, M. W. Schmidt, S. Nagase, *Organometallics* **2001**, *20*, 1646.
[25] F. A. Cotton, A. H. Cowley, X. Feng, *J. Am. Chem. Soc.* **1998**, *120*, 1795.
[26] R. Ponec, G. Yuzhakov, X. Gironés, G. Frenking, *Organometallics* **2004**, *23*, 1790.
[27] H. J. Schnöckel, H.-J. Himmel, *Chem. Eur. J.* **2002**, *8*, 2397.
[28] A. J. Bridgeman, L. R. Ireland, *Polyhedron* **2001**, *20*, 2841.
[29] I. Mayer, *Chem. Phys. Lett.* **1983**, *97*, 270.
[30] Gaussian 03 (Revision A.01): M. J. Frisch et al., see Supporting Information for full reference.
[31] S. I. Gorelsky, AOMix Rev. 5.44, http://www.obbligato.com/software/aomix/.
[32] P. Pyykkö, S Riedel, M. Patzschke, *Chem. Eur. J.* **2005**, *11*, 3511.
[33] P. Flukiger, H. P. Luthi, S. Portmann, J. Weber, MOLEKEL 4.3, Swiss Center for Scientific Computing, Manno, Switzerland, **2000–2002**.
[34] n designates a lone pair orbital. The subscripts + and − refer to its symmetry (+) or antisymmetry (−) with respect to inversion.
[35] K. W. Klinkhammer, *Angew. Chem.* **1997**, *109*, 2387; *Angew. Chem. Int. Ed. Engl.* **1997**, *36*, 2320.
[36] T. L. Allen, W. H. Fink, P. P. Power, *J. Chem. Soc. Dalton Trans.* **2000**, 407.
[37] M. Ichinohe, M. Igarashi, K. Sanuki, A. Sekiguchi, *J. Am. Chem. Soc.* **2005**, *127*, 9978.
[38] X.-W. Li, W. T. Pennington, G. H. Robinson, *J. Am. Chem. Soc.* **1995**, *117*, 7578.
[39] X.-W. Li, Y. Xie, P. R. Schreiner, K. D. Gripper, R. C. Crittendon, C. F. Campana, H. F. Schaefer, G. H. Robinson, *Organometallics* **1996**, *15*, 3798.
[40] Y. Xie, P. R. Schreiner, H. F. Schaefer III, X.-W. Li, G. H. Robinson, *J. Am. Chem. Soc.* **1996**, *118*, 10635.

 © 2006 Wiley-VCH Verlag GmbH & Co. KGaA, Weinheim 

Photochemistry

DOI: 10.1002/anie.200601615

# Photochemical Upconversion: Anthracene Dimerization Sensitized to Visible Light by a $Ru^{II}$ Chromophore**

*Radiy R. Islangulov and Felix N. Castellano**

Upconversion, the generation of photons with higher energy than the incident light, is intrinsically nonlinear and therefore requires high excitation intensities. Recent developments in this area led by our group and others indicate that a plausible route to lowering the optical power requirements for upconversion lies in harnessing triplet–triplet annihilation (TTA) processes.[1–4] In the sensitized TTA mechanism, upconversion becomes linked to sequential, highly allowed one-photon absorption processes, thereby permitting the use of low-power continuous-wave excitation sources. This strategy has been proved quite effective with the metal-to-ligand charge-transfer (MLCT) sensitizer $[Ru(dmb)_3]^{2+}$ (dmb = 4,4′-dimethyl-2,2′-bipyridine) and 9,10-diphenylanthracene, for which the green-to-blue upconversion can be readily visualized by the naked eye in a lighted room by using a laser pointer.[2] Although this advance has obvious relevance in photonic technologies, there are also important ramifications for preparative chemistry. If the TTA process is selected to produce reactive excited singlet species prone to cycloaddition chemistry, then low-energy photons can be used to drive photochemical reactions that traditionally require high-energy ultraviolet light.[5,6] Herein we describe a representative synthetic application in which visible-light-sensitized TTA upconversion efficiently drives bimolecular [4+4] cycloaddition between two anthracene molecules, accomplished through selective excitation of $[Ru(dmb)_3]^{2+}$.

The photodimerization of anthracene (An) is one of the oldest documented photochemical reactions, the nature of which has been investigated extensively by many researchers.[5,6] In 1983 Saltiel and co-workers clearly established that the formation of An dimers by excitation at 366 nm proceeds readily through TTA.[7] The dimerization of An represents a suitable departure point for the search for a prototype addition reaction amenable to sensitized TTA by $Ru^{II}$ MLCT chromophores.

Equations (1)–(3) provide the sequence of chemical steps necessary for photochemical upconversion in the current study. Selective excitation of $[Ru(dmb)_3]^{2+}$ at a variety of visible wavelengths (457.9 nm, 488 nm, 514.5 nm, or 532 nm) initiates bimolecular triplet–triplet quenching by An [Eq. (1)].[1,2,8] Two molecules of excited triplet An ($^3$An*)

$$[Ru(dmb)_3]^{2+*} + An \rightarrow [Ru(dmb)_3]^{2+} + {}^3An^* \quad (1)$$

can encounter, ultimately resulting in TTA [Eq. (2)].[2,7] The dimer $An_2$ is then produced from theinteraction between an

$${}^3An^* + {}^3An^* \rightarrow {}^1An^* + An \quad (2)$$

excited singlet An ($^1$An*) and an An molecule in the ground state, thereby completing the photochemical upconversion reaction sequence [Eq. (3)]. The $Ru^{II}$ sensitizer is photo-

$${}^1An^* + An \rightarrow An_2 \quad (3)$$

catalytic in nature; its ground state is regenerated following triplet energy transfer [Eq. (1)]. In view of the inherent photochemical and thermal stability of $Ru^{II}$ tris(diimine) complexes, one would expect long-term efficacy and large turnovers in preparative synthetic applications of these chromophores in concert with sensitized photochemical upconversion.

Figure 1 provides representative static UV/Vis absorption data obtained from low-power $Ar^+$ laser photolysis ($\lambda_{ex}$ = 457.9 nm) of a vacuum-degassed solution containing $[Ru(dmb)_3]^{2+}$ and An in relatively dilute concentrations in $CH_3CN$. Selective excitation of the $Ru^{II}$ chromophore leads to the net loss of An. This is conveniently monitored by changes in the characteristic An vibronic absorption bands between 325 and 375 nm. After 70 min of photolysis the

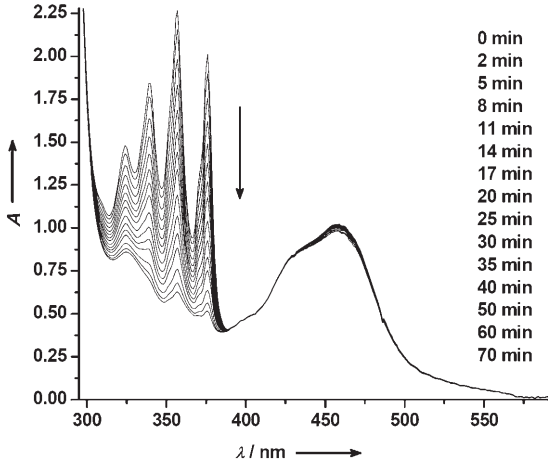


***Figure 1.*** Photolysis of a degassed solution of $[Ru(dmb)_3]^{2+}$ ($5.75\times10^{-5}$ M) and anthracene ($2.55\times10^{-4}$ M) in acetonitrile by continuous-wave $Ar^+$ laser excitation ($\lambda_{ex}$ = 457.9 nm; incident power 13.0 mW). Photolysis times are indicated at the side.

[*] R. R. Islangulov, Prof. F. N. Castellano
Department of Chemistry and Center for Photochemical Sciences
Bowling Green State University
Bowling Green, OH 43403 (USA)
Fax: (+1) 419-372-9809
E-mail: castell@bgnet.bgsu.edu
Homepage: http://www.bgsu.edu/departments/photochem/

[**] F.N.C. gratefully acknowledges financial support from the US Air Force Office of Scientific Research (FA9550-05-1-0276), the US National Science Foundation (CAREER Award CHE-0134782), the American Chemical Society (44138-AC3), and the BGSU Technologies Innovations Enhancement Program.

Supporting information for this article is available on the WWW under http://www.angewandte.org or from the author.


© 2006 Wiley-VCH Verlag GmbH & Co. KGaA, Weinheim

reaction is nearly complete with the low-energy MLCT absorption bands remaining essentially intact.

Figure 2 shows the changes in An concentration as a function of photolysis time at 457.9 nm calculated from the data in Figure 1 and the extinction coefficient for An

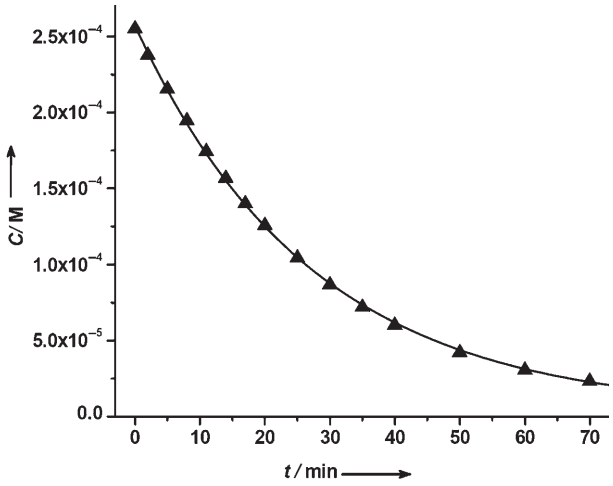


***Figure 2.*** Change in anthracene concentration as a function of photolysis time from the data in Figure 1 ($\varepsilon$(An) at 376 nm = 6450 $M^{-1}$ $cm^{-1}$). The solid line is the first-order least-squares fit.

measured at 376 nm (6450 $M^{-1}cm^{-1}$). The solid line is the first-order least-squares fit to the experimental data points, as the reaction can be considered to take place under pseudo-first-order conditions, in which [An] ≫ [$^1$An*]. Note that $^1$An* forms only as a result of the rate-limiting TTA process [Eq. (2)]. The first-order rate of monomer consumption is consistent with that observed during UV irradiation of An solutions,[9] and we have independently confirmed this finding using acetonitrile as the reaction solvent. We note that Stern–Volmer analysis of the $[Ru(dmb)_3]^{2+}$ luminescence intensity decays measured as a function of An concentration [Eq. (1)] yields $K_{SV} = 4490\,M^{-1}$ with a corresponding bimolecular rate constant of $5.38 \times 10^9\,M^{-1}s^{-1}$, which approaches the diffusion limit in $CH_3CN$. These data are valuable because they directly provide the An concentrations necessary for complete quenching of the $[Ru(dmb)_3]^{2+}$ sensitizers to produce the highest number of $^3$An* molecules which in turn annihilate to form the reactive $^1$An* species. Therefore the quantum efficiency of sensitized photochemical upconversion should scale with the An concentration up to the point at which the production of $^1$An* saturates. It is also known that the quantum yields of direct photochemical An dimerization are sensitive to the monomer concentration.[6,10] Because the photochemically reactive $^1$An* state is so short-lived (approximately 4 ns),[6] relatively large concentrations of ground-state An are necessary to observe efficient dimerization. The ionic nature of $[Ru(dmb)_3]^{2+}$ limited our experiments to $CH_3CN$ solutions, in which the maximum solubility of An is just below 20 mM. According to the Stern–Volmer analysis, 90% of the $[Ru(dmb)_3]^{2+}$ molecules are quenched at approximately 2 mM An as measured under optically dilute conditions (optical density (OD) ≈ 0.1). Although our photolysis experiments utilize higher sensitizer concentrations (OD ≈ 1.0), the Stern–Volmer data imply that working near the An saturation limit will ensure nearly complete quenching of all excited sensitizer molecules. The quantum yields of An dimerization (see the Experimental Section for details) were measured as a function of An concentration at constant sensitizer concentration and incident laser power (Figure 3).

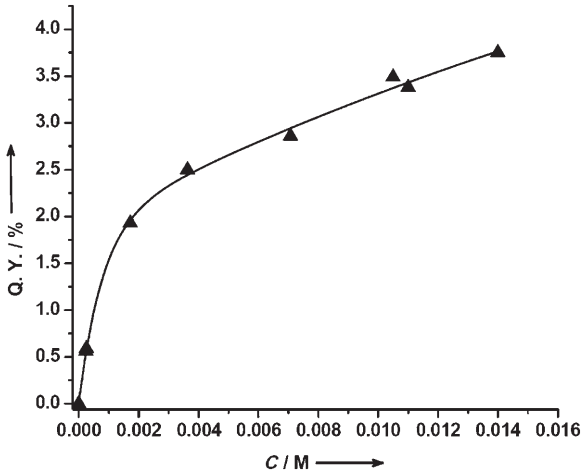


***Figure 3.*** Dependence of the quantum yield (Q.Y.) for anthracene photodimerization on anthracene concentration. Solutions of $[Ru(dmb)_3]^{2+}$ ($5.75 \times 10^{-5}$ M) and anthracene in acetonitrile were irradiated with an $Ar^+$ laser ($\lambda_{ex}$ = 457.9 nm, 13.0 mW).

The dimerization quantum yields sharply increase from 0 to 2.5% between 0 and 3 mM and then slowly rise, ultimately reaching 3.75% at 14 mM in $CH_3CN$, the highest concentration used in this experiment. At low An concentration, the steep slope in Figure 3 likely results from more-efficient production of $^3$An*, as suggested by the Stern–Volmer analysis. At higher An concentrations, the dimerization quantum yield continues to increase linearly with concentration, which is consistent with a dimerization process under strict kinetic control by ground-state An molecules. This finding strongly suggests that the An molecule that reacts in Equation (3) is not the geminate An ground-state molecule produced from annihilation in Equation (2). A limitation of the annihilation approach is that it relies on long-lived excited triplet states to produce excited singlet molecules. This reliance inherently limits the quantum yield of excited singlet-state molecules that result from TTA encounters to a maximum value of 1/9 (11.1%).[7] If the quantum yield for the relevant singlet-state reaction is below unity, the efficiency of the analogous TTA-controlled process will be reduced accordingly, as is likely the case in the present work. Higher concentrations of ground-state An molecules facilitate the quenching of $^3$An*, which diminishes its lifetime and concentration and leads to fewer annihilation events.[7,11] On the basis of these facts, it can be anticipated that increasing the An concentration much beyond that employed in the current work will likely lead to diminished dimerization yields in photochemical upconversion. However, even when these limitations are considered, millimolar concentrations of An

 © 2006 Wiley-VCH Verlag GmbH & Co. KGaA, Weinheim 

are indeed suitable for synthetic chemistry utilizing upconversion phenomena, as described below.

The $^1$H and $^{13}$C NMR spectra of An and the product that precipitates from the MLCT-sensitized TTA reaction mixture containing approximately 14 mM An are provided in the Supporting Information. Both sets of spectra decisively indicate the formation of pure [4+4] An dimers. In the $^1$H NMR spectrum, the characteristic chemical shift of the bridgehead protons are observed as a singlet at $\delta =$ 4.56 ppm.[4] The phenyl protons also display characteristic chemical shifts in comparison with those in the parent An structure. The bridgehead carbons show a resonance at $\delta =$ 53.66 ppm in the $^{13}$C NMR spectrum, which confirms the conversion to the [4+4] dimerized structure.

If the photolysis is carried out in aerated $CH_3CN$, no precipitation occurs after 130 minutes of irradiation, and the low-energy An absorption bands disappear as a function of photolysis time. These observations suggest the efficient formation of endoperoxide and complete suppression of dimer production.[5] Photodimer formation is clearly observed in the deaerated solution in $CH_3CN$, as the nonpolar dimer readily crystallizes during the course of the photolysis. A digital photograph taken after 40 minutes of visible light irradiation (Figure 4) illustrates the extent of reaction and the ease with which sensitized photochemical upconversion takes place.

***Figure 4.*** Photograph of the optical cell containing crystallized anthracene photodimer produced by $Ar^+$ laser photolysis of a solution containing $[Ru(dmb)_3]^{2+}$ ($5.25\times10^{-5}$ M) and anthracene (ca. $1.4\times10^{-2}$ M) in acetonitrile.

The current work establishes the feasibility of applying sensitized TTA in preparative chemistry by using anthracene dimerization as a prototypical reaction. This concept could be extended to other intermolecular cycloaddition reactions, including mixed dimers, to yield new insight into how TTA-driven reactions influence product distributions. In materials science applications, TTA may provide a means of carrying out desired chemical reactions in media that do not permit transmission of ultraviolet light.

## Experimental Section

Anthracene gold label (Aldrich) and spectroscopic-grade acetonitrile (Fisher Chemicals) were used as received. $[Ru(dmb)_3](PF_6)_2$ was prepared according to the published procedure.[12] Static absorption spectra were measured on a HP 8453 diode-array spectrometer. The excitation was accomplished with an argon-ion laser (Coherent Innova 300) whose multiline output was split into the selected wavelength component ($\lambda = 457.9$ nm) by a diffraction grating in concert with several optics. The laser power was measured with a Molectron Power Max 5200 power meter. $^1$H and $^{13}$C NMR were measured on a Bruker 300 spectrometer. All samples in 10-mm pathlength anaerobic quartz cells (home-made) were deoxygenated by five freeze, pump, thaw cycles under pressures of less than $10^{-3}$ mm Hg. Emission lifetimes were measured with an apparatus described previously,[13] by using a nitrogen-pumped broadband dye laser (PTI GL-3300 $N_2$ laser, coumarin 460) as the excitation source.

Quantum yields of anthracene photodimerization were measured by $Ar^+$ laser irradiation (457.9 nm, 13 mW incident power) of deaerated solutions in acetonitrile containing $[Ru(dmb)_3]^{2+}$ (OD at 458 nm maintained at 1.0) and varying An concentrations. The dimerization quantum yield was calculated from the quantum yield for the disappearance of the An monomer at low conversions (< 10%) by using the equation: $\Phi_{dimerization} = 0.5\,\Phi_{An\ loss}$.[9] The quantum yield of An disappearance was determined by evaluating changes in An concentration (mol min$^{-1}$) relative to the number of absorbed photons (mol photons min$^{-1}$) in the constant sample volume. All An concentrations were determined spectrophotometrically at 376 nm, and absorbed photons were determined from the difference between the power of the incident and transmitted light (both measured using the Molectron power meter). When large concentrations of An were utilized, the samples were diluted after photolysis for appropriate concentration determination in the linear range of the diode-array spectrometer.

Received: April 24, 2006
Revised: June 23, 2006
Published online: August 14, 2006

**Keywords:** anthracene · cycloaddition · dimerization · photochemistry · upconversion

[1] D. V. Kozlov, F. N. Castellano, *Chem. Commun.* **2004**, 2860.
[2] R. R. Islangulov, D. V. Kozlov, F. N. Castellano, *Chem. Commun.* **2005**, 3776.
[3] P. E. Keivanidis, S. Baluschev, T. Miteva, G. Nelles, U. Scherf, A. Yasuda, G. Wegner, *Adv. Mater.* **2003**, *15*, 2095.
[4] S. Baluschev, F. Yu, T. Miteva, S. Ahl, A. Yasuda, G. Nelles, W. Knoll, G. Wegner, *Nano Lett.* **2005**, *5*, 2482.
[5] H. Bouas-Laurent, J.-P. Desvergne, A. Castellan, R. Lapouyade, *Chem. Soc. Rev.* **2000**, *29*, 43.
[6] H. Bouas-Laurent, J.-P. Desvergne, A. Castellan, R. Lapouyade, *Chem. Soc. Rev.* **2001**, *30*, 248.
[7] J. L. Charlton, R. Dabestani, J. Saltiel, *J. Am. Chem. Soc.* **1983**, *105*, 3473.
[8] M. Wrighton, J. Markham, *J. Phys. Chem.* **1973**, *77*, 3042.
[9] C. E. Bunker, H. W. Rollins, J. R. Gord, Y.-P. Sun, *J. Org. Chem.* **1997**, *62*, 7324.
[10] Y. C. Yang, D. M. Shold, B. Kim, *J. Am. Chem. Soc.* **1976**, *98*, 6587.
[11] J. Saltiel, G. R. Marchand, R. Debestani, J. A. Pecha, *Chem. Phys. Lett.* **1983**, *100*, 219.
[12] N. H. Damrauer, T. R. Boussie, M. Devenney, J. K. McCusker, *J. Am. Chem. Soc.* **1997**, *119*, 8253.
[13] D. S. Tyson, F. N. Castellano, *J. Phys. Chem. A* **1999**, *103*, 10955.

 © 2006 Wiley-VCH Verlag GmbH & Co. KGaA, Weinheim 

Nanobiotechnology

DOI: 10.1002/anie.200601089

# Proton-Fueled, Reversible Assembly of Gold Nanoparticles by Controlled Triplex Formation**

*Young Hwan Jung, Kyung-Bok Lee, Yang-Gyun Kim,* and Insung S. Choi**

Since the first reports on gold nanoparticles (AuNPs) bearing oligonucleotides (DNA–AuNP conjugates) in 1996,[1] these conjugates have been used intensively to generate self-assembled, networked structures of AuNPs as well as to monitor hybridization/denaturation of oligonucleotides.[1,2] Previously reported approaches to the network formation of AuNPs were generally based on the hybridization of complementary oligonucleotides conjugated to AuNPs, and the one-directional assembly of AuNPs was mainly used for nanometer-scale structuring and biosensing (the disassembly occurred by heating).[2] However, more applications would be envisioned when the programmable, reversible assembly of AuNPs is achieved. To demonstrate reversible assembly/disassembly of DNA–AuNP conjugates, Niemeyer and co-workers used a fueling oligonucleotide that contained a short, dangling-end sequence for the initiation of strand removal from the assembled AuNP structures.[3a] A simpler approach would be the use of protons ($H^+$) as a fuel instead of oligonucleotides to control the structure of DNA and consequently the assembly/disassembly of DNA–AuNP conjugates. The advantages of protons over oligonucleotides have been suggested, including no generation of waste duplex products that poison DNA-based systems.[3b]

[*] Prof. Dr. Y.-G. Kim
Department of Chemistry
Sungkyunkwan University
Suwon 440-746 (Korea)
Fax: (+82) 31-299-6159
E-mail: ygkimmit@skku.edu
Dr. Y. H. Jung, Prof. Dr. I. S. Choi
Department of Chemistry
and School of Molecular Science (BK21)
Center for Molecular Design and Synthesis
KAIST
Daejeon 305-701 (Korea)
Fax: (+82) 42-869-2810
E-mail: ischoi@kaist.ac.kr
Dr. K.-B. Lee
Glycomics Team
Korea Basic Science Institute (KBSI)
Daejeon 305-333 (Korea)

[**] This work was supported by a Korea Research Foundation grant funded by the Korea Government (MOEHRD, Basic Research Promotion Fund; KRF-2005-070-C00078). We thank Professor Younghoon Lee of the Department of Chemistry at KAIST for help with the experiments. Y.-G.K. is grateful for financial support from the Basic Research Program of the Korea Science and Engineering Foundation (grant no. R01-2006-000-11187-0)

Triple-helix DNA (triplex) is a well-documented structure in biology that is formed by the association of a target duplex and a homopyrimidinic "triplex-forming oligonucleotide".[4] Depending on the orientation of the third oligonucleotide with respect to the targeted Watson–Crick duplex, triplexes are classified into parallel and antiparallel structures. The formation of antiparallel triplexes does not require protonation and exhibits pH-independent binding. In contrast, parallel triplexes are critically dependent on the protonation of the imino group (N3) of cytosines at the triplex-forming oligonucleotide. The imino group should be protonated to form the correct Hoogsteen binding with N7 of guanine, and therefore the formation of parallel triplexes can be tuned dynamically by controlled changes in pH value. In other words, parallel triplexes are stable only under acidic conditions and the formation of an oligonucleotide-based triplex provides a powerful tool for genetic manipulation and other applications, such as DNA-based nanomachines.[5–7] We reasoned that the required protonation of the imino group (N3) of cytosines could be utilized for proton-fueled, reversible assembly/disassembly of AuNPs conjugated with oligonucleotides that form triplex structures ("triplex–AuNP conjugates").[8] Herein, we report that the proton-fueled switching of the assembly of AuNPs is realized by the pH-controlled fine-tuning of intermolecular interactions between two triplex-forming oligonucleotide parts.

We formed the triplex–AuNP conjugates by using two different thiolated, single-stranded oligonucleotides, oligo A and oligo B. Oligo A contained a sequence that formed a Watson–Crick hairpin duplex, and oligo B contained a triplex-forming oligonucleotide sequence (Figure 1).[8] Oligo A was a 5′-thiolated oligonucleotide composed of four sections: a 20-nucleotide poly-dA section starting from the 5′ terminus to increase hybridization efficiency,[9] a 12-nucleotide homopurinic section, a central "hinge" made of four dT nucleotides, and a 12-nucleotide homopyrimidinic section ending at the 3′ terminus, capable of forming an intramolecular Watson–Crick duplex with 5′ homopurinic sequences. Oligo B was a 3′-thiolated oligonucleotide whose sequence was composed of a 12-nucleotide homopyrimidinic part and a 20-nucleotide-long poly-dA ending at the 3′ terminus. The

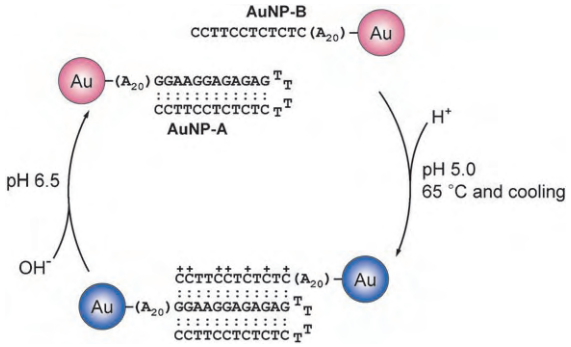


***Figure 1.*** Triplex–AuNP conjugates and their assembly. The protonated cytosine is indicated by +C. One AuNP presented multiple copies of oligonucleotides at its surface; only one of these oligonucleotides is shown for simplicity. The triplex-driven assembly of AuNPs yielded three-dimensional networks of AuNPs.


InterScience
© 2006 Wiley-VCH Verlag GmbH & Co. KGaA, Weinheim

thiol group was located at the 3′ terminus of oligo B, to form a parallel triplex between oligo A and oligo B. Before attachment to AuNPs, the oligo A solution was heated to 90 °C for 5 min, slowly cooled to room temperature, and left in an ice bath for oligo A to hybridize into the intramolecular duplex. The thiol-terminated oligonucleotides (oligo A and oligo B) were then treated with citrate-stabilized AuNPs (15 nm in diameter) in a buffered aqueous solution to obtain a dispersion of AuNPs bearing multiple oligonucleotide molecules per nanoparticle.

The proton-fueled assembly of the triplex–AuNP conjugates was investigated by first mixing together oligo A-attached (AuNP–A) and oligo B-attached AuNPs (AuNP–B) at pH 6.5 (50 mM sodium phosphate buffer containing 10 mM $MgCl_2$) and then acidifying the mixture until pH 5 was reached. The formation of a triplex requires a reduction in the repulsion between the negatively charged phosphate groups of the three strands. The repulsion between these phosphates can be effectively screened by divalent cations, such as $Mg^{2+}$.[10] The UV/Vis absorption spectrum was recorded before the acidification: the maximum absorbance wavelength ($\lambda_{max}$) was 525 nm, indicative of dissociated states of AuNPs (Figure 2). The mixed nanoparticles were assembled

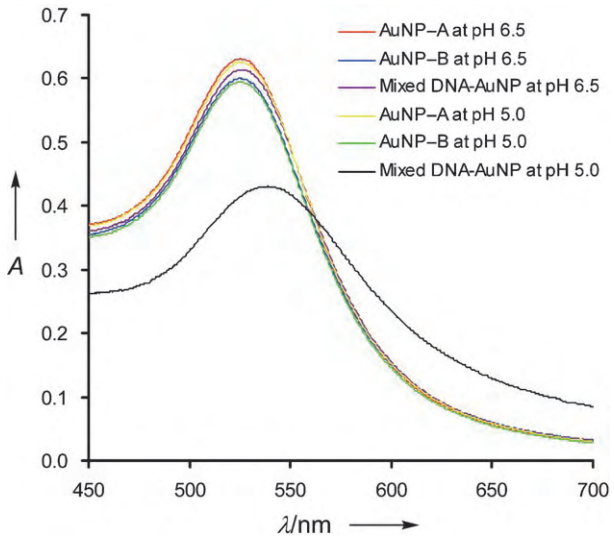


***Figure 2.*** UV/Vis absorption spectra of AuNP–A, AuNP–B, and a mixture of AuNP–A and AuNP–B at pH 6.5 and 5.0.

by heating and slow cooling of the hybridized solution for 48 hours. During the assembly process, the solution changed from the initial red to a reddish-purple color, which indicated that a triplex was formed by two interacting oligonucleotides, oligo A and oligo B, attached to AuNPs. The UV/Vis absorption spectrum also confirmed the proton-fueled assembly of AuNPs; we observed spectral changes in the region of 450–700 nm as a result of the formation of nanoparticle aggregates following the hybridization of the triplex-forming oligonucleotides at pH 5 (Figure 2, black line).

The assembly process also led to a red shift in the surface plasmon resonance from 525 to 537 nm. This absorbance change was the result of the reduced inter-nanoparticle distances through triplex formation.[1,2] As a control experiment, each solution containing AuNP–A or AuNP–B was subjected to a change of pH value from 6.5 to 5, which did not lead to any changes in the UV/Vis spectra. The control experiment confirmed that the observed spectral change resulted from the proton-fueled formation of a triplex between AuNP–A and AuNP–B at pH 5.

Transmission electron microscopy (TEM) experiments were performed to characterize the morphologies of mixed DNA–AuNP composites at pH 6.5 (Figure 3a) and 5.0

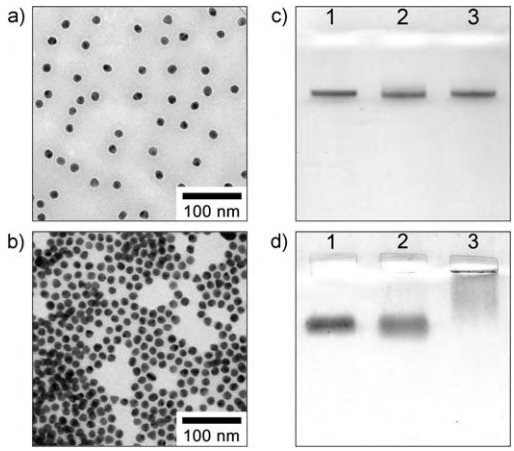


***Figure 3.*** TEM images of mixtures of AuNP–A and AuNP–B at a) pH 6.5 and b) pH 5.0. c) Electrophoretic mobility of AuNP–A (lane 1), AuNP–B (lane 2), and mixed DNA–AuNP (lane 3) at pH 6.5. AuNP solutions were loaded onto agarose gels (1% w/v in 10 mM sodium phosphate, pH 6.5) and subjected to electrophoresis at 100 V for 30 min. d) Electrophoretic mobility of DNA–AuNP conjugates at pH 5.2. Sodium acetate (30 mM) was used instead of sodium phosphate.

(Figure 3b). The TEM image in Figure 3b confirmed the proton-fueled assembly of AuNPs, which indicated that the nanoparticles were linked to each other by hybridization of the triplex-forming oligonucleotide and the hairpin-structured Watson–Crick duplex.

To compare the electrophoretic mobility of triplex-driven aggregates with those of the triplex–AuNP conjugates (AuNP–A and AuNP–B) under the conditions for triplex formation, the resulting aggregate solution was analyzed by electrophoretic mobility shift assay using 1% agarose gel in sodium acetate (30 mM, pH 5.2) as an electrophoresis buffer (Figure 3d). The assembled structure (lane 3) moved slower than AuNP–A (lane 1) and AuNP–B (lane 2), and some aggregates were also observed to stay in the well. In contrast, all of the DNA–AuNP conjugates (AuNP–A, AuNP–B, and mixed DNA–AuNP) had the same mobility in gel electrophoresis at pH 6.5 (Figure 3c).

The repeated switching and pH-dependent reversible assembly/disassembly of triplex–AuNP conjugates were monitored with UV/Vis absorption spectroscopy. The absorbance of the mixed nanoparticle solution was measured while the pH of the sample was repeatedly cycled between 5.0 and

 © 2006 Wiley-VCH Verlag GmbH & Co. KGaA, Weinheim 

6.5 with controlled additions of 1 M HCl and 1 M NaOH. The change in $\lambda_{max}$ value of the nanoparticle solutions was plotted with respect to pH value during six cycles starting at pH 6.5 (Figure 4). At pH 6.5, $\lambda_{max}$ of the mixed nanoparticle solution

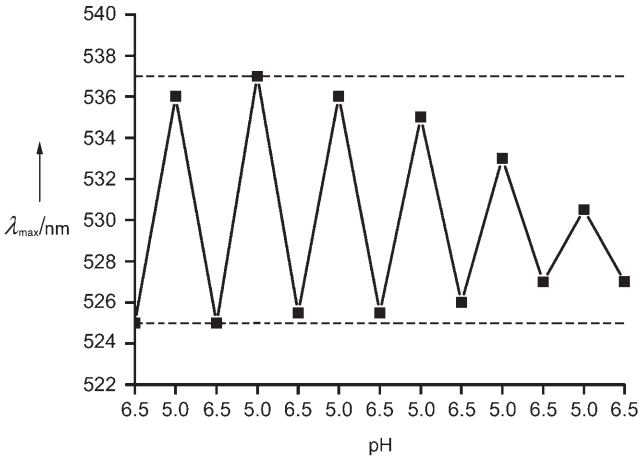


***Figure 4.*** pH-dependent, reversible cycling of the assembly of triplex–AuNP conjugates observed by UV/Vis absorption spectroscopy. The change in the maximum absorbance wavelength ($\lambda_{max}$) of the nanoparticle solutions was plotted with respect to pH value. The initial concentration of each triplex–AuNP conjugate was sodium phosphate buffer (50 mM) with $MgCl_2$ (10 mM). The pH value was cycled between 5.0 and 6.5 by alternating addition of 1 M HCl or 1 M NaOH.

was about 525 nm. This $\lambda_{max}$ value indicated the breakdown of the assembled network of AuNPs by triplex denaturation. Under hybridizing buffer conditions at pH 5.0, $\lambda_{max}$ changed to about 537 nm. This shift in $\lambda_{max}$ synchronized with the induced changes in pH value, and was continually observed during cycling. The gradual decrease in $\lambda_{max}$ at pH 5.0 may have been caused by dilution of the nanoparticle solutions upon addition of acid or base, accumulated NaCl, and partial formation of irreversible aggregates. A gradual increase in the ionic strength as a result of the accumulated NaCl was expected to change the electrostatic potential of the triplex structure and consequently its performance.[10]

In summary, the protonation of the imino group (N3) of cytosines in double-stranded DNA that is required for the formation of a triplex was used to guide the assembly/disassembly of DNA-conjugated AuNPs. This proton-fueled switching of AuNP networks could be useful in various areas of nanobiotechnology. For example, it is possible that structures composed of triplex-forming AuNPs would generate swelling/shrinking of the whole structure in response to changes in pH value, and such variations might be applied to the design of a pH-dependent delivery system for small molecules, such as drugs and probe entities. In addition, a combination of the triplex-forming AuNP networks and other self-assembled nanostructures may lead to hybrids with a structure controlled by the pH-dependent structural change of triplexes.

## Experimental Section

Oligonucleotides were synthesized by Genotech (Korea) on a 1-μmol scale. The thiol-modified oligonucleotides were 48- and 32-base oligonucleotides with the following sequences, respectively; oligo A: 5′-thiol($C_6$)-$A_{20}$GG AAG GAG AGA GTT TTC TCT CTC CTT CC-3′ and oligo B: 5′-CCT TCC TCT CTC $A_{20}$-thiol($C_3$)-3′. Gold colloids (15 nm in diameter) were purchased from BBInternational (UK).

Before using each oligonucleotide, a working stock solution was prepared with Tris–EDTA buffer (10 mM, pH 7.4). Dithiol linkages were cleaved prior to use by adding dithiothreitol (DTT; 1 M, 40 μL) and sodium phosphate buffer (1 M, 68 μL, pH 8.0) to a solution of the oligonucleotide (200 μL, 25 pmol $\mu L^{-1}$). Thiolated oligonucleotides were then desalted on a NAP-25 (Pharmacia, UK) column using sodium phosphate buffer (10 mM, pH 7.0) as the solvent. The resulting fractions were analyzed by UV/Vis absorption spectroscopy with a Shimadzu 2550 spectrophotometer. We added 4.8 nmol of the oligonucleotide to an AuNP solution (3 mL; 2.3 nM). The entire solution was covered with tin foil and stored at room temperature for 16 h. This solution was then brought to sodium phosphate buffer (10 mM, pH 7.0) containing sodium chloride (50 mM). The solution was shaken for another 48 h, and the salt concentration was increased gradually from 50 to 300 mM by adding 2 M NaCl. The solution was then centrifuged at 15000 g for 20 min. The supernatant containing starting material oligonucleotides was removed and the reddish solid at the bottom of the centrifuge tube was dispersed in sodium phosphate buffer (10 mM, pH 7.0). This procedure was repeated and the reddish solid obtained was finally redispersed in sodium phosphate buffer (10 mM, 1.5 mL, pH 7.0).

Hybridization and assembly experiments were carried out with 1 pmol of each triplex–AuNP conjugate (AuNP–A and AuNP–B) in sodium phosphate buffer containing $MgCl_2$. The conjugate was quickly mixed with the same volume of $MgCl_2$ (20 mM) and sodium phosphate (100 mM, pH 5.0). The mixed solution was heated to 65 °C for 5 min, slowly cooled to 37 °C, and then stored at 37 °C for 24 h and at 4 °C for 24 h.

Received: March 20, 2006
Revised: May 29, 2006
Published online: August 4, 2006

**Keywords:** DNA structures · gold · nanoparticles · protonation · self-assembly

[1] a) C. A. Mirkin, R. L. Letsinger, R. C. Mucic, J. J. Storhoff, *Nature* **1996**, *382*, 607–609; b) A. P. Alivisatos, K. P. Johnsson, X. Peng, T. E. Wilson, C. J. Loweth, M. P. Bruchez, Jr., P. G. Schultz, *Nature* **1996**, *382*, 609–611.

[2] a) J. J. Storhoff, R. Elghanian, R. C. Mucic, C. A. Mirkin, R. L. Letsinger, *J. Am. Chem. Soc.* **1998**, *120*, 1959–1964; b) T. A. Taton, C. A. Mirkin, R. L. Letsinger, *Science* **2000**, *289*, 1757–1759; c) N. L. Rosi, C. A. Mirkin, *Chem. Rev.* **2005**, *105*, 1547–1562; d) C. M. Niemeyer, C. A. Mirkin, *NanoBiotechnology: Concepts, Methods and Applications*, Wiley-VCH, Weinheim, **2004**.

[3] a) P. Hazarika, B. Ceyhan, C. M. Niemeyer, *Angew. Chem.* **2004**, *116*, 6631–6633; *Angew. Chem. Int. Ed.* **2004**, *43*, 6469–6471; b) D. Liu, S. Balasubramanian, *Angew. Chem.* **2003**, *115*, 5912–5914; *Angew. Chem. Int. Ed.* **2003**, *42*, 5734–5736.

[4] D. Praseuth, A. L. Guieysse, C. Helene, *Biochim. Biophys. Acta* **1999**, *1489*, 181–206.

[5] a) C. Helene, *Nature* **1998**, *391*, 436; b) P. P. Chan, P. M. Glazer, *J. Mol. Med.* **1997**, *75*, 267–282; c) M. Faria, C. Giovannangeli, *J. Gene Med.* **2001**, *3*, 299–310.

[6] a) Y. Chen, S.-H. Lee, C. Mao, *Angew. Chem.* **2004**, *116*, 5449–5452; *Angew. Chem. Int. Ed.* **2004**, *43*, 5335–5338; b) M.

 © 2006 Wiley-VCH Verlag GmbH & Co. KGaA, Weinheim 

Brucale, G. Zuccheri, B. Samori, *Org. Biomol. Chem.* **2005**, *3*, 575 – 577.
[7] After submission of the manuscript, a related, but different approach to the triplex-driven assembly of AuNPs was reported: M. S. Han, A. K. R. Lytton-Jean, C. A. Mirkin, *J. Am. Chem. Soc.* **2006**, *128*, 4954 – 4955.
[8] D. Murphy, R. Eritja, G. Redmond, *Nucleic Acids Res.* **2004**, *32*, e65.
[9] A. K. R. Lytton-Jean, C. A. Mirkin, *J. Am. Chem. Soc.* **2005**, *127*, 12754 – 12755.
[10] a) A. Ferdous, H. Watanabe, T. Akaike, A. Maruyama, *Nucleic Acids Res.* **1998**, *26*, 3949 – 3954; b) N. Sugimoto, P. Wu, H. Hara, Y. Kawamoto, *Biochemistry* **2001**, *40*, 9396 – 9405.

 © 2006 Wiley-VCH Verlag GmbH & Co. KGaA, Weinheim 

*Surface Chemistry*

DOI: 10.1002/anie.200600692

# Manganese Oxide Nanoparticles Electrodeposited on Platinum Are Superior to Platinum for Oxygen Reduction**

*Mohamed S. El-Deab and Takeo Ohsaka**

A four-electron reduction of molecular oxygen to water at a reasonably low overpotential is the ultimate goal of many investigations. This reaction plays a vital role in electrochemical energy-conversion systems in metal–air batteries and fuel cells. Several attempts have been made at the development of efficient electrocatalysts.[1–18] These include the use of gold-nanoparticle-based electocatalysts which have tunable size and crystallographic orientation.[19–25] The combined use of manganese oxide and cobalt hexadecafluoro or octacyano phthalocyanine has been proposed as novel electrocatalyst for the oxygen-reduction reaction (ORR).[26,27]

Platinum as an electrocatalyst for the ORR is superior to many of the previously investigated electrocatalysts as it supports a direct four-electron reduction of $O_2$ at relatively low overpotentials. However, the Pt surface suffers from the rapid formation of oxides (especially when used in alkaline media), which causes a gradual decrease of the electrocatalytic performance towards the ORR.[28]

Surface oxides and some specifically adsorbed species at the Pt electrode surface impede the parallel adsorption mode of molecular oxygen, which is a prerequisite for the direct four-electron reduction; the overall reaction is retarded and consequently an appreciable amount of the two-electron reduction product of $O_2$, hydrogen peroxide, is produced.[3,7,29]

Recent studies show that alloying Pt with Fe results in significant enhancement of the electrocatalytic ability towards the ORR owing to the sharing of the empty d orbital of each Fe center (an electronic factor).[30] In contrast, the enhanced electrocatalysis of Pt upon alloying with Cr, Co, or Ni originates from one or a combination of the following two reasons: 1) the shrinking of the Pt–Pt interatomic distance brought about by alloying (geometric factor);[29,31] 2) retardation of the poisoning of the Pt electrode surface by inhibiting the formation of adsorbed OH species.[6]

Herein we demonstrate an alternative way of modifying a Pt surface. The Pt electrode surface was modified by the electrodeposition of manganese oxide nanoparticles (nano-MnOx), which was done with the expectation of obtaining a durable electrode with high electrocatalytic activity towards the ORR.

Manganese oxide has been widely used as the main constituent material of air batteries owing to its economical and environmental advantages[32,33] in addition to its catalytic activity for oxygen reduction.[28,34,35] Furthermore, this material exhibits a high efficiency towards the catalytic disproportionation of hydrogen peroxide generated at the surface of a Pt electrode (albeit the hydrogen peroxide formation is very slight).

Figure 1a shows a typical scanning electron microscope (SEM) image obtained for the nano-MnOx/Pt electrode. The MnOx is deposited with a porous texture composed of intersected nanorods (average width of about 20 nm) onto the Pt electrode. This porous texture homogeneously covers the entire surface of the electrode, which enables easy access of the solution species to the underlying Pt substrate through channels across the MnOx nanotexture. Transmission electron microscope (TEM) imaging of the MnOx electrodeposited onto Pt mesh (Figure 1b) indicates that the MnOx forms nanorods with an aspect ratio of about 45. The rate of the propagation of the MnOx crystal exceeds the nucleation rate

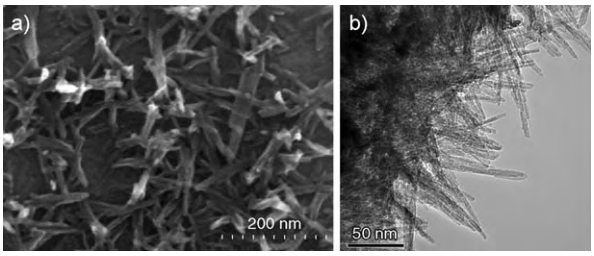


***Figure 1.*** a) SEM image of the nano-MnOx/Pt electrode and b) TEM image of the nano-MnOx/Pt mesh. MnOx nanoparticles were electrodeposited on the Pt electrode or Pt mesh (2000 mesh-grade) from an aqueous solution of $Na_2SO_4$ (0.1 M) containing $Mn(CH_3COO)_2$ (0.1 M) by applying 25 potential cycles between 0 and 0.4 V versus Ag/AgCl/KCl(sat) at 20 $mV s^{-1}$.[36]

[*] Prof. Dr. T. Ohsaka
Department of Electronic Chemistry
Tokyo Institute of Technology
4259 Nagatsuta, Midori-ku, Yokohama 226-8502 (Japan)
Fax: (+81) 45-924-5489
E-mail: ohsaka@echem.titech.ac.jp
Homepage: http://www.echem.titech.ac.jp/~ohsaka/ohsaka.html
Dr. M. S. El-Deab
Department of Chemistry
Faculty of Science
Cairo University, Cairo (Egypt)
E-mail: msaada68@yahoo.com

[**] Financial support by New Energy and Industrial Technology Development Organization (NEDO), Japan is greatly acknowledged.


© 2006 Wiley-VCH Verlag GmbH & Co. KGaA, Weinheim

and thus the formation of the nanorods with a high aspect ratio predominates.[37]

Figure 2 shows typical X-ray diffraction (XRD) patterns of Pt substrates loaded with different amounts of nano-MnOx

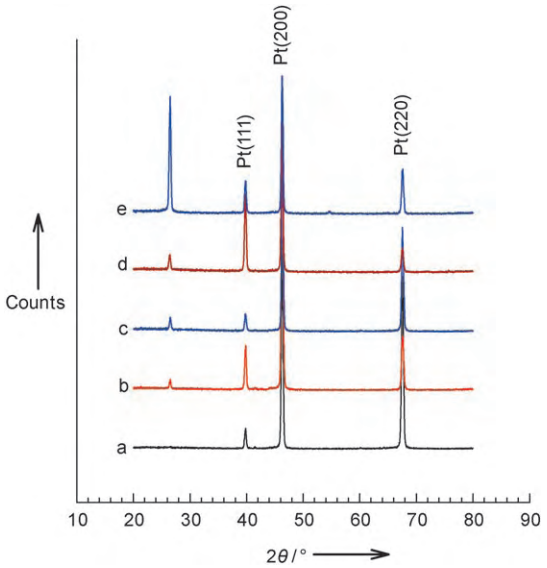


***Figure 2.*** XRD patterns for a) bare Pt, and b–e) nano-MnOx/Pt electrodes. The nano-MnOx/Pt electrodes were prepared in the same way as that described in the caption of Figure 1 with b) 5, c) 25, d) 50, e) 100 potential cycles, respectively.

(patterns b–e) and that of the unloaded Pt substrate (pattern a). The XRD patterns reveal that MnOx is electrodeposited in a crystalline phase giving rise to a sharp peak at a $2\theta$ value of around 26.5°. This peak emerges as MnOx is electrodeposited onto the Pt substrate and corresponds to the $(11\bar{1})$ crystallographic plane of the manganite phase (manganese oxide hydroxide, MnOOH)[38,39].

Steady-state hydrodynamic voltammetry with a rotating ring–disk electrode (RRDE) has long been used to evaluate the electrocatalytic activity of several electrocatalysts towards the ORR.[5–9,19–21,40] Figure 3 shows hydrodynamic voltammograms recorded at 200 rpm for the ORR at a bare Pt disk (curve a; $I_D$ is disk current) and nano-MnOx/Pt disks (curves b and c) with Pt ring electrodes in $O_2$-saturated KOH solution (0.1 M). The Pt ring was potentiostated at +0.5 V. The top curves (a′–c′) represent the corresponding Pt ring currents ($I_R$) arising from the oxidation of hydrogen peroxide, $HO_2^-$, generated at the individual disk electrodes. The ORR current begins to flow at potentials of about +0.025 and +0.05 V (vs. Ag/AgCl) at the nano-MnOx/Pt electrodes prepared by applying 5 (curve b) and 25 (curve c) potential cycles. These potentials are positive by 55 mV (curve b) and 80 mV (curve c) compared to that obtained at the bare Pt electrode (curve a).

The enhancement of the ORR at the nano-MnOx/Pt electrodes is further verified by calculating the number of electrons ($n$) involved in the ORR as it is inherently related to the relative ratio of the disk and ring currents of the RRDE [Eq. (1),[21] in which $n=4$ if $I_R=0$ (i.e., no electrogeneration

$$n = 4-2\,I_R/N\,I_D \qquad (1)$$

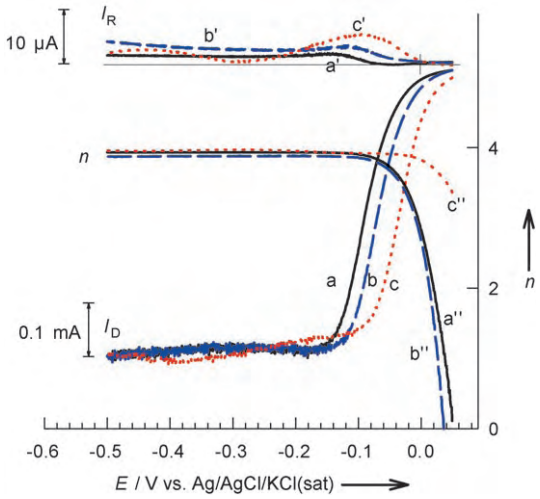


***Figure 3.*** Steady-state voltammograms for the ORR, measured in $O_2$-saturated KOH (0.1 M), at a) bare Pt disk and b,c) nano-MnOx/Pt disk electrodes ($\phi=6.0$ mm). The electrodeposition conditions used for the MnOx preparation were the same as that described in the caption of Figure 1 with b) 5; c) 25 potential cycles. Rotation rate: 200 rpm; potential scan rate of the disk electrode: 10 mV s$^{-1}$. Curves a′–c′ represent the corresponding Pt-ring currents (polarized at +0.5 V). Curves a″–c″ represent the number of electrons ($n$) involved in the ORR at the different disk electrodes.

of hydrogen peroxide) and $n=2$ if the ratio $I_R/NI_D=1$ (i.e., exclusive reduction of oxygen to hydrogen peroxide), and $N$ is the collection efficiency of the RRDE]. Curves a″–c″ of Figure 3 show the variation of $n$ at the bare Pt (a″) and nano-MnOx/Pt disk electrodes (b″ and c″). Curve c″ demonstrates exclusive four-electron reduction of $O_2$ to water (or $OH^-$ in alkaline medium) at the nano-MnOx/Pt electrode at a fairly positive potential compared with that at the bare Pt electrode (curve a″). The enhancement of the ORR in terms of a positive shift of the onset potential with a slight increase in the ring current (curve c′) may suggest a change in the reduction pathway of oxygen upon the electrodeposition of the MnOx nanoparticles onto the Pt surface.

To find out the origin of the ORR enhancement at the nano-MnOx/Pt electrodes, X-ray photoelectron spectroscopy (XPS) measurements of the electrodes were taken and the results are shown in Figure 4 A–C, in which the spectra of Pt 4f, Mn 2p, and O 1s orbitals are obtained at a) bare Pt and b,c) nano-MnOx/Pt surfaces. An inspection of Figure 4 reveals the following points: 1) Figure 4 A (curves a–c) shows that there is no significant change of the binding energies of the 4f orbitals of Pt upon loading MnOx nanoparticles. This fact indicates that the electronic structure of the Pt surface remains unchanged even after loading with nano-MnOx. Thus, the enhancement of the electrocatalytic performance after nano-MnOx loading does not originate from a change in the electronic properties of the Pt surface atoms. 2) Figure 4 B indicates that Mn exists in a cationic state rather than in an elemental state as evidenced from the positive shift of the 2p binding energy of Mn (a shift from 650 and 638.8 eV for $2p_{1/2}$ and $2p_{3/2}$ of elemental Mn to 653.8 and 641.7 eV, respectively, in the sample). 3) The XPS spectrum of the oxygen in MnOx (Figure 4 C) shows a rather broad peak

 © 2006 Wiley-VCH Verlag GmbH & Co. KGaA, Weinheim 

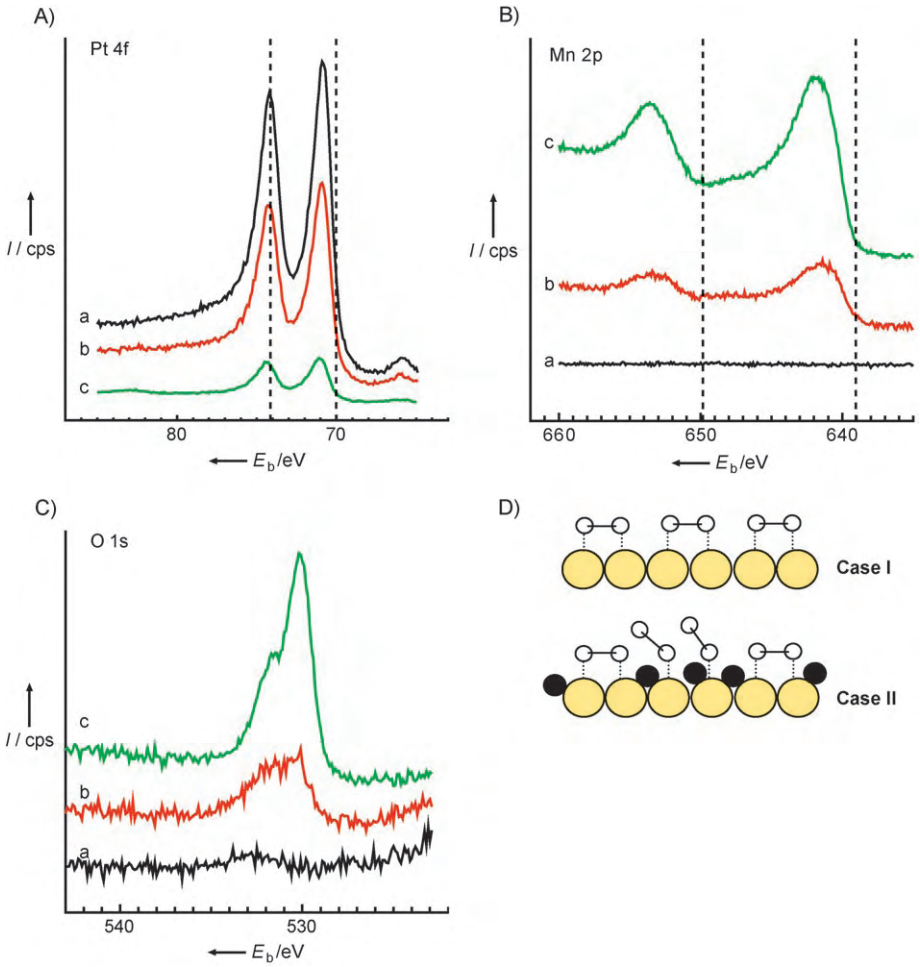


***Figure 4.*** XPS spectra of A) Pt 4f, B) Mn 2p, and C) O 1s obtained for a) bare Pt and b,c) nano-MnOx/Pt electrodes. The electrodeposition conditions used for the MnOx preparation were the same as that described in the caption of Figure 1 with b) 25; c) 100 potential cycles. The dotted lines in Figures 4A and 4B correspond to the binding energies of $4f_{7/2}$ and $4f_{5/2}$ of elemental Pt and $2p_{1/2}$ and $2p_{3/2}$ of elemental Mn, respectively. D) Illustrates the proposed adsorption modes of molecular oxygen (small white circles) at the Pt surface (large yellow circles) in the absence (Case I) and presence (Case II) of nano-MnOx (black circles).

for the low loading of MnOx, which develops into a peak with a shoulder upon increasing the amount of the electrodeposited nano-MnOx (curve c). The origin of this split could be reasonably attributed to the presence of the oxygen in hydroxide and oxide forms in MnOOH.

As the catalytic reaction does not occur at any surface unless at least one of the reactants is chemisorbed, the observed enhancement of the electrocatalysis originates from a change in the adsorption orientation of molecular oxygen at the nano-MnOx/Pt surface. Figure 4D shows a diagram of the adsorption modes of molecular oxygen at bare Pt and nano-MnOx/Pt surfaces. At the bare Pt surface, the parallel adsorption orientation of $O_2$ molecules prevails (as evidenced from the almost-zero ring current in Figure 3, curve a′). Thus, the adsorption of one $O_2$ molecule per pair of Pt active sites is assumed. However, at the nano-MnOx/Pt surface, the adsorbed $O_2$ molecules have a mixed-orientation (i.e., parallel and end-on). The increased ring current provides evidence of end-on orientation, which reflects an increased amount of hydrogen peroxide present (as a two-electron reduction product; compare curves b′ and c′ with curve a′ of Figure 3). The mixed adsorption mode (Case II in Figure 4D) is assumed to result in the nano-MnOx/Pt surface having more adsorbed molecular oxygen species. In this case, the parallel and end-on orientation modes result in the adsorption of four oxygen molecules per three pairs of Pt active sites. Consequently, the higher degree of the adsorption of $O_2$ molecules in the latter case causes an increase in the pre-exponential factor of the Arrhenius equation for the ORR and thus a higher reaction rate is observed as a positive shift of the onset potential of the ORR. A similar explanation has been proposed by Paulus et al.[41] They found Arrhenius apparent activation energies for the ORR at different carbon-supported Pt–Ni and Pt–Co catalysts to be similar to that estimated at a carbon-supported Pt catalyst, although the former catalysts showed a higher catalytic activity than the latter. Thus, the pre-exponential factor in the Arrhenius rate expression has been assumed as the controlling parameter that determines the variations in the observed rates.[41]

In summary, the electrodeposition of manganese oxide nanorods onto Pt electrodes was found to cause a significant positive shift of the onset potential of the ORR compared with that at the bare Pt electrode. The change of the adsorption orientation of oxygen molecules, from the parallel (bridged) orientation at the bare Pt electrode to the mixed orientation of the parallel and end-on modes at the nano-MnOx/Pt electrode, is considered to be the cause for the higher population of oxygen molecules at the MnOx/Pt surface, which results in higher electrocatalysis for the ORR.

Received: February 22, 2006
Revised: June 14, 2006
Published online: August 4, 2006

**Keywords:** adsorption · electrochemistry · heterogeneous catalysis · nanostructures · surface chemistry

[1] "Development of non-platinum-based electrocatalysts for oxygen reduction": T. Ohsaka, M. S. El-Deab in *Recent Research Developments in Electrochemistry, Vol. 7*, Transworld Research Network Publisher, India, **2004**, and references therein.

 © 2006 Wiley-VCH Verlag GmbH & Co. KGaA, Weinheim 

[2] K. Kinoshita, *Electrochemical Oxygen Technology*, Wiley, New York, **1992**.
[3] N. M. Markovic, P. N. Ross, *Surf. Sci. Rep.* **2002**, *45*, 117, and references therein.
[4] C. H. Brian, A. Heinzel, *Nature* **2001**, *414*, 345.
[5] M. Watanabe, H. Igarashi, K. Yoshioka, *Electrochim. Acta* **1995**, *40*, 329.
[6] A. B. Anderson, J. Roques, S. Mukerjee, V. S. Murthi, N. M. Markovic, V. Stamenkovic, *J. Phys. Chem. B* **2005**, *109*, 1198, and references therein.
[7] T. J. Schmidt, U. A. Paulus, H. A. Gasteiger, R. J. Behm, *J. Electroanal. Chem.* **2001**, *508*, 41.
[8] N. M. Markovic, R. R. Adzic, B. D. Cahan, E. Yeager, *J. Electroanal. Chem.* **1994**, *377*, 249.
[9] M. T. Paffet, J. G. Beery, S. Gottesfeld, *J. Electrochem. Soc.* **1988**, *135*, 1431.
[10] F.-P. Hu, X.-G. Zhang, F. Xiao, J.-L. Zhang, *Carbon* **2005**, *43*, 2931.
[11] A. Bergel, D. Feron, A. Mollica, *Electrochem. Commun.* **2005**, *7*, 900.
[12] R. N. Singh, B. Lal, M. Malviya, *Electrochim. Acta* **2004**, *49*, 4605.
[13] H. Dafydd, D. A. Worsley, H. N. McMurray, *Corros. Sci.* **2005**, 47, 3006.
[14] O. S. -Feria, S. Duron, *Int. J. Hydrogen Energy* **2002**, *27*, 451.
[15] Y. Lin, X. Cui, X. Ye, *Electrochem. Commun.* **2005**, *7*, 267.
[16] M. Born, P. Bogdanoff, S. Fiechter, H. Tributsch, *J. Electroanal. Chem.* **2005**, *578*, 339.
[17] J. Hernandez, J. S. -Gullon, E. Herrero, *J. Electroanal. Chem.* **2004**, *574*, 185.
[18] J.-M. Leger, *Electrochim. Acta* **2005**, *50*, 3123.
[19] M. S. El-Deab, T. Ohsaka, *Electrochim. Acta* **2002**, *47*, 4255.
[20] M. S. El-Deab, T. Okajima, T. Ohsaka, *J. Electrochem. Soc.* **2003**, *150*, A851.
[21] M. S. El-Deab, T. Sotomura, T. Ohsaka, *Electrochem. Commun.* **2005**, *7*, 29.
[22] M. S. El-Deab, T. Sotomura, T. Ohsaka, *J. Electrochem. Soc.* **2005**, *152*, C1.
[23] F. Gao, M. S. El-Deab, T. Okajima, T. Ohsaka, *J. Electrochem. Soc.* **2005**, *152*, A1226.
[24] M. S. El-Deab, T. Sotomura, T. Ohsaka, *J. Electrochem. Soc.* **2005**, *152*, C730.
[25] Y. Zhang, S. Asahina, S. Yoshihara, T. Shirakashi, *Electrochim. Acta* **2003**, *48*, 741.
[26] K. Arihara, L. Mao, P. A. Liddell, E. M. -Ochoa, A. L. Moore, T. Imase, D. Zhang, T. Sotomura, T. Ohsaka, *J. Electrochem. Soc.* **2004**, *151*, A2047.
[27] L. Mao, K. Arihara, T. Sotomura, T. Ohsaka, *Electrochim. Acta* **2004**, *49*, 2515.
[28] L. Mao, D. Zhang, T Sotomura, K. Nakatsu, N. Koshiba, T. Ohsaka, *Electrochim. Acta* **2003**, *48*, 1015.
[29] M.-ki Min, J. Cho, H. Kim, *Electrochim. Acta* **2000**, *45*, 4211.
[30] T. Toda, H. Igarashi, M. Watanabe, *J. Electroanal. Chem.* **1999**, *460*, 258.
[31] T. Toda, H. Igarashi, M. Watanabe, *J. Electrochem. Soc.* **1998**, *145*, 4185.
[32] S. L. Brock, N. Duan, Z. R. Tian, O. Giraldo, H. Zhou, S. L. Suib, *Chem. Mater.* **1998**, *10*, 2619.
[33] J. Chen, J. C. Jin, V. Purohit, M. B. Cutlip, S. L. Suib, *Catal. Today* **1997**, *33*, 205.
[34] L. Mao, T. Sotomura, K. Nakatsu, N. Koshiba, D. Zhang, T. Ohsaka, *J. Electrochem. Soc.* **2002**, *149*, A504.
[35] T. Ohsaka, L. Mao, K. Arihara, T. Sotomura, *Electrochem. Commun.* **2004**, *6*, 273.
[36] M.-S. Wu, P.-C. J. Chiang, *Electrochem. Solid-State Lett.* **2004**, *7*, A123.
[37] E. Budevski, G. Staikov, W. J. Lorenz, *Electrochemical Phase Formation and Growth*, VCH, Weinheim, **1996**, chap. 4.
[38] Powder Diffraction File, W. F. McClune, Editor, International Center for Diffraction Data (ICDD), USA, **2003**.
[39] M. J. Garrido, *C. R. Hebd. Seances Acad. Sci.* **1935**, *200*, 69.
[40] E. Higuchi, H. Uchida, M. Watanabe, *J. Electroanal. Chem.* **2005**, *583*, 69.
[41] U. A. Paulus, A. Wokaun, G. G. Scherer, T. J. Schmidt, V. Stamenkovic, N. M. Markovic, P. N. Ross, *J. Phys. Chem. B* **2002**, *106*, 4181.

 © 2006 Wiley-VCH Verlag GmbH & Co. KGaA, Weinheim 

Gold Luminescent Probes

DOI: 10.1002/anie.200601526

# Luminescence Studies of the Intracellular Distribution of a Dinuclear Gold(I) N-Heterocyclic Carbene Complex**

*Peter J. Barnard, Louise E. Wedlock, Murray V. Baker,* Susan J. Berners-Price,* David A. Joyce, Brian W. Skelton, and James H. Steer*

Gold compounds are of significant importance in medicine, primarily for the treatment of rheumatoid arthritis.[1] We have

[*] Dr. P. J. Barnard, L. E. Wedlock, Prof. M. V. Baker, Prof. S. J. Berners-Price, Dr. B. W. Skelton
Chemistry M313
School of Biomedical
Biomolecular and Chemical Sciences
The University of Western Australia
35 Stirling Highway, Crawley, WA 6009 (Australia)
Fax: (+61) 8-6488 1005
E-mail: mvb@chem.uwa.edu.au
sbp@chem.uwa.edu.au
Homepage: http://www.chem.biomedchem.uwa.edu.au/staff/homepages/MurrayBaker
http://www.chem.biomedchem.uwa.edu.au/staff/homepages/SueBernersPrice
Prof. D. A. Joyce, J. H. Steer
Pharmacology Unit
School of Medicine and Pharmacology
The University of Western Australia
35 Stirling Highway, Crawley, WA 6009 (Australia)

[**] Financial support for this work was provided by an Australian Research Council Discovery grant. Use of the ChemMat-CARS Sector 15 at the Advanced Photon Source was supported by the Australian Synchrotron Research Program, which is funded by the Commonwealth of Australia under the Major National Research Facilities Program. Chem-MatCARS Sector 15 is also supported by the National Science Foundation/Department of Energy under Grant Nos. CHE9522232 and CHE0087817 and by the Illinois Board of Higher Education. The Advanced Photon Source is supported by the US Department of Energy, Basic Energy Sciences, Office of Science, under Contract No. W-31109-Eng-38. We thank Dr Ron Clarke for very helpful discussions on the luminescence studies.

Supporting information for this article is available on the WWW under http://www.angewandte.org or from the author.

 WILEY InterScience DISCOVER SOMETHING GREAT

© 2006 Wiley-VCH Verlag GmbH & Co. KGaA, Weinheim

been interested in the development of $Au^I$ complexes of phosphine[2] and more recently N-heterocyclic carbene (NHC) ligands as potential antitumor agents that selectively target the mitochondria of cancer cells.[3]

Recently, we reported the synthesis and structures of a family of fascinating dinuclear $Au^I$–carbene complexes, for example, **1** and **2**.[4] These complexes have demonstrated significant antimitochondrial activity[3] and, interestingly, the cyclophane ligand framework allows fine control over the

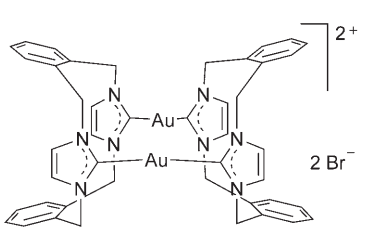


**1**

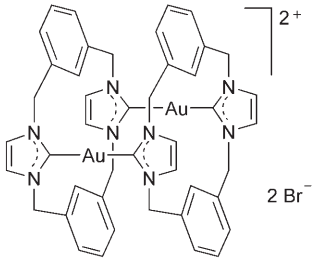


**2**

intramolecular distance between the gold atoms. Compound **1** supports a short Au···Au interaction of 3.0485(3) Å and is luminescent, whereas compound **2**, with a significantly longer Au···Au distance (3.7917(4) Å), is not.[4] The luminescence associated with attractive Au···Au (aurophilic) interactions has been of great interest, both from experimental[5] and theoretical[6] points of view, and complexes possessing such properties offer potential as luminescent display devices and sensors.[7]

Our interest in targeting specific cellular organelles (mitochondria) led us to consider the possibility of exploiting the native luminescence of **1** to determine its intracellular distribution by using fluorescence microscopy. However, the luminescence profile for **1** ($\lambda_{ex}$ 260 nm, $\lambda_{em}$ 400 nm; ex = excitation, em = emission)[4] is unsuitable for such studies, as the high energy excitation would lead to interference from other molecules in the cell.

Previous studies have shown that the excitation and emission energies associated with short Au···Au interactions are, in some cases, red shifted as a result of a contraction of the Au···Au distance.[8,9] Herein, we report studies on a new dinuclear $Au^I$–NHC complex in which the ligand is designed to support a shorter Au···Au distance than that of **1**.

The imidazolium salt, NHC-ligand precursor **3**, was synthesized from an equimolar ratio of 1,3-bis(1-imidazolyl)-propane[10] and α,α′-dibromo-*o*-xylene in refluxing acetonitrile under high dilution conditions. The dinuclear $Au^I$ complex **4** was synthesized from an equimolar ratio of **3** and $(Me_2S)AuCl$ in hot *N*,*N*-dimethylformamide (DMF; ≈90 °C), with sodium acetate acting as a mild base.[4] The imidazolium salt **3** is unsymmetrical about the imidazolium units, resulting in *cis* and *trans* isomers of the dinuclear $Au^I$ complex **4**.

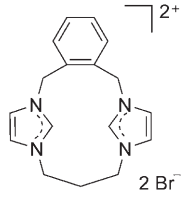


**3**

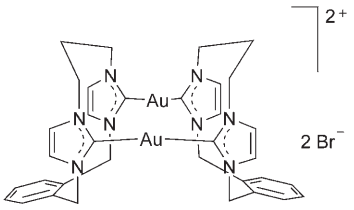


*cis*-**4**

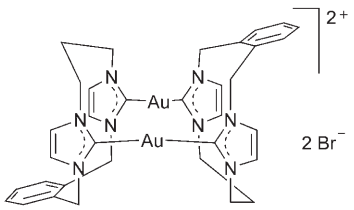


*trans*-**4**

C*is*- and *trans*-**4** cocrystallized as their bromide salts in a 1:1 ratio. Single crystals suitable for X-ray diffraction studies were grown from a methanol solution of both isomers. In the solid state, in space group *C*2/*c*,[11] the cation of *cis*-**4** is disposed about a twofold axis (Au···Au′ 2.9290(4); Au···C 2.035(6), 2.033(6) Å; C–Au–C 177.4(3)°), whereas that of *trans*-**4** is disposed about a crystallographic inversion center (Au···Au′ 2.9582(4); Au···C 2.036(6), 2.029(6) Å; C–Au–C 175.5(3)°), (Figure 1). Deviations of the Au atoms from the $C_3N_2$ carbene planes are $\delta(Au) =$ 0.19(1), 0.21(1) (*trans*); 0.07(1), 0.15(1) Å (*cis*). The *cis* cation of **4** is twisted about the Au···Au line ($\tau$(C–Au···Au–C) 12.6(3)°), which is seemingly a consequence of inter- rather than intramolecular interactions.

The isomeric forms of **4** were separated by fractional crystallization from water, with *trans*-**4** being the less soluble isomer. After recrystallization from ethanol, *cis*-**4** was obtained as a colorless microcrystalline powder and *trans*-**4** as colorless needles. Upon exposure to an ambient atmosphere, crystals of *trans*-**4** rapidly developed a pale green color.[12] The $^1H$ and $^{13}C$ NMR signals for *cis*- and *trans*-**4** (298 K, $CD_3OD$) are sharp. The number of signals detected is the same for each isomer as would be expected for relatively rigid complexes with either a mirror plane (*cis*-**4**) or an inversion centre and a twofold axis (*trans*-**4**) through the Au centers. Consistent with the proposed structures, the $^1H$ NMR signals for the benzylic protons for *cis*- and *trans*-**4** give rise to sharp AX patterns, and the protons in the propylene chain give rise to signals showing splitting patterns with the expected geminal and vicinal couplings.

Aqueous solutions of each isomer display identical electronic absorption (see the Supporting Information) and emission properties and *cis*-**4** was selected for cellular localization studies based on its higher aqueous solubility. In aqueous solution, two emission bands are seen with relative intensities that depend on the excitation wavelength used. With excitation at 313 nm, an emission centered at 396 nm is obtained, whereas excitation at 355 nm yields a band centered at 496 nm, and each of the emission bands show distinct excitation spectra (Figure 2). Very similar spectral properties have been reported previously for a system involving short Au···Au interactions.[9] The emission quantum yield ($\Phi$) is also dependent on the excitation wavelength and values of 0.29 ($\lambda_{ex}$ 313 nm) and 0.98 ($\lambda_{ex}$ 350 nm) were determined by using quinine sulfate in $H_2SO_4$ (0.1M) as a reference. Importantly, the lower energy excitation and emission bands are of suitable wavelengths for cellular distribution studies. A further

 © 2006 Wiley-VCH Verlag GmbH & Co. KGaA, Weinheim 

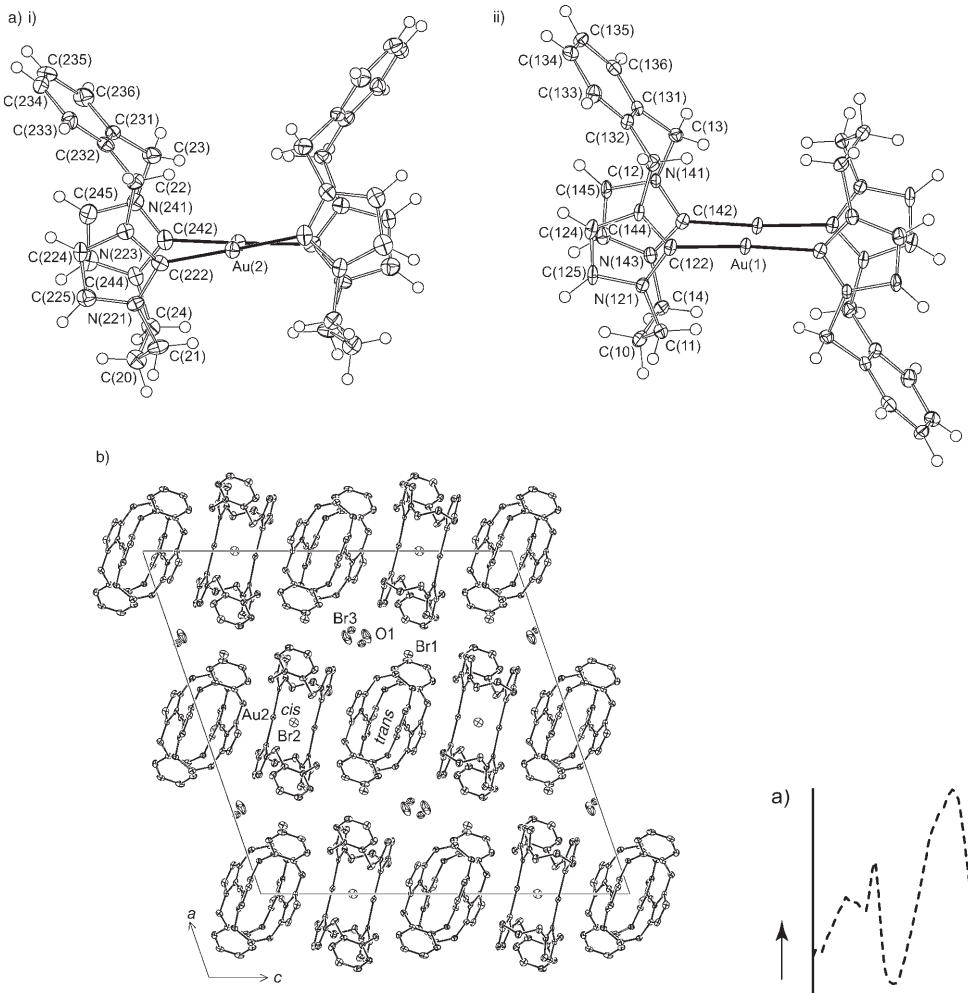


***Figure 1.*** a) The i) *cis*- and ii) *trans*-cations of **4**·$H_2O$. b) Unit cell contents, projected down *b*. Amplitude displacement ellipsoids are depicted at 50% probability; hydrogen atoms, where shown, have arbitrary radii of 0.1 Å.

consideration in assessing the feasibility of such studies is whether the $Au^I$ complex is likely to retain its dinuclear (luminescent) structure under biological conditions as it might be expected that the structure would be degraded by facile ligand exchange reactions with biological thiols. Remarkably, $^1H$ NMR spectroscopy experiments showed no evidence of reaction between *cis*-**4** and glutathione over a period of 28 h (see the Supporting Information).

The uptake and distribution of *cis*-**4** were evaluated in RAW264.7 cells (a mouse macrophage cancer cell line)[13] by using fluorescence confocal microscopy. Figure 3 shows typical brightfield and luminescence images of RAW264.7 cells treated for 15 h with *cis*-**4**. Preserved cell morphology confirmed viability after treatment (Figure 3a). Cellular uptake of *cis*-**4** yielded a clear punctate pattern of luminescence, indicating localization into cellular organelles (Figure 3b). Cell nuclei (identifiable on brightfield images) carried little or no luminescence, indicating that *cis*-**4** was not concentrated in the nucleus. No cellular luminescence was detected in the absence of added gold complex.

Colocalization studies of *cis*-**4** with a lysosomal dye, lysotracker red, and a mitochondrial dye, mitotracker green, provided evidence for localization of *cis*-**4** within lysosomes rather than mitochondria. Luminescence images of RAW264.7 cells treated with *cis*-**4** and lysotracker red (Figure 4b and c) show clear regional colocalization. We observed that the punctate distribution of *cis*-**4** luminescence became less pronounced in cells exposed to lysotracker red, suggesting physicochemical interaction between the two compounds in lysosomes. Mitochondrial mitotracker green luminescence did not colocalize with *cis*-**4** (see the Supporting Information).

Intracellular localization to lysosomes has been noted for several other metal complexes. For example the antiarthritic drug, gold thiomalate (myocrisin), is readily taken up by macrophages and the gold is almost

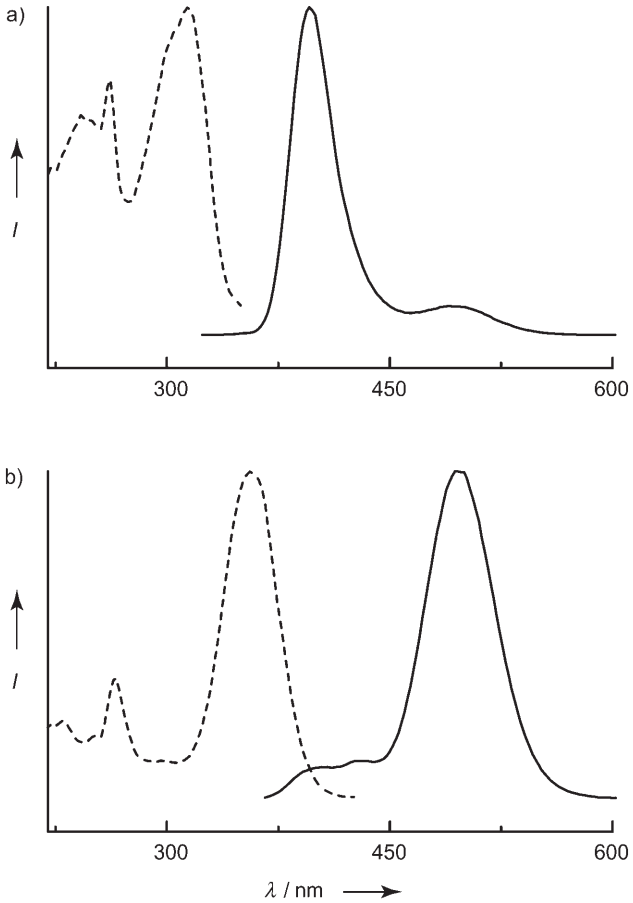


***Figure 2.*** Normalized electronic emission (solid line) and excitation spectra (dashed line) for an aqueous solution of *cis*-**4** ($5\times10^{-5}$ M) at 25 °C, a) $\lambda_{ex}$ 313 nm, $\lambda_{em}$ 396 nm ($\Phi=0.29$) and b) $\lambda_{ex}$ 355 nm, $\lambda_{em}$ 496 nm ($\Phi=0.98$).

 © 2006 Wiley-VCH Verlag GmbH & Co. KGaA, Weinheim 

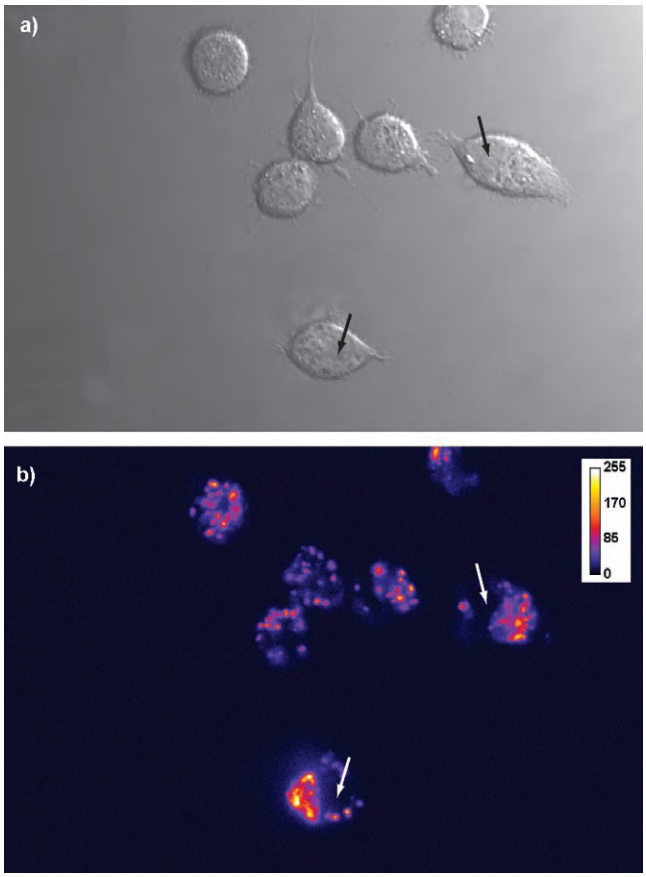


***Figure 3.*** Cellular distribution of *cis*-**4** (200 μM) in RAW264.7 cells after incubation for 15 h at 37 °C; a) brightfield image and b) luminescence image ($\lambda_{ex}$ 351 nm). The black (a) and white (b) arrows mark the position of the nucleus.

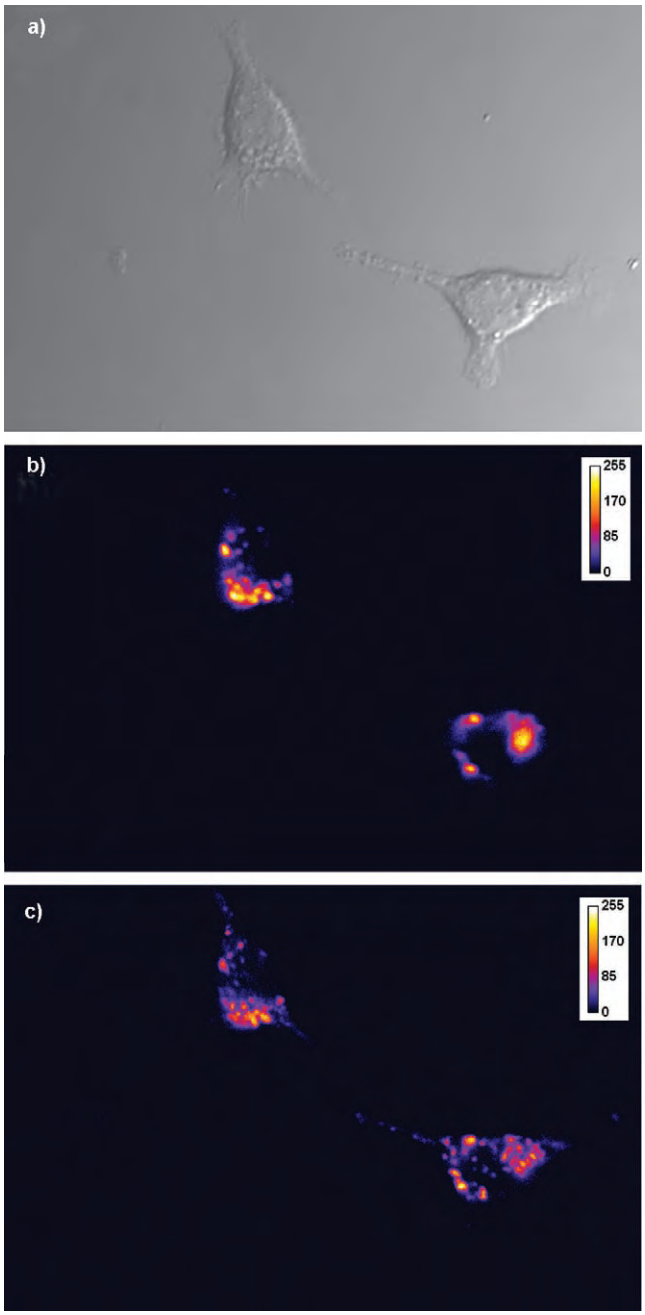


***Figure 4.*** Cellular distribution of *cis*-**4** and lysotracker red in RAW264.7 cells after incubation with *cis*-**4** (15 h, 200 μM) and lysotracker red (20 min, 50 nM) at 37 °C; a) brightfield image and b) luminescence image ($\lambda_{ex}$ 351 nm) showing *cis*-**4** distribution and c) luminescence image ($\lambda_{ex}$ 543 nm) showing lysotracker red distribution.

exclusively deposited in lysosomes.[14] Fluorescence microscopy studies of both zinc–bis(thiosemicarbazone) complexes[15] and a dinuclear platinum complex labeled with a fluorescent tag[16] have shown sequestration of the complexes in lysosomes. These latter studies have demonstrated also that intracellular distribution is strongly dependent on the cell type. RAW264.7 cells were selected for the present study because their adherent properties make them ideal for investigation by confocal microscopy. Notably, *cis*-**4** exhibits only modest cytotoxicity in this cell line ($IC_{50}$ 52 μM, 48 h incubation, see the Supporting Information). Preliminary studies indicate greater potency in other cell lines, such as the human promyelocytic leukaemia cell line, HL 60[17] ($IC_{50}$ 10 μM, 48 h incubation, see the Supporting Information). Further studies are in progress to investigate the intracellular distribution of *cis*-**4** in other cell lines to determine whether a correlation exists between cytotoxicity and localization to mitochondria.

In summary, we have synthesized a dinuclear gold(I) complex in which the bidentate N-heterocyclic carbene ligand has been specifically designed to support Au···Au interactions of a predetermined length. Shortening the Au···Au distance allows the luminescence profile of the resultant dinuclear complex to be red shifted and thereby "tuned" to the desired range. By exploiting the inherent luminescent properties of antimitochondrial dinuclear $Au^I$ complexes, there is potential to investigate their cellular processing in different cancer cell lines by using confocal fluorescence microscopy. This approach is particularly advantageous as it allows cellular imaging studies to be conducted without the need to attach a fluorescent tag. Apart from the synthetic challenges involved in such an approach, the attached emissive group will most likely change the intracellular distribution of the $Au^I$ complex

 © 2006 Wiley-VCH Verlag GmbH & Co. KGaA, Weinheim 

by altering the fundamental properties (e.g. charge, lipophilicity) that determine the potential localization to mitochondria.

## Experimental Section

Full details of the synthesis and spectroscopic characterization of **3** and **4**, the determination of the emission quantum yields for **4**, and the experimental procedures used in the cytotoxicity and confocal microscopy studies are given in the Supporting Information.

Received: April 18, 2006
Revised: June 27, 2006
Published online: August 10, 2006

**Keywords:** bioinorganic chemistry · cellular distribution · gold · luminescent probes · N-heterocyclic carbenes

[1] a) W. F. Kean, L. Hart, W. W. Buchanan, *Br. J. Rheumatol.* **1997**, *36*, 560 – 572; b) C. F. Shaw III, *Chem. Rev.* **1999**, *99*, 2589 – 2600; c) E. R. T. Tiekink, *Crit. Rev. Oncol. Hemat.* **2002**, *42*, 225 – 248.

[2] a) M. J. McKeage, S. J. Berners-Price, P. Galettis, R. J. Bowen, W. Brouwer, L. Ding, L. Zhuang, B. C. Baguley, *Cancer Chemother. Pharmacol.* **2000**, *46*, 343 – 350; b) S. J. Berners-Price, R. J. Bowen, P. Galettis, P. C. Healy, M. J. McKeage, *Coord. Chem. Rev.* **1999**, *185–186*, 823 – 836.

[3] P. J. Barnard, M. V. Baker, S. J. Berners-Price, D. A. Day, *J. Inorg. Biochem.* **2004**, *98*, 1642 – 1647.

[4] P. J. Barnard, M. V. Baker, S. J. Berners-Price, B. W. Skelton, A. H. White, *Dalton Trans.* **2004**, 1034 – 1047.

[5] a) R. L. White-Morris, M. M. Olmstead, F. Jiang, D. S. Tinti, A. L. Balch, *J. Am. Chem. Soc.* **2002**, *124*, 2327 – 2336; b) R. L. White-Morris, M. M. Olmstead, S. Attar, A. L. Balch, *Inorg. Chem.* **2005**, *44*, 5021 – 5029; c) V. W.-W. Yam, C.-L. Chan, C.-K. Li, K. M.-C. Wong, *Coord. Chem. Rev.* **2001**, *216–217*, 173 – 194; d) S.-Y. Yu, Z.-X. Zhang, E. C.-C. Cheng, Y.-Z. Li, V. W.-W. Yam, H.-P. Huang, R. Zhang, *J. Am. Chem. Soc.* **2005**, *127*, 17994 – 17995; e) V. J. Catalano, A. O. Etogo, *J. Organomet. Chem.* **2005**, *690*, 6041 – 6050; f) V. J. Catalano, A. L. Moore, *Inorg. Chem.* **2005**, *44*, 6558 – 6566; g) A. A. Mohamed, I. Kani, A. O. Ramirez, J. P. Fackler, Jr., *Inorg. Chem.* **2004**, *43*, 3833 – 3839.

[6] a) H.-X. Zhang, C.-M. Che, *Chem. Eur. J.* **2001**, *7*, 4887 – 4893; b) W.-F. Fu, K.-C. Chan, V. M. Miskowski, C.-M. Che, *Angew. Chem.* **1999**, *111*, 2953 – 2955; *Angew. Chem. Int. Ed.* **1999**, *38*, 2783 – 2785; c) P. Pyykkö, *Angew. Chem.* **2004**, *116*, 4512 – 4557; *Angew. Chem. Int. Ed.* **2004**, *43*, 4412 – 4456; d) P. Pyykkö, *Inorg. Chim. Acta* **2005**, *358*, 4113 – 4130.

[7] a) M. Bardaji, A. Laguna, *Eur. J. Inorg. Chem.* **2003**, 3069 – 3079; b) M. A. Mansour, W. B. Connick, R. J. Lachicotte, H. J. Gysling, R. Eisenberg, *J. Am. Chem. Soc.* **1998**, *120*, 1329 – 1330; c) V. W.-W. Yam, C.-K. Li, C.-L. Chan, *Angew. Chem.* **1998**, *110*, 3041 – 3044; *Angew. Chem. Int. Ed.* **1998**, *37*, 2857 – 2859; d) V. W.-W. Yam, K.-L. Cheung, E. C.-C. Cheng, N. Zhu, K.-K. Cheung, *Dalton Trans.* **2003**, 1830 – 1835.

[8] a) G. A. Bowmaker in *Gold: Progress in Chemistry Biochemistry and Technology* (Ed.: H. Schmidbaur), Wiley, Chichester, **1999**, pp. 841 – 881; b) Z. Assefa, B. G. McBurnett, R. J. Staples, J. P. Fackler, Jr., *Inorg. Chem.* **1995**, *34*, 75 – 83; c) W. E. van Zyl, J. M. Lopez-de-Luzuriaga, A. A. Mohamed, R. J. Staples, J. P. Fackler, Jr., *Inorg. Chem.* **2002**, *41*, 4579 – 4589; d) N. L. Coker, J. A. Krause Bauer, R. C. Elder, *J. Am. Chem. Soc.* **2004**, *126*, 12 – 13.

[9] Z. Assefa, B. G. McBurnett, R. J. Staples, J. P. Fackler, Jr., *Inorg. Chem.* **1995**, *34*, 4965 – 4972.

[10] M. Luo, S. Guo, C. Zhou, R. Xie, *Heterocycles* **1995**, *41*, 1421 – 1424; K. Sato, T. Onitake, S. Arai, T. Yamagishi, *Heterocycles* **2003**, *60*, 779 – 784.

[11] (*cis*-**4**, *trans*-**4**. 4Br. 2"$H_2O$")$_{0.5} \equiv C_{34}H_{38}Au_2Br_2N_8O$, $M = 1128.5$. Monoclinic $C2/c$, $a = 24.939(1)$, $b = 11.3040(5)$, $c = 25.394(1)$ Å, $\beta = 109.042(2)°$, $V = 6767$ Å$^3$. $\rho_{calcd}$ $(Z = 8) = 2.215$ g cm$^{-3}$. $\mu = 3.9$ mm$^{-1}$; specimen: $0.11 \times 0.03 \times 0.02$ mm$^3$; "$T$"$_{min/max} = 0.78$. $2\theta_{max} = 37°$ (monochromatic synchrotron radiation, $\lambda = 0.48595$ Å); $N_t = 66750$, $N = 7859$ ($R_{int} = 0.048$), $N_o = 6933$; $R = 0.036$, $R_w = 0.072$ ($w = (\sigma^2(F^2) + 32\ F^2)^{-1}$); $T$ ca. 103 K. No hydrogens located in association with "O(1)"; Br(3) is modeled as disordered over a pair of well-separated, inversion related sites (3.291(2) Å). CCDC-295083 contains the supplementary crystallographic data for this paper. These data can be obtained free of charge from The Cambridge Crystallographic Data Centre via www.ccdc.cam.ac.uk/data_request/cif.

[12] The color of **4** in solution is solvent dependent, with colorless solutions formed in organic solvents (methanol, ethanol, dimethyl sulfoxide (DMSO), and DMF) and pale green solutions formed in water. It is possible that the green color of solid samples of *trans*-**4** results from the initially colorless crystals absorbing atmospheric water. The fascinating solvent dependence of the emissive behavior of **4** is currently under further investigation, and the results of these studies will be reported in due course.

[13] P. Ralph, I. Nakoinz, *J. Immunol.* **1977**, *119*, 950 – 954.

[14] J. Aaseth, M. Haugen, Ø. Førre, *Analyst* **1998**, *123*, 3 – 6.

[15] A. R. Cowley, J. Davis, J. R. Dilworth, P. S. Donnelly, R. Dobson, A. Nightingale, J. M. Peach, B. Shore, D. Kerr, L. Seymour, *Chem. Commun.* **2005**, 845 – 847.

[16] a) B. A. Jansen, P. Wielaard, G. V. Kalayda, M. Ferrari, C. Molenaar, H. J. Tanke, J. Brouwer, H. J. Reedijk, *J. Biol. Inorg. Chem.* **2004**, *9*, 403 – 413; b) G. V. Kalayda, B. A. Jansen, C. Molenaar, P. Wielaard, H. J. Tanke, H. J. Reedijk, *J. Biol. Inorg. Chem.* **2004**, *9*, 414 – 422.

[17] a) R. Gallagher, S. Collins, J. Trujillo, K. Mcredie, M. Ahearn, S. Tsai, R. Metzgar, G. Aulakh, R. Ting, F. Ruscetti, R. Gallo, *Blood* **1979**, *54*, 713 – 733; b) S. J. Collins, R. C. Gallo, R. E. Gallagher, *Nature* **1977**, *270*, 347 – 349.

 © 2006 Wiley-VCH Verlag GmbH & Co. KGaA, Weinheim 

Materials Science

DOI: 10.1002/anie.200601617

# Metal-Compound-Induced Vesicles as Efficient Directors for Rapid Synthesis of Hollow Alloy Spheres**

*Xuanjun Zhang and Dan Li**

Vesicles in aqueous solutions are fascinating supramolecular self-assembled structures that have extraordinary potential for applications such as microreactors and nanodevices for encapsulation and controlled release.[1–5] Vesicles can form in dilute solution from different surfactants or phospholipids owing to their amphiphilic character.[6] Some ligands with long alkyl chains can form vesicles upon coordination with metal ions.[7] Vesicles can also form from nanoclusters by self-assembly.[8] Quaternary ammonium ions with short alkyl chains do not form vesicles in the absence of other surfactants. We found that tetrabutylammonium bromide ($Bu_4NBr$) can assembly rapidly into vesicles in water when mixed with some metal compounds such as $PdCl_2$, $K[AuCl_4]$, $AgNO_3$, $K_2[PtCl_4]$, or the mixtures of these compounds. These metal-compound-induced vesicles can be applied as efficient directors for the rapid synthesis of hollow alloy spheres.

The vesicle formation after the addition of metal compounds into a $Bu_4NBr$ solution was evidenced by turbidity of the solutions and the distinct red shifts of the UV/Vis absorption (Figure 1). The absorbance of the $K[AuCl_4]$ solution peaked at around 223 and 304 nm. When mixed with KBr solution, the absorbance peaks shifted to 257 and 381 nm, respectively, which is ascribed to the replacement of the $Cl^-$ ligand by $Br^-$, which has a weaker ligand field and leads to a smaller splitting of the $Au^{III}$ d orbitals. Broad absorption peaks with large red shifts were observed after the addition of $Bu_4NBr$ solution. This phenomenon was also observed for the addition of $Bu_4NBr$ to $PdCl_2$, $AgNO_3$, or the mixtures of these salts, and also led to turbidity of the solutions. The formation of vesicles was visualized by transmission electron microscopy (TEM) and scanning electron microscopy (SEM) measurements. The sizes of the vesicles were found to depend on their composition. Representative TEM images of vesicles induced by $PdCl_2/K[AuCl_4]/AgNO_3$, and $PdCl_2/K[AuCl_4]/AgNO_3/K_2[PtCl_6]$ (Figure 2a and b, respectively) reveal hollow vesicles with sizes of approximately 100 nm and 400–500 nm, respectively. SEM images show that vesicles induced by $PdCl_2/K[AuCl_4]/AgNO_3$ are relatively uniform spheres with sizes agreeing with those observed in the TEM measurements (Figure 2c). In contrast, the vesicles formed in a $K_2[PtCl_4]/Bu_4NBr$ system exhibited a large size distribution (20 nm to 2 μm), and the formation process is relatively slow (more than 20 minutes). Some representative large vesicles (> 1 μm) are shown in Figure 2d;

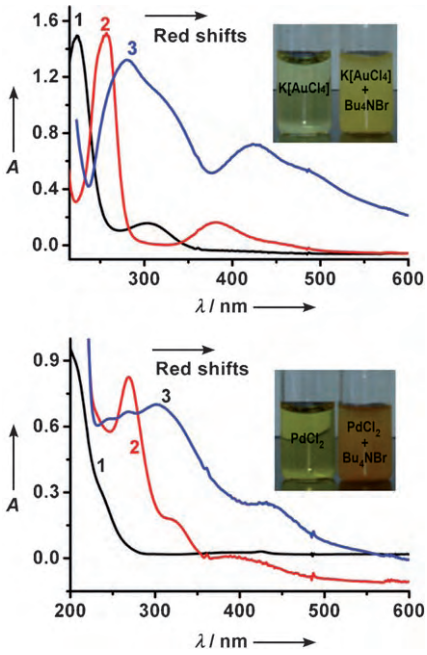


***Figure 1.*** Top: UV/Vis spectra of solutions of $K[AuCl_4]$ (1), $K[AuCl_4]$ + KBr (2), and $K[AuCl_4]$ + KBr + $Bu_4NBr$ (3); Inset: photograph of $K[AuCl_4]$ and $K[AuCl_4]$ + $Bu_4NBr$ solutions. Bottom: UV/Vis spectra of solutions of $PdCl_2$ (1), $PdCl_2$ + KBr (2), and $PdCl_2$ + KBr + $Bu_4NBr$ (3); Inset: photograph of $PdCl_2$ and $PdCl_2$ + $Bu_4NBr$ solutions.

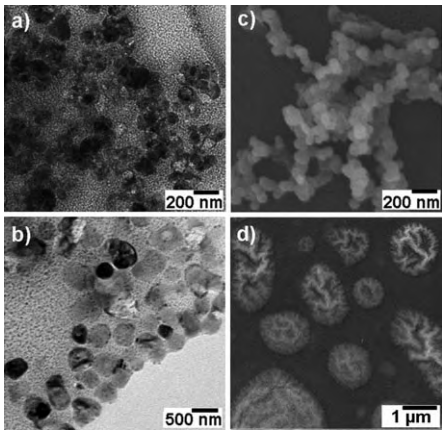


***Figure 2.*** TEM images of vesicles induced by the mixture of $PdCl_2/K[AuCl_4]/AgNO_3$ (a) and $PdCl_2/K[AuCl_4]/K_2[PtCl_6]/AgNO_3$ (b); SEM images of the vesicles induced by $PdCl_2/K[AuCl_4]/AgNO_3$ (c) and $K_2[PtCl_4]$ (d).

[*] Dr. X. Zhang, Prof. Dr. D. Li
Department of Chemistry and Multidisciplinary Research Center
Shantou University
Shantou 515063 (P.R. China)
Fax: (+86) 754-290-2767
E-mail: dli@stu.edu.cn

[**] This work was partly supported by the National Natural Science Foundation of China (Nos. 20571050 and 20271031), the China Postdoctoral Science Foundation, and the NSF of Guangdong Province (No. 05300875).

Supporting information for this article is available on the WWW under http://www.angewandte.org or from the author.


© 2006 Wiley-VCH Verlag GmbH & Co. KGaA, Weinheim

these vesicles have wrinkly surfaces as a result of shrinkage upon drying.

Hollow spheres of nanometer to submicrometer diameter have potential applications in controlled drug release, catalysis, chemical sensors, and cancer hyperthermia,[9] because of their many attractive characteristics, such as low density, larger surface areas, lower amount of material required, and low costs. Also, nanostructured alloys represent an interesting class of materials that exhibit properties distinct from the corresponding monometallic nanoparticles.[10,11] For example, PtRu[11a] and PtRuIr[11b] alloys exhibit enhanced electrocatalytic activity for fuel oxidation relative to pure Pt and are virtually immune to CO poisoning, which is often an intermediate of such reactions. As the properties are strongly dependent on the sizes, compositions, and morphologies of the particles, developing a simple and general approach for hollow alloy spheres with large surface areas and low density is essential for many practical purposes. However, compared with the various morphological controls of semiconductors, metals, and other inorganic materials, the production of bimetallic hollow spheres has met with only very limited success.[12,13] Hitherto, no hollow alloy sphere containing more than two kinds of metals has been reported. A major problem is how to control quick diffusion of different atoms to form homogeneous alloys while simultaneously forming hollow shells.

As $Bu_4NBr$ and some metal compounds or the mixture of these metal compounds can form vesicles with hollow structures, the vesicle surface should consist of numerous aggregated $Bu_4N^+$ cations and metal anions such as $[AuX_4]^-$, $[PdX_4]^{2-}$, $[PtX_6]^{2-}$, and $[Ag_nX_m]^{n-m}$ ($X = Cl$ or Br). When these vesicles are reduced by $NaBH_4$, the newly formed metal nucleation sites with high reactivity are expected to diffuse quickly to form homogeneous alloys on the vesicle template. After growth of these nucleation sites, hollow alloy shells would form. A series of experiments were performed to test this hypothesis. Herein, we select the quaternary alloy AuPdPtAg as an example to demonstrate the efficiency of this novel vesicle-directed alloying strategy.

The hollow alloy spheres were obtained by direct reduction (with $NaBH_4$) of the turbid solution containing $PdCl_2$, $K[AuCl_4]$, $AgNO_3$, $K_2[PtCl_6]$, and $Bu_4NBr$. The structure and morphology of the AuPdPtAg sample were investigated by TEM and SEM. As shown in Figure 3, the centers of the spheres are brighter than the edges, which indicates that their interiors are hollow. The hollow spheres are approximately 500 nm in diameter, which is comparable with the size of the vesicles before reduction. Owing to the very thin shells, some spheres were cracked or collapsed after sonication during purification. Both the selected area electron diffraction (SAED) pattern (Figure 3b) and XRD data (Figure 4a) were consistent with a single-phase face-centered cubic (fcc) structure. The broad peaks in the XRD patterns indicate the small sizes of nanocrystals. The average particle size, calculated from the Scherrer equation, is approximately 4.6 nm. A magnified view of the hollow spheres showed that the shell was composed of many crystallized particles with sizes of 4–7 nm, which agrees well with the XRD data. The high-resolution transmission electron microscopy (HRTEM) image (Figure 3d) of a small particle shows uniform, well-resolved interference fringe spacing (ca. 0.235 nm) and implies that the four kinds of metal atoms diffused quickly to form a homogeneous alloy with highly crystalline structure. The composition was studied by energy-dispersive X-ray

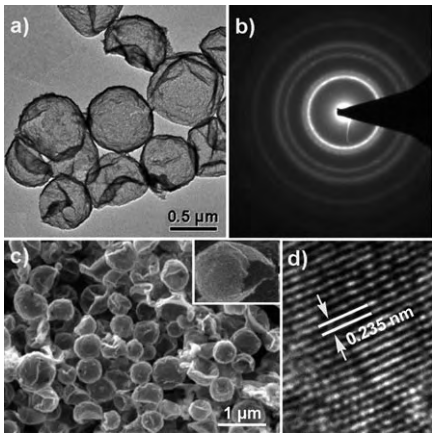


***Figure 3.*** Characterization of hollow AuPdPtAg spheres. a) TEM image; b) SAED pattern; c) SEM image; Inset: enlarged view of a cracked sphere showing the thin shell; d) HRTEM image.

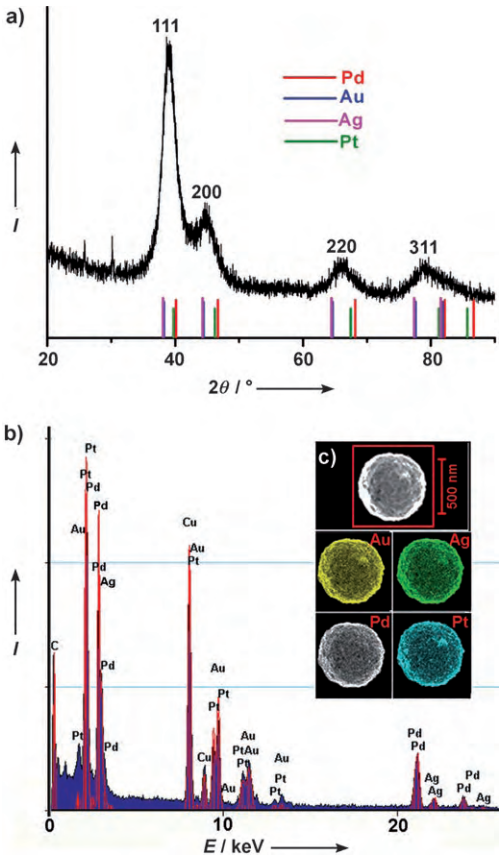


***Figure 4.*** a) XRD pattern; b) EDX spectrum; c) Elemental mapping of hollow AuPdPtAg spheres.

 © 2006 Wiley-VCH Verlag GmbH & Co. KGaA, Weinheim 

(EDX) analysis. All of the Au, Pd, Pt, and Ag peaks could be seen clearly from the spectrum (Figure 4b). Elemental mapping data for a single sphere (Figure 4c) also indicated that the hollow sphere contained all of the four kinds of metals. The average stoichiometry was $Pd_{43}Au_{27}Pt_{19}Ag_{11}$ according to the EDX data. The X-ray photoelectron spectroscopy (XPS) binding energies (see the Supporting Information) were 335.7/341.95, 83.9/87.65, 71.75/75.1, and 368.0/373.95 eV for Pd $3d_{5/2,3/2}$, Au $4f_{7/2,5/2}$, Pt $4f_{7/2,5/2}$, and Ag $3d_{5/2,3/2}$, respectively, with some shifts relative to the data for the pure metals.[14] These shifts are often observed upon alloy formation[13a,14b] and proposed to be due to some interatomic charge donation between different elements, together with some intraatomic charge distribution.[15] As a result, the XRD, SAED, HRTEM, XPS, EDX data coupled with elemental mapping confirmed the formation of hollow spheres of AuPdPtAg alloy.

Some control experiments were implemented to verify this vesicle-directed co-alloying strategy further. It is known that micelles and vesicles formed in water can be destroyed by organic solvents such as alcohols. The result of an experiment in ethanol instead of water (other conditions keep constant) revealed that no hollow sphere formed (see the Supporting Information). Sonication of the reactants (in water) for 2 min before the addition of $NaBH_4$ resulted in some shapeless product, which suggested that the vesicles formed in this system could also be destroyed by sonication. When the experiments were carried out in water by replacing $Bu_4NBr$ with $Et_4NBr$, only a very small amount ($<5\%$) of hollow spheres were produced, and none were produced with $Me_4NBr$, as evidenced by SEM images. This is probably due to the shorter alkyl chains and low hydrophobicity of $Et_4NBr$ and $Me_4NBr$, which cannot assembly effectively into vesicles.

This vesicle-directed alloying strategy has been successfully extended to the synthesis of other bimetallic and multimetallic hollow spheres, such as PdAu, AuPt, AgPd, AuAg, PdAuPt, PdAuAg, PtPdRu, CoPdPt, and AuAgPdPt. Figure 5 shows the TEM and SEM images of some representative examples. Very interestingly, the sizes of the hollow spheres can be tuned by changing the types of metal in the alloys. We found that Ag decreases the size of the spheres, whereas Pt evidently increases the sphere sizes. For example, under the same synthetic conditions, the sizes of AuPdAg and AuPdPt are 90–150 nm and 200–550 nm, respectively. These differences are reasonable, as microstructures of vesicles are often composition-dependent and can be influenced by the geometries, concentrations, and charges of the counteranions or metal ions.[6,7] Although a higher ratio of one metal precursor always leads to a higher ratio of this metal in the final alloys, the metal ratios in hollow alloy spheres are not identical with those in the solution before reduction, probably because of the lattice mismatch of the different metals.

Although some transition-metal compounds such as $CoCl_2$, $RuCl_3$, and $K_2[PtCl_6]$ do not induce vesicle formation in this system, the metals Co, Ru, and Pt alloy efficiently with Au and Pd in systems containing vesicles induced, for example, by $PdCl_2$ and $K[AuCl_4]$ with reduction by $NaBH_4$. The reason is that, in the presence of excess $Bu_4NBr$, these metal compounds can form coordination anions ($[CoX_4]^{2-}$, $[RuX_6]^{3-}$, $[PtX_6]^{2-}$; X = Cl or Br) that can also be efficiently gathered onto the vesicle surface (induced, for example, by $PdCl_2$ and $K[AuCl_4]$) by electrostatic interactions with $Bu_4N^+$ ions on the surface. After reduction, these metal species alloy effectively with others. Hollow alloy spheres of CoPdPt, RuPtPd, AuPt, and others have been prepared in this way.

In conclusion, metal-compound-induced vesicles of $Bu_4NBr$ were used as efficient directors for the rapid synthesis of hollow alloy spheres. This alloying strategy at the vesicle surface is general and has extended to the synthesis of a large variety of binary, ternary, and quaternary intermetallic materials with hollow structures. To our knowledge, this is the first time that different metals have been alloyed on a vesicle surface and that hollow alloy spheres containing more than two kinds of metals have been synthesized. This method could potentially be used for the rapid synthesis of other important alloy catalysts or semiconductors with hollow structures as well as changeable sizes and compositions.

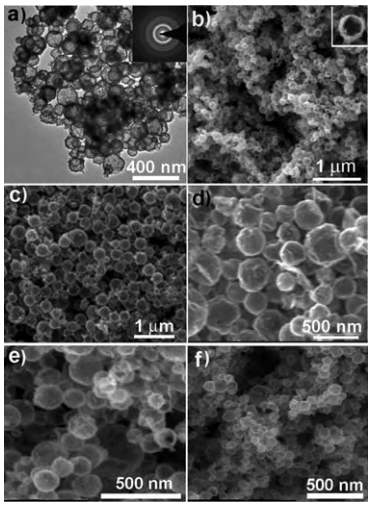


***Figure 5.*** Representative hollow alloy spheres: a) TEM image of AuPdAg; Inset: SAED pattern. SEM images of: b) AuPdAg; Inset: enlarged view of a broken hollow sphere; c) CoPtPd; d) AuPdPt; e) PdAu; f) PdAg.

## *Experimental Section*

Typical synthetic procedure for hollow alloy spheres: AuPdPtAg: An aqueous solution of $Bu_4NBr$ (30 mL, 0.01M) was added to a mixture of $K[AuCl_4]$ (2.4 mL, $5\times10^{-3}$M in $H_2O$), $PdCl_2$ (1.6 mL, 0.01M in acetonitrile), $K_2PtCl_6$ (1.6 mL, $5\times10^{-3}$M in $H_2O$), and $AgNO_3$ (0.8 mL, $5\times10^{-3}$M in $H_2O$). The solution was stirred for 3 min, and a freshly prepared $NaBH_4$ solution (2 mL, 0.1M) was then added quickly. The mixture was stirred vigorous for 1 min, and the product was collected by centrifugation and washed with water. For the vesicle measurements, the solution was used directly for TEM and SEM analysis before addition of $NaBH_4$. When a drop of solution dries, a membrane always forms, which make the SEM analysis difficult. To avoid this problem, a drop of turbid solution was transferred onto a carbon-coated Cu grid, and excess solution was then absorbed and dried with filter paper before the SEM analysis. X-ray power diffraction (XRD) measurements of the samples were performed on a Rigaku D/max rA X-ray diffractometer with graphite-monochromated $Cu_{K\alpha}$ radiation ($\lambda = 1.54187$ Å) at a scanning rate of

 © 2006 Wiley-VCH Verlag GmbH & Co. KGaA, Weinheim 

$0.06°s^{-1}$. X-ray photoelectron spectroscopy (XPS) analysis was performed on VG Escalab 220i-XL spectrometer. TEM, HRTEM, EDX analysis, SAED, and elemental mapping were performed on TECNAI F30 high-resolution transmission electron microscope operated at 300 kV. SEM and field emission scanning electron microscopy (FE-SEM) were performed on JSM 6360 and PHILIPS XL30 scanning electron microscope, respectively. UV/Vis spectra were collected on a Philips PU-8620 UV/Vis spectrophotometer.

Received: April 25, 2006
Revised: July 3, 2006
Published online: August 9, 2006

**Keywords:** alloys · nanostructures · self-assembly · vesicles

[1] For reviews, see: a) D. M. Vriezema, M. C. Aragonès, J. A. A. W. Elmans, J. J. L. M. Cornelissen, A. E. Rowan, R. J. M. Nolte, *Chem. Rev.* **2005**, *105*, 1445, and references therein; b) M. Antonietti, S. Forster, *Adv. Mater.* **2003**, *15*, 1323; c) T. Dwars, E. Paetzold, G. Oehme, *Angew. Chem.* **2005**, *117*, 7338; *Angew. Chem. Int. Ed.* **2005**, *44*, 7174.

[2] a) D. E. Discher, A. Eisenberg, *Science* **2002**, *297*, 967; b) L. F. Zhang, A. Eisenberg, *Science* **1995**, *268*, 1728; c) S. Q. Zhou, C. Burger, B. Chu, M. Sawamura, N. Nagahama, M. Toganoh, U. E. Hackler, H. Isobe, E. Nakamura, *Science* **2001**, *291*, 1944.

[3] a) D. H. W. Hubert, M. Jung, A. L. German, *Adv. Mater.* **2000**, *12*, 1291; b) D. H. W. Hubert, M. Jung, P. M. Frederik, P. H. H. Bomans, J. Meuldijk, A. L. German, *Adv. Mater.* **2000**, *12*, 1286; c) B. M. Discher, Y.-Y. Won, D. S. Ege, J. C.-M. Lee, F. S. Bates, D. E. Discher, D. A. Hammer, *Science* **2001**, *294*, 1143.

[4] T. Ueno, M. Suzuki, T. Goto, T. Matsumoto, K. Nagayama, Y. Watanabe, *Angew. Chem.* **2004**, *116*, 2581; *Angew. Chem. Int. Ed.* **2004**, *43*, 2527.

[5] T. Rispens, J. B. F. N. Engberts, *Org. Lett.* **2001**, *3*, 941.

[6] a) C. A. Bunton, F. Nome, F. H. Quina, L. S. Romsted, *Acc. Chem. Res.* **1991**, *24*, 357; b) R. Zana, J. Schmidt, Y. Talmon, *Langmuir* **2005**, *21*, 11628.

[7] a) T. A. Waggoner, J. A. Last, P. G. Kotula, D. Y. Sasaki, *J. Am. Chem. Soc.* **2001**, *123*, 496; b) X. Luo, S. Wu, Y. Liang, *Chem. Commun.* **2002**, 492; c) T. Owen, R. Pynn, J. S. Martinez, A. Butler, *Langmuir* **2005**, *21*, 12109; d) J. Hao, J. Wang, W. Liu, R. Abdel-Rahem, H. Hoffmann, *J. Phys. Chem. B* **2004**, *108*, 1168.

[8] a) T. Liu, E. Diemann, H. Li, A. W. M. Dress, A. Müller, *Nature* **2003**, *426*, 59; b) T. Liu, *J. Am. Chem. Soc.* **2003**, *125*, 312.

[9] a) F. Caruso, *Chem. Eur. J.* **2000**, *6*, 413; b) E. Mathiowitz, J. S. Jacob, Y. S. Jon, G. P. Carino, D. E. Chickering, P. Chaturvedi, C. A. Santos, K. Vijayaraghavan, S. Montgomery, M. Bassett, C. Morrell, *Nature* **1997**, *386*, 410; c) Y. Hu, X. Q. Jiang, Y. Ding, Q. Chen, C. Z. Yang, *Adv. Mater.* **2004**, *16*, 933; d) C. Loo, A. Lin, L. Hirsch, M.-H. Lee, J. Barton, N. Halas, J. West, R. Drezek, *Technol. Cancer Res. Treat.* **2004**, *3*, 33.

[10] a) F. Maroun, F. Ozanam, O. M. Magnussen, R. J. Behm, *Science* **2001**, 293, 1811; b) S. Sun, C. B. Murray, D. Weller, L. Folks, A. Moser, *Science* **2000**, *287*, 1989.

[11] a) J. Huang, Z. Liu, C. He, L. M Gan, *J. Phys. Chem. B* **2005**, *109*, 16644; b) S. Liao, K.-A. Holmes, H. Tsaprailis, V. I. Birss, *J. Am. Chem. Soc.* **2006**, *128*, 3504.

[12] a) H.-P. Liang, Y.-G. Guo, H.-M. Zhang, J.-S. Hu, L.-J. Wan, C.-L. Bai, *Chem. Commun.* **2004**, 1496; b) H.-P. Liang, L.-J. Wan, C.-L. Bai, L. Jiang, *J. Phys. Chem. B* **2005**, *109*, 7795; c) Y. Sun, B. Wiley, Z.-Y. Li, Y. Xia, *J. Am. Chem. Soc.* **2004**, *126*, 9399.

[13] a) Y. Vasquez, A. K. Sra, R. E. Schaak, *J. Am. Chem. Soc.* **2005**, *127*, 12504; b) P. R. Selvakannan, M. Sastry, *Chem. Commun.* **2005**, 1684; c) G. S. Metraux, Y. C. Cao, R. Jin, C. A. Mirkin, *Nano Lett.* **2003**, *3*, 519; d) J. B. Liu, W. Dong, P. Zhan, S. Z. Wang, J. H. Zhang, Z. L. Wang, *Langmuir* **2005**, *21*, 1683.

[14] a) D. Briggs, M. P. Seah, *Practical Surface Analysis by Auger and X-ray Photoelectron Spectroscopy*, Wiley, Chichester, **1983**, p. 495; b) H. Gao, J. Y. S. Lin, Y. Li, B. Zhang, *J. Membr. Sci.* **2005**, *265*, 142, and references therein.

[15] a) A. Bzowski, T. Sham, *Phys. Rev. B* **1993**, *49*, 7836; b) C.-W. Yi, K. Luo, T. Wei, D. W. Goodman, *J. Phys. Chem. B* **2005**, *109*, 18535.

 © 2006 Wiley-VCH Verlag GmbH & Co. KGaA, Weinheim 

*Hybrid Materials*

DOI: 10.1002/anie.200601878

# Metal–Organic Frameworks as Efficient Materials for Drug Delivery**

*Patricia Horcajada, Christian Serre,* María Vallet-Regí, Muriel Sebban, Francis Taulelle, and Gérard Férey**

Great effort is currently being devoted to the development of methods to control drug release to satisfy the ever-growing demand for prolonged and better control of drug administration. Up until now, two routes have been set up: the "organic route", which uses either biocompatible dendritic macromolecules or polymers[1] and the "inorganic route", in which the hosts are inorganic porous solids, such as zeolites[2] or mesoporous silicate materials.[3] In the first case, a wide range of drugs can be encapsulated but a controlled release is difficult to achieve in the absence of a well-defined porosity.[1] In the second case, this release is performed by grafting organic molecules on the pore walls but implies a decrease in the drug-loading capacity.[4,5] Herein, we introduce a third way: the "hybrid" route. Indeed, a combination of high and regular porosity with the presence of organic groups within

[*] G. Férey
Institut Universitaire de France
Fax: (+33) 1-3925-4358
E-mail: ferey@chimie.uvsq.fr

P. Horcajada, C. Serre, F. Taulelle, G. Férey
Institut Lavoisier, UMR CNRS 8180
Université de Versailles St-Quentin en Yvelines
45 Avenue des Etats-Unis, 78035 Versailles Cedex (France)
Fax: (+33) 139-254-358
E-mail: serrre@chimie.uvsq.fr

P. Horcajada, M. Vallet-Regí
Departamento de Química Inorgánica y Bioinorgánica
Facultad de Farmacia, Universidad Complutense de Madrid (Spain)

M. Sebban, F. Taulelle
Tectospin group of Institut Lavoisier and NMRtec
Versailles (France)

[**] The authors are grateful to E. Fraga (C.A.I. of XRF spectroscopy, Complutense University) for collecting the X-ray fluorescence (XRF) spectra. Ibuprofen was kindly supplied by Laboratorios Dr. Esteve S.A.

Supporting information for this article is available on the WWW under http://www.angewandte.org or from the author.


WILEY InterScience DISCOVER SOMETHING GREAT
© 2006 Wiley-VCH Verlag GmbH & Co. KGaA, Weinheim

the framework may cumulate the advantages to achieve both a high drug loading and a controlled release. Hybrid inorganic–organic solids with large pores exhibit such characteristics and could represent a valuable alternative in such purposes.

Porous hybrid inorganic–organic solids are indeed very important solids because of their potential applications in gas storage,[6] adsorption, separation,[7] or catalysis.[8] Unfortunately, most of them are microporous (pore diameter $< 2$ nm), and the small size of their cavities restricts the choice of incorporated species, induces low diffusion rates, and prevents an efficient and controlled drug delivery. To overcome this major problem, we recently developed a method that combines targeted chemistry and structural computer predictions to obtain mesoporous hybrids with large pores. This approach leads to the characterization of two new cubic (*Fd3m)* zeotypic metal carboxylates, denoted MIL-100 and MIL-101 (MIL = Materials of Institut Lavoisier) and built up from trimers of metal octahedra and di- or tricarboxylic acids.[9] The formula of these acids are: $M^{III}_3OX(H_2O)_2L_n$, $p\,H_2O$ ($M^{III}$ = Cr, X = F, OH) where L = 1,3,5-benzene tricarboxylic acid (BTC) or trimesic acid and $n = 2$ for MIL-100 or L = 1,4-benzenedicarboxylic acid (BDC) or terephthalic acid and $n = 3$ for MIL-101 (Figure 1). They are initially hydrated and exhibit giant pores (∅: 25–34 Å) and unprecedented surface areas (3100–5900 $m^2 g^{-1}$) without any loss of crystallinity after water evacuation. Herein, we describe the study of the adsorption and delivery of an model analgesic and anti-inflammatory drug, Ibuprofen, by MIL-100 and MIL-101. Although the toxicity of chromium compounds is well known,[10] their excellent crystallinity allows a better structural control of the insertion, thus illustrating their use as delivery systems.

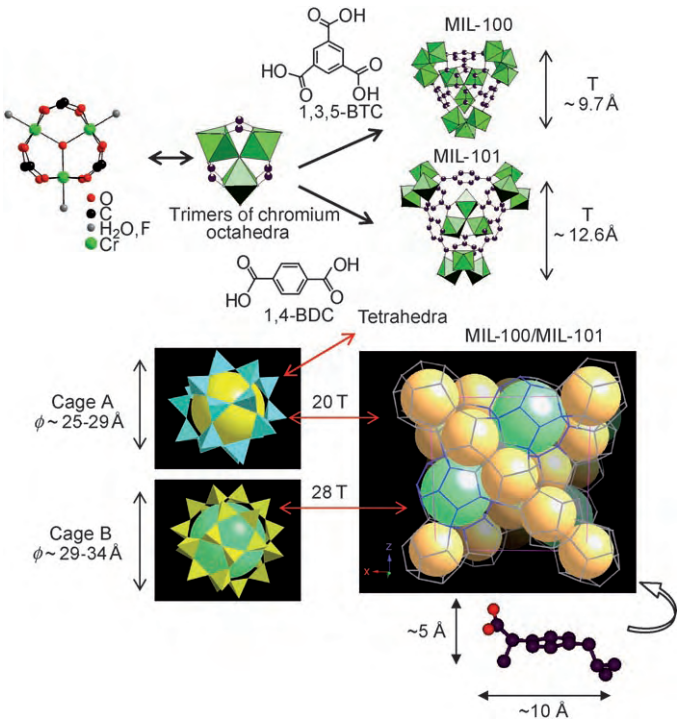


***Figure 1.*** Top: Schematic 3D representation of the tetrahedra (T) built up from trimers of chromium octahedra and 1,4-benzenedicarboxylate moieties or 1,3,5-benzenetricarboxylate groups in MIL-101 and MIL-100, respectively. Bottom: Schematic 3D representation of the mobil-39 (MTN) zeotype architecture of MIL-100 and MIL-101; left: the smaller A cages (yellow spheres with 20 T) and larger B cages (green spheres with 28 T); right: a unit cell (lines connect the T centers).

Ibuprofen was adsorbed by the dehydrated powdered materials from a solution in hexane, and the amount adsorbed was determined by thermogravimetric analysis, UV/Vis spectroscopy, elemental analysis, and X-ray fluorescence; the presence of Ibuprofen was also confirmed by IR spectroscopy. The influence of material dehydration, ratio of Ibuprofen/material, immersion time, and the number of consecutive impregnations on the amount of adsorbed drug was studied (see the Supporting Information).

X-Ray powder diffraction performed on both materials proved that their structures are retained after the drug adsorption. Moreover, $N_2$ adsorption after the incorporation indicates almost no residual porosity. Therefore, the drug completely fills the pores and/or blocks the windows of the cages, thus leaving approximately no accessible pore volume for nitrogen.

The MIL-100 and MIL-101 materials showed remarkable Ibuprofen adsorption (Table 1). However, both materials, which contain different organic components (BTC in MIL-100 and BDC in MIL-101; Figure 1), adsorb drastically different amounts of Ibuprofen as a result of their different pore sizes. On one hand, the MIL-100 matrix has smaller cages (∅: 25 and 29 Å) than MIL-101 despite relatively large pore volumes (8200 and 12700 $Å^3$) and adsorbs 0.35 g of Ibuprofen/gram of dehydrated MIL-100. On the other hand, MIL-101 with its larger cage sizes (∅: 29 and 34 Å; pore volumes: 12700 and 20600 $Å^3$) shows an unprecedented amount of adsorbed drug, larger than the initial matrix weight ($\approx 1.4$ grams of Ibuprofen/gram of dehydrated MIL-101). These findings are very important as only very small amounts of material are required for the administration of high dosages. Structural reasons may explain this discrepancy, particularly the dimensions of the windows of the cages relative to those of Ibuprofen. It must be recalled that both solids, built up from large tetrahedra (T; Figure 1), delimit two types of spherical cages. The smaller (A; 16 in the cubic cell), which is limited by 20 T, exhibits exclusively pentagonal windows with a free aperture $4.8 \times 5.8$ Å (MIL-100) and 12 Å (MIL-101). The

***Table 1:*** Nitrogen adsorption data and the Ibuprofen content of the materials investigated.

| | | MIL-100 | MIL-101 |
|---|---|---|---|
| Starting materials | $S_{langmuir}$ [$m^2 g^{-1}$] | 3340 | 5510 |
| | $V_{meso\text{-}micropore}$ [$cm^3 g^{-1}$] | 1.16 | 2.02 |
| IBU/materials | $S_{langmuir}$ [$m^2 g^{-1}$] | 30 | 6 |
| | $V_{meso\text{-}micropore}$ [$cm^3 g^{-1}$] | 0.03 | 0.02 |
| g IBU/g dehydrated material | | 0.347 | 1.376 |
| Kinetic constant | | $22.9 \pm 2$ | $13.0 \pm 1$ |
| | | $[IBU] = Kt$ | $[IBU] = Kt^{1/2}$ |

 © 2006 Wiley-VCH Verlag GmbH & Co. KGaA, Weinheim 

larger (B; 8 in the cell) with 28 T also possesses hexagonal windows together with the pentagonal ones. The large apertures of the former (8.6 Å and 14.7 × 16 Å for MIL-100 and MIL-101, respectively) allow easy introduction of Ibuprofen, whereas the small dimensions of the pentagonal windows of MIL-100 (close to the Ibuprofen size) are too limited for a valuable introduction of the guest in MIL-100. In other terms, the drastic difference in adsorption between MIL-100 and MIL-101 can be explained by a selective occupation of the larger cages in MIL-100, whereas all the cages are occupied in MIL-101. According to the weight increase, one can estimate that each "small" cage of MIL-101 hosts approximately 56 Ibuprofen molecules and the large cage approximately 92 molecules. This behavior illustrates three facts: 1) the ever-growing need for very large pores, as already claimed by one of us;[11] 2) the hierarchy of mesopores when tunable can act as an internal molecular sieve for a given guest of important dimensions with a selective occupation of the cages—the empty cages remain able to host a different species; and 3) such matrices may provide tools for the study of nanoassemblies of organic compounds and help the development of nano-organic chemistry.

In a second step, solid-state $^1$H and $^{13}$C NMR experiments were performed on Ibuprofen and the anhydrous MIL-100/IBU and MIL-10/IBU (Figure 2). The $^1$H NMR spectra of

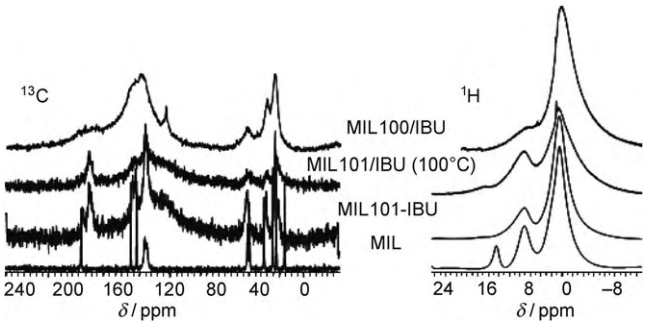


***Figure 2.*** $^{13}$C and $^1$H NMR spectra of Ibuprofen (IBU) and MIL-100 and MIL-101 after the adsorption of Ibuprofen.

Ibuprofen show that it is protonated, whereas $^{13}$C NMR data give the expected information on the different sites. A different behavior is observed for MIL-100/IBU and MIL-101/IBU: whereas two contributions were expected from $^{13}$C NMR data at approximately $\delta = 175$ and 120 ppm (carboxylic and C–H groups, respectively), only the latter exists. The tight bonding of the carboxylic carbon atom to the chromium centers allows paramagnetic relaxation of this carbon atom, which explains the absence of the a contribution at $\delta = 175$ ppm.

The $^1$H NMR spectra after insertion shows that the signal at about $\delta = 14$ ppm, which is characteristic of the protonation of Ibuprofen, disappears. Correlatively, the $^{13}$C NMR spectra indicate that the $CH_3$ group on the α-carbon atom of the carboxylic acid is also strongly shifted upon insertion. Both observations are in agreement with the deprotonation of the carboxylic acid group. This result is important as it is indeed a common practice in medicine formulations to prepare the active pharmaceutical ingredient (API) as a salt for better bioavailability.

Other striking aspects of the $^{13}$C NMR spectra must be mentioned: Although the signal at $\delta = 175$ ppm from the organic linker from the framework reappears, the signals seen in the spectra of Ibuprofen are indicative of some conformational distribution, at variance with the well-defined crystalline order observed in its pure crystal.

As Ibuprofen is being inserted as an anion, several situations may occur to justify the observed changes: 1) the proton may be fixed on the terminal water molecules of the chromium trimeric units and ensure the interaction with anionic Ibuprofen; 2) the latter could to some extent form a complex with the chromium center, thus replacing the bound terminal water molecules as a result of the Lewis acidic character of these sites;[12] or 3) be strongly located close to a proton in the framework. Finally, the broadening of Ibuprofen signals is consistent with the distribution of the interaction types.

MIL-101 and MIL-100 were compacted as cylindrical pieces to study the kinetics of Ibuprofen delivery. The compacting pressures did not affect the integrity of the structure.

Figure 3 displays the kinetics of Ibuprofen delivery to simulated body fluid (SBF)[13] at 37 °C and with continuous stirring. The delivered Ibuprofen concentration was determined by HPLC. In the Ibuprofen delivery from MIL-100 and MIL-101, three stages related to the drug location within the cages can be distinguished. For each type of cage, two situations occur for the guests: when they are close to the walls, the host–guest interaction is governed both by anion–cation electrostatic interactions and π–π interactions between the aromatic rings of Ibuprofen and the organic part of the skeleton, and are therefore dependent on the size of the cage. Once these interactions are fulfilled, the additional Ibuprofen molecules occupy the leaving space of the cavity, with just Ibuprofen–Ibuprofen interactions. This behavior results in three different regimes during the delivery. The initial release of Ibuprofen concerns only the weakly bonded molecules. The kinetics of Ibuprofen delivery for MIL-100 in the first 2 hours are empirically adjusted with regression factors of $> 0.99$ to zero-order kinetics ($[IBU] = Kt$; Table 1), drug-concentration independent, and characteristic of pharmaceutical forms that do not disaggregate.[14] The complete release of Ibuprofen is

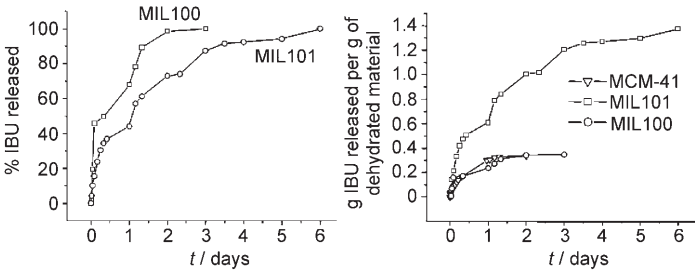


***Figure 3.*** Left: Ibuprofen delivery (% IBU vs *t*) from MIL-101 and MIL-100. Right: Ibuprofen delivery (mg IBU/g dehydrated material vs *t*) from MIL-101 and MIL-100 in comparison with MCM-41.

 © 2006 Wiley-VCH Verlag GmbH & Co. KGaA, Weinheim 

achieved only after 3 days of assays in vitro, thus illustrating the difference in strength of the two types of interactions.

Ibuprofen delivery for MIL-101 in the first stage (8 h) is mainly governed by a diffusion process, which can be predicted by the Higuchi model ($[IBU] = Kt^{1/2}$; Table 1). Considering that the external diffusion process is avoided by constant agitation during the assays, the diffusion process is only due to the drug movements through the windows of the cages. Besides, because of the very high drug content of MIL-101, the concentration of Ibuprofen in the physiological fluid entering the pores is close to saturation; thus, the delivery rate is limited by the dissolution and diffusion process. In this way, Higuchi[14,15] proposed the following equation for the case in which the drug is dissolved in a saturated solution dispersed in a porous matrix:

$$[IBU] = \sqrt{2\,C_0\,\varepsilon\frac{K\,t}{\tau\pi}}$$

where [IBU] is the amount of drug released in time $t$ by surface unity, $C_0$ is the saturated solution concentration, $\varepsilon$ is the matrix porosity, $\tau$ is the tortuosity factor of the capillary system, and $K$ the diffusion constant of the drug molecules in the medium. The $\varepsilon$ value was determined from the $N_2$ adsorption as the accessible surface to the solvent and the $\tau$ value was calculated as the relation between the dimensions of bigger and smaller windows when considering both values as constants and including them in the $K$ constant.

Then, the final drug fraction, probably located close to the cage walls, is delivered more slowly as a consequence of the pore diameter and cation–anion and π–π interactions. Therefore, taking into account the difference in window size of the larger and smaller cages, Ibuprofen placed close to the walls of larger cages would be preponderantly released before those hosted into the smaller cages, thus explaining the last two steps of the delivery. Anyhow, the release concerns the anionic form of Ibuprofen, but it might correspond to its exchange and the anions from the SBF.

It took 6 days to the complete drug release with MIL-101, which may be due to the higher proportion of aromatic rings (Ar) in MIL-101 (Ar/Cr = 1.0 [MIL-101]; Ar/Cr = 0.66 [MIL-100]), which increases the number of interactions between the Ibuprofen and the pore surface of MIL-101. Besides, considering the number of metallic centers per formula unit, with only two Lewis acid sites per trimer (the third site is occupied by an OH or F group), one can estimate that approximately 40% of Ibuprofen is bound to the metal sites, in agreement with the slower delivery of approximately 60% of the drug in the two last steps.

Despite being interesting, the performances of the two first hybrid solids for drug delivery must be compared to those of similar materials with comparable cage sizes. MCM-41,[4] with a pore diameter of 36 Å, was chosen for this purpose. MCM-41 and MIL-100 materials showed very similar Ibuprofen dosage and kinetics. Interestingly, the drug content of MIL-101 is four times larger than in MCM-41 and the delivery rate becomes slower, thus taking 6 days for MIL-101 relative to 2 days for MCM-41. Thus, MIL-101 allows a higher dosage of drug and a longer controlled delivery, which supposes advantages for larger pharmacological molecules.

Herein, we have exposed for the first time the remarkable capacity for drug hosting and controlled delivery of porous metal–organic frameworks. One could criticize the fact that this study is based on chromium materials, well known for their toxicity; nevertheless, homologous nontoxic iron carboxylates (rat oral dose: $DL_{50}(Fe) = 30$ g kg, $DL_{50}$(trimesic acid) = 8.4 g kg, $DL_{50}$(terephthalic acid) = 5 g kg)[16] exist now in the laboratory as well as several porous hybrid iron(III)-based solids that were reported recently[17] and are being tested to obtain controlled delivery systems. Finally, it is of worth to note the enormous possibilities for the design of new hybrid materials, thus altering compositional modifications and creating new topologies[1] adapted to the structure of the drugs and their dosage requirements. In a more general way, this study provides the first elucidation of the interaction between the active ingredient and its excipient that can be designed by using the carboxylic acid group of the ingredient in a porous metal carboxylate. Knowing that about 80% of the APIs have a carboxylic acid group in their formula, a considerable basis for such a strategy has been created.

## Experimental Section

The Supporting Information provides full details of the synthetic methods, Ibuprofen adsorption, and delivery assays, together with the optimization study of Ibuprofen incorporation; determination of the Ibuprofen content by thermogravimetric analysis (TGA), UV/Vis spectroscopy, elemental analysis, and X-ray fluorescence (XRF); and X-ray powder diffraction, $N_2$ adsorption porosimetric, HPLC, IR spectroscopic, and $^1H$ and $^{13}C$ NMR spectroscopic analysis.

Received: May 12, 2006
Published online: August 9, 2006

**Keywords:** controlled delivery · drug delivery · hybrid materials · porous materials

[1] S. Freiberg, X. X. Zhu, *Int. J. Pharm.* **2004**, *282*, 1–18; K. S. Soppimath, T. M. Aminabhavi, A. R. Kulkarni, W. E. Rudzinski, *J. Controlled Release* **2001**, *70*, 1–20.
[2] P. Dhivanand, O. L. Sprockel, *Int. J. Pharm.* **1998**, *167*, 83–96; A. Rivera, T. Farías, *Microporous Mesoporous Mater.* **2005**, *80*, 337–346.
[3] M. Vallet-Regí, A. Rámila, R. P. del Real, J. Perez-Pariente, *Chem. Mater.* **2001**, *13*, 308–311.
[4] B. Muñoz, A. Rámila, J. Perez-Pariente, I. Diaz, M. Vallet-Regi, *Chem. Mater.* **2003**, *15*, 500–503.
[5] P. Horcajada, A. Rámila, G. Férey, M. Vallet-Regí, *Solid State Sci.* **2006**, in press.
[6] G. Férey, M. Latroche, C. Serre, F. Millange, T. Loiseau, A. Percheron-Guégan, *Chem. Commun.* **2003**, 2976–2977; J. L. C. Rowsell, A. R. Millward, K. S. Park, O. M. Yaghi, *J. Am. Chem. Soc.* **2004**, *126*, 5666–5667.
[7] *Handbook of Porous Solids*, *Vol. 3* (Eds: F. Schüth, K. S. W. Sing, J. Weitkamp), Wiley-VCH, Weinheim, **2002**, p. 563.
[8] J. S. Seo, D. Whang, H. Lee, S. I. Jun, J. Oh, Y. J. Jeon, K. Kim, *Nature* **2000**, *404*, 982–986.
[9] G. Férey, C. Serre, C. Mellot-Draznieks, F. Millange, S. Surblé, *Angew. Chem.* **2004**, *116*, 6456–6461; *Angew. Chem. Int. Ed.* **2004**, *43*, 6296–6301; G. Férey, C. Mellot-Draznieks, C. Serre, F.

 © 2006 Wiley-VCH Verlag GmbH & Co. KGaA, Weinheim 

Millange, J. Dutour, S. Surblé, I. Margiolaki, *Science* **2005**, *309*, 2040 – 2042.
[10] R. A. Goyer in *Toxic Effects of Metals. In Casarett and Doull's Toxicology. The Basic science of Poisons* (Ed.: C. D. Klaassen), McGraw-Hill Health Professions Division, New York, **1996** (ISBN 0071054766).
[11] G. Férey, A. K. Cheetham, *Science* **1999**, *283*, 1125 – 1126.
[12] A. Vimont, J.-M. Goupil, J.-C. Lavalley, M. Daturi, S. Surblé, C. Serre, F. Millange, G. Férey, C. N. Audebrand, *J. Am. Chem. Soc.* **2006**, *128*, 3218 – 3227.
[13] T. Kokubo, H. Kushitani, S. Sakka, T. Kitsugi, T. Yamamuro, *J. Biomed. Mater. Res.* **1990**, *24*, 721 – 724.
[14] P. Costa, J. M. Sousa Lobo, *Eur. J. Pharm. Sci.* **2001**, *13*, 123 – 133.
[15] W. I. Higuchi, *J. Pharm. Sci.* **1962**, *51*, 802 – 804.
[16] http://www.ussteel.com/corp/products/msds/3c017.pdf, **2006**; http://www.chemicalland21.com/specialtychem/perchem/TRIMESIC%20ACID.htm, **2006**; http://www.chem.unep.ch/irptc/sids/OECDSIDS/100-21-0.pdf **2006**.
[17] C. Serre, F. Millange, S. Surblé, G. Férey, *Angew. Chem.* **2004**, *116*, 6445 – 6449; *Angew. Chem. Int. Ed.* **2004**, *43*, 6285 – 6289; S. Surblé, C. Serre, C. Mellot-Draznieks, F. Millange, G. Férey, *Chem. Commun.* **2006**, 284 – 286; T. R. Whitfield, X. Wang, L. Liu, A. L. Jacobson, *Solid State Sci.* **2006**, *8*, 1096 – 1103.

 © 2006 Wiley-VCH Verlag GmbH & Co. KGaA, Weinheim 

Combinatorial Chemistry

DOI: 10.1002/anie.200602255

# Direct Monitoring of the Asymmetric Induction of Solid-Phase Catalysis Using Circular Dichroism: Diamine–Cu$^{I}$-Catalyzed Asymmetric Henry Reaction**

*Takayoshi Arai,* Masahiko Watanabe, Akitsugu Fujiwara, Naota Yokoyama, and Akira Yanagisawa*

The catalytic synthesis of chiral molecules is of crucial importance in fine chemistry to ensure the supply of useful and valuable organic compounds.[1] The importance of this research topic has stimulated chemists worldwide to develop numerous methods of asymmetric catalysis, although the process of developing new catalysts involves tedious effort, even when modern methods are used. One way to overcome the time-consuming aspect of the process would be to use the technology of combinatorial chemistry for the discovery and optimization of catalysts.[2]

For the efficient exploration of novel asymmetric catalysts with the combinatorial approach, a convenient technology of high-throughput screening (HTS) is required for the analysis of both catalytic activity (chemical yield) and enantiomeric excess. Although recent remarkable studies[3] have resulted in some useful HTS systems, a more powerful analytical system is required in pursuit of wide application, easy handling, and practical use in broad asymmetric catalysis.[4] Herein, a new HTS system has been developed by coupling circular dichroism (CD) detection and solid-phase reactions (Figure 1). The origin of chirality is restricted in this system by the solid support. When the catalytic asymmetric reaction is examined by using an achiral substrate in solution, no asymmetric induction occurs; therefore, when the solution is analyzed by CD, no significant signal should be detected. Because any two enantiomers have exactly opposite CD values at each wavelength, the CD detector could analyze a single appropriate wavelength and record a positive or negative signal that corresponds to the amount of excess enantiomer.

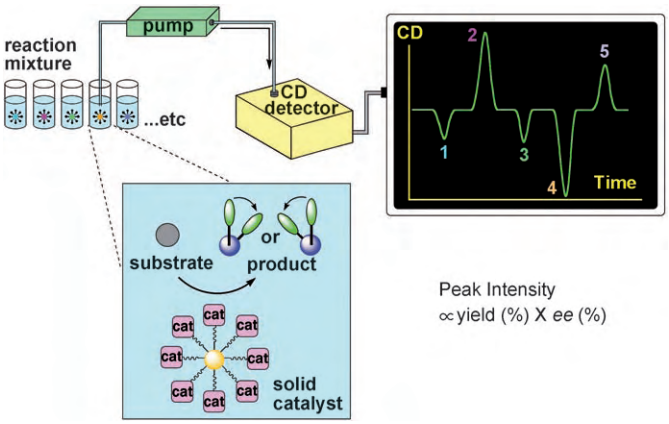


***Figure 1.*** A new high-throughput screening system for analyzing asymmetric induction.

We synthesized chiral amines on polystyrene beads, as outlined in Scheme 1, to demonstrate the newly constructed HTS system. After the introduction of 4-hydroxymethylbenzyl chloride onto the polystyrene beads through formation of a Si–O linkage, the chloromethyl functionality was substituted by 1,3-dimethyl-5-acetylbarbituric acid (DAB)-protected *N*-benzylcyclohexyldiamine.[5] Deprotection of the DAB group with hydrazine gave the diamine ligand **L1**, and further alkylation of the terminal primary amine gave the corresponding ligands **L2**–**L4**. Conversion and product purity were analyzed at each synthetic step by $^{1}$H NMR spectroscopic analysis of the released products.[6]

[*] Prof. Dr. T. Arai, Prof. Dr. A. Yanagisawa
Department of Chemistry
Faculty of Science, Chiba University
Inage, Chiba 263-8522 (Japan)
Fax: (+81) 43-290-2889
E-mail: tarai@faculty.chiba-u.jp
M. Watanabe, A. Fujiwara, N. Yokoyama
Graduate School of Science and Technology
Chiba University
Inage, Chiba 263-8522 (Japan)

[**] This work was supported by a Grant-in Aid for Scientific Research from the Ministry of Education, Science, Sports, Culture and Technology of the Japanese Government and the Industrial Technology Research Grant Program in 2006 from the New Energy and Industrial Technology Development Organization (NEDO) of Japan.

Supporting information for this article is available on the WWW under http://www.angewandte.org or from the author.


InterScience
© 2006 Wiley-VCH Verlag GmbH & Co. KGaA, Weinheim

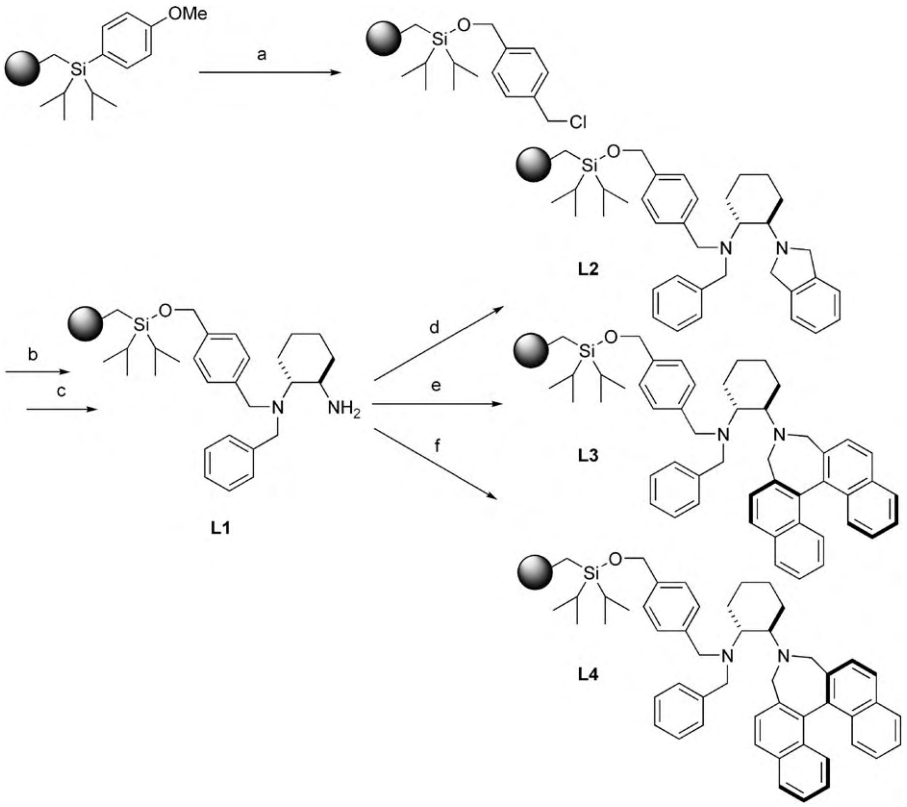


***Scheme 1.*** Synthesis of polymer-supported chiral ligands. a) TfOH, 2,6-lutidine, $CH_2Cl_2$; then 4-chloromethylbenzyl alcohol; b) DAB-protected chiral diamine, 2,6-lutidine, NaI, DMF; c) $H_2NNH_2$–$H_2O$, THF; d–f) corresponding alkyl bromide, $Et_3N$, $CH_2Cl_2$. DMF = *N*,*N*-dimethylformamide, TfOH = trifluoromethanesulfonic acid.

With the polymer-supported chiral diamine ligands **L1**–**L4** in hand, the desired Cu catalysts **C1**–**C12** were prepared on a solid support using three kinds of Cu salts (Figure 2). In all cases, the polystyrene beads turned green, which suggested the formation of Cu–diamine complexes. Among the several types of asymmetric reaction examined, the Henry reaction

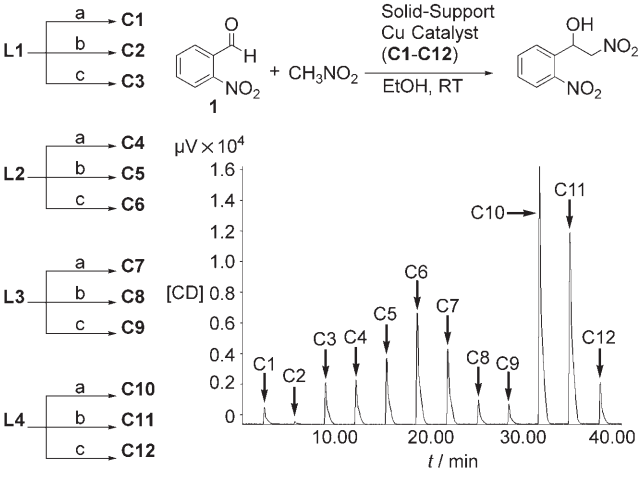


***Figure 2.*** Catalytic asymmetric Henry reaction. The CD was operated at 254 nm. a) CuCl, 2,6-lutidine, $CH_2Cl_2$; b) $CuCl_2$, 2,6-lutidine, $CH_2Cl_2$; c) $Cu(OAc)_2$, 2,6-lutidine, $CH_2Cl_2$.

was found to be catalyzed by the polymer-supported diamine–Cu complexes.[7,8] After carrying out the asymmetric Henry reaction for 36 hours, each reaction mixture was analyzed by continuous injection to obtain the profile shown in Figure 2 (see the experimental details in the Supporting Information).

The detectable compounds in the reaction mixtures were the targeted product and the starting material. Despite the catalytic success of $Cu(OAc)_2$[7b] in conjunction with **L1** and **L2**, the **L4**–CuCl catalyst (namely, **C10**) was found to be the most effective for this reaction. The positive intensity of the signal operated at 254 nm indicates the formation of Henry adducts enriched with the *S* isomer in the reaction. All the reaction mixtures were purified by the conventional method to confirm the results shown in Figure 2; the chemical yields were determined using column chromatography on silica gel, and the enantiomeric excess was analyzed with chiral HPLC. The results of the more time-consuming analysis are summarized in Table 1. An analysis of the **C10**-catalyzed Henry reaction by using conventional methods showed a chemical yield of over 99% with 68% *ee*. It is noteworthy that the CD signals obtained demonstrated considerable sensitivity, even with low levels of enantiomeric excess.

A reaction with a good yield but with low enantiomeric excess should result in a CD signal of low intensity. In the same manner, when catalytic activity is low, thus resulting in a low yield, the intensity of the CD signal is low, even with high enantiomeric excess. The CD signal is of maximum intensity only when both the chemical yield and enantiomeric excess are at their highest. A precise expression of CD signal

***Table 1:*** Chemical yields and *ee* values for the Cu-catalyzed asymmetric Henry reaction.

| Entry | Catalyst | Yield of **1** [%] | *ee* [%] | ACY [%] |
|---|---|---|---|---|
| 1 | **C1** | 18 | 3 | 7 |
| 2 | **C2** | trace | – | 0 |
| 3 | **C3** | 52 | 20 | 32 |
| 4 | **C4** | 15 | 59 | 30 |
| 5 | **C5** | 48 | 6 | 17 |
| 6 | **C6** | 95 | 32 | 55 |
| 7 | **C7** | 91 | 3 | 17 |
| 8 | **C8** | 16 | 7 | 11 |
| 9 | **C9** | 63 | 5 | 18 |
| 10 | **C10** | >99 | 68 | 83 |
| 11 | **C11** | 50 | 68 | 58 |
| 12 | **C12** | 66 | 5 | 18 |

 © 2006 Wiley-VCH Verlag GmbH & Co. KGaA, Weinheim 

intensity is represented by Equation (1), in which the square root of the chemical yield multiplied by the enantiomeric excess is defined as the asymmetric conversion yield (ACY).

$$\mathrm{ACY}\ [\%] = \sqrt{\mathrm{yield}\ [\%] \times ee\ [\%]} \qquad (1)$$

The most efficient asymmetric catalyst should give the target product in good yield with high enantiomeric excess. This principle is of fundamental importance, although it has not so far been clearly stated. Our HTS system allows us to determine the catalysts that meet the criterion of this new definition of ACY. The **C10**-catalyzed Henry reaction recorded equates to an ACY value of 82%.

Although Mikami, Ding, and Reetz recently reported pioneering studies on the application of CD–HPLC in a new HTS system, their system requires the use of achiral HPLC to separate the product from the chiral ligands.[9] The system currently under discussion does not require any pretreatment of the sample (e.g., quenching) and time-consuming purification, and the efficiency of asymmetric induction can be clearly monitored without chromatographic separation. The success of continuous introduction of the reaction mixtures into the CD detector for the ready comparison of the relative intensity of CD signals is remarkable.

Inspired by the success of exploring the promising asymmetric catalyst, the well-defined ligand **L5** was then prepared by solution synthesis. The **L5**–CuCl complex was revealed as an efficient catalyst that provided the Henry adduct in quantitative yield with 65% *ee* at room temperature. When the reaction was carried out in *n*PrOH, the use of only 2 mol% catalyst was enough to promote the reaction in 96% yield, and the enantiomeric excess of the adduct was improved to 77% *ee* (ACY = 86%).

Furthermore, with the employment of the $C_2$-symmetric concept for decreasing the number of catalyst–substrate interactions, which consequently removes competing reaction pathways, ligand **L6** was prepared as a crystalline compound.[10] Finally, the $C_2$-symmetric **L6**–CuCl catalyst provided the Henry adduct in quantitative yield with up to 90% *ee* (ACY = 94%). This reaction is the first success of an asymmetric Henry reaction catalyzed by diamine–$Cu^I$ (Scheme 2).

The scope of the asymmetric Henry reaction was studied on various aldehydes using the well-defined **L6**–CuCl catalyst. As summarized in Table 2, high *ee* values were obtained even at room temperature for various aromatic aldehydes. The reaction was promoted even in the presence of 1 mol% catalyst and gave the nitroaldol product with the highest enantiomeric excess of 92% (Table 2, entry 2). Not only electron-deficient substrates (Table 2, entries 1–3), but *o*-methoxybenzaldehyde was also converted into the corresponding adduct in 82% yield with 90% *ee* (Table 2, entry 4). Moreover, the aliphatic aldehydes were smoothly converted into the nitroaldols in good yield and with high enantiomeric excess (Table 2, entries 6–8).

In conclusion, our new HTS system analyzes asymmetric induction in catalytic enantioselective synthesis by direct introduction of the reaction mixture into a CD detector. In this new HTS system, the Henry reaction catalyzed by the chiral diamine–$Cu^I$ complex was successfully developed. It is of note that this achievement is impossible to realize without use of the HTS system. This direct monitoring system is of obvious application to the ongoing search for outstanding catalysts among the many contenders and also provides an efficient method of analyzing catalytic asymmetric reactions.

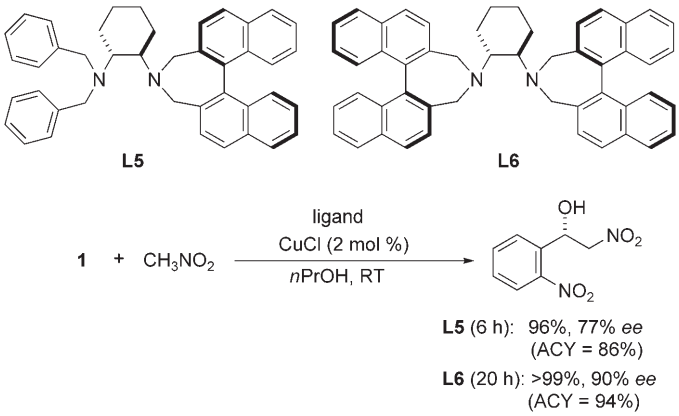


***Scheme 2.*** Catalytic asymmetric Henry reaction using the well-defined solution-phase catalyst.

***Table 2:*** **L6**–CuCl-catalyzed asymmetric Henry reaction.

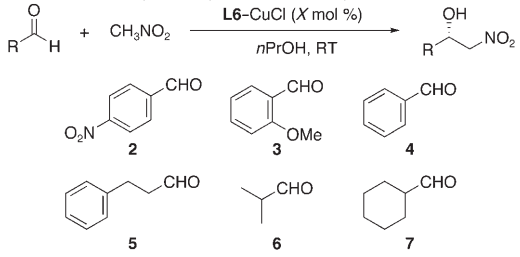


| Entry | Aldehyde | *X* [mol%] | *t* [h] | Yield [%][a] | *ee* [%][b] |
|---|---|---|---|---|---|
| 1 | **1** | 2 | 20 | >99 | 90 |
| 2 | **1** | 1 | 24 | 66 | 92 |
| 3 | **2** | 3 | 16 | >99 | 80 |
| 4 | **3** | 5 | 96 | 82 | 90 |
| 5 | **4** | 5 | 48 | 66 | 86 |
| 6 | **5** | 5 | 48 | 85 | 86 |
| 7 | **6** | 5 | 48 | >99 | 86 |
| 8 | **7** | 2 | 120 | 99 | 90 |

[a] Yield of the isolated product. [b] The enantioselectivity was determined by HPLC analysis with a Chiralcel OD-H column.[7b]

Received: June 6, 2006
Published online: August 9, 2006

**Keywords:** asymmetric catalysis · circular dichroism · combinatorial chemistry · high-throughput screening · solid-phase synthesis

[1] Recent representative books on asymmetric catalysis: a) *Comprehensive Asymmetric Catalysis, Vol. I–III* (Eds.: E. N. Jacob-

 © 2006 Wiley-VCH Verlag GmbH & Co. KGaA, Weinheim 

sen, A. Pfaltz, H. Yamamoto), Springer, Berlin, **1999**; b) *Catalytic Asymmetric Synthesis* (Ed.: I. Ojima), 2nd ed., Wiley-VCH, New York, **2000**.

[2] Recent representative books on combinatorial chemistry: a) *Combinatorial Chemistry* (Ed.: H. Fenniri), Oxford University Press, Oxford, **2000**; b) *Solid-Phase Synthesis and Combinatorial Technologies* (Ed.: P. Seneci), Wiley-Interscience, New York, **2000**; c) *Handbook of Combinatorial Chemistry, Vol. 1 & 2* (Eds.: K. C. Nicolaou, R. Hanko, W. Hartwig), Wiley-VCH, Weinheim, **2002**.

[3] a) M. A. Evans, J. P. Morken, *J. Am. Chem. Soc.* **2002**, *124*, 9020 – 9021; b) F. Taran, C. Gauchet, B. Mohar, S. Meunier, A. Valleix, P. Y. Renard, C. Créminon, J. Grassi, A. Wagner, C. Mioskowski, *Angew. Chem.* **2002**, *114*, 132 – 135; *Angew. Chem. Int. Ed.* **2002**, *41*, 124 – 127; c) M. T. Reetz, M. H. Becker, H. W. Klein, D. Stöckigt, *Angew. Chem.* **1999**, *111*, 1872 – 1875; *Angew. Chem. Int. Ed.* **1999**, *38*, 1758 – 1761.

[4] a) M. T. Reetz, *Angew. Chem.* **2002**, *114*, 1391 – 1394; *Angew. Chem. Int. Ed.* **2002**, *41*, 1335 – 1338; b) M. Tsukamoto, H. B. Kagan, *Adv. Synth. Catal.* **2002**, *344*, 453 – 463; c) M. T. Reetz, *Angew. Chem.* **2001**, *113*, 292 – 320; *Angew. Chem. Int. Ed.* **2001**, *40*, 284 – 310.

[5] E. T. da Silva, E. L. S. Lima, *Tetrahedron Lett.* **2003**, *44*, 3621 – 3624.

[6] J. A. Tallarico, K. M. Depew, H. E. Pelish, N. J. Westwood, C. W. Lindsley, M. D. Shair, S. L. Schreiber, M. A. Foley, *J. Comb. Chem.* **2001**, *3*, 312 – 318.

[7] $Cu^{II}$-catalyzed asymmetric Henry reaction: a) C. Christensen, K. Juhl, K. A. Jørgensen, *Chem. Commun.* **2001**, 2222 – 2223; b) D. A. Evans, D. Seidel, M. Rueping, H. W. Lam, J. T. Shaw, C. W. Downey, *J. Am. Chem. Soc.* **2003**, *125*, 12692 – 12693; c) S.-F. Lu, D.-M. Du, S.-W. Zhang, J. Xu, *Tetrahedron: Asymmetry* **2004**, *15*, 3433 – 3441; d) C. Gan, G. Lai, Z. Zhang, Z. Wang, M.-M. Zhou, *Tetrahedron: Asymmetry* **2006**, *17*, 725 – 728.

[8] Selected examples of a catalytic asymmetric Henry reaction: a) H. Sasai, T. Suzuki, S. Arai, T. Arai, M. Shibasaki, *J. Am. Chem. Soc.* **1992**, *114*, 4418 – 4420; b) B. M. Trost, V. S. C. Yeh, *Angew. Chem.* **2002**, *114*, 889 – 891; *Angew. Chem. Int. Ed.* **2002**, *41*, 861 – 863; c) T. Ooi, K. Doda, K. Maruoka, *J. Am. Chem. Soc.* **2003**, *125*, 2054 – 2055; d) Y. Kogami, T. Nakajima, T. Ashizawa, S. Kezuka, T. Ikeno, T. Yamada, *Chem. Lett.* **2004**, *33*, 614 – 615; e) C. Palomo, M. Oiarbide, A. Laso, *Angew. Chem.* **2005**, *117*, 3949 – 3952; *Angew. Chem. Int. Ed.* **2005**, *44*, 3881 – 3884; f) T. Marcelli, R. N. S. van der Haas, J. H. van Maarseveen, H. Hiemstra, *Angew. Chem.* **2006**, *118*, 943 – 945; *Angew. Chem. Int. Ed.* **2006**, *45*, 929 – 931.

[9] a) K. Ding, A. Ishii, K. Mikami, *Angew. Chem.* **1999**, *111*, 519 – 523; *Angew. Chem. Int. Ed.* **1999**, *38*, 497 – 501; b) K. Mikami, R. Angelaud, K. Ding, A. Ishii, A. Tanaka, N. Sawada, K. Kudo, M. Senda, *Chem. Eur. J.* **2001**, *7*, 730 – 737; c) M. T. Reetz, K. M. Kühling, H. Hinrichs, A. Deege, *Chirality* **2000**, *12*, 479 – 482; d) J. Long, J. Hu, X. Shen, B. Ji, K. Ding, *J. Am. Chem. Soc.* **2002**, *124*, 10 – 11.

[10] J.-L. Vasse, R. Stranne, R. Zalubovskis, C. Gayet, C. Moberg, *J. Org. Chem.* **2003**, *68*, 3258 – 3270.

 © 2006 Wiley-VCH Verlag GmbH & Co. KGaA, Weinheim 

Molecular Mechanics

DOI: 10.1002/anie.200601764

# Auxetics at the Molecular Level: A Negative Poisson's Ratio in Molecular Rods

*Nir Pour, Lior Itzhaki, Benaya Hoz, Eli Altus, Harold Basch, and Shmaryahu Hoz**

Auxetic materials are materials that, counterintuitively, become thicker when stretched and thinner when compressed (negative Poisson's ratio). Examples found up to now have been based mainly on the microgeometry of the material. Using quantum mechanical computations we have identified the first molecular systems, poly[*n*]prismanes ($n = 3$–6), that manifest auxetic behavior at the molecular level. The magnitude of the negative Poisson's ratio in these prismanes ranges from 7 to 15%.

Most materials become thinner when longitudinally stretched and thicker when compressed; that is, they have a positive Poisson's ratio. The latter is defined as the ratio of a lateral contraction to the longitudinal extension during the stretching of a material.[1] Normally, a Poisson's ratio ranges between 0.2 and 0.5. The cork stopper used in wine bottles is an example of a material having a near-zero Poisson's ratio. This characteristic is essential because, otherwise, when pressed against the bottle the cork would have to become thicker, making the seal impossible. In 1987, the first material with a negative Poisson ratio (now called an auxetic material[2]), a foam, was reported by Lakes.[3] The new horizons that were opened by the discovery of auxetic materials induced a major upsurge in structural engineering technologies, with uses ranging from nuclear reactors to the fixing of walls of blood vessels.[4]

The major cause for a negative Poisson's ratio is the microstructure of the material (inverted honeycomb geometry, etc.).[4] It has been suggested that a solid with a porosity of less than 40% cannot be auxetic unless the solid is intrinsically auxetic at the molecular level.[5] Needless to say, high porosity may impair many applications because of low strength and so on. Yet, no molecule is so far known to display auxetic behavior. Herein, we report that molecular rods with a prismanic structure provide the first case of auxetic behavior at the molecular level. It should be pointed

[*] N. Pour, L. Itzhaki, B. Hoz, Prof. H. Basch, Prof. S. Hoz
Department of Chemistry
Bar-Ilan University
Ramat-Gan 52900 (Israel)
Fax: (+972) 3-535-1250
E-mail: shoz@mail.biu.ac.il
Prof. E. Altus
Faculty of Mechanical Engineering
Technion
Israel Institute of Technology
Haifa, 32000 (Israel)

Supporting information for this article is available on the WWW under http://www.angewandte.org or from the author.


© 2006 Wiley-VCH Verlag GmbH & Co. KGaA, Weinheim

out that in addition to foams, a negative Poisson's ratio has been reported for certain crystals[6] in specific directions and is also predicted for extreme states of matter such as the cores of white dwarfs and the outer crusts of neutron stars.[7]

The equilibrium structure and the effect of stretching and compressing various prismanic rods were computed using quantum mechanicals . The procedure follows very closely the one we have recently used.[8] The common feature displayed by all the prismanes is that while the two end rings exhibit normal behavior, the internal rings are auxetic. Namely, they expand upon stretching and contract upon compression. The computations were performed at the B3LYP/6-31G* level using the Gaussian 03[9] program. In the first step, each rod structure was fully optimized. Then, the distance between the corresponding atoms on the two capping rings were fixed at a given length, either shorter (compression) or longer (stretching), and all the other degrees of freedom were reoptimized with respect to the energy. The strained structures were found to have only positive frequencies. The auxetic behavior was found to be independent of method and basis set since sample calculations using AM1, B3LYP/6-31G, MP2/6-31G*, BPW91/6-31G*, and B3LYP/6-311G(2df,2p) all revealed the same phenomenon (Supporting Information).

In Figure 1, the ring bond lengths of deca[3]prismane[10] are plotted as a function of the percent change in the length of the molecular rod. The Poisson's ratio calculated for the

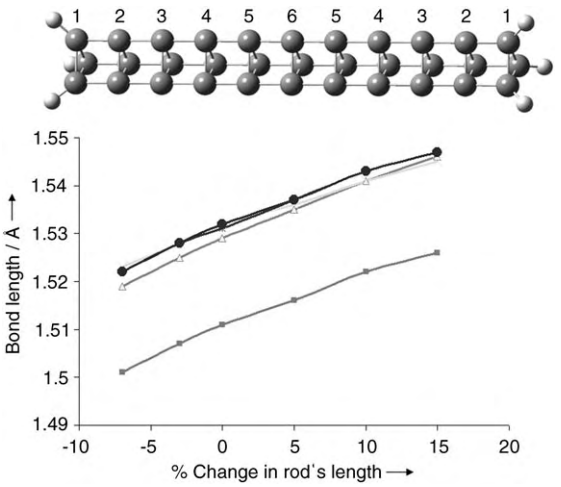


***Figure 1.*** Variation in the internal cyclopropane bond length as a function of the percent change in the length of deca[3]prismane (numbering is according to the scheme shown). The upper group of lines is for rings numbered 3, 4, 5, and 6, the lower line is for ring number 2. The length of the fully optimized rod is 16.001 Å.

internal rings varies from −7% to −9% and averages −7.5%. Figure 1 shows that the Poisson's ratio over the whole range of rod length (−7% to +15%) is remarkably constant, despite the large change of energy involved (up to 300 kcal $mol^{-1}$ for the 15% stretching). As mentioned before, the capping rings (numbered 1 in Figure 1) have a normal Poisson's ratio whereas all the nine internal rings have a negative ratio.

The constancy of this auxetic effect for the internal rings is remarkable when compared to the various porous foams. Using the two-dimensional classical example of reenterant honeycomb (Figure 2),[2] it is clear that the auxetic effect will initially be large and will gradually decay as the dent in the hexagon flattens out.

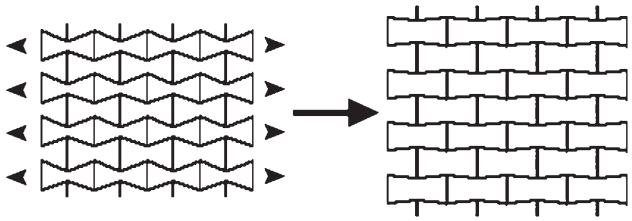

***Figure 2.*** A two-dimensional model for a reenterant honeycomb.

In Table 1, the average Poisson's ratio over all the internal rings is given for a series of prismanes with different numbers of rings as a function of length of the rod. These values were

***Table 1:*** Average Poisson's ratio over all the internal rings for a series of prismanes over the range 97%–105% (energies are given in the Supporting Information).

| No. of rings | △ | □ | ⬠ | ⬡ |
|---|---|---|---|---|
| 3 | −0.071 | −0.066 | −0.115 | −0.133 |
| 4 | −0.081 | −0.079 | −0.131 | −0.156 |
| 5 | −0.083 | −0.079 | −0.112 | |
| 6 | −0.078 | −0.064 | −0.091 | |
| 7 | −0.075 | | | |
| 8 | −0.081 | | | |
| 9 | −0.077 | | | |
| 10 | −0.068 | | | |
| 11 | −0.073 | | | |
| Averages: | −0.076 | −0.072 | −0.112 | −0.144 |

determined over the range 97%–105% (for the sake of simplicity, since the rods are not cylindrical and two radii can be attributed to them, the C–C bond length was used for the calculation of the Poisson's ratio; this procedure yields results very close to a Poisson's ratio based on each of the radii).

The data show that [3]- and [4]prismanes (based on cyclopropane and cyclobutane, respectively) have nearly the same auxetic effect, whereas the rods consisting of cyclopentane and cyclohexane rings display a significantly higher effect culminating in [6]prismane with four rings, which has a negative Poisson's ratio of 15%. Interestingly, in spite of their nonplanar geometry, cyclohexane and cyclopentane are fully planar in the derived prismanes.

An unresolved conundrum is the origin of this phenomenon. It is certainly not a result of some sort of internal compensation between the contraction of the two external rings and the expansion of the inner ones. This cause can be ruled out because the Poisson's ratio of the inner rings

 © 2006 Wiley-VCH Verlag GmbH & Co. KGaA, Weinheim 

remains constant (see Figure 1) regardless of the length of the rod (the number of the rings in the rod) while the contraction of the two external rings is also constant ($0.053 \pm 0.007$) over the whole range of rod length (Supporting Information). One would expect that the expansion of the rings would be accompanied by an increase in the p-orbital character in the bonds within the rings. Surprisingly, NBO analysis shows that upon stretching, the s component increases for bonding within the ring while the interlayer bonds become enriched with the p component. Examples of the changes in hybrid-

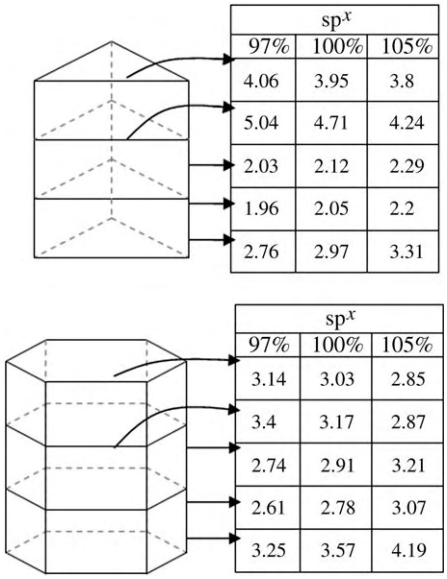

| | $sp^x$ | | |
|---|---|---|---|
| | 97% | 100% | 105% |
| | 4.06 | 3.95 | 3.8 |
| | 5.04 | 4.71 | 4.24 |
| | 2.03 | 2.12 | 2.29 |
| | 1.96 | 2.05 | 2.2 |
| | 2.76 | 2.97 | 3.31 |

| | $sp^x$ | | |
|---|---|---|---|
| | 97% | 100% | 105% |
| | 3.14 | 3.03 | 2.85 |
| | 3.4 | 3.17 | 2.87 |
| | 2.74 | 2.91 | 3.21 |
| | 2.61 | 2.78 | 3.07 |
| | 3.25 | 3.57 | 4.19 |

***Figure 3.*** Variation of the p character ($x$) in the bonds of tri[3]prismane and tri[6]prismane as a function of the percent of stretching (105%) or compression (97%).

ization upon stretching and compression are given in Figure 3 for tri[3]prismane and tri[6]prismane.

It is interesting to note that the normal Poisson's ratio of the capping rings increases also with the ring size. Its value is 0.053, 0.097, 0.126, and 0.15 for the [3]-, [4]-, [5]-, and [6]prismanes, respectively.

These molecular rods display an additional interesting feature. Namely, in spite of the differences in the sizes of the rings, and therefore in the nature of the bonds within the rings which affects the hybridization of the bonds connecting the rings along the rod, the energy for stretching these rods is proportional to the number of bonds stretched, regardless of the size of the rings they connect. This aspect is demonstrated in Figure 4 for a stretching of 5%. The slope of the line is about 1.44 kcal mol$^{-1}$. Thus, stretching of tetra[3]prismane (with $4 \times 3 = 12$ interlayer connecting bonds with a hybridization of $sp^{2.15}$ each; NBO analysis) and tri[4]prismane (with $3 \times 4 = 12$ interlayer connecting bonds with hybridization of $sp^{2.34}$ each; NBO analysis) by 5% produces the same energy cost (ca. 21 kcal mol$^{-1}$).

More than 30 years ago, Woodward and Hoffman referred to prismanes as "an angry tiger unable to break out of a paper cage."[11] Indeed, except for the basic ones,[12] not very many

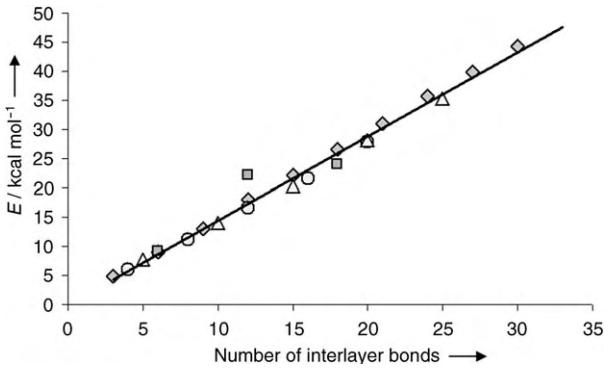


***Figure 4.*** Energy needed to stretch various [$n$]prismanes by 5% as a function of the number of bonds connecting the layers; diamonds: [3]prismane; circles: [4]prismane; triangles: [5]prismane; squares: [4]prismane.

have been synthesized. We hope that our findings will catalyze the efforts in this direction.

Received: May 4, 2006
Published online: August 14, 2006

**Keywords:** ab initio calculations · auxetic materials · molecular mechanics · nanostructures · poly[$n$]prismanes

[1] *CRC Handbook of Chemistry and Physics*, 67th ed., CRC, Boca Raton, FL, **1986–1987**, F97.
[2] K. E. Evans, M. A. Nkansah, I. J. Hutchinson, S. C. Rogers, *Nature* **1991**, *353*, 124.
[3] R. S. Lakes, *Science* **1987**, *235*, 1038–1040.
[4] A. Alderson, *Chem. Ind.* **1999**, 385, and references therein.
[5] M. L. Dunn, H. Ledbetter, *J. Mater. Res.* **1995**, *10*, 2715–2722.
[6] A. Yeganeh-Haeri, D. J. Weidner, J. B. Parise, *Science* **1992**, *257*, 650–652.
[7] R. H. Baughman, S. O. Dantas, S. Stafström, A. A. Zakhidov, T. B. Mitchell, D. H. E. Dubin, *Science* **2000**, *288*, 2018–2022.
[8] L. Itzhaki, E. Altus, H. Basch, S. Hoz, *Angew. Chem.* **2005**, *117*, 7598–7601; *Angew. Chem. Int. Ed.* **2005**, *44*, 7432–7435.
[9] Gaussian 03 (Revision B.04): M. J. Frisch et al., see the Supporting Information.
[10] R. M. Minyaev, V. I. Minkin, T. N. Gribanova, A. G. Starikov, R. Hoffmann, *J. Org. Chem.* **2003**, *68*, 8588–8594.
[11] R. B. Woodward, R. Hoffmann, *The Conservation* of *Orbital Symmetry*, Verlag Chemie, Weinheim, **1970**, pp. 107–112.
[12] G. Mehta, S. Padma in *Carbocyclic Cage Compounds*, (Eds.: E. Osawa, O. Yonemitsu), Wiley-VCH, Weinheim, **1992**.

 © 2006 Wiley-VCH Verlag GmbH & Co. KGaA, Weinheim 

Organocatalysis

DOI: 10.1002/anie.200602207

# Highly Efficient Asymmetric Michael Addition of Aldehydes to Nitroalkenes Catalyzed by a Simple *trans*-4-Hydroxyprolylamide**

*Claudio Palomo,* Silvia Vera, Antonia Mielgo, and Enrique Gómez-Bengoa*

Methods based exclusively on organocatalysts have become of major significance in synthetic chemistry.[1] The Michael addition of carbonyl compounds to nitroalkenes[2] is a challenging benchmark for such a development owing to its potential for the construction of a C–C bond with simultaneous generation of up to three adjacent stereogenic centers and because of the pivotal importance of the nitro group as a precursor to many functionalities.[3] While bifunctional thioureas[4] and chiral Brønsted bases[5] have been developed to control the stereochemistry of the process with malonate esters and related methylene-active substrates,[6] stereocontrol during the reaction involving aldehydes and ketones is most often effected from chiral cyclic secondary amines via enamine formation.[7] However, despite the recent efforts in the area, unmet challenges remain with regard to substrate generality and reaction selectivity, including both diastereo- and enantioselectivity.[8] For example, proline[8a–c] and several diamine/protonic acid catalysts[8d–h] are capable of promoting the reactions with ketones, but with aldehydes poor chemical and stereochemical results are produced (*syn*/*anti* 80:20 to 90:10; 70–75% *ee*). The groups of Kotsuki and Ley have described a pyrrolidine–pyridine/protonic acid system[8i] and a homoprolinetetrazole catalyst,[8j,k] which also provide excellent results for ketones. However, very poor enantioselectivities (22–37% *ee*) are observed when an aldehyde is used as the substrate. Highly diastereo- and enantioselective conjugate additions involving aldehydes were reported by the groups of Hayashi and Wang using a diphenylprolinol silyl ether[8l] and a pyrrolidine–sulfonamide,[8m] respectively. Nonetheless, one drawback is the need for a large excess of the aldehyde substrate, generally 10 equivalents, which becomes a serious limitation in the case of aldehydes that are not commercially available. Most importantly, the catalysts are effective in reactions with nitrostyrenes, but with β-alkyl-substituted nitroalkenes moderate yields (50%)[8l] or essentially no enantioselectivity (22% *ee*)[8m] is produced. The need for high catalyst loading, typically 15–20 mol%, is another important inconvenience related to most of the above approaches,[8] specially when the reactions have to be scaled up. Most recently, an attractive organocatalytic Michael reaction in brine was disclosed.[8n] Again, low diastereo- and enantioselectivities (*syn*/*anti* 60:40, 38–74% *ee*) are observed when aldehydes are employed. Herein we report a new catalyst design (**B**, Figure 1) which provides a highly efficient solution to these problems.

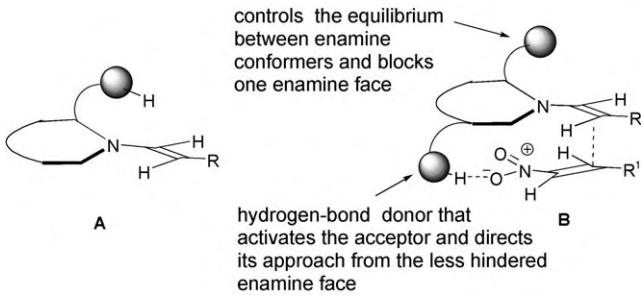


***Figure 1.*** Features of the catalyst design.

The basis of our proposal stems from the observation that in the majority of the above catalyst systems a hydrogen-bond donor at the α-position of the pyrrolidine nitrogen atoms (**A**, Figure 1) is introduced to help the catalytic reaction to proceed.[9] This observation can be correlated to the amine-catalyzed aldol additions wherein a hydrogen-bond motif arising from the same position is involved in a half-chair, six-membered transition state during the catalytic cycle,[10] thus suggesting that the self-aldol reaction[11] in competition with the Michael addition could be the reason for most of the observed problems of the latter. Our hypothesis was that if the design outlined for **B** in Figure 1, wherein the α-hydrogen-bond donor is omitted, could be operative, the aldol reaction might be kept at a minimum whilst the Michael addition should proceed with a high degree of diastereo- and enantiocontrol. To evaluate this hypothesis, *trans*-4-hydroxyprolylamides were selected as potential candidates, as they meet the proposed structural requirements and, in turn, are readily available from commercial sources.

To get initial information on the above assumptions, catalysts **14**–**20** (Scheme 1) were prepared and screened for the reaction of *trans*-nitrostyrene with two representative aldehydes, butyraldehyde **1a** and isovaleraldehyde **1d**. With catalysts **14** and **15**, which lack hydrogen-bond donors, the reaction proceeded to give adducts **8a** and **8d** with good diastereoselectivity, albeit with poor enantioselectivity (Table 1, entries 1 and 2). To our delight, when the same reactions were carried out in the presence of *trans*-4-hydroxyprolylamides **16**, **17**, and **18**, adducts **8a** and **8d** were produced with similar diastereoselectivity levels but, most significantly, with much better enantioselectivities

[*] Prof. Dr. C. Palomo, S. Vera, Dr. A. Mielgo, Dr. E. Gómez-Bengoa
Departamento de Química Orgánica I
Facultad de Química
Universidad del País Vasco. Apdo. 1072.
20080 San Sebastián (Spain)
Fax: (+34) 943-015-270
E-mail: claudio.palomo@ehu.es

[**] This work was financially supported by The University of the Basque Country (UPV/EHU) and the Ministerio de Educación y Ciencia (MEC, Spain). A predoctoral grant to S.V. from MEC is also acknowledged. We also thank M. Alcalá and A. Lizarraga for their help with some experimental work and the SGI/IZO-SGIker UPV/EHU for allocation of computational resources.

Supporting information for this article is available on the WWW under http://www.angewandte.org or from the author.


InterScience
© 2006 Wiley-VCH Verlag GmbH & Co. KGaA, Weinheim

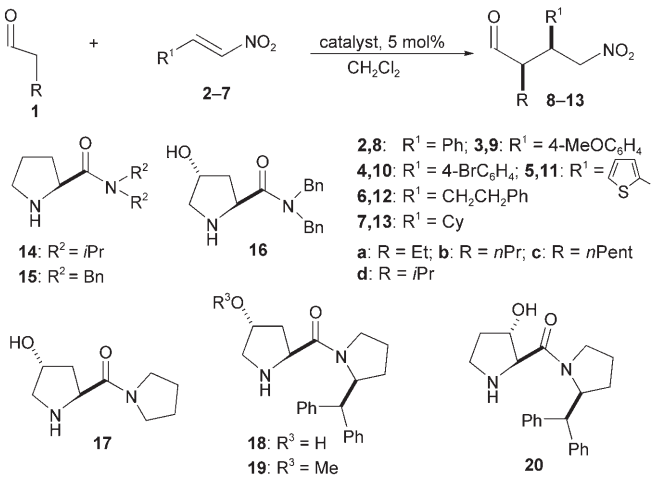


***Scheme 1.*** Catalytic asymmetric conjugate additions of aldehydes to nitroalkenes. Bn = benzyl; Cy = cyclohexyl.

***Table 1:*** Catalyst screening for reaction of **1a** and **1d** with *trans*-β-nitrostyrene (**2**).[a]

| Entry | Cat. | Product **8a** (R = Et, $R^1$ = Ph) Conv. [%][b] | d.r.[c] (*syn*/*anti*) | *ee* [%][c] | Product **8d** (R = *i*Pr, $R^1$ = Ph) Conv. [%][b] | d.r.[c] (*syn*/*anti*) | *ee* [%][c] |
|---|---|---|---|---|---|---|---|
| 1 | **14** | >99 | 92:8 | 60 | >99 | 98:2 | 40 |
| 2 | **15** | >99 | 92:8 | 60 | 99[d] | 98:2 | 60 |
| 3 | **16** | >99 | 98:2 | 86 | 50 | 96:4 | 90 |
| 4 | **17** | >99[e] | 98:2 | 92 | 75 | 98:2 | 90 |
| 5 | **18** | >99[e] | 98:2 | 94 | >99 | 95:5 | 91 |
| 6 | **19** | n.r.[f] | – | – | n.r. | – | – |
| 7 | **20** | >99[e] | 96:4 | 40 | >99 | 90:10 | 70 |

[a] Reactions conducted on a 0.25-mmol scale with a tenfold excess of aldehyde and $Cl_2CH_2$ as solvent. [b] Determined by $^1$H NMR spectroscopy (500 MHz) after 20–24 h at room temperature. [c] Determined by HPLC. See the Supporting Information for further details. [d] After 60 h at room temperature. [e] After 2 h at room temperature. [f] n.r. = no reaction.

(Table 1, entries 3–5). Interestingly, in no case was the corresponding aldol adduct observed despite the excess of aldehyde employed.[12] On the other hand, the fact that no reactions were observed with methyl ether **19** (Table 1, entry 6) further establishes the importance of the hydroxy group not only for reaction stereocontrol, but also for catalyst activity. Furthermore, the position of the hydroxy group in the catalyst seems also to be important as the 3-hydroxyproylamide derivative **20** led to lower enantio- and diastereoselectivities (Table 1, entry 7).

Results from the reaction of several aldehydes and nitroalkenes promoted by catalysts **16** and **18** are summarized in Table 2. While both catalysts provided comparable *syn*/*anti* selectivity ratios, the latter was most effective in terms of reaction enantioselectivity (Table 2, entries 7/8, 10/11, and 14/15). The optimum results were achieved when the reactions were carried out in $CH_2Cl_2$ at room temperature in the presence of 10 mol% of catalyst **18** for β-branched aldehydes (Table 2, entries 8 and 13) and 5 mol% for linear-chain aldehydes at 0°C. To the best of our knowledge, this finding

***Table 2:*** Michael addition reactions of aldehydes to nitroalkenes catalyzed by **16** and/or **18**.[a]

| Entry | Cat.[b] | Product **8–13** | *T* [°C] | *t* [h] | Yield[c] [%] | d.r.[d] (*syn*/*anti*) | *ee* [%] |
|---|---|---|---|---|---|---|---|
| 1 | **18**(10) | 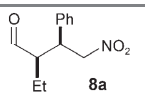 **8a** | RT | 2 | 75 | 98:2 | 94 |
| 2 | **18**(5) | | 0 | 20 | 90[e] | 99:1 | >99 |
| 3 | **18**(10) | 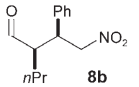 **8b** | RT | 2.5 | 67 | 90:10 | 94 |
| 4 | **18**(10) | | 0 | 20 | 72 | 95:5 | 96 |
| 5 | **18**(5) | 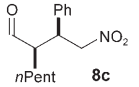 **8c** | 0 | 20 | 70[e] | 99:1 | 96 |
| 6 | **18**(5) | | 0 | 20 | 87[f] | 90:10 | 99 |
| 7 | **16**(10) | 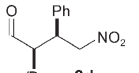 **8d** | RT | 20 | 66[g] | 97:3 | 93 |
| 8 | **18**(10) | | RT | 20 | 75 | 95:5 | 91 |
| 9 | **18**(5) | 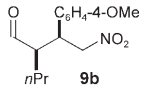 **9b** | 0 | 20 | 72[e] | 96:4 | >99 |
| 10 | **16**(10) | 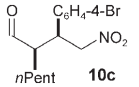 **10c** | 0 | 20 | 90[g] | 92:8 | 76 |
| 11 | **18**(5) | | 0 | 20 | 70 | 97:3 | 98 |
| 12 | **18**(5) | 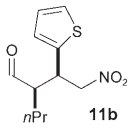 **11b** | 0 | 20 | 70 | >99:1 | 94 |
| 13 | **18**(10) | 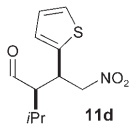 **11d** | RT | 14 | 76 | 94:6 | 92 |
| 14 | **16**(10) | 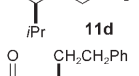 **12b** | 0 | 20 | 90[g] | 97:3 | 86 |
| 15 | **18**(5) | | 0 | 20 | 72 | >99:1 | >99 |
| 16 | **18**(5) | 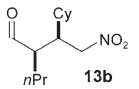 **13b** | 0 | 20 | 75 | >99:1 | >99 |

[a] Reactions conducted on a 1-mmol scale in $CH_2Cl_2$ (1 mL) when 10 mol% is used and $CH_2Cl_2$ (0.5 mL) when 5 mol% of catalyst is used. [b] Number in parenthesis refers to the catalyst loading in mol%. [c] Yield of isolated product after column chromatography. [d] Determined by chiral high-performance liquid chromatography. [e] Reaction conducted on a 3-mmol scale using 1.2 equivalents of aldehyde. [f] Reaction conducted on a 20-mmol scale. [g] Conversion determined by $^1$H NMR spectroscopy.

represents the lowest catalyst/substrate ratio employed in enamine-based Michael additions. Under these conditions, the enantioselectivities obtained were above 90% for essentially all substrates that were explored, including β-alkyl-substituted nitroalkenes, which gave adducts with diastereomeric ratios greater than 99:1 and enantioselectivities of up to 99% (Table 2, entries 15, 16).[13] Furthermore, in these reactions only a slight excess of the aldehyde substrate (1.5–2.0 equiv) is employed, but nearly equimolar amounts are also tolerated with equal efficiency (Table 2, entries 2, 5, and 9). The utility of this approach is illustrated in the reaction of heptanal with nitrostyrene performed on a 20-mmol scale (Table 2, entry 6), which provided **8c** with no significant detrimental effect on yield or stereoselectivity. Moreover, the

 © 2006 Wiley-VCH Verlag GmbH & Co. KGaA, Weinheim 

catalyst can be easily recovered in 70–80% yield after the reaction by simple aqueous acid/base work up, which is an additional aspect of the approach that is of practical importance.

The excellent chemical and stereochemical efficiency observed in these Michael reactions is also of particular interest in that it may provide a simple route to 3,4-disubstituted pyrrolidines[8d] or, as shown in Scheme 2, to γ-butyrolactones, which are common structural units of natural products.[14]

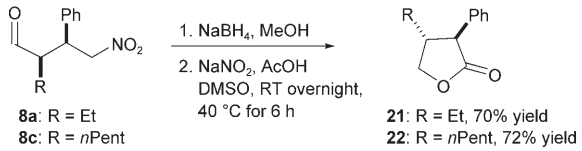


***Scheme 2.*** Elaboration of the Michael adducts.

To better understand the efficiency of the present model the reaction between propionaldehyde and 1-nitropropene catalyzed by *N*,*N*-dimethyl-*trans*-4-hydroxyprolylamide was studied by DFT calculations at the B3LYP/6-31G* level. Concordant with our initial hypothesis, the results show that the OH group helps to discriminate between the two possible transition-state (TS) models **C** and **D** by 2.1 kcal mol$^{-1}$ (Figure 2) and that in the absence of a hydrogen-bond donor, the reactions promoted by the naked prolylamide derivative or the OMe derivative are $10^3$ times slower.[15]

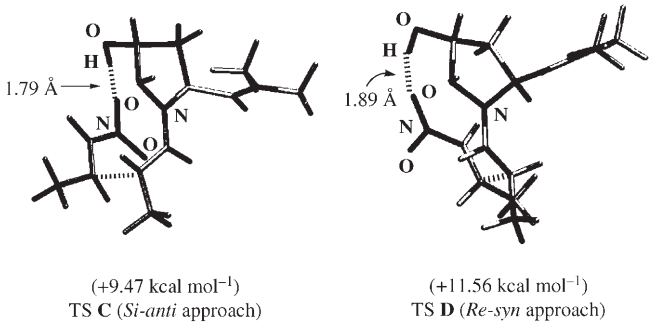


***Figure 2.*** Models for the TS in the catalytic addition of propionaldehyde to 1-nitropropene.

In conclusion, we have documented a new model for the catalytic asymmetric Michael addition of aldehydes to nitroalkenes which holds several interesting features: a) Michael adducts with very high diastereo- and enantioselectivity and a broad range of β-substitution patterns are accessible; b) the catalyst, which in most cases is used in only 5 mol%, is readily available and recoverable; and c) almost equimolar amounts of the aldehyde donor can be employed.

Received: June 2, 2006
Published online: August 4, 2006

**Keywords:** asymmetric synthesis · Michael addition · nitro compounds · organocatalysis · synthetic methods

[1] For general reviews on asymmetric organocatalysis, see: a) P. I. Dalko, L. Moisan, *Angew. Chem.* **2001**, *113*, 3840–3864; *Angew. Chem. Int. Ed.* **2001**, *40*, 3726–3748; b) J. Seayad, B. List, *Org. Biomol. Chem.* **2005**, *3*, 719–724; c) A. Berkessel, H. Gröger, *Asymmetric Organocatalysis: From Biomemetic Concepts to Applications in Asymmetric Synthesis*, Wiley-VCH, Weinheim, **2005**.

[2] a) For recent reviews on conjugate addition to nitroalkenes, see: O. M. Berner, L. Tedeschi, D. Enders, *Eur. J. Org. Chem.* **2002**, 1877–1894; b) V. V. Perekalin, E. S. Lipina, V. M. Berestovitskaya, D. A. Efremov in *Nitroalkenes, Conjugated Nitro Compounds*, Wiley, **1994**; for a general review on enantioselective conjugate addition, see: c) M. P. Sibi, S. Manyem, *Tetrahedron* **2000**, *56*, 8033–8061.

[3] a) G. Rosini in *Comprehensive Organic Synthesis*, *Vol. 2* (Eds.: B. M. Trost, I. Flemming, C. M. Heathcock), Pergamon, New York, **1991**, pp. 321–340; b) F. A. Luzio, *Tetrahedron* **2001**, *57*, 915–945; c) N. Ono, *The Nitro Group in Organic Synthesis*, Wiley-VCH, New York, **2001**.

[4] For a review on stereoselective reactions using thioureas: Y. Takemoto, *Org. Biomol. Chem.* **2005**, *3*, 4299–4306; for recent examples on thiourea-catalyzed conjugate additions, see: a) T. Okino, Y. Hoashi, T. Furukawa, X. Xu, Y. Takemoto, *J. Am. Chem. Soc.* **2005**, *127*, 119–125; b) S. H. McCooey, S. J. Connon, *Angew. Chem.* **2005**, *117*, 107–110; *Angew. Chem. Int. Ed.* **2005**, *44*, 6367–6370; c) J. Wang, H. Li, W. Duan, L. Zu, W. Wang, *Org. Lett.* **2005**, *7*, 4713–4716; S. J. Connon, *Chem. Eur. J* **2006**, *12*, 5418–5427.

[5] For reviews, see: a) S. France, D. J. Guerin, S. J. Miller, T. Lectka, *Chem. Rev.* **2003**, *103*, 2985–3012; b) T. Ishikawa, T. Irobe, *Chem. Eur. J.* **2002**, *8*, 552–557; for recent examples on Lewis base promoted additions, see: c) H. Li, Y. Wang, L. Tang, L. Deng, *J. Am. Chem. Soc.* **2004**, *126*, 9906–9907; d) H. Li, Y. Wang, L. Tang, F. Wu, X. Liu, C. Guo, B. M. Foxman, L. Deng, *Angew. Chem.* **2005**, *117*, 107–110; *Angew. Chem. Int. Ed.* **2005**, *44*, 105–108.

[6] For reactions catalyzed by chiral Lewis acids, see: a) D. M. Barners, J. Ji, M. G. Fickes, M. A. Fitzperald, S. A. King, H. E. Morton, F. A. Plagge, M. Preskill, S. H. Wagaw, S. J. Wittenberger, J. Zhang, *J. Am. Chem. Soc.* **2002**, *124*, 13097–13105; b) M. Watanabe, A. Ikagawa, H. Wang, K. Murata, T. Ikariya, *J. Am. Chem. Soc.* **2004**, *126*, 11148–11149; c) D. A. Evans, D. Seidel, *J. Am. Chem. Soc.* **2005**, *127*, 9958–9959.

[7] For reviews, see: a) E. R. Jarvo, S. D. Miller, *Tetrahedron* **2002**, *58*, 2481–2495; b) B. List, *Tetrahedron* **2002**, *58*, 5573–5590; c) B. List, *Acc. Chem. Res.* **2004**, *37*, 548–557; d) B. List, *Chem. Commun.* **2006**, 819–824.

[8] For L-proline, see: a) B. List, P. Pojarliev, H. J. Martin, *Org. Lett.* **2001**, *3*, 2423–2425; b) D. Enders, A. Seki, *Synlett* **2002**, 26–28; c) P. Kotrusz, S. Toma, H.-G. Schmalz, A. Adler, *Eur. J. Org. Chem.* **2004**, 1577–1583; for diamine/protonic acid catalysts, see: d) J. M. Betancort, C. F. Barbas III, *Org. Lett.* **2001**, *3*, 3737–3740; e) N. Mase, R. Thayumanavan, F. Tanaka, C. F. Barbas III, *Org. Lett.* **2004**, *6*, 2527–2530; f) J. M. Betancort, K. Sakthivel, R. Thayumanavan, F. Tanaka, C. F. Barbas III, *Synthesis* **2004**, 1509–1521; g) O. Andrey, A. Alexakis, G. Bernardinelli, A. Tomassini, *Adv. Synth. Catal.* **2004**, *346*, 1147–1168; h) S. Luo, X. Mi, L. Zhang, S. Liu, H. Xu, J-P. Cheng, *Angew. Chem.* **2006**, *118*, 3165–3169; *Angew. Chem. Int. Ed.* **2006**, *45*, 3093–3097; for pyrrolidine–pyridine/protonic acid systems, see: i) T. Ishii, S. Fujioka, Y. Sekiguchi, H. Kotsuki, *J. Am. Chem. Soc.* **2004**, *126*, 9558–9559; for homoprolinetetrazole derivative, see: j) A. J. A. Cobb, D. A. D. Longbottom, D. M. Shaw, S. V. Ley, *Chem.*

 © 2006 Wiley-VCH Verlag GmbH & Co. KGaA, Weinheim 

*Commun.* **2004**, 1808 – 1809; k) C. E. T. Mitchell, A. J. A. Cobb, S. V. Ley, *Synlett* **2005**, 611 – 614; for diphenylprolinol silyl ethers, see: l) Y. Hayashi, H. Gotog, T. Hayashi, M. Shoji, *Angew. Chem.* **2005**, *117*, 4284 – 4287; *Angew. Chem. Int. Ed.* **2005**, *44*, 4212 – 4215; for a pyrrolidine–sulfonamide catalyst, see: m) W. Wang, J. Wang, H. Li, *Angew. Chem.* **2005**, *117*, 1393 – 1395; *Angew. Chem. Int. Ed.* **2005**, *44*, 1369 – 1371 ; n) N. Mase, K. Watanabe, H. Yoda, K. Takabe, F. Tanaka, C. F. Barbas III, *J. Am. Chem. Soc.* **2006**, *128*, 4966 – 4967.

[9] For reviews on hydrogen bonding in organocatalysis, see: a) P. R. Schreiner, *Chem. Soc. Rev.* **2003**, *32*, 289 – 296; b) P. M. Pihko, *Angew. Chem.* **2004**, *116*, 2110 – 2113; *Angew. Chem. Int. Ed.* **2004**, *43*, 2062 – 2064; c) C. Bolm, T. Rantanen, I. Schiffers, L. Zani, *Angew. Chem.* **2005**, *117*, 1788 – 1793; *Angew. Chem. Int. Ed.* **2005**, *44*, 1758 – 1763; d) M. S. Taylor, E. N. Jacobsen, *Angew. Chem.* **2006**, *118*, 1550 – 1573; *Angew. Chem. Int. Ed.* **2006**, *45*, 1520 – 1543; e) T. Akiyama, J. Itoh, K. Fuchibe, *Adv. Synth. Catal.* **2006**, *348*, 999 – 1010.

[10] a) B. List, R. A. Lerner, C. F. Barbas III, *J. Am. Chem. Soc.* **2000**, *122*, 2395 – 2396; for mechanistic studies on enamine-based aldol reactions, see: b) S. Bahmanyar, K. N. Houk, *J. Am. Chem. Soc.* **2001**, *123*, 11273 – 11283; c) B. List, L. Hoang, H. J. Martin, *Proc. Natl. Acad. Sci. USA* **2004**, *101*, 5839 – 5842; d) C. Allemann, R. Gordillo, F. R. Clemente, P. H.-Y. Cheong, K. N. Houk, *Acc. Chem. Res.* **2004**, *37*, 558 – 569.

[11] For some examples that document chiral amine-based aldehyde–aldehyde aldol reactions, see: a) A. B. Northrup, D. W. C. MacMillan, *J. Am. Chem. Soc.* **2002**, *124*, 6798 – 6799; b) A. B. Northrup, I. K. Mangion, F. Hettche, D. W. C. MacMillan, *Angew. Chem.* **2004**, *116*, 2204 – 2206; *Angew. Chem. Int. Ed.* **2004**, *43*, 2152 – 2154; c) J. Casas, M. Engqvist, I. Ibrahem, B. Kaynak, A. Cordova, *Angew. Chem.* **2005**, *117*, 1367 – 1369; *Angew. Chem. Int. Ed.* **2005**, *44*, 1343 – 1345.

[12] Control experiments conducted without nitroalkene revealed the complete absence of self-aldol reaction. Concurrent with this research, a related design which works for the *anti*-Mannich reaction has been reported: S. Mitsumori, H. Zhang, P. H.-Y. Cheong, K. N. Houk, F. Tanaka, C. F. Barbas III, *J. Am. Chem. Soc.* **2006**, *128*, 1040 – 1041.

[13] This catalytic system seems to be less effective for ketones; for instance, using catalyst **18** (10 mol%) and cyclohexanone (3 equiv) at room temperature gave d.r. 83:17 and 20% *ee*; using tetrahydrothiopyran-4-one (10 equiv) at 0°C gave d.r. >99:1 and 60% *ee*. For recent catalysts for ketone additions, see: homoproline: a) D. Terakado, M. Takano, T. Oriyama, *Chem. Lett.* **2005**, *34*, 962 – 963; chiral ionic liquids: b) S. Luo, X. Mi, L. Zhang, S. Liu, H. Xu, J.-P. Cheng, *Angew. Chem.* **2006**, *118*, 3237 – 3241; *Angew. Chem. Int. Ed.* **2006**, *45*, 3093 – 3097; amine–thiourea catalysts: c) H. Huang, E. Jacobsen, *J. Am. Chem. Soc.* **2006**, *128*, 7170 – 7171; d) S. B. Tsogoeva, S. Wei, *Chem. Commun.* **2006**, 1451 – 1453; primary amines: e) Y. Xei, A. Córdova, *Chem. Commun.* **2006**, 460 – 462; triamines: f) M.-K. Zhu, L.-F. Cun, A.-Q. Mi, Y.-Z. Jiang, L.-Z. Gong, *Tetrahedron: Asymmetry* **2006**, *17*, 491 – 493.

[14] For a review, see: a) S. S. C. Koch, A. R. Chamberlin, *Studies in Natural Products Chemistry, Vol. 16* (Ed.: Atta-ur-Rahman), Elsevier, Amsterdam, **1995**, pp. 687 – 725; for leading references, see: b) R. B. Chhor, B. Nosse, S. Sörgel, C. Böhm, M. Seitz, O. Reiser, *Chem. Eur. J.* **2003**, *9*, 260 – 270.

[15] For details, see the Supporting Information.

 © 2006 Wiley-VCH Verlag GmbH & Co. KGaA, Weinheim 

Germylidyne Complexes

DOI: 10.1002/anie.200602061

# Activation of Aryl Germanium(II) Chlorides by $[Mo(PMe_3)_6]$ and $[W(\eta^2\text{-}CH_2PMe_2)H(PMe_3)_4]$: A New Route to Metal–Germanium Triple Bonds**

*Alexander C. Filippou,* Nils Weidemann, Athanassios I. Philippopoulos, and Gregor Schnakenburg*

Homoleptic trimethylphosphane complexes of transition metals, such as $[Mo(PMe_3)_6]$ (**2**-Mo)[1] and $[W(PMe_3)_6]$ (**2**-W),[2] form a class of rare and very reactive compounds.[3–5] The high reactivity of these complexes originates from the combination of strong σ-donor and weak π-acceptor properties of the $PMe_3$ ligand, which leads to very electron-rich metal centers[6] that are capable of activating σ bonds. A consequence of the high reactivity of the metal centers and the steric pressure caused by the $PMe_3$ ligands in the complexes $[M(PMe_3)_6]$ (M = Mo, W) is the facile dissociation of one $PMe_3$ ligand to afford, through an intramolecular C–H bond activation, the cyclometalated products $[M(\eta^2\text{-}CH_2PMe_2)H(PMe_3)_4]$.[1,2] The complexes $[M(PMe_3)_6]$ and their cyclometalation products are subject to various ligand displacement and oxidative addition reactions.[7] We report here a new reaction type of these electron-rich metal complexes that involves a Ge–Cl bond heterolysis of an aryl germanium(II) chloride to form metal–germanium triple bonds.

A new method was developed for the synthesis of the starting materials $[Mo(PMe_3)_6]$ (**2**-Mo) and $[W(\eta^2\text{-}CH_2PMe_2)H(PMe_3)_4]$ (**2**-W-c) involving the reduction of *trans*-$[MCl_2(PMe_3)_4]$ (**1**-M; M = Mo, W)[8,9] with sodium

[*] Prof. Dr. A. C. Filippou, G. Schnakenburg
Institut für Anorganische Chemie
Rheinische Friedrich-Wilhelms-Universität Bonn
Gerhard-Domagk-Strasse 1, 53121 Bonn (Germany)
Fax: (+49) 228-73-5327
E-mail: filippou@uni-bonn.de

N. Weidemann
Institut für Chemie
Humboldt-Universität zu Berlin
Brook-Taylor Strasse 2, 12489 Berlin (Germany)

Dr. A. I. Philippopoulos
Institute of Physical Chemistry
NCSR Demokritos
Ag. Paraskevi Attikis, 15310 Athens (Greece)

[**] We are grateful to the Humboldt-Universität zu Berlin and the Deutsche Forschungsgemeinschaft (project FI 445/6-1) for the generous financial support of this work, Dr. B. Ziemer and P. Neubauer for technical assistance with the X-ray diffraction studies, Dr. U. Hartmann and U. Kätel for the elemental analyses, and Dr. C. Mügge, W.-D. Bloedorn, A. Thiesies, C. Schmidt, and K. Prochnicki for NMR experiments. N.W. thanks the Fonds der Chemischen Industrie for a fellowship.

Supporting information for this article is available on the WWW under http://www.angewandte.org or from the author.

 © 2006 Wiley-VCH Verlag GmbH & Co. KGaA, Weinheim 

powder in THF in the presence of excess $PMe_3$.[10] This method offers several advantages compared to the published methods.[1,7a,b,11] Complex **2**-Mo was thereby obtained as a beige solid in about 60% yield,[12] and complex **2**-W-c as a bright yellow, very air-sensitive solid in 93% yield. Complex **2**-Mo reacts with one equivalent of the aryl germanium(II) chloride $Ge(C_6H_3\text{-}2,6\text{-}Trip_2)Cl$ (**3**; $Trip = C_6H_2\text{-}2,4,6\text{-}iPr_3$)[13] in toluene to give selectively upon elimination of two $PMe_3$ ligands the germylidyne complex **4**-Mo-Cl, which was isolated as a brown, air-sensitive, crystalline solid in 67% yield [Eq. (1)].[10] No intermediates were observed in this reaction, which is complete within two hours at room temperature.[14]

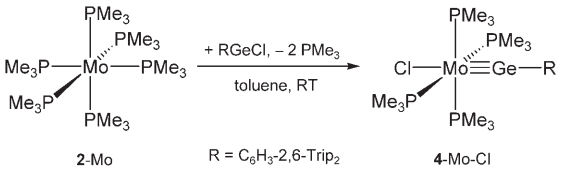


(1)

In contrast, treatment of **2**-W-c with one equivalent of **3** in pentane at −20 °C afforded selectively a thermolabile, very air-sensitive, green product, which was identified by X-ray crystallography and NMR spectroscopy to be the tungsten(II) hydrido–germylidene complex **5**-W-Cl (Scheme 1).[10] Conversion of **2**-W-c into **5**-W-Cl is probably initiated by an insertion of **3** into the W–C bond of **2**-W-c.[15] Heating of complex **5**-W-Cl in toluene at 50 °C gave selectively the brown, air-sensitive germylidyne complex **4**-W-Cl in an unprecedented 1,2-elimination reaction, in which a Ge–C bond is cleaved by a W–H functionality (Scheme 1).[10] This rearrangement reaction occurs also in the solid state when samples of **5**-W-Cl are heated slowly in vacuum to 125 °C. Alternatively, the germylidyne complex **4**-W-Cl can be directly obtained in 64% yield upon heating an equimolar mixture of **2**-W-c and **3** in toluene at 50 °C (Scheme 1).

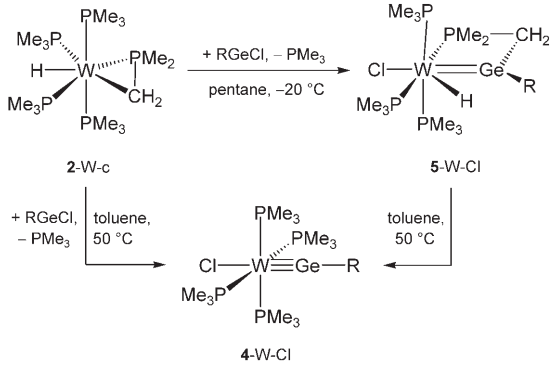


***Scheme 1.*** Stepwise transformation of **2**-W-c into the germylidyne complex **4**-W-Cl. $R = C_6H_3\text{-}2,6\text{-}Trip_2$.

Complexes **4**-M-Cl (M = Mo, W) and **5**-W-Cl were fully characterized.[10] Both germylidyne complexes are thermally stable solids which are very soluble in pentane and decompose upon melting at 142 °C (**4**-Mo-Cl) and 184 °C (**4**-W-Cl). The hydrido–germylidene complex **5**-W-Cl can be stored for a few hours at room temperature. However, its green solutions in toluene or pentane turn gradually brown at ambient temperature as a result of formation of **4**-W-Cl. The molecular structure of **4**-W-Cl was determined by single-crystal X-ray diffraction and exhibits an octahedral complex of roughly $C_{2v}$ symmetry in which the germylidyne and the chlorido ligands are in a *trans* arrangement (Ge-W-Cl 179.3(1)°, Figure 1).[10,16]

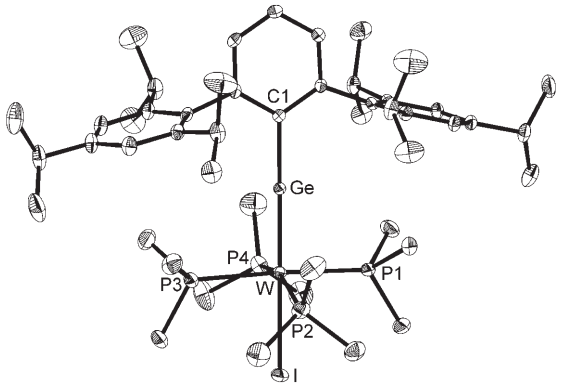


***Figure 1.*** DIAMOND plot of the molecular structure of **4**-W-I in the solid state. Thermal ellipsoids are set at the 30% probability level. Hydrogen atoms are omitted for clarity. Selected bond lengths [Å] and bond angles [°] of **4**-W-I [values for **4**-W-Cl are given in square brackets]: W-Ge 2.3206(4) [2.338(1)], W-I 2.8797(5) [W-Cl 2.540(3)], W-P1 2.4711(8) [2.473(4)], W-P2 2.4967(8) [2.498(4)], W-P3 2.4888(8) [2.473(3)], W-P4 2.4883(8) [2.477(4)], Ge-C1 2.004(2) [1.982(10)]; W-Ge-C1 175.79(7) [177.9(3)], Ge-W-I 177.592(9) [Ge-W-Cl 179.3(1)], Ge-W-P1 90.81(2) [92.55(9)], Ge-W-P2 102.36(2) [101.69(9)], Ge-W-P3 91.96(2) [91.73(8)], Ge-W-P4 97.39(2) [99.30(8)].

Complex **4**-W-Cl features a nearly linear coordinated germanium atom (W-Ge-C1 177.9(3)°) and a W–Ge triple-bond length of 2.338(1) Å, which compares well with those of *trans*-$[X(PMe_3)_4W{\equiv}Ge\text{-}C_6H_3\text{-}2,6\text{-}Trip_2]$ (X = I, W–Ge 2.3206(4) Å, Figure 1; X = H, W–Ge 2.324(1) Å, Figure 2), but is slightly

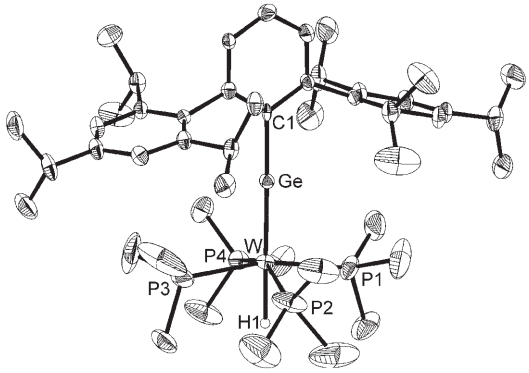


***Figure 2.*** DIAMOND plot of the molecular structure of **4**-W-H in the solid state. Thermal ellipsoids are set at the 30% probability level. Hydrogen atoms except H1 are omitted for clarity. Selected bond lengths [Å] and bond angles [°]: W-Ge 2.324(1), W-H1 1.78(9), W-P1 2.457(3), W-P2 2.442(2), W-P3 2.429(3), W-P4 2.443(2), Ge-C1 1.977(6); W-Ge-C1 178.9(2), Ge-W-H1 179(3), Ge-W-P1 97.31(7), Ge-W-P2 102.53(7), Ge-W-P3 97.24(7), Ge-W-P4 103.49(6).

 © 2006 Wiley-VCH Verlag GmbH & Co. KGaA, Weinheim 

larger than those of the germylidyne complexes *trans*-[X-(dppe)$_2$W≡Ge($\eta^1$-$C_5Me_5$)] (X = Cl, Br, I, NCO, dppe = $Ph_2PCH_2CH_2PPh_2$, W–Ge 2.293(1)–2.3060(9) Å)[17] and [Cp(CO)$_2$W≡Ge-$C_6H_3$-2,6-$Mes_2$] (W–Ge 2.277(1) Å).[18]

Consistent with the molecular structure shown in Figure 1, the $^{31}P\{^1H\}$ NMR spectra of the germylidyne complexes **4**-Mo-Cl and **4**-W-Cl display a singlet resonance at $\delta = -2.7$ and $-31.0$ ppm ($^1J(W,P) = 262$ Hz), respectively, and their $^1H$ NMR spectra show the expected number and multiplicity of signals for the *m*-terphenyl substituent and the $PMe_3$ ligands of *trans*-configured, $C_{2v}$-symmetric complexes.[10] Compound **5**-W-Cl is the first example of a tungsten hydrido–germylidene complex to be characterized by X-ray crystallography.[10,19] Its molecular structure shows a pentagonal bipyramidal, roughly $C_s$-symmetric complex, with two $PMe_3$ ligands (P2 and P4) occupying the apical positions (P2-W-P4 173.46(3)°). The other tungsten-bonded atoms (Ge, P1, Cl, P3, and H54) lie in the equatorial plane of the bipyramid (Figure 3).[20] Complex **5**-W-Cl features a planar four-membered metallacycle (W-Ge-C37-P1 torsion angle: 0.6(2)°) that incorporates a germanium atom in trigonal-planar coordination (sum of interligand angles: 360°). The steric pressure exerted by the *m*-terphenyl substituent increases significantly one of the external bond angles at germanium (W-Ge-C1 159.8(1)°), which in turn leads to a small endocyclic bond angle at germanium (W-Ge-C37 97.8(1)°), thus increasing the ring strain. The W–Ge bond length of **5**-W-Cl (2.4543(4) Å) is one of the smallest to be reported so far for a tungsten–germanium double bond,[21] and lies between those reported for W–Ge triple bonds (2.277(1)–2.338(1) Å, see above) and W–Ge single bonds (2.493(2)–2.681(3) Å).[15f,g,18] The hydrido ligand could be located in the difference Fourier map and lies in the equatorial plane (W–H54 1.73(4) Å). This bond length lies in the range found for W–H bonds by neutron diffraction (1.715(4)–1.778(3) Å).[22] The orientation of the W–H54 vector and the Ge–H54 separation of 2.36(4) Å, which is considerably larger than that expected for a Ge–H single bond (1.53–1.62 Å),[23] do not indicate any bonding interaction between the hydrido ligand and the unsaturated germanium center.

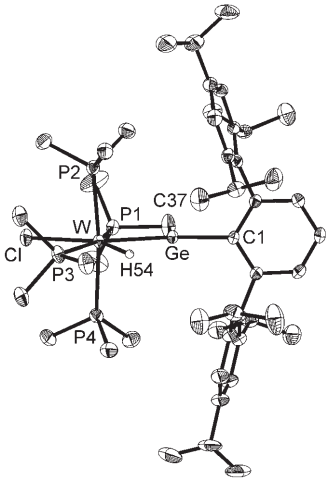


***Figure 3.*** DIAMOND plot of the molecular structure of **5**-W-Cl in the solid state. Thermal ellipsoids are set at the 30% probability level. Hydrogen atoms except H54 are omitted for clarity. Selected bond lengths [Å] and bond angles [°]: W-Ge 2.4543(4), W-Cl 2.5217(9), W-H54 1.73(4), W-P1 2.4806(9), W-P2 2.480(1), W-P3 2.507(1), W-P4 2.470(1), Ge-C1 2.022(3), Ge-C37 2.034(4), P1-C37 1.818(4); W-Ge-C1 159.8(1), W-Ge-C37 97.8(1), C1-Ge-C37 102.4(2), Ge-W-H54 66(1), Ge-W-Cl 148.48(2), Ge-W-P1 67.86(2), Ge-W-P2 93.22(2), Ge-W-P3 133.46(2), Ge-W-P4 93.28(3), Cl-W-P1 80.62(3), Cl-W-P2 87.12(3), Cl-W-P3 78.06(3), Cl-W-P4 87.73(3), P1-W-P2 91.77(3), P1-W-P4 91.36(3), P2-W-P3 87.36(3), P2-W-P4 173.46(3), W-P1-C37 103.2(1), Ge-C37-P1 91.1(2).

The NMR and IR spectra corroborate the solid-state structure of **5**-W-Cl.[10] The $^{31}P\{^1H\}$ NMR spectrum displays three resonance signals at $\delta = -36.2$ ($PMe_2$, $^1J(W,P_X) = 214$ Hz), $-34.4$ ($2 \times PMe_3$, $^1J(W,P_M) = 243$ Hz), and $-32.7$ ppm ($1 \times PMe_3$, $^1J(W,P_A) = 163$ Hz) with the multiplicity pattern of an $AM_2X$ spin system ($^2J(P_A,P_M) = 28$ Hz, $^2J(P_A,P_X) = 111$ Hz, $^2J(P_M,P_X) = 20$ Hz). The hydrido signal appears in the $^1H$ NMR spectrum at $\delta = 0.49$ ppm as a doublet of doublets of triplets ($^2J(P,H) = 70.8$ Hz, $^2J(P,H) = 17.6$ Hz, $^2J(P_M,H) = 15.1$ Hz, $^1J(W,H) = 14.9$ Hz), and the IR spectrum of **5**-W-Cl exhibits one $\nu$(W–H) absorption band at 1812 $cm^{-1}$, which lies in the frequency range of W–H stretching modes of terminal hydrido ligands.[17c,24]

Complex **4**-W-Cl is a useful starting material for the preparation of other tungsten germylidyne complexes. Thus, treatment of **4**-W-Cl with an excess of KNCS in THF at ambient temperature afforded the isothiocyanato complex **4**-W-NCS, which was isolated as a dark brown solid in 88% yield (Scheme 2). Complex **4**-W-NCS can also be prepared in 55% yield from **5**-W-Cl and KNCS in THF at ambient temperature. Similarly, the reaction of **4**-W-Cl with an excess of LiI in diethyl ether gave selectively the iodido derivative **4**-W-I (Scheme 2). Complex **4**-W-I was isolated in 79% yield as a red-brown, microcrystalline solid, which melts at 194 °C and starts decomposing at 198 °C. Unexpectedly, treatment of **4**-W-Cl with $LiNMe_2$ afforded selectively the hydrido–germylidyne complex **4**-W-H (Scheme 2). Two equivalents of $LiNMe_2$ were required according to NMR spectroscopy for the quantitative consumption of **4**-W-Cl, which probably proceeds via a dimethylamido complex intermediate that undergoes β-hydride elimination. Complex **4**-W-H was isolated as a crystalline, red-brown, very air-sensitive solid,

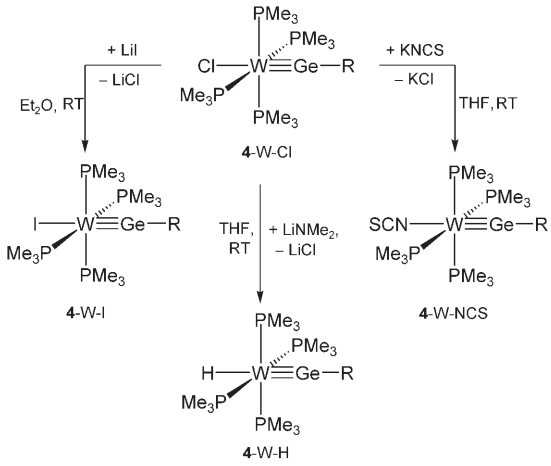


***Scheme 2.*** Chloride substitution reactions of the germylidyne complex **4**-W-Cl. R = $C_6H_3$-2,6-$Trip_2$.

 © 2006 Wiley-VCH Verlag GmbH & Co. KGaA, Weinheim 

which decomposes upon melting at 189 °C. Complexes **4**-W-X (X = NCS, I, H) were fully characterized.[10] The molecular structures of **4**-W-I and **4**-W-H (Figures 1 and 2, respectively) reveal the same bonding features of the germylidyne ligand as **4**-W-Cl, including the almost-linear coordination geometry at germanium (W-Ge-$C_{aryl}$: 175.79(7)° (**4**-W-I), 178.9(2)° (**4**-W-H)) and the very short W–Ge bonds (2.3206(4) Å (**4**-W-I), 2.324(1) Å (**4**-W-H)).[25] The solid-state Raman spectrum of **4**-W-H displays a ν(W–H) band at 1658 $cm^{-1}$,[26] which appears at higher energy than that of *trans*-[H(dmpe)$_2$W≡CMes] (ν(W–H) 1600 $cm^{-1}$; dmpe = $Me_2PCH_2CH_2PMe_2$).[27] This observation suggests that the germylidyne ligand exerts a weaker *trans* influence than the carbyne ligand.[17c] In the $^1$H NMR spectrum of **4**-W-H the hydrido ligand gives rise to a quintet signal at $\delta = -5.56$ ppm ($^2J$(P,H) = 30.6 Hz, $^1J$(W,H) = 61.2 Hz). The $^{31}$P{$^1$H} NMR spectra of the germylidyne complexes display one singlet resonance for the $PMe_3$ ligands at $\delta = -28.2$ (**4**-W-NCS), −46.8 (**4**-W-I), and −30.6 ppm (**4**-W-H), thus confirming the *trans* configuration of the complexes. The $^{31}$P NMR signal is in all cases flanked by a pair of tungsten satellites, and the $^1J$(W,P) coupling constants have similar values (**4**-W-NCS 257 Hz, **4**-W-I 256 Hz, **4**-W-H 252 Hz) compared to that of **4**-W-Cl (262 Hz). Finally, the $^{13}$C{$^1$H} NMR spectra of all germylidyne complexes exhibit a characteristic low-field signal for the germanium-bonded $C_{aryl}$ atom at $\delta = 177.1$ (**4**-W-Cl), 176.6 (**4**-W-NCS), 174.4 (**4**-W-I), and 178.1 ppm (**4**-W-H), which appears at slightly lower field than that of **3** ($\delta = 164.6$ ppm).

This work demonstrates that reactions of organogermanium(II) chlorides with electron-rich metal complexes can follow unprecedented pathways, finally leading to compounds with metal–germanium triple bonds. This work complements our recent studies on the activation of organotetrel(II) halides by $d^6$ metal centers, which have culminated in the isolation of compounds featuring triple bonds to linear-coordinated germanium, tin, and lead centers.[17,28] Extension of the methodology presented here to Group 8 metals is quite appealing, and should lead to ylidyne complexes of metals with a different d-electron configuration and coordination sphere. Efforts in this direction are in progress.

Received: May 23, 2006
Published online: August 22, 2006

**Keywords:** germanium · hydride ligands · molybdenum · multiple bonds · tungsten

[1] a) F. G. N. Cloke, K. P. Cox, M. L. H. Green, J. Bashkin, K. Prout, *J. Chem. Soc. Chem. Commun.* **1982**, 393; b) M. Brookhart, K. Cox, F. G. N. Cloke, J. C. Green, M. L. H. Green, P. M. Hare, J. Bashkin, A. E. Derome, P. D. Grebenik, *J. Chem. Soc. Dalton Trans.* **1985**, 423; c) V. J. Murphy, G. Parkin, *J. Am. Chem. Soc.* **1995**, *117*, 3522.

[2] D. Rabinovich, R. Zelman, G. Parkin, *J. Am. Chem. Soc.* **1992**, *114*, 4611.

[3] For M = Fe, Ru, only the cyclometalation products [M(η$^2$-$CH_2PMe_2$)H($PMe_3$)$_3$] are known: a) J. W. Rathke, E. L. Muetterties, *J. Am. Chem. Soc.* **1975**, *97*, 3272; b) H. H. Karsch, H.-F. Klein, H. Schmidbaur, *Chem. Ber.* **1977**, *110*, 2200; c) H. Werner, R. Werner, *J. Organomet. Chem.* **1981**, *209*, C60. For M = Os, both compounds, [Os($PMe_3$)$_5$] and its cyclometalation product [Os(η$^2$-$CH_2PMe_2$)H($PMe_3$)$_3$], exist: d) H. Werner, J. Gotzig, *Organometallics* **1983**, *2*, 547; e) S. P. Ermer, R. S. Shinomoto, M. A. Deming, T. C. Flood, *Organometallics* **1989**, *8*, 1377.

[4] For the synthesis and reactions of [Co($PMe_3$)$_4$], see: a) H.-F. Klein, *Angew. Chem.* **1971**, *83*, 363; *Angew. Chem. Int. Ed. Engl.* **1971**, *10*, 343; b) H.-F. Klein, H. H. Karsch, *Chem. Ber.* **1975**, *108*, 944; c) H.-F. Klein, R. Hammer, *Angew. Chem.* **1976**, *88*, 61; *Angew. Chem. Int. Ed. Engl.* **1976**, *15*, 42; d) R. Hammer, H.-F. Klein, *Z. Naturforsch. B* **1977**, *32*, 138.

[5] Selected references for the complexes [M($PMe_3$)$_4$] (M = Ni, Pd, Pt): a) C. A. Tolman, *J. Am. Chem. Soc.* **1970**, *92*, 2956; b) H.-F. Klein, H. Schmidbaur, *Angew. Chem.* **1970**, *82*, 885; *Angew. Chem. Int. Ed. Engl.* **1970**, *9*, 903; c) D. H. Gerlach, A. R. Kane, G. W. Parshall, J. P. Jesson, E. L. Muetterties, *J. Am. Chem. Soc.* **1971**, *93*, 3543; d) W. Kuran, A. Musco, *Inorg. Chim. Acta* **1975**, *12*, 187; e) H.-F. Klein, H. H. Karsch, *Chem. Ber.* **1976**, *109*, 2515; f) B. E. Mann, A. Musco, *J. Chem. Soc. Dalton Trans.* **1980**, 776; g) H. Werner, W. Bertleff, *Chem. Ber.* **1983**, *116*, 823; h) R. Benn, H. M. Büch, R.-D. Reinhardt, *Magn. Reson. Chem.* **1985**, *23*, 559; i) D. Milstein, *J. Chem. Soc. Chem. Commun.* **1986**, 817; j) A. G. Avent, F. G. N. Cloke, J. P. Day, E. A. Seddon, K. R. Seddon, S. M. Smedley, *J. Organomet. Chem.* **1988**, *341*, 535; k) H.-F. Klein, B. Zettel, U. Flörke, H.-J. Haupt, *Chem. Ber.* **1992**, *125*, 9; l) W. Lin, S. R. Wilson, G. S. Girolami, *Inorg. Chem.* **1997**, *36*, 2662; m) H. Yamashita, M. Tanaka, M. Goto, *Organometallics* **1997**, *16*, 4696.

[6] The term electron-rich metal center is used here to indicate the presence of filled metal-centered molecular orbitals at high energy in these complexes.

[7] a) V. C. Gibson, C. E. Graimann, P. M. Hare, M. L. H. Green, J. A. Bandy, P. D. Grebenik, K. Prout, *J. Chem. Soc. Dalton Trans.* **1985**, 2025; b) M. L. H. Green, G. Parkin, M. Chen, K. Prout, *J. Chem. Soc. Dalton Trans.* **1986**, 2227; c) D. Rabinovich, R. Zelman, G. Parkin, *J. Am. Chem. Soc.* **1990**, *112*, 9632; d) T. Hascall, V. J. Murphy, G. Parkin, *Organometallics* **1996**, *15*, 3910; e) K. E. Janak, J. M. Tanski, D. G. Churchill, G. Parkin, *J. Am. Chem. Soc.* **2002**, *124*, 4182; f) G. Zhu, J. M. Tanski, D. G. Churchill, K. E. Janak, G. Parkin, *J. Am. Chem. Soc.* **2002**, *124*, 13658; g) T. Hascall, M.-H. Baik, B. M. Bridgewater, J. H. Shin, D. G. Churchill, R. A. Friesner, G. Parkin, *Chem. Commun.* **2002**, 2644; h) G. Zhu, G. Parkin, *Inorg. Chem.* **2005**, *44*, 9637.

[8] E. Carmona, J. M. Marin, M. L. Poveda, J. L. Atwood, R. D. Rogers, *Polyhedron* **1983**, *2*, 185.

[9] P. R. Sharp, J. C. Bryan, J. M. Mayer, *Inorg. Synth.* **1990**, *28*, 326.

[10] The Supporting Information contains detailed experimental procedures for the preparation and the analytical and spectroscopic characterization of the starting materials **2**-Mo and **2**-W-c and of all products. It also contains the NMR spectroscopic data of **3**. CCDC-608272 (**4**-W-Cl·*n*-$C_5H_{12}$), CCDC-608273 (**4**-W-I·0.5*n*-$C_5H_{12}$), CCDC-608274 (**4**-W-H), and CCDC-608275 (**5**-W-Cl·*n*-$C_5H_{12}$) contain the supplementary crystallographic data for this paper. These data can be obtained free of charge from The Cambridge Crystallographic Data Centre via www.ccdc.cam.ac.uk/data_request/cif.

[11] The advantages of the new method are the following: a) the use of $PMe_3$ as solvent is avoided, and b) the starting materials **1**-Mo and **1**-W can be readily obtained in good overall yields starting from $MoCl_5$ and $WCl_6$, respectively.

[12] Depending on the work-up conditions, either pure **2**-Mo or a mixture of **2**-Mo and its cyclometalation product [Mo(η$^2$-$CH_2PMe_2$)H($PMe_3$)$_4$] (**2**-Mo-c) was isolated (see the Supporting Information).

[13] a) L. Pu, M. M. Olmstead, P. P. Power, B. Schiemenz, *Organometallics* **1998**, *17*, 5602.

[14] The outcome of the reaction with **3** is the same when starting either from pure **2**-Mo or a mixture of **2**-Mo and its cyclo-

 © 2006 Wiley-VCH Verlag GmbH & Co. KGaA, Weinheim 

metalation product [Mo($\eta^2$-$CH_2PMe_2$)H($PMe_3$)$_4$] (**2**-Mo-c); see the Supporting Information).

[15] Insertions of germanium(II) halides in metal–carbon bonds are rare: a) J. D. Cotton, G. A. Morris, *J. Organomet. Chem.* **1978**, *145*, 245; b) J. Satgé, *Chem. Heterocycl. Comp.* **2000**, *35*, 1013. More common are insertions of germanium(II) halides in metal–heteroatom, metal–metal, or metal–hydrogen bonds: c) P. Rivière, J. Satgé, A. Boy, *J. Organomet. Chem.* **1975**, *96*, 25; d) A. Castel, P. Rivière, J. Satgé, J. J. E. Moreau, R. J. P. Corriu, *Organometallics* **1983**, *2*, 1498; e) A. C. Filippou, J. G. Winter, G. Kociok-Köhn, I. Hinz, *J. Organomet. Chem.* **1997**, *544*, 225; f) A. C. Filippou, J. G. Winter, G. Kociok-Köhn, C. Troll, I. Hinz, *Organometallics* **1999**, *18*, 2649, and references therein; g) A. C. Filippou, P. Portius, J. G. Winter, G. Kociok-Köhn, *J. Organomet. Chem.* **2001**, *628*, 11.

[16] The *m*-terphenyl substituent adopts in all germylidyne complexes an eclipsed conformation with respect to the {WX($PMe_3$)$_4$} fragment (X = Cl, I, H), as evidenced by the interplane angle (**4**-W-Cl 1.8(3)°, **4**-W-I 3.60(7)°, **4**-W-H 7.9(2)°) between the least-square plane through the tungsten atom, germanium atom, and the central aryl ring carbon atoms, and the least-square plane of the atoms Ge, W, P1, and P3. It should be also noted that all germylidyne complexes show a similar geometric deviation of the $WP_4$ core from planarity. The two *trans*-located $PMe_3$ ligands which are oriented perpendicular to the germanium-bonded phenyl ring (P2 and P4 in Figure 1 and Figure 3) are bent more strongly away from the germylidyne ligand than the other two $PMe_3$ ligands (P1 and P3).

[17] a) A. C. Filippou, A. I. Philippopoulos, P. Portius, D. U. Neumann, *Angew. Chem.* **2000**, *112*, 2881; *Angew. Chem. Int. Ed.* **2000**, *39*, 2778; b) A. C. Filippou, P. Portius, A. I. Philippopoulos, *Organometallics* **2002**, *21*, 653; c) A. C. Filippou, A. I. Philippopoulos, P. Portius, G. Schnakenburg, *Organometallics* **2004**, *23*, 4503.

[18] L. Pu, B. Twamley, S. T. Haubrich, M. M. Olmstead, B. V. Mork, R. S. Simons, P. P. Power, *J. Am. Chem. Soc.* **2000**, *122*, 650.

[19] Only one hydrido–germylidene complex, [{PhB($CH_2PPh_2$)$_3$}($H)_2$Ir=$GeMes_2$], has been reported so far: J. D. Feldman, J. C. Peters, T. Don Tilley, *Organometallics* **2002**, *21*, 4065.

[20] The maximum deviation of the atoms W, Ge, P1, Cl, P3, and H54 from the least-square plane is less than 10 pm.

[21] The W–Ge bond length of **5**-W-Cl compares well with that of the germylidene complex [($\eta^5$-$C_5Me_4Et$)$W(CO)_2$(=$GeMe_2$)$GeMe_3$] (W–Ge 2.459(2) Å: K. Ueno, K. Yamaguchi, H. Ogino, *Organometallics* **1999**, *18*, 4468), but is smaller than those of other tungsten germylidene complexes (W–Ge 2.505(2)–2.632(2) Å): a) G. Huttner, U. Weber, B. Sigwarth, O. Scheidsteger, H. Lang, L. Zsolnai, *J. Organomet. Chem.* **1985**, *282*, 331; b) P. Jutzi, B. Hampel, K. Stroppel, C. Krüger, K. Angermund, P. Hofmann, *Chem. Ber.* **1985**, *118*, 2789; c) P. Jutzi, B. Hampel, M. B. Hursthouse, A. J. Howes, *J. Organomet. Chem.* **1986**, *299*, 19; d) W.-W. du Mont, L. Lange, S. Pohl, W. Saak, *Organometallics* **1990**, *9*, 1395; e) N. Tokitoh, K. Manmaru, R. Okazaki, *Organometallics* **1994**, *13*, 167.

[22] R. Bau, M. H. Drabnis, *Inorg. Chim. Acta* **1997**, *259*, 27.

[23] The experimental value for the Ge–H bond length of $GeH_4$ is 1.5251(5) Å: J. H. Callomon, E. Hirota, K. Kuchitsu, W. J. Lafferty, A. G. Maki, C. S. Pote, *Structure Data of Free Polyatomic Molecules*, Landolt-Börnstein, New Series II, Vol. 7 (Eds. K.-H. Hellwege, A. M. Hellwege), Springer, Berlin, **1976**. The calculated value for the Ge–H bond length of $GeH_2$ ranges from 1.584 to 1.617 Å: Q.-S. Li, R.-H. Lü, Y. Xie, H. F. Schaefer III, *J. Comput. Chem.* **2002**, *23*, 1642.

[24] M-H-E three-center interactions (M = Mo, E = Ge; M = W, E = Si) give rise to ν(M-H-E) absorption bands at considerably lower wave numbers: a) J. L. Vincent, S. Luo, B. L. Scott, R. Butcher, C. J. Unkefer, C. J. Burns, G. J. Kubas, A. Lledós, F. Maseras, J. Tomàs, *Organometallics* **2003**, *22*, 5307; b) T. Watanabe, H. Hashimoto, H. Tobita, *Angew. Chem.* **2004**, *116*, 220; *Angew. Chem. Int. Ed.* **2004**, *43*, 218.

[25] It is noticeable that the W–Ge triple-bond length of **4**-W-H does not differ from those of **4**-W-X (X = Cl, I), despite the presence of a hydrido ligand which exerts a strong *trans* influence. This finding suggests that the σ-bonding part of the W–Ge bond, which is expected to be weakened in **4**-W-H by the hydrido ligand, has a minor influence on the W–Ge triple-bond length.

[26] The W–H stretching mode of **4**-W-H was also observed in the IR spectrum at 1654 $cm^{-1}$ (Supporting Information).

[27] F. Furno, T. Fox, H. W. Schmalle, H. Berke, *Organometallics* **2000**, *19*, 3620.

[28] a) A. C. Filippou, P. Portius, A. I. Philippopoulos, H. Rohde, *Angew. Chem.* **2003**, *115*, 461; *Angew. Chem. Int. Ed.* **2003**, *42*, 445; b) A. C. Filippou, A. I. Philippopoulos, G. Schnakenburg, *Organometallics* **2003**, *22*, 3339; c) A. C. Filippou, H. Rohde, G. Schnakenburg, *Angew. Chem.* **2004**, *116*, 2293; *Angew. Chem. Int. Ed.* **2004**, *43*, 2243; d) A. C. Filippou, N. Weidemann, G. Schnakenburg, H. Rohde, A. I. Philippopoulos, *Angew. Chem.* **2004**, *116*, 6674; *Angew. Chem. Int. Ed.* **2004**, *43*, 6512; e) A. C. Filippou, G. Schnakenburg, A. I. Philippopoulos, N. Weidemann, *Angew. Chem.* **2005**, *117*, 6133; *Angew. Chem. Int. Ed.* **2005**, *44*, 5979.

 © 2006 Wiley-VCH Verlag GmbH & Co. KGaA, Weinheim 

*Carbocyclization*

DOI: 10.1002/anie.200602035

# Gold(I)-Catalyzed Cyclizations of Silyl Enol Ethers: Application to the Synthesis of (+)-Lycopladine A**

*Steven T. Staben, Joshua J. Kennedy-Smith, David Huang, Britton K. Corkey, Rebecca L. LaLonde, and F. Dean Toste**

The construction of carbocycles containing quaternary stereocenters continues to be an important synthetic challenge.[1] We recently described the gold(I)-catalyzed cyclizations of

[*] S. T. Staben, J. J. Kennedy-Smith, D. Huang, B. K. Corkey, R. L. LaLonde, Prof. Dr. F. D. Toste
Department of Chemistry
University of California
Berkeley, CA 94720 (USA)
Fax (+1) 510-643-9480
E-mail: fdtoste@uclink.berkeley.edu

[**] We gratefully acknowledge the University of California, Berkeley, NIHGMS (R01 GM073932-01), Merck Research Laboratories, Bristol-Myers Squibb, Amgen Inc., DuPont, GlaxoSmithKline, Eli Lilly & Co., Pfizer, AstraZeneca, and Roche for financial support. J.J.K.-S. thanks Eli Lilly & Co. for a graduate fellowship. We thank Lauren A. Young for the preparation of tributylallenylstannane.

Supporting information for this article is available on the WWW under http://www.angewandte.org or from the author.


© 2006 Wiley-VCH Verlag GmbH & Co. KGaA, Weinheim
InterScience

enolizable β-keto esters and β-diketones onto appended alkynes as a method for cyclopentene formation.[2] Although broadly applicable to the diastereoselective formation of a variety of cyclic and bicyclic systems, the method is limited to the synthesis of quaternary carbon atoms that bear two carbonyl functionalities. Our proposed mechanism for these transformations involves the addition of the enol tautomer of the keto ester to a gold(I)-complexed alkyne and the subsequent protonolysis of the resulting vinyl–gold(I) species. On the basis of this hypothesis, we envisioned taking advantage of the well-precedented nucleophilicity of silyl enol ethers as "frozen enol equivalents" in gold(I)-catalyzed cyclization reactions.[3,4] Described herein is the development of the gold(I)-catalyzed cyclization of silyl enol ethers onto alkynes and allenes and the application of this carbon–carbon bond-forming reaction to an expedient total synthesis of (+)-lycopladine A.[5]

Several issues must be confronted in employing silyl enol ethers in gold(I)-catalyzed reactions. First, unlike enol nucleophiles, the silylated counterparts lack the proton source necessary for the protonolysis of the vinyl–gold(I) intermediate. Thus, an external proton source is required to complete the catalytic cycle. The competitive reaction of this proton source[6,7] and the electrophilic cationic gold(I) species[8] with the highly nucleophilic silyl enol ether must be avoided. With this in mind, we examined the feasibility of the gold(I)-catalyzed 5-*exo* cyclization of silyl enol ether **1** with water as the external proton source. A catalytic amount of $[Ph_3PAuCl]/AgBF_4$ in a 10:1 dichloromethane/water mixture at 40 °C for 30 minutes provided bicyclic ketone **2** in 78% yield of the isolated product [Eq. (1); OTf = trifluoromethanesulfonate]. The identity of the counterion proved to be key as other complexes (namely, $ClO_4$, $SbF_6$, and OTf salts) produced the desired cyclized product with varying amounts of hydrolyzed enol ethers. Additionally, we found that methanol could be substituted as the proton source with only a slight deterioration in the yield of the isolated product **2**.

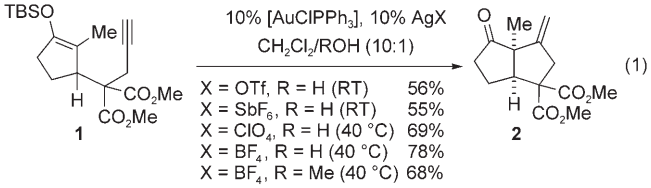

(1)

Under these conditions, the gold(I)-catalyzed *exo*-dig cyclization proved to be general in scope (Table 1, entries 1–8). Alkyl, aryl, and hydrogen substitution was tolerated at the α-position in the completely diastereoselective formation of bicyclic systems. For example, the gold(I)-catalyzed cyclization of enol ether **3** afforded bicyclic product **4**, which contains three consecutive all-carbon quaternary stereocen-

***Table 1:*** Scope of Au$^{I}$-catalyzed carbocyclizations of silyl enol ethers and alkynes[a].

| Entry | Substrate | | | | Product | Yield [%] |
|---|---|---|---|---|---|---|
| 1 | 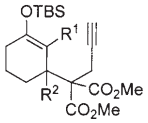 | **3** | $R^1$ = Me | $R^2$ = Me | 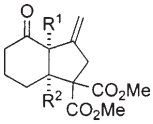 **4** | 90 |
| 2 | | **5** | $R^1$ = Ph | $R^2$ = H | | **6** 83 |
| 3 | 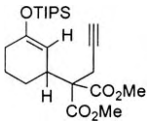 | **7** | | | 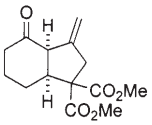 **8** | 83[b] |
| 4 | 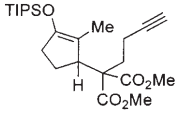 | **9** | | | 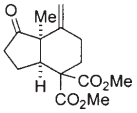 **10** | 94 |
| 5 | 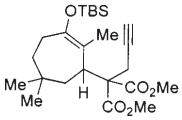 | **11** | | | 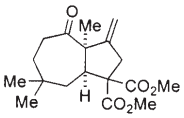 **12** | 80 |
| 6 | 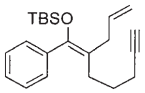 | **13** | | | 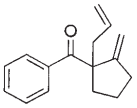 **14** | 77[c] |
| 7 | 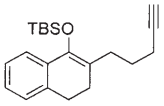 | **15** | | | 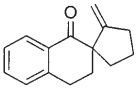 **16** | 91[c] |
| 8 | 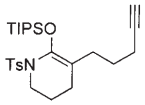 | **17** | | | 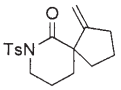 **18** | 75[c] |
| 9 | 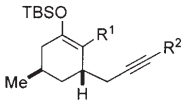 | **19** | $R^1$ = allyl | $R^2$ = H | 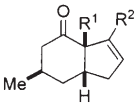 **20** | 77 |
| 10 | | **21** | $R^1$ = | $R^2$ = Ph | | **22** 85 |
| 11 | | **23** | R = 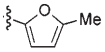 | | | **24** 73 |
| 12 | 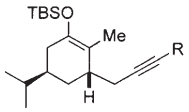 | **25** | R = | | 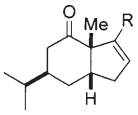 **26** | 75 |
| 13 | | **27** | R = 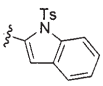 | | | **28** 91 |

[a] Reaction conditions: $[AuClPPh_3]$ (10 mol%), $AgBF_4$ (10 mol%), silyl enol ether (0.4 M) in $CH_2Cl_2/H_2O$ (10:1), 40 °C. [b] Reaction carried out in toluene/MeOH (10:1, 0.4 M) at room temperature, and the product was isolated as a 9:1 mixture with the corresponding enone. [c] Reaction conditions: $[AuClPPh_3]$ (10 mol%) and AgOTf (10 mol%) in $CH_2Cl_2$/MeOH (10:1), 0 °C. TIPS = triisopropylsilyl, Ts = *p*-toluenesulfonyl.

 © 2006 Wiley-VCH Verlag GmbH & Co. KGaA, Weinheim 

ters, in 90% yield (Table 1, entry 1). Furthermore, the mildness of the reaction conditions is highlighted by the fact that non-quaternary α-stereocenters can be created diastereoselectively with minimal isomerization of the *exo*-methylene unit into conjugation with the ketone function (Table 1, entry 3). Furthermore, *exo*-methylene cyclohexane **10** was prepared in 94% yield through a gold(I)-catalyzed 6-*exo*-dig cyclization (Table 1, entry 4). The gold(I)-catalyzed reaction also operates effectively with acyclic silyl enol ether **13**, thus affording *exo*-methylene cyclopentane **14** in 77% yield (Table 1, entry 6). Moreover, the reaction can be employed to construct spirocyclic ketone **16** and amide **18** in 91 and 75% yield, respectively (Table 1, entries 7 and 8).

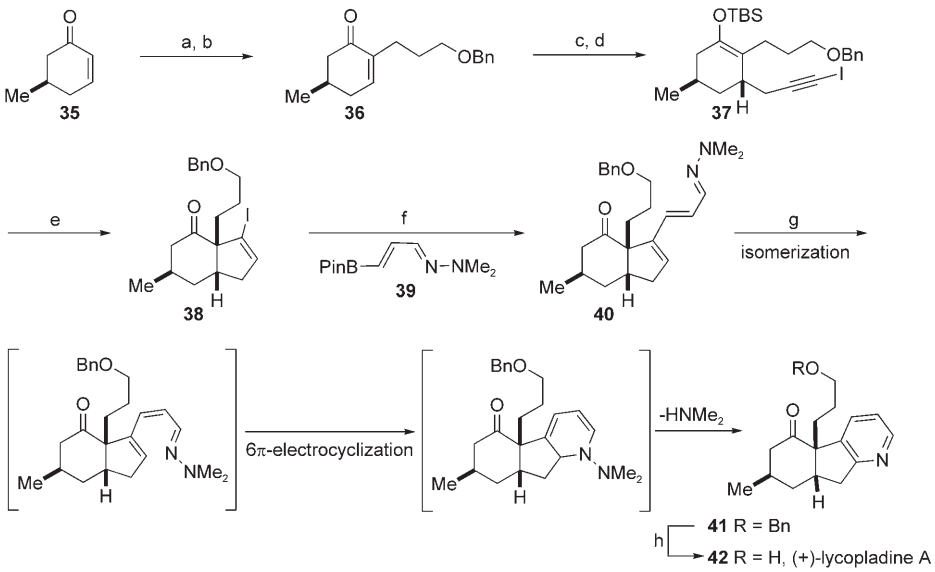


***Scheme 1.*** Synthesis of (+)-lycopladine A. Reagents and conditions: a) $I_2$ (0.6 equiv), $PhI(OCOCF_3)_2$ (0.6 equiv), pyridine, $CH_2Cl_2$, room temperature (85%); b) $(BnOCH_2CH_2CH_2)_3B$, $[PdCl_2(dppf)]$ (5 mol%), $AsPh_3$ (5 mol%), $Cs_2CO_3$, DMF, THF, $H_2O$ (72%); c) tributylallenylstannane, TBSOTf, $CH_2Cl_2$, −78→−10°C (93%); d) NIS, $AgNO_3$, DMF, 0°C→RT (82%); e) $[AuClPPh_3]/AgBF_4$ (10 mol%), $CH_2Cl_2$/MeOH (10:1), 40°C (95%); f) **39**, $[Pd(PPh_3)_4]$ (5 mol%), NaOMe, MeOH/PhH (83%); g) $PhCH_3$, 190°C, 4 h (60%); h) 10% Pd/C, 1,4-cyclohexadiene, EtOH (75%). Bn = benzyl, DMF = dimethylformamide, dppf = 1,1′-bis(diphenylphosphino)ferrocene, NIS = *N*-iodosuccinimide, Pin = pinacol.

We envisioned that this catalyst system might be extended to allow the construction of cyclopentenes, with control of the location of the double bond, simply by varying the electrophilic component. Gratifyingly, silyl enol ethers also participated as nucleophiles in gold(I)-catalyzed 5-*endo*-dig additions to alkynes, which allows for the production of a variety of systems bearing endocyclic olefins (Table 1, entries 9–13). Notably an aryl iodide, a functional group susceptible to oxidative addition by other $d^{10}$-transition-metal catalysts, remains untouched in the $Au^I$-catalyzed process (Table 1, entry 10). Additionally, a variety of heteroaromatic groups were well tolerated at the acetylenic position (Table 1, entries 11–13). Moreover, similar conditions can be employed for the use of allenes as the electrophilic partner in a 5-*endo*-trig cyclization [Eqs. (2) and (3); TBS = *tert*-butyldimethylsilyl].[9] For example, allene **31** smoothly underwent a gold(I)-catalyzed cyclization to afford bicylic cyclopentenes **32** in 72% yield. Therefore, the combination of the gold(I)-catalyzed alkyne and allene cyclization reactions allows for the construction of cyclopentenes with control of the position of the unsaturation (compare **20** with **32**).

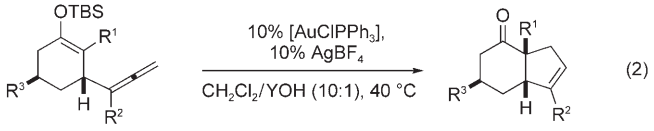


(2)

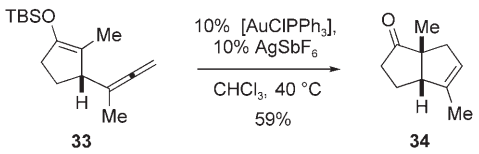


(3)

The utility of the gold(I)-catalyzed method for the formation of non-ester-bearing all-carbon quaternary centers was immediately realized in an expedient total synthesis of the recently isolated fawcettimine alkaloid (+)-lycopladine A (**42**). Isolated from *Lycopodium complantum*, lycopladine A (**42**) shows modest but selective cytotoxicity against murine lymphoma L1210 cells and possesses an unprecedented $C_{16}N$-type alkaloid skeleton, including a novel pyridyl-fused hydrindanone core.[5] We envisioned that a gold(I)-catalyzed 5-*endo*-dig cyclization could be employed to construct the hydrindanone core of lycopladine A. To this end, cyclohexenone **36** was obtained through iodination[10] and subsequent B-alkyl Suzuki–Miyaura coupling[11] of readily obtainable (*R*)-(+)-5-methyl-2-cyclohexen-1-one (**35**;[12] Scheme 1). Conjugate propargylation of tributylallenylstannane promoted by *tert*-butyldimethylsilyl trifluoromethanesulfonate (TBSOTf)[13] followed by iodination of the resultant terminal alkyne[14] diastereoselectively furnished iodoacetylene **37** and set the stage for the key gold(I)-catalyzed 5-*endo*-dig cyclization. Reaction of silyl enol ether **37** under our optimized conditions gave hydrindanone vinyl iodide **38** in 95% yield as a single diastereomer. Vinyl iodide **38** underwent Suzuki coupling with boronic ester **39**[15] to afford *N*,*N*′-dimethylhydrazone **40** in 83% yield. Notable is the consecutive use of two catalytic reactions mediated by $d^{10}$ metals with orthogonal reactivity ($Au^I$ and $Pd^0$), thus allowing rapid and convergent access to all of the carbon atoms of lycopladine. Thus, heating **40** promoted a cascade sequence involving double-bond isomerization, 6π electrocyclization, and elimi-

 © 2006 Wiley-VCH Verlag GmbH & Co. KGaA, Weinheim 

nation of dimethylamine to generate pyridyl-fused product **41** in 60% yield.[16] The benzyl ether protecting group was removed under conditions for transfer hydrogenation to complete the asymmetric total synthesis of (+)-lycopladine A (**42**) and thereby establish the absolute stereochemistry of this alkaloid.

In summary a gold(I)-catalyzed addition of silyl enol ethers to alkynes and allenes has been developed. The reaction allows for the diastereoselective synthesis of a variety of bicyclic frameworks containing all-carbon quaternary centers. Taken together, the gold(I)-catalyzed 5-*exo*-dig, 5-*endo*-dig, and 5-*endo*-trig pentannulation reactions provide access to cyclopentenes with control of the position of the double bond. The utility of these reactions was demonstrated by an efficient total synthesis of (+)-lycopladine A (8 steps, 17% overall yield from enone **35**) which takes advantage of the orthogonal reactivity of the $Au^I$ and $Pd^0$ centers towards unsaturated iodides.[17] Further demonstration of the utility of these cyclopentene annulation reactions, including additional application to the fawcettimine alkaloids, is in progress and will be reported in due course.

Received: May 22, 2006
Published online: August 4, 2006

**Keywords:** alkaloids · carbocyclization · gold · homogeneous catalysis · silyl enol ethers

[1] a) L. E. Overman, C. J. Douglas, *Proc. Natl. Acad. Sci. USA* **2004**, *101*, 5363; b) I. Denissova, L. Barriault, *Tetrahedron* **2003**, *59*, 10105; c) J. Christoffers, A. Mann, *Angew. Chem.* **2001**, *113*, 4725; *Angew. Chem. Int. Ed.* **2001**, *40*, 4591; d) E. J. Corey, A. Guzman-Perez, *Angew. Chem.* **1998**, *110*, 402; *Angew. Chem. Int. Ed.* **1998**, *37*, 388; e) K. Fuji, *Chem. Rev.* **1993**, *93*, 2037.

[2] a) J. J. Kennedy-Smith, S. T. Staben, F. D. Toste, *J. Am. Chem. Soc.* **2004**, *126*, 4526; b) S. T. Staben, J. J. Kennedy-Smith, F. D. Toste, *Angew. Chem.* **2004**, *116*, 5464; *Angew. Chem. Int. Ed.* **2004**, *43*, 5350.

[3] For transition-metal-promoted reactions of silyl enol ethers with alkynes/allenes, see: a) J. Drouin, M. A. Boaventura, J.-M. Conia, *J. Am. Chem. Soc.* **1985**, *107*, 1726; b) J. Drouin, M. A. Boaventura, *Tetrahedron Lett.* **1987**, *28*, 3923; c) H. Huang, C. Forsyth, *J. Org. Chem.* **1995**, *60*, 2773; d) K. Maeyama, N. Iwasawa, *J. Am. Chem. Soc.* **1998**, *120*, 1928; e) K. Imamura, E. Yoshikawa, V. Gevorgyan, Y. Yamamoto, *Tetrahedron Lett.* **1999**, *40*, 4081; f) N. Iwasawa, Maeyama, H. Kusama, *Org. Lett.* **2001**, *3*, 3871; g) N. Iwasawa, T. Miura, K. Kiyota, H. Kusama, K. Lee, P. H. Lee, *Org. Lett.* **2002**, *4*, 4463; h) T. Miura, K. Kiyota, H. Kusama, K. Lee, H. Kim, S. Kim, P. H. Lee, N. Iwasawa, *Org. Lett.* **2003**, *5*, 1725.

[4] For gold-catalyzed reactions involving enol ethers, see: a) J. W. Dankwardt, *Tetrahedron Lett.* **2001**, *42*, 5809; b) C. Nevado, D. J. Cárdenas, A. M. Echavarren, *Chem. Eur. J.* **2003**, *9*, 2627; c) B. D. Sherry, F. D. Toste, *J. Am. Chem. Soc.* **2004**, *126*, 15978; d) M. H. Suhre, M. Reif, S. F. Kirsch, *Org. Lett.* **2005**, *7*, 3925.

[5] K. Ishiuchi, T. Kubota, H. Morita, J. Kobayashi, *Tetrahedron Lett.* **2006**, *47*, 3287.

[6] Hydrolysis of an enol acetate in the presence of gold(I) has been proposed in gold-catalyzed reactions: a) X. Shi, D. J. Gorin, F. D. Toste, *J. Am. Chem. Soc.* **2005**, *127*, 5802; b) L. Zhang, S. Wang, *J. Am. Chem. Soc.* **2006**, *128*, 1442.

[7] Addition of alcohols to enol ethers is proposed in the gold(I)-catalyzed formation of ketals from alkynes: a) J. H. Teles, S. Brode, M. Chabanas, *Angew. Chem.* **1998**, *110*, 1475; *Angew. Chem. Int. Ed.* **1998**, *37*, 1415; ; b) S. Antoniotti, E. Genin, V. Michelet, J.-P. Genêt, *J. Am. Chem. Soc.* **2005**, *127*, 9976.

[8] For reaction of gold(I) complexes with enol ethers to generate gold(I) enolates, see: a) A. N. Nesmeyanov, E. G. Perevalova, K. I. Grandberg, V. P. Dyadchenko, *Izv. Akad. Nauk SSSR Ser. Khim.* **1974**, 2872; b) Y. Ito, M. Inouye, M. Suginome, M. Murakami, *J. Organomet. Chem.* **1988**, *342*, C41; for related reactions with $Pd^{II}$, see: Y. Ito, T. Hirao, T. Saegusa, *J. Org. Chem.* **1978**, *43*, 1011.

[9] For examples involving allene activation by $Au^I$, see: a) L. Zhang, *J. Am. Chem. Soc.* **2005**, *127*, 16804; b) A. W. Sromek, M. Rubina, V. Gevorgyan, *J. Am. Chem. Soc.* **2005**, *127*, 10500; c) N. Morita, N. Krause, *Angew. Chem.* **2006**, *118*, 1930; *Angew. Chem. Int. Ed.* **2006**, *45*, 1897; .

[10] R. Benhida, P. Blanchard, J.-L. Fourrey, *Tetrahedron Lett.* **1998**, *39*, 6849.

[11] S. Chemler, D. Trauner, S. J. Danishefsky, *Angew. Chem.* **2001**, *113*, 4676; *Angew. Chem. Int. Ed.* **2001**, *40*, 4544.

[12] D. Caine, K. Procter, A. Cassell, *J. Org. Chem.* **1984**, *49*, 2647.

[13] J. Haruta, K. Nishi, S. Matsuda, S. Akai, Y. Tamaura, Y. Kita, *J. Org. Chem.* **1990**, *55*, 4853; for the synthesis of the tributylallenyltin reagent, see: Y. Ueno, M. Okawara, *J. Am. Chem. Soc.* **1979**, *101*, 1893.

[14] H. Hofmeister, K. Annen, H. Laurent, R. Wiechert, *Angew. Chem.* **1984**, *96*, 720; *Angew. Chem. Int. Ed. Engl.* **1984**, *23*, 727.

[15] B. B. Toure, D. G. Hall, *J. Org. Chem.* **2004**, *69*, 8429.

[16] For related pyridine syntheses, see: a) T. Hosokawa, N. Shimo, K. Maeda, A. Sonoda, S.-I. Murahashi, *Tetrahedron Lett.* **1976**, 383; b) W. Verboom, P. J. S. S. Van Eijk, P. G. M. Conti, D. N. Reinhoudt, *Tetrahedron* **1989**, *45*, 3131; c) K. Tanaka, H. Mori, M. Yamamoto, S. Katsumura, *J. Org. Chem.* **2001**, *66*, 3099.

[17] For additional applications of Au-catalyzed reactions in natural product synthesis, see: a) J. Zhu, A. R. Germain, J. A. Porco, Jr., *Angew. Chem.* **2004**, *116*, 1259; *Angew Chem. Int. Ed.* **2004**, *43*, 1239; b) A. Fürstner, P. Hannen, *Chem. Commun.* **2004**, 2546; c) K. Sato, N. Asao, Y. Yamamoto, *J. Org. Chem.* **2005**, *70*, 8981; d) G. Dyker, D. Hildebrandt, *J. Org. Chem.* **2005**, *70*, 6093; e) A. Fürstner, P. Hannen, *Chem. Eur. J.* **2006**, *12*, 3006; f) C. Fehr, J. Galindo, *Angew. Chem.* **2006**, *118*, 2967; *Angew. Chem. Int. Ed.* **2006**, *45*, 2901; g) A. S. K. Hashmi, L. Ding, J. W. Bats, P. Fischer, W. Frey, *Chem. Eur. J.* **2003**, *9*, 4339.

 © 2006 Wiley-VCH Verlag GmbH & Co. KGaA, Weinheim 

Asymmetric Catalysis

DOI: 10.1002/anie.200601855

# β-Disubstituted Allylic Chlorides: Substrates for the Cu-Catalyzed Asymmetric $S_N2'$ Reaction**

*Caroline A. Falciola, Karine Tissot-Croset, and Alexandre Alexakis**

Metal-promoted asymmetric catalysis has proven to be an efficient method in carbon–carbon bond-forming reactions to obtain optically enriched compounds. Allylic substitution has attracted much attention and great effort has been put into controlling the chemo-, regio-, and enantioselective outcome of the reaction.[1] Extensive accounts report a wide variety of metals that use soft nucleophiles for the reaction (Pd, Ir, Mo, Rh, Ru).[2] In contrast, copper allows the use of hard, nonstabilized nucleophiles, such as small alkyl groups in the form of organometallic species.[3] Among the broad range of reagents available, the use of Grignard reagents in the catalyzed asymmetric allylic substitution reaction was first reported by Bäckvall et al.,[4] with chiral copper thiolates yielding moderate *ee* values. This pioneering work was soon followed by a report from Dübner and Knochel,[5] who disclosed a different system based on diorganozinc reagents. Other ligands have been introduced for the stereoselective allylic addition of organomagnesium reagents, such as chiral diaminocarbenes by Okamoto et al.,[6] and more recently ferrocenic bidentate phosphines by Feringa et al.[7]

In the past few years, our group has reported highly regio- and enantioselective Cu-phosphoramidite catalytic reactions for the substitution of allylic chlorides by organomagnesium reagents.[8] This methodology was applied, in particular, to the formal synthesis of profen molecules by the highly efficient and valuable stereoselective allylic addition of MeMgBr with *ee* values up to 96%.[9] Subsequently, we focused on the application of our procedure to diverse substrates, and report herein the unprecedented Cu-catalyzed asymmetric allylic alkylation of β-disubstituted allylic halides.

The Cu-catalyzed asymmetric $S_N2'$ reaction has mostly been limited to disubstituted olefinic systems.[10,11] Type A substrates (Scheme 1) that lead to chiral quaternary centers through catalytic allylic alkylation are scarcely documented, with the exception of reports from Hoveyda and co-workers who reached excellent enantioselectivities on γ-disubstituted allylic phosphates.[12,13] Other than the results reported by Woodward and co-workers on the stereoselective addition to Baylis–Hillman-derived allylic electrophiles,[14] copper-catalyzed asymmetric allylic alkylation on type B substrates, the β-disubstituted olefinic system, has not previously been described.

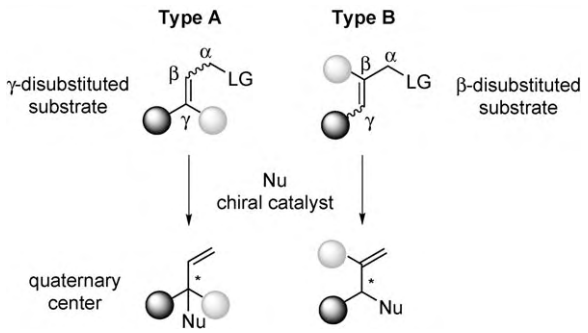


***Scheme 1.*** Asymmetric allylic alkylation of γ- and β-disubstituted allylic substrates. LG = leaving group, Nu = nucleophile.

Preliminary experiments for this study started with a short screening of biphenol-[15] and binaphthol-based[8b,16] phosphoramidite ligands (Scheme 2) on *trans*-(3-chloro-2-methyl-prop-1-enyl)benzene (**1**), the β-methylcinnamyl chloride (Scheme 3). The results are summarized in Table 1. The allylic substitution of **1** by the slow addition of ethylmagnesium bromide, catalyzed by copper thiophene carboxylate (CuTC; 1 mol%) and different phosphoramidite ligands (1.1 mol%), gave adducts with poor-to-good γ/α ratios and provided high enantiomeric excess up to 96% *ee* with ligand **L6** (Table 1, entry 6).

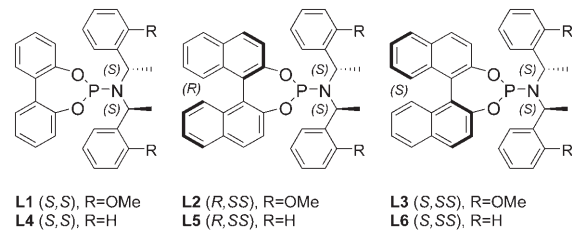


***Scheme 2.*** Chiral phosphoramidite ligands applied in the Cu-catalyzed asymmetric substitution.

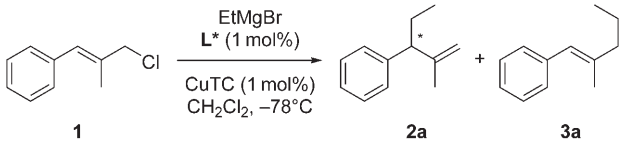


***Scheme 3.*** Asymmetric $S_N2'$ reaction on β-methylcinnamyl chloride. L* = **L1**–**L6**.

Interestingly, the biphenol ligands **L1** and **L4** did not give product **2a** with the same absolute configuration, which is in accordance with our previous studies.[8a–c] Although we had

[*] C. A. Falciola, K. Tissot-Croset, Prof. Dr. A. Alexakis
Department of Organic Chemistry
University of Geneva
30 quai E. Ansermet, 1211 Geneva 4 (Switzerland)
E-mail: alexandre.alexakis@chiorg.unige.ch

[**] We thank the Swiss National Research Foundation (no. 200020-105368) and COST action D24/003/01 (OFES contract no. C02.0027) for financial support, and BASF for the generous gift of chiral amines.

Supporting information for this article is available on the WWW under http://www.angewandte.org or from the author.

 © 2006 Wiley-VCH Verlag GmbH & Co. KGaA, Weinheim 

***Table 1:*** Screening of phosphoramidite ligands in the asymmetric CuTC-catalyzed allylic alkylation with EtMgBr (Scheme 3; L* = **L1**–**L6**).

| Entry[a] | Ligand | Conv. [%][b] | **2a**/**3a**[c] | *ee* [%][d] |
|---|---|---|---|---|
| 1 | **L1** (*S,S*) | >99 | 89:11 | 81(−) |
| 2 | **L2** (*R,SS*) | >99 | 73:27 | 61(−) |
| 3 | **L3** (*S,SS*) | >99 | 87:13 | 80(−) |
| 4 | **L4** (*S,S*) | >99 | 65:35 | 53(+) |
| 5 | **L5** (*R,SS*) | >99 | 30:70 | 27(−) |
| 6 | **L6** (*S,SS*) | >99 | 87:13 | 96(+) |
| 7[e] | **L6** (*S,SS*) | >99 (87) | 92:8 | 98(+) |

[a] Conditions: **1** (1 mmol), CuTC (1 mol%), and L* (1.1 mol%) in $CH_2Cl_2$ (2 mL) at −78 °C with addition of EtMgBr in $Et_2O$ (1.2 equiv) over 1 h. [b] Conversion determined by GC–MS (in parentheses, yield of isolated product after purification by column chromatography on silica gel). [c] Ratio determined by GC–MS and $^1$H NMR spectroscopy. [d] Enantiomeric excess determined by chiral GC. [e] 3 mol% of CuTC and 3.3 mol% of L*.

shown that **L3** was the best ligand in different reactions with copper or iridium catalysis,[8a,b] we observed a lower enantioselective outcome of the substitution, with 80% *ee* (Table 1, entry 3). The hypothetically coordinating *ortho*-methoxy substituents seem to play a detrimental role.[17] An optimal amount (3 mol%) of CuTC/**L6** resulted in improved selectivities of 92% in favor of the γ product and 98% *ee* (Table 1, entry 7). By accelerating the reaction and thus preventing the formation of a dialkyl–cuprate complex in the reaction medium, the catalyst loading is an important parameter that favors the formation of the branched product (**2a**).[2,9,18]

To broaden the scope of the reaction, other Grignard reagents were tested and gave equally good asymmetric results (Table 2). Nonetheless, not being satisfied with the preliminary regioselectivity of **2d** and **2e** (Table 2, entries 3 and 6), we performed a slower addition of the Grignard reagents (Table 2, entries 4 and 7) and found a desirable improvement in regioselectivity (to 89 and 87% γ selectivity for **2d** and **2e**, respectively), while slightly raising the enantiomeric excess. By analogy to our previous finding, one-pot ring-closing metathesis with the Grubbs second-generation catalyst proceeded quantitatively on **2d** and **2e** without any loss of enantioselectivity in products **4d** and **4e** (with regard to open-chain intermediates; Table 2, entries 5 and 8).[19]

***Table 2:*** Enantioselective Cu-catalyzed allylic alkylation on **1** with RMgX.

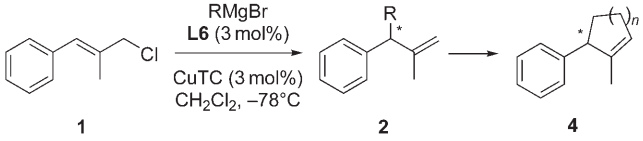


| Entry[a] | RMgX | Yield [%][b] | Product | $S_N2'/S_N2$[c] | *ee* [%][d] |
|---|---|---|---|---|---|
| 1 | *n*-propyl-MgBr | 85 | **2b** | 84:16 | 97(+) |
| 2 | *n*-pentyl-MgBr | 83 | **2c** | 83:17 | 96(+) |
| 3 | 3-butenyl-MgBr | 84 | **2d** | 79:21 | 95(+) |
| 4[e] | 3-butenyl-MgBr | 84 | **2d** | 89:11 | 97(+) |
| 5[f] | – | 69 | **4d** | 89:11 | 97(+) |
| 6 | 4-pentenyl-MgBr | 87 | **2e** | 82:18 | 93(+) |
| 7[e] | 4-pentenyl-MgBr | 87 | **2e** | 87:13 | 96(+) |
| 8[f] | – | 68 | **4e** | 87:13 | 96(+) |

[a] Conditions: **1** (1 mmol), CuTC (3 mol%), and **L6** (3.3 mol%) in $CH_2Cl_2$ (2 mL) at −78 °C with addition of RMgBr in $Et_2O$ (1.2 equiv) over 1 h. [b] Yields of isolated products of the mixture of regioisomers after purification by column chromatography on silica gel. [c] Ratio determined by GC–MS and $^1$H NMR spectroscopy. [d] Enantiomeric excess determined by chiral GC. [e] Addition of RMgBr over 4 h. [f] After completion of the $S_N2'$ reaction, addition of the Grubbs second-generation catalyst (6 mol%) at room temperature.

In addition, we proceeded by functionalizing the aryl moiety of the allylic substrate and varied the β substituent (Scheme 4). The enantioselectivities are within the excellent results obtained previously, between 92 and 96% *ee*. The *para*-chloro electron-withdrawing group (**5a**) does not influence the regioselective outcome of the allylic alkylation. However, the *para*-methyl substituent (**5b**) penalizes the reaction and the branched product **6b** is obtained with 84% selectivity.

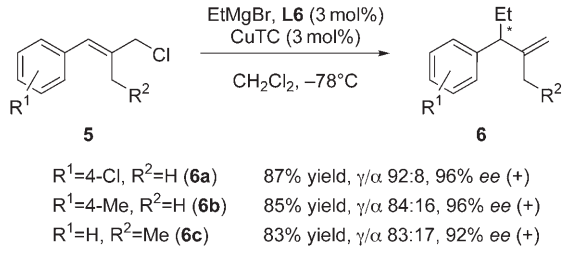


***Scheme 4.*** Enantioselective Cu-catalyzed allylic alkylation on **5a**–**c** with EtMgBr.

In addition, we proceeded by functionalizing the aryl moiety of the allylic substrate and varied the β substituent (Scheme 4). The enantioselectivities are within the excellent results obtained previously, between 92 and 96% *ee*. The *para*-chloro electron-withdrawing group (**5a**) does not influence the regioselective outcome of the allylic alkylation. However, the *para*-methyl substituent (**5b**) penalizes the reaction and the branched product **6b** is obtained with 84% selectivity.

To confirm the efficiency of the copper-catalyzed procedure with the phosphoramidite ligand **L6**, we examined another very interesting class of β-disubstituted allylic substrates, the aliphatic endocyclic allylic chlorides **7a**,**b** (Scheme 5). Some years ago, Gais and co-workers reported the diastereoselective addition of various organocuprates and organocopper reagents to optically active endocyclic allylic sulfoximines, and they obtained $S_N2'$ rearrangement products with low-to-high enantioselectivities (36–90% *ee*).[20] Other

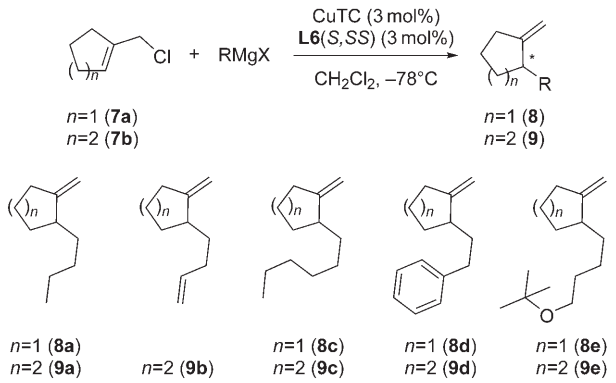


***Scheme 5.*** Formation of α-substituted chiral *exo*-methylenic cyclic compounds.

 © 2006 Wiley-VCH Verlag GmbH & Co. KGaA, Weinheim 

***Table 3:*** Asymmetric CuTC-catalyzed allylic alkylation on endocyclic allylic chlorides **7a**,**b** with RMgX (Scheme 3; L* = **L2**–**L6**).

| Entry | Substrate | *n* | R | L* | Conv. [%][a] | $S_N2'/S_N2$[b] | *ee* [%] |
|---|---|---|---|---|---|---|---|
| 1 | **7a** | 1 | **8a** | **L5** | >99 | 63:37 | 29 (*S*+) |
| 2 | **7a** | 1 | **8a** | **L6** | >99 | 96:4 | 98 (*S*+) |
| 3 | **7a** | 1 | **8c** | **L6** | >99 (44) | 97:3 | 98 (*S*+) |
| 4[c] | **7a** | 1 | **8c** | **L6** | >99 (91) | 98:2 | 98 (*S*+) |
| 5 | **7a** | 1 | **8d** | **L6** | >99 | 97:3 | 98 (*R*+) |
| 6 | **7a** | 1 | **8e** | **L6** | 96 (60) | 98:2 | 98 (+)[d] |
| 7 | **7b** | 2 | **9a** | *ent*-**L2** | >99 | 70:30 | 88 (+) |
| 8 | **7b** | 2 | **9a** | *ent*-**L3** | 75 | 44:56 | 10 (+) |
| 9 | **7b** | 2 | **9a** | **L6** | 73 | 81:19 | 98 (+) |
| 10 | **7b** | 2 | **9b** | **L6** | >99 (83) | 97:3 | 99.2 (+) |
| 11 | **7b** | 2 | **9c** | **L6** | >99 (67) | 97:3 | 98 (+) |
| 12 | **7b** | 2 | **9d** | **L5** | >99 | 72:28 | 87 (*R*) |
| 13 | **7b** | 2 | **9d** | **L6** | >99 (78) | 85:15 | 99.4 (*S*) |
| 14 | **7b** | 2 | **9e** | **L5** | 94 | 73:27 | 74 (−) |
| 15 | **7b** | 2 | **9e** | **L6** | >99 | 91:9 | 98.8 (+) |

[a] Conversion determined by GC–MS (in parentheses, yield of isolated products after purification by column chromatography on silica gel). [b] Ratio determined by $^1$H NMR spectroscopy and GC–MS. [c] Reaction with 4 mmol of material; addition of RMgX over 4 h. [d] Determined by GC analysis of **8f** (R = $(CH_2)_4OCOCF_3$).

than these results, there are no accounts of copper-catalyzed asymmetric $S_N2'$ alkylation with chiral external ligands on such allylic derivatives.

We were gratified to see that the addition of different Grignard reagents with 3 mol% of the copper catalyst proceeded highly selectively toward the γ substitution and delivered adducts **8** and **9** with excellent enantiomeric excess up to >99%. Here again, a small panel of phosphoramidite ligands were tested for their asymmetric induction of the allylic substitution, but it was clear from Table 3 that ligand **L6** (*S*,*SS*) once more was the most successful. As concerns the five-membered-ring substrate **7a**, constant *ee* values of 98% were obtained, independent of the organomagnesium reagent used (Table 3, entries 2–5). In the larger-scale synthesis of the chiral adduct **8c** (Table 3, entry 4) and allowing a slower addition time of the Grignard reagent (to prevent the reaction temperature from rising), we obtained excellent matching selectivities toward the γ product (98:2) and the enantiomeric excess (98%). The six-membered-ring allylic chloride **7b** afforded equally good *ee* values and γ selectivities according to the RMgX. The highest noteworthy enantioselectivity for such a reaction was recorded for the addition of 3-butenylmagnesium bromide on **7b** with 3 mol% CuTC/**L6** loading, to afford **9b** with 99.2% *ee* and a 97:3 branched-to-linear ratio (Table 3, entry 10). All the products obtained in this series are valuable starting materials for more elaborate chiral synthons. For example, the *n*-hexyl adduct (Table 3, entry 4) is a precursor for the formal asymmetric synthesis of lepadiformine.[21,22] Other useful transformations can be envisioned on the exocyclic double bond, such as oxidation to a ketone or selective epoxidation.

In conclusion, we have demonstrated that the asymmetric methodology developed previously by our group can be efficiently applied on more substituted allylic patterns with phosphoramidite ligand **L6** (*S*,*SS*) and a copper-catalyst loading as low as 3 mol%. Two different classes of β-disubstituted substrates, cinnamyl derivatives and aliphatic endocyclic allylic chlorides, afforded both excellent regio- and enantioselectivities. *Ee* values of up to 98 and >99%, respectively, were obtained in both applications.

## *Experimental Section*

CuTC (3 mol%) and chiral ligand (3.3 mol%) were charged in a dried Schlenk tube under inert gas and suspended in $CH_2Cl_2$ (2 mL). The mixture was stirred at room temperature for 30 min, followed by addition of the allylic chloride (1 mmol) at room temperature before cooling the mixture to −78°C in an ethanol–dry ice bath. The Grignard reagent (3M in diethyl ether, 1.2 equiv) diluted in $CH_2Cl_2$ (0.6 mL) was added over 60 min with a syringe pump. Upon completion of the addition, the reaction mixture was left a further 4 h at −78°C. The reaction was quenched by the addition of aqueous HCl (1N, 2 mL) and then $Et_2O$ (10 mL). The aqueous phase was separated and further extracted with $Et_2O$ (3×3 mL). The combined organic fractions were washed with brine (5 mL), dried over anhydrous sodium sulfate, filtered, and concentrated in a vacuum. The oily residue was purified by flash column chromatography. Gas chromatography on a chiral stationary phase showed the enantiomeric excess of the $S_N2'$ product.

Received: May 11, 2006
Published online: August 4, 2006

**Keywords:** alkylation · allylic compounds · asymmetric catalysis · copper · nucleophilic substitution

[1] a) B. M. Trost, C. Lee in *Catalytic Asymmetric Synthesis* (Ed.: I. Ojima), 2nd ed., Wiley, New York, **2000**, p. 593; b) A. Pfaltz, M. Lautens in *Comprehensive Asymmetric Catalysis I–III* (Eds.: E. N. Jacobsen, A. Pfaltz, H. Yamamoto), Springer, Berlin, **1999**, p. 833.

[2] For reviews of asymmetric allylic alkylation with various metals, see: a) H. Miyabe, Y. Takemoto, *Synlett* **2005**, 1641; b) B. M. Trost, *J. Org. Chem.* **2004**, *69*, 5813; c) B. M. Trost, M. L. Crawley, *Chem. Rev.* **2003**, *103*, 2921; d) R. Takeuchi, *Synlett* **2002**, 1954.

[3] For recent reviews of asymmetric Cu-catalyzed allylic alkylation, see: a) A. Alexakis, C. Malan, L. Lea, K. Tissot-Croset, D. Polet, C. Falciola, *Chimia* **2006**, *60*, 124; b) H. Yorimitsu, K. Oshima, *Angew. Chem.* **2005**, *117*, 4509; *Angew. Chem. Int. Ed.* **2005**, *44*, 4435; c) A. Kar, N. P. Argade, *Synthesis* **2005**, 2995.

[4] a) M. Van Klaveren, E. S. M. Persson, A. del Villar, D. M. Grove, J. E. Bäckvall, G. van Koten, *Tetrahedron Lett.* **1995**, *36*, 3059; b) A. S. E. Karlstrom, F. F. Huerta, G. J. Meuzelaar, J. E. Bäckvall, *Synlett* **2001**, 923.

[5] a) F. Dübner, P. Knochel, *Angew. Chem.* **1999**, *111*, 391; *Angew. Chem. Int. Ed.* **1999**, *38*, 379; b) F. Dübner, P. Knochel, *Tetrahedron Lett.* **2000**, *41*, 9233.

[6] a) S. Tominaga, Y. Oi, T. Kato, D. K. An, S. Okamoto, *Tetrahedron Lett.* **2004**, *45*, 5585; b) S. Okamoto, S. Tominaga,

 © 2006 Wiley-VCH Verlag GmbH & Co. KGaA, Weinheim 

N. Saimo, K. Kase, K. Shomoda, *J. Organomet. Chem.* **2005**, *690*, 6001.
[7] F. Lopez, A. W. van Zijl, A. J. Minaard, B. L. Feringa, *Chem. Commun.* **2006**, 409.
[8] a) K. Tissot-Croset, D. Polet, S. Gille, C. Hawner, A. Alexakis, *Synthesis* **2004**, 2586; b) K. Tissot-Croset, D. Polet, A. Alexakis, *Angew. Chem.* **2004**, *116*, 2480; *Angew. Chem. Int. Ed.* **2004**, *43*, 2426; c) A. Alexakis, K. Croset, *Org. Lett.* **2002**, *4*, 4147; d) A. Alexakis, C. Malan, L. Lea, C. Benhaim, X. Fournioux, *Synlett* **2001**, 927.
[9] K. Tissot-Croset, A. Alexakis, *Tetrahedron Lett.* **2004**, *45*, 7375.
[10] a) H. Malda, A. W. van Zijl, L. A. Arnold, B. L. Feringa, *Org. Lett.* **2001**, *3*, 1169; b) A. W. Van Zijl, L. A. Arnold, A. J. Minnaard, B. L. Feringa, *Adv. Synth. Catal.* **2004**, *346*, 413.
[11] a) U. Piarulli, P. Daubos, C. Claverie, C. Monti, C. Gennari, *Eur. J. Org. Chem.* **2005**, 895; b) U. Piarulli, P. Daubos, C. Claverie, M. Roux, C. Gennari, *Angew. Chem.* **2003**, *115*, 244; *Angew. Chem. Int. Ed.* **2003**, *42*, 234; c) U. Piarulli, C. Claverie, P. Daubos, C. Gennari, A. J. Minnaard, B. L. Feringa, *Org. Lett.* **2003**, *5*, 4493; d) S. Ongeri, U. Piarulli, M. Roux, C. Monti, C. Gennari, *Helv. Chim. Acta* **2002**, *85*, 3388.
[12] With chiral Schiff base ligands: a) K. E. Murphy, A. H. Hoveyda, *Org. Lett.* **2005**, *7*, 1255; b) M. A. Kacprzynski, A. H. Hoveyda, *J. Am. Chem. Soc.* **2004**, *126*, 10676; c) C. A. Luchaco-Cullis, H. Mizutani, K. E. Murphy, A. H. Hoveyda, *Angew. Chem.* **2001**, *113*, 1504; *Angew. Chem. Int. Ed.* **2001**, *40*, 1456.
[13] With chiral NHC ligands: a) J. J. Van Veldhuizen, J. E. Campbell, R. E. Giudici, A. H. Hoveyda, *J. Am. Chem. Soc.* **2005**, *127*, 6877; b) A. O. Larsen, W. Leu, C. N. Oberhuber, J. E. Campbell, A. H. Hoveyda, *J. Am. Chem. Soc.* **2004**, *126*, 11130.
[14] a) C. Borner, P. J. Goldsmith, S. Woodward, J. Gimeno, S. Gladiali, D. Ramazzoti, *Chem. Commun.* **2000**, *24*, 2433; b) K. Biswas, C. Boerner, J. Gimeno, P. J. Goldsmith, D. Ramazzotti, A. L. K. So, S. Woodward, *Tetrahedron* **2005**, *61*, 1433; c) P. J. Goldsmith, S. J. Teat, S. Woodward, *Angew. Chem.* **2005**, *117*, 2275; *Angew. Chem. Int. Ed.* **2005**, *44*, 2235.
[15] A. Alexakis, S. Rosset, J. Allamand, S. March, F. Guillen, C. Benhaim, *Synlett* **2001**, 1375.
[16] B. L. Feringa, M. Pineschi, L. A. Arnold, R. Imbos, A. H. M. De Vries, *Angew. Chem.* **1997**, *109*, 2733; *Angew. Chem. Int. Ed. Engl.* **1997**, *36*, 2620.
[17] The analogous *p*-OMe ligands were also tested and gave similar results to **L4** (52% *ee*), **L5** (26% *ee*), and **L6** (96% *ee*).
[18] J.-E. Bäckvall, M. Sellén, B. Grant, *J. Am. Chem. Soc.* **1990**, *112*, 6615.
[19] The Grubbs first-generation catalyst gave poor results.
[20] a) H.-J. Gais, H. Müller, J. Bund, M. Scommoda, J. Brandt, G. Raabe, *J. Am. Chem. Soc.* **1995**, *117*, 2453; b) J. Bund, H.-J. Gais, S. Erdelmeier, *J. Am. Chem. Soc.* **1991**, *113*, 1442.
[21] a) P. Schär, P. Renaud, *Org. Lett.* **2006**, *8*, 1569; b) E. Nyfeler, P. Renaud, *Abstracts of Papers, SCS Fall Meeting 2005*, EPFL, Lausanne, Switzerland, October 13, **2005**, ORGN-278; c) P. G. Reddy, S. Baskaran, *J. Org. Chem.* **2004**, *69*, 3093.
[22] For a short review on marine alkaloid synthesis, see: P. Schär, S. Cren, P. Renaud, *Chimia* **2006**, *60*, 131.

 © 2006 Wiley-VCH Verlag GmbH & Co. KGaA, Weinheim 

Emission-Control Catalysts

DOI: 10.1002/anie.200503938

# Self-Regenerating Rh- and Pt-Based Perovskite Catalysts for Automotive-Emissions Control**

*Hirohisa Tanaka,* Masashi Taniguchi, Mari Uenishi, Nobuhiko Kajita, Isao Tan, Yasuo Nishihata, Jun'ichiro Mizuki, Keiichi Narita, Mareo Kimura, and Kimiyoshi Kaneko*

Automotive catalysts deteriorate as a result of a decrease in the active surface area of the precious metals, this is caused by the growth of grains under the inherent redox environment of exhaust gases at high temperatures of up to 1000 °C. To compensate for this deterioration, conventional catalysts are loaded with an excess amount of precious metals, although this leads to over-consumption and supply problems. Self-regenerating catalysts, which suppress the grain growth of precious metals, have recently been successfully developed and are based on the repeated movement of the precious metals in and out of perovskite oxides between a solid solution and metallic nanoparticles during the natural changes in the redox conditions.[1] Herein, we report for the first time that this self-regenerating function is realizable in Pt and Rh, as well as in Pd.

It has been predicted that the demand for precious metals for automotive catalysts will increase, and that these metals will soon be in short supply as a result of the growth in the number of automobiles in China and India and the global

[*] Dr. H. Tanaka, M. Taniguchi, Dr. M. Uenishi, N. Kajita, Dr. I. Tan
Advanced Research & Development Division
Daihatsu Motor Co., Ltd.
Ryuo, Gamo, Shiga 520-2593 (Japan)
Fax: (+81) 748-17-1064
E-mail: hirohisa_tanaka@mail.daihatsu.co.jp

Dr. Y. Nishihata, Dr. J. Mizuki
Kansai Photon Science Institute
Japan Atomic Energy Agency
Kouto, Sayo, Hyogo 678-5148 (Japan)

K. Narita, M. Kimura
Research & Development Division
Cataler Corporation
Chihama, Kakegawa, Shizuoka 437-1492 (Japan)

K. Kaneko
Fine Chemicals Research Laboratories
Hokko Chemical Industry Co., Ltd.
Toda, Atsugi, Kanagawa 243-0023 (Japan)

[**] We thank Prof. Emeritus Dr. M. Misono (Univ. of Tokyo) and Prof. Dr. T. Kobayashi (AIST) for their advice on catalyst research, and Dr. T. Uruga, Mr. K. Kato, and Ms. Y. Okajima (SPring-8) for their help with the XAFS experiments. We also thank Mr. A. Hirai, Mr. N. Sato, Mr. H. Suzuki, and Mr. S. Matsueda (Cataler), Mr. S. Mitachi and Mr. S. Araki (Hokko Chem.), and Dr. N. Kawase (NTC), Mr. K. Mitsumori, Mr. I Takahashi, and Mr. K. Naito (Daihatsu) for their cooperation in catalyst research and development. This work was supported by the Japan Ministry of Education, Culture, Sports, Science and Technology; KAKENHI (15350090).


WILEY InterScience DISCOVER SOMETHING GREAT
© 2006 Wiley-VCH Verlag GmbH & Co. KGaA, Weinheim

strengthening of emission controls. Three precious metals, namely Pd, Rh, and Pt, are used in catalytic converters for gasoline automobiles. Of these, Pt is expected to be in particularly short supply as it is also used as a catalyst for diesel engines and will soon be in demand as an electrode catalyst for fuel cells. The amount of Rh available from mining is limited, and the supply of Rh has been especially unstable in recent years. In automotive catalysts, Pd shows the biggest deterioration among these precious metals because it has the lowest melting point. To solve this problem, a technology based on the self-regenerating function of Pd-perovskite was introduced.[1,2] The possibility of applying this catalyst technology to Pt and Rh as well would solve the issue of supply and demand for precious metals and have a marked socio-economic effect.

The structure of perovskite, which has the generalized formula $ABO_3$, where A is the larger cation and B is the smaller cation, is adaptable and gives rise to materials that have a wide array of properties.[3] Many combinations of elements form perovskites, and these can be partially substituted when the tolerance factors are met. To maintain electroneutrality, three combinations are possible: $A^{1+}B^{5+}O_3$, $A^{2+}B^{4+}O_3$, and $A^{3+}B^{3+}O_3$. $BaTiO_3$ (an $A^{2+}B^{4+}O_3$ combination) is an electroceramic that is used in capacitors and transducers but not as a catalyst. $LaCoO_3$ is an $A^{3+}B^{3+}O_3$ perovskite whose catalytic properties have attracted attention since the 1970s,[4] and $LaFe_{0.95}Pd_{0.05}O_3$ has been used industrially as a three-way catalyst for gasoline automotive-emission control since October 2002.

To study the self-regenerating properties, perovskite catalysts containing Pd, Rh, or Pt were prepared by the alkoxide method.[1] X-ray absorption fine structure (XAFS) measurements were carried out on samples that were oxidized (O), reduced (OR), and re-oxidized (ORO). The X-ray absorption near-edge structure (XANES) spectrum at the Rh K-edge (23.220 keV) for $LaFe_{0.95}Rh_{0.05}O_3$ after each treatment is shown in Figure 1a, and the calculated radial structure function around Rh is shown in Figure 1b. The local

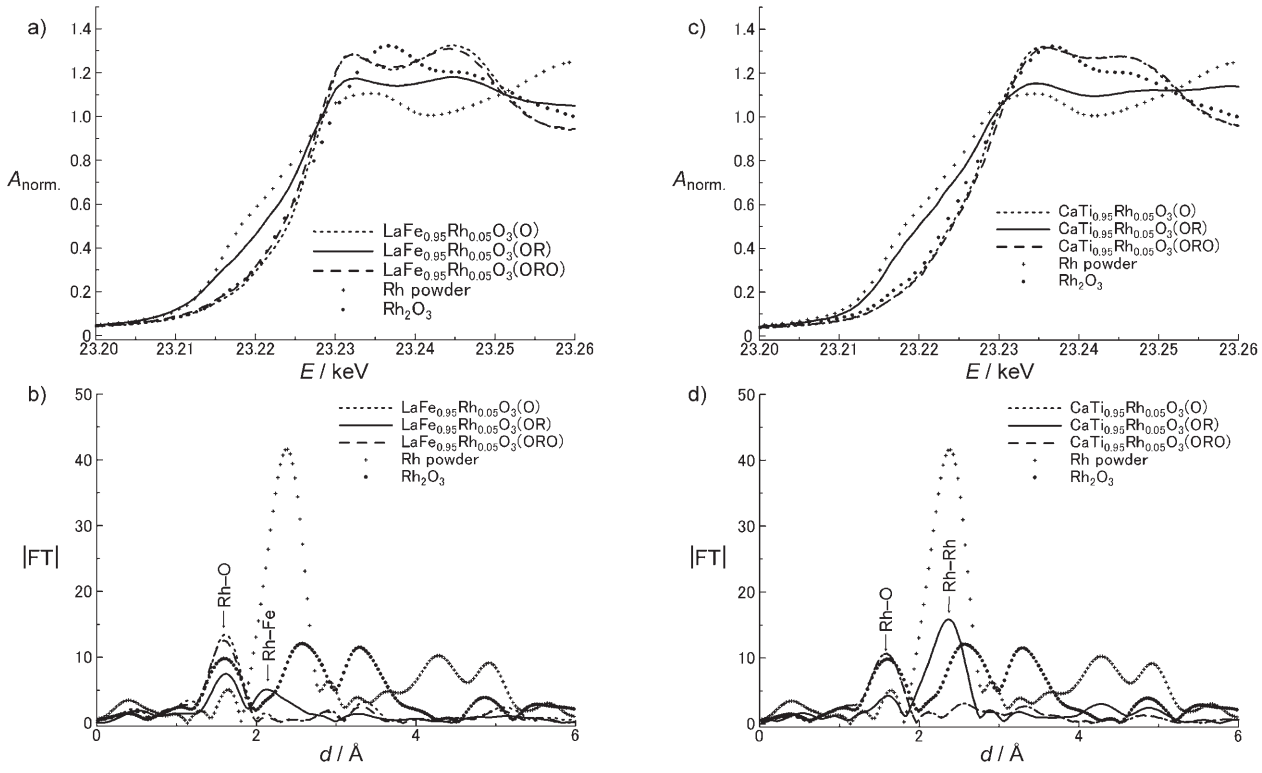


| Sample | Shell | CN | IAD (Å) | D-WF (Å²) | R-factor (%) |
|---|---|---|---|---|---|
| O | Rh-O | 6* | 2.041(6) | 0.0025(7) | 1.4 |
| OR | Rh-O | 3.1(3) | 2.046(9) | 0.0025* | 5.0 |
| | Rh-Fe | 1.2(3) | 2.575(9) | 0.0033(15) | |
| ORO | Rh-O | 5.8(3) | 2.038(5) | 0.0025* | 1.4 |

| Sample | Shell | CN | IAD (Å) | D-WF (Å²) | R-factor (%) |
|---|---|---|---|---|---|
| O | Rh-O | 6* | 2.028(6) | 0.0052(7) | 1.2 |
| OR | Rh-O | 1.8(1) | 2.022(6) | 0.0052* | 0.3 |
| | Rh-Rh | 5.1(2) | 2.676(2) | 0.0062(2) | |
| ORO | Rh-O | 6.0(1) | 2.030(3) | 0.0052* | 0.3 |

*: Fixed parameter, CN: coordination number, IAD: interatomic distance, D-WF: Debye-Waller factor.

***Figure 1.*** Comparison of the X-ray absorption data for $LaFe_{0.95}Rh_{0.05}O_3$ and $CaTi_{0.95}Rh_{0.05}O_3$, together with $Rh_2O_3$ and Rh powder as reference materials. XANES spectra were measured near the Rh K-edge for $LaFe_{0.95}Rh_{0.05}O_3$ (a) and $CaTi_{0.95}Rh_{0.05}O_3$ (c). The valence state of Rh changes reversibly in a redox cycle. The radial structure function around Rh was calculated as the magnitude of the Fourier transform (FT) of the $k^3$-weighted EXAFS oscillations for $LaFe_{0.95}Rh_{0.05}O_3$ (b) and $CaTi_{0.95}Rh_{0.05}O_3$ (d). The results of parameter fitting are shown in the tables. The parameters marked with * were fixed. The coordination number (CN) for Rh–O bonding should be six in the perovskite structure, and the decrease of this number after reduction indicates the separation of Rh from the structure.

 © 2006 Wiley-VCH Verlag GmbH & Co. KGaA, Weinheim 

structure parameter estimated by extended X-ray absorption fine structure (EXAFS) analysis is given in the tables in Figure 1.[5] All the Rh in $LaFe_{0.95}Rh_{0.05}O_3$ is present as a solid solution in perovskite after oxidation, and only 37% of the Rh becomes isolated as metallic nanoparticles even after reduction at 800°C. Moreover, it becomes clear that Rh forms an alloy with Fe. Replacement of the perovskite with $CaTiO_3$ decreases the Rh–O bonding and increases the Rh–Rh bonding after reduction (Figure 1d). In this case about 73% of the Rh is separated from the perovskite to form metallic Rh nanoparticles. The XANES spectrum at the Rh K-edge for reduced $CaTi_{0.95}Rh_{0.05}O_3$ shifts towards the energy for metallic Rh powder, thus implying that a greater proportion of Rh is in the metallic state (Figure 1c). The edge positions of Rh for oxidized and re-oxidized $CaTi_{0.95}Rh_{0.05}O_3$ are slightly higher than that of the trivalent Rh seen in $Rh_2O_3$.

To determine whether Rh and Pt form a solid solution with the perovskite structure or not an X-ray anomalous diffraction (XAD) study was carried out. Figure 2 shows the powder X-ray diffraction (XRD) pattern in the limited range of momentum transfer $Q$ for $CaTi_{0.95}Rh_{0.05}O_3$ and $CaTi_{0.95}Pt_{0.05}O_3$ after oxidation. Two Bragg reflections from the sample can be assigned to the pseudocubic cell of the perovskite structure. The structure factor for the (100) reflection can be expressed approximately in the form: $F(100) \propto |f_A - f_B - f_O|$, where $f_A$, $f_B$, and $f_O$ are the atomic scattering factors for the A-site, B-site, and oxygen atoms, respectively. The insets in Figure 2 represent the energy dependence of the (100) reflection intensity near the Rh K-edge and the Pt $L_{III}$-edge (11.562 keV), respectively. The dip of the X-ray intensity near the edge energy clearly indicates that both Rh and Pt occupy the B-site of the $CaTiO_3$-type perovskite structure since $|f_{Ca}|$ is always less than $|f_{Ti}|$ in this energy range.

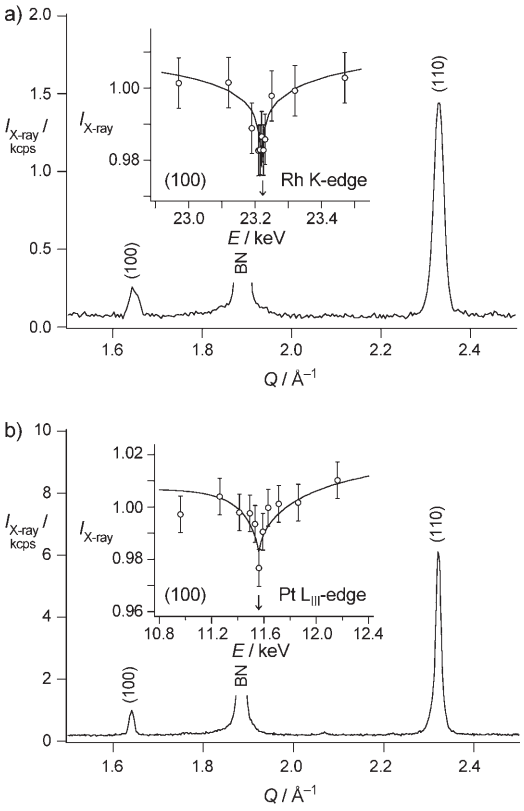


***Figure 2.*** X-ray powder diffraction patterns of $CaTi_{0.95}Rh_{0.05}O_3$ (a) and $CaTi_{0.95}Pt_{0.05}O_3$ (b) around the Bragg reflections (100) and (110) for the pseudocubic cell of the perovskite structure. The oxidized samples contain BN as a binder. The insets give the energy dependence of the (100) reflection intensity near the absorption edges for Rh and Pt, respectively.

The proportion of precious metal present in the perovskite lattice as a solid solution was calculated from the coordination number of the first nearest neighbor with oxygen (Pd–O, Rh–O, or Pt–O bonds) and is given in Figure 3 for various combinations of precious metals with perovskite-type oxides. Under oxidizing conditions, $LaFe_{0.95}Pd_{0.05}O_3$, $CaTi_{0.95}Rh_{0.05}O_3$, $SrTi_{0.95}Rh_{0.05}O_3$, $BaTi_{0.95}Rh_{0.05}O_3$, $CaTi_{0.95}Pt_{0.05}O_3$, and $CaZr_{0.95}Pt_{0.05}O_3$ form perfect solid solutions and show a large difference in the proportion of precious metal present in the perovskite lattice during the redox alternations. This difference is defined the self-regeneration ratio. The $A^{2+}B^{4+}O_3$ perovskites, with $CaTiO_3$, a natural mineral, as a component, have not been considered to have catalytic activity. However, we show in this study that various oxides, including an $A^{2+}B^{4+}O_3$ combination, can be used as catalyst materials, as can an $A^{3+}B^{3+}O_3$ perovskite.

The effect on the suppression of growth of Pt grains in an actual engine exhaust gas was investigated. $CaTi_{0.98}Pt_{0.02}O_3$ and Pd/$\gamma$-$Al_2O_3$ catalysts were exposed to engine exhaust gas at 900°C for 100 h. The Pt grains were then observed by TEM (Figure 4). The Pt grains on alumina grew to over 100 nm, whereas only fine metallic grains about 1–3 nm in diameter were found on the perovskite surface.

We have therefore demonstrated that a precious-metal-containing perovskite catalyst can function as an "intelligent" catalyst that regenerates itself to maintain a high activity in a cycle that involves a solid solution and segregation even in a harsh redox environment at high temperatures.[1] The following considerations are important when designing an intelligent catalyst: the oxide, which makes the perovskite component, should maintain a stable structure so that it can capture and release the precious metal at high temperatures under a redox environment. Under reducing conditions, the precious metal emerges from the oxide to form metallic clusters or nanoparticles that demonstrate a higher catalytic activity. At the same time, the perovskite oxide releases oxygen and retains its electroneutrality. This release of oxygen is detectable by a weight change.[6] Under oxidizing conditions, the precious metal and oxygen are reabsorbed into the perovskite oxide. The precious metal repeats the cycle of forming a solid solution and segregation as a result of the inherent cycling between an oxidizing and a reducing environment.

In conclusion, the precious metals Pd, Rh, and Pt can all be used in new self-regenerating catalysts that suppress the grain growth. Although perovskite-type oxides are very useful because of their structural stability and their abundance of combinations, the possibility of using other oxides with different crystal structures cannot be neglected. Moreover, a self-regenerating Pd-perovskite catalyst has been reported by

 © 2006 Wiley-VCH Verlag GmbH & Co. KGaA, Weinheim 

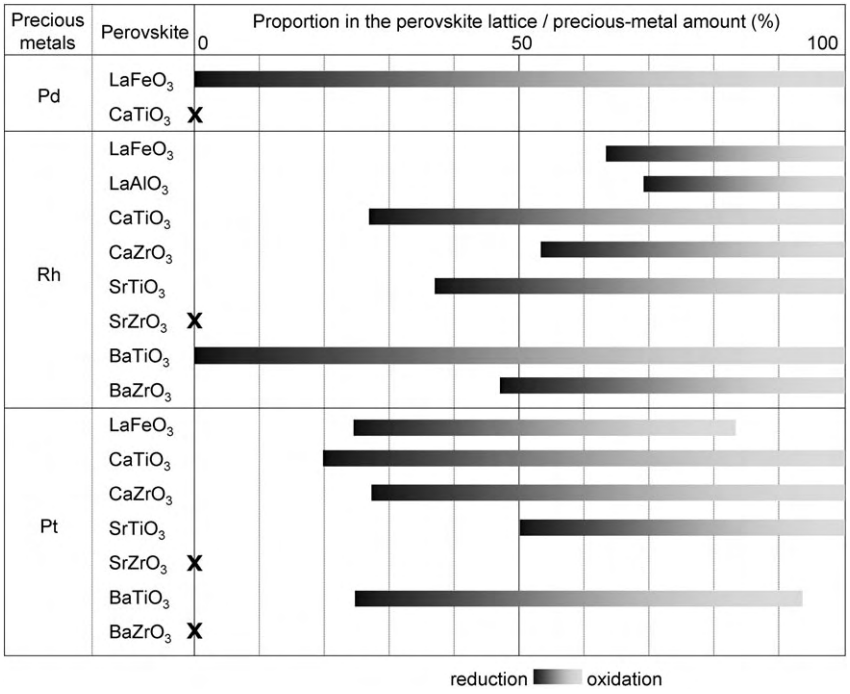


***Figure 3.*** Comparison of the solid solution of the precious metal for various perovskites. A longer bar indicates a better self-regeneration performance. **X** indicates that the precious metal does not form a solid solution with the perovskite.

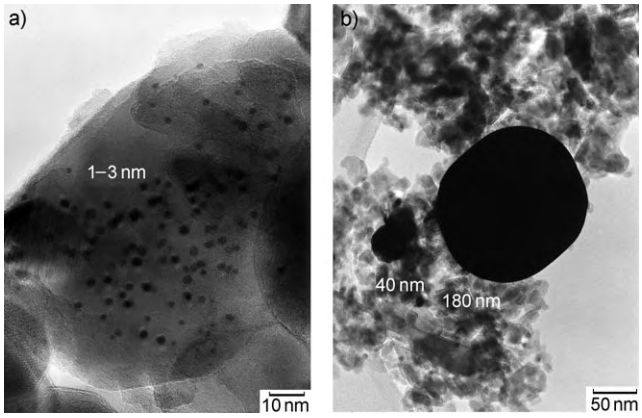


***Figure 4.*** TEM images of Pt grains of catalysts aged in engine exhaust at 900 °C for 100 h. $CaTi_{0.95}Pt_{0.05}O_3$ (a) was observed at a magnification of 400 000 and Pt/$\gamma$-$Al_2O_3$ (b) at a magnification of 100 000.

the group of Ley and Smith to show a high activity and a long life in organic synthesis reactions, such as the Suzuki coupling.[7] The application of this technology could be extended to diesel after-treatment and to pharmaceutical synthesis, and this technology may solve the socio-economic issues relating to the supply and demand of precious metals.

## Experimental Section

*Preparation of powder catalysts*: All the precious-metal-containing perovskite catalysts were prepared by the alkoxide method.[1] Metal ethoxyethylates $[M(OC_2H_4OC_2H_5)_3]$ (M = $La^{3+}$, $Fe^{3+}$, or $Al^{3+}$) or metal isopropoxides $[M^{x+}\{OCH(CH_3)_2\}_x]$ (M = $Ca^{2+}$, $Sr^{2+}$, $Ba^{2+}$, $Ti^{4+}$, or $Zr^{4+}$)} were dissolved in toluene. The precious-metal acetylacetonate $[M^{x+}(CH_3COCHCOCH_3)_x]$ (M = $Pd^{2+}$, $Rh^{3+}$, or $Pt^{2+}$) was also dissolved in toluene. The amount of each precious metal was adjusted to 5 atom% of that of the B-site element of the perovskite structure. Precipitates containing the precious metal were obtained upon hydrolysis with deionized water. The precursor was dried and then calcined at 800 °C for 2 h in air to obtain a perovskite powder catalyst containing homogeneously distributed precious metal. To prepare the conventional catalysts, powdered $\gamma$-$Al_2O_3$ (SSA = 120 $m^2g^{-1}$) was impregnated with dilute aqueous $Pd(NO_3)_2$, $Rh(NO_3)_3$, or $(NH_3)_2Pt(NO_2)_2$, dried, and calcined at 500 °C for 1 h in air.

*XAFS and XAD analyses*: The thermal treatment of the catalyst for X-ray measurements was carried out in three steps.[1] The powdered catalyst was sequentially oxidized (O) in air at 800 °C for 1 h, reduced (OR) in 2.5% $H_2$ and 7.5% CO balanced with $N_2$ at 800 °C for 1 h, and then re-oxidized (ORO) in air at 800 °C for 1 h. After each step the sample was cooled to room temperature under the same atmosphere to make sure that its state did not change, and then pressed into pellets. XAFS measurements were carried out in transmission mode at the BL01B1 beamline of the SPring-8 8 GeV synchrotron radiation source in Japan. EXAFS oscillations were analyzed with the standard procedure, using the FEFF code.[1] XAD measurements on $CaTi_{0.95}Rh_{0.05}O_3$ and $CaTi_{0.95}Pt_{0.05}O_3$ oxidized at 800 °C were carried out at the same beamline to determine the distribution of Rh and Pt in the perovskite crystal structure.

*Rapid ageing of monolithic catalysts*: $CaTi_{0.98}Pt_{0.02}O_3$ and Pt/$\gamma$-$Al_2O_3$ catalysts were coated on the inner wall of a monolithic honeycomb substrate (80 mm in diameter and 95 mm in length with a grid of 64 cells $cm^{-2}$) containing the same amounts of Pt (3.37 mg $cm^{-3}$).[1] The two monolithic catalysts were attached to each side-bank in the exhaust system of an automotive 4-L V8 engine for simultaneous ageing treatment. The monolithic catalysts were then exposed to high-temperature exhaust gas at 900 °C for 100 h by alternating a large redox fluctuating atmosphere ($\Delta\lambda = \pm 4\%$ at 0.6 Hz) around the stoichiometric point for 870 s and an oxidating atmosphere for 30 s. This ageing procedure is widely accepted as simulating a driving strategy that achieves high fuel economy by introducing fuel cut-off during deceleration.

Received: November 7, 2005
Revised: February 22, 2006
Published online: August 14, 2006

**Keywords:** green chemistry · heterogeneous catalysis · perovskites · platinum · rhodium

[1] Y. Nishihata, J. Mizuki, T. Akao, H. Tanaka, M. Uenishi, M. Kimura, T. Okamoto, N. Hamada, *Nature* **2002**, *418*, 164–167.
[2] H. Tanaka, I. Takahashi, M. Kimura, H. Sobukawa in *Science and Technology in Catalysts 1994* (Eds.: Y. Izumi, H. Arai, M. Iwamoto), Kodansya-Elsevier, Tokyo, **1995**, pp. 457–460; H. Tanaka, M. Uenishi, I. Tan, M. Kimura K. Dohmae, *Top. Catal.* **2001**, *16/17*, 63–70; H. Tanaka, M. Uenishi, I. Tan, M. Kimura, Y. Nishihata, J. Mizuki, *SAE Paper* (Society of Automotive Engineers, Inc., Warrendale, Pennsylvania) **2001**, *2001-01-1301*; H.

 © 2006 Wiley-VCH Verlag GmbH & Co. KGaA, Weinheim 

Tanaka, M. Taniguchi, N. Kajita, M. Uenishi, I. Tan, N. Sato, K. Narita, M. Kimura, *Top. Catal.* **2004**, *30/31*, 389 – 396.
[3] R. M. Hazen, *Sci. Am.* **1988**, *258*(6), 52 – 61; L. G. Tejuca, J. L. G. Fierro, J. M. D. Tascon in *Advances in Catalysis*, *Vol. 36* (Eds.: D. D. Eley, H. Pines, P. B. Weisz), Academic Press, San Diego, **1989**, pp. 237 – 328.
[4] D. B. Meadowcroft, *Nature* **1970**, *226*, 847 – 848; W. F. Libby, *Science* **1971**, *171*, 499 – 500; T. Nitadori, M. Misono, *J. Catal.* **1985**, *93*, 459 – 466.
[5] M. Newville, *J. Synchrotron Radiat.* **2001**, *8*, 322 – 324; J. J. Rehr, J. Mustre de Leon, S. I. Zabinsky, R. C. Albers, *J. Am. Chem. Soc.* **1991**, *113*, 5135 – 5140.
[6] M. Uenishi, H. Tanaka, M. Taniguchi, I. Tan, Y. Sakamoto, S.-i. Matsunaga, K. Yokota, T. Kobayashi, *Appl. Catal. A* **2005**, *296*, 114 – 119.
[7] M. D. Smith, A. F. Stepan, C. Ramarao, P. E. Brennan, S. V. Ley, *Chem. Commun.* **2003**, 2652 – 2653; S. P. Andrews, A. F. Stepan, H. Tanaka, S. V. Ley, M. D. Smith, *Adv. Synth. Catal.* **2005**, *347*, 647 – 654.

 © 2006 Wiley-VCH Verlag GmbH & Co. KGaA, Weinheim 

*Synthetic Methods*

DOI: 10.1002/anie.200601699

# $Pd(OAc)_2$-Catalyzed Coupling/Cyclization of 2,3-Allenoic Acids and Methyl Propiolate: Observation of Double 1,7-Hydrogen Shifts**

*Zhenhua Gu and Shengming Ma**

*Dedicated to Professor Xikui Jiang on the occasion of his 80th birthday*

Transition-metal-catalyzed reactions of allenes have received much attention from many synthetic organic chemists.[1–2] Both we and Hashmi et al. established the homo- or hetero-dimerization reaction of two functionalized allenes.[3] Recently, we paid attention to the coupling/cyclization reaction between allenes and alkynes.[4] Herein, we report a coupling/cyclization process between 2,3-allenoic acids and methyl propiolate, in which the π bond in some of the 1:2 addition products "migrated" through double 1,7-hydrogen migrations.

A mixture of 2,3-allenoic acid **1a** and methyl propiolate (**2**) in the presence of 5 mol% of $Pd(OAc)_2$ was stirred in $CCl_3Me$ at 35 °C for 12 h to afford (*E*)-**4a** in 10% yield and the cycloisomerization product **3a** in 40% yield (Table 1, entry 1). $MeCCl_3$ is better than other solvents, such as $CH_3COOH$, benzene, dimethylformamide (DMF), dimethyl sulfoxide (DMSO), $ClCH_2CH_2Cl$, and so forth (see the Supporting Information). When 1.0 equivalent of $BF_3{\cdot}Et_2O$ was added, the yield of **4a** was improved to 40%. Quite surprisingly, instead of the normal 1:2-product **6a**, we also detected the formation of the unexpected 1:2 adduct **5a** in 15% yield, as confirmed by NMR and IR spectroscopic and mass-spectrometric analysis (Table 1, entry 2). Compound **5a** may be considered to be the "π-bond migration" product of **6a**. $BF_3{\cdot}Et_2O$ (10 mol%) led to lower yields of **4a** and **5a** (Table 1, entry 3), and to our disappointment, simple increasing of the loading of **2** could not efficiently improve the yield of **5a**. Furthermore, we even observed the formation of the normal 1:3 adduct **7a** when 8.0 equivalents of **2** were applied (Table 1, entry 4). $PdCl_2$ was not an efficient catalyst (Table 1, entry 5), and when 1.0 equivalent of $[Sc(OTf)_3]$ (Tf = trifluoromethanesulfonyl) was used as the additive, the reaction could afford **5a** in 37% yield, with a 1:11 ratio of **4a**/**5a**, which was contaminated with **3a** in 51% yield (Table 1, entry 6). Unfortunately, 10 mol% of $[Sc(OTf)_3]$ could only afford **4a**

***Table 1:*** The coupling/cyclization reaction of 2,3-allenoic acid **1a** and methyl propiolate (**2**).

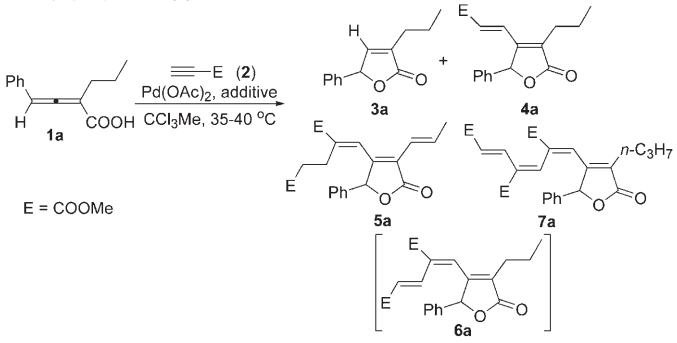


| Entry | Equivalents of **2** | Additive (mol%) | *t* [h] | Yield [%][a] | | | |
|---|---|---|---|---|---|---|---|
| | | | | **3a** | **4a** | **5a** | **7a** |
| 1[b] | 1.0 | – | 12 | 40 | 10 | – | – |
| 2 | 1.0 | $BF_3{\cdot}Et_2O$ (100) | 12 | 28 | 40 | 15 | – |
| 3 | 1.0 | $BF_3{\cdot}Et_2O$ (10) | 24 | 43 | 27 | 6 | – |
| 4 | 8.0 | $BF_3{\cdot}Et_2O$ (100) | 14 | 20 | 22 | 28 | 3 |
| 5[c] | 1.0 | $BF_3{\cdot}Et_2O$ (100) | 12 | 8 | 6 | 2 | – |
| 6 | 3.0 | $[Sc(OTf)_3]$ (100) | 18 | 51 | 3 | 37 | 5 |
| 7 | 3.0 | $[Sc(OTf)_3]$ (10) | 12 | 28 | 35 | 20 | – |
| 8 | 5.0 | $[Sc(OTf)_3] + BF_3{\cdot}Et_2O$[d] | 12 | 14 | 4 | 71 | – |

[a] Yields were determined by $^1H$ NMR spectroscopic analysis with $CH_2Br_2$ as the internal standard. [b] A yield of 14% for starting material **1a**, as determined by $^1H$ NMR spectroscopic analysis. [c] $PdCl_2$ was used as the catalyst, a yield of 67% for starting material **1a**, as determined by $^1H$ NMR spectroscopic analysis. [d] $[Sc(OTf)_3] = 30$ mol%, $BF_3{\cdot}Et_2O = 4.0$ equiv (for details of the procedure see the Experimental Section).

[*] Z. Gu, Prof. Dr. S. Ma
State Key Laboratory of Organometallic Chemistry
Shanghai Institute of Organic Chemistry
Chinese Academy of Sciences
354 Fenglin Lu, Shanghai 200032 (P.R. China)
Fax: (+86) 21-6416-7510
E-mail: masm@mail.sioc.ac.cn

[**] Financial support from the National Natural Science Foundation of China (20121202 and 20332060) and Shanghai Municipal Committee of Science and Technology is greatly appreciated. We thank Mr. Xuefeng Jiang for checking the results of entries 3 and 5 in Table 1 and Scheme 4.

Supporting information for this article is available on the WWW under http://www.angewandte.org or from the author.


InterScience
© 2006 Wiley-VCH Verlag GmbH & Co. KGaA, Weinheim

and **5a** in 35 and 20% yield, respectively (Table 1, entry 7). It was reported that the Lewis acid coordinates preferentially with the methyl acrylate derivatives rather than **2**;[5] thus, an excess amount of $BF_3{\cdot}Et_2O$ was added to release $[Sc(OTf)_3]$ from the products. Further studies showed that when a mixture of **1a** and 2.0 equivalents of **2** was added by a syringe pump to a mixture of 3.0 equivalents of **2**, 30 mol% of $[Sc(OTf)_3]$, 4.0 equivalents of $BF_3{\cdot}Et_2O$, and 5 mol% $Pd(OAc)_2$ in 1.0 mL of $Cl_3CMe$, **5a** was formed in 71% yield, as shown by NMR spectroscopic analysis with **5a**/**4a** = 16:1 (Table 1, entry 8).

We next tested the generality of this type of "π-bond migration" reaction: This transformation is general when the α-substitutent of 2,3-allenoic acids is either an *n*-propyl, *n*-butyl, or *n*-pentyl group (Table 2, entries 1–3, 4–7, and 8, respectively). The reaction afforded **5** in moderate yields with **4**/**5** = 1:9–1:16 when the $R^2$ function is either a phenyl, 4-halophenyl, 1′-naphthyl, or methyl group. It should be noted that the two noncyclic C–C double bonds are exclusively in the *E* form.

There are three significant issues within this transformation: 1) Is **6a** the precursor of **5a**? If yes, is the metal necessary for this transformation? 2) Where did the two hydrogen atoms of the propyl group of **1a** go? 3) Where did the three hydrogen atoms in **5a** (two at the 4′-position and one at the 3′-position) come from? In fact, when R = Me, we obtained the normal 1:2 adduct **6i** as expected. It is noteworthy that the normal adduct **6j** was formed as the major product even when R = Et; the "π-bond migration" adduct, if any, was formed in less than 5% yield (Scheme 1). The structures of **4** and **5** were further established by X-ray diffraction studies of **4i** and **5c**.[6]

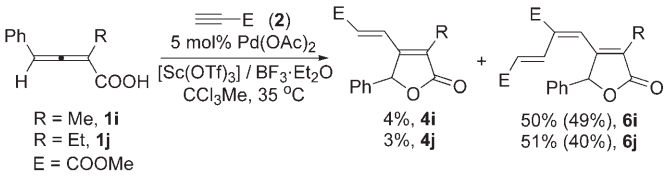


***Scheme 1.*** The reaction of **1i** and **1j** with propiolate. The yields were determined by $^1H$ NMR spectroscopic analysis with $CH_2Br_2$ as the internal standard. The yields of the isolated products are given in parenthesis.

Although we failed to obtain the pure product **6a**, we isolated a mixture of **5a** and **6a** in a ratio of 1:1.27 when the reaction was conducted at 12°C for 5 h. Quite interestingly, it was observed that **6a** can be converted into **5a** in $CDCl_3$ at 25°C in the absence of any metallic catalyst. Nevertheless, complete conversion could not be achieved even at a higher temperature or over a longer reaction time (Figure 1). These results indicate that **6** may be the precursor of **5**.

The deuterium incorporation in $[D_1]$**4a** and $[D_1]$**5a** was approximately 72 and 68%, respectively, when $[D_1]$**1a** was used as the substrate to react with **2** in $Cl_3CMe/CD_3CO_2D$ (10:1). It should be noted that the deuterium atom in $[D_1]$**5a** is at the 4′-position (Scheme 2). On the contrary, when $[D_2]$**1a** was treated with **2**, one of the deuterium atoms was completely transferred to the 3′-position in product $[D_2]$**5a**. These experimental findings reveal that one of the hydrogen atoms at the 4′-position comes from the acidic environment whereas one of the two hydrogen atoms at the 3′-position comes from the 2-position of the propyl group (Scheme 3).

In addition, it should be noted that under similar conditions with **1k** 8% of the normal 1:2 adduct **6k** remained even after stirring at 35°C for 69 h (Scheme 4).

Based on these experimental results, we proposed the following mechanism: the cyclic oxypalladation of $PdX_2$ with $[D_2]$**1a** would form the intermediate **8**.[7] The subsequent stereoselective *cis* carbopalladation of **8** with the C–C triple bond of **2** would form intermediate **9**, which may afford $[D_2]$**4a** through protonolysis, while regenerating the $Pd^{II}$ catalyst.[4a,8] The *cis* carbopalladation of **9** with the second molecule of **2** would form intermediate **10**. The subsequent protonolysis of **10** may form *Z*,*E*,*E*-triene $[D_2]$**6a**. The thermal antarafacial 1,7-hydrogen migration of *Z*,*E*,*E*-triene $[D_2]$**6a** would form the intermediate *E*,*E*,*E*-triene **11**, which may afford $[D_2]$**5a** through the second 1,7-hydrogen migration (Scheme 5).[9–11]

***Table 2:*** The coupling/cyclization reaction of **1** with methyl propiolate (**2**).[a]

| Entry | Substrate **1** | Products **4** | **5** | **4**/**5** | Yield of **5** [%][b] |
|---|---|---|---|---|---|
| | 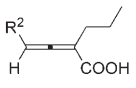 | 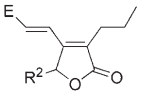 | 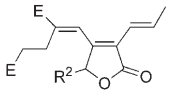 | | |
| 1 | $R^2$ = Ph **1a** | **4a** | **5a** | 1:16 | 71 (54) |
| 2 | $R^2$ = 4-Br-$C_6H_4$ **1b** | **4b** | **5b** | 1:11 | 75 (53) |
| 3[c] | $R^2$ = 1′-naphthyl **1c** | **4c** | **5c** | 1:9 | 52 (45) |
| | 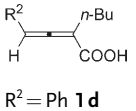 | 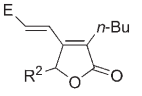 | 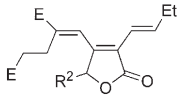 | | |
| 4 | $R^2$ = Ph **1d** | **4d** | **5d** | 1:10 | 65 (47) |
| 5 | $R^2$ = 4-Br-$C_6H_4$ **1e** | **4e** | **5e** | 1:12 | 71 (51) |
| 6 | $R^2$ = 4-Cl-$C_6H_4$ **1f** | **4f** | **5f** | 1:14 | 70 (60) |
| 7[d] | $R^2$ = Me **1g** | **4g** | **5g** | 1:9 | 58 (44) |
| | 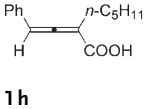 | 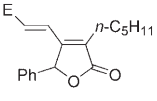 | 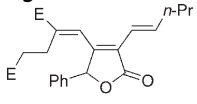 | | |
| 8 | **1h** | **4h** | **5h** | 1:11 | 64 |

[a] The reaction was carried out using 0.25 mmol of **1**, 5.0 equivalents of **2**, 5 mol% of $Pd(OAc)_2$, 30 mol% of $[Sc(OTf)_3]$, and 4.0 equivalents of $BF_3{\cdot}Et_2O$ in $Cl_3CMe$ (2.2 mL) (see the Experimental Section for details of the procedure). [b] Yields were determined by $^1H$ NMR spectroscopic analysis with $CH_2Br_2$ as the internal standard; yields of the isolated products are given in parenthesis. [c] An approximate 9% yield of 1:3 adduct **7c** was detected by $^1H$ NMR spectroscopic analysis. [d] [**2**] = 7.0 equiv.

 © 2006 Wiley-VCH Verlag GmbH & Co. KGaA, Weinheim 

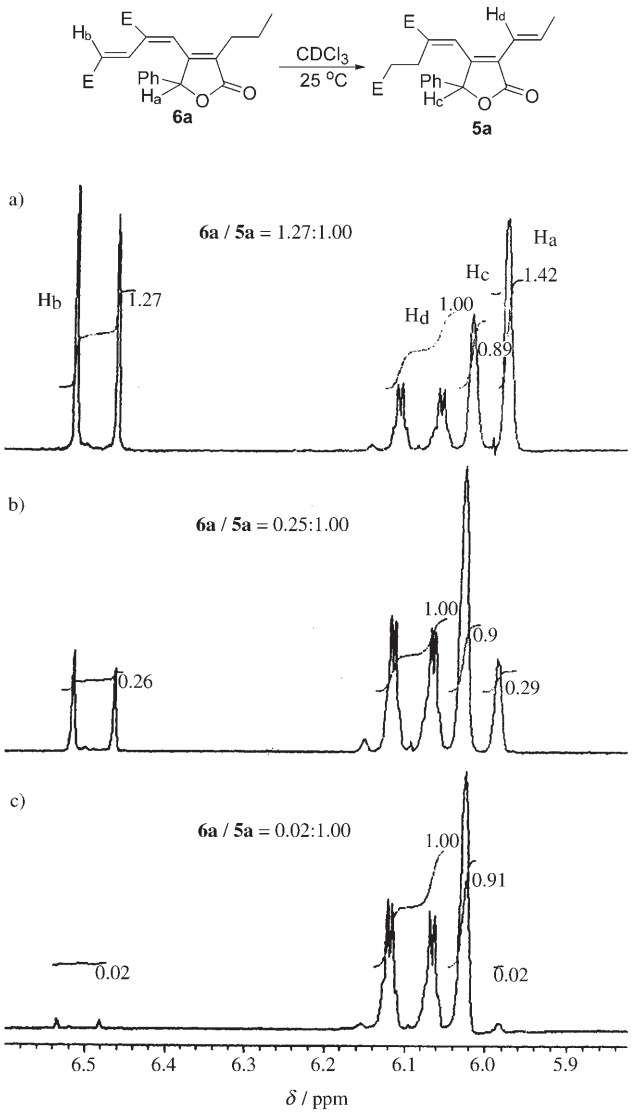


***Figure 1.*** The $^1$H NMR (300 MHz) spectra of the mixture of **5a** and **6a** in $CDCl_3$ at 25 °C. $^1$H NMR spectra of the reaction mixture obtained a) immediately after isolation, b) after 6 h, and c) after 27 h.

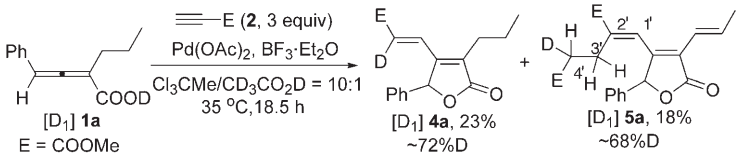


***Scheme 2.*** The reaction of [$D_1$]**1a** with **2**.

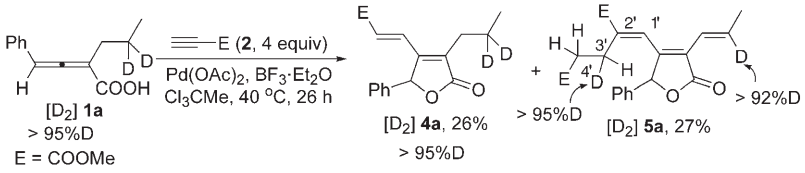


***Scheme 3.*** The reaction of [$D_2$]**1a** with **2**.

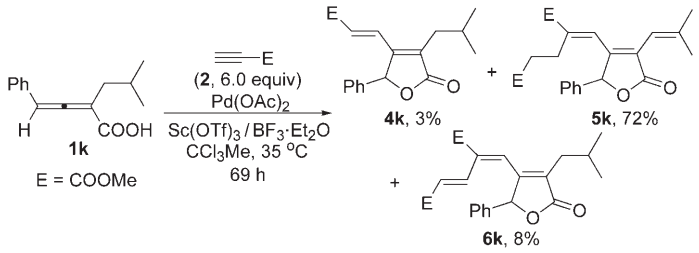


***Scheme 4.*** The reaction of **1k** with **2**. The yields were determined by $^1$H NMR spectroscopic analysis with $CH_2Br_2$ as the internal standard.

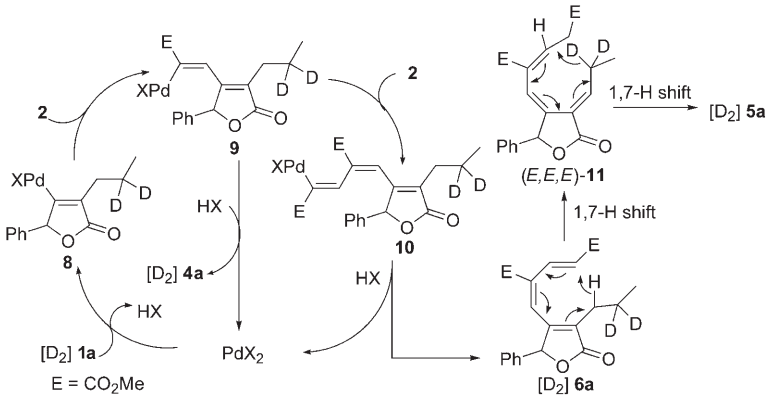


***Scheme 5.*** A plausible catalytic cycle.

In conclusion, we have developed a $Pd(OAc)_2$-catalyzed coupling/cyclization reaction of 2,3-allenoic acids with methyl propiolate in the presence of $[Sc(OTf)_3]/BF_3{\cdot}Et_2O$. In this transformation, we observed the "π-bond migration" in some of the products, which may proceed through double 1,7-hydrogen migrations. Further studies in this area are being pursued in our laboratory.

## Experimental Section

Typical experimental procedure for the coupling cyclization of 2,3-allenoic acids **1** with methyl propiolate (**2**): A solution of **1a** (50 mg, 0.248 mmol) and **2** (42 mg, 0.50 mmol) in $Cl_3CMe$ (1.2 mL) was added by a syringe pump (0.06 mL $h^{-1}$) to a mixture of **2** (63 mg, 0.75 mmol), $[Sc(OTf)_3]$ (37 mg, 0.075 mmol), $BF_3{\cdot}Et_2O$ (124 μL, 1.00 mmol, 4.0 equiv), and $Pd(OAc)_2$ (3 mg, 0.0134 mmol) in $Cl_3CMe$ (1.0 mL) at 40 °C with stirring. After the addition, the reaction mixture was stirred at 40 °C for 13 h. After complete consumption of the starting material, as determined by TLC, the reaction mixture was filtered through a short column of silica gel, evaporated, and analyzed by $^1$H NMR spectroscopic analysis with $CH_2Br_2$ (9 μL, 0.129 mmol) as the internal standard. The ratio of **4a**/**5a** = 1:16, the yield of **5a** as determined by NMR spectroscopy was 71%. The residue was purified by flash chromatography on silica gel (eluent: petroleum ether/ethyl acetate (10:1)) to afford **5a** as a liquid (49 mg, 54%) and **4a** as a solid. **4a**: M.p. 97–99 °C (ethyl acetate/petroleum ether); $^1$H NMR (300 MHz, $CDCl_3$): $\delta$ = 7.52 (d, $J$ = 15.9 Hz, 1H), 7.43–7.33 (m, 3H), 7.30–7.18 (m, 2H), 5.93 (s, 1H), 5.82 (d, $J$ = 15.9 Hz, 1H), 3.72 (s, 3H), 2.55 (t, $J$ = 7.5 Hz, 2H), 1.78–1.62 (m, 2H), 1.02 ppm (t, $J$ = 7.5 Hz, 3H); $^{13}$C NMR (75.4 MHz, $CDCl_3$): $\delta$ = 13.9, 21.9, 26.0, 52.1, 82.4, 125.6, 127.7, 129.2, 129.8, 131.9, 134.8, 135.9, 151.7, 165.8,

 © 2006 Wiley-VCH Verlag GmbH & Co. KGaA, Weinheim 

172.7; MS(EI): *m/z* 286 ($M^+$, 5.20), 181 (100); IR (KBr): $\tilde{\nu}$ = 1759, 1724, 1614, 1313, 1204, 1169, 1003 $cm^{-1}$; elemental analysis (%) calcd for $C_{17}H_{18}O_4$: C 71.31, H 6.34; found: C 71.24, H 6.36. **5a**: oil; $^1H$ NMR (300 MHz, $CDCl_3$): $\delta$ = 7.45–7.33 (m, 3H), 7.28–7.10 (m, 4H), 6.11 (d, $J$ = 15.6 Hz, 1H), 6.05 (s, 1H), 3.77 (s, 3H), 3.64 (s, 3H), 2.51 (t, $J$ = 7.5 Hz, 2H), 2.09 (t, $J$ = 7.5 Hz, 2H), 1.93 ppm (d, $J$ = 6.6 Hz, 3H); $^{13}C$ NMR (75.4 MHz, $CDCl_3$): $\delta$ = 19.6, 24.4, 32.3, 51.6, 52.4, 82.7, 118.9, 126.3, 127.2, 129.06, 129.10, 129.6, 134.6, 136.6, 136.9, 151.1, 166.5, 171.0, 172.5 ppm; MS(EI): *m/z* 370 ($M^+$, 10.61), 105 (100); IR (neat): $\tilde{\nu}$ = 1761, 1736, 1718, 1437, 1257, 1197, 1103 $cm^{-1}$; HRMS (MALDI/DHB) calcd for $C_{21}H_{22}O_6Na$: [$M^+$+Na] 393.1309; found: 393.1312.

Received: April 29, 2006
Published online: August 9, 2006

**Keywords:** allenes · cyclization · lactones · palladium · propiolates

[1] For books, see: a) *The Chemistry of the Allenes*, *Vol. 1* (Eds.: S. R. Landor), Academic Press, London, **1982**; b) *Modern Allene Chemistry*, *Vols. 1–2* (Eds.: N. Krause, A. S. K. Hashmi), Wiley-VCH, Weinheim, **2004**; c) H. F. Schuster, G. M. Coppola, *Allenes in Organic Synthesis*, Wiley, New York, **1984**; d) *The Chemistry of Ketenes, Allenes, and Related Compounds* (Ed.: S. Patai), Wiley, New York, **1980**, Part 1.

[2] For some of the most recent reviews, see: a) R. Zimmer, C. U. Dinesh, E. Nandanan, F. A. Khan, *Chem. Rev.* **2000**, *100*, 3067; b) A. Hoffmann-Röder, N. Krause, *Angew. Chem.* **2004**, *116*, 1216; *Angew. Chem. Int. Ed.* **2004**, *43*, 1196; c) H.-U. Reissig, W. Schade, M. Okala-Amombo, R. Pulz, A. Hausherr, *Pure Appl. Chem.* **2002**, *74*, 175; d) S. Ma, *Chem. Rev.* **2005**, *105*, 2829.

[3] a) A. S. K. Hashmi, *Angew. Chem.* **1995**, *107*, 1749; *Angew. Chem. Int. Ed. Engl.* **1995**, *34*, 1581; b) A. S. K. Hashmi, T. L. Ruppert, T. Knöfel, J. W. Bats, *J. Org. Chem.* **1997**, *62*, 7295; c) A. S. K. Hashmi, L. Schwarz, J.-H. Choi, T. M. Frost, *Angew. Chem.* **2000**, *112*, 2382; *Angew. Chem. Int. Ed.* **2000**, *39*, 2285; d) S. Ma, Z. Yu, *Angew. Chem.* **2002**, *114*, 1853; *Angew. Chem. Int. Ed.* **2002**, *41*, 1775; e) S. Ma, Z. Gu, Z. Yu, *J. Org. Chem.* **2005**, *70*, 6291.

[4] For carbometalation of electron-deficient alkynes, see: a) C. Jia, W. Lu, J. Oyamada, T. Kitamura, K. Matsuda, M. Irie, Y. Fujiwara *J. Am. Chem. Soc.* **2000**, *122*, 7252; b) Z. Shi, C. He, *J. Org. Chem.* **2004**, *69*, 3669; c) M. T. Reetz, K. Sommer, *Eur. J. Org. Chem.* **2003**, 3485.

[5] B. B. Snider, D. J. Rodini, R. S. E. Conn, S. Sealfon, *J. Am. Chem. Soc.* **1979**, *101*, 5283.

[6] See the Supporting Information for the crystal data and ORTEP representations of **4i** and **5c**. CCDC 295216 and 295217 (**4i** and **5c**, respectively) contain the supplementary crystallographic data for this paper. These data can be obtained free of charge from The Cambridge Crystallographic Data Centre via www.ccdc.cam.ac.uk/data_request/cif.

[7] a) Y. Tamaru, H. Higashimura, K. Naka, M. Hojo, Z. Yoshida, *Angew. Chem.* **1985**, *97*, 1070; *Angew. Chem. Int. Ed. Engl.* **1985**, *24*, 1045; b) R. D. Walkup, M. D. Mosher, *Tetrahedron Lett.* **1994**, *35*, 8545; c) K. Imi, K. Imai, K. Utimoto, *Tetrahedron Lett.* **1987**, *28*, 3127; d) T. Wakabayashi, Y. Ishii, K. Ishikawa, M. Hidai, *Angew. Chem.* **1996**, *108*, 2268; *Angew. Chem. Int. Ed. Engl.* **1996**, *35*, 2123; e) S. Ma, *Acc. Chem. Res.* **2003**, *36*, 701, and references therein.

[8] a) Z. Wang, X. Lu, *Chem. Commun.* **1996**, 52; b) Z. Wang, Z. Zhang, X. Lu, *Organometallics* **2000**, *19*, 775.

[9] For the stereochemistry of the thermal antarafacial [1,7]-hydrogen migration, see: a) C. A. Hoeger, W. H. Okamura, *J. Am. Chem. Soc.* **1985**, *107*, 268; b) B. A. Hess, Jr., *J. Org. Chem.* **2001**, *66*, 5897.

[10] a) I. D. Gridnev, M. E. Gurskii, A. V. Ignatenko, Y. N. Bubnov, Y. V. Il'ichev, *Organometallics* **1993**, *12*, 2487; b) W. H. Okamura, H. Y. Elnagar, M. Ruther, S. Dobreff, *J. Org. Chem.* **1993**, *58*, 600; for molecular orbital (MO) calculations, see: B. A. Hess, Jr., L. J. Schaad, J. Panŏir, *J. Am. Chem. Soc.* **1985**, *107*, 149.

[11] T. L. Gilchrist, R. C. Storr, *Organic Reactions and Orbital Symmetry*, Cambridge University Press, Cambridge, UK, **1972**.

 © 2006 Wiley-VCH Verlag GmbH & Co. KGaA, Weinheim 

*Hydrogen Storage*

DOI: 10.1002/anie.200601434

# Storing and Releasing Hydrogen with a Redox Switch**

*Simon K. Brayshaw, Jennifer C. Green, Nilay Hazari, J. Scott McIndoe, Frank Marken, Paul R. Raithby, and Andrew S. Weller**

Hydrogen storage is an area of intense current interest, which is driven by the requirements for reversible storage of dihydrogen for future energy applications.[1] Chemisorption of dihydrogen in the form of light metal hydrides is one approach to the problem of storing large amounts of $H_2$ reversibly.[2] Physisorption of dihydrogen onto porous network materials such as activated carbon, metal–organic framework (MOF) materials,[3] or related systems[4,5] presents an alternative method, and MOF systems that incorporate open metal sites (such as $Ni^{2+}$, $Cu^{2+}$, and $Mg^{2+}$)[5–8] have recently attracted attention because of the stronger binding of $H_2$ with the metal–ligand framework.[8] Although significant and elegant advances have been made in both areas,

[*] Dr. S. K. Brayshaw, Dr. F. Marken, Prof. P. R. Raithby, Dr. A. S. Weller
Department of Chemistry
University of Bath
Bath, BA2 7AY (UK)
Fax: (+44) 1225-386-231
E-mail: a.s.weller@bath.ac.uk

Prof. J. C. Green, N. Hazari
Inorganic Chemistry Laboratory
South Parks Road, Oxford OX1 3QR (UK)

Prof. J. S. McIndoe
Department of Chemistry
University of Victoria
PO Box 3065, Victoria, BC V8W3V6 (Canada)

[**] We thank the EPSRC (grant GR/T10169), the Royal Society, and the Rhodes Trust for support, Dr Damien Murphy (Cardiff University) for providing the EPR spectra, and the Oxford Supercomputing Centre for computational facilities.

Supporting information for this article is available on the WWW under http://www.angewandte.org or from the author.


© 2006 Wiley-VCH Verlag GmbH & Co. KGaA, Weinheim

challenges still remain. Metal hydrides require temperature cycling to promote loss of hydrogen, as hydrogen is chemisorbed (binding energies greater than 100 kJ mol$^{-1}$). Although porous networks show reversible $H_2$ uptake without temperature cycling, they generally require an overpressure to retain $H_2$, because reducing the partial pressure results in loss of $H_2$ (i.e., there is no hysteresis between the absorption and desorption isotherms); this is because dihydrogen is physisorbed[9] (binding energies less than 10 kJ mol$^{-1}$). Although these MOF materials can uptake $H_2$ very well at 77 K,[7,10] adsorption drops dramatically (less than 0.3%) at ambient temperature. MOF systems that show hysteresis have been described recently. These materials retain $H_2$ at reduced pressure (ca. 0.01 atm); however, they only operate at 77 K.[11] In view of the current state of this research, a material that is both a true store of hydrogen under ambient conditions of temperature and pressure and that releases the stored $H_2$ without significant external energy input would be of fundamental interest.

We report herein what we believe to be a novel mechanism for hydrogen storage and subsequent release. The system consists of molecular clusters in which $H_2$ is adsorbed at binding energies intermediate between the accepted limits for chemi- and physisorption. These clusters retain the stored dihydrogen even at low pressure, which makes them genuine hydrogen stores, but they can release $H_2$ rapidly (on the millisecond timescale) when triggered by a simple redox process. Moreover, these processes occur under the attractive conditions of 298 K and 1 atm $H_2$ and can be triggered either chemically or electrochemically. Although cluster species with hydride ligands are common,[12–17] the reversible uptake and release of $H_2$ on molecular clusters is rare and examples have generally required relatively forcing conditions (vacuum, heat, photolysis, or addition of an external hydrogen acceptor) to release the stored $H_2$.[18–20]

We recently reported the synthesis of a new class of rhodium clusters, exemplified by $[Rh_6(PCy_3)_6H_{12}][BAr^F{}_4]_2$ (**A**) ($[BAr^F{}_4] = [B\{C_6H_3(CF_3)_2\}_4]^-$; Cy = cyclohexyl), which have molecular geometries that feature an octahedral hexarhodium core and a trialkyl phosphine ligand radiating from each metal vertex,[19,21,22] thus shrouding the metal core with a hydrocarbon shell. These dicationic clusters are completed by twelve hydrogen atoms that bridge each Rh–Rh edge in the octahedron. Calculations[21] show that there is only a modest energy gap (0.3 eV) between the highest occupied molecular orbital (HOMO) and a degenerate set of two low-lying unoccupied molecular orbitals (LUMOs, Figure 1). Thus, these clusters are predisposed to receive four extra electrons. We have shown that these electrons can come from two $H_2$ molecules (i.e. two bonding electron pairs) and that the addition of $H_2$ to **A** affords the 16-hydrogen-atom cluster $[Rh_6(PCy_3)_6H_{16}][BAr^F{}_4]_2$ (**B**), in which the HOMO–LUMO energy gap is much larger (1.3 eV). The uptake of two molecules of $H_2$ is facile (both in the solution and the solid state) and can be reversed by placing **B** under a dynamic vacuum (ca. $6\times10^{-6}$ atm, $t_{1/2} = 48$ h). Under ambient conditions (1 atm argon, 298 K), cluster **B** retains the two absorbed $H_2$ molecules for weeks with no partial pressure of $H_2$.[21]

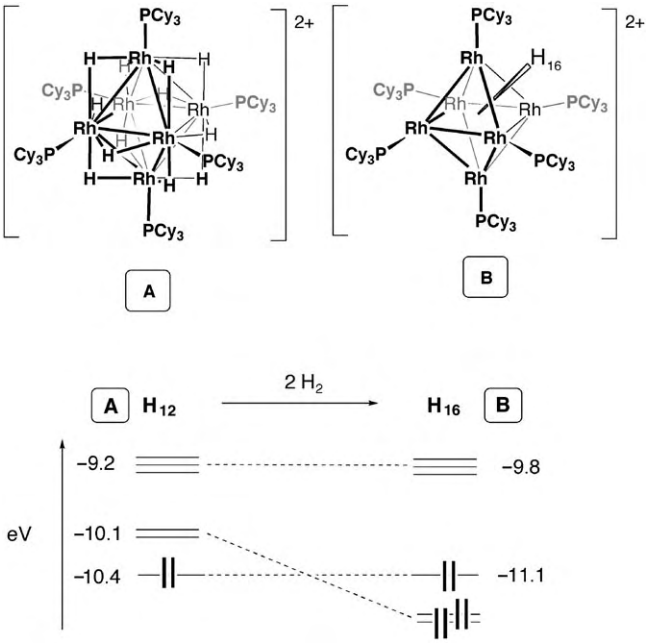


***Figure 1.*** Frontier molecular orbital energy diagram for **A** and **B**.

Inspection of the MO diagram for **B** suggests that the addition of one electron would result in the population of a high-lying orbital and that this could destabilize the cluster, which would result in $H_2$ loss to reestablish a large HOMO–LUMO gap. Exactly this process does in fact occur, and it can be readily followed chemically and electrochemically by using standard spectroscopic and electrochemical techniques. On a preparative scale the addition of the reducing agent $[Cr(\eta^6\text{-}C_6H_6)_2]$ ($E_{1/2} = -1.15$ V relative to ferrocene/ferrocenium) to a solution of **B** in $CH_2Cl_2$ results in a paramagnetic species that we have unequivocally characterized as $[Rh_6(PCy_3)_6H_{14}][BAr^F{}_4]$ (**C**) by following the reaction with electrospray ionisation mass spectrometry (ESI-MS). These spectra show the clean formation of **C**, a monocation with fourteen hydrides associated with a $\{Rh_6(PCy_3)_6\}$ core (Figure 2). As might be expected, $^1$H NMR spectroscopy of paramagnetic **C** is relatively uninformative and the hydride signals are not observed. However, H/D exchange experiments using $D_2$ show the formation of $HD_{(g)}$ and $H_{2(g)}$, which is consistent with accessible dihydrogen ligands on the cluster surface,[23] as are theoretical calculations (see below). Attempts to isolate **C** in pure form on a preparative scale by repeated recrystallization to remove the reductant always led to the loss of $H_2$ and isolation of the twelve-hydride monocationic cluster $[Rh_6(PCy_3)_6H_{12}][BAr^F{}_4]$ (**D**). The "uncharged-with-$H_2$" starting material **A** is simply returned by oxidation of **C** with $[Fe(\eta^5\text{-}C_5H_5)_2][PF_6]$ ($E_{1/2} = 0.00$ V), as monitored by NMR spectroscopy and ESI-MS. Oxidation of **C** thus results in the elimination of a further equivalent of $H_2$, and a complete hydrogen store and release cycle is completed in solution for two molecules of $H_2$ per cluster by a simple redox process.

This redox-triggered release of $H_2$ can also be followed electrochemically. Figure 3 shows the cyclic voltammogram of **B** (in $CH_2Cl_2$, $[NBu_4][BAr^F{}_4]$ electrolyte, glassy carbon

 © 2006 Wiley-VCH Verlag GmbH & Co. KGaA, Weinheim 

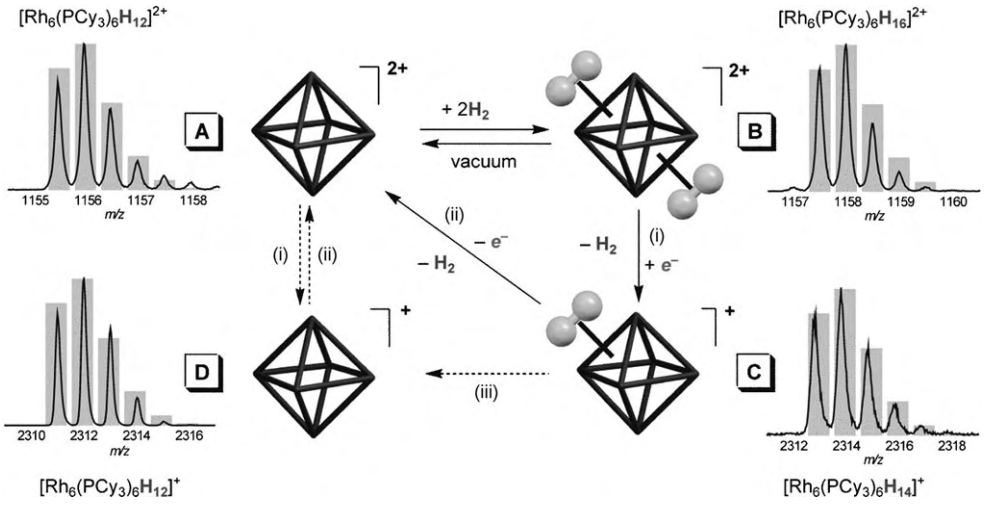


***Figure 2.*** Redox triggered hydrogen storage/release cycle. i) $[Cr(\eta^6\text{-}C_6H_6)_2]$; ii) $[Fe(\eta^5\text{-}C_5H_5)_2][PF_6]$; iii) $-H_2$, glassy carbon electrode. Insets show ESI-MS data (positive-ion mode) of cluster species for each step with the observed isotope pattern overlaid with that predicted (gray bars). See the Supporting Information for full spectra.

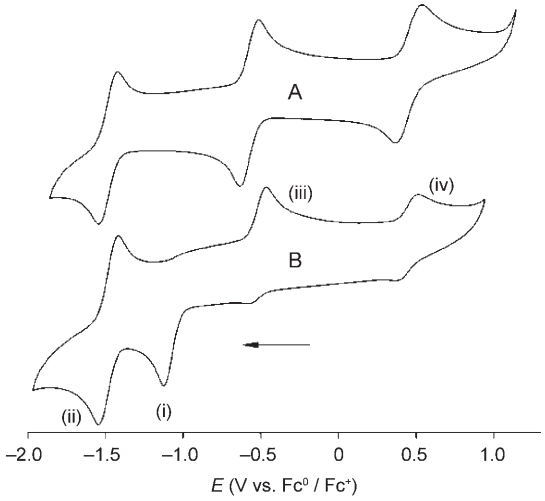


***Figure 3.*** Top: Cyclic voltammogram of $[Rh_6(PCy_3)_6H_{12}]^{2+}$ (**A**) (which is also identical to those of **C** and **D**) showing the three electrochemical processes (two reversible reductions and one quasireversible oxidation). Bottom: Cyclic voltammogram of **B** showing the irreversible reduction (i) and subsequent electrochemistry associated with **A** (ii–iv). See the Supporting Information for full experimental details.

electrode, sweep rate $100\,mV\,s^{-1}$). Cluster **B** undergoes an irreversible one-electron reduction at $E_{1/2} = -1.00$ V, relative to ferrocene/ferrocenium, which is consistent with the irreversible elimination of $H_2$. By progressively increasing the scan rate to $10\,V\,s^{-1}$ and observing the back oxidation, a half-life for the unstable reduced species of 170 ms ($k = 4\,s^{-}$ at 293 K) was obtained. There are also three reversible one-electron processes at $E_{1/2} = -1.51$, $-0.59$, and $+0.44$ V, which are also observed for **A**[24] and **D**, the latter related to **C** by the simple loss of one $H_2$ molecule. Presumably under electrochemical conditions, **C** undergoes facile loss of $H_2$ to form **D**, and this suggestion is supported by the small calculated energy difference between these two species (0.12 eV, see below) and our observation that $H_2$ is slowly lost from **C** in bulk solution. Cluster **D** can be formed independently in excellent yield by chemical reduction of **A** with $[Cr(\eta^6\text{-}C_6H_6)_2]$ (see the Supporting Information for full characterization, including the X-ray crystal structure). Overall, the electrochemical behavior of **B** can be summarized as the irreversible loss of two molecules of $H_2$ upon reduction at the carbon electrode to give **D**, which is directly related to the starting cluster **A** by simple oxidation. Although there is a subtle change in the order of events between the bulk chemical and electrochemical processes, the overall redox hydrogen storage/release cycle holds for both: the reduction of **B** and subsequent reoxidation to afford **A** is effectively quantitative, repeatable, and involves two equivalents of $H_2$ per cluster per cycle.

Full geometry optimizations and calculations of the relative Gibbs free energies were performed using density functional theory (DFT) (see the Supporting Information for details) on the model system $[Rh_6(PH_3)_6H_x]^{n+}$ ($x = 12, 14, 16$; $n = 1, 2$). The relative energies of the possible intermediates in this cycle (Gibbs free energy at 298.15 K, taking into account solvent effects ($CH_2Cl_2$), zero-point energy, and entropy) are shown in Figure 4. The addition of two molecules of $H_2$ to $[H_{12}]^{2+}$ (**A**) to give $[H_{16}]^{2+}$ (**B**) is an overall exothermic process, which is consistent with the experimentally observed formation of **B** on exposure to $H_2$ (the "charged-with-$H_2$"

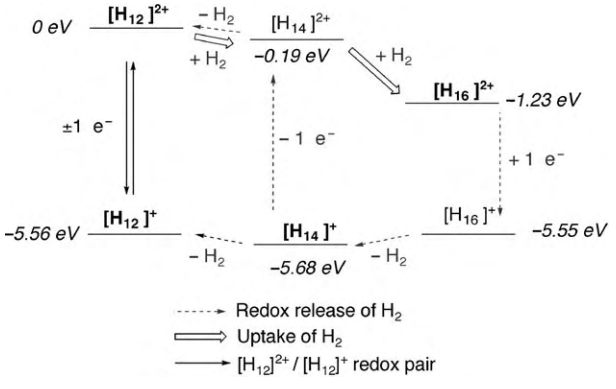


***Figure 4.*** Calculated energies (eV) relative to **A** ($[H_{12}]^{2+}$) for the cluster hydride species in the storage/release cycle. Molecular species in bold face were observed spectroscopically and in some cases [**A**, **B**,[21] and **D** (this work)] determined by X-ray diffraction. Energies quoted take into account the Gibbs free energy of gaseous $H_2$ where appropriate. $PCy_3$ was replaced by $PH_3$ in the model systems.

 © 2006 Wiley-VCH Verlag GmbH & Co. KGaA, Weinheim 

state). A reasonable supposition is that this proceeds via an intermediate dicationic species with fourteen hydrides, namely $[Rh_6(PH_3)_6H_{14}]^{2+}$ ($[H_{14}]^{2+}$). The average interaction energy of the two extra $H_2$ molecules with the cluster was determined to be 0.62 eV (60 kJ mol$^{-1}$) per dihydrogen. This is comparable with the binding energy both calculated and experimentally determined for dihydrogen bound to a single metal center (60–100 kJ mol$^{-1}$),[23] and DFT calculations and H/D exchange experiments both strongly suggest two dihydrogen ligands on the cluster surface of this sixteen-hydride species.[21] Addition of one electron to $[H_{16}]^{2+}$ results in $[Rh_6(P(PH_3)_3)_6H_{16}]^{+}$ ($[H_{16}]^{+}$), which is unstable towards $H_2$ loss to afford $[H_{14}]^{+}$ and $H_2$. The calculated structure of $[H_{14}]^{+}$ reveals a relatively close H–H contact on the cluster surface (1.06 Å), which is suggestive of a dihydrogen ligand. Oxidation of $[H_{14}]^{+}$ yields $[Rh_6(PH_3)_6H_{14}]^{2+}$ ($[H_{14}]^{2+}$). Although this species is marginally lower in energy than $[H_{12}]^{2+}$, there must be only a small barrier towards $H_2$ loss, which can be overcome simply by loss of hydrogen to the bulk solution. The barrier to loss of $H_2$ from $[H_{14}]^{+}$ must be larger, as cluster **C** is observed experimentally in bulk solution by ESI-MS. Although the precise mechanism of $H_2$ loss is currently uncertain, the correlation between experiment and theory is reasonable, especially given that the approximations involved in using $PH_3$ instead of $PCy_3$ mean that kinetic factors towards $H_2$ loss may not be modeled accurately. Importantly, the experimental observations show unequivocally that the overall hydrogen storage/release cycle (**A**⇄**B**) involves two molecules of $H_2$ per cluster irrespective of the precise mechanistic details.

The hydrogen storage capacity of **A** (0.1 % w/w) is modest, as the cluster and associated anions have high molecular mass, and this value is clearly not sufficient for practical purposes (the US Department of Energy 2010 target is 6 % w/w [25]). However, the ability to store $H_2$ without a partial pressure of $H_2$ (and even under dynamic vacuum) at 298 K, coupled with the very rapid redox-promoted release of $H_2$, is unique. These attractive features result from the electronic and steric properties of the metal cluster, namely: 1) two low-lying unoccupied molecular orbitals available for the uptake of bonding electron pairs from $H_2$; 2) the resulting calculated binding energy of $H_2$ to the cluster of 60 kJ mol$^{-1}$ (lying at a value intermediate between physi- and chemisorption regimes); and 3) the kinetic stabilization afforded against facile hydrogen loss by the trialkyl phosphine groups. These results suggest that future strategies involving redox-switchable metal clusters in hydrogen storage materials or hydrogen spillover systems[26] could well prove worthwhile.

Received: April 11, 2006
Published online: August 4, 2006

**Keywords:** cluster compounds · density functional calculations · electrochemistry · hydrogen storage

[1] L. Schlapbach, A. Zuttel, *Nature* **2001**, *414*, 353.
[2] F. Schüth, B. Bogdanovic, M. Felderhoff, *Chem. Commun.* **2004**, 2249.
[3] J. L. C. Rowsell, O. M. Yaghi, *Angew. Chem.* **2005**, *117*, 4748; *Angew. Chem. Int. Ed.* **2005**, *44*, 4670.
[4] N. B. McKeown, B. Gahnem, K. J. Msayib, P. M. Budd, C. E. Tattershall, K. Mahmood, S. Tan, D. Book, H. W. Langmi, A. Walton, *Angew. Chem.* **2006**, *118*, 1836; *Angew. Chem. Int. Ed.* **2006**, *45*, 1804.
[5] S. S. Kaye, J. R. Long, *J. Am. Chem. Soc.* **2005**, *127*, 6506.
[6] P. M. Forster, J. Eckert, J. S. Chang, S. E. Park, F. G. , A. K. Cheetham, *J. Am. Chem. Soc.* **2003**, *125*, 1309.
[7] B. Chen, N. W. Ockwig, A. R. Millward, D. S. Contreras, O. M. Yaghi, *Angew. Chem.* **2005**, *117*, 4823; *Angew. Chem. Int. Ed.* **2005**, *44*, 4745.
[8] M. Dinca, J. R. Long, *J. Am. Chem. Soc.* **2005**, *127*, 9376.
[9] J. L. C. Roswell, E. C. Spencer, J. Eckert, J. A. K. Howard, O. M. Yaghi, *Science* **2005**, *309*, 1350.
[10] a) G. Ferey, M. Latroche, C. Serre, F. Millange, T. Loiseau, A. Percheron-Guegan, *Chem. Commun.* **2003**, 2976; b) G. Férey, C. Mellot-Draznieks, C. Serre, F. Millange, J. Dutour, S. Surblé, I. Margiolaki, *Science* **2005**, *309*, 2040; c) A. G. Wong-Foy, A. J. Matzger, O. M. Yaghi, *J. Am. Chem. Soc.* **2006**, *128*, 3494.
[11] X. Zhao, B. Xiao, A. J. Fletcher, K. M. Thomas, D. Bradshaw, M. J. Rosseinsky, *Science* **2004**, *306*, 1012.
[12] J. M. Bemis, L. F. Dahl, *J. Am. Chem. Soc.* **1997**, *119*, 4545.
[13] M. H. Chisholm, K. S. Kramer, *Chem. Commun.* **1996**, 1331.
[14] L. F. Chen, F. A. Cotton, W. T. Klooster, T. F. Koetzle, *J. Am. Chem. Soc.* **1997**, *119*, 12175.
[15] P. Braunstein, L. A. Oro, P. R. Raithby, *Metal Clusters in Chemistry*, Wiley-VCH, Weinheim, **1999**.
[16] H. Suzuki, T. Kakigano, K. Tada, M. Igarashi, K. Matsubara, A. Inagaki, M. Oshima, T. Takao, *Bull. Chem. Soc. Jpn.* **2005**, *78*, 67.
[17] T. H. Lemmen, K. Folting, J. C. Huffman, K. G. Caulton, *J. Am. Chem. Soc.* **1985**, *107*, 7774.
[18] R. D. Adams, B. Captain, M. D. Smith, *Angew. Chem.* **2006**, *118*, 1127; *Angew. Chem. Int. Ed.* **2006**, *45*, 1109.
[19] S. K. Brayshaw, M. J. Ingleson, J. C. Green, P. R. Raithby, G. Kociok-Köhn, J. S. McIndoe, A. S. Weller, *Angew. Chem.* **2005**, *117*, 7035; *Angew. Chem. Int. Ed.* **2005**, *44*, 6875.
[20] R. D. Adams, B. Captain, *Angew. Chem.* **2005**, *117*, 2587; *Angew. Chem. Int. Ed.* **2005**, *44*, 2531.
[21] S. K. Brayshaw, M. J. Ingleson, G. Kociok-Köhn, J. C. Green, J. S. McIndoe, P. R. Raithby, A. S. Weller, *J. Am. Chem. Soc.* ***2006***, *128*, 6247.
[22] M. J. Ingleson, M. F. Mahon, P. R. Raithby, A. S. Weller, *J. Am. Chem. Soc.* **2004**, *126*, 4784.
[23] G. J. Kubas, *Metal Dihydrogen and σ-Bond Complexes*, Kluwer Academic/Plenum Publishers, New York, **2001**.
[24] These redox events correspond to $[Rh_6(PCy_3)_6H_{12}]^{0/}[Rh_6(PCy_3)_6H_{12}]^{+}$ $E_{1/2} = -1.51$, $[Rh_6(PCy_3)_6H_{12}]^{+/}[Rh_6(PCy_3)_6H_{12}]^{2+}$ $E_{1/2} = -0.59$, and the quasireversible $[Rh_6(PCy_3)_6H_{12}]^{2+/}[Rh_6(PCy_3)_6H_{12}]^{3+}$ $E_{1/2} = +0.44$ V. Full characterization (including X-ray crystal structures, EPR studies, magnetic properties, and DFT calculations) of these species will appear in a full paper. For a recent example of related electrochemical behavior in early-transition-metal clusters, see: E. J. Welch, C. L. Yu, N. R. M. Crawford, J. R. Long, *Angew. Chem.* **2005**, *117*, 2605; *Angew. Chem. Int. Ed.* **2005**, *44*, 2549.
[25] Basic Research Needs for the Hydrogen Economy; http://www.eere.energy.gov/hydrogenandfuelcells/pdfs/hydrogen_posture_plan.pdf.
[26] Y. Li, R. T. Yang, *J. Am. Chem. Soc.* **2006**, *128*, 726.

 © 2006 Wiley-VCH Verlag GmbH & Co. KGaA, Weinheim 

*Mg/Air Battery Materials*

DOI: 10.1002/anie.200600099

# Metallic Magnesium Nano/Mesoscale Structures: Their Shape-Controlled Preparation and Mg/Air Battery Applications**

*Weiyang Li, Chunsheng Li, Chunyuan Zhou, Hua Ma, and Jun Chen**

Metal nano/mesoscale structures have received intense attention because of the novel physical and chemical properties that are not present in their corresponding macroscale structures.[1–4] Magnesium is one of the most intriguing alkaline-earth metals and has found applications in the fields of $H_2$ storage, organic synthesis, biochemistry, and as an electrode material.[5–8] With respect to Mg nanomaterials, most studies have focused on the fabrication of Mg nanoparticles[9] and related nanocomposites by high-energy milling methods.[10] It should also be noted that theoretical research on Mg nanowires has been done by computer simulation.[11] However, to the best of our knowledge, there are no reports in the literature on the preparation of Mg nano/mesostructures with controlled shape and morphology.

The field of electrochemical storage and generation of energy in batteries is gaining tremendous importance for powering high-tech electronic devices and for enabling a greener transportation industry.[12] Among various batteries, the Mg/air battery system has the advantages of a high theoretical voltage (3.09 V) and energy density (3910 $Wh\,kg^{-1}$), low cost, light weight, and environmental friendliness.[13] It is a special feature of the Mg/air battery that only the active component of the negative electrode (Mg) needs to be stored in the battery, while the reactant ($O_2$) for the positive (bifunctional oxygen-diffusion) electrode during discharge is drawn from the air by a reduction reaction.[14] It is therefore of great scientific and technological importance to improve the properties of the Mg electrode so as to enhance the performance of Mg/air batteries. Herein, we describe the first example of the shape-controlled preparation of Mg nano/mesoscale structures and their promising properties for application in Mg/air batteries.

The various Mg structures were prepared by a simple vapor-transport approach using commercially available Mg powder and no templates or catalysts (see Supporting Information). The size and morphology of the products are predominantly controlled by the experimental conditions (see Supporting Information). The evaporation temperature was fixed at 850 and 950 °C, and the products were deposited in the cooler region of the stainless-steel tube at a temperature of around 300 °C.

Figures 1a and b show typical SEM images of the as-synthesized Mg spheres (sample A) and plates (sample B) prepared at an evaporation temperature of 850 °C with different flow rates of Ar gas (sample A: 400 $cm^3\,min^{-1}$; sample B: 800 $cm^3\,min^{-1}$). It can be seen that both the spheres and the plates are distributed homogeneously over a wide area. The spheres are polyhedra with a diameter of approximately 200–500 nm and the plates have a smooth surface and a regular hexagonal shape with a diameter in the range of 150–460 nm. When the evaporation temperature was increased to 950 °C, Mg nanorods (sample C) and sea-urchin-like nanostructures (sample D) were obtained at Ar flow rates of 400 and 800 $cm^3\,min^{-1}$, respectively. Figure 1c displays a representative SEM image of the as-prepared Mg nanorods, which reveals that the sample contains short,

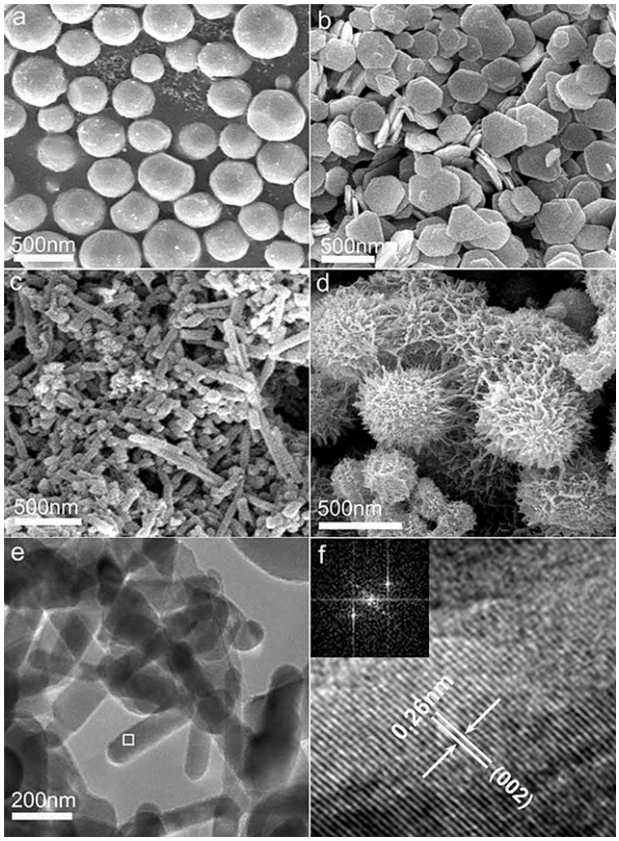


***Figure 1.*** Typical scanning electron microscopy (SEM) images of the as-prepared Mg products: sample A (a), sample B (b), sample C (c), sample D (d); representative transmission electron microscopy (TEM) image of sample C (e) and high-resolution transmission electron microscopy (HRTEM) image (f) of the white square marked in (e); the inset in (f) shows the corresponding fast Fourier transform (FFT) pattern.

[*] W. Li, C. Li, C. Zhou, Dr. H. Ma, Prof. Dr. J. Chen
Institute of New Energy Materials Chemistry
Nankai University
Tianjin 300071 (P.R. China)
Fax: (+86) 22-2350-9118
E-mail: chenabc@nankai.edu.cn

[**] This work was supported by the NSFC (20325102 and 90406001) and the 973 Program (2005CB623607). W.L. and C.L. contributed equally to this work. We are also very grateful to the reviewers for their valuable suggestions.

Supporting Information for this article is available on the WWW under http://www.angewandte.org or from the author.

 © 2006 Wiley-VCH Verlag GmbH & Co. KGaA, Weinheim 

uniform, rodlike structures with a length of approximately 200–500 nm. The SEM image of the Mg sea-urchin-like nanostructures (Figure 1 d) shows their prickly, spherical morphology with very fine whiskerlike fibrils of several tens of nanometers in length. Moreover, these nanowhiskers are interconnected to form a porous network architecture. The TEM image of sample C (Figure 1 e) shows that the diameter of the nanorods is in the range 70–100 nm. The HRTEM image in Figure 1 f shows clear fringes with an interplanar spacing of 0.26 nm, which corresponds to the separation between the (002) lattice planes. These are aligned perpendicular to the longitudinal direction of the rod, which suggests that the nanorods grow along the [001] direction.

When maintaining the experimental conditions for preparing the above four different Mg structures but extending the heating time to 2 h, various other Mg micro/nanostructures with different sizes and morphologies were obtained (see Supporting Information). The prevailing growth morphology of the as-prepared Mg micro/nanostructures is strongly influenced by the degree of supersaturation in the vapor-transport approach, and this is mainly controlled by the experimental parameters, including both the evaporation and deposition temperature, the flow rate of the carrier gas, and the heating time.[15]

Figure 2 shows representative XRD patterns of the as-prepared Mg structures. It can be seen that the positions of the characteristic peaks of the four products are identical. All

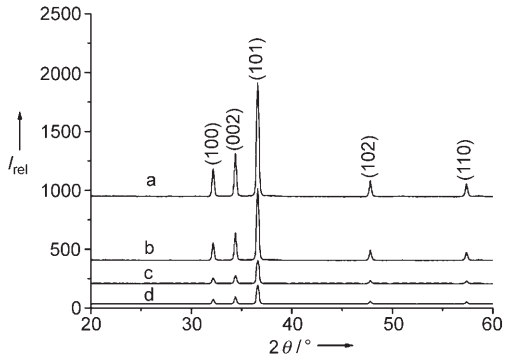


***Figure 2.*** X-ray diffraction (XRD) patterns of the as-prepared Mg products: sample A (a), sample B (b), sample C (c), and sample D (d).

the diffraction peaks can be readily indexed on the basis of the hexagonal close-packed structure of Mg (ICDD-JCPDS 35-0821). No peaks from other phases can be detected, thus indicating that the products are of high purity. According to the present observations, a lower evaporation temperature leads to the formation of products with a larger grain size (samples A and B), while a higher evaporation temperature leads to a smaller grain size (samples C and D). BET nitrogen-adsorption measurements show that the specific surface areas of samples A–D are 8.4, 15.6, 47.2, and 130.6 $m^2 g^{-1}$, respectively.

With respect to metal/air batteries, considerable research effort has been devoted to the study of the performance of Zn/air and Al/air batteries.[16] However, only a few studies have focused on Mg/air batteries.[17] The electrochemical reactions of the Mg/air battery can be expressed by Equations (1)–(3).

$$(+)\ O_2 + 2H_2O + 4e^- \rightarrow 4OH^- \quad \Phi^\circ = 0.40\ V \tag{1}$$

$$(-)\ 2Mg + 4OH^- \rightarrow 2Mg(OH)_2 + 4e^- \quad \Phi^\circ = -2.69\ V \tag{2}$$

$$\text{Overall}\ \ 2Mg + O_2 + 2H_2O \rightarrow 2Mg(OH)_2 \quad E^\circ = 3.09\ V \tag{3}$$

The major problem in using Mg/air batteries is the low Coulombic efficiency of the traditional Mg plate electrode and the high level of polarization during the discharge process. The electrolyte for Mg/air batteries, which is a critical factor that influences their electrochemical performance, must also satisfy the objectives of low anodic polarization, a uniform corrosion rate of Mg, and fast sedimentation of the final anodic product ($Mg(OH)_2$) in the electrolyte.

Figure 3 I displays the linear sweep voltammograms (current density ($J$) versus potential ($\Phi$)) of Mg electrodes made from commercial Mg powder in three different electrolytes: $Mg(ClO_4)_2$ (1.6 M) (a), a mixed solution containing $Mg(NO_3)_2$ (2.6 M) and $NaNO_2$ (3.6 M) (b), and 14 wt % NaCl (c). The anodic dissolution current densities of the Mg electrodes in the three electrolytes all increase as the potential sweeps from −1.5 to −0.5 V. As for electrolyte c, the anodic dissolution current density increases quickly at

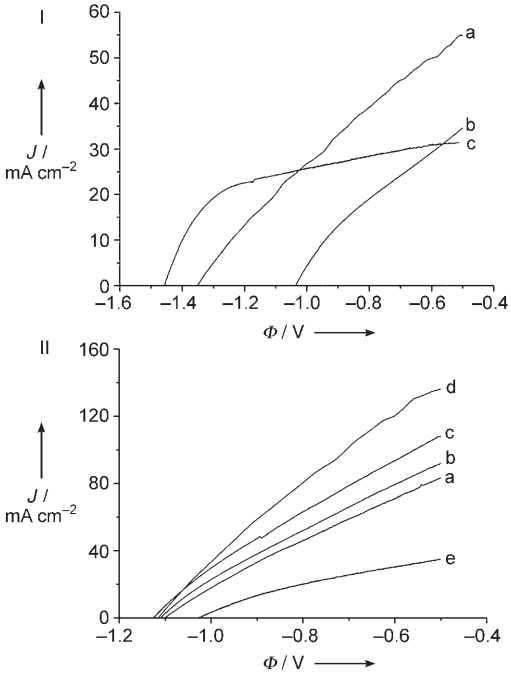


***Figure 3.*** I) Linear sweep voltammograms of Mg electrodes made from commercial Mg powder in three different electrolytes: $Mg(ClO_4)_2$ (1.6 M) (a), a mixed solution of $Mg(NO_3)_2$ (2.6 M) and $NaNO_2$ (3.6 M) (b), and 14 wt% NaCl (c); II) linear sweep voltammograms of different Mg electrodes made from the various as-prepared Mg structures: sample A (a), sample B (b), sample C (c), sample D (d), and commercial Mg powder (e) with a mixed electrolyte solution of $Mg(NO_3)_2$ (2.6 M) and $NaNO_2$ (3.6 M). Scan rate: 20 $mV s^{-1}$; potential range: −1.50 to −0.50 V versus Ag/AgCl saturated with KCl.

 © 2006 Wiley-VCH Verlag GmbH & Co. KGaA, Weinheim 

first in the potential range −1.45 to −1.25 V and then slows down when the potential sweeps to more positive values; this behavior is due to the formation of a passive film of $Mg(OH)_2$ on the Mg electrode surface. In electrolytes a and b, however, no obvious passivation phenomena are observed. Moreover, the starting potentials of the Mg anodic dissolution in the three electrolytes are quite different (−1.35, −1.03, and −1.45 V for electrolytes a, b, and c, respectively). Although a more negative anodic dissolution potential indicates a higher open circuit voltage for the Mg/air battery, the corrosion problem of Mg electrodes, which reduces the shelf life and operating life of the battery, is much more acute in electrolytes a and c. The overall reaction for the corrosion of a Mg electrode can be expressed by Equation (4).

$$Mg + 2\,H_2O \rightarrow Mg(OH)_2 + H_2\uparrow \quad (4)$$

With regard to electrolytes a and c, a large number of bubbles can be seen around the Mg electrode during our experiment, thus indicating the rapid release of $H_2$ gas and serious self-discharge problems; few bubbles were observed in electrolyte b. It has been demonstrated in detail by Sathyanarayana and co-workers[17] that a mixed electrolyte containing $Mg(NO_3)_2$ and $NaNO_2$ is better than a variety of other electrolytes (especially conventional halide or perchlorate electrolytes) in terms of low corrosion rate on open circuit, which can keep the Mg anode in an activated state for about a year, high Faradaic efficiency for Mg anodic dissolution (higher than 90% at a current density of above 20 mA cm$^{-2}$), and uniform pattern of corrosion. Consequently, an electrolyte of $Mg(NO_3)_2$ and $NaNO_2$ solution should be suitable for a Mg/air battery containing Mg anodes with a high surface area, especially those made from Mg nanomaterials. Moreover, Mg/air batteries are generally operated either as "reserve" batteries, in which the electrolyte solution is added to the cell only when required to begin the discharge, or as "mechanically rechargeable" batteries, which have replacement anode units available. With respect to our laboratory-made Mg/air batteries, the controllable air vent is closed during battery storage and the anode is isolated from the electrolyte fluid prior to the first or successive uses of the cell. Therefore, the self-discharge problem can be readily controlled and inhibited to some extent.

Figure 3 II shows the linear sweep voltammograms of different Mg electrodes made from various as-synthesized Mg nano/mesostructures and commercial Mg powder in an electrolyte of $Mg(NO_3)_2$ (2.6 M) and $NaNO_2$ (3.6 M). The starting potentials of the Mg anodic dissolution for the electrodes made from Mg nano/mesostructures are shifted to more negative potentials of approximately −1.10 to −1.13 V compared with the value of −1.03 V for the commercial Mg powder electrode. Furthermore, the anodic dissolution current densities of the electrodes made from the Mg nano/mesostructures are much higher than that of the electrode made from the Mg powder; the sequence of current densities from highest to lowest is d > c > b > a > e. These results indicate that the electrochemical activity of vapor-deposited Mg structures is significantly higher than that of commercial Mg powder.

Figure 4 shows representative discharge curves (cell potential ($E$) versus discharge time ($t$)) for Mg/air batteries made from samples A and D, at a constant current of 0.5 mA

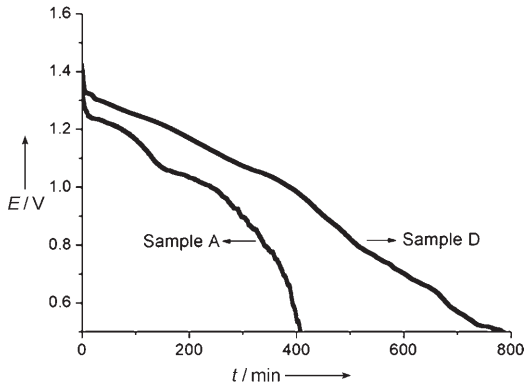


***Figure 4.*** Representative discharge curves of the Mg/air batteries made from samples A and D, at a constant current of 0.5 mA and a temperature of 25 °C.

and a temperature of 25 °C in the voltage range 1.5–0.5 V. The open-circuit voltage of the battery made from sample D is approximately 1.42 V and is higher than that of the battery made from sample A (approximately 1.36 V). In addition, the battery made from sample D also exhibits a higher discharge voltage and a much longer discharge time than the battery made from sample A, thus indicating its higher energy density. The discharge curves of the batteries made from samples B and C show similar voltage profiles to those of samples A and D; the discharge times of samples B and C are approximately 480 and 620 min, respectively.

Table 1 summarizes the energy densities of the Mg/air batteries made from the as-synthesized Mg structures at different discharge current densities. The energy densities of all the batteries decrease with increasing discharge current density. The Mg/air battery made from sample D shows the highest energy density among the four batteries. At a current density of 50 mA cm$^{-2}$, the energy density of the Mg/air battery made from sample D is still 305 W h kg$^{-1}$, approximately 54.0% of its energy density at 5 mA cm$^{-2}$, while those of the Mg/air batteries made from samples A–C are approximately 24.6, 30.3, and 43.9% of their energy densities at 5 mA cm$^{-2}$, respectively. It is therefore apparent that the sequence of high-rate discharge ability from best to worst is D > C > B > A.

According to the results presented above, the Mg/air batteries made from vapor-deposited Mg nano/mesostruc-

***Table 1:*** Energy densities of the Mg/air batteries made from the various as-prepared Mg structures, at different discharge current densities.

| Mg structure | Energy density [W h kg$^{-1}$] at discharge current densities [mA cm$^{-2}$] of | | | |
|---|---|---|---|---|
| | 5 | 10 | 25 | 50 |
| Sample A | 285 | 230 | 153 | 70 |
| Sample B | 346 | 282 | 197 | 105 |
| Sample C | 455 | 385 | 283 | 200 |
| Sample D | 565 | 494 | 402 | 305 |

 © 2006 Wiley-VCH Verlag GmbH & Co. KGaA, Weinheim 

tures, especially the battery made from the Mg sea-urchin-like nanostructures, display much better electrochemical properties (high gravimetric energy density) than the various existing power sources (see Supporting Information). It is generally believed that chemical and physical properties can be altered considerably when downsizing materials into the nanoscale region. With decreasing particle size, an increasing proportion of the total number of the atoms lie near or at the surface, thus making the materials more active for the electrochemical reaction and significantly enhancing the utilization efficiency of the Mg electrode. Furthermore, the battery made from the Mg sea-urchin-like nanostructures exhibits the best high-rate discharge capability, which is critical for high-power-output battery systems. This may be attributable to the porous and network structure of these nanostructures, which contributes to the low anodic polarization/corrosion of Mg and fast sedimentation of the anodic product ($Mg(OH)_2$) in the electrolyte. The polarization of the Mg electrode increases with increasing discharge current density. The high specific surface areas of the Mg sea-urchin-like nanostructures can help to reduce the real current density for the electrode during the discharge process and lead to a relatively low level of polarization for the Mg electrode, which is favorable for improving the energy density and high-rate discharge capability of the battery.

## Experimental Section

The experimental setup consisted of a conventional tube furnace (68.0 cm in length, 40.0 cm in diameter), a horizontal stainless-steel tube (80.0 cm in length, 1.6 cm in diameter), and a gas-flow control system (see Supporting Information). In a typical preparation, Mg powder (99.8% purity, Alfa Aesar) was put into a W boat at the center of the stainless-steel tube. The tube furnace was heated at a rate of 30 °C $min^{-1}$ to a temperature of 850 or 950 °C and maintained at this temperature for 1 h, under a constant flow of high-purity Ar (>99.995%). The flow rates of Ar were controlled at 400 or 800 $cm^3$ $min^{-1}$ during the heating process. Silver-gray wool-like products were obtained on the surface of the substrate in the cooler region of the stainless-steel tube at a deposition temperature of approximately 300 °C. After the chamber had cooled naturally to ambient temperature, the products were collected and kept in a vacuum desiccator for further analysis.

The as-prepared samples were characterized by powder XRD (Rigaku D/max-2500 X-ray generator, $Cu_{K\alpha}$ radiation), SEM (Philips XL-30 and JEOL JSM-6700F field emission), TEM and HRTEM (FEI Tecnai 20, 200 kV), and BET nitrogen adsorption/desorption measurements (Shimadzu-Micromeritics ASAP 2010 Instrument).[18]

Magnesium electrodes were prepared in a glove box filled with Ar (99.995%) by filling a glass tube (2.1 mm in diameter) containing a Cu wire as collector with a mixture of 65 wt% active materials (vapor-deposited Mg products or commercial Mg powder), 25 wt% acetylene black, and 10 wt% poly(tetrafluoroethylene) (PTFE) solution. The electrochemical properties of these electrodes were investigated with a Parstat 2273 potentiostat/galvanostat analyzer (AMTECT Company) in an electrochemical cell that contained the Mg working electrode, a Pt counter electrode, and a Ag/AgCl-KCl (saturated) reference electrode.

The laboratory-made Mg/air batteries were assembled with a Mg anode and an air cathode. The Mg anode was prepared in a glove box filled with Ar (99.995%) in the presence of an $O_2$ scavenger and an Na drying agent. The air electrodes were composed of two layers: an $La_{0.6}Ca_{0.4}CoO_3$ perovskite catalyst layer on the electrolyte side and a hydrophobic gas-diffusion layer on the gas side.[19] The electrolyte was a mixed solution containing $Mg(NO_3)_2$ (2.6 M) and $NaNO_2$ (3.6 M). The batteries were tested with an Arbin charge–discharge device.

Received: January 10, 2006
Revised: June 11, 2006
Published online: August 4, 2006

**Keywords:** batteries · electrochemistry · magnesium · materials science · nanostructures

[1] a) C. Burda, X. B. Chen, R. Narayanan, M. A. El-Sayed, *Chem. Rev.* **2005**, *105*, 1025; b) C. T. Campbell, *Science* **2004**, *306*, 234.
[2] a) F. Raimondi, G. G. Scherer, R. Kotz, A. Wokaun, *Angew. Chem.* **2005**, *117*, 2228; *Angew. Chem. Int. Ed.* **2005**, *44*, 2190; b) H. P. Liang, H. M. Zhang, J. S. Hu, Y. G. Guo, L. J. Wan, C. L. Bai, *Angew. Chem.* **2004**, *116*, 1566; *Angew. Chem. Int. Ed.* **2004**, *43*, 1540.
[3] Y. N. Xia, P. D. Yang, Y. G. Sun, Y. Y. Wu, B. Mayers, B. Gates, Y. D. Yin, F. Kim, H. Q. Yan, *Adv. Mater.* **2003**, *15*, 353.
[4] a) X. G. Wen, Y. P. Fang, S. H. Yang, *Angew. Chem.* **2005**, *117*, 3628; *Angew. Chem. Int. Ed.* **2005**, *44*, 3562; b) S. R. C. Vivekchand, G. Gundiah, A. Govindaraj, C. N. R. Rao, *Adv. Mater.* **2004**, *16*, 1842.
[5] a) R. W. P. Wagemans, J. H. van Lenthe, P. E. de Jongh, A. J. van Dillen, K. P. de Jong, *J. Am. Chem. Soc.* **2005**, *127*, 16675; b) H. Imamura, T. Nobunaga, M. Kawahigashi, S. Tsuchiya, *Inorg. Chem.* **1984**, *23*, 2509.
[6] a) P. Dai, P. H. Dussault, T. K. Trullinger, *J. Org. Chem.* **2004**, *69*, 2851; b) B. Bogdanović, *Angew. Chem.* **1985**, *97*, 253; *Angew. Chem. Int. Ed. Engl.* **1985**, *24*, 262.
[7] J. A. Cowan, *The Biological Chemistry of Magnesium*, VCH Publishers, New York, **1995**.
[8] a) D. Aurbach, Z. Lu, A. Schechter, Y. Gofer, H. Gizbar, R. Turgeman, Y. Cohen, M. Moshkovich, E. Levi, *Nature* **2000**, *407*, 724; b) A. Brenner, *J. Electrochem. Soc.* **1996**, *143*, 3133.
[9] Y. K. Zhang, S. J. Liao, Y. H. Fan, *J. Nanopart. Res.* **2001**, *3*, 23.
[10] a) L. Lu, M. O. Lai, W. Liang, *Compos. Sci. Technol.* **2004**, *64*, 2009; b) J. L. Bobet, E. Grigorova, M. Khrussanova, M. Khristov, P. Stefanov, P. Peshev, D. Radev, *J. Alloys Compd.* **2004**, *366*, 298.
[11] H. Li, F. Pederiva, G. H. Wang, B. L. Wang, *J. Appl. Phys.* **2004**, *96*, 2214.
[12] a) M. Winter, R. J. Brodd, *Chem. Rev.* **2004**, *104*, 4245; b) J. M. Tarascon, M. Armand, *Nature* **2001**, *414*, 359.
[13] D. Linden, T. B. Reddy, *Handbook of Batteries*, 3rd ed., McGraw-Hill, New York **2002**.
[14] a) A. Weidenkaff, S. G. Ebbinghaus, T. Lippert, *Chem. Mater.* **2002**, *14*, 1797; b) S. Muller, K. Striebel, O. Haas, *Electrochim. Acta* **1994**, *39*, 1661.
[15] Y. D. Yin, G. T. Zhang, Y. N. Xia, *Adv. Funct. Mater.* **2002**, *12*, 293.
[16] a) X. Zhang, S. H. Yang, H. Knickel, *J. Power Sources* **2004**, *128*, 331; b) X. Y. Wang, P. J. Sebastian, M. A. Smit, H. P. Yang, S. A. Gamboa, *J. Power Sources* **2003**, *124*, 278; c) E. Deiss, F. Holzer, O. Haas, *Electrochim Acta* **2000**, *47*, 3995.
[17] a) S. Sathyanarayana, N. Munichandraiah, *J. Appl. Electrochem.* **1981**, *11*, 33; b) R. P. Hamlen, E. C. Jerabek, J. C. Ruzzo, E. G. Siwek, *J. Electrochem. Soc.* **1969**, *116*, 1588.
[18] a) F. Y. Cheng, J. Chen, X. L. Gou, P. W. Shen, *Adv. Mater.* **2005**, *17*, 2753; b) J. Chen, L. N. Xu, W. Y. Li, X. L. Gou, *Adv. Mater.* **2005**, *17*, 582; c) X. Wang, J. Zhuang, J. Chen, K. B. Zhou, Y. D. Li, *Angew. Chem.* **2004**, *116*, 2051; *Angew. Chem. Int. Ed.* **2004**, *43*, 2017.
[19] D. Chartouni, N. Kuriyama, T. Kiyobayashi, J. Chen, *Int. J. Hydrogen Energy* **2002**, *27*, 945.

 © 2006 Wiley-VCH Verlag GmbH & Co. KGaA, Weinheim 

*Solid-State Reactions*

DOI: 10.1002/anie.200600845

# Solid-State Phase Transition of an Inclusion Complex of 5-Methyl-2-pyridone with 1,3,5-Benzenetricarboxylic Acid**

*Shinya Hirano, Shinji Toyota, Fumio Toda,* Kotaro Fujii, and Hidehiro Uekuasa**

Efficient and selective inter- and intramolecular photoreactions of guest compounds in their inclusion complexes with a host compound have long been studied.[1] We reported that photoirradiation of a 1:2 inclusion complex of 5-methyl- (**1a**) and 5-chloro-2-pyridone (**1b**) with a 2,2′-biphenyldicarboxylic acid host (**2**) gives the corresponding *rac-cis-anti* dimer **3a** and **3b**, respectively.[2,3] These [2+2] photodimerization reactions of 2-pyridone derivatives are important as models for DNA damage; this damage occurs by photodimerization of the thymine component of DNA, which is the cause of skin cancer. We also reported [4+4] photodimerizations of 2-pyridone itself (**1c**) and **1b** in their inclusion complexes with **2** and a 1,2,4,5-benzenetetracarboxylic acid host (**4**), respectively, which give the *rac-trans-anti* dimer **5c** and the *meso-cis-syn* dimer **6b**, respectively.[3,4] X-ray analyses of these inclusion complexes showed that the 2-pyridone molecules are ordered at reasonable positions for the corresponding photodimerization reactions in all cases.[2–4]

In some cases, however, the guest molecules are not located at appropriate positions for a photodimerization. Schmidt's rule states that for efficient photodimerization in the solid state, two olefin molecules should be arranged parallel and closer than 4.2 Å in the crystal.[5] Nevertheless, we found that a photochemically unreactive molecular aggregate of **1a** in an inclusion complex with a 1,3,5-benzenetricarboxylic acid host (**7**) can be transformed in the solid state into a reactive aggregate by heating or by contact with MeCN vapor. The mechanism of this novel phase transition was clarified by X-ray analysis.

A 1:1:1 inclusion complex (**8**) of **7**, **1a**, and MeOH, which was prepared as colorless crystals by recrystallization of **7** and **1a** from MeOH, was inert to photoirradiation. Very interestingly, however, the crystal of **8** was transformed by heating or by contact with MeCN vapor into a reactive powder of **9**, the solid-state photoirradiation of which gave the *meso-cis-syn* [4+4] dimer **6a** (Scheme 1). This is the first report of a phase transition in the solid state from photochemically unreactive molecular aggregate into a reactive aggregate caused by heating or contact with solvent vapor.

The phase transition of **8** into **9** did not occur by contact with vapor of EtCN, PhCN, tetrahydrofuran, acetone, $CH_2Cl_2$, $CHCl_3$, or *n*-hexane. This is an interesting example of a solvent effect in the solid state. A similar solvent effect was reported for a solid-state reaction that was accelerated in the presence of a small amount of solvent vapor.[6]

Since **6a** is thermally labile and can be converted easily into the *meso-cis-syn* [2+2] dimer **11**, **6a** was isolated as its stable 1:1:1 inclusion complex **10** consisting of **7**, **6a**, and $H_2O$, which was prepared by recrystallization of the photoirradiated powder of **9** from MeOH. The structure of **6a** was elucidated by comparison of its IR and $^1$H NMR spectra with those of **6b**.[3] The structure of **6a** was finally confirmed by X-ray analysis of **10** (Figure 1). However, the simulated powder X-ray diffraction (PXRD) pattern of **10** was different from that of photoirradiated powder of **9** (see the Supporting Information). Heating of the thermally labile **6a** as **10** in $CD_3COOD$ at 70 °C for 2 h gave **11** in quantitative yield. The structure of **11** was elucidated by comparison of its $^1$H and $^{13}$C NMR spectra with those of **3a**.[2,3] The *meso-cis-syn* dimer **11** is the first example of a [2+2] photodimer of 2-pyridone that has a *cis-syn* configuration. Compound **11** has the same configuration as that of the thymine dimer produced by photodimerization of the thymine component of a nucleotide in DNA.[7]

To know the mechanism of the unreactive-to-photoreactive phase transition of **8** into **9**, the crystal structure of **8** was studied by X-ray analysis. As shown in the packing diagram of **8** (Figure 2), molecules of **1a, 7**, and MeOH aggregate by forming four kinds of hydrogen bonds: COOH(**7**)···O=C(**1a**), C=O(**7**)···HN(**1a**), COOH(**7**)···OHMe, and C=O(**7**)···HOMe. The shortest contact between the reaction centers of two symmetry-related molecules of **1a** is C3–C6′ (=C6–C3′) = 5.04 Å. This distance is too far for reaction. Even if a [4+4] photodimerization of **1a** can be effected, the *trans-anti* dimer **5a** should be produced instead of *cis-syn* dimer **6a**, as is expected from the molecular ordering shown in Figure 2.

As the crystal of **8** did not retain its single crystalline form after the thermal phase transition at 120 °C, attempts to obtain single crystals suitable for X-ray diffraction were unsuccessful. The results of thermogravimetry and differential thermal analysis (TG/DTA) show that the phase transition is associated with the loss of MeOH molecules from **8** (see the Supporting Information), which is the cause of the disintegration of the single crystal. The decreasing weight corresponded to one MeOH molecule in the asymmetric unit. The phase transition was confirmed by the PXRD pattern of **8**

[*] S. Hirano, Prof. Dr. S. Toyota, Prof. Dr. F. Toda
Department of Chemistry
Okayama University of Science
Ridai-cho, Okayama 700-0005 (Japan)
Fax: (+81) 86-256-9604
E-mail: toda@chem.ous.ac.jp
K. Fujii, Prof. Dr. H. Uekuasa
Department of Chemistry and Materials Science
Tokyo Institute of Technology
Ookayama 2, Meguro-ku, Tokyo 152-8551 (Japan)
Fax: (+81) 3-5734-3529
E-mail: uekusa@cms.titechl.ac.jp

[**] S.T. and F.T. are grateful for the financial support from MEXT.HAITEKU (2001–2005). H.U. is grateful to Professor K. D. M. Harris (Cardiff University, Wales) for supplying the program EAGER for structure solution from powder diffraction data, and to the financial support by Grant-in-Aid for Scientific Research (KAKENHI) in Priority Area "Molecular Nano Dynamics" from MEXT.

Supporting information for this article is available on the WWW under http://www.angewandte.org or from the author.

 © 2006 Wiley-VCH Verlag GmbH & Co. KGaA, Weinheim 

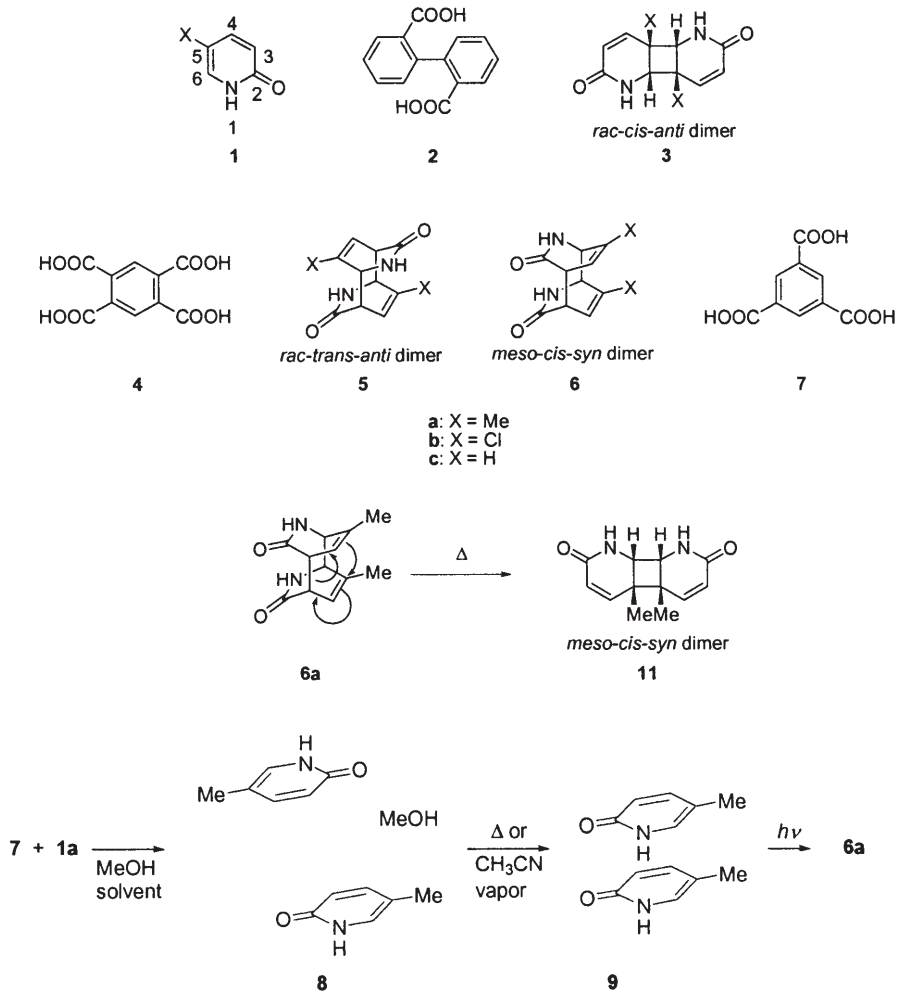


***Scheme 1.*** Transformation from photochemically unreactive **8** into reactive **9** in the solid state. Host **7** is omitted for clarity.

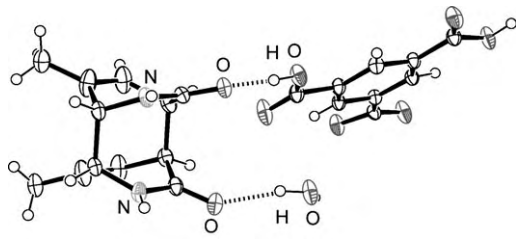

***Figure 1.*** X-ray crystal structure of **10**.

and **9** (Figure 3). As the pattern of **9** is significantly different from that of **8**, we determined the crystal structure of **9** from the PXRD data by using the ab initio method of the program EAGER;[8,9] this program adopts the direct-space strategy[10] for structure solution from powder diffraction data[11] and is based on the use of the genetic algorithm technique[9] for global optimization. The crystal structure was refined by the Rietveld method.

As shown in the packing diagram of **9** (Figure 4), molecules of **1a** and **7** aggregate by forming the four kinds of hydrogen bonds: two COOH(**7**)···O=C(**1a**) bonds, COOH(**7**)···O=C(**7**), and C=O(**1a**)···HN(**1a**). The shortest contact between the reaction centers of two translationally related **1a** molecules is C3–C3′ (= C6–C6′) = 3.84 Å. This distance is close enough for reaction to occur, and two **1a** molecules are arranged so as to give the *cis-syn*-dimer **6a**. These data show that the transformation of **8** into **9** should occur through removal of a methanol molecule and turning of one **1a** molecule about 180° by heating or by contact with MeCN vapor. Photochemically unreactive chalcone derivatives are known to transform both in the solid state and in solution into reactive species in the molten state, and a [2+2] stereoselective photodimerization of chalcones occurrs in the molten state to give *rac-anti*-head-to-head dimers.[12] However, the transformation from the photochemically unreactive **8** into the reactive **9** in the solid state is much more interesting and important.

Although host–guest inclusion crystals are useful for stereoselective template reactions of the guest compounds, the guest molecules are not always ordered at appropriate positions for effective reaction. For example, for [2+2] or [4+4] photodimerization of olefins, the two olefin molecules should be ordered close and parallel to each other. The unsuitable positioning of olefin molecules in the inclusion complex can be changed into an appropriate molecular ordering by phase transition in the solid state. This finding should encourage chemists who have been disappointed with the failure of template

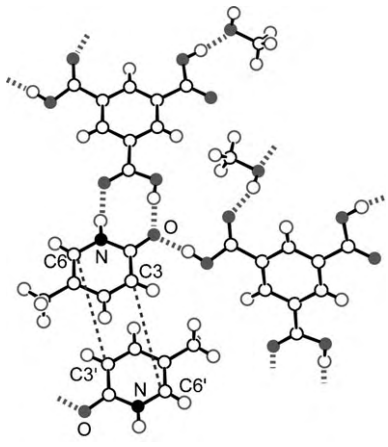


***Figure 2.*** X-ray crystal structure of **8**.

reactions because of inappropriate ordering of the guest molecules.

Knowledge of the three-dimensional crystal structure is of vital importance for the discussion of crystalline-state reaction mechanisms. However, the structural phase transition is

 © 2006 Wiley-VCH Verlag GmbH & Co. KGaA, Weinheim 

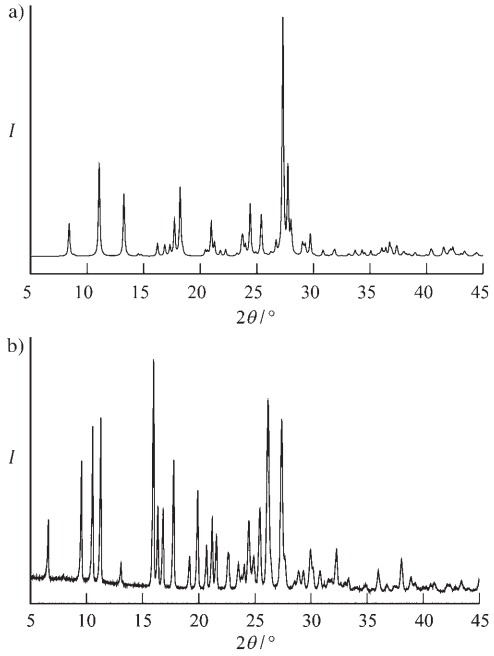


***Figure 3.*** Powder X-ray diffraction pattern of a) **8** (simulation from single-crystal data) and b) **9**.

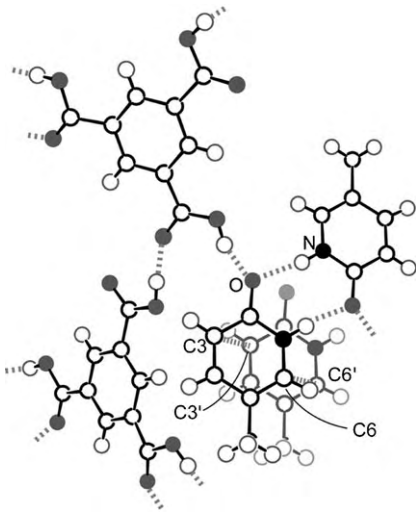


***Figure 4.*** X-ray crystal structure of **9**.

often associated with loss of crystal integrity, and the crystal structure after the phase transition may not be accessible by single-crystal analysis. Even in such a case, a method that enables the ab initio structure determination from a PXRD pattern can be used to elucidate the crystal structure of polycrystalline materials.

## *Experimental Section*

The single-crystal X-ray diffraction data were collected on a Rigaku RAXIS RAPID Imaging Plate diffractometer with $Mo_{K\alpha}$ radiation ($\lambda = 0.71075$ Å) to a maximum $2\theta$ value of 55.0°. The reflection data were corrected for the Lorentz-polarization effects and secondary extinction. No absorption correction was applied. The structure was solved by direct methods using the Sir2004[13] program and refined by the full-matrix least-squares method by using the SHELXL97[14] program. Non-hydrogen atoms were refined anisotropically. Hydrogen atoms were located from the difference Fourier map and refined.

Crystal data for **8**: $C_9H_6O_6{\cdot}C_6H_7NO{\cdot}CH_4O$, $M_r = 351.31$, monoclinic, space group $P2_1/n$, $a = 13.3645(14)$, $b = 7.4825(5)$, $c = 15.9942(19)$ Å, $\beta = 92.852(5)°$, $V = 1597.4(3)$ Å$^3$, $Z = 4$, $\rho_{calcd} = 1.461$ g cm$^{-3}$, $T = 173$ K, number of unique reflections = 3650, $R_{int} = 0.027$ up to $2\theta = 55.0°$, number of parameters = 294, $R_1 = 0.0349$, $wR = 0.0915$, $Gof = 1.056$ for 3124 reflections.

Crystal data for **10**: $C_9H_6O_6{\cdot}C_{12}H_{14}N_2O_2{\cdot}H_2O$, $M_r = 446.41$, triclinic, space group $P\bar{1}$, $a = 7.0942(9)$, $b = 9.6224(8)$, $c = 14.467(2)$ Å, $\alpha = 92.634(6)$, $\beta = 93.240(7)$, $\gamma = 95.754(6)°$, $V = 979.7(2)$ Å$^3$, $Z = 2$, $\rho_{calcd} = 1.513$ g cm$^{-3}$, $T = 173$ K, number of unique reflections = 4505, $R_{int} = 0.026$ up to $2\theta = 55.0°$, number of parameters = 357, $R_1 = 0.0616$, $wR = 0.1559$, $Gof = 1.064$ for 4054 reflections. The large maximum residual electron density (1.2 e Å$^{-3}$) was caused by decomposition of the *meso-cis-syn* [4+4] dimer (**6a**).

The powder X-ray diffraction data of **9** were collected at ambient temperature on a Panalytical X'Pert PRO MRD with reflection mode (parallel $Cu_{K\alpha}$ radiation, $\lambda = 1.54184$ Å; $2\theta$ range 5–70°; step size 0.006°; data collection time 12 h). The powder X-ray diffraction pattern was indexed by using DICVOL04[15] to give the monoclinic unit cell $M_{25} = 45.0$, $F_{25} = 136.2$. The space group was assigned from the results of LeBail fitting ($R_{wp} = 0.0839$) as $P2_1/a$. The space group and cell volume indicates that there is one pair of molecules **1a** and **7** in the asymmetric unit. The genetic algorithm calculation was performed using the program EAGER to solve the structure and determine a total of 15 variables for **1a** and **7**. Final Rietveld refinement was carried out with the GSAS[16] program. $a = 16.713(6)$, $b = 22.089(8)$, $c = 3.8294(14)$ Å, $\beta = 93.631(2)°$, $V = 1409.2(15)$ Å$^3$, $R_{wp} = 0.0780$, $R_p = 0.0581$, $R_B = 0.0505$, $2\theta$ range 5.0–55.0°, 8332 profile points, 124 refined variables. CCDC-263741, -263742, and -602110 contain the supplementary crystallographic data for this paper. These data can be obtained free of charge from The Cambridge Crystallographic Data Centre via www.ccdc.cam.ac.uk/data_request/cif.

The $^1$H and $^{13}$C NMR spectra were measured on a JEOL Lambda-500 spectrometer at 500 MHz. IR spectra were measured on a JEOL FT/IR-460 Plus instrument. Melting points were measured on a Stuart Scientific SMP3 instrument. TG/DTA was performed on a Rigaku Thermo Plus 2 instrument.

Preparation of **8**: A solution of **7** (101 mg, 0.478 mmol) and **1a** (104 mg, 0.948 mmol) in MeOH (4.0 mL) was kept at room temperature for 24 h to give the 1:1:1 inclusion complex **8** as colorless needles (127 mg, 0.361 mmol, 75% yield, m.p. 284–286 °C).

Transformation of **8** into **9**: Compound **8** was heated at 120 °C for 10 min to give the 1:1 inclusion complex **9** as a white crystalline powder (m.p. 289–289.5 °C) in quantitative yield. Contact of **8** with MeCN vapor for 24 h at room temperature also gave **9** quantitatively.

Photoreaction of **9** in the solid state: The crude product obtained by photoirradiation (400-W high-pressure Hg lamp) of powdered **9** (100 mg, 0.313 mmol) in the solid state for 30 h was recrystallized from MeOH to give **10** as colorless block crystals (45.1 mg, 0.101 mmol, 64% yield, m.p. 245.5–282.5 °C (decomp)). $^1$H NMR (500 MHz, $CF_3COOD$): $\delta = 5.75$ (brm, 2H), 4.37 (brm, 2H), 3.81 (dd, $J$ (H,H) = 2.5 and 4.3 Hz, 2H), 2.13 ppm (d, $J$ (H,H) = 1.5 Hz, 6H); $^{13}$C NMR (125 MHz, $CF_3COOD$): $\delta = 20.89$, 50.12, 62.52, 125.02, 148.92, 186.03 ppm.

Thermal conversion of **6a** into **11**: A solution of **10** in $CD_3COOD$ was heated at 70 °C for 2 h to give **11** in quantitative yield. $^1$H NMR (500 MHz, $CF_3COOD$): $\delta = 6.51$ (d, $J$ (H,H) = 10 Hz, 2H), 6.00 (d, $J$ (H,H) = 10 Hz, 2H), 4.23 (s, 2H), 1.38 ppm (s, 6H); $^{13}$C NMR

 © 2006 Wiley-VCH Verlag GmbH & Co. KGaA, Weinheim 

(125 MHz, $CF_3COOD$): $\delta = 22.71$, 48.09, 59.83, 120.52, 151.45, 171.18 ppm.

Received: March 5, 2006
Revised: June 14, 2006
Published online: August 9, 2006

**Keywords:** dimerization · phase transitions · photochemistry · solid-state reactions

[1] F. Toda, *Top. Curr. Chem.* **1988**, *149*, 211 – 238; F. Toda, *Synlett* **1993**, 303 – 312; F. Toda, *Acc. Chem. Res.* **1995**, *28*, 480 – 486; K. Tanaka, F. Toda, *Chem. Rev.* **2000**, *100*, 1025 – 1074; "Organic Photoreaction in the Solid State": K. Tanaka, F. Toda in *Organic Solid-State Reactions* (Ed.: F. Toda), Kluwer, Dordrecht, **2002**, pp. 109 – 158; "Selective Reactions in Inclusion Crystals": Z. Urbanczyk-Lipkowska, F. Toda in *Organic Supramolecular Chemistry* (Eds.: F. Toda, R. Bishop), Wiley, New York, **2004**, pp. 173 – 184; D. B. Varahney, X. Gao, T. Friscic, L. R. MacGillivray, *Angew. Chem.* **2006**, *118*, 662 – 666; *Angew. Chem. Int. Ed.* **2006**, *45*, 646 – 650.
[2] S. Hirano, S. Toyota, F. Toda, *Chem. Commun.* **2005**, 643 – 644.
[3] S. Hirano, S. Toyota, F. Toda, *Heterocycles* **2004**, *64*, 383 – 391.
[4] S. Hirano, S. Toyota, F. Toda, *Mendeleev Commun.* **2004**, 247 – 249.
[5] G. M. J. Schmidt, *Pure Appl. Chem.* **1971**, *27*, 647 – 678.
[6] S. Nakamatsu, S. Toyota, W. Jones, F. Toda, *Chem. Commun.* **2005**, 3808 – 3810.
[7] S. Y. Wang, *Nature* **1963**, *200*, 879 – 880.
[8] S. Habershon, G. W. Turner, B. M. Kariuki, E. Y. Cheung, A. J. Hanson, E. Tedesco, D. Albesa-Jové, M.-H. Chao, O. J. Lanning, R. L. Johnston, K. D. M. Harris, *EAGER—A Computer Program for Direct-Space Structure Solution from Powder X-ray Diffraction Data*, Cardiff University and University of Birmingham.
[9] B. M. Kariuki, H. Serrano-González, R. L. Johnston, K. D. M. Harris, *Chem. Phys. Lett.* **1997**, *280*, 189 – 195; K. D. M. Harris, R. L. Johnston, B. M. Kariuki, *Acta Crystallogr. Sect. A* **1998**, *54*, 632 – 645; S. Habershon, K. D. M. Harris, R. L. Johnston, *J. Comput. Chem.* **2003**, *24*, 1766 – 1774; E. Y. Cheung, S. J. Kitchin, K. D. M. Harris, Y. Imai, N. Tajima, R. Kuroda, *J. Am. Chem. Soc.* **2003**, *125*, 14658 – 14659; D. Albesa-Jové, B. M. Kariuki, S. J. Kitchin, L. Grice, E. Y. Cheung, K. D. M. Harris, *ChemPhysChem* **2004**, *5*, 414 – 418; F. Guo, K. D. M. Harris, *J. Am. Chem. Soc.* **2005**, *127*, 7314 – 7315.
[10] K. D. M. Harris, M. Tremayne, P. Lightfoot, P. G. Bruce, *J. Am. Chem. Soc.* **1994**, *116*, 3543 – 3547.
[11] K. D. M. Harris, M. Tremayne, B. M. Kariuki, *Angew. Chem.* **2001**, *113*, 1674 – 1700; *Angew. Chem. Int. Ed.* **2001**, *40*, 1626 – 1651.
[12] F. Toda, K. Tanaka, M. Kato, *J. Chem. Soc. Perkin Trans. 1* **1998**, 1315 – 1318.
[13] M. C. Burla, R. Caliandro, M. Camalli, B. Carrozzini, G. L. Cascarano, L. De Caro, C. Giacovazzo, G. Polidori, R. Spagna, *J. Appl. Crystallogr.* **2005**, *38*, 381 – 388.
[14] G. M. Sheldrick, SHELXL97. University of Göttingen, Germany. **1997**.
[15] A. Boultif, D. Louër, *J. Appl. Crystallogr.* **2004**, *37*, 724 – 731.
[16] "General Structure Analysis System (GSAS)": A. C. Larson, R. B. Von Dreele, *Los Alamos Sci. Lab. [Rep.] LA* **2000**, 86 – 748.

 © 2006 Wiley-VCH Verlag GmbH & Co. KGaA, Weinheim 

C-Sialylation

DOI: 10.1002/anie.200601209

# Anomeric Acetates of *N*-Acetylneuraminic Acid are Useful *C*-Sialyl Donors in Samarium-Mediated Reformatsky Coupling Reactions**

*Adeline Malapelle, Zouleika Abdallah, Gilles Doisneau, and Jean-Marie Beau**

*N*-Acetylneuraminic acid (Neu5Ac) occurs in a wide range of biologically important glycoconjugates, mostly at the terminal position of oligosaccharides attached to proteins or lipids.[1,2] It is involved in a large number of intercellular events,[2] and molecular tools containing this important motif are needed to devise reagents or probes for biological studies and applications. The α-glycosidic bond of these terminal sialyl residues is, however, fragile in vitro under very mild acidic conditions, and it is cleaved by neuraminidases in vivo. The replacement of the interglycosidic oxygen atom with a carbon atom provides C-linked analogues that are stable towards hydrolysis, as required for various applications such as Neu5Ac-containing antiviral drugs or vaccines.

We have previously established a rapid and stereoselective assembly of C-glycosides through a samarium diiodide[3] promoted Barbier reaction with glycosyl 2-pyridylsulfones without an additive.[4,5] Linhardt and co-workers showed that the procedure worked equally well with **3**, the anomeric 2-pyridylsulfone of Neu5Ac (Scheme 1),[6] as well as with the chlorides (such as **4**) and phenylsulfones of Neu5Ac and other 2-ulosonic esters.[7]

We have also reported that **2**, the anomeric 2-pyridylsulfide *N*-acetyl neuraminic acid derivative, is a useful anionic precursor in a high-yielding samarium-mediated Reformatsky approach for stereoselective α-C-sialylation.[8] All these precursors of the *N*-acetylneuraminyl–samarium(III) species are, in fact, derived from the anomeric acetates **1**. In an effort to simplify further the synthetic sequence, we report herein that these standard peracetylated intermediates, prepared 40 years ago by Kuhn and co-workers,[9] are practical *C*-sialyl donors in samarium-mediated Reformatsky coupling reactions with carbonyl compounds. The possibility of this approach was suggested by the well-documented α-deoxygenation of esters[10] and acetylated carbohydrate lactones[11] with samarium diiodide. This procedure was further devel-

[*] A. Malapelle, Dr. Z. Abdallah, Dr. G. Doisneau, Prof. J.-M. Beau
Université Paris-Sud
Institut de Chimie Moléculaire et des Matériaux associé au CNRS
Laboratoire de Synthèse de Biomolécules
91405 Orsay Cedex (France)
Fax: (+33) 1-6985-3715
E-mail: jmbeau@icmo.u-psud.fr

[**] We thank the Ministère de la Recherche for PhD grants to A.M. and Z.A.

Supporting information for this article is available on the WWW under http://www.angewandte.org or from the author.


WILEY InterScience DISCOVER SOMETHING GREAT
© 2006 Wiley-VCH Verlag GmbH & Co. KGaA, Weinheim

oped by Enholm and co-workers for α-deoxygenation/carbonyl-addition reactions of benzoylated lactones.[12] In an application with O-acetylated 2-ulosonates, Hanessian and Girard have also described an efficient and easy anomeric deoxygenation procedure by using $SmI_2$.[13] For the success of all of these reactions, additives were needed (namely, hexamethylphosphoramide (HMPA)[10–12] or ethylene glycol[13]).

Standard methyl ester formation and peracetylation of Neu5Ac with acetic anhydride/pyridine provided peracetates **1** as an α/β mixture of ≈1:4 (83% from Neu5Ac; Scheme 1).[9]

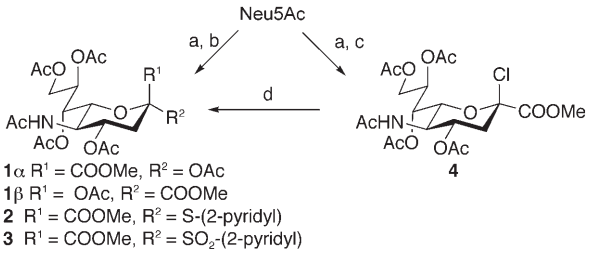


***Scheme 1.*** Synthesis of the Neu5Ac derivatives **1**. a) MeOH, Dowex $H^+$, room temperature, 24 h; b) $Ac_2O$, pyridine, room temperature, overnight; 83% from Neu5Ac; c) $HCl_g$, AcOH/AcCl (1:1), room temperature; d) CsOAc (1.5 equiv), MeCN, room temperature, 74% from Neu5Ac.

The anomers were easily separated by column chromatography to allow the examination of their individual behaviors in the reductive process. For these preliminary studies, larger amounts of the minor isomer **1α** were more conveniently obtained by cesium acetate treatment of chloride **4**, as described earlier (74% yield from Neu5Ac).[14,15]

Separate treatment of a solution of acetate **1α** or **1β** in the presence of cyclopentanone in THF at 20°C with a *freshly* prepared THF solution of $SmI_2$[16] gave the *C*-sialyl derivative **5**, with yields of 97% and 82%, respectively (Table 1, entries 1 and 2). In these experiments, reactions occurred at room temperature in the absence of any additive. However, the time needed for the reduction depended on the anomeric configuration of **1**. The equatorial acetate in **1α** reacted in about 20 min, whereas the reaction needed about 2 h to go to completion with the axial acetate in **1β**. As was expected and in agreement with our previously published results, coupling reactions with a symmetric ketone like cyclopentanone gave **5** as a single diastereomer, with an equatorial orientation of the new C–C bond (see below). Coupling with 4-*tert*-butylcyclohexanone proceeded with equal efficiency (yields of 91% and 83%; Table 1, entries 3 and 4).

Cyclohexanecarbaldehyde (2 equiv) was also a good substrate and provided the coupling products **8** in 87% and 83% yield (Table 1, entries 7 and 8). The coupling products both displayed a standard $_5C^2$-chair conformation as determined by $^1H$ NMR analysis ($J_{3ax,4}$, $J_{4,5}$, and $J_{5,6}$ values of 10.2, 11.8, and 10.5 Hz for one isomer and of 12.0, 10.5, and 10.5 Hz for the other). The expected equatorial orientation of the newly formed C–C bond at the quaternary center was indicated by the large values of $^3J_{C1,H3ax}$.[17] The rate of the acetate reduction was however too slow for coupling with an acyclic ketone such as 3-pentanone or an aliphatic aldehyde such as *n*-octanal; these provided the respective coupling products with much lower efficiency (**7**: 44 and 26% yield; Table 1, entries 5 and 6; **9**: 39 and 33% yield; Table 1, entries 9 and 10). In these reactions, reduction of the carbonyl compound became the major competing pathway.

***Table 1:*** Samarium-induced coupling of acetates **1** with carbonyl compounds.

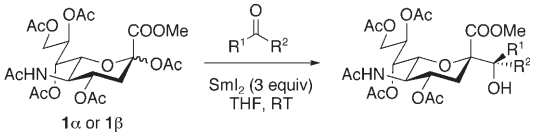


| Entry | Acetate | Carbonyl partner (reaction time) | Product: yield[a] (isomer ratio) |
|---|---|---|---|
| 1 | **1α** | cyclopentanone (0.3 h) | **5**: 97% |
| 2 | **1β** | cyclopentanone (2 h) | **5**: 82% |
| 3 | **1α** | 4-*tert*-butylcyclohexanone (0.3 h) | **6**: 91% |
| 4 | **1β** | 4-*tert*-butylcyclohexanone (2 h) | **6**: 83% |
| 5 | **1α** | 3-pentanone (0.3 h) | **7**: 44%[b] |
| 6 | **1β** | 3-pentanone (2 h) | **7**: 26%[b] |
| 7 | **1α** | cyclohexanecarbaldehyde (0.3 h) | **8**: 87% (1.25:1) |
| 8 | **1β** | cyclohexanecarbaldehyde (2 h) | **8**: 83% (1.25:1) |
| 9 | **1α** | *n*-octanal (0.3 h) | **9**: 39%[b] |
| 10 | **1β** | *n*-octanal (2 h) | **9**: 33% (1:1)[b] |

[a] Yields for isolated products after chromatography on silica gel. [b] Together with reduction product **36** (40–44%; $R^1 = H$, see Scheme 5).

With these preliminary results on the separate anomers **1**, we proceeded to investigate the use of the more practical **1α,β** synthetic mixture. Some results obtained for the reductive coupling with the anomeric 2-pyridylsulfide **2**[8] are also reported for comparison (Table 2, Scheme 2).

The $SmI_2$ treatment of **1α,β** with the same cyclic carbonyl compounds provided results essentially identical to those obtained with the separate anomers in a 2-hour reaction (entries 3 and 4 in Table 1 and entry 3 in Table 2). Under identical conditions, sulfide **2** also provided similar results, although in a very fast reaction, as observed earlier (reduction time $<1$ min; Table 2, entries 2 and 4). Cyclobutanone was also a good substrate for this reaction and provided the *C*-sialyl compound **11** (88 and 96%; Table 2, entries 5 and 6). Coupling of **1α,β** with 1,4-cyclohexanedione (1.4 equiv) provided 30% of the mono-*C*-sialyl product **12** (Table 2, entry 7), whereas sulfide **2** furnished an 89% yield of the same compound (Table 2, entry 8). Sulfide **2** also provided the bis-*C*-sialyl product **13** in a very high yield (98%) when a limiting amount of the diketone was used (0.45 equiv; Table 2, entry 9). Good coupling yields were obtained with cyclohexanecarbaldehyde (75 and 90%; Table 2, entries 10 and 11).

As noticed above with the separate acetates and *n*-octanal, coupling of **1α,β** with aldehyde **14** was not practical (26% yield of **15**; Table 2, entry 12) in comparison with the reaction with sulfide **2**, which furnished **15** in 78% yield. The

 © 2006 Wiley-VCH Verlag GmbH & Co. KGaA, Weinheim 

***Table 2:*** Samarium-induced coupling of acetates **1** and pyridylsulfide **2** with carbonyl compounds. The structural formulae of **12**–**14** and **16**–**21** can be found in Scheme 2.

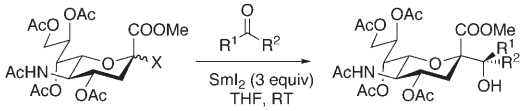


**1**α,β (X = OAc); **2** [X = αS(2-py)]

| Entry | Substrate | Carbonyl partner | Product: yield[a] (isomer ratio) |
|---|---|---|---|
| 1 | **1α,β**[b] | cyclohexanone | **10**: 79% |
| 2 | **2**[c] | cyclohexanone | **10**: 82% |
| 3 | **1α,β** | 4-*tert*-butylcyclohexanone | **6**: 98% |
| 4 | **2** | 4-*tert*-butylcyclohexanone | **6**: 96% |
| 5 | **1α,β** | cyclobutanone | **11**: 88% |
| 6 | **2** | cyclobutanone | **11**: 96% |
| 7 | **1α,β** | 1,4-cyclohexanedione[d] | **12**: 30% |
| 8 | **2** | 1,4-cyclohexanedione[d] | **12**: 89% |
| 9 | **2** | 1,4-cyclohexanedione[e] | **13**: 98% |
| 10 | **1α,β** | cyclohexanecarbaldehyde | **8**: 75% |
| 11 | **2** | cyclohexanecarbaldehyde | **8**: 90%[f] |
| 12 | **1α,β** | **14** | **15**: 26%[g] (1:1) |
| 13 | **2** | **14** | **15**: 78% |
| 14 | **1α,β** | **16** | (**17**: 56%)[h] |
| 15 | **2** | **16** | **18**: 80% (1:1) |
| 16 | **1α,β** | **19** | **20**: 30%[h] (1:1) |
| 17 | **2** | **19** | **20**: 82% (1:1) |

[a] Yields for isolated products after chromatography on silica gel. [b] Used as an α/β mixture with a ratio of 1:4; reaction for 2 h at room temperature. [c] Reaction for about 5 min at room temperature. [d] With 1.4 equivalents of 1,4-cyclohexanedione. [e] With 0.45 equivalents of 1,4-cyclohexanedione. [f] Results taken from reference [8]. [g] Together with reduction product **36** (17%; $R^1 = H$, see Scheme 5). [h] Acetates **1α/β** were recovered (53%, entry 14; 14%, entry 16) with reduction product **36** (24%, entry 14; 21%, entry 16).

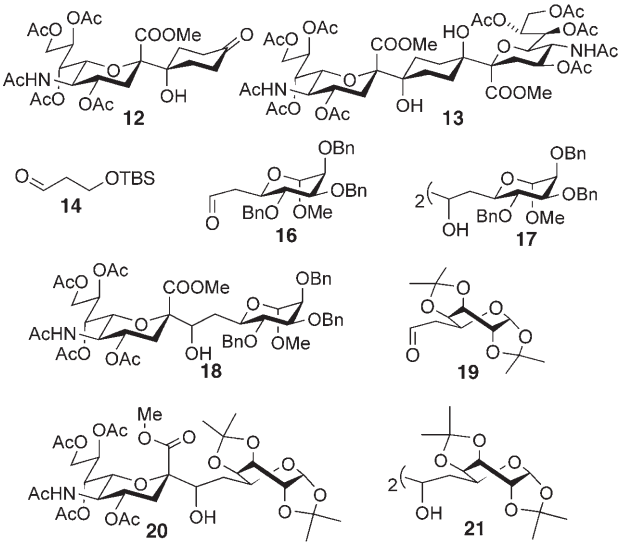


***Scheme 2.*** Formulae of some of the compounds given in Table 2.

superiority of sulfide **2** over acetates **1α,β** was also revealed by using the D-mannose-derived aldehyde **16**.[4f] No coupling occurred in the $SmI_2$-induced reaction with **1α,β**, with the reductive coupling of aldehyde **16** occurring instead to form diol **17**, whereas sulfide **2** supplied the expected compound **18** in 80% yield (Table 2, entries 14 and 15). With the D-galactose-derived aldehyde **19**,[7a] both acetates **1α,β** and sulfide **2** provided the expected compound **20** (in 30 and 82% yield, respectively, Table 2, entries 16 and 17). When acetates **1α,β** are used, the moderate yield is due to the competitive pinacol coupling of aldehyde **19** to diol **21** (30% yield).

The utility of this coupling process with acetates **1α,β** was validated in a fast elaboration of sialoside analogues **24**–**26** (Scheme 3). Coupling of **1α,β** with ketone **22** provided a

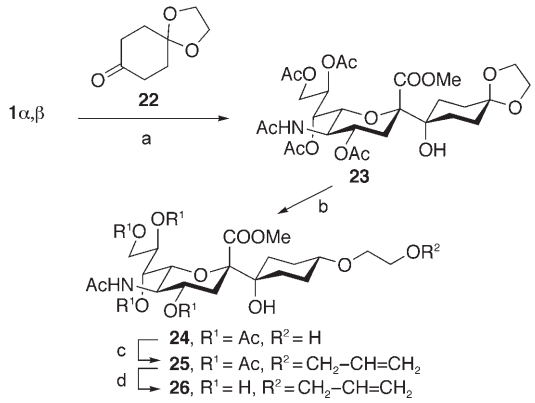


***Scheme 3.*** Synthesis of sialoside analogues. a) $SmI_2$ (3 equiv), THF, room temperature, 85%; b) $BH_3{\cdot}SMe_2$ (1.2 equiv), TMSOTf (1.2 equiv), −78 °C in $CH_2Cl_2$, 4 h, 91%; c) allyltrichloroacetimidate (2 equiv), cat. TfOH, cyclohexane/$CH_2Cl_2$ (2:1), 4 h, 62%; d) $K_2CO_3$/MeOH, room temperature, overnight, 88%. TMSOTf = trimethylsilyl trifluoromethanesulfonate.

single compound **23** (85% yield). Reductive opening of the acetal furnished selectively the equatorial product **24** (91% yield) which could be allylated to give **25** (62%) and then deprotected to form **26** (88% yield). Compounds such as **24**–**26** constitute valuable building blocks to elaborate multivalent sialosides as robust biological probes or potential inhibitors towards sialic acid binding proteins.[18]

The adequacy of other anomeric substituents was also briefly examined, with the $SmI_2$-induced coupling with cyclopentanone serving as a reference reaction (Table 3).

Anomeric α-benzoate **27** did not show an improved reduction rate compared to that with acetate **1α** (reduction in 20 min at room temperature; Table 3, entry 2), whereas the reaction with ethyl xanthate **28**[19] was as fast as with 2-pyridylsulfide **2** or its corresponding sulfone (less than 1 min at room temperature; Table 3, entries 3 and 4). Phenylsulfide **29** reacted very slowly (10–20% yield of **5** with 50% of the starting material recovered after 4 h; Table 3, entry 5) and methyl glycoside **30** was unreactive under identical conditions, even after a prolonged time in the presence of $SmI_2$ (Table 3, entry 7). Increasing the reducing power of $SmI_2$ by adding HMPA[20] or 1,3-dimethyl-3,4,5,6-tetrahydro-2(1*H*)-pyrimidinone[21] (DMPU, 8 equiv with respect to $SmI_2$) restored the reactivity towards phenylsulfide **29**; however, coupling product **5** was obtained in a low yield (25%; Table 3,

 © 2006 Wiley-VCH Verlag GmbH & Co. KGaA, Weinheim 

***Table 3:*** Samarium-induced coupling of different Neu5Ac glycosides with cyclopentanone.

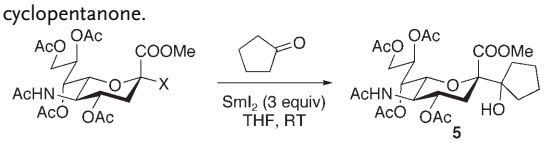


| Entry | Substrate | X | Reaction time | Yield of **5**[a] |
|---|---|---|---|---|
| 1 | **1α** | OAc | 20 min | 97% |
| 2 | **27** | OBz[b] | 20 min | 95% |
| 3 | **28** | S(CS)OEt | <1 min | 94% |
| 4 | **2** | SPy[c] | <1 min | 76% |
| 5 | **29** | SPh | 4 h | 10–20%[d] |
| 6 | **29** | SPh[e] | 2 h | 25%[f] |
| 7 | **30** | OMe[g] | 4 h | n.r.[h] |

[a] Yields for isolated products after chromatography on silica gel. [b] Bz = benzoyl. [c] Py = 2-pyridyl. [d] 50% of **29** was recovered. [e] With HMPA or DMPU (8 equiv). [f] Together with reduction product **36** (65%; $R^1$ = H, see Scheme 5). [g] Experiment done with the β anomer. [h] n.r. = not recovered. Only **30** was recovered (97%), even when DMPU (8 equiv) was added.

entry 6), together with the reduction product **36** ($R^1$ = H in Scheme 4; 65% yield).

The "room-temperature" conditions reported herein and previously with similar compounds,[6–8] which are possible with the "anion-sensitive" *O*-acetyl protecting groups and an amide proton, may suggest a radical mechanism for the crucial carbon–carbon bond formation.[22] In this report, the behavior of the acetylated Neu5Ac derivatives **1**, **2**, and **27**–**30** with different anomeric substituents also provides information on the possible mechanism. The facile reductive process of acetates **1**, which is possible without an additive, may be facilitated by the chelation of the two carbonyl groups with the samarium atom ($Sm^{II}$) with an extra complexation of the endocyclic O6 atom as shown in Scheme 4.

This scheme of tight complexation might increase the reducing ability of $SmI_2$, as most chelating agents do,[23] or facilitate the first electron transfer. It would allow a fast electron transfer within the chelate, which would also be possible with the reactive pyridylsulfide (as in **2**·**Sm** in Scheme 4) but not with the phenylsulfide or the unreactive methyl glycoside (as in **29**·**Sm** and **30**·**Sm** in Scheme 4), unless HMPA or DMPU were present (phenylsulfide **29** only). Owing to the behavior of **29** and **30** in the presence of $SmI_2$ without an additive, we would favor electron transfer in the carbonyl group of the acetate of **1** (as in **1α**·**Sm** in Scheme 4) rather than in the carbonyl group of the methyl ester (as in **29**·**Sm**/**30**·**Sm** in Scheme 4) because in the latter event, enolate **33** could also be formed by cetyl radical reduction (**34** to **35**) and β elimination of X (**35** to **33**; X = SPh or OMe).

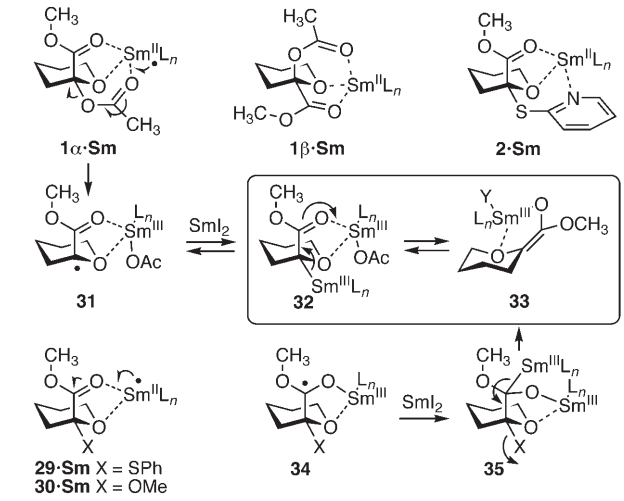


***Scheme 4.*** The proposed complexation scheme for efficient electron transfer and formation of the organosamarium intermediate (in **33**: Y = OAc from **32** or Y = I from **35**). L = ligand.

Finally, addition of $H_2O$ or $D_2O$ (8 equiv with respect to acetates **1**) to the reaction mixture before the introduction of $SmI_2$ strongly interfered with the coupling reaction with cyclobutanone (Scheme 5). This mostly provided both "protonation" products **36** and **37** in a ratio of 2:1[24] (62–64%; 70% deuterium incorporation), together with coupling product **11** (16–18%). This gives evidence that organosamarium intermediate **32** or the corresponding enolate **33** could be generated and be involved in the carbon–carbon bond forming step, provided that the presence of water does not alter the mechanism.[22e,25]

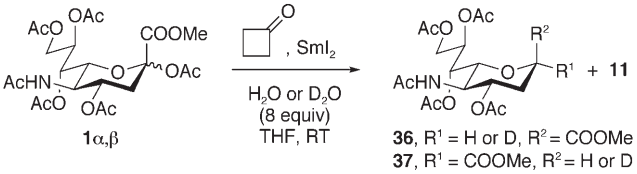


***Scheme 5.*** Samarium-induced coupling of acetates **1** with cyclobutanone in the presence of water (or $D_2O$).

In conclusion, we have shown that the reductive samariation of the peracetates of methyl *N*-acetyl-neuraminate in the presence of cyclic ketones provides a practical, straightforward, and high-yielding solution for stereoselective α-C-sialylation. Based on experimental evidence, we propose that the key carbon–carbon bond forming step occurs through an organosamarium intermediate. This procedure should prove useful in the fast synthesis of simple molecular modules containing stable bioactive sialoside mimetics for biological research.

## *Experimental Section*

**23**: A freshly prepared 0.1M solution of $SmI_2$ in THF (100 mL, 10 mmol of $SmI_2$) was added to a stirred THF (10 mL) solution mixture of acetates **1α,β** (1.77 g, 3.32 mmol) and ketone **22** (1.00 g, 6.64 mmol) at 20°C under Ar. After the mixture had been stirred for 2 h, saturated aqueous $NH_4Cl$ was added and the reaction mixture was extracted three times with $CH_2Cl_2$. The combined organic phases were washed twice with water, dried with $Na_2SO_4$, and evaporated to dryness. Flash chromatography on silica gel (toluene/acetone, 1:1) gave **23** (1.78 g, 85%): $^1$H NMR ($CDCl_3$, 360 MHz): $\delta$ = 5.62 (d, $J$(NH,5) = 9.5 Hz, 1H, NH), 5.52 (ddd, $J$(8,7) = 8.1, $J$(8,9b) = 6.6, $J$(8,9a) = 2.5 Hz, 1H, H-8), 5.39 (dd, $J$(7,8) = 8.1, $J$(7,6) = 1.1 Hz, 1H, H-7), 4.84 (ddd, $J$(4,3ax) = 11.2, $J$(4,5) = 10.4, $J$(4,3eq) = 4.5 Hz, 1H, H-4), 4.43 (dd, $J$(9a,9b) = 12.4, $J$(9a,8) = 2.5 Hz, 1H, H-9a), 4.22–3.97

 © 2006 Wiley-VCH Verlag GmbH & Co. KGaA, Weinheim 

(m, 2H, H-5,6), 4.21 (dd, $J$(9b,9a) = 12.4, $J$(9b,8) = 6.6 Hz, 1H, H-9b), 4.05 (m, 4H, $O(CH_2)_2O$), 3.89 (s, 3H, $COOCH_3$), 2.95 (s, 1H, OH), 2.58 (dd, $J$(3eq,3ax) = 12.8, $J$(3eq,4) = 4.5 Hz, 1H, H-3eq), 2.27, 2.22, 2.15, and 2.12 (4s, 12H, $OCOCH_3$), 1.96 (s, 3H, $NCOCH_3$), 1.94 (dd, $J$(3ax,3eq) = 12.8, $J$(3ax,4) = 11.2 Hz, 1H, H-3ax), 1.93–1.60 ppm (m, 8H, $CH_2$ of cyclohexyl); $^{13}$C NMR ($CDCl_3$, 90 MHz): $\delta$ = 170.8, 170.7, 170.5, 170.1, 169.9, and 169.8 (4$OCOCH_3$, $NCOCH_3$, $COOCH_3$), 108.1 (C of cyclohexyl), 85.7 (C2), 74.1 (COH), 73.1, 70.3, 68.7, 67.7 (C4, C6, C7, C8), 64.9, 63.9 ($OCH_2CH_2O$), 62.9 (C9), 52.2 ($CH_3O$), 49.0 (C5), 32.9 (C3), 29.9, 29.7, 29.2, and 28.9 (4$CH_2$ of cyclohexyl), 22.9, 21.1, 20.7, 20.6, and 20.5 ppm (4$CH_3OCO$, $CH_3CON$); MS (ES): $m/z$ 654 $[M+Na]^+$; HR-MS (ES): calcd for $C_{28}H_{41}NaNO_{15}$: 654.2368; found: 654.2383.

Received: March 27, 2006
Revised: June 13, 2006
Published online: August 9, 2006

**Keywords:** carbohydrates · glycosides · metalation · samarium · sialic acids

[1] *Sialic Acids: Chemistry, Metabolism and Function* (Ed.: R. Schauer), Cell Biology Monograph Series, Vol. 10, Springer, Vienna, **1982**.
[2] a) R. Schauer in *Carbohydrates in Chemistry and Biology*, *Vol. 3* (Eds.: B. Ernst, G. W. Hart, P. Sinaÿ), Wiley-VCH, Weinheim, **2000**, pp. 227–243; b) M. L. Allende, R. L. Proia, *Curr. Opin. Struct. Biol.* **2002**, *12*, 587; c) P. R. Crocker, *Curr. Opin. Struct. Biol.* **2002**, *12*, 609.
[3] For selected recent reviews on the use of $SmI_2$ in organic synthesis, see: a) D. J. Edmonds, D. Johnston, D. J. Procter, *Chem. Rev.* **2004**, *104*, 3371; b) H. B. Kagan, *Tetrahedron* **2003**, *59*, 10351; c) P. G. Steel, *J. Chem. Soc. Perkin Trans. 1* **2001**, 2727; d) A. Krief, A.-M. Laval, *Chem. Rev.* **1999**, *99*, 745; e) G. A. Molander, C. R. Harris, *Tetrahedron* **1998**, *54*, 3321; f) G. A. Molander, C. R. Harris, *Chem. Rev.* **1996**, *96*, 307.
[4] Neutral hexoses: a) D. Mazéas, T. Skrydstrup, O. Doumeix, J.-M. Beau, *Angew. Chem.* **1994**, *106*, 1457; *Angew. Chem. Int. Ed. Engl.* **1994**, *33*, 1383; b) D. Mazéas, T. Skrydstrup, J.-M. Beau, *Angew. Chem.* **1995**, *107*, 990; *Angew. Chem. Int. Ed. Engl.* **1995**, *34*, 909; c) T. Skrydstrup, D. Mazéas, M. Elmouchir, G. Doisneau, C. Riche, A. Chiaroni, J.-M. Beau, *Chem. Eur. J.* **1997**, *3*, 134; d) T. Skrydstrup, O. Jarreton, D. Mazéas, D. Urban, J.-M. Beau, *Chem. Eur. J.* **1998**, *4*, 655; e) O. Jarreton, T. Skrydstrup, J.-M. Beau, *Chem. Eur. J.* **1999**, *5*, 430; f) N. Miquel, G. Doisneau, J.-M. Beau, *Angew. Chem.* **2000**, *112*, 4277; *Angew. Chem. Int. Ed.* **2000**, *39*, 4111.
[5] 2-Deoxy-2-acetamido sugars: a) D. Urban, T. Skrydstrup, C. Riche, A. Chiaroni, J.-M. Beau, *Chem. Commun.* **1996**, 1883; b) D. Urban, T. Skrydstrup, J.-M. Beau, *J. Org. Chem.* **1998**, *63*, 2507; c) L. Andersen, L. M. Mikkelsen, J.-M. Beau, T. Skrydstrup, *Synlett* **1998**, 1393; d) S. Palmier, B. Vauzeilles, J.-M. Beau, *Org. Biomol. Chem.* **2003**, *1*, 1097.
[6] I. R. Vlahov, P. I. Vlahova, R. J. Linhardt, *J. Am. Chem. Soc.* **1997**, *119*, 1480.
[7] a) T. Polat, Y. Du, R. J. Linhardt, *Synlett* **1998**, 1195; b) Y. Du, R. J. Linhardt, *Carbohydr. Res.* **1998**, *309*, 161.
[8] Z. Abdallah, G. Doisneau, J.-M. Beau, *Angew. Chem.* **2003**, *115*, 5367; *Angew. Chem. Int. Ed.* **2003**, *42*, 5209.
[9] R. Kuhn, P. Lutz, D. L. MacDonald, *Chem. Ber.* **1966**, *99*, 611.
[10] K. Kusuda, J. Inanaga, M. Yamaguchi, *Tetrahedron Lett.* **1989**, *30*, 2945.
[11] a) J. Inanaga, J. Katsuki, M. Yamaguchi, *Chem. Lett.* **1991**, 1025; b) S. Hanessian, C. Girard, J. L. Chiara, *Tetrahedron Lett.* **1992**, *33*, 573.
[12] a) E. J. Enholm, S. Jiang, *Tetrahedron Lett.* **1992**, *33*, 6069; b) E. J. Enholm, S. Jiang, *Heterocycles* **1992**, *34*, 2247; c) E. J. Enholm, S. Jiang, K. Aboud, *J. Org. Chem.* **1993**, *58*, 4061.
[13] S. Hanessian, C. Girard, *Synlett* **1994**, 863.
[14] A. Marra, P. Sinaÿ, *Carbohydr. Res.* **1989**, *190*, 317.
[15] A. Lubineau, J. Le Gallic, *J. Carbohydr. Chem.* **1991**, *10*, 263.
[16] P. Girard, J.-L. Namy, H. B. Kagan, *J. Am. Chem. Soc.* **1980**, *102*, 2693.
[17] a) J. Haverkamp, T. Spoormaker, L. Dorland, J. F. G. Vliegenthart, *J. Am. Chem. Soc.* **1979**, *101*, 4851; b) D. W. Norbeck, J. B. Kramer, P. A. Lartey, *J. Org. Chem.* **1987**, *52*, 2174.
[18] a) D. Zanini, R. Roy, *J. Am. Chem. Soc.* **1997**, *119*, 2088, and references therein; b) G. B. Sigal, M. Mammen, G. Dahmann, G. M. Whitesides, *J. Am. Chem. Soc.* **1996**, *118*, 3789.
[19] A. Marra, P. Sinaÿ, *Carbohydr. Res.* **1989**, *187*, 35.
[20] J. Inanaga, M. Ishikawa, M. Yamaguchi, *Chem. Lett.* **1987**, 1485.
[21] E. Hasegawa, D. P. Curran, *J. Org. Chem.* **1993**, *58*, 5008.
[22] For mechanistic studies, see: a) H. B. Kagan, J.-L. Namy, P. Girard, *Tetrahedron* **1981**, *37*, 175; b) J.-L. Namy, J. Collin, C. Bied, H. B. Kagan, *Synlett* **1992**, 733; c) G. A. Molander, L. S. Harring, *J. Org. Chem.* **1990**, *55*, 6171; d) D. P. Curran, T. L. Fevig, M. J. Totleben, *Synlett* **1990**, 773; e) D. P. Curran, X. Gu, W. Zhang, P. Dowd, *Tetrahedron* **1997**, *53*, 9023.
[23] E. Prasad, R. A. Flowers II, *J. Am. Chem. Soc.* **2002**, *124*, 6357, and references therein.
[24] These results parallel the reduction results of Hanessian and Girard[13] when they used $SmI_2$ with ethylene glycol, which provided the two isomers **36** ($R^1$ = H) and **37** ($R^2$ = H) in a ratio of 4:1. However, when the reduction of **1** or **2** was carried out without any other electrophile, addition of a proton source ($H_2O$ or ethylene glycol) after the reduction event provided only product **36** ($R^1$ = H).
[25] As further evidence, the reaction performed in [$D_8$]THF without an electrophile provided after treatment product **36** without deuterium incorporation ($R^1$ = H). This indicates that this compound arises from the protonation of an organosamarium intermediate or the corresponding enolate.

 © 2006 Wiley-VCH Verlag GmbH & Co. KGaA, Weinheim 

*Organocatalysis*

DOI: 10.1002/anie.200601919

# N-Heterocyclic Carbene Catalyzed C–C Bond Cleavage in Redox Esterifications of Chiral Formylcyclopropanes**

*Stephanie S. Sohn and Jeffrey W. Bode**

*Dedicated to Professor Michael P. Doyle*

Ring-opening reactions of small, strained molecules translate the high degree of stereoselectivity inherent in the synthesis of diverse cyclic structures into the establishment of absolute stereochemistry in acyclic systems.[1] A disadvantage of many ring-opening processes, which are formally reduction reactions, is the necessity of stoichiometric reagents that are often expensive or toxic metals. To address this limitation, we recently developed an organocatalytic redox opening of α,β-epoxyaldehydes with concomitant oxidation of the aldehyde and subsequent esterification.[2,3] This efficient process transforms widely available, enantioenriched epoxides into a variety of value-added products, including *anti*-propionate aldol adducts under mild, practical conditions.

In seeking to extend the concept of catalytic cyclic-to-acyclic stereochemical translation of readily prepared, enantiopure starting materials, we were attracted to the recent advances made by Kunz and MacMillan on the direct, highly enantioselective synthesis of formylcyclopropanes with the commercially available organocatalyst (2*S*)-indoline-2-carboxylic acid.[4] We reasoned that an efficient method for redox esterifications that involves opening the cyclopropane unit would result in a concise approach to enantioenriched β-substituted carboxylic acid derivatives, an attractive class of chiral building blocks with few methods for their general, asymmetric preparation.[5] To achieve this transformation, however, we required the cleavage of a carbon–-carbon bond lacking heteroatom functionalities,[6] a process that normally requires strong reducing agents and vigorous conditions even in highly strained systems.[7] We now report the successful development of C–C-bond-cleaving ring-openings of formylcyclopropanes mediated by an N-heterocyclic carbene (NHC) organocatalyst, thus leading to esters and thioesters via the intermediacy of catalytically generated activated carboxylates [Eq. (1); DBU = 1,8-diazabicyclo[5.4.0]undec-7-ene, electron-withdrawing group (EWG) = ketone, ester, amide, or nitro].

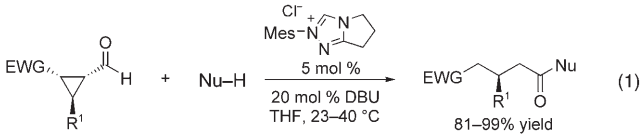


(1)

At the onset of our studies, it was unclear if the stabilized acyl anion equivalents expected to be formed by addition of an NHC catalyst to a formylcyclopropane would lead to ring-opening reactions in preference to benzoin dimerizations,[8] especially under the protic conditions mandated by redox esterification processes. We selected readily prepared, enantiomerically enriched formylcyclopropane **1** as a model substrate for reaction development. Initial efforts confirmed our trepidation that simple thiazolium- and triazolium-derived NHCs would prove inefficient or prefer competing pathways (Scheme 1). However, we were pleased to find that our mesityl-substituted triazolium salt **7**,[3b] which deters

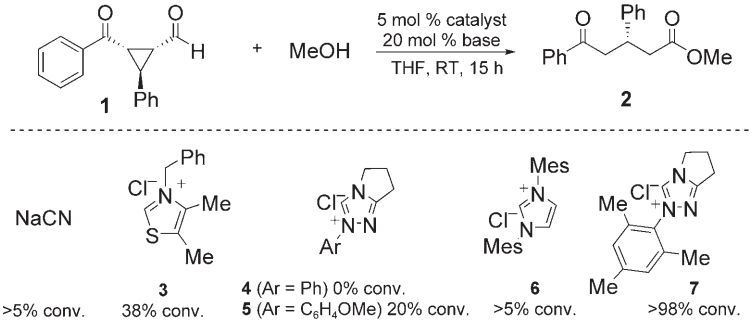


***Scheme 1.*** The influence of NHC precatalysts on catalytic redox esterifications of formylcyclopropane **1**. The starting aldehyde was recovered in reactions with lower conversion. Mes = 2,4,6-trimethylphenyl.

nucleophilic reactions of the catalytically generated acyl anion equivalent, serves as a highly active precatalyst for ring-opening esterifications of formylcyclopropanes in excellent yield. A screen of solvents, bases, reaction temperatures, and catalyst loadings revealed the optimal conditions. Weaker bases ($NEt_3$, Hünig's base) proved less efficient at ambient temperature but worked well at 60 °C. We selected THF as the optimal solvent, but comparable conversions and rates were observed in EtOAc, $CH_2Cl_2$, and toluene. Careful studies using GC and HPLC with chiral columns confirmed the preservation of the stereochemistry at the β-position.

NHC-catalyzed ring-opening reactions of trisubstituted formylcyclopropanes proceeded with a wide range of substitution patterns in the presence of 5 mol % **7** and 20 mol % DBU (Table 1). The necessary substrates were available in a single, convenient step from the corresponding sulfur ylides,

[*] S. S. Sohn, Prof. Dr. J. W. Bode
Department of Chemistry and Biochemistry
University of California
Santa Barbara, CA (USA)
Fax: (+1) 805-893-4120
E-mail: bode@chem.ucsb.edu
Homepage: http://www.chem.ucsb.edu/~bodegroup/

[**] This study was supported by the National Science Foundation (CHE-0449587) and the California Cancer Research Coordinating Committee. J.W.B. is grateful to Amgen and Richard and Leslie Anderson for additional support. We are grateful to Sean Riznikove, John Unger, and Bruce Lipshutz (UCSB) for assistance with the chiral GC analyses.

Supporting information for this article is available on the WWW under http://www.angewandte.org or from the author.

 © 2006 Wiley-VCH Verlag GmbH & Co. KGaA, Weinheim 

***Table 1:*** NHC-catalyzed redox esterifications of chiral, enantiomerically enriched formylcyclopropanes.[a]

| Entry | RCHO | NuH | Product | *T* [°C] | *ee* [%] | Yield [%][b] |
|---|---|---|---|---|---|---|
| 1 | 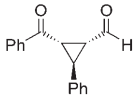 | MeOH | 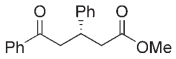 | 23 | 89[c] | 90 |
| | | | | | 89[d] | |
| 2 | 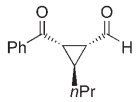 | MeOH | 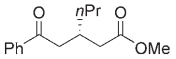 | 40 | 93[c] | 87 |
| | | | | | 90[d] | |
| 3[d] | 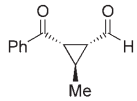 | MeOH | 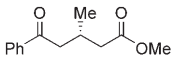 | 40 | 83[c] | 84 |
| | | | | | 77[d,e] | |
| 4 | 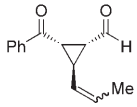 | MeOH | 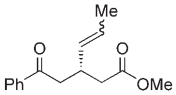 | 40 | 83[c] | 96 |
| | | | | | 81[d] | |
| 5 | 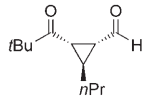 | MeOH | 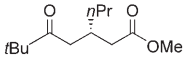 | 40 | 93[c,e] | 95 |
| 6 | 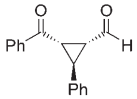 | $C_{12}H_{25}SH$ | 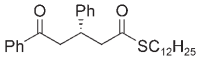 | 23 | 88[c] | 99 |
| | | | | | 88[d] | |
| 7[f] | 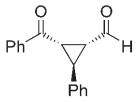 | $H_2O$ | 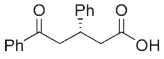 | 23 | 88[c] | 92 |
| | | | | | 87[d] | |

[a] Unless otherwise indicated, all reactions were performed on a 0.2–0.8-mmol scale at 0.5 M in THF with 5 mol% **7** and 20 mol% DBU for 15 h. [b] Yields of the isolated products following chromatography. [c] The *ee* values were assessed by chiral GC or HPLC analysis of the major diastereomer of the starting cyclopropane. [d] The *ee* values were assessed by chiral HPLC or GC analysis of the product ester. [e] Minor cyclopropane diastereomer (≈10%) was present in the starting aldehyde. [f] DBU = 1.2 equiv.

unsaturated aldehydes, and a commercially available amino acid catalyst, thus rendering the two-step MacMillan cyclopropanation/redox ring-opening reaction a highly efficient method for the preparation of acyclic, enantiomerically enriched β-substituted carboxylic acid derivatives. Importantly, this strategy is amenable to a full range of substituent types, including aromatic, aliphatic, and unsaturated moieties. Although we have focused on alcohol nucleophiles, thiols also proved to be highly reactive, thus leading to synthetically useful thioesters poised for further transformation (Table 1, entry 6).[9] Water, in conjunction with 1.2 equivalents of DBU, made possible the direct preparation of the corresponding acid (Table 1, entry 7). At the present stage of development, attempts to use primary or secondary amine nucleophiles led to complex reaction mixtures.

We prepared a range of formylcyclopropanes bearing electron-deficient functional groups to probe the requirements for an electron sink in the cyclopropane substrates (Table 2). These findings suggest a wide scope for interfacing this process with emerging methods for the catalytic, enantioselective synthesis of chiral formylcyclopropanes.[10–12]

The NHC-catalyzed ring-opening reaction leads to the formation of enolate **9**.[13] Under our present conditions, this species is most likely quenched by rapid proton transfer to lead to a more stabilized, catalyst-bound enolate **10** (or its corresponding enol), which undergoes protonation and tautomerization to form acyl triazolium activated carboxylate **11** (Scheme 2). A reaction performed with five equivalents of MeOD resulted in the quantitative incorporation of a single deuterium atom, as a mixture of diastereomers, adjacent to the ketone moiety. Quenching the reaction at partial conversion leads to the recovery of the starting aldehyde deuterated at the acyl carbon atom, thus demonstrating that the NHC catalyst can react reversibly with the formylcyclopropane. These observations would be consistent with a hydride-shift mechanism; however, an experiment in which an enantioenriched substrate gave a racemic product currently disfavors this pathway, at least for the substitution pattern examined.[14]

In summary, we have described the first NHC-organocatalyzed C–C bond-cleavage reaction that is useful for the synthesis of enantiomerically enriched esters and thioesters

 © 2006 Wiley-VCH Verlag GmbH & Co. KGaA, Weinheim 

***Table 2:*** Further scope of NHC-catalyzed redox esterifications of formylcyclopropanes.[a]

| Entry | RCHO | NuH | Product | *T* [°C] | Yield[b] [%] |
|---|---|---|---|---|---|
| 1 | 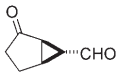 | $C_{12}H_{25}SH$ | 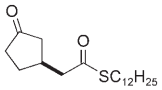 | 40 | 81 |
| 2 | 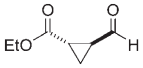 | MeOH | 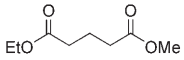 | 23 | 95 |
| 3[d] | 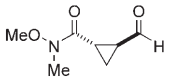 | MeOH | 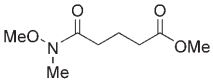 | 23 | 98 |
| 4 | 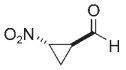 | MeOH | 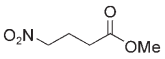 | 23 | 90 |
| 5 | 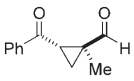 | $C_{12}H_{25}SH$ | 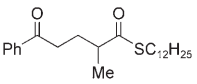 | 23 | 95 |
| 6 | 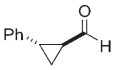 | MeOH | [c] | 60 | – |

[a] Unless otherwise indicated, all reactions were performed on a 0.2–0.8-mmol scale at 0.5 M in THF with 5 mol% **7** and 20 mol% DBU for 15 h. All the starting aldehydes shown in this table were used as racemic mixtures. [b] Yield of the isolated products following chromatography. [c] Only the starting material and benzoin dimer were observed.

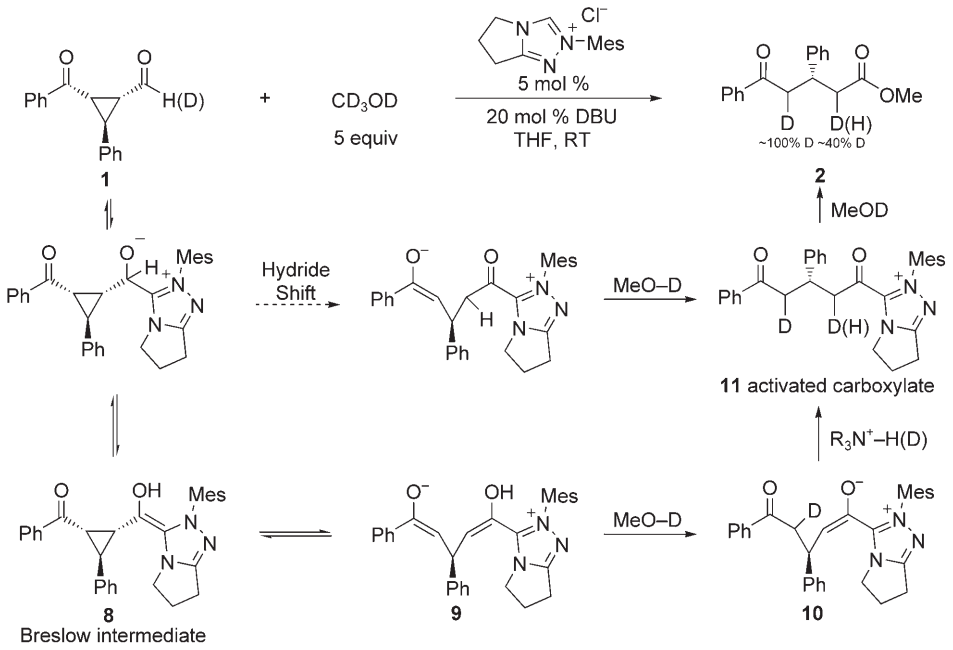


***Scheme 2.*** Reaction pathways for NHC-catalyzed redox reactions of formylcyclopropanes.

from readily available chiral formylcyclopropanes. The overall two-step process for the synthesis of enantioenriched carboxylic acid derivatives is notable for proceeding from simple starting materials under mild, nearly neutral conditions without reagents or reaction by-products.

Received: May 15, 2006
Published online: July 26, 2006

**Keywords:** esterifications · N-heterocyclic carbenes · organocatalysis · ring-opening · synthetic methods

[1] E. J. Corey, X.-M. Cheng, *The Logic of Chemical Synthesis*, Wiley, New York, **1995**.
[2] a) K. Y.-K. Chow, J. W. Bode, *J. Am. Chem. Soc.* **2004**, *126*, 8126–8127; b) K. Zeitler, *Angew. Chem.* **2005**, *117*, 7674–7678; *Angew. Chem. Int. Ed.* **2005**, *44*, 7506–7510.
[3] For other recent examples of organocatalyzed redox esterifications, see: a) N. T. Reynolds, J. Read de Alaniz, T. Rovis, *J. Am. Chem. Soc.* **2004**, *126*, 9518–9519; b) S. S. Sohn, J. W. Bode, *Org. Lett.* **2005**, *7*, 3873–3876; c) A. Chan, K. A. Scheidt, *Org. Lett.* **2005**, *7*, 905–908; d) K. Zeitler, *Org. Lett.* **2006**, *8*, 637–640.
[4] R. K. Kunz, D. W. C. MacMillan, *J. Am. Chem. Soc.* **2005**, *127*, 3240–3241.
[5] R. Shintani, G. C. Fu, *Angew. Chem.* **2002**, *114*, 1099–1101; *Angew. Chem. Int. Ed.* **2002**, *41*, 1057–1059.
[6] Cyclopropanes bearing both an electron-withdrawing group and a heteroatomic functionality, commonly known as donor–acceptor cyclopropanes, undergo a wide range of facile and useful ring opening reactions; for reviews, see: a) H.-U. Reissig, R. Zimmer, *Chem. Rev.* **2003**, *103*, 1151–1196; b) M. Yu, B. L. Pagenkopf, *Tetrahedron* **2005**, *61*, 321–347.
[7] a) W. G. Dauben, E. J. Deviny, *J. Org. Chem.* **1966**, *31*, 3794–3798; b) R. A. Batey, W. B. Motherwell, *Tetrahedron Lett.* **1991**, *32*, 6649–6652.
[8] a) "The Benzoin and Related Acyl Anion Equivalent Reactions": A. Hassner, K. M. L. Rai in *Comprehensive Organic Synthesis* (Eds.: B. M. Trost, I. Fleming), Pergamon, Oxford, **1991**, pp. 1, 541–577; b) D. Enders, T. Balensiefer, *Acc. Chem. Res.* **2004**, *37*, 534–541.
[9] a) H. Tokuyama, S. Yososhima, T. Yamashita, T. Fukuyama, *Tetrahedron Lett.* **1998**, *39*, 3189–3192; b) L. S. Liebeskind, J. Srogl, *J. Am. Chem. Soc.* **2000**, *122*, 11260–11261.
[10] a) C. D. Papageorgiou, S. V. Ley, M. Gaunt, *Angew. Chem.* **2003**, *115*, 852–855; *Angew. Chem. Int. Ed.* **2003**, *42*, 828–831; b) C. D. Papageorgiou, M. A. Cubillo de Dios, S. V. Ley, M. Gaunt, *Angew. Chem.* **2004**, *116*, 4741–4744; *Angew. Chem. Int. Ed.* **2004**, *43*, 4641–4644; c) N. Bremeyer, S. C. Smith, S. V. Ley, M. Gaunt, *Angew. Chem.* **2004**, *116*, 2735–2738; *Angew. Chem. Int. Ed.* **2004**, *43*, 2681–2684.

 © 2006 Wiley-VCH Verlag GmbH & Co. KGaA, Weinheim 

[11] a) C. A. Risatti, R. E. Taylor, *Angew. Chem.* **2004**, *116*, 6839 – 6840; *Angew. Chem. Int. Ed.* **2004**, *43*, 6671 – 6672; b) V. K. Aggarwal, E. Alonso, G. Fang, M. Ferrara, G. Hynd, M. Porcelloni, *Angew. Chem.* **2001**, *113*, 1482 – 1485; *Angew. Chem. Int. Ed.* **2001**, *40*, 1433 – 1436.

[12] Decomposition of diazocarbonyl compounds with chiral metal catalysts provides a versatile entry to enantioenriched cyclopropanes that can be readily transformed into chiral formylcyclopropanes; for selected reviews, see: a) M. P. Doyle, M. A. McKervey, T. Ye, *Modern Catalytic Methods for Organic Syntheses with Diazo Compounds: From Cyclopropanes to Ylides*, Wiley, New York, **1998**; b) M. P. Doyle, D. C. Forbes, *Chem. Rev.* **1998**, *98*, 911 – 936.

[13] For elegant, metal-promoted C–C bond-forming reactions from acyl cyclopropanes; see, for example: a) S. J. Danishefsky, *Acc. Chem. Res.* **1979**, *12*, 66 – 72; b) P. B. Alper, C. Meyers, A. Lerchner, D. R. Siegel, E. M. Carreira, *Angew. Chem.* **1999**, *111*, 3131 – 3134; *Angew. Chem. Int. Ed.* **1999**, *38*, 3186 – 3189; c) M. Lautens, W. Han, *J. Am. Chem. Soc.* **2002**, *124*, 6312 – 6316; d) I. S. Young, M. S. Kerr, *Angew. Chem.* **2003**, *115*, 3379 – 3381; *Angew. Chem. Int. Ed.* **2003**, *42*, 3023 – 3026; e) L. Liu, J. Montgomery, *J. Am. Chem. Soc.* **2006**, *128*, 5348 – 5349.

[14] The enantiomerically enriched substrate was prepared by a chiral NHC-catalyzed kinetic resolution of a racemic mixture of formylcyclopropanes; further studies on the use of chiral NHCs for the enantioselective transformation of formylcyclopropanes will be reported in due course.

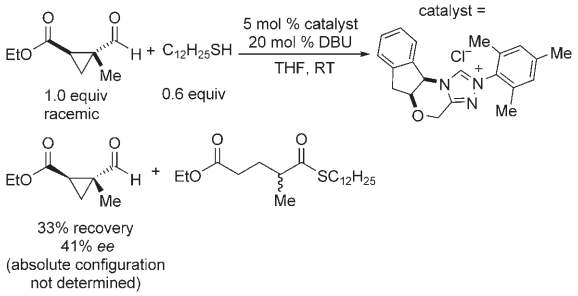


 © 2006 Wiley-VCH Verlag GmbH & Co. KGaA, Weinheim 

Asymmetric Synthesis

DOI: 10.1002/anie.200602129

# Enantioselective Catalytic Intramolecular Cyclopropanation using Modified Cinchona Alkaloid Organocatalysts**

*Carin C. C. Johansson, Nadine Bremeyer, Steven V. Ley, Dafydd R. Owen, Stephen C. Smith, and Matthew J. Gaunt**

New asymmetric methods to generate the cyclopropane motif have attracted widespread attention from the synthetic community owing to their ubiquitous presence in a diverse range of natural products and their crucial role in the mode of action of many therapeutic agents.[1] Furthermore, the rigid structure and strain-driven reactivity make them attractive intermediates in complex molecule synthesis.[2] Because of these important properties and the need for efficient methods for their stereoselective formation, the synthesis of cyclopropane-containing molecules has become a platform for the development of new asymmetric catalytic processes.[3] Notably, in the last few years numerous metal-catalyzed and organocatalytic intermolecular cyclopropanation reactions have been reported that enable the generation of discrete three-membered ring systems with high diastereo- and enantioselectivity.[4] In contrast, there are few corresponding catalytic asymmetric intramolecular reactions. Although recently a number of catalytic diastereoselective intramolecular cyclopropanation processes have been reported,[5] only methods that exploit the metal-catalyzed decomposition of α-diazo-carbonyl compounds lead to a general enantioselective assembly of [*n*.1.0]-bicycloalkane frameworks.[6] The development of a new catalytic enantioselective intramolecular cyclopropanation method would be a valuable tool for the synthetic chemist and would further aid the quest for novel

[*] C. C. C. Johansson, Dr. N. Bremeyer, Prof. Dr. S. V. Ley, Dr. M. J. Gaunt
Department of Chemistry
University of Cambridge
Lensfield Road, Cambridge CB21EW (UK)
Fax: (+44) 1223-336362
E-mail: mjg32@cam.ac.uk

Dr. D. R. Owen
Pfizer Global Research and Development
Sandwich, Kent CT13 9NJ (UK)

Dr. S. C. Smith
Syngenta Jealotts Hill International Research Centre
Bracknell, Berkshire RG42 6EY (UK)

[**] We gratefully acknowledge Pfizer Ltd (Sandwich) for a PhD studentship (C.C.C.J.), Syngenta for a Case Award (N.B.), Novartis for a Research Fellowship (S.V.L.), the Royal Society for University Research Fellowship (M.J.G.), and the EPSRC Mass Spectrometry service at the University of Swansea.

Supporting information for this article is available on the WWW under http://www.angewandte.org or from the author.


WILEY InterScience DISCOVER SOMETHING GREAT
© 2006 Wiley-VCH Verlag GmbH & Co. KGaA, Weinheim

ways to efficiently assemble architecturally complex molecules.[7]

Herein, we describe the development of an organocatalytic enantioselective intramolecular cyclopropanation reaction via ammonium ylides that forms [4.1.0]-bicycloalkanes with high stereoselectivity. The process is catalyzed by novel cinchona alkaloids that were developed through a mechanism-guided design strategy and produce the products in excellent yields and as single diastereomers and with *ee* values usually over 95% (Scheme 1).

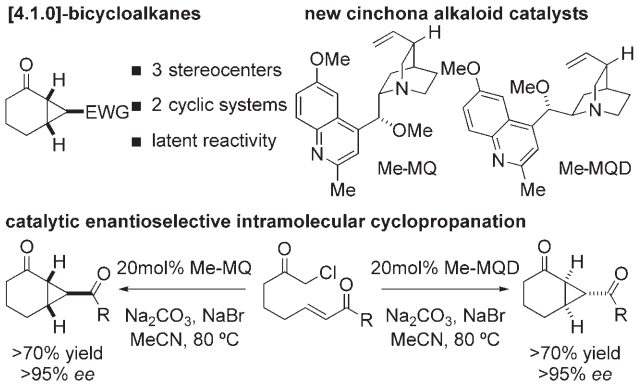


***Scheme 1.*** Enantioselective organocatalytic cyclopropanation. EWG = electron-withdrawing group.

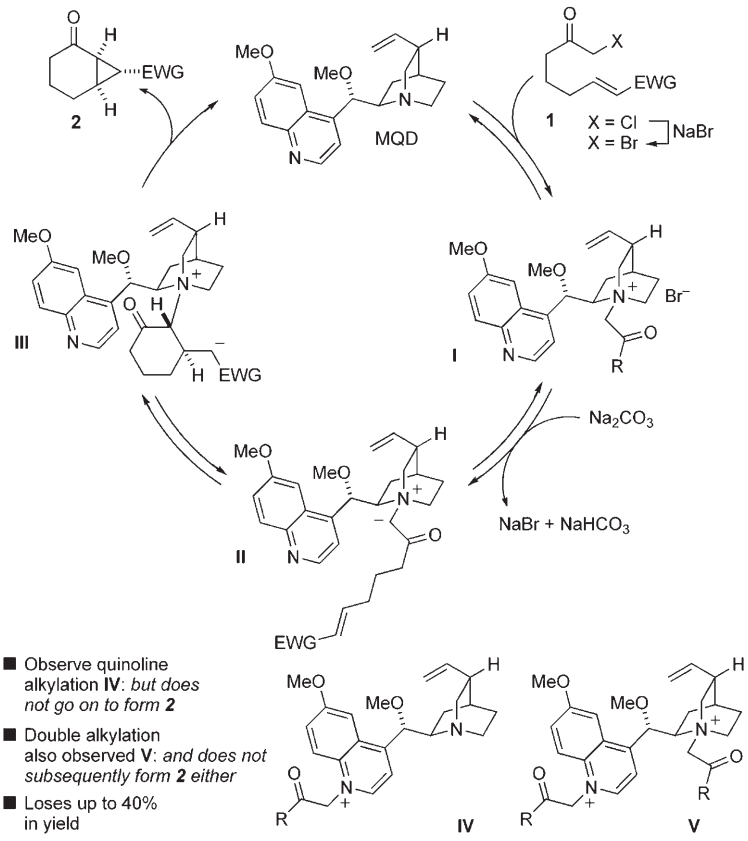


***Scheme 2.*** Catalytic cycle for intramolecular cyclopropanation.

We recently reported that an intramolecular cyclopropanation reaction could be catalyzed by the nucleophilic amine 1,4-diazabicyclo[2.2.2]octane (DABCO). When we replaced DABCO with a catalytic quantity of the chiral quinidine derivative 9-*O*-methylquinidine (MQD; MQ = 9-*O*-methylquinine), the cyclopropane was formed with an excellent *ee* value of 94%, although in poor yield.[8] The corresponding quinine catalyst gave similar results when producing the opposite enantiomer, and frustratingly all attempts to improve the yield and maintain the *ee* value through variation of the conditions were met with failure. It was notable during these optimization studies that in the reaction of **1a** with 20 mol% of the MQD catalyst it was not possible to quantitatively reisolate the catalyst at the end of the process.

We speculated the catalyst was being derailed from its desired mechanistic pathway, thus resulting in a deleterious effect on the yield of the cyclopropane (−)-**2a**. The catalytic cycle for the enantioselective intramolecular cyclopropanation initially involves Finkelstein substitution at the chloroketone unit with sodium bromide (Scheme 2). Displacement of the bromide with the alkaloid catalyst forms the quaternary ammonium salt **I**, which undergoes deprotonation with sodium carbonate to the ylide-type species **II**. Intramolecular conjugate addition forms a new intermediate **III** and subsequently the cyclopropane **2**, thus expelling the catalyst MQD to restart the cycle. Therefore, to investigate the poor yield in this process we analyzed a reaction that was carried out until 60% conversion of the starting material was achieved. From this we could identify the expected salt **I**; however, a complex combination of salts was also obtained. Although we were not able to purify them, we speculate these intermediates result from alkylation at the quinoline nitrogen atom of **IV** and both nitrogen atoms of the alkaloid catalyst **V**.[9a] Importantly, no further cyclopropanation was observed when these salts were resubjected to the reactions conditions. This behavior suggested that the proposed side reaction at the quinoline nitrogen atom consumed both the catalyst and starting material and was responsible for the poor yield in the reaction.[9b]

We therefore speculated that a modified catalyst with substitution at the C2′ position on the quinoline ring would render the nitrogen atom inert and should inhibit this problematic reaction.[10] Towards the synthesis of these catalysts, we found that treatment of the cinchona alkaloid catalysts MQD and MQ with methyl lithium in diethyl ether at room temperature followed by exposure to air or iodine afforded 2′-methyl-9-*O*-methylquinine (Me-MQ) and 2′-methyl-9-*O*-methylquinidine (Me-MQD) in good yield (Scheme 3).

The modified cinchona catalysts were tested in the intramolecular cyclopropanation, and to our delight use of the Me-MQD catalyst resulted in the formation of (−)-**2a** in a high yield (88%) with 97% *ee* (Scheme 4). The Me-MQ catalyst also improved the yield of the reaction to 84%, again with 97% *ee* of the opposite isomer (+)-**2a**.[11] We found that the reaction was most effective when 20 mol% of the cinchona alkaloid catalyst was used.

We next investigated the scope and limitations of this new catalytic asymmetric process. The reaction worked on a range

 © 2006 Wiley-VCH Verlag GmbH & Co. KGaA, Weinheim 

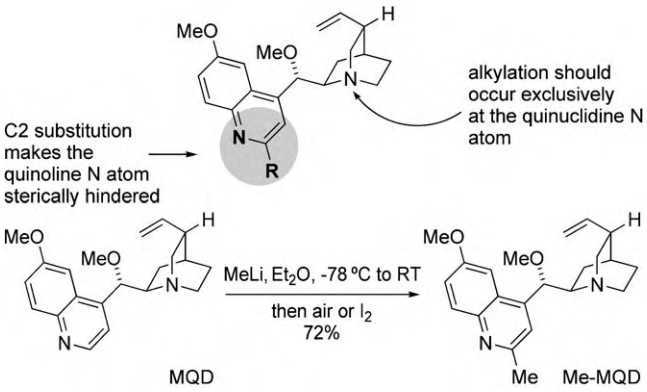


***Scheme 3.*** Synthesis of modified cinchona alkaloid organocatalysts.

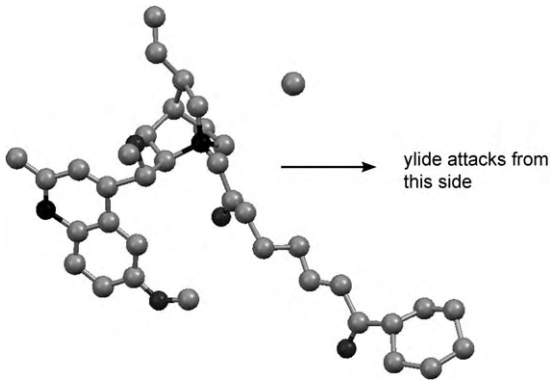


***Figure 1.*** X-ray crystal structure of a Me-MQD salt, **1c**.

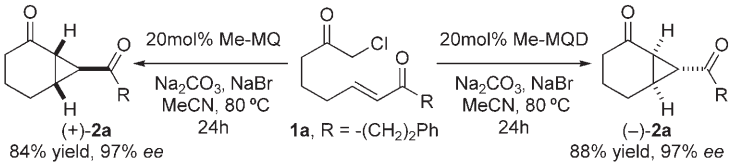


***Scheme 4.*** Cyclopropanation with modified cinchona catalysts.

of systems as shown in Table 1.[12] Enones were the best substrates for this reaction, and a range of substituents could be tolerated, including alkyl (branched and unbranched; entries 1–3 and 10–12), aryl (electron-rich and electron-deficient substituents; entries 4–6 and 13–15) and heteroaryl motifs (entries 7 and 16). In all cases, a single diastereomer was observed. Yields were generally greater than 70%, the enantiomeric excess was >95% in almost all cases, and the bicycloalkanes could be accessed as either enantiomer depending on whether the Me-MQ or Me-MQD catalyst was used. Although the catalytic process works well for the formation of [4.1.0]-bicycloalkanes, the process is unsuccessful under these conditions for the corresponding [3.1.0] system. Formation of a heterocyclic amide product could be achieved with excellent enantiomeric excess, although the turnover in the reaction was surprisingly poor (entry 8). The reaction also works well when the enone is replaced with an α,β-unsaturated diimide (entries 9 and 18), thus providing convenient access to substrates with higher oxidation states. This new enantioselective organocatalytic process represents a facile and efficient method for the synthesis of these useful functionalized molecules in a high-yielding and stereocontrolled manner.

With an efficient new process in hand we investigated the origin of the enantioselectivity. A crystal structure of (+)-**2e** provided the absolute configuration of the cyclopropanes from the quinine series, and the opposite rotation of (−)-**2e** confirmed that the quinidine-based catalysts gave the other enantiomer.[12] Stirring bromoketone **1c** with one equivalent of Me-MQD in acetonitrile afforded the corresponding salt intermediate **1c**, which was crystallized from the same solvent, thus enabling analysis of the structure by X-ray diffraction (Figure 1). This study showed that the ammonium salt adopts a conformation that would give a *Z* enolate on deprotonation with the sodium carbonate. Although we are assuming that the structure suggested by the X-ray diffraction is indeed related to the active conformation in solution, it does allow us to propose a model that is consistent with the formation of the observed enantiomer (Scheme 5). Interestingly, from this model the required enantiomer will form from intramolecular conjugate addition through a boat-type transition state.

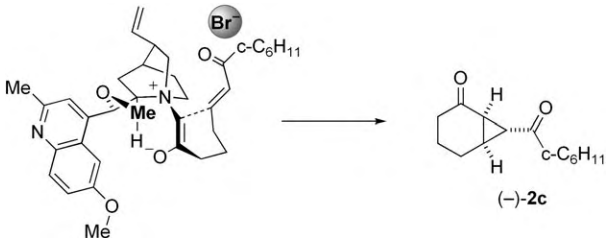


***Scheme 5.*** Proposed origin of enantioselectivity.

Having demonstrated the effectiveness of our new enantioselective organocatalytic cyclopropanation process we turned our attention towards its application in complex molecule synthesis. We were intrigued by the possibility of using these readily accessible cyclopropanes as immediate precursors to polycyclic natural products. Of particular interest were structures such as guanacastapene A[13] and rameswaralide,[14] targets of significant biological interest. Furthermore, these natural products have a common 5–7–6 tricyclic framework, and we envisioned that these structures could be rapidly accessed through our organocatalytic cyclopropanation tactic and an intramolecular metal-catalyzed [5+2] cycloaddition reaction similar to that reported by Trost et al.[15] Accordingly, alkynyl vinyl cyclopropane **5** was synthesized from the corresponding aldehyde through a Wittig olefination. We were able to isolate both the *Z* and *E* isomers from this olefination, which was important as we speculated that the olefin isomers would lead to different diastereomers in the [5+2] cycloadditon. Accordingly, the treatment of (*Z*)-**5** with the ruthenium catalyst **6**[15a,b,16] surprisingly afforded none of the [5+2] cycloaddition prod-

 © 2006 Wiley-VCH Verlag GmbH & Co. KGaA, Weinheim 

***Table 1:*** Scope of the catalytic enantioselective intramolecular cyclopropanation reaction.

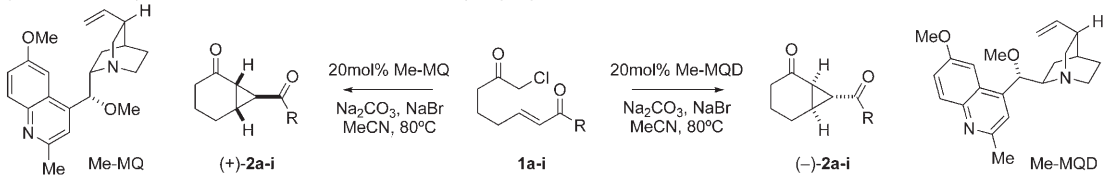


| Entry[a] | | Product | Yield[b] [%] | *ee* [%] | Entry[a] | | Product | Yield[b] [%] | *ee* [%] |
|---|---|---|---|---|---|---|---|---|---|
| 1 | (+)-**2a** | 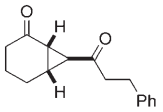 | 84 | 97 | 10 | (−)-**2a** | 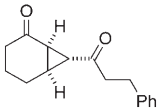 | 75 | 93 |
| 2 | (+)-**2b** | 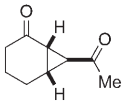 | 68 | 98 | 11 | (−)-**2b** | 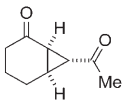 | 65 | 99 |
| 3 | (+)-**2c** | 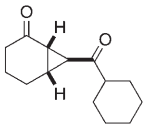 | 79 | 95 | 12 | (−)-**2c** | 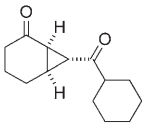 | 71 | 99 |
| 4 | (+)-**2d** | 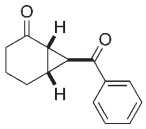 | 78 | 98 | 13 | (−)-**2d** | 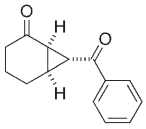 | 85 | 98 |
| 5 | (+)-**2e** | 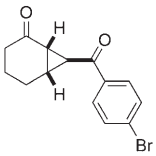 | 83 | 96 | 14 | (−)-**2e** | 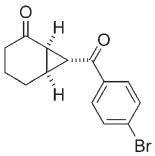 | 88 | 99 |
| 6 | (+)-**2f** | 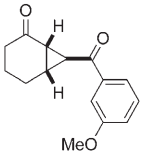 | 77 | 99 | 15 | (−)-**2f** | 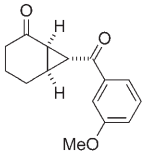 | 83 | 99 |
| 7 | (+)-**2g** | 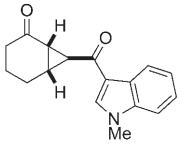 | 95 | 98 | 16 | (−)-**2g** | 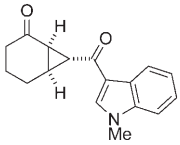 | 85 | 99 |
| 8[c] | (+)-**2h** | 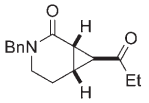 | 27 | 97 | 17[d] | (−)-**2h** | 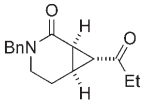 | n.d. | n.d. |
| 9 | (+)-**2i** | 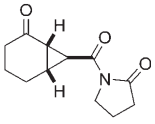 | 77 | 99 | 18 | (−)-**2i** | 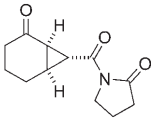 | 87 | 99 |

[a] Reactions run for 36 h. [b] Yield of the isolated product after chromatography. [c] One equivalent of catalyst was used. [d] Reaction not carried out.

uct, thus returning only the starting material. However, treatment of (*E*)-**5** with the same catalyst **6** led to the 5–7–6 ring system as the all *syn*-diastereomer **7**, which resembles the core of rameswaralide.[15a,b] We are further investigating the [5+2] cycloaddition of (*Z*)-**5**, as this process would form the *anti* relationship present in guanacastapene A. However, it is noteworthy that we can assemble the polycyclic framework present in many natural products from readily available starting materials in only four steps[17] by using three catalytic operations that control the installation of five C–C bonds and three stereocenters (Scheme 6).

In summary, we have developed a highly enantioselective catalytic intramolecular cyclopropanation process that uses modified cinchona alkaloids to generate the desired functionalized [4.1.0]-bicycloheptanes in excellent yields and enantioselectivities. The new catalysts contain an alkyl substituent at the C2′ position, thus preventing the quinoline nitrogen atom from interfering in the reaction. We are currently investigat-

 © 2006 Wiley-VCH Verlag GmbH & Co. KGaA, Weinheim 

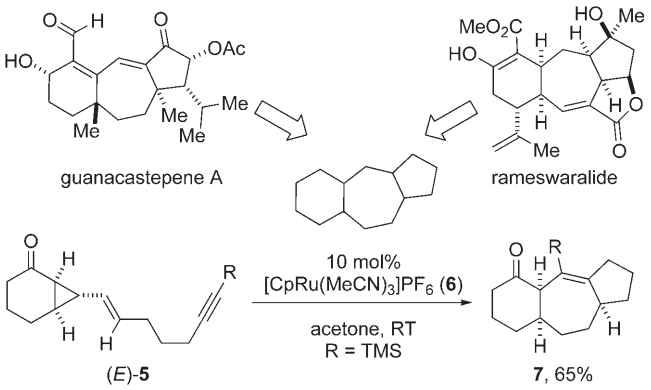


***Scheme 6.*** Catalytic elaboration of [4.1.0]-bicycloalkenes in complex molecule synthesis. Cp = cyclopentadienyl, TMS = trimethylsilyl.

ing the application of this new catalytic reaction in the synthesis of architecturally complex natural products.

## *Experimental Section*

The cinchona alkaloid catalyst (20 mol %) was added to a mixture of the chloroketone **1** (1.0 equiv), sodium bromide (0.25 equiv), and sodium carbonate (1.3 equiv) in anhydrous acetonitrile (0.1M), and the reaction mixture was stirred at 80 °C for 24–36 h until complete, as shown by TLC and LC–mass-spectrometric analysis. The reaction was concentrated and diluted with diethyl ether before filtering through a pad of silica. After concentration of the filtrate the residue was purified by flash column chromatography on silica gel to afford the [4.1.0]-bicycloalkane.

Received: May 28, 2006
Published online: August 4, 2006

**Keywords:** asymmetric synthesis · cinchona alkaloids · cyclopropanation · intramolecular reactions · organocatalysis

[1] a) H.-U. Reissig, R. Zimmer, *Chem. Rev.* **2003**, *103*, 1151; b) J. Pietruszka, *Chem. Rev.* **2003**, *103*, 1051.
[2] W. A. Donaldson, *Tetrahedron* **2001**, *57*, 8589.
[3] For a review, see: H. Lebel, J.-F. Marcoux, C. Molinaro, A. B. Charette, *Chem. Rev.* **2003**, *103*, 977.
[4] For catalytic asymmetric intermolecular cyclopropanation reactions, see: a) B. Moreau, A. B. Charette, *J. Am. Chem. Soc.* **2005**, *127*, 18014; b) M. J. Johansson, D. J. Gorin, S. T. Staben, F. D. Toste, *J. Am. Chem. Soc.* **2005**, *127*, 18002; c) R. K. Kunz, D. W. C. MacMillan, *J. Am. Chem. Soc.* **2005**, *127*, 3240; d) W.-W. Lioa, K. Li, Y. Tang, *J. Am. Chem. Soc.* **2003**, *125*, 13030; e) V. K. Aggarwal, E. Alonso, G. Hynd, K. M. Lydon, M. J. Palmer, M. Porcelloni, J. R. Studley, *Angew. Chem.* **2001**, *113*, 1482; *Angew. Chem. Int. Ed.* **2001**, *40*, 1433; f) C. D. Papageorgiou, M. A. Cubilos de Dios, S. V. Ley, M. J. Gaunt, *Angew. Chem.* **2004**, *116*, 4741; *Angew. Chem. Int. Ed.* **2004**, *43*, 4641.
[5] For examples of catalytic intramolecular cyclopropanation strategies, see: a) A. Fürstner, H. Szilat, F. Steltzer, *J. Am. Chem. Soc.* **2000**, *122*, 6785; b) Y. Harrak, C. Blaszykowski, M. Bernard, K. Cariou, E. Mainetti, V. Mouriers, A. L. Dhimane, L. Fensterbank, M. Malacria, *J. Am. Chem. Soc.* **2004**, *126*, 8656; c) M. R. Luzung, J. P. Markham, F. D. Toste, *J. Am. Chem. Soc.* **2004**, *126*, 10858; d) D. Yang, Q. Gao. C.-S. Lee, K.-K. Cheung, *Org. Lett.* **2002**, *4*, 3271; e) T. Miura, T. Sasaki, T. Harumashi, M. Murakami, *J. Am. Chem. Soc.* **2006**, *128*, 2516.
[6] a) G. Maas, *Chem. Soc. Rev.* **2004**, *3*, 183; b) M. Honma, T. Sawada, Y. Fujisawa, M. Utsugi, H. Watanabe, A. Umino, T. Matsumura, T. Hagihara, M. Takano, M. Nakada, *J. Am. Chem. Soc.* **2003**, *125*, 2860; c) it is also possible to form [*n*.1.0]-bicyclic motifs through the intermolecular cyclopropanation of cyclic alkenes; for examples, see: M. P. Doyle, D. C. Forbes, *Chem. Rev.* **1998**, *98*, 911.
[7] For examples of using strain-driven reactivity, see: a) R. Sarpong, J. T. Su, B. M. Stoltz, *J. Am. Chem. Soc.* **2003**, *125*, 13624; b) P. A. Wender, C. O. Husfild, E. Langkopf, J. Love, *J. Am. Chem. Soc.* **1998**, *120*, 1940.
[8] a) N. Bremeyer, S. C. Smith, S. V. Ley, M. J. Gaunt, *Angew. Chem.* **2004**, *116*, 2735; *Angew. Chem. Int. Ed.* **2004**, *43*, 2681.
[9] a) Based on LC–mass-spectrometric analysis of the mixture; b) quinoline **A**, when treated with **1a** and NaBr in MeCN at 80 °C, leads to an intractable mixture of products and consumes all the starting material; quinoline **B** does not react with **1a** under the same conditions, thus both materials are returned untouched; no cyclopropanantion was observed in these reactions.

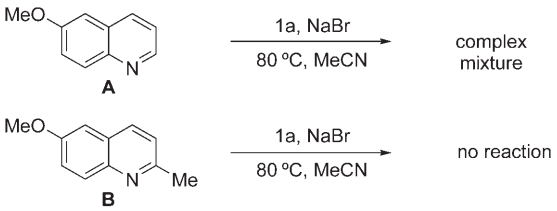


[10] 1′-deazo cinchona alkaloids have been synthesized previously through a nontrivial route: a) C. Exner, A. Pfaltz, M. Studer, H.-U. Blaser, *Adv. Synth. Catal.* **2003**, *345*, 1253; b) E. V. Dehmlow, S. Düttmann, B. Neumann, H.-G. Stammler, *Eur. J. Org. Chem.* **2002**, 2087.
[11] We also tested catalysts containing C2′-Ph (83 % yield, 96 % *ee*), *i*Pr (59 % yield, 98 % *ee*), and *t*Bu (46 % yield, 93 % *ee*), but the Me-MQ/ Me-MQD catalysts gave the best results.
[12] See the Supporting Information for details.
[13] For isolation, see: a) S. F. Brady, M. P. Singh, J. E. Janso, J. Clardy, *J. Am. Chem. Soc.* **2000**, *122*, 2116; for the first synthesis, see: b) S. Lin, G. S. Dudley, D. S. Tan, S. J. Danishevsky, *Angew. Chem.* **2002**, *114*, 2292; *Angew. Chem. Int. Ed.* **2002**, *41*, 2188.
[14] P. Ramesh, N. Srinivasa, Y. Venkateswarlu, M. V. R. Reddy, D. J. Faulkner, *Tetrahedron Lett.* **1998**, *39*, 8217.
[15] For a related example of intramolecular [5+2] cycloadditions, see: a) B. M. Trost, H. C. Shen, *Angew. Chem.* **2001**, *113*, 2375–2378; *Angew. Chem. Int. Ed.* **2001**, *40*, 2313–2316; b) B. M. Trost, H. C. Shen, D. B. Horne, F. D. Toste, B. G. Steinmetz, C. Koradin, *Chem. Eur. J.* **2005**, *11*, 2577; see also: c) P. A. Wender, F. C. Bi, M. A. Brodney, F. Gosselin, *Org. Lett.* **2001**, *3*, 2105, and references therein.
[16] T. P. Gill, K. R. Mann, *Organometallics* **1982**, *1*, 485.
[17] The chloroketone precursors are made through an alkene cross metathesis reaction using the Grubbs second generation catalyst.

 © 2006 Wiley-VCH Verlag GmbH & Co. KGaA, Weinheim 

*Intermolecular Cyclization*

DOI: 10.1002/anie.200602448

# Gold(I)-Catalyzed Intermolecular Cyclopropanation of Enynes with Alkenes: Trapping of Two Different Gold Carbenes**

*Salomé López, Elena Herrero-Gómez, Patricia Pérez-Galán, Cristina Nieto-Oberhuber, and Antonio M. Echavarren**

Transition-metal-catalyzed reactions of 1,6-enynes[1,2] that proceed by the selective coordination of the metal center to the alkyne take place through *exo*-cyclopropyl metal carbenes or the related *endo* intermediates.[2,3] In the absence of nucleophiles, enynes undergo skeletal rearrangement (Scheme 1). Based on kinetic data and DFT calculations, we recently proposed that upon coordination of $Au^I$ to the enyne **I**, the resulting *anti*-cyclopropyl gold(I) carbene **II** rearranges to give **III**, which can undergo demetalation (pathway a) to form the single cleavage rearrangement product **IV**. Alternatively, **III** may undergo a 1,2-shift (pathway b) to form a new gold carbene **V**, which gives double cleavage rearrangement diene **VI** after α-hydrogen elimination. The double cleavage rearrangement can also take place directly from intermediate **II** to give **V**.[4]

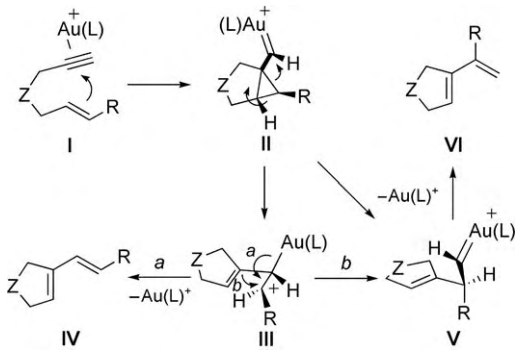


***Scheme 1.*** Skeletal rearrangement of enynes. L = ligand.

Strong evidence for the existence of metal carbenes of type **II** has been obtained by intramolecular trapping with alkenes in ruthenium-,[5] platinum-,[6,7] and gold-catalyzed reactions.[4a,8] We have recently shown that the *anti* arrangement of the carbene and the cyclopropane accounts for the configuration observed in all these intramolecular processes.[8]

We now report that carbenes **II** and **V** can be trapped intermolecularly with a variety of alkenes.[9,10] We also found the first examples of a shift of cyclopropyl gold(I) carbenes. These results support the mechanism proposed for the skeletal-rearrangement of enynes.[4]

We first studied the reaction of enyne **1a** with norbornene in the presence of several gold(I) catalysts **A**–**D** (Table 1). In the absence of norbornene, skeletal rearrangement products **3** and **4** were cleanly obtained in overall quantitative yield with catalyst **A** (Table 1, entry 1).[8] However, when the reaction of **1a** was performed in the presence of norbornene (5 equiv), biscyclopropane **2a** was obtained as the major product (Table 1, entry 2).[11] The configuration of **2a** was determined by a NOESY experiment.[12] Less satisfactory results were obtained with catalysts **B**[13] and **C**, which led to the formation of **3** and **4** (Table 1, entries 3 and 4). Catalyst **C** presumably forms a highly electrophilic $Au^I$ complex in situ, which has a bulky phosphite moiety as the ligand. Attempts at isolating the corresponding cationic complex in acetonitrile have not been yet successful. The best yields of biscyclopropane **2a** were realized with catalyst **D**[14,15] or AuCl (Table 1, entries 5 and 6, respectively).

Although catalysts **D** and AuCl gave satisfactory results in the cyclopropanation of enynes, in general cleaner transformations were achieved with **D**. The scope of this reaction is

***Table 1:*** Gold(I)-catalyzed reaction of enyne **1** with norbornene.[a]

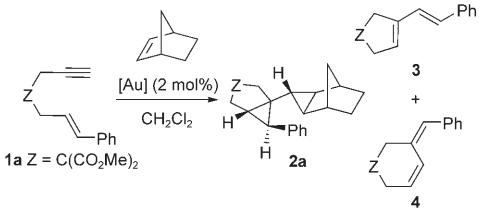


| Entry | [Au] | Norbornene [equiv] | Yield of **2** [%][b] | **3** + **4** Yield [%] | **3** + **4** Ratio[b] |
|---|---|---|---|---|---|
| 1 | **A** | – | – | 99 | 1:1.4 |
| 2 | **A** | 5 | 66 | 29 | 1:1.2 |
| 3 | **B** | 5 | 34 | 62 | 1.1:1 |
| 4 | **C** | 5 | 40 | 52 | 1:1.6 |
| 5 | **D** | 5 | 93 | 3 | >10:1 |
| 6 | AuCl | 5 | 94 | 0[c] | – |

[a] Reactions carried by slow warming from −50 to 23 °C over approximately 15 h with five equivalents of norbornene. [b] Yields and ratios determined by GC for reactions with approximately 100% conversion. [c] Approximately 2% of other uncharacterized products. Mes = mesityl.

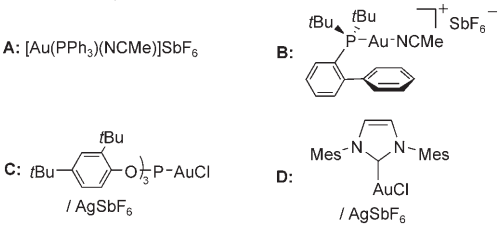


[*] Dr. S. López, E. Herrero-Gómez, P. Pérez-Galán, C. Nieto-Oberhuber, Prof. Dr. A. M. Echavarren
Institute of Chemical Research of Catalonia (ICIQ)
Av. Països Catalans 16
43007 Tarragona (Spain)
Fax: (+34) 977-920-225
E-mail: aechavarren@iciq.es

[**] We are grateful to the MEC (project CTQ2004-02869, Torres Quevedo (contract to S.L. and predoctoral fellowships to E.H.-G., P.P.-G., and C.N.-O.), the AGAUR (2005 SGR 00993), and the ICIQ Foundation for financial support.

Supporting information for this article is available on the WWW under http://www.angewandte.org or from the author.

 © 2006 Wiley-VCH Verlag GmbH & Co. KGaA, Weinheim 

shown in Table 2. A single isomer was obtained in the reactions of **1a–c** with norbornene (Table 2, entries 1–3)[12] and cyclohexene (Table 2, entries 4–6). The yield of the reaction of entry 2 was low as a result of problems encountered in the purification of biscyclopropane **2b**. The reaction of **1a** with styrene provided **4a** in 76% yield (Table 2, entry 7) as a single isomer. Reaction of **1a** with 2-methylpropene and 4-methylpenta-1,3-diene afforded mixtures of two stereoisomers (Table 2, entries 8 and 9, respectively).

The configurations assigned to the major compounds obtained in the intermolecular cyclopropanations follow those assigned in the intramolecular processes,[8] which correspond to the stereochemical model **VII** for the approach of the alkene to the cyclopropyl gold carbene (Scheme 2).[12] This model also explains the regiochemistry observed in the reaction of 4-methylpenta-1,3-diene (Table 2, entry 9), in which the bulky ligand on the Au center directs the cyclopropanation towards the less sterically hindered alkene.

***Table 2:*** Gold(I)-catalyzed reaction of enynes **1a–c** with alkenes.

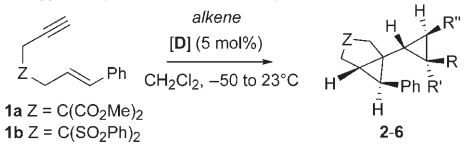


| Entry | Alkene | Enyne | Product | Yield [%][a] |
|---|---|---|---|---|
| 1 | | **1a** | **2a** 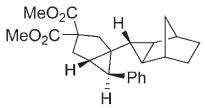 | 67 |
| 2 | | **1b** | **2b** 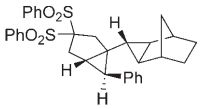 | 31 |
| 3 | | **1c** | **2c** 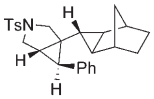 | 73 |
| 4 | | **1a** | **3a** 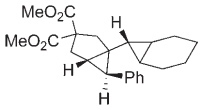 | 77 |
| 5 | | **1b** | **3b** 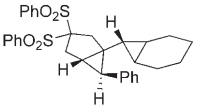 | 53 |
| 6 | | **1c** | **3c** 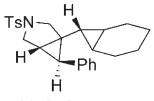 | 75 |
| 7 | | **1a** | **4a** 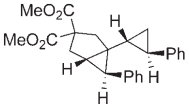 | 76 |
| 8[b,c] | | **1a** | **5a/5a'** 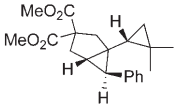 | 52[d] |
| 9[c] | 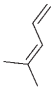 | **1a** | **6a/6a'** 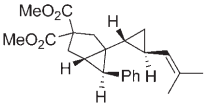 | 60[e] |

[a] Yields of the isolated products are as the average of at least two reactions; reaction time = 15 h, except for entries 2 and 3 (40 h). [b] Reaction carried out with AuCl (2 mol%). [c] Only the major isomer is shown. [d] Ratio of isomers = 3.7:1. [e] Ratio of isomers = 5:1. Ts = *p*-methylphenylsulfonyl.

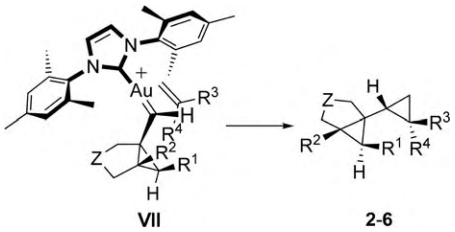


***Scheme 2.*** Model for the stereoselective cyclopropanation of alkenes by cyclopropyl gold carbene **VII**.

The second Au$^{I}$ carbene **V** (Scheme 1) can also be trapped intermolecularly with alkenes. Thus, enynes **1d–e** react with different alkenes to form products **7a–c** through a cyclopropanation reaction of intermediates **VIII** (Scheme 3). In the case of **1e**, the best results were obtained with catalyst **C**, which gave **7** as a 3.3:1 mixture of *cis* and *trans* isomers. In the absence of styrene, **1e** reacts with catalyst **C** to give a 2:1 mixture of *exo* and *endo* skeletal rearrangement products in 87% yield. Configuration of the major stereosiomers **7a–c** were based on the analysis of the coupling constants of the cyclopropane hydrogen atoms and NOESY experiments.

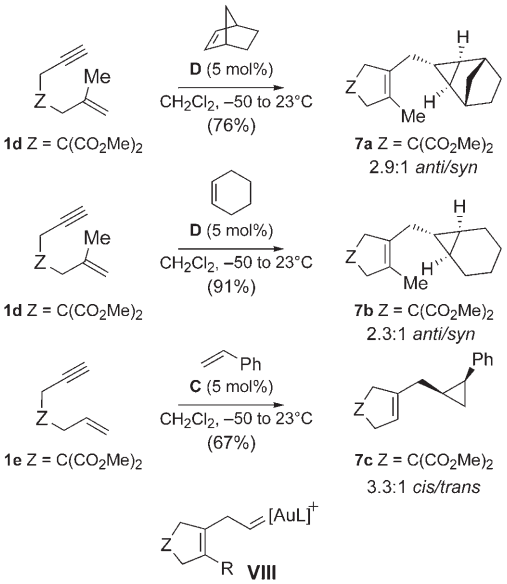


***Scheme 3.*** Gold(I)-catalyzed reaction of enynes **1d,e** with alkenes via carbene **VIII**.

Additional evidence for the involvement of metal carbenes in these reactions was obtained in the reaction of dimeric substrates **8a–c** with cationic Au$^{I}$ catalyst **B**

 © 2006 Wiley-VCH Verlag GmbH & Co. KGaA, Weinheim 

(Scheme 4). Thus, the reaction of **8a** with **B** (5 mol%) for 5 h furnished **9a** and **9′a** in 91% yield. The $^{13}C$ NMR ($CDCl_3$, 100 MHz) spectrum showed only 11 signals. However, in $C_6D_6$

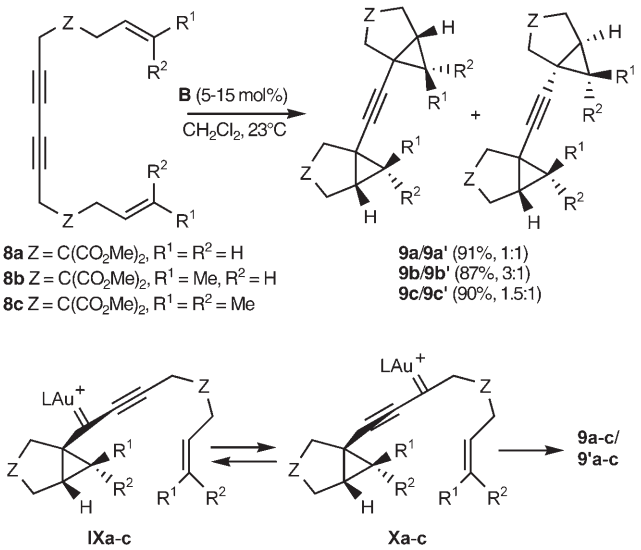


***Scheme 4.*** Cyclopropanation through a [1,3]-metallotropic shift.

(125 MHz), the formation of a 1:1 mixture of *meso*-**9a** and chiral **9a′** was evident by the splitting of three of the carbon signals. On the other hand, **8b** reacted with **B** (15 mol%) for 15 h to give **9b**/**9′b** (90%). Reaction of **8b** with **C** (5 mol%) was completed in 7 h to give **9b**/**9′b** (70%). Similarly, **8c** reacted with **B** (10 mol%) for 24 h to give **9c**/**9′c** (87%). These reactions can be explained by isomerization of the initially formed cyclopropyl gold carbene **IX** to form **X** by a [1,3]-metallotropic shift, followed by intramolecular trapping of the gold carbene by the alkene. This type of [1,3]-metallotropic shift has been observed before for Rh,[16] Cr, Mo, W,[17] and Ru[18,19] carbene complexes.

In summary, we have established the first intermolecular cyclopropanation reactions of enynes with alkenes. This new cyclopropanation[20] allows the synthesis of complex cyclic systems from readily available starting materials with gold(I) catalysts under mild conditions. These results also provide compelling evidence for the existence of metal carbenes of types **II** and **V** in the skeletal rearrangement. We have also provided the first examples of a 1,3-metallotropic shift of $d^{10}$ metal complexes, which further supports the existence of gold carbenes in these reactions.

Received: June 17, 2006
Published online: August 10, 2006

**Keywords:** cyclization · cyclopropanation · enynes · gold · rearrangement

[1] Reviews: a) G. C. Lloyd-Jones, *Org. Biomol. Chem.* **2003**, *1*, 215–236; b) C. Aubert, O. Buisine, M. Malacria, *Chem. Rev.* **2002**, *102*, 813–834; c) S. T. Diver, A. J. Giessert, *Chem. Rev.* **2004**, *104*, 1317–1382; d) A. M. Echavarren, C. Nevado, *Chem. Soc. Rev.* **2004**, *33*, 431–436.

[2] a) M. Méndez, M. P. Muñoz, A. M. Echavarren, *J. Am. Chem. Soc.* **2000**, *122*, 11549–11550; b) M. Méndez, M. P. Muñoz, C. Nevado, D. J. Cárdenas, A. M. Echavarren, *J. Am. Chem. Soc.* **2001**, *123*, 10511–10520; c) C. Nevado, D. J. Cárdenas, A. M. Echavarren, *Chem. Eur. J.* **2003**, *9*, 2627–2635; d) M. P. Muñoz, M. Méndez, C. Nevado, D. J. Cárdenas, A. M. Echavarren, *Synthesis* **2003**, 2898–2902; e) C. Nevado, L. Charruault, V. Michelet, C. Nieto-Oberhuber, M. P. Muñoz, M. Méndez, M.-N. Rager, J. P. Genêt, A. M. Echavarren, *Eur. J. Org. Chem.* **2003**, 706–713; f) C. Nevado, C. Ferrer, A. M. Echavarren, *Org. Lett.* **2004**, *6*, 3191–3194; g) M. P. Muñoz, J. Adrio, J. C. Carretero; A. M. Echavarren, *Organometallics* **2005**, *24*, 1293–1300.

[3] a) C. Nieto-Oberhuber, M. P. Muñoz, E. Buñuel, C. Nevado, D. J. Cárdenas, A. M. Echavarren, *Angew. Chem.* **2004**, *116*, 2456–2460; *Angew. Chem. Int. Ed.* **2004**, *43*, 2402–2406; b) C. Nieto-Oberhuber, M. P. Muñoz, S. López, E. Jiménez-Núñez, C. Nevado, E. Herrero-Gómez, M. Raducan, A. M. Echavarren, *Chem. Eur. J.* **2006**, *12*, 1677–1693.

[4] a) C. Nieto-Oberhuber, S. López, M. P. Muñoz, D. J. Cárdenas, E. Buñuel, C. Nevado, A. M. Echavarren, *Angew. Chem.* **2005**, *117*, 6302–6304; *Angew. Chem. Int. Ed.* **2005**, *44*, 6146–6148; b) C. Nieto-Oberhuber, S. López, E. Jiménez-Núñez, A. M. Echavarren, *Chem. Eur. J.* **2006**, *11*, 5916–5923.

[5] N. Chatani, K. Kataoka, S. Murai, N. Furuakwa, Y. Seki, *J. Am. Chem. Soc.* **1998**, *120*, 9104–9105.

[6] a) E. Mainetti, V. Mouriès, L. Fensterbank, M. Malacria, J. Marco-Contelles, *Angew. Chem.* **2002**, *114*, 2236–2239; *Angew. Chem. Int. Ed.* **2002**, *41*, 2132–2135; b) Y. Harrak, C. Blaszykowski, M. Bernard, K. Cariou, E. Mainetti, V. Mouriès, A.-L. Dhimane, L. Fensterbank, M. Malacria, *J. Am. Chem. Soc.* **2004**, *126*, 8656–8657.

[7] B. P. Peppers, S. T. Diver, *J. Am. Chem. Soc.* **2004**, *126*, 9524–9525.

[8] C. Nieto-Oberhuber, S. López, M. P. Muñoz, E. Jiménez-Núñez, E. Buñuel, D. Cárdenas, A. M. Echavarren, *Chem. Eur. J.* **2006**, *12*, 1694–1702.

[9] Intermolecular trapping of carbenes formed by the Rautenstrauch rearrangement of propargyl carboxylates have been reported: a) M. J. Johansson, D. J. Gorin, S. T. Staben, F. D. Toste, *J. Am. Chem. Soc.* **2005**, *127*, 18002–18003; b) K. Miki, K. Ohe, S. Uemura, *Tetrahedron Lett.* **2003**, *44*, 2019–2022; c) K. Miki, K. Ohe, S. Uemura, *J. Org. Chem.* **2003**, *68*, 8505–8513; see also: d) K. Miki, T. Yokoi, F. Nishino, Y. Kato, Y. Washitake, K. Ohe, S. Uemura, *J. Org. Chem.* **2004**, *69*, 1557–1564; e) K. Miki, F. Nishino, K. Ohe, S. Uemura, *J. Am. Chem. Soc.* **2002**, *124*, 5260–5261.

[10] M. R. Fructos, T. R. Belderrain, P. de Frémont, N. M. Scott, S. P. Nolan, M. M. Díaz-Requejo, P. J. Pérez, *Angew. Chem.* **2005**, *117*, 5418–5422; *Angew. Chem. Int. Ed.* **2005**, *44*, 5284–5288.

[11] For the transition-metal-catalyzed cyclopropanation of norbornenes, see: N.-W. Tseng, J. Mancuso, M. Lautens, *J. Am. Chem. Soc.* **2006**, *128*, 5338–5339, and references therein.

[12] See Supporting Information for additional support of the configurations of biscyclopropanes.

[13] E. Herrero-Gómez, C. Nieto-Oberhuber, S. López, J. Benet-Buchholz, A. M. Echavarren, *Angew. Chem.*, DOI: 10.1002/ange.200601688; *Angew. Chem. Int. Ed.*, DOI: 10.1002/anie.200601688.

[14] C. Nieto-Oberhuber, S. López, A. M. Echavarren, *J. Am. Chem. Soc.* **2005**, *127*, 6178–6179.

[15] P. de Fremont, N. M. Scott, E. D. Stevens, S. P. Nolan, *Organometallics* **2005**, *24*, 2411–2418.

[16] A. Padwa, D. J. Austin, Y. Gareau, J. M. Kassir, S. L. Xu, *J. Am. Chem. Soc.* **1993**, *115*, 2637–2647.

 © 2006 Wiley-VCH Verlag GmbH & Co. KGaA, Weinheim 

[17] J. Barluenga, R. B. de la Rúa, D. de Saá, A. Ballesteros, M. Tomás, *Angew. Chem.* **2005**, *117*, 5061 – 5063; *Angew. Chem. Int. Ed.* **2005**, *44*, 4981 – 4983.

[18] a) W. A. L. van Otterlo, E. L. Ngidi, C. B. de Koning, M. A. Fernandes, *Tetrahedron Lett.* **2004**, *45*, 659 – 662; b) M. Kim, R. L. Miller, D. Lee, *J. Am. Chem. Soc.* **2005**, *127*, 12818 – 12819; c) M. Kim, D. Lee, *J. Am. Chem. Soc.* **2005**, *127*, 18024 – 18025; d) K. Ohe, M. Fujita, H. Matsumoto, Y. Tai, K. Miki, *J. Am. Chem. Soc.* **2006**, *128*, 9270 – 9271; e) E. J. Cho, M. Kim, D. Lee, *Eur. J. Org. Chem.* **2006**, 3074 – 3078.

[19] For related metallotropic rearrangements of alkynyl–Re and alkynyl–Mn carbenes, see: a) C. P. Casey, S. Kraft, D. R. Powell, *J. Am. Chem. Soc.* **2000**, *122*, 3771 – 3772; b) C. P. Casey, S. Kraft, D. R. Powell, *Organometallics* **2001**, *20*, 2651 – 2653; c) C. P. Casey, S. Kraft, M. Kavana, *Organometallics* **2001**, *20*, 3795 – 3799; d) C. P. Casey, S. Kraft, D. R. Powell, *J. Am. Chem. Soc.* **2002**, *124*, 2584 – 2594; e) C. P. Casey, T. L. Dzwiniel, S. Kraft, I. A. Guzei, *Organometallics* **2003**, *22*, 3915 – 3929; f) C. P. Casey, T. L. Dzwiniel, *Organometallics* **2003**, *22*, 5285 – 5290; g) Y. Ortin, A. Sournia-Saquet, N. Lugan, R. Mathieu, *Chem. Commun.* **2003**, 1060 – 1061.

[20] Lead general references: a) H. Lebel, J.-F. Marcoux, C. Molinaro, A. B. Charette, *Chem. Rev.* **2003**, *103*, 977 – 1050; b) W. A. Donaldson, *Tetrahedron* **2001**, *57*, 8589 – 8627.

 © 2006 Wiley-VCH Verlag GmbH & Co. KGaA, Weinheim 

*Single-Molecule Magnets*

DOI: 10.1002/anie.200600712

# Property-Oriented Rational Design of Single-Molecule Magnets: A $C_3$-Symmetric $Mn_6Cr$ Complex based on Three Molecular Building Blocks with a Spin Ground State of $S_t = 21/2$**

*Thorsten Glaser,* Maik Heidemeier, Thomas Weyhermüller, Rolf-Dieter Hoffmann, Holger Rupp, and Paul Müller*

Single-molecule magnets (SMMs) are a class of coordination compounds that attract attention because of their magnetic bistability.[1] These finite-size molecules show a slow relaxation of the magnetization at low temperatures owing to an energy barrier for spin reversal resulting in a hysteresis of the magnetization which is of purely molecular origin.[2,3] SMMs promise access to dynamic random access memory (RAM) devices for quantum computing and to ultimate high-density memory storage devices in which each bit of digital information might be stored on a single molecule.[4] The energy barrier ($D_{S_t}S_t^2$) for spin reversal arises from the combination of a high spin ground state $S_t$ and a magnetic anisotropy of the easy-axis type (negative zero-field splitting parameter $D_{S_t}$). The archetype of SMMs is the family of dodecanuclear manganese complexes, $[Mn_{12}O_{12}(O_2CR)_{16}(OH_2)_4]$, $Mn_{12}$.[2,5] Since the discovery of the fascinating SMM behavior of $Mn_{12}$, a lot of synthetic efforts have been devoted to the preparation of new molecules with an increased anisotropy barrier and impressive new structural motives have been reported.[6]

The necessary requirements for SMMs are a high spin ground state $S_t$ and a strong magnetic anisotropy $D_{S_t}$. To rationally design polynuclear complexes with high spin ground states $S_t$, a control of the exchange couplings is highly desirable. The main component of the magnetic anisotropy of the ground state ($D_{S_t}$) usually comes from the projection of the single-site anisotropies ($D_i$) onto the spin ground state $S_t$, while dipolar and anisotropic interactions yield only minor contributions.[7,8] Since zero-field splittings are tensor quantities, the projection of the single-site zero-field splittings onto the spin ground state may vanish when the metal-ion arrangement approaches a cubic symmetry. Thus, a rational design of SMMs requires a control of the molecular topology which can not be achieved by simply increasing the nuclearity of complexes and using small bridging ligands. Another prerequisite for a SMM to function as a data storage is the minimization of the quantum-mechanical magnetization tunneling which provides an alternative pathway for spin-reversal and thus the loss of information. This tunneling mechanism is directly related to the rhombic component of the magnetic anisotropy expressed by $E_{S_t}$ which is exactly zero for complexes with at least a threefold axis. Thus, there are several requirements for a targeted synthesis of SMMs which must be considered when designing a polynucleating ligand of low flexibility.

We have designed the $C_3$-symmetric triplesalen ligand **C** (Scheme 1) which combines the phloroglucinol bridging unit (**A**) with the coordination environment of a salen ligand (**B**).[9] In trinuclear $Cu^{II}$[10] and $Mo^{V}$[11] complexes the phloroglucinol bridging unit **A** acts as a ferromagnetic coupler by the spin-polarization mechanism. To introduce magnetic anisotropy we have been choosing a salen-like coordination environment **B** which causes a pronounced magnetic anisotropy through its strong ligand field in the basal plane.[8,12] A well documented example is the Jacobsen

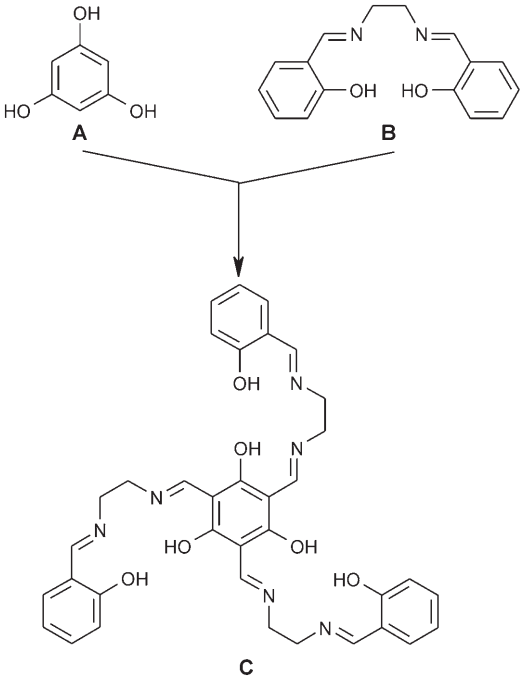


***Scheme 1.*** Components of the $C_3$-symmetric triplesalen ligand **C**.

[*] Prof. Dr. T. Glaser, Dipl.-Chem. M. Heidemeier
Lehrstuhl für Anorganische Chemie I, Fakultät für Chemie
Universität Bielefeld
Universitätsstrasse 25, 33615 Bielefeld (Germany)
Fax: (+49) 521-106-6003
E-mail: thorsten.glaser@uni-bielefeld.de
Dr. T. Weyhermüller
Max-Planck-Institut für Bioanorganische Chemie
45470 Mülheim an der Ruhr (Germany)
Dr. R.-D. Hoffmann
Institut für Anorganische und Analytische Chemie
Westfälische Wilhelms-Universität Münster
48149 Münster (Germany)
Dipl.-Phys. H. Rupp, Prof. Dr. P. Müller
Lehrstuhl für Experimentalphysik, Physikalisches Institut III
Universität Erlangen-Nürnberg
91058 Erlangen (Germany)

[**] This work was supported by the Fonds der Chemischen Industrie, the BMBF, the Dr. Otto Röhm Gedächtnisstiftung, and the DFG (SFB424 and SFB583). We thank Dr. E. Bill (MPI for Bioinorganic Chemistry) for magnetic measurements and valuable discussions.

Supporting information for this article is available on the WWW under http://www.angewandte.org or from the author.

 © 2006 Wiley-VCH Verlag GmbH & Co. KGaA, Weinheim 

catalyst [(salen′)Mn$^{III}$Cl] ($H_2$salen′ = (*R*,*R*)-*N*,*N*′-bis(3,5-di-*tert*-butylsalicylidene)-1,2-cyclohexanediamine)[13] with $S = 2$ and a zero-field splitting of $D = -2.5\ cm^{-1}$.[12,14] It is of note that a dimeric Mn$^{III}$ salen complex already behaves as a SMM.[15]

Metal salen complexes form interesting complexes of varying nuclearity and dimensionality[16] with $[M(CN)_6]^{n-}$. The nuclearity and dimensionality, however, are difficult to control. The reaction of $[Cr(CN)_6]^{3-}$ with $[(salen)Mn(OH_2)]^+$ results in the formation of a heptanuclear complex $[\{(salen)Mn^{III}\}_6\{Cr(CN)_6\}]^{3+}$ which exhibits a high ferrimagnetic spin ground state of $S_t = 21/2$ arising from antiferromagnetic interactions.[17] Although, $[(salen)Mn^{III}]^+$ units are incorporated as a source of single-ion magnetic anisotropy, this heptanuclear complex does not behave as a SMM.[18]

Trinuclear complexes of the *tert*-butyl triplesalen derivative $H_6talen^{tBu_2}$ (Scheme 2a) are not flat but bowl-shaped

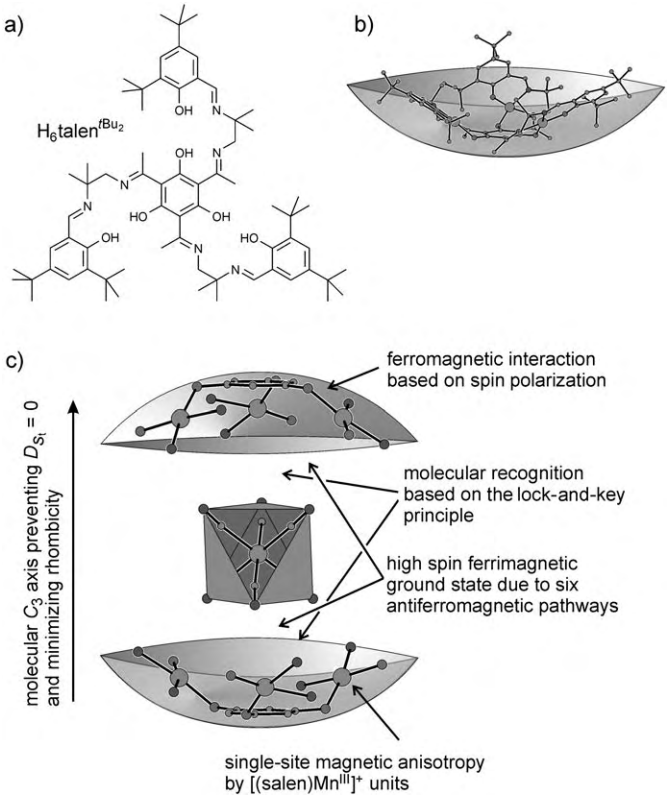


***Scheme 2.*** a) $H_2talen^{tBu_2}$, b) bowl-shaped trinuclear complex with $talen^{tBu_2}$, c) heptanuclear ion $\mathbf{1}^{3+}$. For atom legend, see Figure 1.

(Scheme 2b).[19] This ligand folding preorganizes the three metal ions for a facial coordination by three N donor atoms of a $[M^B(CN)_6]^{n-}$ ion, thus favoring the formation of heptanuclear complexes $M^A{}_6M^B$ by molecular recognition in analogy to the lock-and-key principle (Scheme 2c). We anticipated a heptanuclear $Mn_6Cr$ assembly to fulfill all the requirements for SMMs, namely: 1) a high ferrimagnetic spin ground state of $S_t = 21/2$, 2) the $[(salen)Mn^{III}]^+$ units provide a pronounced single-site $D_i$, 3) the $C_3$ symmetry precludes the compensation of the single-site $D_i$s by projecting onto $S_t$, and 4) the molecular $C_3$ axis enforces $E_{S_t} = 0$ thus minimizing the disrupting tunneling probability.

The reaction of $H_6talen^{tBu_2}$, $Mn(OAc)_2{\cdot}4H_2O$, $K_3[Cr(CN)_6]$, and $NaBPh_4$ in $MeOH/H_2O$ yields, after recrystallization from $MeCN/Et_2O$, large brownish-black crystals of $[\{(talen^{tBu_2})Mn_3\}_2\{Cr(CN)_6\}(MeOH)_3(CH_3CN)_2](BPh_4)_3{\cdot}4\,CH_3CN{\cdot}2\,Et_2O$ (**1**-$(BPh_4)_3{\cdot}4\,MeCN{\cdot}2\,Et_2O$).

The high yield of 78% indicates the success of the anticipated molecular recognition process of the three molecular building blocks. A single $\nu(C{\equiv}N)$ mode at $2153\ cm^{-1}$ implies the presence of a symmetric $\mu_6$-bridging $[Cr(CN)_6]^{3-}$ unit. The MALDI-TOF and ESI mass spectra exhibit prominent ions at *m/z* 2747.0 and 916.3, respectively, with mass and isotope distribution patterns corresponding to $[\{(talen^{tBu_2})Mn_3\}_2Cr(CN)_6]^+$ and $[\{(talen^{tBu_2})Mn_3\}_2\{Cr(CN)_6\}]^{3+}$, respectively.

The molecular structure of $\mathbf{1}^{3+}$ consists of two trinuclear manganese triplesalen complexes bridged by a central $[Cr(CN)_6]^{3-}$ ion as a six-fold connector (Figure 1 and see

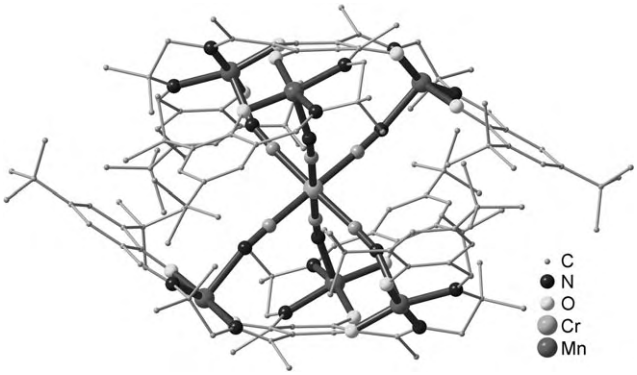


***Figure 1.*** Molecular structure of the ion $[\{(talen^{tBu_2})Mn_3\}_2\{Cr(CN)_6\}]^{3+}$ ($\mathbf{1}^{3+}$) in crystals of **1**-$(BPh_4)_3{\cdot}4\,MeCN{\cdot}Et_2O$. For clarity, the loosely bound solvent molecules have been omitted.

Supporting Information).[20] The manganese ions are in a square-pyramidal coordination geometry in which the $N_2O_2$ donor sets of the salen-like environment form the basal planes and the nitrogen atoms of $[Cr(CN)_6]^{3-}$ units occupy apical positions with Mn–N distances of 2.11–2.23 Å. The remaining coordination sites are either occupied by weakly coordinating MeCN or MeOH molecules or this position remains unoccupied as a result of the π–π stacking of a phenyl ring of one $[BPh_4]^-$ ion with the terminal phenolate donor of the manganese ion. Thus, the Jahn–Teller axes of the Mn$^{III}$ ions are along the Mn–N$^{N{\equiv}C}$ bonds. The different occupation of the sixth positions results in an only approximate $C_3$ symmetry. While as usual the Cr-C≡N connection is almost linear (175–177°), the C≡N-Mn unit is bent with angles of 160–162°. This bending aligns the manganese ions towards the molecular $C_3$ axes. Note that the crystal structure contains two different orientations of $\mathbf{1}^{3+}$ (see Supporting Information). The angle between their pseudo $C_3$ axes is 41.7°.

Temperature-dependent magnetic susceptibility measurements (2–290 K, 0.05 T) on powdered samples of **1**-$(BPh_4)_3$ reveal an effective magnetic moment of $\mu_{eff} = 11.72\,\mu_B$ at

 © 2006 Wiley-VCH Verlag GmbH & Co. KGaA, Weinheim 

290 K, which decreases slightly with decreasing temperature to a minimum of 11.14 $\mu_B$ at 90 K (Figure 2a). Further temperature decrease results in a steep increase of $\mu_{eff}$ to 17.75 $\mu_B$ at 5 K and a small subsequent decrease down to 2 K. This temperature dependence is typical for a ferrimagnetic coupling of the terminal $Mn^{III}$ salen complexes, which enforces an antiparallel orientation of the central $Cr^{III}$ spin ($S_i = 3/2$) with the terminal $Mn^{III}$ spins ($S_i = 2$), resulting in a $S_t = 21/2$ ground state. The low-temperature $\mu_{eff}$ value does not reach the theoretical value of 21.76 $\mu_B$ for $S_t = 21/2$ with $g = 1.98$[21] owing to the combined influence of zero-field splitting, saturation, and intermolecular interactions. Magnetization measurements at variable temperature and variable field indicate that **1**-$(BPh_4)_3$ possess a high anisotropic spin ground state (Figure 2b). The saturation value at 7 T of 18.4 $\mu_B$ in combination with the splitting of the isofield lines confirms a magnetically anisotropic $S_t = 21/2$ system.

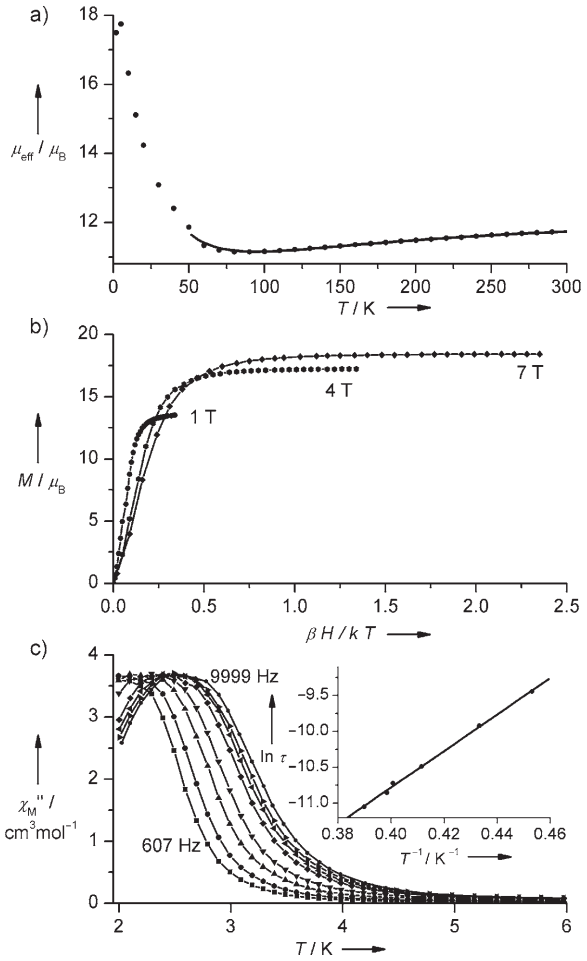


***Figure 2.*** Magnetic measurements on microcrystalline **1**-$(BPh_4)_3$. a) Temperature dependence of $\mu_{eff}$ at 0.05 T: the line is a fit to the experimental data using the spin Hamiltonian and exchange parameters provided in the text. b) Variable temperature–variable field magnetization measurements: the lines are only to guide the eyes. c) Temperature dependence of $\chi_M''$ measured at zero DC field with a 3 G AC field at 607, 1057, 2011, 3247, 5697, 7211, 8231, and 9999 Hz: the lines are only to guide the eyes. Inset: linear fit to the Arrhenius plot ($R = 0.9991$).

To estimate the coupling constants $J_i$ we simulated the temperature dependence of $\mu_{eff}$ with the appropriate Heisenberg–Dirac–van Vleck (HDvV) exchange Hamiltonian [Eq. (1)] using the package MAGPACK.[22]

$$\mathcal{H}_{HDvV} = -2J(\mathbf{S}_1\mathbf{S}_7 + \mathbf{S}_2\mathbf{S}_7 + \mathbf{S}_3\mathbf{S}_7 + \mathbf{S}_4\mathbf{S}_7 + \mathbf{S}_5\mathbf{S}_7 + \mathbf{S}_6\mathbf{S}_7) - 2J'(\mathbf{S}_1\mathbf{S}_2 + \mathbf{S}_2\mathbf{S}_3 + \mathbf{S}_3\mathbf{S}_1 + \mathbf{S}_4\mathbf{S}_5 + \mathbf{S}_5\mathbf{S}_6 + \mathbf{S}_6\mathbf{S}_4) \quad (1)$$

The exchange parameters $J$ and $J'$ describe the coupling between the central $Cr^{III}$ ion and the terminal $Mn^{III}$ ions, and between the $Mn^{III}$ ions of a trinuclear $\{(talen^{tBu_2})Mn_3\}^{3+}$ building block, respectively. We have only used the data above 50 K because at lower temperatures zero-field splitting has a pronounced influence. First attempts to simulate the data by only using $J$ were not satisfactory. Incorporation of $J'$ demonstrated clearly but unexpectedly that $J'$ is antiferromagnetic. The minimum at 90 K and its curvature allowed a relatively precise determination of the coupling constants. Our best simulation using $J = -5.0$ cm$^{-1}$, $J' = -1.03$ cm$^{-1}$, and $g = 1.98$ is shown as a solid line in Figure 2a. This simulation results in a $S_t = 21/2$ spin ground state with the first excited states (four degenerate $S_t = 19/2$) at $+2.64$ cm$^{-1}$. The overall spread of the spin-ladder is 375 cm$^{-1}$ with the $S_t = 27/2$ highest in energy.

AC magnetic susceptibility measurements with zero DC field allowed the slow magnetization relaxation indicative of SMM behavior to be probed. The applied oscillating field probes the dynamics of this reorientation, as the out-of-phase signal ($\chi_M''$) is at maximum when the frequency of the AC field equals the relaxation rate of the magnetization. In Figure 2c, the temperature dependence of $\chi_M''$ at different AC frequencies is shown (measured on a Quantum Design PPMS). Compound **1**-$(BPh_4)_3$ exhibits a frequency-dependent maximum in $\chi_M''$ demonstrating the slow relaxation of the magnetization. The energy barrier $U_{eff}$ is derived from an Arrhenius plot (Figure 2c, inset) as 25.4 K with $\tau_o = 8 \times 10^{-10}$ s.

Although, the occurrence of frequency-dependent $\chi_M''$ maxima is considered as a key signature of a SMM, the conclusive evidence is the presence of hysteresis loops in the magnetization versus DC field data (Figure 3). Single-crystal magnetization data on **1**-$(BPh_4)_3 \cdot 4\,MeCN \cdot 2\,Et_2O$ were mea-

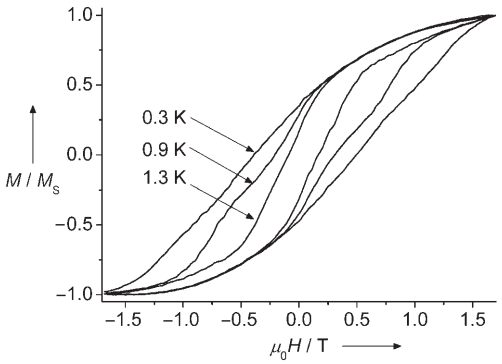


***Figure 3.*** Hysteresis loops at different temperatures measured at a sweep rate of 50.3 mTs$^{-1}$ on a single crystal of **1**-$(BPh_4)_3 \cdot 4\,MeCN \cdot 2\,Et_2O$ oriented at 45° to the long axis.

 © 2006 Wiley-VCH Verlag GmbH & Co. KGaA, Weinheim 

sured using a 2DEG Hall probe magnetometer. Although two orientations of $\mathbf{1}^{3+}$ with an angle of 41.7° prevail in the single crystal, hysteresis loops with significant coercive fields are clearly apparent below 1.5 K.

## Experimental Section

**1**-$(BPh_4)_3$: A solution of $Mn(OAc)_2{\cdot}4H_2O$ (93 mg, 0.41 mmol) in methanol (30 mL) was added to a stirred suspension of $H_6talen^{tBu_2}$ (150 mg, 0.135 mmol) in methanol (30 mL). Heating the mixture to reflux for 15 min resulted in a brown solution which was subsequently treated with a solution of $K_3[Cr(CN)_6]$ (22 mg, 0.068 mmol) in water (3 mL). After addition of $NaBPh_4$ (277 mg, 0.809 mmol) in methanol (30 mL), the reaction mixture was stirred for 16 h giving a precipitate which was collected by filtration and dried in vacuum. This residue was then dissolved in acetonitrile. Upon slow diffusion of diethyl ether into the solution large brownish-black crystals were obtained. The crystallographic and single-crystal magnetization data were obtained from crystals in contact with mother liquor to prevent solvent loss. The product was identified crystallographically as **1**-$(BPh_4)_3{\cdot}4\,MeCN{\cdot}2\,Et_2O$. The other measurements were performed on a vacuum-dried sample. High-vacuum treatments yield a weight loss of 7.39%. This result indicates the complete release of the cocrystallized solvent molecules (calculated weight loss for 4 MeCN and 2 $Et_2O$: 7.44%). The dried sample appears to be hygroscopic and analyzed as **1**-$(BPh_4)_3{\cdot}3\,H_2O$. Yield: 207 mg (78%). ESI-MS ($CH_3CN$): *m/z* (%): 916.3 (100) $[\{(talen^{tBu_2})Mn_3\}_2\{Cr(CN)_6\}]^{3+}$, 1374.7 (78) $[\{(talen^{tBu_2})Mn_3\}_2\{Cr(CN)_6\}]^{2+}$; MALDI-TOF-MS: *m/z* (%): 2747.0 (100) $[\{(talen^{tBu_2})Mn_3\}_2\{Cr(CN)_6\}]^{+}$; IR (KBr): $\tilde{\nu} = 3055$w, 3033w, 2958w, 2905w, 2867w, 2153w, 1609m, 1566 m, 1537m, 1490s, 1427m, 1392m, 1362w, 1340w, 1309w, 1274m, 1252m, 1188m, 1155m, 846m, 703m, 576m, 533w $cm^{-1}$. Elemental analysis (%) calcd for **1**-$(BPh_4)_3{\cdot}3\,H_2O$ ($C_{223}H_{276}N_{20}O_{18}B_3CrMn_6$): C 68.00, H 7.06, N 7.11; found: 67.85, H 6.82, N 6.99.

Received: February 23, 2006
Revised: May 17, 2006
Published online: August 9, 2006

**Keywords:** chromium · magnetic properties · manganese · N,O ligands · single-molecule magnets

[1] G. Christou, D. Gatteschi, D. N. Hendrickson, R. Sessoli, *MRS Bull.* **2000**, *25*, 66 – 71.

[2] a) R. Sessoli, D. Gatteschi, A. Caneschi, M. A. Novak, *Nature* **1993**, *365*, 141 – 143; b) R. Sessoli, H. L. Tsai, A. R. Schake, S. Y. Wang, J. B. Vincent, K. Folting, D. Gatteschi, G. Christou, D. N. Hendrickson, *J. Am. Chem. Soc.* **1993**, *115*, 1804 – 1816.

[3] a) D. Gatteschi, A. Caneschi, L. Pardi, R. Sessoli, *Science* **1994**, *265*, 1054 – 1058; b) S. M. J. Aubin, N. R. Dilley, L. Pardi, J. Krzystek, M. W. Wemple, L. C. Brunel, M. B. Maple, G. Christou, D. N. Hendrickson, *J. Am. Chem. Soc.* **1998**, *120*, 4991 – 5004; c) D. Gatteschi, R. Sessoli, *Angew. Chem.* **2003**, *115*, 278 – 309; *Angew. Chem. Int. Ed.* **2003**, *42*, 268 – 297; d) J. R. Long in *Chemistry of Nanostructured Materials* (Ed.: P. Yang), World Scientific, Hong Kong, **2003**, pp. 291 – 315; e) L. Thomas, F. Lionti, R. Ballou, D. Gatteschi, R. Sessoli, B. Barbara, *Nature* **1996**, *383*, 145 – 147.

[4] a) J. Tejada, E. M. Chudnovsky, E. del Barca, J. M. Hernandez, T. P. Spiller, *Nanotechnology* **2001**, *12*, 181 – 186; b) J. Tejada, *Polyhedron* **2001**, *20*, 1751 – 1756; c) D. D. Awschalom, D. P. Di Vincenzo, J. J. Smyth, *Science* **1992**, *258*, 414 – 421; d) M. N. Leuenberger, D. Loss, *Nature* **2001**, *410*, 789 – 793; e) A. Cornia, A. C. Fabretti, M. Pacchioni, L. Zobbi, D. Bonachi, A. Caneschi, D. Gatteschi, R. Biagi, U. Del Pennino, V. De Renzi, L. Gurevich, H. S. J. van der Zant, *Angew. Chem.* **2003**, *115*, 1683 – 1686; *Angew. Chem. Int. Ed.* **2003**, *42*, 1645 – 1648; f) E. D. Dahlberg, *Phys. Today* **1995**, *48*, 34.

[5] a) T. Lis, *Acta Crystallogr. Sect. B* **1980**, *36*, 2042 – 2046; b) P. D. W. Boyd, Q. Y. Li, J. B. Vincent, K. Folting, H. R. Chang, W. E. Streib, J. C. Huffman, G. Christou, D. N. Hendrickson, *J. Am. Chem. Soc.* **1988**, *110*, 8537 – 8539; c) H. L. Tsai, H. J. Eppley, N. Devries, K. Folting, G. Christou, D. N. Hendrickson, *J. Chem. Soc. Chem. Commun.* **1994**, 1745 – 1746; d) Z. M. Sun, D. Ruiz, E. Rumberger, C. D. Incarvito, K. Folting, A. L. Rheingold, G. Christou, D. N. Hendrickson, *Inorg. Chem.* **1998**, *37*, 4758 – 4759; e) C. Boskovic, E. K. Brechin, W. E. Streib, K. Folting, J. C. Bollinger, D. N. Hendrickson, G. Christou, *J. Am. Chem. Soc.* **2002**, *124*, 3725 – 3736.

[6] a) C. Delfs, D. Gatteschi, L. Pardi, R. Sessoli, K. Wieghardt, D. Hanke, *Inorg. Chem.* **1993**, *32*, 3099 – 3103; b) S. M. J. Aubin, N. R. Dilley, M. W. Wemple, N. B. Maple, G. Christou, D. N. Hendrickson, *J. Am. Chem. Soc.* **1998**, *120*, 839 – 840; c) S. L. Castro, Z. M. Sun, C. M. Grant, J. C. Bollinger, D. N. Hendrickson, G. Christou, *J. Am. Chem. Soc.* **1998**, *120*, 2365 – 2375; d) S. T. Ochsenbein, M. Murrie, E. Rusanov, H. Stoeckli-Evans, C. Sekine, H. U. Güdel, *Inorg. Chem.* **2002**, *41*, 5133 – 5140; e) C. P. Berlinguette, D. Vaughn, C. Canada-Vilalta, J. R. Galan-Mascaros, K. R. Dunbar, *Angew. Chem.* **2003**, *115*, 1561 – 1564; *Angew. Chem. Int. Ed.* **2003**, *42*, 1523 – 1526; f) J. J. Sokol, A. G. Hee, J. R. Long, *J. Am. Chem. Soc.* **2002**, *124*, 7656 – 7657; g) A. J. Tsasiopoulos, A. Vinslava, W. Wernsdorfer, K. A. Abboud, G. Christou, *Angew. Chem.* **2004**, *116*, 2169 – 2173; *Angew. Chem. Int. Ed.* **2004**, *43*, 2117 – 2121; h) E. K. Brechin, E. C. Sanudo, W. Wernsdorfer, C. Boskovic, J. Yoo, D. N. Hendrickson, K. Yamaguchi, H. Ishimoto, T. E. Concolino, A. L. Rheingold, G. Christou, *Inorg. Chem.* **2005**, *44*, 502 – 511; i) R. E. P. Winpenny, *J. Chem. Soc. Dalton Trans.* **2002**, 1 – 10; j) J. C. Goodwin, R. Sessoli, D. Gatteschi, W. Wernsdorfer, A. K. Powell, S. L. Heath, *J. Chem. Soc. Dalton Trans.* **2000**, 1835 – 1840; k) S. Maheswaran, G. Chastanet, S. J. Teat, T. Mallah, R. Sessoli, W. Wernsdorfer, R. E. P. Winpenny, *Angew. Chem.* **2005**, *117*, 5172 – 5176; *Angew. Chem. Int. Ed.* **2005**, *44*, 5044 – 5048.

[7] A. Bencini, D. Gatteschi, *Electron Paramagnetic Resonance of Exchanged Coupled Systems*, Springer, Berlin, **1990**.

[8] A. Bencini, I. Ciofini, M. G. Uytterhoeven, *Inorg. Chim. Acta* **1998**, *274*, 90 – 101.

[9] T. Glaser, M. Heidemeier, T. Lügger, *Dalton Trans.* **2003**, 2381 – 2383.

[10] a) T. Glaser, M. Gerenkamp, R. Fröhlich, *Angew. Chem.* **2002**, *114*, 3984 – 3986; *Angew. Chem. Int. Ed.* **2002**, *41*, 3823 – 3825; b) T. Glaser, M. Heidemeier, S. Grimme, E. Bill, *Inorg. Chem.* **2004**, *43*, 5192 – 5194.

[11] V. A. Ung, A. Thompson, D. A. Bardwell, D. Gatteschi, J. C. Jeffery, J. A. McCleverty, F. Totti, M. D. Ward, *Inorg. Chem.* **1997**, *36*, 3447 – 3454.

[12] B. J. Kennedy, K. S. Murray, *Inorg. Chem.* **1985**, *24*, 1552 – 1557.

[13] W. Zhang, E. N. Jacobsen, *J. Org. Chem.* **1991**, *56*, 2296 – 2298.

[14] a) K. A. Campbell, M. R. Lashley, J. K. Wyatt, M. H. Nantz, R. D. Britt, *J. Am. Chem. Soc.* **2001**, *123*, 5710 – 5719; b) J. Krzystek, J. Telser, *J. Magn. Reson.* **2003**, *162*, 454 – 465.

[15] H. Miyasaka, R. Clerac, W. Wernsdorfer, L. Lecren, C. Bonhomme, K.-i. Sugiura, M. Yamashita, *Angew. Chem.* **2004**, *116*, 2861 – 2865; *Angew. Chem. Int. Ed.* **2004**, *43*, 2801 – 2805.

[16] a) H. Miyasaka, N. Matsumoto, H. Okawa, N. Re, E. Gallo, C. Floriani, *J. Am. Chem. Soc.* **1996**, *118*, 981 – 994; b) H. Miyasaka, N. Matsumoto, N. Re, E. Gallo, C. Floriani, *Inorg. Chem.* **1997**, *36*, 670 – 676; c) N. Re, R. Crescenzi, C. Floriani, H. Miyasaka, N. Matsumoto, *Inorg. Chem.* **1998**, *37*, 2717 – 2722; d) H. Miyasaka, H. Ieda, N. Matsumoto, N. Re, R. Crescenzi, C. Floriani, *Inorg. Chem.* **1998**, *37*, 255 – 263; e) M. Clemente-Leon, E. Coronado, J. R. Galan-Mascaros, C. J. Gomez-Garcia, T. Woike, J. M.

 © 2006 Wiley-VCH Verlag GmbH & Co. KGaA, Weinheim 

Clemente-Juan, *Inorg. Chem.* **2001**, *40*, 87 – 94; f) L. M. C. Beltran, J. R. Long, *Acc. Chem. Res.* **2005**, *38*, 325 – 334.

[17] W. Shen, B. Li, J. Zou, Z. Xu, Y. Yu, S. Liu, *Transition Met. Chem.* **2002**, *27*, 372 – 376.

[18] H. J. Choi, J. J. Sokol, J. R. Long, *Inorg. Chem.* **2004**, *43*, 1606 – 1608.

[19] T. Glaser, M. Heidemeier, R. Fröhlich, P. Hildebrandt, E. Bothe, E. Bill, *Inorg. Chem.* **2005**, *44*, 5467 – 5482.

[20] Crystal data for **1**·4 MeCN·$Et_2O$: $C_{234}H_{288}B_3CrMn_6N_{24}O_{15}$, $M_r$ = 4090.95 g mol$^{-1}$, 0.18 × 0.05 × 0.05 mm$^3$, monoclinic, space group $P2_1$, $a$ = 18.5226(9), $b$ = 35.976(2), $c$ = 18.5435(9) Å, $\beta$ = 107.875(5)°, $V$ = 11 760.3(10) Å$^3$, $Z$ = 2, $\rho_{calcd}$ = 1.155 g cm$^{-3}$, $2\theta_{max}$ = 52.0°, $Mo_{K\alpha}$ radiation ($\lambda$ = 0.71073 Å, $\mu$ = 0.417 mm$^{-1}$, rotating anode 50 kV, 80 mA), $T$ = 100(2) K, 148 117 reflections measured, 43 433 independent reflections, $R1$ = 0.0713, w$R2$ = 0.1759 (35 492 reflections with $I > 2\sigma(I)$). Data were collected on a Nonius Kappa CCD diffractometer. Images were taken at 0.5° stepwise rotation in $\phi$ (1278 images) and $\omega$ (701 images), and at 30 s/frame with a detector-to-crystal distance of 60 mm. Intensity data were processed using Nonius Collect Software. The Bruker-Nonius ShelXTL 6.14 software was used for face-indexed absorption correction of the data set, giving min. and max. transmission factors of 0.918 and 0.980, respectively. The same software package was used for structure solution with direct methods. A recompiled ShelXL97 version was used for full-matrix-refinement of 2568 parameters and 9 restraints against $F^2$. The absolute-structure parameter refined to a value of 0.077(14). All non-hydrogen atoms were refined anisotropically. Hydrogen atoms were placed at calculated positions and refined as riding atoms with isotropic displacement parameters. The positions of two diethyl ether and two methanol molecules of crystallization were found to be not fully occupied. The sum of the corresponding occupation factors was refined to be 1.0, yielding distributions of 0.685/0.315 and 0.655/0.345, respectively. Equal thermal-displacement parameters and restrained bond distances were refined using the EADP and SAME instructions of ShelXL97. The residual max. and min. electron densities were +1.16 and −0.57 e Å$^{-3}$. CCDC-292667 contains the supplementary crystallographic data for this paper. These data can be obtained free of charge from The Cambridge Crystallographic Data Centre via www.ccdc.cam.ac.uk/data_request/cif.

[21] J.-J. Girerd, Y. Journaux in *Physical Methods in Bioinorganic Chemistry* (Ed.: L. Que, Jr.), University Science Books, Sausalito, CA, **2000**, p. 335.

[22] a) J. J. Borrás-Almenar, J. M. Clemente-Juan, E. Coronado, B. S. Tsukerblat, *Inorg. Chem.* **1999**, *38*, 6081 – 6088; b) J. J. Borrás-Almenar, J. M. Clemente-Juan, E. Coronado, B. S. Tsukerblat, *J. Comput. Chem.* **2001**, *22*, 985 – 991.

 © 2006 Wiley-VCH Verlag GmbH & Co. KGaA, Weinheim 

*Phosphorus Nitrides*

DOI: 10.1002/anie.200601670

# The First Structural Characterization of a Binary P–N Molecule: The Highly Energetic Compound $P_3N_{21}$**

*Michael Göbel, Konstantin Karaghiosoff, and Thomas M. Klapötke**

*Dedicated to Professor Karl Otto Christe on the occasion of his 70th birthday*

Compounds of the elements phosphorus and nitrogen can exist either as molecular species or as three-dimensional polymeric solids. Examples of known solid-state compounds include the structurally well-characterized phases of the binary compound $P_3N_5$, which were reported by Schnick et al.[1] In contrast, none of the four binary P–N molecules described in the literature, namely $P_4N_4$,[2] $P(N_3)_3$,[3] $P(N_3)_5$,[4] $P_3N_{21}$,[5] and the ionic compound $(N_5)P(N_3)_6$, have been structurally characterized.[6] As shown by Christe et al. for $(N_5)P(N_3)_6$,[6] the difficulties in the isolation and handling of these compounds arise from their highly endothermic character and their extremely low energy barriers, which lead to an often uncontrollable, explosive decomposition.[7]

Herein, we report the single-crystal X-ray structure of $P_3N_{21}$ (**1**)[8] and, thereby, the first structural characterization of a binary P–N molecule. Although the synthesis of this compound was first reported over 50 years ago through the reaction of hexachlorophosphazene with sodium azide,[5a] compound **1** has only been characterized by elemental analysis,[5a] and vibrational[5b,c] and NMR spectroscopy.[5c] The experimental difficulties involved in the structural characterization of $P_3N_{21}$ are a consequence of its high energy content; our calculated gas-phase enthalpy of formation is $+341.4\ \mathrm{kcal\,mol^{-1}}$.

To obtain as pure a product as possible, a new synthetic strategy for $P_3N_{21}$, in which the azide ($N_3$) group is introduced using trimethylsilylazide, was chosen [Eq. (1)]. The trime-

[*] M. Göbel, K. Karaghiosoff, Prof. Dr. T. M. Klapötke
Department of Chemistry and Biochemistry
Ludwig-Maximilians-Universität Munich
Butenandtstrasse 5–13 (Haus D), 81377 Munich (Germany)
Fax: (+49) 89-2180-77492
E-mail: tmk@cup.uni-muenchen.de

[**] We are grateful to Dr. G. Fischer for the mass spectrometry measurements, T. Kerscher for support with the calculations and Dr. Habil M.-J. Crawford for the English translation of the manuscript. The Cusanuswerk is gratefully acknowledged for the award of a PhD scholarship (M.G.) and the Ludwig-Maximilians-Universität and the Fonds der chemischen Industrie (FCI) are thanked for generous financial support. The Federal Republic of Germany, as well as the Free State of Bavaria, are thanked for providing a single-crystal X-ray diffractometer within the HBFG programme.

Supporting information for this article is available on the WWW under http://www.angewandte.org or from the author.


© 2006 Wiley-VCH Verlag GmbH & Co. KGaA, Weinheim

$$P_3N_3Cl_6 + 6\,(CH_3)_3SiN_3 \rightarrow P_3N_{21}\,(\mathbf{1}) + 6\,(CH_3)_3SiCl \quad (1)$$

thylsilylchloride by-product formed was continuously removed from the equilibrium under the reaction conditions. Owing to its volatility, excess trimethylsilylazide could also be easily removed from the reaction mixture. After sublimation of the product, **1** was obtained in high purity.

The appearance of only one signal at $\delta = 13.6$ ppm ($\Delta\nu_{1/2} = 10$ Hz) in the $^{31}$P NMR spectrum of **1** indicates that a complete chloride–azide exchange occurred. The $^{14}$N and $^{15}$N NMR spectra of **1** are shown in Figure 1. The $^{15}$N NMR

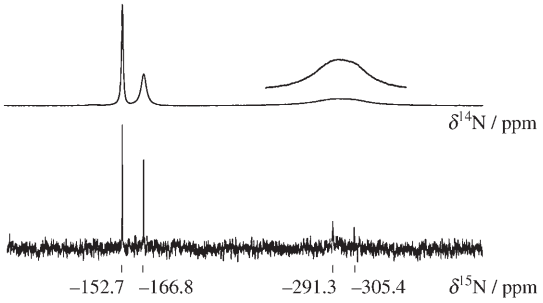


***Figure 1.*** $^{14}$N NMR (top) and $^{15}$N NMR (bottom) spectra of $P_3N_{21}$ in $C_6D_6$. An enlargement of the broad signal at $\delta = -300$ ppm in the $^{14}$N NMR spectrum is also shown.

signal at $\delta = -305.4$ ppm is assigned to the ring nitrogen atoms, by comparison with the chemical shifts of hexasubstituted cyclophosphazenes.[9] The $^{15}$N NMR signals of the covalent azide groups are assigned according to the typical chemical shifts reported for covalent azides:[10] $\delta = -152.7$ ($N_\beta$), $-166.8$ ($N_\gamma$), and $-291.3$ ppm ($N_\alpha$). In the $^{14}$N NMR spectrum, the signals of the ring nitrogen atoms and the $N_\alpha$ atoms appear as a broadened peak at $-300$ ppm.

The Raman and IR spectra of **1** are shown in Figure 2, and a comparison of the experimental and calculated (unscaled) vibrational frequencies is given in Table 1. If standard scaling factors are applied for both calculation methods[11] (BLYP/6-31G(d): 0.9940; B3LYP/6-31G(d): 0.9613), good agreement between the calculated and experimental frequencies is obtained. The vibrational frequencies observed for the liquid phase were assigned by comparison with the frequencies calculated for a molecule of $C_1$ point symmetry, in contrast to the approach reported in the literature,[5b,c] where a $D_{3h}$ molecular symmetry was assumed.

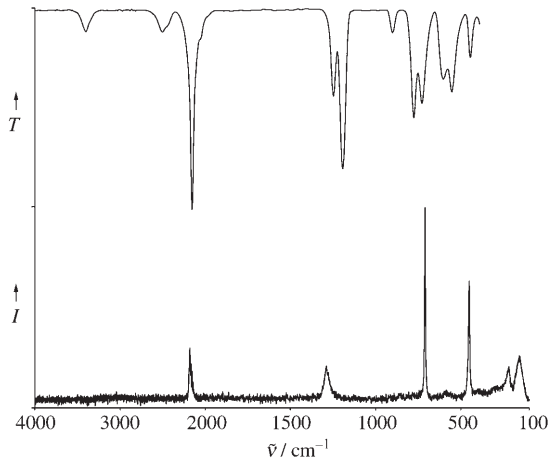


***Figure 2.*** IR (top) and Raman (bottom) spectra of $P_3N_{21}$.

***Table 1:*** Comparison of the experimental and calculated ($C_1$ point group) vibrational frequencies [cm$^{-1}$] and intensities[a] of $P_3N_{21}$.

| Assignment | Experiment | | Calculation | |
|---|---|---|---|---|
| | IR | Raman | BLYP | B3LYP |
| $\nu_{as}N_3 + \nu_sN_3$ | 3406 (w) | | | |
| $2\nu_sN_3$ | 2511 (w) | | | |
| $\nu_{as}N_3$ | 2162 (vs) | 2181 [26] | 2189 (128) [196] | 2318 (172) |
| | | | 2181 (701) [30] | 2308 (1016) |
| | | | 2180 (567) [72] | 2306 (624) |
| | | | 2178 (940) [50] | 2304 (1101) |
| | | | 2175 (303) [25] | 2303 (251) |
| | | | 2173 (83) [8] | 2300 (37) |
| $\nu_sN_3$ | | 1291 [21] | 1275 (13) [51] | |
| | | | 1257 (22) [18] | |
| $\nu_sN_3$ | 1256 (s) | | 1268 (175) [1] | 1336 (191) |
| | | | 1265 (99) [6] | 1333 (103) |
| | | | 1258 (661) [3] | 1324 (848) |
| $\nu_{as}(PN)_{Ring}$ | 1201 (vs) | | 1149 (1536) [1] | 1220 (1793) |
| | | | 1114 (1069) [2] | 1185 (1191) |
| $\nu_{as}(PN)_{Ring}$ | 910 (w) | | 1048 (88) [0] | 1120 (96) |
| $\delta N_3$ | 786 (m) | | 727 (421) [0] | 779 (517) |
| $\delta N_3$ | 739 (m) | | 679 (175) [0] | 729 (232) |
| | | | 672 (191) [1] | 721 (239) |
| $\delta_{bend}(PN)_{ring}$[b] | | 712 [100] | 638 (1) [63] | |
| $\delta_{wag}(PN)_{ring}$,[b] $\delta N_3$ | 614 (m) | | 582 (222) [1] | 617 (222) |
| $\delta_{rock}(PN)_{ring}$,[b] $\delta N_3$ | 564 (m) | | 562 (11) [15] | 567 (137) |
| | | | 533 (148) [0] | 558 (99) |
| | | | 526 (116) [1] | |
| $\delta_{bend}(NPN)$[b] | 456 (w) | 454 [63] | 410 (0) [47] | |
| | | 220 [21] | 298 (2) [1] | |
| $\delta_{twist}(NPN)$[b] | | 160 [26] | 215 (1) [11] | |

[a] The intensities of the calculated IR and Raman spectra are given in (km mol$^{-1}$) and [Å$^4$ amu$^{-1}$], respectively. The IR frequencies calculated using the B3LYP method have very low intensities and are not given.

The lowest-energy conformation calculated for a free $P_3N_{21}$ molecule in the gas phase corresponds to that detected in the solid state by single-crystal X-ray diffraction (Figure 3). The relative arrangement of the azide groups and the (noncrystallographic) $C_1$ symmetry of the molecule are consistent in both structures. $P_3N_{21}$ crystallizes in the space group $P\bar{1}$ with two formula units per unit cell. Three azide groups (N4-N5-N6, N10-N11-N12, and N19-N20-N21) are nearly parallel to the phosphazene ring, as is also found in the calculated gas phase structure. The three remaining azide groups (N7-N8-N9, N13-N14-N15, and N16-N17-N18) are nearly perpendicular to the ring. The $N_\alpha$–$N_\beta$/$N_\beta$–$N_\gamma$ bond lengths and the $N_\alpha$-$N_\beta$-$N_\gamma$ angles are in good agreement with those of other covalently bound azides.[10] The six-membered ring in **1** is nearly planar, with a slight chair conformation, as observed for the phosphazene ring of the $P_3N_3Cl_6$ starting material.[12] The P-N-P/N-P-N angles (120.8(2)–122.9(2)°/117.0(2)–118.2(1)°), as well as the P–N distances (1.556(2)–

 © 2006 Wiley-VCH Verlag GmbH & Co. KGaA, Weinheim 

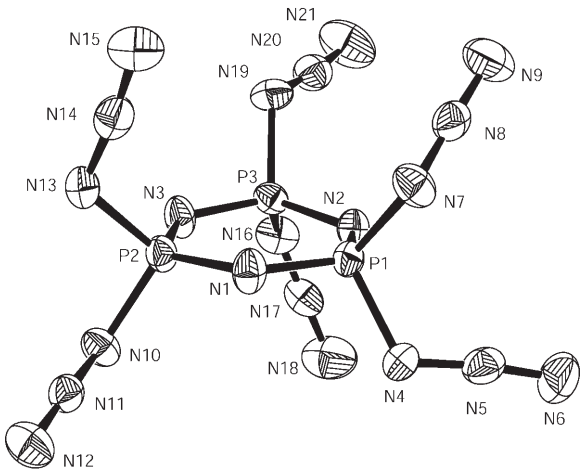


***Figure 3.*** ORTEP representation of the molecular structure of $P_3N_{21}$; thermal ellipsoids are set at 50% probability. Selected bond lengths [Å] and angles [°]: P1–N1 1.558(2), P1–N2 1.576(2), P1–N4 1.666(2), P1–N7 1.671(2), N4–N5 1.218(3), N5–N6 1.117(3), N7–N8 1.203(3), N8–N9 1.114(3); N1-P1-N2 118.2(1), P1-N1-P2 122.1(1), N4-N5-N6 173.4(3), N7-N8-N9 173.5(3), P1-N4-N5 117.7(2), P1-N7-N8 119.2(2), N4-P1-N7 102.2(1), N1-P1-N4 104.5(1), N2-P1-N4 111.9(1), N1-P1-N7 108.9(1), N2-P1-N7 109.8(1).

1.576(2) Å), correspond well with the average values of 121.4/118.4° and 1.58 Å reported for $P_3N_3Cl_6$. In addition, the $N_\alpha$-P-$N_\alpha$ angles (99.2(1)–102.2(1)°) also correspond well with the average Cl-P-Cl angle of 102°. However, the average P–$N_\alpha$ distance in **1** (1.67 Å) is significantly shorter than the corresponding average P–Cl distance in $N_3P_3Cl_6$ (1.97 Å). The P-$N_\alpha$-$N_\beta$ angles are all approximately 120°, suggesting an $sp^2$ hybridization of the $N_\alpha$ atoms.

Furthermore, the identity of $P_3N_{21}$ was confirmed by high-resolution mass spectrometry, which also demonstrated that the compound can be transferred into the gas phase without decomposition. Two signals were observed in the mass spectrum: the first mass peak corresponds to the molecular peak, and the second to a species in which one azide group has been removed from the $P_3N_{21}$ molecule.

The thermal stability of $P_3N_{21}$ was investigated using differential scanning calorimetry (DSC). At a heating rate of $2\,^\circ C\,min^{-1}$, the compound decomposes explosively at an onset temperature of 220 °C. This relatively high decomposition temperature is in contrast with the very high impact sensitivity of the substance at room temperature (< 1 J). Direct heating in a flame also results in an explosive decomposition of the compound with a loud noise and a flash of light.

## Experimental Section

**Caution!** Phosphorus azides are highly endothermic compounds and decompose explosively under various conditions! $P_3N_{21}$ is extremely impact sensitive. Owing to the high energy content of $P_3N_{21}$, explosions can cause substantial damage, even when quantities on the order of 1 mmol are used.[5a] The use of suitable protective clothing, in particular a face shield, ear protectors, a bullet-proof vest, arm protectors, and kevlar gloves, as well as appropriate shoes for protection from electrostatic charge, is mandatory. **Ignoring these safety precautions can result in serious injury!**

$P_3N_3Cl_6$ and trimethylsilylazide were purchased from Aldrich. Propionitrile was dried over $P_4O_{10}$ and distilled prior to use. The Raman spectra were measured using a Perkin Elmer Spectrum 2000R NIR FT-Raman instrument (Nd:YAG Laser (1064 nm)). The IR spectra were recorded using a Perkin Elmer Spectrum One FT-IR instrument. The $^{31}P$, $^{15}N$, and $^{14}N$ NMR spectra were recorded using a Jeol EX 400 NMR spectrometer operating at 28.9 MHz ($^{14}N$), 40.6 MHz ($^{15}N$), or 162.0 MHz ($^{31}P$); the chemical shifts are in ppm relative to nitromethane ($^{14/15}N$) or 85% phosphoric acid ($^{31}P$). The mass spectra were measured using a Jeol MStation JMS-700 spectrometer. The decomposition temperature was determined using a Pyris 6 DSC instrument. The impact sensitivity at room temperature was determined using a Bundesanstalt für Materialforschung und -prüfung (BAM) drop hammer.

$P_3N_{21}$: $P_3N_3Cl_6$ (224 mg, 0.644 mmol) was added to a flame-dried Schlenk flask under argon and dissolved in anhydrous propionitrile (20 mL) at room temperature. Trimethylsilylazide (893 mg, 7.750 mmol) was added dropwise to the stirred solution under a nitrogen purge. A bubbler was connected to the flask, and a slow stream of nitrogen gas was passed continuously through the apparatus. The colorless solution was warmed to 60 °C and stirred for 3 h at this temperature. The now pale yellow solution was then stirred for 19 h at room temperature. The reaction mixture was subsequently concentrated using a rotary evaporator (30 °C, 50 mbar) and the remaining solvent was removed on a high-vacuum line ($1 \times 10^{-3}$ mbar, room temperature, several minutes). The pale yellow liquid obtained was purified by sublimation ($1 \times 10^{-3}$ mbar, 130 °C oil bath, −86 °C cold finger), yielding a colorless liquid. Single crystals of **1** were obtained by the controlled cooling and warming of the substance near its melting point. The substance was repeatedly cooled to −78.5 °C with dry ice and slowly warmed to −17 °C in a cold room, while being monitored with a microscope. As soon as the liquid phase formed, it was again cooled with dry ice. The cycle was repeated until crystals formed. The single crystals of **1** must be handled with great care! Raman (neat, 25 °C): see Table 1; IR (nujol, KBr, background subtracted): see Table 1; $^{31}P$ NMR ($C_6D_6$, 25 °C): $\delta = 13.6$ ppm ($\Delta\nu_{1/2} = 10$ Hz); $^{15}N$ NMR ($C_6D_6$, 25 °C): $\delta = -152.7$ ($N_\beta$), −166.8 ($N_\gamma$), −291.3 ($N_\alpha$), −305.4 ppm ($N_{ring}$); $^{14}N$ NMR ($C_6D_6$, 25 °C): $\delta = -152.7$ ($N_\beta$, $\Delta\nu_{1/2} = 34$ Hz), −166.8 ($N_\gamma$, $\Delta\nu_{1/2} = 115$ Hz), −300 ppm ($N_\alpha/N_{ring}$, $\Delta\nu_{1/2} = 950$ Hz); MS (DEI, 70 eV): *m/z* (%): 387 (39) $[M]^+$, 345 (100) $[M-N_3]^+$; MS (HR): *m/z* calcd for $P_3N_{21}$: 386.9858; found: 386.9851. DSC ($2\,^\circ C\,min^{-1}$): 220 °C (decomp); impact sensitivity: < 1 J.

Computational methods: BLYP and B3LYP density functional theory (DFT) calculations were carried out. The geometry, IR spectrum, and Raman spectrum of **1** were calculated with the Gaussian program,[13] using 6-31G(d) basis sets.

Received: April 27, 2006

**Keywords:** ab initio calculations · azides · phosphorus nitrides · structure elucidation · X-ray diffraction

[1] a) S. Horstmann, E. Irran, W. Schnick, *Angew. Chem.* **1997**, *109*, 1938; *Angew. Chem. Int. Ed. Engl.* **1997**, *36*, 1873; b) K. Landskron, H. Huppertz, J. Senker, W. Schnick, *Angew. Chem.* **2001**, *113*, 2713; *Angew. Chem. Int. Ed.* **2001**, *40*, 2643.

[2] E. H. Kober, H. F. Lederle, G. F. Ottmann, USA Patent US 32918645, **1966**.

[3] X. Zeng, W. Wang, F. Liu, M. Ge, Z. Sun, D. Wang, *Eur. J. Inorg. Chem.* **2006**, 416.

[4] P. Volgnandt, A. Schmidt, *Z. Anorg. Allg. Chem.* **1976**, *425*, 189.

[5] a) C. Grundmann, R. Rätz, *Z. Naturforsch. B* **1954**, *10*, 116; b) F. Räuchle, M. Gayoso, *Ann. Fis.* **1970**, *66*, 241; c) J. Müller, H. Schröder, *Z. Anorg. Allg. Chem.* **1979**, *450*, 149.

 © 2006 Wiley-VCH Verlag GmbH & Co. KGaA, Weinheim 

[6] R. Haiges, S. Schneider, T. Schroer, K. O. Christe, *Angew. Chem.* **2004**, *116*, 5027; *Angew. Chem. Int. Ed.* **2004**, *43*, 4919.
[7] a) I. C. Tornieporth-Oetting, T. M. Klapötke, *Angew. Chem.* **1995**, *107*, 559; *Angew. Chem. Int. Ed. Engl.* **1995**, *34*, 511; b) T. M. Klapötke, *Chem. Ber.* **1997**, *130*, 443; c) I. C. Tornieporth-Oetting, T. M. Klapötke in *Combustion Efficiency and Air Quality* (Eds.: I. Hargittai, T. Vidoczy), Plenum, New York, **1995**, p. 51.
[8] Crystal data for $P_3N_{21}$: Xcalibur S (Oxford Diffraction), $0.26 \times 0.22 \times 0.13$ mm, triclinic, space group $P\bar{1}$, $a = 7.1953(9)$, $b = 7.3718(9)$, $c = 12.994(1)$ Å, $\alpha = 87.41(1)$, $\beta = 78.95(1)$, $\gamma = 89.59(1)°$, $V = 675.8(1)$ Å$^3$, $Z = 2$, $\rho_{calcd} = 1.902$ g cm$^{-3}$, $2\theta_{max} = 52.12°$, $Mo_{K\alpha}$ radiation ($\lambda = 0.71073$ Å), graphite monochromator, $\omega$ scans, $T = 200$ K, 6941 measured reflections, 2657 independent reflections, 2207 with $F_o > 4\sigma(F_o)$, 217 parameters, $R_1 = 0.0375$, $wR_2$(all data) $= 0.0944$, $\mu(Mo_{K\alpha}) = 0.486$ mm$^{-1}$, programs used: SHELXS-97, SHELXL-97 (G. M. Sheldrick, *SHELXS-97*, Program for the solution of crystal structures, Universität Göttingen, **1997**; G. M. Sheldrick, *SHELXL-97*, Program for the refinement of crystal structures, Universität Göttingen, **1997**), refinement on $F^2$, residual electron density: 0.334/−0.321 e Å$^3$. Further details on the crystal structure investigations may be obtained from the Fachinformationszentrum Karlsruhe, 76344 Eggenstein-Leopoldshafen, Germany (fax: (+49) 7247-808-666; e-mail: crysdata@fiz-karlsruhe.de), on quoting the depository number CSD-416415.
[9] B. Thomas, G. Seifert, G. Großmann, *Z. Chem.* **1980**, *20*, 217.
[10] P. Geißler, T. M. Klapötke, H. J. Kroth, *Spectrochim. Acta Part A* **1995**, *51*, 1075.
[11] J. B. Foresman, A. Frisch, *Exploring Chemistry with Electronic Structure Methods*, 2nd ed., Gaussian, Philadelphia, **1996**, p. 64.
[12] G. J. Bullen, *J. Chem. Soc. A* **1971**, 1450.
[13] Gaussian 03 (Revision A.1): M. J. Frisch et al., see Supporting Information.

 © 2006 Wiley-VCH Verlag GmbH & Co. KGaA, Weinheim 

Organozinc Compounds

DOI: 10.1002/anie.200601450

# Efficient Synthesis of Functionalized Organozinc Compounds by the Direct Insertion of Zinc into Organic Iodides and Bromides**

*Arkady Krasovskiy, Vladimir Malakhov, Andrei Gavryushin, and Paul Knochel**

Organozinc compounds are important intermediates in organic chemistry because of their compatibility with many functional groups.[1] The direct insertion of zinc into organic halides is the most attractive and simplest method for the preparation of functionalized organozinc halides.[1] Whereas several polar solvents such as dimethylacetamide, hexamethylphosphoramide, *N*,*N*-dimethylformamide, dimethylsulfoxide, acetonitrile, and tetramethylurea can be used,[2] the most common and convenient is tetrahydrofuran.[3] The preparation of arylzinc iodides in THF from aryl iodides can only be achieved by using Rieke-zinc[1b,4] or requires the presence of electron-accepting substituents in the *ortho* position of the aryl iodides as well as elevated reaction temperatures.[3] The use of Rieke-zinc also allows the preparation of alkylzinc reagents starting from alkyl bromides instead of alkyl iodides.[5] Since the activity of Rieke-zinc decreases with time, the development of a practical procedure for zinc insertion using commercially available zinc dust would be highly desirable.

Recently, we have found that the Br/Mg exchange reaction can be accelerated by adding LiCl.[6] Herein, we report a new protocol for the preparation of functionalized aryl- and alkylzinc compounds by the direct insertion of commercially available Zn powder[7] in the presence of LiCl in THF. Thus, when iodobenzene (**1a**) was treated with commercial zinc powder (3 equiv, 150 mesh, activated by the addition of 1,2-dibromoethane (5 mol%) and TMSCl (1 mol%))[7] only 5% conversion could be reached after 24 h at 50°C. However, in the presence of 1.5 equivalent of LiCl, full conversion into phenylzinc iodide (**1b**) was observed after 7 h at 50°C. Ketone **1c** was obtained in 90% yield after reaction with pivaloyl chloride in the presence of CuCN·2 LiCl. The presence of an electron-withdrawing group at the *ortho* (see **2a**) or *para* positions (see **3a**) considerably increases the rate of insertion, and the corresponding arylzinc

[*] Dr. A. Krasovskiy, V. Malakhov, A. Gavryushin, Prof. Dr. P. Knochel
Ludwig Maximilians-Universität München
Department Chemie & Biochemie
Butenandtstrasse 5–13, Haus F, 81377 München (Germany)
Fax: (+49) 89-218-077-680
E-mail: paul.knochel@cup.uni-muenchen.de

[**] We thank the Fonds der Chemischen Industrie and Merck Research Laboratories (MSD) and the DFG for financial support. We also thank Chemetall GmbH (Frankfurt) and BASF AG (Ludwigshafen) for the generous gift of chemicals.

Supporting information for this article is available on the WWW under http://www.angewandte.org or from the author.


WILEY InterScience DISCOVER SOMETHING GREAT
© 2006 Wiley-VCH Verlag GmbH & Co. KGaA, Weinheim

iodides can be efficiently prepared at room temperature (>98% conversion; Scheme 1). The insertion of zinc in the absence of LiCl can only be accomplished at 70°C with a low yield for *ortho*-trifluoromethylphenyl iodide (**2a**) and no insertion occurs with ethyl 4-iodobenzoate (**3a**; 70°C, 24 h, conversion <5%). The organozinc iodides **2b** and **3b** react cleanly with electrophiles such as tetramethylthiuram disulfide[8] and allyl bromide to afford the corresponding products **2c** and **3c** in yields of 91 and 94%, respectively (Scheme 1).

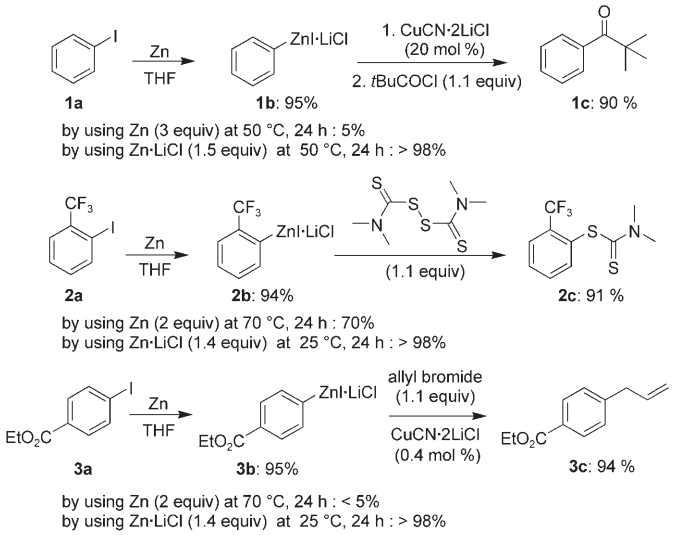


***Scheme 1.*** Insertion of Zn in the presence and absence of LiCl. The specified yields by the formula numbers **1b**–**3b** were determined by titration; the yields >98% were determined by GC analysis.

4-Anisylzinc iodide (**4a**) can be prepared in 93% yield by the insertion of Zn in the presence of LiCl at 50°C in THF (entry 1, Table 1).[9] A broad range of functionalized arylzinc iodides bearing an ester, a nitrile, or an amide group such as **5a**–**8a** can be easily prepared in good yields (92–95%) and treated with electrophiles (entries 2–5, Table 1). A sensitive methyl ketone functionality is also compatible with the mild insertion conditions. 4-Acetylphenylzinc iodide (**9a**) was formed in 87% yield after 3 h at 25°C and a copper-catalyzed acylation led to the diketone **9b** in 88% yield (entry 6, Table 1). Interestingly, even an aldehyde group can be tolerated. Thus, aryl- and heteroarylzinc iodides bearing a formyl group (**10a** and **11a**) were obtained in good yields by a direct zinc insertion reaction at room temperature (entries 7 and 8, Table 1). Transition-metal-catalyzed coupling reactions with ethyl 4-iodobenzoate (1 mol% $[Pd(PPh_3)_4]$) and ethyl 2-bromomethyl acrylate (0.4 mol% of CuCN·2LiCl) led to the desired functionalized aldehydes **10b** and **11b** in yields of 85 and 81%, respectively (entries 7 and 8, Table 1).

The insertion reaction displays an excellent chemoselectivity. Thus, treating 4-bromophenyl iodide (50°C, 6 h) with Zn/LiCl resulted only in insertion into the C–I bond to give the zinc reagent **12a** (96%). Subsequent allylation provides the aryl bromide **12b** in 96% yield (entry 9, Table 1). Moreover, a selective formation of the corresponding monometalated compound is possible in the case of diiodoaryl compounds (**13a**, entry 10, Table 1). A stepwise insertion into 2,5-diiodothiophene (**14a**) allows the introduction of two different electrophiles (Scheme 2). Thus, the reaction of diiodide **14a** with Zn/LiCl followed by a copper(I)-catalyzed acylation led to the ketone **14b**, which can be further functionalized through a zinc insertion/allylation sequence to afford the disubstituted thiophene **14c** in 82% overall yield. Alternatively, the formation of a bismetallic species can be achieved.[10] Thus, 2,2′-diiodobiphenyl (**15a**) reacts smoothly with Zn/LiCl (5 equiv) at 50°C to furnish bis(iodozincio)biphenyl (**15b**) in 94% yield. The corresponding biphenyl derivative **15c** was obtained in 77% yield after a copper(I)-catalyzed coupling with allyl bromide.

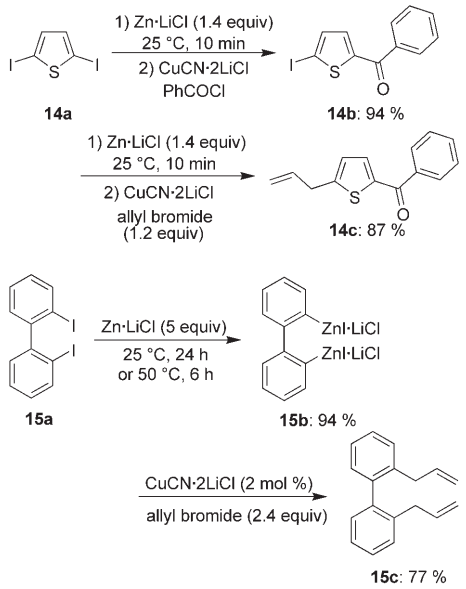


***Scheme 2.*** Chemoselective zinc insertion into diiodides.

A smooth zinc insertion is also observed for heterocyclic iodides. Thus, various iodopyridines and 1-iodoisoquinoline react readily with Zn powder to afford the corresponding heteroarylzinc iodides **16a**–**19a** at RT in yields of greater than 90% (entries 11–14, Table 1). The resulting organozinc compounds were efficiently quenched with a wide range of electrophiles under transition-metal catalysis to give the functionalized aza-heterocycles **16b**–**19b** in yields of 83–90%.

The insertion of Zn into a C–Br bond is also possible in the case of activated aryl- and heteroaryl compounds. Thus, in the presence of LiCl, the functionalized zinc reagent **20b** was formed at room temperature in 91% yield starting from the bromodiester **20a**. Quenching with allyl bromide leads to the allylated diester **20c** in 90% yield. Similarly, the reaction of ethyl 5-bromo-2-furoate (**21a**) with Zn/LiCl furnishes the corresponding furylzinc reagent **21b** in 92% yield after 12 h at 25°C. This compound was successfully coupled with 4-iodobenzonitrile in the presence of $[Pd(PPh_3)_4]$ (1 mol%; Scheme 3).[11]

For the first time, the use of Zn powder in the presence of LiCl allows the expedient preparation of functionalized

 © 2006 Wiley-VCH Verlag GmbH & Co. KGaA, Weinheim 

***Table 1:*** Preparation and reactions of functionalized aryl- and heteroarylzinc reagents.

| Entry | Zinc reagent, yield [%][a] | *T* [°C], *t* [h] | Electrophile | Product, yield [%][b] | Entry | Zinc reagent, yield [%][a] | *T* [°C], *t* [h] | Electrophile | Product, yield [%][b] |
|---|---|---|---|---|---|---|---|---|---|
| 1 | 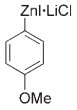 | | | 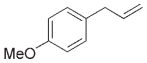 | 8 | 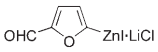 | | 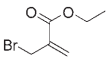 | 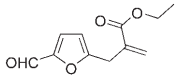 |
| | **4a:** 93 | 50, 90 | AllBr[c] | **4b**: 94 | | **11a**: 83 | 25, 2.5 | | **11b**: 81 |
| 2 | 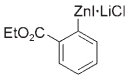 | | | 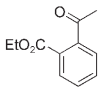 | 9 | 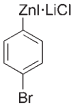 | | | 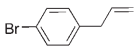 |
| | **5a**: 92 | 25, 1 | AcCl[d] | **5b**: 90 | | **12a**: 96 | 50, 6 | AllBr[c] | **12b**: 96 |
| 3 | 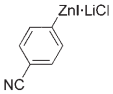 | | 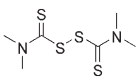 | 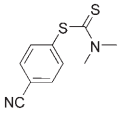 | 10 | 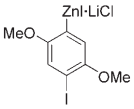 | | | 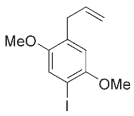 |
| | **6a**: 95 | 50, 3 | | **6b**: 89 | | **13a**: 90 | 50, 120 | AllBr[c] | **13b**: 89 |
| 4 | | | | | 11[e] | 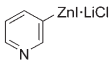 | | 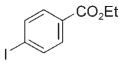 | 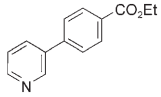 |
| | **7a**: 93 | 50, 6 | PhCOCl[d] | **7b**: 88 | | **16a:** 92 | 25, 8 | | **16b**: 87 |
| 5 | 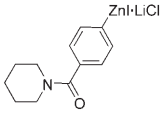 | | | 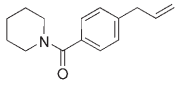 | 12 | 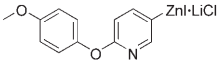 | | | 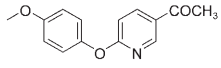 |
| | **8a**: 93 | 25, 24 | AllBr[c] | **8b**: 96 | | **17a:** 90 | 25, 24 | $CH_3COCl$[d] | **17b**: 83 |
| 6 | 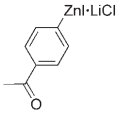 | | | 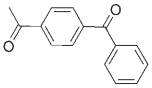 | 13 | 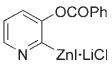 | | | 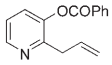 |
| | **9a**: 87 | 25, 3 | PhCOCl[d] | **9b**: 88 | | **18a:** 91 | 25, 12 | AllBr[c] | **18b**: 85 |
| 7[e] | 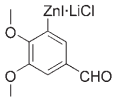 | | 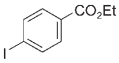 | 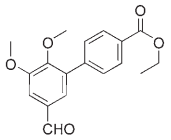 | 14 | 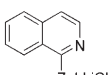 | | | 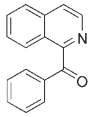 |
| | **10a**: 82 | 25, 12 | | **10b**: 85 | | **19a:** 96 | 25, 12 | PhCOCl[d] | **19b**: 90 |

[a] Yield estimated after titration with $I_2$. [b] Yield of isolated analytically pure product based on the molarity of the zinc reagent. [c] 2 mol% of CuCN·2 LiCl was added. [d] 20 mol% of CuCN·2 LiCl was added. [e] 1 mol% of $[Pd(PPh_3)_4]$ was added.

alkylzinc reagents **22a**–**30a** starting from alkyl bromides (Table 2). Thus, unactivated *n*-octylbromide and 1-bromo-5-chloropentane react cleanly with Zn·LiCl to afford the corresponding alkylzinc reagents in yields of greater than 92%. The reaction with PhCOCl in the presence of catalytic amounts of $Pd^0$ provides ketones **22b** and **23b** in 89% yield (Table 2).[11] The formation of cyclobutylmethylzinc bromide **24a** proceeds without the formation of ring-opening products, thus leading after allylation to the unsaturated ester **24b**. Functionalized alkylzinc compounds such as **25a**–**27a** can also be prepared in high yields. The Pd-catalyzed coupling of these zinc reagents with different ethyl iodobenzoates lead to difunctionalized benzenes **25b**–**27b** in good yields (entries 4–6, Table 2). The insertion reaction is also efficient in the case of secondary alkyl bromides and provides alkylzinc reagents **28a** and **29a** in yields of 96 and 93%, respectively. Adamantylzinc bromide (**30a**) is obtained in 83% yield by the direct insertion of Zn in the presence of LiCl. Secondary alkylzinc reagents **28a**–**30a** show good reactivity towards electrophiles (entries 7–9, Table 2). Finally, zinc insertion in the presence of LiCl allows the smooth preparation of the alkenylzinc reagent **31b** starting from α-bromostyrene (**31a**). Copper(I)-catalyzed acylation with benzoyl chloride leads to the unsaturated ketone **31c** in 81% yield (Scheme 4).

The nature of the activation of the zinc dust with LiCl is speculative. However, it can be envisioned that the role of LiCl is to rapidly remove the formed organozinc reagent from the metal surface by generating highly soluble RZnX·LiCl

 © 2006 Wiley-VCH Verlag GmbH & Co. KGaA, Weinheim 

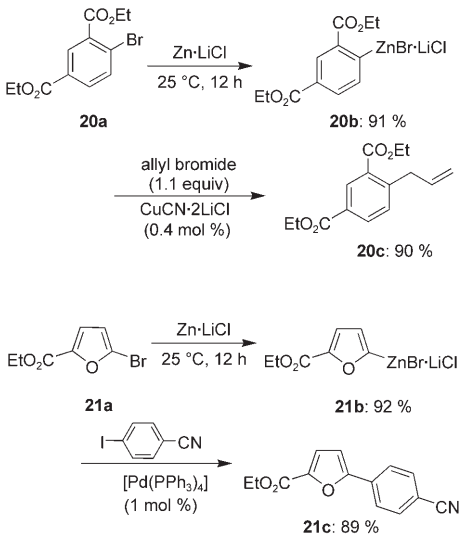


***Scheme 3.*** LiCl-mediated zinc insertion into aryl and heteroaryl bromides.

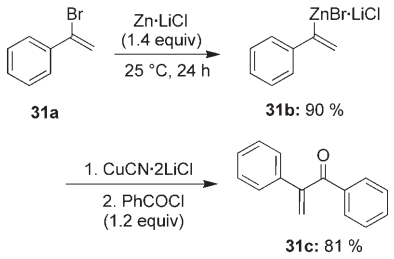


***Scheme 4.*** Insertion of Zn into α-bromostyrene.

complexes, thus allowing a rapid reaction of a further molecule of R–X and thereby avoiding the competitive deactivation of the active metal sites.

In conclusion, we have shown that the use of Zn powder in the presence of LiCl in THF allows a simple, high-yielding preparation of a broad range of functionalized aryl- and heteroarylzinc reagents. The synthesis of the alkylzinc reagents was performed from inexpensive and readily available alkyl bromides. All reactions proceed within a practical temperature range (25–50 °C), and can be extended to large-scale preparation. Extensions of this work are currently underway.[12]

## *Experimental Section*

Typical procedure. Preparation of **3c** (Scheme 1): Anhydrous LiCl (5 mmol) was placed in an Ar-flushed flask and dried for 20 min at 150–170 °C under high vacuum (1 mbar). Zinc powder (7 mmol, 1.4 equiv, 150 mesh, Chemetall, or 325 mesh, Strem) was added under Ar and the heterogeneous mixture of Zn and LiCl was dried again for 10–20 min at 150–170 °C under high vacuum (1 mbar). The reaction flask was evacuated and refilled with argon three times. THF (5 mL) was added and the Zn was activated with $BrCH_2CH_2Br$ (5 mol %) and $Me_3SiCl$ (1 mol %).[7] **3a** (5 mmol) was then added neat at room temperature. The insertion reaction was complete after 24 h (checked by GC analysis of reaction aliquots, the conversion was higher than 98 %). Titration of an aliquot (1 mL) of the organozinc reagent with iodine[13] showed that the concentration of **3b** in THF was 0.83 M. The solution of **3b** (3 mmol, 3.61 mL) was carefully separated from the remaining zinc powder by using a syringe and transferred to another dry and Ar-flushed flask. Allyl bromide (3.3 mmol) was added at −20 °C, followed by CuCN·2 LiCl (one drop of a 1.0 M solution in THF, ca. 0.02 mmol, ca. 0.4 mol %). The reaction mixture was stirred for 1 h at 0 °C and was then quenched with saturated aqueous $NH_4Cl$ solution (5 mL). The aqueous phase was extracted with ethyl acetate (3 × 5 mL) and concentrated in vacuo. The crude residue was purified by flash chromatography ($CH_2Cl_2$) and yielded **3c** (2.82 mmol, 504 mg, 94 %) as a colorless oil.

***Table 2:*** Preparation and reaction of aliphatic zinc reagents.

| Entry | Zinc reagent, yield [%][a] | *T* [°C], *t* [h] | Electrophile | Product, yield [%][b] |
|---|---|---|---|---|
| 1 | *n*-$C_8H_{17}ZnBr\cdot LiCl$ | | | 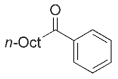 |
| | **22a**: 92 | 50, 24 | PhCOCl[c] | **22b**: 89 |
| 2 | $Cl(CH_2)_5ZnBr\cdot LiCl$ | | | 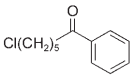 |
| | **23a**: 93 | 50, 12 | PhCOCl[c] | **23b**: 89 |
| 3 | 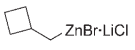 | | 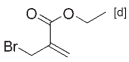 [d] | 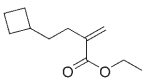 |
| | **24a**: 86 | 50, 50 | | **24b**: 82 |
| 4 | $AcO(CH_2)_4ZnBr\cdot LiCl$ | | 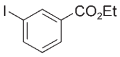 | 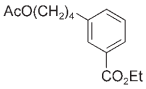 |
| | **25a**: 96 | 50, 3 | | **25b**: 83 |
| 5 | $EtO_2C(CH_2)_3ZnBr\cdot LiCl$ | | 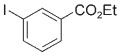 | 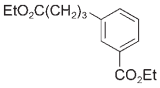 |
| | **26a**: 95 | 50, 1 | | **26b**: 93 |
| 6 | $NC(CH_2)_4ZnBr\cdot LiCl$ | | 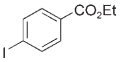 | 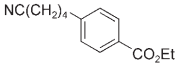 |
| | **27a**: 95 | 50, 6 | | **27b**: 88 |
| 7 | 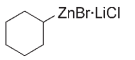 | | PhCOCl[c] | 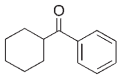 |
| | **28a**: 96 | 50, 24 | | **28b**: 94 |
| 8 | 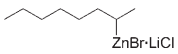 | | PhCOCl[c] | 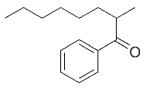 |
| | **29a**: 93 | 50, 18 | | **29b**: 90 |
| 9 | 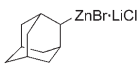 | | 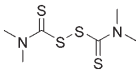 | 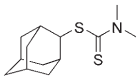 |
| | **30a**: 83 | 50, 24 | | **30b**: 79 |

[a] Yield determined by titration with $I_2$. [b] Yield of isolated analytically pure product based on the molarity of the zinc reagent. [c] 0.1 mol % of $[Pd(dba)_2]$ (dba = *trans*,*trans*-dibenzylideneacetone) and 0.2 mol % of *S*-phos[14] were added. [d] 1 mol % of CuCN·2 LiCl was added.

Received: April 12, 2006
Published online: August 10, 2006

**Keywords:** coupling · homogeneous catalysis · insertion · organozinc compounds · zinc

 © 2006 Wiley-VCH Verlag GmbH & Co. KGaA, Weinheim 

[1] a) "Polyfunctional Zinc Organometallics for Organic Synthesis": P. Knochel, H. Leuser, L.-Z. Gong, S. Perrone, F. F. Kneisel, *Handbook of Functionalized Organometallics*, *Vol. 1* (Ed.: P. Knochel), Wiley-VCH, Weinheim, **2005**, p. 251; b) *Organozinc Reagents* (Eds.: P. Knochel, P. Jones), Oxford University Press, New York, **1999**.

[2] a) K. Tagaki, N. Hayama, S. Inokawa, *Bull. Chem. Soc. Jpn.* **1980**, *53*, 3691; b) K. Tagaki, *Chem. Lett.* **1993**, 469; c) K. Tagaki, Y. Shimoishi, K. Sasaki, *Chem. Lett.* **1994**, 2055; d) T. N. Majid, P. Knochel, *Tetrahedron Lett.* **1990**, *31*, 4413; e) C. Gosmini, M. Amatore, S. Claudel, J. Perichon, *Synlett* **2005**, 2171; f) I. Kazmierski, C. Gosmini, J.-M. Paris, J. Perichon, *Tetrahedron Lett.* **2003**, *44*, 6417.

[3] R. Ikegami, A. Koresawa, T. Shibata, K. Takagi, *J. Org. Chem.* **2003**, *68*, 2195.

[4] a) R. D. Rieke, P. T. Li, T. P. Burns, S. T. Uhm, *J. Org. Chem.* **1981**, *46*, 4323; b) R. T. Arnold, S. T. Kulenovic, *Synth. Commun.* **1977**, *7*, 223.

[5] a) L. Zhu, R. M. Wehmeyer, R. D. Rieke, *J. Org. Chem.* **1991**, *56*, 1445; b) R. D. Rieke, M. V. Hanson, J. D. Brown, Q. J. Niu, *J. Org. Chem.* **1996**, *61*, 2726; c) P. Knochel, M. C. P. Yeh, S. C. Berk, J. Talbert, *J. Org. Chem.* **1988**, *53*, 2390.

[6] a) A. Krasovskiy, P. Knochel, *Angew. Chem.* **2004**, *116*, 3396; *Angew. Chem. Int. Ed.* **2004**, *43*, 3333; b) H. Ren, A. Krasovskiy, P. Knochel, *Chem. Commun.* **2005**, 543; c) H. Ren, A. Krasovskiy, P. Knochel, *Org. Lett.* **2004**, *6*, 4215; d) A. Krasovskiy, B. F. Straub, P. Knochel, *Angew. Chem.* **2006**, *118*, 165; *Angew. Chem. Int. Ed.* **2006**, *45*, 159.

[7] The zinc powder was activated by treatment first with 1,2-dibromoethane and then with chlorotrimethylsilane; see: P. Knochel, M. J. Rozema, C. E. Tucker, *Organocopper reagents* (Ed.: R. J. K. Taylor), Oxford University press, Oxford, **1994**, p. 85.

[8] A. Krasovskiy, A. Gavryushin, P. Knochel, *Synlett* **2006**, 792.

[9] There is only one literature precedent[3] for the direct synthesis of **4a** in an ethereal solvent (24 h, 130 °C in diglyme).

[10] a) J. F. Normant, I. Marek, J. M. Lefrancois, *Pure Appl. Chem.* **1992**, *64*, 1857; b) J. F. Normant, *Acc. Chem. Res.* **2001**, *34*, 640.

[11] "Palladium- or nickel-catalyzed cross-coupling with organometals containing zinc, aluminum, and zirconium: The Negishi coupling": a) E. Negishi, X. Zeng, Z. Tan, M. Qian, Q. Hu, Z. Huang, *Metal-Catalyzed Cross-Coupling Reactions*, *Vol. 2*, *2nd ed.* (Eds.: A. De Meijere, F. Diederich), Wiley-VCH, Weinheim, **2004**, p. 815.

[12] A patent application was filed.

[13] A. Krasovskiy, P. Knochel, S *ynthesis* **2006**, 890.

[14] S. D. Walker, T. E. Barder, J. R. Martinelli, S. L. Buchwald, *Angew. Chem.* **2004**, *116*, 1907; *Angew. Chem. Int. Ed.* **2004**, *43*, 1871.


 © 2006 Wiley-VCH Verlag GmbH & Co. KGaA, Weinheim 

Polymerization

DOI: 10.1002/anie.200601387

# Mechanistic Studies of Catalytic Polyethylene Chain Growth in the Presence of Water**

*Andreas Berkefeld and Stefan Mecking**

Emulsion polymerization of unsaturated monomers is among the most important polymerization processes. With this method aqueous dispersions of surfactant-stabilized polymer particles, with sizes of 50 nm to 1000 nm, are obtained. These dispersions are employed broadly, for example, for environmentally benign coatings. In comparison to traditional free-radical techniques which are employed commercially,[1] the synthesis of polymer dispersions by transition-metal-catalyzed insertion polymerization is complimentary in terms of the polymers accessible, and provides a much broader scope of control of polymer microstructures.[2–5,8] Synthesis of polyethylene dispersions of unusually small particle sizes and defined microstructures has been studied recently.[2g–i]

These versatile transition-metal-catalyzed polymerizations in aqueous systems raise the question of fundamental underlying reaction steps, namely 1) the competition of monomer and water for binding sites at the metal center (that is, reversible blocking of active sites), 2) chain growth in the presence of water, and 3) the reactivity of higher metal alkyl species M−R (R > Me) formed during polymerization towards water in general. Recent theoretical studies indicate that ethylene binding is preferred over water coordination in various catalyst systems, namely neutral nickel salicylaldiminato and cationic palladium or nickel diimine complexes.[6]

As the model system for experimental studies we chose the cationic α-diimine palladium system studied by Brookhart et al., because the palladium alkyl olefin resting states can be detected conveniently by low-temperature NMR spectroscopy.[7,9,10] To enable quantitative studies in homogeneous solution, [D$_8$]THF was employed as a water-miscible solvent with a low freezing point.

Addition of water to a solution of the diethyl ether adduct[7] [($\widehat{\text{NN}}$)PdMe(OEt$_2$)][BAr$_4^F$] (**1**-OEt$_2$), where BAr$_4^F$ = B(3,5-(CF$_3$)$_2$C$_6$H$_3$)$_4$, $\widehat{\text{NN}}$ = ArNC(Me)(Me)CNAr, with Ar = 2,6-*i*Pr$_2$C$_6$H$_3$) in [D$_8$]THF at −60 °C cleanly afforded the water complex **1**-OH$_2$. The relative binding constant of water versus [D$_8$]THF was estimated to be

[*] Dipl.-Chem. A. Berkefeld, Prof. Dr. S. Mecking
Lehrstuhl für Chemische Materialwissenschaft
Fachbereich Chemie
Universität Konstanz
Universitätsstrasse 10, 78457 Konstanz (Germany)
Fax: (+49) 7531-88-5152
E-mail: stefan.mecking@uni-konstanz.de

[**] Financial support by the DFG (Me1388/3-2) is gratefully acknowledged. We thank U. Haunz for technical support, and H. Möller for discussions on NMR spectroscopy.

Supporting information for this article is available on the WWW under http://www.angewandte.org or from the author.

 WILEY InterScience DISCOVER SOMETHING GREAT

© 2006 Wiley-VCH Verlag GmbH & Co. KGaA, Weinheim

$K = 4 \times 10^4$ (THF versus diethyl ether, $K = 4$). Key signals in the $^1$H NMR spectrum (12 equiv water,[13] −60 °C) are $\delta =$ 6.32 (br, s, Pd($CH_3$)($OH_2$)), 2.31 and 2.27 (s, ($H_3$C)CN, $\widehat{NN}$), 0.34 ppm (s, Pd($CH_3$)($OH_2$)) (for complete NMR data see the Supporting Information).[11]

The resonance signal for excess free water occurs at $\delta =$ 3.30 ppm. As the singlet signal of coordinated water is not conclusive, the assignment was confirmed unambiguously by an EXCY NMR exchange experiment on the signals of free and coordinated water (see Supporting Information). This observation of separate signals for free and coordinated water shows that the exchange is slow on the NMR time scale. The corresponding coalescence temperature, $T_C(OH_2)$, was determined to be between 0 and 5 °C. This corresponds to a first-order exchange rate constant $k_C(PdMe, OH_2)$ on the order of $10^3$ s$^{-1}$.[12]

Exposure of **1**-$OH_2$ in [$D_8$]THF to ethylene at −60 °C resulted in its partial conversion into the known[7] olefin complex **1**-$C_2H_4$ (Scheme 1 and Figure 1). At temperatures above −30 °C ethylene insertion occurs. Thus, the insertion of ethylene in the presence of water can be detected and higher alkyl water complexes $[(\widehat{NN})Pd(C_{2n+1}H_{4n+3})(OH_2)]^+$ (**2**-$OH_2$)

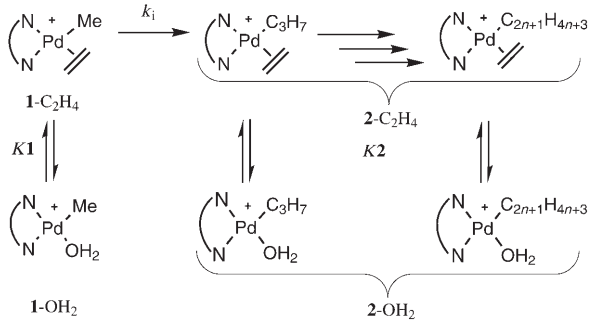


***Scheme 1.*** Exchange of water versus ethylene monomer, and chain growth in the presence of water.

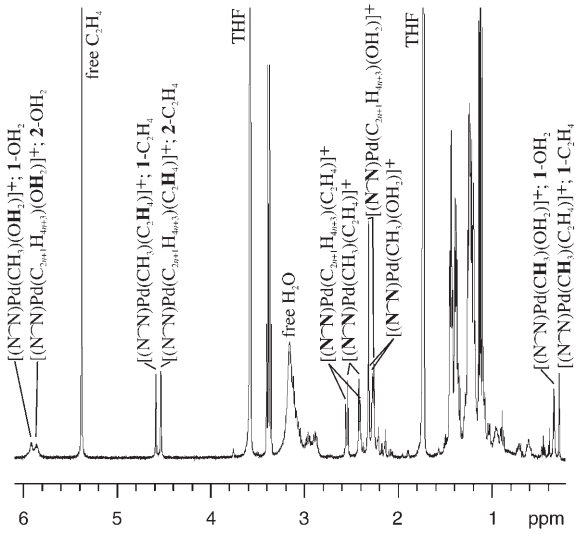


***Figure 1.*** Palladium water and olefin species detected by $^1$H NMR spectroscopy during chain growth (12 equiv ethylene, 3.6 equiv water, −20 °C, [$D_8$]THF).

can be prepared cleanly in the NMR tube (Figure 2). Vice versa, starting from **1**-$OEt_2$, the addition of water after the

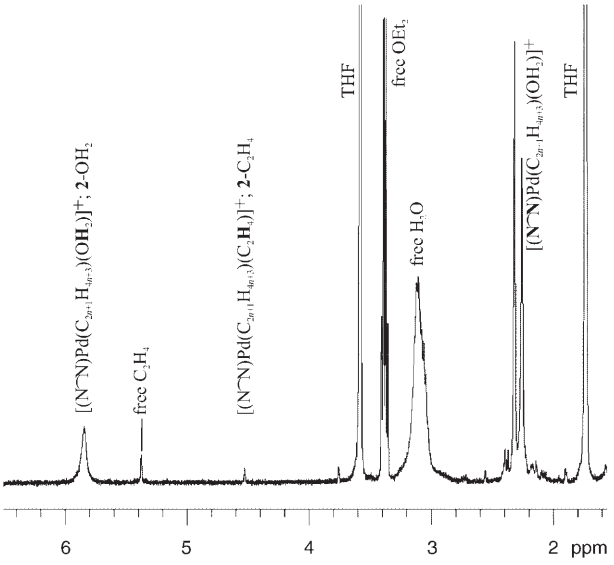


***Figure 2.*** Higher palladium alkyl water species, **2**-$OH_2$, detected by $^1$H NMR spectroscopy after consumption of 24 equiv of ethylene (3.6 equiv water, −20 °C, [$D_8$]THF).

consumption of a defined amount of ethylene also resulted in the clean formation of complexes **2**-$OH_2$. Key $^1$H NMR signals: (3.6 equiv water, −20 °C): $\delta = 5.98$ (br, s, Pd($C_{2n+1}H_{4n+3}$)($OH_2$)), 2.31 and 2.25 ppm (s, $H_3$C)CN, $\widehat{NN}$). Note that the signal of bound water (and also the diimine backbone) in **2**-$OH_2$ are different from the corresponding signals of the methyl complex **1**-$OH_2$ (Figure 1).

The water- versus olefin-binding equilibrium constants (**1**-$OH_2$+$C_2H_4$ ⇄ **1**-$C_2H_4$ + $OH_2$, $K$**1** and **2**-$OH_2$ + $C_2H_4$ ⇄ **2**-$C_2H_4$ + $OH_2$, $K$**2**) were determined at various temperatures (accompanied by olefin insertion at $T > -30$ °C) from integral intensities of the four species involved (Scheme 1, Table 1). The determination of the equilibrium constants $K$ over a range of ethylene and water concentrations demonstrated that $K$ is concentration independent (see Supporting Information). $K$ ranges from 1 to 4 depending on the temperature. That is, on an order of magnitude scale ethylene and water have a similar binding capability in the system studied; ethylene binding is slightly preferred. This finding is surprising as theoretical studies[6] had pointed to a strong preference for ethylene binding.[14] By comparison to other σ-donor ligands, such as diethyl ether or THF, water competes much

***Table 1:*** Relative binding constants ($K$ of water versus ethylene exchange) and rate constants of ethylene insertion ($k_i$).

| $T$ [°C] | $K$[a] | | $k_i$ [$\times 10^{-3}$ s$^{-1}$] | |
|---|---|---|---|---|
| | ($R$=Me) | ($R$>Me) | absence of water | presence of water[b] |
| −60 | 4.7 ± 0.2 | 4.4 ± 0.1 | n.i.[c] | n.i.[c] |
| −20 | 1.9 ± 0.1 | 1.4 ± 0.2 | 2.7 ± 0.1 | 2.2 ± 0.1 |
| −10 | 1.3 ± 0.3 | 1.9 ± 0.1 | 10.3 ± 0.4 | 10.2 ± 0.1 |

[a] Binding equilibrium constants, see Supporting Information. [b] 4–12 equiv water. [c] no insertion occurs.

 © 2006 Wiley-VCH Verlag GmbH & Co. KGaA, Weinheim 

more effectively for coordination at the cationic palladium center. A reasonable explanation might be the low steric hindrance of the water molecule. Notably, relative binding in higher alkyl species ($\mathbf{2}\text{-}OH_2 + C_2H_4 \rightleftarrows \mathbf{2}\text{-}C_2H_4 + OH_2$, $K\mathbf{2}$) does not differ significantly from that for the methyl complex. The temperature dependence of the equilibria is low, as expected; $K$ decreases by a factor of 2 to 3 over a temperature range of 50 K.

It is conceivable that the presence of water has an influence on the migratory-insertion step, for example, as the fifth ligand in five-coordinate intermediates (for example, five-coordinate intermediates are assumed to be the key species in chain transfer in the palladium diimine system[7,10]). Insertion into the Pd–Me bond was monitored in the presence and absence of water by the decrease of the Pd–Me species (see Supporting Information). First-order insertion rate constants determined in the presence (3.6–12 equiv) or absence of water, corrected for the water versus monomer equilibrium, are identical within experimental error (Table 1). This result confirms that water does not affect the crucial migratory insertion step; further, that establishing the $H_2O$ versus $C_2H_4$ binding equilibrium is fast compared to insertion and thus not rate determining. A free enthalpy of $\Delta G^{\neq} = 74\ kJ\,mol^{-1}$ was determined which coincides with a free enthalpy of $73\ kJ\,mol^{-1}$ in $CD_2Cl_2$ solution reported previously.[7]

Alkyl complexes $[(\widehat{NN})Pd(C_{2n+1}H_{4n+3})(OH_2)]^+$ ($\mathbf{2}\text{-}OH_2$), are stable at low temperatures ($< 0\,°C$; Figure 2). At room temperature, decomposition with the formation of a black solid, presumably Pd-black, was observed. Remarkably, the decomposition was accelerated in the simultaneous presence of water and ethylene, even at low temperature. As a conceivable pathway, β-hydride elimination seems unlikely, as no olefin signals are observed in the NMR spectra. Possible explanations are 1) hydrolysis of higher (secondary) alkyl species,[6] 2) reductive coupling of the alkyl fragment to the ligand, or 3) binuclear reductive alkyl-chain coupling.[15] In contrast, the methyl complex, $\mathbf{1}\text{-}OH_2$, was found to be stable in aqueous [$D_8$]THF solution for days at room temperature (10 equiv excess water). No hydrolysis of the Pd–Me bond occurred.

In summary, we have reported the first direct observation of ethylene migratory-insertion chain growth in the presence of water. Higher alkyl species $[(\widehat{NN})PdR(OH_2)]^+$ ($R > Me$) were prepared cleanly. Surprisingly, water can compete with ethylene for the vacant coordination site in the system studied. This situation is true for cationic Pd–Me species and also for higher palladium alkyl species, the latter being the relevant species in chain growth. Insertion rate constants are not affected by the presence of water.

Experimental data can be found in the Supporting Information.

Received: April 7, 2006
Published online: August 9, 2006

**Keywords:** chain growth · homogeneous catalysis · palladium · polymerization · water

[1] a) D. Distler, *Wäßrige Polymerdispersionen*, Wiley-VCH, Weinheim, **1999**; b) R. M. Fitch, *Polymer Colloids: a Comprehensive Introduction*, Academic Press, San Diego, **1997**.

[2] Ethylene polymerization: a) A. Held, F. M. Bauers, S. Mecking, *Chem. Commun.* **2000**, 301–302; b) A. Tomov, J. P. Broyer, R. Spitz, *Macromol. Symp.* **2000**, *150*, 53–58; c) F. M. Bauers, S. Mecking, *Angew. Chem.* **2001**, *113*, 3112–3115; *Angew. Chem. Int. Ed.* **2001**, *40*, 3020–3022; d) R. Soula, C. Novat, A. Tomov, R. Spitz, J. Claverie, X. Drujon, J. Malinge, T. Saudemont, *Macromolecules* **2001**, *34*, 2022–2026; e) F. M. Bauers, M. M. Chowdhry, S. Mecking, *Macromolecules* **2003**, *36*, 6711–6715; f) M. A. Zuideveld, P. Wehrmann, C. Röhr, S. Mecking, *Angew. Chem.* **2004**, *116*, 887–891; *Angew. Chem. Int. Ed.* **2004**, *43*, 869–873; g) L. Kolb, V. Monteil, R. Thomann, S. Mecking, *Angew. Chem.* **2005**, *117*, 433–436; *Angew. Chem. Int. Ed.* **2005**, *44*, 429–432; h) V. Monteil, P. Wehrmann, S. Mecking, *J. Am. Chem. Soc.* **2005**, *127*, 14568–14569; i) I. Göttker-Schnetmann, B. Korthals, S. Mecking, *J. Am. Chem. Soc.* **2006**, *128*, 7708–7709.

[3] Butadiene polymerization: a) H. Ono, T. Kato, *J. Polym. Sci. Part A* **2000**, *38*, 1083–1089; b) V. Monteil, A. Bastero, S. Mecking, *Macromolecules* **2005**, *38*, 5393–5399.

[4] ROMP: a) S.-Y. Lu, P. Quayle, P. C. Booth, S. G. Yeates, J. C. Padget, *Polym. Int.* **1993**, *32*, 1–4; b) I. Kühn, B. Mohr, Y. Durant, R. Schwab, R. Leyrer (BASF), DE 19859191, **2000**; c) J. P. Claverie, S. Viala, V. Maurel, C. Novat, *Macromolecules* **2001**, *34*, 382–388; d) D. Quenemer, A. Chemtob, V. Heroguez, Y. Gnanou, *Polymer* **2005**, *46*, 1067–1075; e) see also: D. M. Lynn, S. Kanaoka, R. H. Grubbs, *J. Am. Chem. Soc.* **1996**, *118*, 784–790.

[5] Review: A. Held, F. M. Bauers, S. Mecking, *Angew. Chem.* **2002**, *114*, 564–582; *Angew. Chem. Int. Ed.* **2002**, *41*, 544–561.

[6] I. H. Hristov, R. L. DeKock, G. D. W. Anderson, I. Göttker-Schnetmann, S. Mecking, T. Ziegler, *Inorg. Chem.* **2005**, *44*, 7806–7818.

[7] L. K. Johnson, C. M. Killian, M. Brookhart, *J. Am. Chem. Soc.* **1995**, *117*, 6414–6415.

[8] For an early work on ethylene polymerization with the cationic complex $[(\widehat{NNN})RhMe(OH_2)_2]^{2+}$ ($\widehat{NNN}$ = triazacyclononane) in an aqueous system to afford a suspension of low-molecular-weight polymer, see L. Wang, R. S. Lu, R. Bau, T. C. Flood, *J. Am. Chem. Soc.* **1993**, *115*, 6999–7000.

[9] D. T. Tempel, L. K. Johnson, R. L. Huff, P. S. White, M. Brookhart, *J. Am. Chem. Soc.* **2000**, *122*, 6686–6700.

[10] L. H. Shultz, D. J. Tempel, M. Brookhart, *J. Am. Chem. Soc.* **2001**, *123*, 11539–11555.

[11] NMR data in other solvents: A. Held, S. Mecking, *Chem. Eur. J.* **2000**, *6*, 4623–4629 and ref. [2a].

[12] H. Friebolin, *Ein- und zweidimensionale NMR - Spektroskopie: eine Einführung*, 3rd. ed., Wiley-VCH, Weinheim, **1999**.

[13] Addition of less than 2 equiv of water gave rise to two singlet signals for coordinated water in a 30:70 ratio ($\delta = 6.055/6.019$ ppm, $-60\,°C$; overall integral intensity of 2H relative to the Pd–Me signal) but only one Pd–Me signal was observed. This finding might result from hydrogen bridges of coordinated water ($Pd(Me)(OH_2)$) to solvent (minor signal) and to water molecules in solution (major signal). Increasing the amount of excess water results in the stepwise disappearance of the signal from the minor species.

[14] The theoretical studies[6] were based on toluene as the solvent, whereas the present studies were carried out in THF as the solvent, which can form hydrogen bridges. This feature may affect the coordination behavior of water.

[15] A. C. Gottfried, M. Brookhart, *Macromolecules* **2003**, *36*, 3085–3100.

 © 2006 Wiley-VCH Verlag GmbH & Co. KGaA, Weinheim 

*Radioactive Peptides*

DOI: 10.1002/anie.200600795

# $^{18}$F-Labeling of Peptides by means of an Organosilicon-Based Fluoride Acceptor**

*Ralf Schirrmacher,* Gerrit Bradtmöller, Esther Schirrmacher, Oliver Thews, Julia Tillmanns, Thomas Siessmeier, Hans G. Buchholz, Peter Bartenstein, Björn Wängler, Christof M. Niemeyer, and Klaus Jurkschat**

Fluorine-18 is among the most commonly used radionuclides for positron emission tomography (PET).[1] This non-invasive imaging technique is capable of providing in vivo information about the distribution of radiolabeled biomolecules by 180° coincidence detection of two simultaneously emitted photons from positron–electron annihilation. Although a number of different radiotracers have been successfully employed in PET, only a few, such as 2-[$^{18}$F]fluoro-2-deoxy-D-glucose (FDG)[2] and [$^{18}$F]fluorodopa,[3] have gained widespread application in nuclear medicine. The reason for this is that the regioselective introduction of $^{18}$F into tracer molecules is often non-specific and radiochemical yields (RCY) of the $^{18}$F-labelled product are low. The introduction of $^{18}F^-$ into tracer molecules requires high temperatures and often leads to undesired by-products.[1] The research over the last decade clearly indicates that the success of PET in nuclear medicine justifies the intense search for versatile labeling formulations for the syntheses of $^{18}$F-radiopharmaceuticals. Especially the development of rational $^{18}$F-labelling strategies for peptides, until now characterized by multistep procedures, is considered to be one of the most important tasks.[4] As an alternative to conventional $^{18}$F-labelling chemistry, the use of [$^{18}$F]fluorosilanes as labeling synthons was first proposed by Rosenthal et al. who treated chlorotrimethylsilane with n.c.a. (no carrier added) $^{18}F^-$ in aqueous acetonitrile isolating the corresponding [$^{18}$F]fluorosilane in 65 % yield.[5] A preliminary in vivo evaluation revealed fast hydrolysis of the compound accompanied by high radioactivity ($^{18}$F) uptake by the bone making it unsuitable as a labeling synthon.

Another approach is based on the work by Pilcher et al.[6] who fluorinated organosilanoles with nonradioactive HF in high yields. An analogous labeling strategy was proposed in a symposium abstract.[7] However, so far no labeling experiments using aqueous $^{18}F^-$/[$^{18}$F]HF solutions have been reported. Most recently Ting et al. used organotriethoxysilanes as labeling precursors for the synthesis of [$^{18}$F]fluorosilanes but no practical application for the synthesis of potential radiopharmaceuticals has been demonstrated.[8]

Herein we report the syntheses of substituted [$^{18}$F]organofluorosilanes using organochlorosilanes as labeling precursors and their in vitro and in vivo stability. As an alternative labeling approach we also describe the $^{18}$F–$^{19}$F isotopic exchange using [$^{19}$F]di-*tert*-butylphenyl fluorosilane as a highly efficient silicon-based fluoride acceptor (SiFA compound). As proof of applicability we transferred the SiFA approach to the development of a simple and practical formulation for the synthesis of a $^{18}$F-labelled SiFA derivatized Tyr$^3$-octreotate, a peptide used in oncology for the visualization of neuro-endocrine tumors.[9]

We synthesized three [$^{18}$F]organofluorosilanes, namely [$^{18}$F]fluorotriphenylsilane (**1**), [$^{18}$F]fluoro-*tert*-butyldiphenylsilane (**2**), and [$^{18}$F]fluorodi-*tert*-butylphenylsilane (**3**), and evaluated their in vitro stability in human serum as well as their in vivo stability in rats, studied by animal-PET. These data are essential for finding the most suitable compound and for evaluating the labeling concept.

The reaction in acetonitrile of the triorganochlorosilanes (5–11.8 μmol mL$^{-1}$) $Ph_3SiCl$, $tBuPh_2SiCl$, and $tBu_2PhSiCl$, with the azeotropically dried complex $^{18}F^-$/Kryptofix2.2.2./$K^+$ at room temperature provided almost quantitatively the corresponding [$^{18}$F]triorganofluorosilanes **1**–**3** (Figure 1), as demonstrated by means of radio-HPLC. Their identities were confirmed by coelution of the radioactive probes spiked with the related nonradioactive $^{19}$F-analogues. The specific activity of **1**, **2**, and **3** was determined using UV-calibration curves and was in the range 1500–1700 GBq μmol$^{-1}$.

To investigate the applicability of the $^{18}$F-labelled compounds for the development of Si–$^{18}$F containing radiopharmaceuticals, their in vitro stability in human serum was investigated (Figure 1). In agreement with previously published data,[10,11] the [$^{18}$F]triphenylfluorosilane **1** was found to be stable for 4 h in neutral water (data not shown) but unstable at pH 7.4–7.6 in human serum. In contrast, the *tert*-

[*] Dr. R. Schirrmacher,[+] Dr. E. Schirrmacher,[+] J. Tillmanns, Dr. T. Siessmeier, Dipl.-Ing. H. G. Buchholz, Prof. Dr. P. Bartenstein
Klinik und Poliklinik für Nuklearmedizin
Johannes Gutenberg Universität Mainz
55131 Mainz (Germany)
Fax: (+49) 6131-172386
E-mail: schirrmacher@klinik.nuklearmedizin.uni-mainz.de
Dipl.-Chem. G. Bradtmöller,[+] Prof. Dr. K. Jurkschat
Lehrstuhl für Anorganische Chemie
Universität Dortmund
44221 Dortmund (Germany)
Fax: (+49) 231-755-5048
E-mail: klaus.jurkschat@uni-dortmund.de
Dr. B. Wängler
Abteilung für Radiopharmazeutische Chemie
Deutsches Krebsforschungszentrum Heidelberg (Germany)
Priv.-Doz. Dr. O. Thews
Institut für Physiology und Pathophysiologie
Universität Mainz (Germany)
Prof. Dr. C. M. Niemeyer
Lehrstuhl für Biologisch-Chemische Mikrostrukturtechnik
Universität Dortmund (Germany)
[+] These authors contributed equally.

[**] This work was supported by the International Isotope Society Central European Division. The authors thank Philips for support and would like to thank Prof. Dr. H. J. Wester (TU Munich) for providing a protocol for oxime ligation. C.M.N. and G.B. acknowledge financial support from the Zentrum für Angewandte Chemische Genomik, a joint research initiative of the European Union and the Ministry of Innovation and Research of North Rhine-Westphalia.

Supporting information for this article is available on the WWW under http://www.angewandte.org or from the author.

 © 2006 Wiley-VCH Verlag GmbH & Co. KGaA, Weinheim 

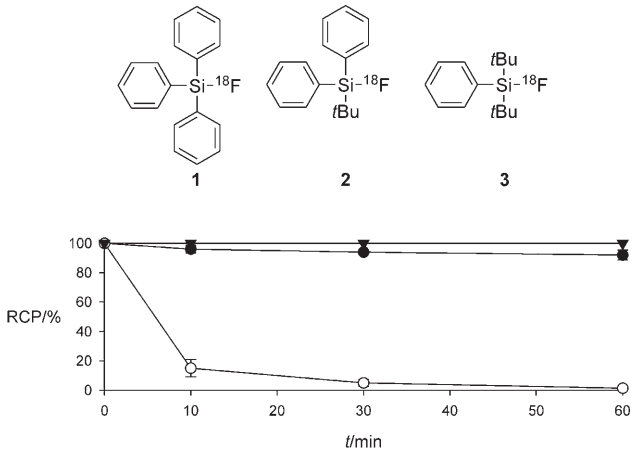


***Figure 1.*** Top: $^{18}$F-fluorosilanes **1**–**3** for in vitro evaluation in human serum and in vivo evaluation in rats by animal PET. Bottom: Only compounds **2** and **3** are stable in human serum (37.4 °C, pH 7.4–7.6; ○ = **1**, ● = **2**, ▼ = **3**). RCP = radiochemical purity.

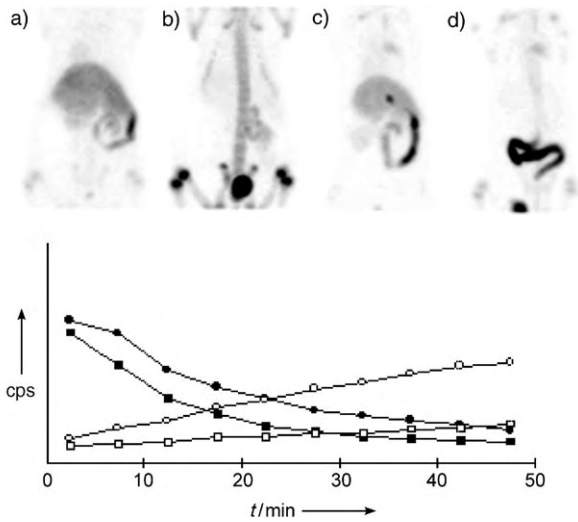


***Figure 2.*** Top: Coronal maximum intensity projections (MIP) of the second frame (5–10 min after injection, a and c) and the last frame (45–50 min after injection, b and d). The data reveal a much higher bone uptake for compound **2** (a, b) than for **3** (c, d). Bottom: Plot of time activity in regions of interest in bone and liver for compound **2** (○ = lumbar vertebra, ● = liver) and **3** (□ = lumbar vertebra, ■ = liver). cps = normalized counts per second.

butyl-substituted derivatives **2** and **3** displayed a high stability in this biological matrix.

Encouraged by these results, we performed the first in vivo animal PET scans with compounds **2** and **3** in healthy Sprague-Dawley rats to investigate the in vivo stability of the Si–$^{18}$F bond. To this end, 20–40 MBq of HPLC-purified **2** and **3**, dissolved in physiological saline/10% ethanol, were injected into the rats and the thoraco-abdominal area was scanned using an animal PET scanner (Philips, Mosaic animal imaging) for 50 min with time frames of 5 min. Because unbound $^{18}F^-$ readily accumulates in bone (osteotropic), the stability of the Si–$^{18}$F bond was determined by measuring the time curve of radioactivity uptake in bone (lumbar vertebra) as a dynamic measurement of Si–$^{18}$F hydrolysis. In contrast to their rather similar in vitro stability (Figure 1), the in vivo stability of **2** and **3** was found to be markedly different. As shown on the PET scans, for the mono-*tert*-butyl-substituted [$^{18}$F]triorganofluorosilane **2**, fast bone uptake of radioactivity was detected, whereas in case of di-*tert*-butyl-substituted compound **3**, only a little uptake in late time frames was observed (Figure 2).

Moreover, PET studies indicated that, probably owing to their high lipophilicity, both compounds are metabolized mainly by the liver. Because **2** is hydrolyzed in vivo to give unbound $^{18}F^-$, the main excretion of radioactivity occurred through the bladder, in contrast to compound **3**, which displayed intestinal excretion (see Supporting Information). To use organosilanes for $^{18}$F-labelling of radiopharmaceuticals, such as peptides for tumor imaging,[12] a suitable labeling strategy must include fast coupling steps to cope with the half-life of 110 min of $^{18}$F. Ideally, as in $^{99m}$Tc-labelling chemistry, no final HPLC purification step should be required for the formulation of the final radiopharmaceutical. Unfortunately, when applying triorganochlorosilanes as precursors for $^{18}$F-labelling reactions, the resulting [$^{18}$F]triorganofluorosilane has to be separated from the triorganochlorosilane by means of HPLC. This step is time consuming, leads to a decreased RCY, and requires a trained radiochemist. Furthermore, organochlorosilanes as well as organoalkoxysilanes are sensitive to hydrolysis, which limits complex syntheses.

Another major problem in conventional $^{18}$F-radiochemistry is that $^{19}$F-compounds to be labeled with $^{18}$F by isotopic exchange reactions are used in high concentrations (usually 10–100 μM) resulting in overall products of low specific activity. Therefore, the application of the concept of isotopic exchange to [$^{18}$F]triorganofluorosilanes would only be meaningful if 1) the concentration of the organofluorosilane is low enough to guarantee a high specific activity, 2) the $^{18}$F–$^{19}$F exchange rate is sufficiently high, and 3) the isotopic exchange reaction is not negatively influenced by various functional groups (such as, $NH_2$, COOH) usually present in biological molecules, such as peptides. To circumvent these difficulties and to reduce the labeling to only one reaction step, preferably excluding HPLC purification, we investigated the reaction of [$^{19}$F]-*t*Bu$_2$PhSiF (**4**) with n.c.a. $^{18}F^-$/Kryptofix 2.2.2./$K^+$ complex in acetonitrile (Figure 3).

The reaction in acetonitrile of compound **4** (1 μg, 4.1 nM) with "dried" n.c.a. $^{18}F^-$/Kryptofix 2.2.2./$K^+$ complex (1 GBq) at room temperature in 100 μL acetonitrile without stirring gave [$^{18}$F]triorganofluorosilane **3** in yields between 80–95% after only 15 min. The specific activity of **3** was in the range of 194–230 GBq μmol$^{-1}$. This exchange reaction is remarkably fast and exceeds the RCY of 50–70% usually obtained by nucleophilic $^{18}$F–$^{19}$F substitution of activated aromatic compounds, which normally requires high reaction temperatures and HPLC purification.[13,14] The specific activity obtained is competitive with clinically used radiotracers, which show specific activities between 100–1000 GBq μmol$^{-1}$. As a result of the very mild reaction conditions, a noteworthy advantage of the SiFA method is the exclusive formation of product **3** (Figure 3). Moreover, the specific activity, which is of crucial importance when imaging saturable neuroreceptors,[15] might

 © 2006 Wiley-VCH Verlag GmbH & Co. KGaA, Weinheim 

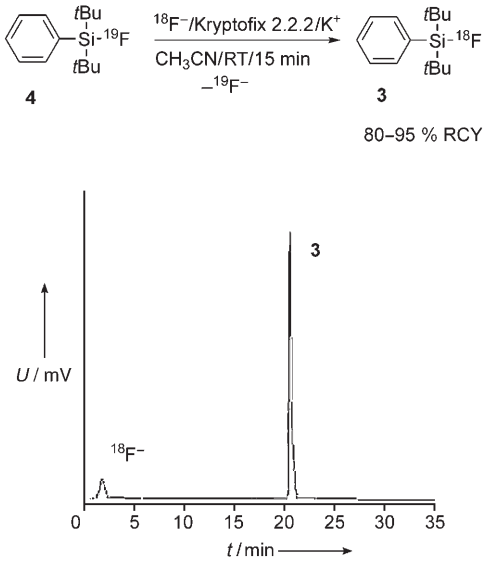


***Figure 3.*** Top: synthesis of **3** using **4** and $^{18}F^-$/Kryptofix2.2.2/$K^+$; Bottom: radio-HPLC chromatogram of the crude reaction mix of **4** (1 μg (4.1 nM)) with $^{18}F^-$/Kryptofix2.2.2/$K^+$ complex (1 GBq) in $CH_3CN$ (100 μL) after 15 min reaction time at room temperature.

be further enhanced by starting with higher amounts of $^{18}F$ radioactivity.

Current conventional methods for the syntheses of $^{18}F$-labelled peptides are based on multistep procedures involving prosthetic groups suitable for bioconjugation, for example, acylation, amidation, alkylation, photochemical conjugation,[4,12] and the recently introduced method of chemoselective oxime formation.[16,17] All these methods are complex, which is a major drawback owing to the short half-life of $^{18}F$. Hence, in contrast to the radiolabeling of peptides with radiometals,[4,12] no suitable robust practical formulation has been described for the routine $^{18}F$-labeling of peptides. Ideally the radiolabeling should proceed directly in the commercially available $^{18}F^-/[^{18}O]H_2O$ solution or in dried $^{18}F^-$/Kryptofix2.2.2/$K^+$ complex in dipolar aprotic solvents. To date, nucleophilic $^{18}F$-fluorination from aqueous solution has been considered impossible because the fluoride ion is highly solvated and thus has low nucleophilicity. To circumvent these problems and to utilize our labeling chemistry described on potential radiopharmaceuticals, we synthesized *p*-(di-*tert*-butylfluorosilyl) benzaldehyde, *p*-($t$Bu$_2$FSi)C$_6$H$_4$C(O)H (**5**, see Supporting Information) which is amenable for chemoselective oxime ligation to aminooxy-functionalized peptides.[16]

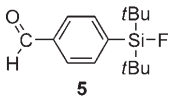

**5**

The organosilicon-functionalized aldehyde **5** was coupled to an aminooxy-derivatized Tyr$^3$-octreotate,[18] a peptide which is used in nuclear medicine,[19] which was synthesized by Fmoc solid-phase-peptide-synthesis (see Supporting Information; Fmoc = (9H-fluoren-9-ylmethoxy)carbonyl) and coupled to compound **5** by oxime formation in acetonitrile/water (90:10) at pH 4, yielding peptide **6** in > 98 % purity after HPLC purification. In a first isotopic exchange experiment we treated **6** (100 μg, 74 nmol) of with $^{18}F^-$/Kryptofix2.2.2./$K^+$ complex (280–360 MBq) in 800 μL acetonitrile for 10–15 min at room temperature yielding [$^{18}F$]**6** in yields between 95–97 % (Scheme 1). This reaction is the fastest,

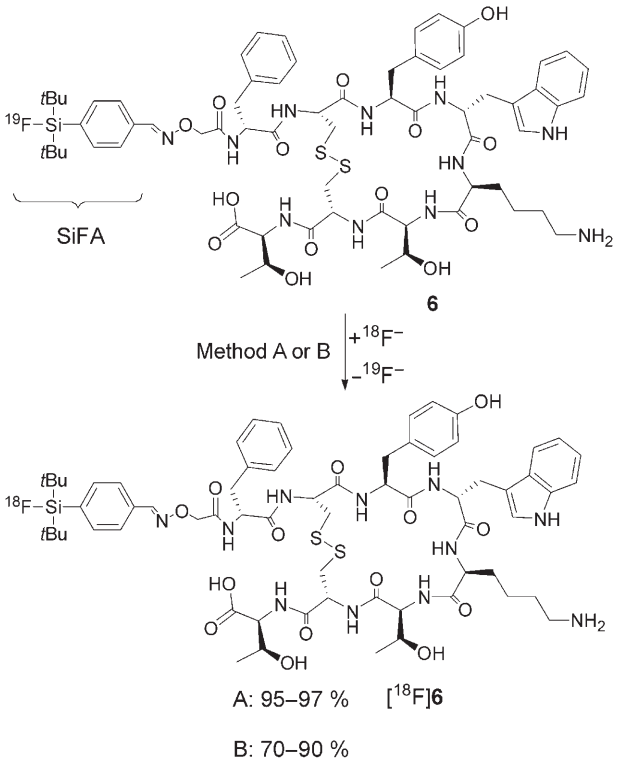


***Scheme 1.*** Synthesis of [$^{18}F$]**6** by two different procedures. Method A: **6** (100 μg, 74 nmol), $^{18}F^-$/Kryptofix2.2.2/$K^+$ (280–360 MBq), $CH_3CN$ (800 μL), room temperature, 10–15 min. Method B: **6** (100 μg, 74 nmol) in $CH_3CN$ (40 μL), $^{18}F^-/[^{18}O]H_2O$ (200–300 μL, 175–250 MBq), 95 °C, 30 min.

most selective and mildest $^{18}F$-labelling chemistry documented to date. To remove the toxic Kryptofix2.2.2, potassium ions and residual $^{18}F^-$, the acetonitrile was diluted with sodium dihydrogenphospate (0.25 N, pH 4.5, 10 mL) and passed through a C-18-solid-phase-extraction cartridge. The radiolabeled peptide [$^{18}F$]**6** was retained on the cartridge (trapping efficiency ≈ 80 %) and washed with water to reduce the amount of residual $^{18}F^-$ to < 1 %. To obtain [$^{18}F$]**6** as an injectable solution, the cartridge was eluted with ethanol (1 mL, elution efficiency ≈ 80 %) and diluted with isotonic saline (9 mL). Notably, the entire experimental procedure took only 25 min and the overall radiochemical yield was between 55–65 % giving [$^{18}F$]**6** in a purity of > 98 %.

To evaluate whether an isotopic exchange also occurs in commercially available $^{18}F^-/[^{18}O]H_2O$, we treated a solution of **6** (100 μg, 74 μmol) in acetonitrile (40 μL) with $^{18}F^-/[^{18}O]H_2O$ (200 μL, 175–250 MBq) at room temperature for 15 min. Only a 5 % yield of [$^{18}F$]**6** was detected by radio-HPLC. However, when conducting this reaction at 95 °C, the desired compound was obtained in yields between 70–90 % (HPLC) within 30 min (Scheme 1). No hydrolysis of the Si–$^{18}F$ bond and no disintegration of peptide **6** was observed

 © 2006 Wiley-VCH Verlag GmbH & Co. KGaA, Weinheim 

during HPLC quality control. Purification was performed in a similar manner as described above by solid-phase extraction using water (5 mL) for dilution. The calculated specific activity of [$^{18}$F]**6** for both methods was 3–5 GBq μmol$^{-1}$ which is sufficient for in vivo PET studies. We anticipate, however, that even higher specific activities should be obtainable by using larger amounts of $^{18}F^-$ for the isotopic exchange.

In conclusion, we have described a rapid and versatile approach for the synthesis of $^{18}$F-labeled peptides as illustrated by the example of a SiFA-derivatized Tyr$^3$-octreotate. This compound was labeled with $^{18}F^-$/Kryptofix2.2.2./$K^+$ complex in acetonitrile at room temperature as well as in aqueous $^{18}F^-$/[$^{18}$O]$H_2O$ solution at 95 °C. We anticipate that the very mild reaction conditions and the fast and efficient labeling make the SiFA strategy a valuable tool for the development of $^{18}$F-radiopharmaceuticals. The in vivo evaluation of compound [$^{18}$F]**6** as a tumor imaging agent is currently under investigation.

## Experimental Section

Syntheses of the organosilanes *t*$Bu_2$PhSiX (X = H,[20] F,[21] Cl,[20] I[21]) and *t*$BuPh_2SiF$[22] have been described elsewhere, however, different procedures were applied herein and all details are given in the Supporting Information, together with the synthetic procedures for *p*-(di-*tert*-butylfluorosilyl) benzaldehyde (**5**) and peptide **6**. Noteworthy, in contrast to earlier reports *t*$Bu_2$PhSiF (**4**) was obtained as crystalline material and its molecular structure was determined by single-crystal X-ray diffraction.[23]

[$^{18}$F]**6**: Method A: Compound **6** (100 μg, 74 nmol) was dissolved in acetonitrile and $^{18}F^-$/Kryptofix2.2.2./$K^+$ complex (280–360 MBq) in acetonitrile was added to obtain a total volume of 800 μL. The solution was kept at room temperature without stirring for 10–15 min, diluted with sodium dihydrogenphospate (0.25 N, pH 4.5, 10 mL) and passed through a C-18-Sepak cartridge (Merck). The cartridge was washed with water (2 mL) and eluted with ethanol (1 mL) to obtain [$^{18}$F]**6** (160–240 MBq) as an injectable solution.

[$^{18}$F]**6**: Method B: Compound **6** (100 μg, 74 nmol) dissolved in acetonitrile (40 μL) was added to $^{18}F^-$/[$^{18}$O]$H_2O$ (200–300 μL; 175–250 MBq; purchased from PetNet Erlangen) and heated at 95 °C for 30 min in a sealed reaction vial. Water (5 mL) was added and the solution was passed through a C-18-SepPac cartridge (Merck). The cartridge was washed with water (2 mL) and eluted with ethanol (1 mL) to obtain [$^{18}$F]**6** (95–150 MBq) as an injectable solution.

Received: March 1, 2006
Revised: June 13, 2006
Published online: August 3, 2006

**Keywords:** fluorination · isotopic labeling · organofluorosilanes · peptides

[1] "Chemistry of Fluorine-18 Radiopharmaceuticals": S. E. Snyder, M. Kilbourn in *Handbook of Radiopharmaceuticals, Radiochemistry and Applications* (Eds.: M. Welch, C. S. Redvanly), Wiley, Chichester, **2003**.
[2] T. Ido, C.-N. Wan, J. S. Fowler, A. P. Wolf, *J. Org. Chem.* **1977**, *42*, 2341.
[3] G. Firnau, C. Nahmias, E. S. Garnett, *Int. J. Appl. Radiat. Isot.* **1973**, *24*, 182.
[4] P. Blower, *Dalton Trans.* **2006**, 1705.
[5] M. S. Rosenthal, A. L. Bosch, R. J. Nickles, S. J. Gatley, *Int. J. Appl. Radiat. Isot.* **1985**, *36*, 318.
[6] A. S. Pilcher, H. L. Ammon, P. DeSong, *J. Am. Chem. Soc.* **1995**, *117*, 5166.
[7] J. C. Walsh, K. M. Akhoon, N. Satyamurthy, J. R. Barrio, M. E. Phelps, S. S. Gambhir, T. Toyokuni, *J. Labelled Compd. Radiopharm.* **1999**, *42*, S1.
[8] R. Ting, M. J. Adam, T. J. Ruth, D. M. Perrin, *J. Am. Chem. Soc.* **2005**, *127*, 13094.
[9] M. de Jong, W. A. P. Breeman, W. H. Bakker, P. P. M. Kooij, B. F. Bernard, L. J. Hofland, T. J. Visser, A. Srinivasan, M. A. Schmidt, J. L. Erion, J. E. Bugaj, H. R. Mäcke, E. P. Krenning, *Cancer Res.* **1998**, *58*, 437.
[10] C. G. Swain, R. M. Esteve, R. H. Jones, *J. Am. Chem. Soc.* **1949**, *71*, 965.
[11] H. Szmant, G. A. Brost, *J. Am. Chem. Soc.* **1950**, *72*, 5763.
[12] "Radiolabeled Peptides for Tumor Imaging": L. C. Knight in *Handbook of Radiopharmaceuticals, Radiochemistry and Applications* (Eds.: M. Welch, C. S. Redvanly), Wiley, Chichester, **2003**.
[13] R. Bolton, *J. Labelled Compd. Radiopharm.* **2002**, *45*, 485.
[14] M. S. Haka, M. R. Kilbourn, G. L. Watkins, S. A. Toorongian, *J. Labelled Compd. Radiopharm.* **1989**, *27*, 823.
[15] "Neurological Applications": N. I. Bohnen in *Principles and Practise of Positron Emission Tomography* (Eds.: R. L. Wahl, J. W. Buchanan), Lippincott Williams & Wilkins, Philadelphia, **2002**, and references therein.
[16] G. Thumshirn, U. Hersel, S. L. Goodman, H. Kessler, *Chem. Eur. J.* **2003**, *9*, 2717.
[17] T. Poethko, M. Schottelius, G. Thumshirn, U. Hersel, M. Herz, G. Henriksen, H. Kessler, M. Schwaiger, H. J. Wester, *J. Nucl. Med.* **2004**, *45*, 892.
[18] Tyr$^3$-octreotate was synthesized by Fmoc solid-phase peptide synthesis according to a published procedure (E. Schirrmacher, R. Schirrmacher, C. Beck, W. Mier, N. Trautman, F. Rösch, *Tetrahedron Lett.* **2003**, *44*, 9143).
[19] C. R. Reubi, M. Gugger, B. Waser, *Eur. J. Nucl. Med.* **2002**, *29*, 855.
[20] T. Kusukawa, W. Ando, *J. Organomet. Chem.* **1998**, *559*, 11.
[21] H.-W. Lerner, S. Scholz, M. Bolte, *Z. Anorg. Allg. Chem.* **2001**, *627*, 1638.
[22] R. Damrauer, R. A. Simon, B. Kanner, *Organometallics* **1988**, *7*, 1161.
[23] G. Bradtmöller, K. Jurkschat, M. Schürmann, *Acta Crystallogr. Sect. E* **2006**, *62*, 1303.

 © 2006 Wiley-VCH Verlag GmbH & Co. KGaA, Weinheim 

Icosahedral Clusters

DOI: 10.1002/anie.200602137

# $Li_{26}$ Clusters in the Compound $Li_{13}Na_{29}Ba_{19}$**

*Volodymyr Smetana, Volodymyr Babizhetskyy, Grigori V. Vajenine, and Arndt Simon**

In recent years, numerous metal-rich nitrides of alkaline-earth metals, particularly of Ba in combination with Na, have been discovered.[1] Extending this chemistry to the heavier homologues of Na proved unsuccessful; however, Li emerged as the most promising candidate for further development of the field, as we found several new subnitride phases of this element. A detailed knowledge of the relevant intermetallic systems is needed to open up this field of research.

In the Na–Ba system, two binary compounds are known,[2] $Na_2Ba$[3] and NaBa[4], and in the Li–Ba system, one compound is known, $BaLi_4$.[5] In contrast, no miscibility exists in the solid-state Li–Na system.[6] Ternary compounds were previously unknown in the Na–Li–Ba system. Herein, we report the first such compound, which, furthermore, exhibits quite unusual structural features. Single crystals of the ternary compound were obtained during an attempt to prepare Li-containing subnitrides. After a composition of $Li_{13}Na_{29}Ba_{19}$ was determined from the crystal-structure analysis, the compound was also obtained in high yield from an appropriate combination of the elements.[7]

$Li_{13}Na_{29}Ba_{19}$ crystallizes in a new structure type of cubic symmetry.[8] The main structural feature of this compound is a $Li_{26}$ cluster formed from four interpenetrating icosahedra (Figure 1). In this cluster, a central $Li_4$ tetrahedron is capped by 4, 6, and $4\times3$ Li atoms above its faces, edges, and vertices, respectively. Such anti-Mackay-type[9,10] $Li_{26}$ clusters have been predicted to be stable in the gas phase,[11] and isostructural $Ar_{26}$[12] and $Ba_{26}$[13] species have been postulated on the basis of cluster distributions in mass spectra of the gaseous elements. In the solid state, the $M_{26}$ cluster of γ-brass ($Cu_5Zn_8$) is well known,[14] but is composed of different atom types. Similarly, the $M_{26}$ cluster of $Ag_4Li_9$ contains both Ag and Li atoms.[15] To our knowledge, $Li_{13}Na_{29}Ba_{19}$ is the first example of a solid with homoatomic $M_{26}$ clusters.

The $4+4$ atoms at the center of the $Li_{26}$ cluster define what is known as a tetrahedral star (*TS*; Figure 1a).[16] Additional capping of the *TS* by 6 Li atoms and 4 $Li_3$ triangles results in four interpenetrating centered $Li_{13}$ icosahedra, (*I*; Figure 1b). The structures of numerous crystalline and quasicrystalline intermetallic phases can be systematized on the basis of *TS*[17] and *I*.[18] Icosahedral $Li_{13}$ fragments are found in the binary compound $BaLi_4$, where they share faces to form infinite chains. Distorted *I* surround Na atoms in the structures of $Na_2Ba$ and NaBa. The structure of NaBa can also be elegantly described with a *TS* framework.[17]

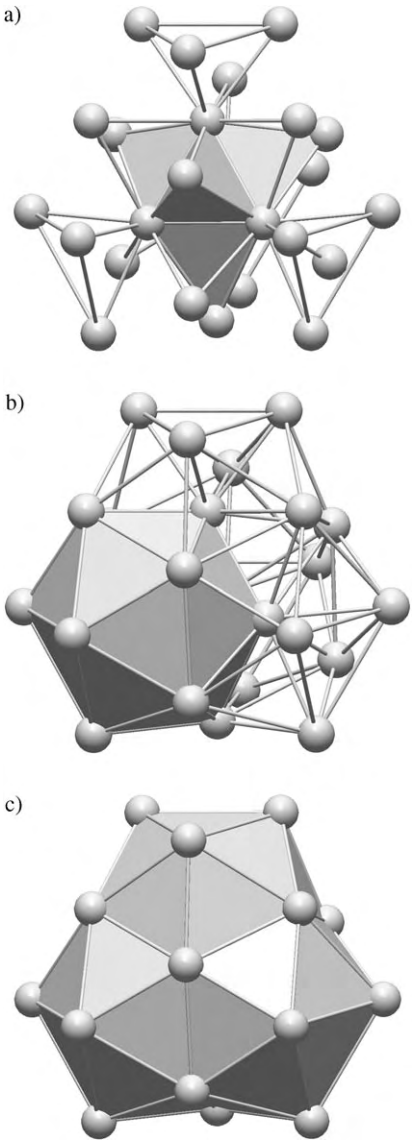


***Figure 1.*** a) Tetrahedral star (*TS*) and b) icosahedral (*I*) fragments of c) the $Li_{26}$ cluster in the intermetallic phase $Li_{13}Na_{29}Ba_{19}$.

The *TS* is composed of 5, and *I* of 20 (slightly distorted) face-sharing tetrahedra. The $Li_{26}$ cluster contains 57 close-packed tetrahedra. This type of close packing of tetrahedra in intermetallic structures was recognized by Frank and Kasper early on. Their approach can also be used to describe the local environments of the Na and Ba atoms in $Li_{13}Na_{29}Ba_{19}$. While the Na atoms are icosahedrally coordinated, larger Frank-Kasper-type polyhedra[19] with 15–17 vertices surround the Ba atoms. In the crystal structure of $Li_{13}Na_{29}Ba_{19}$ (Figure 2), the Na and Ba atoms lie between the $Li_{26}$ clusters, which form a

[*] Dipl.-Chem. V. Smetana, Dr. V. Babizhetskyy, Dr. G. V. Vajenine, Prof. Dr. A. Simon
Max-Planck-Institut für Festkörperforschung
Heisenbergstrasse 1, 70569 Stuttgart (Germany)
Fax: (+49) 711-689-1642
E-mail: a.simon@fkf.mpg.de
Dr. G. V. Vajenine
Institut für Anorganische Chemie
Universität Stuttgart
Pfaffenwaldring 55, 70569 Stuttgart (Germany)

[**] The authors thank C. Hoch for collecting the single-crystal diffraction data and J. Köhler for helpful discussions.

 © 2006 Wiley-VCH Verlag GmbH & Co. KGaA, Weinheim 

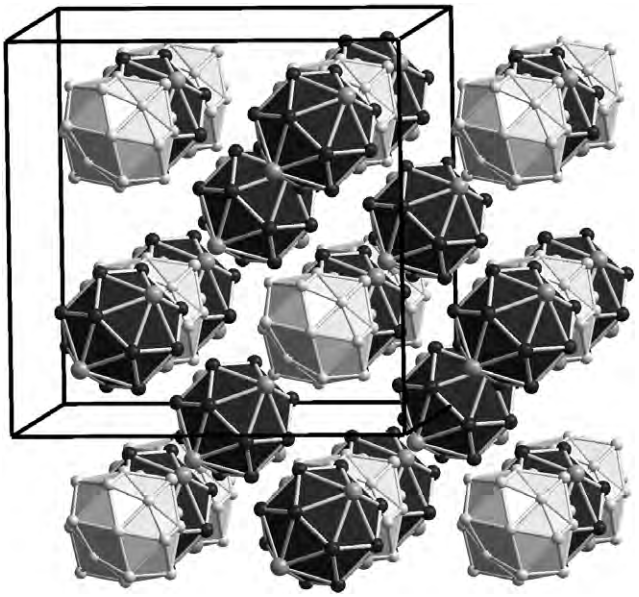

***Figure 2.*** Face-centered cubic arrangement of $Li_{26}$ clusters (light gray) in $Li_{13}Na_{29}Ba_{19}$. The octahedral and half of the tetrahedral voids are occupied by $BaBa_4Na_{12}$ polyhedra (dark gray). The remaining Na and Ba atoms are omitted for clarity. The cubic unit cell of $Li_{13}Na_{29}Ba_{19}$ is shown.

face-centered cubic array (*A* sites). All of the octahedral (*O* sites) and half of the tetrahedral (*T* sites) voids are filled by $BaBa_4Na_{12}$ polyhedra, as in the LiAlSi structure type,[20,21] corresponding to a filled zinc blende or rock salt structure. The resulting formulation of $(Li_{26})_4^A(BaBa_4Na_{12})_4^O(BaBa_4Na_{12})_4^T \cong Li_{13}Na_{12}Ba_5$ accounts for only 5 of 19 Ba atoms and 12 of 29 Na atoms per formula unit. The remaining Na and Ba atoms fill the rest of the space in the unit cell, resulting in a polytetrahedral packing.

The $Li_{26}$ clusters are surrounded by a larger cage of 28 Ba atoms, which consists of 16 triangles and 12 pentagons. All of the pentagons are capped from the inside by peripheral Li atoms of the $Li_{26}$ cluster and from the outside by Na atoms. These capping Na and Li atoms form the only Li–Na contact in the structure, in which the remaining Li and Na atoms are completely separated, consistent with the immiscibility of the two elements in solid state.

The Li–Li (2.94(7)–3.34(2) Å) and Na–Na (3.54(1)–3.78(1) Å) distances are somewhat shorter than the sums of the respective metallic radii, but fall within the range of bond lengths observed for $BaLi_4$[5] and $Na_2Ba$.[3] The only close Li–Na contact (3.19(3) Å) is considerably shorter than the sum of the metallic radii (3.37 Å). All other bonding contacts, Li–Ba (3.84(3)–4.07(3) Å), Na–Ba (3.98(1)–4.48(1) Å), and Ba–Ba (4.405(1)–4.461(1) Å), are comparable with the sums of the respective metallic radii. As is typical for alloys of electropositive elements, the volume of $Li_{13}Na_{29}Ba_{19}$ is only slightly smaller (−3%) than the sum of the volumes of its component elements (Table 1).

The question remains whether the $Li_{26}$ clusters in $Li_{13}Na_{29}Ba_{19}$ represent the upper limit of icosahedrally based Li clusters. In principle, polytetrahedral packing could be continued to yield larger anti-Mackay-type clusters, such as a $Li_{45}$ cluster comprising 13 interpenetrating $Li_{13}$ icosahedra,[9,10] analogous to the $M_{45}$ clusters in $Mg_2Al_5Cu_6$ and $Mg_2Zn_{11}$.[23–25] According to calculations for gas-phase Li clusters, structural strain increases with cluster size, such that Mackay-type icosahedral clusters, followed by a face-centered cubic structure,[11] and finally the body-centered cubic structure of metallic Li are predicted to form.

***Table 1:*** Crystal volumes per formula unit at room temperature for Li, Na, Ba, and their compounds.

| Material | $V = V_{cell}/Z$ [Å$^3$] | $\Delta V$[a] [%] | Ref. |
|---|---|---|---|
| Li | 21.61 | – | [22] |
| Na | 39.50 | – | [22] |
| Ba | 63.44 | – | [22] |
| NaBa | 102.84 | −0.1 | [4] |
| $Na_2Ba$ | 142.00 | −0.3 | [3] |
| $BaLi_4$ | 156.02 | +4.1 | [5] |
| $Li_{13}Na_{29}Ba_{19}$ | 2553.1 | −3.0 | this work |

[a] The percent volume change for $Li_xNa_yBa_z$ is defined as $\Delta V = 100[V(Li_xNa_yBa_z) - xV(Li) - yV(Na) - zV(Ba)]/[xV(Li) + yV(Na) + zV(Ba)]$.

Received: May 29, 2006
Published online: August 9, 2006

**Keywords:** barium · cluster compounds · intermetallic phases · lithium · sodium

[1] A. Simon in *Molecular Clusters of the Main Group Elements* (Eds.: M. Driess, N. Nöth), Wiley-VCH, Weinheim, **2004**, pp. 246–266.
[2] F. A. Kanda, R. M. Stevens, D. V. Keller, *J. Phys. Chem.* **1965**, *69*, 3867–3872.
[3] G. J. Snyder, A. Simon, *Z. Naturforsch. B* **1994**, *49*, 189–192.
[4] G. J. Snyder, A. Simon, *J. Chem. Soc. Dalton Trans.* **1994**, 1159–1160.
[5] F. E. Wang, F. A. Kanda, C. F. Miskell, A. J. King, *Acta Crystallogr.* **1965**, *18*, 24–31.
[6] *Binary Alloy Phase Diagrams* (Ed.: T. B. Massalski), ASM, Metals Park, **1986**, pp. 1491–1492.
[7] Sample A: Ba metal (476 mg; Merck, 99%; distilled twice with intermediate heating at 1270 K in vacuum to remove trace H), Ca metal (12 mg; Merck, 99%; distilled twice), $Ba(N_3)_2$ (129 mg; recrystallized and dried under vacuum), Li metal (28 mg; Merck, 99%), and Na–K alloy (69 at% Na; 1200 mg) were placed in a Ta ampoule in a glove box under an Ar atmosphere. The ampoule was closed by arc welding under an inert atmosphere and sealed inside a Duran glass ampoule. To decompose the azide, the reaction mixture was heated to 670 K at a rate of 10 K h$^{-1}$ and kept at this temperature for 5 days. Then it was cooled to 390 K at 1 K h$^{-1}$ and annealed at this temperature for 1 month. The resulting product, dispersed in excess liquid Na–K alloy, was transferred into a press, in which the greater part of the liquid was extruded at 5 kbar through a small hole. The brittle metallic product isolated consisted of approximately equal amounts of $Li_{13}Na_{29}Ba_{19}$ and $Na_{14}Ba_{14}CaN_6$,[26] according to powder X-ray diffraction analysis. Sample B: Li metal, Na metal (Merck, 99%), and Ba metal were mixed in a 1:3:2 stoichiometry, sealed in Ta and Duran ampoules under Ar (as described above), heated at 670 K for 10 days, and then cooled to room temperature at 1 K h$^{-1}$. According to powder X-ray diffraction

 © 2006 Wiley-VCH Verlag GmbH & Co. KGaA, Weinheim 

analysis, the bulk product contained approximately 60 wt% $Li_{13}Na_{29}Ba_{19}$, along with NaBa. All handling of the reactants and products was performed under purified Ar in a glove box. According to a temperature-dependant Guinier measurement,[27] $Li_{13}Ba_{29}Na_{19}$ begins to decompose at 410 K.

[8] The structure of $Li_{13}Na_{29}Ba_{19}$ was determined from X-ray diffraction data for a single crystal from sample A; data were collected on a STOE IPDS diffractometer; crystal size $0.12 \times 0.13 \times 0.14\ mm^3$, cubic, space group $F\bar{4}3m$, $a = 27.335(2)$ Å, $V = 20424(3)$ Å$^3$, $Z = 8$, $\rho_{calcd} = 2.189\ g\,cm^{-3}$, $2\theta_{max} = 42.0°$, $Ag_{K\alpha}$ radiation, $\lambda = 0.56086$ Å, $\omega$–$\theta$ scan, 293 K, 25544 collected and 1321 unique reflections, empirical absorption correction, $\mu = 3.872\ mm^{-1}$; the crystal structure was solved using direct methods (SHELXS-97[28]), and a full-matrix least-squares refinement on $F^2$ (SHELXL-97[29]; anisotropic for the Ba and Na atoms) was carried out; 65 parameters, $R1\,(I>2\sigma(I)) = 0.0307$, $wR2\,(I>2\sigma(I)) = 0.0483$, $R1$ (all data) $= 0.0484$, $wR2$ (all data) $= 0.0513$, GOF $= 1.006$. Further details on the crystal structure investigations may be obtained from the Fachinformationszentrum Karlsruhe, 76344 Eggenstein-Leopoldshafen, Germany (fax: (+49) 7247-808-666; e-mail: crysdata@fiz-karlsruhe.de), on quoting the depository number CSD-416631.

[9] K. H. Kuo, *Struct. Chem.* **2002**, *13*, 221 – 230.

[10] J. P. K. Doye, D. J. Wales, *J. Chem. Soc. Faraday Trans.* **1997**, *93*, 4233 – 4243.

[11] M.-V. Sung, R. Kawai, J. H. Weare, *Phys. Rev. Lett.* **1994**, *73*, 3552 – 3555.

[12] I. A. Harris, R. S. Kidwell, J. A. Northby, *Phys. Rev. Lett.* **1984**, *53*, 2390 – 2393.

[13] D. Rayane, P. Melinon, B. Cabaud, A. Hoareau, B. Tribollet, M. Broyer, *Phys. Rev. A* **1989**, *39*, 6056 – 6059.

[14] J. K. Brandon, R. Y. Brizard, P. C. Chieh, R. K. McMillan, W. B. Pearson, *Acta Crystallogr. Sect. B* **1974**, *30*, 1412 – 1417.

[15] L. Arnberg, S. Westman, *Acta Chem. Scand.* **1972**, *26*, 1748 – 1750.

[16] K. Schubert, *Kristallstrukturen zweikomponentiger Phasen*, Springer, Berlin, **1964**, p. 150.

[17] U. Häussermann, C. Svensson, S. Lidin, *J. Am. Chem. Soc.* **1998**, *120*, 3867 – 3880.

[18] G. Kreiner, H. F. Franzen, *J. Alloys Compd.* **1995**, *221*, 15 – 36.

[19] F. C. Frank, J. S. Kasper, *Acta Crystallogr.* **1958**, *11*, 184 – 190.

[20] H. Nowotny, F. Holub, *Monatsh. Chem.* **1960**, *91*, 877 – 887.

[21] L. Spina, Y. Z. Jia, B. Ducourant, M. Tillard, C. Belin, *Z. Kristallogr.* **2003**, *218*, 740 – 746.

[22] F. S. Galasso, *Structure and Properties of Inorganic Solids*, Pergamon, Oxford, **1970**, p. 28.

[23] S. Samson, *Acta Chem. Scand.* **1949**, *3*, 809 – 834.

[24] S. Samson, *Acta Chem. Scand.* **1949**, *3*, 835 – 843.

[25] L. Pauling, *Phys. Rev. Lett.* **1987**, *58*, 365 – 368.

[26] U. Steinbrenner, A. Simon, *Angew. Chem.* **1996**, *108*, 595 – 597; *Angew. Chem. Int. Ed. Engl.* **1996**, *35*, 552 – 554.

[27] A. Simon, *J. Appl. Crystallogr.* **1971**, *4*, 138 – 145.

[28] G. M. Sheldrick, SHELXS-97: Program for the Solution of Crystal Structures, University of Göttingen, Germany **1997**.

[29] G. M. Sheldrick, SHELXL-97: Program for the Refinement of Crystal Structures, University of Göttingen, Germany **1997**.

 © 2006 Wiley-VCH Verlag GmbH & Co. KGaA, Weinheim 

Homogeneous Catalysis

DOI: 10.1002/anie.200602261

# Regioselective Iron-Catalyzed Allylic Amination**

*Bernd Plietker**

Catalysis in the presence of inexpensive and nontoxic metals has gained increasing attention in chemical research within the past years. In particular, iron complexes proved to be efficient and selective catalysts for a variety of transformations.[1] With regard to the importance of allylic substitutions in organic synthesis[2] the development of an iron-catalyzed protocol appeared to be a useful extension of the existing methodologies. Recently, we presented the first regioselective, salt-free, iron-catalyzed allylic alkylation of allyl carbonates.[3] In this reaction a new C–C bond is formed with retention of the configuration at the carbon atom that was substituted by the leaving group in the starting material. Aiming to broaden the scope of the reaction and to gain further information on stability and reactivity of the iron catalyst $[Bu_4N][Fe(CO)_3(NO)]$, we further developed this reaction into an iron-catalyzed, allylic amination. Such a reaction has not been developed until now.

Various transition metals are known to catalyze the allylic amination.[4] The classical version in the presence of Pd catalysts, however, exhibits a lack of regioselectivity. In general, the product resulting from an attack of the nucleophile at the sterically less encumbered allyl terminus is formed predominantly. The preparation of higher-substituted, branched amines can be realized in the presence of Ir[5] or Ru catalysts.[6] However, in all of these protocols the substitution pattern in the π-allyl metal intermediate determines the regioselective course of the reaction. The Rh-catalyzed allylic amination on the other hand might be regarded as a complementary procedure.[7] In this reaction both the regio- and stereoselectivity are solely determined by the constitution of the starting material.[8] The new C–N bond is formed selectively at the carbon atom that was substituted by the leaving group in the starting material.

[*] Dr. B. Plietker
Organische Chemie II
FB Chemie
Universität Dortmund
Otto-Hahn-Strasse 6, 44221 Dortmund (Germany)
Fax: (+49) 231-755-3884
E-mail: bernd.plietker@uni-dortmund.de

[**] Financial support from Prof. Dr. N. Krause, the Fonds der Chemischen Industrie, the Deutsche Forschungsgemeinschaft, the Dr.-Otto-Röhm-Gedächtnisstiftung, and the Fonds zur Förderung des wissenschaftlichen Nachwuchses im Fachbereich Chemie der Universität Dortmund is gratefully acknowledged.

Supporting information for this article is available on the WWW under http://www.angewandte.org or from the author.

 © 2006 Wiley-VCH Verlag GmbH & Co. KGaA, Weinheim 

Although allylic substitutions are formally related to C or N nucleophiles, the direct nucleophilicity[9] of the nitrogen atom causes significant mechanistic differences (Scheme 1).

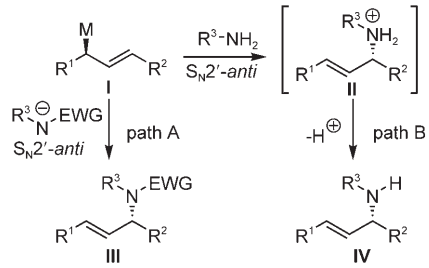


***Scheme 1.*** Mechanistic dichotomy in allylic aminations. EWG = electron-withdrawing group.

Similar to the C nucleophiles, electron-poor secondary amines have to be deprotonated separately or in situ prior to the allylic substitution and then treated with an allyl metal species **I** (Scheme 1, path A). The low tendency of these nucleophiles and the resulting product **III** to coordinate to the metal center is advantageous for the reaction. Similar processes often lead to catalyst inhibition. Electron-rich primary or secondary amines on the other hand can coordinate to a metal center but offer the possibility to act as a direct nucleophile[9] in the reaction with allyl metal species like **I** (Scheme 1, path B). Upon substitution of the metal center, an ammonium cation **II** is formed which is deprotonated in the final step of the mechanism.

Since no iron-catalyzed allyic amination has been described in the literature so far,[10] the similarity of the allylic amination using electron-poor secondary amines (Scheme 1, path A) with the allylic alkylation motivated us to apply this amine class in initial screening experiments (Table 1, entries 1–4). However, the conversion using this nucleophile class was very low. Moreover, a brown solid was formed during the reaction, which indicated probable catalyst decomposition.

The reaction in the presence of primary amines on the other hand (Scheme 1, path B) furnished the desired allyl amine with a high degree of regioselectivity in favor of the *ipso*-substitution product (Table 1, entry 8). A transfer of these results to the amination of less-substituted allyl carbonates, however, proved to be difficult (Scheme 2).[11]

***Table 1:*** Development of the allylic alkylation of amines.

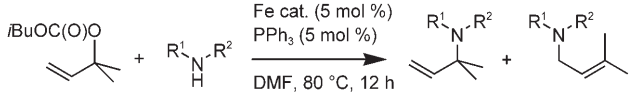


| Entry | $R^1$ | $R^2$ | A/B[a] | Conv. [%][a] |
|---|---|---|---|---|
| 1 | Ph | Ts | n.d.[b] | 8 |
| 2 | Ph | Ms | n.d.[b] | 12 |
| 3 | Ph | Ac | n.d.[b] | – |
| 4 | *n*Bu | Ts | n.d.[b] | – |
| 5 | *n*Pr | *n*Pr | n.d.[b] | – |
| 6 | *n*Bu | H | n.d.[b] | 12 |
| 7 | *t*Bu | H | 96:4 | 23 |
| 8 | Ph | H | 97:3 | 67 |

[a] According to GC integration. [b] Not determined. Ts = *p*-toluenesulfonyl, Ms = methanesulfonyl, Ac = acetyl.

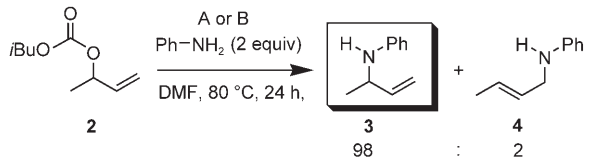


***Scheme 2.*** Iron-catalyzed allylic amination. Conditions: A) Fe cat. (5 mol%), $PPh_3$ (5 mol%), 1 M, 36% yield; B) Fe cat. (5 mol%), $PPh_3$ (5 mol%), Pip·HCl (30 mol%), 10 M, 84% yield.

Again, significant catalyst decomposition was observed. This undesired side effect was retarded upon addition of a catalytic amount of piperidinium chloride (Pip·HCl) as a buffer. This addition in combination with an increase in the substrate concentration led to a significant increase in the conversion (Scheme 2), thus allowing for the regioselective amination of primary and secondary allyl carbonates in good yield (Table 2).

***Table 2:*** Amination of allyl carbonates.[a]

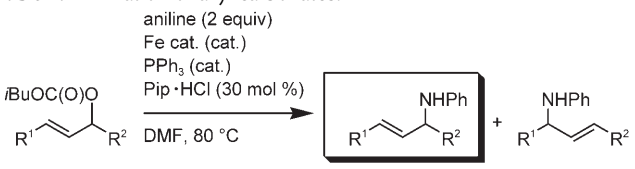


| Entry | Carbonate | Product | *t* [h][b] | Yield [%][c,d] |
|---|---|---|---|---|
| 1 | 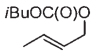 **5** | 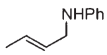 **4** | 48 (5) | 69 (97:3) |
| 2 | 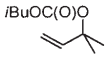 **1** | 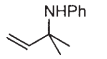 **6** | 6 (2.5) | 87 (98:2) |
| 3 | 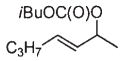 **7** | 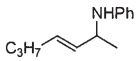 **8** | 48 (5) | 61 (97:3) |
| 4 | 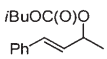 **9** | 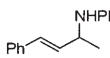 **10** | 24 (5) | 62 (96:4) |
| 5 | **11** | **12** | 24 (5) | 47 (97:3) |

[a] All reactions were performed on a 1-mmol scale. [b] Amount of catalyst in mol% is given in brackets. [c] Yield of isolated product. [d] Regioselectivity of the crude product according to GC integration is given in brackets.

 © 2006 Wiley-VCH Verlag GmbH & Co. KGaA, Weinheim 

In all cases the new C–N bond is formed with very high selectivity at the carbon atom that was substituted by the leaving group in the starting material. However, both reaction time and yield strongly depend on the substitution pattern of the allyl carbonate: the more highly substituted the double bond the slower the reaction proceeds. Whereas monosubstituted olefins are efficiently aminated, the introduction of one more olefinic substituent leads to a significant increase in the reaction time (**2** vs. **7**; Table 2, entry 3).[12] Furthermore, tertiary allyl carbonates are significantly more reactive compared to primary or secondary carbonates (**1**, **2**, and **5**; Table 2). Both steric and electronic effects might account for this finding. Gratifyingly, the longer reaction times had no impact on the regioselectivity of the reactions.

***Table 3:*** Allylation of primary anilines.[a]

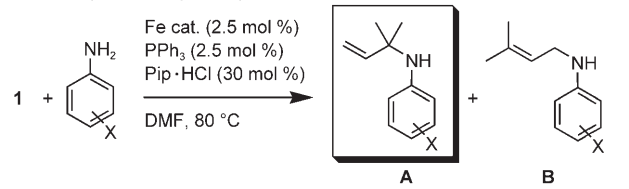


| Entry | Product | *t* [h] | Yield [%][b,c] |
|---|---|---|---|
| 1 | **13** (X = *m*-$CH_3$) | 6 | 85 (97:3) |
| 2 | **14** (X = *p*-$CH_3$) | 6 | 87 (98:2) |
| 3 | **15** (X = *m*-$OCH_3$) | 12 | 87 (97:3) |
| 4 | **16** (X = *p*-$OCH_3$) | 12 | 82 (98:2) |
| 5 | **17** (X = *m*-Cl) | 15 | 71 (96:4) |
| 6 | **18** (X = 3,5-$CH_3$) | 6 | 89 (97:3) |
| 7 | 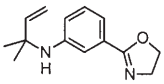 **19** | 6 | 67 (97:3) |
| 8 | 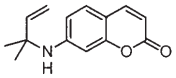 **20** | 6 | 93 (97:3) |

[a] All reactions were performed on a 1-mmol scale. [b] Yield of isolated product. [c] Regioselectivity of the crude product according to GC integration is given in brackets.

Various aniline derivatives are regioselectively allylated under the optimized reaction conditions (Table 3). Chloride, ether, or ester functionalities are tolerated. Even the presence of strongly coordinating functional groups such as the oxazolidinone in **19** does not lead to a reduction of the catalytic activity. However, the reaction time depends strongly on the nucleophilicity of the nitrogen atom. Electron-poor anilines are allylated more slowly, albeit with the same high degree of regioselectivity, compared to the electron-rich derivatives. Whereas *para*- or *meta*-substituted anilines are efficiently transformed into the corresponding products, a substituent in the *ortho* position inhibits the reaction.

As for the iron-catalyzed allylic alkylation, we envisioned a mechanism involving a σ-allyl metal intermediate as the reason for the observed high regioselectivity. If a stereospecific double $S_N2'$-*anti* mechanism takes place, the use of enantiomerically pure allyl carbonates should furnish the corresponding amines with retention of the configuration. Indeed, the allylic amination of (*S*)-**9** occurrs with almost complete chirality transfer and retention of the configuration to give amine (*S*)-**10** (Table 4, entries 1–3). This result

***Table 4:*** Chirality transfer in allylic aminations.

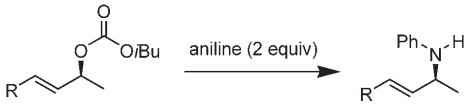


| Entry | R | Substrate (*ee* [%][a]) | Cond.[b] | Product[c] | *ee* [%][a] | Yield [%][d] |
|---|---|---|---|---|---|---|
| 1 | Ph | (*S*)-**9** | A | (*S*)-**10** | 86 | – |
| 2 | | (94) | B | | 83 | 15 |
| 3 | | | C | | 84 | 62 |
| 4 | H | (*S*)-**2** | A | (*S*)-**3** | 87 | – |
| 5 | | (92) | B | | 82 | 36 |
| 6 | | | C | | 80 | 84 |

[a] According to HPLC using Chiracel columns. [b] Conditions: A) 1 mmol substrate, 2 mmol aniline, 250 μL DMF, 80 °C, 5 h; B) 1 mmol substrate, 2 mmol aniline, 10 mol % $[Bu_4N][Fe(CO)_3(NO)]$, 10 mol % $PPh_3$, 250 μL DMF, 80 °C, 5 h; C) 1 mmol substrate, 2 mmol aniline, 5 mol % $[Bu_4N][Fe(CO)_3(NO)]$, 5 mol % $PPh_3$, 30 mol % Pip·HCl, 250 μL DMF, 80 °C, 5 h. [c] The absolute configuration was assigned by comparison to the literature. [d] Yield of isolated product.

corresponds nicely with the observations made in the allylic alkylation of malonic acid derivatives.[3] Interestingly, only a small decrease in the enantiopurity was observed in the allylic amination of (*S*)-**2** (Table 4, entries 4–6). We were pleased to find that the additive had no influence on the chirality transfer.

This result is remarkable since the chirality of the α-carbon atom in the in situ generated σ-allyl iron complex **V** is conserved only through coordination to the C–C double bond, thus preventing fast rotation around the C–C single bond, which would result in a loss of stereochemical information (Scheme 3). Furthermore, with regard to the observed strong substituent effects, a stereospecific ionization by a $S_N2$ mechanism appears improbable.

Herein, our results on the first iron-catalyzed allylic amination of allyl carbonates are summarized. As compared to the already established Rh-catalyzed procedure, this protocol is distinguished in particular by the use of the

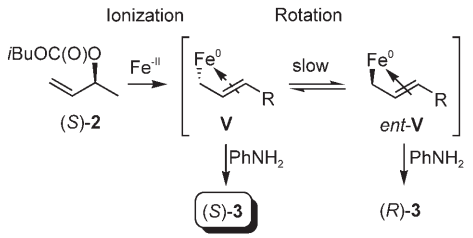


***Scheme 3.*** Stereoselectivity in allylic aminations.

 © 2006 Wiley-VCH Verlag GmbH & Co. KGaA, Weinheim 

inexpensive and nontoxic iron catalyst $[Bu_4N][Fe(CO)_3(NO)]$, the simple working procedure, and the high stereo- and regioselectivity, especially in the amination of higher-substituted allyl carbonates.[13]

Various allyl carbonates are converted under the described conditions into essentially regio- and stereoisomerically pure allyl amines. The use of secondary amines as N nucleophiles proved to be problematic as a result of catalyst decomposition. However, this side reaction is retarded in the presence of catalytic amounts of piperidinium chloride as a buffer. The observations and results obtained within the development of the iron-catalyzed allylic amination allowed for important insights into the stability and reactivity of the iron catalysts. Based on these results, future work will concentrate on the development of CO-free iron(−II) complexes, which might possess higher stability toward basic amines.

## Experimental Section

General procedure for the allylic amination: In a 2-mL Wheaton vial equipped with a stirring bar and a Mininert valve, a mixture of $[Bu_4N][Fe(CO)_3(NO)]$ (20.6 mg, 0.05 mmol), $PPh_3$ (13.2 mg, 0.05 mmol), and Pip·HCl (37.1 mg, 0.3 mmol) in DMF (250 μL) under argon was stirred for 15 min at 80 °C. After cooling to ambient temperature, the yellow-brown suspension was stirred further for 15 min before addition of the aniline derivative (2 mmol) and the allyl carbonate (1 mmol). The closed system was heated at 80 °C until full conversion of the carbonate (TLC analysis). Purification was performed directly by column chromatography ($SiO_2$, isohexane/ethyl acetate) of the cooled reaction mixture. The products were obtained as air- and in some cases light-sensitive, colorless oils.

Received: June 6, 2006
Published online: August 9, 2006

**Keywords:** allylic amination · arylamines · homogeneous catalysis · iron · regioselectivity

[1] a) C. Bolm, J. Legros, J. Le Paih, L. Zani, *Chem. Rev.* **2004**, *104*, 6217; b) A. Fürstner, R. Martin, *Chem. Lett.* **2005**, *34*, 624.

[2] a) Review on asymmetric allylic substitutions: B. M. Trost, M. L. Crawley, *Chem. Rev.* **2003**, *103*, 2921; b) I. D. G. Watson, A. K. Yudin, *J. Am. Chem. Soc.* **2005**, *127*, 17516, and references therein; c) J. W. Faller, J. C. Wilt, *Org. Lett.* **2005**, *7*, 1239.

[3] B. Plietker, *Angew. Chem.* **2006**, *118*, 1497; *Angew. Chem. Int. Ed.* **2006**, *45*, 1469.

[4] Review on allylic aminations: M. Johannsen, K. A. Jørgensen, *Chem. Rev.* **1998**, *98*, 1689.

[5] a) A. Leitner, S. Shekhar, M. J. Pouy, J. F. Hartwig, *J. Am. Chem. Soc.* **2005**, *127*, 15506; b) C. Welter, A. Dahnz, B. Brunner, S. Streiff, P. Dübon, G. Helmchen, *Org. Lett.* **2005**, *7*, 1239, and references therein.

[6] a) R. Hermatschweiler, I. Fernandez, F. Breher, P. S. Pregosin, L. F. Veiros, M. J. Calhorda, *Angew. Chem.* **2005**, *117*, 4471; *Angew. Chem. Int. Ed.* **2005**, *44*, 4397; b) R. Hermatschweiler, I. Fernandez, P. S. Pregosin, E. J. Watson, A. Albinati, S. Rizzato, L. F. Veiros, M. J. Calhorda, *Organometallics* **2005**, *24*, 1809.

[7] a) Review on rhodium-catalyzed allylic substitutions: D. K. Leahy, P. A. Evans in *Modern Rhodium-Catalyzed Organic Reactions* (Ed.: P. A. Evans), Wiley-VCH, Weinheim, **2005**, p. 191; b) P. A. Evans, J. E. Robinson, K. K. Moffett, *Org. Lett.* **2001**, *3*, 3269; c) K. Fagnou, M. Lautens, *Org. Lett.* **2000**, *2*, 2319; d) P. A. Evans, J. E. Robinson, J. D. Nelson, *J. Am. Chem. Soc.* **1999**, *121*, 6761.

[8] P. A. Evans, J. D. Nelson, *J. Am. Chem. Soc.* **1998**, *120*, 5581.

[9] "Direct nucleophiles" are distinguished by the fact that the nucleophilic center does not have to be activated prior to the reaction (through, for example, deprotonation).

[10] Oxidative, iron-catalyzed aminations of unactivated olefins: R. S. Srivastava, K. M. Nicholas, *J. Am. Chem. Soc.* **1997**, *119*, 3302, and references therein.

[11] For a common reaction between iron carbonyl complexes and nitrogen bases, see: a) W. Hieber, N. Kahlen, *Chem. Ber.* **1958**, *91*, 2223; b) W. Hieber, N. Kahlen, *Chem. Ber.* **1958**, *91*, 2234.

[12] A significant influence of the substitution pattern was already observed in the iron-catalyzed allylic alkylation;[3] Evans and Robinson reported on similar results in Rh-catalyzed allylic alkylations.[8] The electronic influence of various substituents on conversion and yield in the stoichiometric amination of π-allyl iron complexes has been described: S. Nakanishi, K. Okamoto, H. Yamaguchi, T. Takata, *Synthesis* **1998**, 1735.

[13] The only broadly applicable procedure for the allylic substitution of higher-substituted allyl carbonates by the mechanism involving a σ-allyl metal fragment to be reported so far was published by Martin et al.: B. L. Ashfeld, K. A. Miller, S. F. Martin, *Org. Lett.* **2004**, *6*, 1321.

 © 2006 Wiley-VCH Verlag GmbH & Co. KGaA, Weinheim 